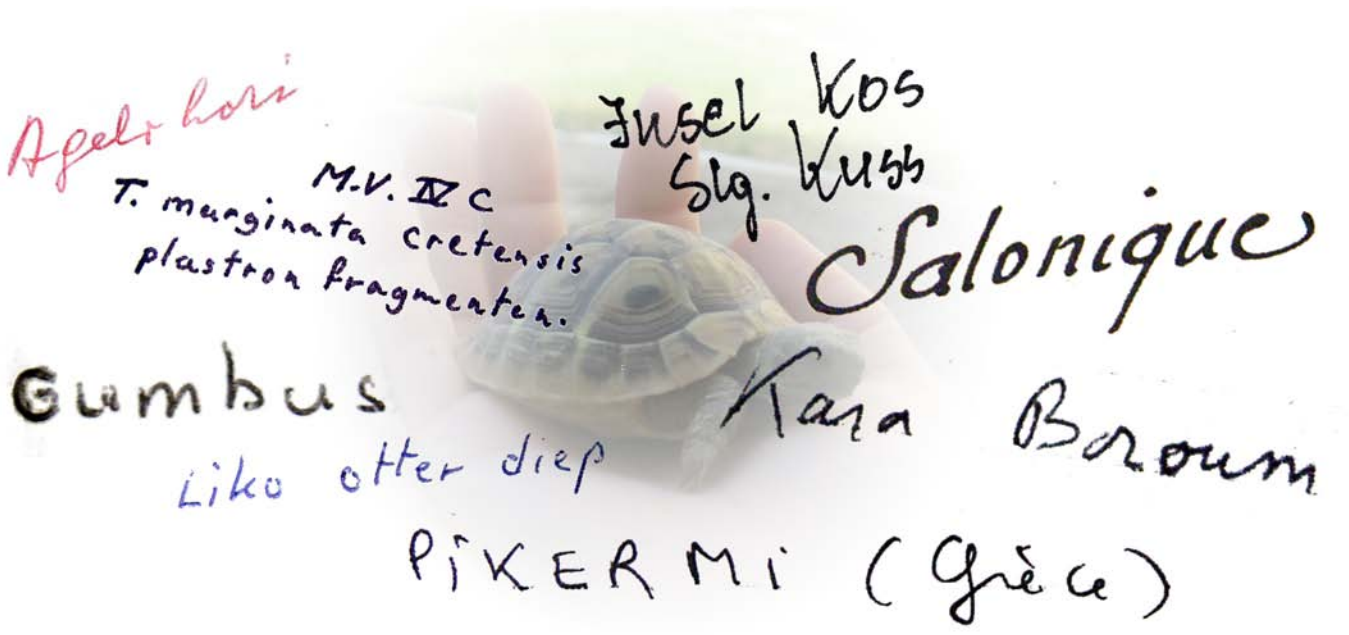
ARISTOTLE UNIVERSITY OF THESSALONIKI
FACULTY OF SCIENCES
SCHOOL OF GEOLOGY

EVANGELOS CH. VLACHOS
MSc Geologist

THE FOSSIL CHELONIANS OF GREECE
SYSTEMATICS - EVOLUTION - STRATIGRAPHY - PALAEOECOLOGY

DOCTORAL THESIS



THESSALONIKI
2015

02/16/2016 Ψηφιακή Βιβλιοθήκη Θεόφραστος - Τμήμα Γεωλογίας - Α.Π.Θ.

Εξώφυλλο: Αποσπάσματα από τις χειρόγραφες ταμπέλες που συνοδεύουν ορισμένα δείγματα τα οποία βρίσκονται σε μουσεία του εξωτερικού. Ελπίζουμε ότι η παρούσα διατριβή θα συμβάλει στην επιστροφή τους σε Ελληνικά ινστιτούτα και μουσεία.

Cover: Parts of the handwritten labels accompanying the fossils studied in this thesis, which are dispersed in various museums in Europe. Hopefully, this work will contribute in the return of those specimens in Greek institutions and museums.

02/16/2016 Ψηφιακή Βιβλιοθήκη Θεόφραστος - Τμήμα Γεωλογίας - Α.Π.Θ.

ΑΡΙΣΤΟΤΕΛΕΙΟ ΠΑΝΕΠΙΣΤΗΜΙΟ ΘΕΣΣΑΛΟΝΙΚΗΣ
ΣΧΟΛΗ ΘΕΤΙΚΩΝ ΕΠΙΣΤΗΜΩΝ
ΤΜΗΜΑ ΓΕΩΛΟΓΙΑΣ

ΕΥΑΓΓΕΛΟΣ Χ. ΒΛΑΧΟΣ
Πτυχιούχος MSc Γεωλόγος

ΟΙ ΑΠΟΛΙΘΩΜΕΝΕΣ ΧΕΛΩΝΕΣ ΤΗΣ ΕΛΛΑΔΑΣ. ΣΥΣΤΗΜΑΤΙΚΗ – ΕΞΕΛΙΞΗ – ΣΤΡΩΜΑΤΟΓΡΑΦΙΑ - ΠΑΛΑΙΟΟΙΚΟΛΟΓΙΑ

ΔΙΔΑΚΤΟΡΙΚΗ ΔΙΑΤΡΙΒΗ

ΘΕΣΣΑΛΟΝΙΚΗ
2015

02/16/2016 Ψηφιακή Βιβλιοθήκη Θεόφραστος - Τμήμα Γεωλογίας - Α.Π.Θ.

Αριθμός Παραρτήματος Επιστημονικής Επετηρίδας Τμήματος Γεωλογίας, Α.Π.Θ., N° 173
Scientific Annals of the School of Geology, Aristotle University of Thessaloniki, N° 173

© Evangelos Ch. Vlachos, 2015
Με επιφύλαξη παντός δικαιώματος. All rights reserved.

THE FOSSIL CHELONIANS OF GREECE.
SYSTEMATICS - EVOLUTION - STRATIGRAPHY - PALAEOECOLOGY

ISBN:

ⓘ evlacho@geo.auth.gr | evlacho@gmail.com

Citation: Vlachos, E., 2015. The fossil chelonians of Greece. Systematics - Evolution - Stratigraphy – Palaeoecology. Scientific Annals of the School of Geology, Aristotle University of Thessaloniki, Greece, 173, 479 pp.

Απαγορεύεται η αντιγραφή, αποθήκευση και διανομή της παρούσας εργασίας, εξ ολοκλήρου ή τμήματος αυτής, για εμπορικό σκοπό. Επιτρέπεται η ανατύπωση, αποθήκευση και διανομή για σκοπό μη κερδοσκοπικό, εκπαιδευτικής ή ερευνητικής φύσης, υπό την προϋπόθεση να αναφέρεται η πηγή προέλευσης και να διατηρείται το παρόν μήνυμα. Ερωτήματα που αφορούν τη χρήση της εργασίας για κερδοσκοπικό σκοπό πρέπει να απευθύνονται προς το συγγραφέα.

Οι απόψεις και τα συμπεράσματα που περιέχονται σε αυτό το έγγραφο εκφράζουν το συγγραφέα και δεν πρέπει να ερμηνευτεί ότι εκφράζουν τις επίσημες θέσεις του Α.Π.Θ.

ARISTOTLE UNIVERSITY OF THESSALONIKI
FACULTY OF SCIENCES
SCHOOL OF GEOLOGY

EVANGELOS CH. VLACHOS
MSc Geologist

THE FOSSIL CHELONIANS OF GREECE
SYSTEMATICS - EVOLUTION - STRATIGRAPHY - PALAEOECOLOGY

Submitted in the School of Geology
Department of Geology
Date of Defence: 13 February 2015

Commitee

Associate Professor Evangelia Tsoukala, School of Geology, Aristotle University of Thessaloniki, Greece (Supervisor)
Professor George Theodorou, Department of Geology & Geoenvironment, National and Kapodistrian University of Athens, Greece
Professor Tassos Kotsakis, Dipartimento di Scienze, University Roma Tre, Italy

Reviewing Committe

Associate Professor Evangelia Tsoukala, School of Geology, Aristotle University of Thessaloniki, Greece
Professor George Theodorou, Department of Geology & Geoenvironment, National and Kapodistrian University of Athens, Greece
Professor Tassos Kotsakis, Dipartimento di Scienze, Università Roma Tre, Italy
Professor George Koufos, School of Geology, Aristotle University of Thessaloniki, Greece
Associate Professor George Syrides, School of Geology, Aristotle University of Thessaloniki, Greece
Associate Professor Massimo Delfino, Dipartimento di Scienze della Terra, Università di Torino, Italy
Independent Researcher A', Dr. Marcelo de la Fuente, CONICET and Museo de Historia Natural de San Rafael, Mendoza, Argentina

02/16/2016 Ψηφιακή Βιβλιοθήκη Θεόφραστος - Τμήμα Γεωλογίας - Α.Π.Θ.

This page has been intentionally left blank

VELOCITATEM SEDENDO

TARDITATEM TEMPERA SURGENDO

MEDIUM TENVERE BEATI



Poliphili Hypnerotomachia (1499)

This page has been intentionally left blank

ACKNOWLEDGMENTS

The present thesis is the result that started many years ago, during my under-graduate studies, when I have decided to start working with fossil turtles. Given the little attention that this group has received in Greece, it was a difficult decision to make. But I had the luck to be accompanied by a supporting family, a generous teacher and numerous respected colleagues. Among all these, the most important person during the last ten years, a major source of inspiration, guidance and support, a respected teacher, a colleague and a friend, has been my supervisor, Ass. Prof. Evangelia Tsoukala. All this work is dedicated to her, along with my deepest respect and appreciation.

We would both like to deeply thank the Supervising and Reviewing Committees for proofing the present thesis.

-

Each and every page of this thesis has a different face, of the numerous people that played a part, minor or major but all equally important, which I will briefly try to mention below. Hopefully I will not forget to mention anyone that has helped during this effort.

Special thanks are due to the Supervising Committee of the thesis, including Prof. George Theodorou and Prof. Anastasios “Tassos” Kotsakis, whose advice, guidance and support were crucial for the completion of this thesis. Due to the efforts of Prof. Theodorou I was able to have access to the wonderful collection of the Paleontological Museum of the University of Athens, as well as to participate in the excavation in Megalopolis (2012), gaining important field experience. Besides Prof. Theodorou, the entire team from AMPG helped me a lot, including Lec. S. Roussakis, Dr. D. Michailidis and PhD candidate V. Mitsopoulou (assistance, material, preparations, discussions). Prof. Kotsakis is an iconic figure of the Greek paleontology and his involvement with the study of turtles in Greece and Italy was of extreme importance for me. Prof. Kotsakis also facilitated my numerous visits to Rome and Italy, arranging many important issues such as accessing specimens and providing useful literature.

The Reviewing Committee comprised of the three members of the Supervising Committee with the addition of four other members: Prof. G. Koufos and Ass. Prof. G. Syrides from LGPUT, Ass. Prof. M. Delfino from University of Torino and the Researcher A’ Dr. M. de la Fuente from CONICET and San Rafael Museum, Argentina. Their critical review and the numerous valuable comments highly improved the final version of the thesis, whereas the useful questions raised during the public defense of the thesis were a major source of inspiration for the future. I would like to deeply thank all the members mentioned above for the honor of being part of the Reviewing Committee.

Many colleagues gratefully provided material for this thesis and/or assisted us in excavations in the area of Thessaloniki, helping also with the preparation of some specimens. I would like to express my sincere thanks to researchers involved and especially to N. Bacharidis, Ch. Plastiras, G. Lazaridis, K. Polydoropoulos, H. Luett, N.

Tsigirliotis, K. Chantzarides, A. Tzanoudakis, A. Xanthis, N. Vassiliadis, N. Bougeli, V. Dimou. Additional new material has been gratefully provided by G. Syrides, K. Vasileiadou, A. Zampetaki, H. Brinkerink, M. Savvelis, A. Bartsiokas, and G. Koufos.

From all the people mentioned above, a special place is reserved for Nikos Bacharidis, a passionate fossil hunter, artist and preparator, responsible for enriching the fossil record of Northern Greece with unique fossils. Our smallest honor to this unique person is to name a new species after him, hoping that his contribution will survive and be mentioned.

In the last part of my personal acknowledgements I would like to mention my friends and colleagues A. Xafis, K. Chatzopoulou, Sp. Pappa and O. Koukousioura for support and important scientific discussions. E. Gregut was the one that suggested working in the large testudinid from Epanomi, which was the start of this beautiful journey. D. Nagel provided key discussions and support over the course of the study. My Dutch colleagues and friends, D. Mol for pushing me to my limits and beyond, R. Bakker, W. van Logchem and H. Wildschut for their help and inspiration. The “Fossilie Schildpadden” event as an invited speaker, in the Natural History Museum of Rotterdam (The Netherlands), organized by D. Mol, Mammuthus Club International, and J. Reumer was a unique experience. And last but not least, my “teacher” Vassilis Makridis for trying to pass onto me all his knowledge and experience.

Finally I would like to dedicate also this thesis to my family for their continuous patience and support in numerous aspects. They were always there when needed, and especially during the times when a scholarship or a grand was not available.

--

Thanks are due to many researchers, individuals, institutions and museums for facilitating, supporting and providing for this study.

For providing access to study material included in this study I would like to thank G. Theodorou, S. Roussiakis, G. Lyras (AMPG), E. Tsoukala, G. Koufos, D. Kostopoulos (LGPUT) M. Mylonas, Ch. Fassoulas (NHMC), T. Syros and the Ephorate of Paleoantrhopology and Speleology of Northern Greece, K. Vitelli and the D’ Ephorate of Nafplion. Material from Crete and stored in the University of Utrecht (the Netherlands) has been gratefully returned to AMPG by H. Brinkerink with the assistance of D. Mol (the Netherlands).

I would like to deeply thank and acknowledge the support and contribution of the staff and members of the School of Geology (AUTH). Access to freely use the facilities of the university was key for the completion of the study. The members of the secretary office, for all the paperwork and support during this lengthy procedure. Access to prepare the thin sections and to use the microscope in the Laboratory of Petrography (AUTH) was granted by Prof. A. Koroneos, and in the Laboratory of Geology (AUTH) by Prof. A. Kilias and Ass. Prof. M. Tranos. I deeply thank the Library of the School of Geology (AUTH) and to S. Mintzaridis for helping with numerous requests on literature and even

more. I would like to draw special attention on their work on the digital library "Theofrastos" that facilitated access in many previous works that are difficult to reach.

For providing access to comparative collections we would like to thank M. Moser (BSPG), E. Cioppi (IGF), K. Rauscher and D. Nagel (IPW), N. Schimdtt-Kittler & K. Grimm (JGU.Geow.Pw); E. Jimenez Fuentes (MCNUS), E. "Dudu" Ruigomez (MEF), D. Schwarz-Wings (MfN), J. Morales and P. Perez Dios (MNCN), R. Allain and B. Battail (MNHN), R. van Zelst (NCB), M. Harzhauser, U. Göhlich and R. Gemel (NHMW), S. Scherrer (NWS), H. Furrer (PIMUZ), R. Boettcher and R. Schoch (SMNS).

Over the course of this study I had the privilege to work and co-operate with and learn from several colleagues in Greece and abroad. I would like to thank F. de Lapparent de Broin for providing the basement and as a major source of inspiration through her works; A. Pérez-García for all the co-operation with the Spanish material; M. Rabi and M. Boehme for their co-operation with the German material; M. Delfino for his collaboration with material from Greece and Italy; G. Iliopoulos for invaluable help with the Cretan material; M. Stiner and N. Munro for the co-operation with the material from Franchthi Cave; G. Georgalis for useful discussions; L. Dotsika regarding information on stable isotopes; A. Plougarlis for preparing thin sections; L. Papadopoulou and M. Zougrou for SEM analysis and assistance with optical microscopy; A. Kalogera for assistance with CT-scans of fossil material; T. Rowe and the Digimorph.org crew for allowing using the ct-scans for comparisons; M. Tranos, E. Thomaidou, A. Batsi, G. Georgiadis, A. Plougarlis and P. Neofotistos for discussions and useful literature on geological issues; I. Cerda for assistance with bone histology and co-operation; D. Pol and M. de la Fuente for useful discussions on cladistics and on South American taxa and invaluable support during my stay in Argentina (austral winter 2014).

The Willy Hennig Society is thanked for sponsoring the free use of the TNT software.

Several grants and awards provided important financial support for the completion of this study. Study of MNCN collections was supported by a Synthesys grant (ES-TAF 2754). Study of German material was supported by the IKYDA 2014 project. Additional support was provided by an Excellence Award of the Research Committee of AUTH (2013).

Nothing would be possible without the critical review, guidance and advice of Juliana Sterli. During a short-term visit in MEF (Trelew, Argentina) she guided me through the process of phylogenetic analysis and she provided information and photographs on extant testudinoids, which were used for the phylogenetic analyses. Her support in nearly every aspect of this thesis was of equal importance as the shell is for a tortoise.

Evangelos Ch. Vlachos

February 13, 2015

Thessaloniki, Greece

This page has been intentionally left blank

ABSTRACT

The present thesis deals with the description of the fossil chelonians of Greece, mainly focusing on the detailed description of thousands individual specimens from more than 40 localities, including many new specimens and nearly all the previously published ones. Also, efforts have been made to place these taxa into a phylogenetic context, and to generate some hypotheses on the distribution, the role of chelonians in biostratigraphy and to explore their paleoecology through histological sections. The Greek paleochelonofauna is the most diverse and best preserved in the South Balkans with numerous testudinids (both small and large in size) and geoemydids. Also present, but to a smaller extent, are the emydids and trionychids, whereas a single pleurodire has been found. In general, the taxonomic diversity described in this thesis is significantly different than previously thought, since several taxa previously mentioned are found not valid, additional taxa have been identified, as well as the presence of at least three new taxa is proposed. Fossil chelonians are present in Greece since the Early Miocene, but their main geographical distribution is established since the Late Miocene. The evolution of several clades is in good accordance with the significant geotectonic and climatic changes that occurred in the circum Mediterranean area. As for the phylogenetic analysis, a new matrix of 81 morphological characters for the testudinids is defined, producing promising results that allow discussion of the phylogenetic relationships and evolutionary history of the major testudinid clades, as well as to investigate the evolution of gigantism in this group. The Greek fossil chelonian assemblage, standing between Eurasia and Africa, is of critical importance for the evolution of various chelonian clades from the beginning of the Neogene and onwards. Finally, as it is evident from the present thesis, the study of fossilized chelonians could provide a significant advance on our knowledge of paleoecology and biostratigraphy of Greece.

Keywords: turtles; tortoises; Testudinidae; Geoemydidae; Trionychidae; Emydidae; Bothremydidae; Mediterranean; Balkans; Phylogeny; Paleogeography; Paleoecology.

02/16/2016 Ψηφιακή Βιβλιοθήκη Θεόφραστος - Τμήμα Γεωλογίας - Α.Π.Θ.

ORGANIZATION OF THE DOCTORAL THESIS

In Chapter 1 introductory information is provided. First, the main objectives of the study are clearly stated (1.1), followed by information on Material & Methods (1.2), i.e. abbreviations, methodology and lists of comparative material. The last two sub-chapters provide information on the extant chelonian fauna of Greece (1.3) and an historical overview of the study of chelonians in Greece.

In Chapter 2 brief geological information is provided for the sites mentioned here.

Chapter 3 contains the main information on the paleontological results, such us the detailed anatomical description of the available specimens of Greece, with anatomical drawings, photographic documentation and measurements.

The remaining chapters analyze and discuss the morphological information in a evolutionary – phylogenetic (Chapter 4), biostratigraphic (Chapter 5) and palaeoecologic (Chapter 6) context.

Chapter 7 summarizes the conclusions of this study.

Chapter 8 provides an extensive summary in Greek language.

In the end of the thesis, the full reference list is followed by an extensive Appendix, with tables of measurements, CT-scan results, and all data concerning the phylogenetic and SEM analyses.

02/16/2016 Ψηφιακή Βιβλιοθήκη Θεόφραστος - Τμήμα Γεωλογίας - Α.Π.Θ.

Table of Contents

Chapter 1. Introduction	**1**
1.1. Objectives	4
1.2. Material and Methods	5
1.2.1. Abbreviations	5
1.2.2. Material	6
1.2.3. Methods	8
1.3. The extant chelonian fauna of Greece	10
1.4. Historical overview of the chelonian research in Greece	18
Chapter 2. Geological information of the fossil chelonian sites of Greece	**21**
2.1. Introduction	22
2.2. Miocene	24
2.3. Pliocene	29
2.4. Pleistocene	35
2.5. Pleistocene/Holocene	41
2.6. Material of uncertain age	42
Chapter 3. Paleontology	**43**
3.1. Introduction	44
3.2. Systematic Paleontology	45
TESTUDINES Batsch, 1788 (sensu Joyce et al., 2004)	45
PLEURODIRA Cope, 1865	45
PODOCNEMIDOIDEA (sensu Gaffney et al., 2006)	45
CRYPTODIRA Cope, 1868	47
TRIONYCHIDAE Gray, 1825	47
TESTUDINIDAE Gray, 1825	52
Titanochelon Pérez-García & Vlachos, 2014	52
Testudo Linnaeus, 1758 sensu lato or *Pantestudo* (sensu Parham et al. 2006)	118
Testudo Linnaeus, 1758 sensu stricto or *Testudo* (sensu Parham et al. 2006)	122
GEOEMYDIDAE Theobald, 1868	235
Mauremys Gray, 1869	235
EMYDIDAE Bell, 1825	275
Emys Duméril, 1805	275
TESTUDOOLITHIDAE indet. (sensu Hirsch, 1996)	282
Chapter 4. Evolution	**289**
4.1. Introduction	290
4.2. A new matrix for testudinids	290
4.3. Phylogenetic analysis of the testudinids from Greece	320
4.4. Phylogenetic analysis of the terrapins from Greece	334
4.5. The bothremydid affinities of the pleurodiran *Nostimochelone lampra*	340
Chapter 5. Biostratigraphy	**343**
5.1. Introduction	344
5.2. Distribution	344
5.3. Comparison of the Greek chelonian assemblage with adjacent areas	349
Chapter 6. Palaeoecology	**355**
6.1. Introduction	356
6.2. The histology of the Gefira trionychid	357
6.3. The histology of the large testudinid, *Titanochelon bacharidisi*	363
6.4. Concluding Remarks	365
Chapter 7. Conclusions	**367**
Chapter 8. Εκτεταμμένη Περίληψη - Extended Summary in Greek	**381**
References	391
List of Tables - List of Figures	405
Appendix	413 - 479

This page has been intentionally left blank

Chapter 1. Introduction

Highlights:

Objectives
Extant chelonian fauna
History of investigations in Greece

02/16/2016 Ψηφιακή Βιβλιοθήκη Θεόφραστος - Τμήμα Γεωλογίας - Α.Π.Θ.

Chapter 1. Introduction

Turtles and tortoises are among the most peculiar and characteristic animals on the planet, mainly because of the presence of a rigid shell that encloses part the neck, girdles and limbs and part of the tail. The turtle shell comprises of the dorsal carapace and the ventral plastron, which are connected laterally in the bridge. The shell leaves an anterior opening for the neck and anterior limbs and a posterior opening for the posterior limbs and tail.

Turtles are successfully surviving in nearly all continents of the planet, except Antarctica, having a remarkable diversity of terrestrial, freshwater and truly marine forms. Their fossil record is extensive, with early representatives even in the Upper Triassic. The origin of turtles, and especially of the shell is, however, a subject of debate (amongst others: Gilbert et al, 2001; Lyson et al, 2010; 2013; Kuratani et al., 2011; and references therein).

Greece is located in the south Balkans area in the eastern Mediterranean Sea, in the crossroads of three continents (Europe, Asia and Africa). The complex terrestrial environments of Greece have emerged from the Alpine orogenesis and the closure of the Tethys ocean in the late Eocene – Oligocene times, and has undergone a series of changes as a result of geological, climate and environmental processes. The present-day environment of Greece is also complex, hosting mountain ranges and extensive low-lands, river and lake systems and a high number of islands of various sizes (some of them volcanic in origin). This complex ecosystem is home to a relatively diverse chelonian fauna with marine, freshwater and terrestrial species.

The purpose of this thesis is to present and document, for the first time, the available fossil record of chelonians in Greece in detail. The main focus is not only in the revision of previously published taxa, but mainly in the detailed description of new material. Most of the specimens come from the Late Miocene and Pliocene, from a number of fossil localities in continental and insular Greece. Previous to the Late Miocene, the known localities are few. In Pleistocene, however, the quantity of localities is relatively numerous, especially those in caves that emerged in Greece due to the extension of the geotectonic environment during Plio-Pleistocene. The Holocene record is also rich, with many archaeological sites with chelonians; some of them are accidental findings whereas others were used a small-game food resources. Besides a food resource, the role of chelonians in antiquity was important in the daily life. Turtles were used as musical instruments (λύρα – lyre) or even depicted in coins (στατήρας – stater) and ceramics. Also, the distinct locomotion of turtles, as a result of the presence of the shell, has given rise to several myths (e.g. Aesop's myth, "The tortoise and the hare") or mathematical problems (e.g. Zeno's paradox, "The Achilles and the tortoise").

Up to now, little attention has been given to the study of the fossil chelonians, especially compared to the vast amount of studies about the fossil mammals from Greece. In most cases, they are short papers where a single specimen is described (e.g. Melentis; Symeonidis and collaborators; see below). Others only mentioned the presence of turtles and tortoises, without giving any morphological information. Recently, a summary table of the fossil chelonian findings is given by Mueller-Töwe et al. (2011). Over the course of this thesis, the process of revising the Greek fossil chelonians is continued, a task that started by the author during his diploma and master thesis (Vlachos 2007; 2011) regarding fossil giant tortoises from Thessaloniki area. The results obtained from the present doctoral thesis can be compared with similar efforts in Italy (Delfino, 2002; Chesi, 2008), France (de Broin, 1977; Hervet,

2003) and Spain (Pérez-García, 2012). Unfortunately, the information on Minor Asia and North Africa is still limited, but several papers provide relevant information (Staesche et al., 2007; Lapparent de Broin, 2000; 2003; 2008; Gmira et al., 2014).

In total, the specimens from more than 40 localities have been studied in this thesis. The study of this material is distributed in several museums and institutions in Greece and Europe. Additionally, comparative material from several European collections has been used. The preliminary results of this doctoral thesis have allowed the publication of several papers (Tsoukala et al., 2011; Vlachos et al., 2014; in press; Vlachos & Tsoukala, in press; Pérez-García & Vlachos, 2014) and a number of oral and poster presentations in international, national conferences and symposiums (Table 1.1).

Table 1.1. List of publications that are related with the present doctoral thesis.

Papers in peer-reviewed journals
The chelonians from the latest Miocene-earliest Pliocene locality of Allatini and Pylea (east Thessaloniki, Macedonia, Greece). Vlachos, E., Delfino, M. & Kotsakis, T. *Comptes Rendus Palevol*, in press.
Testudo cf. *graeca* from the new Late Miocene locality of Platania (Drama basin, N. Greece) and a reappraisal of previously published specimens. Vlachos, E. & Tsoukala, E. *Bulletin of the Geological Society of Greece*, in press.
New generic proposal for the European Neogene large testudinids (Cryptodira) and the first phylogenetic hypothesis for the medium and large representatives of the European Cenozoic record. Pérez-García, A. & Vlachos, E. *Zoological Journal of the Linnean Society*, 2014, 172(3): 653-719.
Cheirogaster bacharidisi sp. nov., a new species of a giant tortoise from the Pliocene of Thessaloniki (Macedonia, Greece). Vlachos, E., Tsoukala, E. & Corsini, J. *Journal of Vertebrate Paleontology*, 2014, 34(3), 560-575.
Elephas antiquus in Greece: New Finds and a reappraisal of older material (Mammalia, Proboscidea, Elephantidae). Tsoukala, E., Mol, D., Pappa, S., Vlachos, E., van Logchem, W., Vaxevanopoulos, M., Reumer, J. *Quaternary International*, 2011, 245: 339-349.
Extended abstracts in conferences
Between the feet of elephants: turtles as a common element of the associated fauna of proboscideans. Vlachos, E. Abstract Book of the VIth International Conference on Mammoths and their Relatives. Scientific Annals of the School of Geology, Special Volume 102: 9.
Abstracts in conferences
Relevance of the Miocene *'Testudo' bolivari* (Cryptodira, Testudinoidea) to understanding the phylogenetic relationships of the testudinids from the Cenozoic of Europe. Pérez-García, A., Vlachos, E., Ortega, F. 74th Meeting of the Society of Vertebrate Paleontology, Berlin, November 2014.
A revision of the chelonian fauna from Allatini (Thessaloniki, Macedonia, Greece, latest Miocene-earliest Pliocene). Vlachos E., Kotsakis, T. & Delfino, M. 11th Annual Meeting of the European Association of Vertebrate Palaeontologists, Torino, June 2014.
Did the Messinian Salinity Crisis allow the migration of large tortoises from Africa to Europe? Pérez-García, A., Murelaga, X. & Vlachos, E. Gondwana 15, Madrid, May 2014.
Las tortugas gigantes del Mioceno medio de la Meseta Castellana: Revisión del (malparado) material clásico. Pérez-Garcia, A. & Vlachos, E. XXIX Jornadas de la Sociedad Española de Paleontología, Cordoba, Spain, October 2013.
Special Remarks on the Posterior Limb morphology of the Giant Continental Tortoises from the Pliocene of Thessaloniki area (Macedonia, Greece). Vlachos, E. Symposium on Turtle Evolution, University of Tübingen, Germany, 2-4 June 2012.
New Finds of Giant Tortoises from Thessaloniki area: the most complete *Cheirogaster* BERGOUNIOUX, 1935 skeleton in Greece. Vlachos, E. & Tsoukala, E. 9th Annual Meeting of the European Association of Vertebrate Palaeontologists, Heraklion, Greece, 2011, Abstract Book, p. 59.

1.1 . Objectives

In the present thesis the entire available fossil chelonian fauna from Greece is studied, in order to answer a series of open questions. The general objectives that are going to be explored in this study are briefly summarized below.

Objective 1: Paleontological study and description of new specimens of turtles and tortoises. A great number of new specimens is presented here. Their description enlightens our knowledge on the morphology and diversity of the chelonian diversity in Greece.

Objective 2: Discovery of new taxa of turtles and tortoises from Greece. The detailed morphological description and comparison of the specimens allow the designation of several new taxa of turtles and tortoises. Whereas some of them have been justified through publication in peer-reviewed journals, others are introduced here for the first time and are in the process of publication.

Objective 3: Revision of previously published specimens from Greece. Nearly all the previously published specimens (some of them are lost or not available) are revised here, providing new information on their morphology and systematic position. An overview of the previously published papers is given in the Chapter 1.4.

Objective 4: Documentation of the diversity of the fossil chelonians of Greece. This is the main objective of the thesis, as the information mentioned in previous works (e.g. Lapparent de Broin, 2001; 2002; Mueller-Töwe et al., 2012; Georgalis & Kear, 2013) barely reflects the true diversity and/or is partly erroneous in some cases. This information will allow comparison with the extant chelonian fauna of South Balkans. An overview of the extant chelonian fauna of Greece is given in the Chapter 1.3.

Objective 5: Description of the evolution of the chelonian clades in Greece, from the Miocene up to the present. The up-to-date knowledge of the morphology and distribution of the various taxa, allows the documentation of the evolution of the turtle lineages in the South Balkans.

Objective 6: Phylogenetic analysis of the small testudinid taxa. Based on a new set of morphological characters will be performed a phylogenetic analysis of the small testudinid taxa from Greece. This analysis will be included in a larger dataset containing various testudinid taxa from all continents.

Objective 7: Phylogenetic analysis of the large testudinid taxa. Based on a new set of morphological characters will be performed a phylogenetic analysis of the large testudinid taxa from Greece. This analysis will be included in a larger dataset containing various testudinid taxa from all continents.

Objective 8: Phylogenetic analysis of the freshwater taxa. Based on a pre-existing matrix (introduced in Hervet, 2003) will be performed the phylogenetic analysis of freshwater taxa, discussing the various problems on the systematics of the *Palaeochelys-Mauremys* clade (sensu Hervet, 2004). Also will be explored the phylogenetic relationships of the only pleurodire from Greece, based on the matrices of Gaffney et al. (2006; 2011).

02/16/2016 Ψηφιακή Βιβλιοθήκη Θεόφραστος - Τμήμα Γεωλογίας - Α.Π.Θ.

Objective 9: Study the bone histology of several taxa. Histological sections could provide valuable data in the morphology of several specimens and they could bring information related with the palaeoecology of these taxa. In the current thesis histological studies have been performed in trionychid and large testudinid samples.

Objective 10: Comparison of the Greek chelonians with those from Minor Asia, Italy, South Balkans and adjacent areas.

Objective 11: Study of the contribution of the fossil chelonians to the biostratigraphy of the Neogene – Quaternary of South Balkans.

Objective 12: Identifying key areas of future research.

1.2. Material and Methods

1.2.1. Abbreviations

Institutional Abbreviations

AMPG, Museum of Palaeontology and Geology of the National and Kapodistrian University of Athens, Greece; **BSPG**, Bayerische Staatssammlung für Paläontologie und Geologie, Munich, Germany; **GNHM**, Goulandris Natural History Museum, Athens, Greece; **GPIT**, Geological and Paleontological Institute of Tübingen, Germany; **IPS**, Institut Català de Paleontologia; **IPW**, Institute of Paleontology, University of Vienna; **JGU.Geow.Pw**, Johannes Guttenberg University, Department of Geosciences, Paleontological Collection, Mainz, Germany; **LGPUT**, Laboratory of Geology and Paleontology of University of Thessaloniki; **MCNUS**, Museum of Salamanca, Spain; **MPEF**, Museo Paleontológico Egidio Feruglio, Trelew, Chubut, Argentina; **MIL**, Paleontological Exhibition of Milia, Grevena, Greece; **NHMC**, Natural History Museum of Crete, Herakleion, Crete, Greece; **NHMW**, Naturhistorisches Museum, Vienna, Austria; **MNCN**, Museo National de Ciencias Naturales, Madrid, Spain; **MNHN**, Muséum National d'Histoire Naturelle, Paris, France; **NCB**, Naturalis Center of Biodiversity, Leiden, The Netherlands; **NWS**, Naturmuseum Winterthur, Switzerland; **PIMUZ**, Paläontologische Institut und Museum, University Zurich, Switzerland; **SMNS**, Staatliche Museum für Naturkunde, Stuttgart, Germany; **STUS**, Sala de las Tortugas de la Universidad de Salamanca, Spain; **VM**, Vrisa Museum of Natural History, Lesvos Island

For the material used in the phylogenetic analysis (see chapter 4): **AMNH**, American Museum of Natural History; **CRI**, Chelonian Research Institute (P. Pritchard), U.S.A.; **FRANK**, Natural History Museum of Frankfurt, Germany; **REP**, Comparative Anatomy Collection, MNHN, Paris; **UCMP**, University of California Museum of Paleontology, U.S.A.; **USNM**, Smithsonian Museum of Natural History, U.S.A; **ZIN**, Zoological Museum of the Russian Academy of Sciences, Moscow, Russia.

Without abbreviations: Museum of Petralona Cave, Chalkidiki; the Ephorate of Paleoanthropology and Speleology, Ministry of Culture, Thessaloniki; the D'

Ephorate of Prehistoric Archaeology, Nafplion, Peloponnesus; the Museum of Theopetra Cave, Kalambaka, Thessaly.

Anatomical Abbreviations

Bony plates are indicated with small letters, scutes with capitals. Palatal ridges and temporal emarginations also with capitals. **ABD**, abdominal; **AN**, anal; **ane**, apertura narium externa; **ap**, apertura postotica; **as**, astragalus; **as+cal**, astragalocalcaneum; **bo**, basioccipital; **bs**, basisphenoid; **cal**, calcaneum; **CE**, cervical; **cm**, condylus mandibularis; **co**, condylus occipitalis; **cos**, costal; **cs**, crista supraoccipitalis; **dc**, distal carpal; **dt**, distal tarsal; **en/ent**, entoplastron; **ep**, epiplastron; **FE**, femoral; **fe**, femur; **fi**, fibula; **fjp**, foramen jugulare posterius; **fm**, foramen magnum; **fnh**, foramen nervi hypoglossi; **fo**, fossa orbitalis; **fp/fpp**, foramen praepalatinum; **fr**, frontal; **fst**, foramen stapedio-temporale; **fti**, fossal temporalis inferior; **fts**, fossa temporalis superior; **GU**, gular; **hyo**, hyoplastron; **hypo**, hypoplastron; **HU**, humeral; **ica**, insicura columella auris; **int**, intermedium; **ju**, jugal; **LAR**, labial ridge; **LIR**, lingual rigde; **LTE**, lower temporal emargination; **MA**, marginal; **mc**, metacarpal; **md**, mandible; **med+lat**, medial + lateral centrale; **MMR**, median maxillary ridge; **mt**, metatarsal; **mx**, maxilla; **ne**, neural; **nu/nuc**, nuchal; **op**, opisthotic; **os**/**ost**, osteoderm; **pa**, parietal; **pal**, palatine; **PEC**, pectoral; **per**, peripheral; **ph**, phalanx; **pla**, plastron; **PLE**, pleural; **prf**, prefrontal; **PMP**, posterior maxillary process; **pmp**, premaxillary pit; **PMR**, premaxilla/maxilla ridge; **po**, postorbital; **pp**, processus postobritalis; **pr**, prootic; **pt**, pterygoid; **pto**, processus trochlearis oticum; **py**, pygal; **qj**, quadratojugal; **qu**, quadrate; **ra**, radius; **SUC**, supracaudal; **soc**, supraoccipital; **sp/spy**, supragygal; **sq**, squamosal; **ti**, tibia; **tp**, processus trochlearis; **tu**, tubercle; **un**, ungual; **UTE**, upper temporal emargination; **VE**, vertebral; **vo**, vomer; **VR**, vomer ridge; **xi**, xiphiplastron.

Other Abbreviations:

Fm, formation; **Mb**, member; **MN**, Mammal Neogene Biozones (after Mein, 1989)

1.2.2. Material

The studied material is given in detail in the description of each taxon. It includes material stored in the collections of AMPG, GNHM, LGPUT, MIL, MNHN, NHMC, NHMW, VM, and additional from the Museum of Petralona Cave, Chalkidiki, the D' Ephorate of Prehistoric Archaeology, Nafplion.

The following specimens were used as comparative material for the purposes of this thesis, with direct observations made by the author:

-AMPG-
specimens of shells of the extant taxa, *Testudo ibera*, *'Testudo' hermanni boettgeri*, *Testudo marginata, Emys orbicularis, Caretta caretta*.

-BSPG-
Geochelone cf. *perpiniana* (in Schleich, 1981, Sandlezhausen; BSPG 1959 II 2034, MN5);

additional material from Sandelzhausen (mentioned in Schleich, 1981; BSPG 1959 II 2033, MN5)

-IPW-
Trionyx sp. (unpublished, Siebenhirten; IPW)
Trionyx rostratus (unpublished, Leithahalk; IPW 1897/II 14)

-LGPUT-
Testudo marginata shell (Mt. Olympus; extant);
'Testudo' hermanni shell (Milia, Grevena; extant);
Testudo graeca shell (Thessaloniki; extant)

-MNCN-
material of *Titanochelon bolivari* (presented in Pérez-García & Vlachos, 2014, see supplementary information for detailed numbers)
Centrochelys sulcata (Algeria, extant)

-MNHN-
"*Cheirogaster*" sp. (Artenay, MNHN AR 538, MN 2)
"*Cheirogaster*" sp. (Bois de Fabregues, MNHN APF 1, MN 6-7)
"*Cheirogaster*" *phosphoritarum* (Quercy, MNHN QU 8747, Oligocene)
"*Cheirogaster*" *eurysternum* (Saint-Gerand-le-Puy, MNHN SG 289-290, MN 2a)
"*Cheirogaster*" sp. (Vauche, MNHN VAU 1, Miocene)
"*Cheirogaster*" sp. (Gypsum, MNHN GY 7, Miocene)
"*Cheirogaster*" *perpiniana* (Perpignan, MNHN 1887-26, Late Pliocene)
"*Testudo*" *gigas* (Bournoncle Saint-Pierre, MNHN.F.BP 2014, Oligocene)
?*Centrochelys* sp. (Irak, Injana, MNHN G 694, lower Miocene)
Centrochelys sp. (Djebel Zelten, MNHN QB 55, MN4)
Chelonoidis nigra (Galapagos, Gallery of Comparative Anatomy, extant)

-NCB-
material of giant tortoises from Indonesia (in Hooijer, 1971)

-NHMW-
cf. *Cheirogaster schafferi* (Szalai, 1931, Samos; NHMW 2009z0103/0001, NHMW 1911/0005/0275, MN12-13)
Testudo antiqua novitensis (Roggendorf; NHMW A-3602, MN6-8?)
Testudo cf. *promarginata* (Prottes, NHMW Prottes 57)
Mauremys cf. *gaudryi* (Kohfidisch, NHMW 1981/24/18, Turolian)
Hadrianus sp. (Prottes; NHMW 1984/67a, Eocene?)

-NWS-
Cheirogaster vitodurana (holotype, in Biedermann, 1862, Wintethur; NWS 13758, MN6)
"*Testudo*" *picteti* (holotype, in Biedermann, 1862, Winterthur; NWS 14900, MN6)

-PIMUZ-
Cheirogaster vitodurana (in Peyer, 1946, Zurich; PIMUZ A/III 661, MN6)
Testudo escheri (in Pictet & Humbert, 1856, Winterthur; PIMUZ A/III 00094, MN6)

-SMNS-
Geochelone sp. (unpublished, Tobel Oelhalde Süd; SMNS 85684, 85685, MN5-6);
Geochelone sp. (Oberkirchberg; SMNS 57201, 57202, 85325, MN4);
Geochelone sp. (unpublished, Langenau; SMNS 52142, 52143, 53518, 53519, 53586, 53662, 53707, 85959, 89577, MN4-6);
Geochelone sp. (unpublished, Essingen; SMNS 50044, 56906, MN4-6)

-STUS-
Titanochelon bolivari (numbers of material in Pérez-García & Vlachos, 2014)

1.2.3. Methods

General: standard paleontological procedures in the study of the fossil and extant specimens were followed. Measurements have been taken using a BMI caliper (0.01 mm precision). Photographs were taken using a SONY Powershot and a NIKON 1 J3 camera. Photographs have been edited using Adobe Photoshop CS5. Drawings were made using Adobe Illustrator CS5. Diagrams were created in Microsoft Excel 2007 and in PaSt software (MAC free version; Hammer et al., 2001). Timescale in figures (including all subdivision and MN zones) has been generated with the TimeScale Creator (freely available at www.stratigraphy.org) routed to the divisions validated by the International Commission of Stratigraphy.

Literature: Skull nomenclature follows Gaffney (1972). Shell nomenclature follows Zangerl (1969). Anatomical descriptions of giant tortoises follow Vlachos et al. (2014) and Pérez-García & Vlachos, 2014. The work of Amiranashvili (2000) is used for the description of shells of *Testudo.* For the study of microscopic thin-sections we follow Scheyer (2007). Taxonomy largely follows Joyce et al. (2004). Useful information about extant taxa is available in http://wbd.etibioinformatics.nl/ (Turtles of the world) by Ernst, Altenburg & Barbour. Geographical ranges of extant taxa largely follow Iverson (1986). Taphonomical nomenclature follows Badgley (1986).

Phylogenetic Analysis: The basis for the morphological matrix of the testudinids is the set of characters introduced by Pérez-García & Vlachos (2014) for the European giant tortoises. This matrix (9 taxa and 36 characters) is expanded with additional characters from Crumly (1982, 1984), Amiranashvili (2000), Gerlach, (2001), Takahashi et al. (2003), Joyce and Bell (2004), and Zacarias et al. (2013). For the analysis of the geoemydids the data matrix introduced by Hervet (2003) is used, following the modifications suggested by Chesi et al. (2009) for *Mauremys portisii* and *Mauremys campanii* (excluding *Borkenia* aff. *B. oschkinisi*). The synonymies proposed by Claude & Tong (2004) have been accepted, i.e. for *Juvemys*, *Francellia*, *Owenemys* and *Euroemys* (junior synonyms of *Palaeoemys*), for *Bergouniouxchelys*, *Cuculemys* and *Provencemys* (junior synonyms of *Palaeochelys*), for *Francellia sallouagmirae* and *Juvemys labarrei* (junior synonyms of *Palaeoemys testudiniformis*) and *Palaeoemys occitana* (junior synonym of *Palaeoemys hessiana*). For the analysis of the pleurodiran material the matrices of Gaffney et al. (2006) and Gaffney et al. (2011) are used. The matrices were created in Mesquite software (Maddison & Maddison, 2008). The cladistic analysis was made with the software TNT (Goloboff et al., 2008a, b). The clade Bremer support and Jackknife and Bootstrap indices were calculated in TNT. The results obtained in this study present an ideal example to be analyzed by using the Dispersal – Extinction – Cladogenesis

Analysis (DEC) model that has been developed by Ree & Smith (2008). The analysis was run in Python v. 2.7.8, by using the Python script (see Suppl. Data for the detailed results), which was generated in the online page http://www.reelab.net/lagrange/configurator/index. First, a matrix with the species ranges across the five different study areas has been uploaded. Second, the tree was uploaded in Newick format with time-calibrated branch lengths, by using the MSM script in TNT (following Pol & Norell, 2001; 2006). Regarding the range constraints, it seems rather improbable that a taxon could be spread in more than two of the defined areas. The DEC model not only will calculate the possible ancestral areas for each node, but more importantly this will be evaluated through the various dispersal constraints raised by the geotectonic evolution of the area since the Eocene. Dispersal constrains are mainly based on Rögl (1999) and Popov et al. (2006).

Thin sections: the thin sections were made following the methodology proposed by Scheyer (2007). The sections were prepared in the Laboratory of Petrography of the School of Geology, Aristotle University of Thessaloniki. The costals were sampled in X (transversely) and L (parallel) sections, following standard petrographic procedure. All bone samples were processed into standard petrographic thin-sections. Therefore, the bone samples (whole shell elements, fragments and drilled cores) had to be stabilized by embedding into synthetic resins (Araldite-2020® or Biresin-L84®). In a second step, the specimens were cut and ground successively with SiC powder (220, 500, 800 and 1000) to eradicate saw marks and smooth out the relief. Third, the bone material was subsequently processed into thin-sections of a thickness around 80 μm or less, again using the SiC grounding powders mentioned above. Because of the highly porous nature and inner vascularization, some specimens had to be impregnated in vacuum several times with synthetic resins (Araldite-2020® or Biresin-L84®). The study of the sections was realized in two LEICA DMLP® compound polarizing microscopes (magnifications: 40x, 100x, 400x; normal transmitted and polarized light) in the Laboratory of Petrography (AUTH) and in the Laboratory of Geology (AUTH). Additional study was made in a LEICA DMLP® compound polarizing microscopes (magnifications: 40x, 100x, 400x; normal transmitted and polarized light) in MEF.

1.3.The extant chelonian fauna of Greece

In this chapter brief information on the extant chelonians of Greece is given. This information is important for the study of the fossil chelonian fauna. The following composition is the result of the evolution of the chelonian lineages in the Mediterranean and South Balkans, shaped by migrations, dispersals, extinctions, and climate changes. In some cases, humans might have played a role in the extinction of some forms and the dispersal of others. This work will be, from paleontological point view, presenting information regarding some taxonomical issues of some taxa, the general morphology of the extant species, and information regarding the range of these forms in Greece, in the present. At the same time, attention will be drawn upon the ecology of each taxon, which will help the analysis of their extinct representatives.

Several summaries and checklists provide a list of the taxa present in Greece. Perhaps one of the most complete and detailed works, is the work of Sillero et al. (2014). From a taxonomic point of view, the contribution of the Turtle Taxonomy Working Group (TTWG) is also useful. According to one of the latest reports of

TTWG (van Dijk et al., 2012) the extant chelonian fauna of Greece consists of the following taxa:

Testudines Batch, 1788

Cryptodira Cope, 1868
Chelonioidea Baur, 1893
Cheloniidae Oppel, 1811
Caretta caretta Linnaeus, 1758
(Nesting site) [Loggerhead Turtle]

Chelonia mydas Linnaeus, 1758
(Foraging site) [Green Sea Turtle]

Dermochelyidae Fitzinger, 1843
Dermochelys coriacea Vandelli, 1761
(Foraging site) [Leatherback Sea Turtle]

Testudinoidea Fitzinger, 1826
Emydidae Rafinesque, 1815
Deirochelyinae Agassiz, 1857
Trachemys scripta elegans Wied, 1839
(Introduced) [Read-eared Slider]

Emydinae Rafinesque, 1815
Emys orbicularis Linnaeus, 1758
[European Pond Turtle]
(*E. o. hellenica* Vallenciennes *in* Bibron & Bory de Saint-Vincent, 1832)

Geoemydidae Theobald, 1868
Mauremys rivulata Vallenciennes *in* Bory de Saint-Vincent, 1833
[Western Caspian Turtle, Balkan Terrapin]

Testudinidae Batsch, 1788
Testudo graeca Linnaeus, 1758
[Spur-thighed Tortoise, Greek Tortoise, Moorish Tortoise]
(*T. g. ibera* Pallas, 1814)

Testudo marginata Schoepff, 1793
[Marginated Tortoise]

'Testudo' hermanni Gmelin, 1789
[Hermann's Tortoise]
('*T*'. *h. boettgeri* Mojsisovics, 1889)

In general, no pleurodirans are present today in Greece. On the other hand the cryptodirans are diverse, showing several marine forms, few freshwater taxa and a significant number of terrestrial tortoises.

As far as the marine turtles are concerned, no fossil specimens are known up to now from Greece. The present geography of Greece, however, in the eastern part of the Mediterranean Sea is one of the places of the world that the cosmopolitan chelonid turtles are found, the Loggerhead Turtle *Caretta caretta* and the Green Sea Turtle *Chelonia mydas*. The two taxa differ much in shell morphology, with *Caretta caretta* being larger and heavier than *Chelonia mydas* (Ernst & Barbour, 1989). From

these two chelonids, only the loggerhead turtles use Greek beaches as nesting sites, and especially those islands in the Ionian Sea (e.g. Zakynthos). For this reason, a Greek non-profit organization named "Archelon" puts a lot of effort in the protection of this species, especially contra to the growing pollution and touristic activities. The other marine turtle is *Dermochelys coriacea*, the single taxon of the family Dermochelyidae. This is also a cosmopolitan taxon, which is characterized by the unique shell structure formed by an association of several small bony plates, covered by a smooth, leather-like skin. On the dorsal view seven longitudinal keels are noted. The entire construction of the shell gives to this taxon a perfect hydrodynamic shape (Ernst & Barbour, 1989). This species is only foraging in Greece in the present.

The terrestrial and aquatic cryptodirans that survive today in Greece show also a decent fossil record that is presented in this thesis. For this reason, information on their extant representatives is needed. In the following paragraphs details on the distribution, taxonomy and phylogeography of these taxa is going to be summarized. This summary is based on the extensive works of U. Fritz and collaborators, who have presented molecular analyses of testudinids, geoemydids and emydids from the Mediterranean area.

Perhaps the most iconic of the small land tortoises from Greece is the Greek Tortoise, *Testudo graeca* Linnaeus, 1758. However, this species contains a complex of subspecies distributed all over Mediterranean, extending in three continents (Europe, Africa, and Asia; Fritz et al., 2007b). The taxonomic history of this group is extremely complex, regarding the actual number of subspecies and the elevation of several subspecies into species level; this complex has been reviewed recently by Fritz et al. (2007b; 2009; and references therein). The Greek Tortoise corresponds to the taxon *Testudo graeca ibera* distributed in Southeast Europe, western Minor Asia, Russian and Caspian Black Sea coast, central Caucasus region (clade C in Fritz et al., 2007b). Fritz et al. (2009) used *Testudo burtschaki* from Caucasus area (Upper Sarmatian–Lower Maeotian), to estimate the split between *T. graeca* and the clade grouping *T. kleinmanni* and *T. marginata* between 10.0–8.0 Ma, with the minimum divergence between *T. graeca* subspecies estimated much later, in the Pliocene. However, Delfino et al. (2009:851) have questioned the inclusion of *T. burtschaki* in the *Testudo* s.s. group, since this taxon has no plastral hinge, stressing the importance of detailed anatomical descriptions of extant *Testudo* species. Fritz et al. (2009) mention also *Testudo eldarica* from the slightly younger strata from Azerbaijan (Maeotian), as one of the oldest members of the *T. graeca* group, following Danilov (2005). These two taxa from Caucasus area need revision before they are used calibration points in molecular clock estimates, following the recommendations by Parham et al. (2012).

Morphologically, *Testudo graeca ibera* is characterized by one thigh-spur made from keratin, on each side posterior to the femur. This character however is not preserved in fossil, and therefore the most common character used to distinguish *Testudo graeca* is the presence of a hypo-xiphiplastral hinge, which creates a movable posterior lobe. This is the main character that defines the *Testudo* s.s. lineage, which also includes *Testudo marginata*, as opposed to the hingeless *'Testudo' hermanni*. Amiranashvili (2000) reviews the shell morphology between *T. graeca* and *T. hermanni*, listing a number of characters that distinguish the two taxa. Besides the presence of the hinge (that could also be present in old females individuals of *T. hermanni*), other important characters (Fig. 1.1) are the divided supracaudal (could be also fused or partially fused sometimes), the narrower and higher peripherals, the

median length of hypoplastron and the position of the humero-pectoral sulcus in *T. hermanni* (see Amiranashvili, 2000).

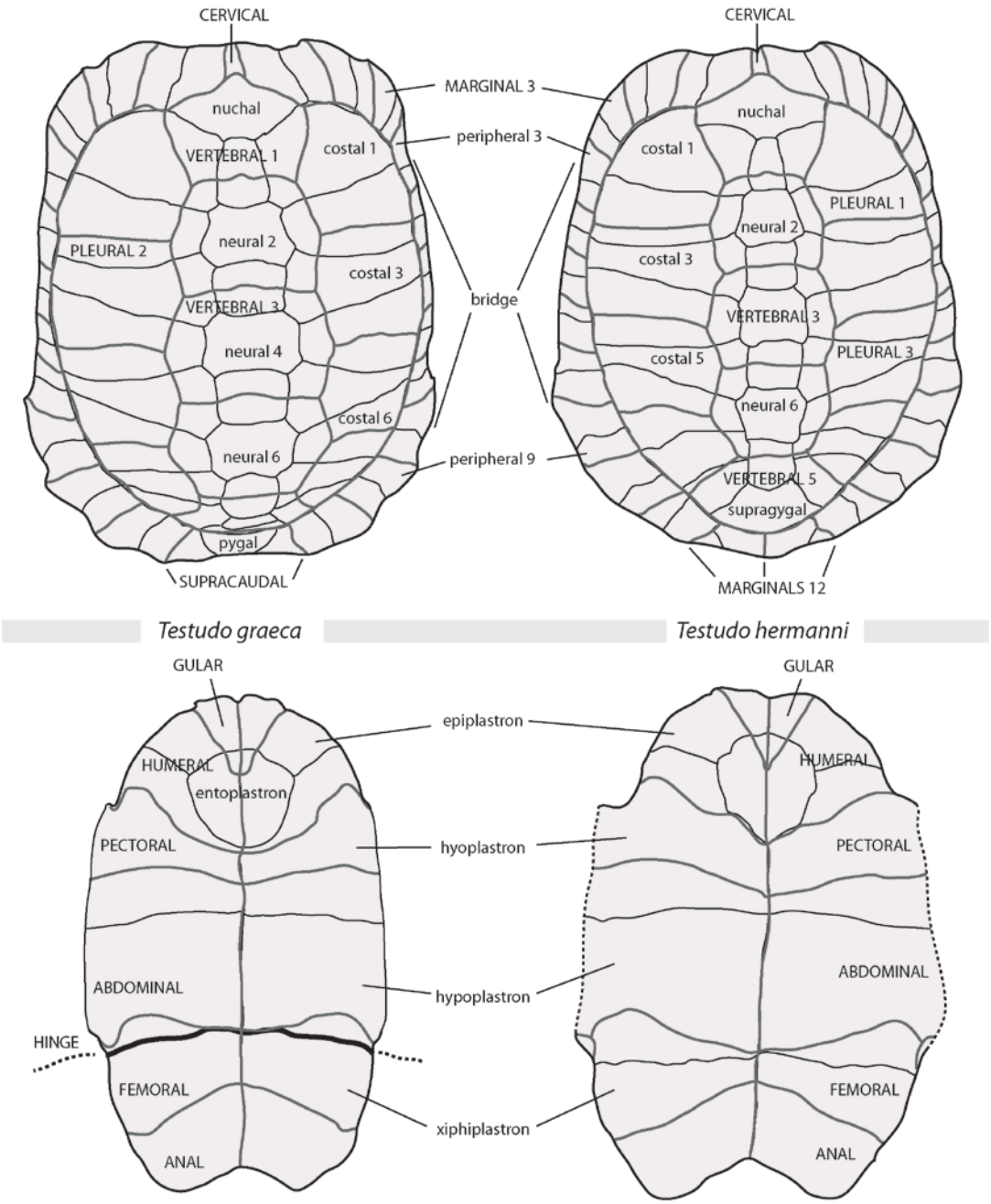


Figure 1.1. Comparative morphology of the carapace and plastron of *Testudo graeca* (based on ZIN 15727) and *'Testudo' hermanni* (based on ZIN 19). The dorsal carapace is figured above, the ventral plastron below. This shell nomenclature is followed in the text.

The other member of the *Testudo s.s.* lineage is the marginated tortoise, *Testudo marginata*. This species is easily recognized by the presence of an elongated posterior carapace, with posterior peripherals and pygal being posteriorly, or even horizontally, flared. This taxon is distributed in continental Greece and in the Balkans (e.g. Albania) and is often encountered in high altitudes. A particular small-sized, "dwarf", population of marginated tortoises in southern Peloponnesus (Mt. Taygetos) was studied by Bour (1996) to erect the species *Testudo weissengeri*. This new

species, which also preserves a flared carapacial margin, has been distinguished from *T. marginata* based on the smaller shell size and differences in colorations, presenting a distinct population on the south Peloponnesus. However, genetic evidence from mitochondrial and nuclear genomic markers showed that *T. weissengeri* is not a distinct evolutionary lineage (Fritz et al., 2005), since no significant genetic differences were noted between *T. weissengeri* and *T. marginata*. Interestingly, Fritz et al. (2006) reported also some different haplotypes for *T. hermanni* population from the same area, compared to the other haplotypes of Hermann's tortoise in continental Greece.

The phylogeography of *'Testudo' hermanni* has been investigated by Fritz et al. (2006). One of the main questions of this study was to define the ranges of the subspecies of the Hermann's tortoises, namely *T. h. hermanni* and *T. h. boettgeri*. These two subspecies have been often elevated to the species level by many researchers, and in some cases a third species has been recognized (*T. hercegovinensis*) for the central Dalmatian populations. The study of the mtDNA by Fritz et al. (2006) concluded that the traditional concept of the two subspecies (*hermanni* and *boettgeri*) should be continued. As far as the phylogeography is concerned, Fritz et al. (2006) show that *T. h. hermanni* is present in Spain, France, Italy and Sardinia. On the other hand, *T. h. boettgeri* ranges in the eastern (Croatia, Romania, Bulgaria, FYROM) and south Balkans (Greece). It seems that the Dinarides and Pindos mountains play an important role in separating the western from eastern haplotypes of *T. h. boettgeri*, whereas a third haplotype is distinguished in south Peloponnesus.

The two subspecies differ much in coloration (yellow and black color pattern in *hermanni*; greenish and not so dark in *boettgeri*) and size (*hermanni* smaller than *boettgeri*). Recently, a new genus has been named for *T. hermanni*, the genus *Eurotestudo* Lapparent de Broin et al. (2006a), accompanied by detailed morphological analysis (Lapparent de Broin et al., 2006b) and a cladistic analysis (Lapparent de Broin et al., 2006c). The main differences distinguishing the *T. hermanni* clade from *T. graeca, T. marginata* and *T. horsfieldi* clades are: the narrowed vertebral series; fusion of suprapygals into a trapezoid; hexagonal pygal with small latero-anterior sides; tendency of having a divided supracaudal; posteriorly pointed triangle in the ventral surface of the gulars (see Lapparent de Broin et al. 2006a for further information). The validity of the new genus was later on challenged by molecular data when Fritz & Bininda-Emmonds (2007) proposed that *Eurotestudo* is not a valid genus based on the analysis of a five-gene dataset.

From the freshwater taxa, *Trachemys scripta* is introduced by man, and will be no further discussed here. The other two taxa, *Emys orbicularis* and *Mauremys rivulata* are usually found in ponds and lakes in Greece, and they also show a decent fossil record. These two taxa are often confused in sites with fragmented remains due to an overall similarity especially in the peripheral plates. *Emys orbicularis*, the European pond turtle, is perhaps the most common taxon found in Holocene deposits and in many archaeological sites. *Emys* is distinguished mainly by the lyre-shaped first vertebral, the presence of a hyo-hypoplastral hinge and the absence of an anal notch. On the other hand, *M. rivulata* has no hinge, and shows a distinct deep and rounded anal notch (Fig. 1.2).

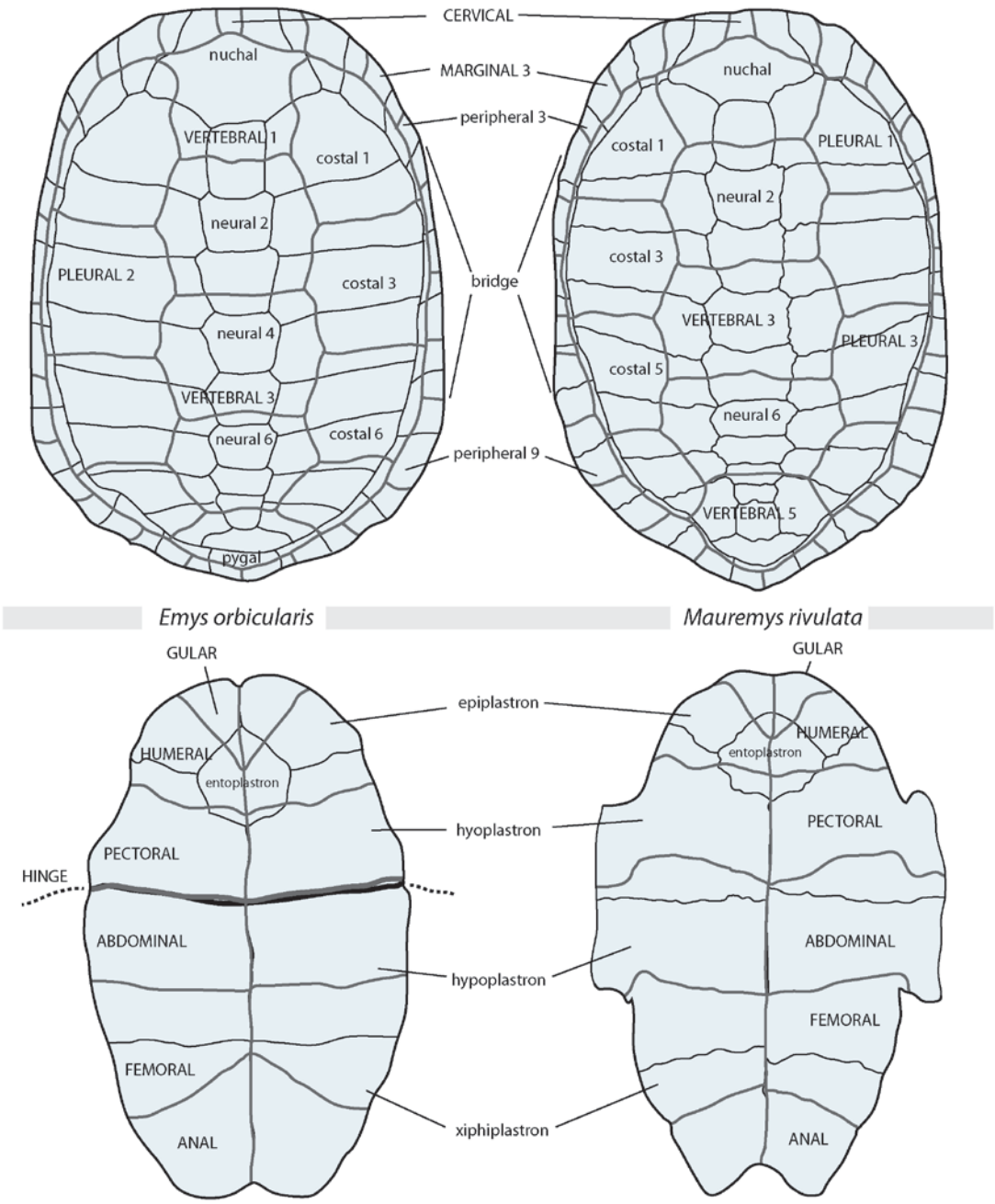


Figure 1.2. Comparative morphology of the carapace and plastron of *Emys orbicularis* (based on REP 35) and *Mauremys rivulata* (REP 48). The dorsal carapace is figured above, the ventral plastron below. This shell nomenclature is followed in the text.

Emys orbicularis has been included in many studies of the climatic changes of the Holocene period. Several mitochondrial works (Lenk et al., 1999; Fritz et al., 2007a; 2009) have indicated a Balkan Glacial refuge for *Emys orbicularis*, from which this taxon expanded into central and northern Europe in warmer periods during Holocene (Sommer et al., 2007). On the other hand, *Mauremys rivulata*, appears to be allopatrically evolved compared to *M. leprosa* and *M. caspica*, with dispersal events that are probably dated in the Neogene (Fritz et al., 2008). Given that the area delimited by South Balkans and Minor Asia is important for the phylogeographic distinction between *M. rivulata* and *M. caspica*, the study of the Greek fossil record could provide useful results on the phylogeographical history of *Mauremys*. The

European Pond Turtle is currently encountered in a wide range, from the Caspian Sea, Azerbaijan, Turkey, eastern Europe, Germany, in southern Europe and in northern Africa (Morocco, Algeria and Tunisia).

Geographical Ranges

In this section the geographical ranges of the extant chelonian fauna of Greece is presented in distribution maps. Special attention has been given to the occurrences of the several taxa in the Greek islands, that are not usually depicted in the distribution maps of widely-distributed atlases and maps (e.g. "Turtles of the World" by Ernst & Barbour, 1989 & Bonin et al., 2006; Iverson, 1992). For this reason an extensive selection of herpetological literature has been examined, and the occurrences of the chelonian taxa in the Greek islands is given below.

The list given below is not exhaustive due to the vast number of herpetological reports that have been published from Greece and in many cases are not accessible or known. However, the distribution maps presented here are considered detailed enough to document the distribution ranges of the extant chelonian taxa. The validity of the species identification of the reports below cannot be tested and is beyond the scope of this study; in the vast majority of reports photographs are missing. Finally, we should mention that most probably many of these occurrences could be the result of human activities, mainly touristic and use of turtles as house pets, as it has been mentioned in many of these reports.

Additional occurrences of the extant chelonian taxa in Greek islands are given below:

'Testudo' hermanni boettgeri: Rhodes (Bader et al., 2009); Kerkyra (Toth et al., 2002; Razzetti et al., 2006); Zakynthos, Keffalonia (Wilson, 2006 and references therein); Ithaki (Valakos et al., 2008);

Testudo graeca ibera: Leros, Simi, Kalymnos, Kos (Dimaki, 2002); Symi (Wilson & Grillitsch, 2009).

Testudo marginata: Lesvos (Hofstra, 2008); Amorgos (Broggi, 2007); Skyros (Broggi, 2006); Kerkyra (Toth et al., 2002)

Mauremys rivulata: Rhodes, Simi (Dimaki, 2002); Kea, Kithnos, Sifnos, (Grillitch & Tiedemann, 1984); Amorgos, Andros, Tenedos, Chios, Crete, Gavdos, Imvros, Ikaria, Lemnos, Lesvos, Milos, Mykonos, Naxos, Paros, Samos, Samothraki, Serifos, Skiathos, Skopelos, Symi, Syros, Thassos, Tilos, Tinos (Broggi, 2012; Valakos et al., 2008); Kerkyra (Toth et al., 2002; Razzetti et al., 2007); Zakynthos, Keffalonia (Wilson, 2007 and references therein); Skyros (Broggi, 2006); Gavdos, Kythera, Crete (Mantziou et al., 2004);

Emys orbicularis: Rhodes (Bader et al., 2009); Kerkyra (Toth et al., 2002; Razzetti et al., 2006); Zakynthos, Keffalonia (Wilson, 2006 and references therein);

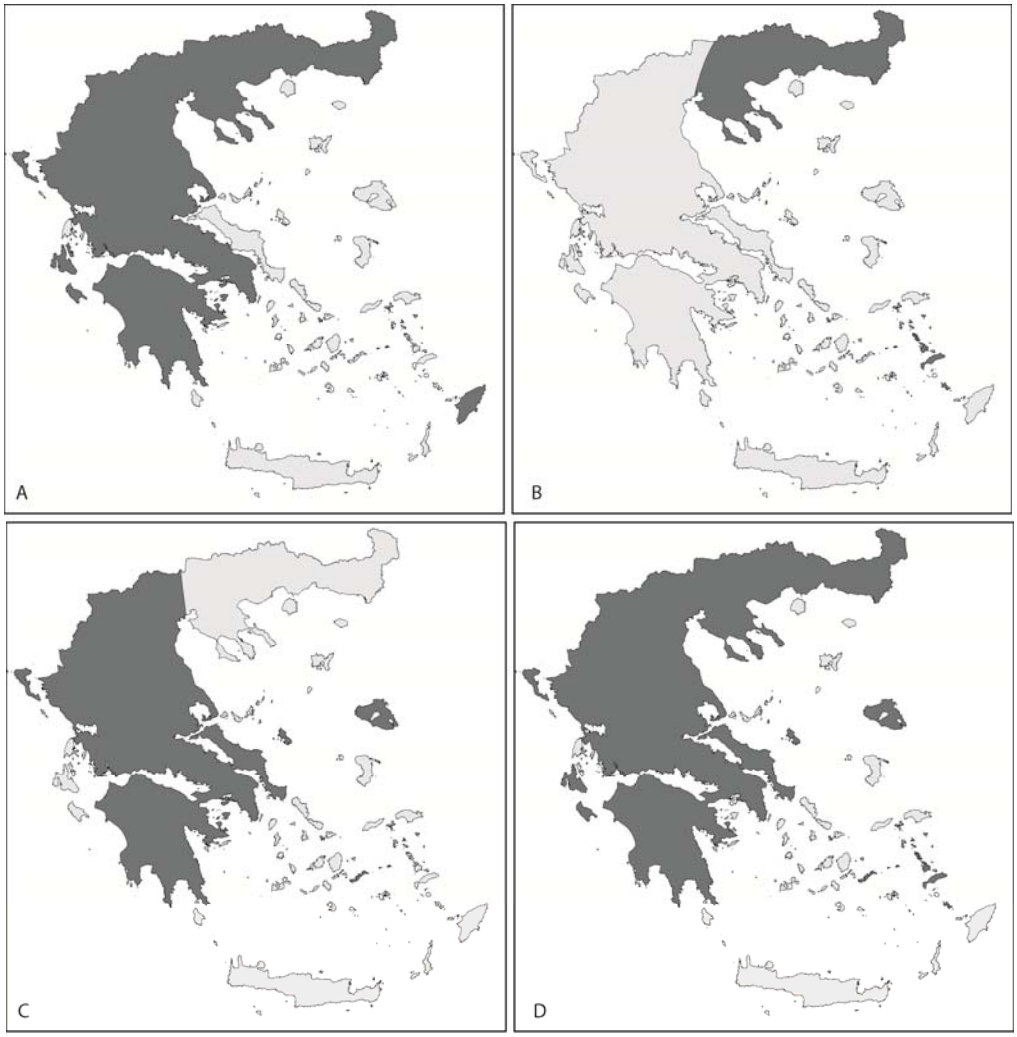


Figure 1.3. The distribution of the extant species of *Testudo* in Greece (dark grey). (A), *'Testudo' hermanni boettgeri*, (B) *Testudo graeca ibera*, (C) *Testudo marginata*, and (D) all *Testudo*. See references in the text.

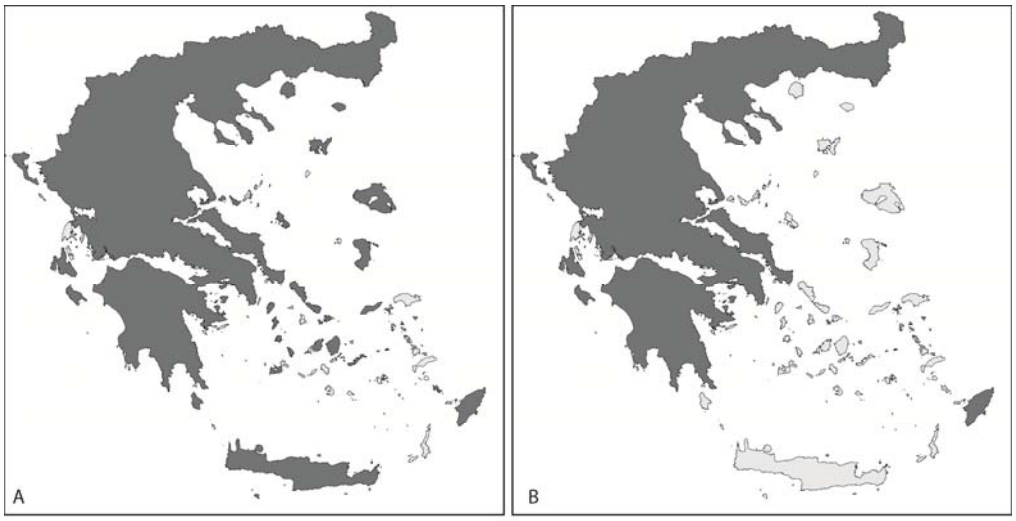


Figure 1.4. The distribution of the extant freshwater turtle species in Greece (dark grey). (A), *Mauremys rivulata*, and (B) *Emys orbicularis*. See references in the text.

1.4. Historical overview of the fossil chelonian research in Greece

In this chapter an historical overview of the research on fossil chelonians in Greece is given. Also, a thorough historical overview of the Greek herpetology is given by Pafilis (2010), covering the study of extant reptiles and amphibians from Greece from the Aristotle's times in antiquity, till the growth of Greek herpetologists after the 1970's. Compared to the growing number of 606 papers on Greek herpetology (from Pafilis, 2010), the papers dealing with fossil specimens are only a handful. Most of them just mention the turtle findings without providing any description or photographs. Few of them attempt to describe the specimens, whereas in some cases new chelonian taxa have been described.

Gaudry made the first description of a fossil chelonian from Greece in the mid 1800's from the Late Miocene site of Pikermi in Attica. In two short publications (Gaudry, 1862a;b) and in his extensive monograph (Gaudry, 1862-1867), he describes a new species of a small tortoise, *Testudo marmorum*, based on three specimens (see Gaudry, 1862-1867:316). Unfortunately, only two specimens have been located in the MNHN collections, which are both figured in all his papers; the third specimen is not figured anywhere.

The next findings are reported just after the World War I, this time from the area of Thessaloniki, in northern Greece. Del Campana (1917; 1919) describes from Capoundjlar (the old Turkish name of the area of Pylea, east Thessaloniki) a shell of *Testudo amiatae* (Del Campana, 1917), and a clutch of eggs of a giant tortoise (Del Campana, 1919). These important specimens are part of the exhibition in IGF (Florence, Italy), and have been revised in the present thesis.

Around the same time, C. Arambourg collected specimens from Thessaloniki area. According to the archive of MNHN, the specimens have been catalogued in 1916 (20 October 1916, collection number MNHN 1916-5) and in 1921 (24 May 1921, collection number MNHN 1921-5). The material has been published later by Arambourg & Piveteau (1929) under the locality name "Salonique", but containing specimens collected from six sites in Axios valley (Ravin X; Ravin des Zouaves; Ravin B; Ravin C; Ravin de Vatilük; Ravin de Konikovo) and one in Thessaloniki area (Falaise de Karabouroun). The former sites are of Late Miocene age (see Koufos, 2006a), whereas the latter is of Late Pliocene age (see Koufos et al., 1991). In the classical monograph of Arambourg & Piveteau (1929) a cranium and limb bones of a large tortoise are identified as *Testudo* sp. In this thesis those specimens are described in detail, along with many specimens without description. As it has been noticed by Vlachos et al. (2014) these specimens are all labeled as "Karabouroun", raising questions about their stratigraphic provenance, which have been always considered of Late Miocene age. The locality Karabouroun corresponds to the Ruscinian locality Megalo Emvolon.

Few years later, a new species of a giant tortoise is described from Samos. Based on an almost complete skull and a complete femur, the species *"Testudo" schafferi* Szalai, 1931 has been erected, from unknown precise locality from the Late Miocene of Samos Island. This material, part of the NHMW collections, is also revised here along with the description of some new specimens discovered in the collection of NHMW in December 2011.

Two internal casts (steinkerns) of testudinids from Chios Island were submitted for publication in winter of 1940 but only published by Paraskevaidis in 1955. Unfortunately, this material was destroyed during bomb attacks in the Museum of Munich during the World War II (footnote in Paraskevaidis, 1955). However, it is

important because is probably of Middle Miocene age, and therefore the oldest record of a terrestrial tortoise in Greece These were initially described as *Testudo* sp. I and *Testudo* sp. II.

Few years later, the same author described some fragments of turtles from a fissure filling in Korydallos, Attica (Paraskevaidis, 1961). However, this material has not been located up to now. Based on the published photographs (Plate XX.4 and Plate XXI.7 in Paraskevaidis, 1961) we can identify some plastron (XX.4) and carapace fragments (XXI.7) of *Testudo*. This material is of Pleistocene age, as it inferred by the presence of an *Ursus* canine.

During the next decades there is an increase in the number of works mentioning and describing fossils of turtles and tortoises, mainly as a result of the work of I. Melentis, F. Bachmayer and N. Symeonidis. Melentis (1966) describes (with drawings but without any photographs) shell fragments of "*Clemmys*" *caspica* from the Pleistocene of Megalopolis basin, in Peloponnesus. However, this material has not been located in the AMPG collections, but the drawings of Melentis (1966) are adequate to allow the study of these specimens in the present thesis.

One year later, Bachmayer reported the first findings of a giant tortoise from Pikermi (Bachmayer, 1967). The material consists of several shell fragments and various post-cranial elements that have been conferred to "*Testudo*" *schafferi* by Bachmayer (1967). In the present thesis, this material has been revised, along with new specimens of giant tortoises from Pikermi. Melentis (1970a,b) reports a specimen of *Testudo marmorum* from the Late Miocene of Halmyropotamos (Evia Island).

Bachmayer & Symeonidis (1970) provided a description of new specimens from the AMPG collections. They mainly described new specimens of *T. marmorum* from Pikermi and a new specimen of *T. amiatae* from Allatini, Thessaloniki. They also provide a summary of the known specimens of chelonians from Greece till then. All this material is revised and described in detail here.

In Crete Island, Bachmayer et al. (1975) described a new subspecies of *Testudo marginata*, *T. m. cretensis*, from Gerani and Zourida caves. This material has been revised here, together with the description of new specimens from these caves. Further specimens of the marginated tortoise are described by Kotsakis in Malatesta et al. (1980) from Simonelli Cave.

Bachmayer & Symeonidis (1975) report *T. marginata* specimens from the Pleistocene of Charkadio Cave in Tilos Island. The few specimens presented by Bachmayer & Symeonidis (1975) are revised here and further aided by the description of numerous new specimens brought to light by systematic excavations in the cave by Prof. G. Theodorou (AMPG).

Another specimen of a giant tortoise from Pikermi area is reported by Bachmayer & Symeonidis (1977), from the Late Miocene locality Liossati (or Kiourka), close to Pikermi in Attica. Bachmayer & Symeonidis (1977) had only provided few photographs of some specimens. In the present thesis, following recent preparation of the specimen, we are able to provide additional information for this individual. The same year, Kretzoi (1977) and later Kretzoi & Poulianos (1981) published a list of the fauna of Petralona Cave, Chalkidiki, N. Greece, noting the presence of tortoises. This material is described here, in detail, for the first time.

In 1979, further fossils of large tortoises are reported from Megalo Emvolon by Bachmayer et al. (1979). These few palm elements and shell remains (AMPG collection) are revised here in the light of new specimens located in the collections of AMPG. In the same paper, Bachmayer et al. (1979) described an almost complete shell of *Testudo* cf. *graeca* (NHMW collection), a specimen that is revised here as

well. Few years later, in 1982, Schleich (1982) described some shell elements of *T. marginata* from the Pleistocene of Lakonia, Peloponnesus.

After a short period of no new discoveries, Rauscher (1995) reports some sub-fossil specimens from Vraona Cave in Attica. The same year, the monograph on the Miocene/Pliocene locality of Maramena, Serres basin is published, were Schmidt – Kittler (1995) reports some indeterminate chelonian specimens. One year later, Brinkerink (1996) provides a summary of the Pleistocene sites of Crete that contain specimens of turtles and tortoises. Most of these specimens remained unpublished and are presented here for the first time.

Lapparent de Broin (2002) described some fragmented specimens of a giant tortoise from the Early Pleistocene of Vatera, Lesvos Island, together with a summary of the known giant tortoises from Europe and adjacent areas. These few specimens represent probably the last continental giant tortoise in Europe and one of the largest known individuals. Few years later, Mueller – Töwe et al. (2011) reported new eggshell remains from the Pliocene of Apolakkia, Rhodes Island. At the same time, they provide an updated list of Greek localities with fossils of chelonians. The same year, Stiner & Munro (2011) provided a taphonomic analysis of the food remains of the Upper Paleolithic – Mesolithic Franchthi Cave, Peloponnesus, reporting numerous shell fragments of turtles and tortoises. This material is revised here. Further specimens of archaeological sites are reported in Klissoura (Starkovich, 2012) and in Kalamakia (Harvati et al., 2013).

The first, and only, pleurodiran from Greece is described by Georgalis et al. (2013), as *Nostimochelone lampra*, from the Early Miocene of Nostimo, Kastoria, N. Greece. One year later, Georgalis & Kear (2013) publish a bibliographic overview of the turtles and tortoises from Greece, expanding the list of Mueller – Töwe et al. (2011). However, this overview is based mainly on published data which are either outdated or partly erroneous in many cases, illustrating the necessity of a detailed review of the Greek fossil chelonian record.

Our contribution to the study of chelonians in Greece started with a diploma (Vlachos, 2007) and a master thesis (Vlachos, 2011), presenting new material from Thessaloniki area. Ultimately, this new information resulted in the description of a new species of a large testudinid from Thessaloniki, "*Cheirogaster*" *bacharidisi* Vlachos et al., 2014. This material is the most complete material of giant tortoises in Greece and one of the most complete in Europe. The material of Thessaloniki provided important information for the revision the European large testudinids presented by Pérez-García & Vlachos (2014). Furthermore, we have also described a shell of *Testudo* sp. (*T. marginata* group) from the Pleistocene site of Xerias, Kavala (Tsoukala et al., 2011).

This page has been intentionally left blank

02/16/2016 Ψηφιακή Βιβλιοθήκη Θεόφραστος - Τμήμα Γεωλογίας - Α.Π.Θ.

Chapter 2. Geological information of the localities with extinct chelonians of Greece

Highlights:

Site Information
Geological Information
Chronological distribution of the localities

02/16/2016 Ψηφιακή Βιβλιοθήκη Θεόφραστος - Τμήμα Γεωλογίας - Α.Π.Θ.

Chapter 2. Geological information of the localities with extinct chelonians of Greece

2.1. Introduction

In total, more than 40 fossil localities from Greece contain fossil specimens of turtles and tortoises. The actual number is certainly far greater if we take into account the Holocene archaeological sites. The available information on archaeological sites is rather uneven and is beyond the scope of this thesis. Nevertheless, some well-known Paleolithic-Neolithic archaeological sites are included here (e.g. Franchthi Caves) because they document the transition from the Pleistocene to the Holocene. In this chapter, an up-to-date list with all the Greek localities containing fossils of turtles and tortoises is presented (Figure 2.1), providing the basic locality information of the material studied. For further information please refer to the cited works and references therein.

The fossils are found in the Neogene-Quaternary deposits that cover numerous basins in the mainland of Greece, as well as smaller surface deposits on the islands (Figure 2.2). The Greek fossil record roughly starts from the Early Miocene, but our knowledge on the lower half of the Miocene is rather poor due to the limited number of localities (only two localities) assigned to that age. During Late Miocene there is a significant number of sites containing giant and small tortoises. More importantly, some of the localities are dated to the boundary of Miocene/Pliocene, allowing the documentation of the chelonian diversity during this significant interval from a paleontological, paleoclimatic and paleogeographic points of view. In the Pliocene, the number of localities increases, mainly as a result of the large numbers of localities in Western Chalkidiki peninsula. During Pleistocene, most of the localities are caves, such as the various karstic sites in Crete Island.

Where available, the geological information of these Neogene deposits comes from works dealing with the mammalian fossils recovered in the various localities. The information inferred by the mammalian fossils allows a better interpretation of the chronology and the paleoenvironment of various localities. In several cases detailed stratigraphy and datings are available. In other cases however such information is lacking. For example, material from two famous localities (Pikermi and Samos) that have been published in the past they come from old collections and its precise locality is not known. The material from “Salonique” (in Arambourg & Piveteau, 1929) could be either from Axios or from Megalo Emvolon (see Vlachos et al., 2014 and this thesis). In those cases however, we provide as detailed information as possible.

In general, the Greek fossil record of turtles is strongly biased towards the terrestrial taxa, whereas the findings of freshwater or littoral taxa are limited. Fossil specimens of truly marine taxa are unknown from Greece. The main reason for this is certainly the collection method. Besides some accidental findings, most of the fossil specimens have been collected during excavation of fossil mammal sites. Moreover, there are no systematic efforts to locate and excavate marine vertebrate sites. For this reason, the results obtained by this study are adequate to document the evolution of the lineages of the terrestrial taxa in considerable detail and the freshwater taxa in a relatively decent level. Our knowledge of the marine fossil chelonian record of Greece is extremely limited.

02/16/2016 Ψηφιακή Βιβλιοθήκη Θεόφραστος - Τμήμα Γεωλογίας - Α.Π.Θ.

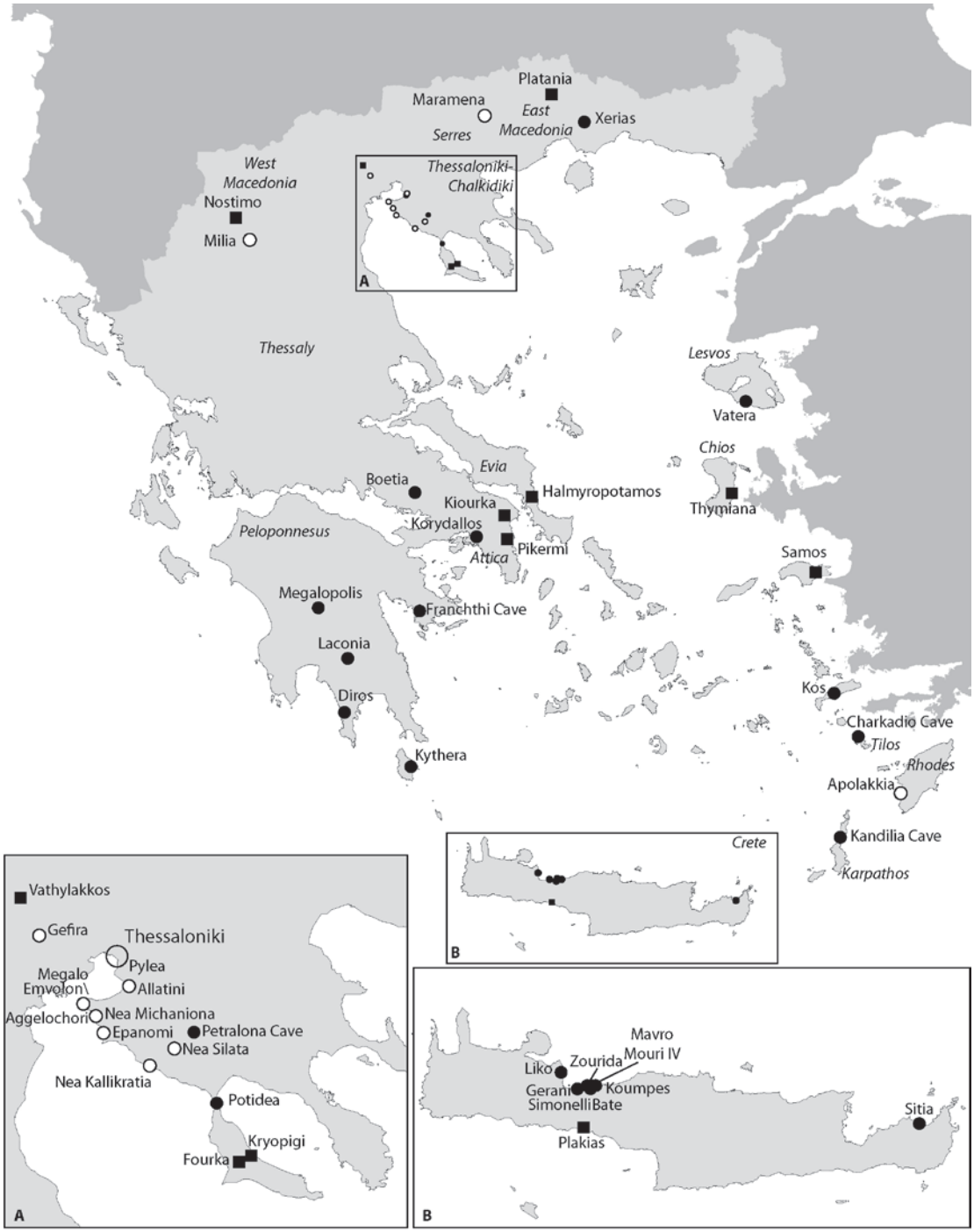


Figure 2.1. Map of Greece with the localities with fossils of turtles and tortoises depicted. (A), detail of the Thessaloniki – Chalkikidi area. (B) detail of Crete Island.
Chronology of the localities (from North to South): Holocene – Pleistocene (solid circle): Franchthi Cave, Charkadio Cave; Pleistocene: Xerias, Petralona Cave, Potidea, Korydallos, Megalopolis, Lakonia, Diros, Vatera, Kandilia Cave, Mavro Mouri IV Cave, Zourida Cave, Gerani IV Cave, Koumpes Cave, Bate Cave, Simonelli Cave, Sitia I; Pliocene (open circle): Gefira, Pylea, Allatini, Megalo Emvolon, Aggelochori, Nea Michaniona, Epanomi, Nea Kallikratia, Milia, Apolakkia; Pliocene – Miocene boundary (open circle): Maramena, Nea Silata; Miocene (solid square): Platania, Vathylakkos, Kryopigi, Fourka, Nostimo, Halmyropotamos, Liossati, Pikermi, Chios, Samos, Plakias.

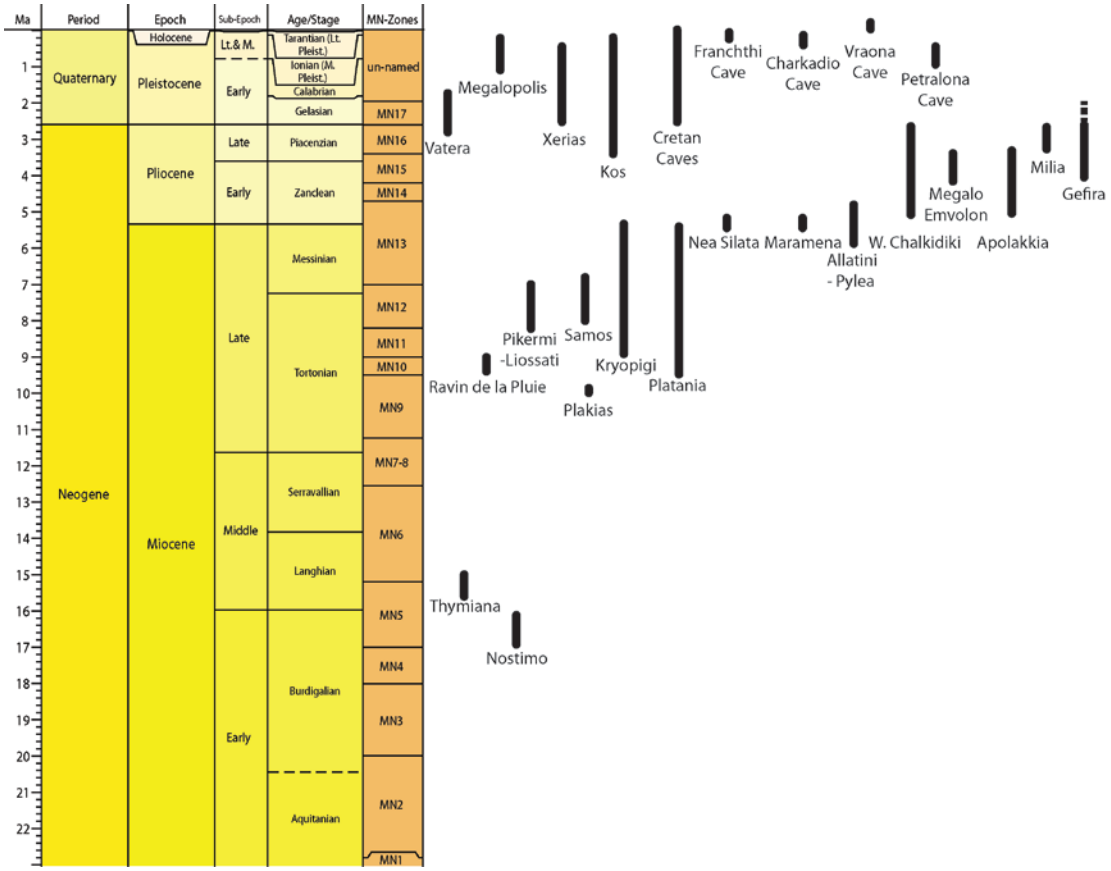


Figure 2.1. Chronological distribution of the main localities with chelonian material from Greece. See text for further details.

2.2. Miocene

The Miocene localities with chelonian fossils in Greece are numerous and widespread. Most of them are from the Late Miocene, including world famous sites such as Samos Island and Pikermi (Attica). Also close to Pikermi, the site Liossati (Kiourka) is known. In the same age and nearby we find the site of Halmyropotamos. Other Late Miocene sites are known in northern Greece, like Vathylakkos (Axios valley) and Kryopigi and Fourka (Kassandra peninsula). Northeast of Thessaloniki, turtles are known in Platania and in Serres basin. Prior to Late Miocene the sites are few, Thymiana (Chios; Middle Miocene) and Nostimo (Kastoria; Lower Miocene).

Nostimo, Kastoria (Lower Miocene)

The site of Nostimo is located near Nostimo village, Kastoria, in northwestern Greece. The material was named as *Nostimochelone lampra* (in Georgalis et al., 2013) and comprises of a partial shell, still resting within the matrix, hindering observations on the dorsal surface of the carapace and visceral surface of the plastron. This material is attributed to the Zeugostasion Formation, which is the primary stratigraphic unit around Nostimo. It comprises mainly sandy marls with intervening thin clastic sandstone and fossiliferous conglomerate layers; the latter are about 1–2 m of thickness and contain numerous bivalves and gastropods. The Zeugostasion Formation forms part of an extensive lower-middle Miocene transgressive series that locally incorporates the underlying Omorfokklissia Formation and terminates with the uppermost Orlia Formation. According to Georgalis et al. (2013; and references

therein) a late Burdigalian age is inferred for the Zeugostasion Formation on the basis of foraminiferal assemblage and Sr isotope data from adjacent sections.

Kryopigi and Fourka, Kassandra peninsula (Late Miocene)

Kryopigi locality is situated in the north part of the Kassandra peninsula, near Thessaloniki and yielded thousands of large mammalian fossils (excavations during 1998-2010). Based on a preliminary faunal list (see Tsoukala & Bartsiokas, 2008 and Lazaridis & Tsoukala, 2014a) the age of the locality is considered as Middle-Late Turolian (MN12-13, Late Miocene). The deposits of Kryopigi locality has been placed in the Triglia Formation (sensu Syrides, 1990), which mainly includes sands with reddish to brownish silts and clays intermixed with pebbles. The chelonian material consists of some osteoderms and possible appendicular element of a large testudinid. The Fourka locality, located towards the western coast of the Kassandra peninsula comprises of several open sand quarries with thick sand deposits, with many scattered fossils.

Platania, Drama (Late Miocene)

Platania village is located in the Drama basin, Northern Greece. It is situated about 30 Km northeastern of Drama city in Eastern Macedonia. Administratively, it belongs to the Municipality of Paranesti. The recently discovered Platania locality has been discovered following information by local people (K. Eleftheriadis and M. Kagiaoglou) to the archaeologist V. Puliudi, as a result of mud collection in the area to build an outdoor mud oven. The fossiliferous site (Fig. 2.3.A) is an exposed slope that was artificially opened during rural road construction, near Platania village (N41º 11’ 48.4’’, E024º 23’ 42.0’’, elevation is 257 m a.s.l., Hellenic Grid, EGSA ’87). The fossils were recovered disarticulated and they show a characteristic blackish color (Fig. 2.3.B) that is related with the presence of high manganese (Mn) concentrations during fossilization processes (I. M. Zougrou, pers. comm.). The sediments cover the lower parts of this sub–basin, which consists of alternations of high metamorphic Paleozoic rocks, such as gneisses, mica schists, marbles, which belong to the Rhodope massif (Fig. 2.32.C, based on Krinidhes sheet, 1:50.000; N.I.G.M.R., 1974; mapping by P. Kronberg, 1962-1970). The fossiliferous site consists mainly of sands and muds, forming two main layers (Fig. 2.3.D). The upper layer consists of consolidated red–brown clayish–sands, with parts that show typical cross–bedding structure. The lower layer with fossils in the lower part is brownish and consists mainly of fine sand with some mud. In this section two layers of conglomerates are distinguished: one consolidated, between the two main layers, and the other thinner, located just above the fossils. These deposits indicate a fluvial environment. Few meters above the fossiliferous site, another outcrop is exposed, representing the deposits just above the PLD section, which are mainly fine–layered yellow–brownish muds, indicating a more lacustrine environment. This material has been preliminary published in Vlachos and Tsoukala (in press). The preliminary study of the mammalian fossils (ET and collaborators, under preparation) has revealed the presence of hipparions, giraffes, rhinoceroses, mastodons, bovids, suids, represented by skulls, mandibles and many complete appendicular elements. The recovered assemblage, in relation with the regional stratigraphy, points out a Late Miocene age.

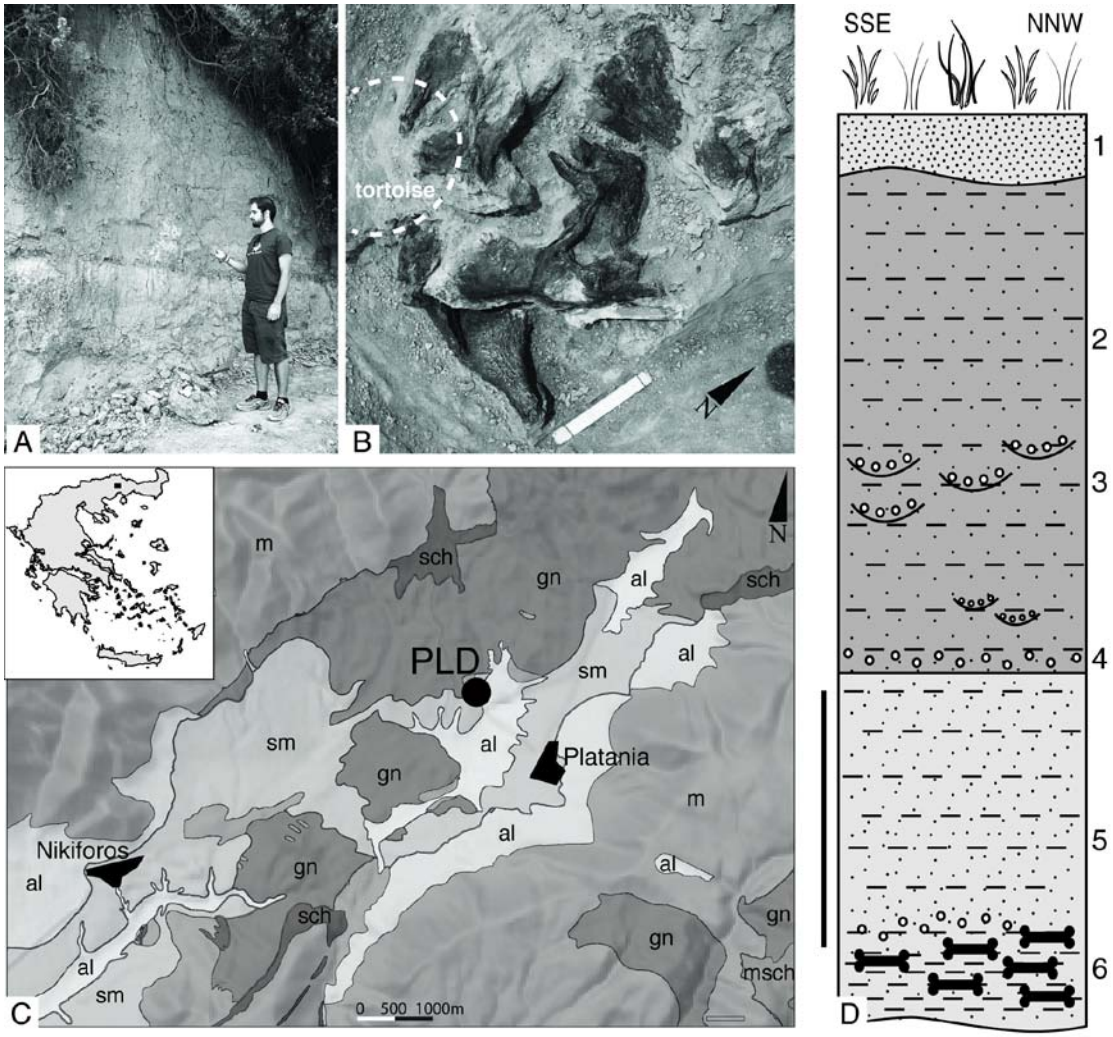


Figure 2.3. The new Late Miocene locality of Platania, Drama basin, Northern Greece. A, photograph of the site. B, the fossils in recovery position, the dotted line indicating the position of the tortoise finding below an hipparion skull, scale bar equals 10 cm. C, simplified geological map of the area (based on Krinidhes sheet, 1:50.000; N.I.G.M.R., 1974; mapping by P. Kronberg, 1962-1970) and map of Greece with the Platania site depicted. D, simplified stratigraphic column of the Platania locality, scale bar equals 1 m. Legend for the geological map: al, Holocene–Quaternary terrestrial and alluvial deposits; gn, gneisses and gneiss–schists; m, marbles; msch, marbles and micaschists; sch, micaschists; sm, Neogene clays, sands, and gravels. Legend for the stratigraphic column: 1, soil; 2, red–brown clayish–sands; 3, cross–bedding; 4, conglomerate; 5, brownish sands and muds; 6, fossils.

Vathylakkos, Axios valley (Late Miocene)

Fossil testudinids have been reported from the Late Miocene of the lower Axios valley. Arambourg & Piveteau (1929) report a testudinid of large size from “Ravin de Vatiluk”. This locality could correspond to one of the Vathylakkos-3 (VAT) locality of the new excavations (see de Bonis et al., 1977; 1988). This material however, as shown by Vlachos et al. (2014) is marked in the collections of MNHN as coming from Megalo Emvolon, a Pliocene locality where Arambourg & Piveteau (1929) also collected fossils. Therefore the stratigraphic provenance of the material of Arambourg & Piveteau (1929) still remains unclear. Recently, García et al. (2011) preliminary reported a possibly new small testudinid species from the Vallesian locality of “Ravin de la Pluie” in lower Axios valley. For further information regarding the stratigraphy

of the localities of lower Axios valley see de Bonis et al., (1988), Koufos & Pavlides (1988), Sen et al. (2000) and Koufos (2006a).

Pikermi, Attica (Late Miocene)

The Late Miocene locality of Pikermi is beyond doubt among the most famous Neogene localities in Europe, with specimens that are dispersed in numerous institution and museum collections all over the world. The Pikermian material is usually a standard reference to any work dealing with fossil mammal remains in the Mediterranean area, and turtles are not an exception. Small and large in size Pikermian testudinids are known from the works of Gaudry (1862a; 1862b; 1862-1867), Bachmayer (1967), Bachmayer & Symeonidis (1970), and the most recent mentions are from Lapparent de Broin (2001; 2002). In our previous work (Vlachos et al., 2014 and Suppl. Info of this article) we point out the necessity of revising the material. The material generally comprises of several shells that are attributed to the small taxon *Testudo marmorum*, and disarticulated appendicular elements of a large testudinid. This material is the result of old collections and the exact stratigraphic placement of the material is not known. The unknown stratigraphic provenance of the Pikermi specimens from the old collections suggests a rather mixed assemblage. This also has been pointed out by the previous authors that were working with specimens from this locality (see Theodorou et al., 2010, Konidaris et al., 2014 and references therein). Currently, the most acceptable dating for this old material is the end of the middle Turolian (MN12, see Konidaris et al., 2014 and references therein). Hopefully, the new excavations that started in Pikermi by AMPG staff (leaded by G. Theodorou, see Theodorou et al., 2010 amongst others) are going to provide key information for clarifying the age and stratigraphic provenance of the "old collections".

Liossati (Kiourka), Attica (Late Miocene)

Bachmayer & Symeonidis (1977) reported the new "Pikermian" locality of Liossati (or Kiourka), which is located north of Athens, near the lake of Marathon relatively close to Pikermi. The presence of fossils of *Hipparion* allows inferring of a Late Miocene age, but further information is not available. From this locality numerous fragments of a large testudinid are recovered, along with further fragments of a smaller individual. In their publication, Bachmayer & Symeonidis (1977), briefly report those specimens, but they provide a detailed analysis of the sediments of the locality. A high percentage of SiO_2 (more than 50%) characterizes the conglomerates of the Kiourka locality.

Halmyropotamos, Evia Island (Late Miocene)

Melentis (1970a,b) reports a specimen from *Testudo marmorum* from the Late Miocene of Halmyropotamos in Evia Island. The first, and most numerous, fossils were discovered in 1916 by Prof. Th. Skoufos and were transported to AMPG. Melentis revisited the site in 1966 and with the assistance of local people he re-discovered the site. The fossiliferous sediment is red-brownish clay with pebbles of various sizes. In this place, Melentis (1970a) reports that he collected from this site several fossils, including teeth of *Hipparion*, bone fragments of Bovidae and an almost complete carapace of *Testudo marmorum.* This specimen, however, has not been located within the AMPG material of Halmyropotamos.

Samos Island (Late Miocene)

The material from Samos presented in the thesis is the result of old collections of fossils in the island. Further specimens of the old collection from Samos come mainly from the excavations during the early 60's by J. Melentis (Melentis, 1968), who founded the museum in Mytilinii to house those fossils.

As a result of recent systematic excavations and investigations of Prof. G. Koufos and collaborators (LGPUT), the detailed lithostratigraphy of the Neogene deposits of the basin is given by Kostopoulos et al. (2009). The known chelonian material from Samos has been attributed to the Late Miocene. Therefore most probably originates from one of the localities of Mytilinii Basin. As it has been explained by Koufos (2009), it is not possible to know the exact location of these findings and most of the collections that exist in several museums in the world could be mixed. In general, the deposits of the Mytilinii basin can be divided into five formations (from bottom to top): 1) the Basal Fm (early Middle Miocene), which contains coarse clastic sediments; 2) The Mavradzei Fm (late Middle Miocene), which contains fossiliferous limestones and clays with lignites; 3) The Hora Fm (early Late Miocene), which contains shallow to deep lacustrine limestones; 4) The Mytilinii Fm (Late Miocene), which contains volcanoclastic sediments. In this formation the famous mammal sites are situated; 5) The Kokkarion Fm (Pliocene), which contains travertine-like limestones. The various mammal assemblages from Samos (based on the new collections cover a large time span from 7.8-7.4 Mya (late MN11) till 6.9-6.7 (latest MN12-early MN13), based on the results of Koufos et al. (2009).

Thymiana, Chios Island (Middle Miocene)

The published material comprised by 2 internal casts (steinkerns) of the shell of two different individuals. They were identified by Paraskevaidis (1955) as *Testudo* sp. I and II. Paraskevaidis (1955) mentions that this material has been deposited in the collections of BSPG circa 1940, but they were lost during the Second World War. Personal communication with Dr. Markus Moser (2011, curator of BSPG at that time) confirmed that such material is not stored in the collections at present. Paraskevaidis (1955) provided a Sarmatian age (Upper Serravalian/ Middle Miocene) for the specimens. Based on the published photographs, we can recognize the typical alternating pattern of testudinids, were costals medially short and laterally long alternate with costals medially long and laterally short. If these specimens would be available, they would be the oldest record of a testudinid in Greece. The only information given by Paraskevaidis regarding the locality is the name "Michalos", which probably corresponds to the clay pit Megas Limnionas in Thymiana, the locality Thymiana B (THB) in Koufos et al. (1995). Melentis & Tobien (1967) report new material from Thymiana. Koufos (2006a) summarizes the stratigraphy of Thymiana locality, based on new excavations, that includes three fossiliferous horizons. The intermediate one contains macromammals, with a possible magnetostratigraphic age of 15.5 Ma (see Koufos, 2006a and references therein). In general, the fauna of Thymiana locality suggests a Late Orleanian (MN5) age.

Plakias, Crete Island (early Late Miocene)

The Late Miocene locality of Plakias is located close to the south coast of Crete, south of Rethymnon city. The locality is already known from the 1970's when de

Bruijn & Meulenkamp (1972) described the first collection of micromammal fossils. Recently, de Bruijn et al. (2012) published a new collection of micromammalian fossils, revising the information from Plakias locality. The information summarized here follows de Bruijn et al. (2012). The material comes from a layer of grayish clays of 25 cm thickness overlying a thicker layer (more than 70 cm) of beige to brown colored clays with calcretes. The chelonian material comes from older collections by Kuss, and it has been stored in the Natural History Museum of Karlsruhe but now it has been returned to NHMC. Based on the new information from Plakias locality, de Bruijn et al. (2012) corroborate with the previous views that the age for this site refers to the lower part of MN9, providing an age of 9.9 Mya.

2.3. Pliocene

Most of the Pliocene localities with chelonians in Greece are located in northern Greece. The majority of the sites are found around the city of Thessaloniki. In Axios valley, the new site of Gefira is located. In the eastern part of the Thessaloniki city, the famous sites of Allatini and Pylea are found. Moreover, the Neogene deposits of Chalkidiki peninsula are quite rich in fossils of chelonians. The main sites are those of Megalo Emvolon, Aggelochori, Nea Michaniona, Epanomi and Nea Kallikratia in the coastal slopes of Western Chalkidiki. Outside Thessaloniki, only two sites are known. In the mainland, turtles and tortoises are found in the famous mastodon site of Milia, in Grevena. In the islands, the only known locality is Apolakkia in Rhodes. Two localities in the area document the boundary of Miocene and Pliocene: Maramena (Serres) and Nea Silata (Chalkidiki).

Nea Silata, Thessaloniki (Miocene/Pliocene boundary)

The fossil locality of Nea Silata is located in a small ravine with steep sides near Nea Silata village, and it belongs to the Silata Member of the Gonia Formation of the Western Chalkidiki deposits (Syrides, 1990). The Gonia Formation (Ruscinian) consists of alternations of lenses and lens-shaped beds of sands, clays, marls, sandstones, gravels and massive marly limestones, with frequent lateral passages and interchanging. These marly limestones divide the formation in three members (Silata Mb., Rhodokipos Mb., Kallikratia Mb.). A total thickness of 100-150 m is possible for this Member. These sediments indicate a fluvial- lacustrine-marshy paleoenvironment. The study of both micro- and macromammals (Vassileiadou et al., 2003; Koufos, 2006b) from Nea Silata suggest an age at the Miocene/Pliocene boundary (MN13/14).

Maramena, Serres basin (Miocene/Pliocene boundary)

The locality of Maramena in Serres basin has been presented in a special monograph (N. Schmidt-Kittler, ed.). The geological information has been described by Schmidt-Kittler et al. (1995). The locality has been discovered during exploration activities for uranium near Christos village, near Serres in the valley of Strymon river. The fossiliferous layer is a greyish blue sandy marl of 2 m thickness. These layers are situated in the upper part of the Lefkon Formation, corresponding the Late Miocene to Pliocene infilling of the Strymon basin. The fossil content of the Maramena locality is diverse, containing some floral remains and numerous faunal remains such us gastropods, bivalves, arthropods, amphibians, reptiles and mammals. The chelonian remains have been preliminary identified as Testudinata indet. The stratigraphic age

of the assemblage is placed between the Turolian – Ruscinian boundary level (MN13/MN14). For a paleoecological aspect, the lacustrine gastropod fauna indicates the presence of stagnant water, the presence of a lake that could become a swamp. The remaining faunal elements indicate both open and closed woodland surroundings. Lefkon Formation is over lied by the Georgios Formation (calcareous limestone and granite breccia; Latest Miocene) and the Spilia Formation (sandstone, conglomerates and travertines; Pliocene) (Armour-Brown et al., 1979).

Allatini/Pylea, Thessaloniki (latest Miocene – earliest Pliocene)

The fossil site of Allatini is among the oldest known sites of Northern Greece. This locality has been cited with a series of names, that all refer to same area in the east part of Thessaloniki city. The name Allatini derives from the private company name that was exploiting the clay pits in the area (Fig. 2.4.A). Close to Allatini, is the area of Pylea, mentioned also as Capundjlar (the Turkish name of Pylea; Fig. 2.4.A). Clay pits existed in Pylea as well, probably yielding many fossil specimens. These two areas are drained by the same hydrographic network, and have been both erroneously grouped in many studies under the name of Allatini. The specimens used in this study probably come from both localities, but is currently impossible to test their actual origin. Based on the available published information we mention here both localities (Allatini and Pylea), located in the east part of Thessaloniki.

The sediments of the study area are part of the Neogene/Quaternary outcrops of the Western Chalkidiki peninsula. These deposits are divided into six formations by Syrides (1990): Antonios Formation (Middle–Late Miocene), Triglia Formation (Vallesian–Early Turolian, Late Miocene), Trilophos Formation (Latest Miocene = Pontian), Gonia Formation (Early–Late Pliocene), Moudania Formation (Pleistocene), and Eleochoria Formation (Late Pleistocene–Holocene) (Fig. 2.4.B). The deposits in Allatini and Pylea are now fully exploited and/or covered by domestic areas, but the majority of them belong to the Trilophos Formation. These well-stratified sediments contain fossiliferous sands, clays, sandstones and limestones with abundant brackish mollusks of Paratethyan origin (Vasileiadou et al., 2003). The Trilophos Formation shows a gradual transition with the overlying fluvial-lacustrine sediments of the Gonia Formation (Fig. 2.4.B), which contains numerous fossils of giant tortoises from the Pliocene (Vlachos et al., 2014). Below Trilophos, the red beds of the Triglia formation lie with an unconformity.

Regarding the place of origin of the specimens used in this study, we can infer the following information. Del Campana (1917, 1919) places the specimens housed in IGF in the locality of Pylea. The testudinid specimen from APMG originates from Allatini (as it is mentioned by Bachmayer and Symeonidis, 1970). Note that the color of the IGF specimen is brownish to reddish, whereas on the other hand the AMPG specimen is grey in color. This is further evidence supporting that the specimens come from different localities. Note that the presence of specimens with reddish color is mention in the nearby locality of Thermi by Stevanovic (1961), with findings of *Hipparion mediterraneum* and *Gazella* cf. *deperdita*. The new specimen of the terrapin from LGPUT originates also from Allatini. As it is mentioned in the handwritten accompanied label (in Greek), the "*freshwater turtle comes from the clay layer b' of the clay pits of Allatini, Thessaloniki, 13 November 1933*". The grey color of the sediment filling the specimens is consistent with Allatini locality. Since both localities are found mainly within Trilophos Formation, it is likely that all the fossils mentioned in this study are found in this formation.

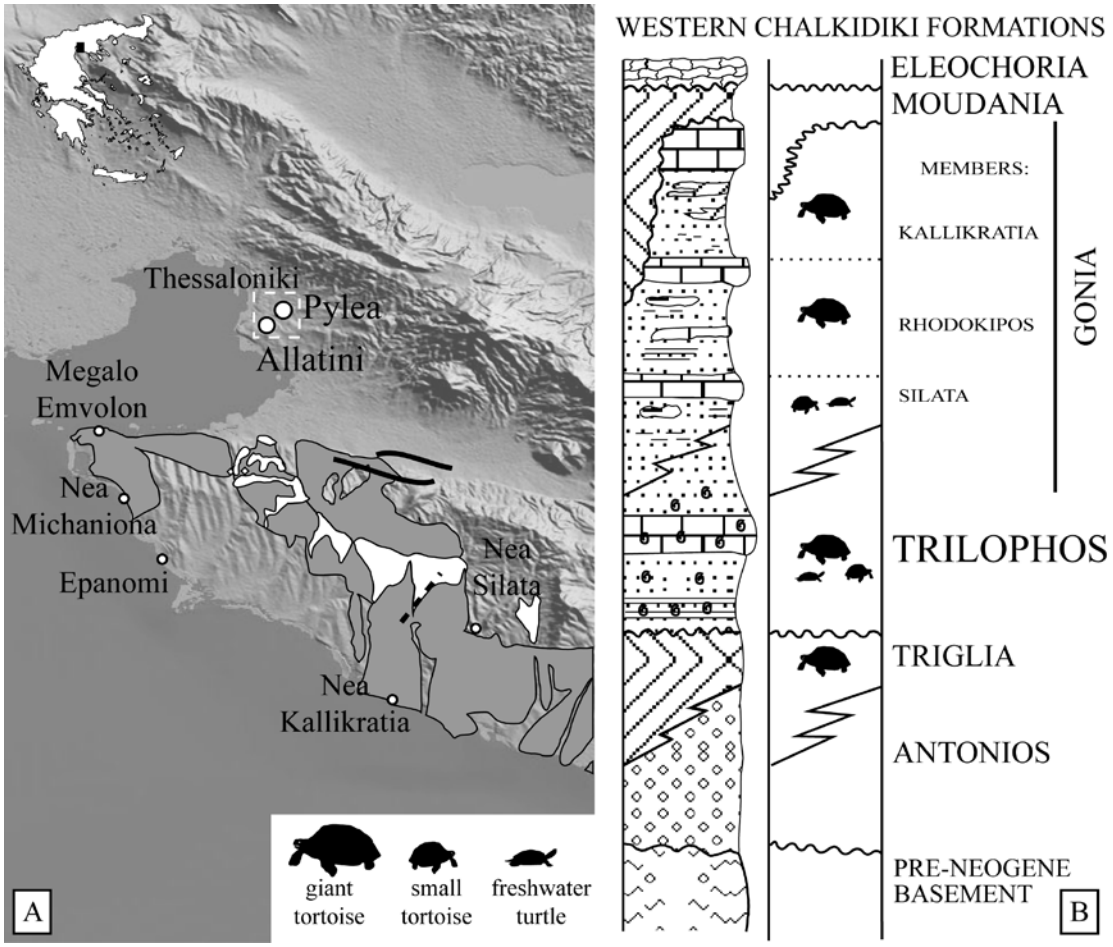


Figure 2.4. A, the position of Pylea and Allatini, east of Thessaloniki city, including other sites containing fossils of turtles and tortoises. Dark grey color indicates the surface exposure of the Neogene deposits. White color indicates the surface exposure of Trilophos formation. B, simplified stratigraphical column (modified after Syrides, 1990 and Vasileiadou et al., 2003) showing the Neogene/Quaternary formations in Western Chalkidiki peninsula. Simplified drawings of turtles indicate the presence of giant and small tortoises, and terrapin in these formations.

Because there is no information available on the discovery and collection of the specimen this claim cannot be tested, unless new specimens are found in situ or the sediment filling the shells is analyzed and compared with sediments collected along the stratigraphic series of the localities mentioned above (something which is out of the scope of this thesis). Therefore, the specimens are highly likely of latest Miocene age but based on the available information we cannot exclude the expansion of their stratigraphic range to the beginning of the Pliocene.

Epanomi; Megalo Emvolon; Aggelochori; Nea Michaniona;
Nea Kallikratia; Thessaloniki, Western Chalkidiki (Pliocene)

Recently, giant tortoises have been collected from three new localities (Epanomi, Nea Kallikratia, and Nea Michaniona) in the coastal area of the western Chalkidiki peninsula, near Thessaloniki (Fig. 2.5.A). The Epanomi site is the most important of all, providing two individuals (I and II in Fig. 2.5.B) with good preservation. Further additional specimens from Nea Kallikratia and Nea Michaniona have also been collected. These new specimens join some fragmented material of large testudinids

and a small tortoise that have been collected and reported from Aggelochori (AMPG) and Megalo Emvolon (AMPG, NHMW). These two names refer to the same area and is unknown whether they are the same or not.

Western Chalkidiki is composed of Neogene/Quaternary sediments (Fig. 2.6.A) which are divided into six formations by Syrides (1990): Antonios Formation (Middle–Late Miocene), Triglia Formation (Vallesian–Early Turolian, Late Miocene), Trilophos Formation (Latest Miocene = Pontian), Gonia Formation (Early–Middle Pliocene), Moudania Formation (Late Pliocene– Early Pleistocene), and Eleochoria Formation (Late Pleistocene–Holocene) (Fig. 2.6B). Up to the present, all of the giant tortoises have been found in the Gonia Formation, which is exposed on almost all the coastal slopes between Megalo Emvolon and Epanomi, in Nea Michaniona and Nea Kallikratia. This formation is complex in structure, with sands, clays, marls, sandstones, gravels in alternating lens-shaped beds, as well as massive marly limestones. Thus, as shown in Fig. 2.6.B, the Formation is divided into three members: the Silata, the Rhodokipos and the Kallikratia members (Syrides, 1990). The main characteristic of this formation is the presence of volcanic pebbles, which probably originated from the Almopia volcanoes (Syrides, 1990). Samples of these pebbles were also collected from the fossil locality Epanomi, providing strong evidence that these deposits belong to the Gonia Formation. This is also confirmed by the sedimentological content of the site (sands, marls, sandstones in alternations), which is similar to the complex structure of this formation (Fig. 2.6.C).

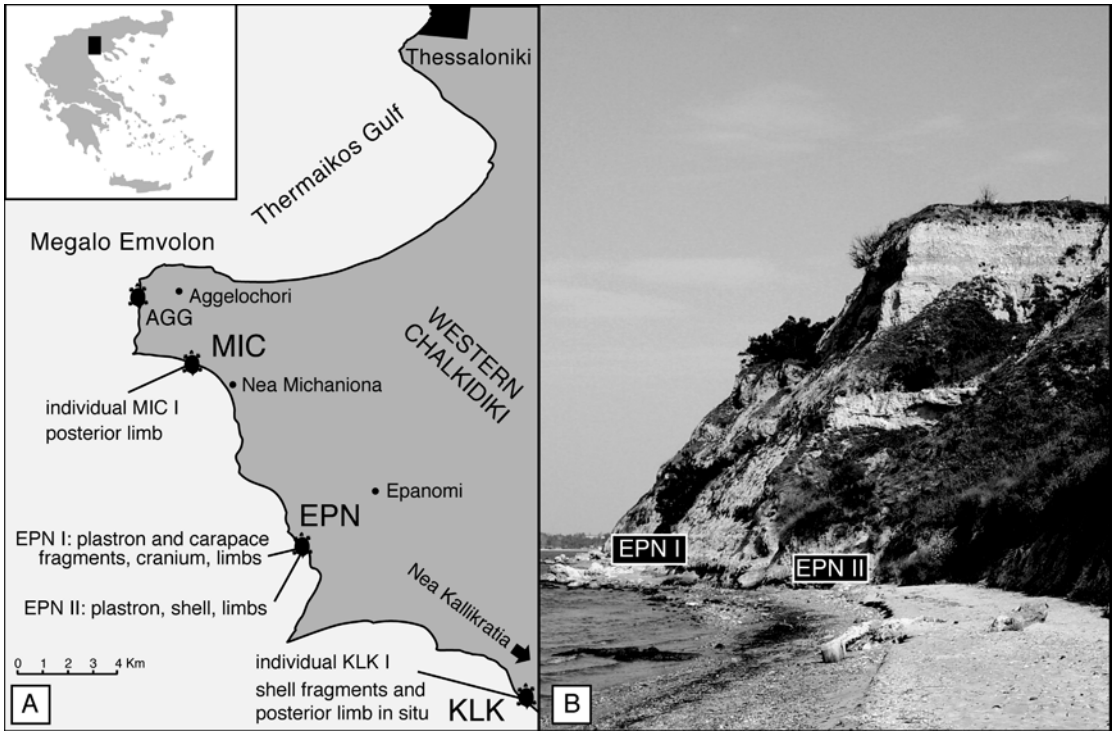


Figure 2.5. The large testudinid sites in Western Chalkidiki peninsula. A, map of the coastal area of western Chalkidiki peninsula, near Thessaloniki, indicating the sites with the Pliocene giant tortoise individuals; B, the locality Epanomi, indicating the recovery positions of individuals EPN I and II. Abbreviations: AGG, Aggelochori; EPN, Epanomi; KLK, Nea Kallikratia; MIC, Nea Michaniona.

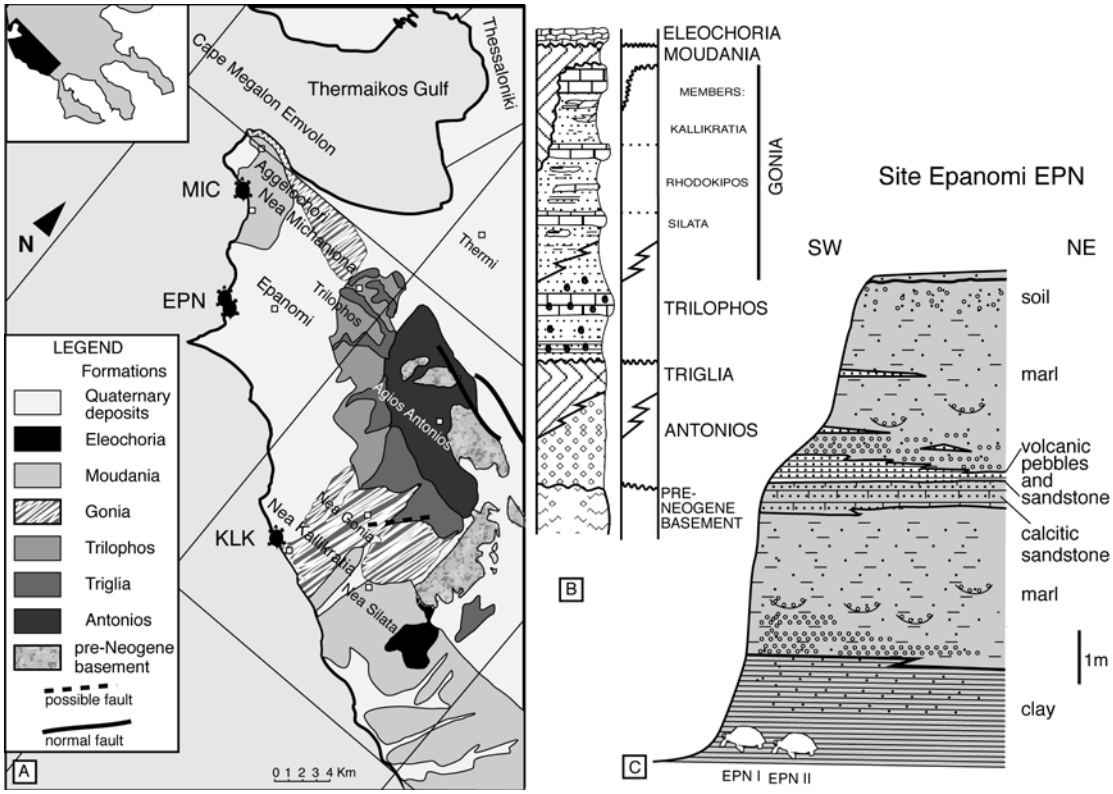


Figure 2.6. Geology of Western Chalkidiki peninsula. A, simplified geological map of western Chalkidiki peninsula, showing the sedimentary formations (modified after Syrides, 1990); B, lithostratigraphical column of western Chalkidiki deposits (modified after Syrides, 1990 and Vasileiadou et al., 2003); C, lithostratigraphical profile of site EPN with indication of giant tortoise findings. Abbreviations: EPN, Epanomi; KLK, Nea Kallikratia; MIC, Nea Michaniona.

Fossil mammal remains are known from these deposits, allowing biostratigraphic inference of the geological age of Gonia Formation. Briefly, the presence of *Dolichopithecus ruscinensis* at Megalo Emvolon suggests a Middle Pliocene (Ruscinian, MN15) age for this section (Koufos et al., 1991). South of Epanomi village, material of *Mammuthus* cf. *meridionalis* and *Equus* sp. suggests a latest Pliocene (MN16) age for this part of the formation (Athanassiou & Kostopoulos, 2010). Finally, analysis of micro-mammalian fauna from Nea Silata locality dates the lower part of the Gonia Formation to the Miocene/Pliocene boundary (MN13/14) (Vasileiadou et al., 2003). So far, the few fossil mammal localities clearly indicate that the Gonia Formation spans the entire Pliocene. The fossil giant tortoise material from Epanomi has been published by Vlachos et al. (2014). New material of large testudinids has been discovered and excavated over the course of this thesis (Fig. 2.7).



Figure 2.7. The new specimen of large testudinid from the Pliocene of Nea Kallikratia. (Above) the front part of the specimen during the excavation; (bleow left) the posterior part of the specimen in the sediment; (below right) the entoplastron revealed during the preparation. Scale bar equals 5 cm.

Gefira, Axios valley, Thessaloniki (Pliocene)

According to Koufos and Pavlides (1988), the deposits between the villages Gefira and Vathylakkos (lower Axios valley) belong to the Gefira Member of Aggelochori Formation, part of the Neogene–Quaternary deposits of the lower Axios valley and they consist mainly of alternated gravels and sands (Fig. 2.8). The Gefira Member overlies the Megalo Emvolon Member and both are included in the Aggelochori Formation. The Megalo Emvolon Member is situated in the cape of Megalo Emvolon (also known as Karaburun or Karabouroun), near Thessaloniki in the western Chalkidiki peninsula, and consists of reddish marls and grey sandy marls alternated with gravels. Koufos and Pavlides (1988) mention that the Megalo Emvolon Member is of an Early Ruscinian age (MN 14), while the Gefira Member is younger and terminates probably in the Pliocene (MN 15–16). The additional material attributed to *Coelodonta antiquitatis praecursor* Guerin, 1980 (MNQ 24), from sand deposits in the same area, show that this formation probably extends up to the Pleistocene (Tsoukala, 1991).

02/16/2016 Ψηφιακή Βιβλιοθήκη Θεόφραστος - Τμήμα Γεωλογίας - Α.Π.Θ.

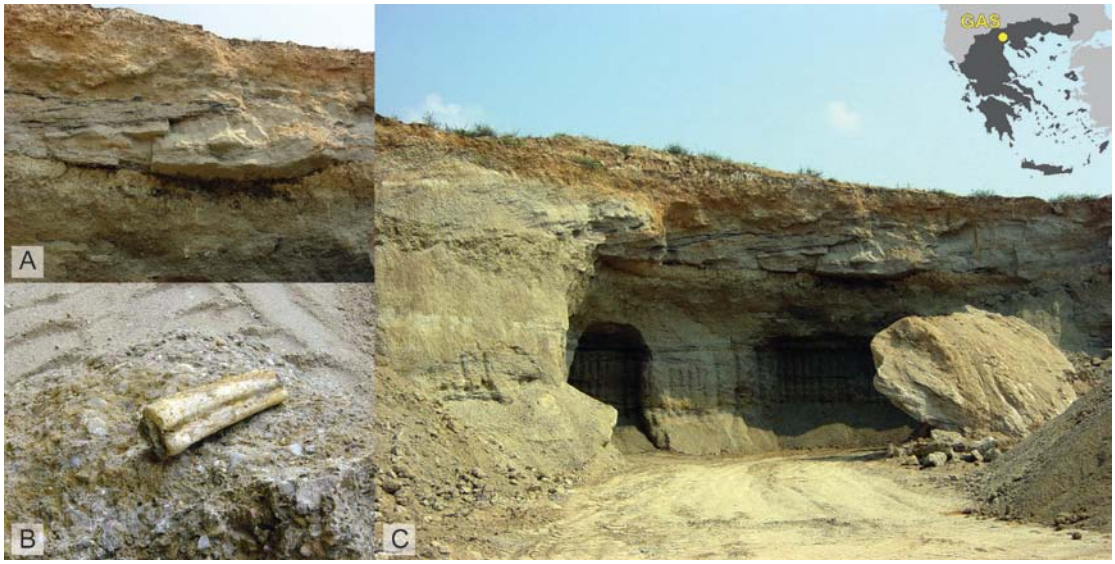


Figure 2.8. The Pliocene locality of Gefira (GAS), in lower Axios valley. A, photograph of the sand deposits that dominate the site. B, fossil mammal bones upon discovery. C, the sand quarry prior to its fully exploitation.

Milia, Grevena, N. Greece (Late Pliocene, Earliest Villafranchian)

The locality of Milia is well-known for its gigantic mastodon fossils that have been described by Tsoukala (2000) and Tsoukala & Mol (in press), its rhino fossils (Guérin & Tsoukala, 2013) and other mammalian taxa that are preliminarily described (carnivores in van Logchem et al., 2010 and Tsoukala et al., 2014; horses in Lazaridis and Tsoukala, 2014b; bovids and cervids in Crégut-Bonnoure and Tsoukala, 2014; Tsoukala, 2005). The testudine remains have been preliminary mentioned in Vlachos (2014). The fossils are recovered mainly in loose sediments of the fluvial and lacustrine deposits of loose conglomerates, clays and sands of various grain sizes in alternations, with red clays in the upper parts of Plio-Pleistocene age, that cover most of the Grevena basin (Brunn, 1956, Savoyat and Monopolis, 1972).

The fossils are found in several localities around the village of Milia (localities Milia 1- Milia 10; Fig. 2.9). The turtle remains in particular are recovered from sandpit localities (Milia 4 and Milia 5) and open localities (e.g. Milia 10). Based on the mammalian fossils, the fauna is of Late Pliocene age (MN16a, Guérin & Tsoukala, 2013). Since the turtle material is recovered together with those fossils, a similar age is proposed for the turtle and tortoise fossils.

Apolakkia, Rhodes Island (Pliocene)

The geological setting of the Apolakkia locality is summarized by Mueller-Töwe et al. (2011). The deposits that are presently exposed in the SW part of Rhodes island belonged to a larger sedimentary basin, and belong to the Apolakkia Formation. It mainly consists of alternations of clays, silts, marls and lignites, whereas in some areas coarse sandstones are found (see Meulenkamp et al. 1972 for further information). Eggshells are known coming from this locality. The eggshells are located in a greenish-grey siltstone (Mueller-Töwe et al., 2011). According to Meulenkamp et al. (1972) the paleoenvironment of the area was generally consisting of rivers, lakes and swamps in a low plain. The age for the material from Apolakkia, based both on the faunal composition and paleomagnetic studies is inferred as

Middle-Late Ruscinian, covering the time span of 5.3-3.4 Mya (see Mueller-Töwe et al., 2011 and references therein).

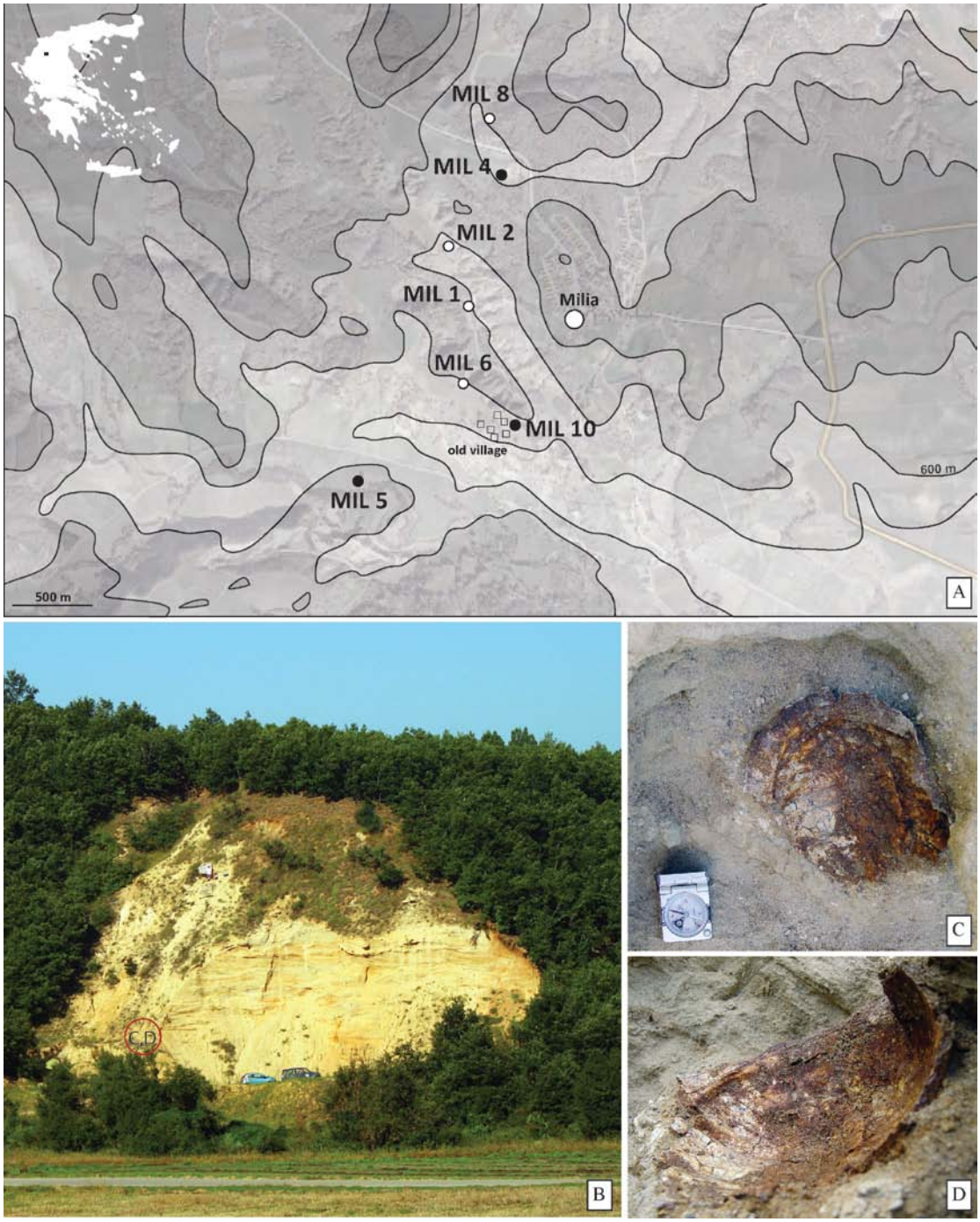


Figure 2.9. The Late Pliocene site of Milia, near Grevena (NW Greece). A, map of the area, showing the fossil localities around the village of Milia. The sites containing fossil chelonians are shown with solid circles. B, site Milia-4, which provided the partial carapace MIL 495. C, the partial carapace MIL 495 on recovery position in visceral and D, on anterior views. Circle marks the position of the carapace finding, shown in C and D.

2.4. Pleistocene

The Pleistocene localities with chelonians in Greece are numerous. The majority of them are cave sites. In mainland Greece the famous caves of Petralona (Chalkidiki)

and Franchthi (Peloponnesus) contain well-preserved specimens. The latter is also of great archaeological interest, since the sediments expand to the Holocene and the presence of humans has been noted in the cave.

Other localities in the mainland include fissure fillings like those of Xerias (Kavala) and Korydallos (Attica), or open sites in Peloponnesus (Megalopolis, Laconia, Diros). Further cave sites are found on islands, like the Charkadio Cave in Tilos, Kandilia Cave in Karpathos, and numerous caves in Crete Island. These caves in Crete (Gerani, Zourida, Bate, Simonelli, Koumpes, Mavro Mouri IV) are located around the city of Rethymnon. Also in Crete, the open site of Sitia is found. Other important open sites are Kos and Vatera (Lesvos). Material of uncertain age is found in Potidea (Chalkidiki), but the morphology of the specimen suggests that most probably is also from the Pleistocene.

Xerias, Kavala; Middle Pleistocene

The tortoise material, associated with specimens of *Elephas antiquus*, has been collected during road construction of the Egnatia National Road in fissure filling deposits in carbonate rocks. The fossils have been preserved in consolidated red calcitic clay (terra rossa). The specimens were collected by Mr. G. Adamidis and subsequently donated to the LGPUT collections. The study of the chelonian material has been preliminary presented in Tsoukala et al. (2011).

Petralona Cave, Chalkidiki (Middle - Late Pleistocene)

The cave of Petralona is situated in Chalkidiki peninsula, near the village of Triglia. It is one of the most famous caves in Greece, not only for touristic reasons, but also due to its important paleontological findings, featuring and almost complete skull of a *Homo heidelbergensis* (Stringer et al., 1979; stored in LGPUT). The fossil fauna consists of numerous fossils, comprising the “old collection” that is stored in LGPUT and the “new collection” stored in the Petralona Museum. The tortoise material is part of the “new collection”, while no chelonian fossils were found in the “old collection”. Tsoukala (1989) in her doctoral thesis that dealt with the detailed study of the “old collection”, as well as in a series of subsequent publications (Rabeder & Tsoukala, 1990; Tsoukala, 1990; Koufos & Tsoukala, 2007; Baryshnikov & Tsoukala, 2010 amongst others) explain the division of the recovered fauna in three biostratigraphic groups of early Middle Pleistocene, late Middle Pleistocene and Late Pleistocene. Kretzoi & Poulianos (1981) mention the tortoise material from the “new collection” as part of the Middle Pleistocene lower vertebrate fauna (see also Kurtén and Poulianos, 1977). Therefore, for the moment, a Middle Pleistocene age could be inferred with caution for the tortoise fossils as well.

Vatera, Lesvos Island; Early Pleistocene

Vatera is located in the south part of Lesvos Island. Near Vatera there are six fossil localities with vertebrate remains. They have been preliminary described in de Vos et al. (2002). The small testudinid material comes from the T-Site, whereas the large testudinid material comes from the F-Site. Note that erroneously Georgalis & Kear (2013) have referred both materials as originating from V-Site. According to de Vos et al. (2002) no chelonian remains are found in V-Site. Lapparent de Broin

(2002) first described those specimens, as belonging to a small and a large testudinid. The fossils have been discovered in the upper parts of the Vatera Formation, consisting of alternations of conglomerates, sandy clays, sandy conglomerates and silt (Drinia et al., 2002). F-Site is a natural outcrop, whereas T-site is a slope that has been exposed by road constructions (see Lyras and van der Geer, 2007). On the study of de Vos et al. (2002) a 2.7 – 1.8 Ma age is provided. Lyras and van der Geer (2007) also provide an approx. age of 2 Ma for this fauna. However, both studies refer it as Late Pliocene. Under the current subdivisions of the Quaternary, the Vatera locality should be referred as Early Pleistocene.

Kos Island (Plio-Pleistocene)

The studied material belongs to the collections made by Kuss in Kos Island (see Kuss, 1973). Although he does not report any turtle remains, he mentions the presence of '*Mastodon' agustidens* and '*Elephas' meridionalis* (Kuss, 1973:60). Further fossil of these proboscideans are reported from Kos (see Doukas & Athanassiou, 2003 and references therein). According to Doukas & Athanassiou (2003) the co-existence of these taxa indicate a Late Pliocene age, but as the stratigraphic position of the specimens is unknown there is no clear conclusion (as in the case of Kos). Therefore, as the exact stratigraphic provenance of the Kos chelonian specimens is unknown, a Late Pliocene – Pleistocene age could be sufficient for the moment.

Charkadio Cave, Tilos Island (Late Pleistocene – Holocene)

The Charkadio Cave is located on the northern part of Tilos Island (Dodecannese Islands) near the village of Megalo Chorio, in an altitude of approximately 120 m. The cave has received considerable attention in the last 40 years, mainly due to the numerous remains of the dwarf elephant. The first data on the stratigraphy of the cave are given by Bachmayer et al. (1984) indicating that the elephant, avian and chelonian remains were restricted to a depth of up to 4 meters, whereas the deer remains are found in deeper layers. This claim is supported also by the C^{14} and U-series dating methods by Bachmayer et al., (1984), which provided a range of 45 ka to 3.5 ka for the elephant remains and 140 ka for the fossil deer. The fossils are located within a considerable layer of fine-grained brownish to gray silt sand sands mixed with tephra grains (Steinhauser et al., 2008). Those elephant remains have been described by Theodorou (1983), and later a new species, *Elephas tiliensis* Theodorou et al., 2007 has been named, declared as the last endemic elephant in the Mediterranean and Europe. The chelonian bones are found scattered and disarticulated along with the elephant bones, therefore a Latest Pleistocene-Holocene age can be inferred for the tortoise material.

Cave sites of Crete (Pleistocene)

Various caves from Crete have provided chelonian material. Most of them are in the surroundings of the town of Rethymnon. The material that is presented here, mostly for the first time, has been collected by various expeditions. Efforts from AMPG provided material from the caves of Gerani and Zourida that led Bachmayer et al. (1975) to the description of the new subspecies *Testudo marginata cretensis*. A Greco/Dutch co-operation (University of Athens / University of Utrecht) resulted in

the collection of numerous material from Gerani, Zourida, Koumpes, Liko, Mavro Mouri IV, and Simonelli caves, as well as from Rethymnon fissure and Sitia (see Brinkerink, 1996). The geological and speleological works of S. Kuss, resulted in the collection of additional fossils from Mavro Mouri, Kalo Choraphi (material not located) and Plakias (material stored in NHMC). Finally, Greco/Italian co-operation (University of Thessaloniki / University of Lincei) discovered new material from Simonelli and "Bate" caves. Below, some brief information on those sites is provided, based on the published works. A significant source of information on Cretan caves can be found in the Bulletin of the Speleological Society of Greece (digitized in digital library "Theofrastos" of AUTH), mainly based on the work of the pioneer speleologist Anna Petrochilou and other collaborators.

However, for the complete evaluation of the Cretan tortoise and turtle material a complete evaluation of the geological information of those sites is necessary. Note that in Georgalis & Kear (2013) the geographical position of most of the Cretan sites around Rethymnon is incorrect. The problem is the uneven available information, as some caves have been extensively investigated, whereas others are only briefly mentioned.

Gerani IV Cave, Crete Island: The material from Gerani presented here, both the holotype and paratype of *T. marginata cretensis* presented in Bachmayer et al. (1975:110), as well as the unpublished material that used to be in Utrecht University, come from Gerani IV Cave, near the village of Gerani, Rethymnon, Crete. It should not be confused with the much larger Gerani Cave that is nearby and has been touristically developed in the past (see below). Due to the importance of the dwarf deer material (e.g. de Vos, 1979 for an earlier view, van der Geer et al., 2014 and references therein for the latest view) the specimens found in Gerani IV cave have been long used for the reconstructions of the isolation of Crete and the effects of island rules on animals. The material of the, so-called, Endemic Cretan Tortoise, is going to be analyzed here. The sediment in which the material has been found is unconsolidated clay capped with a flowstone, within the first 40 cm from the cave fill (van der Geer et al., 2014). Absolute dating in the *Candiacervus* material resulted in an age of 70,000 yr ± 20% (amino acid racemization; in Reese et al., 1996). Based on the taphonomical interpretations in van der Geer et al. (2014), it is most probable that all the material represent one cluster, with minimal postmortem transport and no anthropogenic disturbance. Therefore, a Late Pleistocene age could be inferred for the tortoise material as well. Nearby, the famous touristic Gerani cave is found. Speleological information on this cave is found in Makris (1969) and Petrochilou (1980). The former work is one of the first systematic descriptions of the cave, whereas the latter is much more detailed and contains further information on the results touristic development of the cave. At present, the cave is closed. It is one of the largest caves in Rethymnon area, with a length of 55 m and a surface of 1200 m^2.

Zourida Cave, Crete Island: A relatively detailed description of Zourida Cave can be found in Bachmayer et al. (1975) and Petrochilou (1981). The cave is located on the west side of the Zourida gorge, close to the sea, and contains a lower and an upper chamber. The former is 12 m long and 10 m tall, with numerous boulders covering the floor. In the back of the cave, the red clays are indicated by Bachmayer et al. (1975) as containing the tortoise fossils. The cave roof is composed by conglomerate, containing traces of fossil bones. The upper chamber is accessible through climbing in the entrance and is larger than the lower (23 m long). There is also red clay containing several fossilized bones.

Mavro Mouri IV Cave, Crete Island: Limited information on the Mavro Mouri cave complex is given by Kuss (1970). So far, chelonian remains are known from the cave Mavro Mouri IV and are included in the present thesis. Kuss (1970) reports mixed sediments in the cave, of mainly yellowish sand with coarser and finer parts and horizontal development. Besides the chelonian specimens, the cervid material has received great interest by Dutch researchers, producing numerous publications (see van der Geer et al. 2014 and references therein).

Koumpes Cave, Crete Island: The Koumpes Cave complex (Gumbes I, Gumbes II= Grida Avlaki, Gumpes III in Kuss, 1970) is located in the north shoreline of Crete, few kilometers west of the Rethymnon town. Kuss (1970:78) reports only some bones of *Elephas* in Koumpes III, which is a large cave, right below a nearly flat limestone erosional surface (Terrace sensu Kuss, 1970). Most of the material presented here comes from the cave Koumpes I, as it is inferred by the accompanied information of the fossils.

Simonelli Cave, Crete Island: The morphology of Simonelli Cave has been documented in detail by Malatesta et al. (1980). Simonelli cave is one of the several caves in the limestone cliff west of Rethymnon, reaching a depth of 30 m. It is developed in Miocene limestones and consists of two main chambers, connected by a narrow passage, and its surface is covered by speleothems. Initially, numerous limestone boulders covered the cave floor. The excavations on the first chamber revealed an upper layer of yellowish sands with prehistoric pottery, overlying the reddish clay layer with the bone material, in which the chelonian specimens have been found. Below the fossiliferous layer, a thin layer of yellowish, fine sands overlies a ferruginous clayey earth with scarce limestone fragments. The study of the material from Simonelli Cave indicates a Late Pleistocene age.

“Bate” Cave, Crete Island: Information on the stratigraphy of “Bate” Cave (named after Dorothea Bate) is given by Kotsakis (1977). This cave is also formed in the Miocene limestone of the Rethymnon area, appr. 5 m above sea level. Due to the collapse of the front part of the cave, the cave is partially underwater. The sediment filling the cave is mainly reddish clay with many limestone boulders that have been detached by the roof. The material from “Bate” Cave is of Late Pleistocene age.

Liko Cave, Crete Island: Information of the morphology of Liko Cave is given by Weesie (1982) on the description of a new species of *Athene* (Aves, Strigiformes) from Liko, Gerani and Koumpes cave. The cave is located on the west side of Almyros Gulf, and contains breccious accumulations in the front and in the back parts, excavated in layers. This avian material has been collected during the same expeditions which provided the chelonian material. Based on his work, Weesie (1982) provides a Middle-Upper? Pleistocene age for the *Athene* material. Most of the specimens preserve information of the layer that they were discovered. The tortoise material is found in the layers in Li a, Li b and Li c, whereas the turtle material is found in the layers Li a and Li b. Absolute dating on *Candiacervus* tooth enamel from Liko cave suggests a time range from 105,000 yr ± 20% (units B and C) to 87,000 yr ± 20% (unit D) (amino acid racemization; see van der Geer et al., 2014), indicating a Late Pleistocene age for this material.

Rethymnon fissure, Crete Island: There is no information about this locality, but fossil avian specimens is mentioned in Weesie (1982).

Sitia I, Crete Island

Although Neogene deposits are found in the area of Sitia (or Siteia), mainly with material of deinotheres (e.g. Poulakakis et al, 2002; 2005; Athanassiou, 2004), the chelonian material is the result of the Dutch-team collections on Pleistocene deposits. Since it comes from the locality Sitia I, probably corresponds to Early Pleistocene, i.e. the *Elephas creticus* - *Hippopotamus creutzburgi* fauna, or the *Kritimys* Zone (see Sondaar & van der Geer, 2005 and references therein).

2.5. Pleistocene/Holocene

The Holocene sites with chelonian specimens are numerous, due to the large number of zooarchaeological sites in Greece. The study of turtle and tortoise remains from archaeological sites is not the topic of this study that focuses mainly in the pre-Holocene times. However, over the course of this thesis some material from key sites has been studied that document the transition from the Pleistocene to the Holocene, such as Franchthi Cave in Peloponnesus. Also the material from Vraona Cave is discussed, as it is belongs to recent individuals, being different from the somewhat older material found in this cave. A detailed documentation of the chelonian material from archaeological sites is necessary in the future, in order to understand the interaction with humans and their role as small-game food resources.

Franchthi Cave, Peloponnesus (Paleolithic-Neolithic)

The material has been discovered in cave deposits in the Franchthi cave, which has been developed in Lower Cretaceous limestone. The excavation was carried out in separated lithostratigraphical units (layers P-Z; ranges 106-215+; Stiner & Munro, 2011). Wind blown volcanic ash, originated in Naples, Italy, has allowed radiocarbon datings for the excavated units. Stiner & Munro (2011:620) provide a summary table with dates, stratigraphy and occupation phases for the H1B trench of the cave. This table is used here for reference. For the purposes of this thesis, very important is the recorded boundary of the Pleistocene / Holocene (or Paleolithic / Mesolithic), which could correspond in the boundary between the layer U (151/152-154; 11,700 – 12,500 radiocarbon years BP) and layer V (148-151, undated) in the cave. Besides the numerous findings of turtles and tortoises described here, the faunal material of the cave consists of hundreds of specimens of ungulates, carnivores, small mammals, birds, fishes, and reptiles, which largely represent the diet remains of the humans that occupied the cave (Stiner & Munro, 2011). Furthermore, they showed the evolution of the diet of the Franchthi humans was related with the landscape changes that occurred in the last 40,000 years.

Vraona Cave, Attica

The Vraona Cave is located east of Athens, close to the eastern shore of Attica. The systematic excavations in the cave (collaboration of AMPG and IPW) provided material that has been presented in a special volume (Symeonidis & Rabeder, 1993-1995, Eds). The cave shows an entrance on the top and the bottom of the cave is filled with mixed sediments (sands, conglomerates, clays) and limestone boulders (Verginis, 1993-1995). Within the recovered material some reptilian specimens have been found, studied by Rauscher (1993-1995). The chelonian material consists only of

freshwater taxa, and according to Rauscher (1993-1995) they belong to recent specimens, different from the Holocene/Pleistocene and the Late Pleistocene paleo-faunas that dominate the material.

2.6. Material of uncertain age

Potidea, Kassandra peninsula

According to the poor accompanied information, this almost complete shell comes from the area of Potidea, in the northern part of Kassandra peninsula, Chalkidiki, near Thessaloniki.

Another specimen from old collections, originates from Chalkidiki peninsula (further information not available). On the interior part of the specimen, calcite crystals are preserved on the infill, suggesting that this specimen could be actually deposited in a closed environment.

Chapter 3. Paleontology

Highlights:

Description of new material
Revision of previously published specimens

Podocnemidoideans
Trionychids
Testudinids
Geoemydids
Emydids

Egg-shell specimens

3.1. Introduction

This chapter presents the main part of this study, including the descriptions, comparisons and the analysis of the Greek extinct chelonians. In the following pages one bothremydid, one trionychid, at least nine testudinid, three geoemydid and an emydid taxa are described from numerous fossil specimens. All the descriptions presented here is original work, done in the progress of this study. The majority of the specimens are described for the first time. Only a small amount of the specimens described here have been previously described and published by other authors. All those previously studied specimens have been re-analyzed and revised in this thesis by direct observations. In total, this chapter contains the summary of the morphology of the Greek extinct chelonians, which will be used as a basis for the analyses presented in the following chapters. Only a part of this material has been preliminary published by the author and collaborators during this research.

Briefly, the vast majority of the Greek material belongs to the cryptodiran clade, which is represented by four clades, Trionychidae, Testudinidae, Geoemydidae and Emydidae. All clades that have extant representatives in Greece, are also identified in fossil localities. Among cryptodiran turtles, testudinids appear to be the most diverse clade. The pleurodiran clade is extremely poorly represented in the fossil record of Greece and only one specimen is identified.

A summary table is given at the end of this chapter (Table 3.5, p. 285).

02/16/2016 Ψηφιακή Βιβλιοθήκη Θεόφραστος - Τμήμα Γεωλογίας - Α.Π.Θ.

3.2. Systematic Paleontology

TESTUDINES Batsch, 1788
PLEURODIRA Cope, 1865
PODOCNEMIDOIDEA (sensu Gaffney, Tong, Meylan, 2006)

Nostimochelone lampra **Georgalis, Velitzelos, Velitzelos, Kear (2012) [in Georgalis et al., 2013]**

MATERIAL (Fig. 3.1-3.2): NMP V1, partial carapace and plastron (holotype).

DIAGNOSIS (after Georgalis et al., 2013): *Nostimochelone* is assigned to Podocnemidoidea because it possesses a sutural articulation of the pelvis to the shell, an osseous connection between the carapace and plastron with well-developed axillary and inguinal processes contacting the costal bones, laterally placed, rounded mesoplastra, and an extensive overlap of the pectoral scutes on the entoplastron. Among podocnemidoideans *Nostimochelone* can be diagnosed by the following combination of character states: nuchal wider than long (width = 1.25 x length) with a broadly embayed anterior edge (concavity extending laterally to the medial parts of the first pair of peripherals); a continuous series of six markedly elongate and very narrow neurals with regular, hexagonal outline and short anterolateral sides; anteroposteriorly elongate costal I (midline length = 2.3 x that of costal II) with a concave internal axillary process scar extending to the midline of the plate and laterally crossing the juncture between peripheral II and peripheral III; inguinal buttress contacts costal V but does not extend beyond its lateral extremity; humeral scutes with a midline contact over the entoplastron; pectoral-abdominal sulcus extending well anterior to the mesoplastron.

TYPE LOCALITY: Nostimo, Kastoria, NW Greece.
AGE DISTRIBUTION: Early Miocene (late Burdigalian). Note that in Georgalis et al. (2013:280) in the “Horizon, unit, locality, and age” section, it referred as “late Miocene (late Burdigalian)” which is obviously a mistake.

COMMENTS: This taxon has been recently described in Georgalis et al. (2013), from the Early Miocene of Zeugostasion Formation in Nostimo, Kastoria. The specimen has been found in a hard matrix enclosing the specimen. Up to the present, only the ventral surface of the plastron and the visceral side of the carapace are available for observation (Figure 3.1). This specimen has been attributed to the Zeugostation Formation based on the presence of marine mollusks, shark teeth, and silicified wood in the conglomerate embracing the shell.

This, indeed, enigmatic turtle is clearly a pleurodiran turtle as it is inferred by the presence of a sutured articulation of the pelvis to the shell and the presence of the laterally positioned mesoplastra. In the presence of several other characters, Georgalis et al. (2013) have placed this taxon within Podocnemidoidea, without however performing a phylogenetic analysis. Since the morphological description of the specimen done by Georgalis et al. (2013) is detailed enough and up-to-date, there is no need to revise the morphology of this specimen. In this thesis, an update on the morphology of the neural series (neural 1 is hexagonal, coffin-shaped) (Figure 3.2) and its incorporation into a cladistics framework are provided. *Nostimochelone lampra* was incorporated to the dataset of Gaffney et al. (2006) to explore in a preliminary way its relationships within Pleurodira, showing that is a member of

Bothremydidae. Up to the present, this specimen is the only known pleurodiran turtle in the Greek fossil record, and the oldest known fossil chelonian from Greece.

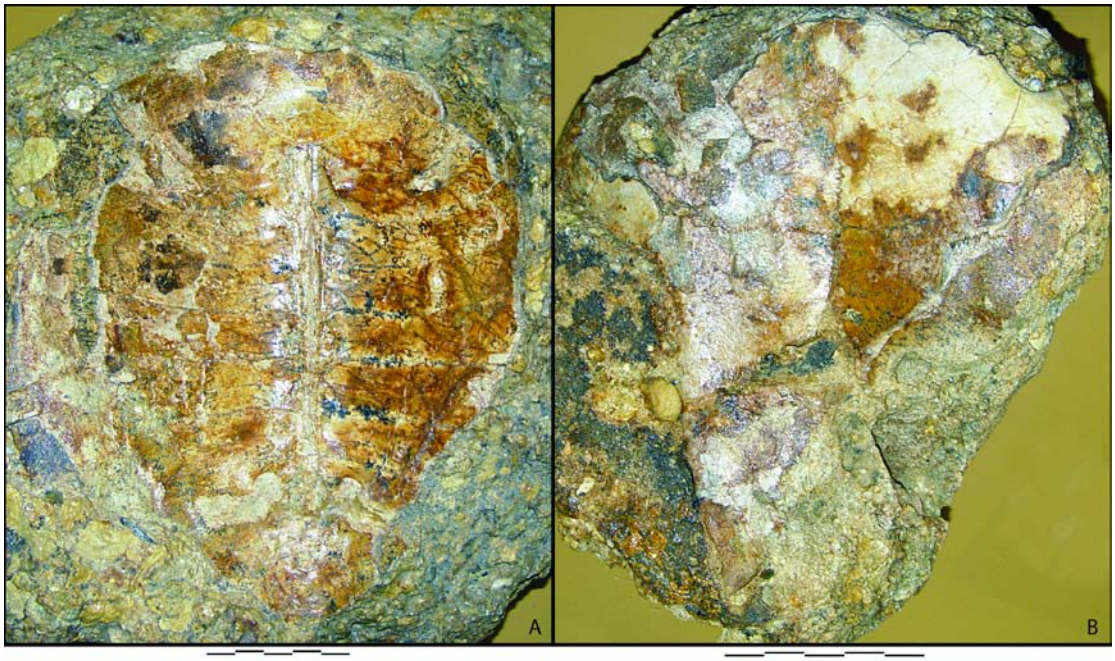


Figure 3.1. *Nostimochelone lampra* Georgalis et al. (2012) from the Late Burdigalian of Nostimo, Kastoria. The holotype and single specimen in (A) visceral view of the preserved carapace and (B) ventral view of the plastron. Scale bar is 5 cm.

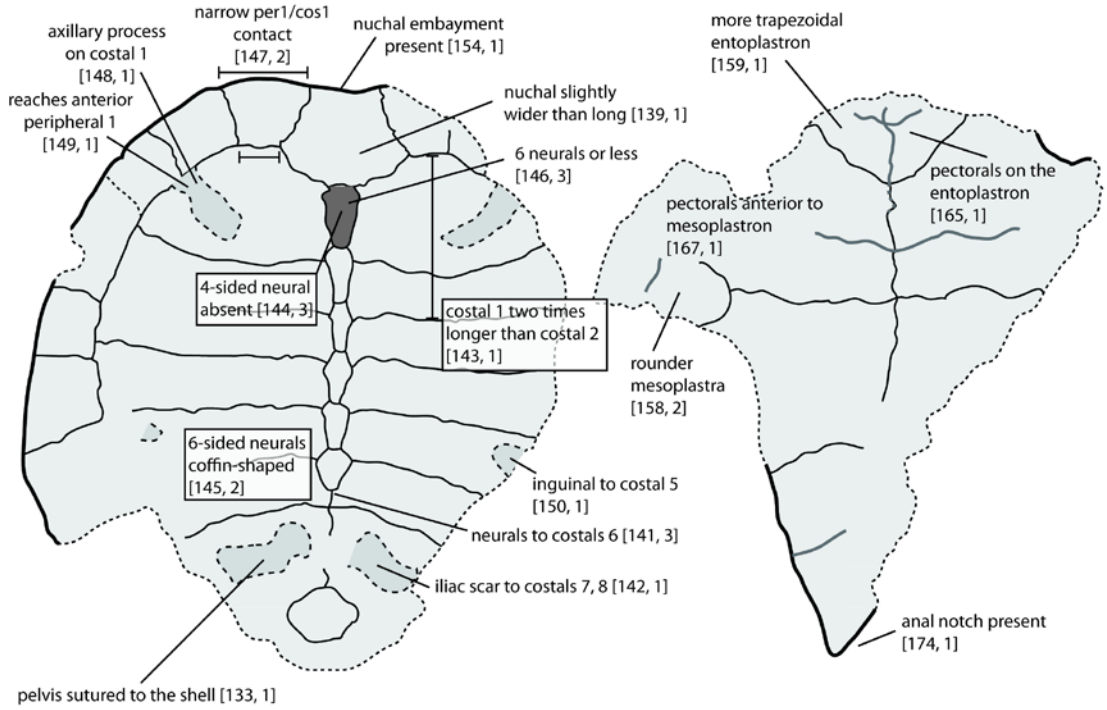


Figure 3.2. Schematic drawings on *Nostimochelone lampra* Georgalis et al. (2012), showing the available character scoring from the matrix of Gaffney et al. (2006). Modified by Georgalis et al. (2013) and personal observations. Explanation in the figure: [number of character in Gaffney et al., 2006, character scoring]

CRYPTODIRA Cope, 1868
TRIONYCHIDAE Gray, 1825

The soft-shelled turtles (Trionychidae Gray, 1825) form a group of highly aquatic cryptodires, which first appeared in the Early Cretaceous of Asia, and spread to the other continents during the Cenozoic (Danilov, 2005; Vitek and Danilov, 2012, and references therein). They possess a flat leathery shell, with a long neck and only three clawed digits in each limb (Meylan, 2006). The surface of the carapace has a distinctive sculpturing, and the absence of scute sulci in dorsal carapace, makes the shell fragments of trionychids easily-recognizable in the fossil record (Meylan, 1987). Although their fossils are very common in Europe, they have been considered absent in the Greek fossil chelonian record (Lapparent de Broin, 2001; Danilov, 2005). Trionychids have received special attention recently due to their distinctive bone histology. Based mainly on the pioneering work of T. Scheyer (Scheyer, 2007; Scheyer et al., 2007; 2012; amongst others) it has become clear that the soft-shelled turtles are characterized by the so-called “plywood” structure in the external cortex of the bone of their shell. This morphology, which can be observed in detailed in thin-sections, is considered as a true synapomorphy of the trionychid clade (Scheyer et al., 2007). Scheyer (2007) and Scheyer et al. (2007) have argued on the biomechanical advantages of the presence of the “plywood” structure but they have pointed out the need of more sampled specimens that would clarify the taxonomic value of this morphology in generic and/or specific level. Histological samples are made on some of the trionychid material studied here. They are presented in a following chapter.

DISTRIBUTION: Gefira, Axios valley, N. Greece and Plakias, Crete Island.

AGE: Pliocene (Gefira) – late Middle Miocene (Plakias).

MATERIAL: (Fig. 3.3-3.4) Gefira, lower Axios valley (Macedonia, Greece): LGPUT GAS 8a (Fig. 2A, B), right part of nuchal; LGPUT GAS 8b (Fig. 2C, D), right part of right first costal; LGPUT GAS 8c (Fig. 2E–G), left second costal; LGPUT GAS 8d (Fig. 3A–D), left part of left fourth costal; LGPUT GAS 8e (Fig 3E–F), right part of left fifth costal. (Fig. 3.5)

Plakias, Crete (2 specimens; temporary numbers): NHMC FS38/01, neural; NHMC FS38/02, hypoplastral process.

DESCRIPTION

Gefira, Axios

The specimens are attributed to Trionychidae on the presence of sculpturing (or ornament), loss of peripherals and the absence of scute sulci in the shell surface. All specimens are heavy mineralized and preserved in very good condition. From the nuchal plate (LGPUT GAS 8a) the right part is preserved, showing that the anterior carapace margin is shallowly concave, while the width is at least three times longer than the length of the plate (Fig. 3.3.A). The remaining preserved elements are from the costals. The right part of the right first costal (LGPUT GAS 8b) is preserved (Fig. 3.3.B), which has a well-developed sutural surface for contact with the nuchal. The sculpturing on the dorsal surface is not visible in some parts probably as a result of

erosion. The left second costal (LGPUT GAS 8c) is found almost complete (Fig. 3.3.C); only a small part of the anterior medial margin is missing. The dorsal surface exhibits distinctive sculpturing (or ornament), consisting of small pits that are found either isolated or connected in larger associations (Fig. 3.3.C1). This pattern is quite similar to that observed in several other Trionychidae, both in fossil and extant forms. This costal plate is longer laterally than medially. The anterior border is shallowly concave, whereas the posterior border for the third costal is almost straight. Ventrally, the ends of the costal ribs can be observed. The ends of the costal rib are convex but they do not project laterally.

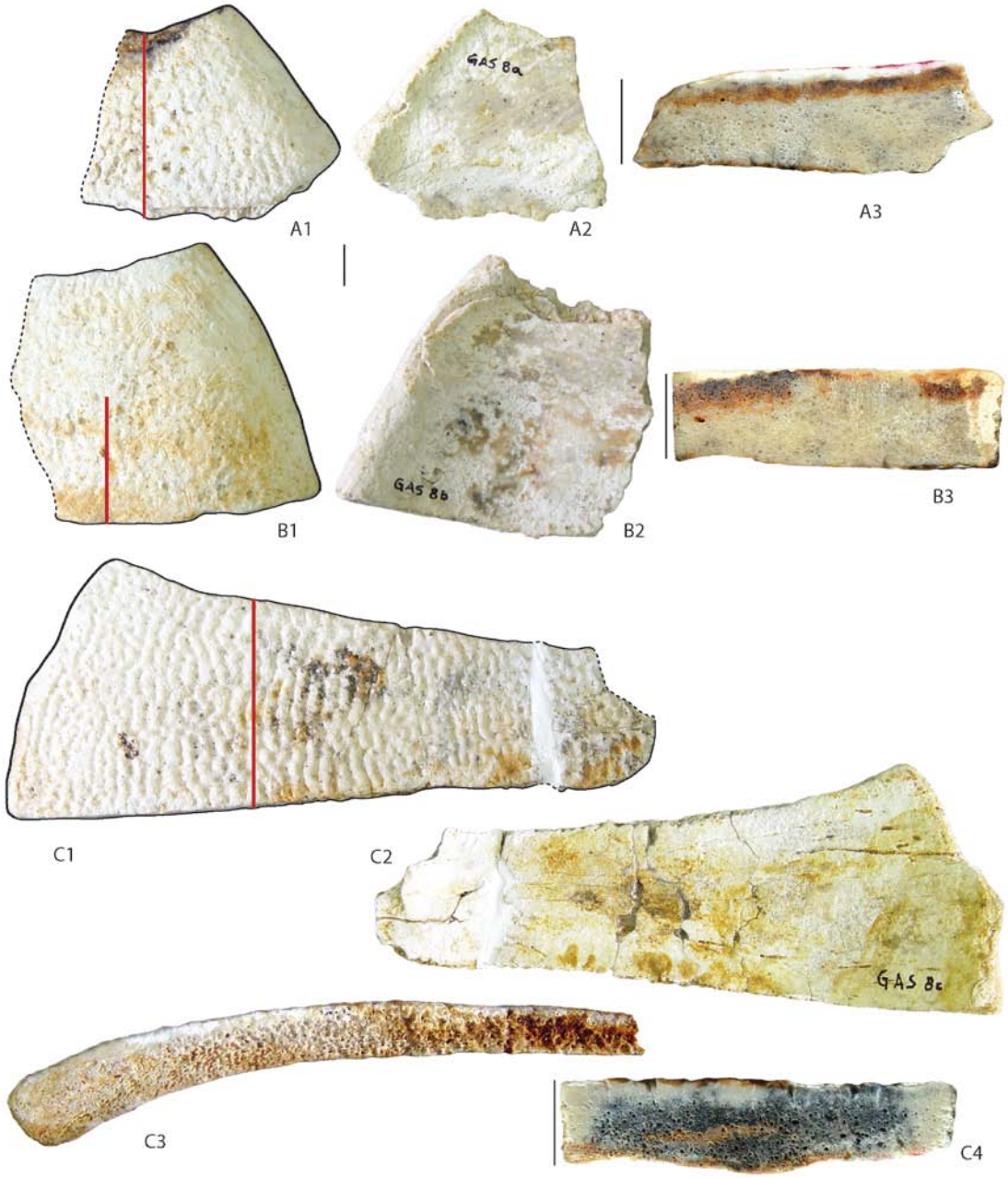


Figure 3.3. Trionychidae from Gefira locality, Pliocene, N. Greece. Carapace plates in (A) LGPUT GAS 8a, nuchal in A1, dorsal, A2, visceral views and in A3, cross-section. (B) LGPUT GAS 8b, 1st right costal plate in B1, dorsal, B2, visceral views and in B3, cross-section. (C) LGPUT GAS 8c, 2nd left costal plate in C1, dorsal, C2, visceral, C3, posterior views and C4, cross-section. Scale bar equals 10 mm. The line indicates the sectioned plane.

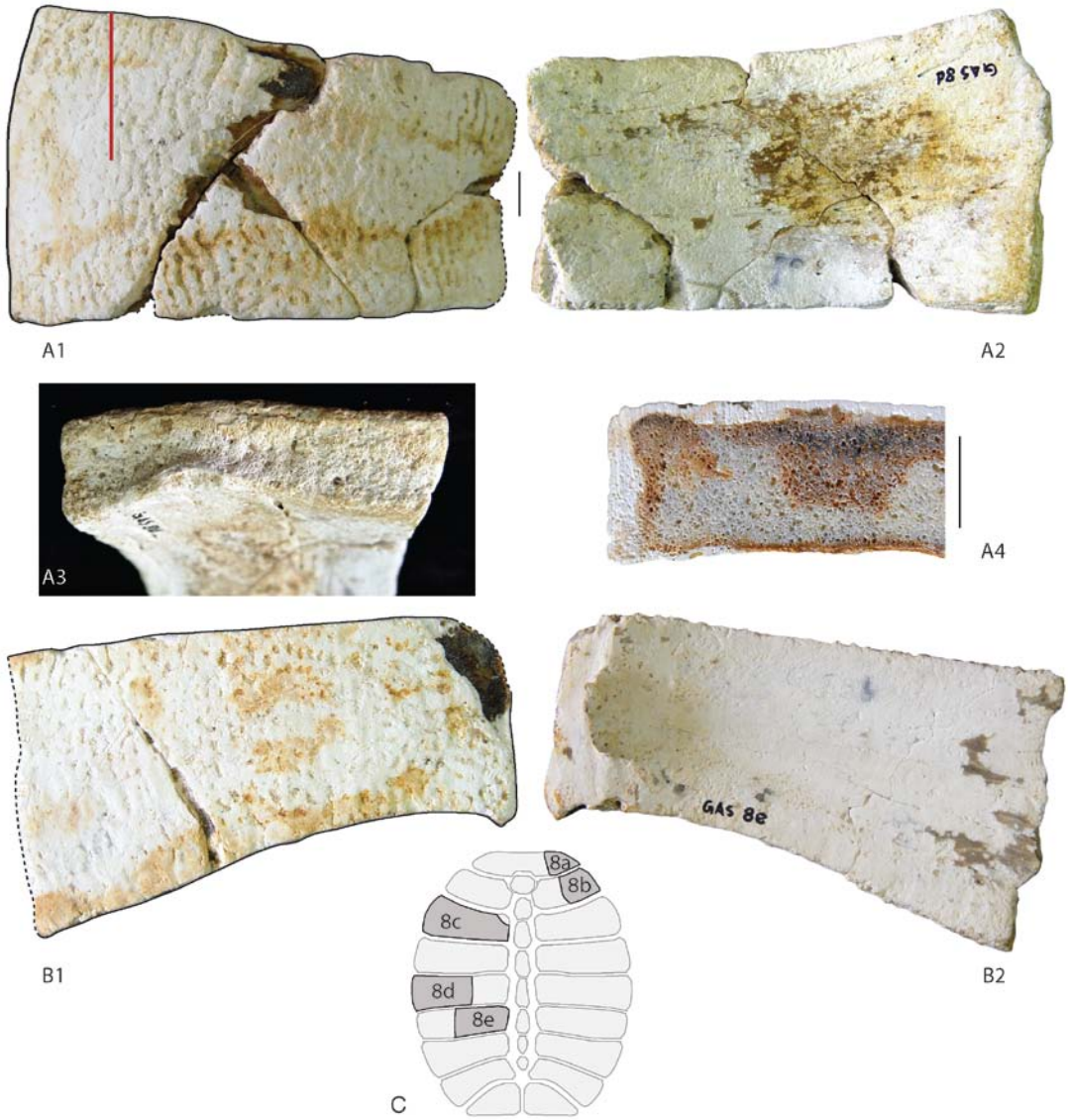


Figure 3.4. Trionychidae from Gefira locality, Pliocene, N. Greece. Carapace plates in (A) LGPUT GAS 8d, left 4th costal plate in A1, dorsal, A2, visceral, A3, lateral, and A4, cross-section. (B) LGPUT GAS 8e, 5th left costal plate in B1, dorsal, and B2, visceral views. (C) drawing, showing the position of the studied specimens on a generalized trionychid carapace. Scale bar equals 10 mm. The line indicates the sectioned plane.

Based on this complete plate, the transverse profile of the carapace is broadly convex (Fig. 2F). The thickness of the plate is varies from 9.1 mm medially to 9.4 mm laterally (Table 1). From the left fourth costal (LGPUT GAS 8d) the left part is preserved (Fig. 3A–D). Both the anterior and posterior borders are straight, whereas the lateral edge of the costal is medially concave in transverse view (Fig. 3C). The dorsal surface is eroded, but the sculpturing is visible. From the left fifth costal (LGPUT GAS 8e) the right part is preserved (Fig. 3E–F). The anterior border is straight, whereas the posterior is anteriorly convex. Again, the sculpturing on the dorsal surface is partially eroded. The medial margin is preserved, showing a long neural with straight lateral borders. In the remaining costal plates the medial margin is not preserved, disallowing the estimation of the shape of the corresponding neurals. The lateral ends of the costals are rounded and show no evidence of a sutural surface, suggesting the loss of peripherals. The dimensions of the preserved parts are given in

Table 1. All the plates have a similar size and morphology and were found in the same locality. They do not preserve overlapping parts of the carapace, and show similar state of fossilization and color. These allow us to conclude that they most probably belong to the same individual (Fig. 3.5.C), that exceeded 400 mm in carapacial length (Table 1 for measurements).

Table 3.1. Measurements of the preserved parts of the Gefira trionychid carapace.

LGPUT:	GAS 8a	GAS 8b	GAS 8c	GAS 8d	GAS 8e
(in mm)	nuchal (right part)	1st right costal (right part)	2nd left costal (almost complete)	4th left costal (left part)	5th left costal (right part)
preserved length	42.9	61	33.7	55.3	48.1
preserved width	63.9	66.7	149.9	121.4	114.4
thickness	10.6–13.2	10.4–12.1	9.1–9.4	7.1–11	6.8–7.3

Comment: The morphology of the preserved carapace fragments of the Gefira individual allows attribution to a single individual of Trionychidae, based on the absence of scute sulci and the sculpturing on the outer shell surface; they are too few to allow further identification. Gardner and Russel (1994), showed that the several carapacial features are quite variable and therefore cannot be of high diagnostic value. Especially the sculpturing is only diagnostic up to Family level. Lapparent de Broin (2001) reports that most fossil trionychids from the Tertiary of Europe are too poorly preserved to be identified as members of the *Trionyx* s.l. group, whereas the presence of *Rafetus* cannot be excluded. The group *Trionyx triunguis* s.s. is restricted in Europe to the Pliocene of South France–Italy, while the remaining findings can be referred to *Trionyx* s.l.. Meylan (1987) mentioned that *Trionyx* is characterized by a nuchal that is at least three times wider than long. Consequently, the Gefira trionychid could be a species of *Trionyx* s.l., based on the dimensions of the preserved nuchal, but more specimens are needed to allow a safe generic identification.

Plakias, Crete

NHMC FS38/01 (Fig. 3.5.A): This specimen corresponds to an almost complete neural. Although the specimen is eroded, the shape of the neural appears to be hexagonal with short anterior lateral sides. Viscerally, the attachment for the vertebra is preserved. Dorsally, the distinctive sculpturing of the trionychids is visibly, consisting of small pits.

NHMC FS38/02 (Fig. 3.5.B): This specimen most probably corresponds to a hypoplastral process of a trionychid. It is long and flattened, with an elliptical cross-section.

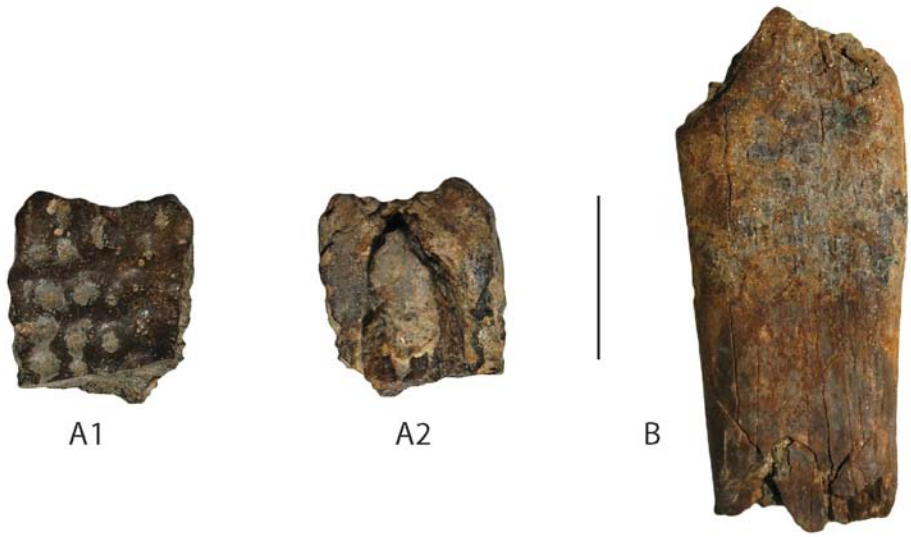


Figure 3.5. Plates of a trionychid from the Middle Miocene site of Plakias, Crete (NHMC collection). A, fragment of a neural plate in A1, dorsal and A2, visceral views. B, part of a hyoplastral process in dorsal view. Scale bar equals 10 mm.

DISCUSSION

Up to the present, fossil trionychids have been unknown from Greece, which was one of the main differences between the Greek and Turkish fossil assemblages (Lapparent de Broin, 2002). This family is also absent in the genuine extant chelonian fauna of Greece, with the only reported members found in the waters near Kos (Taskavak et al., 1999) and other Aegean Islands such as Rhodes, Kalymnos, Leros and Kos (Dimaki, 2002), originating most probably from the Turkish populations. These individuals are usually accidentally caught in fishing nets by local fishers. In Turkey, extant trionychids are represented by two species, *Trionyx triunguis* (Forsskål, 1775) and *Rafetus euphraticus* Dauden, 1802 (Taskavak & Akcinar, 2009).

These, mainly carnivorous, turtles are known for their ability to cover large distances inland; floods and overflows can sweep away the turtles to the ocean and by tolerating salty water they can insert into another river system (Taskavak and Akcinar, 2009 and references therein). Soft-shelled turtles usually prefer rivers and lakes with sandy bottoms, that are very important for their hatchlings (Plummer et al., 2008). Gefira deposits are characterized by large quantities of sands, while the presence of *Anancus arvernensis* reveals the presence of significant bodies of water and large quantities of plants during the Pliocene in the area. This paleoenvironment is consistent with an ecosystem in that trionychids are normally adapted. Moreover, the fact that these findings are reported from the mainland of Greece allows us to assume that the presence of a Trionychidae in the Pliocene is not random like in present-day fauna, but an original member of the Greek fossil chelonian fauna. The fossiliferous sediments of Plakias are interpreted by de Bruijn et al. (2012) as “floodplain deposits” indicating an area next to a river system. This is also an environment where trionychids could thrive. Also, the finding of a trionychid of appr. 10 Mya in Plakias roots the presence of trionychids in Greece in the early Late Miocene, suggesting a diachronic presence of this clade in the South Balkans. However, given the increased mobility of soft-shelled turtles, more specimens are certainly needed to establish the distribution and systematic position of the Greek trionychids.

02/16/2016 Ψηφιακή Βιβλιοθήκη Θεόφραστος - Τμήμα Γεωλογίας - Α.Π.Θ.

TESTUDINIDAE Gray, 1825

TITANOCHELON Pérez-García & Vlachos, 2014

The taxonomy of the large testudinids in Europe has always been problematic. Provisionally, nearly all taxa have been assigned to *Testudo*. After the work of Auffenberg (1974) many scholars used his proposal to group all large testudinids into the genus *Geochelone*. The work of Fritz & Bininda-Emonds (2007) however, proved that this taxon is paraphyletic. At the same time, de Broin (1977) had introduced the use of the French *Cheirogaster* Bergounioux (1935) with an emended diagnosis and later (Lapparent de Broin, 2001; 2002) nearly all large testudinids were assigned to *Cheirogaster*. Lately, our work (Vlachos et al., 2014) pointed out the problems of this assignment. Finally, the re-discovery and description of the putatively lost material of "*Testudo*" *bolivari* from Spain, has allowed Pérez-García & Vlachos (2014) to propose an alternative taxonomy, by erecting the new genus *Titanochelon* and revising most of the Neogene large testudinids. In this work, we follow Pérez- García & Vlachos (2014) and include some information about this recently described genus. For further information see Pérez-García & Vlachos (2014) and their supplementary data. The study of the Greek *Titanochelon bacharidisi* Vlachos et al., 2014 has played an important role in the revision of the European large testudinids.

TYPE SPECIES: *Titanochelon bolivari* (Hernández–Pacheco, 1917)

INCLUDED SPECIES IN THE GENUS: *Titanochelon bolivari* (Hernández–Pacheco, 1917), *Titanochelon eurysternum* (Gervais, 1848–1852), *Titanochelon ginsburgi* (Broin, 1977), *Titanochelon vitodurana* (Biedermann, 1862), *Titanochelon leberonensis* (Depéret, 1890), *Titanochelon schafferi* (Szalai, 1931), *Titanochelon perpiniana* (Depéret 1885), *Titanochelon bacharidisi* (Vlachos et al, 2014).

PROBABLY INCLUDED SPECIES: cf. *Titanochelon gymnesicus* (Bate, 1914).

DIAGNOSIS: Western Euroasiatic (from Western Europe to Minor Asia) Neogene large testudinid (shell from more than 1 m up to 2 m long), with frontals narrower than prefrontals, causing a gentle constriction of the frontals in dorsal view, sharing the following exclusive combination of characters: long crista supraoccipitalis; presence of an elliptical to circular premaxillary pit; relatively low carapace; wide shell; nuchal plate as wide as long or wider than long; eight neural plates, the first one being rectangular; longer than wide first neural, the second and fourth neurals octagonal, with the greatest width of the second one situated in its rear half, the third and fifth neurals rectangular, wider than long, and the sixth to eighth neurals hexagonal, being the length their latero–anterior margins similar to that of the latero–posterior ones; absence of pointed tips in the carapacial rim in the region of contact of the sulci between the marginal scutes and the lateral border of the anterior and posterior peripherals; two suprapygals, the first embrassing the lenticular second one; longer than wide pygal; absence of cervical scute; coincidence between the medial margins of all the marginals and the suture between the costal and peripheral plates; significant distance between the second pair of marginals and the nuchal plate; fourth to sixth marginals in contact with the second pleural scute; presence of a supracaudal scute; second suprapygal crossed by the vertebro–supracaudal sulcus; absence of plastral hinges; wide plastral lobes, at least in the region of contact with the plastral

bridge; anterior plastral lobe longer than the posterior lobe; convex to flat dorsal lip of the epiplastra; absence of ventral relief in the area covered by the gular scutes; angle between the sagittal axis and the gular–humeral sulcus of 45º or more acute; humero–pectoral sulcus perpendicular to the axial plane in the medial region, but with a well developed lateral change of curvature; very short pectoral scutes in the sagittal plane, but markedly expanded, towards the anterior region, laterally; presence of a single pair of inguinal scutes; males with a well developed ventral thickening in the area covered by the anal scutes; curved diaphysis of the humerus and femur; fused astragalus and calcaneum.

DISTRIBUTION: Neogene (Early Miocene to Early Pleistocene) of Europe (Portugal, Spain, France, Switzerland, Germany, Greece, Bulgaria), European Turkey and Minor Asia. This taxon could be also present in the Pleistocene of some Mediterranean Islands (Baleares Islands and Malta).

Titanochelon bacharidisi (Vlachos, Tsoukala, Corsini, 2014)

MATERIAL:

Epanomi, western Chalkidiki, N. Greece (3 individuals; 292 specimens):

Individual EPN I, LGPUT EPN 100–199, female individual, holotype of *T. bacharidisi* (Fig. 3.6-3.13):
LGPUT EPN 100, Carapace (left and right peripherals); LGPUT EPN 101, Plastron; LGPUT EPN 102, Cranium and mandible; LGPUT EPN 103, Right Humerus; LGPUT EPN 104, Left Humerus; LGPUT EPN 105, Left Scapula; LGPUT EPN 105a, Left Coracoid; LGPUT EPN 106, Right Scapula; LGPUT EPN 106a, Right Coracoid; LGPUT EPN 107, Right Femur; LGPUT EPN 108, Right Tibia; LGPUT EPN 109, Right Fibula; LGPUT EPN 110, Left Femur; LGPUT EPN 111, Left Tibia; LGPUT EPN 112, Left Fibula; LGPUT EPN 113, Right Radius; LGPUT EPN 114, Left Radius; LGPUT EPN 115, Pelvis; LGPUT EPN 116, Cervical vertebra; LGPUT EPN 117, Cervical vertebra; LGPUT EPN 121, Right Intermedium; LGPUT EPN 122, Right Medial and Lateral centrale; LGPUT EPN 123, Right Metacarpal; LGPUT EPN 124, Right Distal carpal; LGPUT EPN 125, Right Metacarpal; LGPUT EPN 126, Phalanx I; LGPUT EPN 127, Right Metacarpal; LGPUT EPN 128, Crural osteoderm; LGPUT EPN 129, Carpal indet; LGPUT EPN 130, Carpal indet; LGPUT EPN 131, Anterior claw; LGPUT EPN 132, Anterior claw; LGPUT EPN 133, Anterior claw; LGPUT EPN 134, Half–pointed osteoderm; LGPUT EPN 135, Left Medial and Lateral centrale; LGPUT EPN 136, Left Intermedium; LGPUT EPN 137, Carpal element?; LGPUT EPN 138, Anterior claw; LGPUT EPN 139, Anterior claw; LGPUT EPN 140, Half–pointed osteoderms; LGPUT EPN 141, Anterior claw; LGPUT EPN 142, Half–pointed osteoderm; LGPUT EPN 143, Phalanx I; LGPUT EPN 144, Metacarpal right; LGPUT EPN 145, Phalanx I; LGPUT EPN 146, Right Metacarpal; LGPUT EPN 147, Left Metacarpal; LGPUT EPN 148, Phalanx I; LGPUT EPN 149, Left Metacarpal; LGPUT EPN 150, Right Astragalo–calcaneum; LGPUT EPN 151, Right 4th distal tarsal; LGPUT EPN 152, Metatarsal; LGPUT EPN 153, Right Distal tarsal; LGPUT EPN 154, Right Distal tarsal; LGPUT EPN 155, Right Distal Tarsal; LGPUT EPN 156, Phalanx I; LGPUT EPN 157, Crural osteoderm; LGPUT EPN 158, Right Distal tarsal; LGPUT EPN 159, Phalanx I; LGPUT EPN 160, Tubercle and associated osteoderms; LGPUT EPN 161, Left

Metatarsal; LGPUT EPN 162, Posterior claw; LGPUT EPN 163, Left Metatarsal; LGPUT EPN 164, Phalanx I; LGPUT EPN 165, Anterior claw; LGPUT EPN 166, Left Metatarsal; LGPUT EPN 167, Left 4th distal tarsal; LGPUT EPN 168, Left Distal tarsal; LGPUT EPN 169, Left Distal tarsal; LGPUT EPN 170, Anterior claw; LGPUT EPN 171, Phalanx I; LGPUT EPN 172, Right Metatarsal; LGPUT EPN 173, Left Distal tarsal; LGPUT EPN 174, Posterior claw; LGPUT EPN 175, Phalanx I; LGPUT EPN 176, Left Ulna (fragment); LGPUT EPN 177, Left Distal tarsal; LGPUT EPN 178, Left Distal carpal; LGPUT EPN 179, Left Distal carpal; LGPUT EPN 180, Left Metacarpal; LGPUT EPN 181, Left Metacarpal; LGPUT EPN 182, Left Metacarpal; LGPUT EPN 183, Carpal indet; LGPUT EPN 184, Bony tubercle; LGPUT EPN 185–197, Caudal vertebras; LGPUT EPN 198, Mandible (anterior part); LGPUT EPN 199a, Half–pointed osteoderm; LGPUT EPN 199b, Half–pointed osteoderm; LGPUT EPN 199c, Half–pointed osteoderm; LGPUT EPN 199d, Crural osteoderm; LGPUT EPN 199e, Crural osteoderm; LGPUT EPN 199f, Pointed osteoderm; LGPUT EPN 199g, Pointed osteoderm; LGPUT EPN 199h, Pointed osteoderm; LGPUT EPN 199i, Pointed osteoderm.

Individual EPN II, LGPUT EPN 200–287, male individual, paratype of *T. bacharidisi* (Fig. 3.14-3.17):
LGPUT EPN 200, Right Humerus (distal); LGPUT EPN 201, Right Radius; LGPUT EPN 202, Right Ulna; LGPUT EPN 203, Left Humerus (diaphysis); LGPUT EPN 204, Left Radius; LGPUT EPN 205, Left Ulna; LGPUT EPN 206, Right Scapula; LGPUT EPN 207, Right Coracoid; LGPUT EPN 208, Left Scapula; LGPUT EPN 209, Left Coracoid; LGPUT EPN 210, Right Pubic fragment; LGPUT EPN 211, Pelvic fragment; LGPUT EPN 212, Right Femur; LGPUT EPN 213, Right Tibia; LGPUT EPN 214, Right Astragalo–calcaneum; LGPUT EPN 215, Anterior claw; LGPUT EPN 216, Anterior claw; LGPUT EPN 217, Anterior claw; LGPUT EPN 218, Anterior claw; LGPUT EPN 219, Anterior claw; LGPUT EPN 220, Phalanx I; LGPUT EPN 221, Phalanx I; LGPUT EPN 222, Phalanx I; LGPUT EPN 223, Phalanx I; LGPUT EPN 224, Phalanx I; LGPUT EPN 225, Right Distal Carpal; LGPUT EPN 226, Right Intermedium; LGPUT EPN 227, Right Metacarpal; LGPUT EPN 228, Right Metacarpal; LGPUT EPN 229, Right Distal carpal; LGPUT EPN 230, Metacarpal right; LGPUT EPN 231, Pointed osteoderm; LGPUT EPN 232, Half–pointed osteoderm; LGPUT EPN 233, Half–pointed osteoderm; LGPUT EPN 234, Pointed osteoderm; LGPUT EPN 235, Pointed osteoderm; LGPUT EPN 236, Pointed osteoderm; LGPUT EPN 237, Flat osteoderm; LGPUT EPN 238, Pointed osteoderm; LGPUT EPN 239, Half–pointed osteoderm; LGPUT EPN 240, Half–pointed osteoderm; LGPUT EPN 241, Half–pointed osteoderm; LGPUT EPN 242, Half–pointed osteoderm; LGPUT EPN 243, Half–pointed osteoderm; LGPUT EPN 244, Pointed osteoderm; LGPUT EPN 245, Pointed osteoderm; LGPUT EPN 246, Flat osteoderm; LGPUT EPN 247, Pointed osteoderm; LGPUT EPN 248, Half–pointed osteoderm; LGPUT EPN 249, Flat osteoderm; LGPUT EPN 250, Half–pointed osteoderm; LGPUT EPN 251, Pointed osteoderm; LGPUT EPN 252, Pointed osteoderm; LGPUT EPN 253, Half–pointed osteoderm; LGPUT EPN 254, Half–pointed osteoderm; LGPUT EPN 255–259, Flat osteoderms; LGPUT EPN 260, Half–pointed osteoderm; LGPUT EPN 261–271, Flat osteoderms; LGPUT EPN 272, Pointed osteoderm; LGPUT EPN 273, Half–pointed osteoderm; LGPUT EPN 274, Phalanx I; LGPUT EPN 275, Flat osteoderm; LGPUT EPN 276, Right Fibula; LGPUT EPN 277, Bone fragment indet; LGPUT EPN 278, Bone fragment indet; LGPUT EPN 279, Bone fragment indet; LGPUT EPN 280, Right Medial and Lateral

centrale; LGPUT EPN 281, Right Metacarpal; LGPUT EPN 282, Right Metacarpal; LGPUT EPN 283, Carapace fragment; LGPUT EPN 284, Posterior carapace; LGPUT EPN 285, Plastron; LGPUT EPN 286, Inguinal process fragment (8^{th} – 9^{th} peripheral); LGPUT EPN 287, Right anterior peripheral fragment (2^{nd} – 3^{rd} peripheral).

Individual EPN III (Fig. 3.18):
LGPUT EPN 99, left femur.

Nea Kallikratia, western Chalkidiki, N. Greece (2 individuals; 30+ specimens):
KLK I individual (Fig. 3.19): LGPUT KLK 501, Carapace fragments; LGPUT KLK 502, Plastron fragments; LGPUT KLK 503, Left Humerus proximal; LGPUT KLK 504, Right Femur; LGPUT KLK 505, Right Tibia; LGPUT KLK 506, Right Fibula; LGPUT KLK 507, Right Astragalo–calcaneum; LGPUT KLK 508, Right 1^{st} distal tarsal; LGPUT KLK 509, Right 2^{nd} distal tarsal; LGPUT KLK 510, Right 4^{th} distal tarsal; LGPUT KLK 511, Right 5^{th} distal tarsal; LGPUT KLK 512, Right 1^{st} metatarsal; LGPUT KLK 513, Right 2^{nd} metatarsal; LGPUT KLK 514, Right 3^{rd} metatarsal; LGPUT KLK 515, Right 4^{th} metatarsal; LGPUT KLK 516, Right Phalanx I; LGPUT KLK 517, Right Phalanx I; LGPUT KLK 518, Right Phalanx I; LGPUT KLK 519, Right Phalanx I; LGPUT KLK 520, Right Claw; LGPUT KLK 521, Right Claw; LGPUT KLK 522, Right Claw; LGPUT KLK 523, Thigh tubercle; LGPUT KLK 524, Thigh tubercle; LGPUT KLK 525, Osteoderm; LGPUT KLK 526, Osteoderm; LGPUT KLK 527, Osteoderm; LGPUT KLK 528, Osteoderm; LGPUT KLK 529, pelvis. KLK II individual (Fig. 3.20): LGPUT KLK 500, plastron.

Nea Michaniona, western Chalkidiki, N. Greece (1 individual; 19 specimens):
(Fig. 3.21-3.22) LGPUT MIC 301, Left Femur; LGPUT MIC 302, Left Tibia; LGPUT MIC 303, Left Fibula (same individual, in articulation); LGPUT MIC 304, pelvis fragment; LGPUT MIC 305, pelvis fragment; LGPUT MIC 306, pelvis fragment; LGPUT MIC 307, pelvis fragment; LGPUT MIC 308, costal fragment; LGPUT MIC 309, fibula; LGPUT MIC 310, metacarpal; LGPUT MIC 311, osteoderm; LGPUT MIC 312, thigh tubercle; LGPUT MIC 313, pisiform; LGPUT MIC 314, plastron fragment; LGPUT MIC 315, plastron fragment; LGPUT MIC 316, pelvis fragment; LGPUT MIC 317, pelvis fragment; LGPUT MIC 318, pelvis fragment; LGPUT MIC 319, plastron fragment.

Aggelochori/Megalo Emvolon, western Chalkidiki, N. Greece (>4 individuals; 37 specimens) (Fig. 3.23-3.26):
LGPUT collection: LGPUT AGG 420, femur diaphysis; LGPUT AGG 421, plastron fragment; LGPUT AGG 422, bone fragment. AMPG collection: AMPG 1925, left epiplastron; AMPG 1926, left xiphiplastron; AMPG 1927, left metatarsal; AMPG 1928, phalanx; AMPG 1929, phalanx; AMPG 1930, ungual; AMPG 1931, hyoplastron fragment; AMPG 1932, right hypoplastron fragment; AMPG 1933, plastron fragment; AMPG 1934, carapace fragment; AMPG 1935, plastron fragment; AMPG 1936, left ulna distal part; AMPG 1937, left ulna distal part; AMPG 1938, pelvis fragment; AMPG 1939, ungual; AMPG 1940, ungual; AMPG 1941, pointed osteoderm; AMPG 1942, left metatarsal; AMPG 1943, right metacarpal; AMPG 1944, metacarpal; AMPG 1945, metacarpal; AMPG 1946, rounded osteoderm; AMPG 1947, right intermedium; AMPG 1948, distal carpal; AMPG 1949, distal carpal; AMPG 1950, pointed osteoderm; AMPG 1951, half-pointed osteoderm; AMPG 1952, pointed osteoderm; AMPG 1953, half-pointed osteoderm; AMPG 1954,

tail vertebra; AMPG 1955, tail vertebra; AMPG 1969, right humerus diaphysis of a juvenile individual; AMPG 1970, nuchal fragment.

EMENDED DIAGNOSIS: Given that the description of "*Cheirogaster*" *bacharidisi* was done before the description of *Titanochelon*, we give here an emended diagnosis for *T. bacharidisi*. A member of *Titanochelon* based on the presence of frontals narrower than prefrontals, causing a gentle constriction of the frontals in dorsal view; long crista supraoccipitalis; presence of an elliptical to circular premaxillary pit; relatively low carapace; wide shell; absence of pointed tips in the carapacial rim in the region of contact of the sulci between the marginal scutes and the lateral border of the anterior and posterior peripherals; two suprapygals, the first embrassing the lenticular second one; longer than wide pygal; absence of cervical scute; coincidence between the medial margins of all the marginals and the suture between the costal and peripheral plates; presence of a supracaudal scute; second suprapygal crossed by the vertebro–supracaudal sulcus; absence of plastral hinges; wide plastral lobes, at least in the region of contact with the plastral bridge; anterior plastral lobe longer than the posterior lobe; convex to flat dorsal lip of the epiplastra; absence of ventral relief in the area covered by the gular scutes; angle between the sagittal axis and the gular–humeral sulcus of 45º or more acute; humero–pectoral sulcus perpendicular to the axial plane in the medial region, but with a well developed lateral change of curvature; very short pectoral scutes in the sagittal plane, but markedly expanded, towards the anterior region, laterally; presence of a single pair of inguinal scutes; males with a well developed ventral thickening in the area covered by the anal scutes; curved diaphysis of the humerus and femur; fused astragalus and calcaneum. *Titanochelon bacharidisi* is defined by the following combination of characters: fossa orbitalis in midway between the apertura narium externa and the posterior tip of the squamosal; elements of the zygomatic arch thick and short; squamosal processes converging posteriorly towards the midline; extended ventral emargination; posterior rim of carapace without indentations in supracaudal-11th marginal sulcus; rounded anterior lobe without gular projection anteriorly; short gulars contacting the anterior part of the entoplastron; entoplastron covered medially only by humeral scutes, and its posterior border coinciding with the humero-pectoral sulcus; obtuse and reduced xiphiplastral notch.

DESCRIPTION

Epanomi

Epanomi (EPN) is the type locality of *Ti. bacharidisi*, mainly providing two individuals (the holotype and the paratype), and several other isolated elements.

Individual EPN I, LGPUT EPN 100–199, female individual, holotype of *Ti. bacharidisi*:

Shell Remains

LGPUT EPN 100: From the carapace only few parts are preserved, such as the bridge on both sides in connection with plastron and another fragment that probably comes from the posterior rim (Fig. 3.6). All the carapacial elements are highly eroded and no sulci and only few parts of the sutures can be identified. Although the dorsal part is missing, the carapace was probably low, as it is estimated by the preserved peripherals and the height of the scapula (Fig. 3.6. E-F).

LGPUT EPN 101: The holotype preserves a nearly complete plastron, since only the anteriormost part of the epiplastron is missing (Fig. 3.6.A-B). Because of the mounting strategy, only the visceral view is available for observation. Most of the postcranial skeleton is preserved on the visceral surface of the plastron, providing evidence for rapid burial of the individual. The holotype has short anterior and posterior lobes relative to the total length of the plastron (ca. 30 cm each). The plastron has an approximate length of 115 cm. Viscerally, an epiplastral lip and deep excavation, characteristic of most terrestrial tortoises, is noted on the dorso-visceral surface of the anterior part of the lobe.

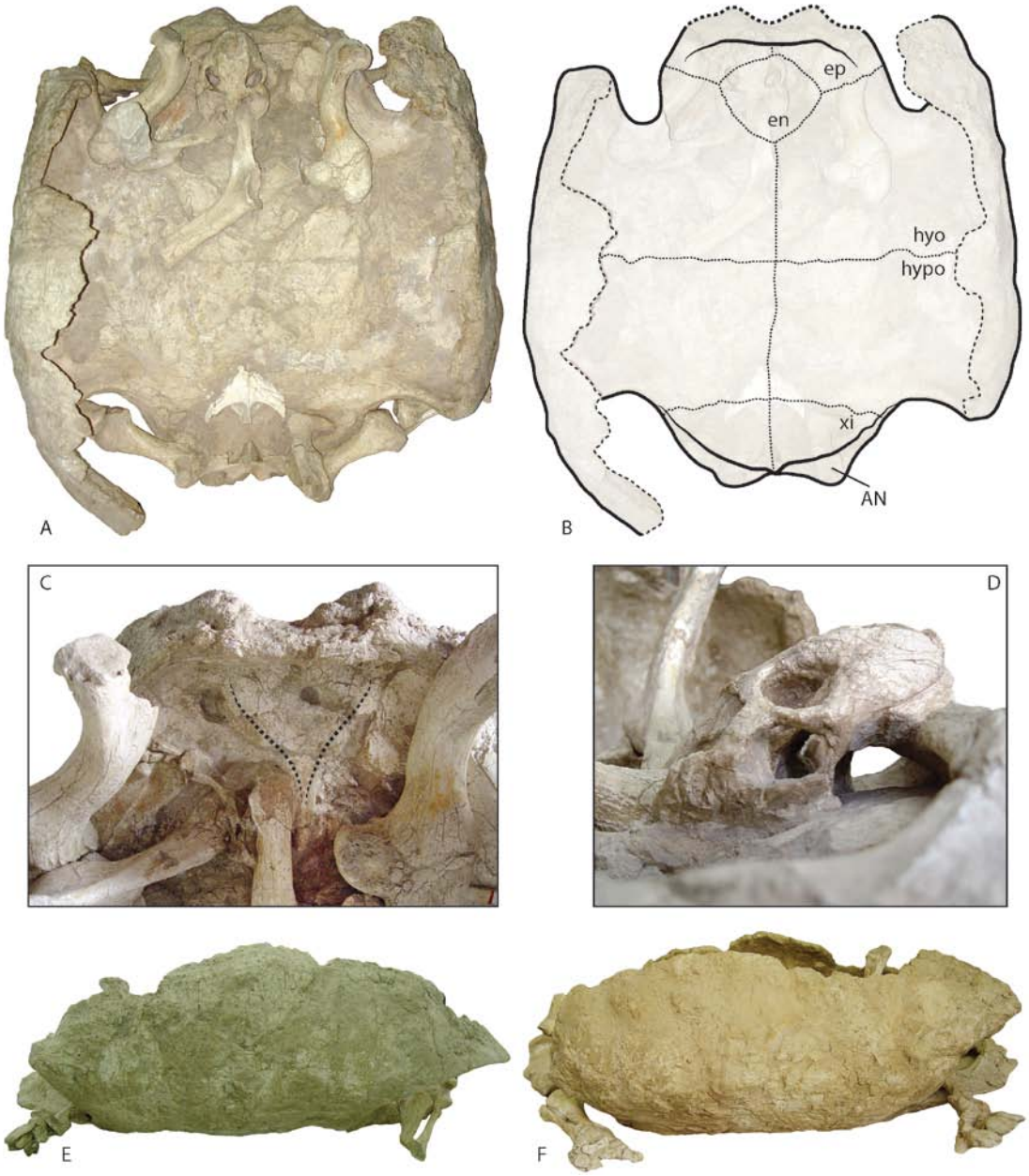


Figure 3.6. *Titanochelon bacharidisi* (Vlachos et al., 2014) from the Pliocene of Epanomi (Thessaloniki). Shell remains from the holotype in (A) plastron and (B) drawing of the plastron in visceral view. (C) detail of the visceral view of the entoplastron showing the ridges (dashed line). (D) detail of the skull in the recovery position. E, left and F, right lateral views. Length of the plastron is 115 cm.

The excavation forms a weak gular pocket. The dorsal surface of the lip is slightly convex. The entoplastron is relatively small in visceral view, showing two elongated ridges that crossed also onto the epiplastra. The hyo- and hypoplastra are quite long and wide, representing most of the surface of the plastron. The xiphiplastra are short and limited to the posterior part of the lobe, preserving an anal notch (length of anal notch is 3.5 cm). The posterior lobe borders converge posteriorly. The plastron of the holotype is rather flat, almost of the same length (measured at midline) and width (measured across the hyo-hypoplastral suture), and has thin xiphiplastral extremities. These three characters, which were noted by Bourgat and Bour (1983) for the female *T. perpiniana*, allow us to infer that EPN I is a female individual. The plastral formula (measured across the midline) is: Hyoplastra ≈ Hypoplastra >> Epiplastra > Xiphiplastra > Entoplastron. Abdominals > Femorals ≈ Humerals >> Gulars > Anals.

Scull and Mandible

LGPUT EPN 102: The skull is preserved (Fig. 3.8-3.9), together with some parts of the mandible, which upon discovery were preserved in the anterior region of the plastron (Fig. 3.6. D). It is 210 mm in length. The dorsal region of skull is nearly complete, and lacks only the anterior-most area and a part of the right prootic–opisthotic area. Much of the anterior palate is missing (Fig. 3.7.A-B). The EPN I skull is slightly deformed on the left zygomatic arch and in the condylus occipitalis area. The sutures between the cranial bones are mostly fused, indicating an adult individual. Upon the initial description of the specimen (Vlachos et al., 2014) we were unable to observe any sutures on the dorsal side of the specimen. The assistance of CT-scans (Fig. 3.8.F) allowed the identification of some cranial sutures on the dorsal side. Anteriorly, where the sutures are clearly visible, the maxillae are medially separated by the premaxillae, the latter being dorsally projected. The fossa orbitalis is located approximately midway between the apertura narium externa and the midpoint of the line connecting posterior tips of the squamosals. The prefrontals are wide, followed by narrower frontals. Medially the prefrontals are longer than the frontals, the latter showing a pointed anterior part. The well-developed processus trochlearis oticum is preserved only on the left side, being wider than long. The squamosals converge posteriorly towards the midline, are thin and pointed, being extended well beyond the condylus occipitalis. The crista supraoccipitalis is long and arched, covering the condylus occipitalis and being slightly bended inwards. The presence of keels is noted on each lateral side of the crista supraoccipitalis. Elements of the zygomatic arch are thick and short, partially preserved on the right side, but complete on the left. The ventral rim of the zygomatic arch is elevated posteriorly. On the ventral side (Fig. 3.8.C-D), some remains of the mandible are preserved anteriorly and in the middle part (in the condylus mandibularis area). The palate is anteriorly incomplete, but the large right foramen palatinum posterius can be observed. On the palate, remains of the lingual and median maxillary ridges are noted, showing the presence of triturating ridges. A clear longitudinal ridge is formed on the ventral side of the vomer. The pterygoids are incompletely preserved. Moreover, both sides exhibit no contact between the jugal and the pterygoid. Although the sutures are not visible on the posterior part, the basisphenoid probably shows a U-shape, developing two lateral extensions posteriorly that surround the anterior part of the basioccipital. The suture between the basisphenoid and the basioccipital is developed as a ridge, and the basioccipital is depressed. The condylus occipitalis is rounded, and the foramen magnum is dorsoventrally expanded. Although the sutures between the bones are not clearly visible, we are able to describe the upper and lower temporal emargination of the cranium (Fig. 3.8).

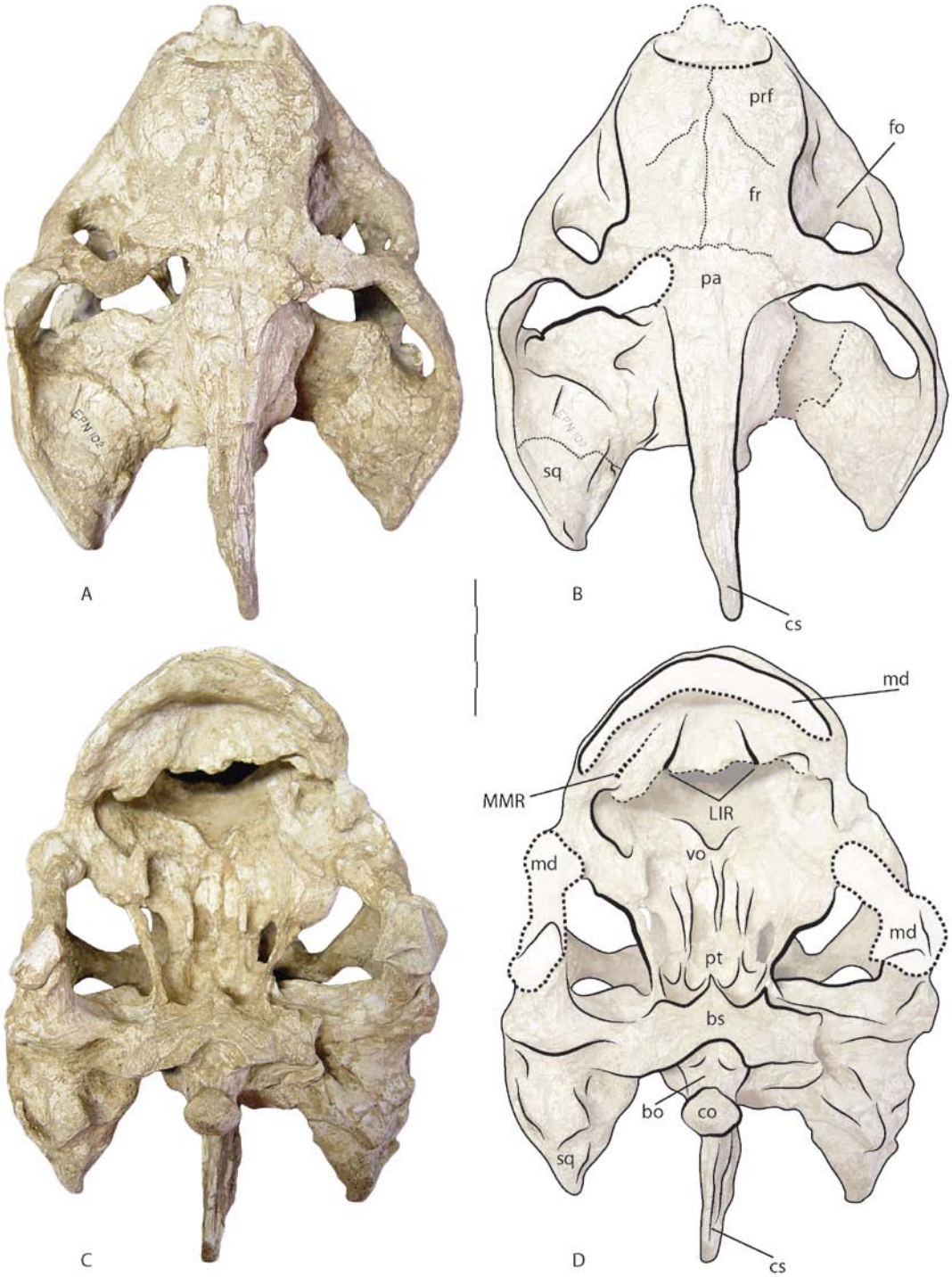


Figure 3.7. *Titanochelon bacharidisi* (Vlachos et al., 2014) from the Pliocene of Epanomi (Thessaloniki). LGPUT EPN 102, the cranium of the holotype in (A) dorsal and (B) drawing of the dorsal view. (C) ventral and (D) drawing of the ventral view. Scale bar equals 5 cm. For abbreviations see Material & Methods.

The upper temporal emargination is extensive, with a large quadratojugal and no jugal contribution. It affects the supraoccipital, parietal, quadratojugal and squamosal, being wide and long.

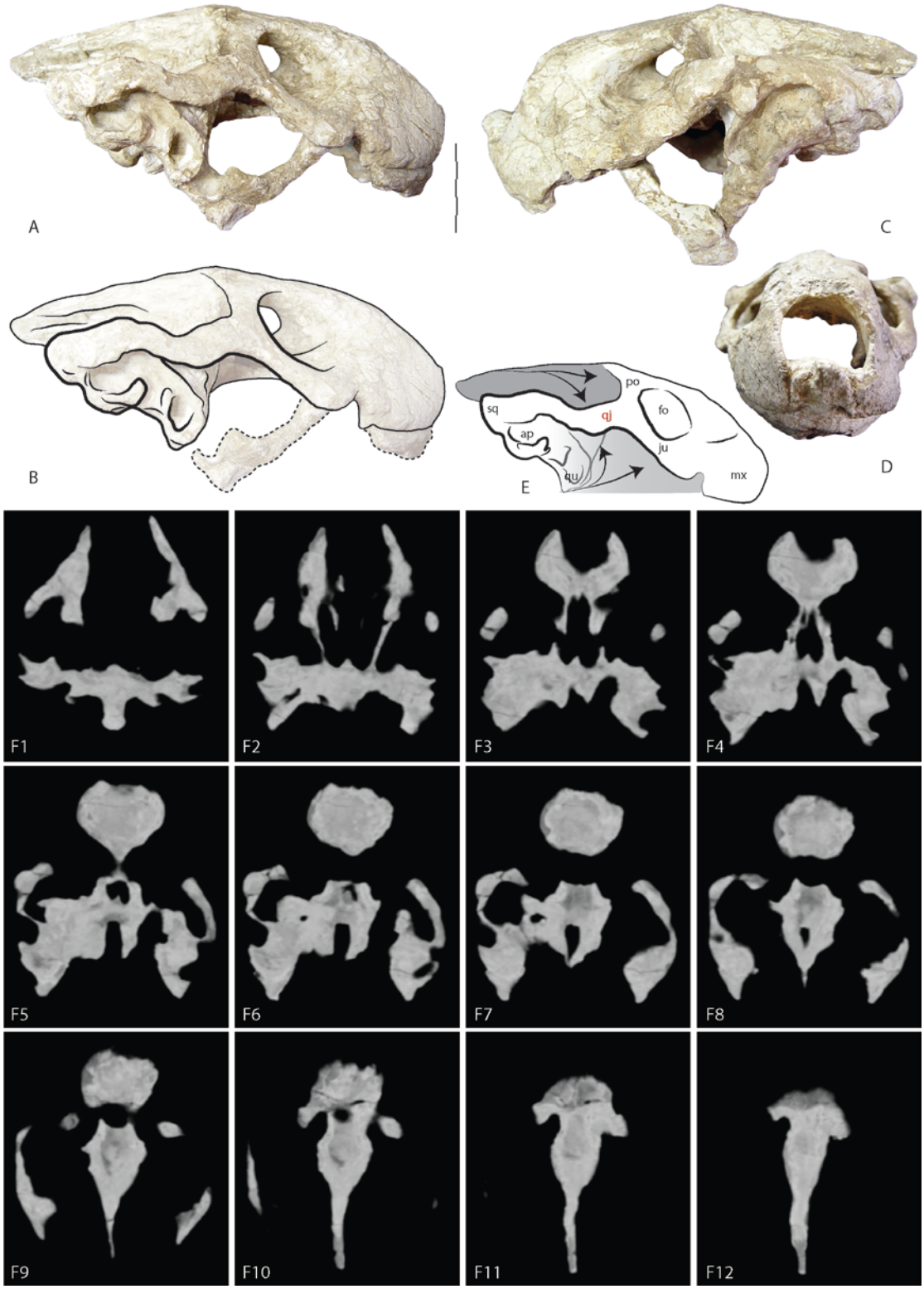


Figure 3.8. *Titanochelon bacharidisi* (Vlachos et al., 2014) from the Pliocene of Epanomi (Thessaloniki). LGPUT EPN 102, the cranium of the holotype in (A) right lateral and (B) drawing of the right lateral view. (C) left lateral and (D) anterior views. (E) schematic drawing of the right lateral view showing the upper and lower temporal emargination with grey color (not in scale). (F) horizontal slices of the CT-scans of the specimens, showing the presence of sutures (see Appendix for CT-scan sections). Scale bar equals 5 cm. For abbreviations see Material & Methods.

The quadratojugal is heavily reduced, not only by the upper temporal emargination but also due to the extensive lower temporal emargination. The ventral reduction of the quadratojugal is also observed on the left side. The lower temporal emargination also affects the anterior side of the quadrate, that is greatly reduced. To our knowledge, this morphology has not been observed in any other cranium of *Titanochelon*, or any other tortoise. Normally the quadratojugal develops a ventral process along the anterior rim of the cavum tympanii, that in some species even reaches the quadrate (see character 11 in Joyce and Bell, 2004). The closest condition of such an extended lower temporal emargination is found in *Gopherus* spp., where the quadrate is also greatly reduced. In the *Gopherus* tortoises however, a small part of the quadrate is still visible on lateral view.

LGPUT EPN 198 (Fig. 3.7 & Fig. 3.8): Some parts of the mandible of the mandible are preserved along with the cranium. The anterior part of the mandible is preserved on the palate and the posterolateral parts are preserved in the area of condylus mandibularis. Due to the preservation, further information is not available.

Cervical Column

LGPUT EPN 116: This specimen corresponds to a cervical vertebra recovered below the crista supraoccipitalis of the cranium. The preservation status does not allow further description.

LGPUT EPN 117: This specimen corresponds to a cervical vertebra recovered below the right scapula. The preservation status does not allow further description.

LGPUT EPN 185–197: The caudal column is represented by twelve caudal vertebrae, each of which exhibits a simple procoelous morphology, with an anteriorly concave and posteriorly convex body, and a long dorsal arch with well–preserved anterior and posterior zygapophyses. Transverse processes decrease in length towards the end of the tail. The total length of the centrum varies from 10–30 mm.

Anterior Limb

LGPUT EPN 106 & 106a (Fig. 3.9.B): The right scapula is also resting on the visceral side of the plastron, but is moved from its anatomical position towards the midline. The coracoid is situated below the scapula, close to its anatomical position. The morphology is similar to the morphology of the left shoulder girdle (see above).

LGPUT EPN 105 & 105a (Fig. 3.9.B): The left scapula and the associated coracoid are preserved on their anatomical position on the left side of the anterior lobe in articulation with the left humerus. The scapula is situated vertically, preserving a long acromion process antero–medially, at an angle of 130º. The coracoid is short, with a narrow neck and expanded, fan-shaped end. The angle between the scapula and the coracoid is the same (130º), whereas the angle between the acromion and the coracoid is rather low (60º). Both the scapula and the coracoid are connected in a broad symphyseal area, forming an elongated, rounded glenoid cavity.

LGPUT EPN 176: This specimen corresponds to the distal part of the left ulna.



Figure 3.9. *Titanochelon bacharidisi* (Vlachos et al., 2014) from the Pliocene of Epanomi (Thessaloniki). Appendicular elements of the holotype: A, LGPUT EPN 102, right humerus in (A1) posterior, (A2) anterior, (A3) ventral and (A4) dorsal views. B, postero-dorsal view of the shell, showing the recovery position of both scapulas, the left humerus and the cranium. C, LGPUT EPN 110, left femur in (C1) dorsal, (C2) posterior and (C3) ventral views. D, LGPUT EPN 107, the right femur in (D1) recovery position articulated with the pelvis and tibia-fibula, (D2-3) posterior views. E, LGPUT EPN 111-112, left tibia and fibula in articulation with the femur, dorsal view. Scale bar equals 5 cm.

LGPUT EPN 103 (Fig. 3.9.A): This specimen corresponds to an almost complete right humerus, missing only the minor trochanter. In the proximal region, the major trochanter is well-developed, almost parallel to the diaphysis, extending beyond the height of the humeral head. The humeral head is elliptical to rounded, with a weak neck. The diaphysis of the bone shows a considerable degree of curvature along its length, and is elliptical in cross section. The ulnar and radial condyles form a wide trochlea. Their size is almost equal, forming a rather symmetrical distal. Dorsally, a strong, elongated ectepicondylar groove is present.

LGPUT EPN 104: This specimen corresponds to an almost complete humerus, missing some parts of the distal end. It is preserved in its recovery position on the anterior opening and in articulation with the left scapula. Its morphology is similar with the right humerus (see above).

LGPUT EPN 113: The right radius is preserved complete, along with associated carpal elements and osteoderms. It is straight and rather robust, having an expanded proximal end. The distal part is also expanded, showing a tall surface for the distal articulation for the ulna. The proximal articulation is broadly concave, whereas the distal cannot be observed because it is covered by the carpal elements.

LGPUT EPN 114: The left radius is preserved almost complete, missing only a part of the proximal articulation. As is the case in the right radius, several carpal, metacarpal elements and osteoderms are preserved in association. The distal articulation for the ulna is tall, and on the distal part a significant tubercle is noted, projecting disto-laterally. The distal articulation cannot be observed.

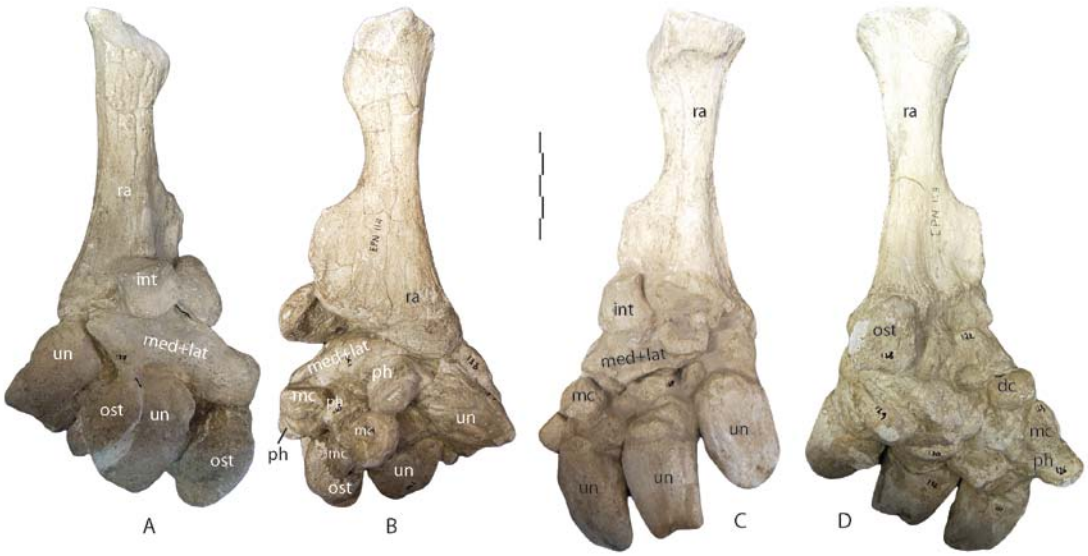


Figure 3.10. *Titanochelon bacharidisi* (Vlachos et al., 2014) from the Pliocene of Epanomi (Thessaloniki). The anterior limb associations of the holotype: left anterior limb in (A) dorsal and (B) ventral views. Right anterior limb in (C) dorsal and (D) ventral views. Scale bar equals 5 cm.

LGPUT EPN 121 (Fig. 3.10): The right intermedium is preserved complete in association with the right radius and most of the right carpus. It is tall and triangular with a rounded distal articular surface for the fused centralia.

LGPUT EPN 122 (Fig. 3.10): The right medial and lateral centrale is preserved complete in association with the remaining carpal elements. The recovery position does not allow a detailed description, but certainly the two central carpals are fused.

LGPUT EPN 123 (Fig. 3.10): This right metacarpal is preserved on the dorsal side of the preserved carpus, being tall and almost cubic. The proximal articulation is concave, whereas the distal is slightly convex.

LGPUT EPN 124 (Fig. 3.10): This distal carpal is preserved on the ventral side of the right limb. It shows the typical morphology with a discoid proximal and a distal protuberance.

LGPUT EPN 125 (Fig. 3.10): This right metacarpal is preserved on the ventral side of the right limb. It is flattened and discoid, with a concave proximal and a convex distal side.

LGPUT EPN 126 (Fig. 3.10): This anterior phalanx is preserved on the latero-ventral side of the right limb. It is relatively short and wide, with a distal convex articular surface for the ungual.
LGPUT EPN 127 (Fig. 3.10): This right metacarpal is flattened and large, visible on the dorsal side of the right limb, below the fused medial and lateral centrale. Further description is not possible.

LGPUT EPN 129, 130 (Fig. 3.10): Two carpal elements that are preserved on the ventral side of the right limb. They are possibly metacarpals, but due to the recovery position and preservation is not possible to make a precise identification.

LGPUT EPN 131, 132, 133 (Fig. 3.10): Three complete anterior unguals from the right limb, preserved more or less in their anatomical position. They are long and wide, with a rounded tip.

LGPUT EPN 135 (Fig. 3.10): The fused left medial and lateral centrale is preserved in association with many other carpal elements and the left radius. Due to its recovery position is not possible to observe the articular surfaces, but on the dorsal side the suture between the medial and lateral centrale is partly visible.

LGPUT EPN 136 (Fig. 3.10): The left intermedium is preserved more or less in its anatomical position, between the distal part of the radius and the fused medial and lateral centrale. It shows a concave proximal surface and a triangular srocc-section.

LGPUT EPN 137 (Fig. 3.10): This is probably a distal carpal preserved on the distal side of the fused medial and lateral centrale, but the preservation status does not allow further description and a confident identification.

LGPUT EPN 138, 139, 141 (Fig. 3.10): Three anterior unguals are preserved in the left anterior limb, showing the typical wide morphology with the rounded tip.

LGPUT EPN 143, 145, 148 (Fig. 3.10): Three anterior phalanges are preserved on the left anterior limb, being rather short and wide with a concave proximal surface for the metacarpals and a convex distal for the unguals.

LGPUT EPN 144, 146, 149 (Fig. 3.10): These three metacarpals are preserved in the anterior limb association, but its recovery position does not allow further description.

LGPUT EPN 147 (Fig. 3.10): This left metacarpal is preserved in the anterior limb association, but its position does not allow further description.

LGPUT EPN 165, 170, 171, 175 (Fig. 3.12.G): The anterior unguals are always shorter and more rounded than the posterior ones. They show a concave proximal articular surface for the posterior phalanx.

LGPUT EPN 178, 179 (Fig. 3.12. A-B): The distal carpals show two main parts: a thick disc distally that is articulated with the metacarpals with a convex surface and a ventro-proximal tubercle. These two parts form a concave distal articular surface for the first row of carpals.

LGPUT EPN 180, 181, 182: The metacarpals are simple in morphology, each one exhibiting simple discoid morphology with convex proximal and distal articular surfaces.

Posterior Limb

LGPUT EPN 115: The pelvis is preserved fragmented, resting on the posteriormost part of the posterior plastral lobe. Most of the pubio-ischiatic plate is preserved, together with the distal part of the right ilium (Fig. 3.6.A). These three elements contribute equally to form a deep spherical acetabulum, which is preserved on the right side in articulation with the femur. Anteriorly, the pubic sends latero-posteriorly a rounded pectineal process that is preserved *in situ*.

LGPUT EPN 107 (Fig. 3.9.D): The right femur is preserved in its anatomical position in articulation with the pelvis on the posterior side of the shell. The femur is quite robust with a significant curvature in the distal part of the diaphysis. The elliptical femoral head is oriented perpendicular to the diaphysis, in dorsal view. In ventral view, the trochanters are fused, forming a broad concavity in the proximal face (intertrochanteric fossa). The distal end of the femur is broad. The ventral side is characterized by a strong concavity formed by the larger tibial and the smaller fibular condyles, connected by a thin ridge.

LGPUT EPN 110 (Fig. 3.9.C): The left femur is preserved almost complete, missing only the femoral head and a part of the fused trochanters. It is preserved in articulation with the tibia and the fibula. The morphology is similar with the right femur (see above).

LGPUT EPN 108 (Fig. 3.11): The right tibia is preserved complete, in articulation with the fibula and most of the remaining tarsus. The tibia shows a robust proximal part with a triangular cross-section. The cnemial crest is rounded and broad. The proximal articular surface is slightly concave. The diaphysis of the bone is slightly curved, having a small lateral process. The distal end shows two convex surfaces, articulating with the astragalus.

LGPUT EPN 111 (Fig. 3.9.E): The left tibia is preserved almost complete, in articulation with the left femur, missing only the distal part. It shows a broad proximal end with a triangular cross section. The tibial protuberance is broad, with a wrinkled surface for the patellar tendon. The diaphysis shows a small degree of torsion.

LGPUT EPN 109 (Fig. 3.11): The right fibula is preserved complete, being articulated with the tibia proximally and with the fused astragalus and calcaneum distally. In the proximal part, sediment is still preserved between the two elements. The diaphysis of the bone is rather straight, having a proximal slightly concave articular surface and a more expanded distal one, that is strongly convex to articulate in the fusion of astragalus and calcaneum.

LGPUT EPN 112 (Fig. 3.9.E): The left fibula is preserved almost complete, articulation with the femur and tibia. It is thin and elongated, with a small proximal part and a wider distal part. The distal epiphysis bears convex articular surface for the astragalo-calcaneum, and articulates with the symphyseal area
LGPUT EPN 150 (Fig. 3.11): The fused right astragalo–calcaneum is preserved complete, in articulation with the tibia and fibula proximally and several tarsal elements distally. The two tarsal elements are fused, preserving the suture between them. The astragalus is much larger than the calcaneum, which shows a rather narrow neck with the astragalus. The proximal surfaces for the tibia and fibula are generally concave. The distal surfaces are convex in the astragalus for the distal tarsals and concave in the fusion for the 4^{th} distal tarsal. On the dorsal side a large foramen is noted.

LGPUT EPN 151 (Fig. 3.11): The 4^{th} distal tarsal from the right side is preserved complete in the posterior limb association, in a nearly anatomical position below the fusion of the astragalus and calcaneum. This element is much larger than the rest distal tarsals, having a convex proximal and distal articular surface.

LGPUT EPN 152 (Fig. 3.11): This specimen corresponds to an almost complete metatarsal from the right side, preserved on the dorsal side of the limb association. It is rather elongated, with a wider proximal part with a concave articular surface and a narrower distal end with a convex articular surface. Based on the comparative material that has been studied, it seems rather probable that it corresponds to the 4^{th} metatarsal bone.

LGPUT EPN 153, 154, 155, 158 (Fig. 3.11): These four elements are distal tarsals from the right side, being preserved with the remaining tarsal bones in the posterior limb association. They are discoid and flattened, with a concave proximal and a convex distal end.

LGPUT EPN 156 (Fig. 3.11): This specimen corresponds to a complete posterior phalanx, preserved in the posterior limb association. It is elongated and narrow, with a concave proximal and a convex distal end.

LGPUT EPN 159 (Fig. 3.11): This specimen corresponds to the proximal part of a posterior phalanx.

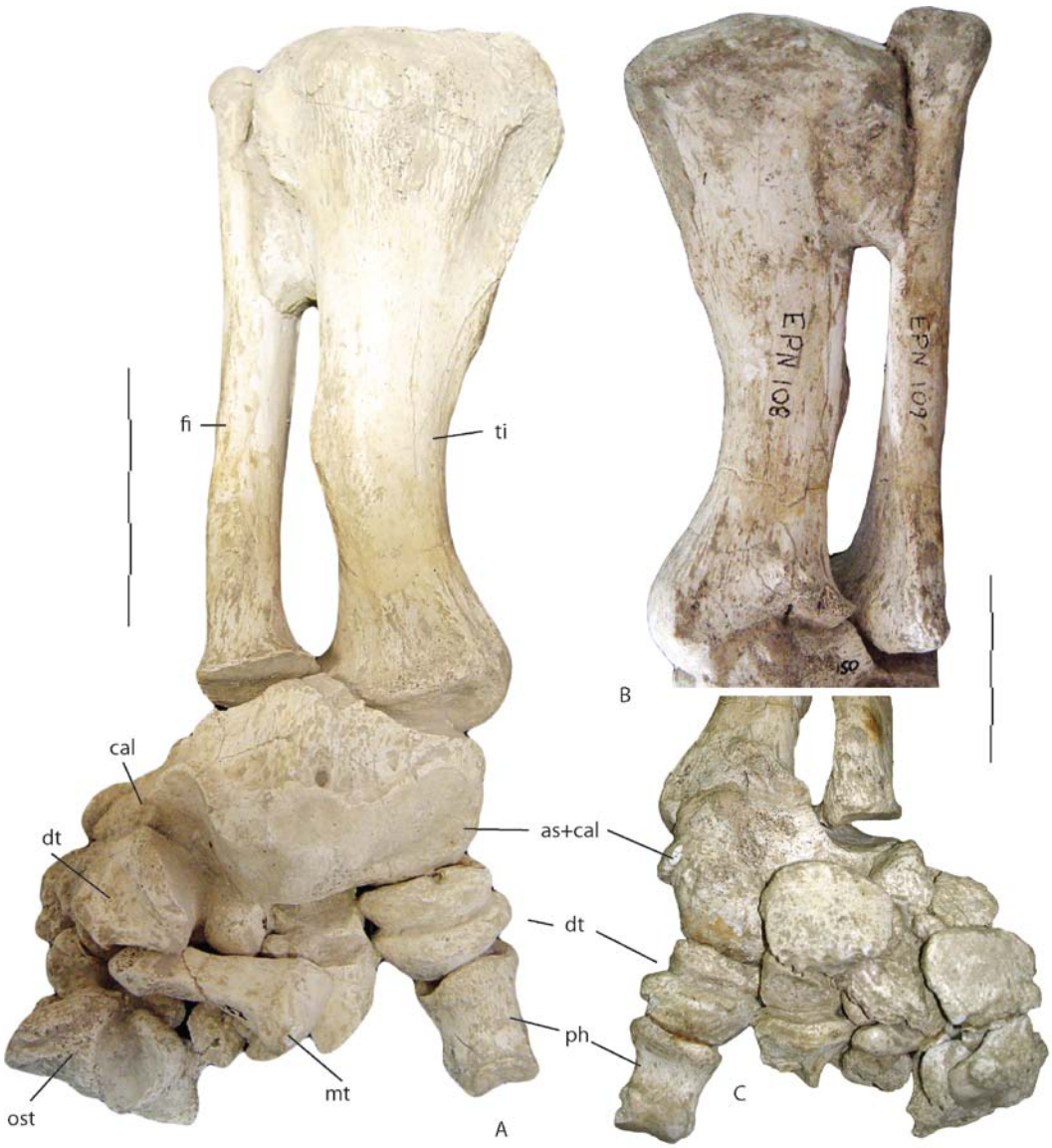


Figure 3.11. *Titanochelon bacharidisi* (Vlachos et al., 2014) from the Pliocene of Epanomi (Thessaloniki). The right posterior limb association of the holotype: A, dorsal view. B, the tibia and fibula in ventral view. C, the tarsus in ventral view. Scale bar equals 5 cm. For abbreviations see Material & Methods.

LGPUT EPN 161, 163, 166, 172 (Fig. 3.12. C-E): Several isolated metatarsal bones are preserved in the holotype. The metatarsals are wide proximally, with a concave articular surface and a convex distal end, which exhibits a small concavity for articulation with the proximal phalanx. They are highly asymmetrical elements, that slightly overlap each other when articulated.

LGPUT EPN 162, 174 (Fig. 3.12.H): The posterior unguals are always longer and more pointed than the anterior ones. The show a concave proximal articular surface for the posterior phalanx.

LGPUT EPN 164 (Fig. 3.12.F): The phalanges of the posterior limb are always longer than those of the anterior limb. They exhibit an elliptical concave proximal articular surface and a well-developed convex distal surface for the ungual.



Figure 3.12. *Titanochelon bacharidisi* (Vlachos et al., 2014) from the Pliocene of Epanomi (Thessaloniki). Carpal and tarsal elements of the holotype: A, LGPUT EPN 178, left distal tarsal in (A1) distal and (A2) lateral views. B, LGPUT EPN 179, left distal tarsal in (B1) distal and (B2) lateral views. C, LGPUT EPN 166, left metatarsal in (C1) dorsal, (C2) ventral, and (C3) anterior views. D, LGPUT EPN 163, left metatarsal in (D1) dorsal, (D2) ventral, and (D3) anterior views. E, LGPUT EPN 161, left metatarsal in (E1) dorsal, (E2) ventral, and (E3) anterior views. F, LGPUT EPN 164, posterior phalanx in (F1) dorsal, (F2) ventral, and (F3) anterior views. G, LGPUT EPN 165, anterior ungual in (G1) dorsal, and (G2) ventral views. H, LGPUT EPN 162, posterior ungual in (G1) dorsal, and (G2) ventral views. Scale bar equals 5 cm.

LGPUT EPN 167: This specimen probably corresponds to a complete left 4th distal tarsal, due to its size. But the preservation does not allow further description.

LGPUT EPN 168, 169, 173, 177: The distal tarsals exhibit a thin discoid shape with a concave proximal and a convex distal surface.

Osteoderms

LGPUT EPN 128 (Fig. 3.10): This crural osteoderm is preserved on the ventral side of the right limb, covering part of the distal radius. It is flattened and rounded.

LGPUT EPN 157 (Fig. 3.11): This is a crural osteoderm preserved on the posterior side of the limb association. It is rounded and flat.

LGPUT EPN 134 (Fig. 3.10): This is a half–pointed osteoderm, preserved in the distal part of the left radius. It is flattened and preserves a small and rounded tip.

LGPUT EPN 140, 142 (Fig. 3.10): Two half–pointed osteoderms are preserved between the anterior unguals of the left limb, being flattened with a half-pointed tip.
LGPUT EPN 160: This specimen corresponds to an association of several rounded conical osteoderms. One of them is slightly enlarged compared to the rest, resembling a conical tubercle.



Figure 3.13. A-B, LGPUT EPN 184, thigh bony tubercle of the holotype of *Titanochelon bacharidisi* (Vlachos et al., 2014) from the Pliocene of Epanomi (Thessaloniki). C, the bony thigh tubercles of extant *Centrochelys sulcata* from Algeria (in MNCN) with remnants of soft tissue and keratin. Scale bar is 5 cm.

LGPUT EPN 184 (Fig. 3.13.A-B): This specimen corresponds to a complete bony thigh tubercle that has been found separated close to the posterior limb. This element is identical to the thigh tubercle from Nea Kallikratia that is found in anatomical position in the right posterior limb of the KLK I individual. The thigh tubercle of the EPN I individual shows a wide and rounded part, leading to a pointed tip. Possibly this tubercle was covered by keratin as in the extant *Centrochelys sulcata* (Fig. 3.13.C).

LGPUT EPN 199a-i: Several isolated osteoderms are preserved, including several half-pointed and some flattened ones.

Individual EPN II, LGPUT EPN 200–287,
male individual, paratype of *Ti. bacharidisi*:

Shell remains

LGPUT EPN 283: This specimen corresponds to a fragment from the carapace, possibly from the axillary notch area.

LGPUT EPN 284 (Fig. 3.15.A-B): This specimen corresponds to the posterior part of the carapace. The posterior carapace rim is continuous, without indentations in the supracaudal-11th marginal sulcus. The posterior rim is curved inwards and no pygal notch is present. Although the dorsal surface is eroded, is possible to observe some of the sutures. The two suprapygals form one trapeze: the first is larger and embraces the second, which is lenticular in shape. The pygal plate is strongly convex and trapezoid in shape, with posteriorly converging lateral borders. The second suprapygal is overlapped by the vertebro-supracaudal sulcus. The marginals 12 are fused into a supracaudal both dorsally and viscerally.

LGPUT EPN 285 (Fig. 3.15.C-F): The paratype preserves most of the plastron. It was found very close to the shoreline, and part of the specimen has been destroyed by exposure to seawater. The plastron of the paratype only misses the left anterior region and the ventral side is available for observation. The postcranial elements were disarticulated on the visceral surface of the plastron, indicating that some time had passed between death and final burial. The lobes of the paratype are long (ca. 40 cm each), compared to the length of the plastron (112 cm). Dorsally, an epiplastral lip and deep excavation, characteristic of most terrestrial tortoises, is noted on the dorso-visceral surface of the anterior part of the lobe. The excavation forms a step-like morphology. The dorsal surface of the lip is slightly convex. The entoplastron is relatively small in visceral view. Ventrally it is larger in size and wider than long, with angular posterior borders. The hyo- and hypoplastra are quite long and wide, representing most of the surface of the plastron. The xiphiplastra are short and limited to the posterior part of the lobe, preserving an anal notch (length of anal notch is 3.5 cm). The anal notch is more pronounced in the paratype than in the holotype, in being deeper and with greater angle between the thick xiphiplastral extremities (ca. 150º). In the xiphiplastra there is a pronounced narrowing in femoro–anal sulcus and the lateral borders in the anal part are almost parallel. The gulars are short, and contact the anterior border of entoplastron. Humerals cover the entire entoplastron medially, and the posterior epiplastra and anterior hyoplastra laterally. The humero-pectoral sulcus is straight medially, and curved towards the axillary notch. Medially, the pectoro-abdominal sulcus is slightly concave. The pectorals are very short, covering a small part of the hyoplastra. The abdominals are long and form the largest scales of the plastron, covering the posterior hyoplastra and anterior hypoplastra. Abdomino-femoral sulcus is posteriorly curved on both lateral sides. Femorals cover most of the posterior lobe, except for the terminus that is covered by short anals. The anal part of the xiphiplastra is ventrally thickened. In the paratype, the plastron is rather longer than wide, shows a ventral depression in the posterior part, and preserves thick xiphiplastral extremities. All the above, as well as the incomplete ossification of bony sutures, indicate a sub-adult male individual. The plastral formula (measured across the midline) is: HyoplastraHypoplastra >> Epiplastra > Xiphiplastra > Entoplastron. Abdominals > Femorals ≈ Humerals >> Gulars > Anals.

LGPUT EPN 286: This specimen corresponds to a fragment of the inguinal process fragment (8^{th} – 9^{th} peripheral).

LGPUT EPN 287: This specimen corresponds to the a right anterior peripheral fragment (possibly 2^{nd} – 3^{rd} peripheral).

Anterior Limb

LGPUT EPN 200 (Fig. 3.15.C): This specimen corresponds to the distal part of a quite robust right humerus. From the preserved part we can infer that the diaphysis of the humerus was curved. The ulnar and radial condyles form a wide trochlea, being almost equal in size forming a rather symmetric distal end. Dorsally, a strong, elongated ectepicondylar groove is present.

LGPUT EPN 201 (Fig. 3.15.E): The right radius of the paratype is preserved complete. The radius is straight, with narrow diaphysis and broad epiphyses. The proximal end articulates with the entire width of the distal part of the humerus with an elongated surface, which is composed of two concave surfaces. The distal part has only a deep, elongate, and concave articular surface for the fused medial and lateral centrale. In the distal part, the radius articulates with the ulna with an elongated and narrow surface.

LGPUT EPN 202 (Fig. 3.15.F): The right ulna is preserved complete. It shows a broad proximal and narrow distal part, and the external face is curved in dorsal view. The proximal articular surface for the humerus is concave. The distal articular surface is convex with short transverse diameter. The lateral part of the bone has a triangular cross-section. The ulna articulates with the radius at two points: proximally with an almost triangular articulation surface, and distally with an elongated, narrow surface. The tear-shaped notch between them is longer than wide.

LGPUT EPN 203 (Fig. 3.15.D): The left humerus preserves only the diaphysis. The diaphysis has a considerable degree of curvature along its length, and is elliptical in cross section.

LGPUT EPN 204: From the left radius only the diaphysis is preserved. The morphology is similar with the right radius (see above).

LGPUT EPN 205: From the left ulna only a fragment of the distal part is preserved, being thin and curved.

LGPUT EPN 206 (Fig. 3.15.A): From the right scapula, most of the scapular prong and the acromion is preserved. The scapula is situated vertically, preserving a long acromion process antero–medially, at an angle of 130º. The angle between the acromion and the coracoid is rather low (60º). Both the scapula and the coracoid are connected in a broad symphyseal area, forming an elongated, rounded glenoid cavity.

LGPUT EPN 207 (Fig. 3.15.B): The right coracoid is preserved complete. The coracoid is short, with a narrow neck and expanded, fan-shaped end. The angle between the scapula and the coracoid is 130º.

LGPUT EPN 208: Most of the left scapula is preserved, missing the ends of the scapula and acromion. The morphology is similar with the right one, with the wide angle between the scapula and the acromion and the elongated, rounded glenoid cavity.

LGPUT EPN 209: From the left coracoid only the medial part is preserved.

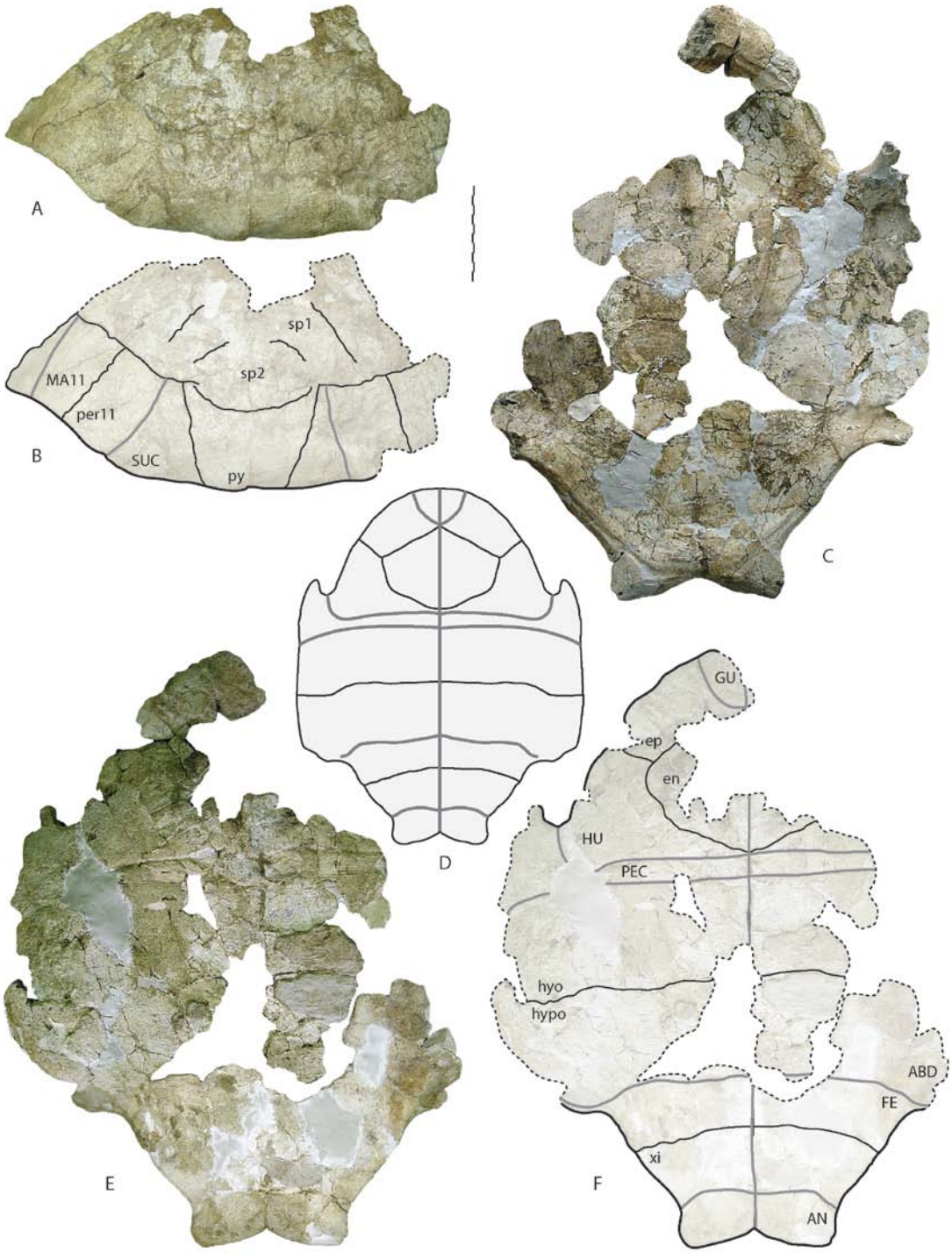


Figure 3.14. *Titanochelon bacharidisi* (Vlachos et al., 2014) from the Pliocene of Epanomi (Thessaloniki). Shell remains of the paratype: A-B, LGPUT EPN 284, posterior carapace in dorsal view. C-F, LGPUT EPN 285, plastron in (C) visceral, (D) reconstruction of ventral, and (E-F) ventral views. Scale bar is 10 cm. For abbreviations see Material & Methods.

LGPUT EPN 215, 216, 217, 218, 219 (Fig. 3.16.G): Several unguals are preserved from the anterior limb. The anterior unguals are shorter compared to the posterior ones, being broader and nearly straight. They show a concave articular surface for the phalanges.

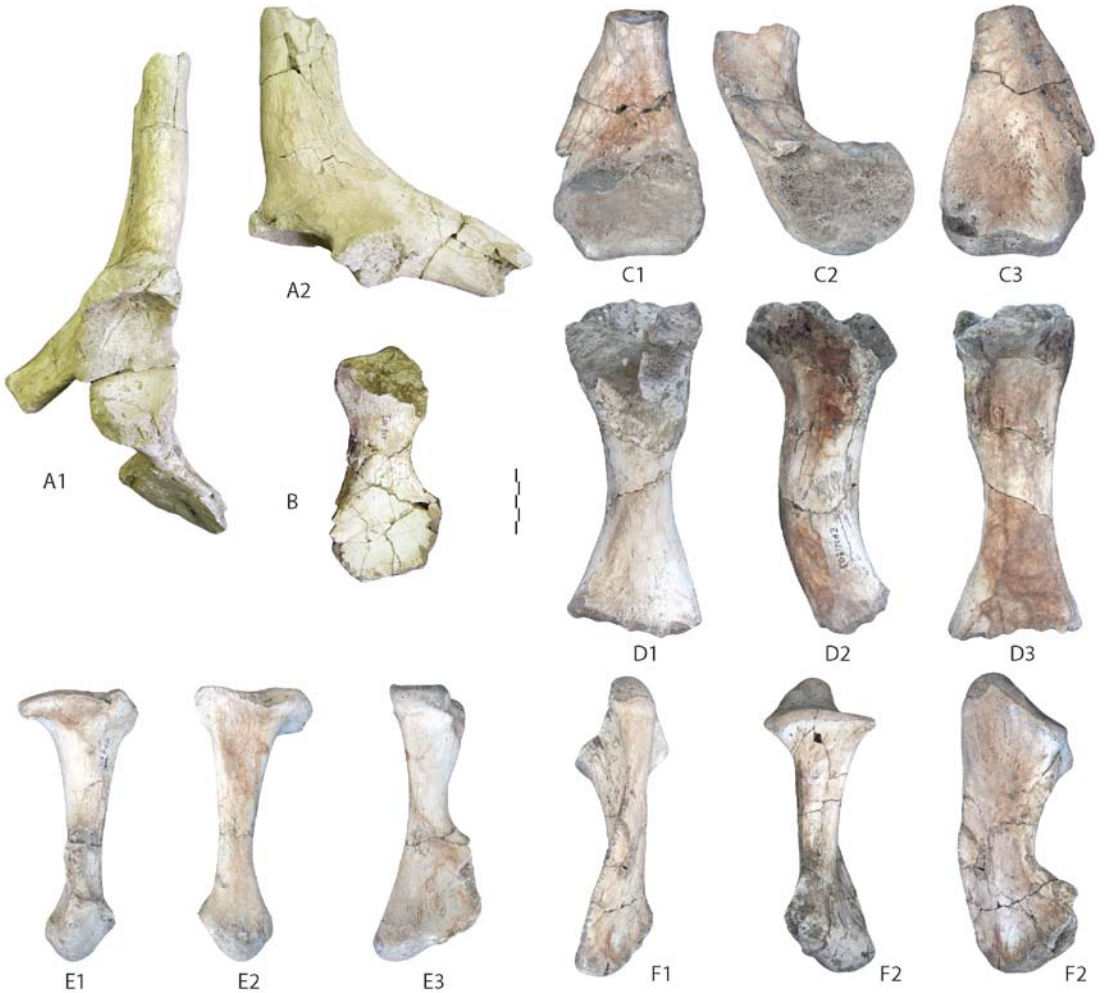


Figure 3.15. *Titanochelon bacharidisi* (Vlachos et al., 2014) from the Pliocene of Epanomi (Thessaloniki). Anterior limb elements of the paratype: A, LGPUT EPN 206, right scapula in (A1) lateral and (A2) anterior view. B, LGPUT EPN 207, right coracoid in dorsal view. C, LGPUT EPN 200, in (C1) ventral, (C2) anterior and (C3) dorsal views. D, LPGUT EPN 203, left humerus in (D1) ventral, (D2) anterior and (D3) dorsal views. E, LGPUT EPN 201, right radius in (E1) medial, (E2) lateral, and (E3) ventral views. F, LGPUT EPN 202, right ulna in (F1) lateral, (F2) medial, and (F3) dorsal views. Scale bar equals 5 cm.

LGPUT EPN 220, 221, 222, 224, 274 (Fig. 3.16.F): Several phalanges of the anterior limb are preserved. The first phalanx that has a broad and concave proximal surface and a convex distal surface for the unguals. In the proximal part a dorsal process is developed. In general, they are much shorter than the posterior ones.

LGPUT EPN 225, 229 (Fig. 3.16.C): The second carpal row comprises five distinct distal carpals. Each one is composed of two main parts: a thick disc distally that is articulated with the metacarpals with a convex surface and a ventro-proximal tubercle. These two parts form a concave distal articular surface for the first row of carpals.

LGPUT EPN 226 (Fig. 3.16.A): This specimen corresponds to a complete right intermedium. The intermedium articulates with both medial and lateral centrale, proximal to the suture. The intermedium also articulates with the distal parts of radius and ulna, and it is triangular in cross–section. It shows expanded articular surfaces both proximally and distally. Laterally, there is a broad surface for the ulnare.

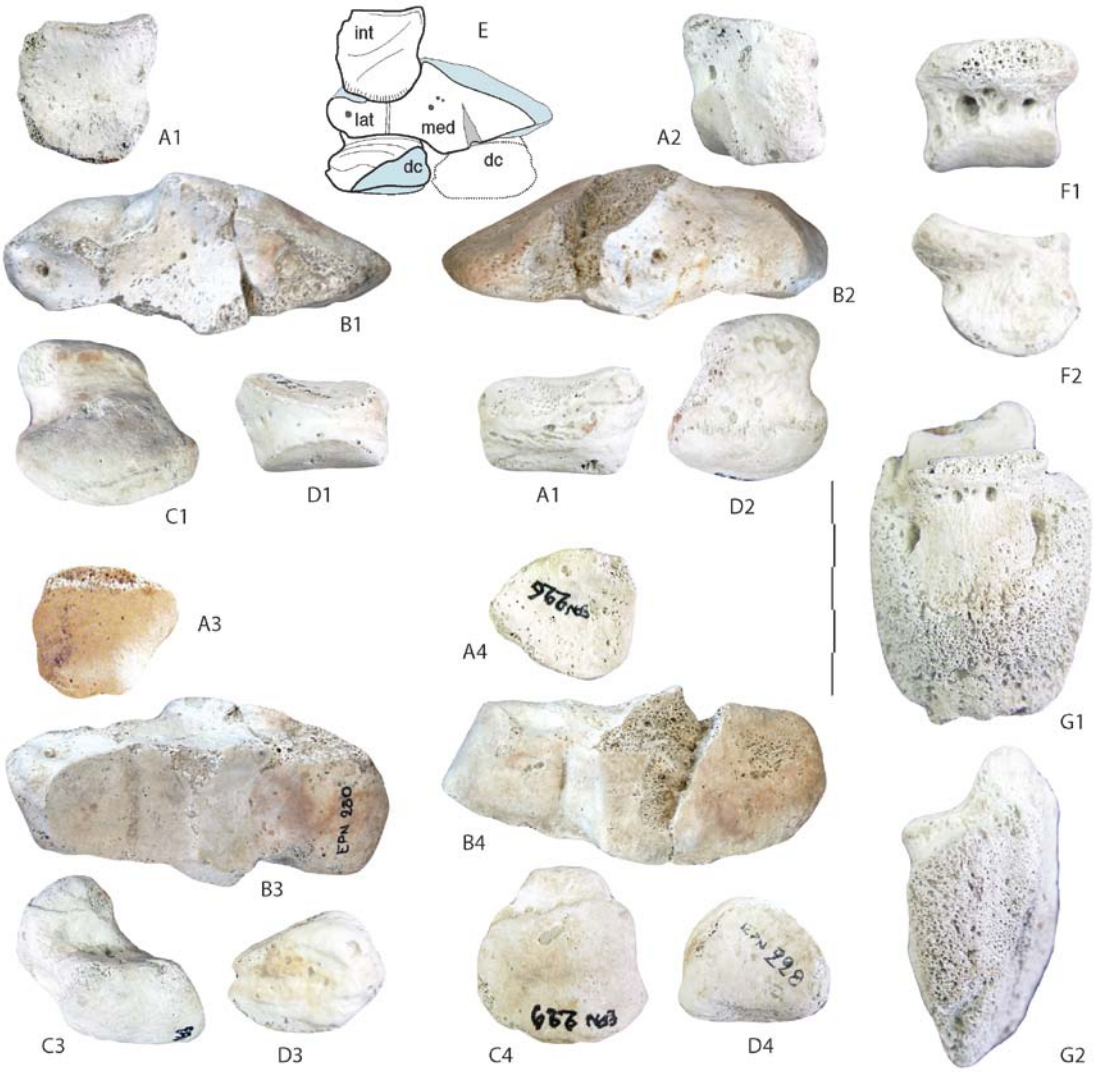


Figure 3.16. *Titanochelon bacharidisi* (Vlachos et al., 2014) from the Pliocene of Epanomi (Thessaloniki). Carpal elements of the paratype: A, LGPUT EPN 226, right intermedium in (A1) dorsal, (A2) anterior, (A3) lateral and (A4) medial views. B, LGPUT EPN 280, right medial and lateral centrale in (B1) dorsal, (B2) anterior, (B3) lateral and (B4) medial views. C, LGPUT EPN 229, right distal carpal in (C1) dorsal, (C2) anterior, (C3) anterior and (C4) posterior views. D, LGPUT EPN 228, right metacarpal in (D1) dorsal, (D2) anterior, (D3) anterior and (D4) posterior views. E, reconstruction of carpal articulation of the carpals. F, LGPUT EPN 220, anterior phalanx in (F1) dorsal and (F2) lateral views. G, LGPUT EPN 216, ungual in (G1) ventral and (G2) lateral views. Scale bar is 5 cm. For abbreviations see Material & Methods.

LGPUT EPN 227, 228, 230, 281, 283 (Fig. 3.16.D): The metacarpals exhibit a simple discoid morphology with convex proximal and distal articular surfaces. The dorsal side is shorter than the ventral one.

Posterior Limb

LGPUT EPN 210: This specimen corresponds to a right pubic fragment, but further description is not possible.

LGPUT EPN 211: This specimen corresponds to a fragment of the pelvis.

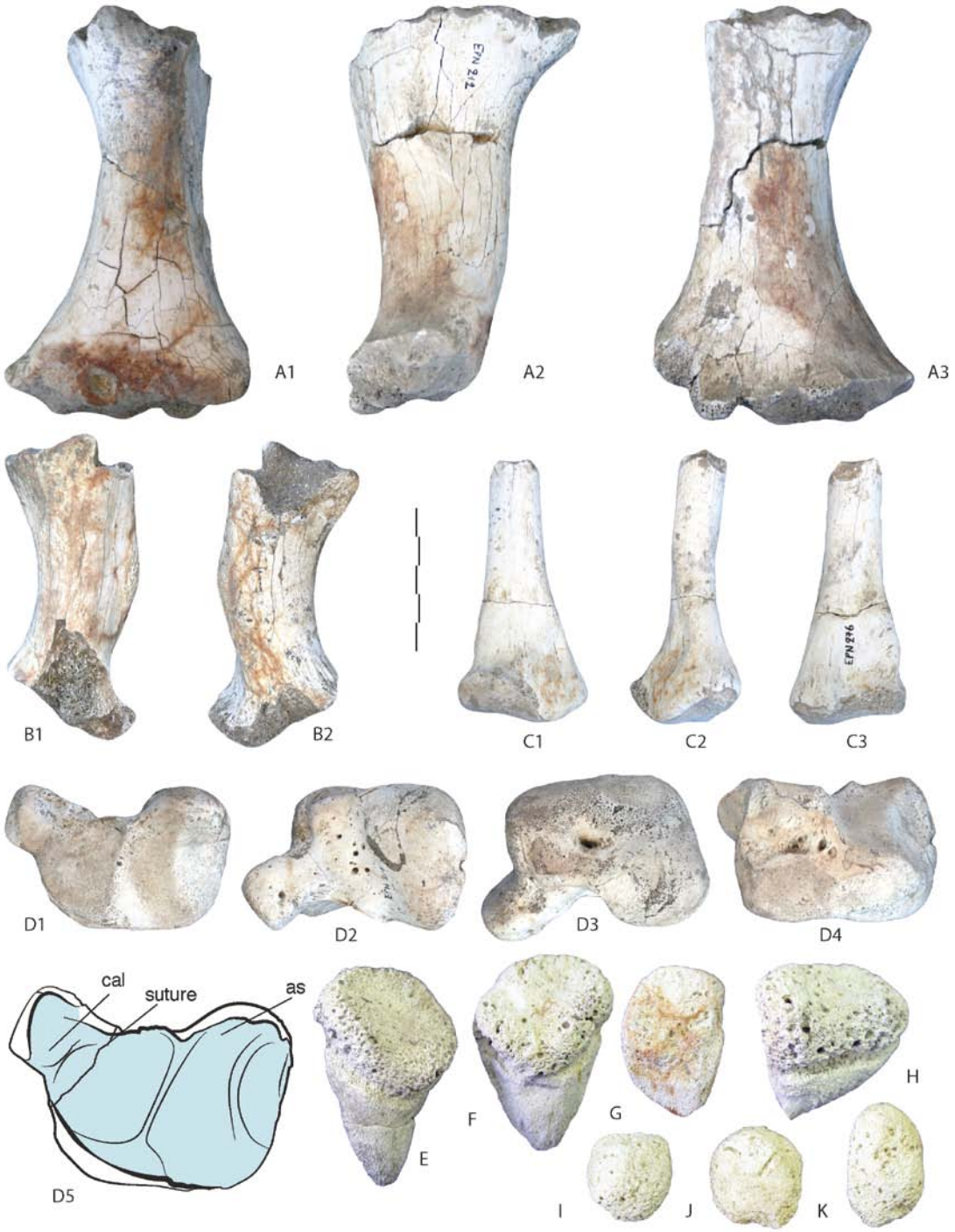


Figure 3.17. *Titanochelon bacharidisi* (Vlachos et al., 2014) from the Pliocene of Epanomi (Thessaloniki). Posterior limb elements of the paratype: A, LGPUT EPN 212, right femur in (A1) dorsal, (A2) posterior, and (A3) ventral views. B, LGPUT EPN 213, right tibia in (B1) dorsal and (B2) ventral views. C, LGPUT EPN 276, right fibula in (C1) dorsal, (C2) lateral and (C3) ventral views. C, LGPUT EPN 214, right astragalo-calcaneum in (C1) dorsal, (C2) anterior, (C3) ventral, (C4) posterior and (D5) reconstruction of dorsal views. E-F, pointed osteoderms. G-H, half-pointed osteoderms. I-K, flattened osteoderms. Scale bar equals 5 cm. For abbreviations see Material & Methods.

LGPUT EPN 212 (Fig. 3.17.A): This specimen corresponds to the medial diaphysis of a right femur. The femur is quite robust with curvature in the distal part of the diaphysis. The distal end is wide.

LGPUT EPN 213 (Fig. 3.17.B): This specimen corresponds to the middle and distal part of the right tibia. The diaphysis of the bone is curved, showing a significant lateral process in the middle part. The distal end shows a rounded articular surface for the astragalus.

LGPUT EPN 214 (Fig. 3.17.D): This specimen corresponds to a complete right astragalo–calcaneum. This fused element preserves the suture between the astragalus and calcaneum. The astragalus is the larger part of the fused element, whereas the calcaneum is quite small, being developed laterally with a narrow neck. The sitibia and fibula articulate in several shallowly concave surfaces. The ventral part of the astragalo-calcaneum is convex for the articulation of the distal tarsals.

LGPUT EPN 231-273, 275 (Fig. 3.17.E-K): Numerous osteoderms are preserved in the paratype. Some of them show a pointed tip (e.g. Fig. 3.17.E-F), whereas other are wider with a less pronounced tip (e.g. Fig. 3.17.G-H). Some osteoderms are small and flattened with a rounded outline (e.g. Fig. 3.17.I-K).

LGPUT EPN 276 (Fig. 3.17.C): This specimen corresponds to an almost complete right fibula, missing only the proximal part. The fibula is thin and elongated, with a small proximal part and a wider distal part. The distal epiphysis bears convex articular surface for the astragalo-calcaneum, and articulates with the symphyseal area.

LGPUT EPN 277-279: Indeterminate bone fragments.

LGPUT EPN 280 (Fig. 3.16.B): This specimen corresponds to a complete right medial and lateral centrale. The two fused elements preserve the suture. The medial centrale articulates with the radius with a convex surface, whereas the lateral articulates with the intermedium with a shallowly concave surface. The ventral side shows several concave surfaces for the distal carpals.

Individual EPN III:

LGPUT EPN 99 (Fig. 3.18): This specimen corresponds to an almost complete left femur, with the distal part missing. The elliptical femoral head is oriented perpendicular to the diaphysis, in dorsal view. The diaphysis corresponds to a rather robust bone, showing a curvature towards the distal part. In ventral view, the trochanters are fused, forming a broad concavity in the proximal face (intertrochanteric fossa).



Figure 3.18. *Titanochelon bacharidisi* (Vlachos et al., 2014) from Epanomi (Thessaloniki). LGPUT EPN 99, left femur of another individual in A, dorsal, B, ventral and C, anterior views. Scale bar equals 5 cm.

Nea Kallikratia

From Nea Kallikratia at least two individuals are preserved. The first (KLK I) preserves several parts of the carapace and plastron, some appendicular elements and an almost complete right posterior limb in articulation. The second (KLK II) preserves most of the plastron and some parts of the carapace, as well as some appendicular elements.

Individual KLK I:

LGPUT KLK 501: Several parts from the carapace are preserved. The largest is the right posterior carapacial rim, probably from the partial 7th till the 9th peripheral. Part of the inguinal notch is preserved viscerally. The peripherals are tall and short. The scute sulci are eroded and not visible, but it appears that the peripherals show weak protrusions in the sulci. The posterior peripherals have been almost perpendicularly oriented.

LGPUT KLK 502 (Fig. 3.19.A): Several parts of the plastron are preserved. The right hyoplastron area with the axillary notch is preserved in relatively good condition. The ventral side is highly eroded, but the imprints of the humero-pectoral and the pectoro-abdominal sulcus are faintly visible. From the preserved part we can infer that the pectorals were short. Another fragment is from the right hypoplastron, preserving the inguinal notch. No connection is found between this specimen and the right carapacial rim described above. The best-preserved specimen from the plastron is the posterior part of the xiphiplastra. The specimen is slightly deformed. Although the middle part of the xiphiplastra is thin (appr. 5 mm), the xiphiplastral processes are thickened. This indicates probably a male individual.

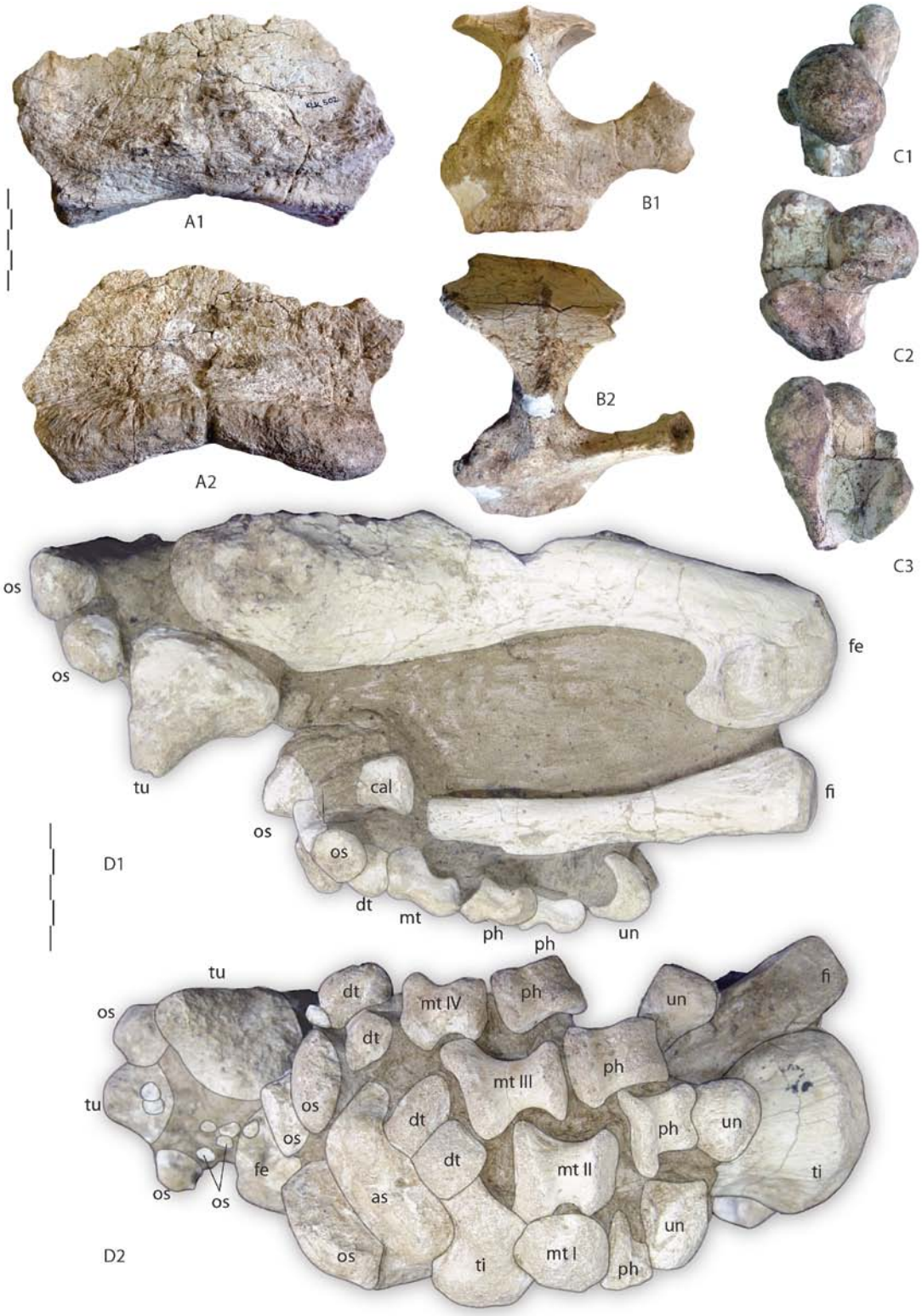


Figure 3.19. *Titanochelon bacharidisi* (Vlachos et al., 2014) from the Pliocene of Nea Kallikratia (Thessaloniki). KLK I individual: A, LGPUT KLK 502, xiphiplastra in (A1) visceral and (A2) ventral view. B, LGPUT KLK 529, partial pelvis in (B1) dorsal and (B2) dorso-lateral view. C, LGPUT KLK 503, left humerus in (C1) anterior, (C2) ventral and (C3) posterior views. D, LGPUT KLK 504-528, right posterior limb in articulation in (D1) dorsal view and (D2) posterior view. Scale bar equals 5 cm. For abbreviations see Material & Methods.

Ventrally, the limit between the femoral and the anal scutes are partially visible. The femoro-anal sulcus is straight, and the anals are short covering the posteriormost part of the xiphiplastra.

LGPUT KLK 503 (Fig. 3.19.C): This specimen corresponds to the proximal part of the left humerus. The humeral head is elliptical, being developed at an angle compared with the diaphysis. Lateral to humeral head a small lateral shoulder process is developed. The two trochanters are different in size. The major trochanter is thickened and extends well beyond the height of the humeral head. The minor is thin, developed till the middle of the humeral head, in the height of the shoulder process.

LGPUT KLK 504 – 528 (Fig. 3.19.D): This specimen corresponds to an almost complete right posterior limb, with the various elements preserved in anatomical position, enabling a detailed description. Lacking are the caput femori, one distal tarsal (probably the 3rd), the 5th metatarsal along with the possible associated 5th phalanx, a claw (probably the 3th), as well as the tips of the remaining unguals of the pes. The femur is straight, showing a small degree of curvature in the distal part. Proximally, the trochanters are fused. The tibia is straight, with a wide proximal part and a rounded and broad cnemial crest. The fibula is thin and straight. The astragalus is fused with the calcaneum, but its recovery position does not allow further description.

The first four digits are preserved in parallel rows to each other, with the 5th (normally much reduced) separated from the rest. The 4th distal tarsal is positioned close to astragalus-calcaneum contact and articulates with the 5th distal tarsal. There is a small overlap between the metatarsals. The large number of bony osteoderms is striking and the pes appears to have been covered by them. The largest number of osteoderms are found on the posterior thigh, i.e., crural bones. Immediately behind the femur, an enlarged, pointed bony structure is found, accompanied by a single more rounded osteoderm. These appear to be two bony crural spurs, quite similar to those found in the African spurred tortoise, *Centrochelys sulcata* Miller, 1779, and other terrestrial Testudinidae, such as *Testudo graeca* s.s. Additional medium sized, rounded osteoderms have been found near the tubercles, as well as much smaller ones in the vicinity of the main bony tubercle.

LGPUT KLK 529 (Fig. 3.19.B): This specimen corresponds to a partial pelvis. The specimen is partly deformed. Most of the pubio-ischiatic plate is preserved, which is curved. The pubic bones are thin and relatively flat. The ischium is thickened posteriorly but thin laterally. The pubo-ischiatic foramen is large, circular to elliptical, being longer than wide.

Individual KLK II:

LGPUT KLK 500: This specimen has been discovered in two pieces. The anterior and middle part of the shell has been removed from the sediment and was vertically rooted to the beach surface, whereas the posterior part was still in the sediment. Several parts of the carapace and the bridge are preserved. Also many appendicular elements are found in the interior of this specimen (humerus, femur, pelvis, parts of the tail). This individual preserves almost the entire plastron, since only some parts of the hypoplastra are missing. The lobes of the paratype are long compared to the length

of the plastron. Viscerally, an epiplastral lip and deep excavation is noted with a slightly convex dorsal surface. The epiplastra are short and wide. The entoplastron is slightly wider than long in ventral view. The hyo- and hypoplastra are quite long and wide, representing most of the surface of the plastron.

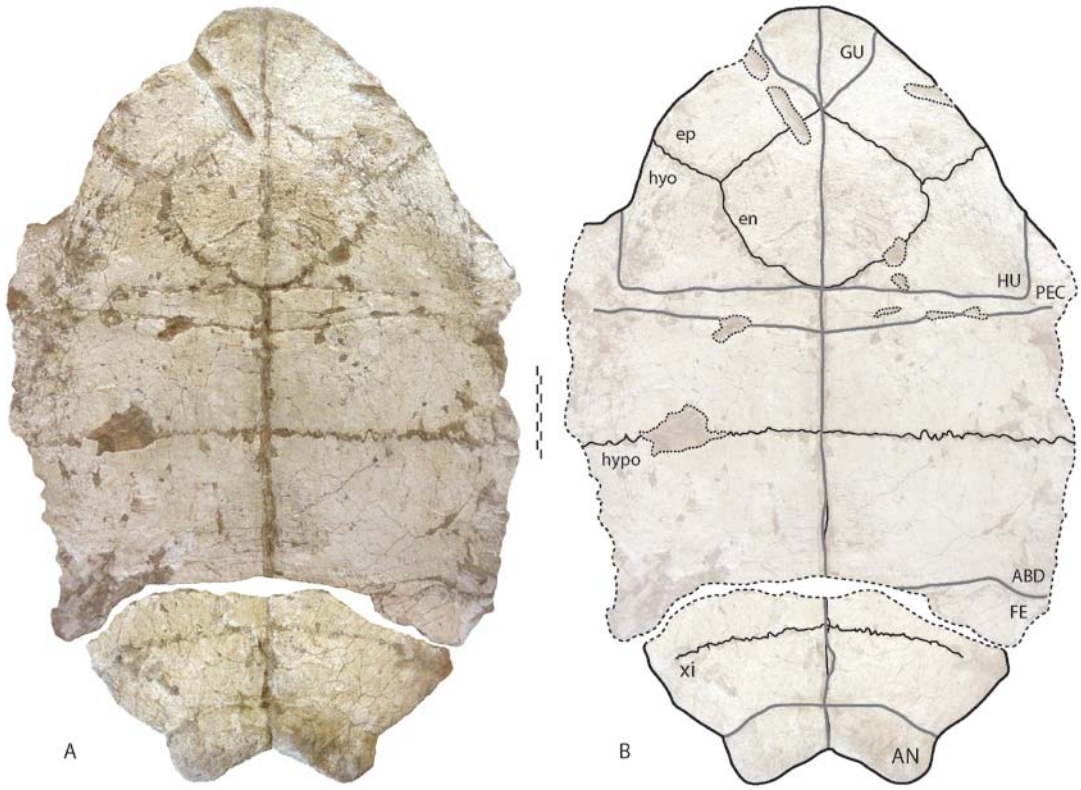


Figure 3.20. *Titanochelon bacharidisi* (Vlachos et al., 2014) from the Pliocene of Nea Kallikratia. LGPUT KLK 500, plastron of the KLK II individual in (A) ventral and (B) drawing of the ventral view. Scale bar equals 10 cm. For abbreviations see Material & Methods.

The xiphiplastra are short and limited to the posterior part of the lobe, preserving a wide anal notch. The gulars are short, developed only in the anteriormost part of the lobe and contact the anterior border of entoplastron. The humerals cover the entire entoplastron medially, and the posterior epiplastra and anterior hyoplastra laterally. The humero-pectoral sulcus is straight medially, and develops a significant change in curvature towards the axillary notch. Medially, the pectoro-abdominal sulcus is slightly concave posteriorly. The pectorals are very short, covering a small part of the hyoplastra. The abdominals are long and form the largest scales of the plastron, covering the posterior hyoplastra and anterior hypoplastra. The abdomino-femoral sulcus is medially straight and posteriorly curved laterally. Femorals cover most of the posterior lobe, except for the posterior part that is covered by short anals. The anal part of the xiphiplastra is ventrally thickened. The plastral formula (measured across the midline) is: Hyoplastra ≈ Hypoplastra >> Epiplastra > Xiphiplastra > Entoplastron. Abdominals > Femorals ≈ Humerals >> Gulars > Anals.

Nea Michaniona

Individual MIC I: various elements have been collected in Nea Michaniona that could belong to the same individual as they have been collected from the same area, they could correspond to individuals of the same size and do not preserve overlapping parts of the skeleton. Compared to the size of similar skeletal elements from Epanomi and Nea Kallikratia, the bones from Nea Michaniona are much more robust and almost twice in size, indicating a much larger individual.

LGPUT MIC 301, 302, 303 (Fig. 3.21.C): This specimen corresponds to a partial left posterior limb, preserving the medial and distal part of the femur (LGPUT MIC 301), and the proximal parts of the tibia (LGPUT MIC 302) and fibula (LGPUT MIC 303) in articulation. The femur shows a curvature in the distal part, which is massive and wide. The proximal part of the tibia is wide, triangular in cross-section, having a broad cnemial crest. The fibula is much smaller and almost straight. On the dorsal side of the articulation (Fig. 3.21.C3) an enlarged bony part is noted, which is irregular in shape. Although its limits with the tibia and fibula can be traced, it appears that it is fused with the distal part of the femur. Based on the lack of comparable material we cannot confirm whether this represents an irregular growth (pathology) or not.

LGPUT MIC 304 – 307, 316 – 318 (Fig. 3.22.A-B): Several parts of a massive pelvis are preserved, but their preservation does not allow further description. One of them (Fig. 3.22.B) corresponds to a possible acetabulum.

LGPUT MIC 308 (Fig. 3.21.B): This specimen corresponds to the distal part of a costal plate. Dorsally this plate is crossed by the pleural sulci. This specimen has been sampled for histological observations (see relevant chapter).

LGPUT MIC 309 (Fig. 3.22.D): This specimen corresponds to the distal part of a right fibula. It is rather straight, having an expanded distal end with a convex articular surface for the astragalocalcaneum. The articular surface is slightly expanded dorsally.

LGPUT MIC 310 (Fig. 3.22.E): This specimen corresponds to a partial metacarpal. Its dorsal side is shorter than the ventral, making the bone pyramidal in shape. The proximal surface is rather straight, whereas the distal is concave.

LGPUT MIC 311 (Fig. 3.22.F): This specimen corresponds to a flattened and rounded osteoderm.

LGPUT MIC 312 (Fig. 3.22.G): This specimen corresponds to an almost complete bony thigh tubercle. It is conical with a pointed tip and a robust distal part.

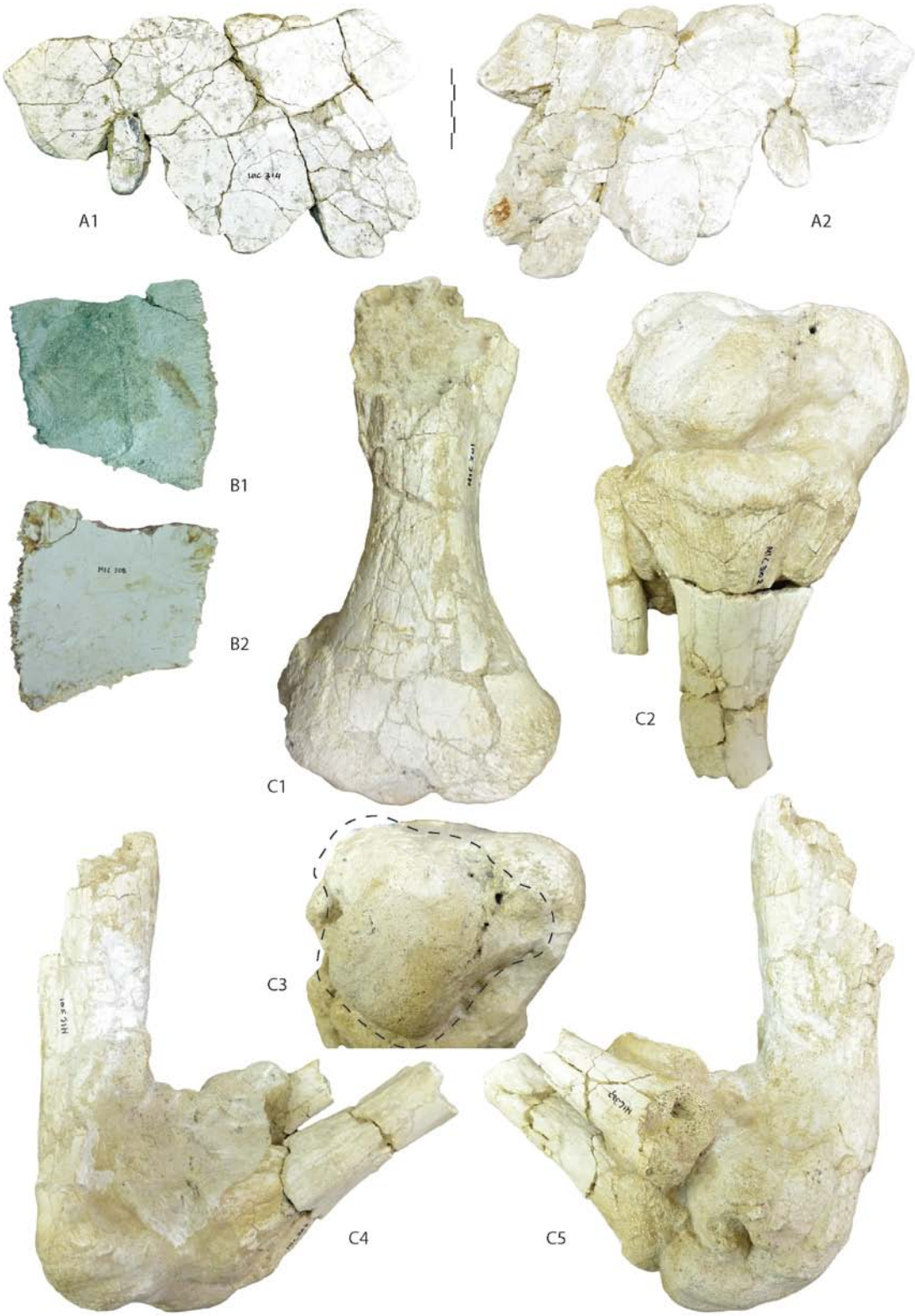


Figure 3.21. *Titanochelon bacharidisi* from the Pliocene of Nea Michaniona (Thessaloniki). A, LGPUT MIC 314, plastron fragment in (A1) visceral and (A2) ventral view. B, LGPUT MIC 308, costal fragment in (B1) dorsal and (B2) visceral view. C, LGPUT MIC 301-303, let posterior limb in articulation in (C1) dorsal view of the femur, (C2) dorsal view of the tibia and fibula, (C3) dorsal view of the irregular bony part of the articulation, (C4) posterior view and (C5) anterior view. Scale bar equals 5 cm.

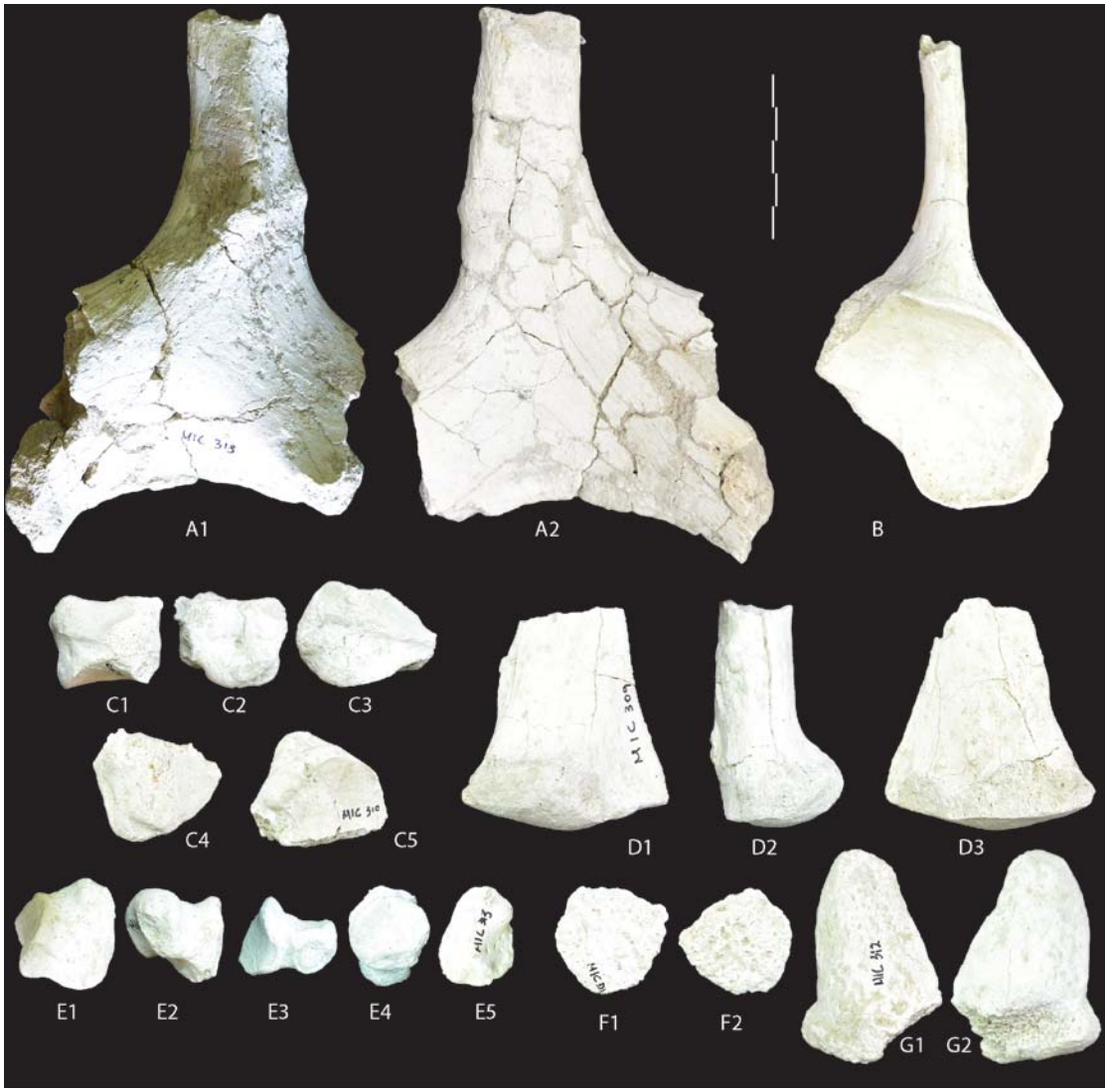


Figure 3.22. *Titanochelon bacharidisi* (Vlachos et al., 2014) from the Pliocene of Nea Michaniona (Thessaloniki). A, LGPUT MIC 318, pelvis fragment. B, LGPUT MIC 319, acetabulum in lateral view. C, LGPUT MIC 310, metacarpal in (C1) dorsal, (C2) medial, (C3) lateral, (C4) distal and (C5) proximal views. D, LGPUT MIC 309, fibula in (D1) dorsal, (D2) lateral and (D3) ventral views. E, LGPUT MIC 313, pisiform in (E1) dorsal, (E2) proximal, (E3) distal, (E4) medial and (E5) latero-ventral views. F, LGPUT MIC 311, osteoderm in (E1) dorsal and (E2) ventral views. F, LGPUT MIC 312, thigh tubercle. Scale bar equals 5 cm.

LGPUT MIC 313 (Fig. 3.22.E): This specimen corresponds to a complete pisiform. It shows a concave surface to articulate with the lateral distal part of the ulna. Distally, it shows a rather flat circular articular surface indicating that there has been a good articulation between the pisiform and the distal tarsal 5. Ventrally and laterally, a rounded elongated tubercle is noted.

LGPUT MIC 314 – 315, 319 (Fig. 3.21.A): Several indeterminate fragments of the plastron are preserved. Their preservation does not allow further description.

Aggelochori/Megalo Emvolon

LGPUT collection

The available material from Aggelochori is rather poor. A small fragment from the plastron is the only available information on the shell. The only identifiable specimen is the diaphysis of a femur (Fig. 3.23), that is straight medially and curved distally.



Figure. 3.23. *Titanochelon bacharidisi* (Vlachos et al., 2014) from the Pliocene of Aggelochori/Megalo Emvolon (Thessaloniki; LGPUT collection). A diaphysis of a femur in A, dorsal, B, lateral and C, ventral views. Scale bar equals 5 cm.

AMPG collection

AMPG 1925 (Fig. 3.24.B): This specimen corresponds to a complete left epiplastron. The plate is wider than long. Viscerally it preserves a thick and rounded epiplastral lip. The dorsal surface of the epiplastral lip is convex. Posterior to the lip, a significant gular pocket is formed. Ventrally, the medial part of the entoplastron is covered by long and narrow gulars that clearly do not overlap the entoplastron. Based on the preserved entoplastron we can reconstruct a rather rounded anterior lobe, but with a straight anterior boundary (the area covered by the gulars).

AMPG 1926 (Fig. 3.24.C): This specimen corresponds to a partial left xiphiplastron, with the lateral and anterior part missing. The anals cover the posterior part of the xiphiplastron, and the femoro-anal sulcus is slightly rounded, especially in the lateral part. Viscerally, the anals cover a significant portion of the posterior border of the xiphiplastron, but they do not meet in the midline. The xiphiplastral extremities are rather thin and rounded. This suggests that this specimen probably belongs to a female individual.

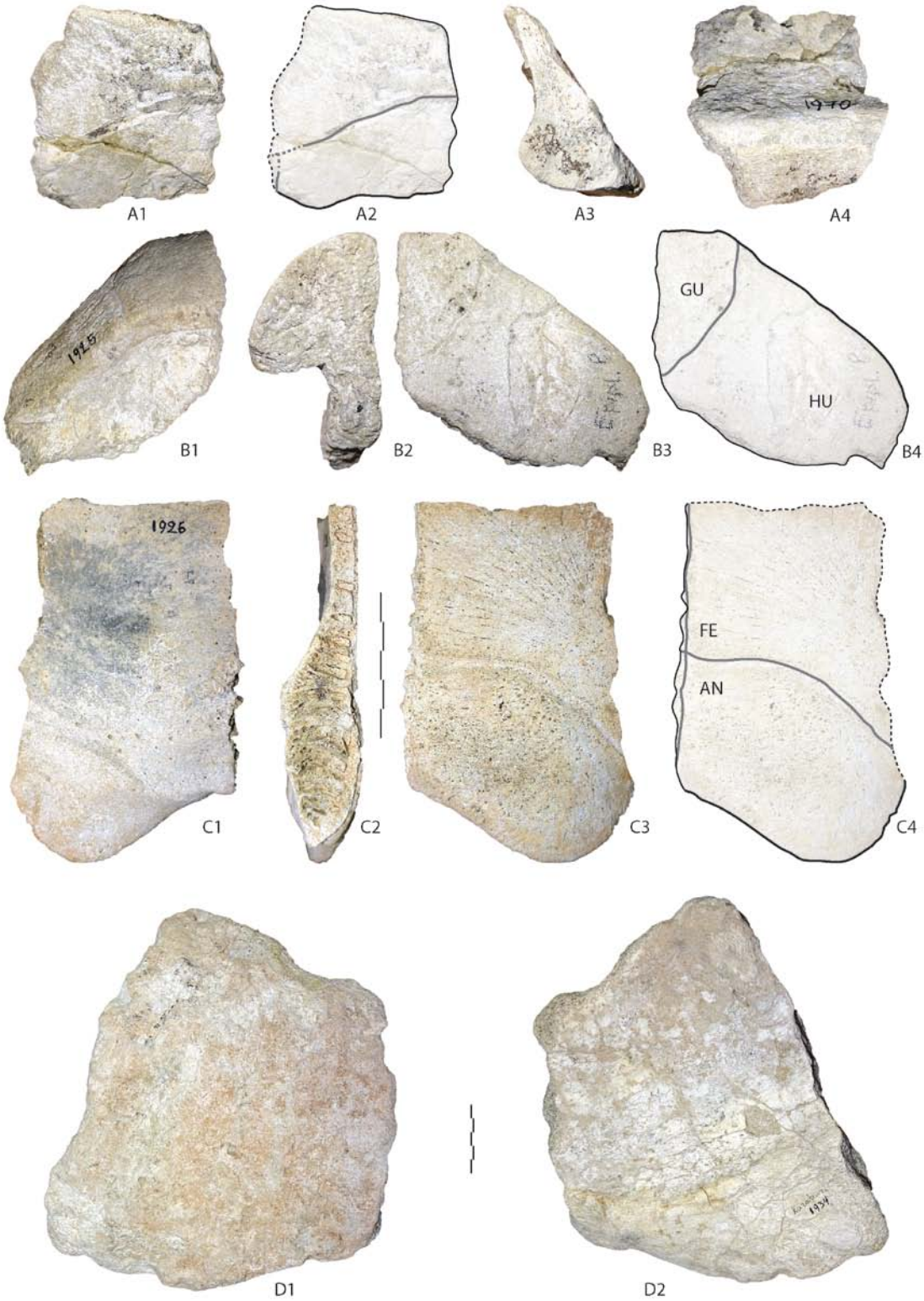


Figure 3.24. *Titanochelon bacharidisi* (Vlachos et al., 2014) from Aggelochori/Megalo Emvolon (AMPG collection). Shell material in A, AMPG 1970, partial nuchal plate in (A1,2) dorsal, (A3) lateral and (A4) visceral views. B, AMPG 1925, left epiplastron in (B1) visceral, (B2) medial, and (B3,4) ventral views. C, AMPG 1926, left xiphiplastron in in (C1) visceral, (C2) medial, and (C3,4) ventral views. D, AMPG 1934, carapace fragment in (D1) dorsal and (D2) visceral views. Scale bar equals 5 cm. For abbreviations see Material & Methods.

AMPG 1927 (Fig. 3.25.J): This specimen corresponds to a complete left metatarsal. It has a wide proximal part, with a concave articular surface for the distal tarsal and a distal part with a convex articular surface for the phalanx. Based on the preserved metatarsal we can estimate that the metatarsal were slightly overlapping each other.

AMPG 1928 (Fig. 3.25.L): This specimen corresponds to a complete phalanx, with a concave proximal surface for the metacarpal and a convex distal surface for the ungual. It is slightly asymmetrical.

AMPG 1929 (Fig. 3.25.M): This specimen corresponds to a complete phalanx, taller than AMPG 1928. It shows a concave proximal surface for the metacarpal and a convex distal surface for the ungual.

AMPG 1930 (Fig. 3.25.N): This specimen corresponds to a complete ungual. It is long, narrow and shows a rather pointed end, suggesting that it could be an element of the posterior limb. The proximal articular surface for the phalanx is concave.

AMPG 1931: This specimen corresponds to a fragment of the plastron. Based on the thickness, curvature and the available comparative material, this could be a fragment of the hyoplastron of a large testudinid. Further identification is not possible.

AMPG 1932: This specimen corresponds to a fragment of the right hypoplastron, as it is inferred by the presence of the part in the beginning of the lobe, right after the end of the inguinal notch. The ventral side is eroded, and no sulci are visible. Based on the preserved size we can estimate that belonged to a large testudinid.

AMPG 1933: This specimen corresponds to an unidentifiable fragment of the plastron of a large testudinid. Further description is not possible.

AMPG 1934 (Fig. 3.24.D): This specimen corresponds to a carapace fragment, probably for the anterior part. Most of the surface is eroded and no sulci are visible, hindering further identification. However it is possible to note the peripheral lip. Based on the preserved part, and compared with the known material this could belong to a testudinid of large size, probably reaching 1m in shell length.

AMPG 1935: This specimen corresponds to an unidentifiable fragment of the plastron of a large testudinid. Further description is not possible.

AMPG 1936 (Fig. 3.25.D): This specimen corresponds to the medial and distal part of a left ulna. The cross-section of this element is triangular. Based on the preserved part we can estimate the presence of a tear-shaped fenestra between the radius and ulna. Further description is not possible.

AMPG 1937: This specimen corresponds to the medial and distal part of a left ulna. The cross-section of this element is triangular. Based on the preserved part we can estimate the presence of a tear-shaped fenestra between the radius and ulna. Further description is not possible.

AMPG 1938: This specimen probably corresponds to a fragment of the pelvis, but the preserved part does not allow further description and identification.

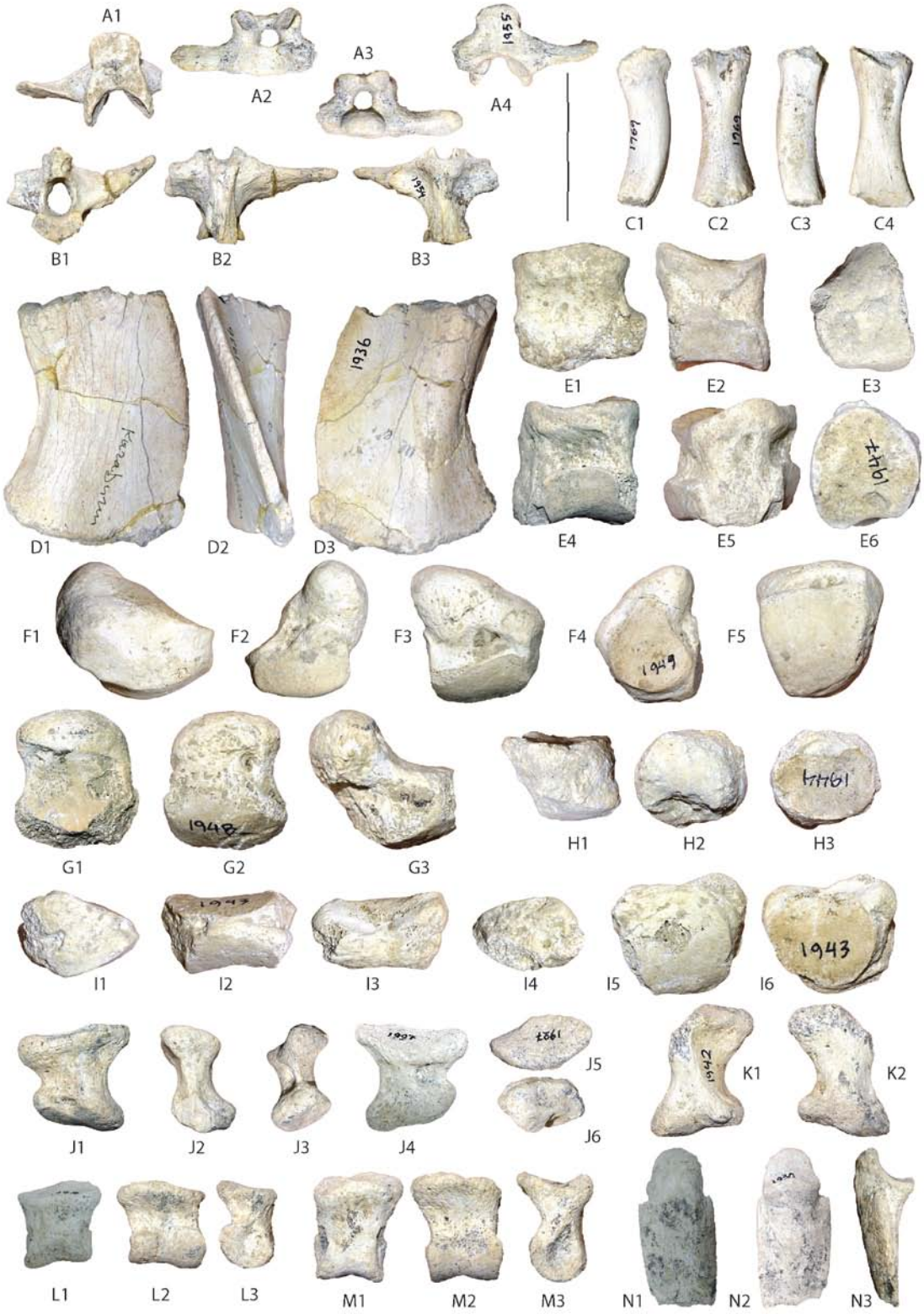


Figure 3.25. *Titanochelon bacharidisi* (Vlachos et al., 2014) from the Pliocene of Aggelochori/ Megalo Emvolon (AMPG collection). A, AMPG 1955, caudal vertebra in (A1) dorsal, (A2), posterior, (A3) anterior, and (A4) ventral views. B, AMPG 1954, caudal vertebra in (B1) dorsal, (B2), posterior, (B3) anterior, and (B4) ventral views. C, AMPG 1969, right humerus in (C1) posterior, (C2) ventral, (C3) anterior and (C4) dorsal views. D, AMPG 1936, part of left ulna in (D1) ventral, (D2) posterior and (D3) dorsal views. E, AMPG 1947, right intermedium in (E1) ventral, (E2) medial, (E3) distal, (E4) lateral, (E5)

dorsal and (E6) proximal views. F, AMPG 1949, distal carpal in (F1) lateral, (F2) medial, (F3) ventral, (F4) proximal and (F5) distal views. G, APMG 1948, distal carpal in (G1) proximal, (G2) ventral and (G3) lateral views. H, AMPG 1944, metacarpal in (H1) lateral, (H2) distal and (H3) proximal views. I, AMPG 1943, right metacarpal in (I1) lateral, (I2) dorsal, (I3) ventral, (I4) medial, (I5) distal and (I6) proximal views. J, AMPG 1927, metatarsal in (J1) dorsal, (J2), lateral, (J3) medial, (J4) ventral, (J5) proximal and (J6) distal views. K, AMPG 1942, metatarsal in (K1) dorsal and (K2) ventral views. L, AMPG 1928, phalanx in (L1) dorsal, (L2) ventral and (L3) lateral views. M, AMPG 1929, phalanx in (M1) dorsal, (M2) ventral and (M3) lateral views. N, AMPG 1930, ungual in (N1) dorsal, (N2) ventral and (N3) lateral views. Scale bar equals 5 cm.

AMPG 1939: This specimen corresponds to an almost complete ungual. It is long and wide, suggesting that it could be an element of the anterior limb. The proximal articular surface for the phalanx is slightly concave.

AMPG 1940: This specimen corresponds to an almost complete ungual. It is long and wide, suggesting that it could be an element of the anterior limb. The proximal articular surface for the phalanx is slightly concave.

AMPG 1941 (Fig. 3.25.E): This specimen belongs to a complete pointed osteoderm that is long and narrow.

AMPG 1942 (Fig. 3.25.K): This specimen corresponds to an almost complete left metatarsal, missing only a part of the proximal surface. It has a wider proximal part, with a concave articular surface for the distal tarsal and a narrower distal part with a convex articular surface for the phalanx.

AMPG 1943 (Fig. 3.25.I): The specimen corresponds to a complete right metacarpal. It shows a slightly concave surface proximally for the distal carpals and a distal convex surface for the first phalanx. The anterior part is shorter than the taller posterior part. It is rather flattened.

AMPG 1944 (Fig. 3.25.H): This specimen corresponds to an almost complete metacarpal. It is tall and narrow, showing a slightly concave surface proximally and a convex articular surface distally.

AMPG 1945: This specimen corresponds to a fragmented complete metacarpal. It is tall, showing a slightly concave surface proximally and a convex articular surface distally.

AMPG 1946 (Fig. 3.26.F): This specimen corresponds to a rounded osteoderm, being flattened, and longer than wide.

AMPG 1947 (Fig. 3.25.E): This specimen corresponds to a complete right intermedium. It is rather robust and shows a triagonal to rounded cross–section. Proximally it has a concave articular surface for the ulna. Medially it shows a slightly concave surface for the radius. Distally and medially it has a slightly concave surface for the medial and lateral centrale.

AMPG 1948 (Fig. 3.25.G): This specimen corresponds to a complete distal carpal. It is tall and narrow. The proximal surface is strongly concave. It shows a large protuberance proximally and a discoid part distally. Ventrally, there is a convex surface for the metacarpals.

AMPG 1949 (Fig. 3.25.F): This specimen corresponds to a complete and well-preserved distal carpal. It is rather tall and narrow. The proximal surface is convex to flat in some places. It shows a large protuberance proximally and a discoid part distally. Ventrally, there is a convex surface for the metacarpals.

AMPG 1950 (Fig. 3.26.A): This specimen corresponds to a pointed osteoderm. It is long, thick, narrow and shows a pointed tip.

AMPG 1951 (Fig. 3.26.D): This specimen corresponds to a partial half-pointed osteoderm, being rather wide and thick.
AMPG 1952 (Fig. 3.26.B): This specimen corresponds to a pointed osteoderm. It is long, thick, narrow and shows a pointed tip.

AMPG 1953 (Fig. 3.26.C): This specimen corresponds to a complete half-pointed osteoderm, being long and narrow.

AMPG 1954 (Fig. 3.25.B): This specimen corresponds to an almost complete tail vertebra, missing only one of the transversal processes. It shows the typical morphology, being procoelous with a short centrum. The transversal process is long.

AMPG 1955 (Fig. 3.25.A): This specimen corresponds to an almost complete tail vertebra, missing only one of the transversal processes. It shows the typical morphology, being procoelous with a short centrum. The transversal process is long.

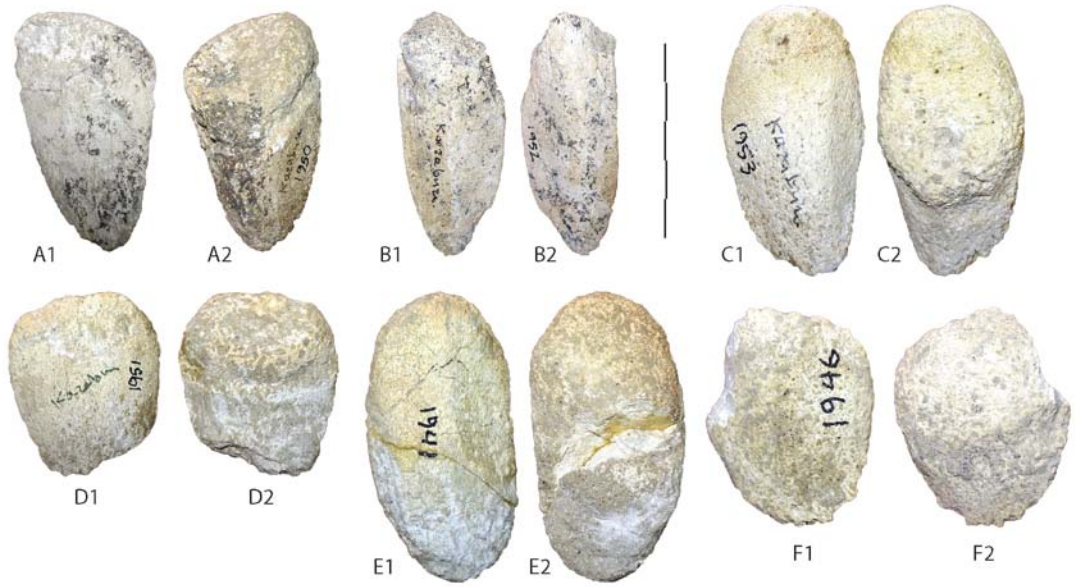


Figure 3.26. *Titanochelon bacharidisi* (Vlachos et al., 2014) from the Pliocene of Aggelochori/ Megalo Emvolon (AMPG collection). Osteoderms in A, AMPG 1950, pointed osteoderm in (A1) dorsal and (A2) ventral views. B, AMPG 1952, pointed osteoderm in (B1) dorsal and (B2) ventral views. C, AMPG 1953, pointed osteoderm in (C1) dorsal and (C2) ventral views. D, AMPG 1951, half-pointed osteoderm in (D1) dorsal and (D2) ventral views.

E, AMPG 1941, half-pointed osteoderm in (E1) dorsal and (E2) ventral views. F, AMPG 1946, half-pointed osteoderm in (F1) dorsal and (F2) ventral views.

AMPG 1969 (Fig. 3.25.C): This specimen corresponds to the diaphysis of a right humerus. Both epiphyses are missing. The diaphysis shows only a small degree of curvature. Based on the small size we can estimate that this specimen could belong to a juvenile individual.

AMPG 1970 (Fig. 3.24.A): This specimen corresponds to the right part of a nuchal. Based on the preserved part we can reconstruct a wider than long or as long as wide nuchal plate. The nuchal lip is thick and is horizontally developed. In the dorsal side we can trace the sulcus between the first vertebral and the first peripheral. Also in the medial side the sulcus between the first two peripherals is noted (although partially eroded), providing evidence the cervical scute is absent.

REMARKS: The locality of Aggelochori (also known as Megalo Emvolon or Karaburun) has been exploited by many researchers in the past and a lot of material is dispersed in various collections in Greece and abroad. The material here corresponds mainly to collections made by F. Bachmayer in the 70's, with most of the material being stored in AMPG. The most important specimens have been reported in Bachmayer et al. (1979). From the material presented in that paper, only the shell of the small testudinid (presented below) is stored in the collections of NHMW. From the remains of the large testudinid, Bachmayer et al. (1979) preliminary described some specimens as "*Testudo*" sp. and figured the two plastral remains (Plate VI in Bachmayer et al., 1979) and some elements of the digit (Plate VII in Bachmayer et al., 1979). The mounting of the digit is erroneous as it shows the presence of two distal phalanges between the metatarsal and the ungual, when obviously this testudinid possessed only one distal phalanx. The remaining material is presented, figured and described here for the first time.

These specimens from Aggelochori can be safely attributed to *Titanochelon bacharidisi*, based on the morphology of the gulars that do not cover the entoplastron. Furthermore, the preserved elements of the appendicular skeleton are fairly similar with the type material of *Ti. bacharidisi* from Epanomi. Moreover, the locality of Aggelochori is within the same stratigraphic formation (Gonia formation, sensu Syrides, 1990), which is characterized by the presence of *Ti. bacharidisi*. All the above provide clear evidence for the identification of this material. Some of the preserved shell material and the partial humerus are of particular interest, because they probably belong to a juvenile individual (both plastral specimens could be part of the same individual), based on the small size and the incomplete ossification of the medial suture (in the xiphiplastron). This could be the first specimen of a juvenile individual of *Ti. bacharidisi*. Most of the material belongs to one (or more) individuals of large size that could reach the length of the Epanomi individuals (i.e. 1–1.2m).

COMMENTS: Part of the presented information on the morphology of *Ti. bacharidisi* has been presented in Vlachos (2011) and Vlachos et al. (2014), but in this thesis all this information is revised and further expanded with the inclusion of more specimens from the collections of LGPUT and AMPG. In the review of Georgalis & Kear (2013), the authors provide information for the material from Epanomi, Nea Michaniona, Aggelochori and Nea Michaniona. This information is based on Vlachos

(2011) but it is reproduced or interpreted by Georgalis & Kear (2013) erroneously. First of all, they provide a Latest Miocene/ Earliest Pliocene age for the specimens, in contrast with the true Pliocene age of this taxon as shown in Vlachos (2011) and Vlachos et al. (2014). Furthermore, they attribute this material to *Cheirogaster* cf. *schafferi*, without any morphological justification, neglecting all the differences described in Vlachos (2011). Also, they provide an erroneous size for the Epanomi individual (150 cm, instead of 115 cm), which raises questions about the validity of their speculative results on the gigantism listed in that paper.

Titanochelon* cf. *bacharidisi

DISTRIBUTION: Salonique (sensu Arambourg & Piveteau, 1929). The specimens could be either from the Axios valley or from Megalo Emvolon (see Vlachos et al., 2014)

AGE: ?Late Miocene – Pliocene? (see Vlachos et al., 2014). This material has been considered Late Miocene in age (Lapparent de Broin, 2001, 2002), probably because most of Arambourg and Piveteau's (1929) material originates from various Late Miocene localities in Axios valley, Greece. In some cases, even a precise locality has been mentioned (Vathylakkos-3, in Georgalis & Kear, 2013) but without any convincing information. Nevertheless, a portion of the material described in Arambourg and Piveteau (1929) was collected from Megalo Emvolon (French name for the site: Falaise de Karaburun, with discoveries of a giant Testudo sp.), which is of a younger, Ruscinian age (Pliocene, MN15, Koufos et al., 1991). Subsequently, this site yielded further elements of a giant tortoise (Bachmayer et al., 1979). Also, more specimens from this locality are presented here for the first time. Considering the interpretation of Arambourg and Piveteau's (1929) work, and the associated labels of the tortoise fossils (MNHN 1921-5-SLQ collection; in most specimens "Karaburun" is written) it seems likely that this tortoise was collected from Megalo Emvolon deposits and, therefore, is of Pliocene age. During the visit in MNHN the original archives of the museum were checked and especially the catalog of incoming fossil material. Unfortunately, in the collection numbers of Arambourg and Piveteau, no mention of tortoise material was found. Therefore, we cannot conclusively exclude subsequent mixing of this material. For all the above, it seems as best solution to expand the Late Miocene age to the Pliocene, pending further evidence that could resolve this issue.

MATERIAL (Fig. 3.27-3.30):

MNHN SLQ 995, cranium; MNHN SLQ 996, humerus; MNHN SLQ 997, humerus distal part; MNHN SLQ 998, radius; MNHN SLQ 999, ulna; MNHN SLQ 1000, ulna; MNHN SLQ 1001, ulna; MNHN SLQ 1002, ulna; MNHN SLQ 1003, radius; MNHN SLQ 1004, osteoderm; MNHN SLQ 1005, osteoderm; MNHN SLQ 1006, osteoderm; MNHN SLQ 1007, osteoderm; MNHN SLQ 1008, osteoderm; MNHN SLQ 1009, osteoderm; MNHN SLQ 1010, osteoderm; MNHN SLQ 1011, osteoderm; MNHN SLQ 1012, osteoderm; MNHN SLQ 1013, osteoderm; MNHN SLQ 1014, osteoderm; MNHN SLQ 1015, osteoderm; MNHN SLQ 1016, osteoderm; MNHN SLQ 1017, osteoderm; MNHN SLQ 1018, osteoderm; MNHN SLQ 1019, osteoderm; MNHN

SLQ 1020, osteoderm; MNHN SLQ 1021, osteoderm; MNHN SLQ 1022, osteoderm; MNHN SLQ 1023, ungual.

DESCRIPTION

MNHN SLQ 995 (Fig. 3.27-3.28): This specimen corresponds to an incomplete skull, from which the right anterior and the left posterior parts are missing. The preservation of the skull is not so good in order to be able to clearly observe the sutures. The specimen is deformed, having a transverse breakage in the breakage causing a small distortion in the posterior part. The skull is long and short. The sutures are partially visible in some cases.

Skull roof and braincase: The anterior part is highly eroded and we cannot notice the apertura narium externa. The anterior part of the skull, from the postorbitals and anteriorly Represents the anterior half of the skull. The braincase elements represent the posterior half of the skull in dorsal view. The limit between the prefrontals and the frontals is visible and is almost straight. The prefrontals appear to be medially as long as laterally long, and they contribute in the formation of the antero-medial rim of the fossa orbitalis. Similarly, the frontals appear to be of equal medial and lateral length, and they contribute in the formation of the medial part of the rim of the fossa orbitalis. The posterior part of the rounded fossa orbitalis is made by the postorbital bone, that is short and rather flat. In the medial part of the frontals a small constriction is noted, making the prefrontals slightly wider than the frontals. The parietals are wide, and they develop a posterior process to reach the supraoccipital. The supraoccipital is elongated, forming a long, and relatively straight crista supraoccipitalis that extends beyond the level of squamosals. Although incomplete, we can notice an extensive upper temporal emargination. The limits of the right squamosal with the opisthotic and the quadrate can be observed. The posterior tip of the squamosal is enlarged and rounded. The zygomatic area is only partially visible on the left side. On the right side the otic chamber is preserved. In the otic chamber we notice the deep antrum postoticum and a strong insisura columellae auris. Posteriorly, below the crista supraoccipitalis we notice a deep foramen magnum. Below the foramen magnum, a long, with a rounded elliptical shape, condylus occipitalis is developed. The processus paraoccipitalis is strong and contacts the squamosal. The state of preservation of the specimen does not allow a confident assessment of the ventral temporal emargination.

Palatal elements: The sutures between the elements of the palate and the ventral skull are not visible, therefore the position of the various elements can only be estimated. Anteriorly a deep premaxillary pit is probably present. The palate is marked by the presence of well-distinct ridges. None of the ridges shows the presence of tooth-like tubercles (sensu Gerlach, 2001). The labial ridge is strong and marks the rim of the palate, whereas is much taller compared to the rest. In the palate we notice the median maxillary ridge and the lingual ridge that are well-developed. The lingual ridge is much longer than the medial, reaching the pterygiods. Anteriorly they are connected via a round transverse ridge. The surface between the ridges is shallowly concave. Medial to the lingual ridges we notice the paired foramina praepalatinum. Between the lingual ridge and he vomer we notice a strong groove that could lead to the apertura narium interna. Posterior to the palate we notice a large fossa temporalis interior. In the anterior part, the pterygoid process is noted.

02/16/2016 Ψηφιακή Βιβλιοθήκη Θεόφραστος - Τμήμα Γεωλογίας - Α.Π.Θ.

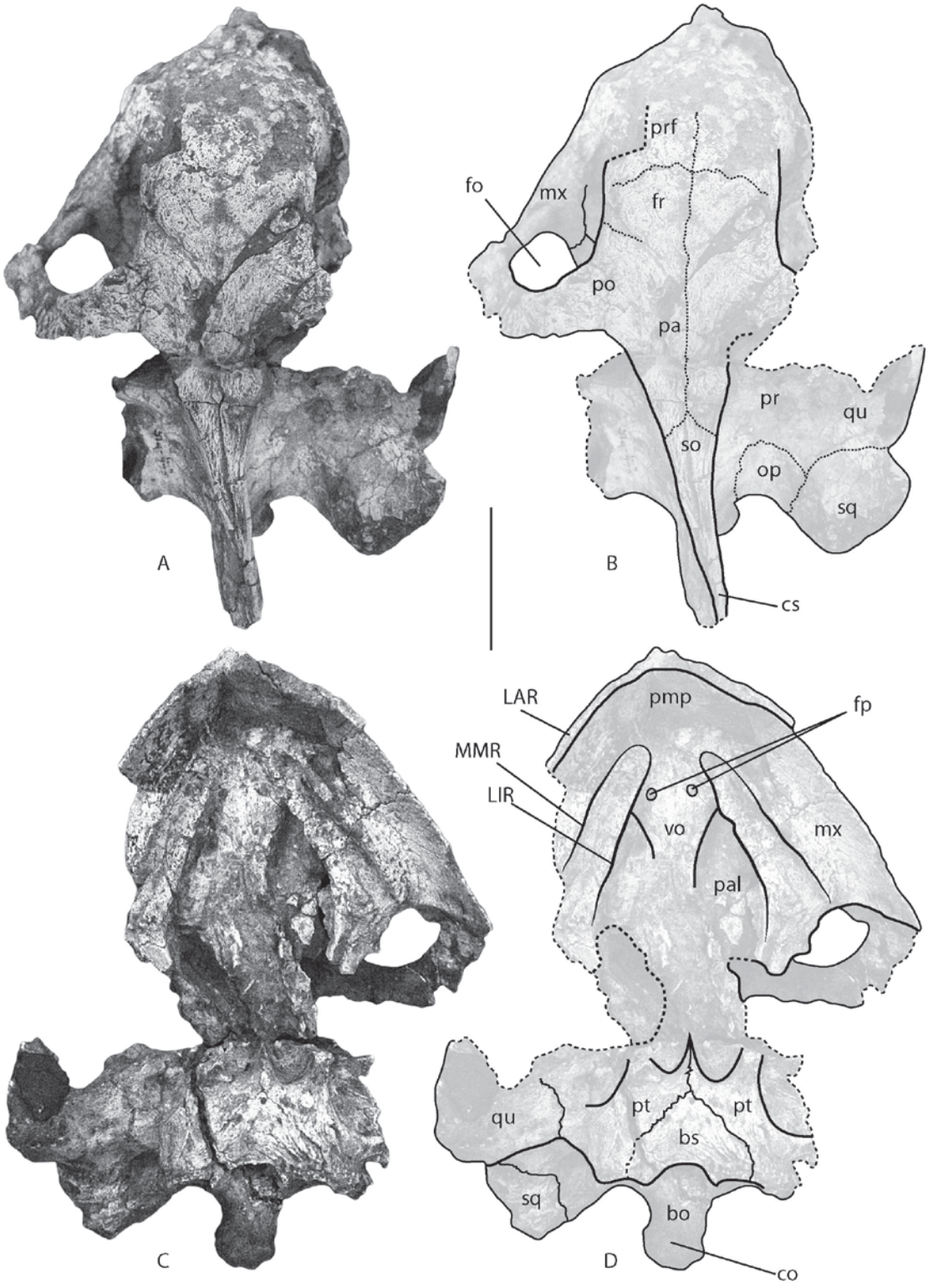


Figure 3.27. *Titanochelon* cf. *bacharidisi* from Salonique (sensu Arambourg & Piveteau, 1929). MNHN 1921-5-SLQ-995, the cranium in (A-B) dorsal and (C-D) ventral views. Scale bar equals 5 cm. For abbreviations see Material & Methods.

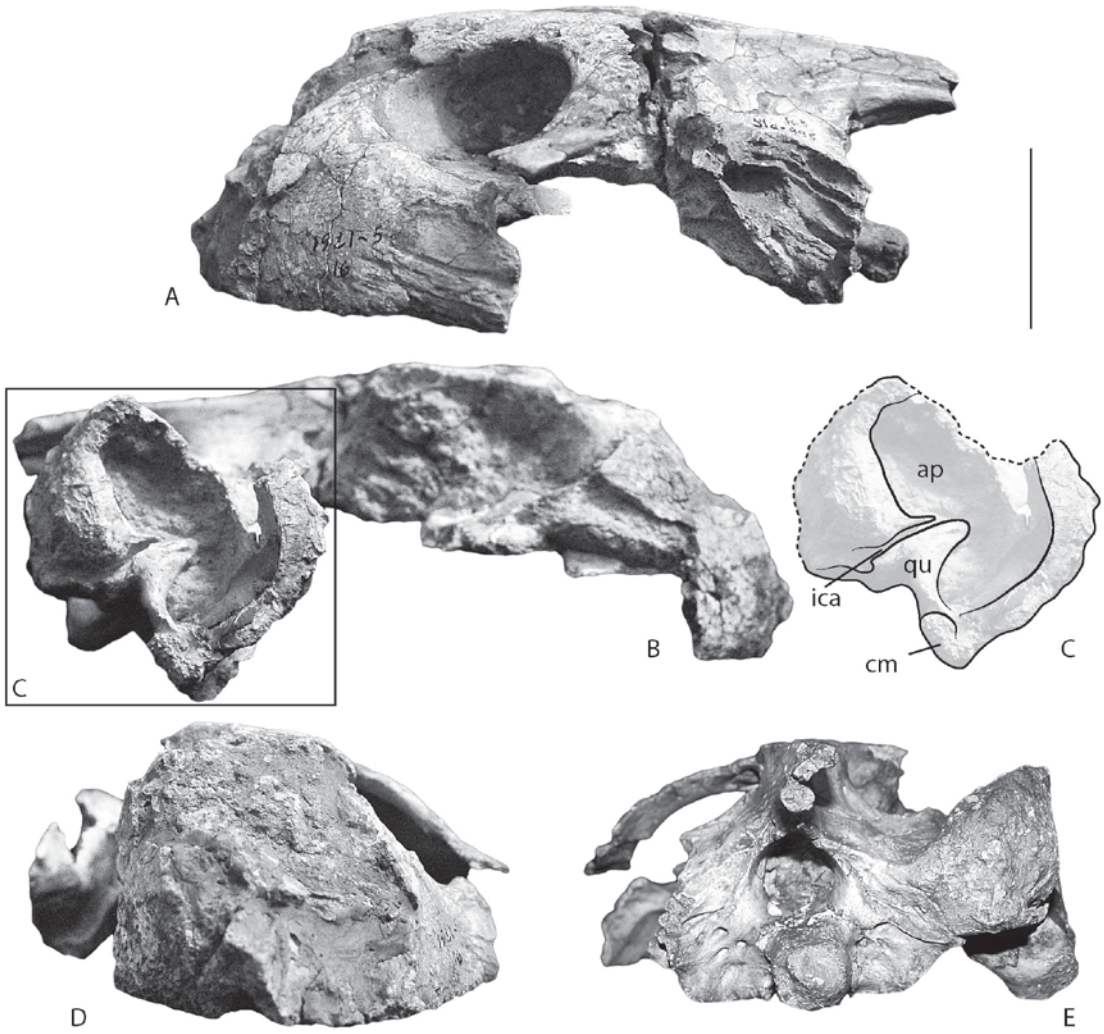


Figure 3.28. *Titanochelon* cf. *bacharidisi* from Salonique (sensu Arambourg & Piveteau, 1929). MNHN 1921-5-SLQ-995, the cranium in (A) left lateral, (B) right lateral, (C) detail of the right ear area, (D) anterior and (D) posterior views. Scale bar equals 5 cm. For abbreviations see Material & Methods.

MNHN SLQ 996 (Fig. 3.29.A): This specimen corresponds to an almost complete humerus. In the proximal part the trochanters are missing, but a rounded elliptical head is developed perpendicular to the diaphysis in lateral view. The neck is well-developed. The diaphysis is moderately curved. The distal part is missing, but from the preserved part we can estimate that it was wide.

MNHN SLQ 997 (Fig. 3.29.B): This specimen corresponds to the distal part of the diaphysis of a humerus.

MNHN SLQ 998 (Fig. 3.29.D): This specimen corresponds to a left radius. The proximal part is fragmented. The radius is straight, with a narrow diaphysis. The proximal articulation is formed by two concave surfaces for the distal humerus. The distal part shows a deep, elongate, and concave articular surface for first row of carpal bones.

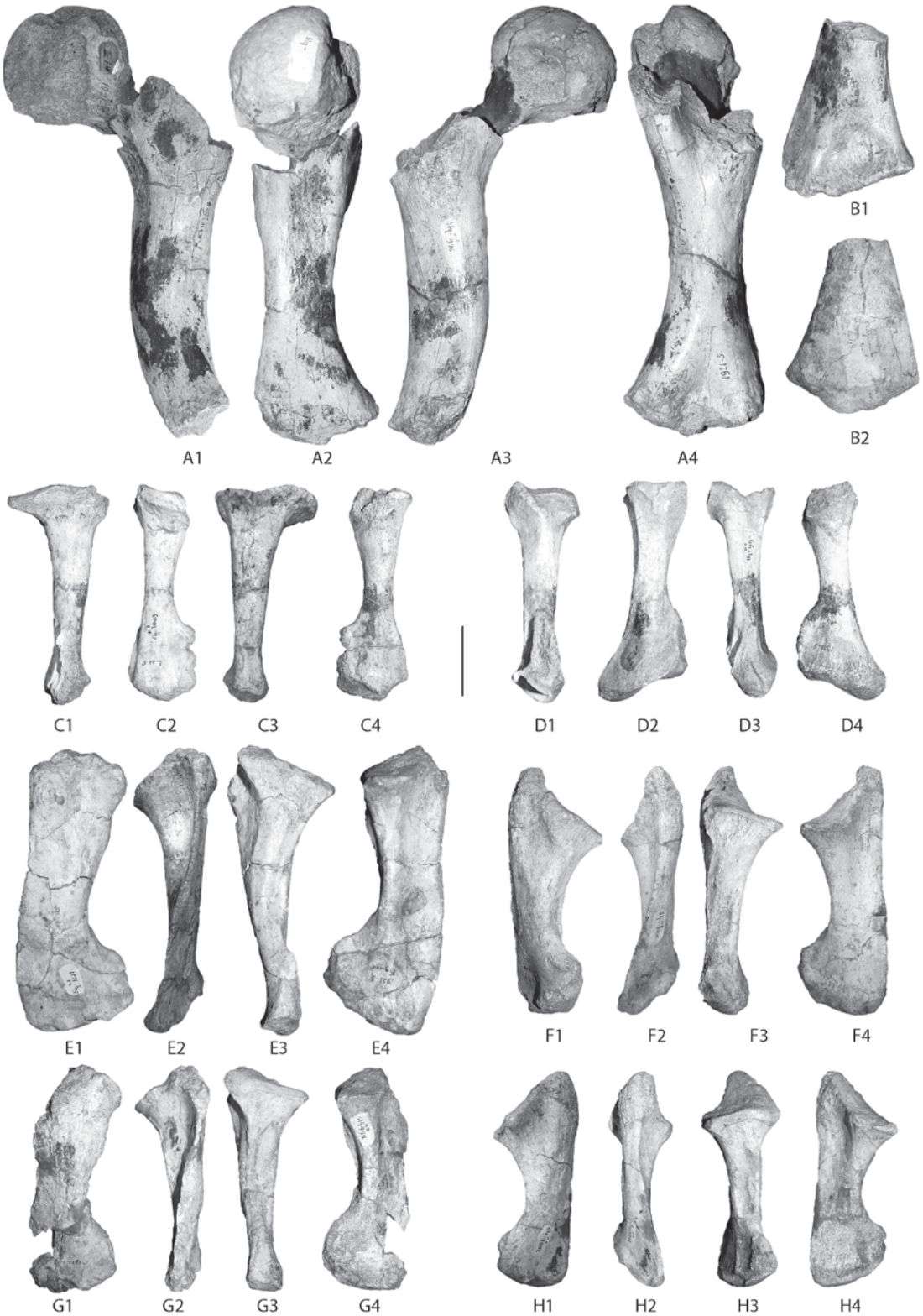


Figure 3.29. *Titanochelon* cf. *bacharidisi* from Salonique (sensu Arambourg & Piveteau, 1929). Appendicular elements in A, MNHN SLQ 996, left humerus in (A1) posterior, (A2) dorsal, (A3) anterior and (A4) ventral views. B, MNHN SLQ 997, distal humerus in (B1) dorsal and (B2) ventral views. C, MNHN SLQ 1003, right radius in (C1) medial, (C2) dorsal, (C3) lateral and (C4) ventral views. D, MNHN SLQ, left radius in (D1) medial, (D2) dorsal, (D3) lateral and (D4) ventral views. E, MNHN SLQ 1001, right ulna in (E1) ventral, (E2) lateral, (E3) medial and (E4) dorsal views. F, MNHN SLQ 1000, right ulna in (F1) ventral, (F2) lateral, (F3) medial and (F4) dorsal views. G, MNHN SLQ 999, right ulna in (G1)

ventral, (G2) lateral, (G3) medial and (G4) dorsal views. H, MNHN SLQ 1002, left ulna in (H1) ventral, (H2) lateral, (H3) medial and (H4) dorsal views. Scale bar equals 5 cm.

MNHN SLQ 999 (Fig. 3.29.G): This specimen corresponds to a right ulna. The distal part is fragmented. The ulna has broad proximal and narrow distal part, and the external face is curved in dorsal view. The proximal articular surface for the humerus is concave. The distal articular surface is convex with short transverse diameter. The lateral part of the bone has a triangular cross-section.

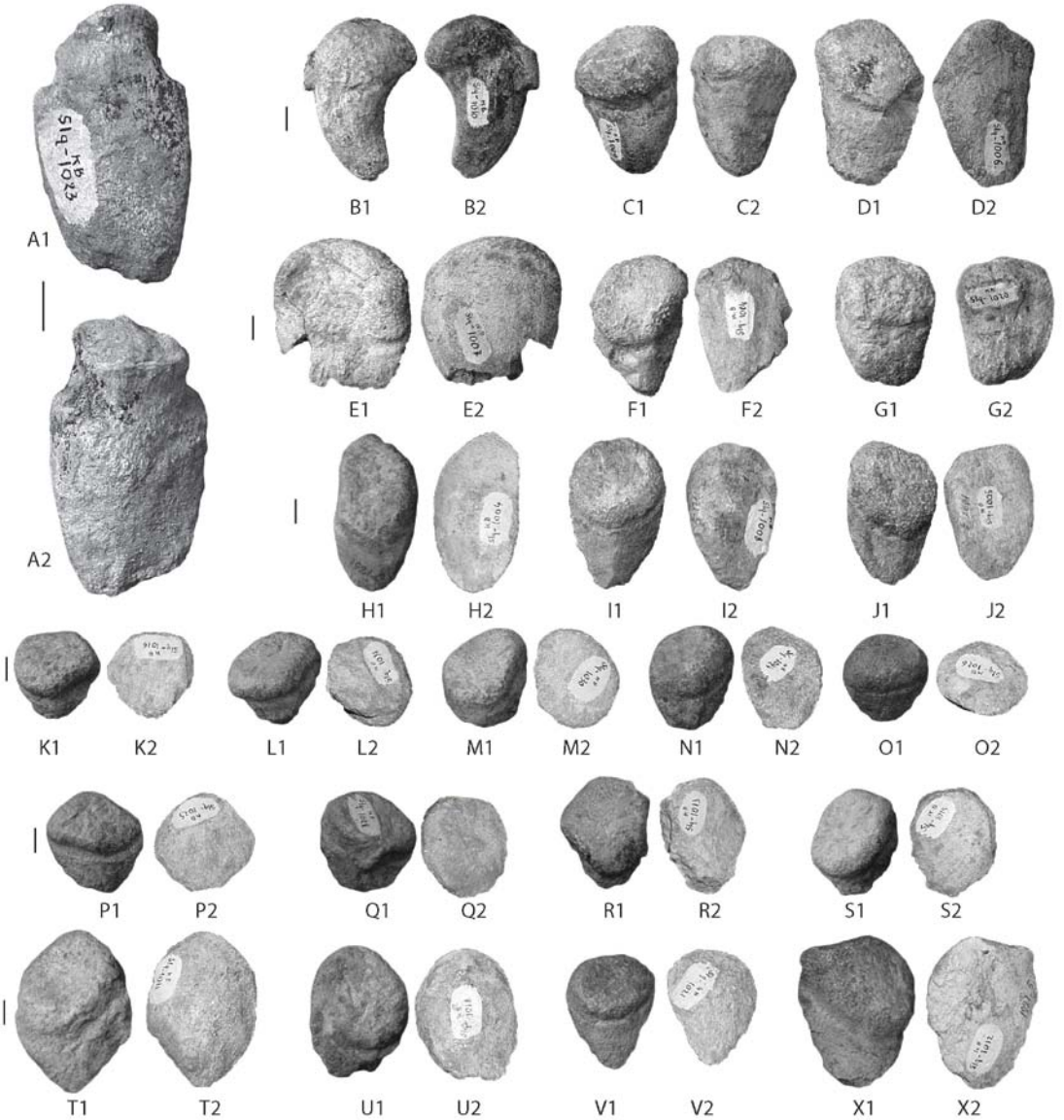


Figure 3.30. *Titanochelon* cf. *bacharidisi* from Salonique (sensu Arambourg & Piveteau, 1929). Ungual and osteoderms in A, AMPG 1023, ungual in (A1) dorsal and (A2) ventral views. B-X, osteoderms. Numbers: B, AMPG 1010; C, AMPG 1009; D, AMPG 1006; E, AMPG 1007; F, AMPG 1014; G, AMPG 1020; H, AMPG 1004; I, AMPG 1008; J, AMPG 1005; K, AMPG 1016; L, AMPG 1031; M, AMPG 1030; N, AMPG 1024; O, AMPG 1026; P, AMPG 1025; Q, AMPG 1028; R, AMPG 1013; S, AMPG 1015; T, AMPG 1011; U, AMPG 1018; V, AMPG 1021; X, AMPG 1012. Scale bar equals 1 cm.

MNHN SLQ 1000 (Fig. 3.29.F): This specimen corresponds to a complete right ulna. The ulna has broad proximal and narrow distal part, and the external face is curved in dorsal view. The proximal articular surface for the humerus is concave. The distal articular surface is convex with short transverse diameter. The lateral part of the bone has a triangular cross-section. When articulated, the radius and ulna leave a fenestra between them that is longer than wide.

MNHN SLQ 1001 (Fig. 3.29.E): This specimen corresponds to a complete right ulna. The ulna has broad proximal and narrow distal part, and the external face is curved in dorsal view. The proximal articular surface for the humerus is concave. The distal articular surface is convex with short transverse diameter. The lateral part of the bone has a triangular cross-section.

MNHN SLQ 1002 (Fig. 3.29.H): This specimen corresponds to a complete left ulna. The ulna has broad proximal and narrow distal part, and the external face is curved in dorsal view. The proximal articular surface for the humerus is concave. The distal articular surface is convex with short transverse diameter. The lateral part of the bone has a triangular cross-section.

MNHN SLQ 1003 (Fig. 3.29.C): This specimen corresponds to a right radius. The distal part is incomplete. The radius is straight, with a narrow diaphysis. The proximal articulation is formed by two concave surfaces for the distal humerus. The proximal part is wide with a lateral extensions of the articular surface. The distal part shows an elongated concave articular surface for first row of carpal bones.

MNHN SLQ 1004 – 1022, 1024 – 1031 (Fig. 3.30): In the material from Salonique several osteoderms are known. One of them (Fig. 3.30.B; MNHN SLQ 1010) is quite large, with a pointed conical shape. This resembles the thigh tubercles of *Ti. bacharidisi*, that have been found either separated (e.g. Epanomi) or in their anatomical position (e.g. Nea Kallikratia). Most of the remaining osteoderms are large and ointed (e.g. Fig.3.30.C, D, F). Others are enlarged and rounded (e.g. Fig. 3.30.E). Finally some of them are half-pointed (e.g. Fig. 3.30.K, L).

MNHN SLQ 1023 (Fig. 3.30.A): This specimen corresponds to a complete ungual. Based on its great length and the rather pointed end, it could be an element of the posterior limb. The proximal articular surface for the phalanx is slightly concave.

Comments: There are some similarities between the cranium from Salonique and the cranium of *Ti. bacharidisi* from Epanomi. The frontal – prefrontal area is similarly shaped, whereas both skulls show a similarly developed crista supraoccipitalis. The skull from Epanomi however shows a longer skull roof area and pointed converging squamosals. Also, the state of preservation of the Salonique skull does not allow a clear documentation of the lower temporal emargination, but it appears that is not so extensive as in the Epanomi skull. At the same time, this skull is greatly different from the skull of *Ti. schafferi* from Samos. Also the bones are different from those of *Titanochelon* sp. from Pikermi. On the other hand, the post-cranial elements from Salonique are fairly similar morphologically and metrically with those of *Ti. bacharidisi*. Moreover, a thigh tubercle is present in the Salonique material, which is one of the morphological characteristics of *Ti. bacharidisi*. Another problem of the specimens of Salonique is their unclear stratigraphic position. However it seems quite

possible that they originate from Megalo Emvolon (see Vlachos et al., 2014), which could place them between the stratigraphic and geographic range of *Ti. bacharidisi*. Therefore, and based on the few similarities on the shape of the skull mentioned above, we can only identify the classic material of Arambourg & Piveteau (1929) from Salonique as *Titanochelon* cf. *bacharidisi*. Based on the preserved material, the fossil specimens from Salonique correspond to at least three different large tortoise individuals as it is inferred by the right ulna.

In the review of Georgalis & Kear (2013), the material of Arambourg & Piveteau (1929) is also noted, but confusion surrounds the locality. Regarding the material of the giant tortoise, they list it as belonging to the Vathylakkos formation (and therefore of Late Miocene). They identified this as *Cheirogaster* cf. *schafferi*. The material of the small tortoise is listed as found in the locality "Falaise de Karabouroun" (Megalo Emvolon), but as belonging to Vathylakkos formation, which led Georgalis & Kear (2013) to provide a Late Miocene age for this material as well. Also, without any morphological justification, this material is referred by Georgalis & Kear (2013) to *Testudo* cf. *marmorum*. As it has been shown by Vlachos et al. (2014) and also here, it is not possible to provide a safe estimation of the locality, but most probably this material is from Megalo Emvolon and therefore of Pliocene age.

Titanochelon schafferi **(Szalai, 1931)**

DISTRIBUTION: Samos Island (precise locality unknown).

AGE: Late Miocene.

MATERIAL (Fig. 3.31-3.33):

NHMW 2009z0103/0001, skull; NHMW 1911/0005/0275, left femur; (temp. numbers) NHMW 1911/1, distal carpal; NHMW 1911/2, phalanx; NHMW 1911/3, osteoderm.

DESCRIPTION

NHMW 2009z0103/0001 (Fig. 3.31, 3.32): This specimen corresponds to a complete skull. As it has been mentioned in Vlachos et al. (2014), the extent of the restoration is not known in this specimen. The skull is long and short, wider posteriorly. Generally, no deformation is observed in this specimen. The sutures are partially visible only on the dorsal side.

Skull roof and braincase: Anteriorly, a wide and short apertura narium externa is noted. The rim of the apertura narium externa is rounded. The skull roof elements form a triangular anterior part of the skull. The anterior part of the skull, from the postorbitals and anteriorly is located in the anterior third of the skull. The braincase elements represent the other two-thirds of the skull in dorsal view. The sutures between the cranial bones are visible mainly in the anterior part. The prefrontals are medially short and laterally long, and they form the antero-medial rim of the fossa orbitalis. Alternatively, the frontals are medially long and laterally short, and they contribute in the formation of the medial part of the rim of the fossa orbitalis. The fossa orbitalis is rounded and is located in the anterior third of the skull. The posterior part of the fossa orbitalis is made by the postorbital bone, that is short and rather flat.

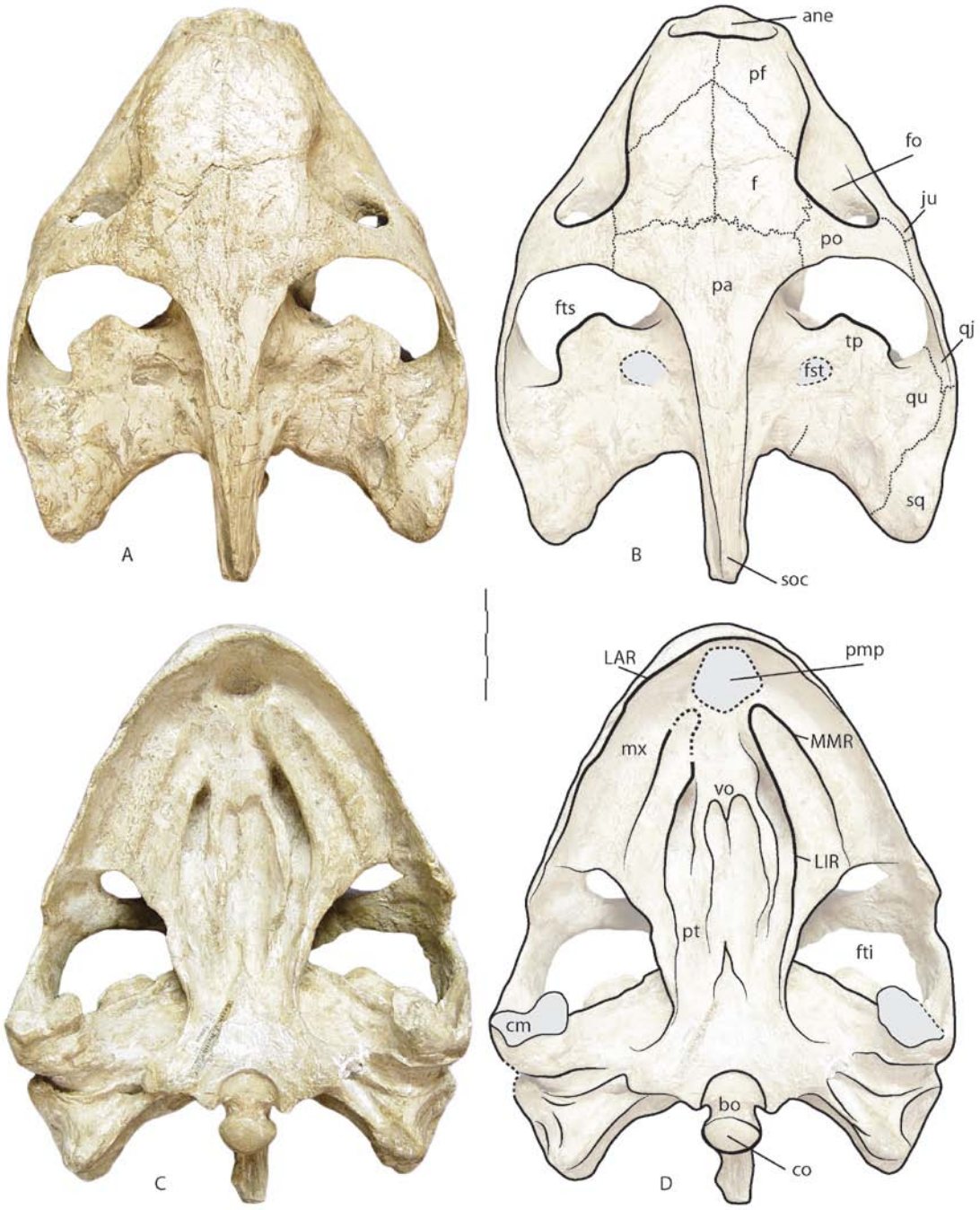


Figure 3.31. *Titanochelon schafferi* (Szalai, 1931) from the Late Miocene of Samos Island. NHMW 2009z0103/0001, the skull in (A-B) dorsal and (C-D) ventral views. Scale bar equals 5 cm. For abbreviations see Material & Methods.

In the medial part of the frontals a trasverse constriction is noted, making the prefrontals wider than the frontals. The parietals are wide, but their posterior suture with the supraoccipital is not visible. Laterally, the parietal is sutured with the thin postorbital. The supraoccipital is elongated, forming a long, and relatively straight crista supraoccipitalis that extends beyond the level of squamosals. The posterior two-thirds of the skull is marked by the presence of long and wide fossa temporalis superior that is limited medio-anteriorly by the postorbital, parietal and supraoccipital. Laterally is limited by the postorbital, the quadratojugal and the squamosal, whereas posteriorly is open. The large fossa temporalis superior is the result of the upper

temporal emargination. As far as the sutures of the braincase elements are concerned, only the limits of the right squamosal can be observed, being long and narrow, with extensive dorsal covering. Anteriorly it makes contact with the quadratojugal. The posterior tip of the squamosal is enlarged and rounded. The lateral sides of the squamosals are developed almost parallel to each other. The prootic – opisthotic area is long, and a large and wide trochlear process is formed, probably with a contribution of the quadrate. Posterior to the trochlear process a large concavity is noted that corresponds to the foramen stapedio-temporale. Laterally, a large tri-radiate zygomatic arch is formed by the postorbital dorsally, the quadratojugal posteriorly and the jugal anteriorly. The zygomatic arch is tall and thin. As a result of preservation, the sutures between these three elements are not always clear. However, we can clearly observe the suture between the postorbital with the quadratojugal. The quadratojugal is flat and forms two processes. The dorsal process extends posteriorly to reach the squamosal. The ventral process extends ventrally to reach the quadrate. On the other hand the limit between the postorbital and the jugal are not so clear. Most probably, the jugal makes contact with both the postorbital and the quadratojugal. Posteriorly, the quadrate is massive and makes contact with the quadratojugal antero-dorsally and the squamosal postero-dorsally, enclosing the otic chamber. Postero-ventrally it forms a pointed processus articularis and ventrally a strong condylus mandibularis. In the otic chamber we notice the deep antrum postoticum and a strong insisura columellae auris. Posteriorly, below the crista supraoccipitalis we notice a deep foramen magnum. Below the foramen magnum, a long, with a rounded elliptical shape, condylus occipitalis is developed. The processus paraoccipitalis is strong and contacts the squamosal. On each side of the condylus occipitalis we find two foramina, that could correspond to the foramen nervi hypoglossi and the foramen jugulare posterius, but the preservation and the lack of comparative material does not allow us to make a confident identification. The ventral part of the skull is marked by the presence of the lower temporal emargination that slightly affects the quadrate, but affects mostly the quadratojugal and the jugal. Ventrally, the sutures between the elements of the braincase are not visible.

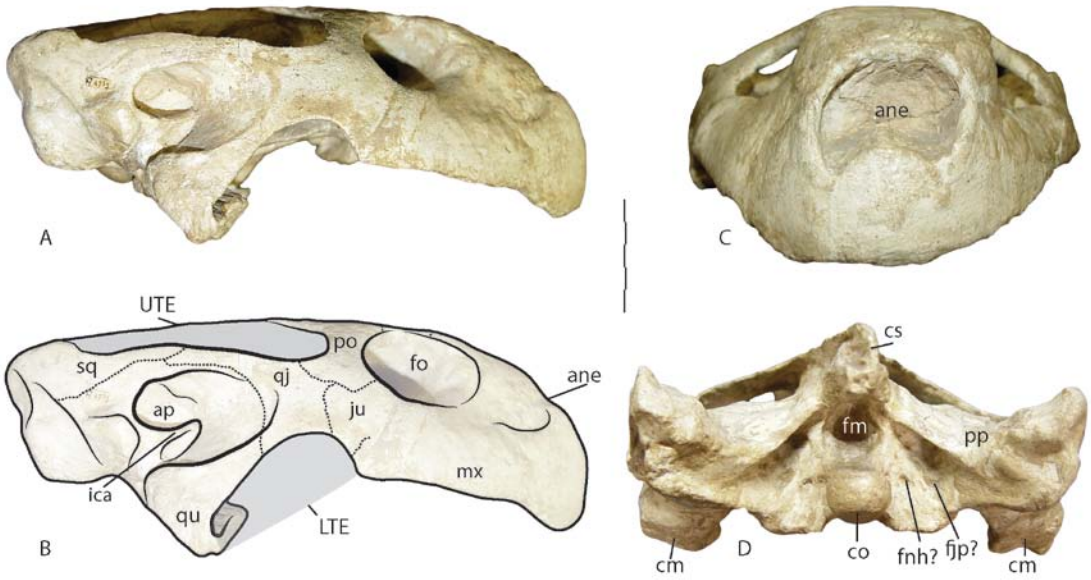


Figure 3.32. *Titanochelon schafferi* (Szalai, 1931) from the Late Miocene of Samos Island. NHMW 2009z0103/0001, the skull in (A-B) right lateral, (C) anterior and (D) posterior views. Scale bar equals 5 cm. For abbreviations see Material & Methods.

Palatal elements: The sutures between the elements of the palate and the ventral skull are not visible, therefore the position of the various elements can only be estimated. Anteriorly a deep premaxillary pit is noted. The palate is marked by the presence of well-distinct ridges. The ridges from the left side are more prominent compared to those from the left side are weak. This could be the result of differential preservation. None of the ridges shows the presence of tooth-like tubercles (sensu Gerlach, 2001). The labial ridge is strong and marks the rim of the palate, whereas is much taller compared to the rest. In the palate we notice the median maxillary ridge and the lingual ridge that are well-developed. The lingual ridge is much longer than the medial, reaching the pterygiods. Anteriorly they are connected via a round transverse ridge. The surface between the ridges is shallowly concave. Between the lingual ridge and he vomer we notice a strong groove that could lead to the apertura narium interna. The vomer develops three processes that extend posteriorly. The medial is weak, whereas the lateral are longer. Interestingly, it is not possible to observe the paired foramina praepalatinum in the anterior part of the palate. This could be either the result of preservation, or they could be concealed by the lingual extensions of the maxillary ridges (see character 28 in Gerlach, 2001). Similarly, the foramen palatinum posterius is not visible in the palate. Posterior to the palate we notice a large fossa temporalis interior.

NHMW 1911/0005/0275 (Fig. 3.33.A): This specimen corresponds to an almost complete left femur of massive size; only on part of the trochanter is missing. The femur is straight throughout the diaphysis. The proximal part is massive and wide. The trochanters are fused. The femoral head is elliptical in shape, longer than wide. Compared to the diaphysis it is oriented with a wide angle, almost perpendicular. Between the head and the trochanters, a wide and deep fossa is noted. The diaphysis is much thinner, circular to elliptical in diameter. The distal part is also wide and massive. The tibular and fibular condyles are of similar size. Posteriorly they are joined by a thin ridge, which creates a deep concavity.

NHMW 1911/1 (Fig. 3.33.B): This specimen corresponds to a complete distal carpal. It is tall and narrow. It shows a large protuberance proximally and a discoid part distally. Ventrally, there is a convex to flat surface for the metacarpals.

NHMW 1911/2 (Fig. 3.33.C): This specimen corresponds to a complete phalanx of the anterior limb, with a concave proximal surface for the metacarpal and a convex distal surface for the ungual. The proximal part of the phalanx is tall.

NHMW 1911/3 (Fig. 3.33.D): This specimen corresponds to a large osteoderm that is longer than wide, flattened and rounded.



Figure 3.33. *Titanochelon schafferi* (Szalai, 1931) from the Late Miocene of Samos Island. Appendicular elements in A, NHMW 1911/0005/0275, left femur in (A1) dorsal, (A2) posterior, (A3) ventral and (A4) anterior views. Scale bar equals 5 cm. B, distal carpal in (B1) ventral, (B2) lateral, (B3) dorsal and (B4) proximal views. C, anterior phalanx in (C1) distal, (C2) medial and (C3) lateral views. D, osteoderm in (D1) dorsal and (D2) ventral views. Scale bar equals 1 cm.

Titanochelon sp.

DISTRIBUTION: Pikermi and Liossati (Kiourka) in Attica.

AGE: Late Miocene.

MATERIAL (Fig. 3.34-3.37):
Pikermi (Late Miocene): AMPG 1871, left ulna; AMPG 2072, right ulna; AMPG 1872, left radius; AMPG 1873, ungual; AMPG PA 2935/91, ungual; AMPG 2073, ungual; AMPG 1874, ulnare?; AMPG 1875, distal carpal; AMPG 1877, phalanx; AMPG 1878, metacarpal; AMPG 1879, metacarpal; AMPG 1880, left epiplastron; AMPG 1881, peripheral; AMPG 1882, shell fragment; AMPG 1883, carapace fragment; AMPG 1884, costal fragment; AMPG 2074, distal carpal; AMPG 2075, right intermedium; AMPG 2078, metacarpal; AMPG 2079, ungual; AMPG 2077, 23+ osteoderms; AMPG PA 1851/91, phalanx; AMPG 1868/91, shell elements of a small-sized individual.

Kiourka (Late Miocene) (Fig. 3.38): AMPG 2070, several fragments of the shell of one individual.

DESCRIPTION

Pikermi

AMPG 1871 (Fig. 3.35.B): This specimen corresponds to a complete left ulna. The ulna is straight, with small curvature in the distal part. The proximal is roughly triagonal, narrow and long. The proximal articulation for the humerus is slightly concave. The distal part is narrower and longer than the proximal, showing a convex articulation surface.

AMPG 2072 (Fig. 3.35.C): This specimen corresponds to an almost complete right ulna. The ulna is straight, with small curvature in the distal part. The proximal is roughly triagonal, narrow and long. The proximal articulation for the humerus is slightly concave. The distal part is narrower and longer than the proximal, showing a convex articulation surface.

AMPG 1872 (Fig. 3.35.A): This specimen corresponds to an almost complete left radius; only the proximal part is missing. The shaft is circular in diameter, and narrow. The distal part of the radius is enlarged, being long and narrow with a convex articular surface. The articulation area with the ulna is tall. When articulated, the radius and ulna show a short, tear-shaped, fenestra between them. The distal part of the articulated radius and ulna is not straight, but leaves a broad space for the articulation of the first carpal row.

AMPG 1873 (Fig. 3.35.O): This specimen corresponds to an almost complete ungual. It is short and wide with a rounded tip. The proximal surface for the phalanx is concave. This ungual is from the anterior limb.



Figure 3.34. *Titanochelon* sp. from the Late Miocene of Pikermi (Attica). Shell elements in A-C, AMPG 1880, left epiplastron in (A) visceral and (B-C) ventral views. D-E, AMPG 1883, carapace fragment. F-G, AMPG 1881, peripheral fragment in (F) dorsal and (G) visceral views. H-I, AMPG 1882, shell fragment. J-K, AMPG 1884, costal fragment in (J) dorsal and (K) visceral views. Scale bar is 5 cm.

AMPG PA 2935/91 – 2073 (Fig. 3.35.N, P): This specimen corresponds to almost complete unguals. It is short and wide with a rounded tip. The proximal surface for the phalanx is concave. This ungual is from the anterior limb.

AMPG 1874 (Fig. 3.35.D): This specimen corresponds to a complete ulnare. It is cubic in shape, taller than wide. Proximally, the ulnare articulates with the ulna with an elongated concave surface. Medially, it articulates with the intermedium with two small and flat surfaces. Distally, it shows two slightly concave surfaces, which are developed in obtuse angle.

AMPG 1875 (Fig. 3.35.F): This specimen corresponds to a complete distal carpal. It shows a small protuberance proximally and a discoid part distally. Compared to the other distal carpal, the distal discoid part is highly asymmetric with longer medial and much shorter lateral part. Ventrally there is a convex to flat surface for the metacarpals.

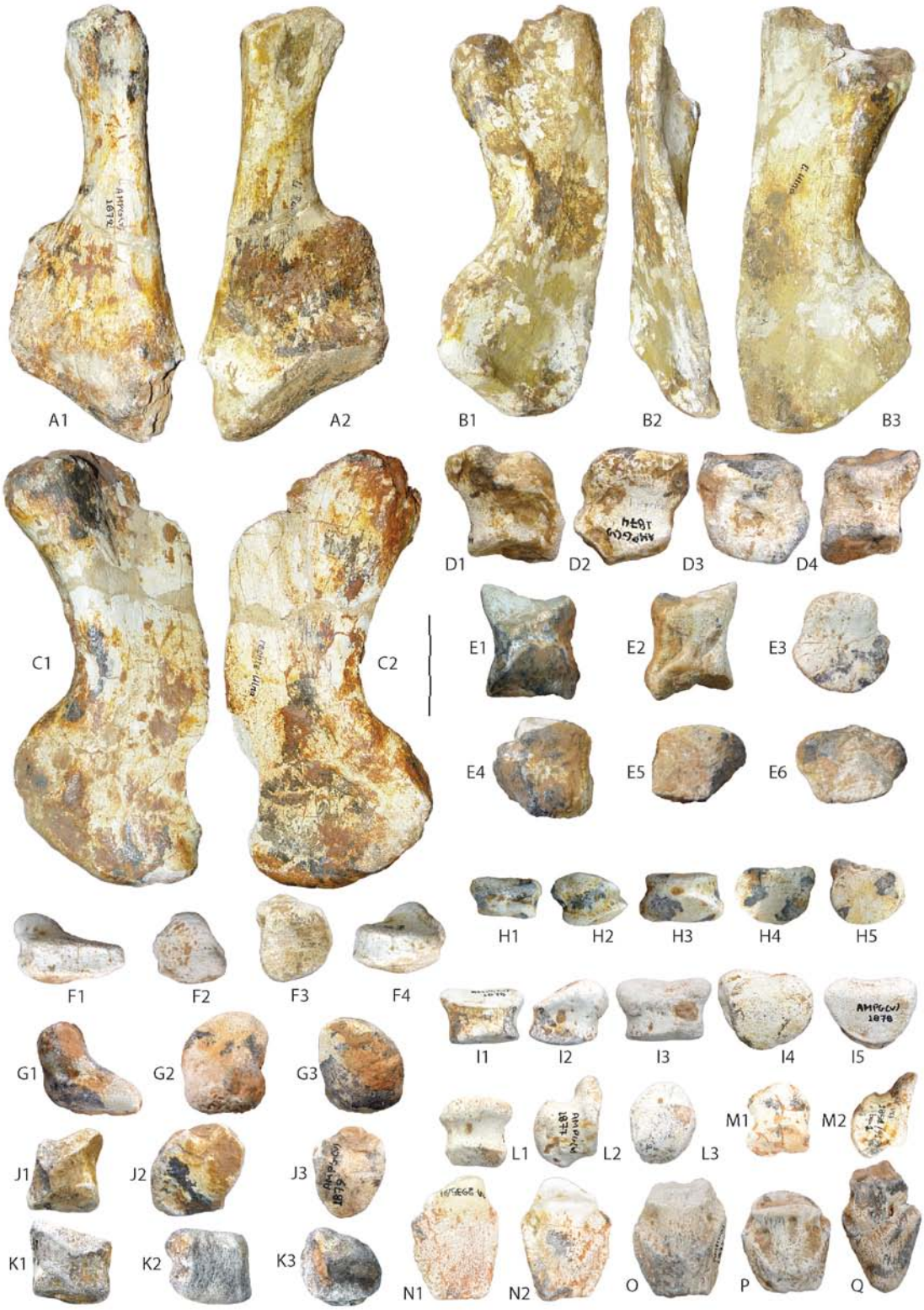


Figure 3.35. *Titanochelon* sp. from the Late Miocene of Pikermi (Attica). Appendicular elements in A, AMPG 1872, left radius in (A1) ventral and (A2) dorsal views. B, AMPG 1871, left ulna in (B1) dorsal, (B2) lateral and (B3) ventral views. C, AMPG 2072, right ulna in (C1) ventral and (C2) dorsal views. D, AMPG 1874, ulnare in (D1) medial, (D2) dorsal, (D3), ventral and (D4) lateral views. E, AMPG 2075, right intermedium in (E1) medial, (E2) lateral, (E3) dorsal, (E4) ventral, (E5) proximal and (E6) distal views. F, AMPG 1875, distal carpal in (F1) dorsal, (F2) proximal, (F3) distal and (F4) lateral views. G, AMPG 2074, distal carpal in (G1) lateral, (G2) proximal and (G3) distal views. H, AMPG 2076, metacarpal in

(H1) ventral, (H2) medial, (H3) dorsal, (H4) distal and (H5) proximal views. I, AMPG 1878, metacarpal in (I1) ventral, (I2) medial, (I3) dorsal, (I4) distal and (I5) proximal views. J, AMPG 1878, metacarpal in (J1) medial, (J2) proximal and (J3) distal views. K, AMPG 2078, metacarpal in (K1) medial, (K2) lateral and (K3) distal views. L, AMPG 1877, phalanx in (L1) dorsal, (L2) lateral and (L3) distal views. M, AMPG PA 1851/91, phalanx in (M1) dorsal and (M2) lateral views. N, AMPG PA 2935/91, ungual in (N1) dorsal and (N2) ventral views. O, AMPG 1873, ungual in ventral view. P, AMPG 2073, ungual in ventral view. Q, AMPG 2079, ungual in ventral view. Scale bar equals 5 cm.

AMPG 1877 (Fig. 3.35.L): This specimen corresponds to a complete phalanx of the anterior limb, with a concave proximal surface for the metacarpal and a convex distal surface for the ungual.

AMPG 1878 – 1879 (Fig. 3.35.I-J): This specimen corresponds to a complete metacarpal. It shows a convex surface proximally for the distal carpals and a distal convex surface for the first phalanx.

AMPG 1880 (Fig. 3.34.A-C): This specimen corresponds to an almost complete left epiplastron, with only a small part of the antero-medial border missing. The epiplastron is long and wide. Viscerally, the epiplastra are thickened, forming a long slightly convex epiplastral lip, without any gular pocket. Ventrally, the gulars are narrow and long, overlapping the anterior part of the entoplastron. The gularo-humeral sulcus is nearly straight and causes a constriction in the epiplastra. Therefore, the anterior part of the epiplastra is protruded anteriorly.

AMPG 1881 (Fig. 3.34.F-G): This specimen corresponds to a peripheral. The marginal sulci are partially visible as a result of erosion. The peripheral is moderately flared.

AMPG 1882 (Fig. 3.34.H-I): This specimen corresponds to a fragment of the shell. Further description is not possible.

AMPG 1883 (Fig. 3.34.D-E): This specimen corresponds to a fragment of the carapace. Further description is not possible.

AMPG 1884 (Fig. 3.34.J-K): This specimen corresponds to medial and lateral part of a costal. No sulci are observed dorsally. The inserted rib is noted viscerally.

AMPG 2074 (Fig. 3.35.G): This specimen corresponds to a complete distal carpal. It is tall and narrow. It shows a large protuberance proximally and a discoid part distally. Ventrally, there is a convex to flat surface for the metacarpals.

AMPG 2075 (Fig. 3.35.E): This specimen corresponds to a complete right intermedium. It shows a triagonal cross–section. Proximally, it shows a concave articular surface for the ulna. Proximo-medially it shows a slightly concave surface for the radius. Distally it shows a concave surface for the centrales.

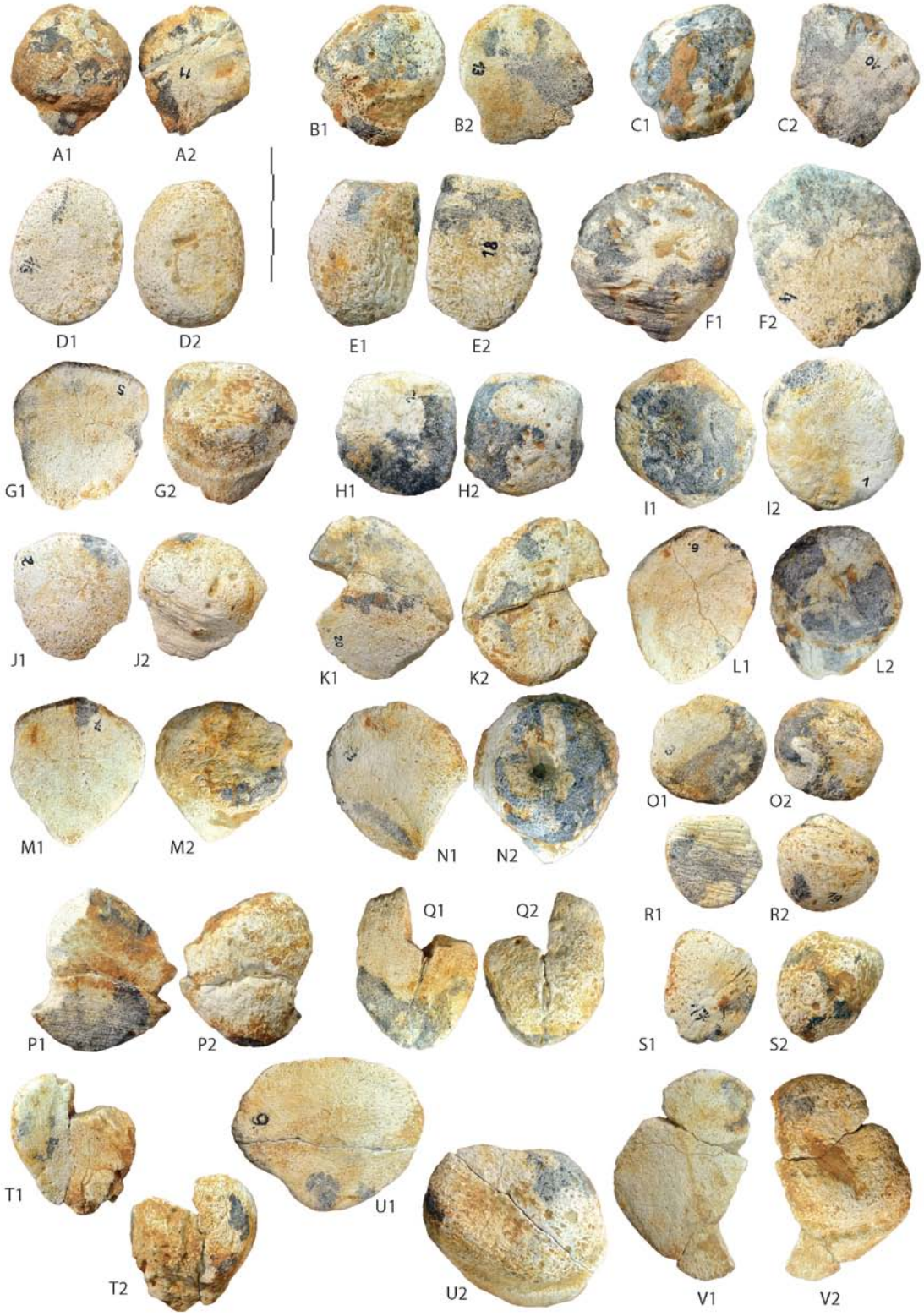


Figure 3.36. *Titanochelon* sp. from the Late Miocene of Pikermi (Attica). A-V, AMPG 2077, Osteoderms in various views. Scale bar equals 5 cm.

AMPG 2076 (Fig. 3.35.H): This specimen corresponds to a complete metacarpal. It shows a convex surface proximally for the distal carpals and a distal convex surface for the first phalanx.

AMPG 2077: Several osteoderms are known from Pikermi. They are all large in size and flattened. Two types of osteoderms are noted, half-pointed osteoderms (e.g. Fig. 3.36.J, U) or rounded ones (Fig.3.36.O-P).

AMPG PA 1851/91 (Fig. 3.35.M): This specimen corresponds to a complete phalanx.

Comment: The above mentioned material from Pikermi is of similar size, morphology and type of fossilization. Since it does not preserve overlapping parts of the skeleton, it could belong to the same individual of a giant tortoise.

AMPG 1868/91 (Fig.3.37): This specimen consists of various shell elements that belong to the same individual. Based on the size and the thickness of the plates we can estimate that they belong to a small-sized, young, individual. Two fragments from the carapace are of particular size to allow further detailed description, whereas the rest are small fragments of the same carapace that we cannot find any connections.

The first fragment corresponds to a part of the neural series. Viscerally, the attachments for the vertebra are visible in most preserved plates. From the first plate, only the posterior part is preserved. This part shows no vertebra attachments viscerally. Therefore, this part could be the posterior part of a nuchal plate. This is in accordance with the configuration of the remaining neural plates. Posterior to the nuchal, parts of the first four neurals are noted. From the neural 1 the middle part is preserved. The plate appears to be longer than wide, having a concave anterior border for the nuchal. It is crossed transversely by the vertebral sulcus. The neural 2 preserves the middle and right part. It is octagonal in shape, having a concave anterior and nearly straight posterior border. It is wider than long. The neural 3 preserves also the middle and right part. It is quadrangular with rounded edges, wider than long. It is crossed transversely by the vertebral sulcus, which is anteriorly convex in the middle. The neural 4 preserves only the anterior part, but most probably is octagonal. The medial parts of the costals 2-4 are preserved. As we can infer from the shape of costal 3, the costals showed the alternating pattern of costals medially short with one sutured area alternated with costals medially long with three sutured areas. This alternating pattern corresponds to the quadrangular/octagonal neurals.

The second fragment corresponds to a part of the carapacial margin, showing four consecutive peripherals. The margin is thickened, and the peripherals are only slightly flared. They are crossed by the marginal sulci. There is good coincidence between the costo-peripheral sutures and the pleuro-marginal sulci.

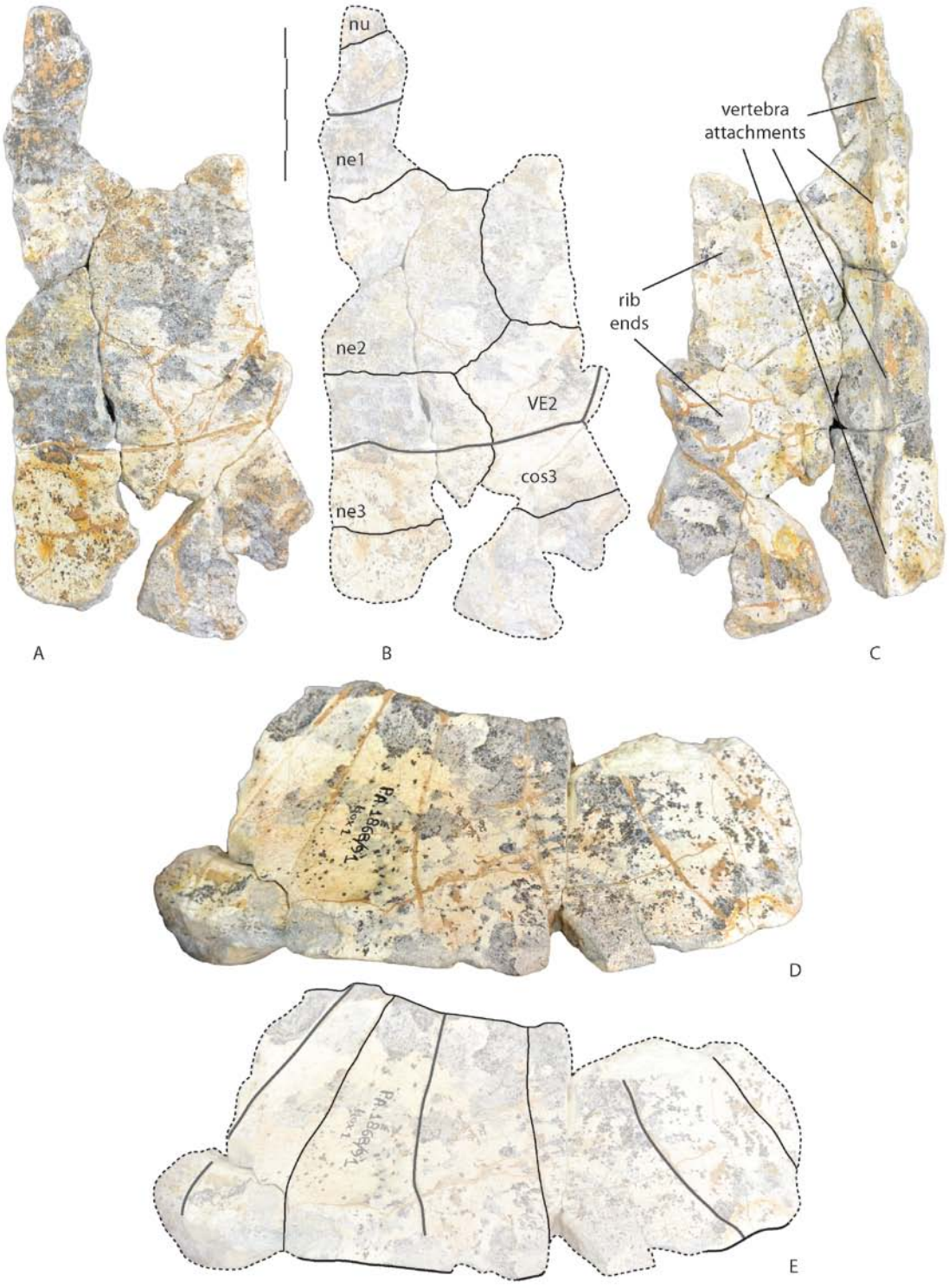


Figure 3.37. *Titanochelon* sp. from the Late Miocene of Pikermi (Attica). AMPG 1868/91, shell material of a juvenile individual in A-C, fragment of the dorsal carapace in (A-B) dorsal and (C) visceral views. D-E, part of the posterior peripheral rim. Scale bar equals 5 cm. For abbreviations see Material & Methods.

Kiourka (Liossati, Attica)

The material from the Late Miocene locality of Kiourka (or Liossati), near Pikermi in Attica is highly fragmented (Fig. 3.38). Despite my efforts and the efforts of the stuff of AMPG is not possible to connect the numerous shell fragments in a way that would allow any description. The specimens correspond probably to the same individual of medium-size, which could reach one meter in length. Several specimens preserve sutures and sulci but they are too few to allow a clear identification. Some specimens are more complete. A complete peripheral is preserved (Fig. 3.38.A), being medially short and laterally long. A part of the epiplastron (Fig. 3.38.B) preserves some of the sulci covering the epiplastral lip. Also a part of the hyoplastron is identified (Fig. 3.38C). Some caudal vertebrae are recovered (e.g. Fig. 3.38.D), preserving mainly the centrum and missing the transversal processes.

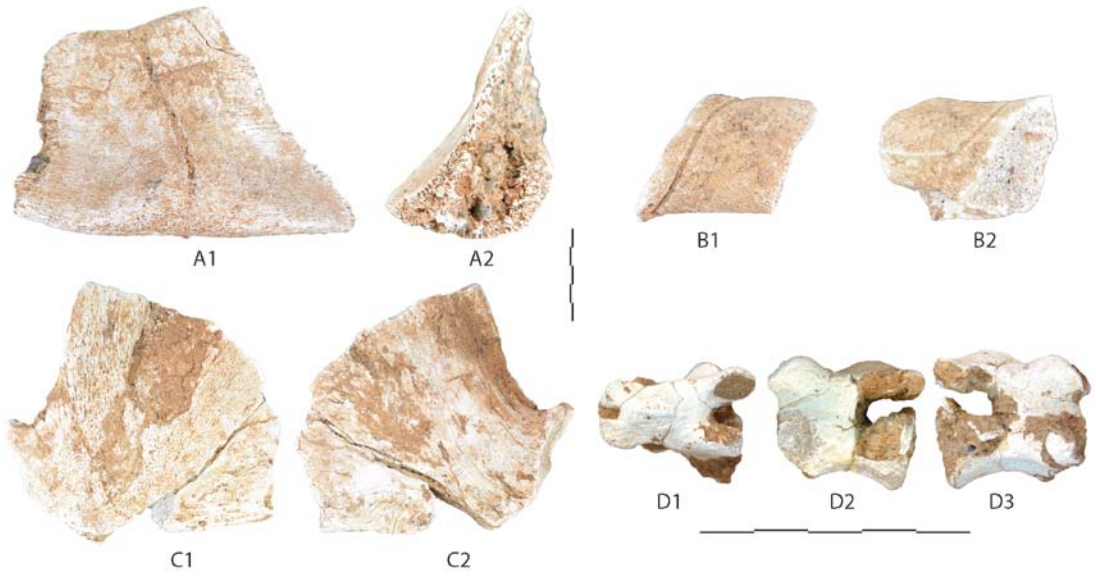


Figure 3.38. *Titanochelon* sp. from the Late Miocene of Kiourka (Liossati), near Pikermi (Attica). AMPG 2070: A, peripheral plate in (A1) dorsal and (A2) lateral views. B, plastron fragment. C, hyoplastron fragment in (C1) ventral and (C2) visceral views. D, caudal vertebra in (D1) dorsal, (D2) left lateral and (D3) right lateral views. Scale bar equals 5 cm.

COMMENTS: The presence of a giant tortoise in the Late Miocene site of Pikermi was first reported by Bachmayer (1967), who presented few fragments from the shell, limb bones and osteoderms. All these specimens, as well as several others not presented by Bachmayer (1967), have been revised and described here in detail. For example, the specimen AMPG 1880 was reported by Bachmayer (1967) as parts of the costals 7 and 8. Here we show that this specimen corresponds actually in the left epiplastron. Few years later, Bachmayer & Symeonidis (1977) reported another finding of a giant tortoise from the locality Kiourka (or Liossati), close to Pikermi. This fragmented specimen is also analyzed here. At the same time, new important specimens from Pikermi are presented. For example, the specimen AMPG 1868/91, which was discovered and preserved in excellent condition by S. Roussiakis (AMPG), shows the only known example of the neural series of a giant tortoise from Greece. All this new and updated information, aided by the knowledge on comparative material from Greece which is now available, allows us to update the taxonomic status of the large testudinid from Pikermi.

Bachmayer (1967) attributed the specimens to *Testudo* cf. *schafferi* but without any morphological evidence, since the material from Pikermi is not comparable with the known material from Samos. Lapparent de Broin (2002) also lists this as cf. *Cheirogaster* cf. *schafferi* (or as ?*Cheirogaster* cf. *schafferi* in Lapparent de Broin, 2001). However, even with the updated information presented here is not possible to find comparable preserved parts between the Samos and the Pikermi material. The only exceptions are the new carpal elements reported from Samos, i.e. the distal carpal and the phalanx. Similar elements exist in Pikermi. Also similar in size, the Samos elements are always taller and narrower than those from Pikermi. However, such elements are not enough to form the basis of a taxonomic distinction but they show however some differences between the material from Pikermi and Samos. The Samos material on the other hand is clearly distinguished by comparable fossils in Thessaloniki area, from localities like Salonique (sensu Arambourg & Piveteau, 1929) or Epanomi, Nea Michaniona and Nea Kallikratia in western Chalkidiki. These differences have been first reported by Vlachos et al. (2014) and are further supported here. It seems likely that the Samos large testudinid is more related with Minor Asia, than with the South Balkans area. Based on all the above, and on all the available fossils, we suggest that a relationship between the Pikermi and Samos large testudinids should not be continued unless new findings with comparable parts show this similarity.

Leaving the obvious difference in size aside, the Pikermi form is also different from *Ti. bacharidisi*. The epiplastron from Pikermi shows a shallow epiplastral excavation and a narrowing of the anterior lobe at gularo-humeral sulcus, causing a protrusion of the epiplastral lip. This protrusion is missing in *Ti. bacharidisi*. The preserved sulci show that the anterior part of the entoplastron was overlapped by the gulars. The entoplastron of *Ti. bacharidisi* however is covered only by the humerals. The radius from Pikermi is more robust, showing a large and wide distal part. At the same time, the distal articulation with the ulna in the Pikermi form is much taller than in *Ti. bacharidisi*. The Pikermi intermedium (AMPG 2075) is quite large, almost cubic, with an angular articular surface for the medial and lateral centrale, whereas it is triangular with rounded articular surface for the fused medial and lateral centrale in *Ti. bacharidisi*. The distal carpals of Pikermi are taller and much narrower than in *Ti. bacharidisi*. Based on the few available comparable skeletal elements we can infer that the morphology of the anterior limb of the Pikermi form was different from the Pliocene form *Ti. bacharidisi*. The differences in the morphology of the epiplastra are even greater between the two forms.

Summarizing, there is no sufficient evidence to relate the Pikermi form with the *Ti. schafferi* from Samos, and at the same time the Pikermi specimens are different from the comparable parts in *Ti. bacharidisi*. However, due to the limited information on the shell is not possible to identify the Pikermi form in the species level. Therefore, it is identified as *Titanochelon* sp..

Titanochelon sp.

In this section we describe several isolated specimens from various localities in Greece. This material is scarce and the information is limited. Although the taxonomic identification is only up to the generic level, these findings are important because indicate the presence of large testudinids in new localities.

MATERIAL:

Vatera, Lesvos Island (Early Pleistocene; 9 specimens): PO 067 F, phalanx; PO 071 F, osteoderm; PO 073 F, osteoderm; PO 127, osteoderm; PO 176 F, phalanx; PO 184 F, left tibia; PO 186 F, left femur; PO 188 F, phalanx; PO 254 F, osteoderm.

Milia, Grevena, W. Macedonia (Late Pliocene; 2 specimens) (Fig. 3.39): MIL 1511, right coracoid fragment; MIL 1834, possible rounded osteoderm.

Kryopigi, Kassandra peninsula, Chalkidiki (Middle-Late Turolian, MN12-13, Late Miocene; 3 specimens) (Fig. 3.40): LGPUT KRY 4206, tibia fragment; LGPUT KRY 4481, half-pointed osteoderm; LGPUT KRY 4430, half-pointed osteoderm.

Fourka, Kassandra peninsula, Chalkidiki (Late Miocene; 1 specimen) (Fig. 3.40): LGPUT FRK 26, fragment of plastral lobe.

DESCRIPTION

Vatera, Lesvos Island

The large testudinid material from Vatera is limited and preserves only few elements from the appendicular skeleton. The left partial femur preserves only the diaphysis, and it appears to be rather straight with a curvature distally. The left tibia preserves only the middle and distal part. A lateral tuberosity is seen on the distal part, and the distal articulation is double for the fused astragalo-calcaneum. From the carpal one possible ulnare is preserved. It is cubic in shape, taller than wide. Proximally, the ulnare articulates with the ulna with an elongated concave surface. Medially, it articulates with the intermedium with two small and flat surfaces. Distally, it shows two nearly straight surfaces, which are developed in wide angle between them. Several unguals and osteoderms are also present. One of the osteoderms is enlarged, conical in shape and with a pointed tip, resembling a thigh bony tubercle.

Based on the available material is difficult to find the affinities of these specimen. Lapparent de Broin (2002) identified this as cf. *Cheirogaster* aff. *schafferi*, given the few similarities in the femur, the similar inferred size and the geographic proximity with the Samos form. The comparable element with the Pikermi form is the ulnare being slightly different in the Lesvos form, in being more asymmetric, showing different proximal and distal articular surfaces. However, all the preserved elements barely preserve any diagnostic features to allow attribution to one or another taxon. Therefore, based on the available information the large testudinid from Lesvos can only be identified as *Titanochelon* sp.

Milia, Grevena, W. Macedonia

MIL 1511 (Fig. 3.39): This specimen corresponds to the proximal part of the right coracoid. It is large and wide, triagonal in cross-section, and it shows a shallowly concave articular surface for the humeral head, whereas the symphyseal area with the scapula is broken. The coracoid shows a narrow and long neck, leading to the medial part of the bone, which is flattened and with elliptical cross-section.

MIL 1834: This specimen corresponds to a fragment of a porous, flat and rounded element. Based on the available material and the structure of the broken inner surface, this specimen could be a rounded osteoderm of a giant tortoise.

Comment: The material from the Late Pliocene site of Milia is too scarce to allow a confident identification. It indicates, however, the presence of large testudinids in Western Macedonia for the first time. The size and morphology of the preserved coracoid is similar to that of the Pliocene species *Ti. bacharidisi*, present in northern Greece.



Figure 3.39. *Titanochelon* sp. from the Late Pliocene of Milia (Grevena). Right coracoid in (A) dorsal, (B) anterior, (C) ventral, (D) posterior views and (E) detail of the articulation. Scale bar equals 5 cm.

Kryopigi, Kassandra peninsula, Chalkidiki

LGPUT KRY 4206 (Fig. 3.40.A): This specimen corresponds to the proximal and medial part of a tibia. The specimen is eroded. The proximal part is wide, with triagonal cross-section and a significant cnemial crest. The diaphysis of the bone is slightly curved.

LGPUT KRY 4481 (Fig. 3.40.B): This specimen corresponds to a complete half-pointed osteoderm. It is long and narrow, relatively flattened. Anteriorly, the pointed surface is short.

LGPUT KRY 4430 (Fig. 3.40.C): This specimen corresponds to a complete half-pointed osteoderm. It is short and wide, relatively flattened. Anteriorly, the pointed surface is short.

COMMENT: Although the preserved material from Kryopigi is rather scarce, this is the first confirmed record of a giant tortoise from Kassandra peninsula. These specimens expand the presence of giant tortoises in Chalkidiki to the Miocene. Up to

now, giant tortoises were known from the Pliocene of western Chalkidiki. Compared to the known osteoderms of the Pliocene *Ti. bacharidisi*, the osteoderms from Kryopigi are much larger, indicating a larger individual than the appr. 120 cm long *Ti. bacharidisi*.

Fourka, Kassandra peninsula, Chalkidiki

LGPUT FRK 26 (Fig. 3.40.D): This specimen corresponds to a fragment of the lip of a plastral lobe, most probably from the anterior one. Although the material is extremely poor, it confirms the presence of large testudinids in the Late Miocene of Kassandra peninsula.

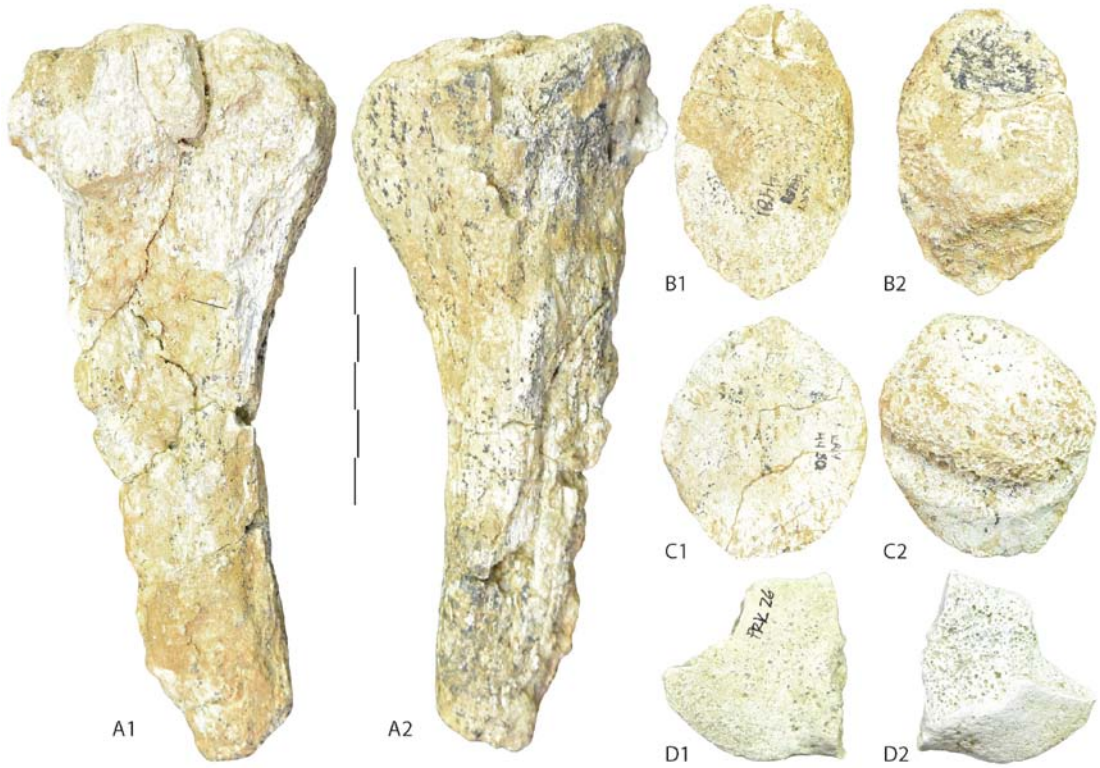


Figure 3.40. *Titanochelon* sp. from the Late Miocene of Kassandra peninsula (Chalkidiki, Thessaloniki). Kryopigi: A, LGPUT KRY 4206, tibia in (A1) dorsal and (A2) ventral views. B, LGPUT KRY 4481, half-pointed osteoderm in (B1) dorsal and (B2) ventral views. C, LGPUT KRY 4430, half-pointed osteoderm in (C1) dorsal and (C2) ventral views. Fourka: D, LGPUT FRK 26, fragment of epiplastral lip in (D1) ventral and (D2) visceral views. Scale bar equals 5 cm.

DISCUSSION

Fossils of large testudinids are relatively abundant in the Neogene fossil record of Greece. In the late Miocene the presence of giant tortoises of the genus *Titanochelon* is established in Pikermi, Samos, and Kassandra peninsula. The Pliocene localities are larger in number, preserving several specimens. Most of the localities are found near Thessaloniki, in Western Chalkidiki peninsula, with Epanomi, Aggelochori/Megalo Emvolon, Nea Michaniona and Nea Kallikratia, with further specimens from Milia and Apolakkia. Uncertainty surrounds both the stratigraphic provenance and the geological age of the "Salonique" material of Arambourg & Piveteau (1929) as it has been explained above. Most probably this material comes from the Pliocene of Megalo Emvolon (Karabouroun) but more evidence is needed for clear conclusion. Undescribed specimens are also mentioned in Makrygialos (Sylvestrou, 2002). The latest occurrence of a giant tortoise in Greece is from the Early Pleistocene of Lesvos Island, from Vatera locality. At least two species are represented in the fossil material from Greece, *Titanochelon bacharidisi* from the Pliocene and *Titanochelon schafferi* from the Late Miocene, based on the current known distribution.

The Pliocene *Ti. bacharidisi* has been originally described in Vlachos et al. (2014) from Epanomi, Nea Michaniona and Nea Kallikratia (near Thessaloniki). Its presence on these localities has been further confirmed with new specimens presented here. Also, this species is present in Aggelochori/Megalo Emvolon based on the specimens presented here. Also, most probably the "Salonique" material of Arambourg & Piveteau (1929), regardless its provenance and age, could be referred to this species as well. Outside Greece, the Late Pliocene material from Tenevo, Bulgaria (Boev, 2008; Stoyanov, 2009) can be also attributed to *Ti. bacharidisi*. This species presents a peculiar morphology of the lower temporal emargination in the skull of the holotype that needs to be confirmed by further specimens. It preserves fossil material of several individuals preserving nearly the entire skeleton and information on sexual dimorphism and intraspecific variation, that allows a detailed comparison with known European large testudinids.

The cranium of *Ti. bacharidisi* differs from the cranium of *Ti. schafferi* in several aspects. *Titanochelon bacharidisi* shows a curved crista supraoccipitalis that is bended inwards, short and thick zygomatic elements, as well as long and pointed squamosals that extend beyond the level of condylus occipitalis. The position of the orbits, relative to the entire length, are anteriorly placed in the Samos species, compared to the posterior placement in *Ti. bacharidisi*. The cranium of *Ti. schafferi*, shows a lesser degree of both upper and lower temporal emargination. It should be noted that the Samos cranium is partially restored. Since the precise extent of the restoration is not known, the morphological comparisons with this specimen are incomplete. Also, the distal femur from Samos is almost straight, unlike the curved distal part of the femur of *Ti. bacharidisi*.

Among the various *Titanochelon* spp., *Titanochelon perpiniana* from the Early Pliocene of Perpignan (France; see Bourgat & Bour, 1983 and references therein) is perhaps the closest in morphology with *Ti. bacharidisi*. Both species show an entoplastron that is not covered by the gular scutes, but in *Ti. perpiniana* the humerals are expanded on the medial part of the epiplastra. In constrast, the gulars of *Ti. bacharidisi* are touching medially the anterior part of the entoplastron, and the humerals cover only the entoplastron medially. The skull of *Ti. perpiniana* is different from *Ti. bacharidisi* in the position of the orbits, being placed more anteriorly and in

02/16/2016 Ψηφιακή Βιβλιοθήκη Θεόφραστος - Τμήμα Γεωλογίας - Α.Π.Θ.

the relative proportions of the cranium. The preserved part of the crista supraoccipitalis is straight, whereas the posterior tips of the squamosals are slightly converging, but not to the degree seen in *Ti. bacharidisi*. They are also thick and rounded, thus differing from the thin and pointed squamosals of *Ti. bacharidisi*. The lower temporal emargination in *Ti. perpiniana* is less emarginated than in *Ti. bacharidisi*. The plastron of *Ti. perpiniana* is similar in length with that of *Ti. bacharidisi*, but the anterior and posterior lobes are relatively longer in *Ti. perpiniana*. The epiplastral lip projects anteriorly, with a shallow pocket, that exhibits the step-like morphology of EPN II but differs from the female EPN I, which exhibits a more pronounced gular pocket. The posterior lobe of the plastron is similar to that of EPN I, differing only in the anal notch which is deeper and wider in *Ti. perpiniana*. Differences also occur in the post-cranial elements, such as the coracoid being polygonal-shaped in the Perpignan form, whereas it is fan-shaped in *Ti. bacharidisi*. Finally, the femur is straighter in *Ti. perpiniana* than in *Ti. bacharidisi*.

Compared to the Middle Miocene Swiss taxon, *Ti. vitodurana* (Winterthur and Zurich, Switzerland; see Biedermann, 1862 and Peyer, 1946), *Ti. bacharidisi* differs mainly in the plastron morphology, since in *Ti. vitodurana* the anterior part of the entoplastron is overlapped by the gular scutes. In general, *Ti. vitodurana* shows several similarities with the Spanish taxon, *Ti. bolivari.*

The Miocene Spanich taxon *Titanochelon bolivari* (see Pérez-García & Vlachos, 2014 and references therein) is quite different from *Ti. bacharidisi* both in the shell morphology, as well as in the shape of the appendicular elements. The entoplastron of *Ti. bacharidisi* is covered only by the humeral scutes, with its anterior end contacting the gulars and the posterior end contacting the humero–pectoral sulcus, whereas in *Ti. bolivari* the anterior part of the entoplastron is overlapped by the gular scutes. Also, the anal scutes of the female individuals of *Ti. bolivari* show the typical omega-shape, a condition not observed in *Ti. bacharidisi*. The cranium from Epanomi is also quite different from *Ti. bolivari* in the posteriorly positioned orbits, the pointed squamosals that project beyond the condylus occipitalis, the bended crista supraoccipitalis and the extend upper and lower temporal emarginations. Further differences are found in the appendicular elements. The angles between scapula, acromion and coracoid of *Ti. bolivari* are similar with *Ti. bacharidisi*, but the coracoid of *Ti. bacharidisi* is much more robust and the distal end of this element is much narrower compared to *Ti. bolivari*. The coracoid of *Ti. bolivari* shows a much longer neck as well. All the differences on the asymmetrical articulation of the humerus, radius and ulna, clearly distinguish the anterior limb of *Ti. bolivari* from *Ti. bacharidisi*. The intermedium of *Ti. bolivari* is similar with the intermedium of *Ti. bacharidisi* in shape and morphology, especially due to the triagonal cross–section. However, the articular surface in the medial side in *Ti. bolivari* makes contact with the radius, while in *Ti. bacharidisi* it articulates entirely with the fused medial and lateral centrale. This difference is because of the fusion of centrales in *Ti. bacharidisi*. The lateral centrale of *Ti. bolivari* is significantly different from that of *Ti. bacharidisi*. In *Ti. bacharidisi* the lateral centrale is fused with the medial, and shows a slightly concave distal articular surface. Similarly, the medial centrale is also different. Moreover, both dorsal and ventral articular surfaces are convex in *Ti. bacharidisi*. Finally, the distal carpals of *Ti. bolivari* are different from the distal carpals of *Ti. bacharidisi* in the morphology of the proximal part. In *Ti. bacharidisi* they are almost symmetric, quadrangular in shape, contrarily to those of *Ti. bolivari*. The *Ti. bolivari* femur is straighter compared to the femur of *Ti. bacharidisi*, that shows also a curvature in the distal part. Moreover, the ridge that

connects the tibial and fibular condyles is weak in *Ti. bolivari*, contrary to the more prominent ridge in *Ti. bacharidisi* which creates a deep concavity. The femoral head of *Ti. bolivari* is developed with a wide angle with the diaphysis (about 140º). On the other hand, the femur of *Ti. bacharidisi* shows a femoral head developed almost perpendicular to the diaphysis. The astragalocalcaneum of *Ti. bolivari* is significantly different from that of *Ti. bacharidisi*. In *Ti. bacharidisi* there is a significant constriction in the symphysis and the suture is clearly visible. Moreover, the *Ti. bolivari* astragalocalcaneum is proportionally different, being much narrower and more elongated than that of *Ti. bacharidisi*. The distal part is also different. In *Ti. bacharidisi* there is only one broad articular surface for the distal tarsals, while in *Ti. bolivari* we find a much more complex morphology with a combination of convex and concave surfaces.

The Sandelzhausen tortoise (Middle Miocene; Schleich, 1981) is different from *Ti. bacharidisi* in having a significant gular projection of the epiplastral lip (ca. 190 mm), the presence of a very deep epiplastral excavation, and an almost flat dorsal surface of the epiplastral lip. The posterior lobe has posteriorly converging borders and a very weak (almost nonexistent) anal notch. The preserved limbs are morphologically similar to *Ch. bacharidisi*, although proportionally smaller in size; the only significant difference is in the fused astragalo-calcaneum, which does not preserve the suture in the Sandelzhausen tortoise.

Contrary to the condition seen in the Pikermi large testudinid, *Ti. bacharidisi* differs in the gulars not overlapping the entoplastron, contrary to the condition seen in the Pikermi taxon. The radius from Pikermi is more robust and shows a taller contact with the ulna, and the ulna is much thinner and straighter than in *Ti. bacharidisi.* The intermedium from Pikermi is more robust, and quadrangular in cross-section. The distal carpals are thinner and longer.

The Samos giant tortoise, *Ti. schafferi*, preserves only a cranium and a femur for comparison, but these elements show significant differences from *Ti. bacharidisi.* The skull of *Ti. schafferi* shows a straight crista supraoccipitalis, high and thin zygomatic elements in a ‘T’ shape, and nearly parallel squamosals. In this specimen, the lower temporal area is less emarginated, in contrast with the EPN I cranium, where the ventral reduction of cranial bones is extensive. Also, the position of the orbits is different in the Samos specimen, in which they are located more anteriorly. Another difference is in the squamosal area. The squamosals of the Samos specimen are rounded, not pointed, and less extended. Also, the width of the posterior tips of squamosals compared to the maximum width is longer than in *Ti. bacharidisi*. Another difference is seen in the distal femur from Samos (NHMW 1911/0005/0275) which is straight without curvature, unlike the curved distal femur of *Ti. bacharidisi*. Vlachos et al. (2014) have argued that the differences between the two taxa could be explained by the separation of the southern Balkans (*Ti. bacharidisi*) and Asia Minor (*Ti. schafferi*) during most of the Neogene.

The cranium of *Ti. schafferi* shows the cranial characters of *Titanochelon* in the shape of frontals/prefrontals and in the palatal area, but certainly shell material is needed in order to fully document the morphology of this taxon and highlight its differences with the remaining European large testudinids. Crucial to the discussion surrounding *Ti. schafferi,* is the description of more material from the Late Miocene of mainland Greece. For example, the Pikermi form as it has been explained before, does not preserve comparable elements with the Samos form, but is certainly different from *Ti. bacharidisi*. Hopefully, the description of new material in the future will allow a better estimation of the diversity of the Greek large tortoises in the Neogene.

TESTUDO Linnaeus, 1758 sensu lato or *PANTESTUDO* (sensu Parham et al. 2006)

Testudo is an iconic name, first named by Linnaeus (1758) and since then it dominates the chelonian literature. One of the open debates for example, refers on whether is possible to use *Testudo* as the name of both the family *Testudinidae* and the order Testudines (see Dubois & Bour, 2010 and references therein). Parham et al. (2006) have converted the ICZN genus name *Testudo* into a phylogenetically defined clade name as "the crown clade arising from the last common ancestor of *Testudo graeca* Linnaeus, 1758; *Testudo marginata* Schoepff, 1792; and *Testudo kleinmanni* Lortet, 1883". See the phylogenetic analysis (next chapter) for further information.

'Testudo' hermanni Gmelin, 1789

Recently, Lapparent de Broin et al. (2006a, b, c) proposed *Eurotestudo* Lapparent de Broin et al., 2006a as a new genus name for the *hermanni* group. This new genus has been demonstrated by a detailed morphological description and a cladistic analysis. The *hermanni* group represents a clade with a sister-group relationship with the *graeca-marginata* clade. Genetic analyses (Fritz & Bininda-Emmonds, 2007) however, do not support the distinction of the genus *Eurotestudo*, and *T. hermanni* is included in the genus *Testudo*, along with *T. boettgeri, T. graeca, T. marginata* and *T. kleinmanni*. Although the morphological evidence presented by Lapparent de Broin et al. (2006a, b, c) is convincing and particularly useful in fossil specimens, due to the lack of a genetic support the use of '*Testudo*' will be continued for '*T*'. *hermanni* (see Chapter 4 for further comments on the taxonomy). Fritz et al. (2006) have presented the range phylogeography of '*T*'. *hermanni*, showing that in eastern Mediterranean and in Balkans the subspecies '*T*'. *hermanni boettgeri* occurs. Since most of the differences between '*T*'. *h. hermanni* and '*T*'. *h. boettgeri* are found in coloration, it is not possible to distinguish the subspecies in the extinct specimens presented in this study.

DIAGNOSIS (based on Lapparent de Broin, 2006a and Amiranashvili, 2000): narrowed vertebral series, narrower than the costal series as a whole; fusion of the suprapygals into a trapezoid with a straight posterior border; the quadrangular pygal becomes hexagonal with small latero-anterior sides and which are sometimes covered by the 11th marginals; tendency in having a divided supracaudal, externally and eventually internally; ventral surface of the gulars, making a posteriorly pointed triangle, frequently ventrally in relief relative to horizontal plan; hypo-xiphiplastral suture distant from the corner of the inguinal notch; medial length of xiphiplastron less than maximal width (in females), or nearly half the maximal width (in males).

AGE: Recent – Pleistocene.

MATERIAL: Chalkidiki (1 specimen) (Fig. 3.41): LGPUT MP 40, an almost complete shell. The specimen comes from the Pleistocene of Chalkidiki peninsula, but a precise locality is unknown.

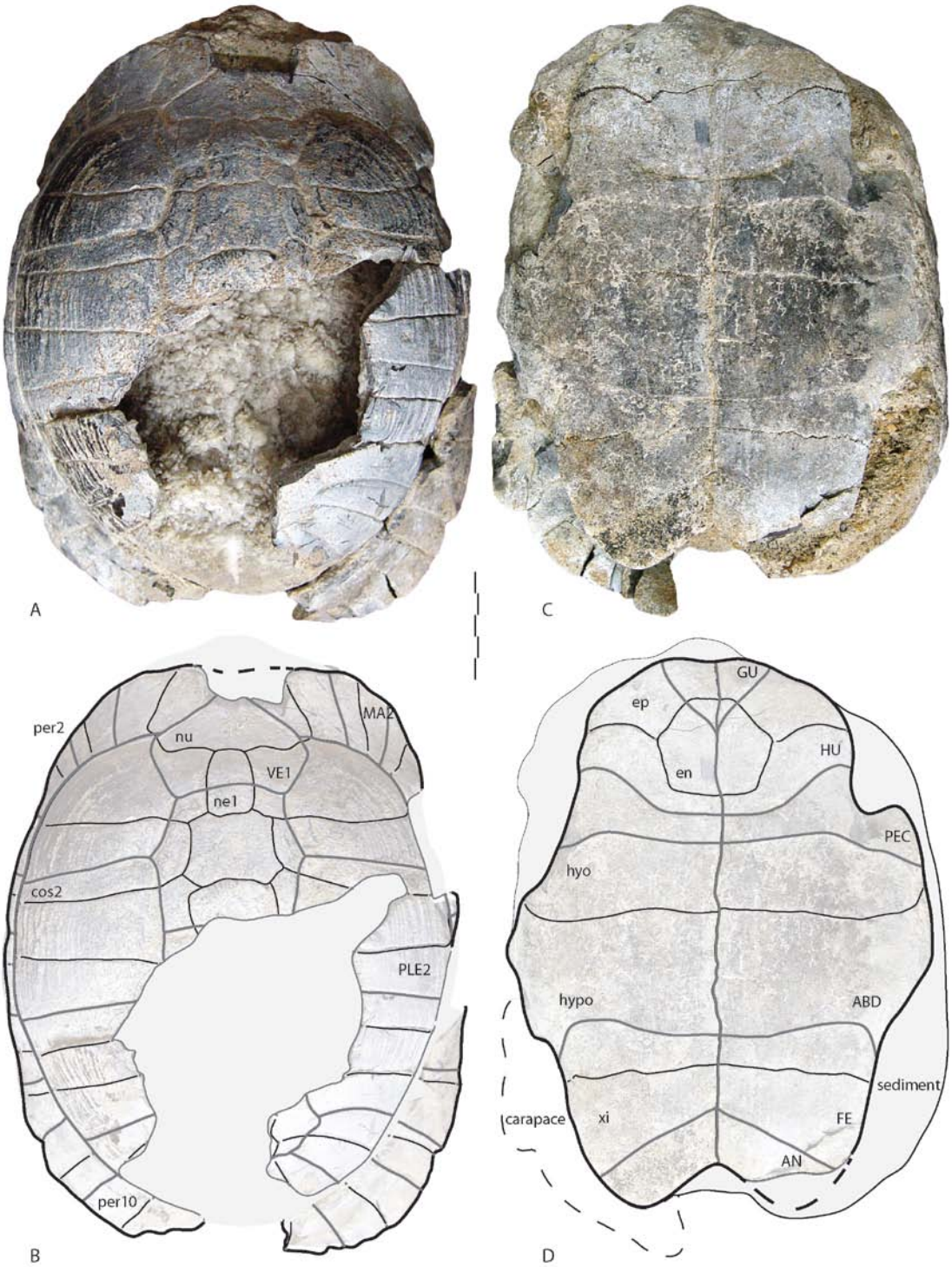


Figure 3.41. '*Testudo*' *hermanni* Gmelin, 1789 from the ?Pleistocene of Chalkidiki. LGPUT MP 40, shell in (A) dorsal, (B) drawing of dorsal carapace, (C) ventral and (D) drawing of ventral plastron views. Scale bar equals 5 cm. For abbreviations see Material & Methods.

LGPUT MP 40 (Fig. 3.41): Most of the shell is preserved, along with the in-filling sediment. In the dorsal side, on the outer surface of the in-filling sediment calcite crystals have been formed. This is an indication that the specimen might have been

fossilized in a cave. Part of the nuchal, and parts of the medial and posterior plates are missing form the carapace. The plastron is almost complete, only the tip of the left xiphiplastron is missing.

Carapace: The nuchal is partially preserved, but it is much wider than long. The nuchal is roughly octagonal. The neural 1 is quadrangular, longer than wide, with narrower anterior border. The neural 2 is octagonal, having a narrower anterior and a wider posterior side. The neural 3 is quadrangular, wider than long, with rounded edges. Costal 1 is larger than the remaining costals, making contact with the nuchal, the neurals 1 and 2, and the first three peripherals. The remaining costals show an alternating pattern, of costals being medially short and laterally long (costal 2, 4, 6) and costals being medially long and laterally short (costals 3, 5, 7). Peirpherals are long and narrow, whereas the posterior peripherals appear to have been bended inwards. Vertebrals are narrow, much narrower than the pleurals. The anterior part of the vertebral 1 is much narrower than the posterior one. The limits between the vertebrals cross transversely the neural 1 and neural 3. The pleurals are quadrangular. The limits between the pleurals cross the costals 2, 4, 6. There is good coincidence between the costo-peripheral suture and the pleuro-marginal sulcus. The marginals are long and narrow.

Plastron: The anterior lobe is short and wide, with a rounded rim. The epiplastra are short, but very wide, covering most of the rim of the anterior lobe. The entoplastron is hexagonal, as wide as long. The anterior and posterior borders are straight. The hyo- and hypoplastra are long and wide, being relatively flat. The hypo-xiphiplastral suture is situated posterior to the end of the bridge and the hypoplastra contribute to the formation of the posterior lobe. The posterior lobe is short and wide. A deep anal notch is noted posteriorly. Gulars are long and wide, covering the medial part of the epiplastra and the anterior part of the entoplastron. The gularo-humeral sulcus is V-shaped and straight on each side, forming an acute angle with the midline. The humerals are long and wide, covering the medial and posterior entoplastron, and the anterior part of the hyoplastra. The humero-pectoral sulcus is medially straight and laterally convex, situated posterior to entoplastron. The pectorals are medially short and laterally longer. The abdominals are long and wide, the largest scutes of the plastron, covering the posterior hyoplastra, and the anterior and medial parts of the hypoplastra. The pectoro-abdominal sulcus is nearly straight. The femorals are medially shorter than laterally, covering the posterior hypoplastra and the anterior half of the xiphiplastra. The abdomino-femoral sulcus if slightly concave medially and strongly convex laterally, being situated anterior to the hypo-xiphiplastral suture. The anals are short, covering the posterior part of the lobe. The femoro-anal sulcus is straight on each side, forming an obtuse angle with the midline. All the above suggest the absence of a hypo-xiphiplastral hinge in this specimen.

'Testudo' cf. *hermanni*

MATERIAL: Franchthi Cave, Peloponnesus (Holocene/Pleistocene, 50+ specimens) (Fig. 3.42): The material has no individual specimen numbers, as is the common practice in many archaeological sites with animal remains. The description is going to be general about the taxon, and where necessary to mention individual specimens the lithostratigraphical unit will be mentioned (e.g. 155).

DESCRIPTION: The material of '*Testudo'* from Franchthi Cave is not enough to provide a confident specific identification. The partial anterior carapace (168 Unit; Fig. 3.42) shows a narrow and long cervical scute and narrow vertebrals, which could indicate the presence of '*Testudo' hermanni*.

COMMENT: Franchthi Cave is within the range of extant *T. h. boettgeri*, whereas *Testudo graeca ibera* is mainly found in Northern Greece. Additionally, we didn't find any specimens indicative of *Testudo marginata*. Based on the available material we could identify the terrestrial tortoises from Franchthi Cave as *Testudo* cf. *hermanni.* For further information please see chapter on *Emys orbicularis* (below).

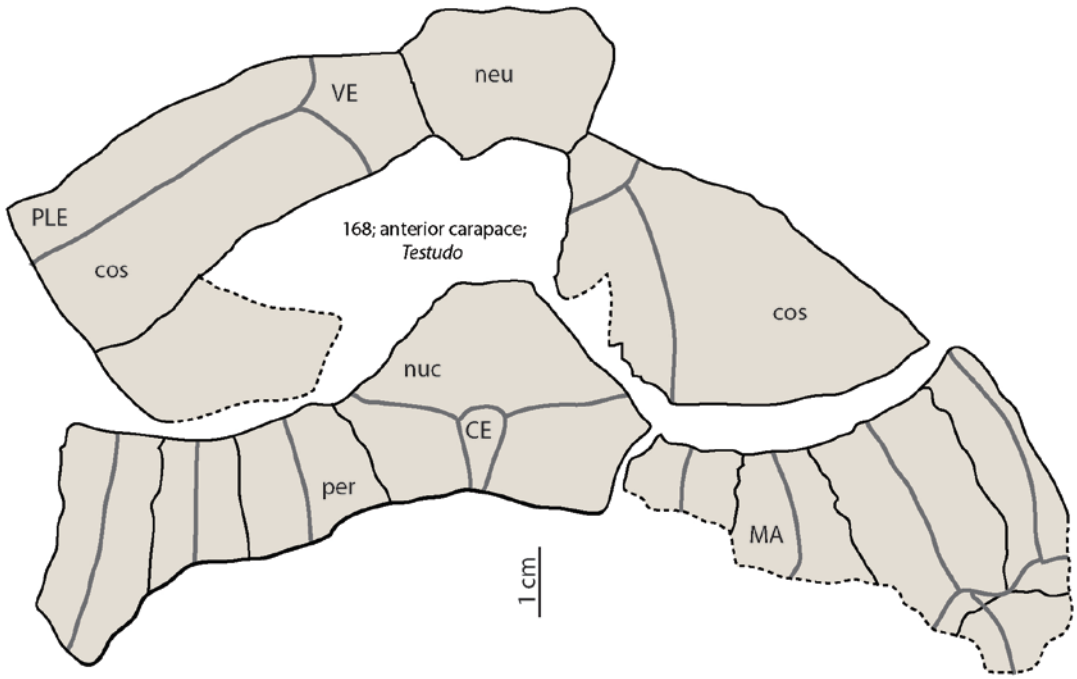


Figure. 3.42. Schematic drawing of the partial anterior carapace of *Testudo* cf. *hermanni* from the Epigravettian (Occupation phase 4, Unit 168) of Franchthi Cave (Peloponnesus). Scale bar equals 1 cm. For abbreviations see Material & Methods.

TESTUDO Linnaeus, 1758 sensu stricto or *TESTUDO* (sensu Parham et al. 2006)

Testudo graeca s.l. Linnaeus, 1758

Testudo graeca is an iconic tortoise species, first named by Linnaeus (1758) and since then it dominates the chelonian literature. This species it the type of the genus *Testudo* and marks the so-called *Testudo* s.s. lineage (sensu Lapparent de Broin et al., 2006b) defined by the presence of the hypo-xiphiplastral hinge.

DIAGNOSIS (based on Lapparent de Broin, 2006a and Amiranashvili, 2000): member of *Testudo* with: wide vertebral series; suprapygals usually not fused; quadrangular pygal; fused marginals 12 into a supracaudal; presence of a hypo-xiphiplastral hinge; presence of spur thighs made from keratin (N/A in fossils).

AGE: Recent – Pleistocene (Petralona Cave, Chalkidiki; Potidea, Chalkidiki) – Pliocene (Megalon Emvolon/Aggelochori, Thessaloniki; "Salonique") – Late Miocene (Allatini and Pylea, Thessaloniki)

MATERIAL:
Petralona Cave (3 specimens) (Fig. 3.43-3.45): TB 68 K87 (shell, male individual); TB 1499 K90 (shell, female individual); TB 580 (partial shell, juvenile individual).

Potidea (1 specimen) (Fig. 3.46): LGPUT MP 41 (partial shell).

Aggelochori/Megalo Emvolon (13 specimens) (Fig. 3.47-3.48): NHMW 1980z0069/0000, complete shell; AMPG 1956, right epiplastron; AMPG 1957, pygal; AMPG 1958, peripheral; AMPG 1959, costal fragment; AMPG 1960, plastron fragment; AMPG 1961, costal fragment; AMPG 1962, right hypoplastron; AMPG 1963, plastron fragment; AMPG 1964, right xiphiplastron fragment; AMPG 1965, left hypoplastron fragment; AMPG 1966, right xiphiplastron fragment; AMPG 1967, right xiphiplastron fragment; AMPG 1968, left xiphiplastron fragment.

Salonique (sensu Arambourg & Piveteau, 1929; 3 specimens) (Fig. 3.49): MNHN SLQ 1024, posterior carapace; MNHN SLQ 1025, anterior plastron; MNHN SLQ 1026, anterior plastron.

Pylea (1 specimen) (Fig. 3.50): IGF 11602, partial shell.

Allatini (1 specimen) (Fig. 3.51): AMPG 1970/2, partial shell.

Vatera, Lesvos Island (Early Pleistocene; 2 specimens) (Fig. 3.52): PO 098 T, partial shell; PO (uncatalogued), partial carapace.

DESCRIPTION

Petralona Cave

TB 68 K87 (Fig. 3.43): This specimen is preserved almost complete. Only some parts of the left costals and the posterior lobe of the plastron are missing.

Carapace: The carapace is tall and rounded, and the posterior part widens right after the end of the bridge. The nuchal is hexagonal, wider than long. The anterior nuchal border is sinuous, creating a small notch in the cervical scute and one small notch on each side on the nuchal-peripheral 1 suture. The neural 1 is quadrangular, sub-rounded, much longer than wide. The neural 2 is octagonal, the anterior part being narrower than the posterior. The neural 3 is quadrangular, sub-rounded and much wider than long. The neural 4 is octagonal, wider than long, and the anterior and posterior sides are of equal width. Although some neurals are missing (probably the neurals 5-6) the specimen appears to have only 7 neurals. The neural 7 is hexagonal, longer than wide. The suprapygal area is not preserved complete, and therefore is not possible to now if there are one or two suprapygals. Most probably there is a single suprapygal, trapezoid, with narrow anterior and wide posterior sides. The pygal is long and narrow, trapezoid, with wider anterior and narrow posterior end. The costal 1 is the largest costal, making contact with the nuchal, neurals 1-2, and peripherals 1-3. Costals 2-6 show an alternating pattern following the alternation of octagonal/quadrangular neurals. Costal 2, costal 4 and costal 6 are shorter medially and longer laterally, alternated with costal 3 and costal 5 that are medially long and laterally short. The peripherals are long and narrow. They show pointed tips in the in the limits of the marginals. Posteriorly, peripherals 9-11 and the pygal are bended inwards. As far as the scute sulci are concerned, anteriorly a long and wide cervical is present. The vertebrals are wide, as wide as the pleurals. Vertebral 1 is narrower than the rest, having a rounded anterior border on the nuchal and a straight to sinuous posterior border. The limit between the first two vertebrals crosses the neural 1 transversely. The vertebrals 2 and 3 are hexagonal, sub-rounded and they cover neurals and medial parts of the costals. The limit between the vertebral 2 and 3 crosses the neural 3 transversely. In the middle the limit shows a small convexity. The limit between the vertebral 3 and 4 crosses the neural 5 transversely. Vertebral 4 is also hexagonal with a narrower posterior part. The limit between the vertebral 4 and 5 crosses the neural 7 transversely. Vertebral 5 covers the posterior part of the neural 7, the last costals and the suprapygal. It is trapezoid, with narrow anterior and wide posterior sides. The pleurals are rectangular, with pleural 1 being the largest. The limits between the pleurals cross the costals 2, 4, 6, and 8. Marginals are long and narrow. All along the periphery of the carapace (except the nuchal), we notice good coincidence between the costo-peripheral suture and the pleuro-marginal sulcus. Marginals 12 are fused into a single supracaudal that is trapezoid with narrow anterior and wide posterior sides.

Plastron: The epiplastra are short and wide, covering the anterior part of the lobe. Viscerally, the epiplastra are thick, creating a convex epiplastral lip with a deep gular pocket. The entoplastron is long and narrow, roughly hexagonal with sinuous anterior border. The hyo- and hypoplastra are long and wide, displaying a medial convavity. This indicates that this is a male individual, as it is also inferred by the general shape of the shell that is longer than wide. The posterior suture of the hypoplastra is rounded. The xiphiplastra are not present, but they should constitute the entire posterior lobe. Gulars are short and wide, covering the medial part of the epiplastra and the anterior part of the entoplastron. The remaining part of the entoplastron is covered medially by the humerals, which are long and wide. The humero-pectoral sulcus is broadly concave and is situated posterior to the entoplastron. Laterally, the humero-pectoral sulcus is strongly convex. The pectorals are short but wide. The pectoro-abdominal sulcus is nearly straight.

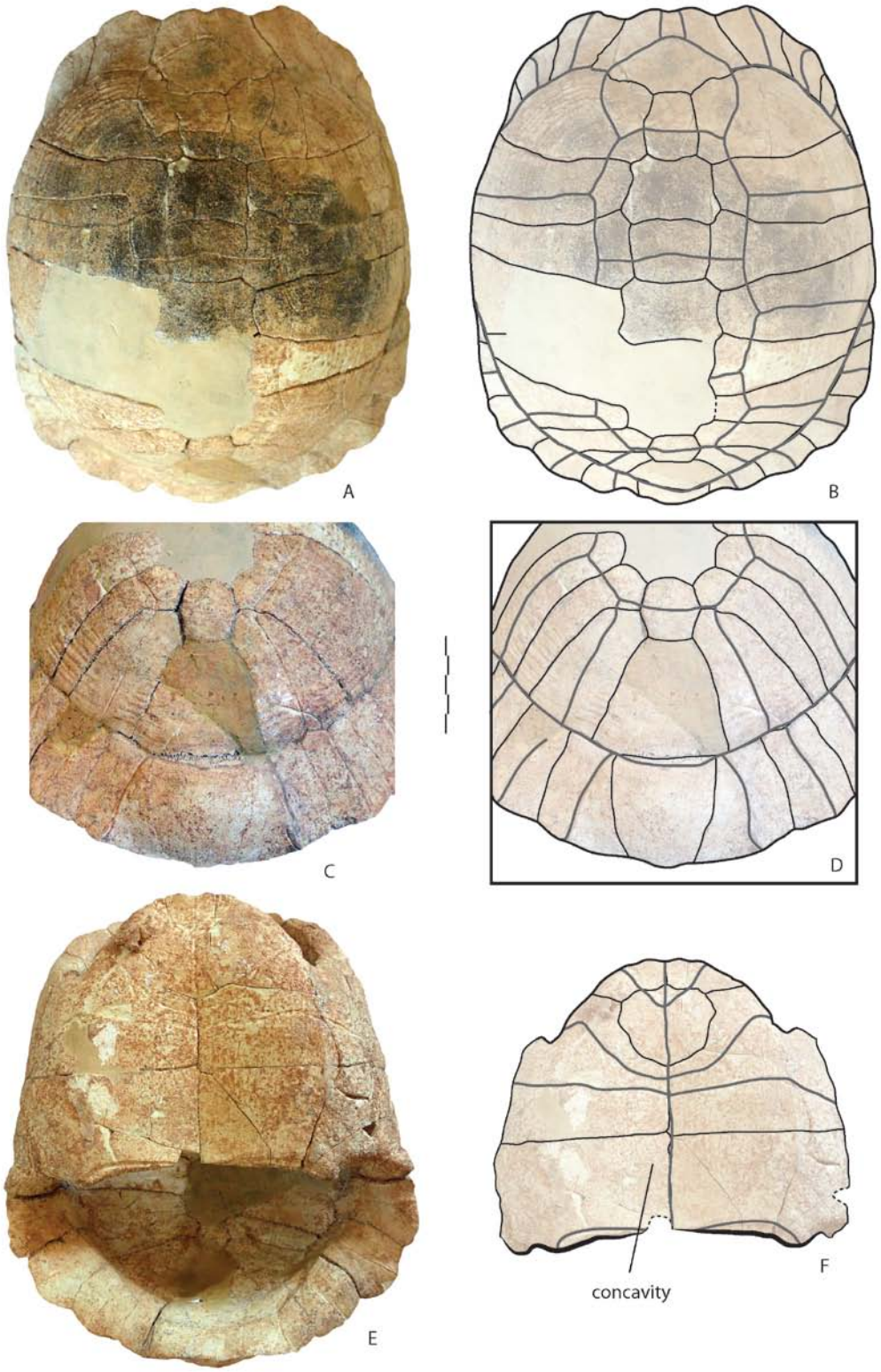


Figure 3.43. *Testudo graeca* Linnaeus, 1758 from the Pleistocene of Petralona Cave (Chalkidiki). TB 68 K87, partial shell in (A) dorsal, (B) drawing of dorsal, (C) posterior, (D) drawing of posterior, (E) ventral and (F) drawing of ventral views. Scale bar equals 5 cm.

The abdominals are the largest scutes preserved, covering the posterior half of the hyoplastra and nearly all the surface of the hypoplastra. Only the postero-lateral part of the hypoplastra is covered by the femorals. The abdomino-femoral sulcus is strongly convex laterally, but is situated on the posterior hypoplastral suture medially.

All the above mentioned morphologies in the posterior hypoplastra and the absence of xiphiplastra in this specimen, suggest a mobile posterior lobe and the presence of a hypo-xiphiplastral hinge.

TB 1499 K90 (Fig. 3.44): This shell is partially complete. From the carapace, the left anterior part is missing, together with some parts of the carapacial rim. From the plastron, few parts are preserved, such as the axillary part of the right hyoplastron, most of the hypoplastra and most of the posterior lobe. The missing parts have been filled with plaster.

Carapace: The carapace is tall and rounded. The nuchal is partially preserved, being wider than long. The neural 1 is quadrangular, sub-rounded, longer than wide. The neural 2 is octagonal, the anterior side being narrower than the posterior. The neural 3 is quadrangular, sub-rounded and wider than long. The neural 4 is octagonal, wider than long, and the anterior and posterior sides are of equal width. The neural 5 is quadrangular, sub-rounded and wider than long. The neural 6 is octagonal, with the anterior part being wider than the posterior one. The neural 7 is hexagonal, being longer than wide. In this specimen two suprapygals are present. The first suprapygal is small, hexagonal and rounded, slightly wider than long. The suture with the second suprapygal shows a small medial convexity. The second suprapygal is larger, wider than long, trapezoid with wide posterior side. On the other hand the pygal, that is also trapezoid in shape, has a wide anterior and a narrow posterior side. Costals 2-6 show an alternating pattern following the alternation of octagonal/quadrangular neurals. Costal 2, costal 4 and costal 6 are shorter medially and longer laterally, alternated with costal 3 and costal 5 that are medially long and laterally short. The peripherals are long and narrow. They show pointed tips in the in the limits of the marginals. Posteriorly, peripherals 9-11 and the pygal are bended inwards. Anteriorly a long and wide cervical is present. The vertebrals are wide, as wide as the pleurals. Vertebral 1 is narrower than the rest, but its limit cannot be clearly observed. The limit between the first two vertebrals crosses the neural 1 transversely. The vertebrals 2 and 3 are hexagonal, sub-rounded and they cover neurals and medial parts of the costals. The limit between the vertebral 2 and 3 crosses the neural 3 transversely. In the middle the limit shows a small convexity. The limit between the vertebral 3 and 4 crosses the neural 5 transversely. Vertebral 4 is also hexagonal with a narrower posterior part. The limit between the vertebral 4 and 5 crosses the neural 7 transversely. Vertebral 5 covers the posterior part of the neural 7, the last costals and the suprapygals. It is trapezoid, with narrow anterior and wide posterior sides. The pleurals are rectangular, with pleural 1 being the largest. The limits between the pleurals cross the costals 2, 4, 6, and 8. Marginals are long and narrow. All along the periphery of the carapace (except the nuchal), we notice good coincidence between the costo-peripheral suture and the pleuro-marginal sulcus. Marginals 12 are fused into a single supracaudal that is trapezoid with narrow anterior and wide posterior sides.

Plastron: In the preserved part of the right hyoplastron, the lateral part of the humero-pectoral sulcus is noted. The preserved parts of the hypoplastra are flat, suggesting that this is a female individual. This is also confirmed by the shape of the shell that is almost of similar length and width.

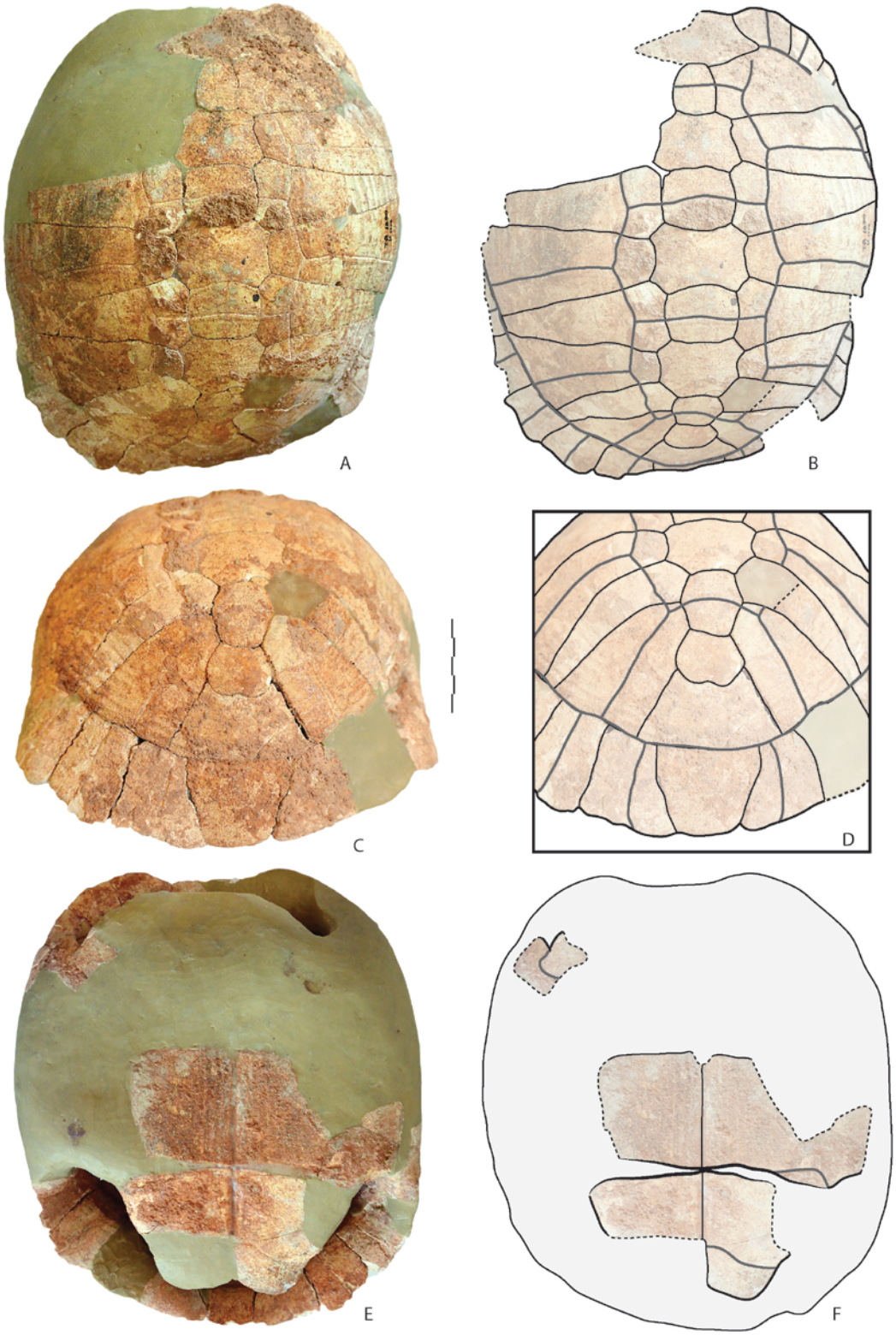


Figure 3.44. *Testudo graeca* Linnaeus, 1758 from the Pleistocene of Petralona Cave (Chalkidiki). TB 1499 K90, partial shell in (A) dorsal, (B) drawing of dorsal, (C) posterior, (D) drawing of posterior, (E) ventral and (F) drawing of ventral views. Scale bar equals 5 cm.

The hypoplastra are covered by the abdominals in almost their entire surface, except for the postero-lateral part that is covered by the femorals. The abdomino-femoral sulcus is strongly convex laterally, but coincides with the posterior hypoplastral suture medially. At the same time, the posterior lobe is made entirely by the

xiphiplastra and is wider than long. Note as well, that in this specimen the xiphiplastra are not tightly sutured with the hypoplastra, and plaster has been used to connect them.These features suggest the presence of a hypo-xiphiplastral hinge. The femorals cover most of the posterior lobe and larger than the anals, that cover the posterior part of the lobe. The femoro-anal sulcus is curved, being convex medially and slightly concave laterally. Posteriorly a wide anal notch is present.

TB 580 (Fig. 3.45): This specimen is partially complete, preserving the anterior and most of the left part of the carapace, as well as the anterior half of the plastron. The outer surface is eroded and observation on sutures and sulci are rather difficult. The small size of the specimen (6.3 cm) suggests that this is a juvenile individual. The shell is tall and rounded. On the carapace we can observe the alternating pattern of the costals, suggesting that this is a *Testudo* s.l. On the plastron is impossible to notice any sutures and sulci, as a result of the preservation, but is evident the presence of a mobile posterior lobe. Although the posterior lobe is missing, the straight posterior limit of the hypoplastra, situated right after the end of the bridge, evidences the presence of a mobile posterior lobe.

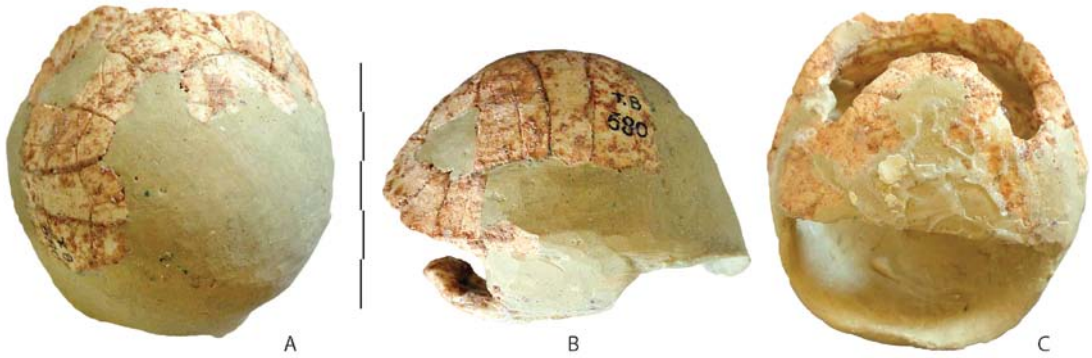


Figure 3.45. *Testudo graeca* Linnaeus, 1758 from the Pleistocene of Petralona Cave (Chalkidiki). TB 580, partial shell of a juvenile individual in (A) dorsal, (B) left lateral and (C) ventral views. Scale bar equals 5 cm.

Comments: The presence of small parts of stalagmitic material and the apparent similarities on color and type of fossilization with the other fossils found in Petralona cave, allow us to conclude that these specimens could be found inside the cave sediments and/or the cave floor. In Petralona Cave, many fossil mammal specimens have been found on the cave floor, being covered by calcitic material (see Tsoukala, 1990). These specimens belong to a male, a female and a juvenile individual. The morphology of these three specimens is in accordance with their attribution to the same taxon. The presence of a mobile posterior lobe of the plastron is a clear character that allows their attribution to *Testudo graeca*. We can notice that the hypo-xiphiplastral hinge is present and functioning in both sexes and in the juvenile individuals as well. In general, the morphology of these shells is fairly similar with the extant *T. graeca/ibera* surviving in Greece. Based on remarks on the vertebrate fauna of Petralona Cave by Kretzoi & Poulianos (1981), the chelonian fauna of the cave consisted of *Testudo graeca = Testudo* sp. (‘*T’. hermanni-graeca* group) and of a giant *Testudo* species. Clearly the small tortoises are members of the *T. graeca* lineage, whereas no record of a fossil giant tortoise has been found in the collections of the museum of Petralona Cave.

Potidea

LGPUT MP 41 (Fig. 3.46): This specimen consists of a partial shell. The effect of deformation is strong on this specimen. Many plates have been moving from their original position, overlapping others. In the posterior part of the carapace, a breakage is evident along the suture of the costals 7 – neural 7(?). The whole shell is compressed. In the plastron, most of the hyoplastra are missing, along with the entire posterior lobe. The in-filling sediment has been preserved, not allowing the observation of the visceral sides.

Carapace: The nuchal is wider than long, with a straight anterior border. The neural 1 is incomplete, but from the preserved part it is evident that it is quadrangular, longer than wide. The neural 2 is octagonal. The neurals 3-4 cannot be observed. Neural 5 is quadrangular, possibly longer than wide. Neural 6 is octagonal, wider than long. Neural 7 is hexagonal, slightly wider than long. Two suprapygals are present, the first being smaller than the second. Both are trapezoid with narrower anterior sides. Costals show an alternating pattern following the alternation of octagonal/quadrangular neurals. Costals that are shorter medially and longer laterally, alternate with costals being medially long and laterally short. Peripherals are long and narrow. Posteriorly, peripherals 9-11 and the pygal are bended inwards. A short and wide cervical is present anteriorly. Vertebrals are slightly narrower than then the pleurals. The limits of the vertebrals cross transversely the neural 1, neural 3, neural 5 and the first suprapygal. The pleurals are rectangular and their limits cross the costals 2, 4, 6 and 8. Marginals are long and narrow. Posteriorly, marginals 12 are fused into a supracaudal. The limits of the pleurals and the marginals coincide with the sutures between the costals and the peripherals all around the carapace.

Plastron: The epiplastra are short and wide, covering the anterior border of the lobe. From the preserved part we can see that the epiplastra are thickened, forming a convex epiplastral lip viscerally. The entoplastron is hexagonal, long and narrow. The hyo- and hypoplastra are long wide. Although not recovered, the posterior lobe seems to have been made entirely by the xiphiplastra. The gulars are short and wide, covering the medial part of the epiplastra and the anterior part of the entoplastron. The remaining part of the entoplastron is covered medially by the humerals that are long and wide. The humero-pectoral sulcus is broadly concave and is situated posterior to the entoplastron. Laterally, the humero-pectoral sulcus is strongly convex. The pectorals are short but wide. The pectoro-abdominal sulcus is slightly convex laterally. The abdominals are the largest scutes preserved, covering the posterior half of the hyoplastra and nearly all the surface of the hypoplastra. Only the postero-lateral part of the hypoplastra is covered by the femorals. The abdomino-femoral sulcus is strongly convex laterally, but is situated on the posterior hypoplastral suture medially. All the above-mentioned morphologies in the posterior hypoplastra and the absence of xiphiplastra in this specimen, suggest a mobile posterior lobe and the presence of a hypo-xiphiplastral hinge.

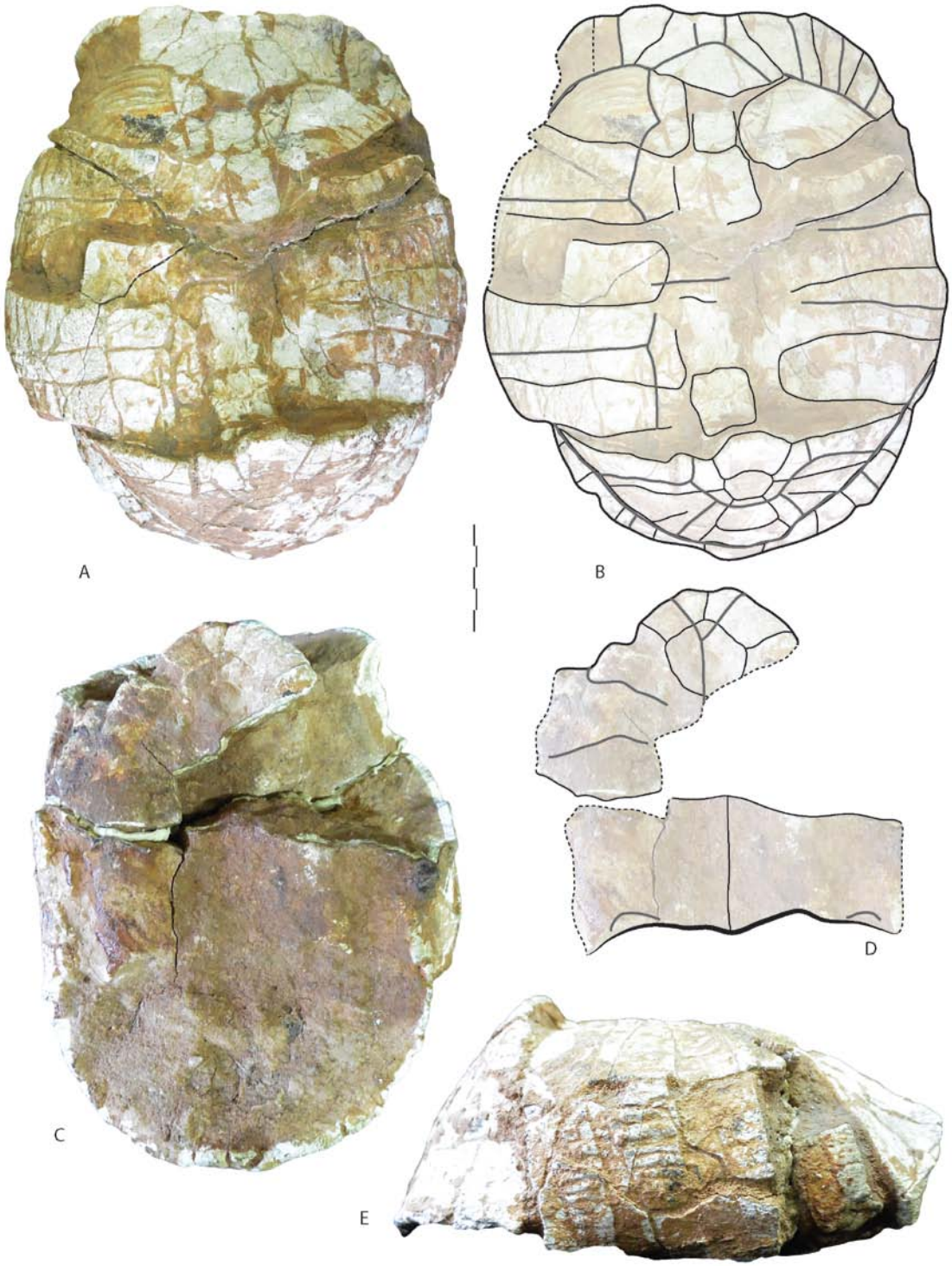


Figure 3.46. *Testudo graeca* Linnaeus, 1758 from the Pleistocene of Potidea (Chalkidiki). LGPUT MP 41, partial shell in (A) dorsal, (B) drawing of dorsal, (C) ventral, (D) drawing of ventral and (E) right lateral views. Scale bar equals 5 cm.

Aggelochori/Megalo Emvolon

NHMW 1980z0069/0000 (Fig. 3.47): The specimen is complete, and the in-filling sediment is preserved in the interior of the shell. There is a slight deformation in the specimen as it is inferred from the presence of a transverse fracture along the anterior border of costals 4 and neural 4. Ventrally, the xiphiplastra are recovered slightly misplaced from their original position. The specimen has a dark coloration, especially in the plastron. This has been indicated by Bachmayer et al., 1979 (who first described this specimen) as indicative of the coloration of the "Maurische Landschildkröte". Obviously, this coloration is the result of the fossilization and/or diagenetic process and not a remnant of the scute coloration of this tortoise.

Carapace: The carapace is elongated, tall and rounded. The nuchal is hexagonal, wider than long. The anterior nuchal border is straight. The specimen has 7 neurals. The neural 1 is quadrangular, sub-rounded, longer than wide. Neurals 2-3 are partially visible. The neural 2 is octagonal, the anterior part being narrower than the posterior. The neural 3 is quadrangular, sub-rounded and much wider than long. The neural 4 is octagonal, wider than long, and the anterior and posterior sides are of equal width. Neural 5 is quadrangular, wider than long. Neural 6 is hexagonal, with short anterior lateral sides. The neural 7 is quadrangular, slightly longer than wide. Two suprapygals are present. The first suprapygal is smaller and trapezoid. The second, also trapezoid, is much larger. Both have wider posterior sides. The pygal is long and narrow, trapezoid, with wider anterior and narrow posterior end. The costal 1 is the largest costal, making contact with the nuchal, neurals 1-2, and peripherals 1-3. Costals 2-6 show an alternating pattern following the alternation of octagonal/quadrangular neurals. Costal 2, costal 4 and costal 6 are shorter medially and longer laterally, alternated with costal 3 and costal 5 that are medially long and laterally short. The costal 7 medially contacts only the neural 7. The peripherals are long and narrow. They show pointed tips in the in the limits of the marginals. Posteriorly, peripherals 9-11 and the pygal are bended inwards. As far as the scute sulci are concerned, anteriorly a long and wide cervical is present. The vertebrals are wide, as wide as the pleurals. Vertebral 1 is narrower than the rest, having a rounded anterior border on the nuchal and a straight to sinuous posterior border. The limit between the first two vertebrals crosses the neural 1 transversely. The vertebrals are hexagonal, sub-rounded and they cover neurals and medial parts of the costals. The limit between the vertebral 2 and 3 crosses the neural 3 transversely. In the middle the limit shows a small convexity. The limit between the vertebral 3 and 4 crosses the neural 5 transversely. Vertebral 4 is also hexagonal with a narrower posterior part. The limit between the vertebral 4 and 5 crosses the neural 7 transversely. Vertebral 5 covers the posterior part of the neural 7, the last costals and the suprapygal. It is trapezoid, with narrow anterior and wide posterior sides. The pleurals are rectangular, with pleural 1 being the largest. The limits between the pleurals cross the costals 2, 4, 6, and 8. Marginals are long and narrow. All along the periphery of the carapace (except the nuchal), we notice good coincidence between the costo-peripheral suture and the pleuro-marginal sulcus. Marginals 12 are fused into a single supracaudal that is trapezoid with narrow anterior and wide posterior sides. There is a small constriction on the marginal 11-supracaudal sulcus on each side.

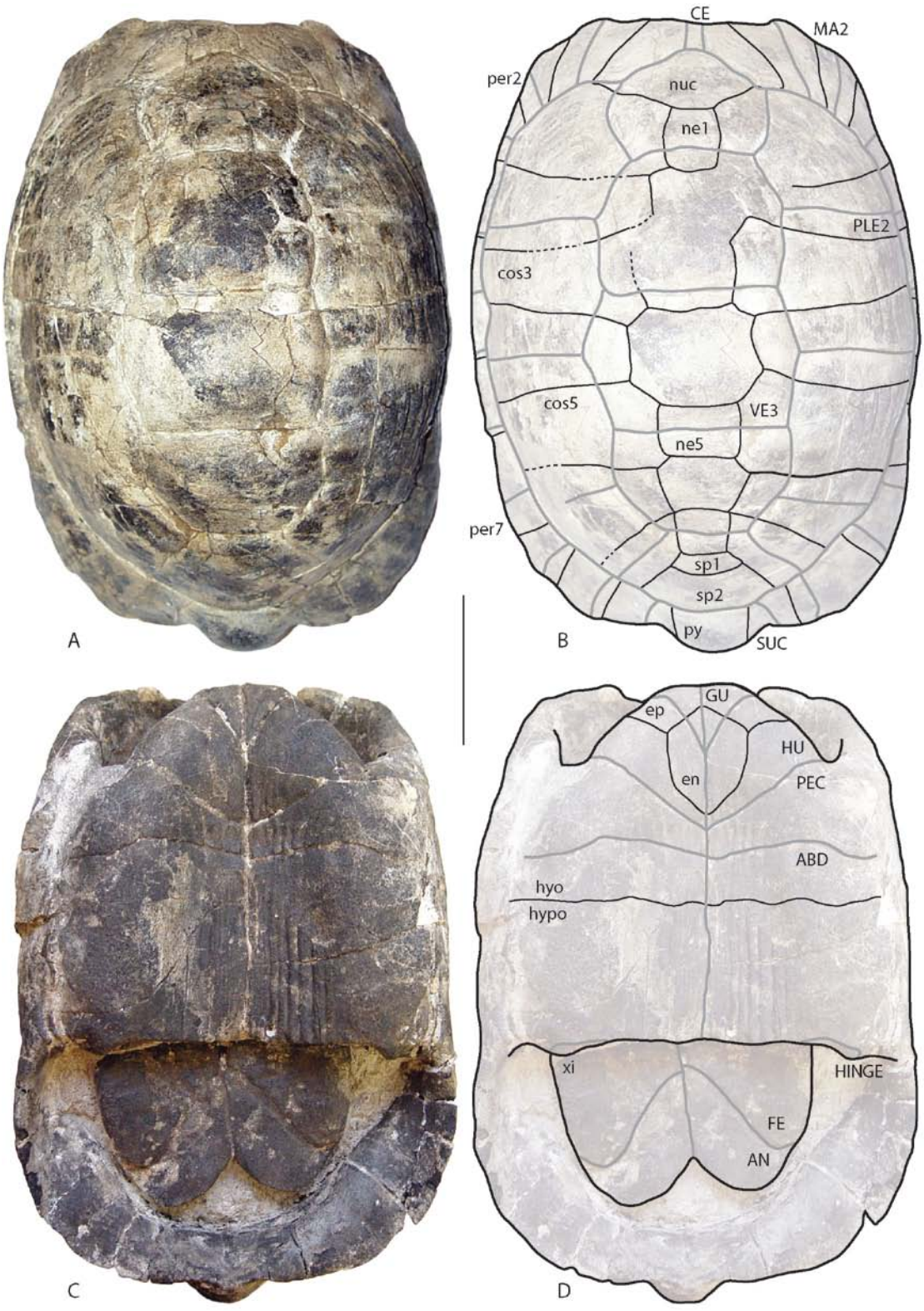


Figure 3.47. *Testudo graeca* Linnaeus, 1758 from the Pliocene of Aggelochori/Megalo Emvolon (Thessaloniki). NHMW 1980z0069/0000, almost complete shell in (A) dorsal, (B) drawing of dorsal, (C) ventral and (D) drawing of ventral views. Scale bar equals 5 cm. For abbreviations see Material & Methods.

Plastron: The epiplastra are short and wide, covering the anterior part of the lobe. Viscerally, the epiplastra are thick, creating a convex epiplastral lip. The entoplastron

is long and narrow, roughly hexagonal with straight borders. The hyo- and hypoplastra are long and wide, displaying a medial convavity. This indicates that this is a male individual, as it is also shown by the general shape of the shell that is longer than wide. The hypoplastra end right in the end of the bridge and do not contribute in the formation of the posterior lobe. The posterior lobe is long and wide, and is formed entirely by the xiphiplastra. The lateral sides are straight and nearly parallel to each other. The posterior lobe is recovered misplaced from its original position. Posteriorly a deep and angular anal notch is noted. The gulars are short and wide, covering the medial part of the epiplastra and the anterior part of the entoplastron. The remaining part of the entoplastron is covered medially by the humerals that are long and wide. The humero-pectoral sulcus is V-shaped and is situated posterior to the entoplastron. Laterally, the humero-pectoral sulcus is convex. The pectorals are short but wide. The pectoro-abdominal sulcus is nearly straight, showing a shallow medial concavity. The abdominals are the largest scutes preserved, covering the posterior half of the hyoplastra and nearly all the surface of the hypoplastra. Only the postero-lateral part of the hypoplastra is covered by the femorals. The abdomino-femoral sulcus is slightly convex laterally, but is situated on the posterior hypoplastral suture medially. The femorals are short medially and long laterally. On the contrary, the anals are medially long and laterally short. The femoro-anal sulcus is V-shaped, being strongly convex to angular medially and strongly concave laterally. All the above-mentioned morphologies in the posterior hypoplastra and the misplaced posterior lobe, suggest a mobile posterior lobe and the presence of a hypo-xiphiplastral hinge.

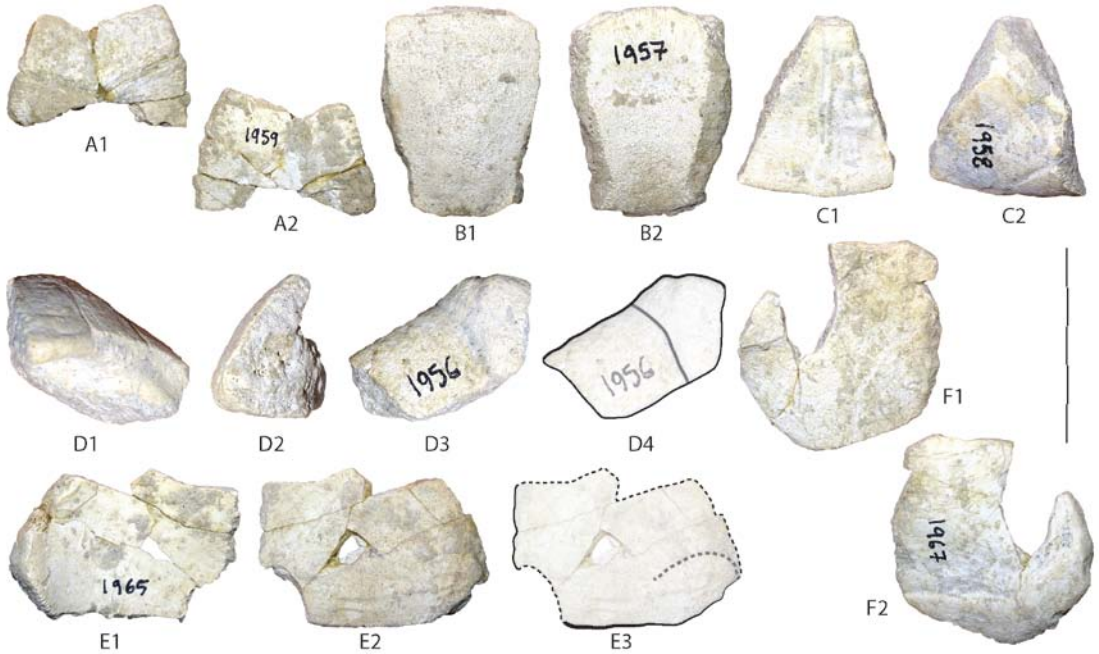


Figure 3.48. *Testudo graeca* Linnaeus, 1758 from the Pliocene of Aggelochori/Megalo Emvolon (Thessaloniki). AMPG collection: A, AMPG 1959, costal fragment in (A1) dorsal and (A2) visceral views. B, AMPG 1957, pygal in (B1) dorsal and (B2) visceral views. C, AMPG 1958, peripheral in (C1) dorsal and (C2) visceral views. D, AMPG 1956, right epiplastron in (D1) visceral, (D2) medial, (D3) ventral and (D4) drawing of the ventral views. E, AMPG 1965, left hypoplastron fragment in (E1) visceral, (E2) ventral and (E3) drawing of the ventral views. F, AMPG 1967, right xiphiplastron in (F1) ventral and (F2) visceral views. Scale bar equals 5 cm.

AMPG 1956 (Fig. 3.38.D): This specimen corresponds to a complete right epiplastron. Viscerally, a thick epiplastral lip with a convex surface is noted. Posterior to lip, a gular pocket is formed. Ventrally, the long and narrow gulars cover the medial parts of the epiplastron and overlap the anterior part of the entoplastron. The anterior outline of the lobe is rather straight.

AMPG 1957 (Fig. 3.38.B): This specimen corresponds to a complete pygal plate. It is quadrangular with wider anterior and narrower posterior sides. It is much longer than wide. Both ventrally and viscerally the twelfth marginals are fused into a supracaudal. Based on the preserved part we can estimate that the posterior carapace border was turned inwards.

AMPG 1958 (Fig. 3.38.C): This specimen corresponds to a complete peripheral. The medial part is much narrower than the lateral one, indicating that most probably belongs to one of the last peripherals (e.g. peripheral 11). It is crossed by the marginal sulci and it is apparent the costo-peripheral suture coincides with the pleuro-marginal sulcus.

AMPG 1959 (Fig. 3.48.A): This specimen corresponds to the medial part of a costal plate. It is dorsally short and becomes longer laterally, indicating the typical shape of the testudinid costals. Dorsally is crossed by the vertebral/pleural sulci.

AMPG 1960: This specimen, based on the smooth and rather flat surface, probably corresponds to a plastron fragment. Further description is not possible.

AMPG 1961: This specimen corresponds to a medial fragment of a costal plate, as indicated by the inserted rib viscerally and the presence of a pleural sulcus on the dorsal side.

AMPG 1962: This specimen corresponds to the lateral fragment of a right hypoplastron. It is rather thick and rounded and resembles the morphology of the hypoplastral part of the hypo-xiphiplastral hinge. However, the preserved part is small to allow further description.

AMPG 1963: This specimen, based on the smooth and rather flat surface, probably corresponds to a plastron fragment. Further description is not possible.

AMPG 1964: This specimen corresponds to the posterior part of the right xiphiplastron. Further description is not possible.

AMPG 1965 (Fig. 3.38.E): This specimen corresponds to the posterior part of the left hypoplastron. The preserved part shows a ventral convexity, indicating that it could belong to a male individual. Laterally we can trace the abdomino-femoral sulcus, being strongly convex. Also, the posterior border of the plate is situated in the end of the bridge, and is thick and rounded. Although the ventral surface of the specimen is eroded and further information is not available, we can safely assume that a hypo-xiphiplastral hinge was present in this specimen.

AMPG 1966: This specimen corresponds to the posterior part of the right xiphiplastron. Further description is not possible.

AMPG 1967 (Fig. 3.38.F): This specimen corresponds to an almost complete right xiphiplastron, with only some parts from the middle of the plate missing. The plate is longer than wide, reconstructing a rather long and wide posterior lobe. The specimen is eroded and no sulci can be confidently identified on the ventral side. Posterior a short and wide anal notch is noted. The xiphiplastron display a small degree of concavity.

AMPG 1968: This specimen corresponds to a fragment of a left xiphiplastron. The plate is longer than wide, reconstructing a rather long and wide posterior lobe. The specimen is eroded and no sulci can be confidently identified on the ventral side.

Salonique (sensu Arambourg & Piveteau, 1929)

MNHN SLQ 1024 (Fig. 3.49.A-B): The posterior carapace is preserved, from the left costal 6 and the right costal 7, until the posterior end. The posterior part of the shell is rounded. The posterior carapacial rim, including the pygal, is bended inwards. The last neural is preserved, probably being hexagonal. Most probably two suprapygals are preserved, the first much smaller, both trapezoid with narrower anterior sides. The pygal is trapezoidal, with wider anterior side. The suture between the peripherals 11 and the pygal is sigmoidal. The preserved costals, are slightly longer medially than laterally, corresponding most probably to hexagonal neurals. The peripherals are long and narrow. The vertebral 5 is trapezoidal, narrower anteriorly. It covers the posterior half of the last neurals, the posterior half of the last costals and the suprapygals. The pleurals are rectangular. The marginals are long and narrow. The marginals 12 are fused into a trapezoid supracaudal. There is good coincidence between the suprapygal-pygal suture and the vertebra-supracaudal sulcus, as well as between the costo-peripheral suture and the pleuro-marginal sulcus.

MNHN SLQ 1025 (Fig. 3.49.C-E): The anterior and medial part of the plastron is preserved. The posterior hypoplastra and the posterior lobe are missing. The epiplastra are short and wide, covering the anterior part of the lobe. The overall shape of the anterior lobe is rounded. Viscerally, the epiplastra are thick, creating a convex epiplastral lip, with a deep gular pocket. The entoplastron is long and wide, roughly hexagonal with rounded borders. The hyo- and hypoplastra are long and wide, displaying a medial convavity. This indicates that this is a male individual, as it is also shown by the general shape of the shell that is longer than wide. The gulars are short and wide, covering the medial part of the epiplastra and the anterior part of the entoplastron. The remaining part of the entoplastron is covered medially by the humerals that are long and wide. The humero-pectoral sulcus is wide, gently concave and is situated posterior to the entoplastron. The pectoro-abdominal sulcus is nearly straight, showing a shallow medial concavity, and being slightly convex laterally. The abdominals are the largest scutes preserved, covering the posterior half of the hyoplastra and all the preserved surface of the hypoplastra.

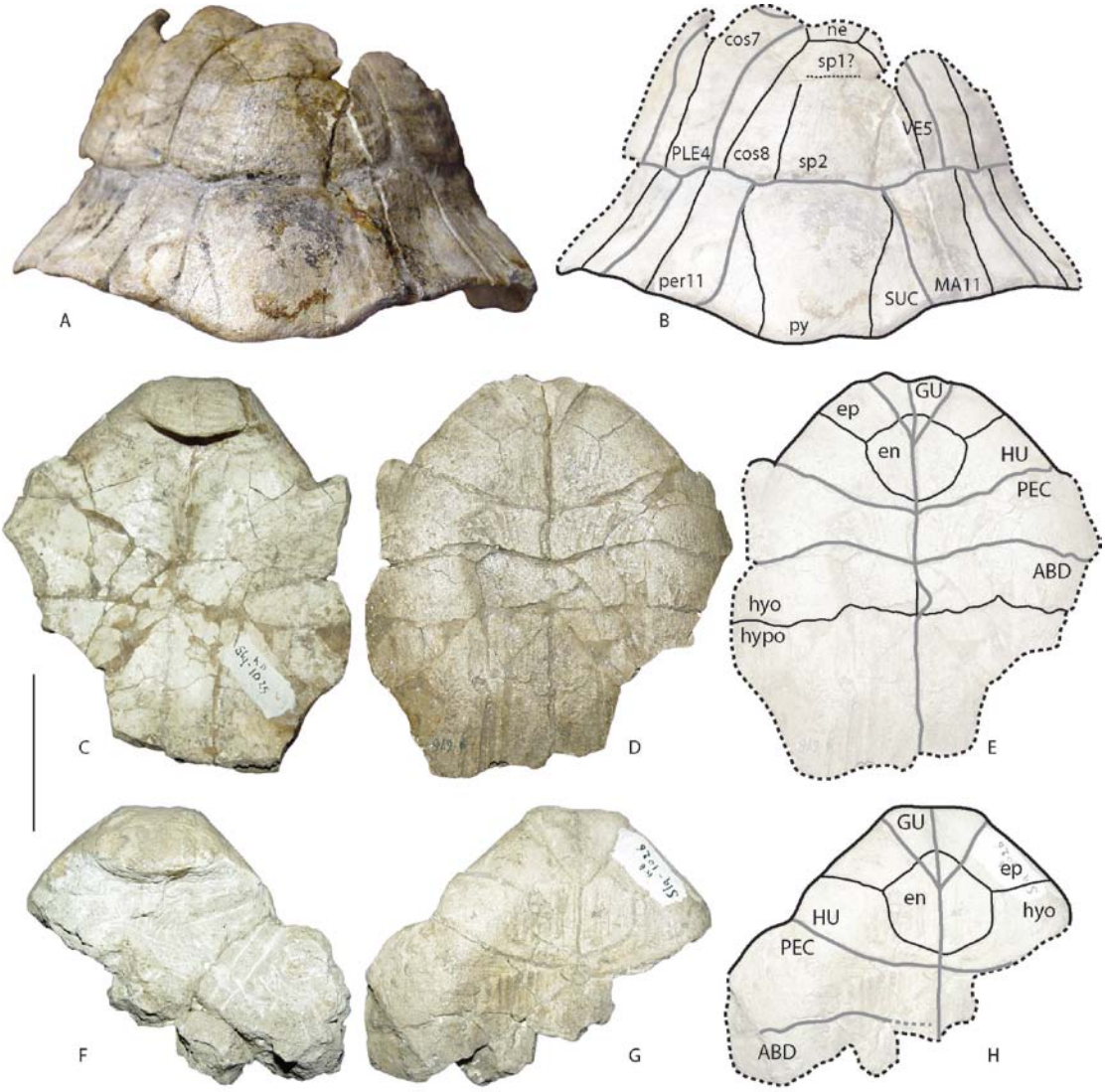


Figure 3.49. *Testudo graeca* Linnaeus, 1758 from the Pliocene of "Salonique" (sensu Arambourg & Piveteau, 1929). A-B, MNHN SLQ 1024, posterior carapace in (A) posterior and (B) drawing of the posterior views. C-E, MNHN SLQ 1025, anterior plastron in (C) visceral, (D) ventral and (E) drawing of the ventral views. F-H, MNHN SLQ 1026, anterior plastron in (F) visceral, (G) ventral and (H) drawing of the ventral views. Scale bar equals 5 cm. For abbreviations see Material & Methods.

MNHN SLQ 1026 (Fig. 3.49.F-H): The anterior part of the plastron is preserved. The left hyoplastron, the hypoplastra and the posterior lobe are missing. The epiplastra are short and wide, covering the anterior part of the lobe. The overall shape of the anterior lobe is rounded, with a straight anterior border. Viscerally, the epiplastra are thick, creating a convex epiplastral lip, with a deep gular pocket. The rest of the visceral surface is covered by sediment. The entoplastron is long and wide, hexagonal with straight borders. The hyoplastra are long and wide, displaying a medial convavity. This indicates that this is a male individual, as it is also shown by the general shape of the shell that is longer than wide. The gulars are short and wide, covering the medial part of the epiplastra and the anterior part of the entoplastron. The remaining part of the entoplastron is covered medially by the humerals that are long and wide. The humero-pectoral sulcus is wide, gently concave and is situated posterior to the

entoplastron. The pectoro-abdominal sulcus is nearly straight, showing a shallow medial concavity, and being slightly convex laterally.

Pylea

IGF 11602 (Fig. 3.50): The specimen is almost complete. The lithified sediment preserved inside the shell masks the morphology of the visceral surfaces of the bones. Most plates of the carapace are preserved (Fig. 3.50.A), apart from the left anterior carapacial margin and the entire posterior carapacial margin (partial seventh and complete eighth costals; posterior peripherals; suprapygals). The right bridge is also missing, but the imprints of the bony plates that formed the bridge can be observed on the sediment filling the shell. The scute sulci are clearly visible on the entire surface of the carapace, but the bony sutures are not clearly visible on the anterior part (Fig. 3.50.B). The plastron is almost completely preserved (Fig. 3.50.C), lacking only some small parts of the xiphiplastra and hypoplastra. Parts of the medial and hypo-xiphiplastral sutures are covered by sediment. The shell is slightly deformed and compressed. The most significant deformation affects the plastron, which is deeply concave because its central area is depressed; proof of the existence of this deformation is furnished by a V-shaped space that separates the epiplastra in anterior view.

Carapace: The nuchal outline is only partially visible, but indicates that the nuchal is slightly wider than long and hexagonal in shape. The anterior border of the nuchal is nearly straight, lacking a nuchal notch.

The first four vertebrals are preserved. The vertebral scutes are wide, approximately equaling the pleurals in width, but appear significantly broader than the pleurals in dorsal view. The first vertebral overlaps the nuchal, first peripherals, first neural, and first costals. It is longer than wide and has convex lateral margins. The sulcus between the first and second vertebrals crosses the first neural and is slightly wavy. The second vertebral is slightly longer than wide, and the anterior part of this scute is narrower than the posterior part. The second vertebral covers the posterior part of the first neural, the second neural, the anterior part of the third neural, and the medial parts of the first three costals. The sulcus between the second and third vertebrals becomes anteriorly convex over a short interval crossing the midline. The third vertebral is slightly wider than long, covering the posterior part of the third neural, the fourth neural, and the anterior part of the fifth neural, as well as medial parts of the third to fifth costals. The sulcus between the third and the fourth vertebrals is straight. The fourth vertebral is longer than wide, with a narrow posterior end. It covers the posterior part of the fifth neural, the sixth neural, and the anterior part of the seventh neural, as well as the medial parts of the fifth to seventh costals. The area of the shell overlain by the fifth vertebral is not preserved.

The pleurals cover only the costal plates, as the pleuro-marginal sulci roughly coincide with the costo-peripheral sutures. The first two pairs of pleurals are longer than wide, whereas the last two are wider than long (although this is uncertain in the case of the last pair because of imperfect preservation). The first pleural covers the first costal, and the anterior part of the second costal. The second pleural covers the posterior part of the second costal, the third costal and the anterior part of the fourth costal.

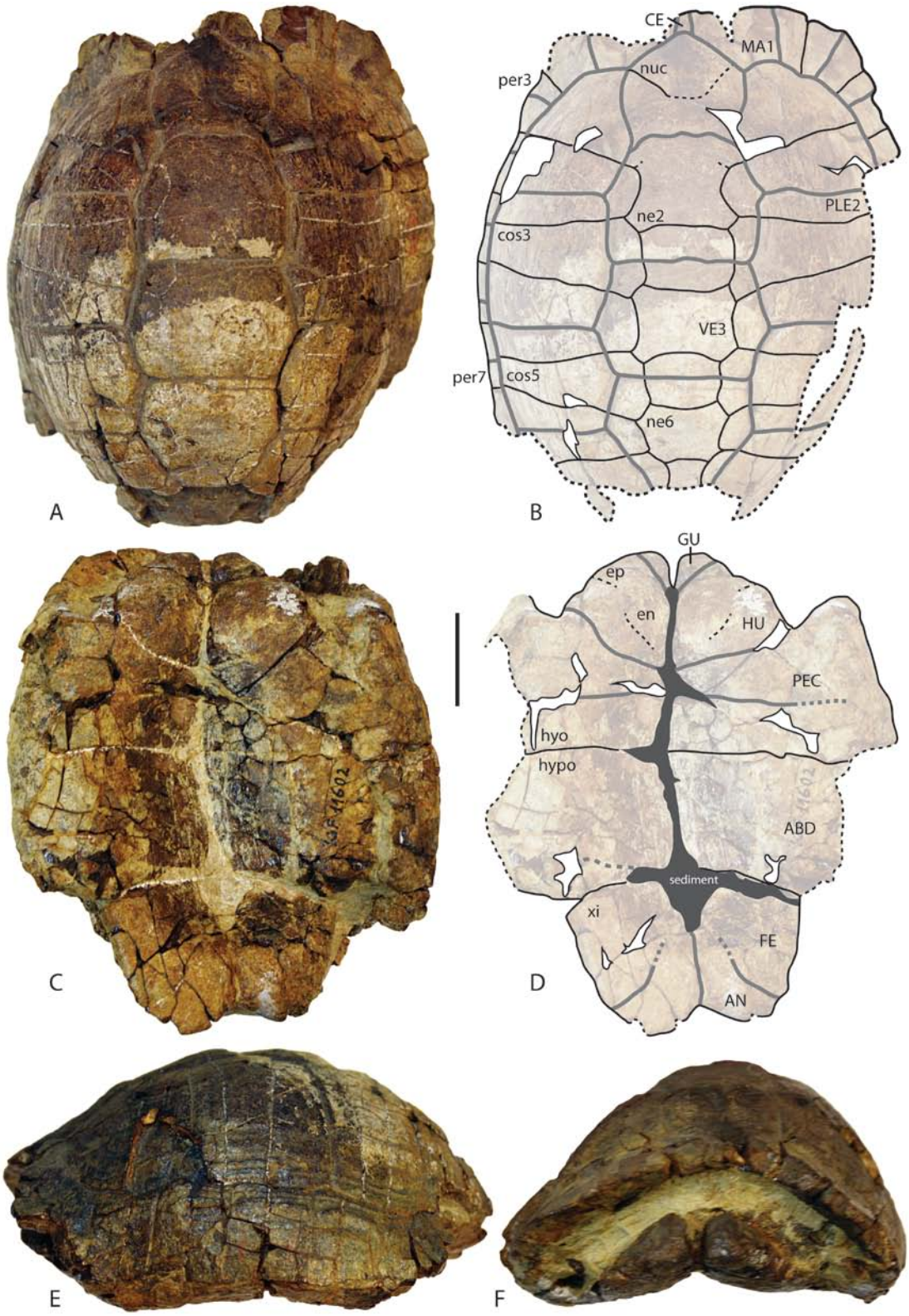


Figure 3.50. *Testudo graeca* Linnaeus, 1758 from the uppermost Miocene – lowermost Pliocene of Pylea (Thessaloniki). IGF 11602, partial shell in (A) dorsal, (B) drawing of dorsal, (C) ventral, (D) drawing of ventral, (E) left lateral and (F) anterior views. Scale bar equals 5 cm. For abbreviations see Material & Methods.

The third pleural covers the posterior part of the fourth costal, the fifth costal and the anterior part of the sixth costal. The fourth pleural covers the posterior part of

the sixth costal, as well as the seventh costal, although not all of the area covered by the fourth pleural is preserved. The marginal scutes are morphological similar to the peripherals. The anterior marginals are wide and short, whereas those of the bridge area are much taller than long.

Plastron: The paired epiplastra have convex ventral surfaces and are greatly thickened in the area corresponding to the epiplastral pads. In lateral view, their anterior portion is clearly deflected dorsally. Because the shell is filled with sediment, it is not possible to evaluate the presence and degree of development of the gular pocket, which is usually present when the epiplastral pads are as well developed as is the case in this specimen. The epiplastra are short and wide, and are restricted to the anterior part of the lobe. The anterior edge of the lobe is approximately convex. The posterior margins of the epiplastra cannot be confidently observed. The margins of the entoplastron are not clear, but this plate is probably broad and rhomboid. The entoplastron probably contributes to the dorsally deflected portion of the anterior lobe.

The hyoplastra and the hypoplastra are the largest plates of the plastron, and are long and wide. They are medially depressed, but it is not possible to infer if this is an effect of deformation or an indication that this specimen represents a male. The anterior suture between the hyoplastra and the entoplastron is not clearly visible. The hyo-hypoplastral suture is straight. The midline suture separating the left and right hyo- and hypoplastra is covered by sediment. The posterior margin of the hypoplastra is mostly covered by sediment as well, but the visible part indicates that this suture is located close to the end of the bridge. Therefore, the hypoplastra do not contribute to the posterior lobe of the plastron. The xiphiplastra are slightly longer than broad. Compared to the hypoplastra, they are relatively long, constituting the entire posterior lobe. The lateral edge of each xiphiplastron is rather straight anteriorly, becoming convex only towards the posterior tip. A wide (appr. 120 degrees) but relatively shallow anal notch separates the posterior parts of the two xiphiplastra.

The gulars are wide and short, covering the epiplastra. They converge posteriorly and probably cover the anterior part of the entoplastron. The humerals are wide and anteroposteriorly short, covering the posterior parts of the epiplastra, the entoplastron and the anterior parts of the hyoplastra. The humero-pectoral sulcus has a wide V-shape, and crosses the hyoplastra posterior to the entoplastron. The pectorals are the anteroposteriorly shortest scutes of the plastron, but they are very wide. They cover only the middle parts of the hyoplastra. The abdominals are the longest scutes of the plastron, covering the posterior parts of the hyoplastra and nearly all of the hypoplastra. Medially, the posterior ends of the abdominals apparently coincide with those of the hypoplastra. Laterally, they contact the anterior parts of the femorals, which prevent them from covering the posterolateral corners of the hypoplastra. The femorals cover the anterior parts of the xiphiplastra, whereas a small part of each femoral, strongly convex in shape, covers the posterolateral part of the corresponding hypoplastron. As a result of the presence of the hinge, the median part of the abdomino-femoral sulcus coincides with the hypo-xiphiplastral suture. The medial parts of the femorals are anteroposteriorly shorter than the lateral parts. The anals cover the posterior parts of the xiphiplastra. Although they are not completely visible, they appear to be medially long and laterally short. The femoro-anal sulcus is slightly anteriorly concave.

Allatini

AMPG 1970/2 (Fig. 3.51): The shell is partially preserved, and its internal surface is covered by lithified sediment. The right side of the carapace is almost complete, lacking only a part of the first costal. The right side is preserved from the third till the eighth costal (Fig. 3.51.A-D). The pygal – suprapygal area is fragmented and incomplete, with only a part of the suprapygal being visible. Only a part of the anterior lobe of the plastron is preserved (Fig. 3.51.E-F). The sutures and sulci are not entirely visible in some areas, such as the medial region of the carapace and the hyoplastral region.

Carapace: Only the posterior part of the first neural is preserved, but this plate was probably quadrangular and very wide. The second neural is hexagonal, with short posterolateral sides. The third neural is quadrangular, and markedly wider than long. The fourth neural is partially visible in this specimen, and possibly deformed. However, it displays an octagonal shape. The fifth neural is quadrangular and longer than wide, with rounded lateral sides. The sixth neural is hexagonal, and wider than long. The seventh neural is also hexagonal, but is narrower in proportion to its length than the sixth. The eighth neural is also hexagonal, but markedly longer than wide. Only a partial suprapygal is preserved. Its state of preservation does not allow its morphology to be clearly assessed, but the suprapygal is probably single and pyramidal in shape, with a narrow anterior end and a wide posterior one. The right costals (from the second to the sixth) show the alternating pattern that is typical of testudinids, as plates that are medially short and laterally long alternate with ones that are medially long and laterally short. The only preserved peripherals are those on the posterior part of the left side. They are short, tall and almost vertically oriented.

Four vertebrals are preserved, and only the first is missing. The vertebrals are wide, being almost equal in width to the pleurals in dorsal view. The second vertebral covers the posterior part of the first neural, and the entirety of the second and third neurals. The third vertebral covers the posterior part of the third neural, the fourth neural, and the anterior part of the fifth neural. The sulcus between the second and third vertebrals is slightly convex anteriorly. The fourth vertebral is longer than wide, covering the posterior part of the fifth neural, all of the sixth and seventh neurals, and the anterior part of the eighth neural. The sulcus between the third and fourth vertebrals is again convex anteriorly. The pleurals show the typical morphology for *Testudo*. They cover only the costals, are quadrangular, and are slightly wider than long. The pleuro-marginal sulcus coincides with the costo-peripheral suture in the preserved portion of the carapace. The marginal scutes are similar in shape to the peripherals, being short and tall.

Plastron: The epiplastra are narrow and anteroposteriorly short. Although covered with sediment, both epiplastra are thickened anteriorly, suggesting the presence of an epiplastral lip. The entoplastron is wider than long, being rhomboid to subcircular in shape. Among the scutes, only the gulars are clearly distinguishable. They are long and narrow, covering the anterior part of the entoplastron. The humero-pectoral sulcus is preserved only on one side, and is only partially visible, but is located posterior to the entoplastron.

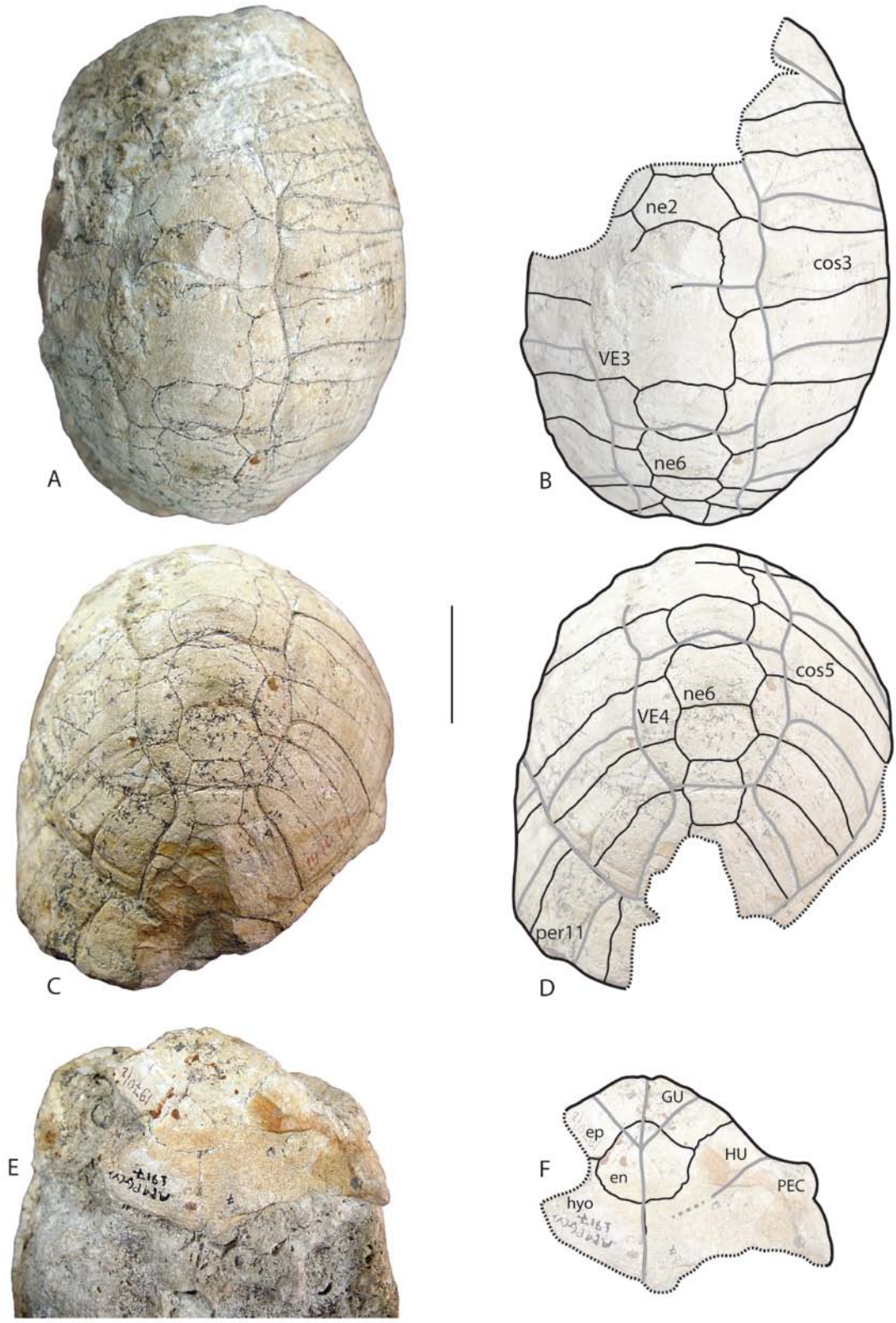


Figure 3.51. *Testudo graeca* Linnaeus, 1758 from the uppermost Miocene – lowermost Pliocene of Allatini, Thessaloniki, Greece. AMPG 1970/2, partial shell in (A) dorsal, (B) drawing of dorsal, (C) posterodorsal, (D) drawing of posterodorsal, (E) ventral and (F) drawing of ventral views. Scale bar equals 5 cm. For abbreviations see Material & Methods.

Vatera, Lesvos Island

The small testudinid material from the locality of Vatera in Lesvos Island consists of two partial specimens. The first specimens is a partial carapace with the infilling sediment. The preservation status does not allow further description. The second specimen is a partial shell, preserving several parts of the carapace and plastron (Fig. 3.52). From the carapace, the anterior and middle part is preserved, missing the left anterior rim. From the plastron, both epiplastra and the posterior lobe are missing.

Carapace: The nuchal is hexagonal, wider than long. The anterior nuchal border is straight. Only the first five neurals are preserved. The neural 1 is quadrangular, sub-rounded, longer than wide. The neural 2 is octagonal, the anterior part being narrower than the posterior. The neural 3 is quadrangular, sub-rounded and much wider than long. The neural 4 is octagonal, wider than long, and the anterior and posterior sides are of equal width. Neural 5 is quadrangular, wider than long. The costal 1 is the largest costal, making contact with the nuchal, neurals 1-2, and peripherals 1-3. Costals 2-6 show an alternating pattern following the alternation of octagonal/quadrangular neurals. Costal 2, costal 4 and costal 6 are shorter medially and longer laterally, alternated with costal 3 and costal 5 that are medially long and laterally short.

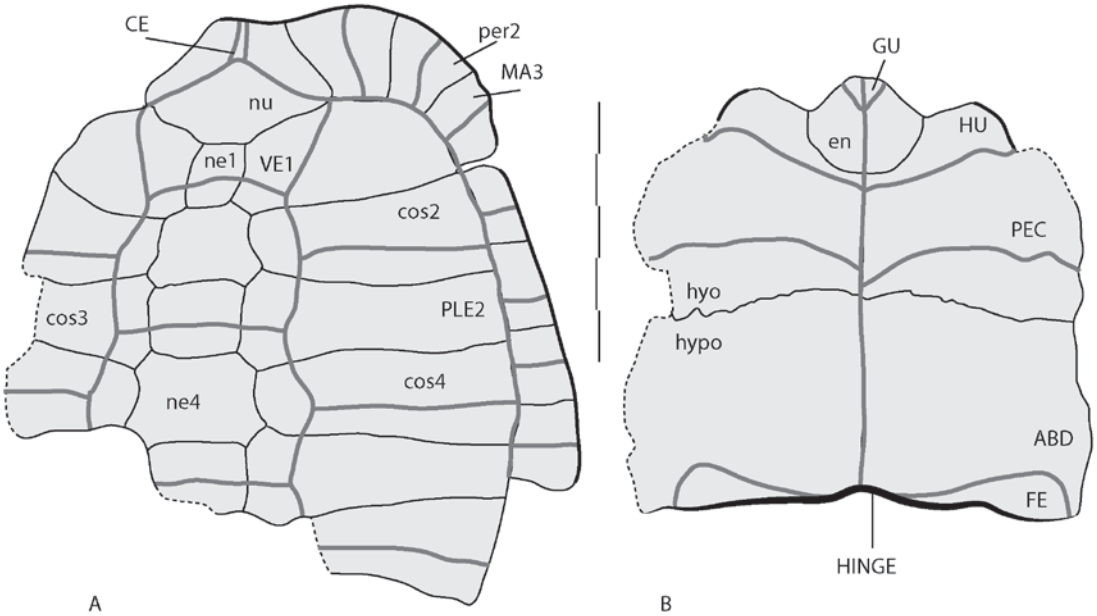


Figure 3.52. *Testudo graeca* Linnaeus, 1758 from the Early Pleistocene of Vatera, Lesvos Island. PO 168, partial shell in (A) drawing of dorsal and (B) drawing of ventral views. Largely based on Lapparent de Broin (2002) and personal observations. Scale bar equals 5 cm. For abbreviations see Material & Methods.

As far as the scute sulci are concerned, anteriorly a long and narrow cervical is present. The vertebrals are wide, as wide as the pleurals. Vertebral 1 is narrower than the rest, having a rounded anterior border on the nuchal and a straight to sinuous posterior border. The limit between the first two vertebrals crosses the neural 1 transversely. The vertebrals are hexagonal, sub-rounded and they cover neurals and medial parts of the costals. The limit between the vertebral 2 and 3 crosses the neural

3 transversely. In the middle the limit shows a small convexity. The limit between the vertebral 3 and 4 crosses the neural 5 transversely. The limits between the pleurals cross the costals 2, 4, and 6. Marginals are long and narrow. All along the periphery of the carapace (except the nuchal), we notice good coincidence between the costo-peripheral suture and the pleuro-marginal sulcus.

Plastron: The entoplastron is long and narrow, roughly hexagonal with rounded borders. The hyo- and hypoplastra are long and wide, displaying a medial convavity. This indicates that this is a male individual. The hypoplastra end right in the end of the bridge and do not contribute in the formation of the posterior lobe. The posterior lobe must have been formed entirely by the xiphiplastra. The gulars are long, covering the anterior part of the entoplastron. The remaining part of the entoplastron is covered medially by the humerals that are long and wide. The humero-pectoral sulcus is wide V-shaped and is situated posterior to the entoplastron. Laterally, the humero-pectoral sulcus is convex. The pectorals are short but wide. The pectoro-abdominal sulcus is sinuous. The abdominals are the largest scutes preserved, covering the posterior half of the hyoplastra and nearly all the surface of the hypoplastra. Only the postero-lateral part of the hypoplastra is covered by the femorals. The abdomino-femoral sulcus is slightly convex laterally, but is situated on the posterior hypoplastral suture medially. All the above-mentioned morphologies in the posterior hypoplastra suggest a mobile posterior lobe and the presence of a hypo-xiphiplastral hinge.

DISCUSSION

The *T. graeca* complex has a convoluted taxonomic history, characterized by numerous nominal species and subspecies (see for example Fritz et al., 2007b, and references therein). In many cases, characters relating to scute coloration or keratinous features (thigh-spurs in *T. graeca*) are used to distinguish the subspecies, but such characters are not preserved in fossil specimens. For example, although *ibera* is normally considered as a subspecies of *Testudo graeca*, it has been elevated to the species level by some authors (e.g. Perälä, 2001 amongst others). According to Perälä (2001) *T. graeca* s.l. is paraphyletic to the species level, being a composite of several species (i.e. the previous subspecies elevated to the species level). Mitochondrial works however (e.g. Fritz et al., 2007b; 2009) found support of a monotypic *T. graeca* and for its subspecies. Given that the available material for this thesis contains only shell remains and no skulls, further identification the studied material from the *T. graeca* complex is not possible. Therefore all these specimens are tentatively referred to *T. graeca* sensu lato.

All the above-mentioned specimens can be referred to Testudinidae, among other features, based on the presence of a thickened epiplastral lip and the alternating pattern of the costals. The presence of a cervical scute, the pattern of the neural plates, the fact that the costo-peripheral sutures coincide with the pleuro-marginal sulci, and the fact that the gulars cover the anterior part of the entoplastron (among other features) indicate that they belong to the genus *Testudo* (e.g. Mlynarski, 1976; Lapparent de Broin et al., 2006a,b,c; and references therein). In most cases the presence of a hypo-xiphiplastral hinge and the fused marginals 12 have been confirmed, allowing attribution to *Testudo graeca.*

The updated morphological description presented above allows the revision of previously published information. For example, the material from Allatini/Pylea has

been provisionally attributed to the Late Miocene species *Testudo amiatae* Pantanelli, 1893a by Del Campana (1917). This taxon was described on the basis of a relatively well-preserved shell from "Fosso Merlaccione" close to Cinigiano (Tuscany, Italy; Pantanelli, 1893a, b), now housed in the collections of the Museo di Paleontologia dell'Università di Modena with the collection number MPUM 25. Auffenberg (1974) lists *T. amiatae* as a junior synonym of *T. antiqua*. Chesi (2008) redescribed the holotype and remarked that it represents a small *Testudo*-like male, being a domed shell 140 mm long, 110 mm wide and 84 tall. The plastron is moderately concave, with a wide anal notch. MPUM 25 is further characterized by broad vertebrals and a sutural connection between the hypoplastra and xiphiplastra. The absence of a hinge is also supported by the considerable distance between the abdomino-femoral sulci and the hypo-xiphiplastral sutures. Chesi tentatively accepted the validity of *T. amiatae*, but questioned its generic identification and suggested that it could belong to the *Testudo hermanni*-*Testudo horsfieldi* lineage because of the sutural relationships between the hypoplastra and xiphiplastra. As described above, the Allatini material clearly differs from *T. amiatae* and cannot be referred to this species. *Testudo amiatae* is therefore known only from its type locality (despite being abundant, all other fossil *Testudo* specimens from Tuscany are referred to extant species or remain unidentified at the species level; Chesi, 2008; Rook et al., 2013).

A recent attempt by Georgalis and Kear (2013) to summarize the fossil turtles of Greece only complicated our scientific understanding of the Allatini fauna. First of all, the site was erroneously placed by these authors in the Mygdonia basin, rather than within the city limits of Thessaloniki (see our Fig. 1A). Second, there was no mention of the giant tortoise eggs (in Del Campana, 1919). Finally, they confused the Athens specimen (described by Bachmayer and Symeonidis, 1970) with the Florence specimen (studied by Del Campana, 1917). In detail, they write: "[…] the only other extinct small-bodied testudinid species documented from Greece is *T. amiatae* from the latest Miocene (Messinian-Zanclean) Trilophos Formation of Allatini, near Thessaloniki (Campana, 1917). This taxon was first described from Tuscany […], with the only known Greek specimen […] consisting of a poorly-preserved shell (AMPG(y) 1917/1970/2) referred solely on the basis of its immobile xiphiplastra, a distinguishing feature of *Testudo* sensu lato […]. However, our inspection of AMPG(y) 1917/1970/2 found the posterior plastron to be missing, thus its taxonomic assignment is impossible to substantiate." (Georgalis & Kear, 2013:304). Therefore, it is clear that these authors inspected the AMPG specimen (first described by Bachmayer and Symeonidis, 1970) as the original specimen in del Campana (1917). Indeed the posterior plastron is missing in the Athens specimen, but is preserved complete in the Florence specimen studied by del Campana (1917)

The information presented implies that the tortoises from Allatini/Pylea should be attributed to the *Testudo* s.s. lineage, and in particular to *Testudo graeca*. Among other features, the wide vertebrals of the carapace are characteristic of *Testudo* s.s., and differ from the narrower vertebrals of *Testudo hermanni* (Amiranashvili, 2000; Lapparent de Broin et al., 2006b). Further evidence comes from the plastron. Several characters suggest the presence of a hypo-xiphiplastral hinge in the Florence specimen (for details on the morphology of the hinge in *Testudo* s.s., see Lapparent de Broin et al., 2006b). First, the posterior lobe is formed entirely by the xiphiplastra and is elongated compared to the hypoplastra. In all hingeless taxa, the anterior part of the posterior lobe is contributed by the hypoplastra. Second, the extent to which the femoral scutes cover the posterior parts of the hypoplastra is much reduced medially. Third, the posterior lobe is preserved slightly misplaced, indicating a loose connection

with the hypoplastra. Finally, the abdomino-femoral sulcus coincides medially with the hypo-xiphiplastral suture, as is typical in taxa with a hinge (Amiranashvili, 2000; Lapparent de Broin et al., 2006b; Delfino et al., 2009). For all the above, a conclusive remark is that the species *Testudo amiatae* is not present in the Greek fossil record.

The Florence and Athens specimens display some important morphological differences with regard to the bony elements of the carapace, despite similarities in the positions of the scute sulci of the carapace and the morphology of the plastron that strongly support their referral to the same species. In particular, the neural series is different. In the Florence specimen we observe the typical differentiated condition of *Testudo* with alternating quadrangular and octagonal neurals. The Athens specimen on the other hand, shows a less differentiated (more primitive) neural series. The second neural is hexagonal. Unfortunately, this region cannot be clearly studied in the Florence specimen, but a hexagonal second neural (or even an octagonal one with very short anterolateral sides) is a relatively normal feature that can be found in several extant specimens of *Testudo graeca*. Moreover, the sixth and seventh neurals of the Athens specimen are also hexagonal, a condition that is rare in the *Testudo* s.s. lineage (Lapparent de Broin et al., 2006b: 334). Similarly, the sulci separating the vertebrals differ in position between the Athens and Florence specimens, being located near the posterior margin of the neurals in the Florence specimen.

The most relevant comparison that can be made is to the complete shell from the Pliocene of Megalo Emvolon, which was described as *Testudo* cf. *graeca* by Bachmayer et al. (1979). The specimen presents enough morphological information to be attributed to *Testudo graeca*. This specimen (NHMW 1980z0069/0000) is more similar to the Florence specimen than the Athens specimen in having a well-differentiated neural region, which differs in only in two minor respects. First, the fourth neural of the Megalo Emvolon specimen is significantly wider than the other neurals, a condition not observed in the Florence specimen. Second, the sulci between the vertebrals in the Megalo Emvolon specimen are straight, in contrast with the wavy condition in the Florence specimen. Few differences in plastron morphology exist between the two specimens as well, and these concern mainly the shape of the entoplastron. In the Megalo Emvolon specimen, the entoplastron is much narrower and longer than in either of the specimens from Allatini and Pylea.

The specimens from “Salonique” have been previously identified as *Testudo* sp. but their overall morphology allows identifying them as members of the *Testudo graeca* lineage. Therefore, based on the information gained from the material coming from across the boundary of Mio-Pliocene (Allatini/Pylea) and from the Pliocene localities (Aggelochori/Megalo Emvolon; “Salonique”) confirm the presence of the spur-thighed tortoise in the Pliocene. These specimens are almost identical in morphology with the Pleistocene specimens described above, such as those from Petralona Cave, Potidea and Vatera, proving that this species was continuously present in northern Greece at least for the last 5.33 million years.

However, many Mio-Pliocene *Testudo* fossils remain unidentified at the species level, so that the actual oldest record of *T. graeca* remains an open question. In other words, how far back in time can we confidently identify this taxon based on morphological characters that can be found in fossils? In the next section some material from the Late Miocene of Platania is described, which could be associated with the *T. graeca* lineage, but the preservation of the specimen does not allow a clear conclusion. Hopefully, more specimens from the Late Miocene times will be described in the future in order to allow establishing the oldest record of this taxon, a result that would be useful for the study of the divergence times of this clade.

02/16/2016 Ψηφιακή Βιβλιοθήκη Θεόφραστος - Τμήμα Γεωλογίας - Α.Π.Θ.

Extinct specimens of *Testudo* s.s. are difficult to be confidently identified into the subspecies level in many cases, like in *T. g. ibera*, because the differences are found on characters that are not preserved in fossils (e.g. coloration). Fritz et al. (2009) used *Testudo burtschaki* from Caucasus area (Upper Sarmatian–Lower Maeotian), to estimate the split between *T. graeca* and the clade grouping *T. kleinmanni* and *T. marginata* between 10.0–8.0 Ma, with the minimum divergence between *T. graeca* subspecies estimated much later, in the Pliocene. However, Delfino et al. (2009:851) have questioned the inclusion of *T. burtschaki* in the *Testudo* s.s. group, since this taxon has no plastral hinge, stressing the importance of detailed anatomical descriptions of extant *Testudo* species. Fritz et al. (2009) mention also *Testudo eldarica* from the slightly younger strata from Azerbaijan (Maeotian), as one of the oldest members of the *T. graeca* group, following Danilov (2005). These two taxa from Caucasus area need revision before they are used as molecular clock estimates, following the recommendations by Parham et al. (2012) for the use of fossils for temporal calibrations. The same is true for most Late Miocene *Testudo* specimens, because most of the available information is outdated. In the next chapter the phylogenetic relationships within Testudinidae are explored, by analyzing extant and extinct taxa from a morphological point of view.

One of the major problems of the use of fossils in such calibrations is the incorrect placement of a specimen as the oldest record of this clade (Parham et al., 2012:348). Future research should focus in the clarification of the taxonomic status of the Late Miocene – Pliocene *Testudo* s.s. specimens of the circum-Mediterranean area. Many specimens are known. In Italy, the only record of *Testudo* s.s. is *Testudo pecorinii* Abbazzi, Carboni, Delfino, Gallai, Lecca and Rook, 2008, from the Late Pliocene of Capo Mannu. Unfortunately, the preserved parts in the holotype of *T. pecorinii* do not allow further comparison with the Platania specimen. In Western Europe, *Testudo graeca* has been proposed as introduced by humans in Holocene times (Moralez Pérez & Serra, 2009). In North Africa, the oldest reliable record of a hinged *Testudo* is from Ahl Al Oughlam (Morocco, Pliocene, see Gmira et al., 2013) and possibly from Ichkeul (Tunisia, Pliocene), probably originated from the Palaearctic (Lapparent de Broin, 2000). Future research should focus on the detailed description of the hinged specimens from the area between Caucasus, South Balkans and Turkey, to provide new information on the probably oldest records of *Testudo* sensu stricto. In Turkey for example, Staesche et al. (2007) reported the presence of *Testudo* sp. cf. *graeca* since MN6 (Astaracium) from Ankara–Kalecik–Çandir. This material is not figured to be able to confirm their identification, whereas the figured specimens from other Turkish localities could be attributed to *Testudo* sensu lato.

From a distributional point of view, it is surprising that the distribution of the fossil *T. graeca* is within the boundaries of the extant *T. graeca* in Greece (see Chapter 1.3). All the fossil specimens that have been attributed to *T. graeca* do not reach beyond the area of Thessaloniki, as the extant *T. graeca.* Of course further sampling should corroborate with this result.

Testudo cf. *graeca*

MATERIAL: Platania, Drama (Late Miocene; 2 specimens) (Fig. 3.53-3.55): LGPUT PLD 70, partial shell; LGPUT PLD 71, right humerus, proximal part.

DESCRIPTION

LGPUT PLD 70: This partial shell consists of the anterior carapacial margin and the right bridge, the left posterior carapacial margin and most of the plastron. The right xiphiplastron is missing. This, black in color, specimen has been recovered in natural position, but the visceral side of the plastron is eroded and almost empty of appendicular elements. The only exception is a partial right humerus, found inside this specimen. Moreover, all the breaks of the carapace are either on sutural surfaces, or are eroded. Based on the above, we assume that the shell has undergone some modification prior to burial, but only for a short period. This is because the mobile xiphiplastra, which are connected with the plastron with a hinge, were not found disarticulated.

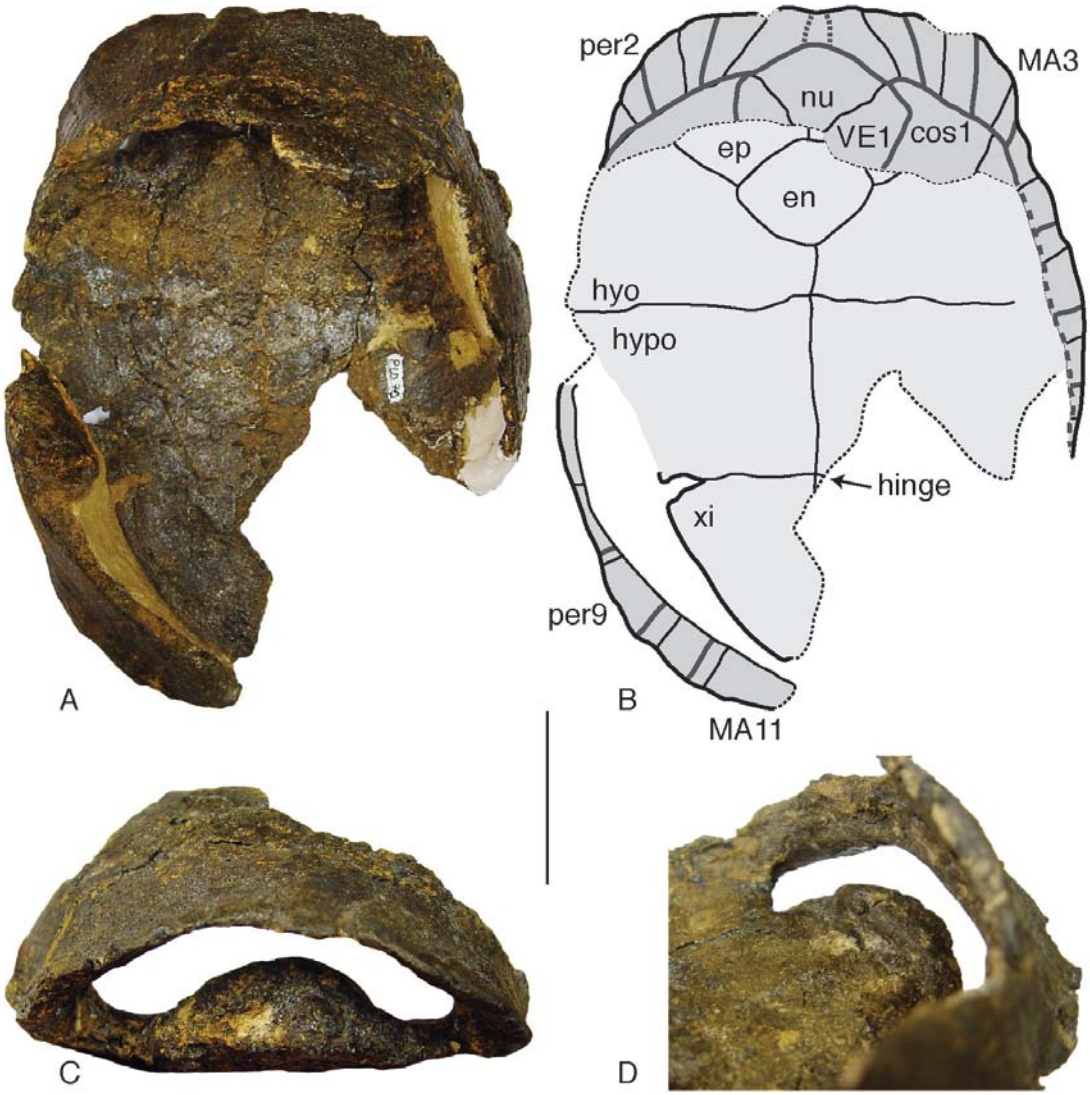


Figure 3.53. *Testudo* cf. *graeca* from the Late Miocene of Platania (Drama basin, Northern Greece). LGPUT PLD 70, partial carapace and plastron in (A) dorsal, (B) drawing of the dorsal, (C) anterior and (D) right dorso–lateral views. Scale bar equals 5 cm. For abbreviations see Material & Methods.

Carapace (Fig. 3.53): From the carapace, the anterior margin with the nuchal is preserved with most of the right bridge, i.e. from the partial 3rd left till the anterior region of the 7th right peripheral. The nuchal is hexagonal in shape, with a narrow posterior part. Anteriorly, a very weak and wide, almost non–existent, nuchal notch is present. Only some parts of the left and right 1st costals are preserved. Posteriorly, only the left carapacial margin is preserved, from the 6th to 11th peripheral. Anterior and posterior peripherals are long and narrow, whereas those from the bridge area are much taller. From the shape of the 11th peripheral we can estimate that the pygal is trapezoid in shape, with narrower posterior end. Based on the curved shape of the preserved 11th peripheral, we can assume that the pygal was also curved inwards. This is commonly found in *Testudo graeca* and *"Testudo" hermanni* (both in males and females), but not in *Testudo marginata*, where the pygal is posteriorly flared. The nuchal is crossed by the vertebro–marginal sulcus in the anterior part and, despite the fact the anterior margin is eroded, the presence of a cervical scute can be confirmed. The cervical is probably longer than wide. Throughout the preserved parts, the costo–peripheral suture coincides with the pleuro–marginal sulcus, which is a typical character of most testudinids.

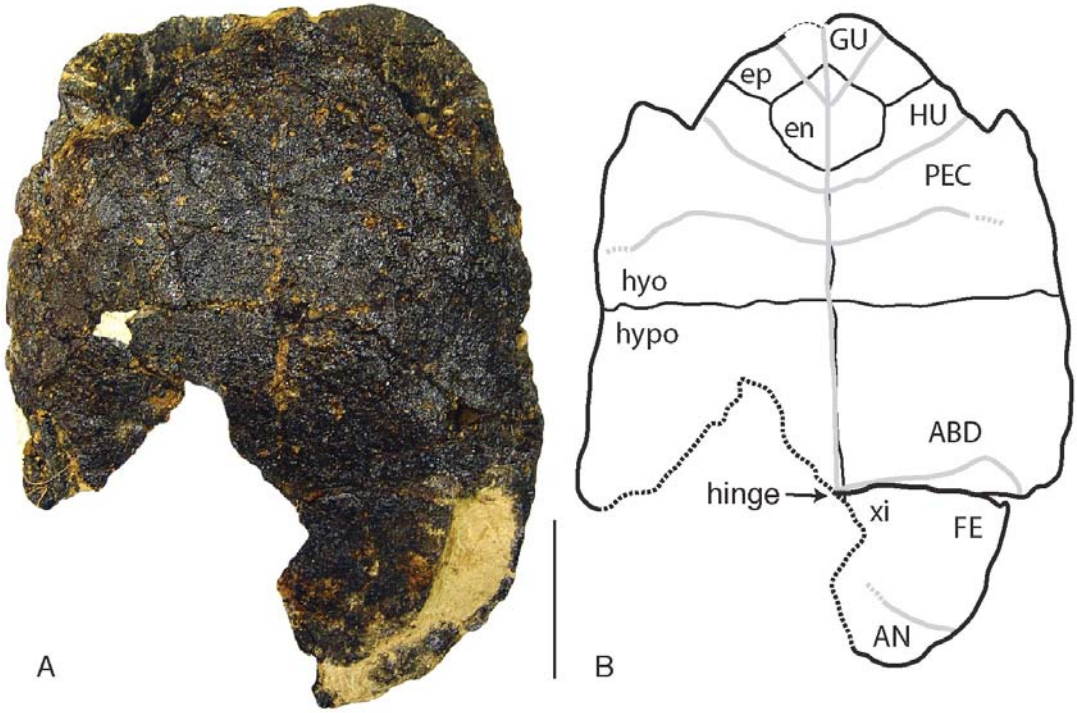


Figure 3.54. *Testudo* cf. *graeca* from the Late Miocene of Platania (Drama basin, Northern Greece). LGPUT PLD 70, plastron in (A) ventral and in (B) drawing of the ventral views. Scale bar equals 5 cm. For abbreviations see Material & Methods.

Plastron (Fig. 3.54): Most of the plastron is preserved, whereas only the right xiphiplastron is missing. The epiplastra are short, forming a very thick epiplastral lip with a deep pocket. The epiplastral lip is convex. In ventral view, the entoplastron is hexagonal. Hyo– and hypoplastra are the largest plates of the plastron. The medial part of the hyo- and hypoplastra is flat, indicating that the Platania tortoise is a female individual; normally, the male individuals show a deep concavity in their plastron. Xiphiplastra are longer than wide, representing the entire length of the posterior lobe. Posteriorly, the xiphiplastra show a very wide and short anal notch. The gular scutes are longer than wide, covering the medial part of the epiplastra and the anterior part of

the entoplastron. The shape of the humero–pectoral sulcus is wide V–shaped, located on the hypoplastra and being posterior to the entoplastron. The pectoro–abdominal sulcus is sigmoidal in shape, being concave in the medial part and convex laterally. The pectorals are short and wide, whereas the abdominals are the longest scutes in the plastron. The abdomino–femoral sulcus coincides medially with the hypo–xiphiplastral suture; laterally it is located in the posterior parts of the hypoplastra, being strongly convex. This morphology, which is noted in many extant and extinct *Testudo* s.s., indicates the presence of a movable hinge between the hypo– and xiphiplastra. The anals are longer medially and shorter laterally, while the femoro–anal sulcus is slightly concave on each side.

Appendicular skeleton (Fig. 3.55): Only the proximal part of the right humerus is preserved. This element has been recovered in anatomical position, resting on the visceral side of the right epiplastron. The trochanters are partially preserved, but they are developed sub–parallel to each other. The humeral head is spherical. From the preserved part we can estimate the shaft of the bone that is curved. In general, the morphology of the PLD humerus is similar to the morphology of the extant *Testudo graeca*.

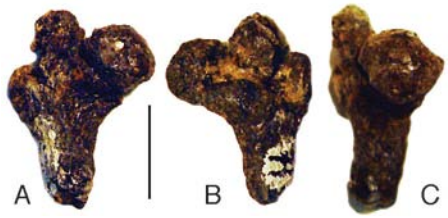


Fig. 3.55. *Testudo* cf. *graeca* from the Late Miocene of Platania (Drama basin, Northern Greece). Proximal part of the right humerus (LGPUT PLD 71) of the specimen in (A) posterior, (B) anterior and (C) dorsal views. Scale bar equals 1 cm.

Comments: This specimen has been described in detail by Vlachos & Tsoukala (in press). Detailed comparisons indicate that the Platania specimen is consistent with the morphology of *T. graeca* lineage (based on the evident hypo-xiphiplastral hinge and the pygal which is curved inwards). The limited information, however, on the morphology of the carapace of this specimen does not allow a confident assessment to this taxon. Based on the preserved parts, the Platania tortoise can be identified for the moment as *Testudo* cf. *graeca*, but is clearly different from the other taxa found in the Late Miocene (*T. marmorum* and the new testudinid from Ravin de la Pluie). The Platania tortoise could be one of the oldest *T. graeca* in Greece and South Balkans, but more specimens are needed, together with the detailed study of the associated fauna that is going to provide more accurate information on the geological age of the specimen. Finally, the Platania specimen is useful for the estimation of the paleozoogeographical range of the genus *Testudo* in Greece. The Platania tortoise is the northernmost chelonian finding, extending the range of *Testudo* to Drama basin. Before this discovery, the northernmost finding was from Xerias locality, in Kavala region of Pleistocene age (Tsoukala et al., 2011). This material consists of a compressed shell of *Testudo* sp. which, based on the presence of hypo–xiphiplastral hinge and widened posterior carapace, could be associated with the marginated tortoise and not with *T. graeca*.

Testudo marginata Schoepff, 1793

AGE: Recent – Pleistocene (Cave sites in Rethymnon area, Crete Island such as Gerani, Zourida, Koumpes, Liko, Mavro Mouri IV, Simonelli, Bate; Kos Island; Charkadio Cave, Tilos Island)

MATERIAL:

Gerani Cave, Crete (1 specimen) (Fig. 3.56-3.57): AMPG 3/1974, shell.

Zourida Cave, Crete (9 specimens) (Fig. 3.58-3.59): AMPG 2071, almost complete carapace; AMPG 577, posterior carapace; AMPG 578, fragment of the posterior lobe; AMPG 600, left hyoplastron fragment; AMPG 601, plastron fragment; AMPG 602, left humerus; AMPG 603, right femur; AMPG 604, left scapula; AMPG 605, right humerus.

Koumpes Cave, Crete (18 specimens) (Fig. 3.60-3.61): AMPG 576, left part of a shell; AMPG 579, costal fragment; AMPG 580, right epiplastron; AMPG 581, peripheral; AMPG 582, plastron fragment; AMPG 583, costal fragment; AMPG 584, hyo/hypo fragment; AMPG 585, hyo/hypo fragment; AMPG 586, plastron fragment; AMPG 587, plastron fragment; 595, costal fragment; 596, left epiplastron fragment; 597, right humerus; 598, femur diaphysis; 599, femur head; 618, left hypoplastron fragment; 619, peripheral; 620, humerus diaphysis.

Liko Cave (70 specimens) (Fig. 3.62-3.64): AMPG 551, left shell part; AMPG 552, part of the bridge; AMPG 553, costal; AMPG 554, peripheral; AMPG 555, right xiphiplastron; AMPG 556, suprapygal; AMPG 557, peripheral; AMPG 558, peripheral fragment; AMPG 559, costal fragment; AMPG 560, left hypoplastron fragment; AMPG 561, plastron fragment; AMPG 562, costal fragment; AMPG 563, peripheral; AMPG 564, hyo/hypo fragment; AMPG 565, costal fragment; AMPG 566, costal fragment; AMPG 567, left hypoplastron fragment; AMPG 568, peripheral; AMPG 569, left epiplastron; AMPG 570, plastron fragment; AMPG 571, costal fragment; AMPG 572, anterior plastral lobe; AMPG 573, peripheral & costal fragment; AMPG 574, peripheral; AMPG 575, left hyoplastron; AMPG 588, hyoplastron fragment; AMPG 589, entoplastron; AMPG 590, peripheral; AMPG 591, suprapygal; AMPG 592, costal fragment; AMPG 593, tibia; AMPG 594, posterior ungual; AMPG 610, left hypoplastron fragment; AMPG 611, left hyoplastron fragment; AMPG 612, costal fragment; AMPG 613, cervical vertebra; AMPG 614, 1st dorsal vertebra; AMPG 615, left shoulder girdle; AMPG 616, humerus; AMPG 617, pelvis fragment; AMPG 625, scapula; AMPG 626, peripheral; AMPG 627, costal; AMPG 628, costal fragment; AMPG 672, costal fragment; AMPG 673, plastron fragment; AMPG 674, coracoid; AMPG 675, femur fragment; AMPG 676, femur fragment; AMPG 677, tibia distal part; AMPG 732, plastron fragment; AMPG 733, plastron fragment; AMPG 734, plastron fragment; AMPG 780, peripheral 11; AMPG 781, peripheral 8; AMPG 782, peripheral; AMPG 783, shell fragment; AMPG 784, costal fragment; AMPG 785, costal fragment; AMPG 787, humerus; AMPG 797, costal fragment; AMPG 798, costal fragment; AMPG 799, peripheral; AMPG 800, peripheral; AMPG 801, left epiplastron; AMPG 802, carapace fragment; AMPG 803, carapace fragment; AMPG 804, carapace fragment; AMPG 805, carapace fragment;

AMPG 806, costal fragment; AMPG 807, peripheral; AMPG 808, ulna; AMPG 809, tibia; AMPG 810, fibula.

Mavro Mouri IV, Crete (122+ specimens) (Fig. 3.65-3.66): NHMC FS38/60, anterior lobe; NHMC FS38/61, right hyoplastron; NHMC FS38/62, left hyoplastron; NHMC FS38/63, right hyoplastron; NHMC FS38/64, anterior peripherals; NHMC FS38/65, posterior peripherals; NHMC FS38/66, peripheral; NHMC FS38/67, xiphiplastron fragment; NHMC FS38/68, xiphiplastron fragment; NHMC FS38/69, hyoplastron fragment; NHMC FS38/70, left humerus fragment; NHMC FS38/71, right humerus fragment; NHMC FS38/72, humerus diaphysis; NHMC FS38/73, humerus diaphysis; NHMC FS38/74, humerus diaphysis; NHMC FS38/75, humerus diaphysis; NHMC FS38/76, scapula fragment; NHMC FS38/77, femur diaphysis; NHMC FS38/78, group of 9 fragments; AMPG 678, right hyoplastron; AMPG 679, left hyoplastron; AMPG 680, left hypoplastron; AMPG 681, left hypoplastron; AMPG 682, left hyoplastron; AMPG 683, right hyoplastron; AMPG 684 right hyoplastron; AMPG 685, left hyoplastron; AMPG 686, costal fragment; AMPG 687, peripheral; AMPG 688, peripheral; AMPG 689, costal fragment; AMPG 690, posterior peripheral; AMPG 691, posterior peripheral; AMPG 692, posterior peripheral; AMPG 693, posterior peripheral; AMPG 694, posterior peripheral; AMPG 695, posterior peripheral; AMPG 696, peripheral; AMPG 697, posterior peripheral; AMPG 698, costal fragment; AMPG 699, costal fragment; AMPG 700, costal fragment; AMPG 701, costal fragment; AMPG 702, peripheral fragment; AMPG 703, peripheral; AMPG 704, peripheral fragment; AMPG 705, costal fragment; AMPG 706, costal fragment; AMPG 707, peripheral fragment; AMPG 708, carapace fragment; AMPG 709, neural fragment; AMPG 710, peripheral; AMPG 711, right hyoplastron; AMPG 712, hypoplastron fragment; AMPG 713, left hyoplastron; AMPG 714, peripheral; AMPG 715, costal fragment; AMPG 716, left 7th peripheral; AMPG 717, right epiplastron; AMPG 718, left epiplastron; AMPG 719, left epiplastron; AMPG 720, left hyoplastron; AMPG 721, right 3rd peripheral; AMPG 722, left 3rd peripheral; AMPG 723, left hyoplastron; AMPG 724, peripheral; AMPG 725, peripheral; AMPG 726, costal fragment; AMPG 727, humerus diaphysis; AMPG 728, cervical vertebra; AMPG 729, vertebra fragment; AMPG 730, osteoderm; AMPG 731, ungual; AMPG 742, left xiphiplastron fragment; AMPG 743, left xiphiplastron fragment; AMPG 744, plastron fragment; AMPG 745, hypoplastron fragment; AMPG 746, peripheral fragment; AMPG 747, plastron fragment; AMPG 750, left epiplastron; AMPG 751, left and right epiplastron; AMPG 752, entoplastron fragment; AMPG 755, nuchal; AMPG 756, posterior peripheral; AMPG 757, costal fragment; AMPG 758, hyoplastron fragment; AMPG 759, left hyoplastron; AMPG 760, hypoplastron fragment; AMPG 761, hyoplastron fragment; AMPG 762, plastron fragment; AMPG 763, plastron fragment; AMPG 764, plastron fragment; AMPG 765, plastron fragment; AMPG 766, plastron fragment; AMPG 767, plastron fragment; AMPG 768, plastron fragment; AMPG 769, plastron fragment; AMPG 770, plastron fragment; AMPG 771, plastron fragment; AMPG 772, plastron fragment; AMPG 773, plastron fragment; AMPG 774, plastron fragment; AMPG 775, plastron fragment; AMPG 776, plastron fragment; AMPG 777, plastron fragment; AMPG 794, hyoplastron fragment; AMPG 795, plastron fragment; AMPG 796, plastron fragment; AMPG 811, group appr. 100 frs; AMPG 812, peripheral fragment; AMPG 813, costal fragment; AMPG 814, 8th costal fragment; AMPG 815, costal fragment; AMPG 816, neural fragment;

AMPG 817, costal fragment; AMPG 818, ilium fragment; AMPG 854, anterior lobe; AMPG 855, right xiphiplastron.

Simonelli Cave, Crete (4 specimens) (Fig. 3.67): AMPG 606, right humerus; AMPG 607, humerus diaphysis; AMPG 607, distal femur; AMPG 608, sacral vertebra.

Kos Island (1 specimen) (Fig. 3.68): NHMC FS38/8, left hyoplastron.

Charkadio Cave, Tilos (114 specimens) (Fig. 3.69-3.75): inventory under prep. (AMPG collection).

Poulion Cave, Boetia (15 specimens; some numbers to be given) (Fig. 3.76): right humerus complete; 7th left peripheral; entoplastron complete; 282, left humerus (distal missing); 283, left humerus (distal missing; young); 284, femur (distal part); 285, femur diaphysis; 286, femur diaphysis; 287, right humerus (proximal part); 288, right humerus diaphysis; 289, right humerus (young); 290, left humerus (juvenile); 291, right humerus (juvenile); 292, right humerus (juvenile); 293, left humerus (juvenile).

Kythera Island (3 specimens; numbers to be given) (Fig. 3.77): left humerus (distal missing, large size); left humerus (proximal part, large size); right radius.

DESCRIPTION

Gerani Cave, Crete

AMPG 3/1974: This specimen was described as the holotype of the endemic taxon *Testudo marginata cretensis* Bachmayer et al., 1975. See below for comments regarding the validity of this subspecies. The specimen is preserved almost complete. For the carapace only some plates are missing from the anterior, from the right bridge and from the medial parts. From the plastron only some parts of the medial hyo- and hypoplastra are missing. The specimen is very fragile and is safely put in a metal skeleton. This, however, does not allow observation of the visceral sides.

Carapace (Fig. 3.56): The nuchal is partially preserved but is wider than long. The neural 1 is hexagonal, longer than wide, with short posterior lateral sides. The posterior part of the neural 1 is wider than the anterior one. The neural 2 is octagonal with rounded edges, slightly wider than long. Neural 3 is quadrangular, wider than long. Neural 4 is octagonal, wider than long. Neural 5 is quadrangular, wider than long, whereas the posterior part is narrower than the anterior. Neural 6 is hexagonal, wider than long, wider than neural 5 and with short anterior lateral sides. Neural 7 is also hexagonal, narrower than neural 6. In the neurals crossed by the vertebral sulci (neurals 1, 3, 5) pointed dorsal bumps are noted. The suprapygal pygal area is incomplete, however we can note the presence of a small trapezoid suprapygal 1. The costals are well differentiated to match the alternating pattern of the neurals. The costal 1 is quite large, making contact with the nuchal, the first two neurals, the costal 2 and the peripherals 1-3. Costal 2 is trapezoid, being shorter medially and longer laterally. Costal 4 shows a similar shape, and they are alternated with the costals 3 and 5 that are medially longer and laterally shorter. Costals 6 and 7 are different in shape, showing a double medial suture for the hexagonal neurals. The peripherals are quite long. The anterior peripherals, as well as the posterior ones, are flared. Especially the posterior ones are quite elongated and flared posteriorly. The same is true for the

pygal that is as long as wide. This orientation of the posterior border creates the characteristic posterior carapace of *T. marginata*. In this specimen however, the posterior rim is not horizontally flared.

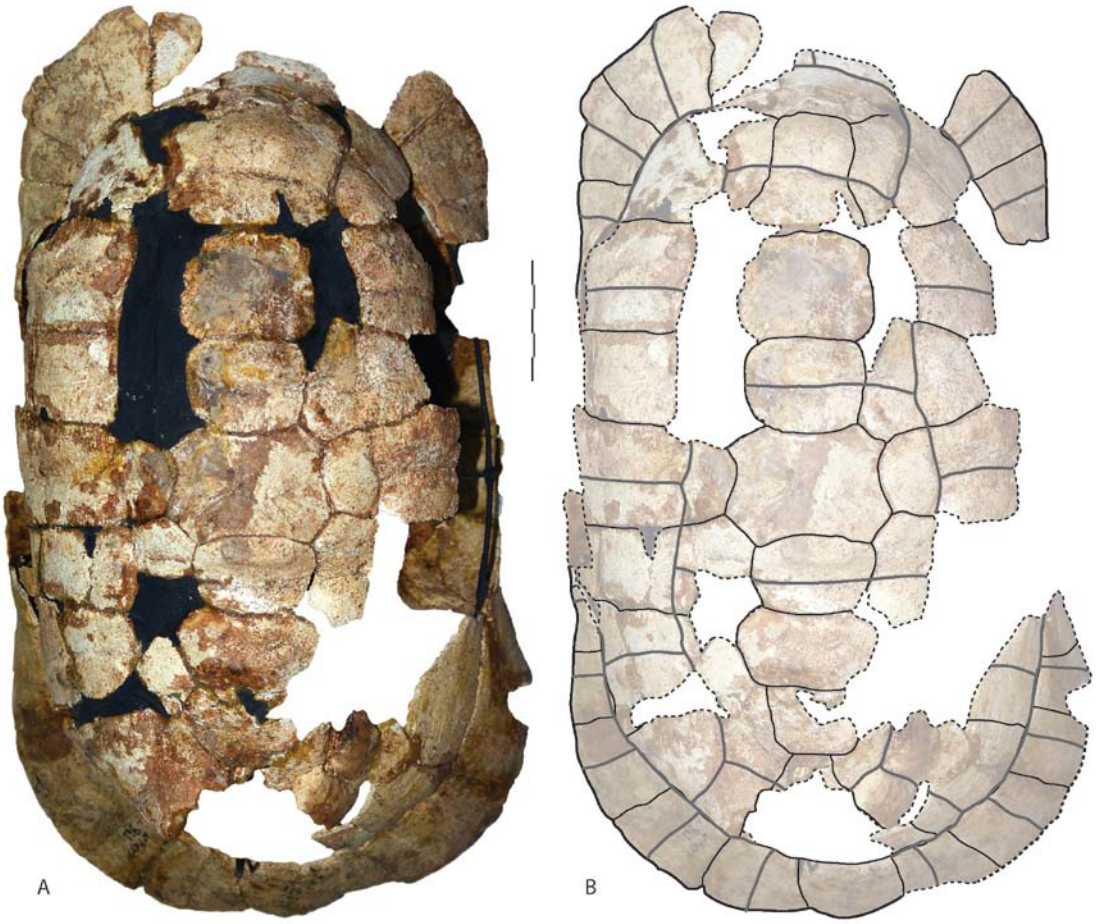


Figure 3.56. *Testudo marginata cretensis* Bachmayer et al., 1975 (AMPG 3/1974) from the Pleistocene of Gerani Cave (Crete). Carapace of the holotype in (A) dorsal and (B) drawing of the dorsal view. Scale bar equals 5 cm.

Although the anterior part of the nuchal is not preserved, the posterior part of a long and narrow cervical is present. The vertebrals are hexagonal, wider than long. Their sulci cross longitudinally neural 1, neural 3, neural 5 and probably the suprapygal 1. In the limits of the vertebrals, dorsal bumps are formed in the neurals. Pleurals are rectangular, crossing costals 2, 4 and 6. The limits of the pleurals with the marginals show a good coincidence with the sutures between the costals and the peripherals. Marginals are long and narrow. The marginals 12 are fused into a wide, trapezoid supracaudal.

Plastron: The anterior lobe of the plastron is short and wide, whereas the posterior lobe is longer. The epiplastra are short and narrow. Viscerally, a thick convex epiplastral lip is formed, with a deep gular pocket. The entoplastron is wide and short, roughly hexagonal with a narrowed posterior part. The hyo- and hypoplastra are long and wide. The posterior lobe is formed entirely by the xiphiplastra, and is not sutured with the hypoplastra. Posteriorly, a wide and shallow anal notch is formed. The gulars are narrow and long, covering the medial epiplastra and the anterior part of the entoplastron. The gularo-humeral sulcus is V-shaped, forming an acute angle with the midline. The rest of the entoplastron is covered by the humerals. The humero-pectoral

sulcus is broadly concave in the midline, strongly convex laterally. It is situated medially on the posterior end of the entoplastron. The limits between the pectorals and the abdominals cannot be confidently observed. The femorals show a small covering on the lateral posterior parts of the hypoplastra, whereas medially the abdomino-femoral sulcus coincides with the posterior hypoplastral suture. The anterior part of the posterior lobe is covered by the femorals that are short medially and long laterally. Alternatively, the anals are medially long and laterally short. Therefore, the femoro-anal sulcus is pointed anteriorly, being strongly convex medially and slightly concave laterally on each side. The absence of tight suture between the hypoplastra and the posterior lobe, the long xiphiplastra forming the entire posterior lobe and the small covering of the femorals on the hypoplastra are morphologies suggesting a mobile posterior lobe. Therefore, the presence of a hypo-xiphiplastral hinge can be hypothesized for this specimen.



Figure 3.57. *Testudo marginata cretensis* Bachmayer et al., 1975 (AMPG 3/1974) from the Pleistocene of Gerani Cave (Crete). Plastron of the holotype in (A) ventral and (B) drawing of the ventral view. Scale bar equals 5 cm.

Comments: we notice some changes compared with the figure 2 in Bachmayer et al. (1975), especially in the shape of the neural 1. Bachmayer et al. (1975) indicate this as rectangular, whereas actually is hexagonal. The shape of the first neural is subject to variation in *T. marginata*. For example it is hexagonal in the recent *T. marginata* in figure 3 of Bachmayer et al. (1975).

Zourida Cave, Crete

AMPG 2071 (Fig. 3.58): This specimen has been also described by Bachmayer et al. (1975) as belonging to *T. marginata cretensis*. A drawing of the dorsal carapace is provided here for the first time. It is an almost complete carapace, missing only some plates that have been reconstructed with plaster.

Carapace: The nuchal is wider than long, showing a small nuchal notch in the area of the cervical scute. The neural 1 is partially preserve, probably being longer than wide, with wider posterior side than the anterior one. The neural 2 is octagonal, wider than long. Neural 3 is quadrangular, longer than wide. Neural 4 is octagonal, slightly wider than long. Neural 5 is quadrangular, slightly longer than wide. Neural 6 is hexagonal, wider than long, wider than neural 5 and with short anterior lateral sides. Neural 7 is also hexagonal, narrower than neural 6. In the neurals crossed by the vertebral sulci (neurals 1, 3, 5) dorsal bumps are noted. The suprapygal pygal area is incomplete, however we can note the presence of a single trapezoid suprapygal. The costal 1 is quite large, making contact with the nuchal, the first two neurals, the costal 2 and the peripherals 1-3. Costals 2 and 4 are shorter medially and longer laterally, alternating with the costals 3 and 5 that are longer medially and shorter laterally. This alternating pattern is typical for the testudinids, to match the octagonal/quadrangular neurals. Costals 6 and 7 are different in shape, showing a double medial suture for the hexagonal neurals. The peripherals are quite long.

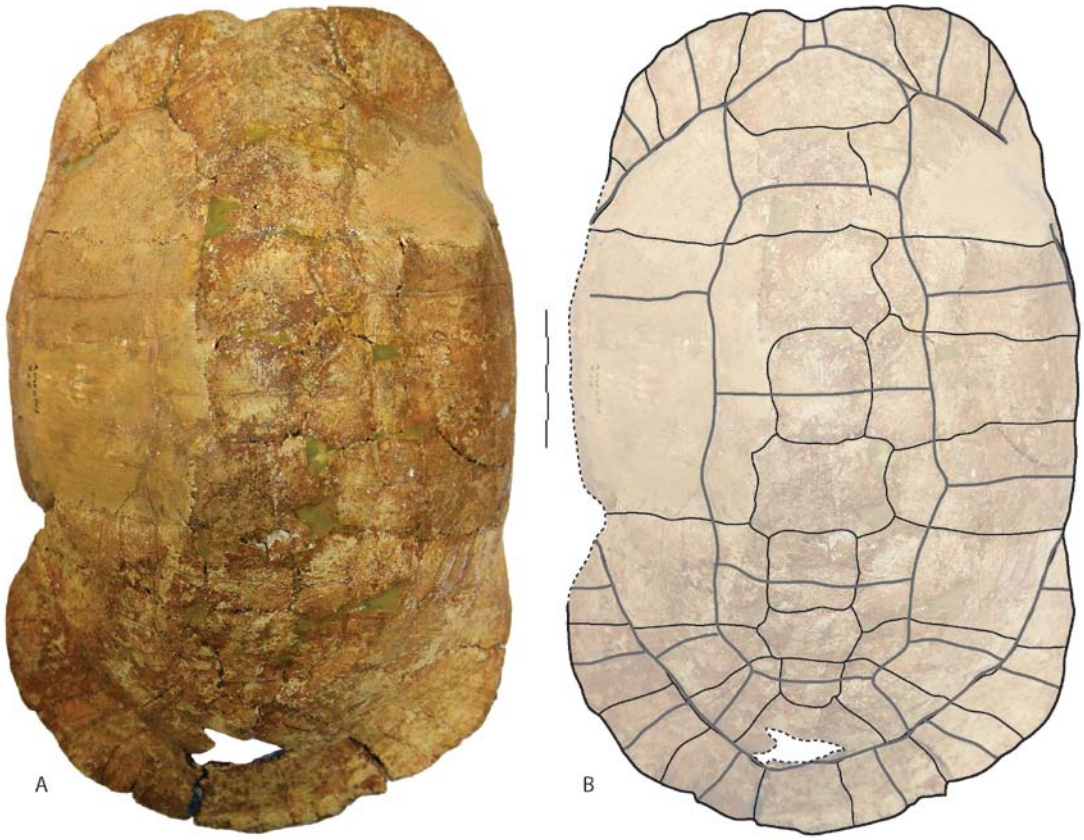


Figure 3.58. *Testudo marginata cretensis* Bachmayer et al., 1975 from the Pleistocene of Zourida Cave (Crete). Carapace of the paratype in (A) dorsal and (B) drawing of the dorsal view. Scale bar equals 5 cm.

The anterior peripherals, as well as the posterior ones, are flared. Especially the posterior ones are quite elongated and flared posteriorly. The same is true for the

pygal, that is as wider than long, with wider posterior side. The posterior rim of the carapace is horizontally flared. A short and narrow cervical is present anteriorly, showing a shallow nuchal notch. The vertebrals are hexagonal, wider than long. Their sulci cross longitudinally neural 1, neural 3, neural 5 and probably the suprapygal 1. In the limits of the vertebrals, dorsal bumps are formed in the neurals. Pleurals are rectangular, crossing costals 2, 4, 6 and 7. The limits of the pleurals with the marginals show a good coincidence with the sutures between the costals and the peripherals. Marginals are long and narrow. The marginals 12 are fused into a wide, trapezoid supracaudal. The anterior side of the supracaudal is narrower than the posterior.

AMPG 577 (Fig. 3.59.A-G): Most of the posterior carapace is preserved. Parts of the last costals are found on each side of a single trapezoid suprapygal. On the visceral side of the last costals we find the end of the sacral vertebrae. The peripherals are long and narrow. The pygal is trapezoid, being slightly wider posteriorly. The last vertebral scute covers the suprapygal and the posterior parts of the last costals. There is good coincidence between the costo-peripheral sutures and the pleuro-marginal sulci. The same is true for the suprapygal-pygal suture and the vertebra-supracaudal sulcus. The marginals are long and narrow. The marginals 12 are fused into a trapezoid supracaudal, with wider posterior part. Viscerally, however the suprapygal is divided.

AMPG 578 (Fig. 3.59.H-J): The posterior parts of both xiphiplastra are preserved, showing a deep anal notch posteriorly. The xiphiplastra are wide. Ventrally, the femoro-anal sulcus is noted, being convex medially and concave laterally. The anals are longer medially, but laterally are short.

AMPG 600: A small fragment of the left hyoplastron, preserving the lip of the visceral covering of the humerals.

AMPG 601: An unidentified fragment of the plastron, as it is inferred by the shape and morphology of the visceral side.

AMPG 602 (Fig. 3.59.L): The proximal and medial part of the left humerus is preserved. The head is spherical. The two trochanters are slightly diverging to parallel. The major trochanter extends well beyond the humeral head. The diaphysis is strongly curved. Preserved length: 52 mm.

AMPG 603 (Fig. 3.59.N): The proximal and medial part of the right femur is preserved. The head is elliptical in shape, being orientated with an obtuse angle with the midline. The trochanters are fused. The diaphysis is straight in the preserved part. Preserved length: 44 mm.

AMPG 604 (Fig. 3.59.K): Most of the left scapula is preserved. The acromion is missing. The scapular prong extends vertically, and is straight. Preserved length: 41 mm.

AMPG 605 (Fig. 3.59.M): The proximal and medial part of the right humerus is preserved, but the minor trochanter is missing. The specimen is eroded. The head is spherical. The major trochanter extends well beyond the humeral head. The diaphysis is curved. Preserved length: 48 mm.

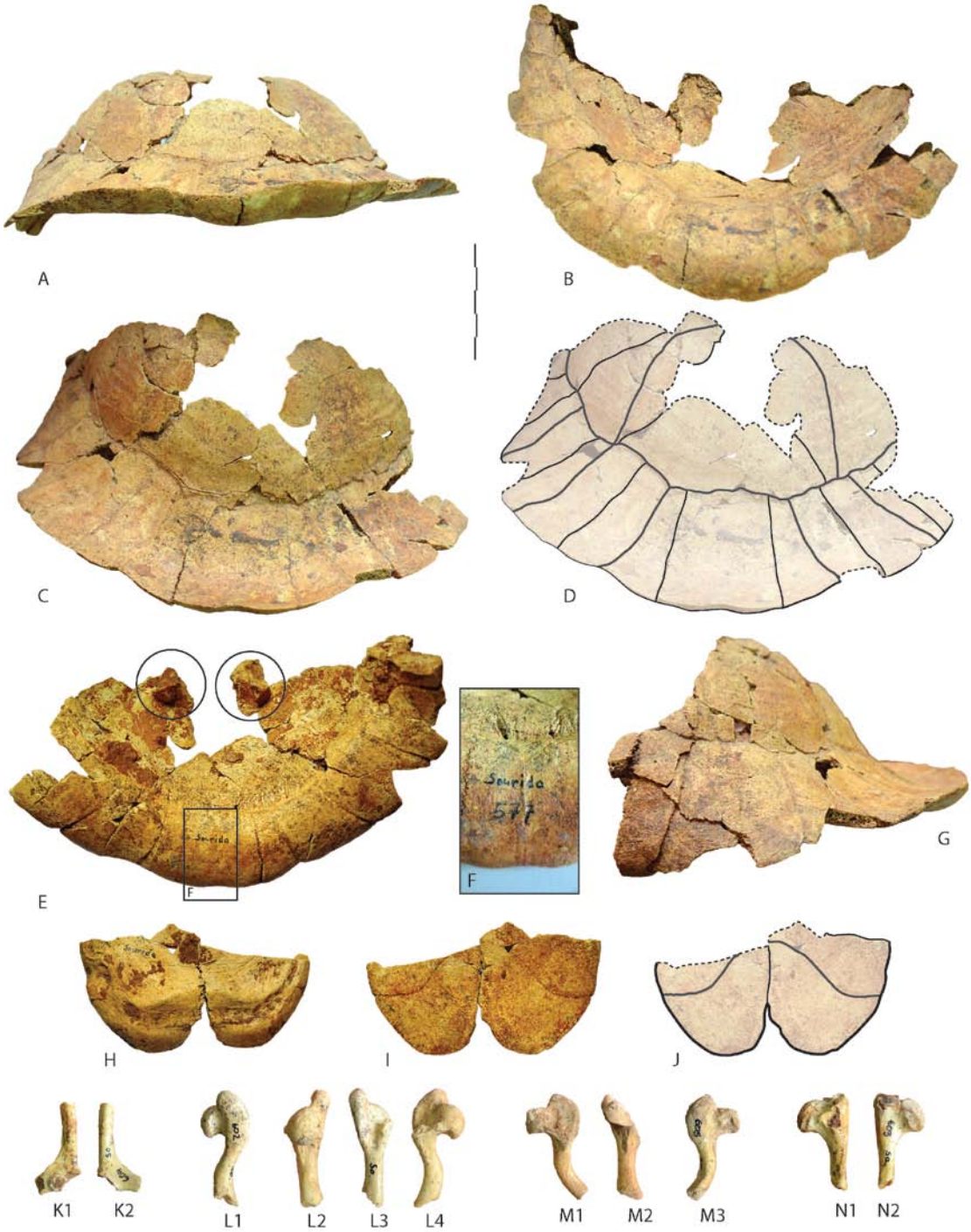


Figure 3.59. *Testudo marginata* Schoepff, 1793 from the Pleistocene of Zourida Cave (Crete). A-G, AMPG 577, posterior carapace in (A) posterior, (B) dorsal, (C) dorso-posterior, (D) drawing of the dorso-posterior, (E) visceral, (F) detail of pygal in visceral and (G) left lateral views. H-J, AMPG 578, posterior lobe in (H) visceral, (I) ventral and (J) drawing of the ventral views. K, AMPG 604, left scapula in (K1) posterior and (K2) anterior views. L, AMPG 602, left humerus in (L1) posterior, (L2) dorsal, (L3) ventral and (L4) anterior views. M, AMPG 605, right humerus in (M1) anterior, (M2) dorsal and (M3) posterior views. N, AMPG 603, right femur in (N1) anterior and (N2) posterior views. Scale bar equals 5 cm.

Comments: The material from Zourida cave can be attributed to the same taxon, *T. marginata*, as it is inferred by the characteristic posterior rim of the carapace. The carapacial rim (peripherals and the pygal) is horizontally flared and in some cases

(AMPG 577) is even more curved. The appendicular elements (AMPG 602-605) could belong to the same individual, since they are morphologically and metrically similar and do not present overlapping parts of the skeleton.

Koumpes Cave

AMPG 576 (Fig. 3.60): The left part of the shell of a marginated tortoise is preserved. From the carapace, the distal parts of the anterior and medial costals are preserved. The costals show the typical alternating pattern of the costals of the testudinids, being alternatively long and short. Almost the entire left peripheral rim is preserved, from the partial peripheral 2 till the peripheral 11. The peripherals are long and narrow. The peripherals of the bridge are tall and narrow. The posterior peripherals are horizontally flared, creating the characteristic posterior carapacial border of the marginated tortoise. There is good coincidence between the costo-peripheral sutures and the pleuro-marginal sulci. In the anterior part of the bridge, in the axillary notch, a single axillary scute is present, being in contact with the marginal 3, the humeral and pectoral scutes.

The left part of the plastron is preserved. The anterior lobe appears to be short and wide. The border of the anterior lobe is rounded. The lateral part of the left epiplastron is preserved, indicating that viscerally a thick epiplastral lip was present. The left part of the entoplastron is preserved. The entoplastron appears to have been hexagonal, wider than long. The hyo- and hypoplastra are long and wide. The hypoplastra end in the end of the bridge, indicating that the posterior lobe has been formed entirely by the xiphiplastra. As far as the scute sulci are concerned, few sulci are observed. The humero-pectoral sulcus is situated medially in the posterior end of the entoplastron, whereas laterally it crosses the hyoplastron to reach the axillary scute. The limits of the pectorals and the abdominals are not visible as a result of the preservation of the specimen. In the posterior part of the hypoplastra however, the abdomino-femoral sulcus is observed, being close to the end of the bridge and strongly convex. All the above suggest the presence of a hypo-xiphiplastral hinge in this specimen.

AMPG 579 (Fig. 3.61.B): The distal part of a costal is preserved, being laterally short.

AMPG 580 (Fig. 3.61.F): Part of the right epiplastron is preserved. Viscerally, based on the preserved part the presence of a thick epiplastral lip can be hypothesized. The epiplastra are short and wide. The entoplastron is wider than long. The gulars are long and narrow, covering the anterior part of the entoplastron.

AMPG 581 (Fig. 3.61.C): An almost entire peripheral is preserved. It is crossed longitudinally by the marginal sulci. A pointed tip is noted in the limits between the marginals in the carapacial rim. Based on the preserved part, the peripheral appears to have been horizontally flared. Moreover, the two sides are not parallel to each other. Compared with the material preserved from this site and other localities from Crete, this peripheral most probably corresponds to the right peripheral 11 of the flared carapacial border of *T. marginata*. Compared to the peripherals of AMPG 576, this peripheral is larger and thicker, corresponding to a large individual.

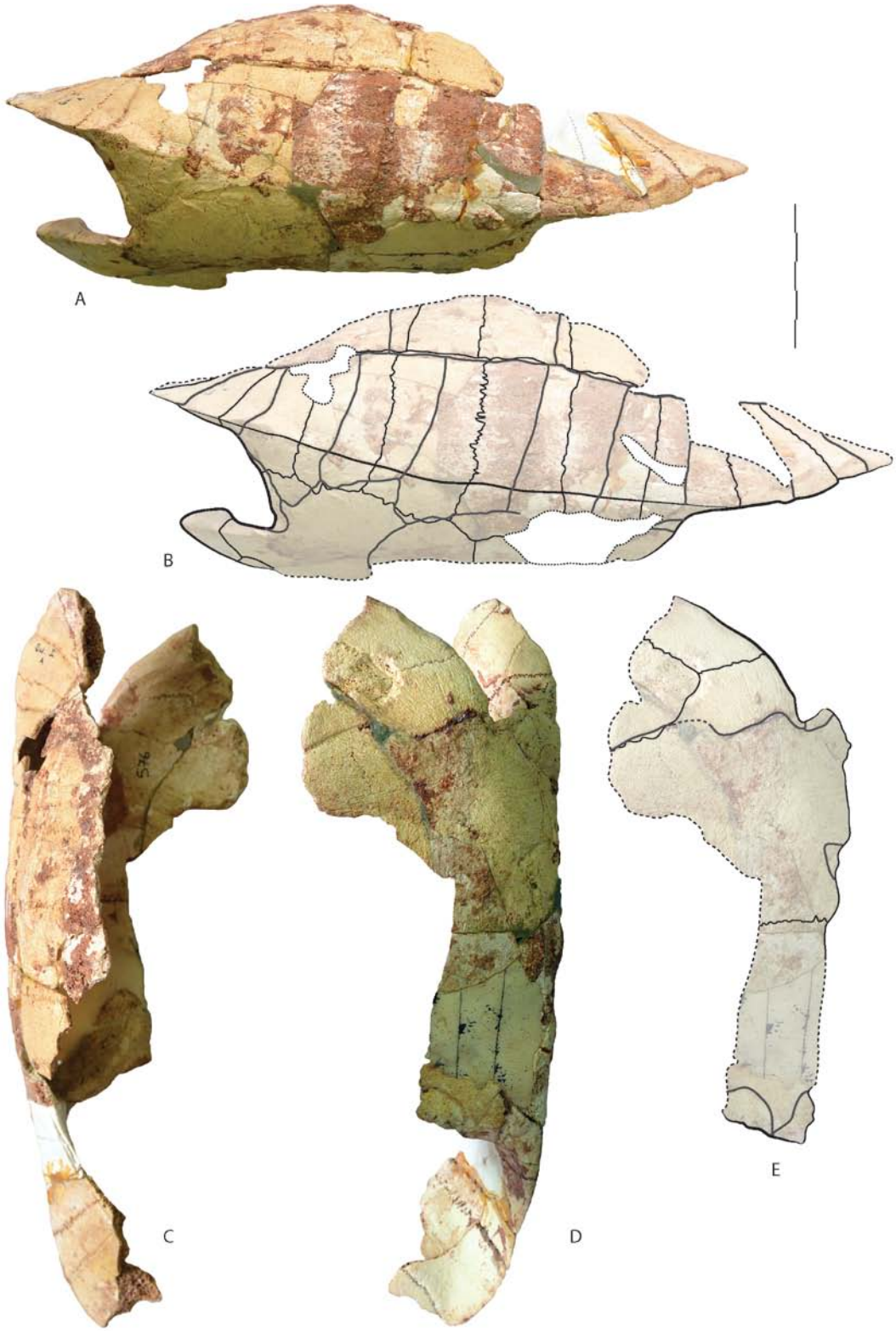


Figure 3.60. *Testudo marginata* Schoepff, 1793 from the Pleistocene of Koumpes Cave (Crete). AMPG 576, partial shell in (A) left lateral, (B) drawing of the left lateral, (C) dorsal, (D) ventral and (E) drawing of the ventral views. Scale bar equals 5 cm.

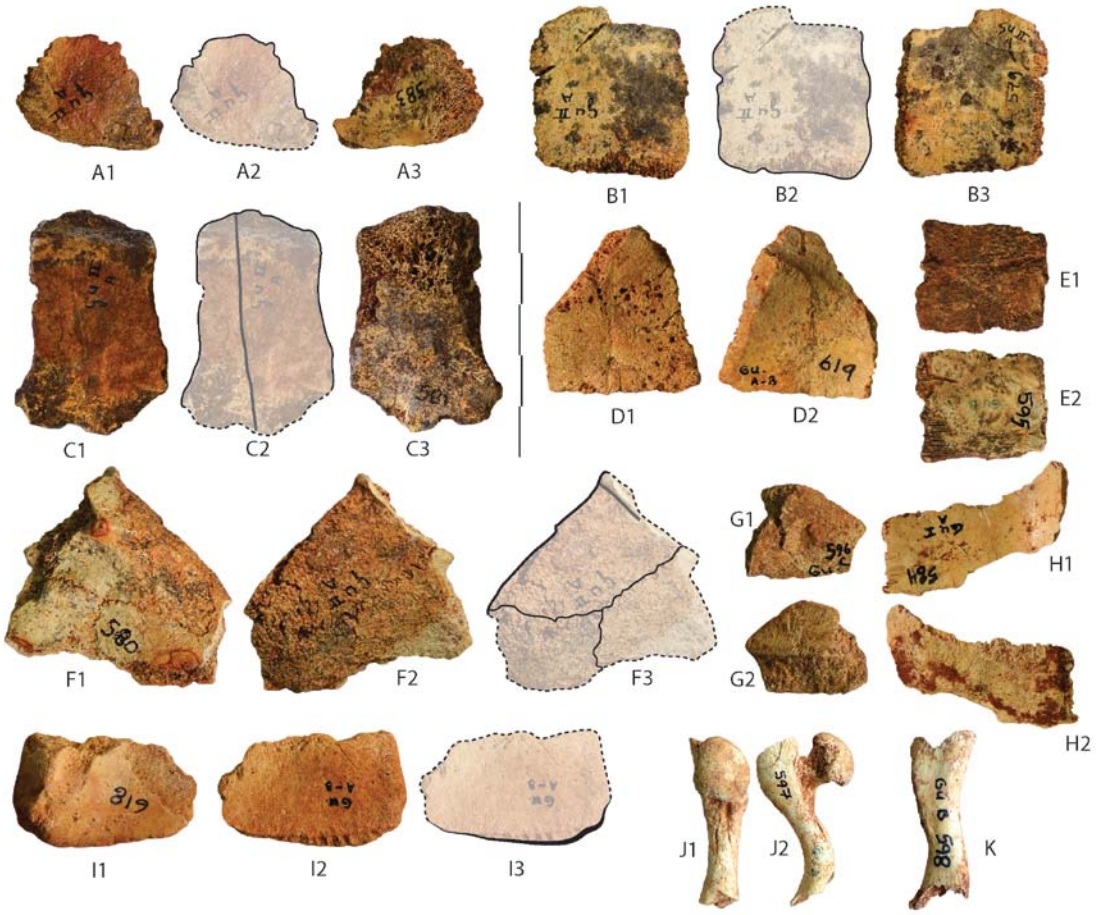


Figure 3.61. *Testudo marginata* Schoepff, 1793 from the Pleistocene of Koumpes Cave (Crete). A, AMPG 583, costal fragment in (A1) dorsal, (A2) drawing of the dorsal and (A3) visceral views. B, AMPG 579, costal fragment in (B1) dorsal, (B2) drawing of the dorsal and (B3) visceral views. C, AMPG 581, peripheral in (C1) dorsal, (C2) drawing of the dorsal and (C3) visceral views. D, AMPG 619, costal in (D1) dorsal and (D2) visceral views. E, AMPG 595, costal fragment in (E1) dorsal and (E2) visceral views. F, AMPG 580, right epiplastron in (F1) visceral, (F2) ventral and (F3) drawing of the ventral views. G, AMPG 596, right epiplastron in (G1) visceral and (G2) ventral views. H, AMPG 584, hyo/hypoplastron in (H1) visceral and (H2) ventral views. I, AMPG 618, left hypoplastron in (I1) visceral, (I2) ventral and (I3) drawing of the ventral views. J, AMPG 597, left humerus in (J1) dorsal and (J2) posterior views. K, AMPG 598, femur in lateral view. Scale bar equals 5 cm.

AMPG 582: This specimen is poorly preserved and sediment is preserved in some parts. Based on the flat and thin surface we can identify this a plastron fragment.

AMPG 583 (Fig. 3.61.A): Based on the preserved part, this specimen could be identified as the medial part of a costal.

AMPG 584 (Fig. 3.61.H): This is specimen is very thin and does not contain any evidence of sulci. Two sides however, show sutural surfaces. Based on the preserved part it could correspond to the medial part of hyo/hypoplastra, but further identification is not possible.

AMPG 585: This specimen is thin and flat, but lacks any diagnostic features. It could correspond to a part of hyo/hypoplastra.

AMPG 586: This specimen corresponds probably to the axillary part of the hyoplastron, as it is inferred by the presence of a process that resembles the axillary process.

AMPG 587: This specimen is thin and flat, but lacks any diagnostic features. Most probably is part of the plastron.

AMPG 595 (Fig. 3.61.E): The distal part of a costal is preserved, being laterally short.

AMPG 596 (Fig. 3.61.G): Part of the right epiplastron is preserved, showing the suture between the epiplastron and the entoplastron, as well as the visceral thickening of the epiplastral lip. Further description is not possible.

AMPG 597 (Fig. 3.61.J): The proximal and medial part of the left humerus is preserved. The head is spherical. The two trochanters are slightly diverging to parallel. The tips of the trochanters are broken. The major trochanter extends well beyond the humeral head. The diaphysis is strongly curved. Preserved length: 34 mm.

AMPG 598 (Fig. 3.61.K): The diaphysis of a femur is preserved, being slightly curved. Preserved length: 35 mm.

AMPG 599: The femoral head is preserved. It is elliptical in shape. Further description is not possible.

AMPG 618 (Fig. 3.61.I): The posterior part of the left hypoplastron is preserved. The posterior suture of the hypoplastron is broad and rounded, indicating the presence of a hinge. The ventral surface is eroded and no sulci can be observed.

AMPG 619 (Fig. 3.61.D): This specimen corresponds to a costal fragment.

AMPG 620: Most of a posterior peripheral is preserved. This peripheral is long and narrow, being crossed by the marginal sulcus. Based on the known material from this site, it resembles in length and morphology the anterior peripherals.

AMPG 621: Part of the diaphysis of a humerus. Further description is not possible.

Liko Cave, Crete

AMPG 551 (Fig. 3.62.A): This specimen preserves the left part of a shell of a tortoise. From the costals, the medial and lateral parts of the left costal 3 to costal 6 are preserved, along with a tiny part of the costal 7. Most of the bridge is preserved. The costal show the alternating pattern known in *T. marginata,* with costals between medially long and laterally short, alternated with costals medially short and laterally long. The costal 3 and costal 5 are crossed by the pleural sulci. The peripherals are tall and narrow. The last preserved peripheral (probably the peripheral 8) displays a widening and a degree of flaring, which is characteristic for the posterior carapace border of *T. marginata*.

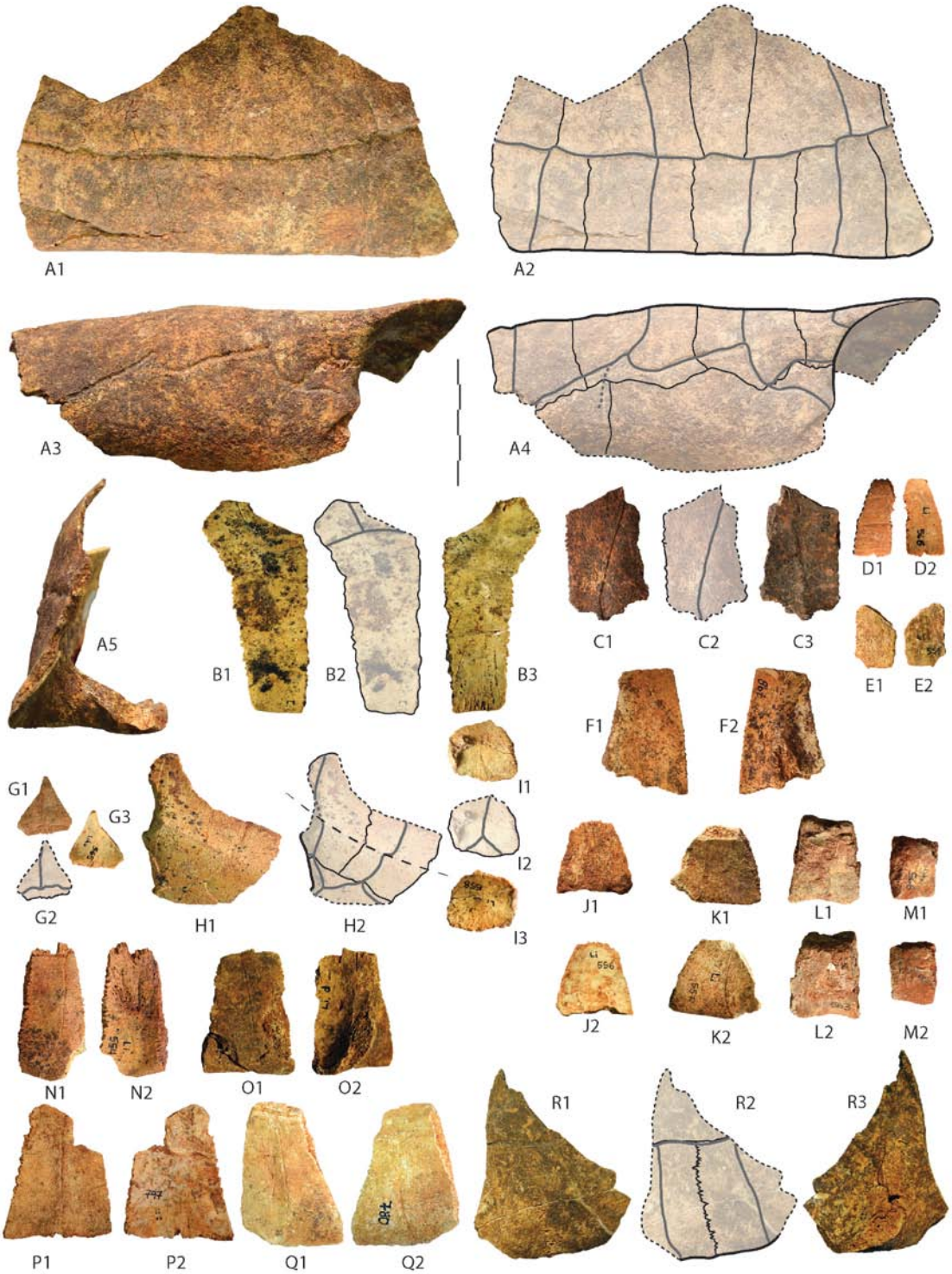


Figure 3.62. *Testudo marginata* Schoepff, 1793 from the Pleistocene of Liko Cave (Crete). A, AMPG 551, left part of the shell in (A1) lateral, (A2) drawing of the lateral, (A3) ventral, (A4) drawing of the ventral and (A5) posterior views. B, AMPG 553, costal in (B1) dorsal, (B2) drawing of the dorsal and (B3) visceral views. C, AMPG 562, costal fragment in (C1) dorsal, (C2) drawing of the dorsal and (C3) visceral views. D, AMPG 566, costal fragment in (D1) dorsal and (D2) visceral views. E, AMPG 559, costal fragment in (E1) dorsal and (E2) visceral views. F, AMPG 798, costal fragment in (F1) dorsal and (F2) visceral views. G, AMPG 595, costal fragment in (G1) dorsal, (G2) drawing of the dorsal and (G3) visceral views. H, AMPG 552, anterior part of the left bridge in (H1) dorsal and (H2) drawing of the dorsal views. I, AMPG 558, peripheral in (I1) dorsal, (I2) drawing of the dorsal and (I3) visceral views. J, AMPG 556, suprapygal in (J1) dorsal and (J2) visceral views. K, AMPG

557, peripheral in (K1) dorsal and (K2) visceral views. L, AMPG 563, peripheral in (L1) dorsal and (L2) visceral views. M, AMPG 568, peripheral in (M1) dorsal and (M2) visceral views. N, AMPG 554, peripheral in (N1) dorsal and (N2) visceral views. O, AMPG 781, peripheral in (O1) dorsal and (O2) visceral views. P, AMPG 797, costal fragment in (P1) dorsal and (P2) visceral views. Q, AMPG 780, peripheral in (Q1) dorsal and (Q2) visceral views. AMPG 573, bridge fragment in (R1) dorsal, (R2) drawing of the dorsal and (R3) visceral views. Scale bar equals 5 cm.

The peripherals of the bridge area are strongly curved ventrally and are tightly sutured with the hyo- and hypoplastra. The marginals cover the peripheral, and their sulci cross them transversely. There is good coincidence between the costo-peripheral sutures and the pleuro-marginal sulci. The sulci between the marginals and the scutes of the plastron are situated on the peripherals. In the posterior part of the bridge, a single inguinal scute is noted. It mainly covers the hypoplastron and is slightly expanded on the sutured peripheral. In the posterior part of the hypoplastron a hinge is formed with the posterior lobe. As a result of erosion, no sulci can be observed on the plastron.

AMPG 552 (Fig. 3.62.H): This specimen represents the anterior part of the left bridge of the shell of a tortoise. Only parts of two peripherals are preserved, being sutured with the lateral part of the left hyoplastron. A crest is noted in the lateral part of the bridge, which is anterodorsally oriented. There is good coincidence between the costo-peripheral sutures and the pleuro-marginal sulci. The sulci between the marginals and the scutes of the plastron are situated on the hyoplastron. A small axillary scute is noted anteriorly.

AMPG 553 (Fig. 3.62.B): An almost complete costal is preserved. Medially is long, whereas laterally is short. On the medial part, the limits between the vertebrals and the pleurals can be observed.

AMPG 554 (Fig. 3.62.N): A tall and narrow peripheral, being crossed by the marginal sulci transversely. The costo-peripheral suture coincides with the pleuro-marginal sulcus.

AMPG 555 (Fig. 3.63.I): This specimen consists of an almost complete right xiphiplastron, missing only some of the medial suture. The suture with the hypoplastron appears to have been broad and rounded, suggesting the presence of a hypo-xiphiplastral hinge. On the posterior end, a deep and wide anal notch is noted. Ventrally, the femorals are medially short and laterally long. Contrary, the anals are medially long and laterally short. The femoro-anal sulcus is V-shaped, anteriorly, being nearly straight on each side.

AMPG 556 (Fig. 3.62.J): A fragment that is relatively flat and thin. It is narrower anteriorly and widens posteriorly, being trapezoid in shape. It is not crossed by any sulci and there is no evidence of a rib in visceral side. Based on the comparative material presented here, this plate could correspond to a single suprapygal.

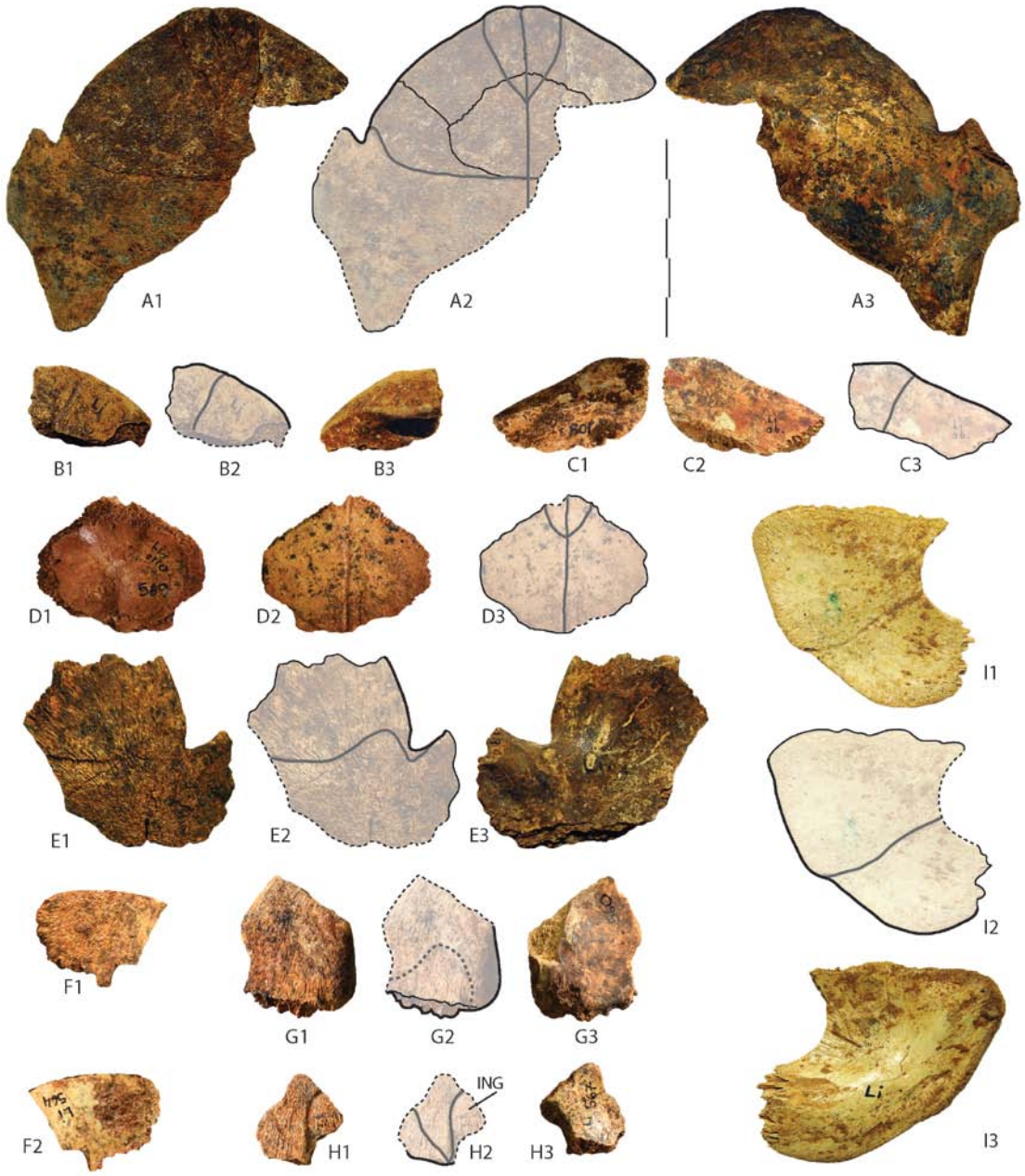


Figure 3.63 *Testudo marginata* Schoepff, 1793 from the Pleistocene of Liko Cave (Crete). A, AMPG 572, anterior lobe in (A1) ventral, (A2) drawing of the ventral and (A3) visceral views. B, AMPG 569, left epiplastron in (B1) ventral, (B2) drawing of the ventral and (B3) visceral views. C, AMPG 801, left epiplastron in (C1) visceral, (C2) ventral and (C3) drawing of the ventral views. D, AMPG 589, entoplastron in (D1) visceral, (D2) ventral and (D3) drawing of the ventral views. E, AMPG 588, left hyoplastron in (E1) ventral, (E2) drawing of the ventral and (E3) visceral views. F, AMPG 564, hyo/hypoplastral fragment in (F1) ventral and (F2) visceral views. G, AMPG 560, left hypoplastron fragment in (G1) ventral, (G2) drawing of the ventral and (G3) visceral views. H, AMPG 567, left hypoplastron fragment in (H1) ventral, (H2) drawing of the ventral and (H3) visceral views. I, AMPG 555, right xiphiplastron in (I1) ventral, (I2) drawing of the ventral and (I3) visceral views. Scale bar equals 5 cm. For abbreviations see Material & Methods.

AMPG 557 (Fig. 3.62.K): A short and narrow peripheral, being crossed by the marginal sulci transversely. It is posteriorly flared.

AMPG 558 (Fig. 3.62.I): A fragment of peripheral from the bridge area, showing the change of curvature towards the plastron. It is crossed by the marginal sulci transversely.

AMPG 559 (Fig. 3.62.E): A small fragment of a costal. It is not crossed by any sulci.

AMPG 560 (Fig. 3.63.G): A small fragment of the posterior area of the left hypoplastron. Although the surface of the specimen is eroded we can observe the imprint of a strongly convex abdomino-femoral sulcus. The posterior part of the hypoplastron is thick and the suture is rounded. The morphology of the preserved part is consistent with the presence of a hypo-xiphiplastral hinge in this specimen.

AMPG 561: A relatively large part of the plastron, as it is inferred by the shape and curvature. Further description is not possible because most of the specimen is covered by calcitic material.

AMPG 562 (Fig. 3.62.C): A fragment of a costal, being crossed by the pleural sulci.

AMPG 563 (Fig. 3.62.L): A tall and narrow peripheral that is partly covered by calcitic material. It is crossed by the marginal sulci transversely, and appears moderately flared.

AMPG 564 (Fig. 3.63.F): A small fragment of the plastron, as it is inferred by the relatively flat shape and the smooth visceral surface. It belongs to the medial part (hyo/hypo) but further identification is not possible.

AMPG 565 (Fig. 3.62.G): A small fragment of a costal, being crossed by the pleural sulci transversely.

AMPG 566 (Fig. 3.62.D): A small fragment of a costal.

AMPG 567 (Fig. 3.63.H): A small fragment of the posterior area of the left hypoplastron. On the ventral side of the specimen we can observe the lateral part of a convex abdomino-femoral sulcus, and the presence of a single inguinal scute. The posterior part of the hypoplastron is thick and the suture is rounded. The morphology of the preserved part is consistent with the presence of a hypo-xiphiplastral hinge in this specimen.

AMPG 568 (Fig. 3.62.M): A short and narrow peripheral, being crossed by the marginal sulci transversely. It is posteriorly flared.

AMPG 569 (Fig. 3.63.B): An almost complete left epiplastron. It is short and wide, showing a thickened visceral part forming a convex epiplastral lip with a gular pocket. Ventrally is covered by long and narrow gulars medially that overlap the anterior part of the entoplastron.

AMPG 570: A relatively flat and thick fragment of the plastron.

AMPG 571: A fragment of a laterally short costal. The surface of the specimen is eroded and further description is not possible.

AMPG 572 (Fig. 3.63.A): Most of the anterior plastral lobe is formed, missing part of the left hyoplastron. The anterior lobe is rounded, short and wide. The epiplastra are short and wide, showing a thickened visceral part forming a convex epiplastral lip with a gular pocket. Ventrally they covered by long and narrow gulars medially that overlap the anterior part of the entoplastron. The entoplastron is wide and short. The humero-pectoral sulcus is broadly concave and is situated medially on the posterior end of the entoplastron.

AMPG 573 (Fig. 3.62.R): A large fragment of the bridge, preserving parts of the peripherals and a fragment of the costal. There is good coincidence between the costo-peripheral sutures and the pleuro-marginal sulci.

AMPG 574: A short and narrow peripheral, being crossed by the marginal sulci transversely. It is posteriorly flared.

AMPG 575: An almost complete left hyoplastron. It is crossed by the humero-pectoral sulcus. This sulcus is strongly curved laterally and is situated posterior to the entoplastron.

AMPG 588 (Fig. 3.63.E): A flat fragment of a hyoplastron. The visceral surface is smooth. Part of the medial suture is preserved. Ventrally it is crossed by the humero-pectoral sulcus.

AMPG 589 (Fig. 3.63.D): A complete entoplastron. The entoplastron is hexagonal, short and wide, being slightly curved. Anteriorly it is overlapped by the gular scutes, whereas the rest is covered by the humerals.

AMPG 590: A fragment of a tall peripheral. It is crossed by the marginal sulci. Based on the preserved part we can infer that this peripheral has been strongly flared.

AMPG 591: A fragment that is relatively flat and thin. It is narrower anteriorly and widens posteriorly, being trapezoid in shape. It is not crossed by any sulci and there is no evidence of a rib in visceral side. Based on the comparative material presented here, this plate could correspond to a single suprapygal.

AMPG 592: A lateral fragment of a costal. Based on the curved lateral end and the absence of sulci crossing, this specimen could correspond to the costal 1.

AMPG 593 (Fig. 3.64.L): A complete right tibia. The tibia is relatively straight in the proximal and medial part, but displays a significant degree of curvature in the distal part. In the distal part of the shaft a rugosity is noted. The proximal part is wide, triangular in cross-section and displays a well-developed and broad cnemial crest. The proximal articular surface is broadly concave. The distal articular surface is more complex, being concave medially and convex laterally.

AMPG 594 (Fig. 3.64.N): A complete ungual. The ungual is long, straight, and with a pointed tip. Based on the length, this ungual is from the posterior limb.



Figure 3.64. *Testudo marginata* Schoepff, 1793 from the Pleistocene of Liko Cave (Crete). A, AMPG 614, cervical vertebra 8 in (A1) anterior, (A2) posterior, (A3) ventral, (A4) left lateral and (A5) dorsal views. B, AMPG 613, cervical vertebra in (B1) anterior, (B2) right lateral, (B3) ventral, (B4) left lateral and (B5) dorsal views. C, AMPG 625, scapula in anterior view. D, AMPG 615, shoulder girdle in (D1) ventral view of the acromion, (D2) anterior and (D3) posterior views. E, AMPG 674, coracoid in (E1) dorsal and (E2) ventral views. F, AMPG 617, ischium in dorsal view. G, AMPG 787, left humerus in (G1) anterior, (G2) dorsal, (G3) ventral and (G4) posterior views. H, AMPG 616, right humerus in (H1) dorsal, (H2) ventral and (H3) posterior views. I, AMPG 808, right ulna in (I1) dorsal, (I2) lateral, (I3) medial and (I4) ventral. J, AMPG 676, left femur in (J1) posterior, (J2) dorsal and (J3) anterior views. K, AMPG 675, femur in (K1) dorsal and (K2) ventral views. L, AMPG 593, right tibia in (L1) dorsal and (L2) ventral views. M, AMPG 809, left tibia in (M1) dorsal, (M2) medial, (M3) lateral and (M4) ventral views. N, AMPG 594, ungual in (N1) dorsal and (N2) ventral views. Scale bar equals 5 cm.

AMPG 610: This is a large fragment of the left hypoplastron of a tortoise. The specimen is eroded and it is not possible to observe the scute sulci limits.

AMPG 611: This is a fragment of the posterior part of the left hypoplastron. Ventrally, a sulcus is noted, most probably of the abdomino-femoral sulcus. The posterior part of the hypoplastron is thick and the suture is rounded. The morphology of the preserved part is consistent with the presence of a hypo-xiphiplastral hinge in this specimen.

AMPG 612: A small fragment of a costal plate. No sulci are noted on the dorsal surface.

AMPG 613 (Fig. 3.64.B): This is an almost complete cervical vertebra, missing only some tips of the processes. The body of the vertebra is long and is amphicoelous. The dorsal processes are relatively long.

AMPG 614 (Fig. 3.64.A): This is an almost complete cervical vertebra 8. The body is short. Posteriorly, two long and curved apophyses are present of the articulation with the dorsal vertebra. The posterior articular surface is convex.

AMPG 615 (Fig. 3.64.D): This is an almost complete shoulder girdle, missing only some part of the coracoid. The specimen is deformed, and therefore is not possible to observe the angles between the shoulder girdle elements.

AMPG 616 (Fig. 3.64.H): This is a complete right humerus. The head is spherical. The two trochanters are slightly diverging to parallel. The major trochanter extends well beyond the humeral head. The diaphysis is strongly curved. Preserved length: 64 mm.

AMPG 617 (Fig. 3.64.F): A part of the ischium is preserved.

AMPG 625 (Fig. 3.64.C): Most of the scapula is preserved, missing only the acromion process. The scapular prong is long and straight, forming a right angle with the acromion.

AMPG 626: A fragment of a long and narrow peripheral is preserved. This peripheral is horizontally flared. No sulci are noted in the preserved part.

AMPG 627, 628, 672, 673: These specimens correspond to small fragments of costals plates.

AMPG 674 (Fig. 3.64.E): This is an almost complete coracoid. Some parts of this element are covered by calcitic material. The neck of the coracoid is long and narrow, whereas the end is wider and rounded. Preserved length: 29 mm.

AMPG 675 (Fig. 3.64.K): The medial and distal part of a femur is preserved. The diaphysis is straight and the distal end is wide. Preserved length: 42 mm.

AMPG 676 (Fig. 3.64.J): The proximal and medial part of a left femur is preserved. The head is rounded and elliptical. Its longer axis is oriented with an obtuse angle

with the midline. The proximal part is wide, and the trochanters are fused. The diaphysis is straight. Preserved length: 44 mm.

AMPG 677: The distal part of a tibia is preserved, largely covered by calcitic material.

AMPG 732 – 734: These specimens correspond to small fragments of the plastron.

AMPG 780 (Fig. 3.62.Q): A complete peripheral is preserved. It is crossed longitudinally by the marginal sulci. Based on the preserved part, the peripheral appears to have been horizontally flared. Moreover, the two sides are not parallel to each other. Compared with the material preserved from this site and other localities from Crete, this peripheral most probably corresponds to the right peripheral 11 of the flared carapacial border of *T. marginata*.

AMPG 781 (Fig. 3.62.O): This is an almost complete peripheral. It is tall and narrow. It is crossed longitudinally by the marginal sulci. Anteriorly it preserves a broad suture, indicating that is the left peripheral 8, and the last one on the left bridge of the shell.

AMPG 782: A part of a peripheral is preserved. It is crossed longitudinally by the marginal sulci. Based on the preserved part, the peripheral appears to have been horizontally flared. Most probably belongs to the posterior peripherals.

AMPG 783: A small fragment of the shell is preserved. Further identification is not possible.

AMPG 784 – 785: These specimens correspond to small fragments of costal plates.

AMPG 787 (Fig. 3.64.G): This is a complete left humerus. The head is spherical. The two trochanters are slightly diverging to parallel. The major trochanter extends well beyond the humeral head. The diaphysis is strongly curved. Preserved length: 60,6 mm.

AMPG 797 (Fig. 3.62.P): A large fragment of a costal is preserved. This costal is laterally long and medially short, and is crossed by pleural sulci.

AMPG 798 (Fig. 3.62.F): A large fragment of a costal is preserved. This costal is laterally long and medially short, whereas is not crossed by any sulci.

AMPG 799: An almost complete peripheral from the bridge area, showing the distal change of curvature for the contact with the plastron. It is crossed by marginal sulci.

AMPG 800: An almost complete peripheral, being crossed by the marginal sulci. It displays a moderate degree of flaring, resembling the anterior peripherals.

AMPG 801 (Fig. 3.63.C): A complete left epiplastron. It is short and wide, showing a thickened visceral part forming a convex epiplastral lip with a gular pocket. Ventrally is covered by long and narrow gulars medially that overlap the anterior part of the entoplastron.

AMPG 802 – 805: These small fragments correspond to parts of the bony plates from the carapace. Further identification is not possible.

AMPG 806: A small fragment of a costal is preserved.

AMPG 807: A part of a peripheral is preserved, largely covered by calcitic material.

AMPG 808 (Fig. 3.64.I): A complete right ulna. The proximal part is wide, whereas the distal is narrow. The proximal articular surface is broadly wide, whereas the distal is convex. The medial part of the bone is curved. The cross-section of the bone is triangular. Laterally a thin crest is formed.

AMPG 809 (Fig. 3.64.M): A complete right tibia. The tibia is relatively straight in the proximal and medial part, but displays a significant degree of curvature in the distal part. In the distal part of the shaft a rugosity is noted. The proximal part is wide, triangular in cross-section and displays a well-developed and broad cnemial crest. The proximal articular surface is broadly concave. The distal articular surface is more complex, being concave medially and convex laterally.

AMPG 810: An almost complete fibula is preserved, but the bone is eroded to allow further description.

Mavro Mouri IV, Crete

Mavro Mouri IV is one of the several caves in Mavro Mouri area in Crete, and the only one among them to provide chelonian remains (Kuss, 1970). This material is the richest known from Crete, and represents nearly all the shell and many appendicular elements of a marginated tortoise. The fossils are stored in the collections of NHMC and AMPG.

NHMC FS38/60 (Fig. 3.65.A): This specimen preserves the entire anterior lobe of the plastron. The lobe is short and wide, having a rounded triangular outline. The epiplastra are short and wide, covering the anterior part of the lobe. Viscerally, the epiplastra are thick, forming a convex epiplastral lip and a significant gular pocket. The entoplastron is hexagonal, slightly wider than long. The anterior parts of the hyoplastra are also preserved. The gulars are narrow and long, covering the medial epiplastra and the anterior part of the entoplastron. The gularo-humeral sulcus is V-shaped, with acute angle with the midline. The humerals medially are slightly shorter than the gulars, covering the remaining part of the entoplastron, whereas laterally they are longer. The humero-pectoral sulcus is nearly straight to slightly sinuous, being situated medially in the posterior end of the entoplastron.

NHMC FS38/61 (Fig. 3.65.B): This specimen corresponds to an almost entire right hyoplastron. It is crossed anteriorly by the humero-pectoral sulcus. Based on the preserved part the sulcus is situated posterior to the posterior end of the entoplastron. The remaining surface of the hyoplastron is eroded and is not possible to confidently observe the pectorals.

NHMC FS38/62 (Fig. 3.65.I): This specimen belongs to the same individual as NHMC FS38/63. It is the anterior and medial part of the left hyoplastron. It is crossed anteriorly by the humero-pectoral sulcus. Based on the preserved part the sulcus is situated posterior to the posterior end of the entoplastron. The pectorals are medially short and laterally longer. The pectoro-abdominal sulcus is slightly convex on each side.

NHMC FS38/63 (Fig. 3.65.I): This specimen belongs to the same individual as NHMC FS38/62. It is the anterior and medial part of the right hyoplastron. It is crossed anteriorly by the humero-pectoral sulcus. Based on the preserved part the sulcus is situated posterior to the posterior end of the entoplastron. The pectorals are medially short and laterally longer. The pectoro-abdominal sulcus is slightly convex on each side.

NHMC FS38/64: This specimen corresponds to a continuous series of anterior peripherals. Based on the available comparative material they are the right peripherals 2-4. They are crossed by the marginal sulci, whereas there is good coincidence between the costo-peripheral sutures and the pleuro-marginal sulci. They are moderately flared.

NHMC FS38/65 (Fig. 3.65.C): This specimen corresponds to a continuous series of posterior peripherals. Based on the available comparative material they are the right peripherals 10-11. The lateral sides of the peripheral 11 are not parallel to each other, indicating that the corresponding pygal must have been trapezoid with narrow posterior side. They are crossed by the marginal sulci, whereas there is good coincidence between the costo-peripheral sutures and the pleuro-marginal sulci. They are long and posteriorly flared.

NHMC FS38/66: A fragment of an anterior peripheral. On the preserved part we cannot observe any evidence of sulci.

NHMC FS38/67 (Fig. 3.65.J): This specimen corresponds to the posterior part of the left xiphiplastron. Based on the preserved part we can infer the presence of a wide anal notch in the posterior part of the posterior lobe. It crossed by the femoro-anal sulcus that is oriented medio-anteriorly. The visceral covering of the anal scutes forms a short, narrow and convex lip on the xiphiplastron.

NHMC FS38/68 (Fig. 3.65.K): This specimen corresponds to the posterior part of the left xiphiplastron. Based on the preserved part we can infer the presence of a wide anal notch in the posterior part of the posterior lobe. The preserved part is not crossed by any sulci. The visceral covering of the anal scutes forms a short, narrow and convex lip on the xiphiplastron.

NHMC FS38/69: A small fragment of the plastron, most probably from the hyoplastral area.

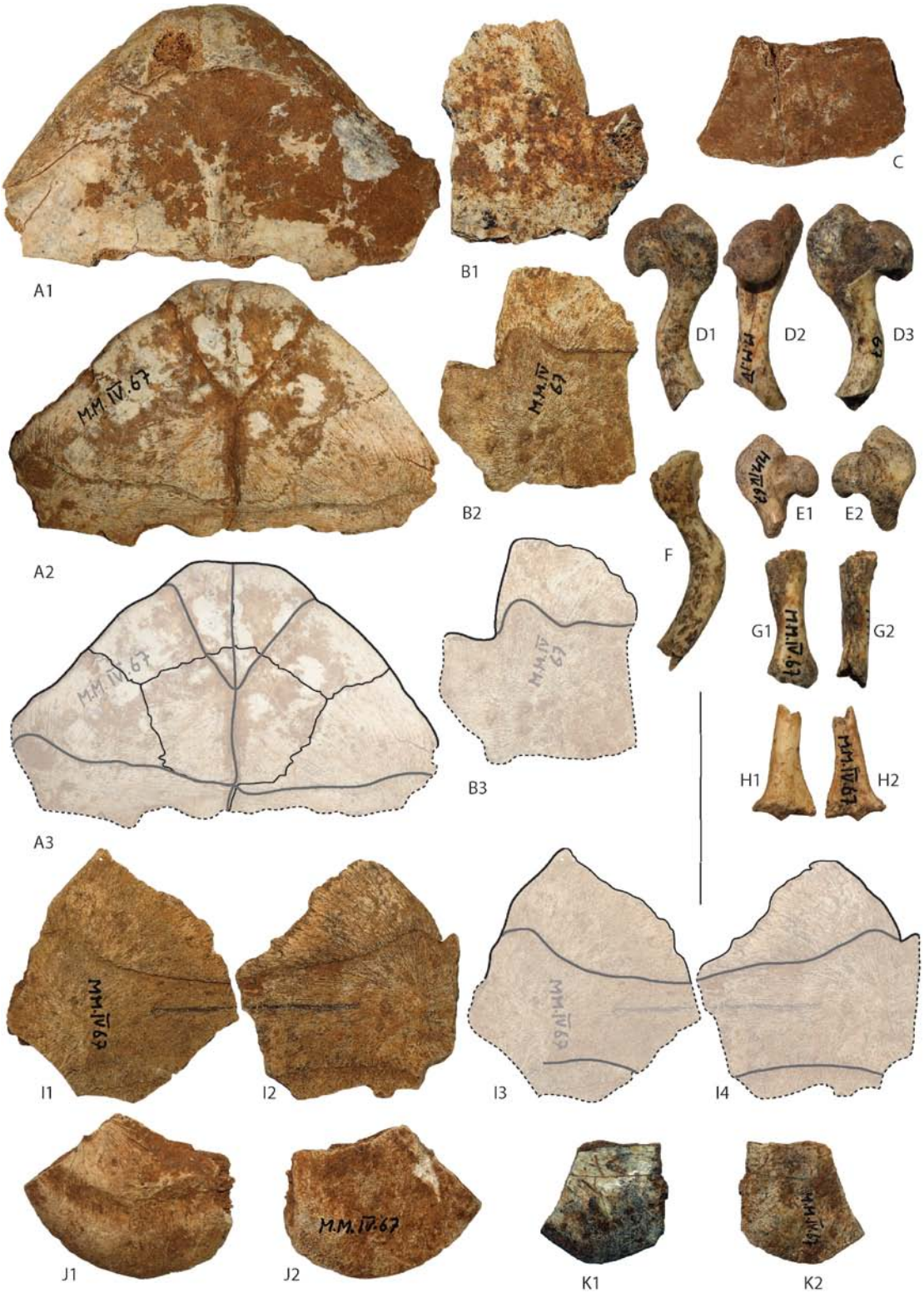


Figure 3.65. *Testudo marginata* Schoepff, 1793 from the Pleistocene of Mavro Mouri IV Cave (Crete). NHMC collection: A, NHMC FS38/60, plastral lobe in (A1) visceral, (A2) ventral and (A3) drawing of the ventral views. B, NHMC FS38/61, left hyoplastron in (B1) visceral, (B2) ventral and (B3) drawing of the ventral views. C, NHMC FS38/65, peripheral in dorsal view. D, NHMC FS38/70, left humerus in (D1) posterior, (D2) dorsal and (D3) anterior views. E, NHMC FS38/71, right humerus in (E1) posterior and (E2) anterior views. F, NHMC FS38/72, humerus in lateral view. G, NHMC FS38/77, femur in (G1) dorsal and (G2) lateral view. H, NHMC FS38/76, ilium in (H1) dorsal and (H2) ventral views. I, NHMC

FS38/62-63, left and right hyoplastra in (I1-2) ventral and (I3-4) drawing of the ventral views. J, NHMC FS38/67, left xiphiplastron in (J1) visceral and (J2) ventral views. K, NHMC FS38/68, left xiphiplastron in (K1) visceral and (K2) ventral views. Scale bar equals 5 cm.

NHMC FS38/70 (Fig. 3.65.D): This specimen corresponds to the proximal and medial part of the left humerus. The head of the humerus is spherical, being developed in right angle with the proximal part of the bone. The two trochanters are unequal in size, and are developed slightly diverging to parallel to each other. The major trochanter extends well beyond the humeral head, whereas the minor is poorly developed in some cases. The diaphysis is strongly curved, especially in the distal part.

NHMC FS38/71 (Fig. 3.65.E): This specimen corresponds to the proximal of the right humerus. The head of the humerus is spherical, being developed in right angle with the proximal part of the bone. The two trochanters are unequal in size, and are developed slightly diverging to parallel to each other. The major trochanter extends well beyond the humeral head, whereas the minor is poorly developed in some cases.

NHMC FS38/72 (Fig. 3.65.F): This specimen corresponds to the diaphysis of a humerus. The diaphysis is strongly curved, especially in the distal part.

NHMC FS38/73: This specimen corresponds to the diaphysis of a humerus. The diaphysis is strongly curved, especially in the distal part.

NHMC FS38/74: This specimen corresponds to the diaphysis of a humerus. The diaphysis is strongly curved, especially in the distal part.

NHMC FS38/75: This specimen corresponds to the diaphysis of a humerus. The diaphysis is strongly curved, especially in the distal part.

NHMC FS38/76 (Fig. 3.65.H): A small fragment of an ilium, which is relatively straight.

NHMC FS38/77 (Fig. 3.65.G): This specimen corresponds to the diaphysis of a femur. The diaphysis is straight, thicker proximally, thinner medially. The distal part widens.

NHMC FS38/78: A group of 9 small fragments of the shell.

AMPG 678 (Fig. 3.66.P): This specimen corresponds to the anterior and medial part of the right hyoplastron. It is crossed anteriorly by the humero-pectoral sulcus. Based on the preserved part the sulcus is situated posterior to the posterior end of the entoplastron. The remaining surface of the hyoplastron is eroded and is not possible to confidently observe the pectorals.

AMPG 679 (Fig. 3.66.O): This specimen corresponds to the anterior part of the left hyoplastron. Anteriorly we notice the suture with the epiplastron and antero-medially with the entoplastron. It is crossed anteriorly by the humero-pectoral sulcus, which is

medially straight and laterally convex. Based on the preserved part the sulcus is situated posterior to the posterior end of the entoplastron.

AMPG 680: This specimen corresponds to a fragment of the left hypoplastron, based on the shape and curvature. As it is not crossed by any sulci, further description is not possible in the preserved part.

AMPG 681: This specimen corresponds to a part of the medial plastral region, most probably from the left hypoplastron. However, in the lack of any sulci ventrally, further description is not possible.

AMPG 682: This specimen corresponds to the anterior part of the left hyoplastron. Anteriorly we can observe the suture with the epiplastron, antero-medially with the entoplastron, and medially with the right hyoplastron. It is crossed anteriorly by the humero-pectoral sulcus, which is medially straight and laterally convex. Based on the preserved part the sulcus coincides medially with the posterior end of the entoplastron.

AMPG 683 – 685: These specimens correspond to small fragments of the right (AMPG 683, 684) and the left hyoplastron (AMPG 685), showing the humero-pectoral sulcus.

AMPG 686: This specimen corresponds to the distal part of a costal plate, being crossed by the pleural sulci transversely. Based on the preserved part, there is good coincidence between the costo-peripheral sutures and the pleuro-marginal sulci.

AMPG 687 (Fig. 3.66.H): Part of a moderately flared peripheral. It is crossed by the marginal sulci, and there is good coincidence between the costo-peripheral sutures and the pleuro-marginal sulci. Medially there is a change in the curvature, whereas anteriorly a broad suture with the successive peripheral is noted. Therefore, this peripheral corresponds to the left peripheral 7, right after the end of the bridge. The change in the curvature indicates that the carapacial rim widens at this point, as in the marginated tortoise.

AMPG 688: This specimen corresponds to a fragment of a peripheral plate.

AMPG 689 : This specimen corresponds to a small fragment of a costal.

AMPG 690: This specimen corresponds to a posterior peripheral, which is long and posteriorly flared. It is crossed by the marginal sulci.

AMPG 691: This specimen corresponds to a posterior peripheral, which is long and posteriorly flared. It is crossed by the marginal sulci.

AMPG 692 - 693: These specimens correspond to long and almost horizontally flared peripherals of the posterior region of the carapace. They are crossed by the marginal sulci.

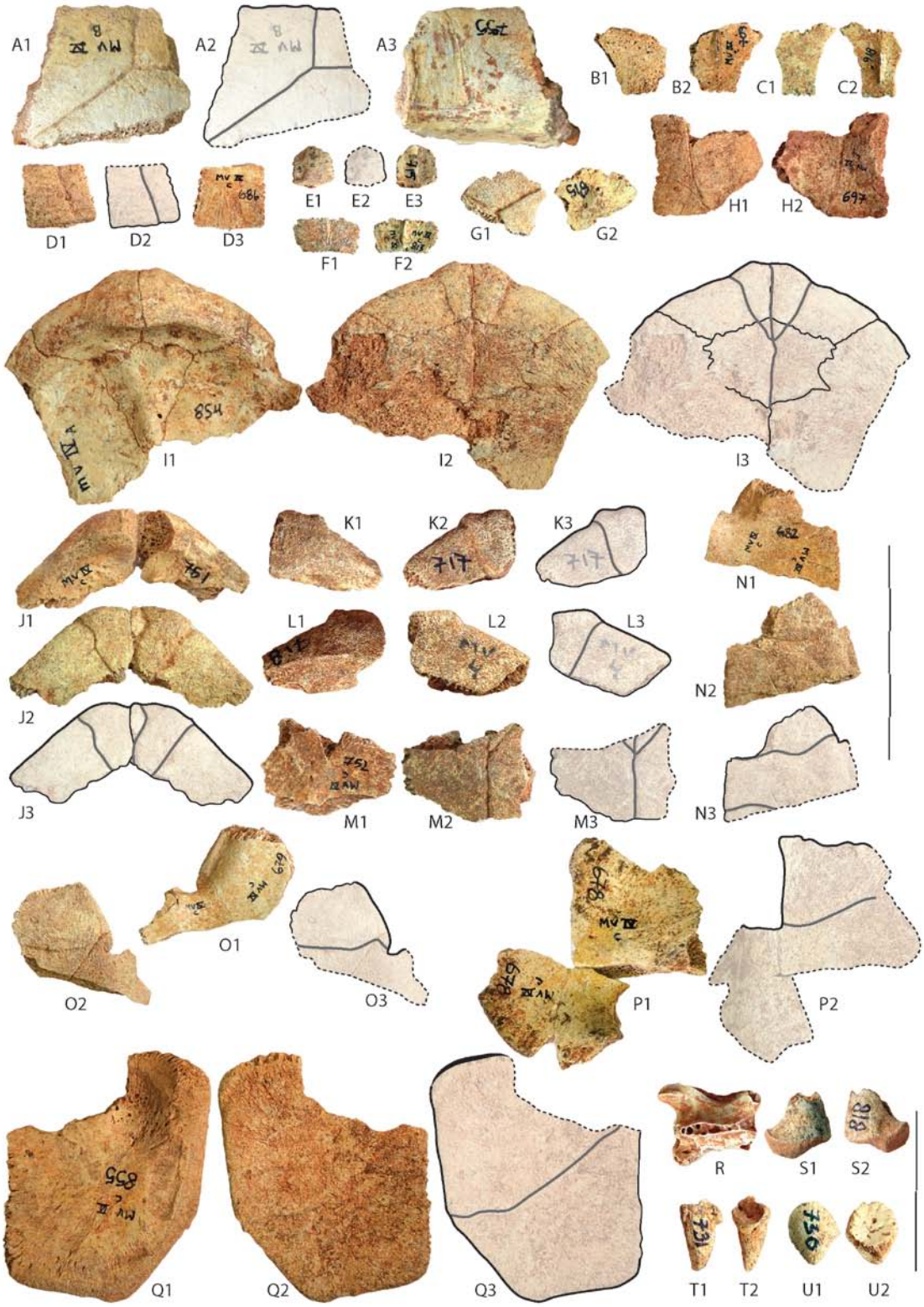


Figure 3.66. *Testudo marginata* Schoepff, 1793 from the Pleistocene of Mavro Mouri IV Cave (Crete). AMPG collection: A, AMPG 755, nuchal fragment in (A1) dorsal, (A2) drawing of the dorsal and (A3) visceral views. B, AMPG 709, neural fragment in (B1) dorsal and (B2) visceral views. C, AMPG 816, neural fragment in (C1) dorsal and (C2) visceral views. D, AMPG 686, costal fragment in (D1) dorsal, (D2) drawing of the dorsal and (D3) visceral views. E, AMPG 715, costal fragment in (E1) dorsal, (E2) drawing of the dorsal and (E3) visceral views. F, AMPG 813, costal fragment in (F1) dorsal and (F2) visceral views. G, AMPG 815, costal fragment in (G1) dorsal and (G2) visceral views. AMPG 697, peripheral in

(H1) dorsal and (H2) visceral views. I, AMPG 854, anterior lobe in (I1) visceral, (I2) ventral and (I3) drawing of the ventral views. J, AMPG 751, left and right epiplastra in (J1) visceral, (J2) ventral and (J3) drawing of the ventral views. K, AMPG 717, right epiplastron in (K1) visceral, (K2) ventral and (K3) drawing of the ventral views. L, AMPG 718, left epiplastron in (L1) visceral, (L2) ventral and (L3) drawing of the ventral views. M, AMPG 752, entoplastron fragment in (M1) visceral, (M2) ventral and (M3) drawing of the ventral views. N, AMPG 682, left hyoplastron in (N1) visceral, (N2) ventral and (N3) drawing of the ventral views. O, AMPG 679, left hyoplastron in (O1) visceral, (O2) ventral and (O3) drawing of the ventral views. P, AMPG 678, right hyoplastron in (P1) visceral and (P2) drawing of the ventral views. Q, AMPG 855, right xiphiplastron in (Q1) visceral, (Q2) ventral and (Q3) drawing of the ventral views. R, AMPG 728, cervical vertebra in dorsal view. S, AMPG 818, ilium in (S1) dorsal and (S2) ventral views. T, AMPG 731, ungual in (T1) dorsal and (T2) ventral views. U, AMPG 730, osteoderm in (U1) dorsal and (U2) ventral views. Scale bar equals 5 cm.

AMPG 694: This specimen corresponds to a long and almost horizontally flared peripheral of the posterior region of the carapace. It is crossed by the marginal sulci, and there is good coincidence between the costo-peripheral sutures and the pleuro-marginal sulci.

AMPG 695: This specimen corresponds to a posterior peripheral, which is long and horizontally flared. It is crossed by the marginal sulci.

AMPG 696: This specimen corresponds to a posterior peripheral, which is long and posteriorly flared. It is crossed by the marginal sulci.

AMPG 697 (Fig. 3.66.H): This specimen corresponds to a posterior peripheral, which is long and posteriorly flared. It is crossed by the marginal sulci.

AMPG 698 – 699: These specimens correspond to fragments of a costal plate, being crossed by the pleural sulci transversely.

AMPG 700: This specimen corresponds to a fragment of a costal plate, being crossed by the pleural sulci transversely.

AMPG 701: This specimen corresponds to a small fragment of a costal.

AMPG 702: This specimen corresponds to a fragment of a peripheral, which is long and moderately flared. It is crossed by the marginal sulci.

AMPG 703: This specimen corresponds to a fragment of a peripheral, which is long and moderately flared. It is crossed by the marginal sulci.

AMPG 704: This specimen corresponds to a small fragment of a peripheral, which is long and moderately flared. It is crossed by the marginal sulci.

AMPG 705 – 706: These specimens correspond to small fragments of a costal.
AMPG 707: This specimen corresponds to a fragment of a peripheral, which is long and moderately flared. It is crossed by the marginal sulci.

AMPG 708: This specimen corresponds to a small fragment of the shell.

AMPG 709 (Fig. 3.66.B): This specimen corresponds to a fragment of an octagonal neural that is not crossed by any sulci. Viscerally we can observe the attachment of the corresponding dorsal vertebra.

AMPG 710: This specimen corresponds to a small fragment of a peripheral, which is long and moderately flared. It is crossed by the marginal sulci.

AMPG 711: This specimen corresponds to the anterior part of the right hyoplastron. It is crossed anteriorly by the humero-pectoral sulcus. Based on the size of the preserved part we can estimate that this specimen belonged to a small-sized individual.

AMPG 712: This specimen corresponds to fragment of the plastron, most probably from the hypoplastron. In the absence of sulci, further description is not possible.

AMPG 713: This specimen corresponds to the anterior part of the left hyoplastron. It is crossed anteriorly by the humero-pectoral sulcus. Based on the size of the preserved part we can estimate that this specimen belonged to a small-sized individual.
AMPG 714: This specimen corresponds to a small fragment of a peripheral, which moderately flared. It is crossed by the marginal sulci.

AMPG 715 (Fig. 3.66.E): This specimen corresponds to a fragment of a costal of a young individual. Viscerally, the inserted rib can be observed. Ventrally is not crossed by any sulci.

AMPG 716: This specimen corresponds to a fragment of the left peripheral 7, located in the end of the bridge. It is crossed by the marginal sulci.

AMPG 717 (Fig. 3.66.K): This specimen corresponds to a complete right epiplastron. The gulars are long and narrow, covering the medial epiplastra and overlapping on the anterior part of the entoplastron. A small constriction is noted in the gularo-humeral sulcus. Viscerally, a thick convex epiplastral lip is formed, with a gular pocket.

AMPG 718 (Fig. 3.66.L): This specimen corresponds to a complete left epiplastron. The gulars are long and narrow, covering the medial epiplastra and expanded on the anterior part of the entoplastron. A small constriction is noted in the gularo-humeral sulcus. Viscerally, a thick convex epiplastral lip is formed, with a deep gular pocket.

AMPG 719: This specimen corresponds to an almost complete right epiplastron. The gulars are long and narrow, covering the medial epiplastra and overlapping on the anterior part of the entoplastron. Viscerally, a thick convex epiplastral lip is formed, with a gular pocket.

AMPG 720: This specimen corresponds to the anterior part of the left hyoplastron. It is crossed anteriorly by the humero-pectoral sulcus. Based on the size of the preserved part we can estimate that this specimen belonged to a small-sized individual.

AMPG 721 – 722: These specimen correspond to small fragments of the right peripheral 3, close to the anterior part of the bridge. They are crossed by the marginal sulci.
AMPG 723: This specimen corresponds to the anterior part of the left hyoplastron. It is crossed anteriorly by the humero-pectoral sulcus. Based on the size of the preserved part we can estimate that this specimen belonged to a small-sized individual.

AMPG 724 – 725: These specimens correspond to fragments of peripherals, which are short and moderately flared. They are crossed by the marginal sulci.

AMPG 726: This specimen corresponds to a costal fragment of a juvenile individual. It is crossed transversely by the pleural sulci.

AMPG 727: This specimen corresponds to the curved diaphysis of a humerus.

AMPG 728 (Fig. 3.66.R): This specimen corresponds to an almost complete procoelous cervical vertebra. The centrum is long, the apophyses are missing, or are fragmented.

AMPG 729: This specimen corresponds to a small fragment of a vertebra.

AMPG 730 (Fig. 3.66.U): A complete half-pointed osteoderm.

AMPG 731 (Fig. 3.66.T): A complete ungual, being long and pointed.

AMPG 742 – 743: These specimens correspond to small fragments of a left xiphiplastron.

AMPG 744: This specimen corresponds to a small plastron fragment.

AMPG 745: This specimen corresponds to a small plastron fragment, most probably of the hypoplastron but further identification is not possible.

AMPG 746: This specimen corresponds to a fragment of a peripheral, which is moderately flared. It is crossed by the marginal sulci.

AMPG 747: This specimen corresponds to a small plastron fragment.

AMPG 750: This specimen corresponds to a fragment of a left epiplastron. The gulars are long and narrow, covering the medial epiplastra and expanded on the anterior part of the entoplastron.

AMPG 751 (Fig. 3.66.J): This specimen corresponds to the left and right epiplastron, forming the anterior part of a wide and rounded lobe. The epiplastra are short and wide. The gulars are long and narrow, covering the medial epiplastra and expanded on the anterior part of the entoplastron. A small irregularity is noted in the right gular scute, being slightly expanded on the left epiplastron. Viscerally, a thick convex epiplastral lip is formed, with a deep gular pocket. Based on the preserved part we can estimate that the entoplastron was short and wide.

AMPG 752 (Fig. 3.66.M): This specimen corresponds to the posterior part of the entoplastron, being overlapped by the gular scutes. The entoplastron is short and wide.

AMPG 755 (Fig. 3.66.A): This specimen corresponds to the anterior part of the nuchal. The nuchal is wide and hexagonal. Anteriorly a long and wide cervical is present. The cervical is present also viscerally. The covering of the marginal 1 is large on the nuchal. The marginal-vertebral sulcus is straight.

AMPG 756: This specimen corresponds to a long and almost horizontally flared peripheral of the posterior region of the carapace. It is crossed by the marginal sulci, and there is good coincidence between the costo-peripheral sutures and the pleuro-marginal sulci.

AMPG 757: This specimen corresponds to a small fragment of a costal.

AMPG 758: This specimen corresponds to the medial part of the hyoplastron. It is crossed anteriorly by the humero-pectoral sulcus. The preserved part is not enough the estimate the side of the plastron that this fragment belongs.

AMPG 759: This specimen corresponds to a fragment of the left hyoplastron. It is crossed anteriorly by the humero-pectoral sulcus.

AMPG 760: This specimen corresponds to a fragment of the right hypoplastron. Although the ventral surface is eroded we can notice the abdomino-femoral sulcus and the limits of a single inguinal scute. The posterior hypoplastral suture is wide and rounded showing the presence of a hypo-xiphiplastral hinge.

AMPG 761: This specimen corresponds to a fragment of the hyoplastron. Further description is not possible, as there is no evidence of sulci in the preserved part.

AMPG 762 – 777 (15 specimens): Small fragments, without any evidence of suture and sulci that belong to the plastron of a tortoise.

AMPG 794: This specimen corresponds to a fragment of the right hyoplastron. Further description is not possible, as there is no evidence of sulci in the preserved part.

AMPG 795 – 796: These specimens correspond to small plastron fragments.

AMPG 811: A group of approximately 100 small fragments of the shell of a tortoise.

AMPG 812: This specimen corresponds to a fragment of a peripheral, which is long and moderately flared. It is crossed by the marginal sulci.

AMPG 813 (Fig. 3.66.F): This specimen corresponds to the medial part of a costal. This costal is medially long and is crossed transversely by the pleural sulci.

AMPG 814: This specimen corresponds to the medial part of the costal 8. Viscerally, we notice the attachment processes of the sacral vertebra.

AMPG 815 (Fig. 3.66.G): This specimen corresponds to the distal part of a costal. This costal is medially long and is crossed transversely by the pleural sulci. There is good coincidence between the costo-peripheral sutures and the pleuro-marginal sulci.

AMPG 816 (Fig. 3.66.C): This specimen corresponds to a fragment of an octagonal neural that is not crossed by any sulci. Viscerally we can observe the attachment of the corresponding dorsal vertebra.

AMPG 817: This specimen corresponds to the medial part of a costal. This costal is medially long and is crossed transversely by the pleural sulci.

AMPG 818 (Fig. 3.66.S): This specimen corresponds to an ilium fragment.

AMPG 854 (Fig. 3.66.I): This specimen preserves almost the entire anterior lobe of the plastron. The lobe is short and wide, having a rounded triangular outlive. The epiplastra are short and wide, covering the anterior part of the lobe. Viscerally, the epiplastra are thick, forming a convex epiplastral lip and a significant gular pocket. The entoplastron is hexagonal, slightly wider than long. The anterior parts of the hyoplastra are also preserved. The gulars are narrow and long, covering the medial epiplastra and the anterior part of the entoplastron. The gularo-humeral sulcus is V-shaped, with acute angle with the midline. The humerals medially are slightly shorter than the gulars, covering the remaining part of the entoplastron, whereas laterally and longer. The remaining part is eroded and we cannot observe the humero-pectoral sulcus.

AMPG 855 (Fig. 3.66.Q): This specimen corresponds to an almost complete right xiphiplastron, since some of the medial part is missing. The posterior lobe is formed entirely by the xiphiplastra, and is not sutured with the hypoplastra. Posteriorly, a wide and deep anal notch is formed. The anterior part of the posterior lobe is covered by the femorals that are short medially and long laterally. Alternatively, the anals are medially long and laterally short. Therefore, the femoro-anal sulcus is slightly concave laterally. The absence of tight suture between the hypoplastra and the posterior lobe and the long xiphiplastra forming the entire posterior lobe suggesting a mobile posterior lobe. Therefore, the presence of a hypo-xiphiplastral hinge can be hypothesized for this specimen.

Simonelli Cave, Crete

AMPG 606 (Fig. 3.67.D): Most of the right humerus is preserved, only the distal part missing. The head is spherical. The two trochanters are slightly diverging to parallel. The major trochanter extends well beyond the humeral head. The diaphysis is strongly curved. Preserved length: 52 mm.

AMPG 607 (Fig. 3.67.C): The curved diaphysis of a humerus is preserved. Preserved length: 27 mm.

AMPG 608 (Fig. 3.67.B): The distal part of the femur is preserved. The femur appears to be straight. Preserved length: 18 mm.

AMPG 609 (Fig. 3.67.A): An entire vertebra is preserved. It shows significant lateral processes and a long procoelous body. It shows no attachments for the carapace. It is one of the sacral vertebras. Preserved length: 21.7 mm.



Figure 3.67. *Testudo marginata* Schoepff, 1793 from the Pleistocene of Simonelli Cave (Crete). AMPG collection: A, AMPG 609, cervical vertebra in (A1) dorsal and (A2) ventral views. B, AMPG 608, femur in (B1) dorsal and (B2) ventral views. C, AMPG 607, diaphysis of a femur in lateral view. D, AMPG 606, right humerus in (D1) dorsal, (D2) posterior, (D3) ventral and (D4) anterior views. Scale bar equals 5 cm.

Comments: The first material mentioned from Simonelli Cave is from Kotsakis (1980). This material (stored in Roma Tre University, Rome, Italy) consists of several limb bones, such as a left femur, three diaphysis of humerus, a tibia, and an ulna. As it has been mentioned by Kotsakis (1980) the morphology of these specimens is consistent with *T. marginata*. The new elements presented here are similar in morphology with the material presented by Kotsakis (1980). No shell remains are known up to now from Simonelli Cave.

Kos Island

NHMC FS38/8 (Fig. 3.68): This specimen corresponds to an almost complete left hyoplastron. The specimen is crossed by the humero-pectoral and the pectoro-abdominal sulci. The humerals are short and the humero-pectoral sulcus is slightly convex medially, showing a strong convexity laterally. It is situated posterior to the entoplastron, on the anterior part of the hyoplastra. The pectorals are much shorter than the humerals medially. The pectoro-abdominal sulcus is slightly concave medially and slightly convex laterally.



Figure 3.68. *Testudo marginata* Schoepff, 1793 from the Pleistocene of Kos Island. NHMC FS38/8, right hyoplastron in (A1) visceral, (A2) ventral and (A3) drawing of the ventral views. Scale bar equals 5 cm.

Charkadio Cave, Tilos

The known chelonian material found in Charkadio Cave consists of 114 specimens. Few specimens have been described by Bachmayer & Symeonidis (1975), which are re-described here in the light of the new specimens discovered by systematic excavations from AMPG (leaded by Prof. G. Theodorou). Few of them are shell elements, whereas most of them belong to the appendicular skeleton. The most common elements are the humerus and the femur. All the material belongs to a single taxon, the marginated tortoise, as it is identified clearly in the few elements of the carapacial margin described below.

Shell elements

Fig. 3.69.A: This specimen is a relatively large and flat shell fragment. Due to the absence of diagnostic features (e.g. sutures, sulci), further identification is not possible.

Fig. 3.69.B: This specimen is an entire peripheral. Since it is partly covered with calcitic material we cannot observe if it is crossed longitudinally by the marginal sulci. No pointed tip is noted in the limits between the marginals in the carapacial rim. There is good coincidence between the costo-peripheral sutures and the pleuro-marginal sulci. Based on the preserved part, the peripheral appears to have been long and vertically oriented. The broad suture on the posterior side allows us to identify this as the peripheral 4 from the right side, right before the start of the bridge.

Fig. 3.69.C.: This specimen is an entire peripheral. It is crossed longitudinally by the marginal sulci. No pointed tip is noted in the limits between the marginals in the carapacial rim. There is good coincidence between the costo-peripheral sutures and the pleuro-marginal sulci. Based on the preserved part, the peripheral appears to have been long and horizontally flared. Moreover, the two sides are not parallel to each other. Compared with the material presented here, this peripheral most probably corresponds to the right peripheral 11 of the flared carapacial border of *T. marginata*.

Fig. 3.69.D: This specimen is an entire peripheral. It is crossed longitudinally by the marginal sulci. No pointed tip is noted in the limits between the marginals in the carapacial rim. There is good coincidence between the costo-peripheral sutures and the pleuro-marginal sulci. Based on the preserved part, the peripheral appears to have been moderately flared. Based on the short length of this peripheral we can conclude that it could belong to the anterior carapacial border.

Fig. 3.69.E: This specimen is a rather large and relatively flat fragment of the plastron. The absence of any sutures and sulci does not allow further identification.

Fig. 3.69.F.: This rather small specimen is flat and preserves a sutured side. Most probably comes from the medial region of the plastron.

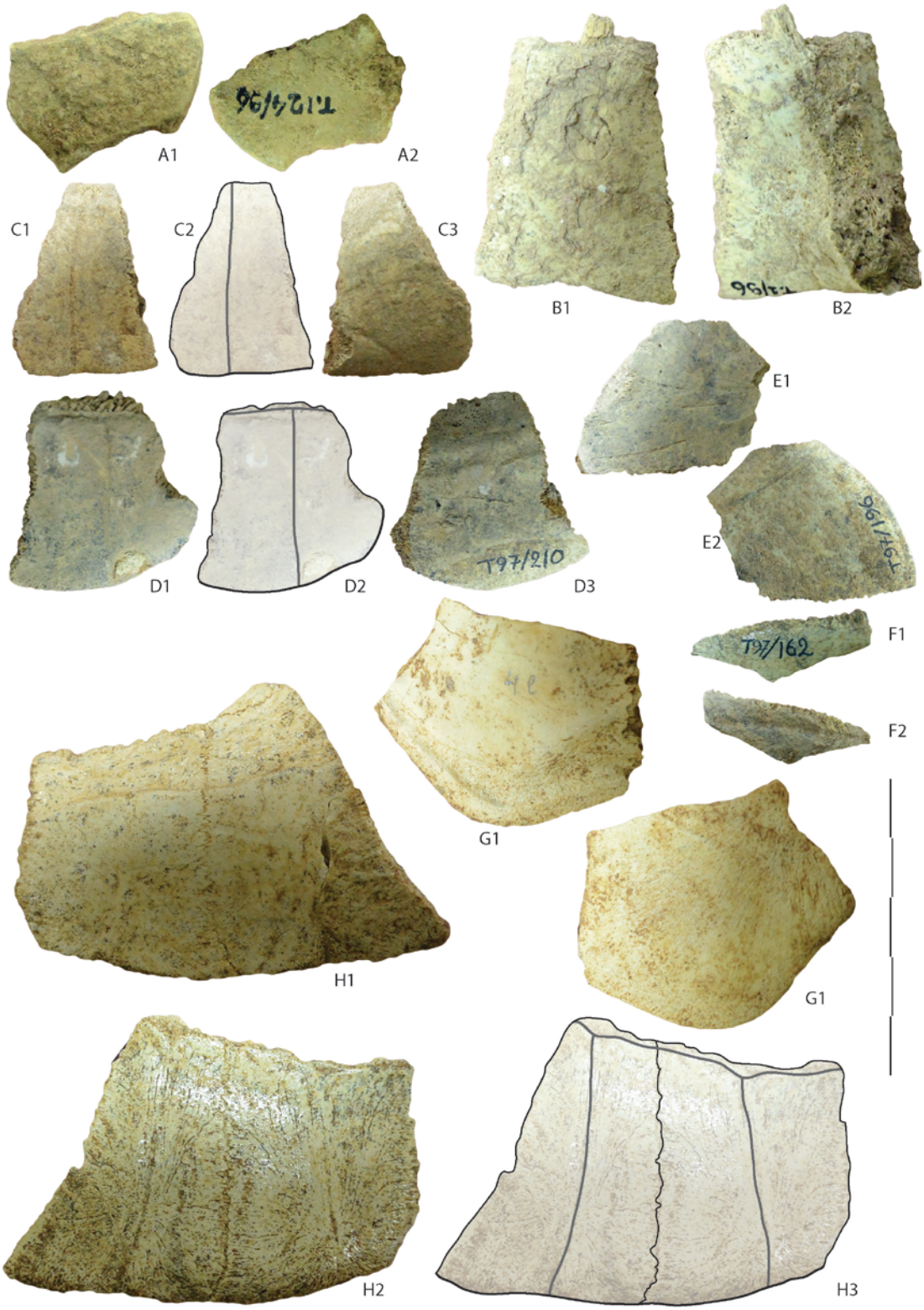


Figure 3.69. *Testudo marginata* Schoepff, 1793 from the Pleistocene/Holocene of Charkadio Cave (Tilos Island). AMPG collection: A, shell fragment in (A1) dorsal and (A2) visceral views. B, peripheral in (B1) dorsal and (B2) visceral views. C, peripheral in (C1) dorsal and (C2) visceral views. D, peripheral in (D1) dorsal and (D2) visceral views. E, plastron fragment in (E1) visceral and (E2) ventral views. F, plastron fragment in (F1) visceral and (F2) ventral views. G, left xiphiplastron in (G1) visceral and (G2) ventral views. H, peripherals in (H1) visceral, (H2) dorsal and (H3) drawing of the dorsal views. Scale bar equals 5 cm.

Fig. 3.69.G: This specimen belongs to a part of the left xiphiplastron. Based on the preserved part we can estimate that the posterior lobe has been long and wide, showing a deep and wide anal notch posteriorly. Ventrally, no sulci can be observed, showing that the anal scutes had a long covering on the posterior part of the posterior lobe. Viscerally, a narrow and convex lip is formed by the visceral covering of the anals to the rim of the plastron.

Fig. 3.69.H: This specimen consists of two continuous peripherals. They are crossed longitudinally by the marginal sulci. No pointed tip is noted in the limits between the marginals in the carapacial rim. There is good coincidence between the costo-peripheral sutures and the pleuro-marginal sulci. Both peripherals appear are long and horizontally flared. Moreover, in one of them the two sides are not parallel to each other. Compared with the material presented here, this peripheral region most probably corresponds to the right peripherals 10-11 of the flared carapacial border of *T. marginata*.

Appendicular elements

Shoulder girdle (Fig. 3.70.A-C): Only 3 specimens belong to the shoulder girdle. There is one left scapula with the acromion (figured by Bachmayer & Symeonidis, 1975). A further finding of a left scapula is found, but part of the acromion is missing. Finally, one fragment of an acromion has been also recovered. The structure of the shoulder girdle is the typical found in small testudinids, showing the triradiate structure of the scapular prong in right angle with the curved acromion. Articulated with the scapula is the coracoid that is missing in the Charkadio Cave material.



Figure 3.70. *Testudo marginata* Schoepff, 1793 from the Pleistocene/Holocene of Charkadio Cave (Tilos Island). AMPG collection: A, left scapula in (A1) posterior and (A2) anterior views. B, acromion in (B1) anterior and (B2) posterior views. C, right scapula in (C1) anterior and (C2) posterior views. D, ilium fragment in dorsal view. E, right radius in (E1) medial, (E2) dorsal, (E3) lateral and (E4) ventral views. F, tibia in (F1) dorsal, (F2) medial, (F3) ventral and (F4) lateral views. G, tibia in dorsal view. H, tibia in (H1) ventral and (H2) dorsal views. Scale bar equals 5 cm.

Humerus (Fig. 3.71): The humerus is the most common element in the chelonian material from Charkadio Cave, counting 69 specimens in total. Several specimens are recovered complete or almost complete (11 of 69; 16%). In those found slightly incomplete, usually the tip of the major trochanter is missing. One of them belongs to a juvenile individual, whereas the rest could be grouped in two size groups, probably related to sexual dimorphism. Most of the preserved humeri (40 of 69; 58%) preserved the proximal part with the head and most of the diaphysis. Additionally, in three specimens that preserve the proximal part, the head is missing. Few specimens (6 of 69; 8%) preserve the diaphysis and the distal part. The remaining specimens (9 of 69; 13%) preserve various parts of the diaphysis. In some cases the preserved part is so small that does not allow a confident identification of the side. In total, the preserved humeri allow a detailed documentation of the morphology of the marginated tortoise from Charkadio Cave. The head of the humerus is spherical, being developed in right angle with the proximal part of the bone. The two trochanters are unequal in size, and are developed slightly diverging to parallel to each other. The major trochanter extends well beyond the humeral head, whereas the minor is much shorter or poorly developed in some cases. The diaphysis is strongly curved, especially in the distal part. Within the studied material, we can observe a small degree of variation in the degree of curvature of the diaphysis. The distal part of the bone is wide and preserves two convex surfaces for the radius and ulna. The radial and ulnar condyles are of equal size and their posterior surface is slightly concave.

Radius (Fig. 3.70.E): Only one radius is found. The bone is straight, showing a narrow diaphysis and wide proximal and distal ends. The proximal surface is concave for the radial condyle, whereas the distal is convex for the carpal elements. Proximally and distally, two articular surfaces for the ulna are noted. The proximal articular surface is short and wide, whereas the distal articular surface is taller and narrower. In between, a long and narrow fenestra is developed.

Pelvis (Fig. 3.70.D): Only one pelvic specimen is found, probably from the ilium, but the preservation status does not allow further description.

Femur (Fig. 3.72): The femur is the second most common element in the material, counting up to 28 specimens. Quite a few of them are preserved complete (9 of 28; 32%). Many (7 of 28; 25%) are found almost complete, missing only the head. Few (3 of 28; 10%) preserve only the proximal part with the femoral head. The remaining specimens (6 of 28; 21%) preserve various parts of the diaphysis with the distal part. The preserved material allows a detailed documentation of the morphology of the femur. The head is rounded and elliptical. Its longer axis is oriented with an obtuse angle with the midline. The proximal part is wide, and the trochanters are fused. The diaphysis is straight, displaying a small degree of curvature in the distal part. The tibial and fibular condyles are large and rounded, creating a shallow concavity in the posterior part.

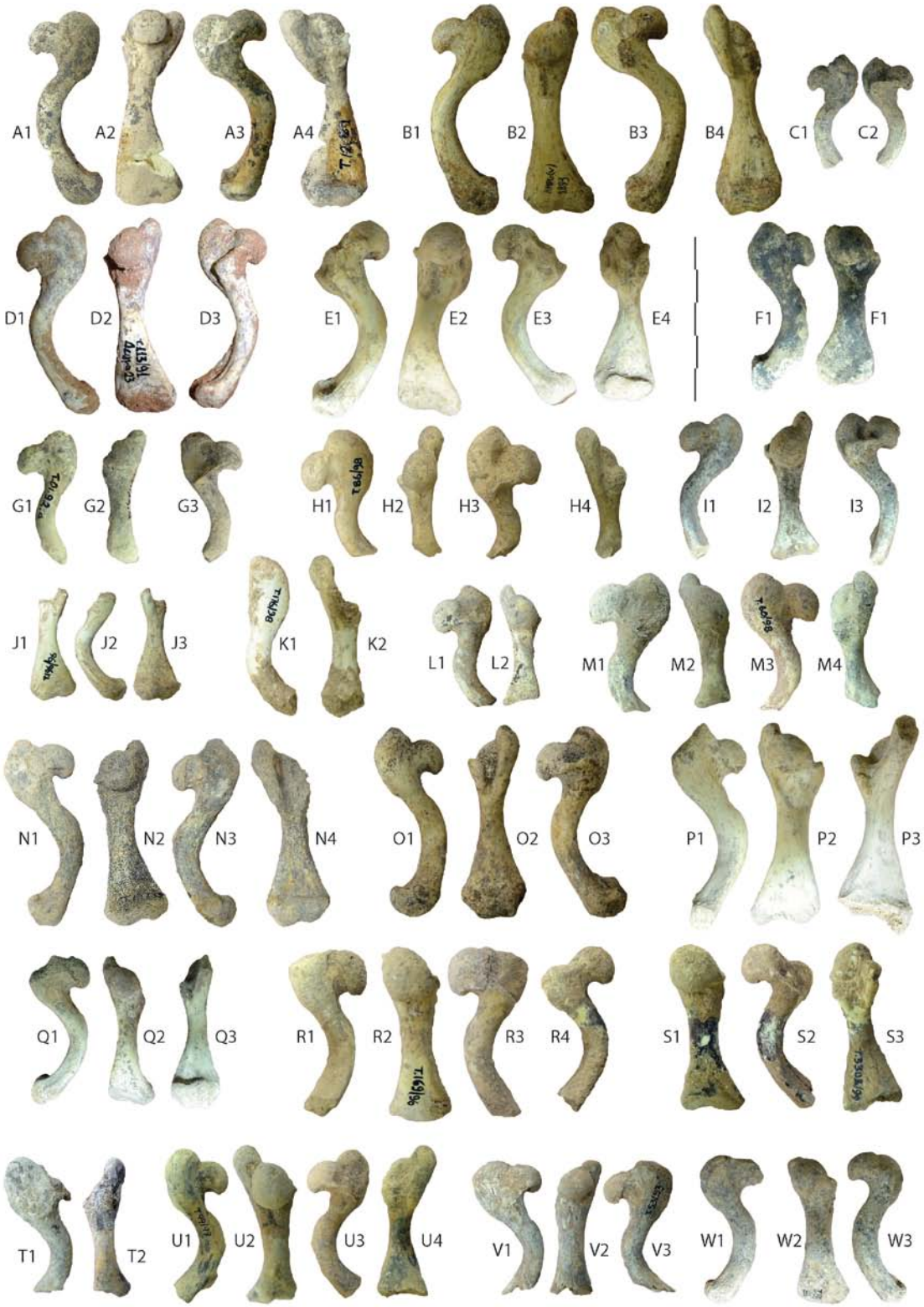


Figure 3.71. *Testudo marginata* Schoepff, 1793 from the Pleistocene/Holocene of Charkadio Cave (Tilos Island). AMPG collection. Left humeri are A, B, C, D, G, H, I, J, L, M. Right humeri are E, F, N, O, P. Views in A are: (A1) posterior, (A2) dorsal, (A3) anterior and (A4) ventral. Scale bar equals 5 cm.

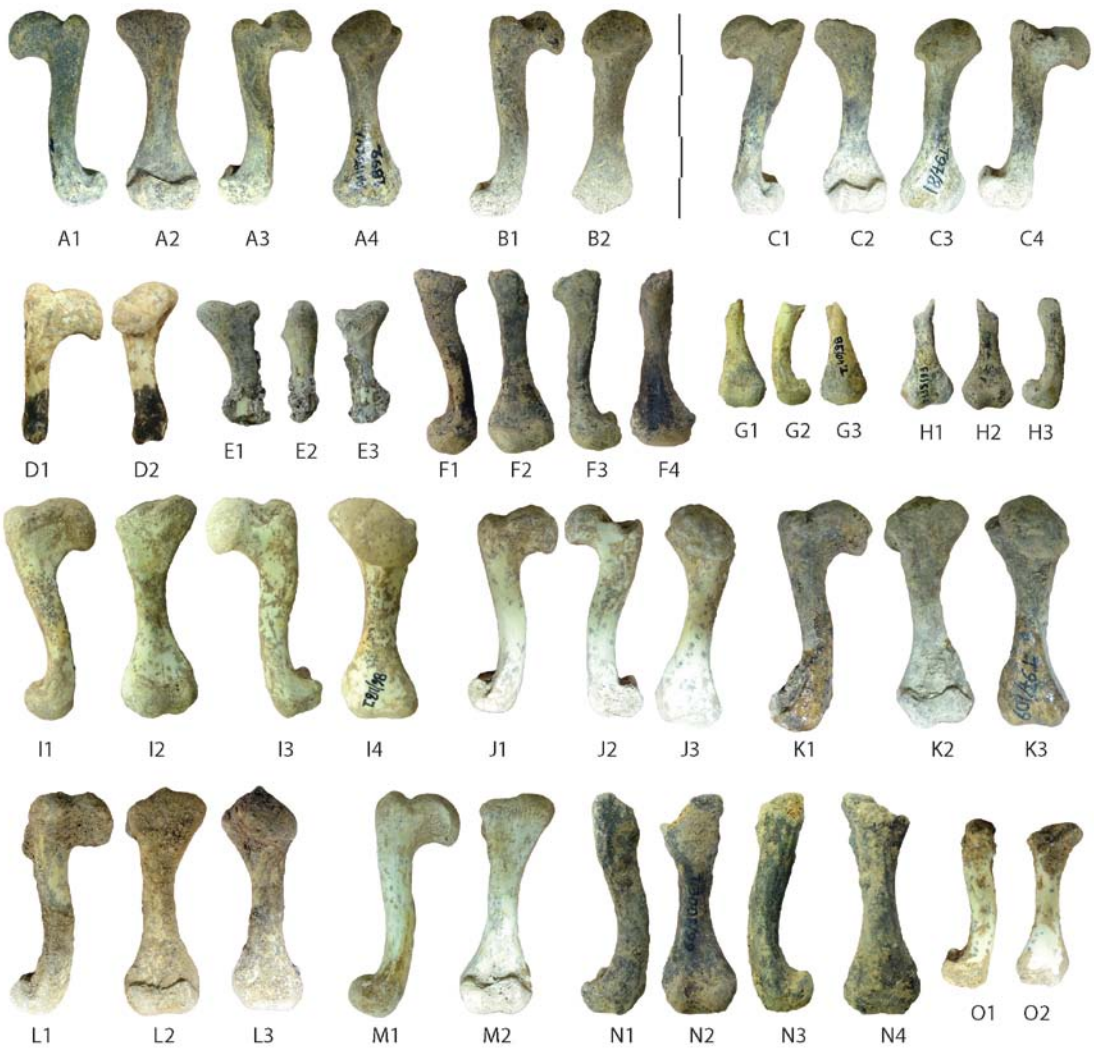


Figure 3.72. *Testudo marginata* Schoepff, 1793 from the Pleistocene/Holocene of Charkadio Cave (Tilos Island). AMPG collection. Left femurs are A, B, C, D. Right femurs are I, J, K, L, M. Views in A are: (A1) posterior, (A2) ventral, (A3) anterior and (A4) dorsal. Scale bar equals 5 cm.

Tibia (Fig. 3.70.F-H): Only 4 specimens belong to the tibia. Two of them are complete, one preserves the proximal part and the diaphysis, and another specimen only the diaphysis and the distal part. The latter specimen is largely covered by calcitic material. The tibia is relatively straight in the proximal and medial part, but displays a significant degree of curvature in the distal part. In the distal part of the shaft a rugosity is noted. The proximal part is wide, triangular in cross-section and displays a well-developed and broad cnemial crest. The proximal articular surface is broadly concave. The distal articular surface is more complex, being concave medially and convex laterally.

Taphonomical Remarks

The skeletal element representation of the *Testudo marginata* from Charkadio Cave is shown in Table 3.2 and in Fig. 3.73. As far as fragmentation is concerned, only 21 specimens (1 scapula, 11 humeri, 9 femori) are found complete, referring to a small percentage to the total number of specimens (18,4%). The degree of

fragmentation however is rather small, as it is shown by the high MNE/NISP ratio (107/114= 93,8%). This means that although most of the specimens are found fragmented, in most cases the breakage occurs in small parts leaving significant portions of the bone unfragmented. This keeps the MNE count close to that of NISP. Comparing the fragmentation pattern between the two most common elements, the humerus and the femur, we notice several significant differences. The humerus appears to have been an element more susceptible to fragmentation compared to the femur. Although in the humerus (Fig. 3.74) the proximal part with the head is overrepresented, being present in 72% of the specimens (50 of 69), the femur shows a different pattern (Fig. 3.75). Only 57% (16 of 28) of the specimens preserve the proximal part with the head. On the contrary, the distal part of the femur is overrepresented, being present in 71% (20 of 28) specimens. Moreover, the diaphysis is frequently recovered without the epiphyses in the humerus.

Table 3.2. Skeletal element representation of the *Testudo marginata* from Charkadio Cave, Tilos Island.

Skeletal Element	NISP	Left	Right	MNI	MNE
Carapace	5	-	-	2	2
Plastron	3	-	-	1	3
Scapula	3	2	-	2	3
Pelvis	1	-	-	1	1
Humerus	69	34	27	34	67
Radius	1	-	1	1	1
Femur	28	15	12	15	26
Tibia	4	3	1	3	4
Total	114	-	-	-	107

The anterior part of the body is much more represented compared to the posterior one, measuring up to 67% of the known appendicular elements (73 of 108 specimens). However, only the humerus is well known, showing a small dominance of the elements from the left side (34 of 61; 55%). The posterior part of the body is less represented (35 of 108; 32%), with the femur being the most dominant. Again the left side of the body is slightly better represented (15 of 27; 55%).

Following Badgley (1986), we choose MNI as the method to estimate the minimum number of individuals of marginated tortoises in Charkadio Cave. This is because the degree of association between the elements is considered high as they are recovered in a cave, in sediment sealed by calcitic layers. Thus, both the degree of peri-mortem transportation and the effect of post-mortem processes is low. The MNI is calculated on the most common element, the humerus. The diagnostic features of this skeletal element, with the difference of the size of the trochanters, makes the identification of the side an easy task. Therefore, the calculation is of the MNI based on the humerus is a confident assessment. Based on the analysis of the recovered assemblage we estimate the presence of at least 34 tortoise individuals (calculated on the left humeri).

.

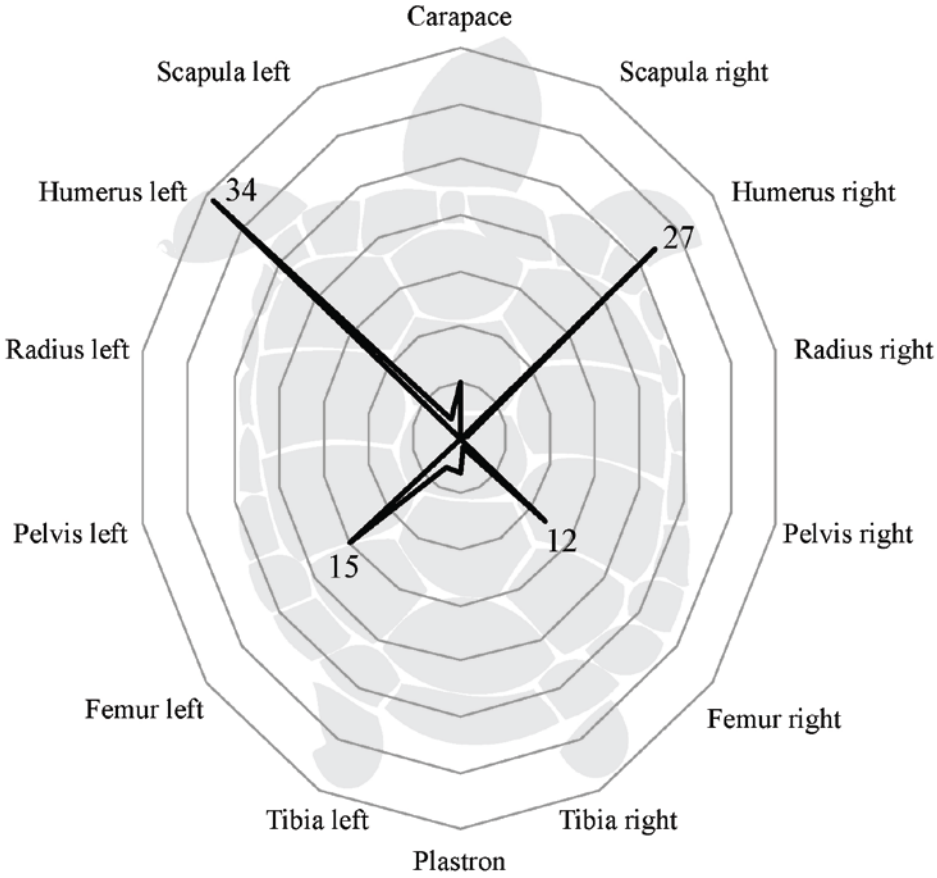


Figure 3.73. Skeletal element representation of the shell fragments and appendicular elements from *Testudo marginata* Schoepff, 1793 from Charkadio Cave, Tilos Island.

Quite recently, Georgalis & Kear (2013:306) commented that "*butchering might explain the unusual taphonomic accumulations of tortoise limb bones in other latest Pleistocene-Holocene cave assemblages around the Aegean (e.g., Charkadio on Tilos*". However, they did not provide any taphonomical evidence for this, but they only gave an example of hunting of large tortoises in Vanuatu islands (in White et al., 2010). Indeed, in this site the shell elements are scarce and survivorship of limb elements is the rule. But the skeletal element representation alone is not enough to connect the two sites. The main reason is the total size difference between the large-bodied tortoises of Vanuatu and the much smaller marginated tortoises of Charkadio Cave. These two taxa occupy a completely different ecological niche and therefore their interaction with the possible humans are not comparable.

Perhaps a comparable site with Charkadio Cave is Franchthi Cave in Peloponnesus. In this site, Stiner & Munro (2011) have proved the human interaction and that in several periods the human that occupied the cave used small animals such as turtles and tortoise as food resources. As it has been preliminary presented by Stiner & Munro (2011) and more detailed in the present thesis, in this site findings of limb bones are scarce. The general rule is to find isolated shell elements, in some cases with scratches and cut marks or even burned. Therefore, comparing the two sites, Charkadio Cave seems to provide the exact opposite image of the human-interacted Franchthi Cave.

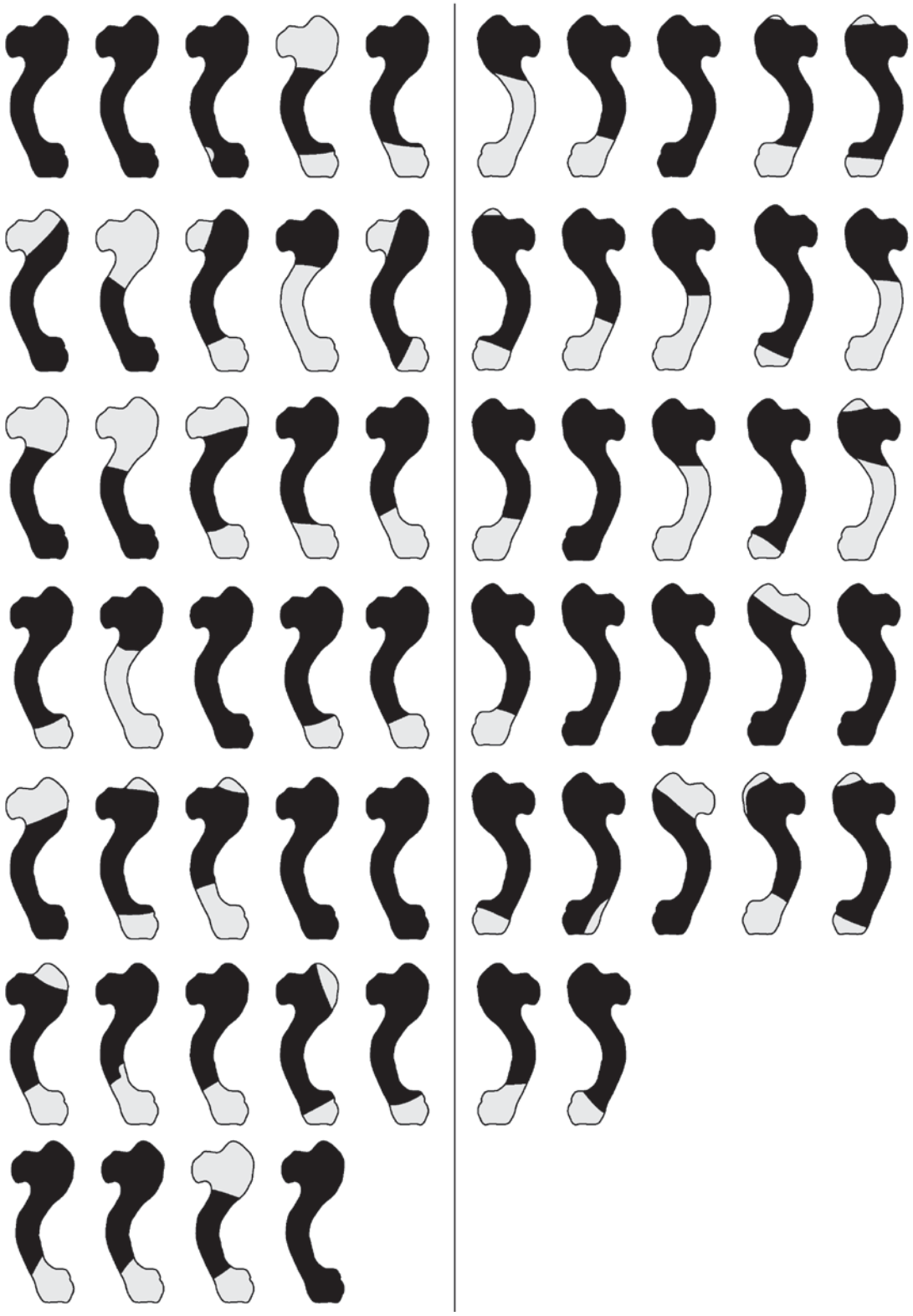


Figure 3.74. Skeletal element representation of the left and right humeri from *Testudo marginata* Schoepff, 1793 from Charkadio Cave, Tilos Island. The preserved bone is colored with black, missing bone with grey colour.

Further evidence does not support human interaction in Charkadio Cave. First and foremost, no human bones are known up to now from the cave. The human presence has only been hypothesized due to the available datings for the elephant

remains of 45 ka to 3.5 ka (Bachmayer et al., 1984). Second, these datings and the abundant fossil material, indicate that this cave has been inhabited by the dwarf elephant species *Elephas tiliensis* Theodorou et al. (2007), and therefore a human occupation at the same time seems improbable. Taphonomical studies on the avian and elephant remains (Michailidis et al., 2014) refutes as well the possible human interaction in the cave. Finally, no cut marks or scratches have been observed in the Charkadio material. Summarizing, all the available data indicate that human did not play any role in the accumulation of the tortoise remains. The degree and the type of fragmentation could be attributed to trampling from the dwarf elephants.

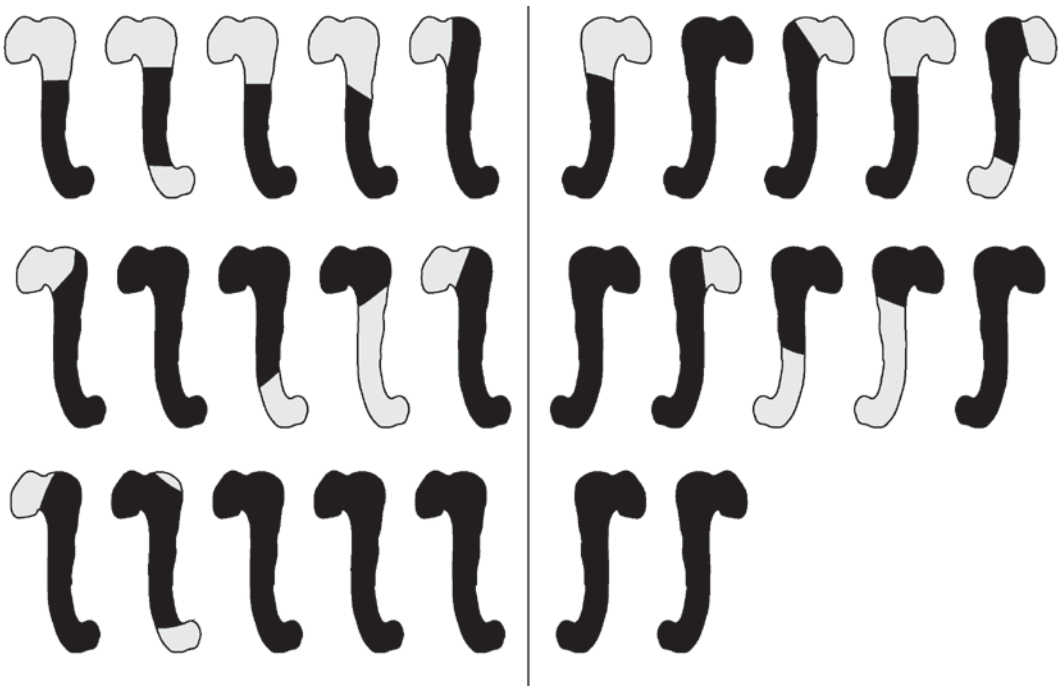


Figure 3.75. Skeletal element representation of the left and right femora from *Testudo marginata* Schoepff, 1793 from Charkadio Cave, Tilos Island. The preserved bone is colored with black, missing bone with grey color.

Right humerus (Fig. 3.76.D): This specimen corresponds to a complete right humerus. The surface of the bone is weathered, resembling bones that have been left exposed. Compared to the weathering stages of Behrensmeyer (1978) the stage of this specimen is intermediate to stage 1 (with cracking parallel to the fiber structure) and stage 2 (presence of flaking in the outer surface with one edge attached to the bone). The head of the humerus is spherical, being developed in right angle with the proximal part of the bone. The two trochanters are different in size, and are developed slightly diverging to each other. The major trochanter extends well beyond the humeral head, whereas the minor is much shorter. The diaphysis is strongly curved, especially in the distal part. The distal part of the bone is wide and preserves two convex surfaces for the radius and ulna. The radial and ulnar condyles are of equal size and their posterior surface is slightly concave. Measurements (mm): L=48,40; PD=18,10; DW=14,02.

Peripheral (Fig. 3.76.A): This specimen corresponds to a complete 7th left peripheral. The plate is tall and short, being developed vertically. On dorsal side the plate is crossed by the marginal sulci, whereas the costo-peripheral suture coincides with the pleuro-marginal sulci. Ventrally, we notice the presence of a sutural surface for the inguinal process that extends dorsally and ends within the limits of the peripheral. Based on the preserved sutural end for the 8th peripheral we can estimate that the posterior part of the carapacial margin has been widened.

Entoplastron (Fig. 3.76.B): This specimen corresponds to a complete entoplastron. The ventral surface of this specimen shows evidence of some cracks that are usually developed after exposure of the specimen on the surface. The weathering stage resembles the stage 1 (after Behrensmeyer, 1978). The entoplastron is relatively thick, wider than long, with an hexagonal and rounded outline in ventral view. The visceral surface is much smaller than the ventral one. The long and pointed entoplastral process is preserve ventrally. Ventrally, the entoplastron is crossed by the medial sulci of the humerals, whereas on the anterior end we notice only a small covering of the gular scutes. Measurements (mm): L=29,05; W=33,98.

282 (Fig. 3.76.C): This specimen corresponds to an almost complete left humerus, with the distal part missing. The head of the humerus is spherical, being developed in right angle with the proximal part of the bone. The two trochanters are unequal, and are developed as slightly diverging to each other. The major trochanter extends well beyond the humeral head, whereas the minor is broken, but it is certainly shorter. The diaphysis is strongly curved, especially in the distal part. Measurements (mm): L(preserved)=50,08; PD=21,92.

283 (Fig. 3.76.H): This specimen corresponds to an almost complete left humerus, with the distal part missing as well as some of the tips of the trochanters. Based on the small size and the slender morphology, and also due to the incomplete ossification of the humeral head we can identify this specimen as belonging to a young individual. The head of the humerus is spherical, being developed in right angle with the proximal part of the bone. The two trochanters are unequal, and are developed as slightly diverging to each other. The major trochanter extends well beyond the humeral head, whereas the minor is broken, but it is certainly shorter. The diaphysis is strongly curved, especially in the distal part. Measurements (mm): L(preserved)=38,14.

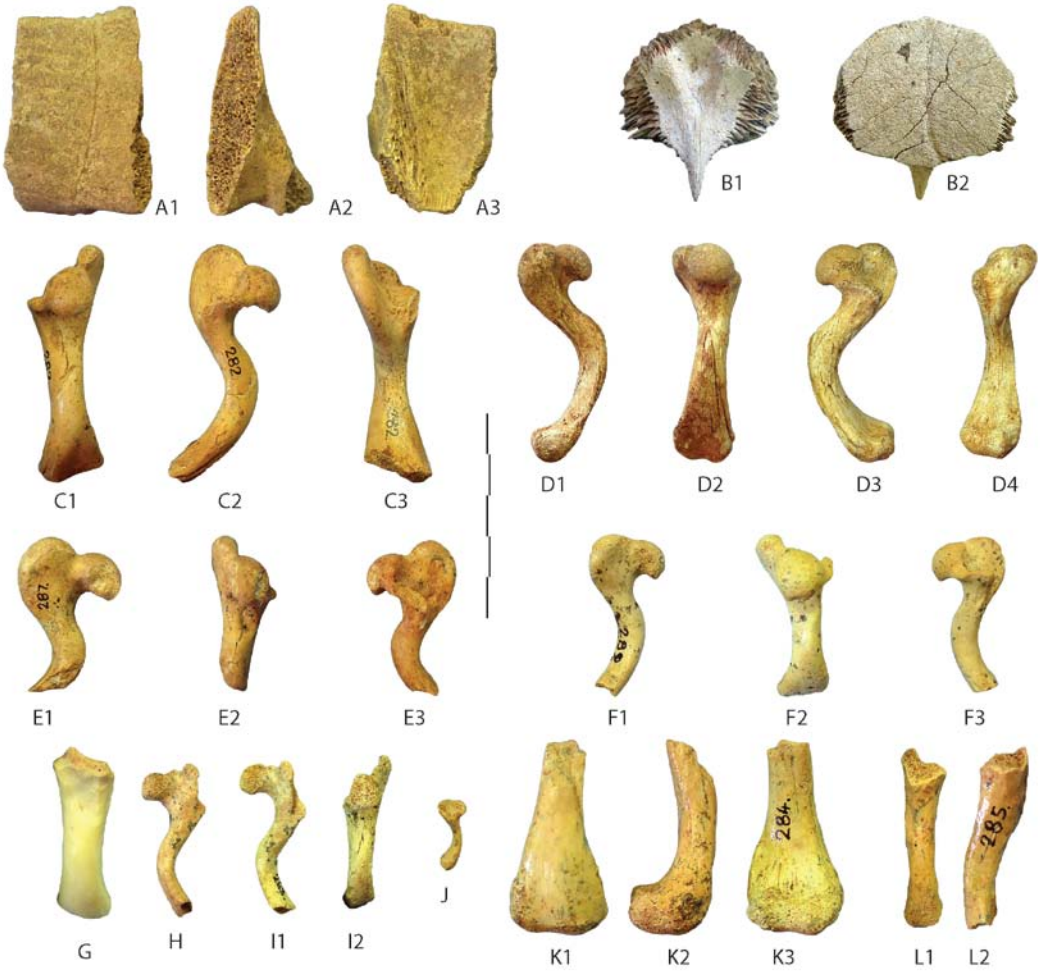


Figure 3.76. *Testudo marginata* Schoepff, 1793 from the Pleistocene of Poulion Cave in Boetia. A, peripheral in (A1) dorsal, (A2) posterior and (A3) visceral views. B, entoplastron in (B1) visceral and (B2) ventral views. C, left humerus in (C1) dorsal, (C2) anterior and (C3) ventral views. D, right humerus in (D1) posterior, (D2) dorsal, (D3) anterior and (D4) ventral views. E, right humerus in (E1) posterior, (E2) dorsal and (E3) anterior views. F, right humerus in (F1) posterior, (F2) dorsal and (F3) anterior views. G, humerus diaphysis. H, left humerus of a juvenile. J, left humerus of a juvenile in (I1) posterior and (I2) dorsal views. J, left humerus of a juvenile. K, femur distal part in (K1) dorsal, (K2) lateral and (K3) ventral views. L, femur in (L1) dorsal and (L2) lateral views. Scale bar equals 5 cm.

284 (Fig. 3.76.K): This specimen corresponds to the distal part of a femur. The diaphysis is straight, displaying a small degree of curvature in the distal part. The tibial and fibular condyles are large and rounded, creating a shallow concavity in the posterior part.

285 (Fig. 3.76.L): This specimen corresponds to a relatively straight diaphysis of a femur.

286: This specimen corresponds to a relatively straight diaphysis of a femur.

287 (Fig. 3.76.E): This specimen corresponds to the proximal part of a right humerus. The head of the humerus is partially broken but it appears to have a spherical shape. The two trochanters are unequal, and are developed as slightly diverging to each

other. The major trochanter extends well beyond the humeral head, whereas the minor is broken, but it is shorter. The diaphysis is strongly curved. Measurements (mm): L(preserved)=36,28; PD (preserved)=20,10.

288 (Fig. 3.76.G): This specimen corresponds to a partial diaphysis of a right humerus.

289: This specimen corresponds to an almost complete right humerus, with the distal part missing. Based on the small size and the slender morphology, we can identify this specimen as belonging to a young individual. The head of the humerus is spherical, being developed in right angle with the proximal part of the bone. The two trochanters are unequal, and are developed as slightly diverging to each other. The major trochanter extends well beyond the humeral head, whereas the minor it is shorter. The diaphysis is strongly curved, especially in the distal part. Measurements (mm): L(preserved)=26,95; PD=13,20.

290 (Fig. 3.76.J): This specimen corresponds to an almost complete left humerus, with the distal part missing. Based on the tiny size and the slender morphology, as well as the incomplete ossification of the humeral head and trochanters we can identify this specimen as belonging to a juvenile individual. The head of the humerus is roughly spherical. The two trochanters are unequal in size. The major trochanter extends well beyond the humeral head, whereas the minor it is shorter. The diaphysis is curved. Measurements (mm): L(preserved)=13,91; PD=5,27.

291: This specimen corresponds to an almost complete right humerus, with the distal part missing. Based on the tiny size and the slender morphology, as well as the incomplete ossification of the proximal part we can identify this specimen as belonging to a juvenile individual. The head of the humerus is missing. The two trochanters are unequal in size. The major trochanter extends well beyond the humeral head, whereas the minor it is shorter. The diaphysis is curved. Measurements (mm): L(preserved)=12,46.

292: This specimen corresponds to an almost complete right humerus, with the distal part missing. Based on the tiny size and the slender morphology, we can identify this specimen as belonging to a juvenile individual. The head of the humerus is spherical to elliptical. The two trochanters are unequal in size. The major trochanter extends well beyond the humeral head, whereas the minor it is shorter. The diaphysis is curved. Measurements (mm): L(preserved)=14,90; PD=7,32.

293: This specimen corresponds to an almost complete left humerus, with the distal part missing. Based on the tiny size and the slender morphology, as well as the incomplete ossification of the humeral head and trochanters we can identify this specimen as belonging to a juvenile individual. The head of the humerus is roughly spherical. The two trochanters are unequal in size. The major trochanter extends well beyond the humeral head, whereas the minor it is shorter. The diaphysis is curved. Measurements (mm): L(preserved)=14,41; PD=5,22.

Kythera Island

Humerus (Fig. A): This specimen corresponds to an almost complete left humerus, with only the distal end missing. The size of this humerus is enormous, much bigger than the remaining specimens. The head of the humerus is spherical, being developed in right angle with the proximal part of the bone. The two trochanters are different in size, and are developed as slightly diverging to each other. The major trochanter extends well beyond the humeral head, whereas the minor is broken, but it is certainly shorter. The diaphysis is strongly curved, especially in the distal part. The distal part of the bone is wide and preserves two convex surfaces for the radius and ulna. The radial and ulnar condyles are of equal size and their posterior surface is slightly concave. A significant ectepicondylar groove is developed. Measurements (mm): L(preserved)=71,43; PD=26,05; DW=21,02.

Humerus (Fig. B): This specimen corresponds to the proximal part of a left humerus, reaching the size of the previous specimen. The head of the humerus is spherical, being developed in right angle with the proximal part of the bone. The two trochanters are different in size, and are developed as slightly diverging to each other. The major trochanter extends well beyond the humeral head, whereas the minor is much shorter. Measurements (mm): L(preserved)=39,38; PD=24,26.

Radius (Fig. C): This specimen corresponds to a complete right radius. The bone is straight, showing a narrow diaphysis and wide proximal and distal ends. The proximal surface is triangular and concave for the radial condyle, whereas the distal is convex for the carpal elements. Proximally and distally, two articular surfaces for the ulna are noted. The proximal articular surface is short and wide, whereas the distal articular surface is taller and narrower. In between, a long and narrow fenestra is developed. Measurements (mm): L=34,13; PD=10,77; DW=14,54.



Figure 3.77. *Testudo marginata* Schoepff, 1793 from the Pleistocene of Kythera Island. A, left humerus in (A1) posterior, (A2) dorsal and (A3) anterior views. B, left humerus in (B1) posterior and (B2) dorsal views. C, right radius in (C1) dorsal, (C2) medial, (C3) lateral, (C4) ventral and (C5) proximal views. Scale bar equals 5 cm.

DISCUSSION

The marginated tortoise, *Testudo marginata*, is one of the traditionally recognized species of *Testudo*, named by Schoeppf in 1792. Among the various species of *Testudo* is certainly the largest, as it could exceed 40 cm in carapacial length. It is distributed across the mainland of Greece and Peloponnesus, and in few Aegean islands. It is also found in Albania. This species is easily recognized by the presence of an elongated carapace with posteriorly flared peripherals and pygal. Among the material presented above, several specimens preserve the posteriorly flared carapace allowing a clear attribution to this taxon. Also, in cases where only limb bones are preserved, they are significantly larger from the size range of *Testudo graeca* and *Testudo hermanni*. The presence of the marginated tortoise is established for the entire Pleistocene with fossils that are within the natural distribution of the extant *T. marginata*. The only significant exception compared with the extant distribution is the presence of this taxon in the south Aegean area in the islands of Kos, Tilos and Crete.

The marginated taxon that has been identified in Crete, is *Testudo marginata cretensis*, a new subspecies described by Bachmayer et al. (1975). In this section some information on the potential validity of this subspecies is provided. It is diagnosed as: "*Neurale I hat eine rechteckige und Neurale II eine achteckige Umrissform. Das Pygale ist vorne und hirten gleich breit. Gulare ist viel schmäler. Der Hinterrand des Xiphiplastrons ist bei der Unterart viel breiter als bei der Art* Testudo marginata" (Bachmayer et al., 1975:111). Based on my observations on the holotype, the neural 1 is hexagonal with short postero-lateral sides, and not rectangular as is described by Bachmayer et al. (1975). Note that Bachmayer et al. (1975:Fig. 3) show the neural region of a recent *T. marginata* as having an hexagonal neural 1. Several other extant specimens that have been examined have rectangular and hexagonal neural 1. In the paratype (from Zourida Cave) the limits of neural 1 are not clearly visible. Therefore, the first character (neural 1 rectangular) for the differential diagnosis of *T. m. cretensis* is subject to the intraspecific variability of *T. marginata*. The second character (neural 2 octagonal) is the normal condition seen not only in *T. marginata* but in other *Testudo* as well. The third character (pygal of equal anterior and posterior width) is even more variable. Although the holotype (Gerani Cave) shows this condition, the paratype (Zourida) shows a pygal that is posteriorly wider (also seen in other specimens from Zourida). In extant specimens of *T. marginata* most of the times there is a pygal that is also posteriorly narrower. The fourth character (narrow gulars) is also quite variable, not only in the studied specimens from Crete, but within *T. marginata* in general. Similar is the variability within *T. marginata* in the last character (wider xiphiplastra). It seems that all these differences can be within the range of the intraspecific variation and/or sexual dimorphism of the marginated tortoise. Also, many of the specimens that have been examined (and also the one figured by Bachmayer et al., 1975:Fig. 3) show many irregularities in the shape of the neurals. For example, in some specimens the last neurals could be missing and the costals contact each other medially.

A recent attempt to define another species within *T. marginata*, was by Bour (1996) with the erection of "dwarf" species of *T. marginata*, named *Testudo weissingeri*. But it mitochondrial studies (Fritz et al., 2005) do not support this distinctiveness. Also, Fritz et al. (2005:399) conclude that: "[…] *tortoises are capable of modifying their morphology within a few hundred or thousand years, due to genetic*

bottlenecks or environ mental pressure. This argues for caution when erecting further new Testudo *species or subspecies without accompanying genetic studies*".

Based on all the available evidence it seems that the small differences observed in the Gerani and Zourida specimens are not adequate enough in order to successfully distinguish the Crete tortoises from *T. marginata*.

Testudo marginata has been traditionally regarded as closely related with the Late Miocene taxon *Testudo marmorum* (Lapparent de Broin, 2001; 2002). In a following section information is provided on the specimens of *Testudo marmorum* and discuss the potential relationship between the two taxa. Also, in a following section some testudinid material is described from the Late Pliocene of Milia that present some similarities with the marginated tortoise.

Regarding the morphological variation in the studied material we can notice several examples. Perhaps the most characteristic is the degree of the flaring of the posterior carapacial rim. For example, some specimens (e.g. Gerani) show a posterior rim that is not horizontally flared, whereas others (e.g. Zourida) show a rim that is horizontal (paratype of *T. m. cretensis*) or even more curved (AMPG 577).

Brinkerink (1996) brings into attention a distal humerus (AMPG 787) from Katharo basin in Crete, suggesting that this is an element of a large *Testudo*. My inspection of the specimen found no similarities with a turtle/tortoise humerus. The diaphysis of the specimen is almost straight, compared to the curved humerus of testudinids. Moreover, there is no ectepicondylar foramen. Finally, a transverse constriction is found that is lacking in chelonian humeri. Therefore, based on the available material we can refute the presence of tortoises in Katharo basin.

Schleich (1982) described some material of *Testudo marginata* from the Pleistocene of Laconia (Peloponnesus). According to the author the original material is stored in the Institute of Geology and Subsurface Research (Athens; now Institute of Geology and Mineral Exploration, IGME), whereas casts of these specimens are stored in BSPG. Personal communication with IGME failed to locate these specimens. Personal observations on the casts in BSPG however, confirm the identifications of Schleich (1982) as a member of *T. marginata*.

Testudo cf. *marginata*

MATERIAL:
Xerias, Kavala (Pleistocene, 1 specimen) (Fig. 3.78): LGPUT XEK 1, a partial shell.

DESCRIPTION

LGPUT XEK 1 (Fig. 3.78): The shell is partially preserved, preserving the right side of the shell, and most of the right side of the plastron. The in-filling sediment is preserved and on the ventral side we can observe the imprints of the plastral sutures. Moreover, few bones have been preserved in the sediment, but the preparation of these bones is rather difficult since the sediment is holding this fragile specimen together. The whole specimen is compressed.

Carapace: The posterior part of the neural 3 is preserved, indicating that it is quadrangular, wider than long. The neural 4 is octagonal, wider than long. The neural 5 is quadrangular, slightly wider than long. Neural 6 is octagonal, with narrower posterior side. Neural 7 is quadrangular with rounded sides. Most probably two suprapygals are present, but this area is highly eroded. The first suprapygal is smaller, quadrangular, whereas the second is larger, trapezoid with narrow anterior and wide posterior ends. The costals show the typical alternating pattern of the testudinids, having costals medially short and laterally long (costals 2, 4, 6) alternated with costals medially long and laterally short (costals 3, 5). Costal 1 is partially preserved. Costal 7 is larger, making contact with the neurals 6-7, the suprapygals, and the posterior peripherals. The posterior peripherals are long and narrow, and they appear to be flat to posteriorly flared. The vertebrals are wider, slightly narrower than the pleurals. The limits between the vertebrals cross the neurals 3, 5, and 7. The pleurals are short and wide, quadrangular, and their limits cross costals 2, 4, 6, and 7.

Plastron: Few plates of the plastron are preserved. The hyo- and hypoplastra are long and wide and relatively flat. On the hyoplastra we notice the humero-pectoral sulcus that joins the marginal sulci of the bridge area. The hypoplastra are long, and they end in the end of the bridge, without any contribution to the posterior lobe. Although the shell is compressed, the carapace on the bridge area appears to have been widened. The posterior lobe is long, formed entirely by the xiphiplastra. At the same time, there is no tight suture with the hypoplastra, and sediment is in between. This suggests that the posterior lobe was movable and the presence of a hypo-xiphiplastral hinge. The femorals show a long covering on the posterior lobe, whereas the anals only cover the posterior part.

COMMENTS: This specimen has been preliminary described in Tsoukala et al. (2011), where it has been already stated that it could be associated with the marginated tortoise, based on the presence of the plastral hinge and the widening of the carapace. Here we present updated information, following subsequent preparation of the specimen, confirming this relationship. Not only the hinge and the shape of the carapace, but also the size of the specimen is consistent with *T. marginata*. The marginated tortoise could reach even 35 to 40 cm in total length, being almost twice the size of the other hinged species in Greece, *T. graeca ibera*. The size of the Xerias specimen (260 mm) allows us to estimate that the total length of the shell could reach 33 to 35 cm. This is in agreement with the size of *T. marginata.* The associated fauna of this tortoise included the straight-tusked elephant (*Elephas antiquus*) and the giant deer (see Tsoukala et al., 2011).

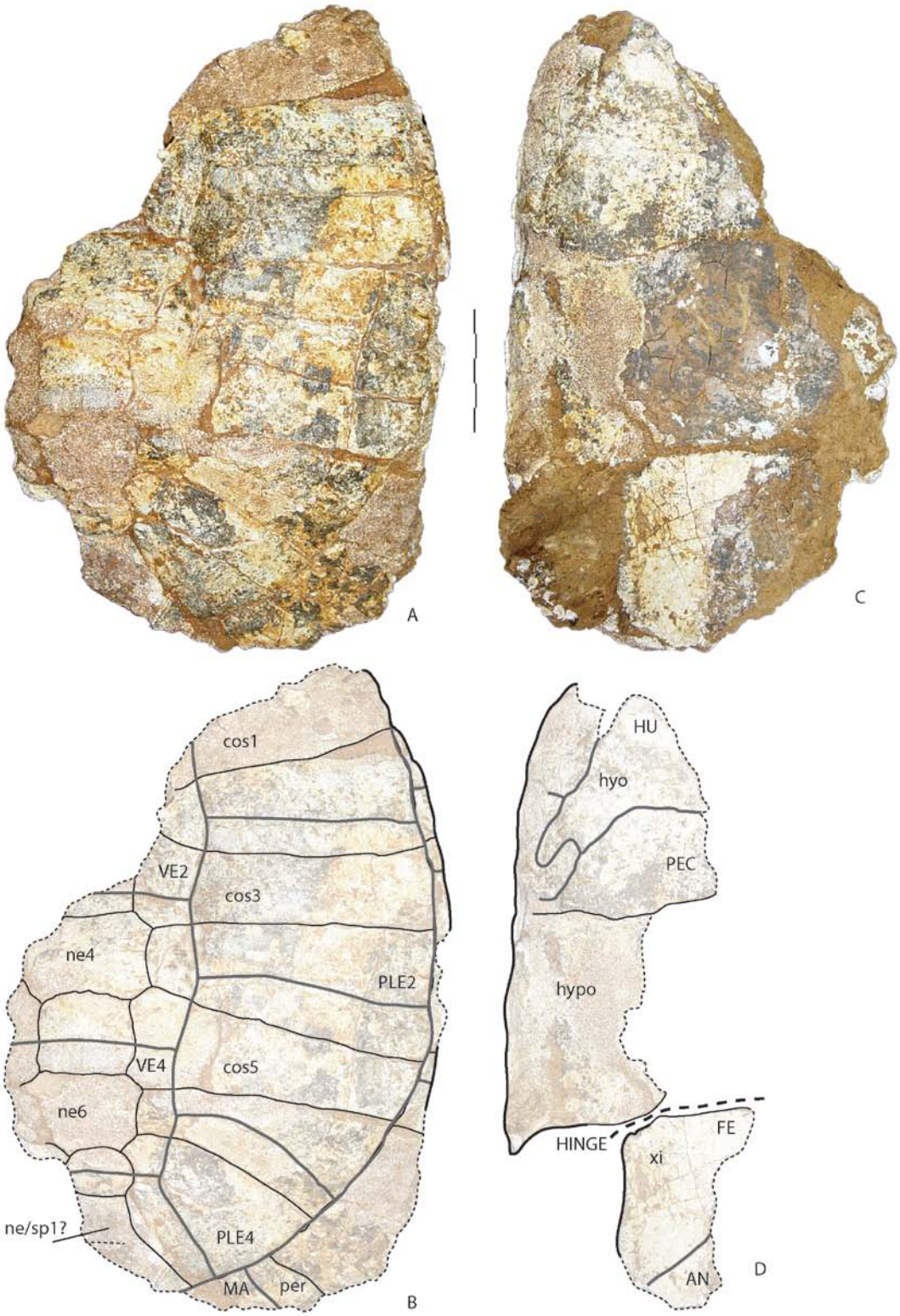


Figure 3.78. *Testudo* cf. *marginata* from the Pleistocene of Xerias (Kavala). LGPUT XEK 1, partial shell in (A) dorsal, (B) drawing of the dorsal, (C) ventral and (D) drawing of the ventral views. Scale bar equals 5 cm. For abbreviations see Material & Methods.

Testudo marmorum Gaudry, 1862a

In the literature mentioning *Testudo marmorum*, we find a confusion concerning the authorship of this taxon name. The reason is that A. Gaudry has named this new taxon in three publications by using more or less the same words: "*J'ai nommé notre tortue de Grèce Testudo marmorum pour rappeler la nature, desroches sur lesquelles elle dut se trainer*" (in Gaudry 1862a:504) or "*J'ai nommé la tortue fossile de l' Attique Testudo marmorum pour rappeler la nature, desroches sur lesquelles elle dut se trainer*" (in Gaudry 1862b:635; Gaudry 1862-1867:317). Most authors mention on of the last two publications for the taxonomic authorship, but our research has shown that Gaudry (1862a) predates both of them. Based on all the above, we choose this as the first mention of the taxon name *Testudo marmorum*.

DISTRIBUTION: Pikermi, Attica. Possibly in Halmyropotamos, Euboea Island, as it is mentioned by Melentis (1970). However, we have been unable to locate the specimens in AMPG, or in the specimens list from Halmyropotamos made by I. Melentis (S. Roussiakis, AMPG, pers. comm.). Therefore the occurrence of *T. marmorum* in Halmyropotamos cannot be confirmed.

AGE: Late Miocene.

ETYMOLOGY: As it mentioned by Gaudry (1862a,b; 1862-1867), the name *marmorum* derives from the Greek word μάρμαρο (marmaro, meaning marble), to recall the nature of the rocks that this animal was walking.

DIAGNOSIS (in Gaudry 1862a,b; 1862-1867): Gaudry finds many similarities between *T. marmorum* and *Testudo marginata* in the shape of the posterior carapace. *Testudo marmorum* is differentiated in having a mobile posterior lobe, which is wider than long compared to the posterior lobe of *T. marginata*. See discussion for further information.

MATERIAL:

Pikermi (6 specimens) (Fig. 3.79-3.85): Besides the holotype MNHN PIK 3683, another specimen, which preserves part of the carapace, is also labeled as TYPE and has the same collection number (figured in Gaudry 1862-1867:Pl. 60.1); AMPG PIK 1970 b, partial shell; AMPG PIK d, partial shell; AMPG PIK e, highly fragmented shell; AMPG PIK g, partial shell.

NOTE: Some specimen from Pikermi that have been described by Bachmayer & Symeonidis (1970) as *Testudo marmorum* are hingeless (AMPG PIK a, c, f), and therefore are described in the following section.

DESCRIPTION

MNHN PIK 3683 (holotype) (Fig. 3.79 & 3.80): Most of the shell is preserved. From the carapace the entire left and the posterior rim is missing. The carapace is deformed, resulting in an overlapping of the costal plates on the neural series. This does not allow a clear description of the neurals. Most of the plastron is preserved, since only

the lateral parts of the hyo- hypoplastra are missing. The sediment filling the shell is preserved, not allowing observation on the visceral sides.

Carapace: Most of the nuchal is preserved, being hexagonal, with a straight anterior border without the presence of a nuchal notch. The nuchal is wider than long. From the neural series only few neural plates can be observed. The first neural is quadrangular, significantly longer than wide. The neurals 2-4 cannot be observed as they are overlapped by the costals as a result of deformation. Based on the alternating shape of the costals, however, we can estimate that the shape of the neurals 2-4 was also alternated between octagonal and quadrangular neurals. Neural 5 is partially visible and is quadrangular, wider than long. Neurals 6-8 are hexagonal, with the shorter lateral sides placed anteriorly. Their widths are not equal, with neurals 6-7 being significantly wider than neural 8. All costals are wider than long, but costals 1 are significantly longer than the rest. Costals 1 make contact with the nuchal, anterior peripherals (probably 1-3) and neurals 1-2. Costals 2-5 show an alternating pattern being medially short and laterally long (costals 2 and 4), alternated with costals being medially long and laterally short (costals 3 and 5). Costals 6-7 are not differentiated, corresponding with the hexagonal neurals. The scute sulci are obscured in dorsal view both because of the above-mentioned deformation, as well as due to erosion. This results in limited available information. Anteriorly, a relatively short and narrow cervical is present. The vertebrals appear to be narrow, much narrower than the pleurals. Neurals 5 and 8 are crossed by the vertebrals sulci.

Plastron: The epiplastra are short and wide, being restricted in the anterior part of the lobe. No anterior notch is noted. The entoplastron is long, narrow and hexagonal. Hyo- and hypoplastra are long and wide. Xiphiplastra are very long, constituting the entire posterior lobe. In the posterior part of the lobe a deep notch is noted. The gulars are long and narrow, covering the anterior part of the entoplastron. The gularo-humeral sulcus forms an acute angle with midline. The rest part of the entoplastron is covered by the humerals. The humero-pectoral sulcus is wide, forming an obtuse angle with the midline, and is located posterior to the entoplastron. The pectorals are short and wide. The pectoro-abdominal sulcus is curved, being concave medially and convex laterally. The abdominals are long, covering the posterior parts of the hyoplastra and nearly the entire ventral surface of the hypoplastra. Only the posterior lateral parts of the hypoplastra are covered by the femorals. The abdomino-femoral sulcus is only visible in the lateral parts of the hypoplastra, whereas medially coincides with the hypo-xiphiplastral suture. The femorals are medially short and laterally long. Alternatively, the anals are medially long and laterally short. Therefore, the femoro-anal sulcus is V-shaped, showing a small degree of curvature.

The medial coincidence of the abdomino-femoral sulcus with the hypo-xiphiplastral suture, the small covering of the femoral onto the hypoplastra, the long xiphiplastra constituting the entire posterior lobe and the absence of a sutured connection between the hypo- and the xiphiplastra (as indicated by the presence of sediment between them) suggest the presence of a hypo-xiphiplastral hinge.

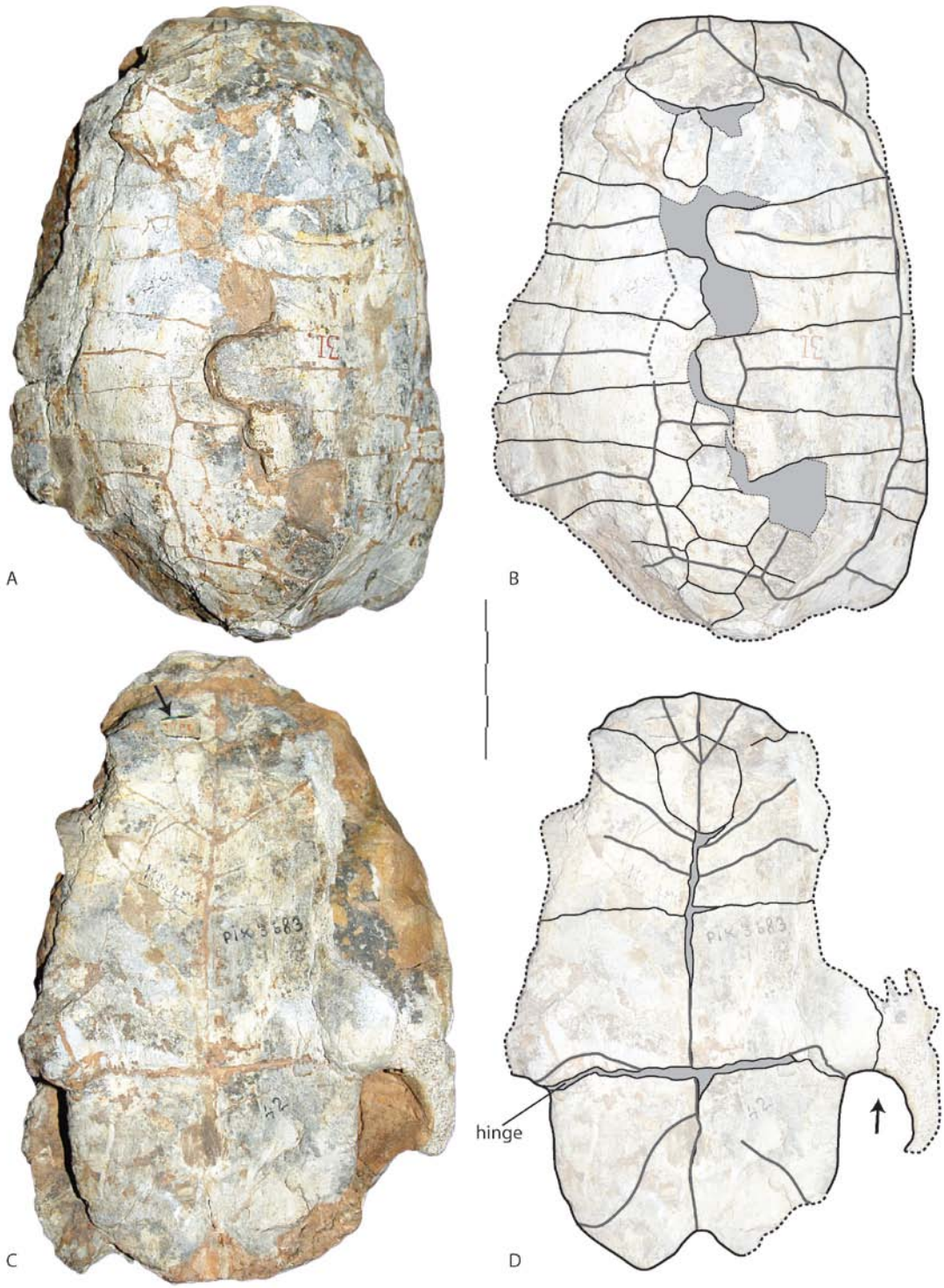


Figure 3.79. *Testudo marmorum* Gaudry, 1862a from the Late Miocene of Pikermi (Attica). MNHN PIK 3683, the holotype in (A) dorsal, (B) drawing of the dorsal, (C) ventral and (D) drawing of the ventral views. Scale bar equals 5 cm. Arrow indicated the widening (see text for further information).

MNHN PIK 3683 (paratype) (Fig. 3.81): Only a part of the carapace is preserved. From the left side only the medial parts of some costals are found. From the right side, some parts of the anterior rim are missing. The right bridge is fragmented. The posterior part is missing. The anterior part of the carapace appears slightly deformed,

whereas the posterior is partially eroded. The sediment filling the shell is preserved, not allowing observation on the visceral sides.

Carapace: The nuchal is hexagonal, longer than wide. The anterior border of the nuchal is straight, but there is a shallow embayment on the anterior carapace border affecting the nuchal and the first peripherals. The neural 1 is octagonal, significantly longer than wide. The neural 2 is octagonal, slightly wider than long. The neural 3 is quadrangular, wider than long. The neural 4 is octagonal, much wider than long, being the largest neural. The neural 5 is quadrangular, wider than long. The posterior part of the neural series is eroded, and it is not possible to make a confident assessment of the morphology of the neural. Most probably the neural 6 is large and hexagonal. The costal 1 much larger than the rest, making contact with the nuchal, neurals 1 and 2, and peripherals 1-3. The costals 2-5 are differentiated, corresponding to the alternated pattern of the octagonal/quadrangular neurals. Costals 2 and 4 are medially short and laterally long, alternated with costals 3 and 5 being medially long and laterally short. The peripherals 1-2 are very long and the peripheral 1 has a long suture with the nuchal. One of the most striking features of this specimen is found in the anterior region of the carapace, on the covering of the scutes. On the anterior part a long and narrow cervical is present. The first vertebral is narrow and as a result, parts of the pleurals 1 cover the edges of the nuchal. The marginals are very long, and the pleuro-marginal sulcus does not coincide with the costo-peripheral suture in the anterior peripherals. Instead, is placed on the medial part of the peripherals. In the bridge area there is good coincidence between the sulci and the sutures. The remaining vertebrals are wider, but all are narrower than the pleurals. Neurals 1, 3, 5 and 7(?) are crossed transversely by the vertebral sulci. Pleurals 2, 4 and 6 are crossed by the pleural sulci.



Figure 3.80. *Testudo marmorum* Gaudry, 1862a from the Late Miocene of Pikermi (Attica). MNHN PIK 3683, the holotype in (A) left lateral, (B) anterior and (C) right lateral views. Scale bar equals 5 cm.

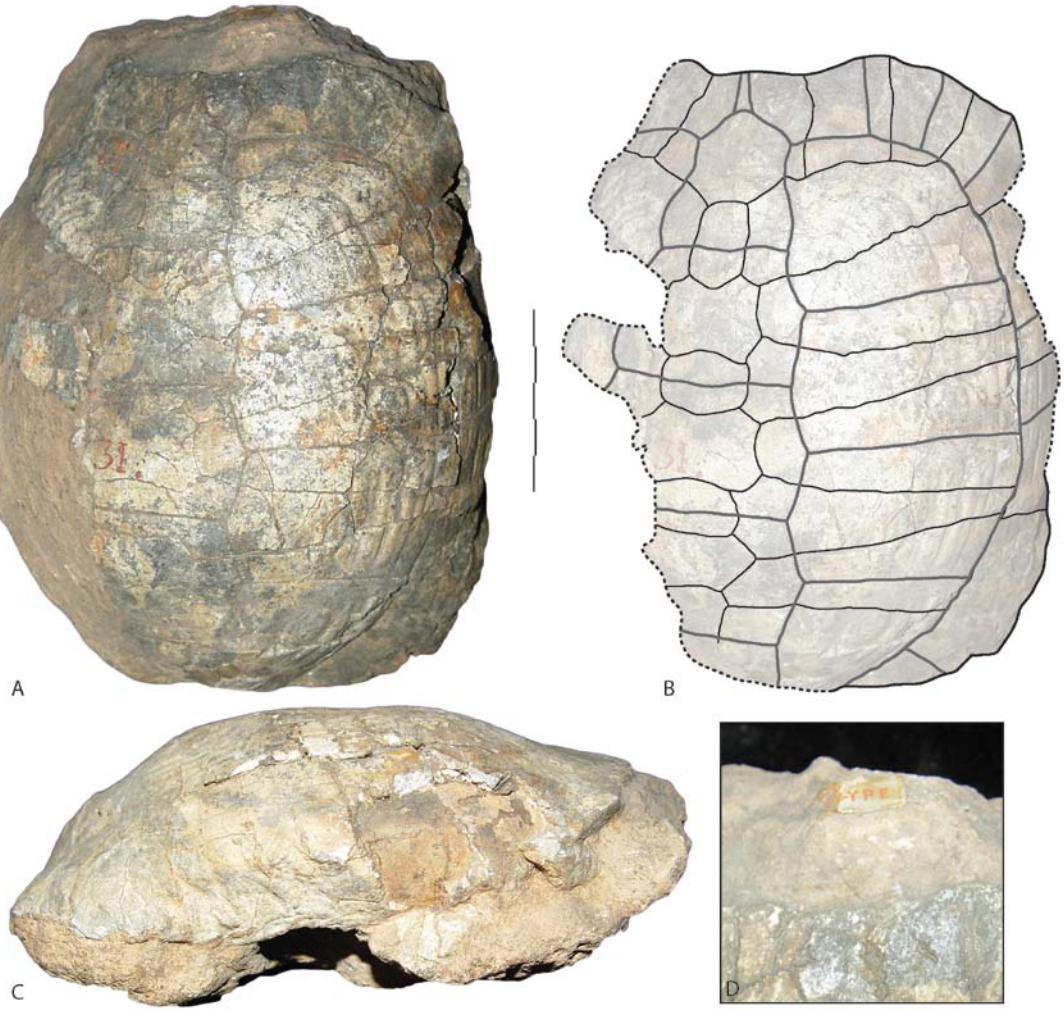


Figure 3.81. *Testudo marmorum* Gaudry, 1862a from the Late Miocene of Pikermi (Attica). MNHN PIK 3683, the paratype in (A) dorsal, (B) drawing of the dorsal, (C) right lateral views. (D) the "TYPE" label in the specimen. Scale bar equals 5 cm.

AMPG PIK 1970b (Fig. 3.82): Most of the shell is preserved, belonging to a juvenile specimen as it is inferred by the small size of the specimen. The left side is preserved complete, whereas the anterior, right and posterior rim is missing. The dorsal surface of the carapace is slightly eroded, which makes the observation of the sutures and sulci easier. The plastron is partially preserved, missing most of the hyoplastra and the right hyoplastron. The sediment filling the shell is preserved, not allowing observation on the visceral sides.

Carapace: The nuchal is hexagonal, being slightly wider than long. Neural 1 is rectangular, much longer than wide. Neural 2 and neural 4 are octagonal. Neural 2 is narrower anteriorly, whereas the sides of the neural 4 are of equal width. Neural 3 and neural 5 are quadrangular and sub-rounded, slightly wider than long. Neural 6 is hexagonal with short anterior sides. The posterior area of the neural series is slightly deformed. The first five costals show an alternating pattern. Costal 2 and costal 4 are medially shorter and laterally longer, whereas the costal 3 and costal 5 are medially longer and laterally shorter. In contrast, costals 6-8 are not differentiated, having medially a long anterior and a short posterior side that contacts with the hexagonal

neural. Anteriorly, a long and narrow cervical is preserved. The vertebrals are narrow compared to the pleurals. The vertebrals are hexagonal and their sulci cross the neural 1, neural 3, neural 5 and neural 8. The pleurals are rectangular and their sulci cross the costal 2, costal 4, costal 6 and costal 8. On the anterior part there is not good coincidence between the costo-peripheral suture. The sulcus of the pleural 1 with the anterior marginals is places on the costal 1, whereas the coincidence starts on peripherals 3-4.

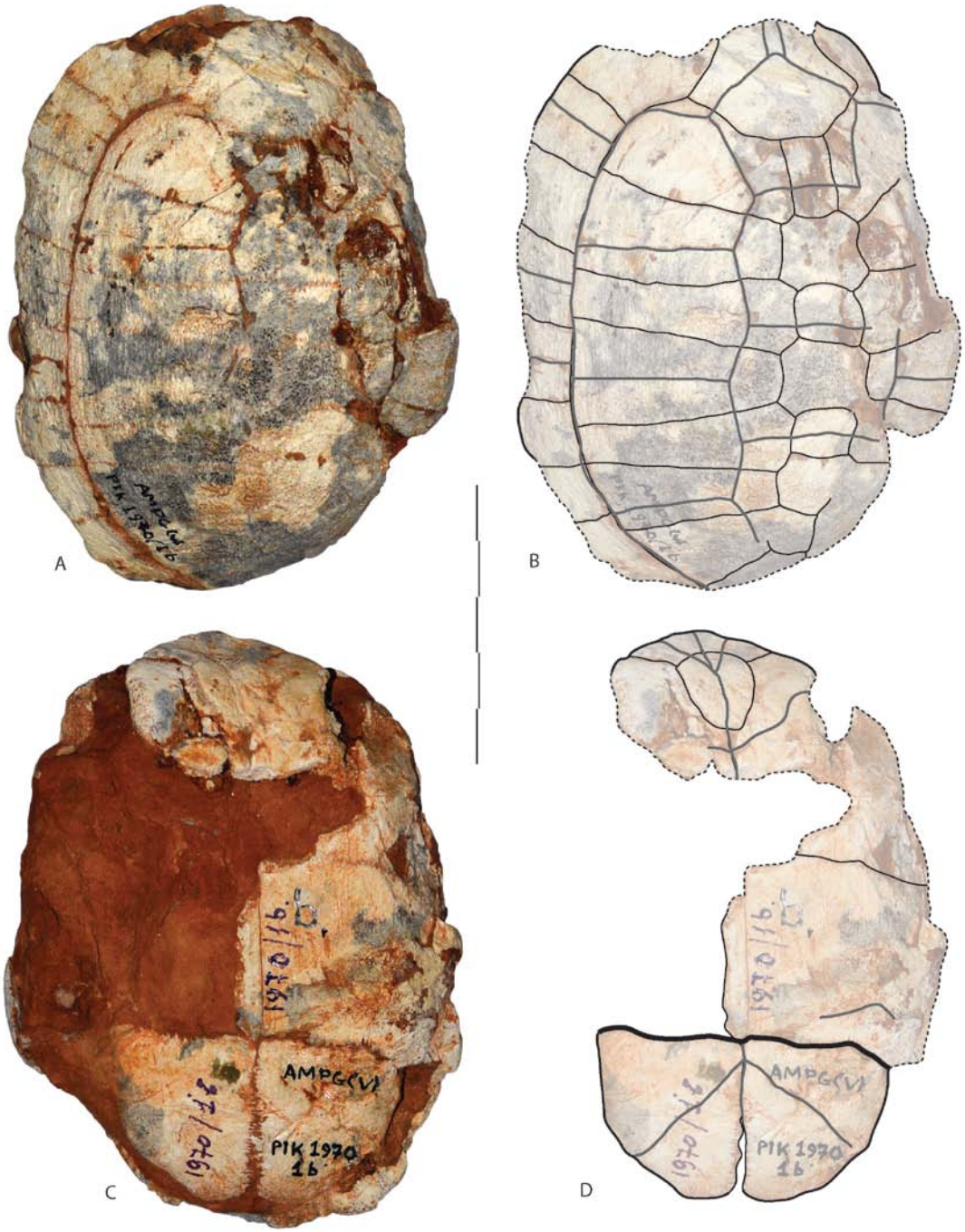


Figure 3.82. *Testudo marmorum* Gaudry, 1862a from the Late Miocene of Pikermi (Attica). AMPG PIK 1970b, a partial shell in (A) dorsal, (B) drawing of the dorsal, (C) ventral and (D) drawing of the ventral views. Scale bar equals 5 cm.

Plastron: The epiplastra are short and narrow, constituting the anteriormost part of the anterior lobe. The shape of the anterior lobe is sub-rounded. The entoplastron is hexagonal and rounded, much narrower than long. Hyo- and hypoplastra are long and wide, being relatively flat throughout their surface. The posterior lobe is made entirely of the xiphiplastra, which are wider than long. No notch is observed in the posterior lobe. The gulars are long and narrow, covering the anterior part of the entoplastron. The gularo-humeral sulcus forms an acute angle with midline. The humerals are medially longer than laterally. The humero-pectoral sulcus is placed posterior to the entoplastron. As a result of erosion is not possible to observe the pectoro-abdominal sulcus. Only a part of the abdomino-femoral sulcus is observed on the left hypoplastron being strongly convex laterally. On the xiphiplastra, femorals are short medially and long laterally, whereas the anals are long medially and short laterally. Therefore, the straight femoro-anal sulcus forms an acute angle with the midline, in a reverse V-shape. The size of the xiphiplastra, constituting the entire posterior lobe and the shape and placement of the abdomino-femoral sulcus indicate the presence of mobile xiphiplastra via a hypo-xiphiplastral hinge.

AMPG PIK 1970d (Fig. 3.83): Most of the shell of the specimen is preserved, along with in the in-filling sediment that does not allow the observation of the visceral sides. Almost the entire rim of the shell is preserved. The middle and posterior part of the carapace is missing. From the plastron, only the xiphiplastra are missing.

Carapace: The nuchal is hexagonal, wider than long. The anterior part is much narrower compared to wide posterior part. The neural 1 is rectangular and sub-rounded, much longer than wide. The neural 2 is octagonal, slightly wider than long. The neural 3 is quadrangular, wider than long with sub-rounded sides. The costals 1 are long and wide, making contact with the nuchal, neurals 1-2 and peripherals 1-3. Costal 2 is medially short and laterally long, whereas the costal 3 is medially long and laterally short. Peripherals are long. Pointed tips are present in the anterior peripherals, on the marginal sulci. Posteriorly a narrow quadrangular pygal is present, with wide anterior and short posterior side. In the anterior part of the carapace there is no coincidence between the pleuro-marginal sulci and the costo-peripheral suture of the peripherals 1-2. The pleuro-marginal sulcus is situated on the peripherals. Anteriorly, a long and narrow cervical is present. The vertebrals are hexagonal, being narrower that the rectangular pleurals. Neural 1 and neural 3 are crossed by the vertebral sulci, whereas the costal 2 is crossed by the pleural sulci. Marginals 12 are fused into a supracaudal scute. The posterior part of the carapacial rim (i.e. peripherals 9-11 and the pygal) is bended inwards.

Plastron: The epiplastra are long and wide. The entoplastron is hexagonal, longer than wide. The hyo- and hypoplastra are long and wide. A concavity is present in the medial parts of the plastron suggesting that this is a male individual. The gulars are long and narrow, covering the anterior part of the entoplastron. The gularo-humeral sulcus forms an acute angle, and a weak constriction on the epiplastra. The humerals are longer medially than the pectorals, which are medially short and wide. The humero-pectoral sulcus is gently concave on each side, situated posterior to the entoplastron. The abdominals are as long as wide, constituting the largest scutes of this plastron. As a result of erosion, the abdomino-femoral sulcus cannot be observed. The length of the abdominals, the shape of the posterior suture of the hypoplastra, and the absence of the xiphiplastra suggest the presence of a mobile posterior lobe and a hypo-xiphiplastral hinge.

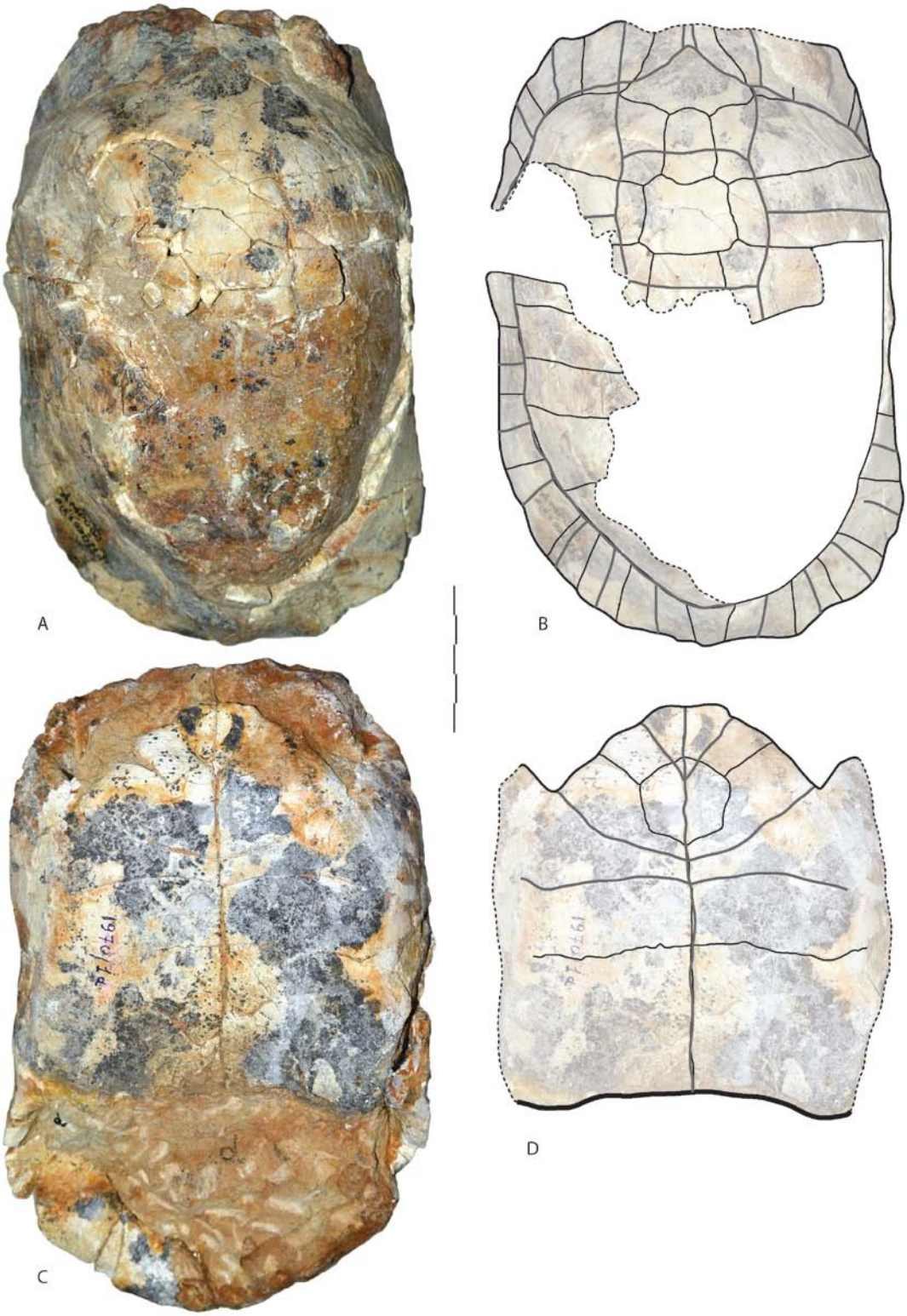


Figure 3.83. *Testudo marmorum* Gaudry, 1862a from the Late Miocene of Pikermi (Attica). AMPG PIK 1970d, a partial shell in (A) dorsal, (B) drawing of the dorsal, (C) ventral and (D) drawing of the ventral views. Scale bar equals 5 cm.

AMPG PIK 1970e (Fig. 3.84): From this individual most of the plates of the shell are found fragmented. The best-preserved specimen is the hyo-hypoplastral part of the plastron. The left part of the entoplastron is also preserved. The humero-pectoral sulcus is concave and situated posterior to the entoplastron. The pectorals are short

and wide. The pectoro-abdominal sulcus is slightly concave medially and convex laterally. The posterior hyoplastra and almost the entire hypoplastra are covered by the abdominal scutes. Only the lateral parts of the hypoplastra are covered by the femoral. The abdomino-femoral sulcus on this part is strongly convex, whereas coincides with the posterior hypoplastral suture medially. This suggests the presence of a hypo-xiphiplastral hinge on this specimen.



Figure 3.84. *Testudo marmorum* Gaudry, 1862a from the Late Miocene of Pikermi (Attica). AMPG PIK 1970e, elements of a partial shell: A-C, costal in (A) dorsal, (B) drawing of the dorsal and (C) visceral views. D-F, partial plastron in (D) visceral, (E) ventral and (F) drawing of the ventral views. Scale bar equals 5 cm.

AMPG PIK 1970g (Fig. 3.85): This specimen preserves the entire plastron, part of the anterior and posterior carapacial rim. The preservation status, deformation, and the fact that the specimen is fixed on plaster basis makes impossible the observation of the ventral side of the plastron. However, it is possible to infer some important morphological information. First of all, the posterior carapacial rim from the peripheral 8 till the trapezoidal pygal is bended inwards. Second, the epiplastra are viscerally thickened forming a convex epiplastral lip and a deep gular pocket. Finally, the xiphiplastra appear to be tightly sutured with the hypoplastra, and therefore the presence of a hypo-xiphiplastral hinge in this specimen is dubious.

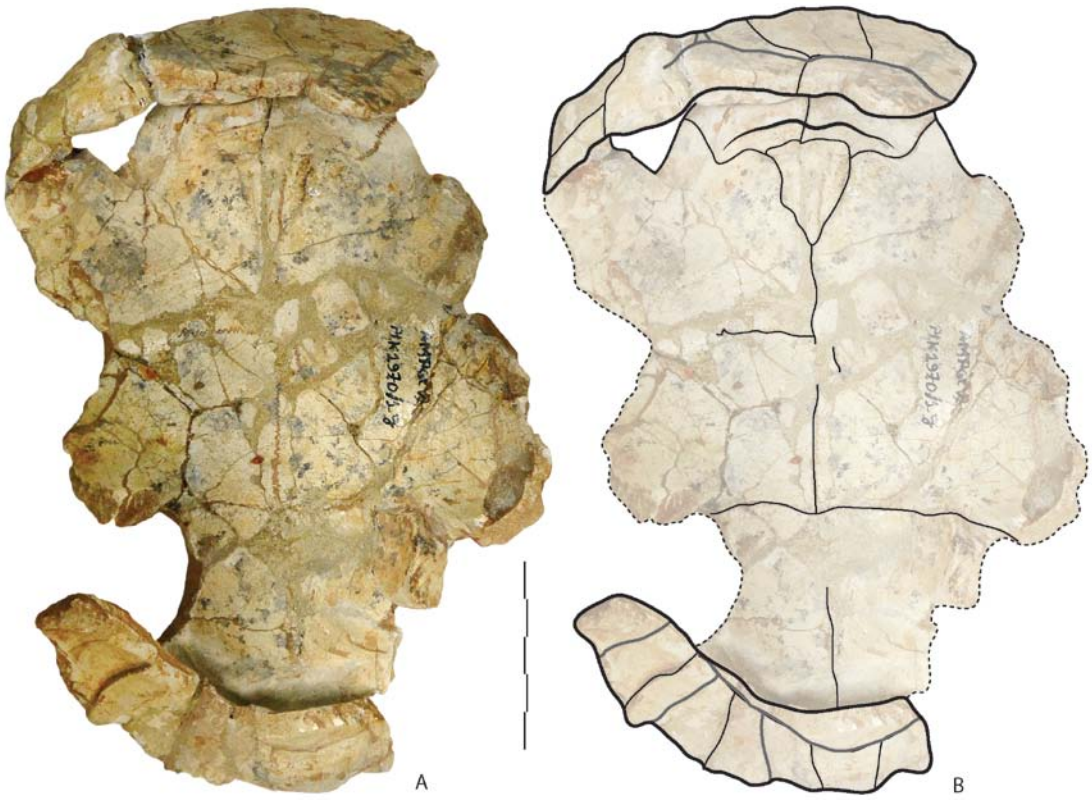


Figure 3.85. *Testudo marmorum* Gaudry, 1862a from the Late Miocene of Pikermi (Attica). AMPG PIK 1970g, a partial shell in (A) dorsal and (B) drawing of the dorsal views. Scale bar equals 5 cm.

DISCUSSION

The material presented in this section has been described and figured in Gaudry (1862a; 1862b; 1862-1867; MNHN specimens) and in Bachmayer & Symeonidis (1970; AMPG specimens). The updated information presented here improves significantly our knowledge of *Testudo marmorum* and the Pikermi testudinids. Perhaps the most important is about the presence of a hypo-xiphiplastral hinge in *Testudo marmorum*. This character is a classical morphological characteristic used to distinguish the *Testudo* s.s. lineage (see Lapparent de Broin et al., 2006b). The presence of mobile xiphiplastra, and therefore the presence of a hinge, has been already noted by Gaudry (1862a; 1862b; 1862-1867) in his diagnosis of *T. marmorum*. Indeed, this is true for the holotype specimen (MNHN PIK 3683) where all the morphological features associated with the hinge are present. This is not the case however with all the AMPG specimens, which have been described in Bachmayer & Symeonidis (1970). In detail, specimens AMPG PIK 1970a, 1970f, and possibly 1970c, do not show the morphology associated with the hinged specimens. In AMPG PIK 1970a and 1970f the posterior lobe is not made entirely by the xiphiplastra, whereas the abdomino-femoral sulcus does not coincides medially with the hypo-xiphiplastral suture. These different morphologies among the AMPG specimens were evident to Bachmayer & Symeonidis (1970) as well, as it shown in their figures 4 and 5, showing the 1970f and 1970e respectively. They attribute this difference to the sexual dimorphism (1970f as male and 1970e as female individual). However, in the present thesis those specimens are treated as belonging to a different taxon from *Testudo marmorum*, and they are described in the following section.

EMENDED DIAGNOSIS: Compared to the information presented by Gaudry, a cervical scute is found present in both MNHN specimens. The cervical scute is rather short and narrow, and maybe this is the reason why Gaudry figured the specimen as having the cervical scute absent. As it is apparent in the MNHN specimens (especially the paratype) and in some AMPG specimens (e.g. AMPG PIK 1970b, d), there is no coincidence between the anterior pleuro-marginal sulci and the costo-peripheral suture, as the marginals are expanded on the peripherals. Also, the vertebral 1 seems to be lyre-shaped in the paratype, and the pleurals 1 cover the lateral parts of the nuchal plate. This is not observed, however, in the AMPG specimens. In the plastron, the gulars are short and narrow, clearly different from the shape of the gular scutes in the hingeless Pikermi specimens described below. Also, the evident hypo-xiphiplastral hinge and its associated morphologies clearly distinguish this taxon from the hingeless Pikermi specimens. Extant *Testudo* is defined by the alternating pattern of octagonal and quadrangular neurals. *Testudo marmorum* shows a less differentiated series where neurals 6-8 are hexagonal with short anterior lateral sides. Based on the available material, the above mentioned combination of characters could be diagnostic for the Late Miocene *T. marmorum*.

RELATIONSHIPS: *Testudo marmorum* has been considered by many authors as a taxon closely related with *Testudo marginata*. But which are the characters that explain this close relationship? Gaudry (1862a; 1862b; 1862-1867) is the first to find similarities between the two taxa. This was because, according to Gaudry, they show the same size and the carapace is of similar shape (besides the presence of the hinge). However, in both cases this is not true. Extant *T. marginata* could reach even 35-40 cm in size, being almost twice the size of *T. marmorum*. The carapace of the marginated tortoise is posteriorly flared, but this flaring is noted in the posteriormost region, i.e. from the peripheral 9 till the pygal. This is because in other *Testudo* s.l. the peripherals 7-8 display a moderate degree of flaring, but the posterior peripherals and the pygal are bended inwards. In the type specimens of *T. marmorum* (MNHN) this part is unknown. Moreover, in the AMPG specimens where this part is preserved (AMPG PIK 1970d, g) the posterior rim is bended inwards and not posteriorly flared as in *T. marginata*. Perhaps the only apparent similarity between the holotype specimen and the marginated tortoise, is that the shell of the holotype widens right after the bridge, as in *T. marginata*. But due to the strong deformation of the shell, as it is emphasized by the overlapping of the costals on the neurals, this observation cannot be trusted. Note that the remaining AMPG specimens do not display a similar widening of the posterior part. This relationship, however, has been followed by several authors. For example, Lapparent de Broin (2001; 2002) mention this relationship, but without providing morphological evidence about it. Georgalis and Kear (2013) explain this due to the "[...] *carapace the flares posteriorly* [...]" (Georgalis and Kear, 2013:304). This flange of the carapace should not be observed in the posterior peripherals 8–10 (as it is noted in Fig. 1C, G in Georgalis and Kear, 2013), since these parts always display some degree of flaring in *Testudo* sensu lato. Instead, the characteristic posterior flaring of *T. marginata* is found in the posterior region of the carapacial margin (peripherals 11 and pygal), in contrast with the other *Testudo*, where it is bended inwards and it is stronger in male individuals. Based on the above we can conclude that *T. marmorum* and *T. marginata* cannot be associated based on the general shell size. In order to investigate of this relationship is true, we have performed a cladistic analysis (see next chapter), focusing on the relationships of *T. marginata*.

'Testudo' sp.

As it has been explained above, the following specimens have been provisionally described as *Testudo marmorum* by Bachmayer & Symeonidis (1970). Due to the fact that these specimens lack a hypo-xiphiplastral hinge (contrary to *T. marmorum*) are described separately in this section. Another specimen from the new excavations in Pikermi is described here.

DISTRIBUTION: Pikermi, Attica.

AGE: Late Miocene.

MATERIAL (4 specimens) (Fig. 3.86-3.89): AMPG PIK a, partial shell; AMPG PIK c, partial plastron; AMPG PIK f, partial shell; AMPG PIK 1630, partial shell in a block of bones.

DESCRIPTION

AMPG PIK 1970a (Fig. 3.86): An almost complete shell preserving most of the carapace and some parts of the plastron. From the carapace, most of the outer rim is missing except from the right posterior peripherals. The dorsal surface of the carapace is preserved in very condition allowing the clear observation on the sutures and sulci. From the plastron only a small part of the right hypoplastron is preserved. The sediment filling the shell is preserved, not allowing observation on the visceral sides.

Carapace: Most of the neural series is preserved. The partial neural 1 is rectangular, longer than wide. The neural 2 and neural 4 are octagonal, being as wide as long. The neural 3 and neural 5 are quadrangular, being as wide as long. The neurals 6-8 are not differentiated, being hexagonal with short lateral anterior sides. The first five costals are differentiated, corresponding to the alternating pattern of the neurals. Costal 2 and costal 4 are medially shorter and laterally longer, whereas the costal 3 and costal 5 are medially longer and laterally shorter. This is not the case for the remaining costals that are sutured with hexagonal neurals. The costals 6-8 therefore are less differentiated, having medially a long anterior and a short posterior side that contacts with the hexagonal neural. The peripherals are long. The vertebrals are narrower than the pleurals. The vertebrals are hexagonal and their sulci cross the neural 1, neural 3, neural 5 and neural 8. The pleurals are rectangular and their sulci cross the costal 2, costal 4, costal 6 and costal 8. In the preserved part, the pleuro-marginal sulci coincide with the costo-peripheral suture. Pointed tips are preserved on the peripheral rim, right on the end of the marginal sulci.

Plastron: only the posterior-lateral part of the right hypoplastron is preserved. Based on the preserved part we see that the posterior lobe is not made entirely by the xiphiplastra. The hypoplastron is crossed by the abdomino-femoral sulcus that is strongly convex. Although the preserved part is small, it seems possible that the sulcus is not situated close to the hypo-xiphiplastral suture. All the above suggest that the presence of a hypo-xiphiplastral hinge in this specimen is dubious.

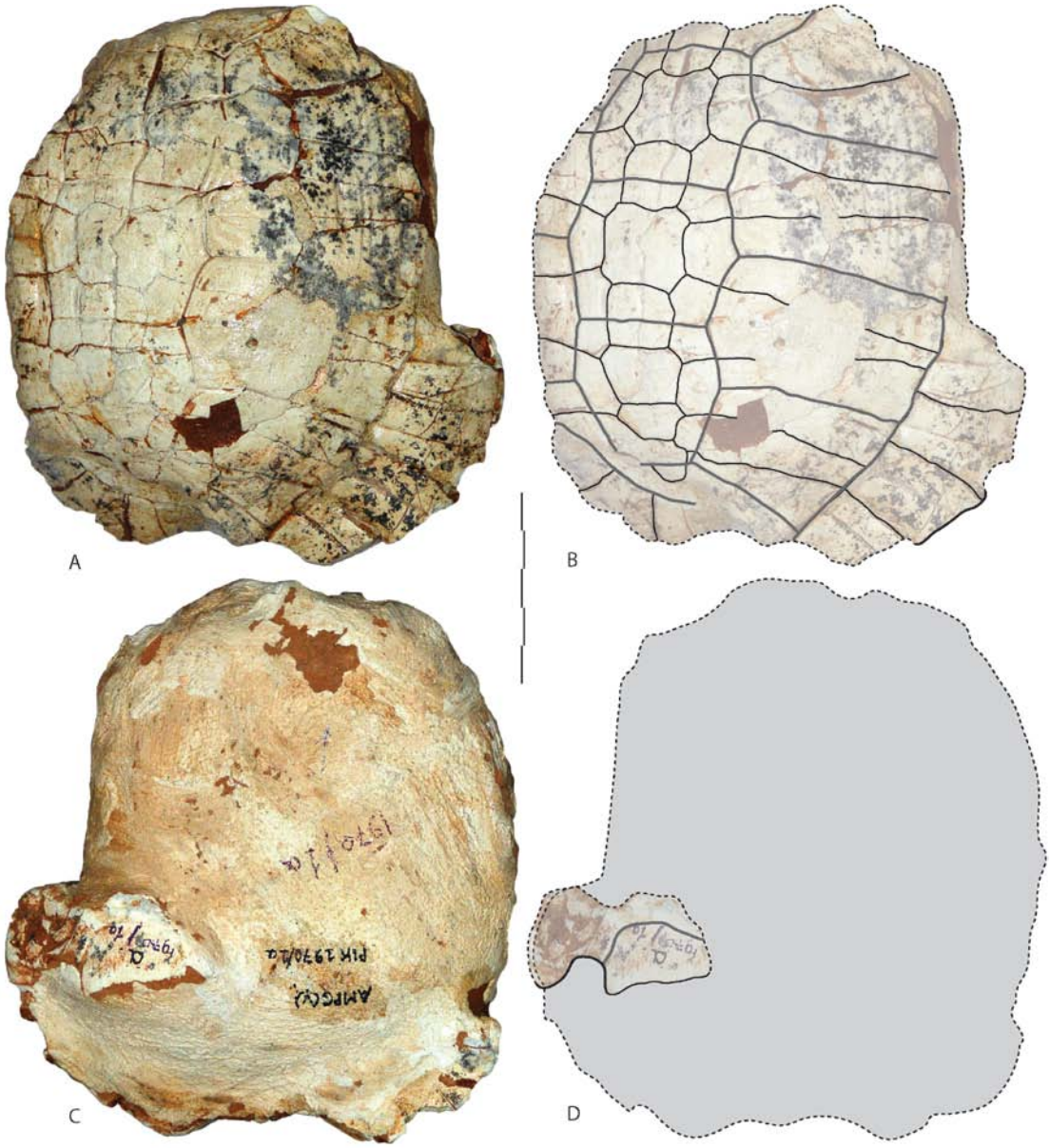


Figure 3.86. AMPG PIK 1970a, a partial shell of a hingeless '*Testudo*' sp. from the Late Miocene of Pikermi (Attica) in (A) dorsal, (B) drawing of the dorsal, (C) ventral and (D) drawing of the ventral views. Scale bar equals 5 cm.

AMPG PIK 1970c (Fig. 3.87): Only the anterior half of the plastron is preserved. The epiplastra are short and wide, constituting most of the anterior rim of the lobe. Viscerally, the epiplastra are thickened, creating a convex epiplastral lip with a deep gular pocket. The entoplastron is octagonal, with sinuous anterior and straight posterior sides. The anterior sides are shorter compared to the posterior ones. The hyoplastra are long and wide. The gulars are long, covering the entire anterior part of the lobe. They cover the anterior part of the entoplastron. The gularo-humeral sulcus is convex anteriorly on each side, forming an acute angle with the midline. A weak gular constriction is noted on the gularo-humeral sulcus. Humerals are longer medially, whereas the pectorals are short. The humero-pectoral sulcus is situated posterior to the entoplastron, is V-shaped and forms an obtuse angle. The pectoro-abdominal sulcus is straight throughout its width.

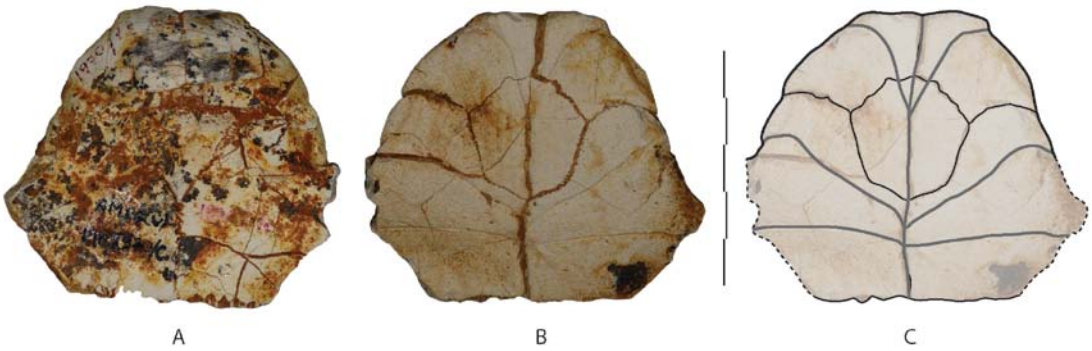


Figure 3.87. AMPG PIK 1970c, a partial plastron of '*Testudo'* sp. from the Late Miocene of Pikermi (Attica) in (A) visceral, (B) ventral and (C) drawing of the ventral views. Scale bar equals 5 cm.

AMPG PIK 1970f (Fig. 3.88): From this specimen most of the carapace and almost the entire plastron (bridge is missing) is preserved. The carapace is preserved with the in-filling sediment and therefore the visceral side cannot be observed. On the other hand, the visceral side of the plastron is available for observation.

Carapace: Most of the nuchal is preserved, being wider than long, and with a straight anterior border. The posterior part of the neural 1 is preserved, showing a quadrangular plate much longer than wide. The neural 2 is octagonal, as wide as long. Neurals 3-4 are missing. Neural 5 is quadrangular, with sub-rounded edges, being wider than long. Neural 6 and 7 are hexagonal with longer posterior lateral sides. They are almost of similar width. The preserved suprapygal is trapezoidal, with wide posterior sides. The first five costals are differentiated, corresponding to the alternating pattern of the neurals. Costal 2 and costal 4 are medially shorter and laterally longer, whereas the costal 3 and costal 5 are medially longer and laterally shorter. The costals 6-8 therefore are not differentiated, having medially a long anterior and a short posterior side. The peripherals are relatively long. Posteriorly a wide trapezoidal pygal is found, which becomes narrower posteriorly. The posterior carapacial rim, made by the peripherals 9-11 and the pygal, is bended inwards. Anteriorly, a short and narrow nuchal is present. In this specimen there is good coincidence between the costo-peripheral sutures and the pleuro-marginal sulci in the anterior part. The vertebrals are hexagonal and narrower than the pleurals. The vertebral sulci cross transversely neural 1 (in the posterior part), neural 3, neural 5 (in the posterior part), and quite possibly the neural 8. The pleural sulci cross the costal 2, costal 4, costal 6 and costal 8. Marginals 12 are fused into a supracaudal.

Plastron: The epiplastra are short and wide, making a sub-rounded anterior lobe, showing a weak anterior notch. Viscerally, the epiplastra are thickened, creating a long convex epiplastral lip with a deep pocket. The entoplastron is hexagonal, with almost straight sides. The entoplastron is longer than wide. Hyo- and hypoplastra are long and wide, being flat throughout their surface. The posterior parts of the hypoplastra contribute in the formation of the posterior lobe, but most of it is made by the xiphiplastra. The xiphiplastra longer than wide, and their lateral sides are gently converging posteriorly. A deep anal notch is noted posteriorly. The gulars are relatively long and narrow, covering the anterior part of the entoplastron. The lateral parts of the gularo-humeral sulcus are convex anteriorly, forming an acute angle with the midline medially.

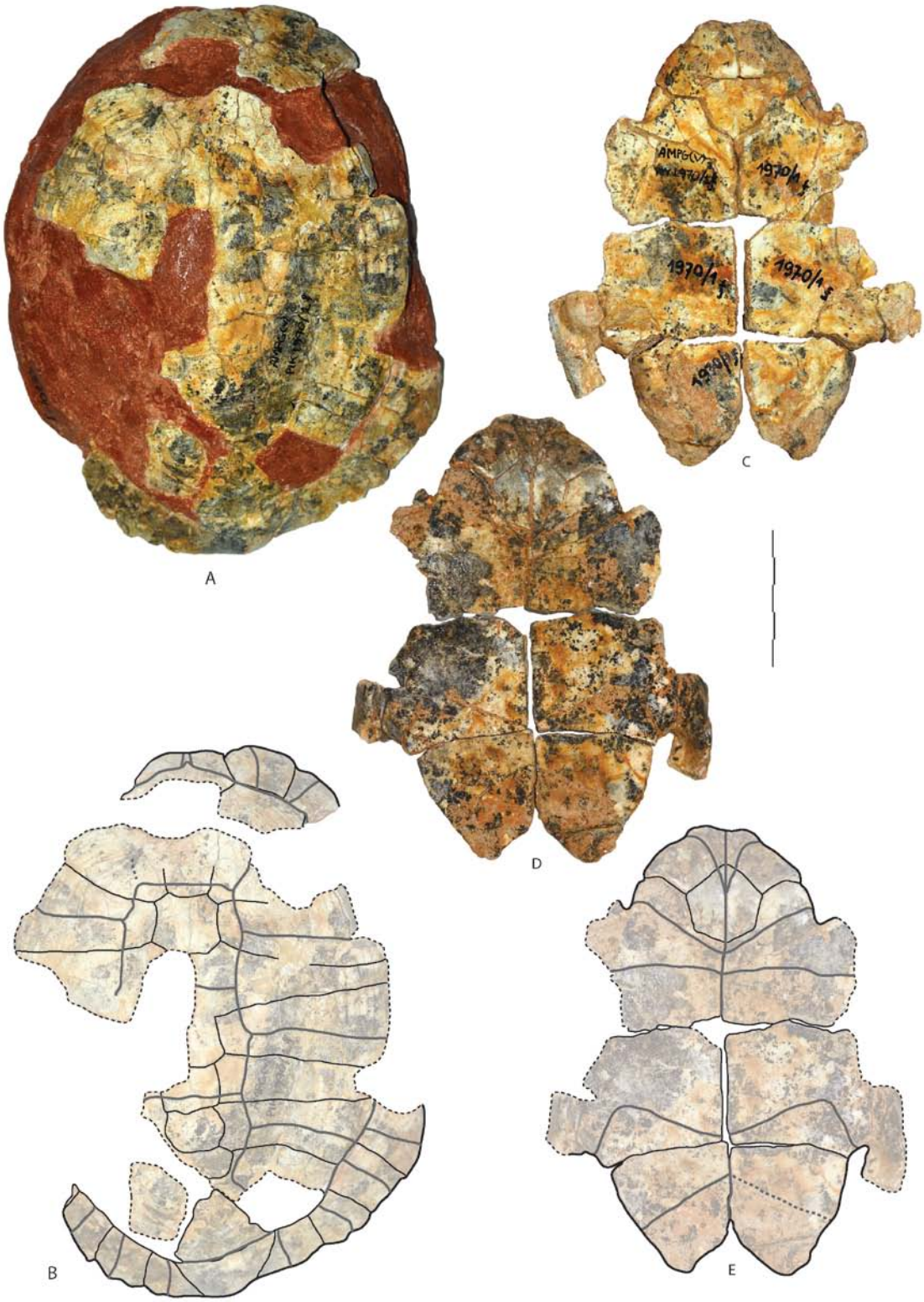


Figure 3.88. AMPG PIK 1970f, a partial shell of a hingeless '*Testudo*' sp. from the Late Miocene of Pikermi (Attica) in (A) dorsal, (B) drawing of the dorsal, (C) visceral plastron, (D) ventral and (E) drawing of the ventral views. Scale bar equals 5 cm.

Laterally, a significant constriction is noted in the gularo-humeral sulcus. The humerals are medially longer, much longer than the pectorals, which are the shorter scutes of the plastron. The humero-pectoral sulcus is concave posteriorly and is situated posterior to the entoplastron. The pectoro-abdominal sulcus is relatively

straight throughout its length. The abdominals are the largest scutes in the plastron, covering the posterior half of the hyoplastra and most of the hypoplastra. The posterior part of the hypoplastra is covered by the femorals. The abdomino-femoral sulcus is strongly convex laterally and gently concave medially. It does not coincide with the hypo-xiphiplastral suture. The femorals are of equal medial width with the anals. The femoro-anal sulcus is straight on each side, forming a reverse V-shape with the midline. The morphology of the posterior part of the plastron suggests that a hypo-xiphiplastral hinge is absent in this specimen, and the hypoplastra are tightly sutured with the xiphiplastra.

AMPG PIK 1630 (Fig. 3.89): This specimen preserves the entire plastron and parts of the anterior carapace. Its recovery position in a big block of bones, hinters most of its relevant morphology. However, the presence of coincidence among the anterior pleuro-marginal sulci and costo-peripheral sutures and the absence of a hypo-xiphiplastral hinge allows association with the hingeless *Testudo* from Pikermi.

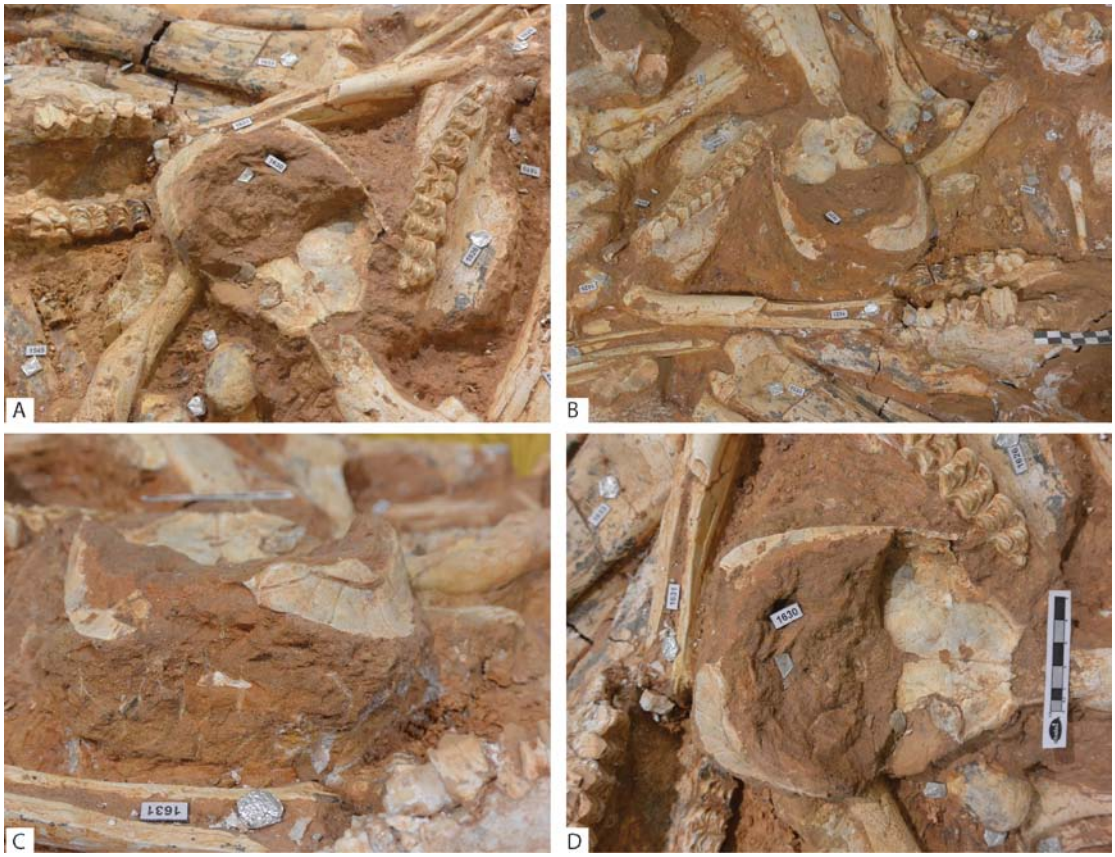


Figure 3.89. AMPG PIK 1630, a partial shell of a hingeless '*Testudo*' sp. from the Late Miocene of Pikermi (Attica) preserved in a big block of a large mammalian bone assemblage. The shell is visible on its dorsal side in (A) postero-lateral, (B) antero-lateral, (C) anterior and (D) dorsal views. Scale bar equals 5 cm.

DISCUSSION

As it has been already discussed in the previous section, these specimens cannot be associated with the Late Miocene *Testudo marmorum*, because they show a good anterior coincidence between the pleuro-marginal sulci and the costo-peripheral suture and they lack a hypo-xiphiplastral hinge. Moreover, the gulars are wider and longer, having curved anteriorly lateral parts. Further study is needed to see if these specimens could belong to a new species or they can be assigned to an existing hingeless taxon.

The revised information on the Miocene '*Testudo' antiqua* by Corsini et al. (2014) shows that the Pikermi hingeless '*Testudo'* sp. differs in the curved gulars (straight borders in '*T'. antiqua*), the longer entoplastron and the deeper anal notch. It further differs from *Paleotestudo canetoniana* (in Pérez-García & Murelaga, 2014) as it lacks protrusions in the peripherals, it has an hexagonal entoplastron, and a nuchal not covered by the pleurals laterally.

02/16/2016 Ψηφιακή Βιβλιοθήκη Θεόφραστος - Τμήμα Γεωλογίας - Α.Π.Θ.

Testudo sp. nov I

LOCALITY: Milia, Grevena, W. Macedonia, N. Greece.

AGE: Late Pliocene; MN 16a.

MATERIAL (Fig. 3.90-3.93): MIL 255, plastron fragment; MIL 256a, neural; MIL 256c, pygal region fragment; MIL 495, posterior carapace; MIL 982d, left hyoplastron fragment; MIL 1168, left epiplastron & entoplastron fragment; MIL 1396, left hyoplastron; MIL 1592, peripheral fragment; MIL 1633, shell fragment; MIL 1638, carapace fragment; MIL 1753, left part of a plastron (in four fragments a, b, c, d); MIL 1937, costal; MIL 1938, left hypoplastron fragment.

DESCRIPTION

MIL 255 (3.92.H): It is fragment of the shell of a tortoise. By the curvature we can assume that it belongs to the carapace. Further identification is not possible.

MIL 256a (3.92.A): This specimen corresponds to an almost complete neural. Viscerally we notice the attachment for the corresponding vertebra. The neural is quadrangular with rounded edges, wider than long. Dorsally it is crossed by the vertebral sulcus, which is strongly convex anteriorly.

MIL 256c (3.92.C): This specimen corresponds to a fragment of the pygal region, preserving the pygal and part of the left peripheral 11. The pygal is trapezoid, with wider anterior side. The pygal, along with the peripheral, are strongly flared posteriorly. Dorsally, it is crossed by the vertebral sulci. No marginals 12 are noted, therefore the presence of a supracaudal is assumed.

MIL 495 (Fig. 3.90): This specimen corresponds to the medial and posterior part of the carapace. The surface of the carapace is fragmented and eroded in some parts. The limits between the plates and the scutes can be observed in most of the surface of the carapace. The shell is rounded in outline and tall in height. The medial and posterior part of the neural series can be described. The neural 4 is octagonal, as long as wide. The neural 5 is quadrangular, wider than long. The neural 6 is roughly octagonal, slightly wider than long. The neural 7 is hexagonal, with short anterior lateral sides. Most probably the neural 8 is present, being quadrangular with rounded edges. It seems that only one suprapygal is present, being trapezoid with narrow anterior and wider posterior part. The costal plates preserve the typical alternating pattern of the testudinids, showing costals that are medially short and laterally long to be alternated with costal that are medially long and laterally short. From the peripheral series, those from the right bridge and the entire posterior rim is preserved. The bridge peripherals are tall and short. The peripherals of the posterior rim are moderately long and posteriorly flared, including also the pygal region. The pygal is trapezoid in shape, with narrow anterior and wider posterior side, thus showing lateral sides that diverge posteriorly. The imprints of the scute sulci are clearly visible as they are deeply pronounced on the plates. The vertebrals are slightly longer than wide, but still narrower than the pleurals. The vertebral sulci cross transversely the neural 3, neural 5, and the last neural plate. In the crossing of the sulci on the neurals, significant dorsal bumps are noted. The pleurals are rectangular, wide and short, crossing the

costals 2, 4, and 6 transversely. The marginals are long and narrow, crossing the peripherals. The marginals 12 are fused into a supracaudal. In the preserved part there is good coincidence between the costo-peripheral suture and the pleuro-marginal sulci.

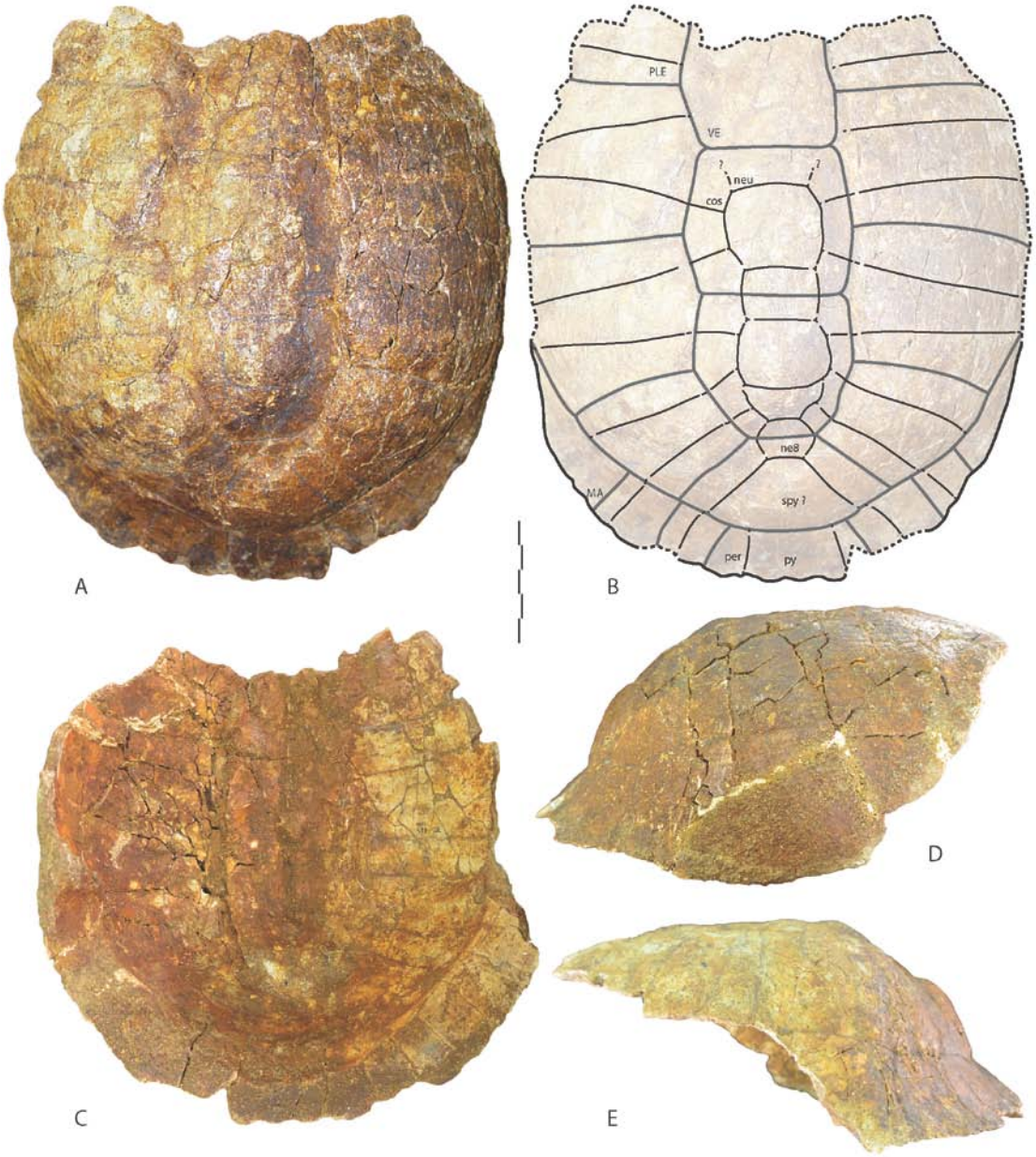


Figure 3.90. *Testudo* sp. nov. from the Late Pliocene of Milia (Grevena). MIL 495, partial carapace in (A) dorsal, (B) drawing of the dorsal, (C) visceral, (D) right lateral and (E) left lateral views. Scale bar equals 5 cm. For abbreviations see Material & Methods.

MIL 982d (3.92.G): This specimen corresponds to a fragment of the left hyoplastron. The specimen is rather flat and small in size. Ventrally, we notice a part of a sulcus, most probably of the humero-pectoral sulcus.



Figure 3.91. *Testudo* sp. nov. from the Late Pliocene of Milia (Grevena). MIL 1753, partial plastron in (A) visceral, (B) ventral, (C) drawing of the ventral, (D) posterior and (E) detail of the left lateral views. Scale bar equals 5 cm. For abbreviations see Material & Methods.

MIL 1168 (3.92.D): It is a fragment of the left anterior lobe, preserving the entire left epiplastron, part of the entoplastron and the anterior part of the left hyoplastron. Dorsally, it is marked by the presence of a thick convex epiplastral lip, which creates a strong gular pocket. Ventrally, the gulars are rather short, restricted in the anterior part of the lobe and overlapping the anterior part of the entoplastron. The remaining part is covered by the humeral scutes that are long. Gular protrusion is absent.

MIL 1396: It is a fragment of the left hyoplastron. Ventrally, it is crossed by the humero-pectoral and the pectoro-abdominal sulci. Pectorals are very short and wide.

MIL 1592: It is a fragment of a peripheral bone. The outer surface is eroded and the identification of the sulci is rather difficult. Only in ventral view a marginal sulcus is noted. This plate is long and flared, consistent with the morphology of the marginated tortoise. By using MIL 495 as comparative material we can identify this plate as a fragment of the right 11th peripheral, but the preservation of the specimen does not allow a clear identification.

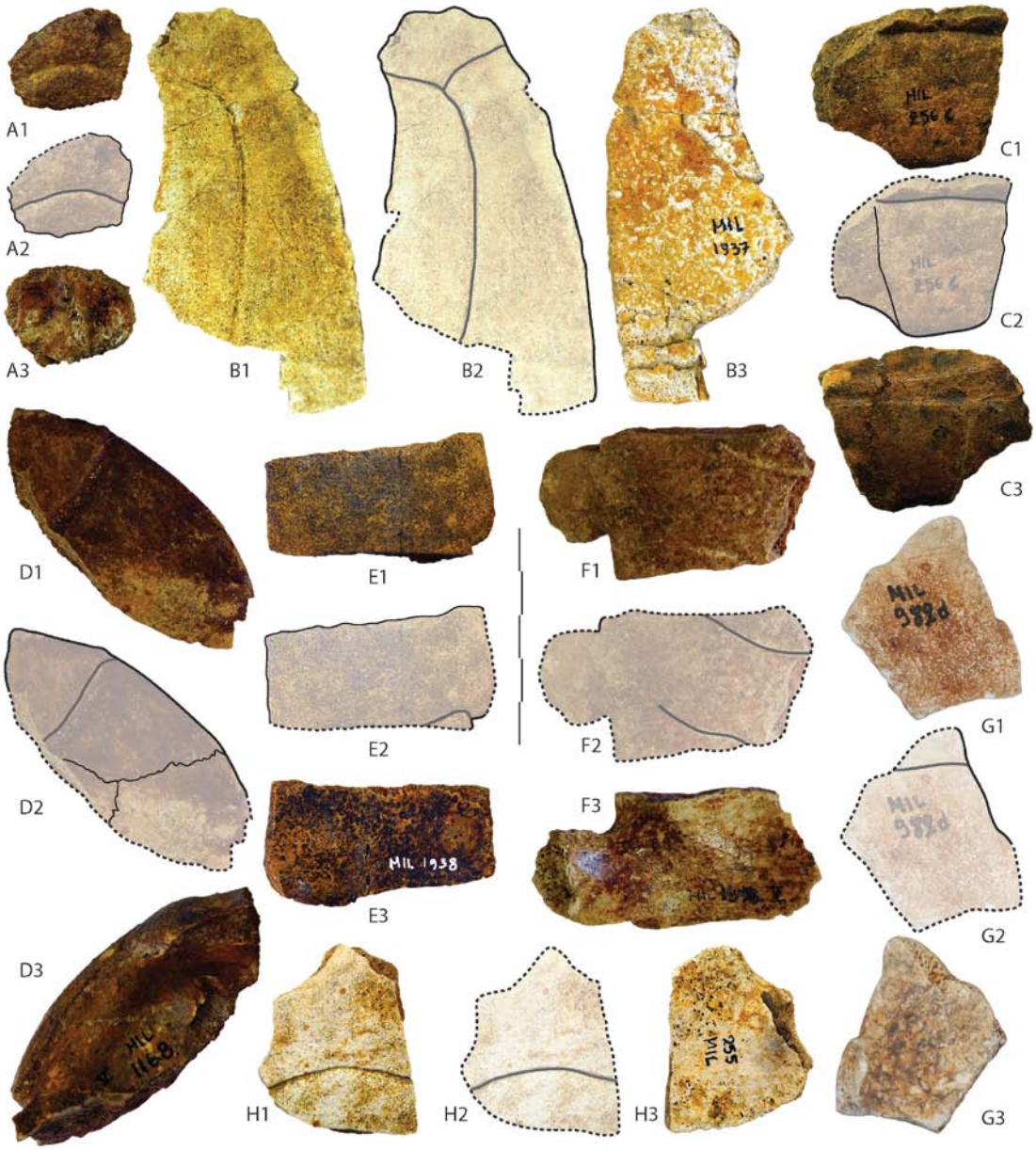


Figure 3.92. *Testudo* sp. nov. from the Late Pliocene of Milia (Grevena). Additional shell material: A, MIL 256a, in (A1) dorsal, (A2) drawing of the dorsal and (A3) visceral views. B, MIL 1937, costal in (B1) dorsal, (B2) drawing of the dorsal and (B3) visceral views. C, MIL 256b, pygal in (C1) dorsal, (C2) drawing of the dorsal and (C3) visceral views. D, MIL 1168, left epiplastron in (D1) ventral, (D2) drawing of the ventral and (D3) visceral views. E, MIL 1938, left hypoplastron fragment in (E1) ventral, (E2) drawing of the ventral and (E3) visceral views. F, left hyoplastron fragment in (F1) ventral, (F2) drawing of the ventral and (F3) visceral views. G, MIL 982d, left hyoplastron fragment in (G1) ventral, (G2) drawing of the ventral and (G3) visceral views. H, MIL 255, shell fragment in (H1) ventral, (H2) drawing of the ventral and (H3) visceral views. Scale bar equals 5 cm.

MIL 1633: It is a small shell fragment. Further identification is not possible.

MIL 1638: It is fragment of the shell of a tortoise and is crossed by a sulcus. By the curvature we can assume that it belongs to the carapace. Further identification is not possible.

MIL 1753 (Fig. 3.91): This specimen corresponds to the left part of a plastron, that is preserved in four fragments. MIL 1753a represents the epiplastron, partial entoplastron and hyoplastron. MIL 1753b represents the anterior part of the hypoplastron. MIL 1753c represents the end of the left bridge, whereas MIL 1753d is a fragment of the hypoplastral region. The anterior lobe of the plastron is short and wide, with a rounded rim. The epiplastra are short and wide, forming a thick convex epiplastral lip viscerally. A deep gular pocket is noted. The entoplastron is longer than wide, roughly hexagonal. The hyo- and hypoplastra are long and wide, showing a moderate concavity ventrally. This suggests that the specimen is probably a male individual. The preserved part of the left bridge shows that the peripherals were tall and short, being moderately flared posteriorly. The gulars are long and narrow, covering the epiplastra and overlapping the anterior part of the entoplastron. The humerals are long, compared to the short pectorals. The humero-pectoral sulcus is laterally convex and medially slightly concave. It is situated on the hyoplastra, posterior to the end of the entoplastron. The pectoro-abdominal sulcus is curved, being concave medially and convex laterally. The abdominals cover the posterior half of the hyoplastra and all the preserved part of the hypoplastra, suggesting a rather long covering of the abdominals. This morphology, together with the thickened plate on the preserved part of the bridge resemble the morphology of the plastra with a movable posterior lobe.

Table. 3.3. Measurements of the left anterior plastron MIL 1753 of *Testudo* sp. Nov. from Milia.

(in mm)	Antero-posterior Length at symphysis	Maximum Width	Thickness
Epiplastron	18,5	45,8	26,5
Epiplastral lip	Length: 32,8, Width: 22,3, Height:29,6		
Entoplastron	41,4	26	12,3-9,4
Hyoplastron	47,3	82,6	6,6-5,4
Hypoplastron	42,8	41,7 (pr)	6,5-6,1
Gular	25,9	22,1	-
Humeral	37,6	56,74	-
Pectoral	20,9	82,2	-
Abdominal	65,6	81,4	-

Abbreviations: pr: preserved.

MIL 1937 (3.92.B): This specimen corresponds to an almost complete costal, missing only the lateral part. The costal is medially short with a single rounded sutured side and laterally is long. Therefore, it presents the typical alternating pattern of the testudinids with costal medially short and laterally long alternating with costals being medially long and laterally short. Viscerally we notice the inserted rib. Dorsally, the vertebrals cover the medial part of the costal and it is crossed transversely by a curved pleural sulcus.

MIL 1938 (3.92.E): This specimen corresponds to the anterior part of the left hypoplastron. The hypoplastron is flat. In the posterior part we notice the presence of a strongly curved abdomino-femoral sulcus.

DISCUSSION

The material presented here has been found in the Late Pliocene site of Milia, Grevena. All the fossils are located in more than 10 sub-sites around the village of Milia, in unconsolidated sand deposits. All these sites are marked by the presence of the Borson's zygodont, *Mammut borsoni* and the rhinoceros species *Dicerorhinus jeanvireti*. Regarding the tortoise specimens, the posterior carapace MIL 495 has been found in the site Milia-4, the left plastron MIL 1753 in the site Milia-10, whereas the remaining isolated fragments in the site Milia-5. Although few of the specimens present overlapping fragments, all the material can be attributed to the same species.

This tortoise material is associated with the marginated tortoise *T. marginata*. This species is found in Greece, in parts of Albania and it has been introduced by humans in Sardinia. It is characterized by the presence of an elongated posterior carapacial lobe, with a peripheral margin that is almost horizontally flared. This distinctive morphology makes the living marginated tortoises and the specimens of its extinct representatives easily recognizable. The other small testudinid species in Greece, *T. graeca* and *T. hermanni*, show a peripheral margin (pygal and last peripherals) that is curved inwards (Fig. 3.93). Thus, they are easily distinguished by *T. marginata*. The Greek fossil record is quite rich in specimens of *T. marginata*, all from the Pleistocene. In the mainland Greece few sites are known, such as Xerias (Kavala; Tsoukala et al., 2011) with a shell showing many similarities with *T. marginata*, and Laconia with fragments of the carapacial margin (Schleich, 1982). On the other hand, numerous specimens of *T. marginata* are found on cave on islands, such as Charkadio Cave, Tilos and various cave in Crete (see previous sections). The Milia marginated tortoise clearly differs from all these specimens in the less flared carapacial margin and in the short posterior carapacial lobe.

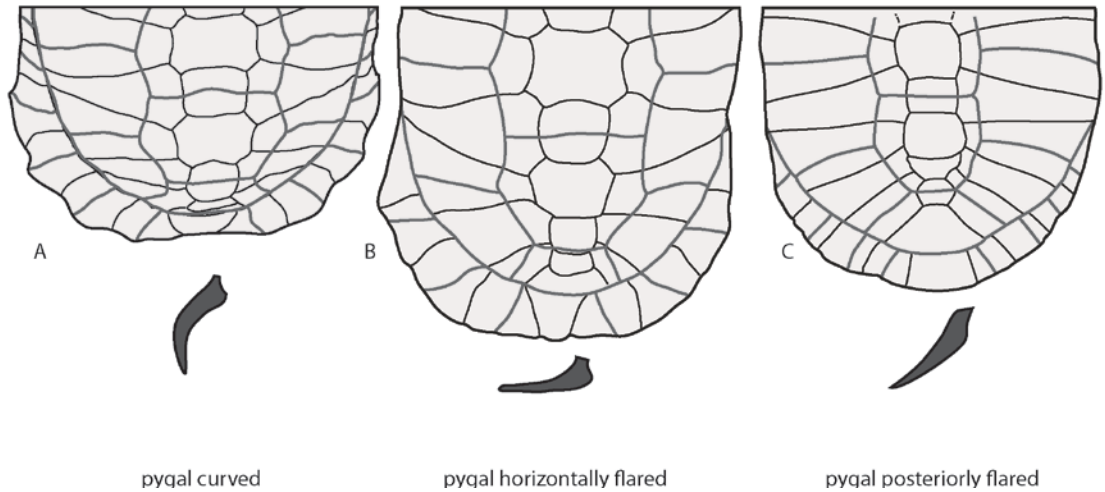


Figure 3.93. Comparison of the morphology of the posterior carapace of (A) extant *Testudo graeca*, (B) extant *Testudo marginata* and (C) the Milia testudinid. Cross-sections of the medial plane of the pygal are shown.

A taxon that has been traditionally associated with the *marginata* group it the *Testudo marmorum* from the Late Miocene of Pikermi (see previous section). The Milia testudinid is different from the marble tortoise in the narrower vertebrals, in the posteriorly flared carapacial margin, the presence of dorsal bumps in the neurals and in the shorter and wider entoplastron.

Another taxon that is of interest, is the recently erected *Testudo weissengeri* by Bour (1996). This new species, which also preserves a flared carapacial margin has been distinguished from *T. marginata* based on the smaller shell size and differences in colorations, presenting a distinct population on the south Peloponnesus. However, genetic evidence from mitochondrial and nuclear genomic markers showed that *T. weissengeri* is not a distinct evolutionary lineage (Fritz et al., 2005).

Based on the above, the *Testudo* sp. from Milia is the only *Testudo* taxon that shows a flared carapacial margin similar to the *T. marginata*. It probably represents a new species that could be diagnosed by the following characters: A member of Testudinidae based on the presence of the alternating pattern of neurals and costals, the octagonal-quadrangular neurals make contact with costals that are medially short and laterally long, alternated with costals that are medially long and laterally short. Differs from extant *Testudo graeca, Testudo hermanni,* and extint *Testudo* spp. and is associated with *Testudo marginata* in the pygal region which is posteriorly flared. Differs from *T. marginata* in the short posterior carapacial lobe, not being elongated, in the narrower vertebrals, shorter peripherals, and in the pygal, which shows lateral sides that diverge posteriorly.

In a following chapter the analysis of its phylogenetic relationships with *T. marginata* and other extant and extinct testudinids is attempted.

'Testudo' sp. nov II

MATERIAL:

Samos (2 specimens) (Fig. 3.94-3.95): AMPG 1999 (complete carapace); MFGUI 22 (anterior half of the shell).

AGE: Late Miocene, MN11 to MN13.

LOCALITY: Samos Island, Aegean Sea, Greece.

DESCRIPTION

AMPG 1999 (Fig. 3.94): The entire carapace has been preserved, except for the pygal-peripheral 11 area. On the interior the in-filling sediment is preserved.

Carapace: The shell is tall, elongated and rounded. The nuchal is wider than long, roughly octagonal. The anterior side is slightly concave. The posterior sides of the nuchal are sinuous and the posterior part of the nuchal is narrow and elongated. Eight neurals are present, showing dorsal bumps on neural 1, 3, 5 and 8, i.e. on the limits of the vertebral sulci. Neural 1 is longer than wide, quadrangular, with rounded edges. The anterior side of the neural 1 is much narrower than the posterior one. Neural 2 is octagonal, with narrow anterior and wider posterior part. Neural 3 is quadrangular, as wide as long. Neural 4 is octagonal, as wide as long, with anterior and posterior sides of equal width. Neural 5 is quadrangular, wider than long. Neural 6 is hexagonal, with short anterior lateral sides. Neural 7 is also hexagonal, smaller than neural 7, with short anterior lateral sides. Neural 8 is small, with a rounded quadrangular shape. Two suprapygals are present, both constituting one trapeze. The first one is much larger, elongated, embracing the second. The second suprapygal is lenticular, wider than long. The costals, following the differentiated neural series, are also differentiated. Costal 1 is long, making contact with the nuchal, the neurals 1-2, and the peripherals 1-3. Costal 2 and costal 4 are medially short and laterally long, alternated with the costal 3 and costal 5 that are medially long and laterally short. Costal 6 and costal 7 are similar in shape, having a double-sutured medial side (longer anteriorly) to make contact with the hexagonal neurals. Costal 8 is smaller, with rounded medial side. It makes contact only with the costal 7 and the suprapygal 1, and not with the neural series. Therefore, the posterior side of the medial border of the costal 7 embraces the costal 8 and makes contact with the suprapygal 1. The peripherals are long and narrow. The peripherals of the bridge are tall.

As far as the scute sulci are concerned, their limits can be clearly noted on the dorsal surface of the carapace. Anteriorly, a cervical scute is present that is shorter anteriorly and wider posteriorly. The first vertebral is smaller than the rest. The vertebrals 2-4 are very wide, even wider than the pleural scutes. Their limits cross transversely the neural 1, neural 3, neural 5 and neural 8. As it has been noted above, dorsal bumps are present on the limits of the vertebrals. The pleurals are generally quadrangular, wider than long, but slightly narrower compared to the vertebrals. There is good coincidence between the costo-peripheral sutures and the pleuro-marginal sulci.

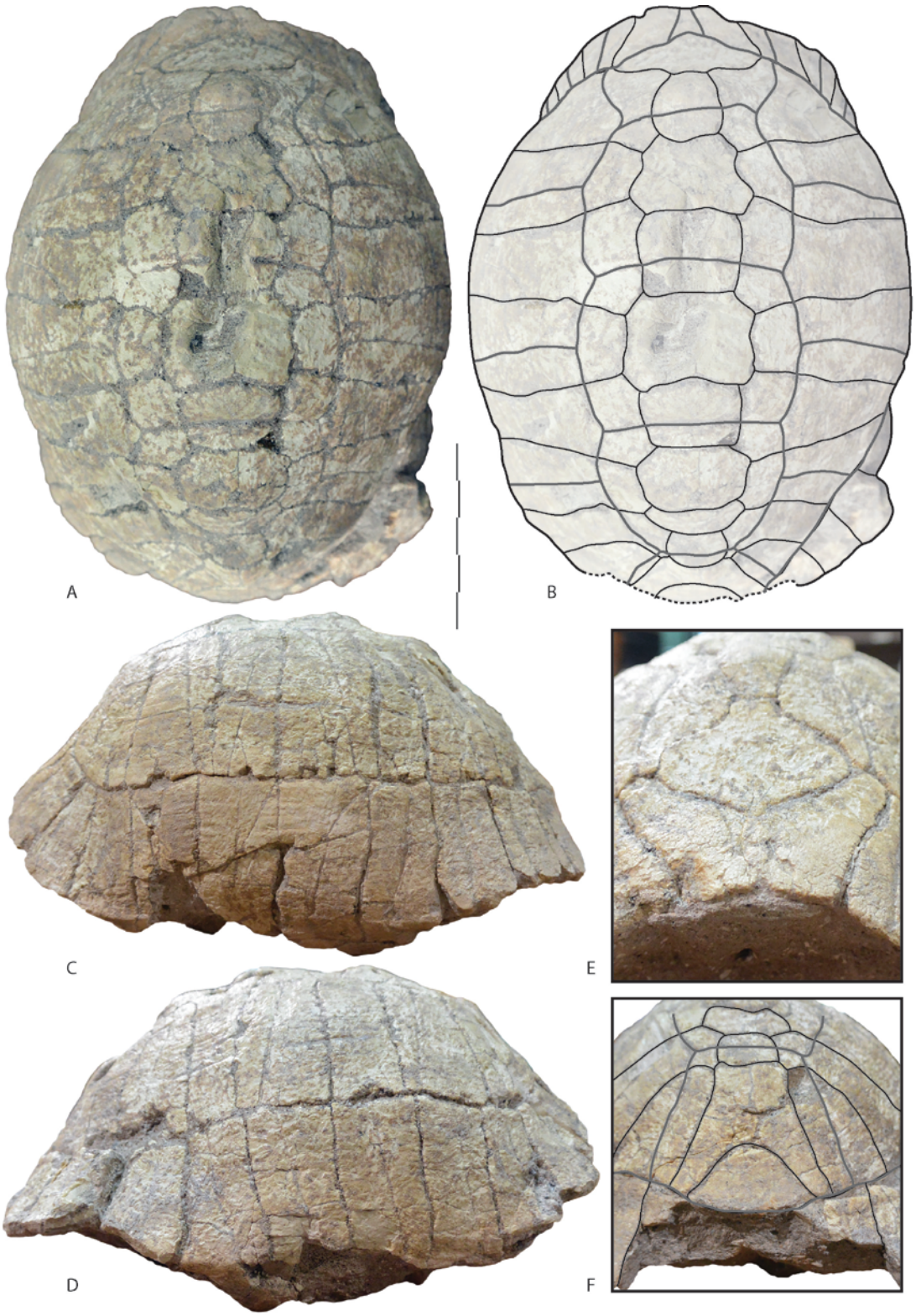


Figure 3.94. '*Testudo*' sp. nov. from the Late Miocene of Samos Island (AMPG collection). The partial shell (AMPG 1999) in (A) dorsal, (B) drawing of the dorsal, (C) left lateral, (D) right lateral, (E) detail of the nuchal and (F) posterior views. Scale bar equals 5 cm.

MFGUI 22 (Fig. 3.95): The anterior half of the shell is preserved, fixed on a permanent basis on the exhibition hall of the Goulandris Museum of Natural History. Therefore, parts of the plastron are not available for observation. Most of the left part of the carapace and the entire posterior part are missing. From the plastron, the posterior lobe is missing.

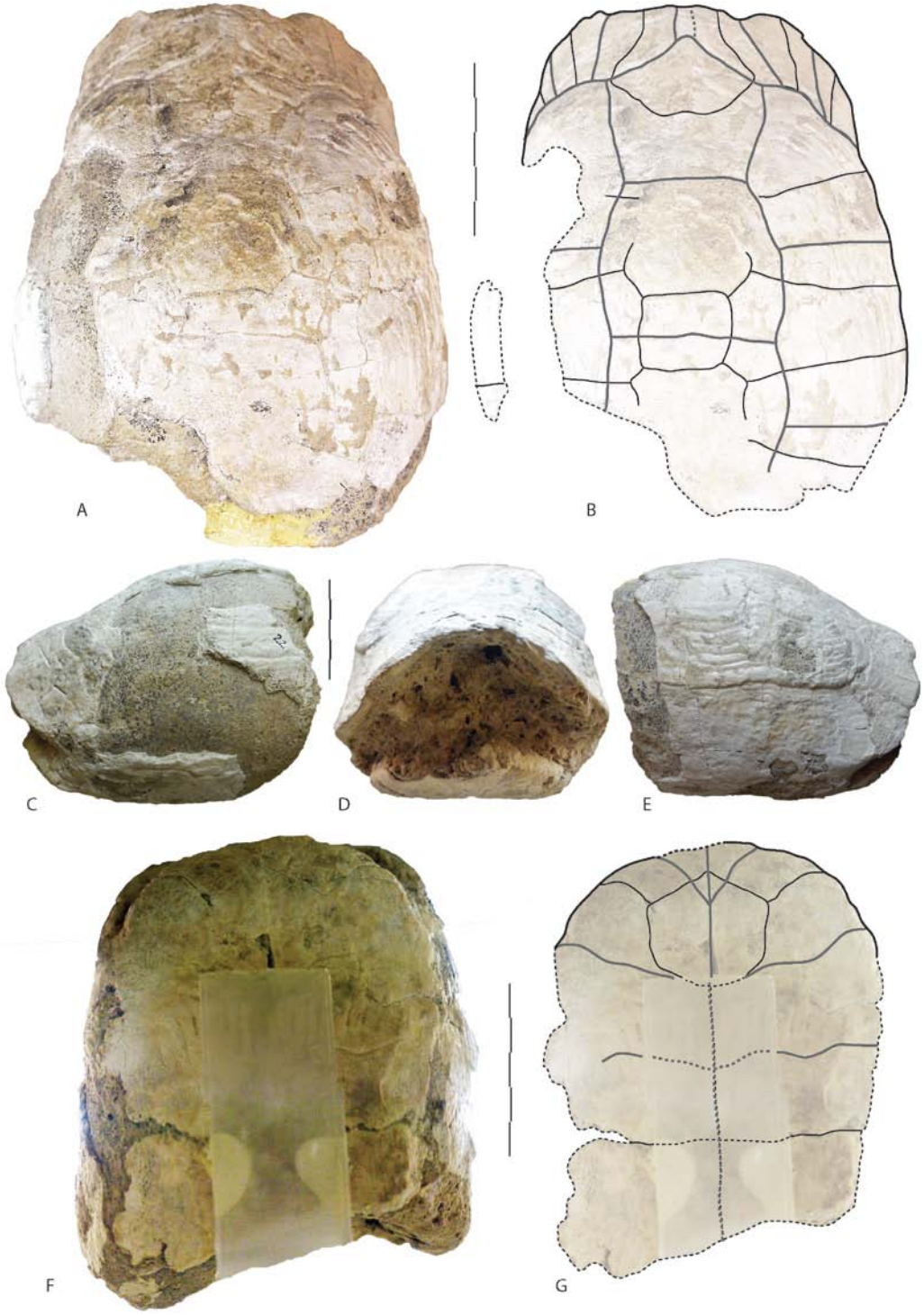


Figure 3.95. '*Testudo*' sp. nov. from the Late Miocene of Samos Island. MFGUI 22, the partial shell in (A) dorsal, (B) drawing of the dorsal, (C) left lateral, (D) anterior, (E) right lateral, (F) ventral and (G) drawing of the ventral views. Scale bar equals 5 cm.

Carapace: The shell is tall, elongated and rounded. The nuchal is wider than long, roughly octagonal. The anterior side is slightly concave. A shallow embayment is present anteriorly, affecting the nuchal and the first peripherals. Neural 2 is octagonal. Neural 3 is quadrangular, as wide as long. Neural 4 is octagonal, as wide as long, with anterior and posterior sides of equal width. Costal 1 is long and wide, but the medial contacts are not visible. Costal 2 and costal 4 are medially short and laterally long, alternated with the costal 3 that is medially long and laterally short. Anteriorly, a narrow cervical scute is present. The first vertebral is smaller than the rest. The vertebrals 2-3 are very wide, even wider than the pleural scutes. Their limits cross transversely the neural 1 and neural 3. The pleurals are generally quadrangular, wider than long, but slightly narrower compared to the vertebrals. There is good coincidence between the costo-peripheral sutures and the pleuro-marginal sulci.

Plastron: The lobe is short, wide and rounded. The epiplastra are short and narrow, covering only the anteriormost part of the lobe. The entoplastron is nearly as wide as long, hexagonal, with straight sides. The hyo- and hypoplastra are long and wide, being flat in the middle part. The gulars are moderately wide and long, covering the medial part of the epiplastra and the anterior part of the entoplastron. The gularo-humeral sulcus is slightly convex on each side, forming an acute angle with the midline. The remaining part of the entoplastron is covered by the long and wide humerals. The humero-pectoral sulcus is nearly straight medially and slightly convex laterally, whereas it is situated medially on the posterior end of the entoplastron. Pectorals are long, of similar length to the humerals, covering the posterior part of the hyoplastra and the anterior half of the hypoplastra.

DISCUSSION

The two specimens from Samos could be attributed to the same taxon based on the overall similarity of the carapace, such as the wide vertebrals compared to the pleurals. However, they display a mosaic of characters that are not encountered in the known specimens of small testudinids from South Balkans. These features are found especially in the AMPG specimen. First of all, the vertebrals 2-4 are particularly wide, slightly wider than the corresponding pleurals. The vertebrals are always narrower than the pleurals in *Testudo* s.s. and especially in the so-called *hermanni* group are particularly narrow (a diagnostic character for this group). The posterior carapace presents also a unique combination of morphologies. Costal 8 is much reduced and does not make contact with the neural series but only with costal 7 and the suprapygal 1. At the same the suprapygal 1 is much larger and embraces the suprapygal 2, which is lenticular in shape.

The MFGUI specimen adds another distinctive character. The pectoral scutes are particularly long medially, being as long as the humerals. This is different than the known condition in *Testudo* where the pectorals are always shorter than the humerals. The known specimens from Samos do not allow a confident conclusion on whether they possessed a movable posterior lobe. However, the absence of the abdomino-femoral sulcus on the preserved part of hypoplastra (almost complete) in the MFGUI specimen resembles the condition in the hinged *Testudo*. In these forms, the femoral covering on the hypoplastra is much reduced, present only in the lateral posterior parts close to the bridge.

02/16/2016 Ψηφιακή Βιβλιοθήκη Θεόφραστος - Τμήμα Γεωλογίας - Α.Π.Θ.

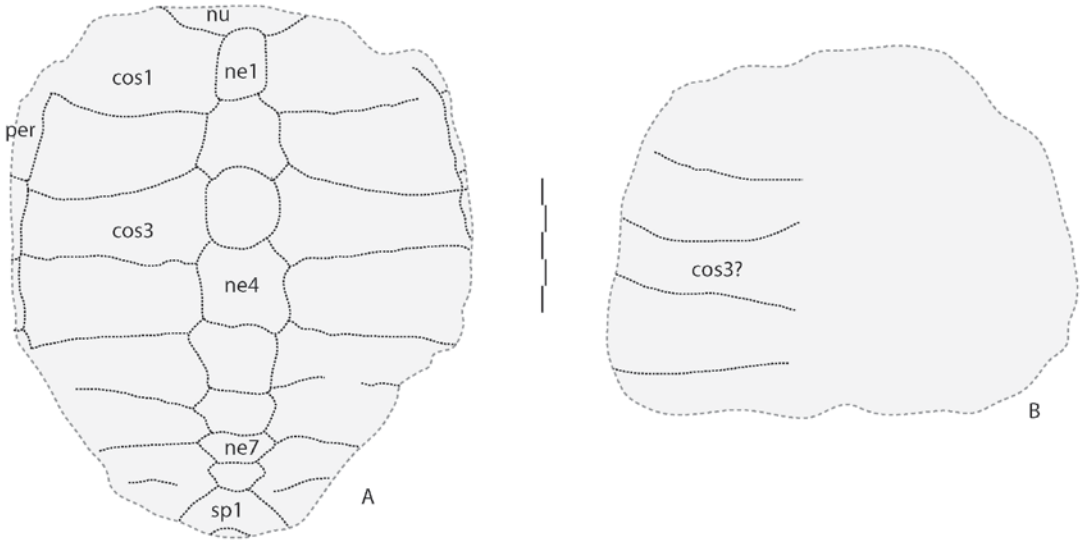


Figure 3.96. The specimens from the ?Middle Miocene of Thymiana, Chios described as *Testudo* sp. I (A) and *Testudo* sp. II (B), based on the photographs by Paraskevaidis (1955).

Other specimens from Greece and adjacent areas could be attributed to this taxon. For example, the two specimens described by Paraskevaidis (1955) from the ?Middle Miocene of Chios are interesting. The published material comprises by 2 internal casts (steinkerns) of the shell of two different individuals. They were identified by Paraskevaidis (1955) as *Testudo* sp. I and *Testudo* sp. II. Paraskevaidis (1955) mentions that this material has been deposited to the collections of BSPG circa 1940, but they were lost during the Second World War. Personal communication with Dr. Markus Moser (2011; curator of BSPG) confirmed that no such material is stored in the collections at present. Paraskevaidis (1955) provided a Sarmatian age (Upper Serravalian/ Middle Miocene) in the specimens. In the Fig. 3.96 an interpretation of the published specimens is given, showing the imprints of the bony plates preserved on the internal cast. These lines are clearly visible in the photographs given by Paraskevaidis (1955). Both specimens preserved the typical alternating pattern of testudinids, consisting of costal plates that are medially short and laterally long alternated with plates that are medially long and laterally short. Although obviously is not safe to make clear comparisons we can document some clear similarities between the Chios testudinids and the new testudinid from Samos. For example, the first four neurals are similarly wide and shaped, with the exception of the third neural in Chios that appears to be more rounded. However, the second neural is similar between the two specimens as it is narrower anteriorly and wider posteriorly. The posterior is strikingly similar, in having a first suprapygal embracing the second one, which appears to be lenticular. Moreover, although not entirely preserved, the morphology of the costals 7 and 8 suggesting a possible contact between the first suprapygal and the costal 7.

Another specimen that could be attributed to this taxon is the almost complete shell from the Turolian (MN11) from Konya-Hatunsaray-Kayadibi (Turkey) described by Staesche et al. (2007). The identification of the specimen as a juvenile member of *Cheirogaster* sp. cf. *bolivari* by Staesche et al. (2007), but in a recent paper we have conclusively shown that it cannot be a juvenile form of any large testudinid (Pérez-García & Vlachos, 2014). This specimen although shows a costal 7-8 association that regularly contacts the neurals, resembles with the taxon described

here in have similarly shaped suprapygals. In the Turkish specimen the first suprapygal embraces the lenticular second one.

As it has been explained elsewhere (e.g. Vlachos et al., 2014) and in many parts of this thesis (e.g. description of the large testudinids from Samos), the island of Samos used to be connected with Minor Asia probably till the Pleistocene, suggesting a closer relationship of its testudinids with the Minor Asian forms than the Balkan ones. For this reason, it is not strange to find similarities with the forms from Chios and Turkish testudinids. Hopefully, the study of numerous undescribed material that exist in Turkish collections will enlighten this matter.

In conclusion, these specimens could be diagnosed as a member of *Testudo*, based on the alternating pattern of medially short and laterally long costals, alternated with costals that are with medially long and laterally short. They differ from other species of *Testudo* based on the following unique combination of characters: wide vertebrals, slightly wider than the pleurals; absence of contact of the costal 8 with the neural series, costal 7 embracing the costal 8 medially making contact with the first suprapygal; suprapygal 1 larger, embracing the lenticular suprapygal 2; pectorals medially as wide as the humerals. In a following chapter the analysis of its relationships within *Testudo* is attempted.

***Testudo* sp.**

Maramena, Serres basin (latest Miocene – Earliest Pliocene; 2 specimens) (Fig. 3.97): JGU.Geow.Pw 216, a rock sample with fragmented fossils, including few chelonian plates; JGU.Geow.Pw 226, a rock sample with fragmented fossils, including mainly chelonian plates.

Serres (Late Miocene; 1 specimen) (Fig. 3.98): AMPG 2000, partial shell

Nea Silata (latest Miocene – Earliest Pliocene) (LGPUT collection, 38 specimens) (Fig. 3.99): SLT 6, costal fragment; SLT 35, peripheral fragment; SLT 111, shell fragment; SLT 180, peripheral; SLT 182, shell fragment; SLT 183, costal fragment; SLT 184, shell fragment; SLT 185, shell fragment; SLT 186, hyoplastron; SLT 187, costal fragment; SLT 188, peripheral; SLT 189, costal; SLT 190, shell fragment; SLT 191, plastron fragment; SLT 192, plastron fragment; SLT 193, peripheral; SLT 194, costal fragment; SLT 195, plastron fragment; SLT 196, peripheral; SLT 197, shell fragment; SLT 198, plastron fragment; SLT 199, plastron fragment; SLT 200, right hyoplastron fragment; SLT 201, plastron fragment; SLT 202, costal fragment; SLT 203, peripheral fragment; SLT 204, shell fragment; SLT 205, shell fragment; SLT 206, shell fragment; SLT 207, shell fragment; SLT 208, shell fragment; SLT 209, shell fragment; SLT 210, shell fragment; SLT 211, shell fragment; SLT 212, shell fragment; SLT 213, shell fragment; SLT 214, shell fragment; SLT 215, shell fragment.

DESCRIPTION

Maramena, Serres basin

The chelonian material from the locality of Maramena is highly fragmented (Fig. 3.97). It consists mainly of isolated plates (that could belong to the same individual) preserved on their recovery position in a grayish clay material.

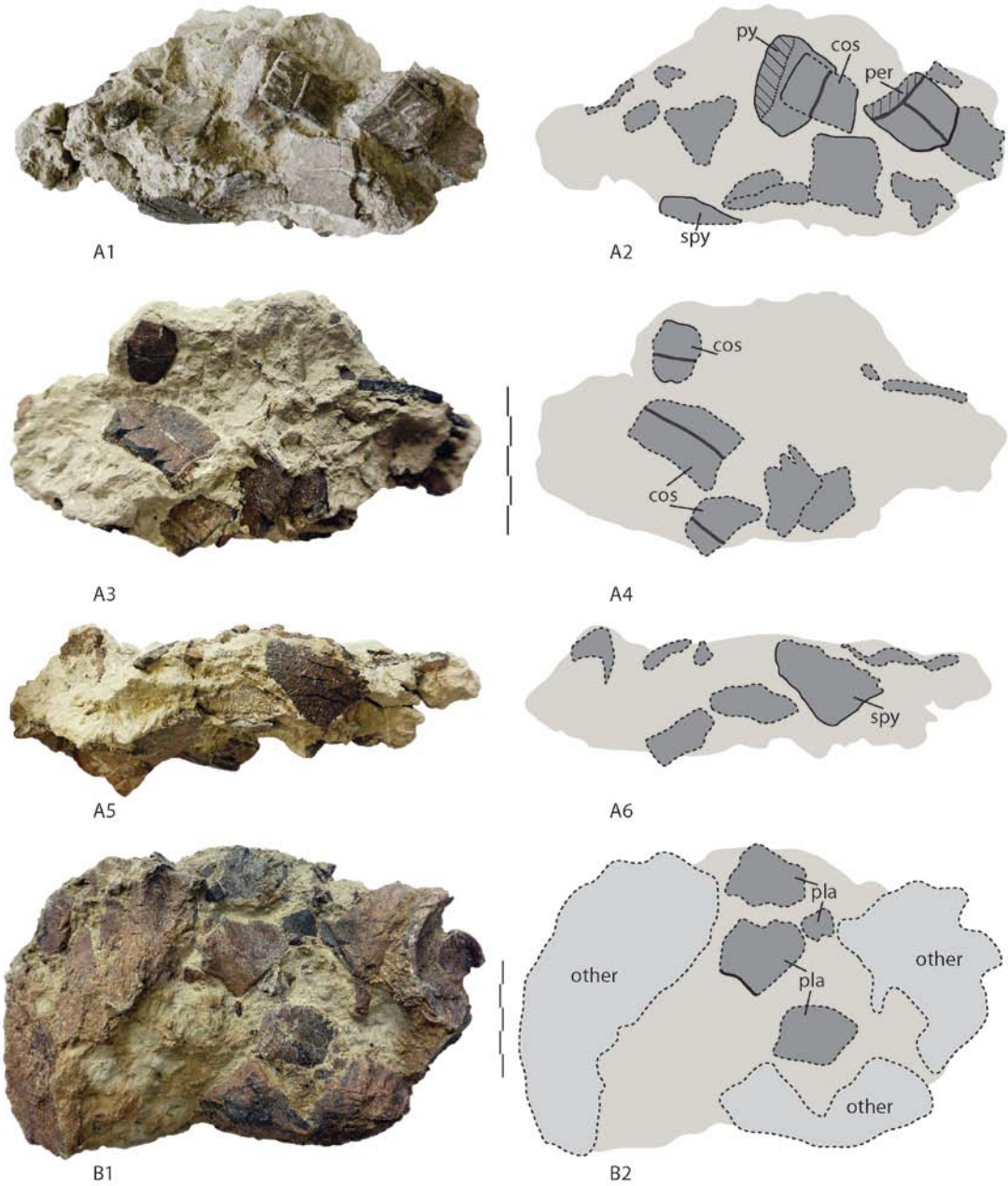


Figure 3.97. *Testudo* sp. from the Miocene/Piocene boundary of Maramena (Serres). A, JGU.Geow.Pw 226, a rock sample with fragmented fossils, including mainly chelonian plates. B, JGU.Geow.Pw 216, a rock sample with fragmented fossils, including few chelonian plates. Chelonian plates are indicated with dark grey. Scale bar equals 5 cm. For abbreviations see Material & Methods.

The preservation status does not allow detailed description. In those plates that we can observe the external surface, we notice the distinctive growth lines of the testudinid shell. The specimen JGU.Geow.Pw 226 contains mainly chelonian plates. Some of them can be further identified. In total we can observe: 1) a pygal plate, with narrower posterior side; 2) a peripheral plate, being crossed by the marginal sulci, with coincidence between the sutures and sulci; 4) a partial suprapygal plate, with any evidence of scute sulci; 5) several costal fragments, being crossed by the pleurals. The morphology of these plates is consistent with *Testudo*. The specimen JGU.Geow.Pw 216 contains only four fragments of chelonian material. Based on the available information they are all identified as plastral elements whose visceral side is visible.

One of them, the largest, preserves part of the border. Further identification is not possible. Based on the available information, the material from Maramena could be only attributed to *Testudo* sp. In the remaining specimens from Maramena in JGU.Geow.Pw, no obvious signs of chelonian material is noted.

Serres

The chelonian material was given to G. Theodorou (AMPG) by Karystineos, and comes from the Miocene of Serres basin. This specimen (Fig. 3.98) corresponds to the infill of a partial shell, that preserves some plates on the dorsal side. In detail, on the anterior part (Fig. 3.98.A-B) most of the neural 1 is preserved, being rectangular and longer than wide, in articulation with a partial octagonal neural 2, both costals 1 (medial parts) and the medial part of the left costal 2. On the left lateral side, a small part of the costal 3 is preserved. On the posterior side (Fig. 3.98.D-E) some neurals are preserved. The anterior one (neural 5 or neural 6) is rectangular, wider than long. The remaining two neurals are hexagonal with short antero-lateral sides. Two suprapygals are preserved, the first being small and rectangular and the second being larger, trapezoid with posterior diverging lateral borders. Some parts of the associated costal are preserved on each side. In ventral view no plates are preserved, but the imprints of the plastral plates are noted (Fig. 3.98.C; see white dashed lines).

The few morphological information that is preserved, allows association with *Testudo*, based on the small size, the alternating neural pattern and the suprapygal area. Although the plastron is not preserved, the imprint of the hypo-xiphiplastral suture is straight and anteriorly positioned, probably indicating long xiphiplastra. These features indicate that this specimen could possess a hinge, but of course there is not way to confirm this attribution. Therefore, based on all the available information this specimen can only be identified to the generic level.

Nea Silata (Thessaloniki)

LGPUT SLT 6 (Fig. 3.99.D): This specimen corresponds to the medial and middle part of a costal plate. The plate is shorter medially and longer laterally. Dorsally is overlapped by the vertebral scute and is crossed longitudinally by the pleural sulci. Viscerally, the rib end is noted.

LGPUT SLT 35: This specimen corresponds to the lateral part of a peripheral. On the dorsal side the distinctive growth lines of the testudinids are noted.

LGPUT SLT 180 (Fig. 3.99.E): This specimen corresponds to an almost complete peripheral plate. The peripheral is thick, showing a pointed tip on the marginal sulci level. Dorsally several growth lines are noted, whereas is crossed only by the marginal sulci and the pleuro-marginal sulcus coincides with the costo-peripheral suture.

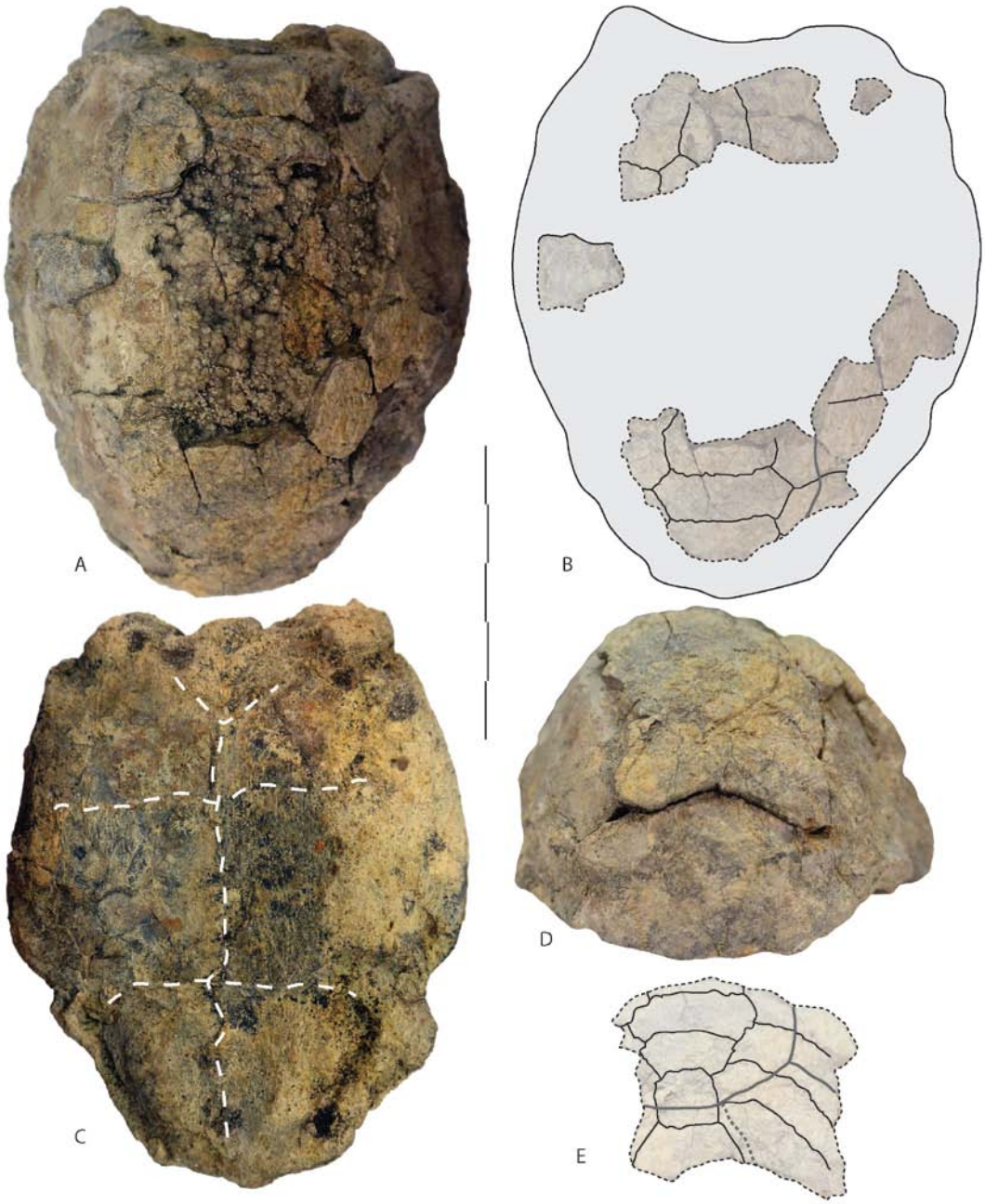


Figure 3.98. *Testudo* sp. from the Miocene of Serres basin (AMPG collection) in (A) dorsal, (B) drawing of the dorsal, (C) ventral, (D) posterior and (E) drawing of the posterior views. Scale bar equals 5 cm. White dashed lines indicate the imprints of the sutures of the plastron.

LGPUT SLT 183 (Fig. 3.99.C): This specimen corresponds to the lateral part of a costal plate. The plate is longer laterally, and probably shorter medially. Dorsally, several distinct growth lines are noted, and the plate is crossed longitudinally by the pleural sulci.

LGPUT SLT 186 (Fig. 3.99.G): This specimen corresponds to a partial left hyoplastron, preserving a part of the axillary notch. The plate is slightly curved. Ventrally, on the anterior part a wavy sulcus is noted, probably corresponding to the humero-pectoral sulcus.

LGPUT SLT 187: This specimen corresponds to a thick fragment of a costal plate. Dorsally is crossed by vertebro-pleural and the pleural sulci and displays prominent growth lines.

LGPUT SLT 188: This specimen corresponds to a complete peripheral. The peripheral plate is slightly taller than wide, whereas it displays a moderate curvature. Dorsally is crossed only by the marginal sulci and the pleuro-marginal sulcus coincides with the costo-peripheral suture.

LGPUT SLT 189 (Fig. 3.99.B): This specimen corresponds to an almost complete costal plate, missing only some of the medial part. Dorsally is crossed by the vertebro-pleural and the pleural sulci. The morphology of the sulci suggest that this could be one of the posterior costals of the carapace (7^{th} or 8^{th}) but is not possible to make a confident identification. Viscerally, the inserted rib is noted.

LGPUT SLT 193: This specimen corresponds to a thick plastron fragment, being crossed by a sulcus ventrally. Further identification is not possible.

LGPUT SLT 192: This specimen corresponds to a small fragment of the right hyoplastron, preserving the end of the axillary buttress viscerally, and being crossed by the humero-pectoral sulcus ventrally. Several growth lines are noted viscerally.
LGPUT SLT 193 (Fig. 3.99.F): This specimen corresponds to a complete peripheral. The peripheral plate is much taller than wide. Dorsally is crossed only by the marginal sulci and the pleuro-marginal sulcus coincides with the costo-peripheral suture.

LGPUT SLT 194 (Fig. 3.99.A): This specimen corresponds to the medial part of a costal. The medial side is long and it is evident that this costal was articulated with three neural plates. Dorsally is crossed by the verterbral and the vertebro-pleural sulci.

LGPUT SLT 195 (Fig. 3.99.H): This specimen corresponds to a thickened plastron fragment. On the ventral side a sulcus in noted, that coincides with the suture. Although the preserved fragment is small, it could correspond to the posterior part of the hypoplastron.

LGPUT SLT 196: This specimen corresponds to a fragment of a curved peripheral. Dorsally, only the marginals are noted. Also, several growth lines are found.

LGPUT SLT 198: This specimen corresponds to a flat small fragment of a plastron. Ventrally no sulci are noted, but several growth lines are found. It probably corresponds to the medial part of hyo/hypoplastra.

LGPUT SLT 199: This specimen corresponds to a thick fragment of a plastron. As no suture or sulci are preserved, further identification is not possible.

LGPUT SLT 200: This specimen corresponds to a small fragment of the right hyoplastron, preserving the end of the axillary buttress viscerally, and being crossed by the humero-pectoral sulcus ventrally.

LGPUT SLT 201: This specimen corresponds to a plastron, probably from a part near the bridge, as it is thickened. Further description is not possible.

LGPUT SLT 202: This specimen corresponds to the medial part of a costal, that is longer medially. From the preserved part, we can infer that this costal was articulating with three neurals.

LGPUT SLT 203: This specimen corresponds to the lateral part of a peripheral. It preserves a thickened part for the bridge on one side. Dorsally is crossed by the marginal sulci.

LGPUT SLT 111, 182, 184, 185, 190, 197, 204 – 215: Those specimens are too poorly preserved to allow a clear identification, as they correspond to small fragment of the carapace and the plastron. Their overall morphology, such as the thickness and the outer surface is consistent with the morphology of a testudinid.

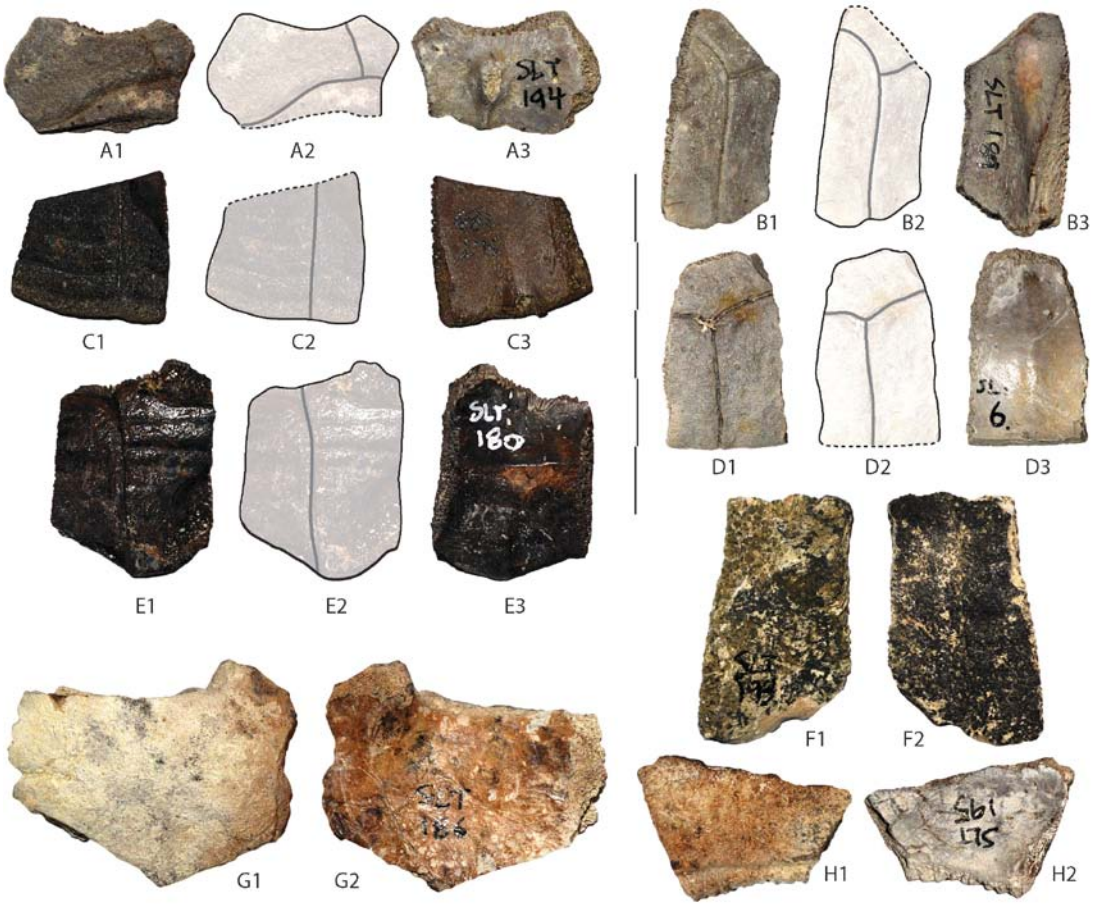


Figure 3.99. *Testudo* sp. from the Late Miocene-Early Pliocene of Nea Silata (Thessaloniki). A, LGPUT SLT 194, costal in (A1) dorsal, (A2) drawing of the dorsal and (A3) visceral views. B, LGPUT SLT 189, costal in (B1) dorsal, (B2) drawing of the dorsal and (B3) visceral views. C, LGPUT SLT 183, costal in (C1) dorsal, (C2) drawing of the dorsal and (C3) visceral views. D, LGPUT SLT 6, costal in (D1) dorsal, (D2) drawing of the dorsal and (D3) visceral views. E, LGPUT SLT 180, peripheral in (E1) dorsal, (E2) drawing of the dorsal and (E3) visceral views. F, LGPUT SLT 193, peripheral in (F1) dorsal, (F2) drawing of the dorsal and (F3) visceral views. G, LGPUT SLT 186, hyoplastron in (G1) dorsal, (G2) drawing of the dorsal and (G3) visceral views. H, LGPUT SLT 195, plastron fragment in (H1) dorsal, (H2) drawing of the dorsal and (H3) visceral views. Scale bar equals 5 cm

COMMENT: All the above mentioned specimens could be attributed to a small testudinid, as they show several morphological characters that allow differentiation of the geoemydid taxon from Nea Silata (see below). These are: the presence of an alternating pattern of neural (rectangular vs. octagonal) and costals (longer medially and shorter laterally) as it is inferred by the shape of the preserved costal specimens; coincidence of the pleuro-marginal sulci and the costo-peripheral suture; presence of pointed tips in some peripherals; thickened shell; outer surface not smooth, with distinct growth lines as in the testudinids. Those characters allow attribution to *Testudo* but further identification is not possible.

Problematic material

- *Testudo* sp. from the Pleistocene of Psychiko: This material has been mentioned by Bachmayer & Symeonidis (1970) as *Testudo* sp., with the original publication cited as Sindowski (1950) (from Bachmayer & Symeonidis, 1970). However, in this publication no turtles are reported, as under Reptilia only some specimens of snakes are mentioned. Georgalis & Kear (2013) continue to report this site as containing tortoise material, as *Testudo* sp. in their Table 1 and as *Testudo graeca* in the text (Georgalis & Kear, 2013:303), but they do not provide any information to support either of the above-mentioned identifications. During the study of AMPG collections no material from Psychiko was found. The presence of fossil tortoises from this locality remains in question.

- *Testudo* sp. from the Pleistocene of Korydallos: This material has been described by Paraskevaidis (1961), was discovered during constructions in a limestone quarry in Korydallos area, near Athens. The fossils were recovered in a limestone breccia with a matrix of terra rossa. The mammalian findings (*Ursus spelaeus*, *Mustella* sp., *Equus caballus* amongst others) clearly indicate a Pleistocene age for the material The tortoise findings are few, corresponding to a plastral fragment and a partial hyoplastron (Taf. XX.7 in Paraskevaidis, 1961) and possibly a part of the anterior carapace (Taf. XXI.4 in Paraskevaidis, 1961) of *Testudo*. Although the material appears to be interesting, Paraskevaidis (1961) did not mention in which collection the specimens are deposited. No such material is found to be stored in the APMG collection up to now (S. Roussiakis, pers. comm.). Also, Paraskevaidis (1961) mentions that the material “belongs to Koula Anastasiou” showing that the material was in a private collection.

GEOEMYDIDAE Theobald, 1868

MAUREMYS Gray, 1869
Mauremys rivulata Vallenciennes *in* Bory de Saint-Vincent, 1833

AGE: Pleistocene – Holocene.

DISTRIBUTION: Crete Island – Kos Island – Peloponnesus.

MATERIAL:
Gerani Cave, Crete (Pleistocene, 2 specimens) (Fig. 3.100): AMPG 852, left hypoplastron; AMPG 853, right hypoplastron.

Rethymnon fissure, Rethymnon, Crete (Pleistocene, 2 specimens) (Fig. 3.100): AMPG 748, peripheral; AMPG 749, costal fragment.

Koumpes Cave, Crete (Pleistocene, 4 specimens) (Fig. 3.101): AMPG 621, fragment of the carapace; AMPG 622, costal; AMPG 623, neural; AMPG 624, peripheral.

Mavro Mouri IV, Crete (Pleistocene, 6 specimens) (Fig. 3.102): AMPG 788, entoplastron; AMPG 789, costal; AMPG 790, costal fragment; AMPG 791, peripheral; AMPG 792, peripheral fragment; AMPG 793, peripheral.

Liko Cave, Crete (Pleistocene, 9 specimens) (Fig. 3.103): AMPG 735, neural; AMPG 736, humerus; AMPG 737, humerus diaphysis; AMPG 738, coracoid; AMPG 739, ungual; AMPG 753, peripheral; AMPG 754, humerus distal part; AMPG 778, right xiphiplastron; AMPG 779, peripheral.

Sitia, Crete (Pleistocene, 72+ specimens) (Fig. 3.104-3.105): AMPG 629, suprapygal 2; AMPG 630, costal; AMPG 631, costal fragment; AMPG 632, costal fragment; AMPG 633, costal fragment; AMPG 634, costal fragment; AMPG 635, peripheral; AMPG 636, right epiplastron; AMPG 637, entoplastron; AMPG 638, hypoplastron fragment; AMPG 639, hypoplastron fragment; AMPG 640, plastron fragment; AMPG 641, plastron fragment; AMPG 642, humerus diaphysis; AMPG 643, femur diaphysis; AMPG 644, costal fragment; AMPG 645, peripheral fragment; AMPG 646, nuchal fragment; AMPG 647, peripheral; AMPG 648, costal fragment; AMPG 649, xiphiplastron fragment; AMPG 650, humerus; AMPG 651, scapula; AMPG 652, costal fragment; AMPG 653, costal fragment; AMPG 654, peripheral; AMPG 655, peripheral fragment; AMPG 656, plastron fragment; AMPG 657, costal fragment; AMPG 658, costal fragment; AMPG 659, costal fragment; AMPG 660, costal fragment; AMPG 661, costal fragment; AMPG 662, costal fragment; AMPG 663, costal fragment; AMPG 664, costal fragment; AMPG 665, pygal; AMPG 666, peripheral; AMPG 667, peripheral; AMPG 668, left epiplastron; AMPG 669, left xiphiplastron fragment; AMPG 670, plastron fragment; AMPG 671, hypoplastron fragment; AMPG 819, peripheral; AMPG 820, peripheral; AMPG 821, peripheral; AMPG 822, peripheral; AMPG 823, peripheral; AMPG 824, peripheral; AMPG 825, peripheral; AMPG 826, peripheral; AMPG 827, left costal; AMPG 828, costal fragment; AMPG 829, costal fragment; AMPG 830, costal fragment; AMPG 831, costal fragment; AMPG 832, costal fragment; AMPG 833, costal

fragment; AMPG 834, plastron fragment; AMPG 835, peripheral; AMPG 836, hyoplastron fragment; AMPG 837, costal fragment; AMPG 838, plastron fragment; AMPG 839, plastron fragment; AMPG 840, plastron fragment; AMPG 841, plastron fragment; AMPG 842, left epiplastron; AMPG 843, left xiphiplastron; AMPG 844, peripheral fragment; AMPG 845, neural fragment; AMPG 846, costal fragment; AMPG 847, hyoplastron fragment; AMPG 848, hyoplastron fragment; AMPG 849, costal fragment; AMPG 850, neural; AMPG 851, costal fragment.

Kos Island (Pleistocene, 29 specimens) (Fig. 3.106): NHMC FS38/9, two sutured peripherals; NHMC FS38/10, peripheral; NHMC FS38/11, peripheral; NHMC FS38/12, costal; NHMC FS38/13, costal; NHMC FS38/14, hyoplastron fragment; NHMC FS38/15, possible costal fragment; NHMC FS38/16, 22 shell fragments.

Megalopolis, Peloponnesus (Pleistocene, 5 specimens)* (Fig. 3.107): AMPG 1966/45, right xiphiplastron; AMPG 1966/46, left xiphiplastron; left xiphiplastron; AMPG 1966/51, left hyoplastron; AMPG 1966/52, right hyoplastron; AMPG 1966/54, right epiplastron.

* These specimens have been published by Melentis (1966), as being part of the collections of AMPG. However, these specimens have not been located in AMPG, despite the numerous efforts of G. Theodorou & S. Roussiakis. Therefore, these descriptions are based on re-interpretations of the initial drawings of Melentis (1966).

DESCRIPTION

Gerani Cave, Crete

AMPG 852 (Fig. 3.100.A1, A3): This specimen corresponds to a complete left hypoplastron. Both the visceral and the ventral surfaces are smooth and the specimen is thin. The femoral covering on the visceral side of the hypoplastra is relatively broad, creating a convex lip. Ventrally, the specimen is crossed by the abdomino-femoral sulcus that is nearly straight to slightly concave medially and broadly convex laterally. The hypoplastra contribute significantly to the formation of the posterior lobe.

AMPG 853 (Fig. 3.100.A2, A4): This specimen corresponds to a complete right hypoplastron. Both the visceral and the ventral surfaces are smooth and the specimen is thin. The femoral covering the visceral side of the hypoplastra is relatively broad, creating a convex lip. Ventrally, the specimen is crossed by the abdomino-femoral sulcus that is nearly straight to slightly concave medially and broadly convex laterally. The hypoplastra contribute significantly to the formation of the posterior lobe.

Comments: These two specimens belong to the same individual. Based on the type of preservation the material is not fossilized and could be recent to sub-recent, as it has been also noted in the first mention of this material by Brinkerink (1996).

Rethymnon fissure

AMPG 748 (Fig. 3.100.B): This specimen is a peripheral short and wide, being crossed by the pleuro-marginal sulcus medially and the marginal sulci transversely. The peripheral is horizontally flared, resembling those in the posterior carapacial rim of a terrapin.

AMPG 749 (Fig. 3.100.C): This specimen is the lateral part of a costal. The specimen is crossed by the pleural sulci. The smooth surface is consistent with that of a terrapin and not of a tortoise.

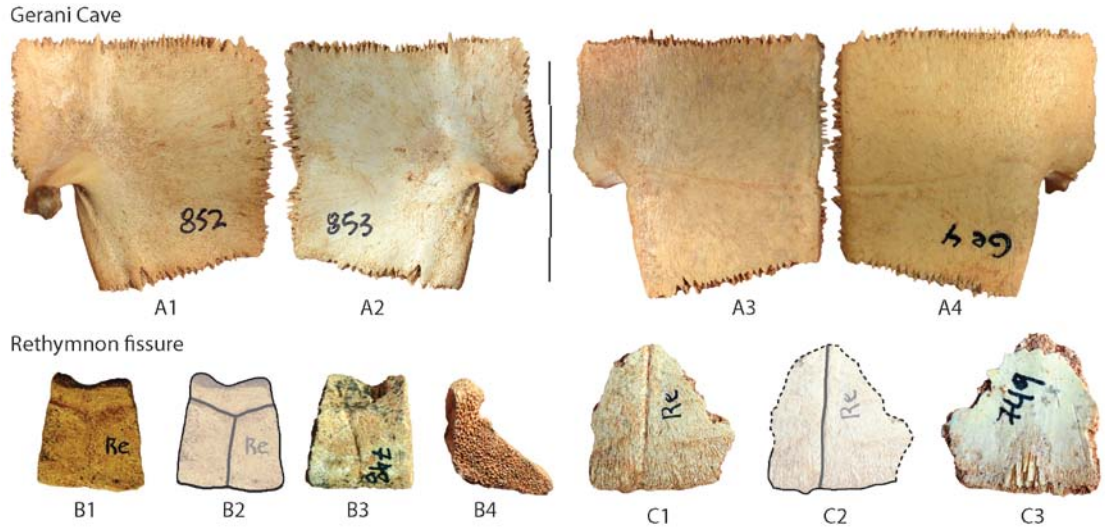


Figure 3.100. *Mauremys rivulata* Vallenciennes *in* Bory de Saint-Vincent, 1833 from Gerani Cave and Rethymnon fissure (Crete). Gerani Cave (recent): A, AMPG 852 & 853, left and right hypoplastra in (A1-2) visceral and (A3-4) ventral views. Rethymnon fissure (Pleistocene): B, AMPG 748, peripheral in (B1) dorsal, (B2) drawing of dorsal, (B3) visceral and (B4) medial views. C, AMPG 749, costal fragment in (C1) dorsal, (C2) drawing of the dorsal and (C3) visceral views. Scale bar equals 5 cm.

Koumpes Cave

AMPG 621 (Fig. 3.101.A): This specimen represents a part of the medial carapace of a terrapin. The presence of rib ends and areas of vertebrae attachments on the visceral side allow the identification of two neurals and a fragment of a costal. The anterior neural is partially preserved, whereas both are hexagonal with short anterior lateral sides. The costal articulates with both neurals, through a long suture with the anterior, and a shorter suture with the posterior one. As far as scute sulci are concerned, the limit of two vertebrals are noted, crossing the anterior neural and the costal.

AMPG 622 (Fig. 3.101.C): This specimen is the medial part of a costal, being crossed by the vertebra-pleural sulcus.

AMPG 623 (Fig. 3.101.D): This specimen is a neural. This neural is hexagonal in shape, with short anterior lateral sides, and is not crossed by any sulci.

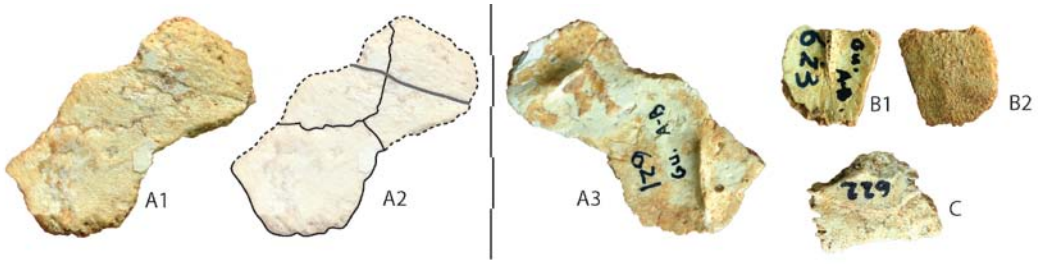


Figure 3.101. *Mauremys rivulata* Vallenciennes *in* Bory de Saint-Vincent, 1833 from the Pleistocene of Koumpes Cave (Crete). A, AMPG 621, neurals and costal fragment in (A1) dorsal, (A2) drawing of the dorsal and (A3) visceral views. B, AMPG 623, neural in (B1) visceral and (B2) dorsal views. C, AMPG 622, costal fragment in dorsal view. Scale bar equals 5 cm.

AMPG 624: This specimen is a fragment of a peripheral. Although no sulci can be observed, the small size, and the degree of flaring is consistent with the morphology of the posterior peripherals of a terrapin.

Mavro Mouri IV

AMPG 788 (Fig. 3.102.C): This specimen corresponds to a complete entoplastron. It is hexagonal, slightly longer than wide. Anteriorly is overlapped by the gular scutes.

AMPG 789 (Fig. 3.102.A): This specimen corresponds to a complete costal. The costal is hexagonal and very wide. The medial and lateral sides are of equal width. The medial side shows one long suture surface anteriorly and one short posteriorly, corresponding to hexagonal neurals. Dorsally, the limits of the vertebrals and the pleural scutes can be observed.

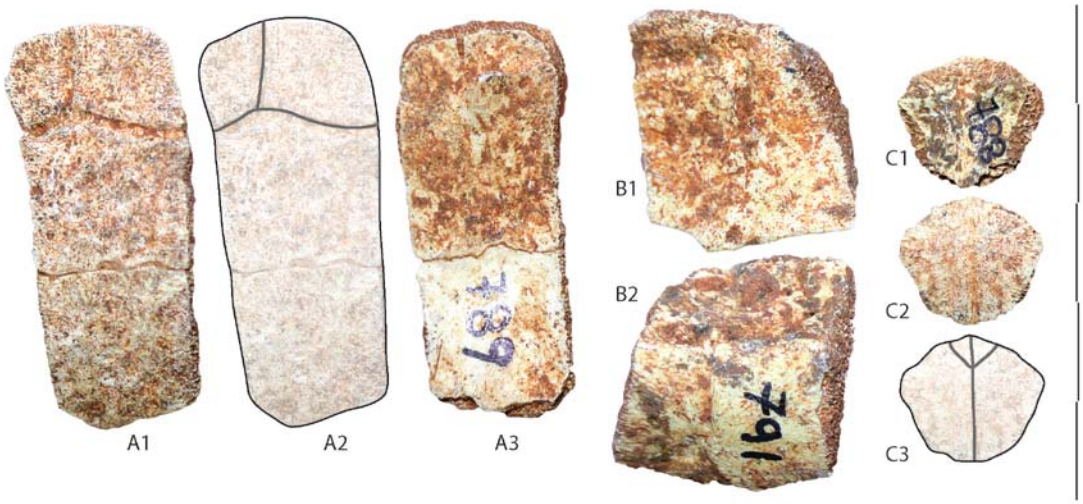


Figure 3.102. *Mauremys rivulata* Vallenciennes *in* Bory de Saint-Vincent, 1833 from the Pleistocene of Mavro Mouri IV Cave (Crete). A, AMPG 789, costal in (A1) dorsal, (A2) drawing of the dorsal and (A3) visceral views. B, AMPG 791, peripheral in (B1) dorsal and (B2) visceral views. C, AMPG 788, entoplastron in (C1) visceral, (C2) ventral and (C3) drawing of the ventral views. Scale bar equals 5 cm.

AMPG 790: This corresponds to a fragment of a costal. It is crossed transversely by the pleural sulci.

AMPG 791 (Fig. 3.102.B): This is an almost complete peripheral. It is short and moderately flared, crossed transversely by the marginal sulci. In the medial part the short overlapping of the pleural scutes is noticed.

AMPG 792: This corresponds to a fragment of a peripheral. It is short and moderately flared, crossed transversely by the marginal sulci.

AMPG 793: This corresponds to a fragment of a peripheral. It is short and moderately flared, crossed transversely by the marginal sulci.

Liko Cave, Crete

AMPG 735 (Fig. 3.103.A): This is a complete neural. It is hexagonal, with short anterior sides, not being crossed by any sulci.



Figure 3.103. *Mauremys rivulata* Vallenciennes *in* Bory de Saint-Vincent, 1833 from the Pleistocene of Liko Cave (Crete). A, AMPG 735, neural in (A1) dorsal and (A2) visceral views. B, AMPG 779, peripheral in (B1) dorsal and (B2) visceral views. C, AMPG 753, peripheral in (C1) dorsal and (C2) visceral views. D, AMPG 778, right xiphiplastron in (D1) visceral, (D2) ventral and (D3) drawing of the ventral views. E, AMPG 738, coracoid of a juvenile in dorsal view. F, AMPG 736, humerus of a juvenile in lateral view. G, AMPG 754, humerus in (G1) dorsal, (G2) posterior and (G3) ventral views. H, AMPG 739, ungual in (H1) ventral and (H2) dorsal views. Scale bar equals 5 cm.

AMPG 736 (Fig. 3.103.F): An almost complete humerus of a juvenile individual. The diaphysis is moderately curved.

AMPG 737: A diaphysis humerus of a juvenile individual that is moderately curved.

AMPG 738 (Fig. 3.103.E): An almost complete coracoid of a juvenile individual. The neck of the coracoid is narrow and long, with a wide distal end.

AMPG 739 (Fig. 3.103.H): A long and pointed ungual of a terrapin.

AMPG 753 (Fig. 3.103.C): A wide and short peripheral, being overlapped by the pleural scutes.

AMPG 754 (Fig. 3.103.G): The medial and distal part of a humerus, being moderately curved.

AMPG 778 (Fig. 3.103.D): An almost complete right xiphiplastron. The anterior part is missing. The lateral sides are converging posteriorly. Posteriorly, a deep and rounded anal notch is noted. The anals are quite long. The femoro-anal sulcus is straight, being oriented anteriorly.

AMPG 779 (Fig. 3.103.B): A complete peripheral of the bridge area. It is overlapped by the pleural scutes. Laterally, it displays a lateral ridge.

Sitia, Crete

AMPG 629 (Fig. 3.104.B): This specimen corresponds to an almost complete suprapygal 2. It is hexagonal with wider anterior part, being wider than long. The plate is also convex in shape. Dorsally is crossed by the vertebro-marginal sulci. Moreover, the presence of two marginals posteriorly (marginals 12) is noted, and the anterior part of the marginal sulcus is preserved in the posterior part of the suprapygal.

AMPG 630 (Fig. 3.104.D): This specimen corresponds to an almost complete costal plate. The medial part shows two sutured sides, one longer and one short, corresponding to hexagonal neurals. Dorsally we can observe the crossing of the vertebral and pleural sulci. The vertebrals are narrower than the pleurals.

AMPG 631 (Fig. 3.104.F): This specimen corresponds to the distal part of a costal. The costal is crossed by the pleural sulci.

AMPG 632: This specimen corresponds to a small fragment of a costal.

AMPG 633 (Fig. 3.104.E): This specimen corresponds to the medial part of a costal. Dorsally, a single sulcus is noted, crossing the plate anterio-posteriorly. Therefore, this specimen could be identified as the costal 8, from the left side. Based on the side it could correspond to a young individual.

AMPG 634: This specimen corresponds to a small costal fragment.

AMPG 635 (Fig. 3.104.Q): This specimen corresponds to a complete peripheral. It is slightly longer than wide and moderately flared. It is crossed by the marginal sulci.

AMPG 636 (Fig. 3.105.A): This specimen corresponds to an almost complete right epiplastron. The epiplastron is long and narrow. Viscerally, a thin lip is formed that is medially concave. Ventrally, the gulars are narrow and long, covering the medial part of the epiplastra and overlapping the anterior part of the entoplastron. The gularo-humeral sulcus is straight and causes a small constriction in the anterior lobe.

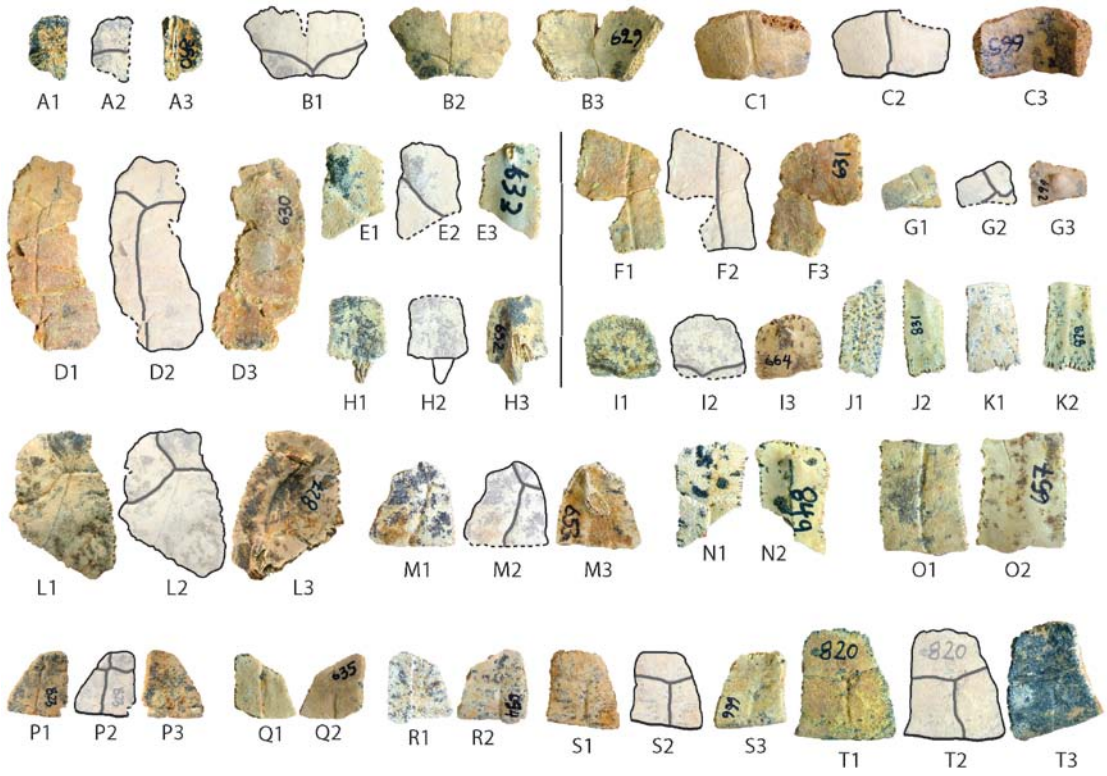


Figure 3.104. *Mauremys rivulata* Vallenciennes *in* Bory de Saint-Vincent, 1833 from the Pleistocene of Sitia (Crete). A, AMPG 850, neural in (A1) dorsal, (A2) drawing of the dorsal and (A3) visceral views. B, AMPG 629, second suprapygal in (B1) drawing of the dorsal, (B2) dorsal and (B3) visceral views. C, AMPG 665, pygal in (C1) dorsal, (C2) drawing of the dorsal and (C3) visceral views. D, AMPG 630, costal in (D1) dorsal, (D2) drawing of the dorsal and (D3) visceral views. E, AMPG 633, costal in (E1) dorsal, (E2) drawing of the dorsal and (E3) visceral views. F, AMPG 631, costal in (F1) dorsal, (F2) drawing of the dorsal and (F3) visceral views. G, AMPG 662, costal in (G1) dorsal, (G2) drawing of the dorsal and (G3) visceral views. H, AMPG 652, costal in (H1) dorsal, (H2) drawing of the dorsal and (H3) visceral views. I, AMPG 664, costal in (I1) dorsal, (I2) drawing of the dorsal and (I3) visceral views. J, AMPG 831, costal in (J1) dorsal, (J2) drawing of the dorsal and (J3) visceral views. K, AMPG 828, costal in (K1) dorsal, (K2) drawing of the dorsal and (K3) visceral views. L, AMPG 827, costal in (L1) dorsal, (L2) drawing of the dorsal and (L3) visceral views. M, AMPG 653, costal in (M1) dorsal, (M2) drawing of the dorsal and (M3) visceral views. N, AMPG 849, costal in (N1) dorsal and (N3) visceral views. O, AMPG 657, costal in (O1) dorsal and (O2) visceral views. P, AMPG 823, peripheral in (P1) dorsal, (P2) drawing of the dorsal and (P3) visceral views. Q, AMPG 635, peripheral in (Q1) dorsal and (Q2) visceral views. R, AMPG 654, peripheral in (R1) dorsal and (R2) visceral views. S, AMPG 666, peripheral in (S1) dorsal, (S2) drawing of the dorsal and (S3) visceral views. T, AMPG 820, peripheral in (T1) dorsal, (T2) drawing of the dorsal and (T3) visceral views. Scale bar equals 5 cm.

AMPG 637 (Fig. 3.105.D): This specimen corresponds to an almost complete entoplastron. It is roughly hexagonal and rounded, with a slightly wider posterior part. Anteriorly is overlapped by the gular scutes, whereas posteriorly is overlapped by the pectorals. The humerals are medially short. The humero-pectoral sulcus is nearly straight medially.

AMPG 638 (Fig. 3.105.E): This specimen corresponds to the lateral part of the right hypoplastron. The specimen is rather flat and is crossed by the abdomino-femoral sulcus.

AMPG 639: This specimen corresponds to a small hypoplastron fragment, based on the shape of the preserved part. Further description, however, is not possible.

AMPG 640: This specimen corresponds to a small plastral fragment.

AMPG 641: This specimen corresponds to a small plastral fragment.

AMPG 642: This specimen corresponds to a diaphysis of a humerus. The diaphysis is moderately curved and belongs to a slender humerus.

AMPG 643: This specimen corresponds to a diaphysis of a femur. The diaphysis is almost straight throughout its length.

AMPG 644: This specimen corresponds to a small costal fragment.

AMPG 645: This specimen corresponds to a small peripheral fragment.

AMPG 646: This specimen is very small, but most probably corresponds to a fragment of the nuchal. The sulci on the dorsal side could represent the cervical and the marginals, but the specimen is too small to allow a confident assessment.

AMPG 647: This is a part of a peripheral. The peripheral is long and narrow, being moderately flared. It is overlapped by the pleural and is crossed by the marginal sulci.

AMPG 648: This specimen corresponds to a small costal fragment.

AMPG 649 (Fig. 3.105.F): This specimen corresponds to a fragment of the left xiphiplastron. Further description is not possible, as the preserved part is small and shows no sulci.

AMPG 650: This specimen corresponds to a diaphysis of a humerus. The diaphysis is moderately curved and rather robust.

AMPG 651: This eroded specimen is part of a scapula. Further description is not possible.

AMPG 652 (Fig. 3.104.H): This specimen corresponds to the lateral part of a costal. It is not crossed by any sulci. Laterally we notice the rib end, indicating a young individual.

AMPG 653 (Fig. 3.104.M): This specimen corresponds to the medial part of a costal. Dorsally is crossed by vertebral and pleural sulci. Viscerally, it shows the attachments of the vertebra. Most probably belongs to the costal 7 or 8.

AMPG 654: This specimen corresponds to a small peripheral fragment.

AMPG 655: This specimen corresponds to a complete peripheral. It is slightly longer than wide and moderately flared. It is crossed by the marginal sulci.

AMPG 656: This specimen corresponds to a fragment of the plastron. It is a fragment of the hyo/hypoplastra, close to the bridge, as it preserves a part of the ascending processes of the bridge. However, the preserved part is too small to allow a more clear identification.

AMPG 657 (Fig. 3.104.O): This specimen corresponds to a middle part of a costal, being crossed by the pleural sulci.

AMPG 658: This specimen corresponds to the medial part of a costal plate. The medial part shows two sutured sides, one longer and one short, corresponding to hexagonal neurals. Dorsally we can observe the crossing of the vertebral and pleural sulci.

AMPG 659 – 661, 663: These specimens correspond to small costal fragments.

AMPG 662 (Fig. 3.104.G): This specimen corresponds to the medial part of a costal plate. The medial part shows two sutured sides, one longer and one short, corresponding to hexagonal neurals. Dorsally we can observe the crossing of the vertebral sulci.

AMPG 664 (Fig. 3.104.I): This specimen corresponds to the medial part of a costal plate. The medial part shows one rounded sutured surface, probably corresponding to the last neurals. Dorsally the crossing of the vertebral sulci can be observed.

AMPG 665 (Fig. 3.104.C): This specimen corresponds to an almost complete pygal plate. The pygal is strongly curved transversely. It is covered only by the marginals 12 and their limit crosses the pygal longitudinally.

AMPG 666 (Fig. 3.104.S): This specimen corresponds to a complete peripheral. The peripheral is long and narrow, being moderately flared. It is overlapped by the pleural and is crossed by the marginal sulci.

AMPG 667: This specimen corresponds to a complete peripheral. The peripheral is long and narrow, being moderately flared. It is overlapped by the pleural and is crossed by the marginal sulci.

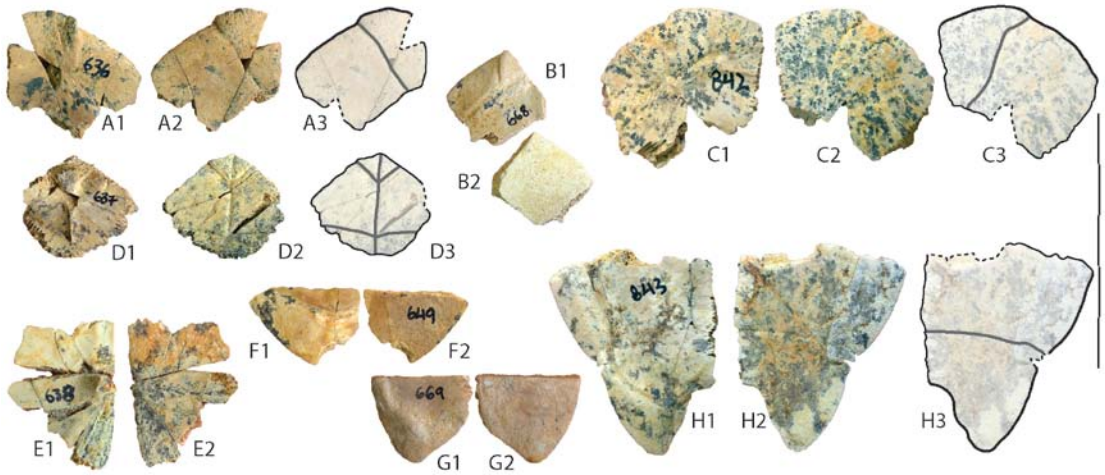


Figure 3.105. *Mauremys rivulata* Vallenciennes *in* Bory de Saint-Vincent, 1833 from the Pleistocene of Sitia (Crete). A, AMPG 636, right epiplastron in (A1) visceral, (A2) ventral and (A3) drawing of the ventral views. B, AMPG 668, left epiplastron fragment in (B1) visceral and (A2) ventral views. C, AMPG 842, left epiplastron in (C1) visceral, (C2) ventral and (C3) drawing of the ventral views. D, AMPG 637, entoplastron in (D1) visceral, (D2) ventral and (D3) drawing of the ventral views. E, AMPG 638, right hyoplastron fragment in (E1) visceral and (E2) ventral views. F, AMPG 649, left xiphiplastron fragment in (F1) visceral and (F2) ventral views. G, AMPG 669, left xiphiplastron in (G1) visceral and (G2) ventral views. H, AMPG 843, left xiphiplastron in (H1) visceral, (H2) ventral and (H3) drawing of the ventral views. Scale bar equals 5 cm.

AMPG 668 (Fig. 3.105.B): This specimen corresponds to a fragment of the left epiplastron. Ventrally no sulci are observed, whereas viscerally the gularo-humeral sulcus is noted.

AMPG 669 (Fig. 3.105.G): This specimen corresponds to the posterior part of the left xiphiplastron. Posteriorly a deep anal notch is noted. The preserved part of the xiphiplastra is not crossed by any sulci indicating that the anals had a long covering on the posterior lobe.

AMPG 670: This specimen corresponds to a small plastron fragment.

AMPG 671: This specimen corresponds to a small fragment of an hypoplastron.

AMPG 819: This specimen corresponds to a fragment of a peripheral. The peripheral is long and narrow, being moderately flared. It is overlapped by the pleurals and is crossed by the pleural and marginal sulci.

AMPG 820 (Fig. 3.104.T): This specimen corresponds to a complete peripheral. The peripheral is rather large, long and narrow, being moderately flared. It is overlapped by the pleural and is crossed by the marginal sulci.

AMPG 821: This specimen corresponds to a fragment of a peripheral. The peripheral is long and narrow, being moderately flared. It is overlapped by the pleurals and is crossed by the pleural and marginal sulci.

AMPG 822: This specimen corresponds to a complete peripheral. The peripheral is long and narrow, being moderately flared. It is overlapped by the pleurals and is crossed by the pleural and marginal sulci.

AMPG 823 (Fig. 3.104.P): This specimen corresponds to a complete peripheral. The peripheral is long and narrow, being moderately flared. It is overlapped by the pleurals and is crossed by the pleural and marginal sulci.

AMPG 824: This specimen corresponds to a complete peripheral. The peripheral is long and narrow, being moderately flared. It is overlapped by the pleurals and is crossed by the pleural and marginal sulci.

AMPG 825: This specimen corresponds to a fragment of a peripheral, from the bridge area. It is overlapped by the pleurals and is crossed by the pleural and marginal sulci.

AMPG 826: This specimen corresponds to a fragment of a peripheral. The peripheral is long and narrow, being moderately flared. It is crossed by the marginal sulci.

AMPG 827 (Fig. 3.104.L): This specimen corresponds to a complete costal. The plate is long and narrow. Dorsally a wide covering of the vertebrals and no pleural sulci are observed. Viscerally, the presence of the rib end is noticed. Based on the outline of the plate, this is the left costal 1.

AMPG 828 (Fig. 3.104.K): This specimen corresponds to the middle part of a costal. It is not crossed by any sulci.

AMPG 829: This specimen corresponds to the medial part of a costal plate. The medial part shows two sutured sides, one longer and one short, corresponding to hexagonal neurals. Dorsally the crossing of the vertebral sulci is observed. Viscerally the rib end is noticed.

AMPG 830: This specimen corresponds to the medial part of a costal. It is crossed by the pleural sulcus.

AMPG 831 – 833 (Fig. 3.104.J): These specimens correspond to the middle part of a costal. It is crossed by the pleural sulcus.

AMPG 834: This specimen corresponds to a small plastron fragment.

AMPG 835: This specimen corresponds to a fragment of a peripheral, from the bridge area. It is overlapped by the pleurals and is crossed by the pleural and marginal sulci.

AMPG 836: This specimen corresponds to an hyoplastral fragment. It is the part of the bridge, preserving the axillary process.

AMPG 837: This specimen corresponds to a small costal fragment.

AMPG 838 – 841: These specimens correspond to small plastral fragments.

AMPG 842 (Fig. 3.105.C): This specimen corresponds to an almost complete left epiplastron. Anteriorly, a shallow notch is noted. The epiplastron is long and narrow. Viscerally, a thin lip is formed that is medially concave. Ventrally, the gulars are narrow and long, covering the medial part of the epiplastra and overlapping the anterior part of the entoplastron. The gularo-humeral sulcus is curved and causes a small constriction in the anterior lobe.

AMPG 843 (Fig. 3.105.H): This specimen corresponds to an almost complete left xiphiplastron. The lateral sides of the posterior lobe are converging posteriorly. On the posterior part, a deep and rounded anal notch is noted. The xiphiplastral extremities are rather pointed. The femorals cover the anterior part of the xiphiplastron, whereas the anals show a long covering on the posterior part of the lobe. The femoro-anal sulcus is straight, being oriented transversely.

AMPG 844: This specimen corresponds to a small peripheral fragment.

AMPG 845: This specimen corresponds to a small neural fragment.

AMPG 846: This specimen corresponds to a small costal fragment.

AMPG 847 – 848: These specimens correspond to small fragment of the hyoplastron.

AMPG 849 (Fig. 3.104.N): This specimen corresponds to the medial part of a costal plate. The medial part shows two sutured sides, one longer and one short, corresponding to hexagonal neurals. Dorsally the crossing of the vertebral sulci is observed. Based on the size it is presumed to be a young individual.

AMPG 850 (Fig. 3.104.A): This specimen corresponds to a part of a neural. The neural is rounded in shape, and is crossed by the vertebral sulci. Dorsally, the crossing of the vertebral sulci is seen.

AMPG 851: This specimen corresponds to a small fragment of a costal.

Kos Island

NHMC FS38/9 (Fig. 3.106.B): This specimen consists of two continuous peripherals in anatomical connection. The peripherals are short and wide, being crossed by the pleuro-marginal sulcus medially and the marginal sulci transversely.

NHMC FS38/10 (Fig. 3.106.C): This specimen is a complete peripheral. It is crossed by the pleuro-marginal sulcus medially and the marginal sulci transversely.

NHMC FS38/11 (Fig. 3.106.D): This specimen is a complete peripheral, probably from the anterior part. It is crossed by the pleural sulci medially, by the pleuro-marginal sulcus longitudinally and the marginal sulci transversely.

NHMC FS38/12 (Fig. 3.106.A): This specimen is an almost complete costal, with only the lateral part missing. It is shorter medially, and longer laterally. In the medial part it shows a concave suture. This could be possibly for the suprapygal. Therefore

this could be the last costal of the shell of a terrapin. It is crossed by the vertebral and pleural sulci.

NHMC FS38/13: This specimen is small and fragmented. The overall morphology is consistent with the morphology of a costal of a terrapin, but further description is not possible.

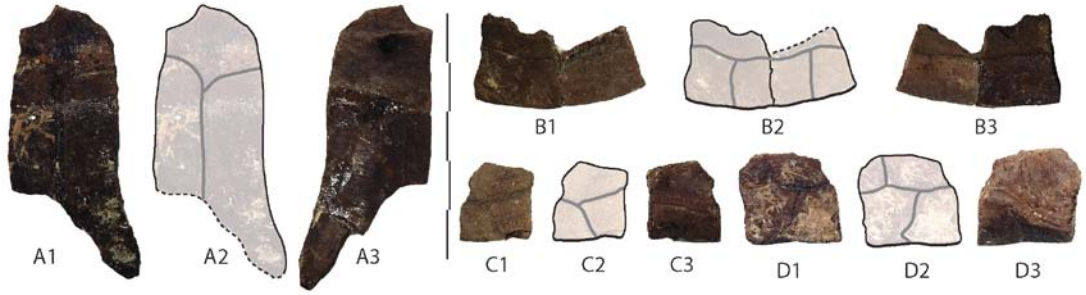


Figure 3.106. *Mauremys rivulata* Vallenciennes *in* Bory de Saint-Vincent, 1833 from the Pleistocene of Kos Island. A, NHMC FS38/12, costal in (A1) dorsal, (A2) drawing of a dorsal and (A3) visceral views. B, NHMC FS38/9, peripherals in (B1) dorsal, (B2) drawing of a dorsal and (B3) visceral views. C, NHMC FS38/10, peripheral in (C1) dorsal, (C2) drawing of a dorsal and (C3) visceral views. D, NHMC FS38/11, peripheral in (D1) dorsal, (D2) drawing of a dorsal and (D3) visceral views. Scale bar equals 5 cm.

NHMC FS38/14: This small specimen resembles the morphology of a plastral fragment and most probably a part of the hyoplastron. The smooth ventral surface is consistent with a terrapin and not with a tortoise.

NHMC FS38/15: This specimen is small and fragmented. The overall morphology is consistent with the morphology of a costal of a terrapin, but further description is not possible.

NHMC FS38/16: Twenty-two (22) fragments of the shell are preserved. They are too small to allow any further identification, but their size and morphology is consistent with that of a terrapin.

Megalopolis, Peloponnesus

AMPG 1966/45 (Fig. 3.107.D; see also Fig. 2A in Melentis, 1966): This specimen corresponds to a complete right xiphiplastron. The plate is crossed by the femoro-anal sulcus in the posterior half of the plate. The femoro-anal sulcus causes a significant constriction laterally. Posteriorly, a wide and angular notch is noted.

AMPG 1966/46 (Fig. 3.107.E; see also Fig. 2B in Melentis, 1966): This specimen corresponds to a complete left xiphiplastron. It is crossed by the femoro-anal sulcus that appears to be rather curvy in morphology. The femoro-anal sulcus causes a significant constriction laterally. Posteriorly, a notch is noted, but it is much narrower and deeper than the anal notch of specimen AMPG 1966/45.

AMPG 1966/51 (Fig. 3.107.B; see also Fig. 5A in Melentis, 1966): This specimen corresponds to an almost complete right hyoplastron, with only some lateral and some medial parts missing. The plate is slightly longer than wide. It is crossed by the

humero-pectoral sulcus anteriorly and by the pectoro-abdominal sulcus posteriorly. Based on the preserved parts of the hyoplastron it can be estimated that the entoplastron was rather wide and crossed by the humero-pectoral sulcus posteriorly.

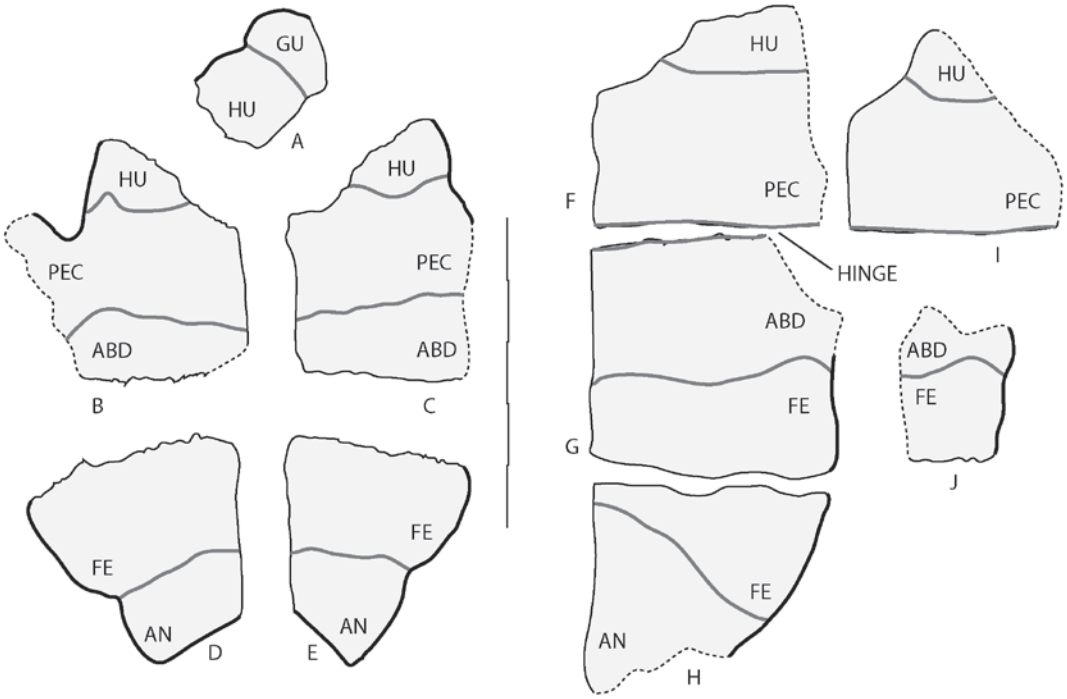


Figure 3.107. Fossil turtle material from the Pleistocene of Megalopolis (Peloponnesus). *Mauremys rivulata* Vallenciennes *in* Bory de Saint-Vincent, 1833: A, AMPG 1966/54, right epiplastron. B, AMPG 1966/51, right hyoplastron. C, AMPG 1966/52, left hyoplastron. D, AMPG 1966/45, right xiphiplastron. E, AMPG 1966/46, left xiphiplastron. *Emys orbicularis* Linnaeus, 1758: F, AMPG 1966/47, left hyoplastron. G, AMPG 1966/48, left hypoplastron. H, AMPG 1966/49, left xiphiplastron. I, AMPG 1966/53, left hyoplastron. J, AMPG 1966/50, left hypoplastron. Scale bar equals 5 cm. Modified from the drawings of the ventral views by Melentis (1966).

AMPG 1966/52 (Fig. 3.107.C; see also Fig. 5B in Melentis, 1966): This specimen corresponds to an almost complete left hyoplastron, with only some lateral parts missing. The plate is significantly longer than wide. It is crossed by the humero-pectoral sulcus anteriorly and by the pectoro-abdominal sulcus posteriorly. Based on the preserved parts of the hyoplastron it can be estimated that the entoplastron was rather wide and has been crossed by the humero-pectoral sulcus posteriorly.

AMPG 1966/54 (Fig. 3.107.A; see also Fig. 7 in Melentis, 1966): This specimen corresponds to a complete right epiplastron. It is as long as wide, reconstructing a rather rounded anterior lobe, showing small constrictions in the gularo-humeral sulcus and anteriorly. The gulars are narrow and wide, overlapping the anterior part of the entoplastron.

DISCUSSION

The phylogeography of the *Mauremys* complex has been recently reviewed by Fritz et al. (2008). In the area of south Balkans, Middle East and Caspian regions two species occur, *M. caspica* and *M. rivulata*. These two taxa have been considered

synonymous but considerable mtDNA differentiation confirms their treatment as full species (Fritz et al., 2008 and references therein). As it is shown in Fritz et al. (2008:Fig. 2), the differences between the two species are practically in the coloration of the plastron, whereas their morphological differences in the suture/sulci pattern are very small. In Greece and in the coastal region of Minor Asia only *Mauremys rivulata* occurs.

Although limited, the specimens presented above allow a safe attribution to the geoemydid *Mauremys* based on the entoplastron being crossed by the gulars anteriorly and by the humero-pectoral sulcus posteriorly, as well as the deep anal notch. The overall similarity (both metrically and morphologically) with extant and extinct members of *M. rivulata*, and the fact that the specimens are of Pleistocene age leaves no room for questioning the attribution to *M. rivulata*. The presence of *M. rivulata* during the Pleistocene is within the extant geographic range of this taxon.

Besides the specimens described above, the presence of *M. rivulata* in the Pleistocene of Crete has been mentioned from Simonelli Cave (note in Kotsakis, 1977) and during the Holocene in Vraona Cave (Rauscher, 1995).

As *M. rivulata* is considered to be adapted to a warm Mediterranean climate, contrary to the adaptation of *M. caspica* to a winter-cold continental climate (Fritz & Wischuf, 1997), its significant presence in the Pleistocene record suggests milder conditions for the South Balkans during the Pleistocene times.

***Mauremys* sp.**

AGE: Late Miocene – Late Pliocene.

MATERIAL:

Milia, Grevena, W. Macedonia (Late Pliocene; 6 specimens) (Fig. 3.108): MIL 818, right hypoplastron; MIL 981, left epiplastron; MIL 1847, left epiplastron; MIL 1927, right hyoplastron fragment; MIL 1928, left epiplastron; MIL 1939, neural; MIL 1940, left hyoplastron fragment.

Plakias, Crete (Late Miocene; 150+ specimens) (Fig. 3.109): NHMC FS38/43, part of anterior lobe; NHMC FS38/44, right xiphiplastron; NHMC FS38/45, left hypoplastron; NHMC FS38/46, group of 15 plastral fragments; NHMC FS38/47, neural; NHMC FS38/48, neural; NHMC FS38/49, neural; NHMC FS38/50, left hyoplastron fragment; NHMC FS38/51, left hypoplastron fragment; NHMC FS38/52, right hypoplastron fragment; NHMC FS38/53, costal fragment; NHMC FS38/54, right hypoplastron fragment; NHMC FS38/55, costal fragment; NHMC FS38/56, costal fragment; NHMC FS38/57, left epiplastron; NHMC FS38/58, left hyoplastron fragment; NHMC FS38/59, group of 23 shell fragments; NHMC FS38/60, right epiplastron; NHMC FS38/61, left epiplastron; NHMC FS38/62, left epiplastron; NHMC FS38/63, costal fragment; NHMC FS38/64, costal fragment; NHMC FS38/65, two costals in association; NHMC FS38/66, right peripheral 1; NHMC FS38/67, right xiphiplastron fragment; NHMC FS38/68, right hypoplastron fragment; NHMC FS38/69, left hyoplastron fragment; NHMC FS38/70, costal fragment; NHMC FS38/71, costal fragment; NHMC FS38/72, costal fragment; NHMC FS38/73, group of appr. 80 shell fragments; NHMC FS38/74, neural fragment; NHMC FS38/75, group of 10 shell fragments; NHMC FS38/76, neural 1; NHMC

FS38/77, costal fragment; NHMC FS38/78, costal fragment; NHMC FS38/79, costal fragment; NHMC FS38/80, costal fragment; NHMC FS38/81, costal fragment; NHMC FS38/82, costal fragment; NHMC FS38/83, costal fragment; NHMC FS38/84, costal fragment; NHMC FS38/85, costal fragment; NHMC FS38/86, costal fragment; NHMC FS38/87, costal fragment; NHMC FS38/88, costal fragment; NHMC FS38/89, costal fragment; NHMC FS38/90, costal fragment; NHMC FS38/91, peripheral fragment; NHMC FS38/92, peripheral fragment; NHMC FS38/93, peripheral fragment; NHMC FS38/94, group of 50 shell fragments.

Milia, Grevena, W. Macedonia

MIL 818 (Fig. 3.108.E): The specimen corresponds to a fragment of the right hypoplastron. The posterior side corresponds to the slightly convex suture with the xiphiplastron. Viscerally, there is a wide covering of the femoral scutes. Ventrally, no sulci are noted indicating that the preserved surface was covered only by the femorals.

MIL 981 (Fig. 3.108.D): This specimen corresponds to a complete left epiplastron. The epiplastron is long and narrow. Viscerally, a long lip is formed, being concave medially. The gular scutes are wide and long, overlapping the anterior part of the entoplastron. The gularo-humeral sulcus is slightly curved. The length of the medial suture of the epiplastra is 21 mm, the maximum width is 44 mm.

MIL 1847 (Fig. 3.108.B): This specimen corresponds to a complete left epiplastron. The epiplastron is long and rather narrow. Viscerally, a long lip is formed, being concave medially and convex laterally. The gular scutes are narrow and long, overlapping the anterior part of the entoplastron. The gularo-humeral sulcus is slightly convex, and causes a slight constriction in the anterior part of the lobe. Therefore, the anterior part of the lobe is protruding. This specimen shows a remarkable size. The length of the medial suture of the epiplastra is 34 mm, the maximum width is 54 mm. This suggests that the width of the anterior lobe could reach 11 cm, making this terrapin among the largest known.

MIL 1927 (Fig. 3.108.F): This specimen corresponds to a fragment of the right hyoplastron. Ventrally, part of a sulcus is noted, probably of the humero-pectoral sulcus.

MIL 1928 (Fig. 3.108.C): This specimen corresponds to an almost complete left epiplastron. The epiplastron is long and narrow. The gular scutes are narrow and long, overlapping the anterior part of the entoplastron. The gularo-humeral sulcus is almost straight. The length of the medial suture of the epiplastra is 21 mm.

MIL 1939 (Fig. 3.108.A): This specimen corresponds to an almost complete neural. The neural is hexagonal in shape, with short anterior lateral processes. The anterior part of the neural is wider than the posterior one. It is not crossed by any sulci.

MIL 1940 (Fig. 3.108.G): This specimen corresponds to a fragment of the left hyoplastron. No sulci are noted in the preserved part and further description is not possible.

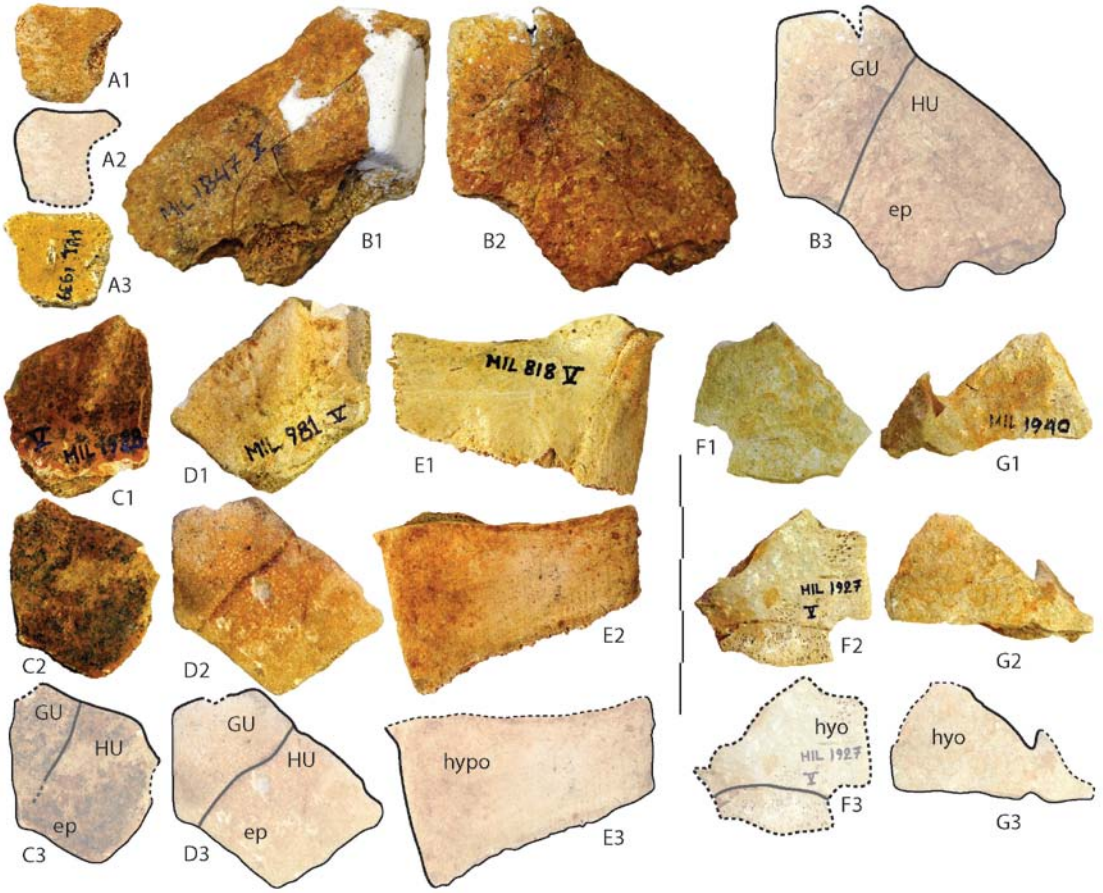


Figure 3.108. *Mauremys* sp. from the Late Pliocene of Milia (Grevena). A, MIL 1939, neural in (A1) dorsal, (A2) drawing of the dorsal and (A3) visceral views. B, MIL 1847, left epiplastron in (B1) visceral, (B2) ventral and (B3) drawing of the ventral views. C, MIL 1928, left epiplastron in (C1) visceral, (C2) ventral and (C3) drawing of the ventral views. D, MIL 981, left epiplastron in (D1) visceral, (D2) ventral and (D3) drawing of the ventral views. E, MIL 818, right hypoplastron in (E1) visceral, (E2) ventral and (E3) drawing of the ventral views. F, right hyoplastron in (F1) visceral, (F2) ventral and (F3) drawing of the ventral views. G, MIL 1940, left hyoplastron in (G1) visceral, (G2) ventral and (G3) drawing of the ventral views. Scale bar equals 5 cm. For abbreviations see Material & Methods.

Comments: The geoemydid material from Milia is relatively scarse and the most diagnostic preserved element is the epiplastron. Fortunately this is also the most common element in the Milia assemblage. The presence of a shallow notch, the constriction in the gularo-humeral sulcus, and the presence of a pointed tip on the visceral surface of the epiplastron, associated the Milia material with the geoemydid *Mauremys* as opposed to emydids. In emydids, the anterior lobe is wheel-rounded and there is less coverage of the gulars viscerally. Identification to the specific level is not possible based on the preserved material. One of the most important observations in the Milia *Mauremys* remains is the size of the specimens. Especially specimen MIL 1847 is, to the extent of my knowledge, among the biggest epiplastra attributed to *Mauremys*. From the literature, Melentis (1966) provides some medial lengths of a recent *M. (Clemmys) caspica* (18,3mm), *Clemmys steinheimensis* (17,5 - 14 - 16,5mm). Both specimens from Milia are larger. MIL 981 has a medial length of 22mm, while MIL 1847 reaches a length of 34,9mm. Gigantic proportions are evident among the animals from Milia, as emphasized by the presence of one of the largest mastodons that ever lived (Tsoukala, 2000; Tsoukala & Mol, in press).

Plakias, Crete

The material from the Late Miocene site of Plakias in South Crete consists of numerous shell fragments of good preservation. Many specimens preserve enough information to be identified, but several are so small that remain identifiable. The description of the identifiable specimens is given below, whereas the unidentifiable shell fragments are grouped together according to size and morphology.

NHMC FS38/43 (Fig. 3.109.K): This specimen corresponds to the right part of the anterior lobe, consisting of the right epiplastron and most of the entoplastron. The epiplastron is long and narrow. Viscerally, a long lip is formed, being concave medially and convex laterally. Anteriorly, a shallow notch is noted. The entoplastron is hexagonal and rounded, being wider posteriorly. The gular scutes are wide and long, overlapping the anterior part of the entoplastron. The gularo-humeral sulcus is slightly convex laterally, and causes a slight constriction in the anterior part of the lobe. The humerals are medially short and laterally longer. The entoplastron is also overlapped by the anterior part of the pectorals. The humero-pectoral sulcus is slightly concave medially.

NHMC FS38/44 (Fig. 3.109.Q): This specimen corresponds to an almost complete left xiphiplastron. The lateral sides of the posterior lobe are converging posteriorly. On the posterior part, a deep and wide anal notch is formed. The xiphiplastral extremities are rounded. The femorals cover the anterior part of the xiphiplastron, whereas the anals show a somewhat long covering on the posterior part of the lobe. The femoro-anal sulcus is slightly convex, being oriented antero-medially.

NHMC FS38/45 (Fig. 3.109.O): This specimen corresponds to an almost complete left hypoplastron. The anterior suture with the hyoplastron is straight, whereas the posterior with the xiphiplastron is slightly convex. The hypoplastron is rather flat. Viscerally, the abdominal forms a wide and slightly convex lip on the posterior lobe. Ventrally, an unusual morphology is noticed. Although the posterior part of the hypoplastron is covered by the abdominal scute, anteriorly there is another sulcus. Normally the hypoplastron is only crossed by the abdomino-femoral sulcus. The double sulci on this hypoplastron can be explained in two ways: first, this could be an anomaly in the growth of the scutes. Second, this could indicate longer pectorals, that are expanded posteriorly to the hypoplastron. This morphology has not been documented so far in a fossil and extant terrapin.

NHMC FS38/46: A group of 15 plastral fragments, small in size.

NHMC FS38/47 (Fig. 3.109.B): This specimen corresponds to a complete neural. It is hexagonal with short anterior lateral sides. It is crossed by the vertebral sulci in the posterior part.

NHMC FS38/48 (Fig. 3.109.A): This specimen corresponds to a complete neural. It is hexagonal with short anterior lateral sides. It is not crossed by any vertebral sulci.

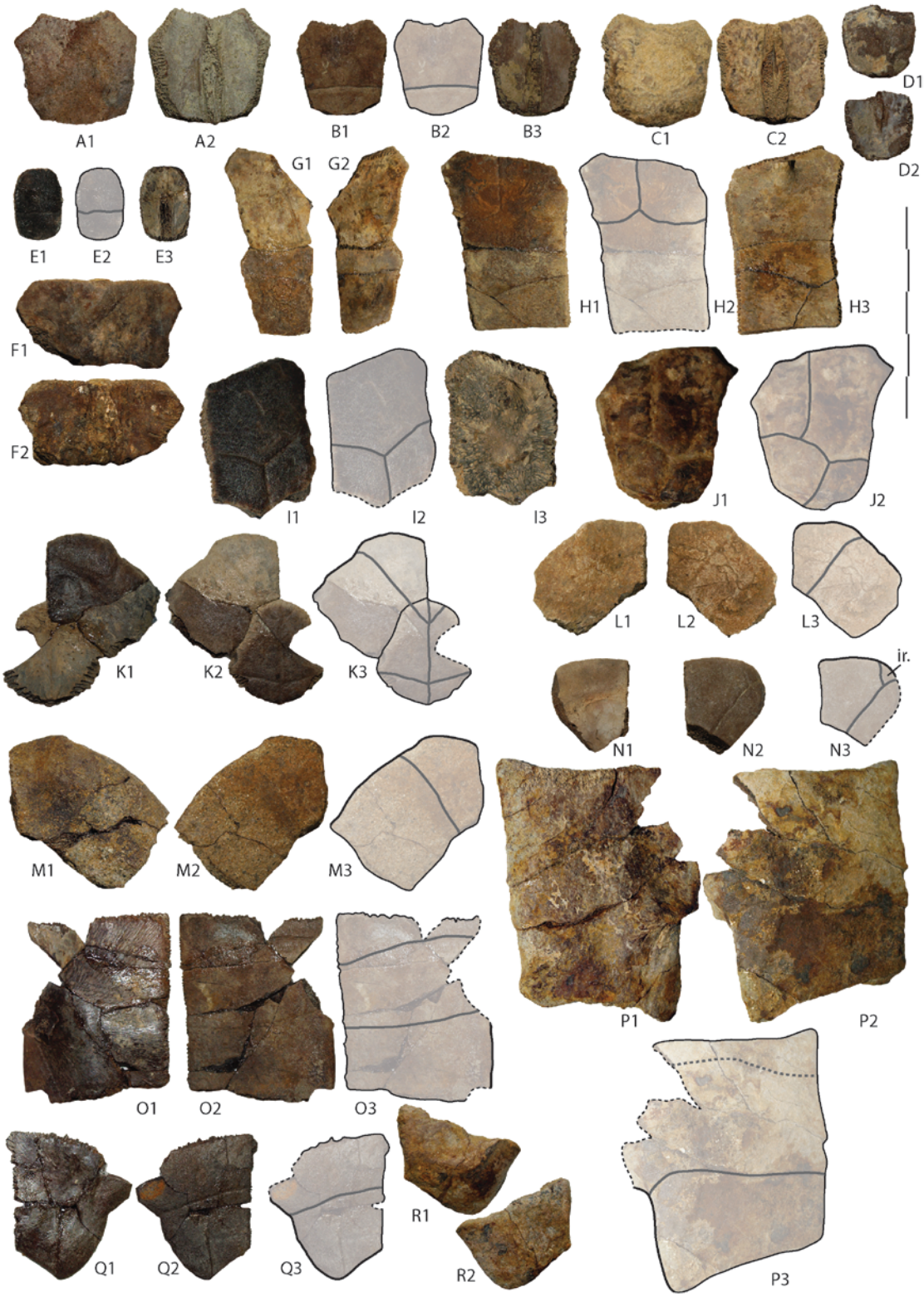


Figure 3.109. *Mauremys* sp. from the Late Miocene of Plakias (Crete Island). NHMC FS/38 collection: A, neural in (A1) dorsal and (A2) visceral views. B, neural in (B1) dorsal, (B2) drawing of the dorsal and (B3) visceral views. C, neural in (C1) dorsal and (C2) visceral views. D, neural in in (D1) dorsal and (D2) visceral views. E, neural in (E1) dorsal, (E2) drawing of the dorsal and (E3) visceral views. F, neural fragment in (F1) dorsal (F3) visceral views. G, two successive neurals in (G1) dorsal and (G2) visceral views. H, costal in (H1) dorsal, (H2) drawing of the dorsal and (H3) visceral

views. I, costal fragment in (I1) dorsal, (I2) drawing of the dorsal and (I3) visceral views. J, peripheral in (J1) dorsal and (J2) drawing of the dorsal views. K, right epiplastron and entoplastron in (K1) visceral, (K2) ventral and (K3) drawing of the ventral views. L, left epiplastron in (L1) visceral, (L2) ventral and (L3) drawing of the ventral views. M, right epiplastron in (M1) visceral, (M2) ventral and (M3) drawing of the ventral views. N, left epiplastron fragment in (N1) visceral, (N2) ventral and (N3) drawing of the ventral views. O, left hypoplastron in (O1) visceral, (O2) ventral and (O3) drawing of the ventral views. P, right hypoplastron in (P1) visceral, (P2) ventral and (P3) drawing of the ventral views. Q, right xiphiplastron in (Q1) visceral, (Q2) ventral and (Q3) drawing of the ventral views. R, right xiphiplastron fragment in (B1) visceral and (B2) ventral views. Scale bar equals 5 cm. Abbreviations: ir, irregular scute growth.

NHMC FS38/49 (Fig. D): This specimen corresponds to a complete neural. It is quadrangular to rounded, with slightly wider anterior part. It is not crossed by any vertebral sulci. A dorsal keel is noted longitudinally.

NHMC FS38/50: This specimen probably corresponds to a left hyoplastron fragment. It is crossed by a sulcus, but the preserved specimen does not preserve any information on the sutures. Therefore, this sulcus cannot be identified with confidence.

NHMC FS38/51: This specimen corresponds to a fragment of the left hypoplastron. The specimen is rather flat. It is crossed by the abdomino-femoral sulcus.

NHMC FS38/52: This specimen corresponds to a fragment of the right hypoplastron. Part of the posterior suture with the xiphiplastron is noted. The preserved part is not crossed by any sulcus.

NHMC FS38/53: This specimen corresponds to a small fragment of a costal plate. The inserted rib can be observed viscerally. No sulci are observed.

NHMC FS38/54: This specimen corresponds to a fragment of the right hypoplastron. The specimen is flat and preserves a part of the abdomino-femoral sulcus.

NHMC FS38/55: This specimen corresponds to a costal fragment, showing a small part of the vertebro-pleural sulcus.

NHMC FS38/56: This specimen corresponds to a costal fragment, being crossed by the vertebro-pleural sulcus.

NHMC FS38/57 (Fig. 3.109.N): This specimen corresponds to an almost complete left epiplastron. The epiplastron is rather long and wide. Viscerally a short and slightly concave lip is formed. It is covered medially by the gulars. An irregular growth of a small scute is noted in the anterior end of the gularo-humeral sulcus.

NHMC FS38/58: A fragment of the plastron, probably corresponding to the left hyoplastron. The preserved part is not crossed by any sulci.

NHMC FS38/59: A group of 23 small, unidentified fragments of the shell.

NHMC FS38/60 (Fig. 3.109.M): This specimen corresponds to the right epiplastron. The epiplastron is long and rather wide. Viscerally, a long lip is formed, being concave medially and convex laterally. The gular scutes are wide and long, overlapping the anterior part of the entoplastron. The gularo-humeral sulcus is slightly convex laterally, and causes a slight constriction in the anterior part of the lobe.

NHMC FS38/61: This specimen corresponds to an almost complete left epiplastron. The epiplastron is long and rather wide. Viscerally, a long lip is formed, being concave medially and convex laterally. The gular scutes are wide and long, overlapping the anterior part of the entoplastron. The gularo-humeral sulcus is slightly convex laterally, and causes a significant constriction in the anterior part of the lobe.

NHMC FS38/62 (Fig. 3.109.L): This specimen corresponds to the left epiplastron. The epiplastron is long and rather wide. Viscerally, a long lip is formed, being concave medially and convex laterally. The gular scutes are wide and long, overlapping the anterior part of the entoplastron. The gularo-humeral sulcus is slightly convex laterally.

NHMC FS38/63 (Fig. 3.109.H): This specimen corresponds to an almost complete costal, missing only the distal part. The medial side shows two sutured surfaces, one long and the other short, corresponding to an hexagonal neural. Dorsally, the sulci between the vertebrals and the pleurals cross the medial part of this costal.

NHMC FS38/64 (Fig. 3.109.I): This specimen corresponds to the medial part of a costal. The medial side shows two sutured surfaces, one long and the other short, corresponding to an hexagonal neural. Dorsally, the sulci between the vertebrals and the pleurals cross the medial part of this costal.

NHMC FS38/65 (Fig. 3.109.G): This specimen corresponds to two successive costals in association. Both show the long and short medial sutures for the corresponding hexagonal neurals. In the preserved part the sulci between the vertebrals and the pleurals can be observed.

NHMC FS38/66 (Fig. 3.109.J): This specimen corresponds to a complete right peripheral 1. Based on the preserved anterior border we can estimate the presence of a wide nuchal notch affecting also the first peripherals. The peripheral is long and narrow. Medially the vertebral 1 and the pleural 1 overlap the peripheral. Also, the sulci between the first two marginals are noted.

NHMC FS38/67 (Fig. 3.109.R): This specimen corresponds to a fragment of the right xiphiplastron. Based on the preserved part, the presence of a wide angular anal notch can be estimated. In the anterior part, a short part of the femoro-anal sulcus is noted.

NHMC FS38/68 (Fig. 3.109.P): This specimen corresponds to an almost complete right hypoplastron. The anterior suture with the hyoplastron is straight, whereas the posterior with the xiphiplastron is slightly convex. The hypoplastron is rather flat. Viscerally, the abdominal forms a wide and slightly convex lip on the posterior lobe. The ventral surface is eroded and therefore the unusual morphology noted in the other

specimen of the left hypoplastron cannot be confidently confirmed. In the posterior part the abdomino-femoral sulcus is clearly visible, whereas in the anterior part the sulcus is not clear as a result of erosion.

NHMC FS38/69: A fragment of the plastron, probably corresponding to the left hyoplastron. The preserved part is not crossed by any sulci.

NHMC FS38/70 – 72: These specimens correspond to a costal fragments, not crossed by any sulci.

NHMC FS38/73: A group of approximately 80 shell fragments.

NHMC FS38/74 (Fig. 3.109.F): This specimen corresponds to a fragment of a neural. It is much wider than long, hexagonal in shape, with shorter anterior lateral sides. Viscerally the attachment for the vertebra is noted. As it is not crossed by any sulci, it could be either the neural 6 or 7.

NHMC FS38/75: A group of 10 small shell fragments.

NHMC FS38/76 (Fig. 3.109.E): This specimen corresponds to a complete neural 1. It is quadrangular with rounded edges, being longer than wide. The posterior part is crossed by the vertebral sulcus that is not straight.

NHMC FS38/77: This specimen corresponds to a small fragment of a costal plate. The inserted rib can be observed viscerally. No sulci are observed.

NHMC FS38/78: This specimen corresponds to a fragment of the medial part of a costal plate, being crossed by the vertebro-pleural sulcus. It connects with an hexagonal neural.

NHMC FS38/79: This specimen corresponds to a fragment of the medial part of a costal plate, being crossed by the vertebro-pleural sulcus. It connects with an hexagonal neural.

NHMC FS38/80: This specimen corresponds to a fragment of the medial part of a costal plate, being crossed by the vertebro-pleural sulcus. It connects with an hexagonal neural.

NHMC FS38/81: This specimen corresponds to a fragment of the medial part of a costal plate, being crossed by the vertebro-pleural sulcus. It connects with an hexagonal neural.

NHMC FS38/82 – 86: These specimens correspond to fragments of the middle part of a costal plate, being crossed by the pleural sulcus.

NHMC FS38/87: This specimen corresponds to a fragment of the medial part of a costal plate, being crossed by the vertebro-pleural sulcus. It connects with an hexagonal neural.

NHMC FS38/88: This specimen corresponds to a small fragment of a costal plate. The inserted rib can be observed viscerally. No sulci are observed.

NHMC FS38/89: This specimen corresponds to a small fragment of a costal plate. The inserted rib can be observed viscerally. No sulci are observed.

NHMC FS38/90: This specimen corresponds to a small fragment of a costal plate. The inserted rib can be observed viscerally. No sulci are observed.

NHMC FS38/91 – 92: These specimens correspond to a small fragment of peripherals. No sulci are observed in the preserved part.

NHMC FS38/93: This specimen corresponds to a fragment of a peripheral, being longer than wide. The marginal sulci are observed in the preserved part.

NHMC FS38/94: A group of 50 shell fragments.

DISCUSSION: Brinkerink (1996) reports that no turtles are known in Crete prior to the Pleistocene. This has been also noted in the bibliographic review of Georgalis & Kear (2013). Therefore the findings from the early Late Miocene of Plakias in South Crete are of particular importance, being the first pre-Pleistocene chelonians from Crete, joining a list of few Greek Late Miocene localities with fossil terrapins. This is also the oldest occurrence of a geoemydid in Greece.

Several characters, such as the entoplastron being crossed by the gulars and the humero-pectoral sulcus and the deep anal notch allow attribution to the Geoemydidae. The preserved material is similar to the known specimen of the only extant and extinct geoemydid genus present in Greece, *Mauremys*, but based on the preserved specimens no further identification is possible.

At the same time, the study of the isolated plates from Plakias has revealed an unusual morphology. The two hypoplastra that are preserved (the one well-preserved and the other partly eroded) provide evidence of long pectorals that are expanded into the hypoplastra. Although the preserved sample is too small to exclude a possible abnormal growth of scutes, the limited available information of the hyoplastra of Plakias seems to agree with the idea of long pectorals in this taxon. The preserve parts have showed only crossing of the humero-pectoral sulcus or no evidence of sulci at all. Based on all the available evidence, it seems likely that the pectorals were indeed long in the terrapin from Plakias. If this is true, then this is a novel morphology for the fossil and extant terrapins. So far, all the known specimens of *Mauremys* have pectorals, either being within the hyoplastra (the majority of extant and extinct terrapins) or coinciding with the hyo-hypoplastral suture medially (e.g. *Mauremys portisii*, see Chesi 2008:Plate 20).

***Mauremys* sp. nov**

Nea Silata (Late Miocene/Early Pliocene; 200+ specimens) (Fig. 3.110-3.112): SLT 1, nuchal; SLT 2, peripheral; SLT 3, first neural; SLT 4, neural; SLT 5, pygal; SLT 7, peripheral; SLT 8, peripheral fragment; SLT 9, costal fragment; SLT 10, peripheral fragment; SLT 11, peripheral fragment; SLT 12, costal fragment; SLT 13, peripheral; SLT 14, costal, juvenile; SLT 15, peripheral; SLT 16, peripheral; SLT 17, left costal; SLT 18, peripheral; SLT 19, peripheral; SLT 20, left costal 7; SLT 21, right costal 7; SLT 22, peripheral fragment, juvenile; SLT 23, peripheral; SLT 24, nuchal fragment; SLT 26, costal fragment; SLT 28, costal fragment; SLT 29, costal fragment; SLT 32, peripheral fragment; SLT 34, peripheral, juvenile; SLT 36, peripheral; SLT 38, costal fragment; SLT 41, peripheral; SLT 42, peripheral; SLT 43, costal fragment; SLT 44, peripheral; SLT 45, plastron fragment; SLT 47, peripheral fragment; SLT 48, left hypoplastron fragment; SLT 49, left xiphiplastron; SLT 50, left xiphiplastron; SLT 51, right epiplastron; SLT 52, entoplastron; SLT 53, right hyoplastron; SLT 54, right xiphiplastron; SLT 55, right xiphiplastron; SLT 56, left costal 8; SLT 57, left epiplastron fragment; SLT 58, left hypoplastron fragment; SLT 59, right hypoplastron fragment; SLT 60, right epiplastron fragment; SLT 61, hyoplastron fragment; SLT 62, hyoplastron fragment; SLT 63, hyoplastron fragment; SLT 64, left xiphiplastron fragment; SLT 65, right hyoplastron fragment; SLT 66, right epiplastron fragment; SLT 67, left xiphiplastron fragment; SLT 68, right epiplastron; SLT 69, left hypoplastron fragment; SLT 70, left epiplastron fragment; SLT 71, left hyoplastron fragment; SLT 73, peripheral; SLT 75, hypoplastron fragment; SLT 79, hyoplastron fragment; SLT 85, nuchal fragment; SLT 86, peripheral; SLT 88, peripheral; SLT 89, peripheral; SLT 91, costal fragment; SLT 94, costal fragment; SLT 98, costal fragment; SLT 100, costal fragment; SLT 103, peripheral fragment; SLT 108, costal fragment; SLT 110, peripheral; SLT 119, costal fragment; SLT 123, suprapygal 1; SLT 127, costal fragment; SLT 134, peripheral plate, juvenile; SLT 174, costal fragment, juvenile; SLT 179, costal juvenile.

Indeterminable shell fragments (SLT): 96, 109, 113, 122, 123, 128, 132, 140, 141, 145, 146, 148, 149, 150, 151, 152, 154, 155, 156, 159, 160, 161, 163, 164, 165, 166, 167, 168, 169, 170.

Indeterminable carapace fragments (SLT): 25, 27, 46, 90, 92, 97, 101, 104, 106, 107, 111, 114, 115, 118, 125, 127, 138, 130, 143, 144, 158, 162, 171, 172, 177, 178.

Small fragments of peripherals (SLT): 30, 31, 33, 37, 87, 95, 102, 112, 117, 120, 121, 122, 131, 139, 142, 158, 175.

Indeterminable plastron fragments (SLT): 40, 72, 74, 76, 77, 78, 80, 81, 93, 99, 105, 116, 124, 126, 147.

Appendicular elements (SLT, no numbers): humerus diaphysis (2); phalanx (3); cervical vertebra (3).

Allatini, Thessaloniki (Late Miocene/Early Pliocene; 1 specimen) (Fig. 3.113): LGPUT GG 23, shell.

Nea Silata, Thessaloniki

As is normally the case, the material from Nea Silata is highly fragmented as a result of the sieving procedure. However, several isolated elements of the shell can be identified and described in detail, allowing the description of the shell morphology of this taxon in detail. Most of the specimens are black in color.

LGPUT SLT 1 (Fig. 110.A): this specimen corresponds to a complete nuchal plate. The nuchal is hexagonal, and is slightly curved transversely, showing a wide nuchal notch anteriorly. Dorsally and anteriorly, a cervical scute is present, which is long and wide, representing approximately 1/3 of the nuchal length. The remaining part of the anterior nuchal is covered by marginals 1. The cervical is present also viscerally. Measurements (mm): Medial length: 28.76 (with notch), 31.91 (no notch); maximum width: 36.53.

LGPUT SLT 2: This specimen corresponds to an almost complete peripheral plate. The plate is gently curved and almost horizontally oriented. Dorsally is crossed by the pleuro-marginal and the marginal sulci. The pleural scutes overlap the peripherals. Measurements (mm): Maximum length: 16.70; maximum width: 20.75.

LGPUT SLT 3 (Fig. 110.C): This specimen corresponds to a complete first neural. Viscerally, the scar of the dorsal vertebra is preserved. The plate is quadrangular with rounded edges, longer than wide. Dorsally, the sulcus of the vertebral 1-2 crosses the plate longitudinally. The sulcus is curved, being convex medially and concave laterally on both sides. Measurements (mm): Length: 13.71; width: 10.68.

LGPUT SLT 4 (Fig. 110.D): This specimen corresponds to a complete neural. This neural is hexagonal with short antero-lateral and longer postero-lateral sides. Its anterior width is larger than the posterior width. It is crossed by the vertebral sulcus transversely, which is anteriorly convex medially and slightly concave laterally. Measurements (mm): Length: 12.82; width: 13.04.

LGPUT SLT 5 (Fig. 110.F): This specimen corresponds to a complete pygal plate. The pygal quadrangular, almost twice wide as long, and is strongly curved transversely. Both dorsally and viscerally is crossed by the marginal 12 sulci. A small pygal notch is noted posteriorly. Measurements (mm): Length: 12.25 (no notch); width: 19.81.

LGPUT SLT 7 (Fig. 111.I): This specimen corresponds to a complete peripheral plate of a large individual. The plate is gently curved and almost vertically oriented. Dorsally is crossed by the pleuro-marginal and the marginal sulci. The pleural scutes overlap the peripherals. Measurements (mm): Length: 21.43; width: 28.85.

LGPUT SLT 8 (Fig. 111.J): This specimen corresponds to an almost complete peripheral plate. The plate is gently curved and almost horizontally oriented. Dorsally is crossed by the pleuro-marginal and the marginal sulci. The pleural scutes overlap the peripherals. Measurements (mm): Maximum length: 21.54; maximum width: 29.30.

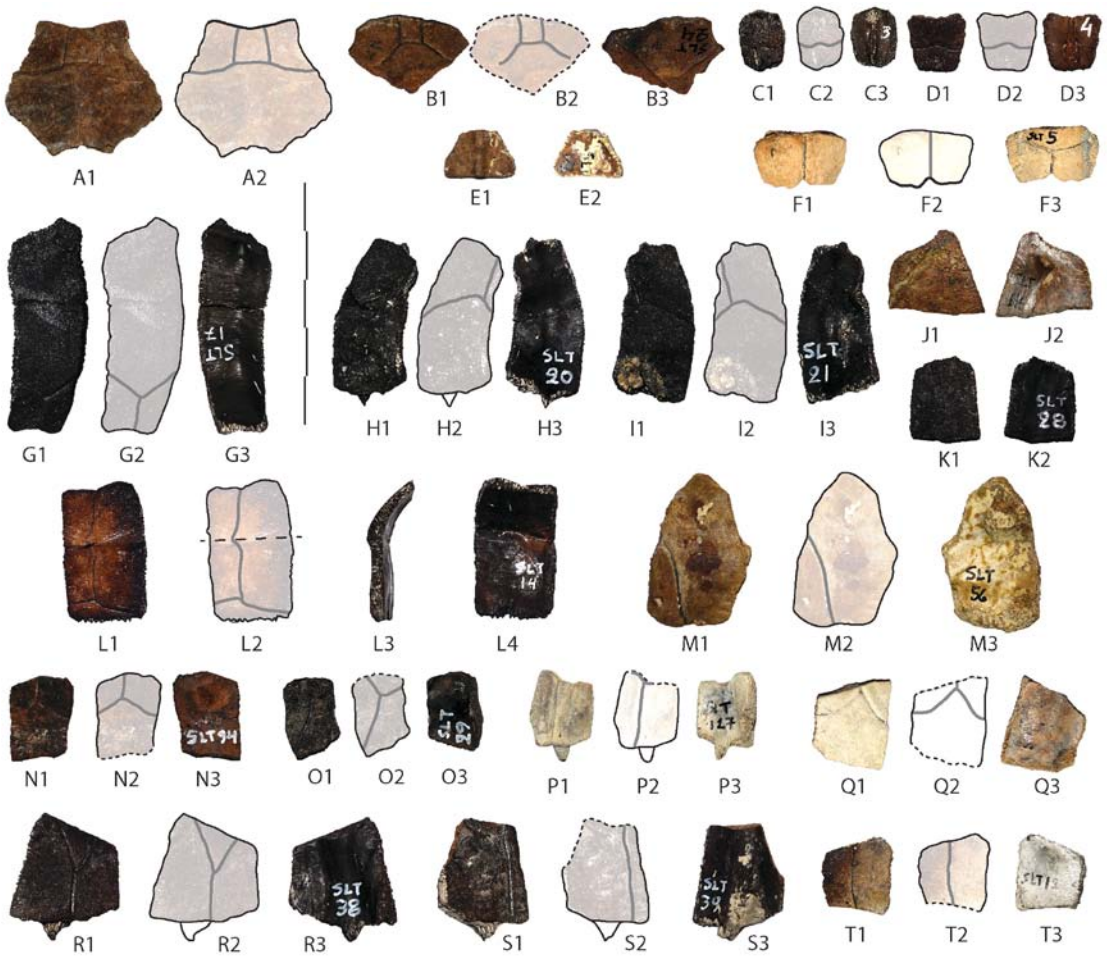


Figure 3.110. *Mauremys* sp. nov. from the Mio-Pliocene boundary of Nea Silata (Thessaloniki). LGPUT collection: A, SLT 1, nuchal in (A1) dorsal and (A2) drawing of the dorsal views. B, SLT 24, nuchal fragment in (B1) dorsal, (B2) drawing of the dorsal and (B3) visceral views. C, SLT 3, neural in (C1) dorsal, (C2) drawing of the dorsal and (C3) visceral views. D, SLT 4, neural in (D1) dorsal, (D2) drawing of the dorsal and (D3) visceral views. E, SLT 123, suprapygal 1 in (E1) dorsal and (E2) visceral views. F, SLT 5, pygal in (F1) dorsal, (F2) drawing of the dorsal and (F3) visceral views. G, SLT 17, costal in (G1) dorsal, (G2) drawing of the dorsal and (G3) visceral views. H, SLT 20, costal in (H1) dorsal, (H2) drawing of the dorsal and (H3) visceral views. I, SLT 21, costal in (I1) dorsal, (I2) drawing of the dorsal and (I3) visceral views. J, SLT 26, costal in (J1) dorsal and (J2) visceral views. K, SLT 28, costal in (K1) dorsal and (K2) visceral views. L, SLT 14, costal in (L1) dorsal, (L2) drawing of the dorsal, (L3) lateral and (L4) visceral views. M, SLT 56, costal in (M1) dorsal, (M2) drawing of the dorsal and (M3) visceral views. N, SLT 94, costal fragment in (N1) dorsal, (N2) drawing of the dorsal and (N3) visceral views. O, SLT 29, costal in (O1) dorsal, (O2) drawing of the dorsal and (O3) visceral views. P, SLT 127, costal in (P1) dorsal, (P2) drawing of the dorsal and (P3) visceral views. Q, SLT 9, costal in (Q1) dorsal, (Q2) drawing of the dorsal and (Q3) visceral views. R, SLT 38, costal in (R1) dorsal, (R2) drawing of the dorsal and (R3) visceral views. S, SLT 39, costal in (S1) dorsal, (S2) drawing of the dorsal and (S3) visceral views. T, SLT 12, costal in (T1) dorsal, (T2) drawing of the dorsal and (T3) visceral views. Scale bar equals 5 cm.

LGPUT SLT 9 (Fig. 110.Q): This specimen corresponds to the middle part of a costal plate. Dorsally, it is crossed by the vertebro-pleural sulci. Based on the preserved part the orientation of the plate is not identified.

LGPUT SLT 10: This specimen corresponds to the lateral part of a long peripheral plate, which appears to be gently curved. Dorsally is crossed by the marginal sulci.

LGPUT SLT 11 (Fig. 111.K): This specimen corresponds to a partial peripheral plate. The plate is gently curved and almost horizontally oriented. Dorsally is crossed by the pleuro-marginal and the marginal sulci. The pleural scutes overlap the peripherals.

LGPUT SLT 12 (Fig. 110.T): This specimen corresponds to the medial part of a costal plate from the left side, having a long anterior and a short posterior medial side to articulate with two successive hexagonal neurals. It is crossed longitudinally by the vertebral sulci.

LGPUT SLT 13 (Fig. 111.G): This specimen corresponds to a complete peripheral plate, from the beginning or the end of the bridge, as it is inferred by the presence of a scar viscerally that could correspond to the axillary or inguinal process. Dorsally is crossed by the pleural, pleuro-marginal and the marginal sulci. The pleural scutes overlap the peripherals. Measurements (mm): Length: 18.06; width: 19.52.

LGPUT SLT 14 (Fig. 110.L): This specimen corresponds to a complete costal plate of a juvenile individual. This is evident by the development of a longitudinal lateral carina. Viscerally, no evidence of the process for the vertebra is found. Dorsally, it is crossed by the vertebral and the vertebro-pleural sulci. Measurements (mm): Maximum length: 17.74; maximum width: 28.14.

LGPUT SLT 15 (Fig. 111.H): This specimen corresponds to a complete peripheral, probably from the posterior carapacial rim. The plate is gently curved. Dorsally is crossed by the pleuro-marginal and the marginal sulci. The pleural scutes overlap the peripherals. Measurements (mm): Length: 18.23; width: 20.86.

LGPUT SLT 16 (Fig. 111.A): This specimen corresponds to a complete peripheral, probably from the posterior carapacial rim. The plate is gently curved. Dorsally is crossed by the pleuro-marginal and the marginal sulci. The pleural scutes overlap the peripherals. Measurements (mm): Length: 13.33; width: 15.66.

LGPUT SLT 17 (Fig. 110.G): This specimen corresponds to a complete costal plate. The presence of a process for the dorsal vertebra ventrally and the double articulation side on one part (with a long anterior and short posterior side, corresponding to two successive hexagonal neurals) confirm that this plate is from the right side of the carapace. It is crossed by the vertebro-pleural and the pleural sulci laterally, suggesting that this shell had extremely wide and short vertebrals. The vertebrals did not reach the costo-peripheral suture. Measurements (mm): Medial length: 16.40; lateral length: 12.23; maximum width: 46.81.

LGPUT SLT 18 (Fig. 111.B): This specimen corresponds to an almost complete peripheral plate, which is slightly curved. Dorsally is crossed by the marginal sulci, and only a small part of the pleuro-marginal sulcus is found medially. Measurements (mm): Length: 14.08; width: 13.32.

LGPUT SLT 19: This specimen corresponds to an almost complete peripheral plate, which is slightly curved. Dorsally is crossed by the marginal sulci. The pleural scutes probably overlap the peripherals. Measurements (mm): Length: 14.62; width: 12.05.

LGPUT SLT 20 (Fig. 110.H): This specimen corresponds to a complete costal 7 from the left side. This costal is medially short, with two sutural sides, whereas laterally is longer. Dorsally, in the medial part is crossed transversely by the vertebral sulcus, and in the middle part by the vertebro-pleural sulcus in the middle. It probably corresponds to the same individual as LGPUT SLT 21. Measurements (mm): Length: 16.14; width: 34.03.

LGPUT SLT 21 (Fig. 110.I): This specimen corresponds to a complete costal 7 from the right side. This costal is medially short, with two sutural sides, whereas laterally is longer. Dorsally, in the medial part is crossed transversely by the vertebral sulcus, and in the middle part by the vertebro-pleural sulcus in the middle. It probably corresponds to the same individual as LGPUT SLT 22. Measurements (mm): Length: 16.12; width: 33.21.

LGPUT SLT 22: This specimen corresponds to an almost complete peripheral plate of a juvenile individual as it is inferred by the small size. Only a part of the rim is missing. Dorsally is crossed by the marginal sulci. Measurements (mm): Length: 10.34; width: 10.96.

LGPUT SLT 23 (Fig. 111.C): This specimen corresponds to a complete peripheral, probably the seventh right one, right after the end of the bridge. Dorsally is crossed by the marginal sulci.

LGPUT SLT 24 (Fig. 110.B): This specimen corresponds to the anterior part of a nuchal plate. A cervical scute is present both dorsally and viscerally. Dorsally is short and wide, whereas viscerally is longer and narrow. Also, the sulci between the first marginals and the first vertebrals are noted.

LGPUT SLT 26 (Fig. 110.J): This specimen corresponds to the medial part of a costal plate. Based on the length of the preserved part (that is much longer by the remaining costals) we can estimate that this could be the first left costal. Viscerally, the rib end is visible. Dorsally, it is crossed by the vertebral and the vertebro-pleural sulci.

LGPUT SLT 28 (Fig. 110.K): This specimen corresponds to the medial part of a costal plate. Viscerally, the rib end is preserved. Dorsally is not crossed by any sulci.

LGPUT SLT 29 (Fig. 110.O): This specimen corresponds to a fragment of a costal plate. Viscerally, the inserted rib is evident. Dorsally, it is crossed by the vertebral and pleural sulci.

LGPUT SLT 32: This specimen corresponds to a partial peripheral plate, probably the first peripheral. The lateral part is missing. In the medial part, we notice the crossing of the vertebro-pleural, pleuro-marginal and marginal sulci.

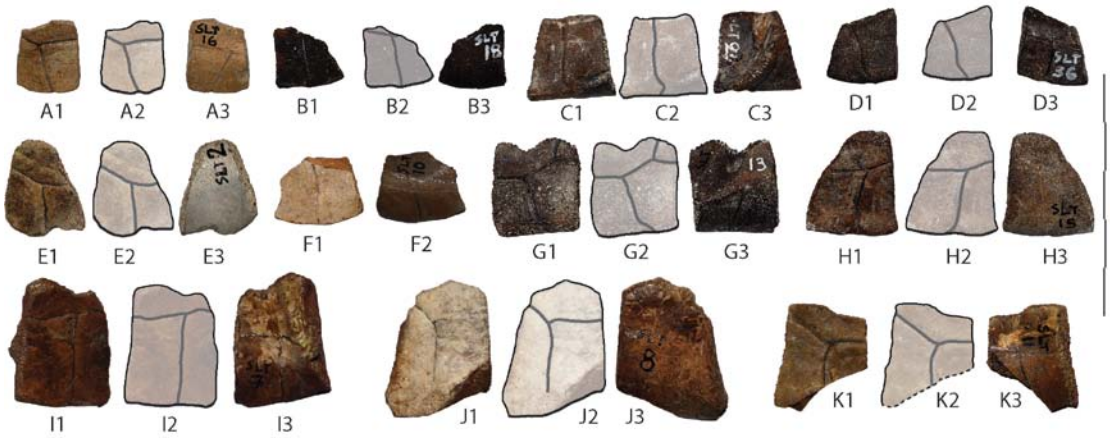


Figure 3.111. *Mauremys* sp. nov. from the Mio-Pliocene boundary of Nea Silata (Thessaloniki). LGPUT collection: A, SLT 16, peripheral in (A1) dorsal, (A2) drawing of the dorsal and (A3) visceral views. B, SLT 18, peripheral in (B1) dorsal, (B2) drawing of the dorsal and (B3) visceral views. C, SLT 23, peripheral in (C1) dorsal, (C2) drawing of the dorsal and (C3) visceral views. D, SLT 36, peripheral in (D1) dorsal, (D2) drawing of the dorsal and (D3) visceral views. E, SLT 2, peripheral in (E1) dorsal, (E2) drawing of the dorsal and (E3) visceral views. F, SLT 10, peripheral in (F1) dorsal and (F2) visceral views. G, SLT 13, peripheral in (G1) dorsal, (G2) drawing of the dorsal and (G3) visceral views. H, SLT 15, peripheral in (H1) dorsal, (H2) drawing of the dorsal and (H3) visceral views. I, SLT 7, peripheral in (I1) dorsal, (I2) drawing of the dorsal and (I3) visceral views. J, SLT 8, peripheral in (J1) dorsal, (J2) drawing of the dorsal and (J3) visceral views. K, SLT 11, peripheral in (K1) dorsal, (K2) drawing of the dorsal and (K3) visceral views. Scale bar equals 5 cm.

LGPUT SLT 36 (Fig. 111.D): This specimen corresponds to a complete peripheral plate, which is rather straight. Dorsally is crossed by the marginal sulci, and only a small part of the pleuro-marginal sulcus is found medially, coinciding with the costo-peripheral suture. Measurements (mm): Length: 14.95; width: 12.23.

LGPUT SLT 38 (Fig. 110.R): This specimen corresponds to the lateral part of a costal plate. Laterally, the rib insertion to the peripheral plate is noted. Dorsally is crossed by the vertebro-pleural and the pleural sulci. The position of the vertebro-pleural sulci indicates that the vertebrals were extremely wide, but not reaching the costo-peripheral suture.

LGPUT SLT 39 (Fig. 110.S): This specimen corresponds to the lateral part of a costal plate. Laterally, the rib insertion to the peripheral plate is noted. Dorsally is crossed by the pleural sulci.

LGPUT SLT 41: This specimen corresponds to a complete peripheral plate. The plate is gently curved towards the rim. Dorsally is crossed by the pleuro-marginal and the marginal sulci. The pleural scutes overlap the peripherals. Measurements (mm): Maximum length: 16.69; maximum width: 17.51.

LGPUT SLT 42: This specimen corresponds to a complete peripheral plate. The plate is thick and is gently curved towards the rim. Dorsally is crossed by the pleural, the pleuro-marginal and the marginal sulci. The pleural scutes overlap the peripherals. Measurements (mm): Maximum length: 17.08; maximum width: 17.77.

LGPUT SLT 43: This specimen corresponds to the medial part of a costal plate. Dorsally is crossed transversely by the vertebral sulci.

LGPUT SLT 44: This specimen corresponds to an almost complete peripheral plate, only a part of the outer rim and of the dorsal surface missing. The plate is gently curved towards the rim. Dorsally is crossed by the pleuro-marginal and the marginal sulci. The pleural scutes overlap the peripherals. Measurements (mm): Maximum length: 17.56; maximum width: 18.08.

LGPUT SLT 45: This specimen corresponds to small flat plastron fragment.

LGPUT SLT 47: This specimen corresponds to a partial peripheral plate. Based on the size and the thickness we can infer that this specimen belong to a large individual. The plate is thick, and dorsally is crossed by the pleural, the pleuro-marginal and the marginal sulci. The pleurals overlap the peripheral plate. Measurements (mm): Maximum length: 18.54; thickness: 10.72.

LGPUT SLT 48 (Fig. 112.J): This specimen corresponds to a partial left hypoplastron, being crossed ventrally by the abdomino-femoral sulcus.

LGPUT SLT 49 (Fig. 112.L): This specimen corresponds to the posterior part of a left xiphiplastron. Posteriorly a narrow, deep and rounded anal notch is noted. The tips of the xiphiplastra are pointed. Ventrally the anals cover the posterior half of the xiphiplastra. The femoro-anal sulcus is almost straight, but it is rounded laterally.

LGPUT SLT 50 (Fig. 112.Q): This specimen corresponds to a complete left xiphiplastron. The lateral borders of the posterior lobe are converging posteriorly. Posteriorly a narrow, deep and rounded anal notch is noted. The tips of the xiphiplastra are pointed. Ventrally the anals cover the posterior half of the xiphiplastra. The femoro-anal sulcus is almost straight.

LGPUT SLT 51 (Fig. 112.A): This specimen corresponds to a complete right epiplastron. A shallow and wide notch is present anteriorly. Viscerally, the medial part of the epiplastral lip is concave. Ventrally is crossed by the gularo-humeral sulcus, which is slightly curved. The gulars have been long and narrow, overlapping the anterior part of the entoplastron. It belongs to the same individual as the entoplastron LGPUT SLT 52. Measurements (mm): Length: 26.09; width: 30.51.

LGPUT SLT 52 (Fig. 112.F): This specimen corresponds to a complete entoplastron. The entoplastron is hexagonal, slightly wider than long. Medially, the gulars cover the anterior third of the entoplastron, whereas the pectorals the posterior third. The gularo-humeral sulci are developed at an acute angle with the midline. The humero-pectoral sulcus is angularly concave medially. Laterally is advanced just before the epiplastron/hyoplastron suture. It belongs to the same individual as the epiplastron LGPUT SLT 51. Measurements (mm): Length: 27.82; width: 33.95.

LGPUT SLT 53 (Fig. 112.H): This specimen corresponds to the posterior part of the right hyoplastron. Medially, the sutural sides for the left hyoplastron and posteriorly

the one for the hypoplastron are preserved. Ventrally, the pectoro-abdominal sulcus is developed transversely, being straight, and medially concave.

LGPUT SLT 54 (Fig. 112.P): This specimen corresponds to a complete right xiphiplastron. The lateral borders of the posterior lobe are converging posteriorly. Posteriorly a narrow, deep and rounded anal notch is noted. The tips of the xiphiplastra are rounded. Ventrally the anals cover the posterior half of the xiphiplastra. The femoro-anal sulcus is almost straight. Measurements (mm): Medial length: 34.68 (with notch), 41.08 (no notch); maximum width: 36.43.

LGPUT SLT 55 (Fig. 112.O): This specimen corresponds to the posterior part of a right xiphiplastron. Based on the preserved part a wide, deep and rounded anal notch could have been present. The tips of the xiphiplastra are pointed. No sulci are observed on the preserved part.

LGPUT SLT 56 (Fig. 110.M): This specimen corresponds to a complete costal 8 from the left side. The plate is curved, and shows a short medial and a longer lateral side. The posterior side shows two sutural sides, indicating that it was articulating with two suprapygals. Dorsally is only crossed by the vertebro-pleural sulcus, which is developed diagonally. Measurements (mm): Length: 19.56; width: 31.97.

LGPUT SLT 57 (Fig. 112.B): This specimen corresponds to the medial part of a left epiplastron. A shallow notch is present anteriorly. Viscerally, the medial part of the epiplastral lip is concave. Ventrally is crossed by the gularo-humeral sulcus, which is slightly curved. The gulars have been long and narrow, overlapping the anterior part of the entoplastron.

LGPUT SLT 58 (Fig. 112.K): This specimen corresponds to the posterior and medial part of the left hypoplastron. It is rather flat, and is ventrally crossed by the femoro-abdominal sulcus.

LGPUT SLT 59 (Fig. 112.M): This specimen corresponds to the anterior and medial part of the right hypoplastron.

LGPUT SLT 60 (Fig. 112.C): This specimen corresponds to the medial part of a right epiplastron. A shallow notch is present anteriorly. Viscerally, the medial part of the epiplastral lip is concave. Ventrally is crossed by the gularo-humeral sulcus, which is slightly curved. The gulars have been long and narrow, overlapping the anterior part of the entoplastron.

LGPUT SLT 61: This specimen corresponds to a small fragment of the lateral part of a right hyoplastron. It is rather flat. Ventrally is crossed by the humero-pectoral sulcus. Further description is not possible.

LGPUT SLT 62: This specimen corresponds to a small lateral fragment of the right hyoplastron. No sulci are observed on the ventral side of the preserved part.

LGPUT SLT 63: This specimen corresponds to a small lateral fragment of the right hyoplastron. No sulci are observed on the ventral side of the preserved part.

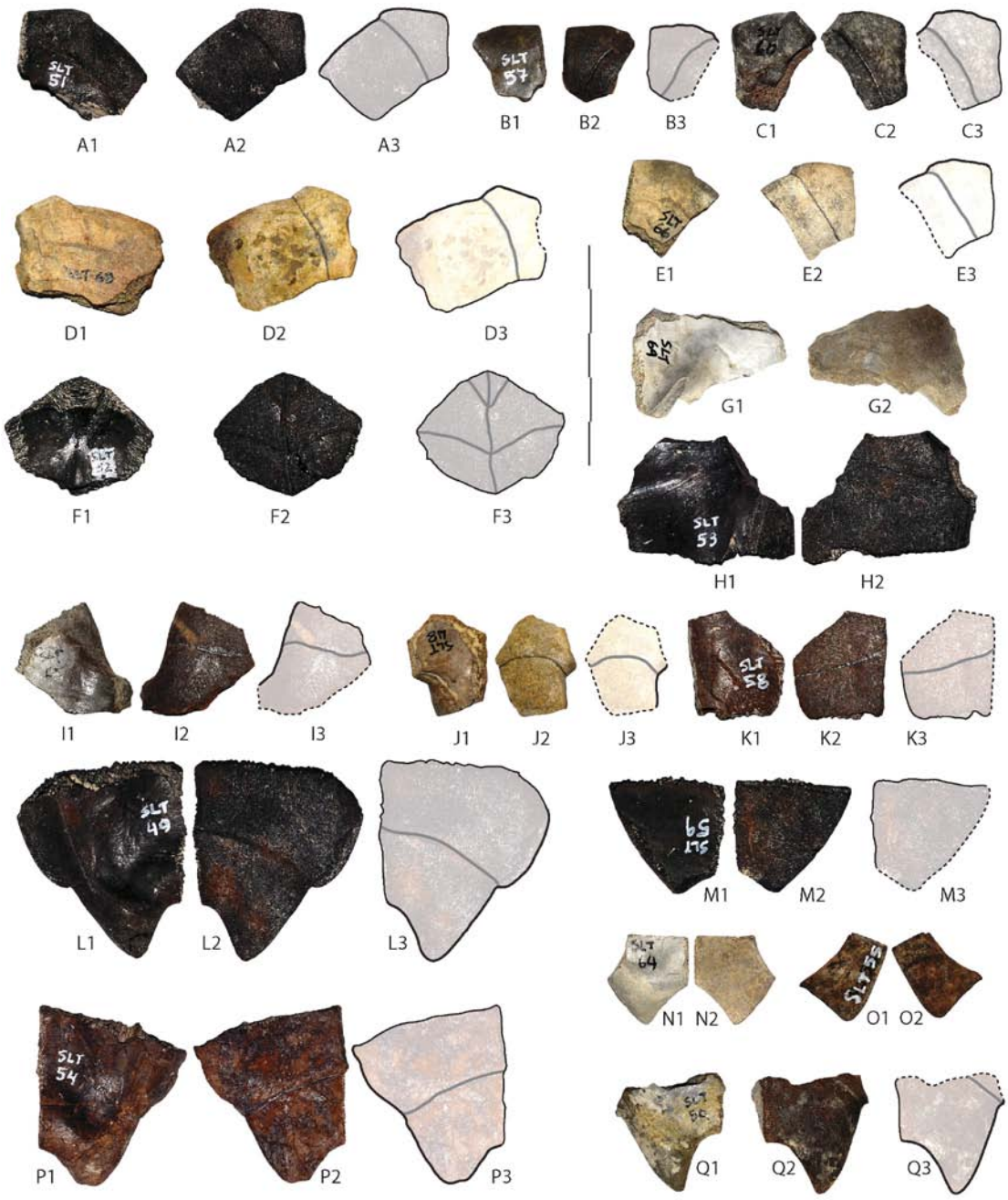


Figure 3.112. *Mauremys* sp. nov. from the Mio-Pliocene boundary of Nea Silata (Thessaloniki). LGPUT collection: A, SLT 51, right epiplastron in (A1) visceral, (A2) ventral and (A3) drawing of the ventral views. B, SLT 57, left epiplastron in (B1) visceral, (B2) ventral and (B3) drawing of the ventral views. C, SLT 60, right epiplastron in (C1) visceral, (C2) ventral and (C3) drawing of the ventral views. D, SLT 68, right epiplastron in (D1) visceral, (D2) ventral and (D3) drawing of the ventral views. E, SLT 66, right epiplastron in (E1) visceral, (E2) ventral and (E3) drawing of the ventral views. F, SLT 52, entoplastron in (A1) visceral, (A2) ventral and (A3) drawing of the ventral views. G, SLT 69, left hypoplastron in (G1) visceral and (G2) ventral. H, SLT 53, right hyoplastron in (H1) visceral, (H2) ventral and (H3) drawing of the ventral views. I, SLT 65, right hyoplastron in (I1) visceral, (I2) ventral and (I3) drawing of the ventral views. J, SLT 48, left hypoplastron in (J1) visceral, (J2) ventral and (J3) drawing of the ventral views. K, SLT 58, left hypoplastron in (K1) visceral, (K2) ventral and (K3) drawing of the ventral views. L, SLT 49, left xiphiplastron in (L1) visceral, (L2) ventral and (L3) drawing of the ventral views. M, SLT 59, left xiphiplastron in (M1) visceral, (M2) ventral and (M3) drawing of the ventral views. N,

SLT 64, left xiphiplastron in (L1) visceral and (L2) ventral views. O, SLT 55, right xiphiplastron in (O1) visceral, and (O2) ventral views. P, SLT 54, right xiphiplastron in (P1) visceral, (P2) ventral and (P3) drawing of the ventral views. Q, SLT 50, left xiphiplastron in (Q1) visceral, (Q2) ventral and (Q3) drawing of the ventral views. Scale bar equals 5 cm.

LGPUT SLT 64 (Fig. 112.N): This specimen corresponds to the posterior part of a left xiphiplastron. Based on the preserved part we can reconstruct a deep and rounded anal notch. The tips of the xiphiplastra are pointed. No sulci are observed on the preserved part.

LGPUT SLT 65 (Fig. 112.I): This specimen corresponds to the anterior part of the right hyoplastron. A part of the buttress is preserved. Medially, the sutural sides for the epiplastron and the entoplastron are noted. Ventrally, the humero-pectoral sulcus is developed transversely, being wavy, and crossing the entoplastron posteriorly.

LGPUT SLT 66 (Fig. 112.E): This specimen corresponds to the medial part of a right epiplastron. A shallow notch is present anteriorly. Viscerally, the medial part of the epiplastral lip is concave. Ventrally is crossed by the gularo-humeral sulcus, which is slightly curved. The gulars have been long and narrow, overlapping the anterior part of the entoplastron.

LGPUT SLT 67: This specimen corresponds to the posterior part of a left xiphiplastron. Based on the preserved part a deep and rounded anal notch could have been present. The tips of the xiphiplastra are pointed. No sulci are observed on the preserved part.

LGPUT SLT 68 (Fig. 112.D): This specimen corresponds to an almost complete right epiplastron. The epiplastron is wider than long, reconstructing a rounded anterior lobe with a faint notch anteriorly. Viscerally, the medial part of the epiplastral lip is concave. Ventrally is crossed by the gularo-humeral sulcus, which is slightly curved. The gulars have been long and narrow, overlapping the anterior part of the entoplastron. Length: 29.60; width: 34.09.

LGPUT SLT 69 (Fig. 112.G): This specimen corresponds to a fragment of the left hypoplastron. Part of the buttress is preserved. Ventrally no sulci are noted.

LGPUT SLT 70: This specimen corresponds to the posterior part of the left epiplastron. No sulci are preserved in the ventral part.

LGPUT SLT 71: This specimen corresponds to a small fragment of the posterior and medial part of a left hyoplastron. It is rather flat. Ventrally is crossed by the pectoro-abdominal sulcus that is oriented diagonally (in the preserved part) and terminates medially very close to the hyo-hypoplastral suture.

LGPUT SLT 73: This specimen corresponds to a complete peripheral from the bridge area. The outer surface is eroded and no sulci are noted as a result.

LGPUT SLT 75: This specimen corresponds to a small fragment of the right hypoplastron. The posterior suture with the xiphiplastron is preserved. Ventrally is crossed by the abdomino-femoral sulcus.

LGPUT SLT 79: This specimen corresponds to a small fragment of a right hyoplastron. Ventrally is not crossed by any sulci.

LGPUT SLT 85: This specimen corresponds to the left part of the nuchal plate. Based on the preserved part we can estimate that the nuchal is hexagonal with a wide notch anteriorly. Although the cervical is preserved only viscerally (due to fragmentation) a cervical was also present dorsally. The antero-lateral parts are covered by the marginals 1 and the remaining parts of the vertebral 1.

LGPUT SLT 86: This specimen corresponds to a complete peripheral, probably from the posterior carapacial rim. The plate is gently curved. Dorsally is crossed by the pleuro-marginal and the marginal sulci. The pleural scutes overlap the peripherals. Measurements (mm): Length: 22.11; width: 21.60.

LGPUT SLT 88: This specimen corresponds to a complete peripheral. The plate is taller than long and is gently curved. Dorsally is crossed by the marginal sulci. The pleural scutes overlap the peripherals. Measurements (mm): Length: 16.69; width: 20.05.

LGPUT SLT 89: This specimen corresponds to a complete peripheral. The plate is only slightly taller than long and relatively straight. Dorsally is crossed by the pleuro-marginal and the marginal sulci. The pleural scutes overlap the peripherals. Measurements (mm): Length: 20.11; width: 21.53.

LGPUT SLT 91: This specimen corresponds to the medial part of a costal plate. Viscerally, the rib end is preserved. Dorsally, the plate is crossed transversely by the vertebral sulci.

LGPUT SLT 94 (Fig. 110.N): This specimen corresponds to the medial fragment of a costal plate. Viscerally, the rib end is preserved. Dorsally, the plate is crossed by the vertebro-pleural and the pleural sulci.

LGPUT SLT 98: This specimen corresponds to the medial part of the costal plate. The medial side is comprised by a double articulation, with a long anterior and short posterior side, corresponding to two successive hexagonal neurals. Viscerally, the rib end is preserved. Dorsally, no evidence of sulci is found.

LGPUT SLT 100: This specimen corresponds to the medial part of the costal plate. The medial side is comprised by a double articulation, with a long anterior and a short posterior sides, corresponding to two successive hexagonal neurals. Viscerally, the rib end is preserved. Dorsally, no evidence of sulci is found.

LGPUT SLT 103: This specimen corresponds to a fragmented peripheral plate. Dorsally is crossed by the pleuro-marginal and the marginal sulci. The pleural scutes overlap the peripherals.

LGPUT SLT 108: This specimen corresponds to the medial part of the costal plate. The medial side is comprised by a double articulation, with a long anterior and a short posterior sides, corresponding to two successive hexagonal neurals. Viscerally, the rib end is preserved. Dorsally, no evidence of sulci is noted.

LGPUT SLT 110: This specimen corresponds to a complete peripheral. The plate is taller than long and gently curved. Dorsally is crossed by the pleuro-marginal and the marginal sulci. The pleural scutes overlap the peripherals. Measurements (mm): Length: 19.41; width: 17.16.

LGPUT SLT 119: This specimen corresponds to the lateral part of the costal plate. Dorsally, it is crossed by the vertebro-pleural sulci.

LGPUT SLT 123 (Fig. 110.E): This specimen corresponds to a complete first suprapygal, probably of a juvenile individual as it is inferred by the presence of a medial carina. The plate is quadrangular, trapezoid, with a narrow anterior and a wide posterior side. It is not crossed by any sulci. Measurements (mm): Length: 9.42; anterior width: 8.61; posterior width: 14.36.

LGPUT SLT 127 (Fig. 110.P): This specimen corresponds to the lateral part of a costal plate. Laterally, the rib insertion to the peripheral plate is noted. Dorsally is crossed by the vertebro-pleural (partially visible) and the pleural sulci. The position of the vertebro-pleural sulci indicates that the vertebrals were extremely wide, but not reaching the peripherals.

LGPUT SLT 134: This specimen corresponds to a complete peripheral plate. Due to small size this specimen can be identified as belonging to a juvenile individual. No sulci are identified dorsally. The carapacial rim is horizontally oriented. Maximum length: 5.12; maximum width: 9.14.

LGPUT SLT 174: This specimen corresponds to an almost complete costal plate of a juvenile individual, as it is inferred by the small size of the specimen. Viscerally, the rib end is preserved. Dorsally, the plate is crossed transversely by the vertebral sulci. Measurements (mm): Length: 7.25; Preserved width: 11.93.

LGPUT SLT 179: This specimen corresponds to an almost complete costal plate of a juvenile individual, as it is inferred by the small size of the specimen. Viscerally, the rib end is preserved. Dorsally, the plate is not crossed by any sulci.

Allatini, East Thessaloniki

LGPUT GG 23 (Fig. 3.113): this specimen was collected in November of 1933 in the clay pits of Allatini, and delivered to the LGPUT. When the fossil was discovered, only the dorsal side was visible, the ventral side being covered with sediment. On the dorsal side, only a few plates were preserved, in their original position (Fig. 3.113.A). However, compression of the specimen caused the missing bony plates to leave clear imprints on the matrix filling the shell, providing additional information on the structure of the carapace. The visceral surface of the left xiphiplastron was also exposed in dorsal view, indicating that at least some of the plastron was preserved (Fig. 3.113.B). The ventral side of the specimen was recently prepared, revealing the nearly complete plastron. Due to the severe compression of the specimen, the surface of the shell is badly fractured, but in most cases the sutures and sulci are clearly visible (Fig. 3.113.C). The only missing parts of the plastron are the right epiplastron and a portion of the left (Fig. 3.113.D).

Carapace: The general shape of the carapace, as inferred from the imprints of the plates on the sediment, resembles that seen in a turtle. The carapace is longer than wide, is relatively flattened (even allowing for the compression it has undergone), and has short and almost horizontally oriented peripherals (those not involved in the bridge). The imprints of the neurals indicate a poorly differentiated neural series, with quadrangular and hexagonal neurals. The first neural appears to be quadrangular, and longer than wide. The second is hexagonal with short anterolateral sides, and slightly wider than long. The fourth is quadrangular. The fifth is hexagonal, with short anterolateral sides, and is slightly longer than wide. This neural is crossed by a sulcus. The remaining neurals appear to be hexagonal, with short anterolateral sides, and markedly wider than long. The costals are not differentiated, all being quadrangular with almost parallel sides. Only one costal, possibly the left fourth costal, is crossed by sulci. Two sulci, which could correspond to the boundaries between a vertebral and two adjacent pleurals, are visible on this plate. If the fourth costal plate is in its correct anatomical position, the vertebrals must have been very short and wide.

Plastron: The partial left epiplastron is thin, without any protruding epiplastral lip, and is covered by the gular scute medially. The part of the plastron covered by the gulars is incompletely preserved, but these scutes appear to be long and narrow. The entoplastron is rhomboidal in shape, being equally long and wide, and is covered by the gulars anteriorly. The humero-pectoral sulcus crosses the posterior part of the entoplastron. The hyo- and hypoplastra are long and wide. The hyoplastra are crossed anteriorly by the humero-pectoral sulcus, whereas the hypoplastra are crossed posteriorly by the pectoro-abdominal sulcus. The xiphiplastra are strongly constricted at the level of the lateral termination of the femoro-anal sulcus. The anals are medially long and laterally short. A deep and somewhat rounded anal notch separates the posterior ends of the xiphiplastra.

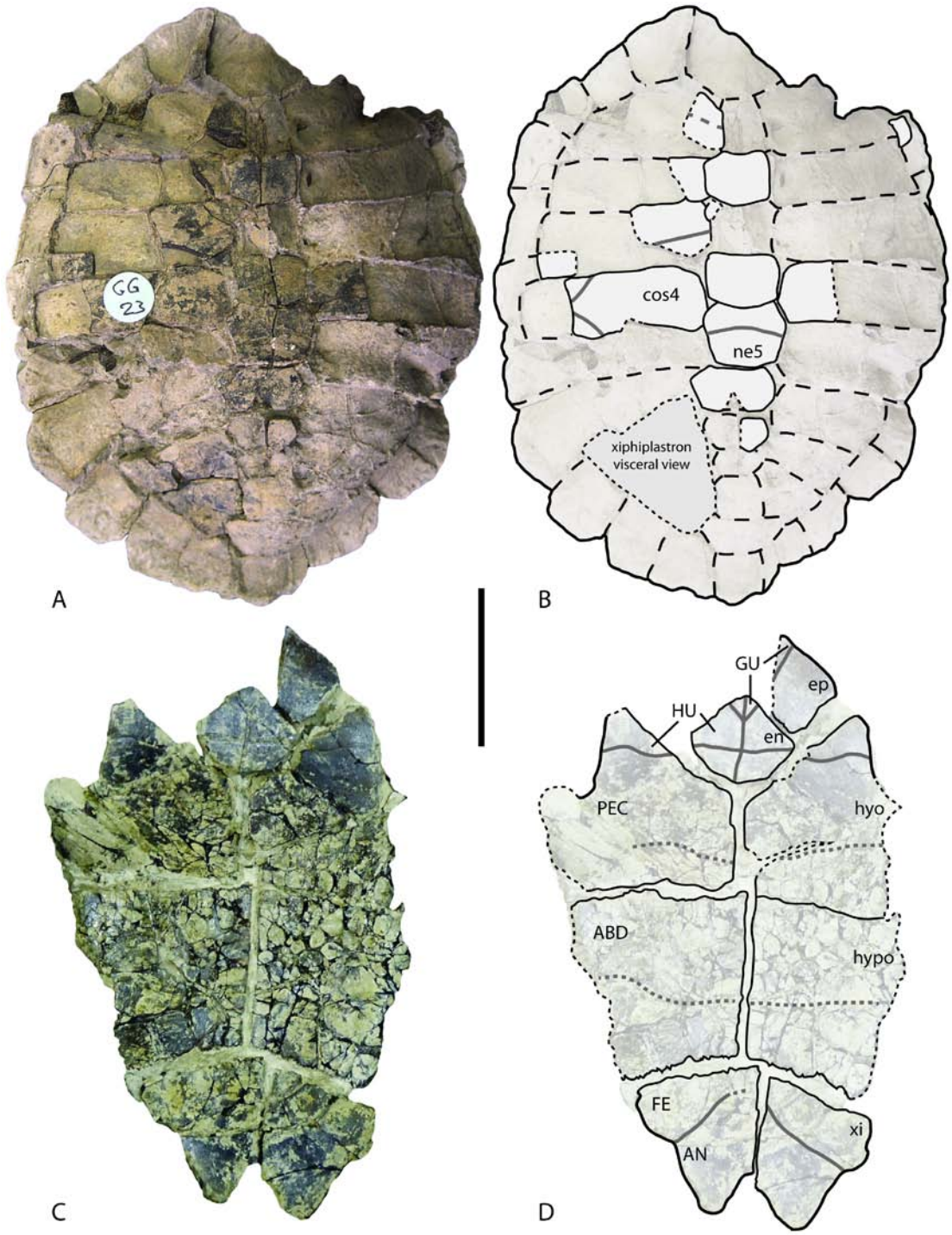


Figure 3.113. *Mauremys* sp. nov. from the uppermost Miocene – lowermost Pliocene of Allatini, Thessaloniki, Greece. LGPUT GG 23, (A) dorsal view of the carapace, (B) simplified drawing of the carapace in dorsal view, (C) ventral view of the plastron and (D) simplified drawing of the plastron in ventral view. Scale bar equals 5 cm. For abbreviations see Material & Methods.

DISCUSSION

The specimens from Nea Silata and Allatini (Thessaloniki) come from the same region and represent roughly the same time period. Their common elements are similar in morphology and they are both united by the presence of wide vertebrals (probably present in the Allatini specimen). Therefore, we can safely assume that they belong to the same taxon. The neural pattern, the entoplastron covered anteriorly by the gular scutes and posteriorly crossed by the humero-pectoral sulcus and the presence of the anal notch allow attribution to Geoemydidae. Among geoemydids there are some taxa that present wide vertebrals as well (Fig. 3.114), summarized by Danilov (2005: Fig. 80).

The Pliocene *Clemmydopsis mehelyi* from Hungary (see Danilov, 2005: Fig. 80A, B) lacks the first pleural scutes, showing very wide vertebrals as a result, being different from the Nea Silata and Allatini geoemydids. Also, the plastron of *Clemmydopsis* shows a short anal notch, different from the condition seen in *Mauremys* and in the Nea Silata and Allatini geoemydids. The Pliocene *Sakya kolakovskii* from Georgia (see Danilov, 2005: Fig. 80C, D) also shows wide vertebrals that reach the lateral parts of the costals, in contact with narrow pleurals. In this case however, the number of vertebrals is higher than normal, showing 10 wide and narrow vertebral scutes. This character clearly suggests that the Nea Silata and Allatini geoemydids cannot be associated with *Sakya*. The Miocene *Sarmatemys lungui* from Moldavia (see Danilov, 2005: Fig. 80E, F) shows some similarities with the Nea Silata and Allatini geoemydids in the shape of the vertebrals and in the shape of the anal notch, but *Sarmatemys* differs in many other aspects: in the carapace, there is no nuchal notch; the cervical and marginals 1 show the same length; there is no inter-pleural sulci cross the costals, as the vertebrals extend up to the costo-peripheral sutures; the configuration of the costal 7/8 in relation with the sulci is different, as the Nea Silata form shows a, *Mauremys*-like, diagonal crossing of the vertebro-pleural sulcus; the pleurals do not overlap the peripherals (only in the anterior area); the entoplastron is not overlapped by the gular scutes; rather straight humero-pectoral sulcus (instead of sinuous as in *Mauremys*). In the all the above-mentioned differences, the Nea Silata and Allatini geoemydids are clearly distinct from *Sarmatemys*. In other words, although the wide vertebrals seems to associate these specimens with *Sarmatemys*-like taxa, nearly all other morphological characters are closer to *Mauremys*.

Extant specimens of *Mauremys* (*M. rivulata*, *M. leprosa)* always have narrow and longer vertebrals. Among the known fossil forms of *Mauremys*, the only taxon in which the vertebrals approach a comparable width is *Mauremys campanii* (see Chesi et al., 2009), but even in this species the vertebrals are still narrower than in the Nea Silata and Allatini specimens. Other fossil *Mauremys* specimens from Italy (e.g. *M. portisii*, *M. etrusca*; see Chesi, 2008) have narrower and longer vertebrals as well. The vertebrals of *Hardella thurjii* are wider than in other extant geoemydids, but still almost twice as long as those of the geoemydids from Thessaloniki.

In the Thessaloniki specimens, the humerals are medially very short, increasing the area of the entoplastron that is covered by the gulars and pectorals. This condition is found only in some species of *Mauremys* (e.g. *Mauremys caspica*, *Mauremys leprosa*, *Mauremys sarmatica*, *Mauremys gaudryi*; see character 49, state 4, and Fig. 3.21 in Hervet, 2003), whereas the gulars and pectorals cover less of the entoplastron in *Mauremys portisii*, *Mauremys pygolopha*, *Mauremys thainensis* and some species of *Palaeochelys*. Another character supporting the taxonomic placement

of the Thessaloniki geoemydids in *Mauremys* is the narrow and deep anal notch. The anal notch of the Allatini *Mauremys* is somewhat rounded as in *M. sarmatica* and *M. pygolopha*, but is more similar to the angular notch seen in *M. caspica* and *M. leprosa*. However, the anal notch is wider in these two extant taxa than in the Allatini geoemydid. Claude et al. (2007) listed a number of additional diagnostic characters of the carapace of *Mauremys* that cannot be observed on the Allatini specimen. Some of them (short anterior marginals; contact of vertebral 1 with marginals 2) can be found in the Nea Silata plates but the disarticulated nature of the specimens does not allow observing all of them.

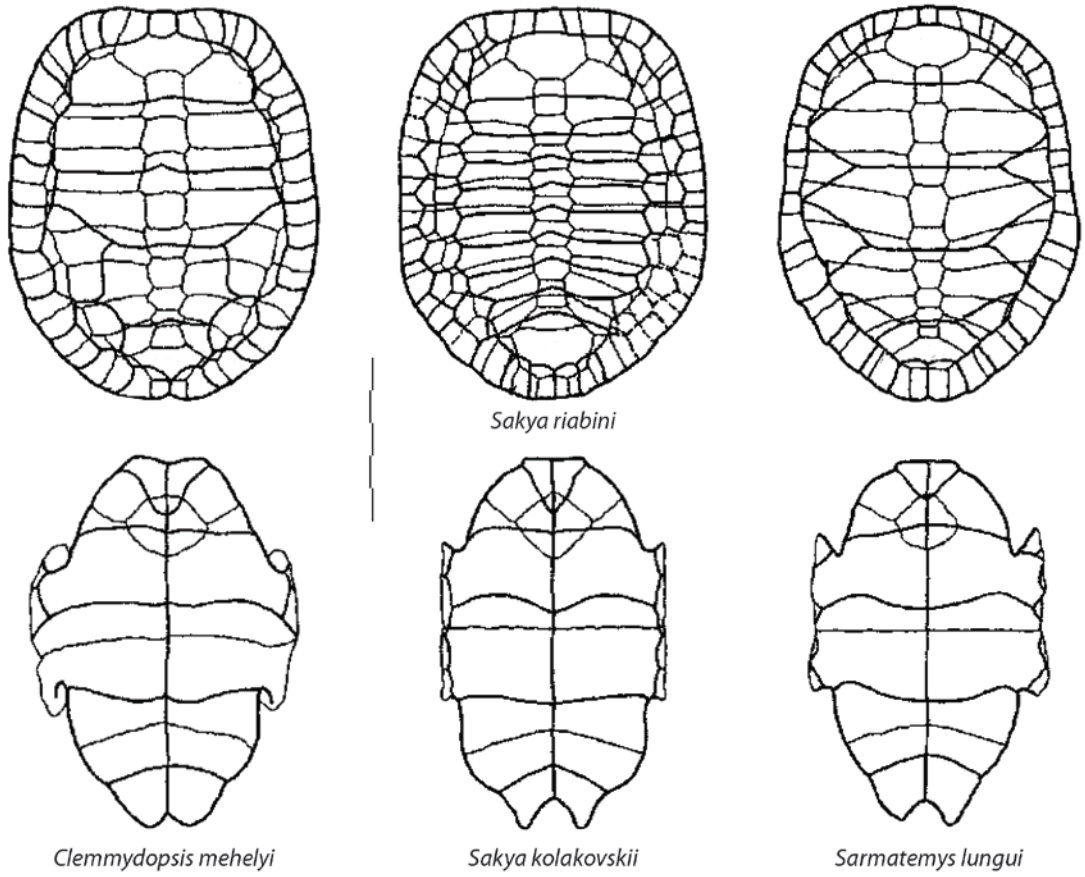


Figure 3.114. Geoemydid taxa with wide vertebral scutes. Figure modified from Danilov (2005:Fig. 80).

Compared to *Mauremys* sp. from San Giovanni di Sinis, Italy (Chesi et al., 2007), the Thessaloniki geoemydids show a deeper and narrower anal notch. Compared to the Late Miocene *Mauremys campanii* (new combination in Chesi et al., 2009), the Thessaloniki geoemydids show a deeper nuchal notch, and a more posteriorly located humero-pectoral sulcus. Among the measurements and ratios used by Chesi et al. (2009), only the ratio of the length of the humerals to that of the entoplastron can be confidently assessed in the Allatini specimen (HuL/Ent = 8.38mm/21.42mm = 0.391). The calculated value of 0.391 is similar to those previously obtained for *M. campanii* ($0.132 < x < 0.5$), *Mauremys gaudryi* (0.352) and *Mauremys sarmatica* ($0.164 < x < 0.586$), but significantly lower than the value for *Mauremys portisii* (0.613) (from Chesi et al., 2009). Also, the median length of the humerals is much shorter than that of the pectorals. The length ratio between these elements cannot be determined precisely, but appears to fall within the range expected

for *Mauremys*. These ratios are not calculated in the Nea Silata material due to the disarticulated nature of the material.

Regarding the Asian *Mauremys*, Takahashi et al. (2013) list a number of differences among hingeless geoemydids from Asia and Europe with an entoplastron crossed by the humero-pectoral sulcus. The main differences are found on the carapace, which is not preserved in the Allatini specimen. The only character that is preserved in this specimen is the length of the entoplastron relative to the interhyoplastral suture (character 8 in Takahashi et al., 2013). The length of the entoplastron in the Allatini specimen is shorter than the interhyoplastral length, similar to *M. japonica* but contrasting the condition in *M. mutica* and *M. yabei*.

Several of the characters mentioned above, however, are potentially subject to the intraspecific variation that is present in *Mauremys*, a matter that has received some attention in the literature. For example, Gómez de Soler et al. (2012) suggested that the differences between the Pliocene *M. gaudryi* and the extant *M. leprosa* were small enough to be attributed to intraspecific variation. The two taxa are indeed fairly similar in many respects, although *M. gaudryi* may differ from *M. leprosa* in having wider cervical, a slightly deeper anal notch, and a humero-pectoral sulcus that is more posteriorly placed on the entoplastron. This example illustrates one of the main problems encountered when comparing fossil and extant taxa, involving the distinction between discrete and continuous characters (see for example the discussion in Escapa & Pol, 2011 and references therein). Most of the differences noted above cannot be adequately coded as discrete characters (e.g. presence/absence) because they are actually changes in the shape that are more appropriately analyzed with a combination of morphometrics and cladistics (see Escapa & Pol, 2011 and references therein).

The isolated plates from Nea Silata represent most of the shell of the geoemydid individual, allowing the reconstruction of the morphology of most of the shell. The peculiar morphology of the Nea Silata geoemydid is the presence of extremely wide vertebral scutes, that cover most of the medial part of the carapace, almost reaching in some cases the lateral parts of the costals. Based on all the comparisons listed above, the Nea Silata and Allatini geoemydids could belong to a new taxon. The relationships of these specimens among other geoemydids are going to be discussed in a following chapter. As it is evident in some of the specimens (e.g. SLT 14 & SLT 123) of the morphology of the juvenile individuals of this taxon can be reconstructed. Most probably, the juvenile individuals were characterized by the presence of three carinas, one in the medial plane, and one on each side. Also, it appears that the relative covering of the vertebral scutes in the juvenile carapace was even larger than in the adult individuals.

EMYDIDAE Bell, 1825

EMYS Duméril, 1805
Emys orbicularis Linnaeus, 1758

MATERIAL:

Franchthi Cave, Peloponnesus (Holocene/Pleistocene, 300+ specimens) (Fig. 3.115-3.119): The material has no individual specimen numbers, as is the common practice in many archaeological sites with animal remains. The description is going to be general about the taxon, and where it is necessary to mention individual specimens and the lithostratigraphical unit, they will be mentioned (e.g. 155).

Megalopolis, Peloponnesus (Pleistocene, 5 specimens)* (Fig. 3.107): AMPG 1966/47, left hyoplastron; AMPG 1966/48, left hypoplastron; AMPG 1966/49, left xiphiplastron; AMPG 1966/50, left hypoplastron; AMPG 1966/53, left hyoplastron.

* These specimens have been published by Melentis (1966), as being part of the collections of AMPG. However, these specimens have not been located in AMPG, despite the numerous efforts of Prof. G. Theodorou & Lec. S. Roussiakis. Therefore, these descriptions are based on re-interpretations of the initial detailed drawings of Melentis (1966).

DESCRIPTION

Franchthi Cave, Peloponnesus

Taxonomic Remarks: In the detailed study of the zooarchaeological material of Franchthi Cave by Stiner & Munro (2011), the chelonians were preliminary identified as *Emys/Mayrymys* (sic) and *Testudo* sp. Based on the re-examination of the material a more accurate identification is provided. Although very fragmentary, the material presents some diagnostic elements. The distinction between the freshwater and the terrestrial taxa can be based on the surface of the elements (smoother in the freshwater taxon) and especially based on the peripherals that are overlapped by the pleural scutes in *Emys/Mauremys*. Generally, the shell elements of *Testudo* are thicker than those of the freshwater taxa. The new identifications are given in Table 3.4.

Table 3.4. Skeletal element representation of the chelonian material from Franchthi Cave.

Carapace					
Nuchal	Neural	Suprapygal	Pygal	Costal	Peripheral
2	29	2	1	105	52
Plastron					
Epiplastron	Entoplastron	Hyoplastron	Hypoplastron	Xiphiplastron	Indet
2	1	2	1	3	5

Nearly all parts of the shell are represented in the material (Fig. 3.115-3.118). The vast majority of the material is fragmented, and no evidence of articulated specimens have been noted. Most of the specimens are identified as parts of costal plates, found complete in juvenile specimens (155; 158), or almost complete in adult ones (e.g. 160) (Fig. 3.116). These costals are sometimes crossed by the pleural sulci

and their medial border (were preserved) shows a short anterior and a longer posterior side, as it is usually the case of costals articulating with hexagonal neurals. The second best represented category is the peripherals. In all the identified peripherals, the pleurals cover the medial parts of the plates. From the remaining parts of the carapace few elements are preserved. Only two specimens of the nuchal plate are known (160; 161; Fig. 3.116), showing a lateral covering of the first pleurals on the nuchal. The cervical scute is long and rather narrow. Interestingly the neural series is very well represented with at least 29 specimens. Some rectangular, longer than wide, first neurals are preserved (160; 161), being crossed by the vertebral sulcus. The remaining neurals are typically hexagonal, with short anterior lateral sides. Some of them are crossed by the sulcus between the vertebrals (e.g. 160; 161), whereas others are not crossed by sulci (e.g. 160). Few remains of suprapygals have been identified (160). One of them is much wider than long, with a narrowed anterior side, and is not crossed by any sulci, being identified as a second suprapygal. The other suprapygal (probably the second as well) is fragmented. It shows the presence of a carina dorsally. One pygal plate has been identified (161; Fig. 3.116), being slightly wider than long. It is overlapped by the fifth vertebral anteriorly, and posteriorly is covered by the twelfth marginals. The plastron is significantly less represented in the studied material. Few diagnostic parts are identified, such as the right xiphiplastron (137; Fig. 3.115) that shows a rounded posterior outline for the lobe indicating that an anal notch is absent. The plate is crossed only by the femoro-anal sulcus. The femorals are medially short and laterally long, whereas the anals are medially long and laterally short. The freshwater material could be referred to *Emys orbicularis* based on several elements: the nuchal plate (160; Fig. 3.116) is wide and laterally overlapped by the first pleural scute. Based on the preserved part the lyre-shaped first vertebral of *E. orbicularis* can be reconstructed. In contrast, in *Mauremys* sp. the nuchal is narrower and not overlapped by the pleurals laterally. Additionally, the xiphiplastron (137; Fig. 3.115) shows no anal notch and a long anal covering ventrally, further confirming the presence of *Emys* in the material. Finally, no hyoplastron crossed by the pectoro-abdominal sulcus is found, confirming the condition seen in *Emys orbicularis* due to the presence of the hyo-hypoplastral hinge. Most of the remaining diagnostic elements (neurals, entoplastron, suprapygals and pygals) are consistent with *E. orbicularis* as well.

Distribution (Fig. 3.119): As far as temporal distribution of the chelonians in the cave is concerned, an update from the distribution shown in Fig. 12 in Stiner & Munro (2011) is provided. The main changes are found on the first record of *Emys orbicularis*. First of all, the costal specimen from unit 173 is attributable to *Testudo* and not to a freshwater taxon, since it preserves a medial side corresponding to the rectangular/octagonal neural pattern of *Testudo.* The oldest findings that could be attributed to *Emys* are the two peripherals from the Epigravetian (165 and 166 units), based on the overlapping of the pleural scutes.
The chelonian specimens in the cave are the remains of small game prey of the early humans inhabiting the cave. Assuming that the relative abundances of the food remains could reflect actual faunal abundances in the area, important conclusions can be found for the presence of *Emys orbicularis*. The European pond turtle shows an impressive expansion during the occupation phase 5 (Epigravettian) somewhat between 13,300 and 12,700 BP, and is absent before 15,000 BP. On the contrary, *Testudo* is present since the “Gravettoid” period, showing its maximum expansion during the occupation phase 4 (Epigravettian), prior to the presence of *Emys*.

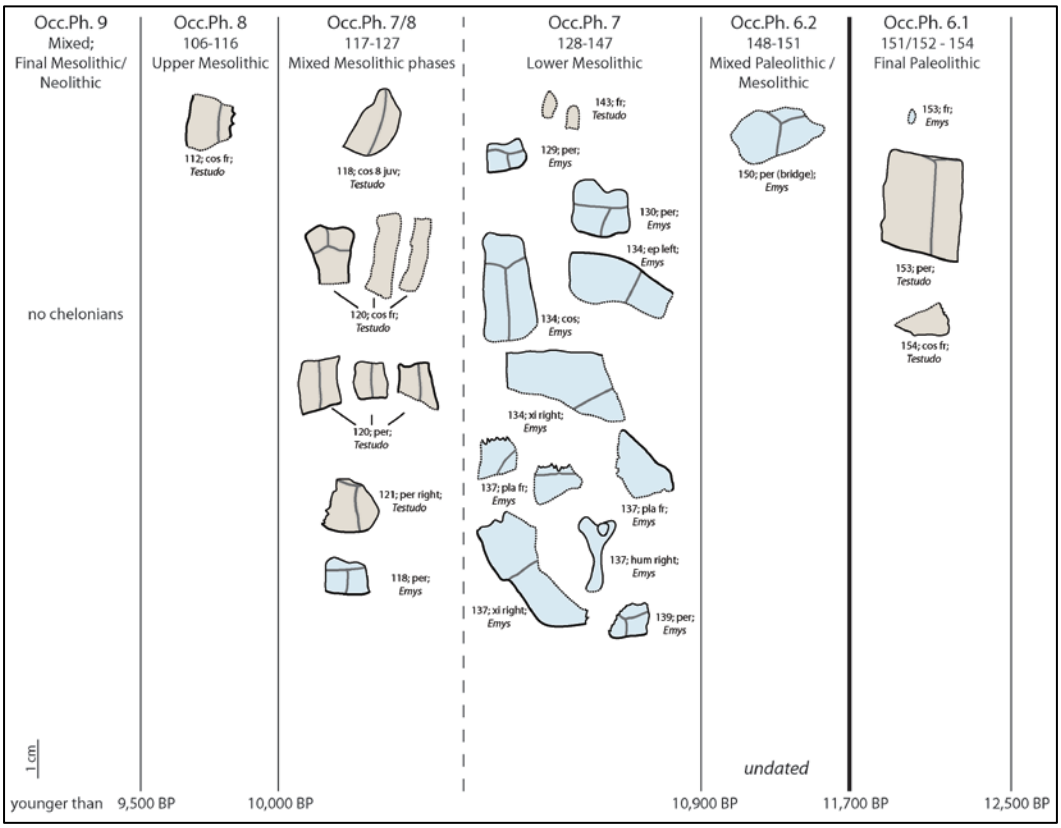


Figure 3.115. *Emys orbicularis* Linnaeus, 1758 (blue) and *Testudo* cf. *hermanni* (brown), from the Pleistocene – Holocene times of Franchthi Cave (Peloponnesus). Occupational phases 9-6, from Final Mesolithic/Neolithic till Final Paleolithic times.

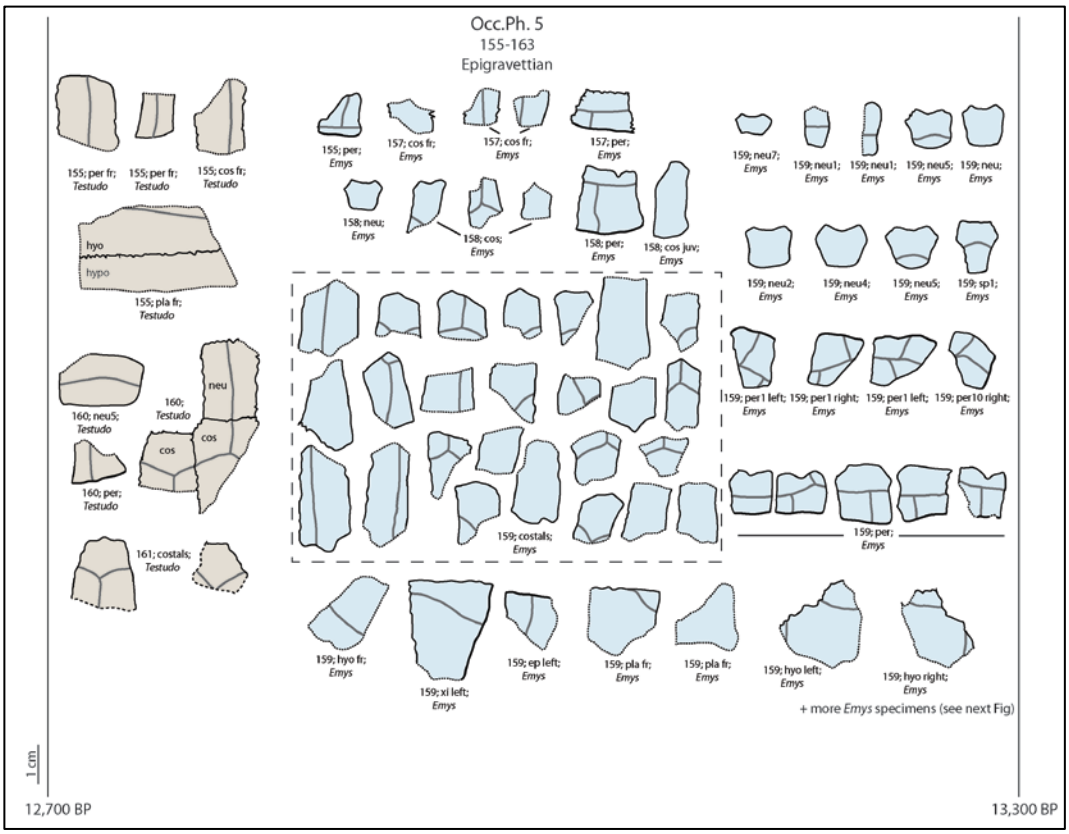


Figure 3.116. Franchthi Cave (Peloponnesus). Occupational phase 5, from the Epigravettian times. (See caption of Fig. 3.115).

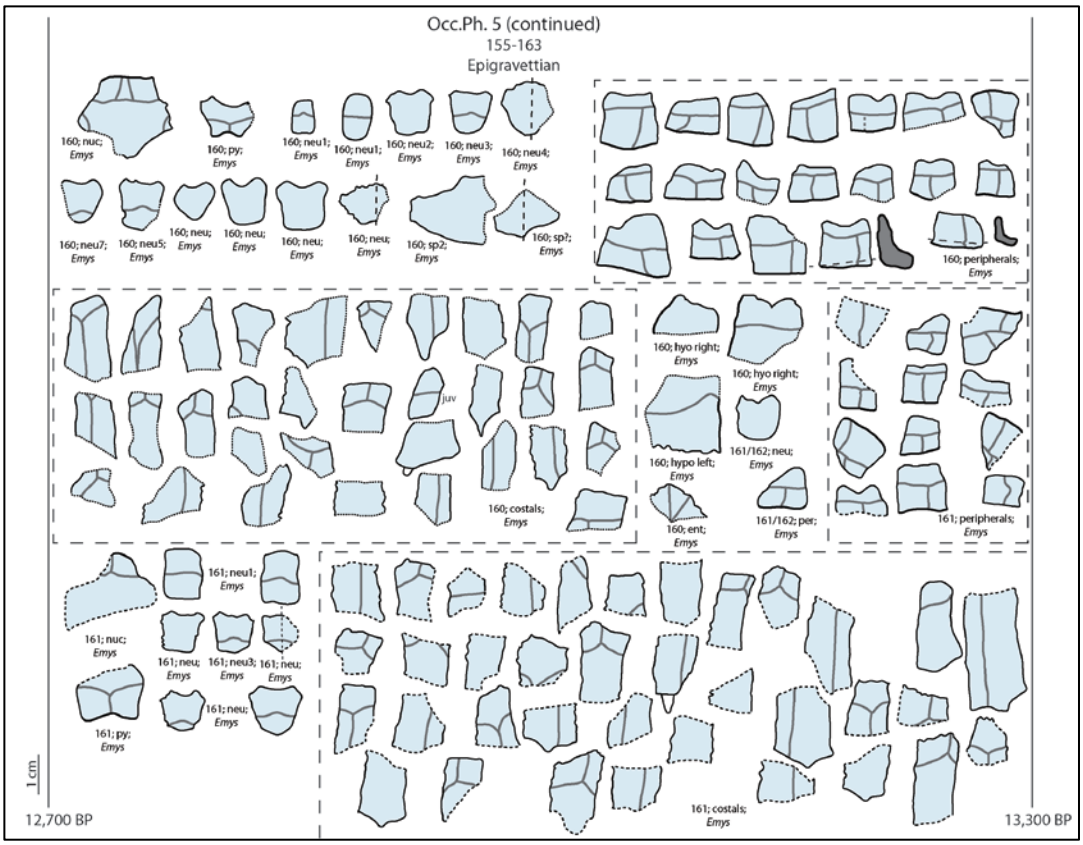


Figure 3.117. Franchthi Cave (Pelopponessus). Occupational phase 5, from the Epigravettian times (continued from previous figure).

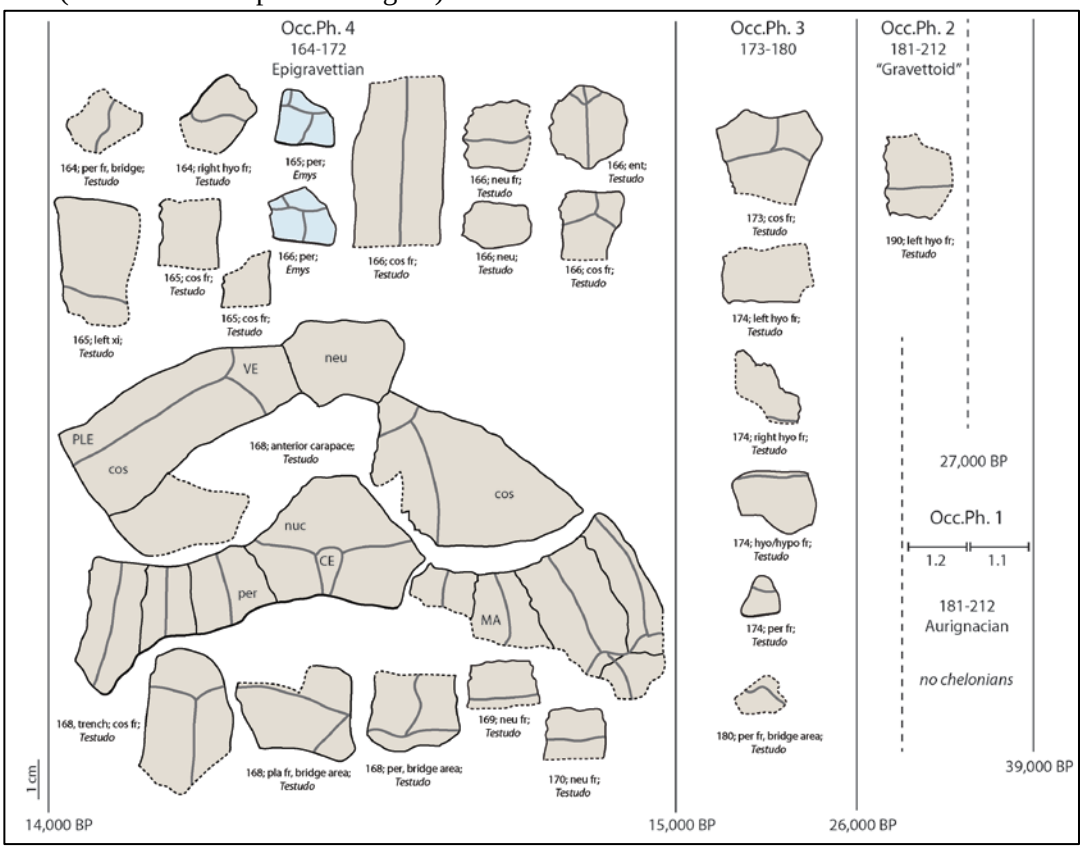


Figure 3.118. Franchthi Cave (Peloponnesus). Occupational phases 4-2, from the Epigravettian till the "Gravettoid" times. (See caption of Fig. 3.115).

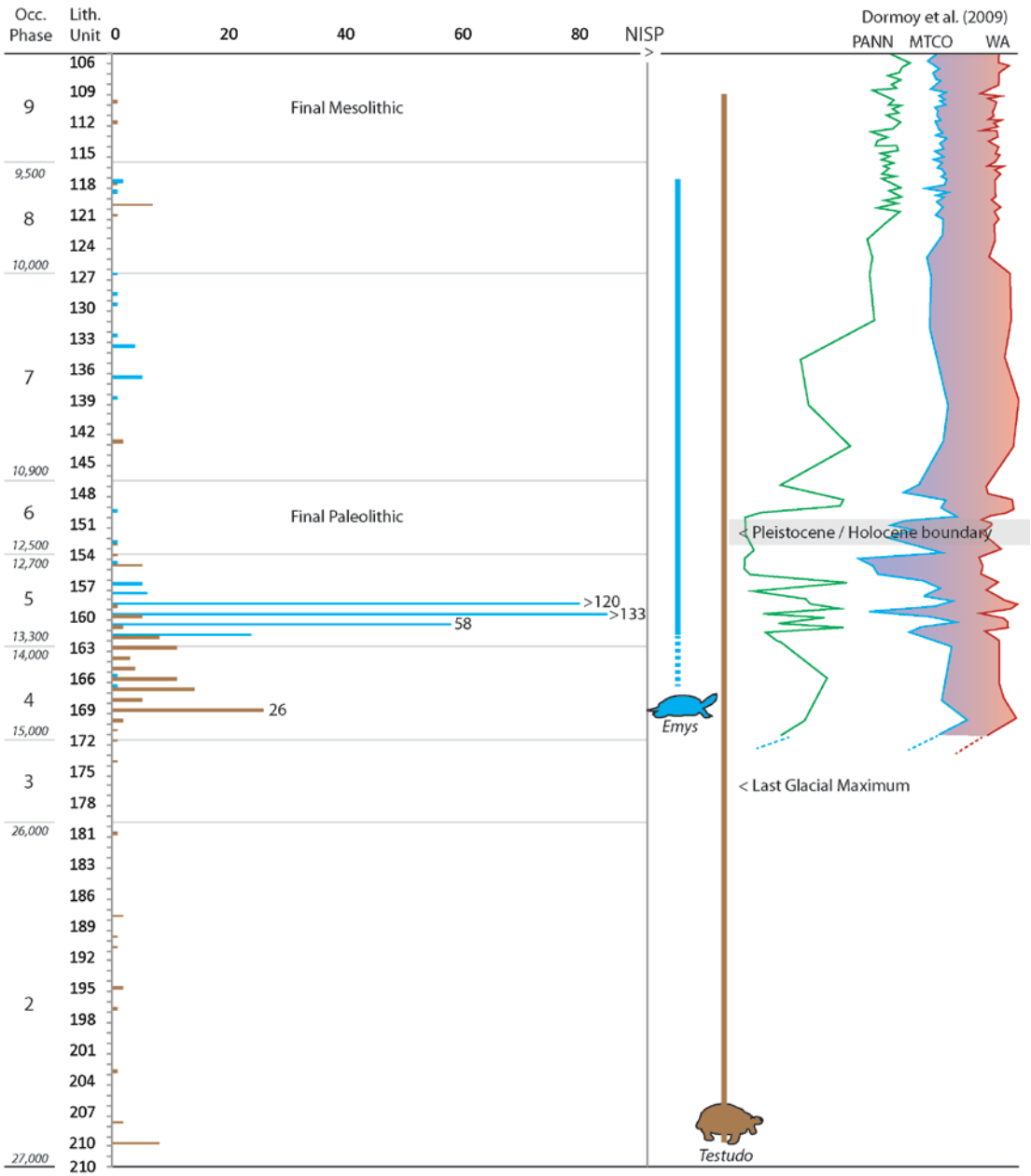


Figure 3.119. Temporal distribution of the chelonians from Franchthi Cave (Peloponnesus). Curves follow Dormoy et al. (2009). Abbreviations: MTCO, mean temperature of the coldest month; MTWA, mean temperature of the warmest month; NISP, Number of identified specimens; PANN, annual precipitation.

Remarks: Several mitochondrial works (Lenk et al., 1999; Fritz et al., 2007a; 2009) have indicated a Balkan Glacial refuge for *Emys orbicularis*, from which this taxon expanded onto central and northern European areas during the favorable conditions of the warmer parts of the Holocene (Sommer et al., 2007). The *E. orbicularis* record of the Franchthi Cave is important, because this is the oldest record of this taxon in Greece. The systematic revision of the chelonian remains (this thesis) shows only the presence of *Mauremys* during the Pleistocene in Liko, Mavro Mouri IV caves and Sitia (Crete Island) and in Kos Island, but not in the mainland. Also, a revision and detailed study of other material from Greek Paleolithic sites is needed, but in most of these sites chelonian remains receive little attention. The presence of remains of *Emys orbicularis* in Franchthi Cave starts after the end of the Last Glacial Maximum and

rapidly increases during the Epigravettian (Late Pleistocene) and towards the end of the Paleolithic (Latest Pleistocene). The climatic reconstruction of the Aegean region during this period (Dormoy et al., 2009 and references therein) shows that the temperatures were increasing towards the Holocene (Fig. 3.119). Between 14,700 and 12,500 BP (Bølling/Allerød period), the marine pollen records show a temperate phase, with warm and moist conditions, with the establishment of a sub-seasonal "Mediterranean" rainfall regime similar to the modern conditions (Dormoy et al., 2009). These conditions would favor the survival, diversification and expansion of the pond turtle in Greece. Indeed, during this period we notice the maximum number of findings from this taxon in Franchthi Cave. Lenk et al. (1999) have indicated the presence of a glacial-pleniglacial refuge of this taxon in Greece. The findings from Franchthi Cave support this claim and document the pre-Holocene early expansion of the European pond turtle.

Megalopolis, Peloponnesus

AMPG 1966/47 (Fig. 3.107.F; see also Fig. 3A in Melentis, 1966): This specimen corresponds to an almost complete left hyoplastron, with some medial parts missing. It is slightly wider than long. Anteriorly it is crossed by the humero-pectoral sulcus. The posterior border appears to be the coincidence of the posterior hyoplastral suture and the posterior pectoral sulcus, resembling the condition noted by the presence of a hyo-hypoplastral hinge. Based on the preserved part can be estimated that the posterior part of the entoplastron was crossed by the humero-pectoral sulcus.

AMPG 1966/48 (Fig. 3.107.G; see also Fig. 3B in Melentis, 1966): This specimen corresponds to an almost complete left hypoplastron, with the antero-lateral corner missing. It is slightly wider than long. It is crossed only by the abdomino-femoral sulcus in the posterior half of the plate. The anterior border appears to be the coincidence of the anterior hypoplastral suture and the anterior abdominal sulcus, resembling the condition noted by the presence of a hyo-hypoplastral hinge.

AMPG 1966/49 (Fig. H; see also Fig. 3C in Melentis, 1966): This specimen corresponds to an almost complete left xiphiplastron, with only the posteriormost part missing. It is slightly wider than long. Posteriorly, an anal notch is absent, indicating a rounded posterior outline for the lobe. The plate is crossed only by the femoro-anal sulcus. The femorals are medially short and laterally long, whereas the anals are medially long and laterally short. Therefore the slightly rounded sulcus is diagonally oriented.

AMPG 1966/50 (Fig. 3.107.I; see also Fig. 6 in Melentis, 1966): This specimen corresponds to fragmented left hyoplastron. It is wider than long. Anteriorly it is crossed by the humero-pectoral sulcus. The posterior border appears to be the coincidence of the posterior hyoplastral suture and the posterior pectoral sulcus, resembling the condition noted by the presence of a hyo-hypoplastral hinge.

AMPG 1966/53 (Fig. 3.107.J; see also Fig. 4 in Melentis, 1966): This specimen corresponds to a small fragment of the left hyoplastron. It is crossed by the abdomino-femoral sulcus. Further description is not possible.

Comments: These specimens have been identified as "*Clemmys*" *caspica* by Melentis (1966), an identification that has been followed in the revision of Georgalis & Kear (2013) as *Mauremys caspica*. However these specimens preserved several characters that allow the attribution to the European pond turtle, *Emys orbicularis*. These are: the presence of a hyo-hypoplastral hinge, overlap of the pectoral scutes on the entoplastron, the absence of anal notch with a rounded posterior lobe, and the medially long anal scutes. It should be noted here, however, that direct observations on these specimens are not possible (see note above) but these characters are clearly seen in the detailed drawings of Melentis (1966). Pending confirmation from the re-discovery of these specimens and/or by the discovery of new ones, they can be tentatively attributed to *E. orbicularis*. Findings of the European pond turtle are not strange in Megalopolis basin, as such findings have been reported (but not studied in detail) by van Vugt et al. (2000). Confirmation of the presence of this taxon in Megalopolis basin is important because it could possibly be the oldest occurrence in Greece.

Concluding Remarks: Although the fossil/subfossil record of the European Pond Turtle (*Emys orbicularis*) in Greece is limited compared to *Mauremys* and *Testudo*, the preserved material from Franchthi cave and Megalopolis basin allows confirmation of this taxon in Greece from the Late Pleistocene at least. These findings provide support for the previous claims of a glacial-pleniglacial refuge of this taxon in Greece. These preliminary findings should spur the description of more findings, especially from archaeological sites and localities.

TESTUDOOLITHIDAE indet. (sensu Hirsch, 1996)

LOCALITY: Pylea, east Thessaloniki; uppermost Miocene – lowermost Pliocene.

IGF 11603 (Fig. 3.120): Six structures that could represent eggs are preserved as internal molds of lithified sediment (Fig. 3.120) that retain on the surface several eggshell fragments (indicated with white color in Fig. 6). Worth noting is that some of the poorly preserved specimens that are partly incomplete, show on the sections fragments of eggshell embedded in the matrix. If the interpretation of these structures is correct, it is therefore necessary to assume a complex taphonomic history.

DESCRIPTION: They are elliptical in shape and somehow flattened. The best-preserved specimens (A-C in Fig. 3.120) have the following dimensions (in mm): A = 61-52-43; B = 59-53-47, C = 60-49-47. The others are too fragmentary and they are not worth measuring. The external surface of the eggshell is light brown in color and generally smooth but in some cases it is slightly pitted.

IDENTIFICATION: All specimens can be referred to the parataxonomic family Testudoolithidae Hirsch, 1996, based on the ellipsoid shape. The preserved eggs are larger than previously known eggs of *Testudo* (e.g. the eggs of *T. marginata* measure 38x32 mm, and those of *T. ibera* measure 35x25 mm; Bonin et al., 2006). In comparison, eggs of extant large testudinids may exceed 50 mm in length (e.g. *Centrochelys sulcata*, *Chelonoidis nigra;* from Bonin et al., 2006). The specimens correspond in their dimensions and external morphology to previously described chelonian eggs from the Pliocene of Apolakkia, Rhodes (Mueller-Töwe et al., 2011) and the Pliocene of Gran Canaria (Hirsch & Lopez-Jurado, 1986). According to Hirsch (1996), turtle eggs are characterized by the presence of an aragonite calcareous shell layer. Therefore, only an X-ray diffraction analysis (following Mueller-Töwe et al., 2011) would confidently identify the IGF specimens. Unfortunately, sampling the IGF specimens for such an analysis was not accepted by IGF over the course of this study (M. Delfino, pers. Comm.). However, the fact that the Pylea deposits belong to the Gonia Formation, which is rich in large tortoise material (see Vlachos et al., 2014), supports the possibility that these structures represent eggs of giant tortoises.

The possible presence of giant tortoise's eggs is among the most interesting features of the Pylea locality. Although these are the first chelonian eggs reported from Greece (in del Campana, 1919), they were not mentioned by Mueller-Töwe et al. (2011) or Georgalis and Kear (2013). In fact, these specimens may represent the oldest Greek record of a giant tortoise. The presence of giant tortoises was further reported in the Thessaloniki area by Arambourg and Piveteau (1929; from Axios or Megalo Emvolon) and by Bachmayer et al. (1979; from Megalo Emvolon). Recently, the new species *Titanochelon bacharidisi* has been reported (Vlachos et al., 2014; also this study) from localities at Epanomi, Nea Michaniona and Nea Kallikratia that, like Megalo Emvolon, are within the Gonia Formation. Unfortunately, no fossil giant tortoise shells are known from Allatini, making it impossible to know if the eggs can be attributed to this species. Together with previously reported eggshell fragments from the Pliocene of Apolakkia (Rhodes Island; Mueller-Töwe et al., 2011), these specimens are the only example of preserved turtle eggshells known from Greece.

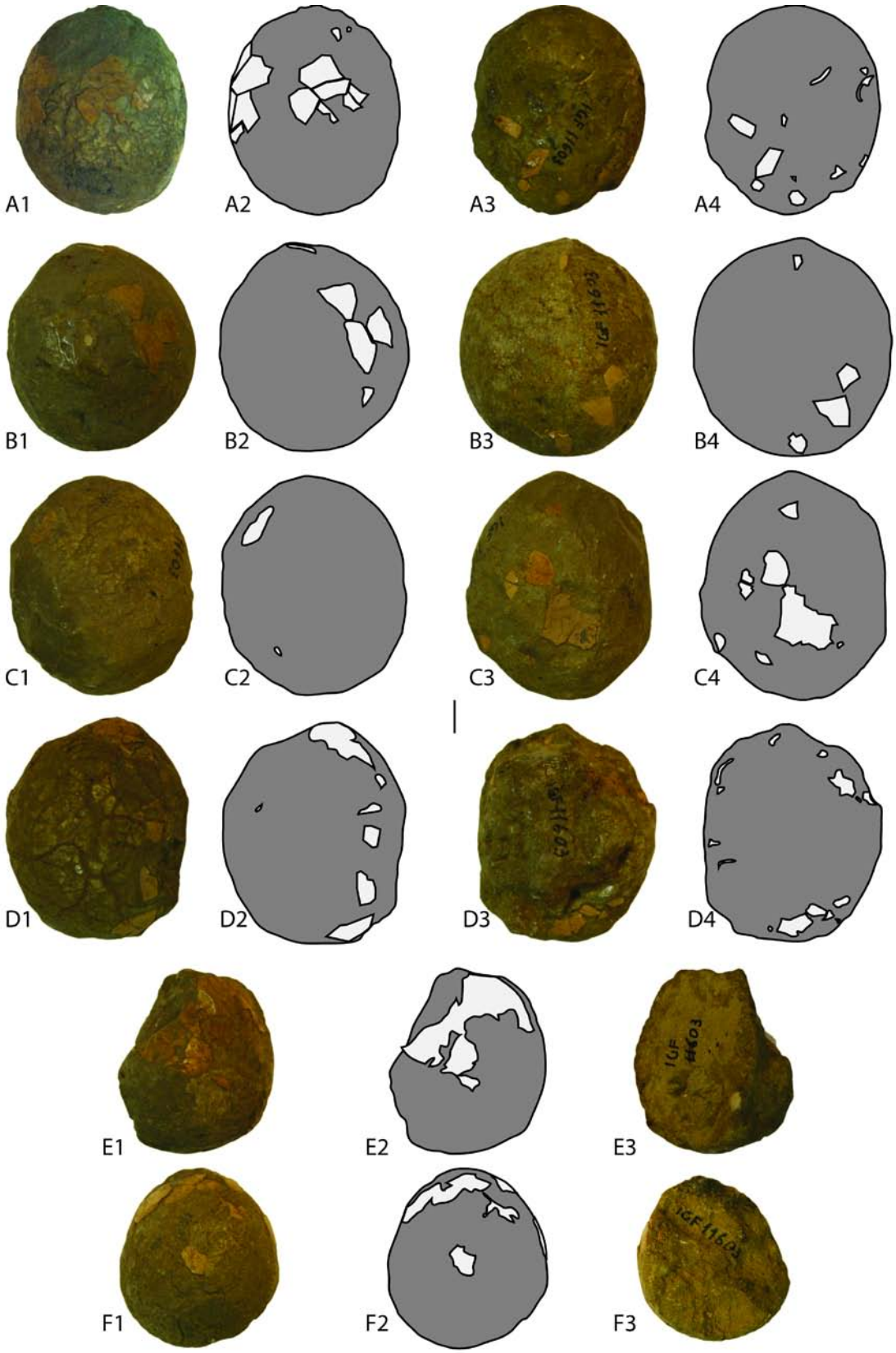


Figure 3.120. A-F, Clutch of possible giant tortoise eggs (IGF 11603) from the uppermost Miocene – lowermost Pliocene of Pylea (Thessaloniki). The simplified drawings indicate the patches of preserved eggshell (white) and the lithified sediment (gray). Scale bar equals 1 cm.

Testudoolithus Hirsch (1996)

LOCALITY: Apolakkia, Rhodes Island; Pliocene.

AMPG 515 – 519 (Fig. 3.121): Clutch of at least five complete eggs

DESCRIPTION: The material has been described in detail by Mueller-Töwe et al. (2011) identified as Testudoolithidae Hirsch, 1996, based on their shape and morphology, and by accompanied X-ray diffraction analysis. The analysis was carried out in a loose eggshell fragment and in the surrounding sediment and showed a high aragonitic content which is a characteristic of testudooolithid eggs (Mueller-Töwe et al., 2011). The eggshell microstructure suggests a rigid eggshell and is very similar to the structure of eggs of extant large testudinid taxa. Whereas the eggs have been laid by a large testudinid individual, Mueller-Töwe et al. (2011) also reported several carapacial fragments from a small individual. My inspection of the specimens suggests that they are too small and fragmentary to allow any identification, but we concur with the view of the authors that this individual is a small tortoise, which is certainly different from the turtle that laid the eggs.



Figure 3.121. Clutch of giant tortoise eggs (AMPG 515-519) from the Pliocene of Apolakkia, Rhodes Island. Scale bar equals 5 cm.

Table 3.5. Summary of the fossil chelonians from Greece, with additional information about the locality, age, initial description and institution.

Locality	Age	First description	Present study	Institution
		Holocene/Pleistocene		
Franchthi Cave, Peloponnesus	Pleistocene/ Holocene	*Testudo* (in Stiner & Munro, 2011)	*Testudo* cf. *hermanni*	D' Ephorate of Archaeology, Nafplion
Franchthi Cave, Peloponnesus	Pleistocene/ Holocene	*Emys/Maurymys* [sic] (in Stiner & Munro, 2011)	*Emys orbicularis*	D' Ephorate of Archaeology, Nafplion
Vraona Cave	Recent	*Emys orbicularis* (in Rauscher, 1995)	*Emys orbicularis*	IPUW
Vraona Cave	Recent	*Clemmys caspica* (in Rauscher, 1995)	*Mauremys rivulata*	IPUW
Charkadio Cave, Tilos Island	Latest Pleistocene	*Testudo marginata* (in Bachmayer & Symeonidis, 1975)	*Testudo marginata*	AMPG
Petralona Cave	Pleistocene	*Testudo graeca* (in Kretzoi, 1977)	*Testudo graeca*	Museum of Petralona Cave
Gerani Cave, Crete Island	Holocene?	-	*Mauremys* sp.	AMPG
Gerani Cave, Crete Island	Pleistocene	*Testudo marginata cretensis* (in Bachmayer et al., 1975)	*Testudo marginata*	AMPG
Zourida Cave, Crete Island	Pleistocene	*Testudo marginata cretensis* (in Bachmayer et al., 1975)	*Testudo marginata*	AMPG
Liko Cave, Crete Island	Pleistocene	*Testudo marginata cretensis* (in Brinkerink, 1996)	*Testudo marginata*	AMPG
Liko Cave, Crete Island	Pleistocene	-	*Mauremys rivulata*	AMPG
Simonelli Cave, Crete Island	Pleistocene	*Testudo marginata* (in Malatesta et al., 1980)	*Testudo marginata*	AMPG
Koumpes Cave, Crete Island	Pleistocene	*Testudo marginata cretensis* (in Brinkerink, 1996)	*Testudo marginata*	AMPG
Koumpes Cave, Crete Island	Pleistocene	-	*Mauremys rivulata*	AMPG
Mavro Mouri IV, Crete Island	Pleistocene	*Testudo* (in Brinkerink, 1996)	*Testudo marginata*	AMPG
Mavro Mouri IV, Crete Island	Pleistocene	-	*Mauremys rivulata*	AMPG
Sitia, Crete Island	Pleistocene	*Clemmys* cf. *caspica* (in Mayhew, 1997)	*Mauremys rivulata*	AMPG
Rethymnon fissure, Crete Island	Pleistocene	cf. *Emys orbicularis* (in Brinkerink, 1996)	*Mauremys rivulata*	AMPG
Bate Cave, Crete Island	Pleistocene	*Testudo marginata cretensis* (in Kotsakis, 1977)	*Testudo marginata*	Roma Tre
Kythera Island	Pleistocene	-	*Testudo marginata*	LGPUT?
Kos Island	Pleistocene	-	*Mauremys rivulata*	NHMC
Kos Island	Pleistocene	-	*Testudo marginata*	NHMC
Megalopolis basin, Peloponnesus	Pleistocene	*Clemmys caspica* (in Melentis, 1966)	*Mauremys rivulata*	AMPG
Megalopolis basin, Peloponnesus	Pleistocene	*Clemmys caspica* (in Melentis, 1966)	*Emys orbicularis*	AMPG

Table 3.5. (continued)

Vatera-F site, Lesvos Island	Early Pleistocene	cf. *Cheirogaster* aff. *schafferi* (in Lapparent de Broin, 2002)	*Titanochelon* sp.	VM
Vatera-T site, Lesvos Island	Early Pleistocene	*Testudo* cf. *graeca ibera* (in Lapparent de Broin, 2002)	*Testudo graeca*	VM
Xerias, Kavala	Pleistocene	*Testudo* sp. (in Tsoukala et al., 2011)	*Testudo* cf. *marginata*	LGPUT
Potidea, Chalkidiki	Pleistocene	-	*Testudo graeca*	LGPUT
Chalkidiki	Pleistocene	-	*Testudo hermanni*	LGPUT
Korydallos	Pleistocene	*Testudo* sp. (in Paraskevaidis, 1961)	*Testudo* sp.	unknown
Lakonia	Pleistocene	*Testudo marginata* (in Schleich, 1982)	*Testudo marginata*	BSPG (cast)
		Pliocene		
Aggelochori/ Megalo Emvolon, Thessaloniki	Pliocene	*Testudo* cf. *graeca* (in Bachmayer et al., 1979)	*Testudo graeca*	NHMW; AMPG
Aggelochori/ Megalo Emvolon, Thessaloniki	Pliocene	*Testudo* sp. (in Bachmayer et al., 1979)	*Titanochelon bacharidisi*	LGPUT; AMPG
Epanomi, Chalkidiki	Pliocene	*Cheirogaster bacharidisi* (in Vlachos et al., 2014)	*Titanochelon bacharidisi*	LGPUT
Nea Michaniona, Chalkidiki	Pliocene	*Cheirogaster bacharidisi* (in Vlachos et al., 2014)	*Titanochelon bacharidisi*	LGPUT
Nea Kallikratia, Chalkidiki	Pliocene	*Cheirogaster bacharidisi* (in Vlachos et al., 2014)	*Titanochelon bacharidisi*	LGPUT
Gefira, Axios valley	Pliocene	-	Trionychidae indet	LGPUT
Milia, Grevena	Late Pliocene	-	*Testudo* sp. nov.	LGPUT
Milia, Grevena	Late Pliocene	-	*Mauremys* sp.	LGPUT
Milia, Grevena	Late Pliocene	-	*Titanochelon* sp.	LGPUT
Apolakkia, Rhodes Island	Early Pliocene	Testudoolithidae indet (in Mueller-Töwe et al., 2011)	*Testudoolithus* sp.	AMPG
Apolakkia, Rhodes Island	Early Pliocene	*Remains of a chelonian taxon* (in Mueller-Töwe et al., 2011)	cf. *Testudo* sp.	AMPG
"Salonique"	Late Miocene – Pliocene?	*Testudo* sp. (small size) (in Arambourg & Piveteau, 1929)	*Testudo graeca*	MNHN
"Salonique"	Late Miocene – Pliocene?	*Testudo* sp. (large size) (in Arambourg & Piveteau, 1929)	*Titanochelon* cf. *bacharidisi*	MNHN
Allatini, Thessaloniki	Latest Miocene/ Earliest Pliocene	-	*Mauremys* sp.	LGPUT
Allatini, Thessaloniki	Latest Miocene/ Earliest Pliocene	*Testudo amiatae* (in Bachmayer & Symeonidis, 1970)	*Testudo graeca*	AMPG
Pylea, Thessaloniki	Latest Miocene/ Earliest Pliocene	*Testudo amiatae* (in del Campana, 1917)	*Testudo graeca*	IGF
Pylea, Thessaloniki	Latest Miocene/ Earliest Pliocene	*Identified as turtle eggs* (in del Campana, 1919)	Testudoolithidae indet.	IGF

Miocene				
Table 3.5. (continued)				
Nea Silata	Latest Miocene/ Earliest Pliocene	-	*Testudo* sp.	LGPUT
Nea Silata	Latest Miocene/ Earliest Pliocene	-	*Mauremys* sp. nov.	LGPUT
Maramena	Latest Miocene/ Earliest Pliocene	Testudinidae indet (in Schmidt-Kittler et al., 1995)	*Testudo* sp.	Mainz
Plakias, Crete Island	Late Miocene	-	*Mauremys* sp.	NHMC
Plakias, Crete Island	Late Miocene	-	Trionychidae indet.	NHMC
Platania, Drama	Late Miocene	-	*Testudo* cf. *graeca*	LGPUT
Kryopigi, Kassandra peninsula	Late Miocene	-	*Titanochelon* sp.	LGPUT
Fourka, Kassandra peninsula	Late Miocene	-	*Titanochelon* sp.	LGPUT
Pikermi, Attica	Late Miocene	*Testudo marmorum* (in Gaudry, 1862a,b)	*Testudo marmorum*	AMPG
Pikermi, Attica	Late Miocene	*Testudo* sp. (in Bachmayer, 1967)	*Titanochelon* sp.	AMPG
Pikermi, Attica	Late Miocene	*Testudo marmorum* (in Bachmayer & Symeonidis, 1970)	*Testudo* sp. (hingeless)	AMPG
Liossati, Kiourka	Late Miocene	*Testudo* sp. (in Bachmayer & Symeonidis, 1977)	*Titanochelon* sp.	AMPG
Samos Island	Late Miocene	*Testudo schafferi* (in Szalai, 1931)	*Titanochelon schafferi*	NHMW
Samos Island	Late Miocene	-	*'Testudo'* sp. nov.	AMPG; GNHM
Serres	Late Miocene	-	*Testudo* sp.	AMPG
Thymiana?, Chios Island	Middle Miocene	*Testudo* sp. I & II (in Paraskevaidis, 1955)	cf. *'Testudo'* sp. nov.	BSPG (lost)
Nostimo, Kastoria	Early Miocene	*Nostimochelone lampra* (in Georgalis et al., 2013)	*Nostimochelone lampra*	NM
Halmyropotamos, Evia Island	Late Miocene	*Testudo marmorum* (in Melentis, 1970)	Not located	unknown

Collections examined with no chelonian findings: Over the course of the present thesis several collections of Greek material housed in Greek and foreign institutions have been examined in order to discover chelonian fossils. In the following collections no chelonian fossils have been noted:

Loutra Almopias Cave (Late Pleistocene; LGPUT LAC); Agios Georgios Cave, Kilkis (Pleistocene; LGPUT SKG); Petralona Cave (Pleistocene; old collection, LGPUT PEC); Thermopigi, Serres (Late Miocene; Museum of Thermopigi SIT); Smari Acropolis, Crete Island (Holocene; Herakleion); Pikermi, Attica (Late Miocene; MNHN, MfN, PIMUZ). Samos Island (Late Miocene; MfN).

This page has been intentionally left blank

02/16/2016 Ψηφιακή Βιβλιοθήκη Θεόφραστος - Τμήμα Γεωλογίας - Α.Π.Θ.

Chapter 4. Evolution

Highlights

A new matrix for testudinids

Phylogeny of testudinids
Phylogeny of geoemydids
The affinities of the only pleurodire of Greece

4.1. Introduction

This chapter deals with the evolution of the Greek chelonians within the current European and Mediterranean context. On the first part of the phylogenetic analysis of large and small testudinids is presented, based on a new morphological matrix of characters. Further analyses are made on the geoemydid taxa and on *Nostimochelone lampra*. On the second part of this chapter, this information is combined with the fossil record (presented in the previous chapter) to present the evolution of the Greek chelonian lineages through time.

In this chapter phylogenetic analyses of the most important components of the Greek fossil chelonian fauna are performed. Our main focus lies on the phylogenetic analyses of the large testudinids of Greece and Europe, which are poorly known. Here a new matrix of morphological characters is presented, with drawings of the various character states. At first, we analyse both large and small-in-size testudinids, but a special focus is drawn upon the complex of the various *Testudo* species from Greece, with particular interest on the phylogenetic relationships of *Testudo marmorum* and *Testudo marginata*. Also, the fossil terrapins from the Late Miocene and Early Pliocene of Greece are analysed as well, in a more general context including many Paleogene and Neogene forms. Finally, the affinities of the only pleurodire taxon from Greece are explored.

4.2. A new matrix for testudinids.

The following phylogenetic analyses are based on a series of characters from the shell, cranium and limb bones. First of all, the characters introduced in several papers for the cladistic analysis of testudinids have been evaluated and reviewed. Such a matrix does not exist in the literature. The doctoral dissertation of Crumly (1984) is a particularly useful source of information, since it contains extensive description of many characters from the shell, skull and the rest of the skeleton for the analysis of land tortoises. However, the problem of this set of characters is mainly on the coding that has been completely revised here. A set of characters that has been used in many studies is that of Takahashi et al. (2003), which is based largely on the works of Crumly (1982; 1984) and Meylan & Sterrer (2000). Regarding the analysis the hinged and hingeless *Testudo* we used many characters proposed by Amiranashvili (2000) and Lapparent de Broin et al. (2006b). The contribution of Gerlach (2001) has been particularly useful for the cranial characters. However, these characters also required some significant revision in order to be described and to properly define the coding. Regarding the inclusion of large testudinids we follow the set of characters introduced by Pérez-García & Vlachos (2014). Finally, several characters from Joyce & Bell (2004) have been used, that are particularly useful for the relationships of the ingroup within Testudinoidea. A great difficulty is found in scoring the cranial characters among the fossil large testudinid taxa, given the inability to observe the cranial sutures. Moreover, skull specimens are only known within *Titanochelon* and in the extant taxa, therefore the inclusion of cranial characters was useful only to discover the relationships in these taxa. Most of the characters in the appendicular skeleton, such as those regarding the fusion of carpals and tarsals, were found to be subject to intraspecific variation and more importantly to the ontogenetic stage of the animal. Following Joyce & Bell (2004) the different states of most characters have been illustrated. Some of them (e.g. from the appendicular skeleton) are relatively straightforward and do not require illustration.

02/16/2016 Ψηφιακή Βιβλιοθήκη Θεόφραστος - Τμήμα Γεωλογίας - Α.Π.Θ.

Drawings based on extant and fossil specimens are presented. This list of characters is not exhaustive, but is only a first attempt to solve the relationships of the European tortoises based on morphological characters, and should be treated as such. For example, this set of characters cannot sufficiently explain groups such as the *Chelonoidis* group, which exhibits a mosaic of characters and significant intra-generic morphological variation. Therefore, the application of this set of characters in testudinid groups outside Europe and Africa should be treated with caution, and additional characters and/or different coding might be required.

Carapace Characters

[1] NUCHAL 1: Shape of the outline of the nuchal plate (see Amiranashvili 2000:1).
Coding: hexagonal (0); octagonal (1).
Comments: the shape of the outline of the nuchal bone is generally hexagonal, contacting the first peripherals, the first pleurals and the first neural (e.g. *T. g. ibera*). In some cases however (e.g. *T. h. boettgeri*), the outline could be octagonal, showing two additional sutural surfaces with the first pleurals. In some cases, the octagonal shape of the nuchal causes a posterior elongation of the nuchal plate towards the first neural.

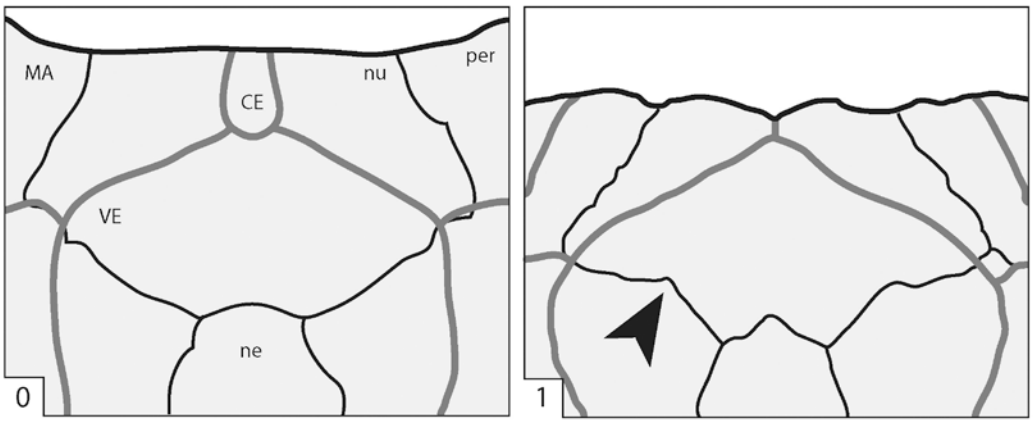


Figure 4.1. Illustration of the different states of the character NUCHAL 1: 0, hexagonal in *Testudo graeca*; 1, octagonal in *Geochelone elegans*.

[2] NUCHAL 2: General shape of the nuchal plate (see Pérez-García & Vlachos, 2014:2).
Coding: markedly wider than long (0); slightly wider than long or as long as wide (1); markedly longer than wide (2).
Comments: this character refers to the general shape of the nuchal plate based on the comparison between the maximum length of the plate measured in the midline (without the affection of the nuchal notch, if present), versus the maximum width (usually noted in the suture with the first peripherals).

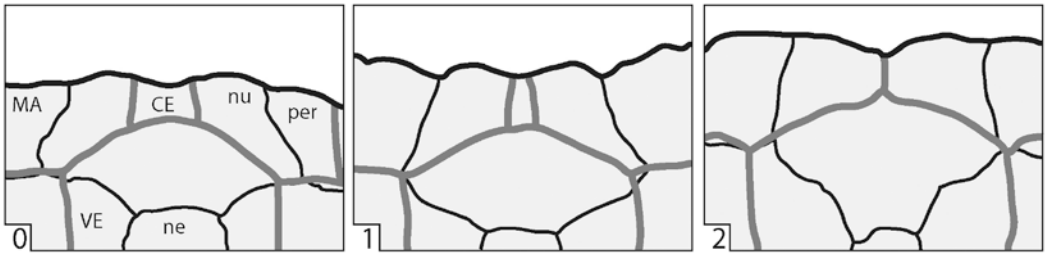


Figure 4.2. Illustration of the different states of the character NUCHAL 2: 0, markedly wider than long in *Gopherus agassizi*; 1, as wide as long in *Testudo graeca*; 2, longer than wide in *Centrochelys sulcata*.

[3] NUCHAL 3: Overlapping of the first pleural on the nuchal plate (see Amiranashvili 2000:4). Coding: first pleural overlaps postero-lateral parts of the nuchal (0); first pleural touches, but it does not overlap the nuchal (1); first pleural is not in contact with the nuchal (2).
Comments: In some cases, the antero-medial parts of the first pleural scute overlap the postero-lateral sides of the nuchal. Although this morphology is usually found in emydids, some testudinids (e.g. *T. h. boettgeri* and *T. kleinmanni*) display it as well, but to a lesser degree. This character could be related with the character 45 of Joyce & Bell, 2004 (width of the anterior part of the first vertebral scute), since when the first vertebral is anteriorly narrowed then the first pleural overlaps the nuchal.

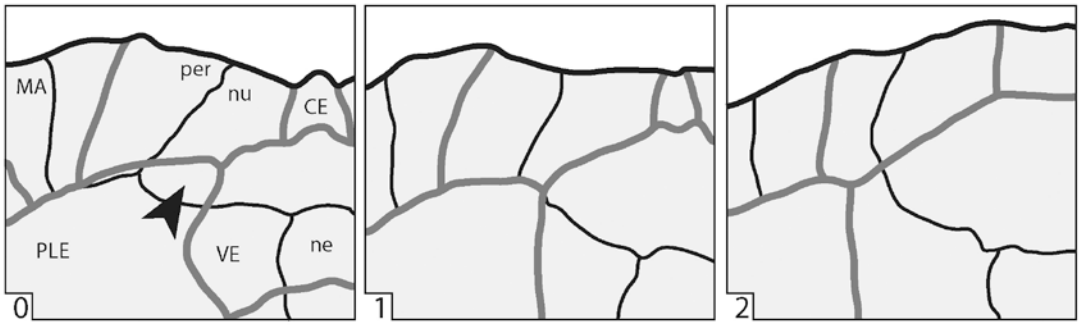


Figure 4.3. Illustration of the different states of the character NUCHAL 3: 0, first pleural overlapping the nuchal in *Testudo kleinmanni*; 1, first pleural touches, but it does not overlap the nuchal *Testudo graeca*; 2, first pleural is not in contact with the nuchal in *Gopherus polyphemus*.

[4] NUCHAL 4: Nuchal notch (see Pérez-García & Vlachos, 2014:1).
Coding: absent (0); shallow (1); deep (2); significant medial protrusion present (3).

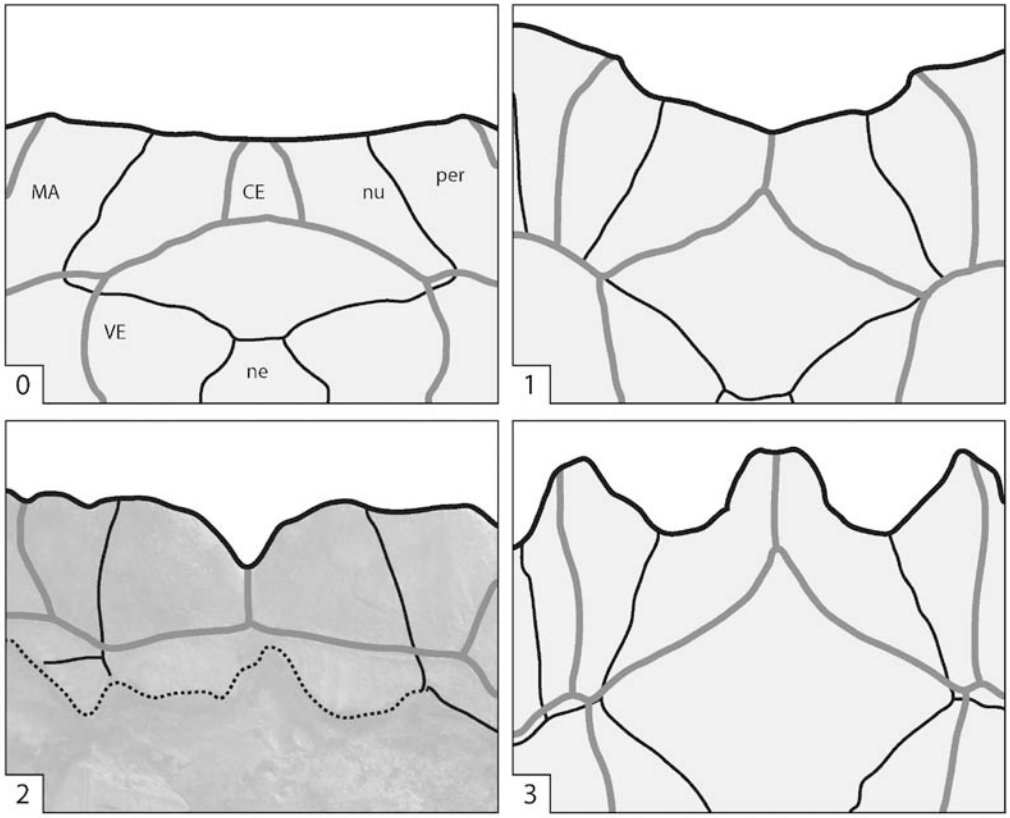


Figure 4.4. Illustration of the different states of the character NUCHAL 4: 0, notch absent in *'Testudo' hermanni*; 1, shallow notch in *Stigmochelys pardalis*; 2, deep notch in the Oligocene *"Testudo" gigas*; 3, medial protrusion (extreme in this case) in *Kinixys erosa*.

Comments: In several forms the anterior border of the nuchal plate could be notched. This character is relatively difficult to code, because of the significant morphological variation. When absent, in some cases a medial protrusion is present in the part that is covered by the cervical. When present it could be shallow and broad, sometimes affecting the first peripherals as well. In other cases, the nuchal notch could be very deep, affecting only the nuchal plate and not the peripherals. Interestingly, the presence of a deep nuchal notch is usually associated with the absence of the cervical scute.

[5] CERVICAL: Presence of a cervical scute on dorsal side of the carapace (see CVS, Crumly, 1984; Takahashi et al., 2003:15; Joyce & Bell, 2004:40; Pérez-García & Vlachos, 2014:14).
Coding: dorsally present (0); absent (1).
Comments: the presence/absence of the cervical scute is among the classic characters used in the analysis of testudinids. Here the simple coding of Joyce and Bell (2004; character 40) is followed. Note however that there are cases were the cervical scute could be present dorsally and absent viscerally.

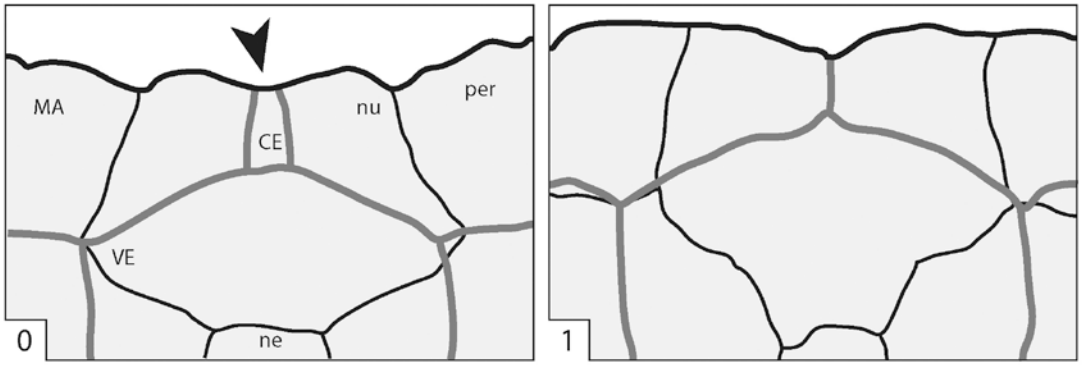


Figure 4.5. Illustration of the different states of the character CERVICAL: 0, dorsally present in *Testudo graeca*; 1, absent in *Centrochelys sulcata*.

[6] NEURAL NUMBER: Number of neural plates (see Amiranashvili, 2000:7; Lapparent de Broin et al., 2006b:5; Pérez-García & Vlachos, 2014:3).
Coding: nine neurals (0); eight neurals (1); seven neurals or less (2).

Comments: In some basal extinct forms there are nine neurals (e.g. *Hadrianus castrensis*; see Pérez-García & Vlachos, 2014). The most common case is the presence of eight neural plates. The fusion of the posterior neurals results in reduction of the number of neurals in 7, and on some extreme cases to less than 7 with costal plates meeting in the midline. We treat this condition as a separate character, following Joyce and Bell (2004; character 39).

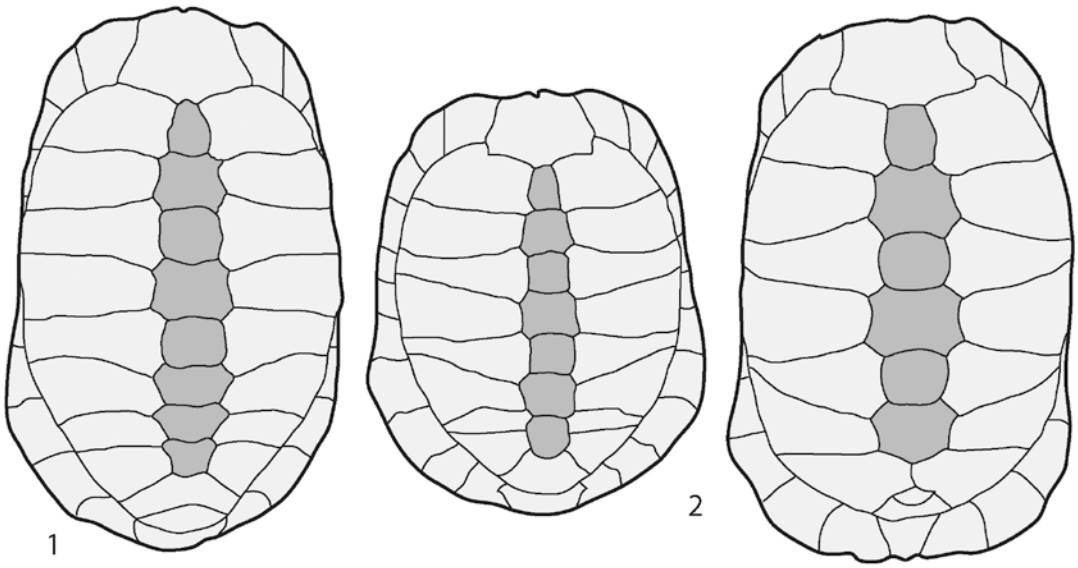


Figure 4.6. Illustration of the different states of the character NEURAL NUMBER: 1, eight neurals in *Indotestudo elongata*; 2, seven neurals or less in *'Testudo' hermanni* (seven) and in *Testudo marginata* (six). For state 0, see *Hadrianus castrensis* in de Broin (1977).

[7] NEURAL 1: Shape of the first neural (see Pérez-García & Vlachos, 2014:6).
Coding: hexagonal, short sides positioned posteriorly (0); rectangular (1).

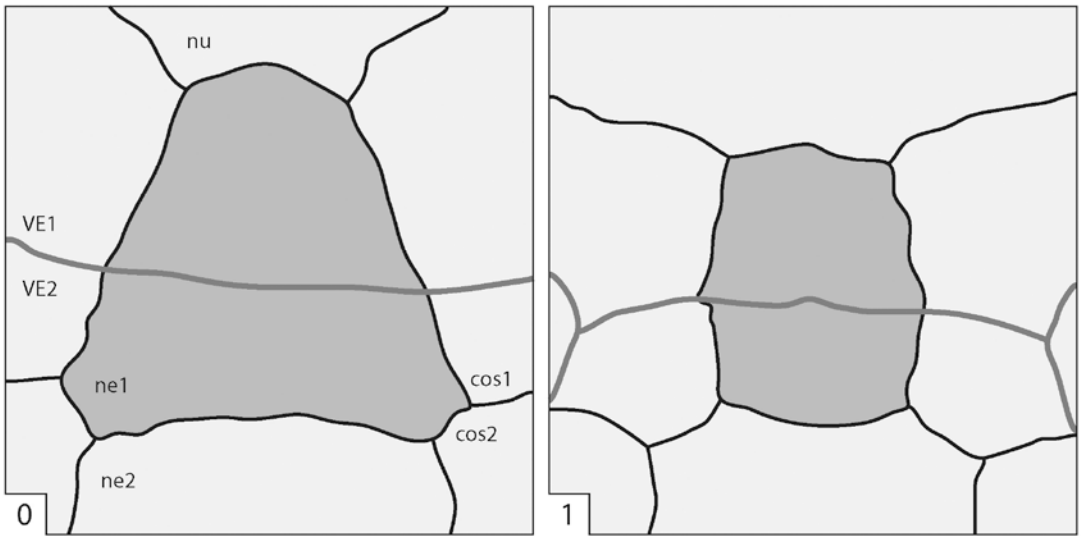


Figure 4.7. Illustration of the different states of the character NEURAL 1: 0, hexagonal in *Gopherus polyphemus*; 1, rectangular in *Testudo marginata.*

[8] NEURAL 2: Shape of the second neural (see Joyce & Bell, 2004:37; Pérez-García & Vlachos, 2014:7).
Coding: rectangular (0); hexagonal, short sides positioned anteriorly (1); hexagonal, short sides positioned posteriorly (2); octagonal (3).
Comments: based on the coding introduced by Joyce and Bell (2004; character 37), we have added another one for a rectangular second neural. A rectangular second neural is not present in extant testudinids, but is found in the fossil *Achilemys cassouleti*.

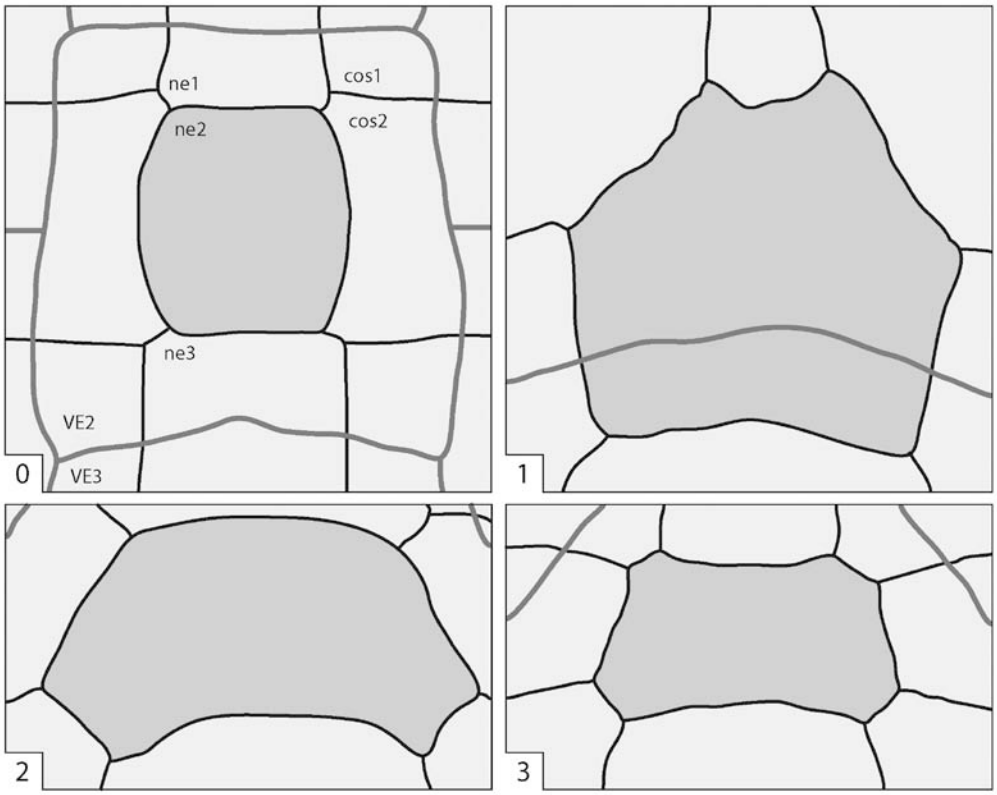


Figure 4.8. Illustration of the different states of the character NEURAL 2: 0, rectangular in *Achilemys cassouleti*; 1, hexagonal, short sides positioned anteriorly in *Psammobates tentorius*; 2, hexagonal, short sides positioned posteriorly in *Geochelone elegans*; 3, octagonal in *Stigmochelys pardalis.*

[9] NEURAL 3: Shape of the third neural (see Joyce & Bell, 2004:38; Pérez-García & Vlachos, 2014:8).
Coding: hexagonal (0); rectangular (1); octagonal (2).

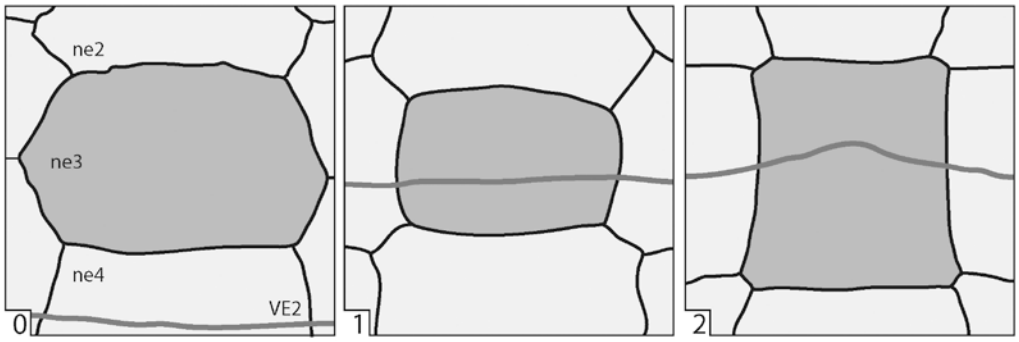


Figure 4.9. Illustration of the different states of the character NEURAL 3: 0, hexagonal in *Kinixys beliana*; 1, rectangular in *Testudo graeca*; 2, octagonal in *Achilemys cassouleti*.

[10] NEURAL 4: Shape of the fourth neural (see Pérez-García & Vlachos, 2014:9).
Coding: rectangular (0); hexagonal (1); octagonal (2).

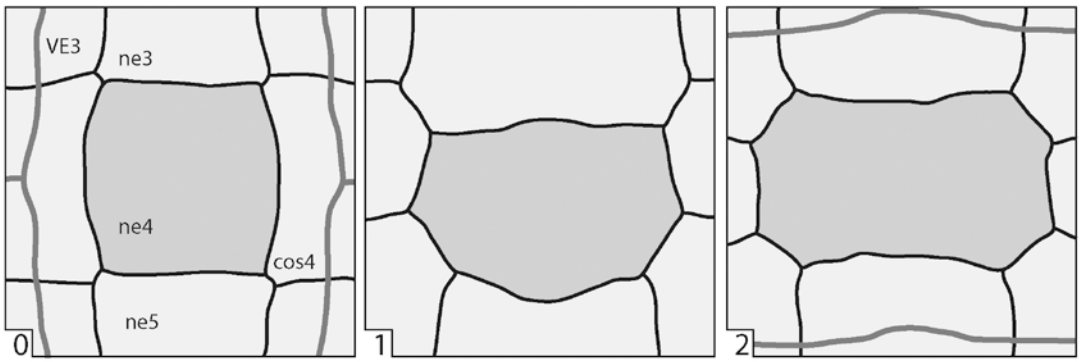


Figure 4.10. Illustration of the different states of the character NEURAL 4: 0, rectangular in *Achilemys cassouleti*; 1, hexagonal in *Kinixys erosa*; 2, octagonal in *Stigmochelys pardalis.*

[11] NEURAL 5: Shape of the fifth neural (see Pérez-García & Vlachos, 2014:10).
Coding: hexagonal (0); rectangular (1).

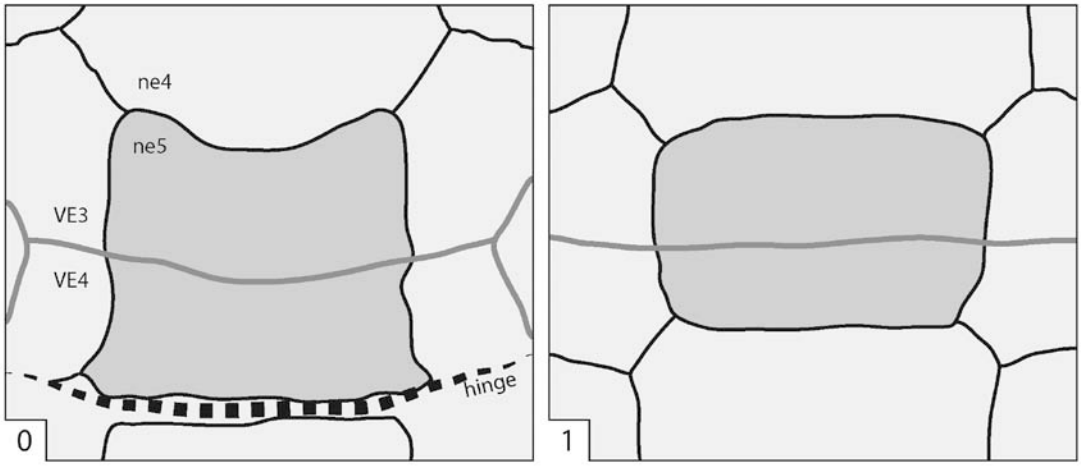


Figure 4.11. Illustration of the different states of the character NEURAL 5: 0, hexagonal in *Kinixys erosa*; 1, rectangular in *Testudo graeca.*

[12] COSTAL: Medial contact of the seventh and/or eighth costal plates (see Joyce & Bell, 2004:39).
Coding: absent (0); present (1).

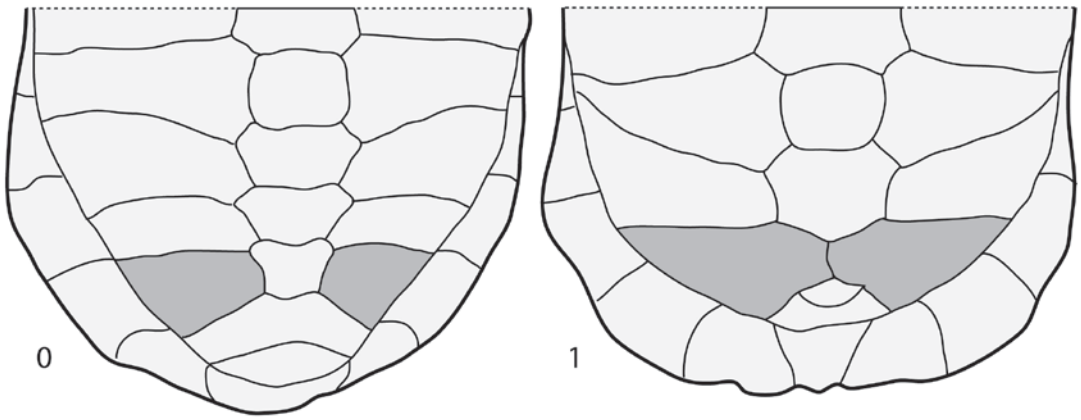


Figure 4.12. Illustration of the different states of the character COSTAL: 0, absent in *Stigmochelys pardalis*; 1, present in *Testudo marginata.*

[13] SUPRAPYGAL: Number and shape of the suprapygal bones (see PYP, Crumly, 1984; Amiranashvili, 2000:12; Lapparent de Broin et al., 2006b:6, 7; Pérez-García & Vlachos, 2014:11).
Coding: two, the contact between the suprapygals is straight and perpendicular to the axial plane (0); two, the two suprapygals together constitute one trapeze and the first suprapygal embraces the lenticular second one (1); one, suprapygals fused, constituting one trapeze (2).
Comments: Many characters have been proposed to explain the variation in this region. As it has been extensively described by Lapparent de Broin et al. (2006b), the variation of this region within *Testudo* s.l. is high, but in other groups (e.g. *Titanochelon*) the variation is much less (Pérez-García & Vlachos, 2014). Here the available characters are combined to account for the number and shape of the suprapygals at the same time.

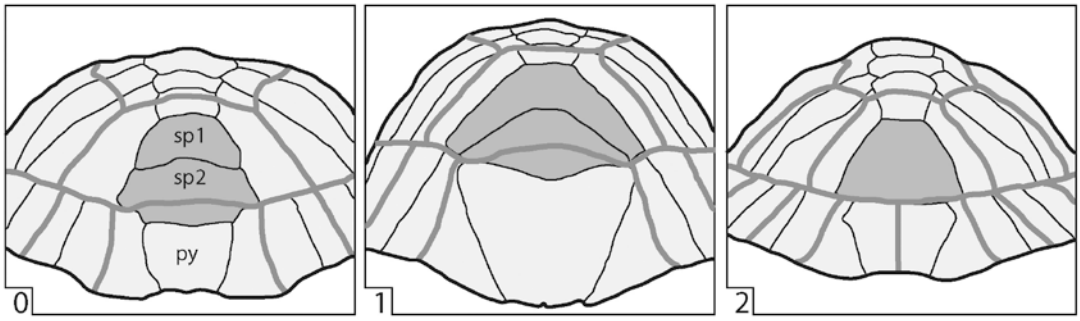


Figure 4.13. Illustration of the different states of the character SUPRAPYGAL: 0, two suprapygals with straight contact in *Gopherus polyphemus*; 1, two suprapygals, the first embracing the second, in *Stigmochelys pardalis*; 2, one suprapygal in *'Testudo' hermanni*.

[14] PYGAL: Pygal shape (see Lapparent de Broin et al., 2006b:8).
Coding: quadrangular (without small latero-anterior borders) (0); quadrangular or hexagonal with small latero-anterior borders (1).

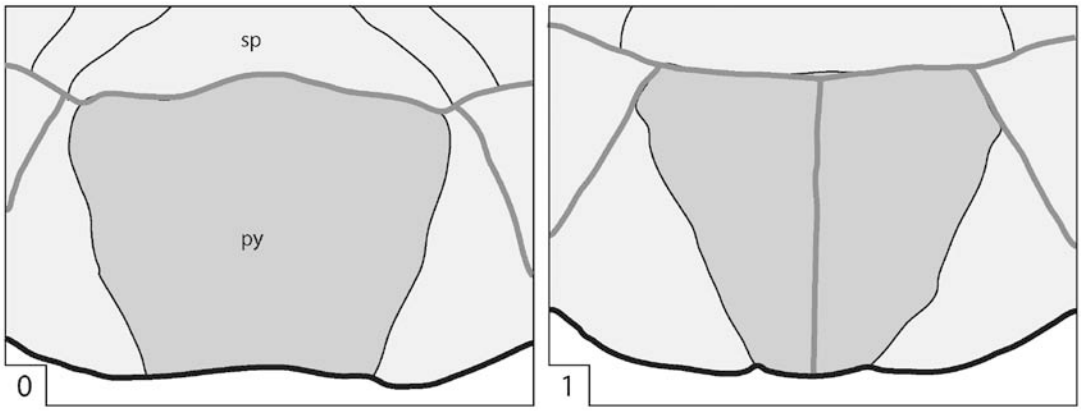


Figure 4.14. Illustration of the different states of the character PYGAL: 0, without latero-anterior border in *Indotestudo elongata*; 1, with latero-anterior borders in *'Testudo' hermanni*.

[15] VERTEBRAL 1: Width of the vertebrals in respect with the pleurals (see Amiranashvili, 2000:15, 16; Lapparent de Broin et al., 2006b:14).
Coding: wide vertebrals, wider than the pleurals (0); wide vertebrals, almost equal to the pleurals (1); narrow vertebrals, narrower than the pleurals (2).

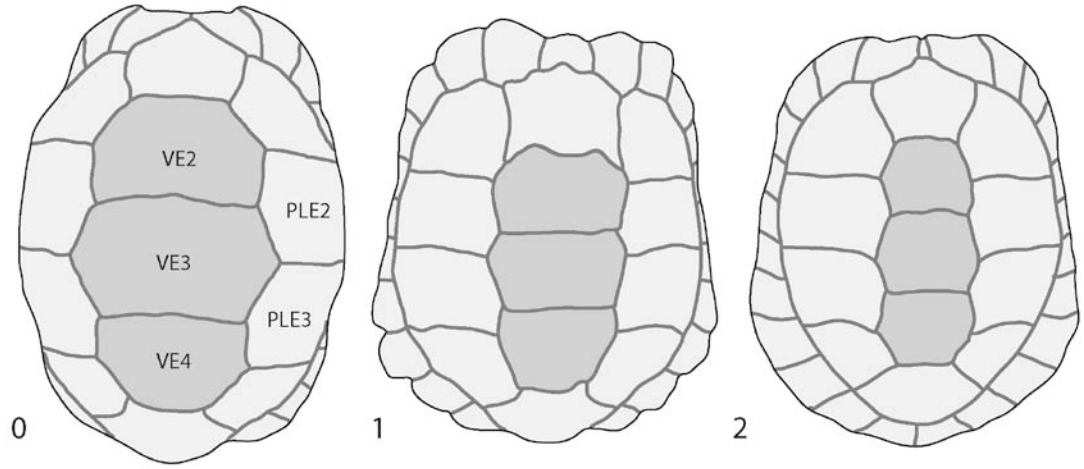


Figure 4.15. Illustration of the different states of the character VERTEBRAL 1: 0, vertebrals wider than pleurals in *Stigmochelys pardalis*; 1, vertebrals almost equal to pleurals in *Manouria impressa*; 2, vertebrals narrower than pleurals in *'Testudo' hermanni*.

[16] VERTEBRAL 2: Overlapping of fifth vertebral on suprapygal (see Lapparent de Broin et al., 2006b:6).
Coding: the posterior sulcus of the fifth vertebral overlaps the anterior part of the pygal (0); the posterior sulcus of the fifth vertebral crosses the suprapygal transversely (1); the posterior sulcus of the fifth vertebral coincides with the suprapygal-pygal suture (2).
Comments: the degree of overlapping of the fifth vertebral is quite variable. In Lapparent de Broin et al. (2006b) this morphology is combined with the morphology of the suprapygal area. Since the shape of the suprapygals has been defined independently (see previous character), a different coding is proposed here.

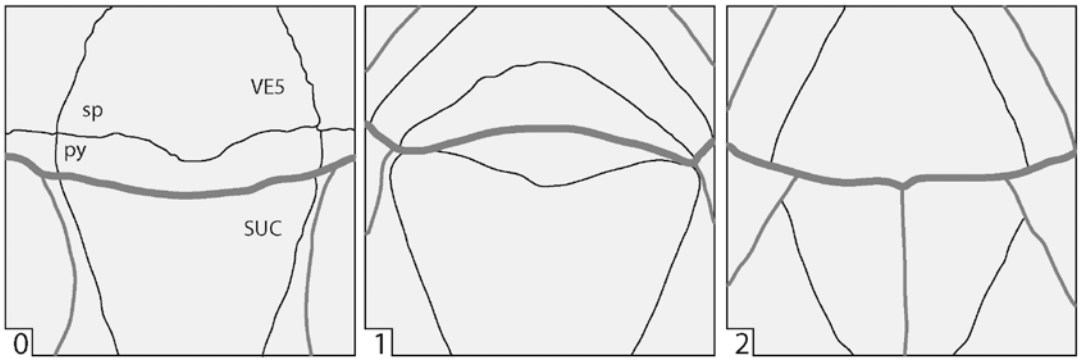


Figure 4.16. Illustration of the different states of the character VERTEBRAL 2: 0, vertebral 5 overlapping the anterior pygal in *Kinixys erosa*; 1, vertebral 5 crossing the suprapygal transversely in *Stigmochelys pardalis*; 2, coinciding with the suprapygal-pygal suture in *'Testudo' hermanni*.

[17] SUPRACAUDAL 1: Fusion of twelfth marginals into a supracaudal, dorsally (see SSP, Crumly, 1984; Amiranashvili, 2000:18; Takahashi et al., 2003:27; Joyce & Bell, 2004:49; Lapparent de Broin et al., 2006b:15, 16; Pérez-García & Vlachos, 2014:19).
Coding: two twelfth marginals present dorsally (0); twelfth marginals fused into a single supracaudal dorsally (1).
Comments: this is a classic character used in testudinids, but is variable on whether the twelfth marginals are fully fused, both dorsally and viscerally. Although we could make only one character with combined states, here the characters are separated (as in

Lapparent de Broin et al., 2006b but with a simpler coding) for dorsal and visceral sides. This will make these characters particularly useful in fossils where only one side is available for observation and will help to document better the variation.

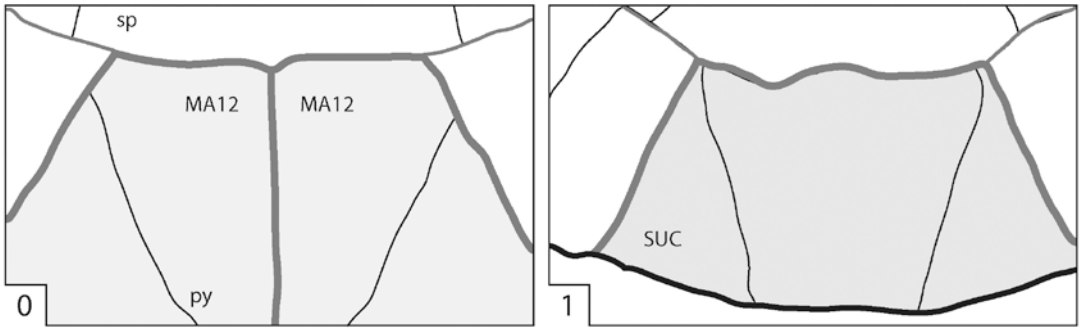


Figure 4.17. Illustration of the different states of the character SUPRACAUDAL 1: 0, marginal 12 present in *'Testudo' hermanni*; 1, fused into a supracaudal in *Testudo graeca*.

[18] SUPRACAUDAL 2: Fusion of twelfth marginals into a supracaudal, viscerally (see previous character).
Coding: two twelfth marginals present viscerally (0); twelfth marginals fused into a supracaudal viscerally (1).

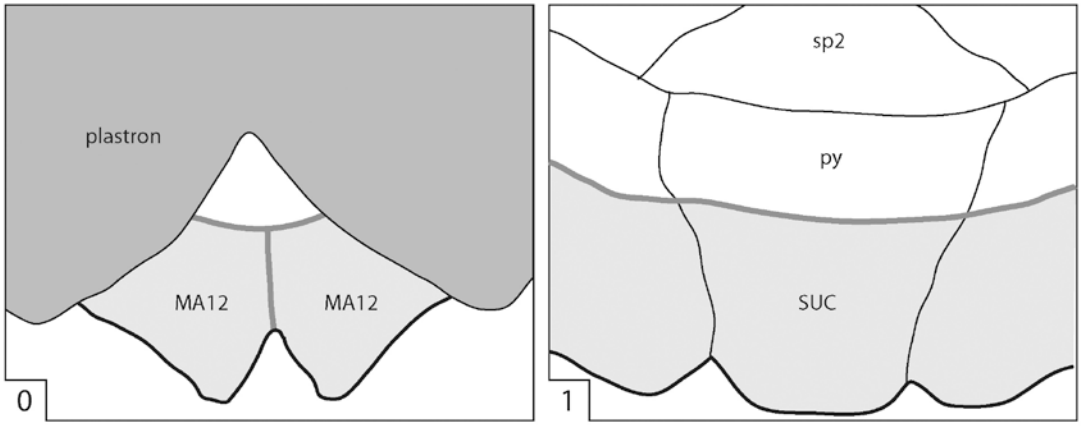


Figure 4.18. Illustration of the different states of the character SUPRACAUDAL 2: 0, marginal 12 present viscerally in *Manouria impressa*; 1, marginals fused into a supracaudal in *'Testudo' hermanni*.

[19] COINCIDENCE: Coincidence between the costo-peripheral suture and the pleuro-marginal sulcus, in the anterior peripherals (1-4) (see Amiranashvili, 2000:19; Lapparent de Broin et al., 2006:4; Pérez-García & Vlachos, 2014:15).
Coding: absent (0); present (1).

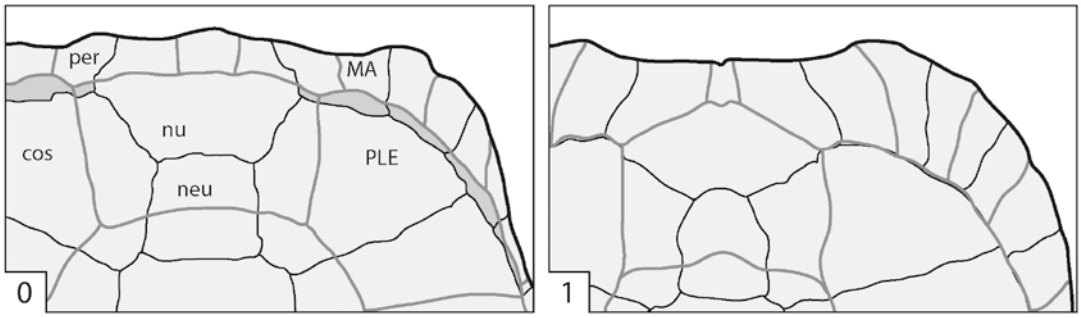


Figure 4.19. Illustration of the different states of the character COINCIDENCE: 0, absent in *Gopherus berlandieri*; 1, present in *'Testudo' hermanni*.

[20] PERIPHERAL: Protrusions on the peripherals, at the limit with the sulci between the marginal (Pérez-García & Vlachos, 2014:12,13).
Coding: absent or poorly developed (0); well developed (1).

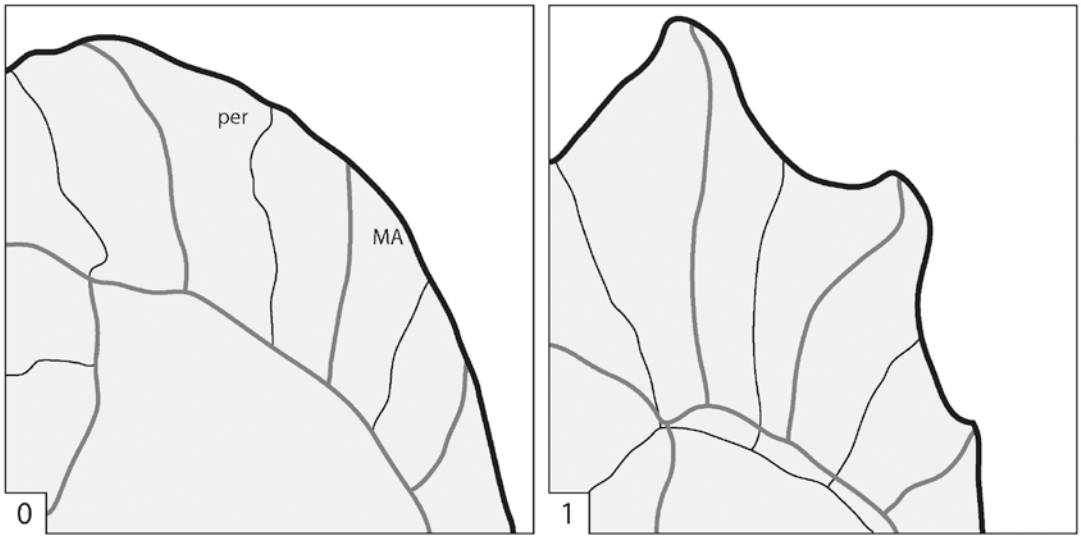


Figure 4.20. Illustration of the different states of the character PERIPHERAL: 0, absent or poorly developed in *'Testudo' hermanni*; 1, well developed in *Kinixys erosa*.

[21] MARGINAL 1: Contact of the second marginals with the lateral margin of the nuchal (Pérez-García & Vlachos, 2014:16).
Coding: absent (0); present (1).

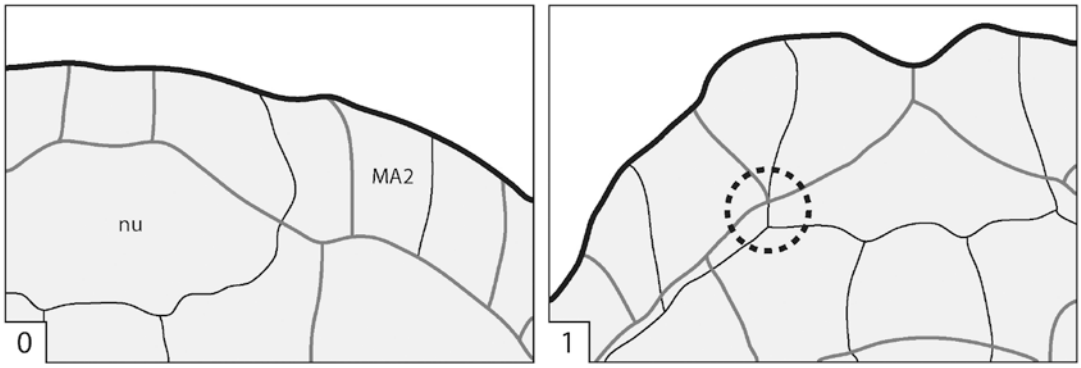


Figure 4.21. Illustration of the different states of the character MARGINAL 1: 0, absent in *Gopherus polyphemus*; 1, present in *Cheirogaster maurini*.

[22] MARGINAL 2: Contact of the second marginals with the first vertebral scute (Joyce & Bell, 2004:47; Pérez-García & Vlachos, 2014:17).
Coding: absent (0); present (1).

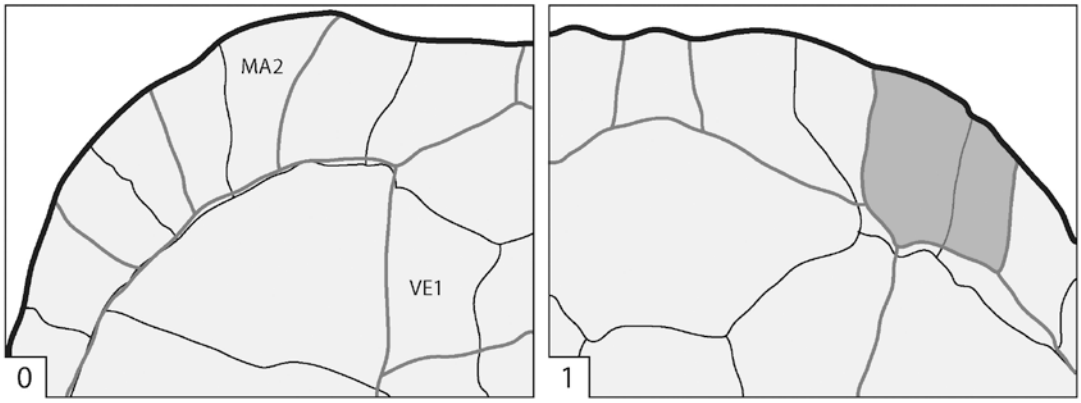


Figure 4.22. Illustration of the different states of the character MARGINAL 2: 0, absent in *'Testudo' hermanni*; 1, present in *Mauremys caspica*.

[23] MARGINAL 3: Contact of the fourth marginals with the second pleural scutes (Pérez-García & Vlachos, 2014:18).
Coding: absent (0); present (1)



Figure 4.23. Illustration of the different states of the character MARGINAL 3: 0, absent in *Testudo graeca*; 1, present in *Gopherus polyphemus*.

[24] MARGINAL 4: Contact of the sixth marginals with the third pleural scute.
Coding: absent (0); present (1)

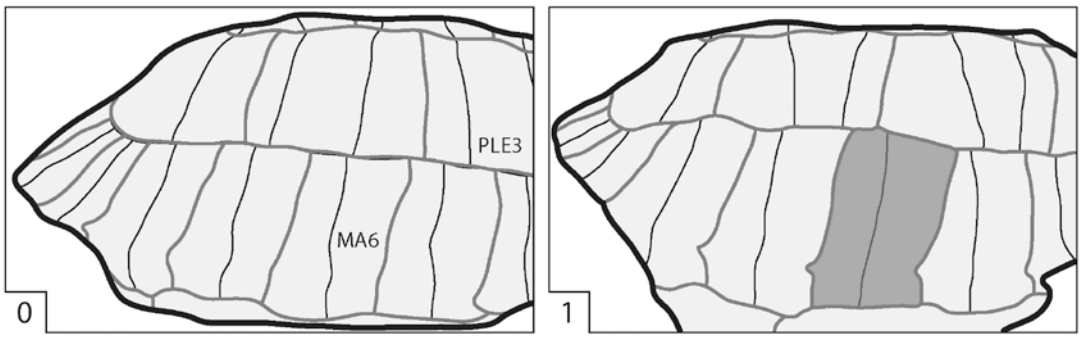


Figure 4.24. Illustration of the different states of the character MARGINAL 4: 0, absent in *Testudo graeca*; 1, present in *Gopherus polyphemus*.

[25] CARAPACIAL HINGE: presence of a carapacial hinge (CRH, Crumly, 1984).
Coding: absent (0); present (1).

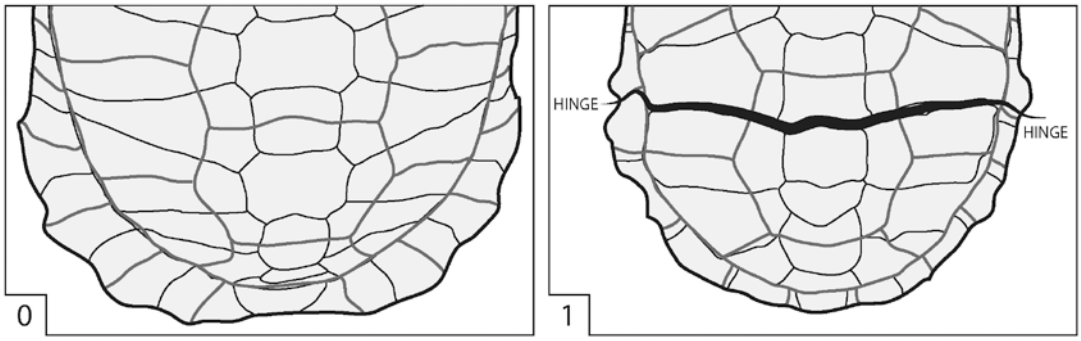


Figure 4.25. Illustration of the different states of the character CARAPACIAL HINGE: 0, absent in *Testudo graeca*; 1, present in *Kinixys erosa*.

[26] BORDER: shape of the posterior shell border (see Lapparent de Broin et al., 2006:2).
Coding: posterior border curved inwards (0); posterior border posteriorly flared (1).
Comments: the posterior border of the carapace, i.e. pygal and the 9-11 peripherals, could be either curved inwards (moderately or strongly depending also on the sex) or it could be posteriorly (and even horizontally in some cases) flared.

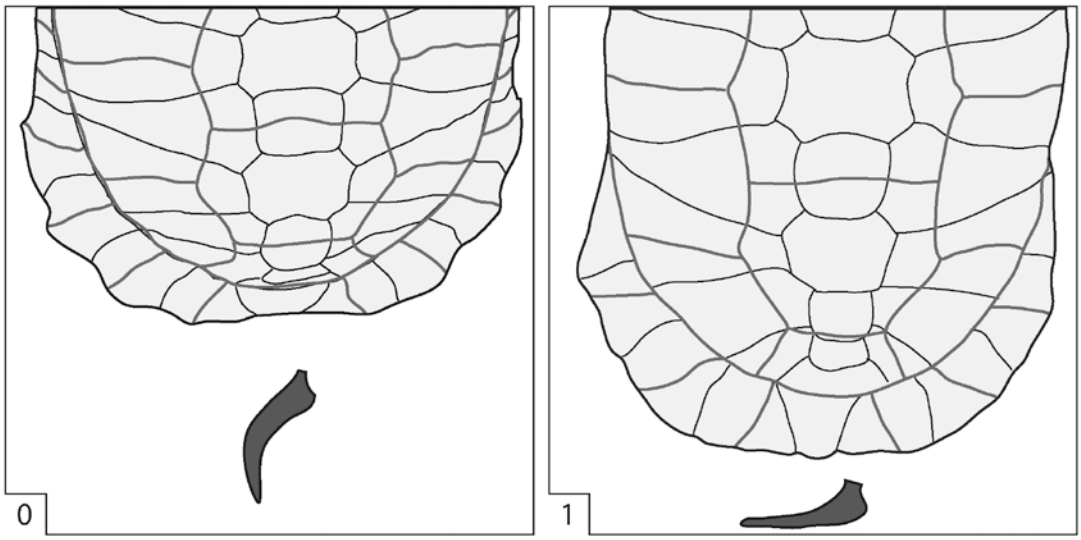


Figure 4.26. Illustration of the different states of the character BORDER: 0, posterior border curved inwards (see cross-section) in *Testudo graeca*; 1, posterior border posteriorly flared (see cross-section) in *Testudo marginata*.

Plastron

[27] ANTERIOR LOBE: Shape of the anterior lobe (Amiranashvili, 2000:22; Pérez-García & Vlachos, 2014:21).
Coding: subrounded to straight (0); medially notched (1); trilobed (2); triagonal (3).

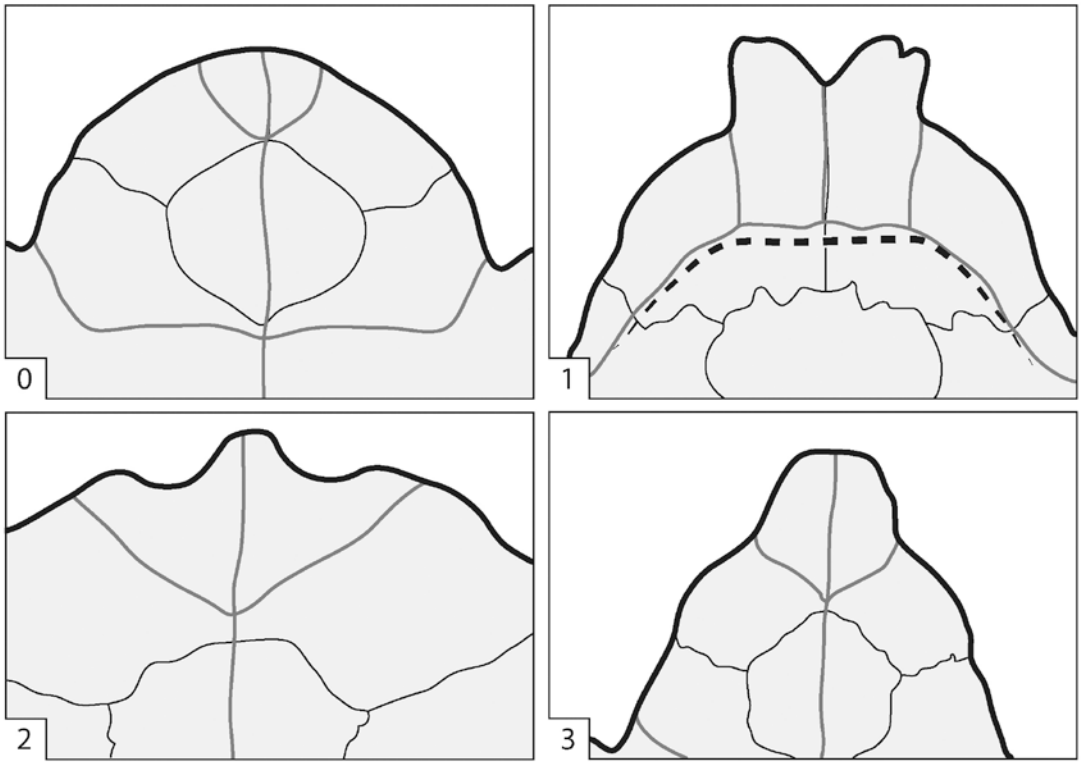


Figure 4.27. Illustration of the different states of the character ANTERIOR LOBE: 0, subrounded to straight in *Stigmochelys pardalis*; 1, medially notched in *Centrochelys sulcata*; 2, trilobed in *Kinixys erosa*; 3, triagonal in *Gopherus agassizii*.

[28] GULAR PROTRUSION: Well-developed gular protrusion, caused by constriction in the gularo-humeral sulcus (see PLC, Crumly, 1984; Pérez-García & Vlachos, 2014:22).
Coding: absent (0); present (1).

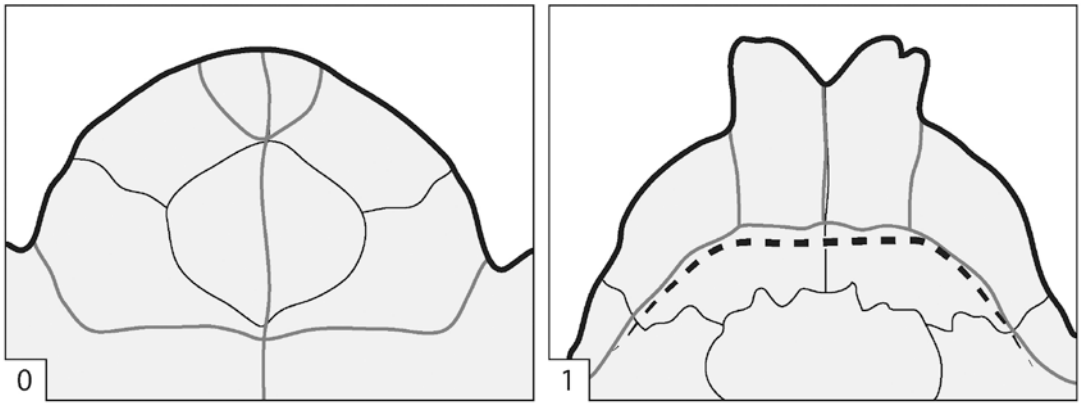


Figure 4.28. Illustration of the different states of the character GULAR PROTRUSION: 0, absent in *Stigmochelys pardalis*; 1, present in *Centrochelys sulcata*.

[29] EPIPLASTRON 1: Presence of an epiplastral lip (Amiranashvili, 2000:23; Takahashi et al., 2003:28; Joyce & Bell, 2004:59; Lapparent de Broin et al., 2006b:9).
Coding: absent or poorly developed (0); present (1).
Comments: in some cases the visceral part of the epiplastra is thickened forming a lip, which sometimes preserves a gular pocket.

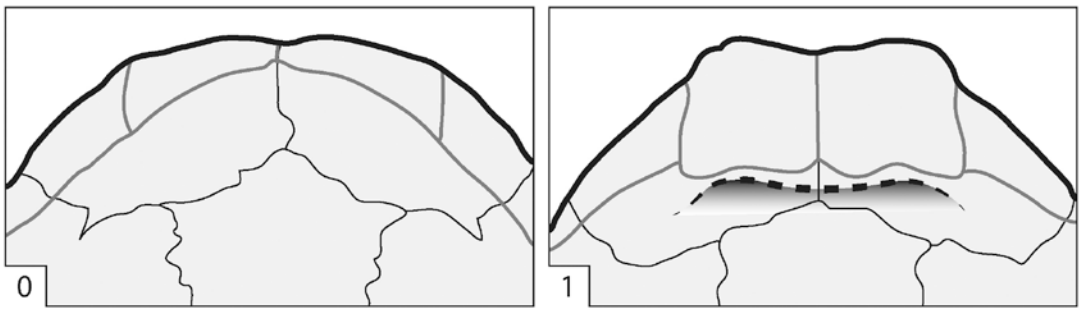


Figure 4.29. Illustration of the different states of the character EPIPLASTRON 1: 0, absent in *Emys orbicularis*; 1, present in *Testudo graeca*.

[30] EPIPLASTRON 2: Shape of the dorsal lip of the epiplastra (Pérez-García & Vlachos, 2014:23).
Coding: concave (0); convex to flat (1).

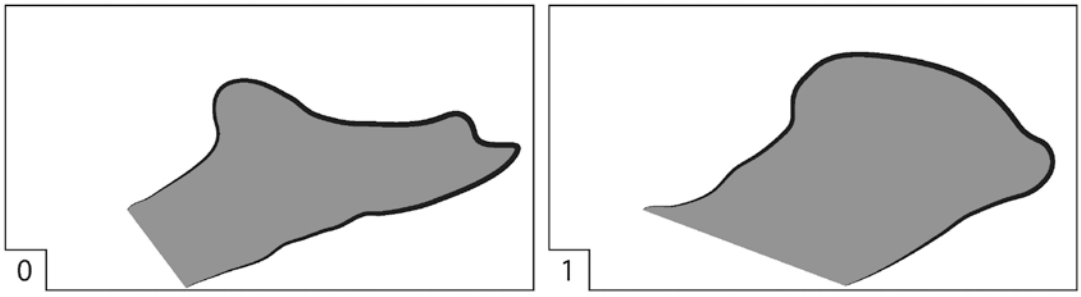


Figure 4.30. Illustration of the different states of the character EPIPLASTRON 2: 0, concave epiplastral in *Gopherus agassizii* (cross-section); 1, convex in *Testudo graeca* (cross-section).

[31] GULARS 1: Gulars in contact with the entoplastron or covering this plate (see GSE, Crumly, 1984; Amiranashvili, 2000:25; Takahashi et al., 2003:29; Pérez-García & Vlachos, 2014:24).
Coding: not in contact (0); in contact with the anterior margin (1); covering the anterior area (2).

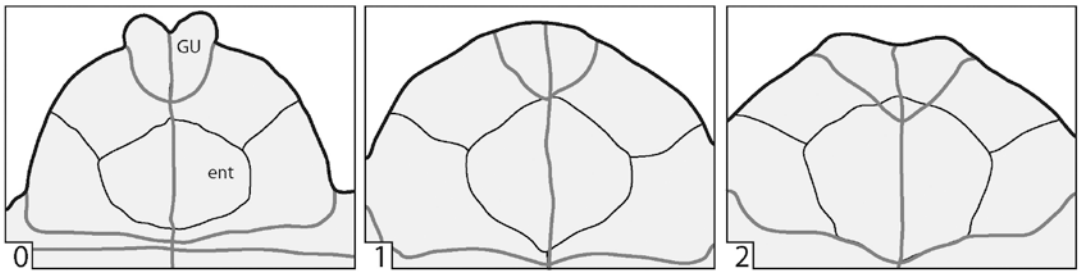


Figure 4.31. Illustration of the different states of the character GULARS 1: 0, not in contact in *Centrochelys sulcata*; 1, in contact with the anterior margin in *Stigmochelys pardalis*; 2, covering the anterior area in *Testudo graeca*.

[32] GULARS 2: Angle between the sagittal axis and the gular–humeral sulcus (see GSE, Crumly, 1984; Pérez-García & Vlachos, 2014:28).
Coding: 45º or more obtuse (0); more acute (1).



Figure 4.32. Illustration of the different states of the character GULARS 2: 0, 45º or more obtuse in *Manouria impressa*; 1, more acute in *Testudo graeca*.

[33] HUMERALS: Median length of humerals, compared to the median length of gulars (Amiranashvili, 2000:28)
Coding: humerals equal or smaller than the gulars (0); humerals longer than the gulars (1).

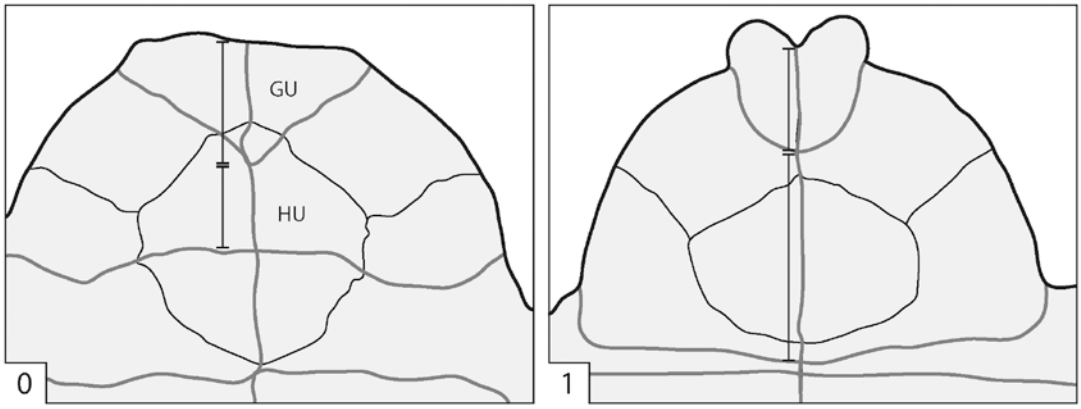


Figure 4.33. Illustration of the different states of the character HUMERALS: 0, humerals equal or smaller than the gulars in *Indotestudo elongata*; 1, humerals longer than the gulars in *Centrochelys sulcata*.

[34] HUMERO-PECTORAL 1: Position of the humero-pectoral sulcus relative to the entoplastron (Amiranashvili, 2000:32; Joyce & Bell, 2004:60).
Coding: posterior to the entoplastron (0); coinciding medially with the posterior suture of the entoplastron (1); crossing the entoplastron (2).

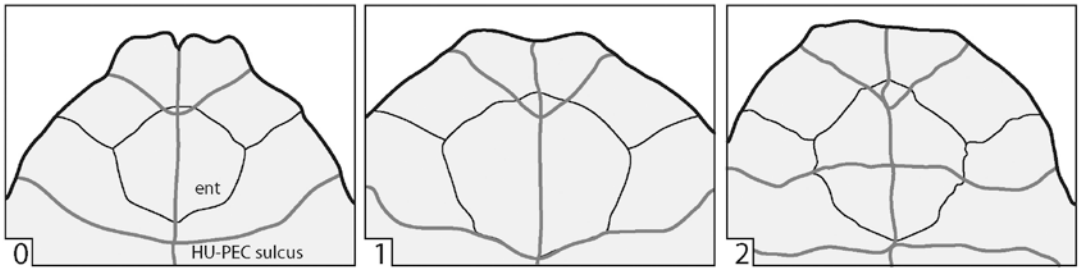


Figure 4.34. Illustration of the different states of the character HUMERO-PECTORAL 1: 0, posterior to the entoplastron in *Gopherus polyphemus*; 1, coinciding medially with the posterior suture of the entoplastron in *Testudo graeca*; 2, crossing the entoplastron in *Indotestudo elongata*.

[35] HUMERO-PECTORAL 2: Humero-pectoral sulcus shape (see PEC, Crumly, 1984; Amiranashvili, 2000:34, Takahashi et al., 2003:30; Pérez-García & Vlachos, 2014:25).
Coding: not perpendicular to the axial plane, rounded or forming a wide angle (0); perpendicular to the axial plane, relatively straight throughout its width (1); perpendicular to the axial plane, with a well-developed lateral change of curvature (2).

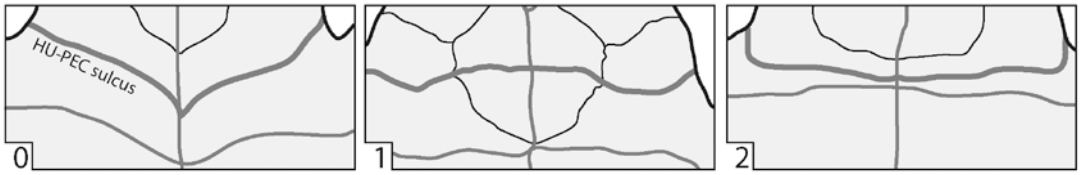


Figure 4.35. Illustration of the different states of the character HUMERO-PECTORAL 2: 0, not perpendicular to the axial plane, rounded or forming a wide angle in *Psammobates tentorius*; 1, perpendicular to the axial plane, relatively straight throughout its width in *Indotestudo elongata*; 2, perpendicular to the axial plane, with a well-developed lateral change of curvature in *Centrochelys sulcata*.

[36] PECTORALS: Medial length of pectorals (see Amiranashvili, 2000:33; Pérez-García & Vlachos, 2014:26).
Coding: long (0); short (1).

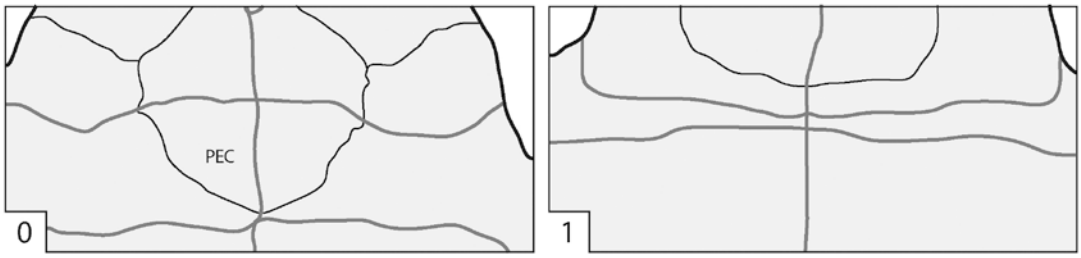


Figure 4.36. Illustration of the different states of the character PECTORALS: 0, medially long in *Indotestudo elongata*; 1, short in *Centrochelys sulcata*.

[37] PLASTRAL HINGE: Presence of a hypo-xiphiplastral hinge in the posterior lobe (see PPH, Crumly, 1984; Amiranashvili, 2000:40; Lapparent de Broin et al., 2006b:3; Pérez-García & Vlachos, 2014:27; closely related morphological characters Amiranashvili 2000:37, Amiranashvili 2000:39, Lapparent de Broin et al., 2006b:11).
Coding: absent (0); present, between hyoplastra and hypoplastra (1); present, between hypoplastra and xiphiplastra (2).

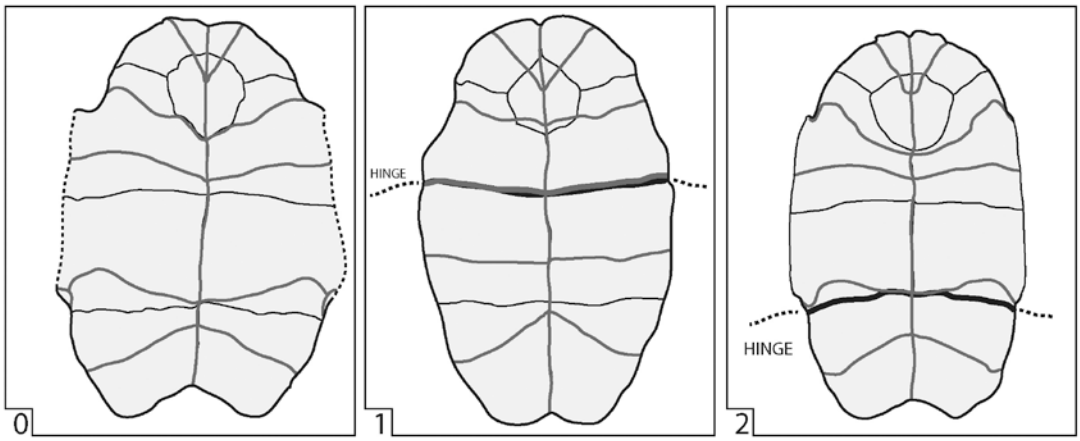


Figure 4.37. Illustration of the different states of the character PLASTRAL HINGE: 0, absent in *'Testudo' hermanni*; 1, between hyo- and hypoplastra in *Emys orbicularis*; 2, between hypo- and xiphiplastra in *Testudo graeca*.

[38] FEMORO-ANAL: Shape of the femoro-anal sulcus (Amiranashvili, 2000:42).
Coding: forms an acute angle with the axial plane (0); it is straight or slightly rounded, developed mainly perpendicular with the axial plane (1); forms S-shaped curve laterally (2).

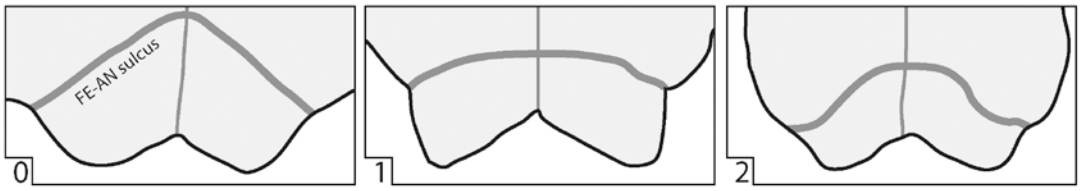


Figure 4.38. Illustration of the different states of the character FEMORO-ANAL: 0, forms an acute angle with the axial plane in *Chersina angulata*; 1, it is straight or slightly rounded, developed mainly perpendicular with the axial plane in *Stigmochelys pardalis*; 2, forms S-shaped curve laterally in *Testudo graeca*.

[39] MEDIAN LENGTH OF ANAL SCUTE: (see Amiranashvili, 2000:44).
Coding: shorter than the median length of femoral (0); longer than the medial length of femoral (1).

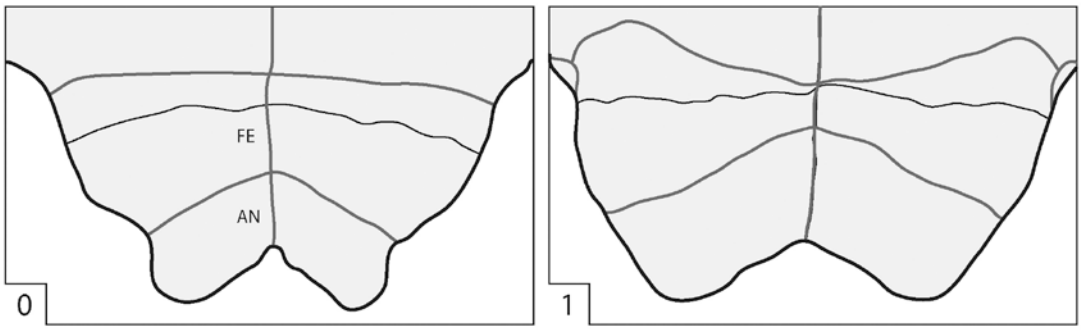


Figure 4.39. Illustration of the different states of the character MEDIAN LENGTH OF ANAL SCUTE: 0, shorter than the median length of femoral in *Gopherus agassizii*; 1, longer than the medial length of femoral in *'Testudo' hermanni*.

Cranium

[40] FRONTAL 1: Frontal participation to the orbital rim (Gerlach, 2001:1; Joyce & Bell, 2004:3).
Coding: frontal participates to the formation of the orbital rim (0); frontal excluded from the orbit (1).
Comments: we follow the coding of Joyce & Bell (2004) instead of that of Lujan et al. (2014).

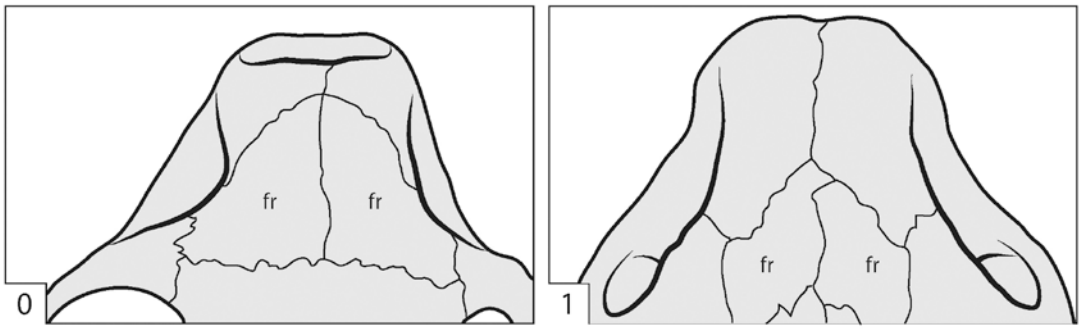


Figure 4.40. Illustration of the different states of the character FRONTAL 1: 0, frontal participating in the orbit in *Chelonoidis nigra*; 1, not in *Centrochelys sulcata*.

[41] FRONTAL 2: median length of frontals, compared to the prefrontals (Gerlach, 2001:4).
Coding: frontals longer than prefrontals (0); prefrontals longer than frontals (1).

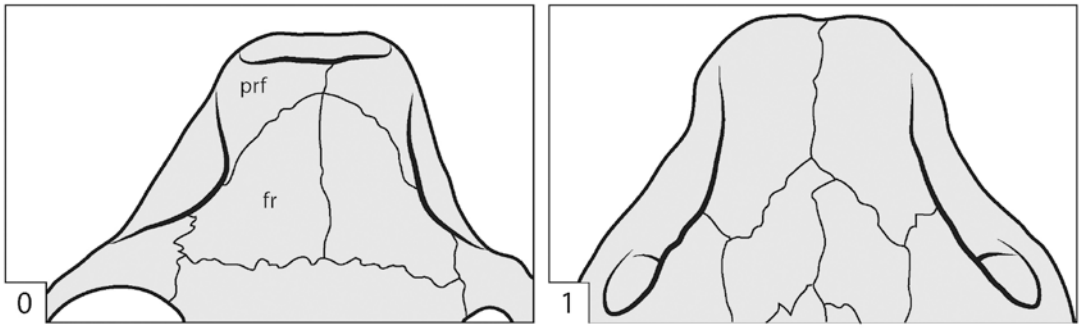


Figure 4.41. Illustration of the different states of the character FRONTAL 2: 0, frontals longer than prefrontals in *Chelonoidis nigra*; 1, frontals shorter than prefrontals in *Centrochelys sulcata*.

[42] INFERIOR DESCENDING PROCESSES OF THE FRONTAL: Modified by Joyce & Bell (2004:2) regarding the ventral closure of the processes (Gerlach, 2001:3, see below).
Coding: absent, or very small (0); present, well-developed (1)
Comments: In most turtles, a gutter (the sulcus olfactorius) is formed along the ventral surface of the frontals. This gutter transmits the olfactory nerve. The lateral rims of the sulcus sometimes form processes that descend ventromedially to surround the nerve from below (processus circumolfactorius in Gerlach, 2001:2, Joyce & Bell, 2004:2).

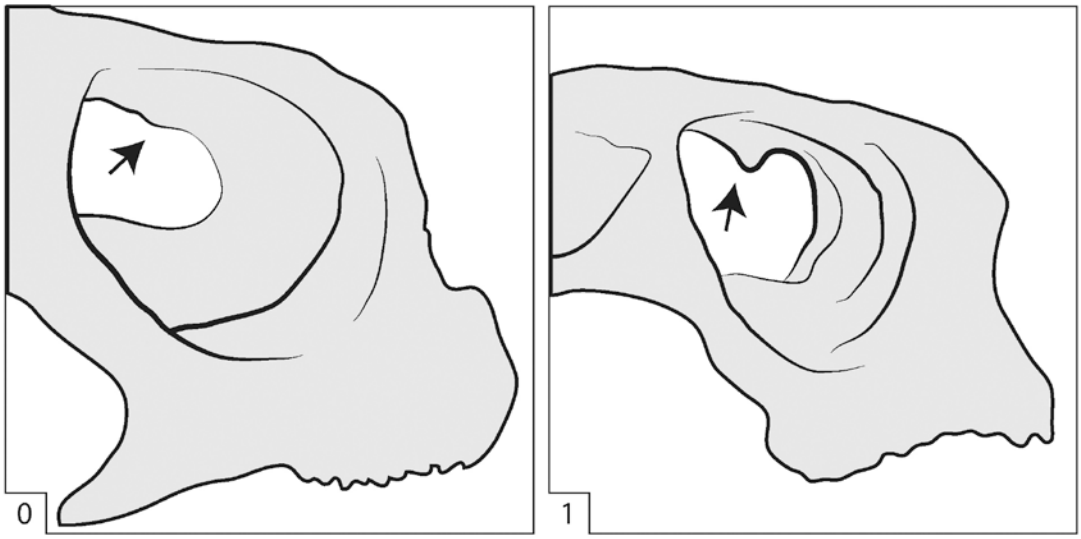


Figure 4.42. Illustration of the different states of the character INFERIOR DESCENDING PROCESSES OF THE FRONTAL: 0, almost absent in *Gopherus agassizi*; 1, well-developed in *'Testudo' hermanni*.

[43] SULCUS OLFACTORIUS: (Gerlach, 2001:3).
Coding: ventrally open (0); ventrally nearly closed (1).
Comments: the sulcus olfactorius, which extends from the cavum cranii to the fossa nasalis, is surrounded by the processus circumolfactorius. It could be ventrally open or nearly closed.

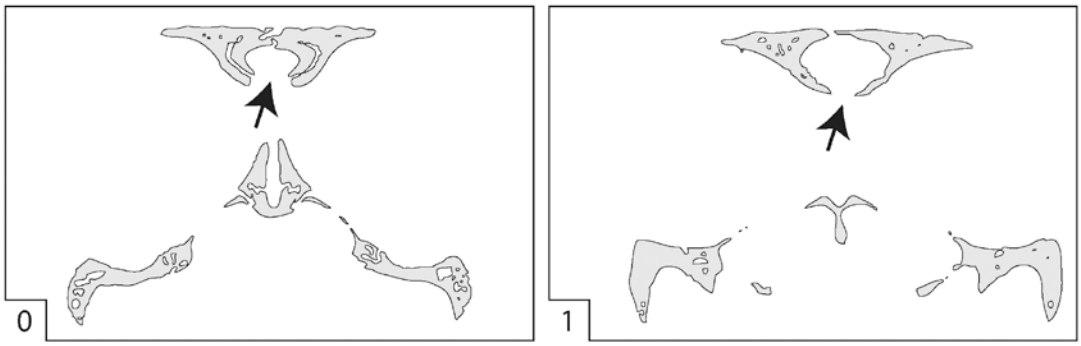


Figure 4.43. Illustration of the different states of the character SULCUS OLFACTORIUS: 0, open in *Emys orbicularis*. (modified from coronal slice 63 available in http://digimorph.org/specimens/Emys_orbicularis/); 1, nearly closed in *Gopherus polyphemus* (modified from coronal slice 118 available in http://digimorph.org/specimens/Gopherus_polyphemus/). The CT-scans are available by Dr. Heather A. Jamniczky, Dr. Anthony P. Russell, University of Calgary, 2007, "*Gopherus polyphemus*" & "*Emys orbicularis*", Digital Morphology. Accessed December 15, 2014 at http://digimorph.org/specimens/. Used with permission (Dr. T. Rowe)

[44] FOSSA ORBITALIS: Position of fossa orbitalis (A), relative to the total length (B) of the cranium, from the anterior tip to the end of the condylus occipitalis (Pérez-García & Vlachos, 2014:31).
Coding: placed on the anterior half (0); placed on the posterior half (1).

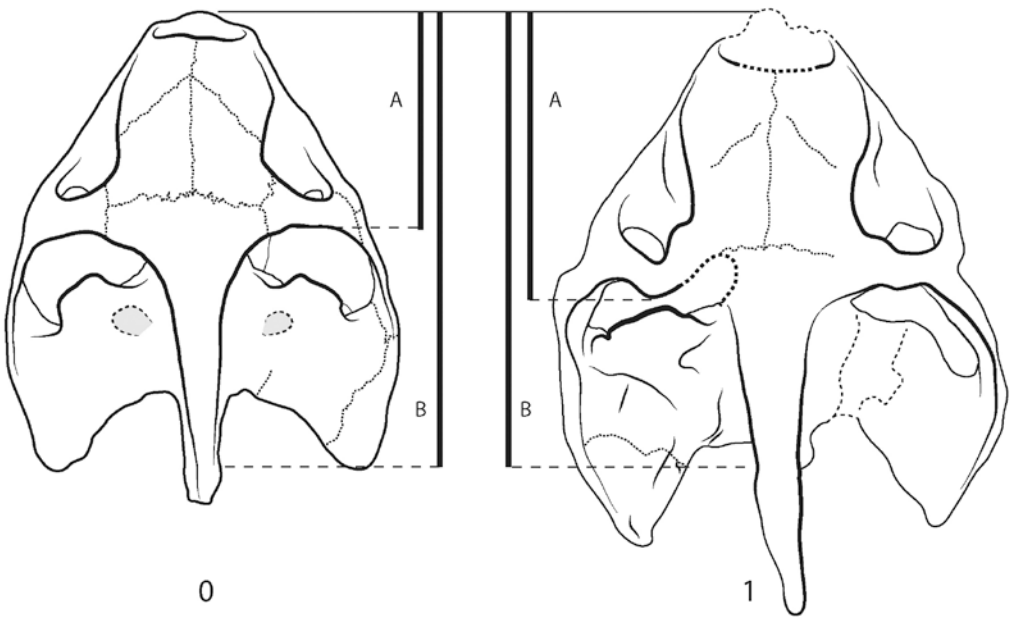


Figure 4.44. Illustration of the different states of the character position of FOSSA ORBITALIS: 0, placed on the anterior half in *Titanochelon schafferi*; 1, placed on the posterior half in *Titanochelon bacharidisi*.

[45] LOWER TEMPORAL EMARGINATION: (Pérez-García & Vlachos, 2014:32).
Coding: small (0); extensive (1).
Comments: Lower temporal emargination can be extensive, causing an extreme reduction of the quadratojugal, that could even cause a loss of the contact with the quadrate in lateral view (e.g. *Gopherus* and the extinct *Titanochelon bacharidisi*).

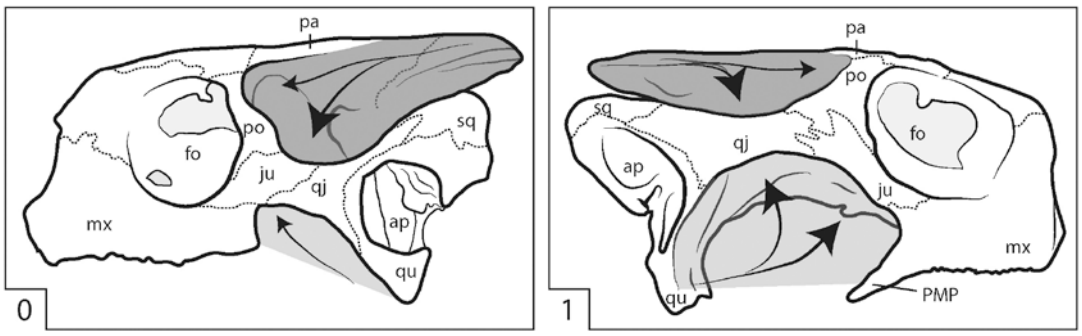


Figure 4.45. Illustration of the different states of LOWER TEMPORAL EMARGINATION: 0, small in *Centrochelys sulcata*; 1, extensive in *Gopherus polyphemus*.

[46] MAXILLA-PREMAXILLA SYMPHYSIS HEIGHT: Height of the symphysis of the maxilla/premaxilla compared to the height of the fossa nasalis (see Gerlach, 2001:10).
Coding: short, shorter than the height of fossa nasalis (0); short, shorter than the height of fossa nasalis, but with the development of a dorsal projection (1); high, taller than the height of fossa nasalis (2).

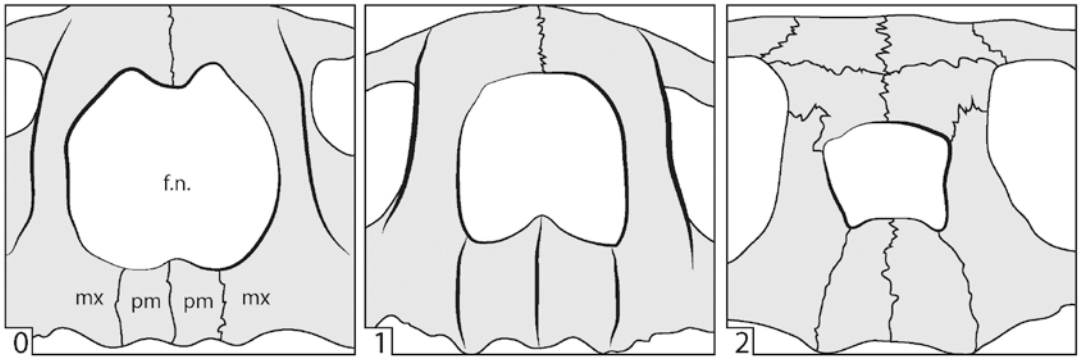


Figure 4.46. Illustration of the different states of MAXILLA-PREMAXILLA SYMPHYSIS HEIGHT: 0, short in *'Testudo' hermanni*; 1, short, but with a dorsal projection in *Centrochelys sulcata*; 2, tall in *Indotestudo elongata*.

[47] PREMAXILLA RIDGE: Presence of a longitudinal ventral ridge along premaxillary symphysis (Gerlach, 2001:11).
Coding: absent (0); present (1).

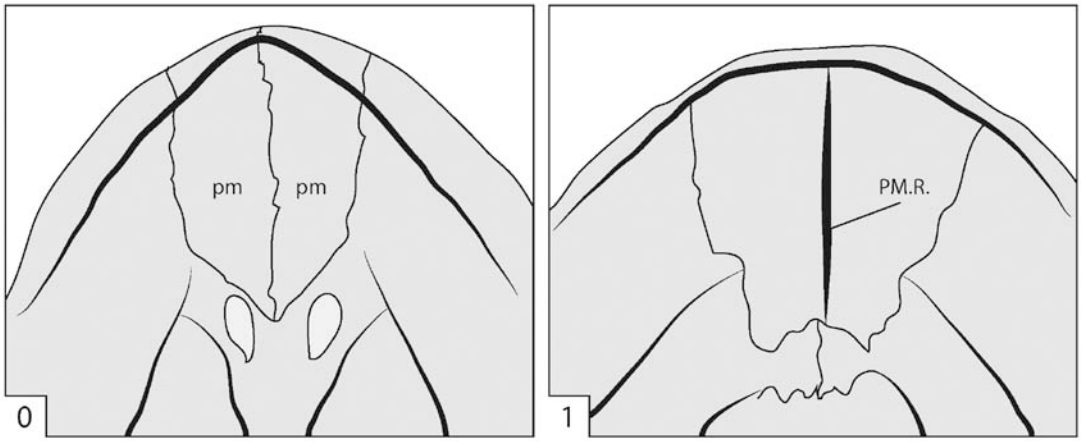


Figure 4.47. Illustration of the different states of PREMAXILLA RIDGE: 0, absent in *'Testudo' hermanni*; 1, present in *Gopherus polyphemus*.

[48] PREMAXILLARY PIT: Presence of a premaxillary pit on the ventral part of the premaxillae that could be circular or elliptical.
Coding: absent (0); present (1).

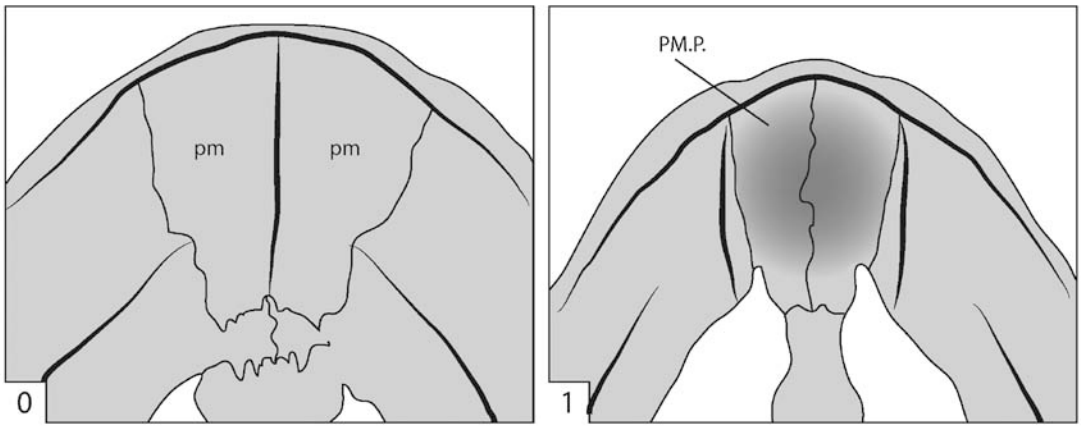


Figure 4.48. Illustration of the different states of PREMAXILLARY PIT: 0, absent in *Gopherus polyphemus*; 1, present in *Centrochelys sulcata*.

[49] PREMAXILLA-MAXILLA RIDGE: Presence of a longitudinal ventral ridge along premaxilla-maxilla suture (Gerlach, 2001:12; “transverse ridge” of Takahashi et al, 2003).
Coding: absent (0); present (1).

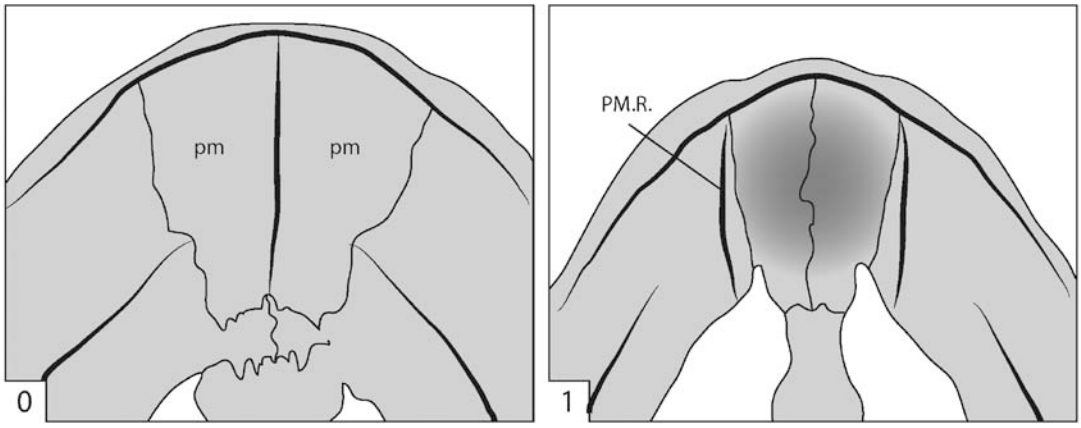


Figure 4.49. Illustration of the different states of PREMAXILLA-MAXILLA RIDGE: 0, absent in *Gopherus polyphemus*; 1, present in *Centrochelys sulcata*.

[50] NUMBER OF TRITURATING RIDGES: number of triturating ridges on the maxilla (Takahashi et al., 2003).
Coding: one, labial (0); three (1).

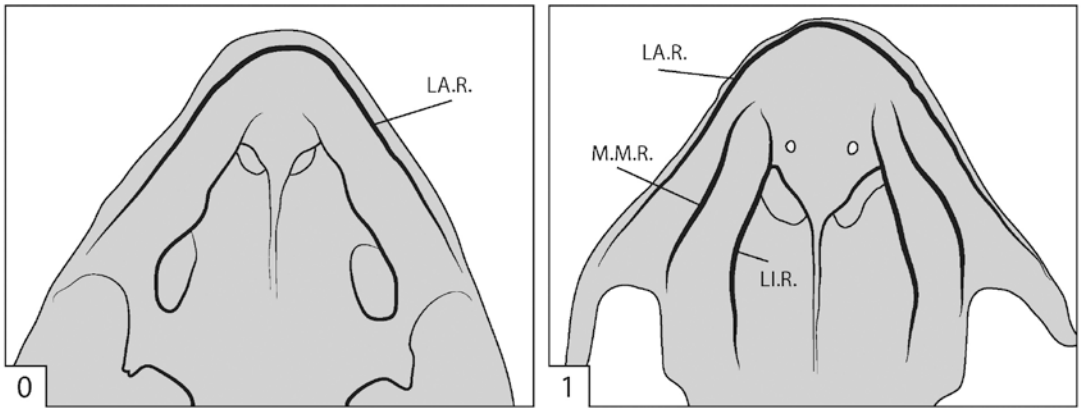


Figure 4.50. Illustration of the different states of NUMBER OF TRITURATING RIDGES: 0, one in *Mauremys caspica*; 1, three in *Testudo graeca*.

[51] EXTENT OF LINGUAL RIDGE: Extent of the lingual ridge on premaxilla (modified by Gerlach, 2001:13).
Coding: no, restricted to maxilla (0); yes, extending onto premaxillae (1).

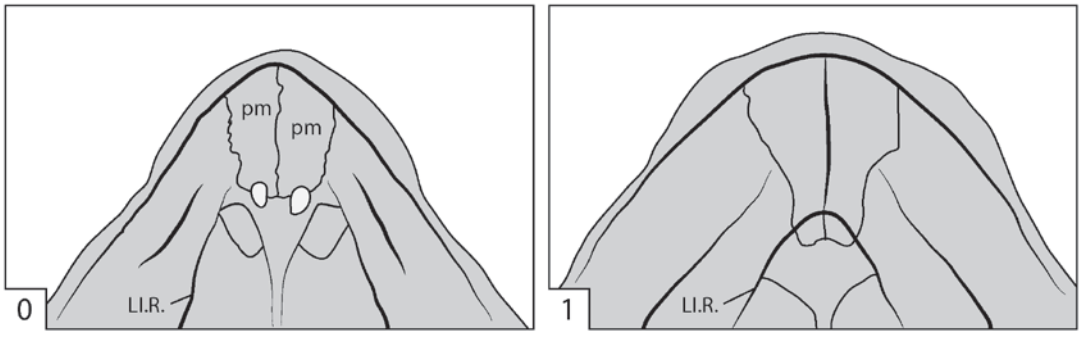


Figure 4.51. Illustration of the different states of EXTENT OF LINGUAL RIDGE: 0, restricted to maxilla in *'Testudo' hermanni*; 1, extending to premaxilla in *Gopherus polyphemus*.

[52] LABIAL RIDGE: Tooth-like tubercles on the labial ridge (modified by Gerlach, 2001:14 and Gerlach 2001:15).
Coding: absent (0); present (1).

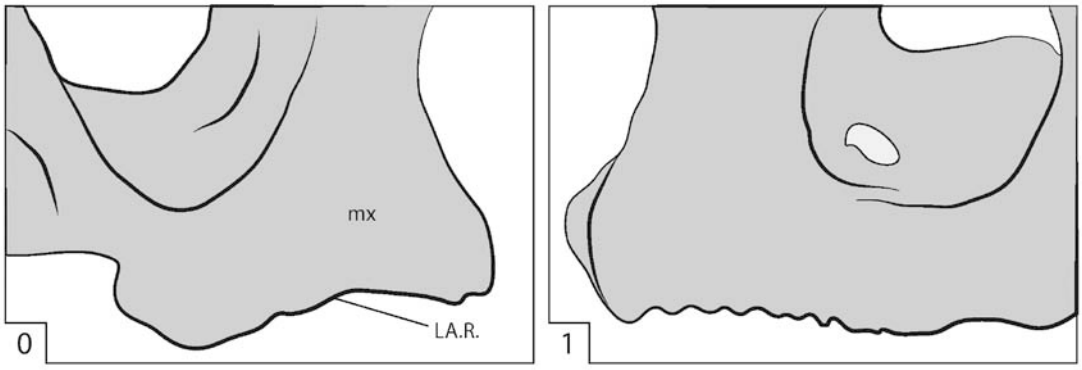


Figure 4.52. Illustration of the different states of LABIAL RIDGE: 0, no tubercles in *'Testudo' hermanni*; 1, tooth-like tubercles in *Centrochelys sulcata*.

[53] POSTERIOR MAXILLARY PROCESS: the posterior maxillary process is defined as the posterior elongation of the maxilla below the jugal, forming an extension of the labial ridge (PMP, Crumly, 1984; Takahashi et al., 2003:7).
Coding: absent (0); present (1).

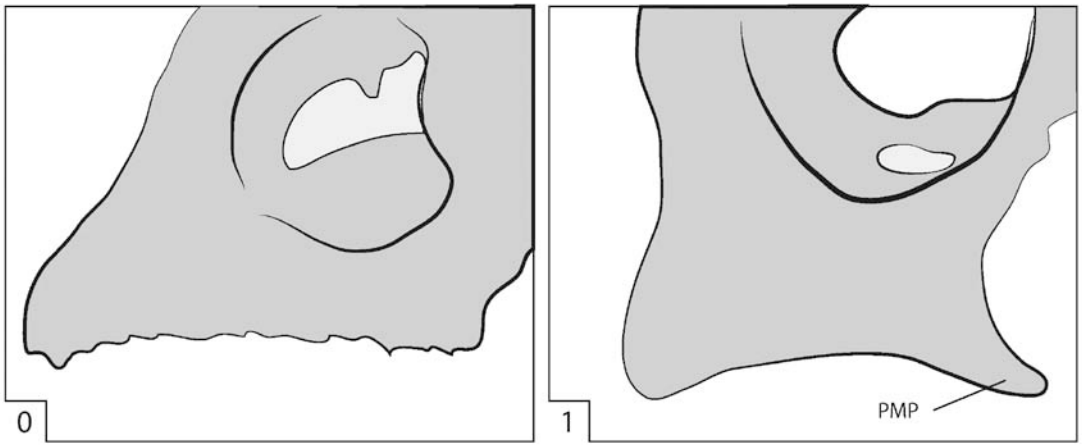


Figure 4.53. Illustration of the different states of POSTERIOR MAXILLARY PROCESS: 0, absent in *Stigmochelys pardalis*; 1, present in *Gopherus polyphemus*.

[54] MEDIAN MAXILLARY RIDGE: Presence of a median maxillary ridge, between the lingual and the labial ridges on the palate (Takahashi et al., 2003:4; see also TR, Crumly, 1984;).
Coding: absent (0); present, restricted to maxilla (1); present, extends to the premaxilla (2).

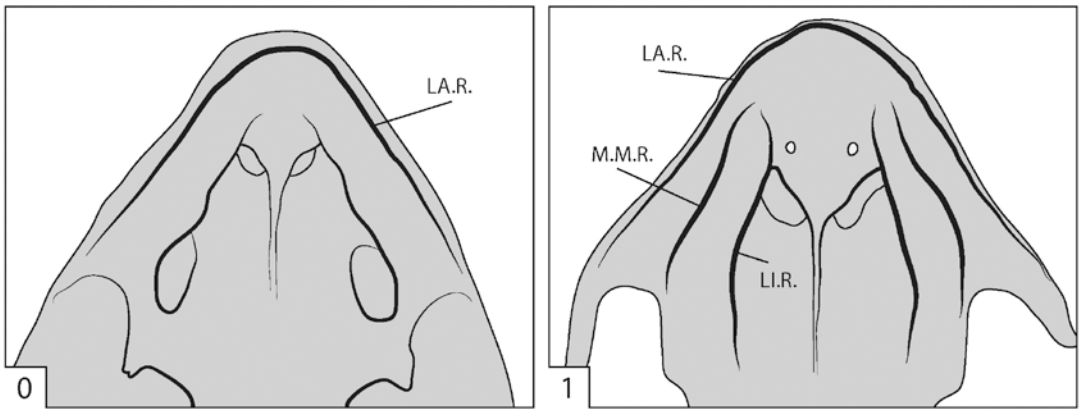


Figure 4.54. Illustration of the different states of MEDIAN MAXILLARY RIDGE: 0, absent in *Mauremys caspica*; 1, present in *Testudo graeca*.

[55] MAXILLARY RIDGES: Tooth-like tubercles on the maxillary alveolar ridge (Gerlach, 2001:17).
Coding: absent (0); present (1).

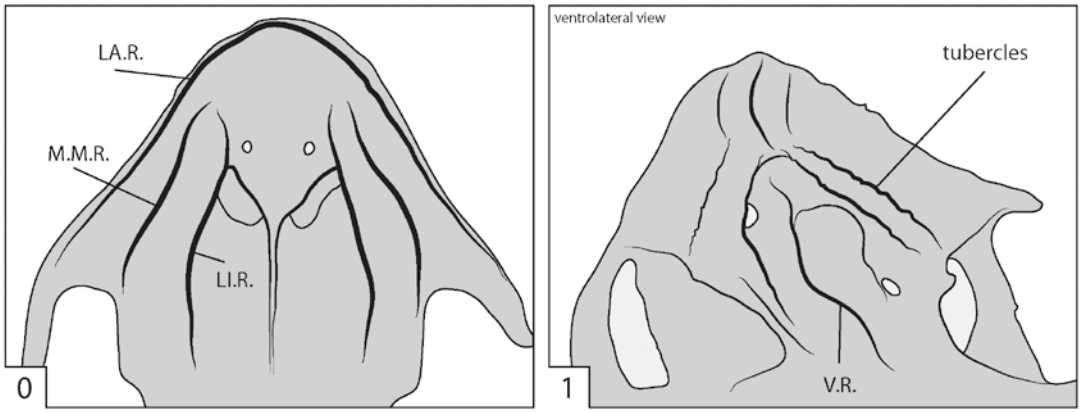


Figure 4.55. Illustration of the different states of MAXILLARY RIDGES: 0, absent in *Testudo graeca*; 1, present in *Gopherus polyphemus*.

[56] VOMER RIDGE: presence of a ventral ridge on vomer (Gerlach, 2001:22).
Coding: absent (0); present (1).

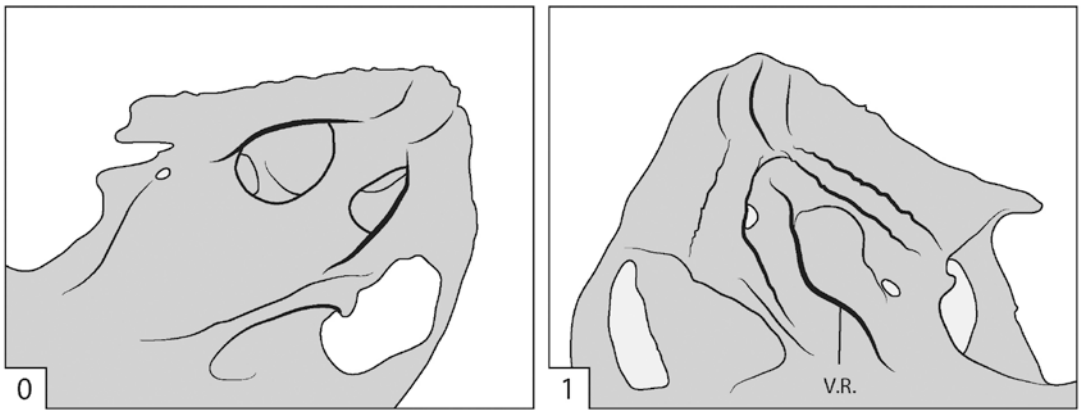


Figure 4.56. Illustration of the different states of VOMER RIDGE: 0, absent in *Kinixys erosa*; 1, present in *Gopherus polyphemus*.

[57] VOMER: Posterior extent of the vomer till the basisphenoid (modified by Gerlach, 2001:24; based on Takahashi et al., 2003:10).
Coding: vomer short, not dividing the palatines (0); vomer dividing the palatines, not the pterygoids (1); vomer diving part of the pterygoids, not reaching the basisphenoid (2); vomer dividing palatines and pterygoids, reaching the basisphenoid (3).

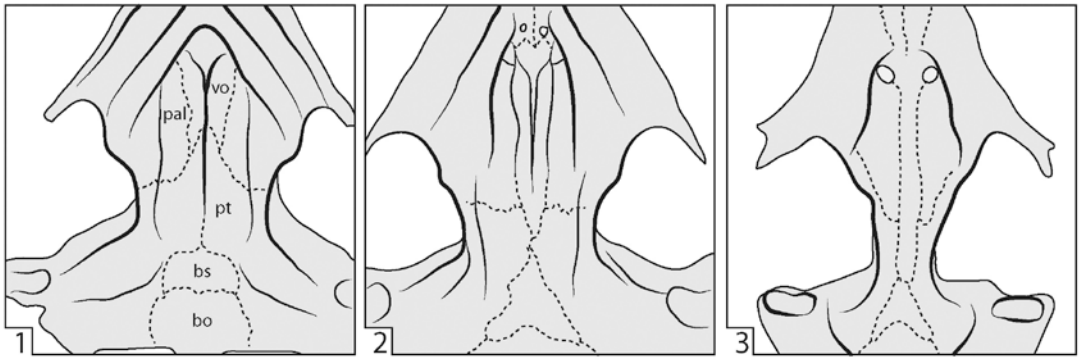


Figure 4.57. Illustration of the different states of VOMER (state 0 not figured): 1, vomer dividing the palatines, not the pterygoids in *Gopherus polyphemus*; 2, vomer diving part of the pterygoids, not reaching the basisphenoid in *Centrochelys sulcata*; 3, vomer dividing palatines and pterygoids, reaching the basisphenoid in *Geochelone elegans*.

[58] CONTACT PTERYGOID-BASIOCCIPITAL: (see BP, Crumly, 1984; Joyce & Bell, 2004:21).
Coding: present (0); absent (1).

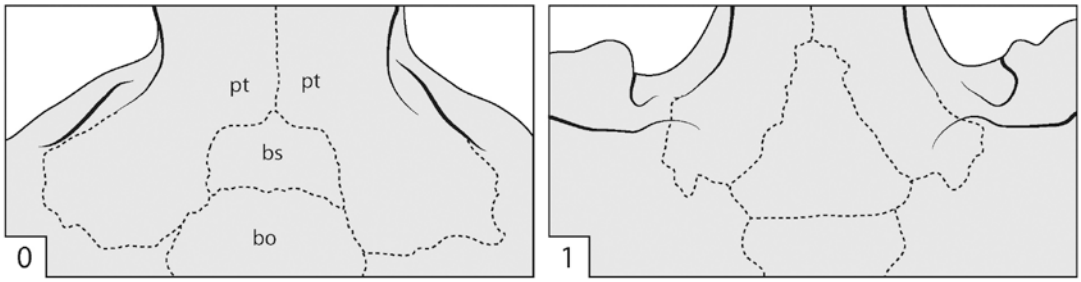


Figure 4.58. Illustration of the different states of CONTACT PTERYGOID-BASIOCCIPITAL: 0, present in *Gopherus polyphemus*; 1, absent in *Chrysemys picta*.

[59] FORAMEN PRAEPALATINUM: Position of foramina praepalatina in ventral view (modified by Gerlach, 2001:28).
Coding: visible (0); not visible in ventral view - foramina may be concealed by lingual extensions of the maxillary alveolar ridges (1).

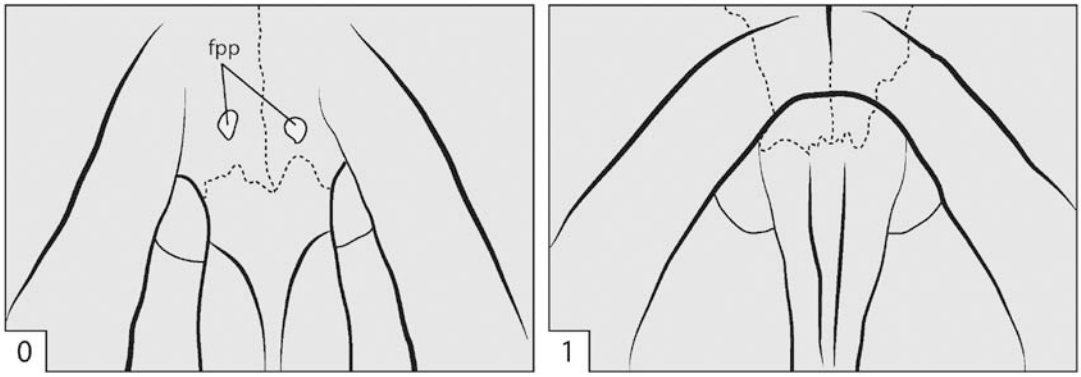


Figure 4.59. Illustration of the different states of FORAMEN PRAEPALATINUM: 0, visible in *Centrochelys sulcata*; 1, not visible in *Gopherus polyphemus*.

[60] EXTENSION OF SQUAMOSALS: Extension of the squamosals in relation with the condylus occipitalis (modified by Gerlach, 2001:38).
Coding: not extending (0); extending beyond the condylus occipitalis (1).

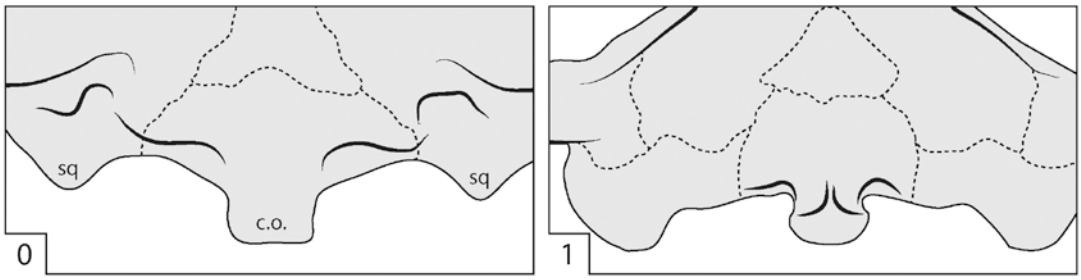


Figure 4.60. Illustration of the different states of EXTENSION OF SQUAMOSALS: 0, not extending in *Centrochelys sulcata*; 1, extending beyond the condylus occipitalis in *Gopherus polyphemus*.

[61] CRISTA SUPRAOCCIPITALIS 1: Length of the crista supraoccipitalis, in relation with the condylus occipitalis (modified by Gerlach, 2001:42).
Coding: not extending (0); extending beyond the condylus occipitalis (1).

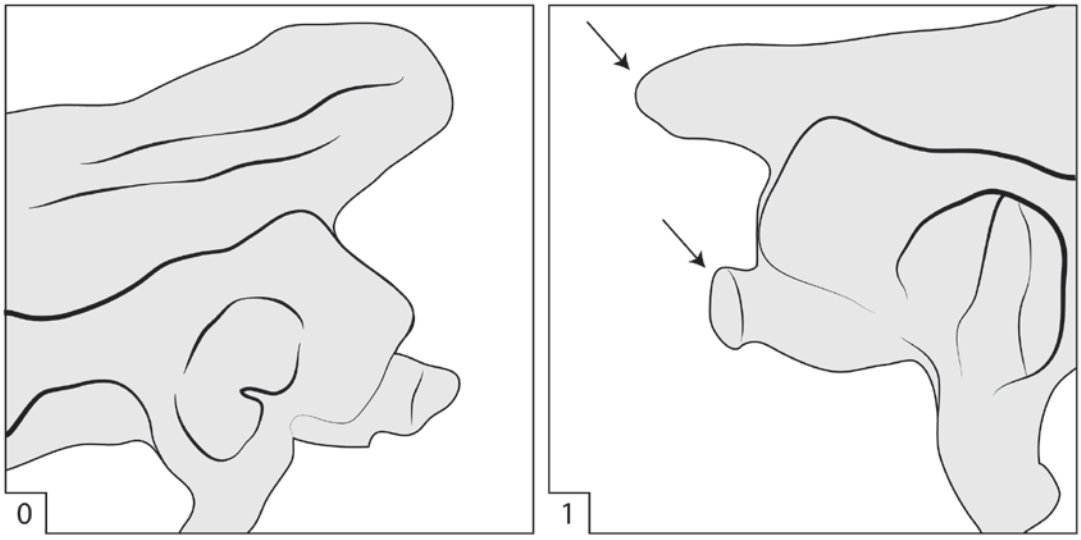


Figure 4.61. Illustration of the different states of CRISTA SUPRAOCCIPITALIS 1: 0, not extending in *Malacochersus tornieri*; 1, extending beyond the condylus occipitalis in *'Testudo' hermanni*.

[62] CRISTA SUPRAOCCIPITALIS 2: Presence of horizontal keels in crista supraoccipitalis (Gerlach, 2001:43).
Coding: absent (0); present (1).

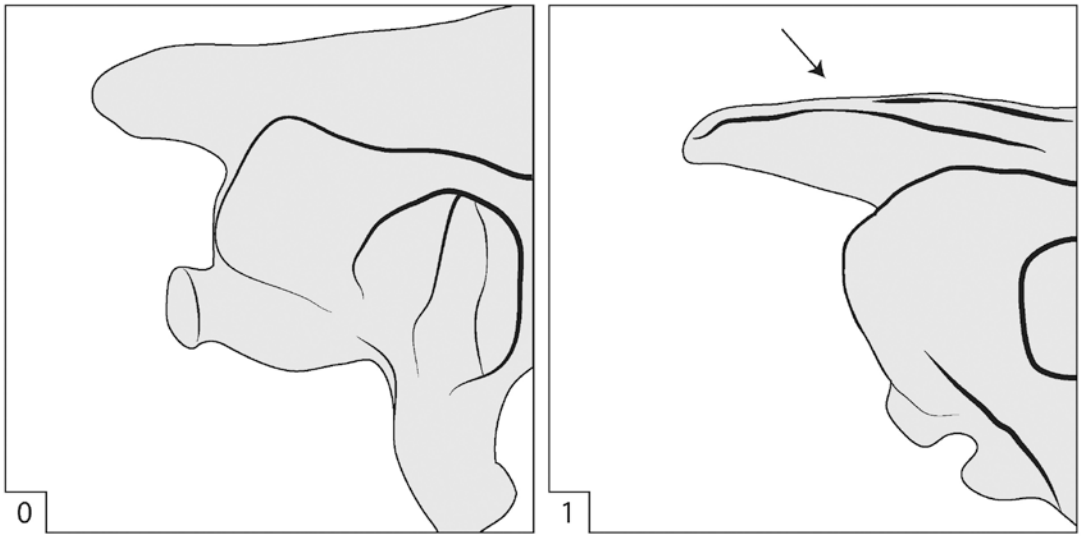


Figure 4.62. Illustration of the different states of CRISTA SUPRAOCCIPITALIS 2: 0, absent in *'Testudo' hermanni*; 1, present in *Chelonoidis nigra*.

[63] CRISTA SUPRAOCCIPITALIS 3: Shape of crista supraoccipitalis (Pérez-García & Vlachos, 2014:30).
Coding: straight (0); bended inwards (1); elevated posteriorly (2).



Figure 4.63. Illustration of the different states of CRISTA SUPRAOCCIPITALIS 3: 0, straight in *Centrochelys sulcata*; 1, bended inwards in *Gopherus polyphemys*; 2, elevated posteriorly in *Kinixys erosa*.

[64] PARIETAL: Contact between the parietal and the quadrate, partially covering the prootic (modified by Gerlach, 2001:45).

Coding: absent (0); present (1).

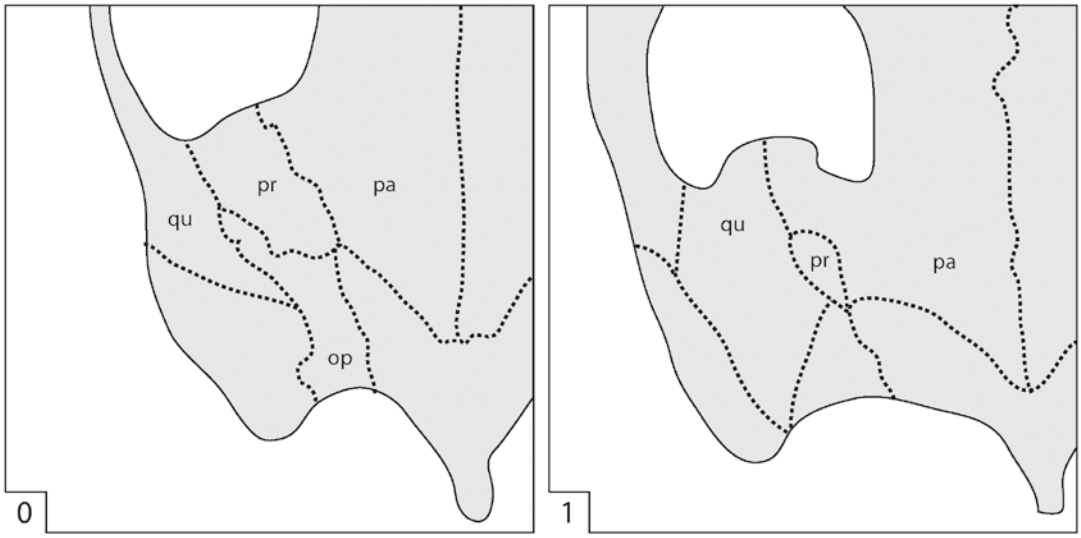


Figure 4.64. Illustration of the different states of PARIETAL: 0, absent in *'Testudo' hermanni*; 1, present in *Testudo graeca*.

[65] OPISTHOTIC: degree of expansion of the opisthotic in posterior view (modified by Gerlach, 2001:50).

Coding: not expanded, fenestra postotica open (0); expanded, could contact exoccipital (1) expanded, contacting the pterygoid (2).

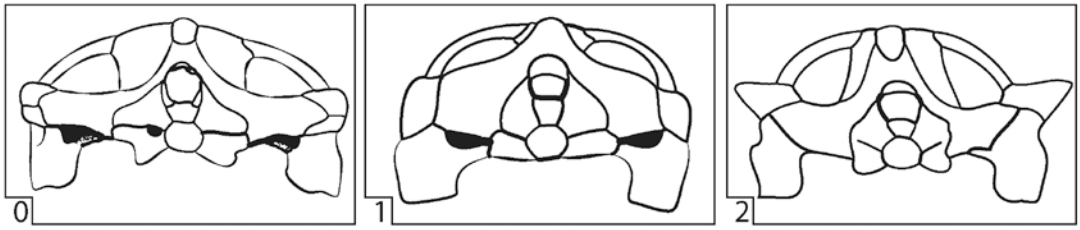


Figure 4.65. Illustration of the different states of OPISTHOTIC (modified by Gerlach, 2001): 0, not expanded, fenestra postotica open in *Dipsochelys dussumieri*; 1, expanded, could contact exoccipital in *Gopherus polyphemus*; 2, expanded, contacting the pterygoid in *Chelonoidis carbonaria*.

[66] PROCESSUS TROCHLEARIS OTICUM: Extension of processus trochlearis oticum (see TP, Crumly, 1984; Gerlach, 2001:54).

Coding: absent, or small (0); large (1).



Figure 4.66. Illustration of the different states of PROCESSUS TROCHLEARIS OTICUM: 0, absent in *Gopherus polyphemus*; 1, present in *Chelonoidis nigra*.

[67] FORAMEN NERVI TRIGEMINI: Number of foramen nervi trigemini (see Gerlach, 2001:56).
Coding: one (0); two (1).

Skeleton

[68] HUMERUS 1: Diaphysis of the humerus (CRE, Crumly, 1984; Pérez-García & Vlachos, 2014:33).
Coding: slightly curved (0); well-developed curvature (1).

[69] HUMERUS 2: Shape of the distal end of the humerus (Pérez-García & Vlachos, 2014:34).
Coding: symmetric (0); asymmetric (1).

[70] HUMERUS 3: presence of latissimus dorsi scar (LDS, Crumly, 1984;).
Coding: absent or reduced (0); present (1).

[71] HUMERUS 4: major trochanter of the humerus, in relation with the humeral head (Takahashi et al., 2003:22).
Coding: short, not extending beyond the humeral head (0); long, extending beyond the humeral head (1).

[72] SCAPULA: Glenoid fossa of the scapula (Pérez-García & Vlachos, 2014:35).
Coding: relatively short (0); elongated (1).

[73] CORACOID: Shape of the coracoid end (Takahashi et al., 2003:21).
Coding: long and narrow (0); fan shaped (1).

[74] FEMUR 1: Angle between the femoral head and the diaphysis of the femur (Pérez-García & Vlachos, 2014:36).
Coding: relatively large angle (0); femoral head developed almost perpendicular to the diaphysis (1).

[75] FEMUR 2: Union of the trochanters of the femur in ventral view (Takahashi et al., 2003:26; Lapparent de Broin et al., 2006:17).
Coding: not fused (0); fused (1).

[76] CARPALS 1: medial and lateral centrale fusion (CNF, Crumly, 1984).
Coding: not fused (0); fused (1).

[77] CARPALS 2: fusion of ulnare and intermedium (FUI, Crumly, 1984).
Coding: not fused (0); fused (1).

[78] MANUS: phalangeal number in the manus (PHN, Crumly, 1984).
Coding: two phalanges in all digits (0); one phalanx in fifth finger (1); one phalanx in first and fifth fingers (2); one phalanx in second and fifth finger (3).

[79] TARSALS: fusion of calcaneus and astragalus (CA, Crumly, 1984).
Coding: not fused (0); fused (1).

[80] PES: fifth phalanx in the pes (FP, Crumly, 1984).
Coding: present (0); absent (1).

[81] THIGH SPURS: Presence of thigh spurs, posterior to the femur (HSP, Crumly, 1984)
Coding: absent (0); present (1).

4.3. Phylogenetic analysis of the testudinids from Greece

The outgroup taxa: As outgroup taxa two extant representatives within Testudinoidea have been used, the emydid *Chrysemys picta* and the geoemydid *Mauremys caspica*. For the scoring, photographs of several specimens have been used, for *C. picta* (AMNH 75250; FMNH 22224; USNM 63078) and for *M. caspica* (USNM 167562).

The ingroup extant taxa: Many extant representatives of testudinids have been used in this analysis, trying to include most of the diversity in this clade. Photographs and direct observations were used. *Manouria impressa* (UCMP 136588; REP 63); *Geochelone elegans* (USNM 167557); *Stigmochelys pardalis* (UCMP 119051); *Indotestudo elongata* (UCMP 119050, 520645; ZIN 6978); *Indotestudo forstenii* (FRANK 73267); *Centrochelys sulcata* (MNCN 58823; REP 179, 180); *Agrionemys horsfieldii* (Mlynarksi, 1966 & information on digimorph.org for the cranium); *'Testudo' hermanni* (REP 3, 26; USNM 102222; ZIN 29; specimens in LGPUT uncatalogued); *Testudo graeca* (ZIN 15727, 18242; USNM 76506; FRANK 67588; REP 73; specimens in LGPUT uncatalogued); *Testudo marginata* (USNM 499029; ZIN 3941; specimens in LGPUT uncatalogued); *Testudo kleinmanni* (ZIN 9446; information in Delfino et al. 2009); *Kinixys erosa* (USNM 63483, 109687, 109696); *Gopherus agassizii* (UCMP 119060, 119066, 222094); *Gopherus polyphemus* (AMNH 73053; USNM 61059, 167526); *Astrochelys radiata* (USNM 167657); *Chelonoidis chilensis* (MPEF specimens); *Chelonoidis nigra* (VCCDRS 860-875; MNHN 1883-230); *Chelonoidis denticulata* (CRI 284, 287, 2489, 6374, 7702; UCMP 138687; USNM 73932); *Chelonoidis carbonaria* (AMNH 7042, 7043, 62583-62590; UCMP 119049, 119049, 137990). Information from the drawings, photographs and descriptions of Crumly (1984), Gerlach (2001) and Joyce & Bell (2004) is also used.

The ingroup fossil taxa: For the various species of *Titanochelon*, direct observation on the specimens listed in Material & Methods are made. For *Ti. bolivari* Luján et al. (2014) is also used. For *Cheirogaster maurini* and '*Ergilemys' bruneti* the information in de Broin (1977) is used. For *Gigantochersina ammon* Andrews (1906) is used. For "*Testudo*" *gigas* direct observation on the holotype specimen in MNHN are made. For *Namibchersus namaquensis* Lapparent de Broin (2003; 2008) is used. For *Paleotestudo canetoniana* Pérez-García & Murelaga (2013) is used. For '*Testudo' antiqua* Corsini et al (2014) is used. For *Impregnochelys pachytestis* Meylan & Auffenberg (1986) is used. For '*Achilemys' cassouleti* Claude & Tong (2004) is used. The full matrix consists of 38 taxa and 81 characters is given in Appendix. Also in the Appendix the number of nodes and the list of synapomorphies for each analysis are given.

Results:

Analysis #1: This analysis includes all taxa except the testudinids from Milia and Samos, and *Paleotestudo canetoniana* that will be analyzed separately below. The Traditional Search with TBR in TNT (1000 replicates) resulted in 6 trees with a best score of 296 steps (80 hits out of 1000). The Consistency Index (CI) is 0.341 and the Retention Index (RI) is 0.548. In general, the support (calculated with bootstrap GC values, jackknife GC values and Bremer supports) of most clades is relatively low. The exception is in the *Gopherus* clade showing strong support, and *Indotestudo*, some *Testudo*, *Titanochelon* and *Chelonoidis* that is moderate for a cladogram with

many fossils. The strict consensus tree is given is given in Figure 4.67. The number of nodes and the detailed synapomorphies of the consensus tree are given in Appendix. Most of the nodes of the trees are fully resolved, except for the taxa recovered in basal positions, such as the extant *Kinixys erosa* and the fossil '*Achilemys' cassouleti*, '*Hadrianus' castrensis* and *Cheirogaster maurini*. *Manouria impressa* is recovered as basal to a larger clade containing the remaining extant and extinct testudinid taxa. Several well-recognized clades from the Americas and Asia are recovered here as monophyletic, like the *Indotestudo* clade (with moderate support), the *Gopherus* clade (with high support) and the *Chelonoidis* clade (with moderate support). The Asian *Indotestudo* clade is defined by 4 synapomorphies, such as the obtuse angle between the gulars, the perpendicular humero-pectoral sulcus, the nearly straight femoro-anal sulcus, the loss of posterior maxillary process and the open fenestra postotica. The North American *Gopherus* clade is characterized by 9 synapomorphies, such as the triagonal anterior plastral lobe, the concave epiplastral lip, the gulars contacting the anterior margin of the entoplastron, the wide angle of the humero-pectoral sulcus, the longer prefrontals, the nearly closed sulcus olfacturius, the extensive lower temporal emargination, the presence of a premaxillary ridge and the lingual ridge extending onto premaxillae. The South American *Chelonoidis* clade is characterized by 4 synapomorphies, such as the absence of contact between the pleural 1 and the nuchal, the wide vertebrals, the obtuse angle of the gulars and the opisthotic contacting the pterygoid.

A newly described clade, *Titanochelon*, that includes most of the Neogene large testudinids (Pérez-García & Vlachos, 2014) is also recovered here as monophelytic. It is characterized by 2 synapomorphies, the contact between the pleural 2 and the marginal 4 and the contact between the pleural 3 and the marginal 6. This clade is within a larger clade that contains extant large testudinids from Africa (*Stigmochelys pardalis* and *Centrochelys sulcata*), the Oligocene '*Testudo' gigas* from France, and *Chelonoidis*, suggesting a complex biogeographic history that will be explored below.

The extant species of *Testudo* are recovered in a monophyletic clade, including the extinct *Testudo marmorum*, as a sister group of *Indotestudo*. *Testudo* is characterized by 3 synapomorphies, the reduced number of neurals, the long anal scutes and the reduced phalangeal number. Interestingly, the recently revised *'Testudo' antiqua* from the Miocene (by Corsini et al., 2014) is recovered outside the [*Testudo* + *Indotestudo*] clade, a result that will be further tested below with the addition of more *Testudo* species. *Kinixys erosa* and *Geochelone elegans* are recovered in basal positions.

Compared to Maximum Parsimony results from a recent molecular analysis that contains the taxa analyzed here (Fritz & Bininda-Emmonds, 2007 and Le et al., 2006), this morphological analysis agrees in several aspects. For example, a key point is in the intra-relationships of *Testudo* and its sister-group relationship with *Indotestudo.* Another important similarity is the sister-group of *Chelonoidis* with African taxa. Fritz & Bininda-Emmonds (2007) recovered *Chelonoidis* with *G. elegans* and *C. sulcata*. In our analysis however, only the *Centrochelys* sister-group relationship is recovered, as *G. elegans* is recovered in a basal position. Note that in the work of Fritz & Bininda-Emmonds (2007), *Kinixys* is recovered as the sister-group of *Chelonoidis* in the Maximum Likelihood and Bayesian analysis. Similar results are obtained by Le et al. (2006) In this analysis is in a basal position. Regardless the position of *Kinixys*, the close relationship of *Chelonoidis* with African

taxa based on morphological characters is demonstrated for the first time, as Gerlach (2001) recovered a close relationship with the North American *Gopherus*.

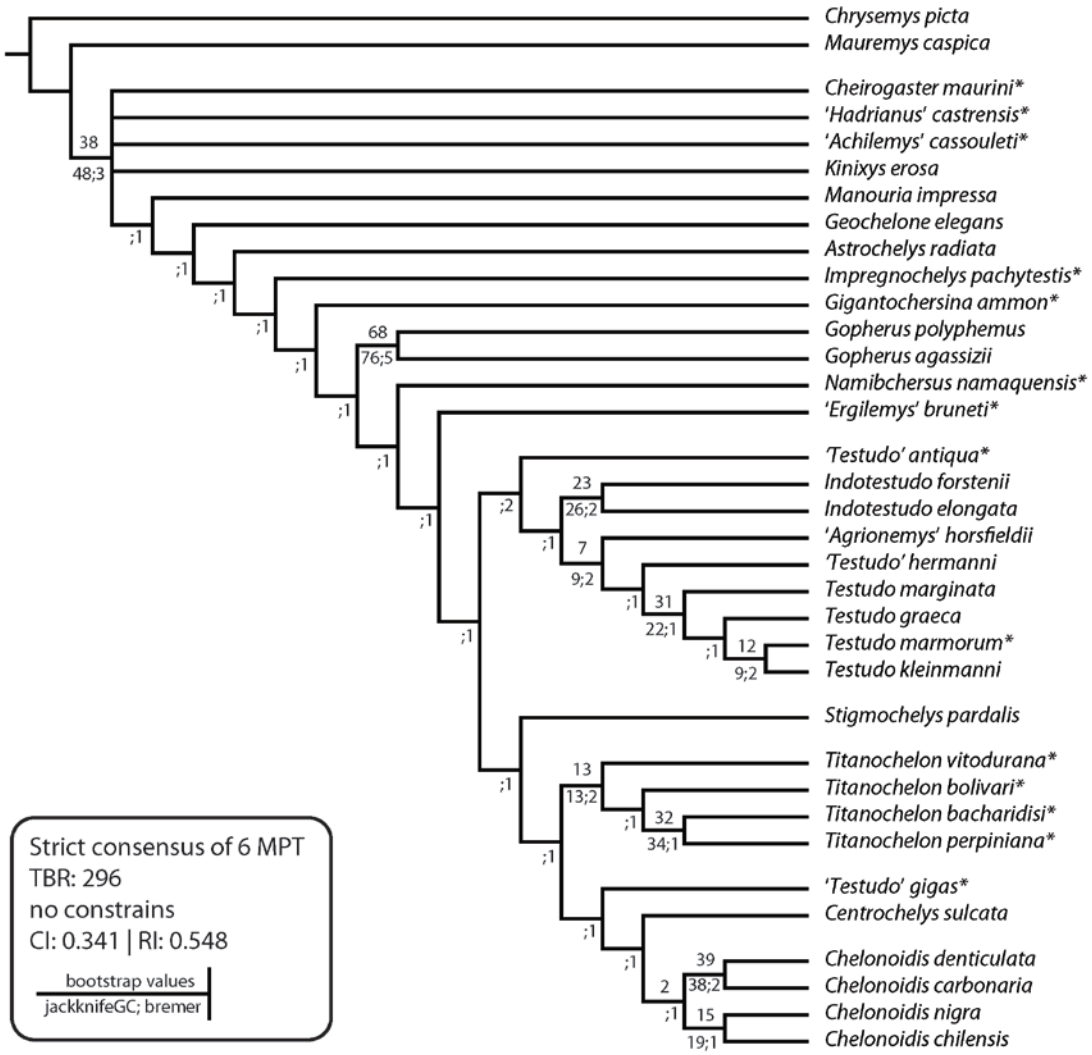


Figure 4.67. The strict consensus of 6 MPT of several extant and extinct testudinid taxa, based on the character defined above. Fossil taxa are indicated with an asterisk.

The low support in the various nodes and the several differences compared with molecular phylogenies illustrates two problems: first, the inclusion of fossil taxa usually lowers the support due to missing characters and second, the issue of homoplasy that is a common problem within testudinids. A possible way to tackle this issue is to use a "molecular scaffold" to constrain the morphological analysis (see Crawford et al., 2014 and references therein). From the two available molecular phylogenies (Fritz & Bininda-Emmonds, 2007 and Le et al., 2006) the MP result of Fritz & Bininda-Emmonds (2007) is chosen to constrain the initial analysis, since it contains a similar taxon sampling of the extant species. All the extant lineages are constrained, and the fossil ones were left free to flow anywhere in the cladogram. The result is given in Figure 4.68.

Analysis #2: The result is a single MPT of 315 steps with a CI of 0.321 and a RI of 0.503. The topology of the constrained tree differs in several aspects compared with the analysis #1. The most important difference is the derived position of *Kinixys erosa*, which carries together in derived positions Late Eocene taxa like *Cheirogaster*

maurini and *Gigantochersina ammon* that were previously recovered basally (Fig. 4.68). This pushes back the origin of most testudinid lineages to the Middle-Late Eocene (Fig. 4.69).

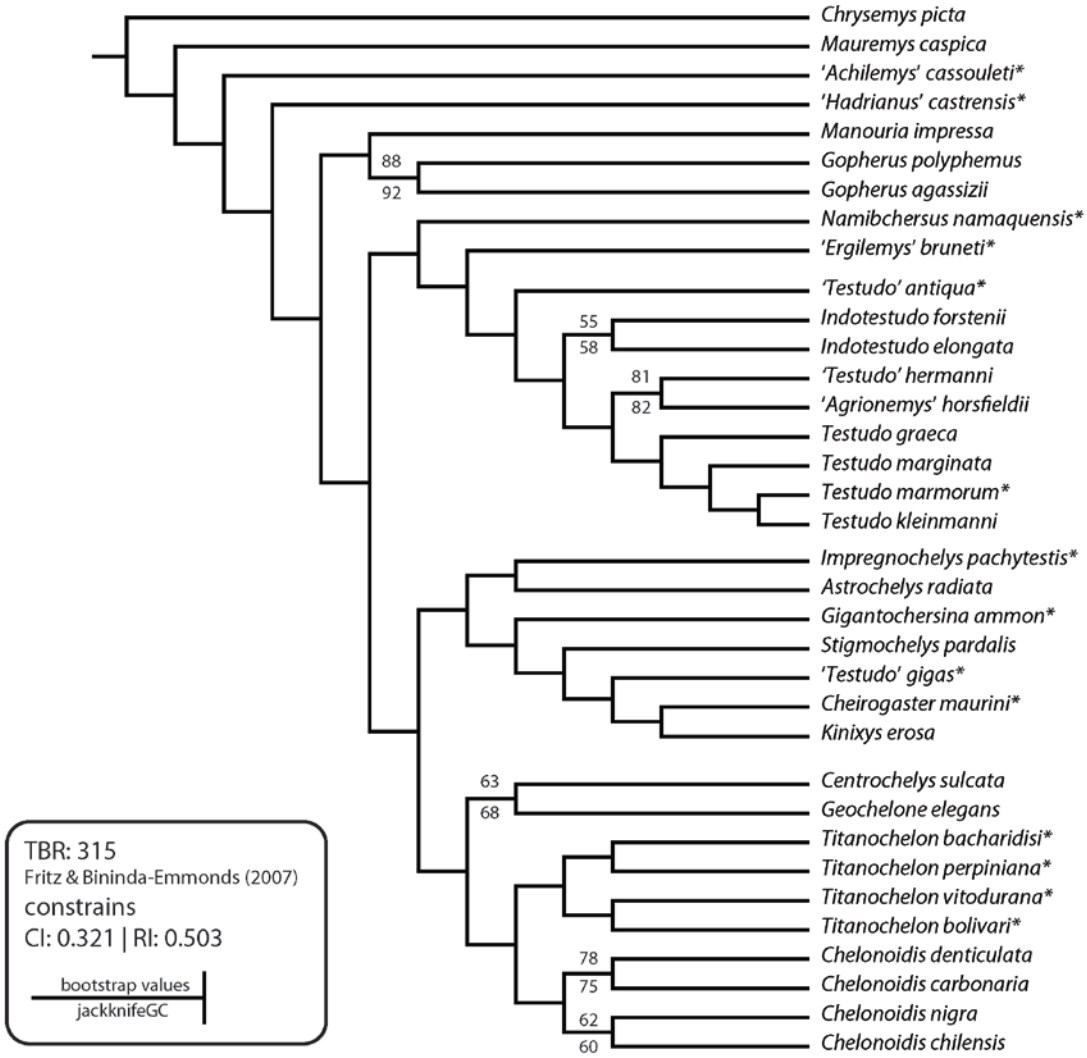


Figure 4.68. Analysis #2 with the molecular constrains from Fritz & Bininda-Emmonds (2007). Fossil taxa are indicated with an asterisk.

The *Manouria* clade could reach to the Late Eocene, but the fossils attributed to *Manouria* are numerous and require revision (see Discussion in Takahashi et al., 2003). The presence of *Gopherus laticuneus* in the Early Oligocene of Colorado (see Reynoso & Montellano, 2004 and references therein), roots the *Gopherus* lineage at least in the beginning of Oligocene. The *Testudo+Indotestudo* clade appears to have a long ghost lineage in the Early Miocene, but actually numerous small testudinids (*Paleotestudo canetoniana*, '*Testudo' promarginata* and others) exist from this period. Their revision could allow a confident placement in a phylogenetic context and fill this gap. Similar is the case with the ghost lineage from the Late Eocene till the Oligocene (prior to '*Ergilemys' bruneti*). For example, Lapparent de Broin et al. (2006b) report that the Late Eocene '*Testudo' insolitus* from Mongolia might be related with *Ergilemys*. The available information of the Mongolian taxon is scarse and it didn't allow a confident placement in this analysis. The grouping of *Impregnochelys pachytestis* and *Astrochelys radiata* suggests the presence of a Miocene ghost lineage for the latter. As no fossils are known to confirm or refute this

result, this result is interpreted with caution. Similar is the fate of the *Stigmochelys* lineage that is not known confidently beyond the appr. 4 my of Laetoli with *St. brachygularis* (Harrison, 2011). But Lapparent de Broin (2000) explains that numerous fossils exist from the Miocene of Africa that could be attributed to the extant African lineages. *Centrochelys* is surely present since the early Middle Miocene of Djebel Zelten (Lapparent de Broin, 2000; 2002). Regarding *Titanochelon*, only four taxa preserve enough information to be scored and confidently placed within this phylogeny, but fragmented fossils from the Early Miocene of France (e.g. from Saint-Gérand-le-Puy) could be attributed to this clade (pers. observations), allowing tracing the root of this lineage in the beginning of Miocene. This is in accordance with its sister-group taxon in the constrained analysis, *Chelonoidis*, which is confidently known from the Early Miocene with *Ch. gringorum* (Simpson, 1942).

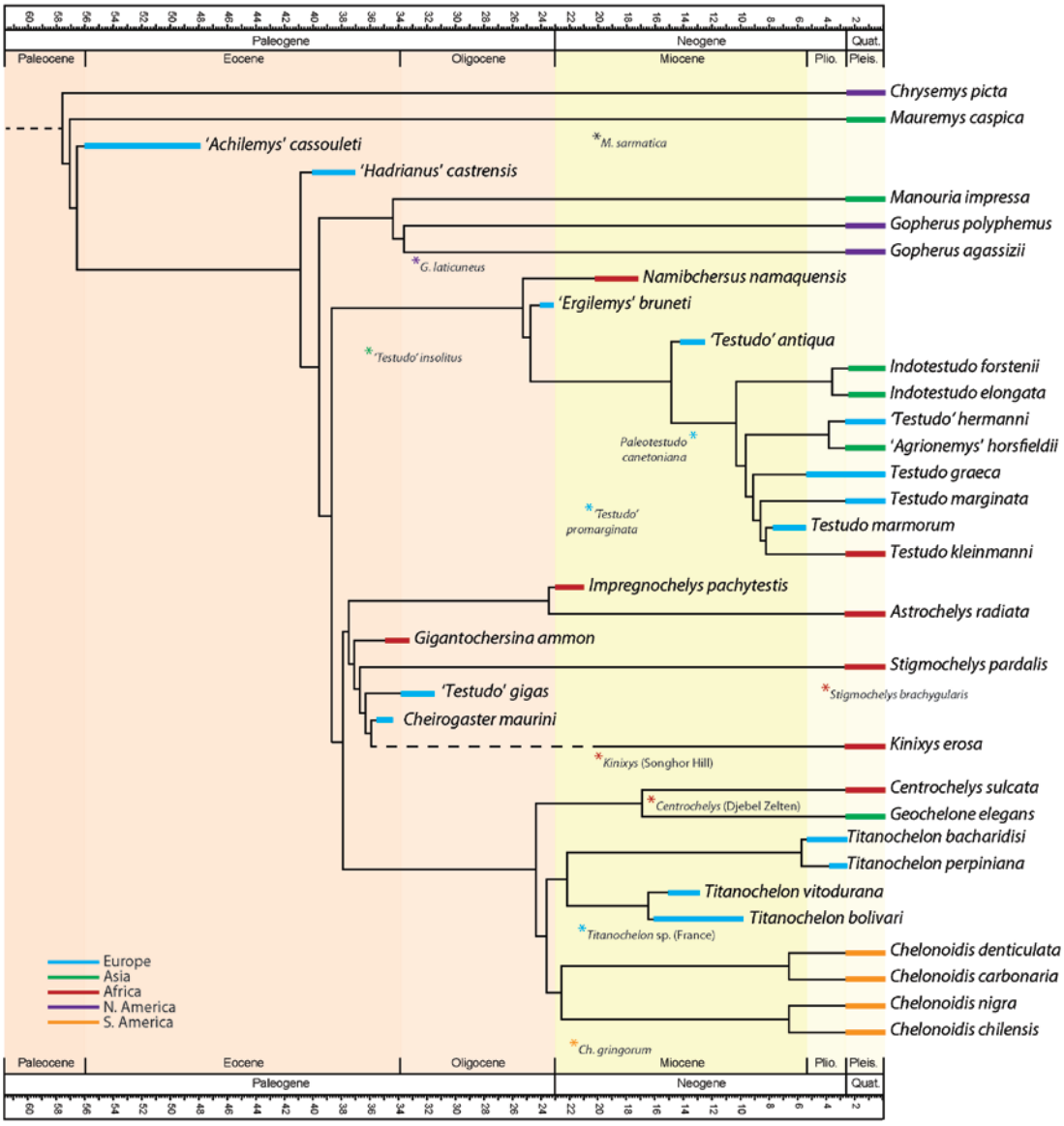


Figure 4.69. The time calibrated constrained tree of the Analysis #2 (see Fig. 4.68).

Another important difference compared to the unconstrained analysis is that the South American testudinids show a sister-group relationship with *Titanochelon*. This result should be interpreted with caution, as no fossils of the *Chelonoidis* clade are included that might alter this relationship. These two clades are sister to the

[*Centrochelys* + *Geochelone*] clade and all-together are nested within a larger clade with many African large and medium-sized testudinids (e.g. *Gigantochersina*, *Stigmochelys*) and medium-sized European testudinids (*Cheirogaster*, '*Testudo' gigas*).

The topology of the *Testudo* + *Indotestudo* remains almost unchanged, with the only exception of the sister-group relationship of *'Testudo' hermanni* and *'Agrionemys' horsfieldii*, which is, of course, enforced by the molecular constrains. Again, *'Testudo' antiqua* is not recovered within *Testudo*.

Remarks: This is the first large-scale phylogenetic analysis of extant and extinct testudinids, including both large and small-in-size forms, based on a new matrix of characters from the carapace, plastron, cranium and limb bones. The first results presented above allow some important concluding remarks. Given that this attempt is mainly focused on the Greek and European forms, results regarding larger groups should be viewed a source of inspiration for further steps. These should include the enlargement of the analyzed matrix with more characters and taxa (both extant and extinct) and a total evidence analysis.

The Greek taxa: Several results can be drawn for the taxa from Greece analyzed in the present thesis. Among the small testudinids, *'Testudo' hermanni*, *Testudo graeca*, *Testudo marginata* and *Testudo marmorum* have been analyzed. The most important conclusion perhaps, is that *Te. marmorum* shows, both in the unconstrained and in the constrained analysis, a sister-group relationship with the North African *Te. kleinmanni*. This contrasts previous hypotheses (e.g. Lapparent de Broin, 2001; 2002; 2006b), which regarded *Te. marmorum* as a close relative of the marginated tortoise. This has been due to the supposable presence of posteriorly flared carapacial margin in *Te. marmorum*, but in the previous chapter it is shown that this is not the case. Instead, *Te. marmorum* is grouped with *Te. kleinmanni* forming a clade that is supported by 3 synapomorphies, such as the pleural 1 overlapping the postero-lateral parts of the nuchal, the absence of pointed tips in the peripherals and the position of the humero-pectoral position posterior to the entoplastron. Interestingly, their first synapomorphy is a reversal (from the plesiomorphic condition found in the outgroup and in '*Achilemys' cassouleti*). Also their last synapomorphy is again a reversal, shared with many more taxa this time. Since they are recovered in a derived position within *Testudo*, this should push back the origin of the extant *Testudo* lineages of Greece prior to the Late Miocene.

From the large testudinids, only *Titanochelon bacharidisi* has been included. Unfortunately, *Titanochelon schafferi* preserves only limited information on the cranium and it could not be confidently resolved at this stage of the phylogenetic analysis. The large testudinid from the Pliocene of Greece is recovered as sister-group of *Ti. perpiniana* in an identical topology as in the analysis of Pérez-García & Vlachos (2014). However, this clade is now placed within a larger taxon sampling and allows better estimations of its position (see next section). Ultimately, it is more than clear from the above-mentioned analysis that the large and small testudinid lineages of Greece are not closely related to each other and they share most probably a different origin and biogeographical history that could be traced in the Late Eocene.

Taxonomic Implications: Although this is only the first attempt to analyze so many extinct and extant testudinid taxa at once, the character sampling allows the analysis of several fossils that have been left out of previous studies because they preserved

only shell remains. Therefore, our knowledge on the relationships of the Paleogene testudinid taxa (that preserved only the shell) has been rather poor. With this analysis as a starting point we can conclude on some taxonomic issues that should be further tested in the future. These results are mainly drawn based upon the constrained analysis presented above (Fig. 4.70).

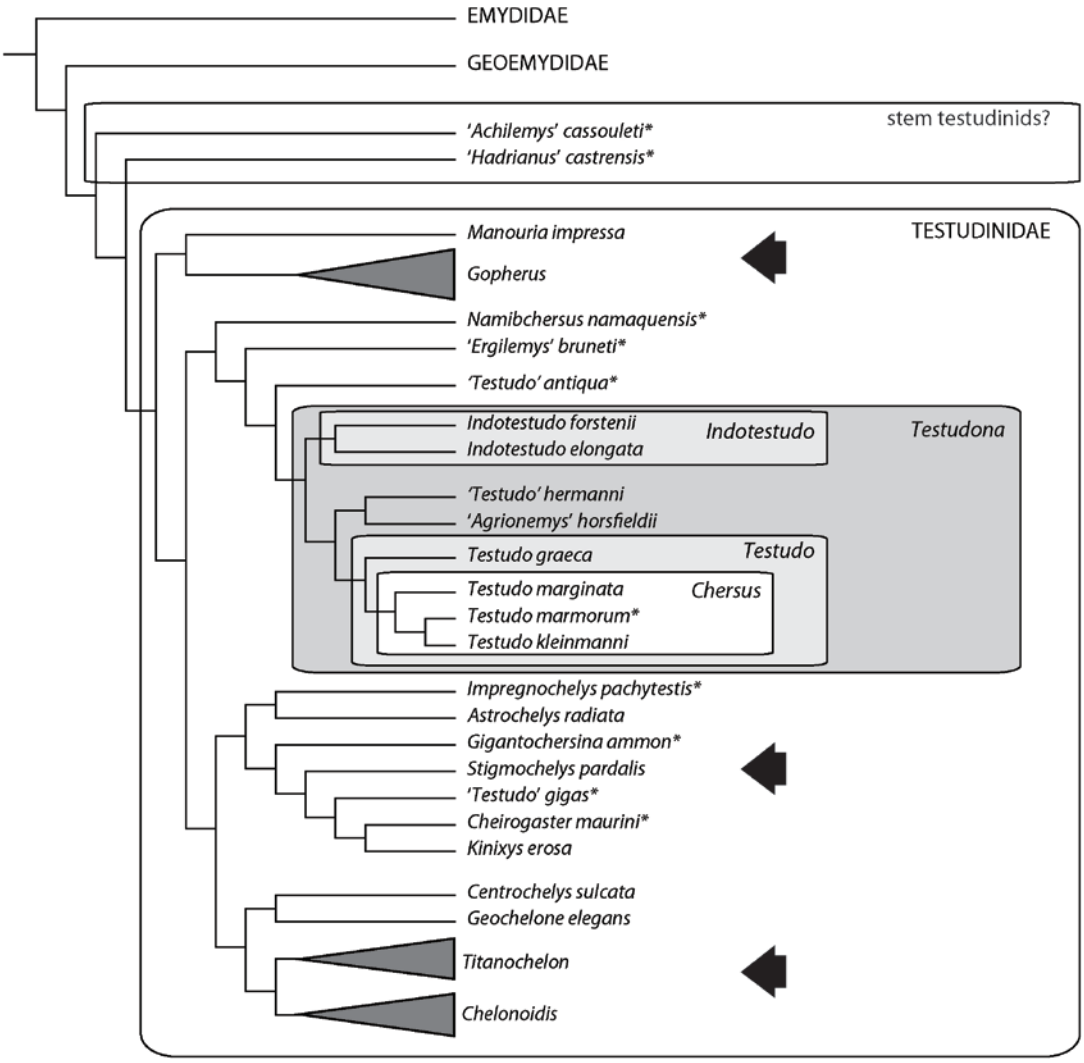


Figure 4.70. The taxonomy of Testudinidae based on the present analysis #2. Fossil taxa are indicated with an asterisk.

The clade Testudinidae is phylogenetically defined as "[…] the crown clade arising from the last common ancestor of *Testudo graeca* Linnaeus, 1758, *Manouria* (orig. *Testudo*) *emys* (Schlegel and Müller, 1844), and all other valid species listed in Appendix 8 […]" (Joyce et al., 2004:1005). As expected, this clade is fully recovered in our analysis (both constrained and unconstrained). The analysis presented here shows that some fossil taxa from the Paleogene of Europe, the Early Eocene '*Achilemys' cassouleti* and the Late Eocene '*Hadrianus' castrensis* could belong to the panstem of Testudinidae. In fact, both taxa are in need of a major revision, as they have been described as belonging to 'genera' originally described in other continents. In my opinion the future study of those taxa, their comparison with the original *Hadrianus* and *Achilemys*, analyzed in a broader scale including more testudinoids will shed light in the early evolution of testudinids.

Within the clade Testudinidae, other phylogenetically defined clades have been named and converted by J. Parham in Parham et al. (2006), the most of them recovered here as well, both in the constrained and in the unconstrained analysis. The clade *Testudona*, defined as "the crown clade arising from *Malacochersus* [orig. *Testudo*] *tornieri* (Siebenrock, 1903), *Testudo graeca* Linnaeus, 1758 *Agrionemys* [orig. *Testudo*] *horsfieldii* (Gray, 1844), and *Indotestudo* [orig. *Testudo*] *elongata* (Blyth, 1853)" (Parham et al., 2006:59) is clearly recovered, nested within a clade containing [*Manouria* + *Gopherus*] and a larger one with the African endemics, the South American tortoises and most fossil forms from Europe and Africa. Within *Testudona*, the clade *Indotestudo*, defined as "the crown clade arising from the last common ancestor of *Indotestudo* [orig. *Testudo*] *elongata* (Blyth, 1853), *Indotestudo* [orig. *Testudo*] *forstenii* (Schlegel and Müller, 1844), and *Indotestudo* [orig. *Testudo*] *travancorica* (Boulenger, 1907)" (Parham et al., 2006:59) is recovered as well in both analyses. The clade *Testudo*, defined as "the crown clade arising from the last common ancestor of *Testudo graeca* Linnaeus, 1758; *Testudo marginata* Schoepff, 1792; and *Testudo kleinmanni* Lortet, 1883" (Parham et al., 2006:59) is again recovered in both analyses, including the fossil *Testudo marmorum* as a sister-group of *Te. kleinmanni*.

The clade *Chersus*, defined as "the crown clade arising from the last recent common ancestor of *Testudo marginata* Schoepff, 1792; and *Testudo kleinmanni* Lortet, 1883" (Parham et al., 2006:59) is only recovered in the constrained analysis, as in the unconstrained it is recovered as synonymous with the clade *Testudo*.

The clade containing '*Testudo' hermanni* and '*Agrionemys' horsfieldi*, is recovered only in the constrained analysis as a sister to *Testudo*. In the unconstrained analysis these two taxa are located in the stem of *Testudo*. On the contrary, Parham et al. (2006) recovered this clade as sister to *Indotestudo* and they mention the intention of Lapparent de Broin et al. (2006a) to name a new ICZN name for '*Te*.' *hermanni*. This happened one year later with *Eurotestudo* (Lapparent de Broin et al., 2006 a,b,c) but Fritz & Bininda-Emmonds (2007) showed with a molecular analysis that this genus might not be necessary. In their analysis (which is followed here for the constrains), '*Te*.' *hermanni* and '*A*.' *horsfieldi* are a sister-group of the remaining extant *Testudo*, and these authors include them in this genus. The results presented here show, from a morphological point of view with molecular constrains, that perhaps the defined clades of Parham et al. (2006) were defined based only on few analyzed taxa. Given that the main idea of the phylogenetic nomenclature is to promote stability and avoid constant changes, for the moment these two taxa ('*Te*.' *hermanni* and '*A*.' *horsfieldi*) are understood as members of *Pantestudo*. Of course those thoughts should be further tested before the testudonan classification is clarified.

Several fossil taxa are recovered in the stem of *Testudona*, such as the Europeans Middle Miocene '*Testudo' antiqua* and the Oligocene '*Ergilemys' bruneti*, and the African Middle Miocene *Namibchersus namaquensis*. These results should stimulate further analyses in order to clarify whether some of these forms (or other fossil taxa) are within *Testudona* or on its stem. Such studies will enlighten the early history of this clade that appears to be placed in the Oligocene.

The fact that most of the clades defined by Parham et al. (2006) are recovered from morphology is fortunate, given that the morphological signal usually produced by the testudinids is weak and complex (e.g. see Joyce & Bell, 2004). Further works could help defining additional large clades within Testudinidae (some possible clades

are shown with the black arrows in Fig. 4.70) in order to better understand the evolutionary history of testudinids.

Evolutionary implications: This section introduces some ideas regarding the main evolutionary events that can be inferred from the analysis made above. Those implications should be treated with caution and for this reason the evolutionary scenario of the major clades is discussed. This is based on the general topology of the tree and by applying the Dispersal-Evolution-Cladogenesis (DEC) method. First of all, although the DEC results are presented on both the constrained (Fig. 4.71.A) and the unconstrained (Fig. 4.71.B) analyses, the main discussion is made on the constrained one. Although the general topology of the trees of the main extant clades (except *Kinixys*, discussed above) is roughly similar, the placement of the fossils on the constrained is better. This is not only because a "molecular scaffold" has been used, but also because their placement creates shorter "ghost" lineages. However is worthy to discuss the results on the unconstrained analysis for comparison. It should be noted however that from the 6 MPT of the unconstrained analysis, the tree #5 is selected for the reason that the DEC analysis requires a non-polytomous tree (Ree & Smith, 2008). The difference among the trees is on the placement of the basal taxa. Although *Ch. maurini* and *K. erosa* are recovered as basal in this analysis, their placement differs in the trees. This tree is selected because is the only one in which they are sister-groups, resembling the condition on the constrained tree. This is only for the visual impact and consistency, as the results on the DEC analysis are the same.

What is evident from both analyses is the rapid diversification of the main clades before the Late Eocene, as in the Late Eocene all the major clades are already present (Fig. 4.71). This diversity has been recorded with fossils in North America for example. Estes & Hutchinson (1980) document the presence of '*Geochelone'* in the Early Eocene of Ellesmere Island in the Canadian Artic Archipelago. This Northern finding could be correlated with the early dispersal of testudinoids in the Early Eocene after the Paleocene/Eocene Thermal Maximum (Crawford et al., 2014). Also Holroyd et al. (2001) document a rapid increase in the abundance of testudinids in the late Early Eocene. In Eurasia, Lapparent de Broin (2000) suggests a Late Eocene – Early Oligocene dispersal event from Europe to Africa with *G. ammon*. These results are also in accordance with the Paleocene (60.6 Mya and older) origin of testudinids (Lourenço et al., 2012). Also Le et al. (2006) bring together molecular evidence to trace the origin of Testudinidae in the late Mesozoic-early Cenozoic of Asia + North America + Africa, whereas they are the first to suggest an African origin of the extant testudinid lineages (except *Manouria* + *Gopherus*). They also report that the dispersal of the clades in North America, Europe and Africa has been already achieved in the Eocene times.

The DEC analysis was run as explained in the Material & Methods and the detailed results are given in the Appendix. Although the ability to add dispersal constrains on the analysis is a powerful feature of this method (Ree & Smith, 2008) no such constrains are included for two main reasons. First, the user usually needs to upload dispersal constrains based on paleogeography. Our efforts on quantifying the dispersal methods of testudinids are rather poor, as testudinids are known for their ability to float as well as to disperse by using land bridges. Therefore, adding constrains for this group is a rather complicated issue and other factors should be also considered (temperature, precipitation, locomotion). Since this would be complicated even for a small region (e.g. Mediterranean) for the entire Cenozoic, the task is even harder in a worldwide scale. Second, these dispersal constrains are used by the script

in relation with the calibrated tree, in order to calculate in each node the possibility for dispersal in given areas.

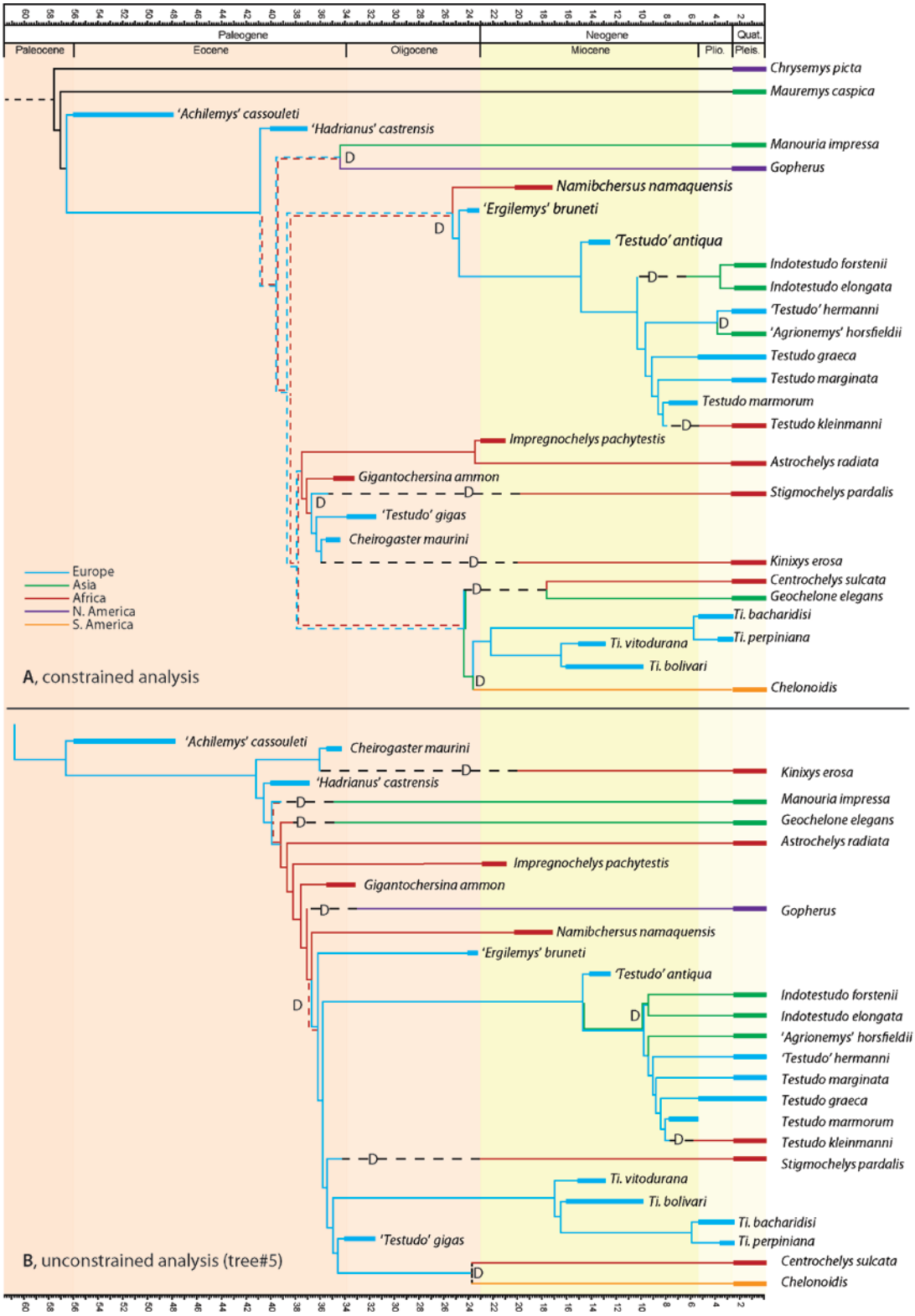


Figure 4.71. The Dispersal-Evolution-Cladogenesis (DEC) analysis on the (A) constrained and (B) unconstrained analysis of the testudinids. No dispersal constrains have been applied.

In the present case however, the calibration is done based on the oldest age of the terminal taxa. Since some clades only include extant taxa, its posterior calibration

would not reflect their real temporal distribution and the results of the analysis would be erroneous. For these reasons, it seems rather difficult at the moment to fully analyze the dispersal of the various testudinid clades. Nevertheless, an analysis without any constrains is performed, i.e. to calculate the ancestral areas for the split based on the tree topology (Fig. 4.71). For the reasons explained above only the results in clades with numerous fossil representatives are considered that would allow a correct posterior calibration. Others (e.g. *Chelonoidis*, *Gopherus*) without any fossils included in the analysis, probably do not reflect their real biogeographic history.

Based on the results of the DEC on the constrained analysis, three points should be emphasized. First of all, regarding the origin of the major testudinid lineages, the analysis cannot fully resolve the ancestral areas, but it provides the two highest possibilities for Europe and Africa. Therefore it could be likely that indeed those lineages originate from Africa. Second, it seems possible that *Testudona* could originate from Europe, which would imply subsequent dispersal event to Asia for *Indotestudo* and '*A.*' *horsfieldi* and to Africa for *Te. kleinmanni*. Although the ancestral area of the stems of *Testudona* clade are not fully resolved between Europe and Africa (they show similar possibilities), a possible African ancestry would agree with the this novel scenario proposed by Le et al. (2006). Finally, it is likely that both Europe and Africa have played an important role on the early biogeographic evolution of the testudinid lineages as we can trace dispersals from Africa to Europe (with '*Te*.' *gigas* and *Ch. maurini*) and subsequent dispersals to Africa (*Kinixys*). Also the area of Mediterranean shows important dispersal events within *Testudona* and should be further analyzed in detail in the future.

Shell size evolution: One of the classic recurring subjects on the study of the testudinid evolution is the study on giantism (sensu Gould & McFadden, 2004). Two main ideas are usually used. The first idea behind it is the so-called 'Cope's rule', i.e. a general size increase of a phyletic line. The study of Moen (2006) on the application of this rule on the cryptodiran turtles showed that their evolution does not follow any pattern of size increase consistent with Cope's rule. The second idea is the so-called 'island rule', i.e. a trend of dwarfism of large animals and a gigantism of small animals that are isolated in islands. On a recent paper, Itescu et al. (2014) find that turtles disagree with this rule, as for example the ancestors of the large Galápagos tortoises must have been already large prior to colonization with the large size aiding the dispersal.

As it is clearly stated by Gould & McFadden (2004) such studies make no sense without a phylogeny. Therefore the question towards giantism or nanism (sensu Gould & McFadden, 2004) is addressed here, based on the calibrated constrained analysis. To do that a shell size character is simply mapped (0, 0-40cm long; 1, 40-80cm long; 2, >80cm long) on the constrained analysis using TNT. The scope of this action is to observe the optimization of such character in a existing phylogeny and try to infer the most parsimonious evolution of the shell size. '*H.*' *castrensis*, '*E.*' *bruneti*, *I. pachytestis*, *S. pardalis*, *C. sulcata*, '*Te.*' *gigas* and *Ch. maurini* are coded as 1. *G. ammon*, *Titanochelon* and *C. nigra* are coded as 2. The remaining taxa have been codes as 0. The result is given in Fig. 4.72.

Although the taxon sampling should clearly by larger in order to make a more confident assessment, the emerging picture from these results is striking. It appears that the most parsimonious solution is that the ancestral condition for most testudinid clades is to be small in the Eocene times, and that the large (40-80 cm) and giant

(more than 80 cm) sizes have evolved independently in many occasions and in many continents.

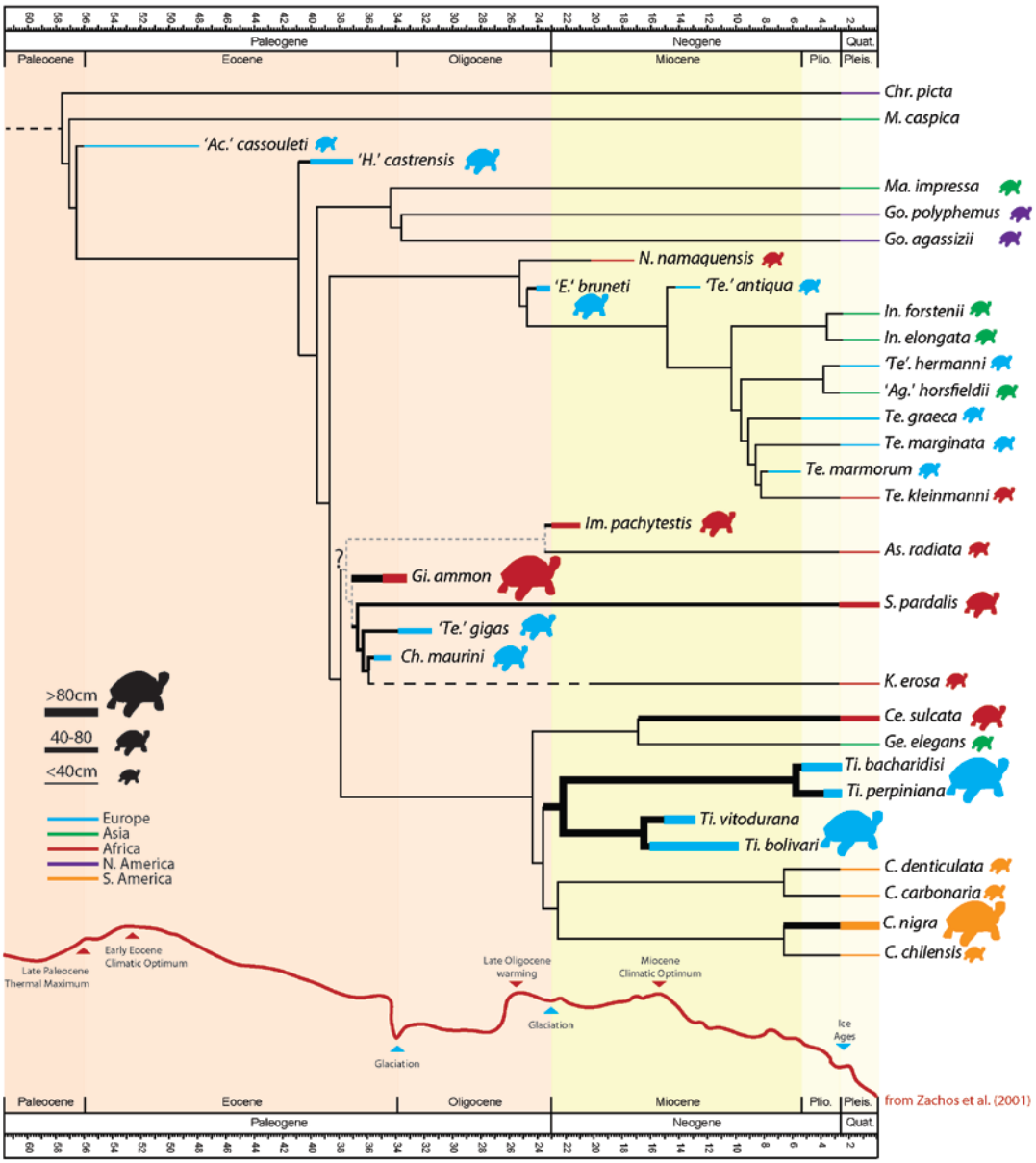


Figure 4.72. Mapping of the shell size on the constrained analysis and comparison with the global climatic evolution from Zachos et al. (2001). Grey dotted line indicates ambiguous optimization.

The exception is the clade containing some of the oldest testudinids in Europe and Africa (*G. ammon*, *Ch. maurini*, *"Te." gigas*) and several other African extant and extinct taxa, whose ancestral condition is ambiguous between the small and large size. In this clade, is likely that the small size is secondarily retained in *A. radiata* and *K. erosa*. This could indicate a trend towards nanism for this clade. Within this clade, the fossil *I. pachytestis* and the extant *S. pardalis* retain the large size.

Giantism appears to be lineage-specific for *Titanochelon* and *Ch. nigra*. All the representatives of *Titanochelon* are large-in-size and some forms (not included in this analysis due to fragmentation) are even large than 150 cm (Samos, Lesvos and possibly Las Higuerelas forms; Lapparent de Broin, 2002). The results for the *Chelonoidis* clade should be however interpreted with caution, as many large-sized

fossil taxa that could belong to this clade are not included in this analysis. The early representatives of this clade were middle-sized (*C. gringorum*, Simpson, 1942 amongst others) or giant (*C. gallardoi*; Rovereto, 1914), whereas most extant *Chelonoidis* are small-in-size. Giantism occurs in the Miocene times in the early representatives of *Centrochelys* (Djebel Zelten). However, *Centrochelys* is smaller today than in the past (Lapparent de Broin and van Dijk, 1999). On the other hand, the clade *Testudona* and its stems are likely to be small and they even show a trend towards nanism, as *Te. kleinmanni* among the smallest testudinids at present. However, giantism is noted at least in one stem *Testudona* with '*E.*' *bruneti*.

It is possible that the shell size evolution is tied with the global climatic evolution. The large and giant size evolved in the Eocene times could be triggered by the favorable conditions in the Early Eocene and afterwards. On the beginning of Oligocene the onset of Oligocene glaciations caused a global cooling (Zachos et al., 2001) that could generally favor a smaller size for the testudinids. Indeed, many clades that seem to originate in Oligocene times (e.g. *Testudona*, *Gopherus+Manouria*), show only small-in-size individuals today and in the fossil record. Giantism re-appears in the Miocene times, a phenomenom that could be favored by the Miocene Climatic Optimum conditions. These speculative results suggest that the general trend on the testudinid size evolution is towards nanism, a trend that could be tied with the global climatic evolution.

Of course, in many lineages giantism appears sporadically and specific clades might pertain large sizes, with a nanism (e.g. the *G. ammon* clade) or giantism trend (*Titanochelon*). These results should be further tested on each clade in detail, as the evolution of the shell size in each lineage could be more complex and other factors could have played a role. For example, Georgalis & Kear (2013:308) suggest that within *Titanochelon* giantism could be explained by metabolic factors and/or to be affected by dietary reasons as a response to large-scale vegetation changes. Certainly these ideas are promising and could explain lineage-specific changes, but they should be further tested in a larger phylogenetic context. Moreover, individual focus should be drawn upon the estimation of the shell size based on fragmentary material, which could allow the inclusion of many incomplete specimens in this scenario. A trend towards nanism is interesting and need to be further tested, as it has been recorded in other animal groups (e.g. trend toward nanism in varanids in Gould & McFadden, 2004). The same authors showed also that Cope's rule is not applied in horses as well, as the giantism is recovered autapomorphically in many lineages.

Analysis #3: In this section the phylogenetic relationships of some small testudinid taxa from Greece are investigated. These specimens have been described in the previous chapter and could belong to new species. These are the specimens from the Late Pliocene site Milia and the partial shell from the Late Miocene of Samos. These specimens were analyzed with a matrix of 38 taxa and 81 characters (see Appendix), including *Paleotestudo canetoniana*. The results are given in Fig. 4.73, showing only the relevant clade. The unconstrained analysis resulted in 12 MPT, of 301 steps (TBR), with a CI 0.336 and a RI 0.536. The general topology of the various clades is the same as in the Analysis #1. The constrained analysis resulted in 4 MPT, of 320 steps (TBR), with a CI 0.316 and a RI 0.492. The general topology of the various clades is the same as in the Analysis #1 and Analysis #2 respectively. In both analyses both taxa from Milia and Samos are within *Testudona*, the Milia testudinid being recovered within *Testudo*. In the unconstrained analysis (Fig. 4.73.A) the Samos testudinid is grouped with *A. horsfieldii*, whereas in the constrained analysis is

recovered in the stem of *Testudo*. Another difference between the two analyses, regards the position of *P. canetoniana*, that is recovered either in the stem of *Testudona* or in the stem of *Testudo*. Regarding the Greek taxa, based on the Analysis #3 is clear that the Samos testudinid is situated in the stem of *Testudo*. Given that this specimen could in fact represent a Minor Asian taxon (see previous chapter) then further study of Turkish specimens would be important to clarify the early evolutionary stages of *Testudo* in that region. On the other hand, the Milia testudinid is nested within *Testudo*. The interrelationships within this clade are not fully resolved, as the Milia testudinid is either grouped with *Te. kleinmanni* (in 2 trees) or with *Te. marginata* (in 2 trees). The grouping with *Te. kleinmanni* is not supported by any synapomorphies, whereas the sister-group relationship with the marginated tortoise is supported by 1 synapomorphy, the posteriorly flared carapacial margin. This sister-group relationship is also recovered in the unconstrained analysis in 6 trees. This character is also recovered as an autapomorphy of the African taxon *Kinixys erosa*, suggesting a possible homoplasy of this character within Testudinidae. Although the analysis is not conclusive, it seems that the best-supported hypothesis for the Milia testudinid is a member of the *Te. marginata* lineage.

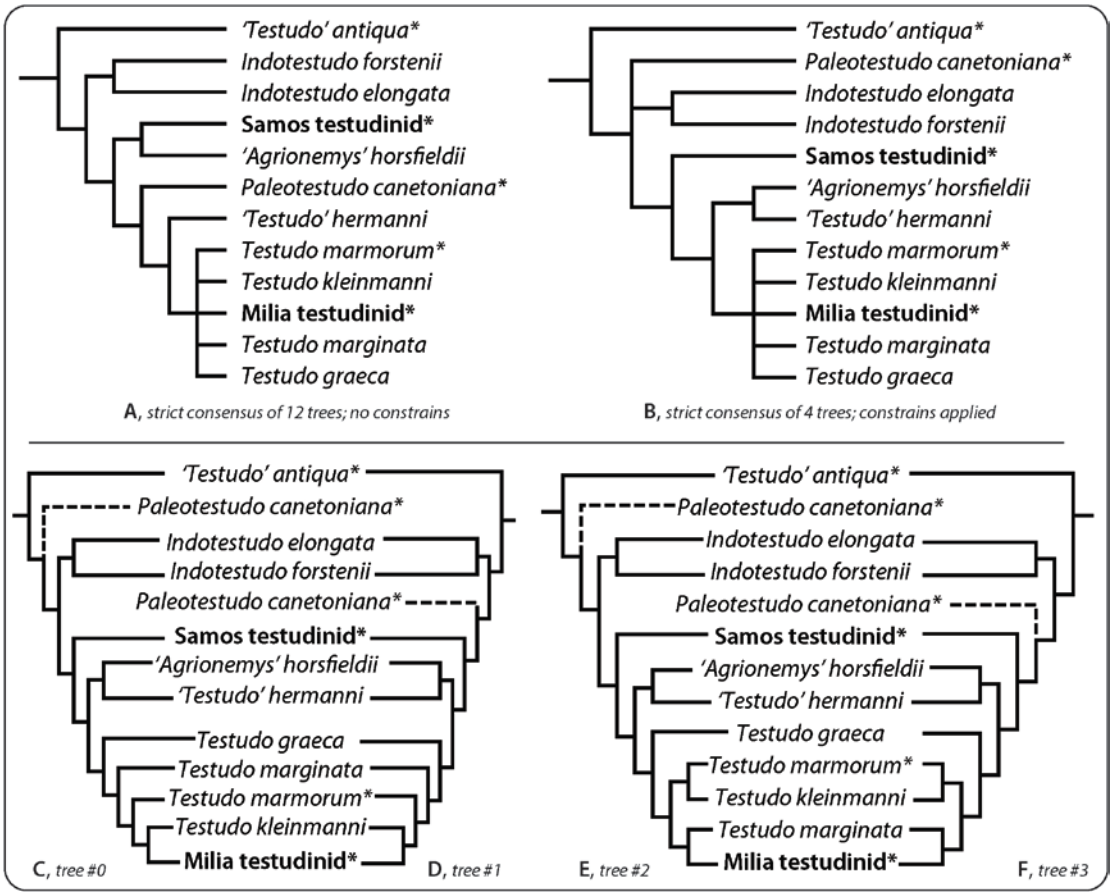


Figure 4.73. Phylogenetic analyses of the Milia and Samos testudinids. A, strict consensus of 12 MPT of the unconstrained analysis. B, strict consensus of 4 MPT of the constrained analysis. C-D, the 4 MPT of the constrained analysis. Fossil taxa are indicated with an asterisk.

In conclusion, the relationships within *Testudona* are still blurry regarding the inclusion of several fossil forms (e.g. *P. canetoniana*) and future work should try to include in this matrix several of these fossil forms within *Testudona*, as those analyzed by Lapparent de Broin et al. (2006c) and Corsini et al. (2014). This would

help to understand the relationships of this clade, as the main difference of my analysis with the above-mentioned works is the placement of '*Te'. antiqua* on the stem of *Testudona*. Although my results highly contrast the broadly accepted placement of '*Te'. antiqua*, they are in accordance with the molecular rate estimates (not based on fossils) of the basal polytomy of testudonans of 6.0 – 9.4 Mya by Parham et al. (2006). If '*Te'. antiqua* is placed within *Testudona*, then it would push back the origin of testudonans at least 5 million years.

4.4. Phylogenetic analysis of the terrapins from Greece

The peculiar morphology of the vertebral scutes seems to distinguish the Nea Silata and Allatini geoemydids from known extant and extinct forms, suggesting that the Late Miocene *Mauremys* from the Thessaloniki area could belong to a new species. However, the specimens from Nea Silata are disarticulated and the Allatini specimen is too poorly preserved, since many diagnostic parts of the carapace are missing. Therefore, although the morphology of this taxon can be reconstucted, this result should be interpreted with caution till an articulated specimen is found. Nevertheless, an attempt will be made in this session to assess the phylogenetic position of this taxon, within known extant and extinct geoemydids from Europe. Hopefully new specimens will allow a more detailed description, and a more secure taxonomic identification, in the future.

The data matrix of Hervet (2003) is used, which has been designed to explain the diversity of the Eocene – Oligocene taxa that have been formerly included in the "*Palaeochelys* s.l. – *Mauremys*" group. Since the characters have only been published in French, in the thesis of Hervet (2003), they are listed here in English (see Table 4.1). The modifications suggested by Chesi et al. (2009) for *Mauremys portisii* and *Mauremys campanii* (excluding *Borkenia* aff. *B. oschkinisi*) are incorporated.

The proposal by Claude & Tong (2004) that the following species represent junior synonyms of other taxa are preliminary accepted: *Juvemys*, *Francellia*, *Owenemys* and *Euroemys* (junior synonyms of *Palaeoemys*); *Bergouniouxchelys*, *Cuculemys* and *Provencemys* (junior synonyms of *Palaeochelys*); *Francellia sallouagmirae* and *Juvemys labarrei* (junior synonyms of *Palaeoemys testudiniformis*); and *Palaeoemys occitana* (junior synonym of *Palaeoemys hessiana*).

Ideally, the matrix should included more fossil and extant geoemydid taxa from Asia, in order to be able to document the entire diversity of the group. Therefore, the results listed below can place the Nea Silata geoemydid within the European context, but further sampling will be required in the future. The data matrix contains 30 taxa and 54 characters (see Appendix). A traditional search with TNT v. 1.0 (Goloboff et al., 2008a,b), using a tree-bisection algorithm with 1,000 replicates is performed. All characters were considered unordered and equally weighted. A total of 12 most parsimonious trees, each having a length of 146 steps, were recovered. The CI is 0.582 and the RI is 0.802. The strict consensus tree is shown in Fig. 4.74.

Table 4.1. Morphological characters used in the analysis, based on Hervet (2003: 201-237; original characters in French). These are brief and simplified descriptions; please see Hervet (2003) for detailed information and drawings of the alternative character states.

0, Presence of inframarginal scutes: (0) yes; (1) no, presence only of axillary and inguinal scutes.

1, Length of the contact of the axillary process with the first costal (COS1): (0) no contact; (1) long process, touching a third to half of the COS1; (2) narrow process, touching a third of PL1; (3) narrow process, touching less than a third of COS1; (4) narrow process, touching only an extremity of COS1.

2, Contact of the inguinal process with the fifth and/or sixth costal: (0) no contact; (1) long process, touching a third to half of the pleurals; (2) narrow process, touching less than a third of the pleurals.

3, Axillary and inguinal notches: (0) large; (1) reduced.

4, Nuchal notch: (0), wide notch, affecting the first and second peripherals as well; (1) reduced, affecting the first peripheral and sometimes the second; (2) almost absent.

5, Contact of the first vertebral with the nuchal: (0), narrow vertebral, the first pleurals cover the lateral parts of the nuchal; (1) wide vertebral, extending on first peripherals and the pleuro-marginal sulcus crosses the peripheral; (2) wide, could extend behind the suture of the first two peripherals.

6, Width/length ratio of the first vertebral: (0) below 1.2; (1) between 1.2 and 1.7; (2) above 1.7.

7, Contact of the first vertebral with the second marginal: (0), absent; (1) large contact.

8, Shape of the first vertebral: (0) lyre-shaped; (1) straight lateral borders that diverge anteriorly; (2) rounded lateral borders that converge anteriorly.

9, Width of the second and third vertebral in respect to the nuchal: (0) always below 75%; (1) more than 70%.

10, Width of the vertebral in respect to the pleurals: (0) narrow; (1) wide, width of third vertebral/width of second and third pleurals more than 80%; (2) wider, width of third vertebral/width of second and third pleurals more than 100%

11, Width of fourth and fifth vertebral: (0) fifth vertebral wider than the fourth; (1) fifth vertebral narrower than the fourth.

12, Width of the cervical in respect to the nuchal (cervical width/ nuchal width): (0) less than 25%; (1) more than 25%.

13, Covering of the cervical viscerally: (0) short; (1) long.

14, Covering to the first and second marginals viscerally on the nuchal and on the border: (0) long on nuchal and reducing towards the border, small or absent on the border; (1) well developed on nuchal and moderate on the border; (2) well developed on the nuchal, more developed on the border.

15, Contact between the costals 1-2 and the peripherals: (0) costals 1-2 suture in the middle of peripheral 3; (1) costals 1-2 suture roughly corresponds to the peripheral 3-4 suture.

16, Correspondence of the costal sutures with the peripheral sutures in the anterior

carapace: (0) good correspondence in general; (1) weak correspondence.

17, Position of the pleuro-marginal sulci on the peripherals (excluding peripherals 11 and the pygal): (0) pleuro-marginal sulcus crossing the peripherals, marginals 1-3 always being shorter than peripherals 1-2; (1) coincidence (excluding the pygal and peripheral 11, and moderate coincidence of marginals 1-3 anteriorly).

18, Contact between the marginal 1 and/or marginal 2 and the costal 1: (0) absent or sometimes present (intraspecific variation); (1) always present.

19, Contact between the pleural 3 and the marginal 6: (0) absent; (1) present.

20, Contact between the pleural 4/vertebral 5 sulcus and the marginal 10: (0) absent, sulcus on marginal 11; (1) present, sulcus on marginal 10/11 or on marginal 10.

21, Position of vertebral 5 in respect to the suprapygal 2 and the pygal: (0) marginals 12 sulcus is short and marginals are on the same level as the suprapygal/pygal suture; (1) marginals 12 sulcus is short, but the marginals extend on the suprapygals; (2) vertebral 5 does not extend on the pygal.

22, Shape of the nuchal: (0) short, wider than long, with wide anterior border; (1) long, moderately wide, with wide anterior border; (2) long, moderately wide, but with narrower anterior border than state 1; (3) long, longer than wide, with narrow anterior border.

23, Neural series: (0) completely irregular; (1) neural 1 is quadrangular and neurals 2-8 hexagonals with short anterior lateral borders.

24, Shape of suprapygals 1: (0) trapezoidal, with a wide posterior side; (1) trapezoidal, with narrow posterior side (more rectangular).

25, Shape of suprapygals 2: (0) inversed trapezoidal; (1) trapezoidal to hexagonal; (2) hexagonal, with anterolateral and posterolateral borders of equal width; (3) hexagonal, with longer posterolateral borders.

26, Shape of pygal: (0) long, as long as wide or longer than wide; (1) short, wider than long, rectangular; (2) short, much shorter than state 1.

27, Shape of the anterior lobe of the plastron: (0) quadrangular to slightly trapezoidal; (1) trapezoidal.

28, Size of the plastron in respect with the carapace: (0) shorter, the lobes not reaching the level of the marginals; (1) long, the anterior and/or the posterior lobe reaching the level of the marginals.

29, Type of dorsal epiplastral lip: (0) weakly developed medially and laterally; (1) epiplastral lip developed, but is non-existent in the symphysis; (2) epiplastral lip more developed than in state 1, as well as in the posterior ends of the epiplastra; (3) epiplastral lip even more developed, with the presence of two thickenings one each side, medially of the humero-pectoral sulcus.

30, Length of the gularo-humeral sulcus in respect to the width of the gulars: (0) less than 0.2; (1) between 0.2 and 0.3; (2) more than 0.3.

31, Elongation of the epiplastral lip in the symphysis: (0) absent; (1) present.

32, Position of the posterior point of the gulars in respect with the entoplastron: (0) contacting the entoplastron, often with the presence of a small entoplastral scute; (1) not contacting the entoplastron; (2) covering the anterior area of the entoplastron.

33, Comparison of the width and length of gulars (length/width ratio): (0) less than 45%; (1) more than 45 %.

34, Angle of the gularo-humeral sulci: (0) almost 180°; (1) equal or more than 90°;

(2) always below 90°.

35, Shape of the gularo-humeral sulcus: (0) straight or sinuous; (1) becomes narrower towards the medial part.

36, Narrowing of the anterior lobe at gularo-humeral sulcus: (0) absent or slightly developed; (1) present.

37, Shape of the anterior lobe: (0) straight to slightly rounded; (1) well rounded.

38, Length of the abdominal and femoral scutes (abdominal/femoral length ratio): (0) more than 175%; (1) less than 175%.

39, Length of the humeral and pectoral scutes (humeral/pectoral length ratio): (0) more than 70%; (1) less than 70%.

40, Length of the gular and humeral scutes (gular/humeral length ratio): (0) less or equal than 100%; (1) more or equal than 100%.

41, Length of the humeral scute relative to the entoplastron (humeral/entoplastron length ratio): (0) more than 70%; (1) less than 70%.

42, Length of the gular scute relative to the length of the anterior lobe, measured till the axillary process (humeral/anterior lobe length ratio): (0) less than 30%; (1) between 30 and 45%; (2) more than 40%.

43, Shape of entoplastron: (0) long and oval; (1) rhomboid; (2) piriform.

44, Orientation of the epi-hyoplastral suture in ventral view: (0) diverges posteriorly; (1) almost perpendicular; (2) converge posteriorly.

45, Length of epiplastra in symphysis: (0) short; (1) long; (2) elongated.

46, Median length of hyoplastra in the posterior border of the entoplastron in respect to the axillary notches: (0) hyoplastra medially long and the posterior border of the entoplastron is situated anterior to the axillary notches; (1) hyoplastra medially short and the posterior border of the entoplastron is situated slightly anterior to the axillary notches; (2) hyoplastra medially much shorter and the posterior border of the entoplastron is situated posterior to the axillary notches;

47, Length of the hyoplastron in the symphysis in respect to the length of the anterior lobe (hyoplastron/anterior lobe length ratio): (0) more than 55%; (1) less than 55%.

48, Shape of the humero-pectoral sulcus: (0) sinuous; (1) rounded; (2) straight or slightly sinuous.

49, Position of the humero-pectoral sulcus medially, in respect with the entoplastron: (0) posterior to the entoplastron; (1) still posterior to the entoplastron, but in a more advanced position compared to the previous state; (2) in contact with the posterior end of the entoplastron; (3) crossing the posterior part of the entoplastron; (4) in an advanced position on the entoplastron.

50, Length of the bridge in respect to the length of the plastron (till the xiphiplastral tips, bridge/plastron length ratio): (0) less than 20%; (1) more than 40%; (2) between 30 and 40%.

51, Thickening of the lip covered by the humeral and femoral scutes in visceral view: (0) slight to moderate; (1) moderate to large.

52, Anal notch: (0) large and wide, sometimes deep; (1) narrow and deep.

53, Size of anal scute in respect to the xiphiplastron: (0) anals cover more than 80% of the xiphiplastra; (1) anals cover less than 80% of the xiphiplastra.

The Nea Silata specimen is clearly a member of the *Mauremys* clade, and in particular the clade containing *M. leprosa, M. caspica, M. gaudryi, M. campanii* and *M. portisii*, being clearly separated from the older forms like *Mauremys sarmatica* and *Mauremys pygolopha*. The Allatini specimen occupies different positions within the *Mauremys* clade: either outside to the clade containing *M. leprosa, M. caspica, M. gaudryi*, and *M. campanii*, or as the sister taxon of *M. caspica*, or as the sister of one of the two Italian taxa, the Early Pliocene *M. portisii*.

.

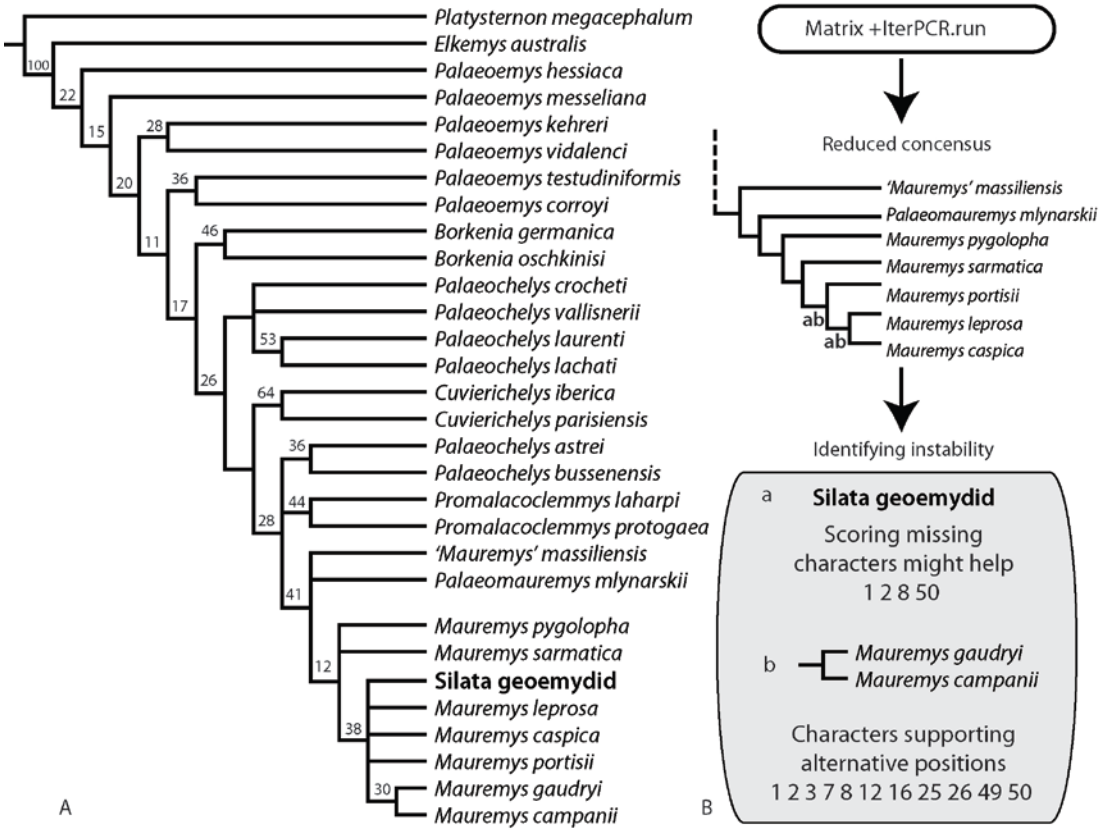


Figure 4.74. A, Strict consensus tree of the phylogenetic analysis of the Nea Silata geoemydid with many European fossil geoemydids, based on the matrix of Hervet (2003). Numbers indicate Bootstrap values. B, Implementation of the IterPCR script (Pol & Escapa, 2009), identifying the instability of the tree.

To further analyze this instability, the iterPCR script developed by Pol & Escapa (2009) has been employed. This script not only analyzes the positions of unstable taxa, but also reports the characters that support alternative placements. Furthermore, it identifies characters that, if coded, could potentially resolve the positions of taxa for which many codings are lacking (Pol & Escapa, 2009). The script also produces a reduced consensus tree without the unstable taxa (Fig. 4.74.B). The iterPCR results showed that the Nea Silata geoemydid, and the clade containing *M. campanii* and *M. gaudryi* were all unstable, but for different reasons. The Nea Silata geoemydid was found to be unstable as a result of missing data, mainly pertaining to carapace characters (1, 2, 50, 80). New material from the same locality or nearby sites will hopefully help to resolve this issue in the future. On the other hand, *M. campanii* and *M. gaudryi* were found to be unstable because of several characters (1, 2, 3, 7, 8, 12, 16, 25, 26, 49, 50) that could be scored but supported alternative positions for these two taxa. Based on all available published information,

and on direct observations, the scorings taken from previous analyses for *M. gaudryi* (Hervet, 2003) and *M. campanii* (Chesi et al., 2009) are correct. Therefore, this instability as an indication that the characters used in the analysis, although useful for analyzing relationships at the generic level and above, were unable to provide good resolution at the specific level. Hopefully our results will encourage a search for further characters that might be of use in resolving species-level relationships within *Mauremys*

Based on the above, it is clear that more specimens must be described from nearby localities exposing Early Miocene – Late Miocene boundary strata in northern Greece in order to shed light on faunal changes across this boundary. This analysis also highlights the problematic state of the taxonomy of European geoemydids. For example, some taxa that are placed within *Mauremys* in our analysis (e.g. *Palaeomauremys mlynarskii*) or *Mauremys massiliensis* need revision. Also, taking into account the synonymies suggested by Claude & Tong (2004) this analysis reveals that *Palaeochelys* may be polyphyletic, and *Palaeoemys* paraphyletic. However, this analysis includes only European taxa, and therefore fails to encompass the entire diversity and range of *Mauremys* given that this genus has numerous representatives in Asia as well. Hervet (2004) suggested the presence of a *Palaeochelys* s.l. – *Mauremys* lineage, contradicting both molecular phylogenetic analysis of geoemydids and the Asian fossil record (see Claude et al., 2007 and references therein). For example, molecular evidence suggests that the clade containing *M. caspica* and *M. rivulata* has a sister-group relationship with a clade containing such Asian taxa as *M. annamensis*, *M. mutica* and *M. pritchardi* (Spinks et al., 2004), and the position of *M. leprosa* is not fully resolved. Similar results were also obtained by Barth et al. (2004). Phylogenetic relationships within *Mauremys*, and the Geoemydidae in general, could be better resolved by analyzing further morphological characters to the morphological matrix introduced by Hervet (2003), and by including extant and extinct Asian geoemydids, and combine the results with the information produced by molecular studies. Such an analysis is far beyond the scope of this thesis, but is needed in order to fully understand the geoemydid phylogenetic relationships.

4.5. The bothremydid affinities of the pleurodiran *Nostimochelone lampra*

The most complete and widely used matrices for the pleurodiran clades are those of Gaffney et al. (2006; particularly useful for bothremydids, euraxemydids and araripemydids) and of Gaffney et al. (2011; particularly useful for podocnemidids). The first matrix contains 175 characters whereas the second 74 characters. Both matrices focus on the morphology of the skull (120 cranial characters in Gaffney et al., 2006 and 54 characters in Gaffney et al., 2011). Instead, the shell morphology is underestimated with only 21 and 13 characters respectively. Given the inability to score characters concerning the dorsal side of the carapace it becomes immediately understood that the available information for *N. lampra* is limited.

The reader should note, however, that also Georgalis et al. (2013) used and discussed several characters of Gaffney et al. (2006) and Lapparent de Broin & Murelaga (1999). By doing so, they have confirmed the placement of the taxon within Podocnemidoidea. However, simply discussing the various synapomorphies or symplesiomorphies, without performing a parsimony analysis, is not enough to access the relationships of a taxon. The matrix of Lapparent de Broin & Murelaga (1999) contains also several shell characters, but the use the Gaffney et al. (2006; 2011) matrices is justified on the basis of the broader sampling. Gaffney et al. (2006; 2011)

sample nearly the entire diversity of pleurodirans, producing a well-supported phylogenetic hypothesis for the ingroup taxa. In this robust framework, hopefully even this limited information could be enough in order to preliminary assess the relationships of this enigmatic pleurodiran turtle.

Scoring (on the character matrix of Gaffney et al., 2006; summarized in Fig. 3.101):

(Characters 1-132 scored as "?")

	135	140	145	150	155	160	165	170	175
Nostimochelone lampra	1??	???1?	31132	32111	???1?	??21?	1???1	?1???	???1?

Most of the morphological characters have clear scorings, but attention should be raised on two important points. First, most of the carapacial characters are designed to be scored on the dorsal side of the carapace. Although no significant changes in the shape of the plates dorsally and ventrally is known, small differences might occur on the size (usually smaller in ventral side). Second, the shape of the first neural needs revising. Georgalis et al. (2013:282) interpret the first neural as being 4-sided, based on the contact with four surrounding plates. In their diagnosis, however, they state: "[…] *a continuous series of six markedly elongate and very narrow neurals with regular, hexagonal outline and short anterolateral sides* […]" (Georgalis et al., 2013:279). My direct observations on the specimen show the presence of small anterolateral sides on this neural, resembling the typical 6-sided coffin-shaped neurals of *Nostimochelone*. When the first neural is 4-sided, the anterior and posterior borders are usually of equal width, and most times narrower than the middle width of the plate. In this case however, the anterior border is much wider than the posterior, as it is commonly found in 6-sided neurals. Although my primary scoring is based on the interpretation of the first neural as 6-sided, a test-analysis is made with the first neural interpreted as 4-sided. Thus, the state of the character 144 is changed from 3 to 0 in the test analysis.

The inclusion of *N. lampra* in the character matrix of Gaffney et al. (2011) does not provide any robust results. The analysis (traditional search, 1000 replicates, TBR algorithm) results in 90 most parsimonious trees of 176 steps. The position of *N. lampra* is uncertain as it jumps around the cladogram, nearly in any clade, without producing any synapomorphies with other taxa or clades. The results from the inclusion of *N. lampra* in the Gaffney et al. (2006) are significantly better, since *N. lampra* is placed better in the cladogram. In total, the analysis of a matrix of 46 taxa and 175 characters (traditional search, 1000 replicates, TBR algorithm) produces 4 most parsimonious trees of 410 steps (Fig. 4.75). The CI is 0.590 and the RI is 0.800. The general topology of the trees is in good accordance with the data of Gaffney et al. (2006) recovering the various clades described there.

In all trees, *N. lampra* is recovered within family Bothremydidae (sensu Gaffney et al., 2006). In 2 of the 4 MPT's, *N. lampra* is recovered within the clade Bothremydini, as the sister-group of *Araiochelys hirayamai* and as basal to the clade containing [*A. hirayamai* + *Elochelys convenarum*] with two synapomorphies (146, 6 neurals; 167, pectorals anterior to the entoplastron). In the remaining trees, *N. lampra* is placed due to the same synapomorphies (146, 6 neurals; 167, pectorals anterior to the entoplastron) within the clade Kurmademymini. Given the uncertainty of the character of the first neural shape (explained above), based on our interpretation and that of Georgalis et al. (2013), another analysis is made with the first neural interpreted as 4-sided. In this analysis (4 MPT's, 409 steps) the results are the same.

Note that *A. hirayamai* possess a 4-sided first neural, but this character is always recovered as homoplastic in both analyses.

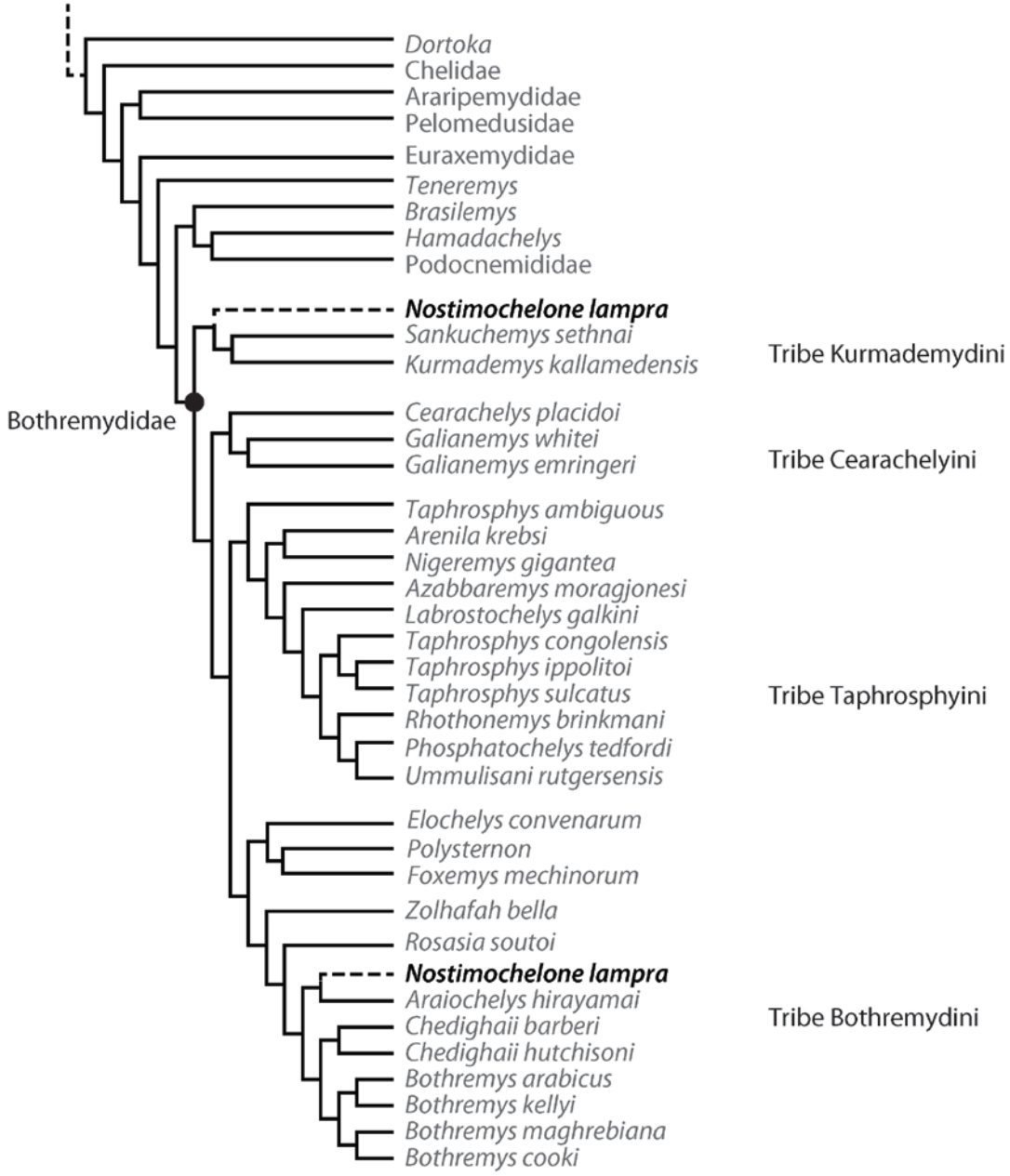


Figure 4.75. A composite cladogram from the 4 MPT of the *Nostimochelone lampra* in the matrix of Gaffney et al. (2006), showing the two positions of the taxon within Bothremydidae.

The clade Bothremydidini shows a temporal distribution from the Late Cretaceous till the Ypresian (Gaffney et al., 2006) and is one of the most abundant group of turtles in the Late Cretaceous fossil sites of Western Europe (Pérez-García, et al., 2012). The results of the analysis clearly indicate that the preserved information on the holotype of *N. lampra* is not enough to clarify the systematic position of this taxon within Podocnemidoidea, as the recovered position is only based on few shell characters, within a matrix that mainly contains cranial characters. However, the available information suggests some shell affinities with the clade Bothremydini, which need to be evaluated by future findings.

This page has left intentionally blank

Chapter 5. Biostratigraphy

Highlights

Geographical Distribution
Temporal Distribution

Contribution to biostratigraphy

Diversity

5.1. Introduction

This chapter follows the description of the available chelonian specimens from Greece (Chapter 3) and their analysis in a broader phylogenetic context (Chapter 4). The description of new specimens from new localities and the revision of previously published specimens allow a better understanding of geographical and temporal distribution of chelonian lineages in Greece. Also the updated information presented in this thesis allows discussing the potential contribution of the fossil chelonians in the biostratigraphy of Greece.

5.2. Distribution

In general, the fossil chelonians of Greece show a widespread distribution both in continental Greece, as well as in many Aegean Islands. The number of fossil localities with chelonian specimens is much smaller compared to the fossil mammalian localities but it follows, more or less their temporal and geographical distribution. For these comparisons two of the most recent summaries of the localities will be used, the one of Tsoukala (1992) for the Pleistocene and the one of Koufos (2006) for the Neogene localities. When possible, a confirmation of the presence of chelonians in most of these sites is made, not only based on the published information but also by looking at the fossil collections. Also, it should be pointed out that the actual number of fossiliferous localities is greater than those listed in the above-mentioned publications. The geographical distribution of the presence of chelonians through time is shown in Fig. 5.1.

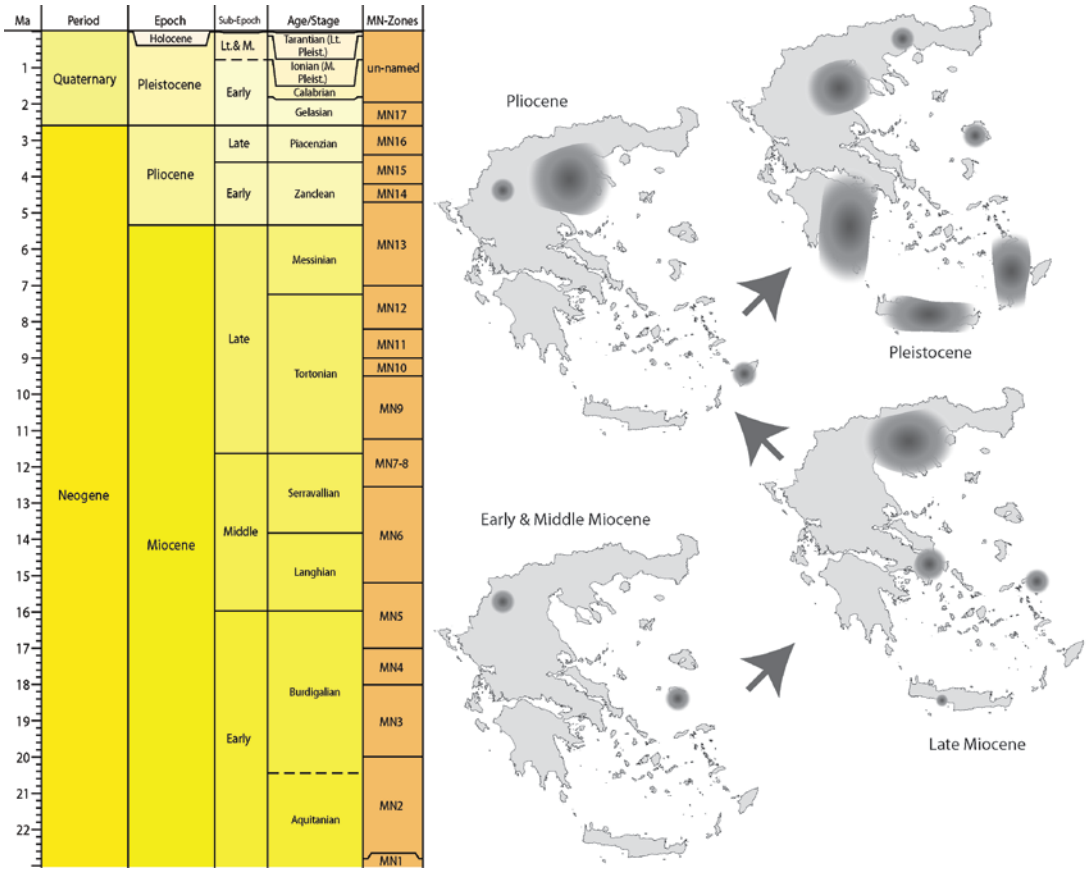


Figure 5.1. The geographical distribution of the chelonian lineages during Neogene/ Quaternary.

In the Early-Middle Miocene of Greece the fossiliferous localities in Greece are relatively few and so are the localities with chelonian remains. Only two localities are known, the Nostimo locality in NW Greece (with no mammalian fossils) and Thymiana from Chios Island. In the fosFARbase database of Böhme & Ilg (2003) unpublished emydid remains from the MN4 of Aliveri and unidentified specimens from the MN4 of Karydia are mentioned by M. Böhme, but these specimens were not available for this study. Although these preliminary identifications cannot be confrimed, this shows that the actual number of localities could be greater. Also the confirmation of the presence of emydid remains in the Early-Middle Miocene would be important, since the only confirmed emydid remains come from the Pleistocene (Fig. 5.2). The Nostimo locality contains the remains of the only pleurodire known from Greece, which shows bothremydid affinities (see Chapter 4). The material from Thymiana is lost (see Chapters 2 & 3) but is important as it could be the oldest testudinid in Greece and possibly close in morphology with a new Late Miocene testudinid from Samos.

Right in the beginning of the Late Miocene, the locality of Plakias in southern Crete is key, as it contains both trionychid and geoemydid specimens which are the southernmost chelonian findings in Greece (Fig. 5.1 & 5.2). Most Late Miocene localities in Greece are found after MN9, and similarly a significant number of fossil localities with extinct chelonians is found. Most of them are found in northern Greece and also in the classical localities of Pikermi and Samos. The taxonomic diversity increases in the Late Miocene compared to the Middle Miocene, as both small and large testudinids are found, as well as aquatic taxa (geoemydids). This certainly the result of the increasing number of fossil localities in the Late Miocene. The large testudinids are found in at least three areas, but most probably they do not belong to the same species. In Samos Island, *Titanochelon schafferi* has been named, but the lack of shell information does not allow confirming its affinities. The large testudinid from Pikermi preserves shell and appendicular elements but no comparable parts are found with Samos's form. These forms, along with the few specimens from Kassandra peninsula, mark the appearance of large testudinids in Greece at least in the MN11. At the same time the small testudinids flourished, found also in Pikermi and Samos, as well as in several localities in northern Greece (Fig. 5.2). Besides the material from the sites described in this thesis, it should be mentioned that more material exists, such as the possible new species from the Late Vallesian of Ravin de la Pluie (MN10) in Axios valley (preliminary mentioned by García et al., 2011; pending publication).

Several localities are known from the boundary of the Miocene and Pliocene. Nea Silata and Maramena are biostratigraphically dated to this boundary based on micromammalian fossils, whereas Allatini and Pylea (Latest Miocene-Earliest Pliocene) could represent this boundary based on the regional stratigraphy of Chalkidiki (see Chapter 2 for further details). Interestingly all these localities are found in northern Greece.

The Pliocene fossil localities are generally fewer compared to the Miocene ones (Koufos, 2006) and therefore is not strange that the number of chelonian localities decreases. Interestingly, except the locality of Apolakkia in Rhodes Island with remains of testudinid eggs and shell remains, the remaining sites are found in Northern Greece. A turnover is noted in the testudinid lineages with the appearance of *Ti. bacharidisi*, with a strong presence in western Chalkidiki. Also, in the Late Miocene *Te. marmorum* has disappeared and early representatives of *Te. graeca* are

found within the boundaries of the range of the extant taxon. Also, close relatives of the marginated tortoise are found in Milia (MN 16a).

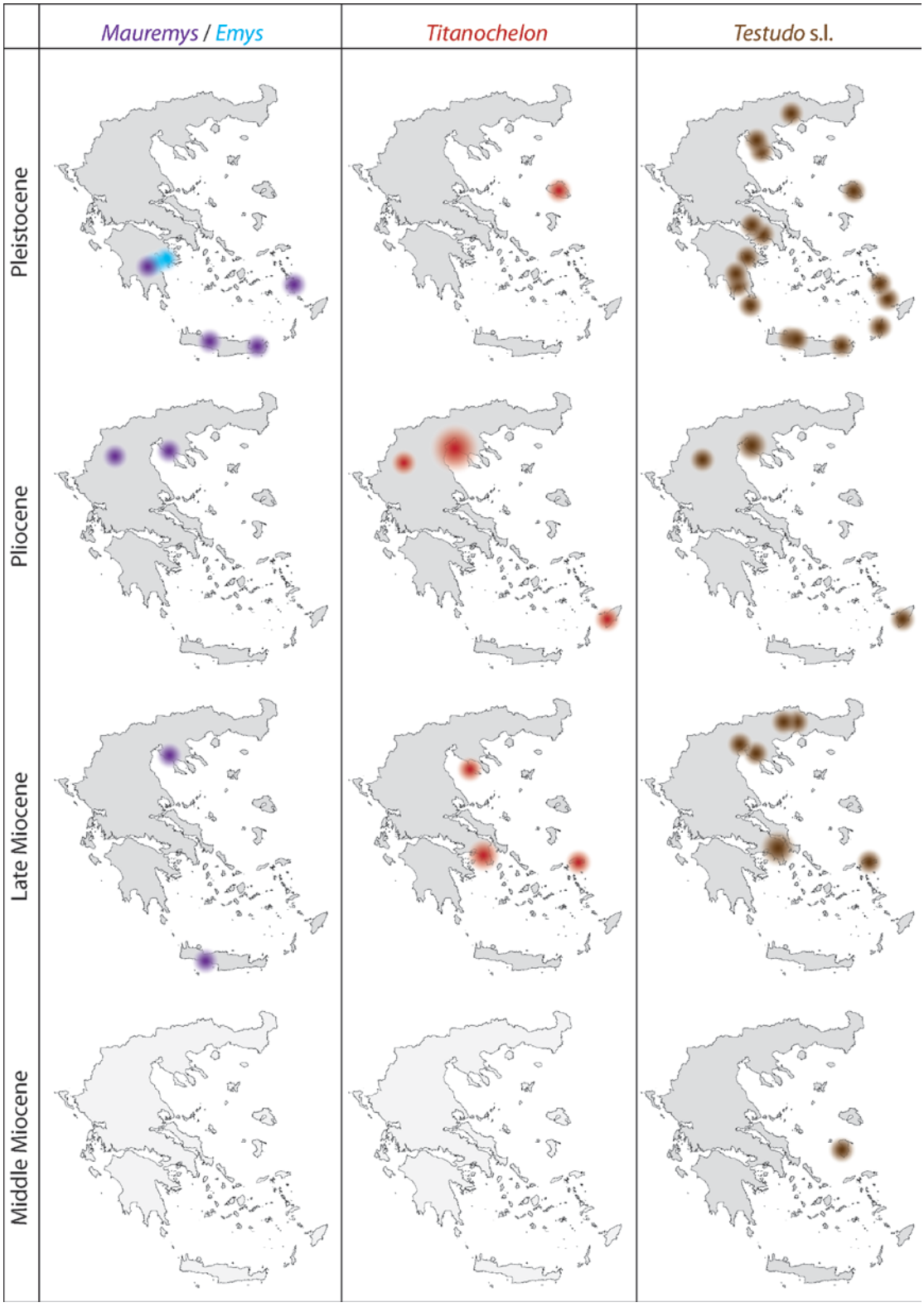


Figure 5.2. Map of Greece with the geographical distribution of the main chelonian clades through time.

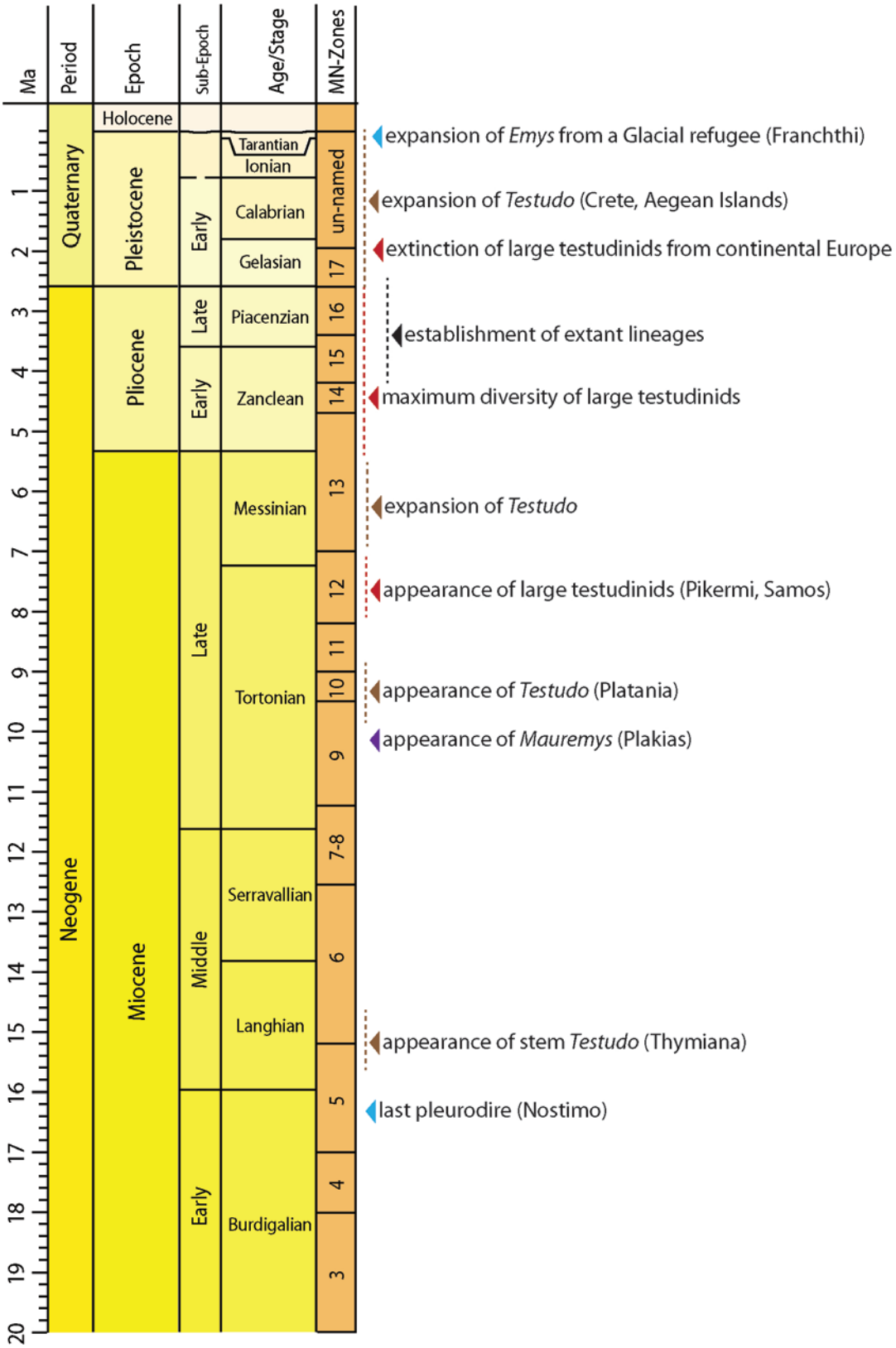


Figure 5.3. The main biostratigraphic events marking the chelonian lineages of Greece.

During the Pleistocene, numerous localities are known, many coming from cave environments (Tsoukala, 1992). Therefore is not strange that several fossil localities are also noted. The extant lineages are already established in the continental

and insular Greece. In the beginning of Pleistocene the large testudinids become extinct, with the last European representative of this clade is found in Lesvos Island.

The study of the Greek chelonians allows the suggestion of several events that are key for the evolution of turtles in Greece. These results should provide the basis for future studies that will seek to analyze these events in detail. First of all, the presence of a pleurodire in the Early Miocene is rather unusual and could correspond to one of the last pleurodires in the European continent (Georgalis & Kear, 2013). Shortly after the disappearance of pleurodires in Greece we have the appearance of terrestrial testudinids in Chios, taxa that could belong to the stem of *Testudo*. The appearance of true *Testudo* is found later in the Late Miocene with *Testudo marmorum* and fragmented remains of *Testudo* sp. At the same time, the first geoemydids and the first large testudinids appear in the fossil record of Greece. Towards the latest Miocene the range of *Testudo* increases, and is found in most parts of Continental Greece. In the Pliocene, the material from Thessaloniki area allows studying the maximum of the diversity in large testudinids, whereas at the same time the presence of the extant chelonian clades is established.

The small testudinids are found widespread all over Continental Greece and in several islands. In Northern Greece, representatives of *Te. graeca* and *'Te.' hermanni* are found. On the other hand, the testudinids found in Peloponnesus, Crete and other southern Aegean islands are mostly attributed to the marginated tortoise. Also, several sites contain specimens of *M. rivulata*, and in two sites (Franchthi Cave & Megalopolis) remains of *Emys orbicularis* are found. These last findings confirm previous suggestions that *Emys* has been retracted in the South Balkans as a Glacial refugee (Fritz et al., 2007), from which expanded northwards during the warmer parts of the Holocene. At the same time, the range of *Mauremys* is significantly reduced compared to the Pliocene, as it is found only in southern Greece and especially in Peloponnesus, Crete and Kos Island. Still, the range of *Mauremys* is much larger than the range of *Emys*.

These events are summarized in Fig. 5.3. Information on most of these events can be found in the literature. For example, the Balkan Glacial refugee of *E. orbicularis* is mentioned by Fritz et al. (2007; 2009). Regarding testudinids, more information is available. Lapparent de Broin (2002) mentioned that the Lesvos large testudinid is the last continental representative in Europe. Indeed, no younger specimens are found in Greece or in Europe, except some fragmentary material in Mediterranean Islands (see discussion in Pérez–García & Vlachos, 2014).

So far, the use of chelonians in biostratigraphy has been limited. Indeed chelonians have a different rhythm of evolution compared to the mammalian taxa (that are usually used in biostratigraphy). Therefore, it seems that turtles and tortoises cannot compete with the mammal fossils from a biostratigraphic point of view. Nevertheless, in Greece, we can observe some groupings that at least allow us to use chelonians effectively to define the epochs in the Neogene and Quaternary times (Fig. 5.4). Given that chelonians show a good fossil record and most of the times even small fragments can be confidently identified, their potential use in the biostratigraphy could be of some importance.

Holocene: Most probably, the presence of *Emys orbicularis* defines the Latest Pleistocene and the Holocene times. This taxon showed a retracted distribution during the Ice Ages of the Pleistocene and the Balkans are considered a Glacial refugee during the Latest Pleistocene (Fritz et al., 2007).

Pleistocene: The Pleistocene Epoch in Greece is defined by the presence of the extant taxa. In particular, *Mauremys rivulata*, *'Testudo' hermanni* and *Testudo marginata* are present only since the beginning of Pleistocene and usually co-exist with one-another in several localities. Also, the Pleistocene is characterized by the absence of large testudinids in Continental Greece, and the absence of trionychids.

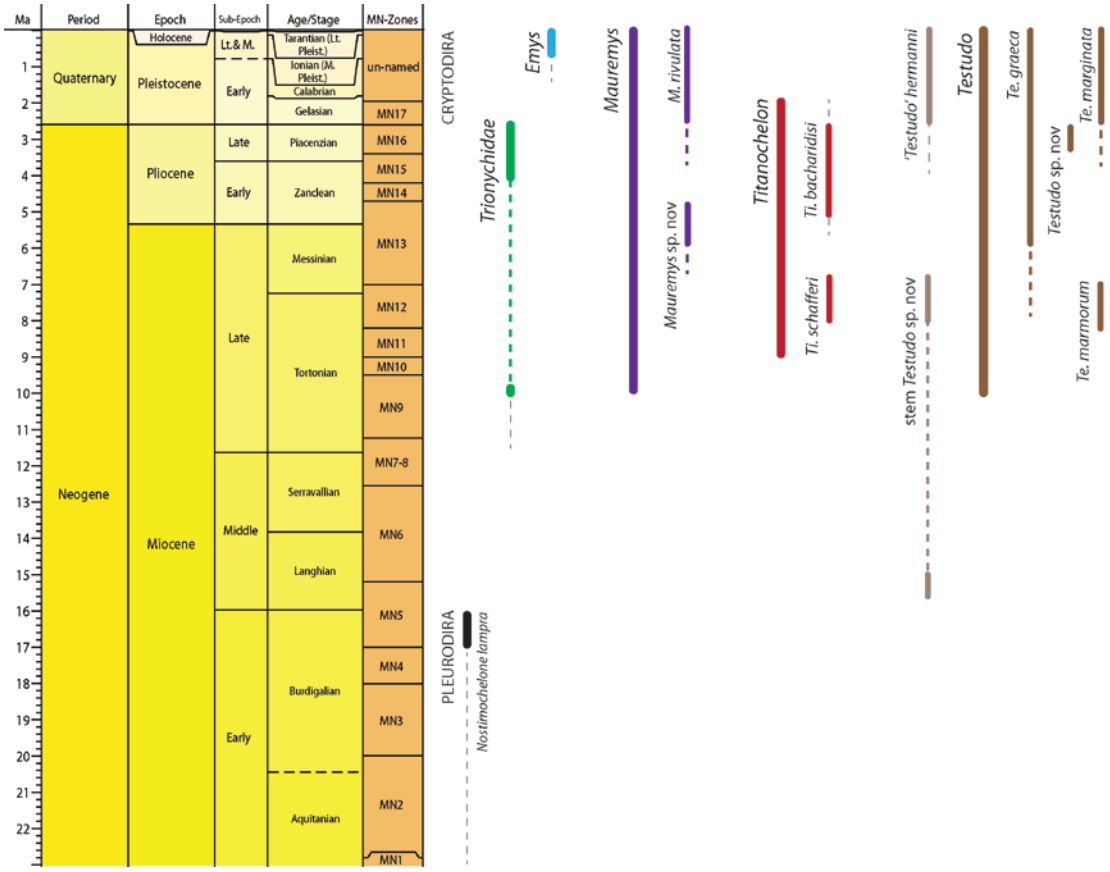


Figure 5.4. The biostratigraphical distribution of the Greek chelonian taxa.

Most probably, the presence of large testudinid fossils indicate a pre-Pleistocene age.

Pliocene: The Pliocene epoch is characterized by the presence of the large testudinid taxon *Titanochelon bacharidisi*. The small testudinid *Testudo graeca* certainly characterizes the entire Pliocene, but it is expanded in the Pleistocene and up to the present.

Late Miocene: The Late Miocene is characterized by the presence of the large testudinid *Titanochelon schafferi* and the small testudinid taxon *Testudo marmorum*.

5.3. Comparison of the Greek chelonian assemblage with adjacent areas

The most relevant comparisons of the Greek fossil chelonian fauna could be done with the paleoherpetofauna from Italy. The Italian fossil record covers a similar timespan as the Greek one, compared to the fossil record of other countries like France and Spain that is greatly expanded to the Paleogene and Mesozoic. Also, the Italian fossil record has been recently revised, mainly by the works of M. Delfino and

F. Chesi and previous efforts of T. Kotsakis. Therefore, it is possible to compare in detail the Greek fossil record with the Italian one.

At family level, the Italian chelonian record is richer than the Greek record. As it is summarized in Chesi (2008; and references therein), the pleurodirans are more diverse with clear members of Bothremydidae and Podocnemididae, whereas in Greece only the enigmatic *Nostimochelone lambra* has been found. However, in the present thesis it is shown that most probably this taxon could be a member of the bothremydid clade.

The Italian cryptodires are also more diverse, in terms of the presence of marine forms of Chelonidae and Dermochelydae. The trionychid specimens are few in Greece, whereas in Italy at least two species are recognized. The emydids are poorly known in both countries, with only few specimens of the European pond turtle. Geoemydids are far more diverse in Italy, with at least 6 different species, compared to the only 2 species reported in Greece.

Table 5.1. Comparisons between the Greek and Italian fossil chelonians (based on Chesi, 2008)

Taxa	Greece	Italy
	PLEURODIRA	
Bothremydidae	*Nostimochelone lampra*	Bothremydidae indet.
Podocnemididae	-	*Neochelys capellinii* *Erymnochelys* sp.
	CRYPTODIRA	
Chelonidae	-	*Trachyaspis lardyi*
Dermochelydae	-	*Psephophorus polygonus*
Emydidae	*Emys orbicularis*	*Emys* cf. *E. orbicularis*
Geoemydidae	*Mauremys rivulata* *Mauremys* sp.1	*Bergouniouxchelys vallisnerii* cf. *Geoemyda* sp. *Mauremys campanii* *Mauremys etrusca* *Mauremys portisii* *Mauremys* sp.
Testudinidae	*'Testudo' hermanni* *Testudo graeca* *Testudo marginata* *Testudo marmorum* *Testudo* sp.1 (Milia) *Testudo* sp.2 (Samos) *Testudo* sp.3 (Axios) *Titanochelon bacharidisi* *Titanochelon schafferi*	*'Testudo' hermanni* *"Testudo" amiatae* *Testudo pecorinii* *"Testudo globosa"* ?*Titanochelon* sp.
Trionychidae	Trionychidae indet.	*Trionyx pliopedemontanus* *Trionyx capellinii*

On the other hand, the Greek testudinids are more diverse than the Italian ones. The hingeless taxa are more frequent in Italy, whereas in contrast, Greece is richer in hinged taxa. In both countries *'Testudo' hermanni* is found, but the Italian fossil record is richer. Another hingeless taxon is known from Italy, *"Testudo" amiatae,* also previously reported from Greece. A revision of the Pylea fauna however, has shown that this taxon is not present in Greece. Finally, the third hingeless taxon from Italy is *"Testudo globosa"*. The only hinged taxon from Italy is *Testudo pecorinii*. In Greece however, several hinged taxa are identified, such as *Testudo graeca, Testudo marmorum* and *Testudo marginata*. Furthermore, the two new taxa reported from Milia and Samos on the basis of carapacial remains (so that

we can identify if they are hinged or not) and the new, but yet unpublished, *Testudo* s.s. from Axios (Garcia et al., 2011), show that the testudinid diversity was even greater during the Neogene.

Besides the Italian chelonian assemblages, the Greek fossil chelonian fauna is the most diverse and rich compared with the adjacent areas in the South Balkans and Asia Minor. This results perhaps correlates with the limited interest in the study of chelonians in these areas:

From Bulgaria, only some remains of a large testudinid from the Pliocene of Tenevo have been reported (Boev, 2008; Stojanov, 2009). These specimens have been attributed to *Titanochelon bacharidisi* by Vlachos et al. (2014). From FYROM, the Eocene geoemydid '*Temnoclemmys' mazedonica* has been mentioned by Pašic & Klinčarski (1954), but needs revision (D. Petrovic, Museum of Natural History of Belgrade, pers. comm.). Also in Serbia, only *Mauremys serbica* has been mentioned as well as other unpublished material of large testudinids and trionychids (D. Petrovic, Museum of Natural History of Belgrade, pers. comm.). In European Turkey, Nicholas (1978) reports some fragmentary specimens of a large testudinid from the Late Miocene of Kucuk-Cekmece. Staesche et al. (2007) describe more specimens from the Miocene of Minor Asia. They report many specimens of large testudinids, which they identify as *Geochelone* cf. *bolivari*, but Pérez-García & Vlachos (2014) show that they do not share morphological similarities with the Spanish taxon. They also show that a possible juvenile specimen of *Geochelone* cf. *bolivari* in Staesche et al. (2007) belongs to a small testudinid taxon. Staesche et al. (2007) further report *Testudo* cf. *graeca*, *Mauremys* cf. *caspica*, *Clemmydopsis* cf. *turnauensis* and *Trionyx triunguis*. Certainly, the material from Turkey needs revision and more specimens need to be described.

Besides the overall diversity of the Greek chelonians, it is important to see how diversity is evolved through time. In order to depict these changes the diversity curve command in PaSt software (Hammer et al., 2001) is used, that analyzes a Presence/Absence matrix (Table 5.2), and produces the diversity curves as in Fig. 5.5.

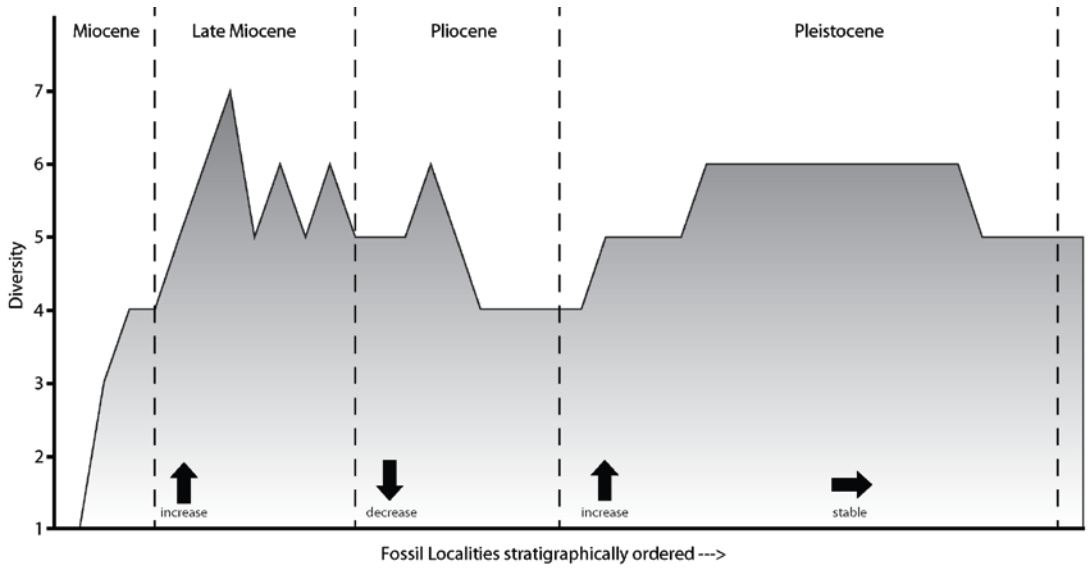


Figure 5.5. Diversity curves of the Greek chelonian taxa diversity through time. Data drawn from Table 5.2. Numbers in the vertical axis indicate number of taxa.

This figure suggests a significant increase in the diversity during Late Miocene, which is probably the highest ever noticed in Greece. Many testudinid (small and large) and aquatic taxa are present during this period. Towards the end of the Pliocene the diversity decreases, mainly in the aquatic taxa. A second increase in the diversity of chelonian taxa is observed in the Pleistocene, where the diversity is almost similar as today, with only a small decrease noticed. In the extant fauna, several marine taxa are living in Greece but they were not included in this analysis due to their absence from the fossil record. These changes could be correlated with several events that are known in the Neogene, such as the cooling in the Plio-Pleistocene times and the Messinian Salinity Crisis. However, due to the absence of absolute datings of the material that could allow a precise placement in time and therefore a robust analysis of the diversity, it would be difficult to further analyze these results.

Table 5.2. Presence/Absence (1/0) data of the Greek fossil chelonians.

	Bothremydidae	Trionychidae	*Emys orbicularis*	*Mauremys rivulata*	*Mauremys* sp. nov	*Mauremys* sp.	*'Testudo' hermanni*	*Testudo graeca*	*Testudo marginata*	*Testudo marmorum*	*Testudo* sp.I	*Testudo* sp.II	*Testudo*.sp.	*Titanochelon bacharidisi*	*Titanochelon schafferi*	*Titanochelon* sp.
Present Taxa	0	0	1	1	0	0	1	1	1	0	0	0	0	0	0	0
Vraona Cave	0	0	1	1	0	0	0	0	0	0	0	0	0	0	0	0
Franchthi_Cave	0	0	1	0	0	0	1	0	0	0	0	0	0	0	0	0
Charkadio Cave	0	0	0	0	0	0	0	0	1	0	0	0	0	0	0	0
Petralona Cave	0	0	0	0	0	0	0	1	0	0	0	0	0	0	0	0
Gerani Cave	0	0	0	0	0	1	0	0	1	0	0	0	0	0	0	0
Zourida Cave	0	0	0	0	0	0	0	0	1	0	0	0	0	0	0	0
Liko Cave	0	0	0	1	0	0	0	0	1	0	0	0	0	0	0	0
Simonelli Cave	0	0	0	0	0	0	0	0	1	0	0	0	0	0	0	0
Koumpes Cave	0	0	0	1	0	0	0	0	1	0	0	0	0	0	0	0
Mavro Mouri IV	0	0	0	1	0	0	0	0	1	0	0	0	0	0	0	0
Sitia	0	0	0	1	0	0	0	0	0	0	0	0	0	0	0	0
Rethymnon	0	0	0	1	0	0	0	0	0	0	0	0	0	0	0	0
Kythera	0	0	0	0	0	0	0	0	1	0	0	0	0	0	0	0
Kos	0	0	0	1	0	0	0	0	1	0	0	0	0	0	0	0
Megalopolis	0	0	1	1	0	0	0	0	0	0	0	0	0	0	0	0
Vatera	0	0	0	0	0	0	0	1	0	0	0	0	0	0	0	1
Xerias	0	0	0	0	0	0	0	0	1	0	0	0	0	0	0	0
Potidea	0	0	0	0	0	0	0	1	0	0	0	0	0	0	0	0
Chalkidiki	0	0	0	0	0	0	1	0	0	0	0	0	0	0	0	0
Lakonia	0	0	0	0	0	0	0	0	1	0	0	0	0	0	0	0
Megalo Emvolon	0	0	0	0	0	0	0	1	0	0	0	0	0	1	0	0
Epanomi	0	0	0	0	0	0	0	0	0	0	0	0	0	1	0	0

Michaniona	0	0	0	0	0	0	0	0	0	0	0	0	0	1	0	0
Kallikratia	0	0	0	0	0	0	0	0	0	0	0	0	0	1	0	0
Gefira	0	1	0	0	0	0	0	0	0	0	0	0	0	0	0	0
Milia	0	0	0	0	0	1	0	0	0	0	1	0	0	0	0	1
Salonique	0	0	0	0	0	0	0	1	0	0	0	0	0	1	0	0
Allatini	0	0	0	0	1	0	0	1	0	0	0	0	0	0	0	0
Pylea	0	0	0	0	0	0	0	1	0	0	0	0	0	0	0	0
Silata	0	0	0	0	1	0	0	0	0	0	0	0	1	0	0	0
Maramena	0	0	0	0	0	0	0	0	0	0	0	0	1	0	0	0
Pikermi	0	0	0	0	0	0	0	0	0	1	0	0	1	0	0	1
Liossati	0	0	0	0	0	0	0	0	0	0	0	0	0	0	0	1
Samos	0	0	0	0	0	0	0	0	0	0	0	1	0	0	1	0
Serres	0	0	0	0	0	0	0	0	0	0	0	0	1	0	0	0
Platania	0	0	0	0	0	0	0	1	0	0	0	0	0	0	0	0
Kryopigi	0	0	0	0	0	0	0	0	0	0	0	0	0	0	0	1
Fourka	0	0	0	0	0	0	0	0	0	0	0	0	0	0	0	1
Plakias	0	1	0	0	0	1	0	0	0	0	0	0	0	0	0	0
Thymiana	0	0	0	0	0	0	0	0	0	0	0	1	0	0	0	0
Nostimo	1	0	0	0	0	0	0	0	0	0	0	0	0	0	0	0

This page has been left intentionally blank

Chapter 6. Palaeoecology

Highlights

Histology of trionychid
Histology of large testudinid
Contribution of fossil chelonians to paleoecology

02/16/2016 Ψηφιακή Βιβλιοθήκη Θεόφραστος - Τμήμα Γεωλογίας - Α.Π.Θ.

6.1. Introduction

One of the paleoecological approaches performed in this thesis is the study of histological thin sections of fossil and extant specimens from Greece. In total two fossil taxa, the trionychid from the Late Pliocene of Gefira, N. Greece and the large testudinid *Titanochelon bacharidisi* from the Pliocene of Nea Michaniona, N. Greece, have been analyzed. The histological work has been done in co-operation with I. Cerda (CONICET, Cipoletti, Río Negro, Argentina) and the work presented in this chapter is part of two papers that are in preparation (Vlachos, Cerda & Tsoukala, in prep.). The sampled sections have been analyzed with Scanning Electron Microscopy (SEM) by Dr. L. Pappadopoulou (School of Geology, AUTH) and that it will be further analyzed by MSc M. Zougrou (Department of Physics, AUTH). Although the results are included in the Appendix, only results that are relevant with the structure of the shell of the sampled taxa are discussed here.

A novel approach on the study of paleoecology of chelonians has been made by the doctoral thesis of Scheyer (2007) and several papers that followed it (Scheyer et al., 2007; Scheyer et al., 2012; Delfino et al., 2013), where the histology could be used to infer the paleoecology of extinct turtles. Table 6.1 summarizes the results of Scheyer (2007), showing the four different ecological categories.

Table 6.1. Ecological categories of turtles, based on their bone histology (based on Scheyer, 2007).

Ecological Categories	Histology		
	External Cortex	Cancellous Bone	Internal Cortex
Terrestrial [massive appearance under microscope]	well developed; thick, weakly vascularised cortices	primary short and thick bone trabeculae; small vascular spaces	well developed; thick, weakly vascularised cortices
Semiaquatic to mainly aquatic [compact appearance]	Increased Vascularization; Vascular canals; Primary Osteons	conspicuous transition with the cortices	Increased Vascularization; Vascular canals; Primary Osteons
Fully aquatic [reduction of compact bone layers]	Seldom reduced; strong vascularization	High degree of organization of trabeculae	Strongly reduced to Almost completely reduced
Extreme adaptation to aquatic/marine environment [homogeneous spongy appearance]	Reduction in thickness of the cortices; Strong vascularisation; Loss of compact nature of the cortices; **No possible distinction of the bone tissue in cortical bone and cancellous bone in many cases**		

6.2. The histology of the Gefira trionychid

The soft-shelled turtles are characterized by the presence of the plywood structure in the external cortex of their carapace plates, which probably adds strength to the shell structure (see Scheyer, 2007). For the Gefira trionychid we sampled all but one plate (LGPUT GAS 8e), which was eroded. All the sampled plates showed evidence of the plywood structure on the external cortex, but the best preservation was found on the costal 3 (LGPUT GAS 8c) (Fig. 6.1).

Up to the present, fossil trionychids have been unknown from Greece, which was one of the main differences between the Greek and Turkish fossil assemblages (Lapparent de Broin, 2002). This family is also absent in the genuine extant chelonian fauna of Greece, with the only reported members found in the waters near Kos (Taskavak et al., 1999) and other Aegean Islands such as Rhodes, Kalymnos, Leros and Kos (Dimaki, 2002), originating most probably from the Turkish populations. These individuals are usually accidentally caught in fishing nets by local fishers. In Turkey, extant trionychids are represented by two species, *Trionyx triunguis* (Forsskål, 1775) and *Rafetus euphraticus* Dauden, 1802 (from Taskavak and Akcinar, 2009).



Figure 6.1. The costal 3 of the Gefira trionychid, showing the external (ECO) and the internal (ICO) cortex, surrounding the cancellous bone (CB). The cross-section of the rib is also observed. Scale bar equals 10 mm.

These, mainly carnivorous, turtles are known for their ability to cover large distances inland; floods and overflows can sweep away the turtles to the ocean and by tolerating salty water they can insert into another river system (Taskavak and Akcinar, 2009 and references therein). Soft–shelled turtles usually prefer rivers and lakes with sandy bottoms, that are very important for their hatchlings (Plummer et al., 2008). Gefira deposits are characterized by large quantities of sands, while the presence of *Anancus arvernensis* reveals the presence of significant bodies of water and large quantities of plants during the Pliocene in the area. This paleoenvironment is consistent with an ecosystem in that trionychids are normally adapted. Moreover, the fact that these findings are reported from the mainland of Greece allows us to assume that the presence of a Trionychidae in the Pliocene is not random, like in present–day fauna (trionychids are distributed in Minor Asia, but they could be found in the Aegean randomly), but an original member of the Greek fossil chelonian fauna.

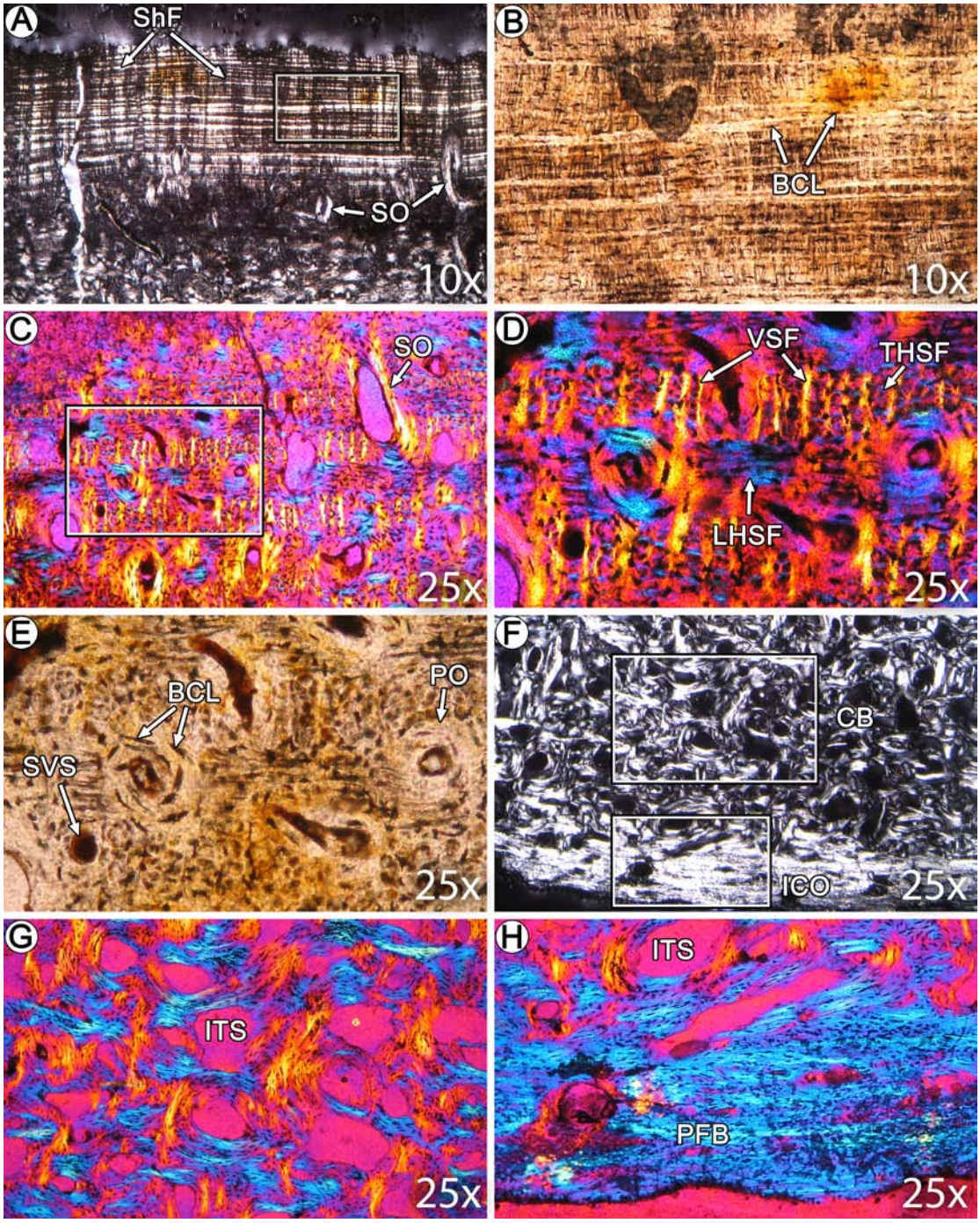


Figure 6.2. Bone shell histology of Trionychidae from Gefira locality, Pliocene, N. Greece. A, outer region of the external cortex composed of lamellar bone tissue in LGPUT GAS 8c. Note the abundance of Sharpey's fibers oriented perpendicularly to the surface. Cross-polarized light. B, detailed view of the same specimen (box inset in A). Normal transmitted light. C, general view of the inner portion of the external cortex LGPUT GAS 8b. Structural fibers are organized forming a plywood arrangement. Cross-polarized light with lambda compensator. D, E, detailed view of the same specimen (box inset in C) viewed under cross-polarized light with lambda compensator (D) and normal transmitted light (E). F, general view of the transition between the cancellous bone and the internal cortex in LGPUT GAS 8b. Cross polarized light. G, detailed view of the cancellous bone (large box inset in F). Cross-polarized light with lambda compensator. H, detailed view of the internal cortex (small box inset in F), which is entirely composed of parallel fibred bone. Cross-polarized light with lambda compensator. Abbreviations: BCL: bone cell lacunae; CB: cancellous bone; ICO: internal cortex; ITS: inter-trabecular spaces; LHSF: horizontally oriented structural fibers

longitudinally sectioned; PFB: parallel fibered bone; PO: primary osteons; ShF: Sharpey's fibers; SO: secondary osteons; SVS: simple vascular space; THSF: horizontally oriented structural fibers transversally sectioned; VSF: vertically oriented structural fibers. [This figure is made by Dr. I. Cerda for the publication that is in prep.]

All plates exhibit a diploe structure, in which two cortices (external and internal) frame an internal core of cancellous bone. The external cortex (ECO) is composed by two distinct zones (outer and inner). The outer zone cortical bone is composed of avascular lamellar bone tissue, in which each lamella follows the external surface outline (Fig. 6.2A). Bone cell lacunae are flattened or circular in section. Sharpey's fibres are present throughout the whole outer zone (Fig. 6.2.B). These extrinsic fibres are long and they insert perpendicularly to the outer surface. In LGPUT GAS 8a, long Sharpey's fibres are also present in the (anterior) margin. Primary vascular spaces are absent. Few secondary osteons are scattered in some regions of the outer cortex. The inner zone is composed by intercrossed structural fibre bundles (SFB sensu Scheyer and Sander, 2004). While in some areas (e.g. in the boundary with the outer zone) these fibres exhibit a disorganized arrangement, in others they show the typical "plywood" organization described previously for trionychid taxa (Scheyer, 2007; Scheyer et al., 2007; Scheyer et al., 2012; Delfino et al., 2013). This plywood pattern consists in three orthogonal systems of fibre bundles; one vertical and two horizontal (Fig. 6.2.C-E). Horizontal systems are organized in successive layers. In each layer, fibre bundles are mutually parallel, but the direction changes from one layer to the next, forming angles of 90 degrees. These layers are crossed perpendicularly by a vertical system of fibre bundles. Transversally sectioned horizontal systems possess a quadrangular shape. Bone cell lacunae show a prolate ellipsoid shape and they are oriented following the arrangement of the fibres in which they are imbedded. The inner zone is vascularised by simple vascular canals and primary and secondary osteons. The transition between the external cortex and the cancellous bone is not clearly defined because of the amount of scattered secondary osteons and erosion cavities.

The cancellous bone consists of short and thick trabeculae and relatively small intertrabecular spaces (Fig. 6.2.F). Some of these small spaces coalesce to form larger spaces of irregular shape. In the LGPUT GAS 8b, a large subcircular space is present within the cancellous tissue. Some variation with regard to the degree of development of the cancellous bone is observed. In LGPUT GAS 8c the internal spaces of the "cancellous" bone are relatively smaller and less abundant compared with the other plates and the entire plate exhibits a rather compact structure. Bony trabecuale are exclusively composed of secondary lamellar bone tissue formed during different generation of continuous resorption and deposition (Fig. 6.2.G).

The internal cortex (ICO) is relatively thin and consists of avascular parallel fibred bone (Fig. 6.2.H). The ICO contains at least ten lines of arrested growth (LAGs), which are more clearly observed using a high contrast in the normal light incidence. The morphology of the preserved carapace fragments of the Gefira individual allows attribution to a single individual of Trionychidae, based on the absence of scute sulci, loss of peripherals and the sculpturing on the outer shell surface. Given the scarcity of the material further identification is not possible beyond the family level. Gardner and Russel (1994), showed that the several carapacial features are quite variable and therefore cannot be of high diagnostic value. Especially the sculpturing is only diagnostic up to family level. The other line of evidence for the

attribution of the Gefira individual to the Trionychidae family comes from the bone shell histology. In this sense, the “plywood” arrangement of the structural fibers in the inner portion of the external cortex is considered an exclusive histological character of this group (Scheyer et al., 2007; Delfino et al., 2013).

The histological data obtained from the Gefira trionychid are not only valuable for the systematic assignment of the material, but also allows the discussion of other issues, including inter-elemental and inter-specific variation of the shell histology. Regarding the degree of histological inter-elemental variation within the shell, previous studies (Scheyer et al., 2007; Delfino et al., 2010) showed that, with the exception of the prenuchal bones of *Cyclanorbis senegalensis*, which possess SFB in both external and internal cortices, the main histological features in the plates are invariable. The most distinctive histological variation in our sample was recorded in the anterior margin of the nuchal plate (LGPUT GAS 8a), which possesses abundant and long Sharpey’s fibers. These extrinsic fibers are continuous with those observed in the outer portion and they are possibly related with the anchoring between the shell and the epidermis.

Histological descriptions of trionychid bone shell elements has been provided by previous studies (Scheyer et al., 2007; Delfino et al., 2010; Hirasawa et al., 2013; Lyson et al., 2013), which allow a comparison with the Gefira sample. Since no histological descriptions of trionychid nuchal plates exist to our knowledge, we restrict the comparison only to the costal bones. The main histological variations appear to be related with the relative thickness of the internal cortex and the plywood layer of structural fibers. Whereas in the Gefira bones the internal cortex occupies around the 5% of the thickness of the plates, this value is notably increased (around 25%) in other taxa in other taxa (e.g. cf. *Aspideretoides* sp.). Regarding the relative proportion of the plywood layer, this is comparatively lower (10%) in the Gefira trionychid compared with other taxa (25% in cf. *Aspideretoides* sp.). These variations could be related to different, non-mutually exclusive causes, including biomechanical and ontogenetic factors.

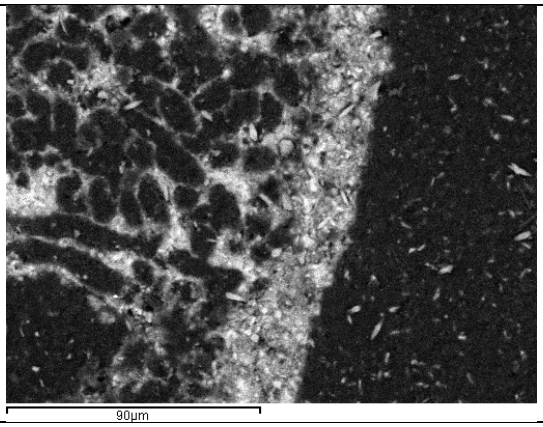
The thin sections have been analyzed through Scanning Electron Microscopy (SEM). Although the analysis of the SEM results is part of another study by M. Zougrou, Table 2 shows that the composition of the external cortex is similar with the part of the costal with the “plywood” structure. Therefore, we cannot observe any significant changes between the compositions of these two areas and the only differences lie in the structure of the fibers. On the other hand, the material filling the osteon is significantly different from the surroundings. The entire results of the SEM analysis are given in the Appendix.

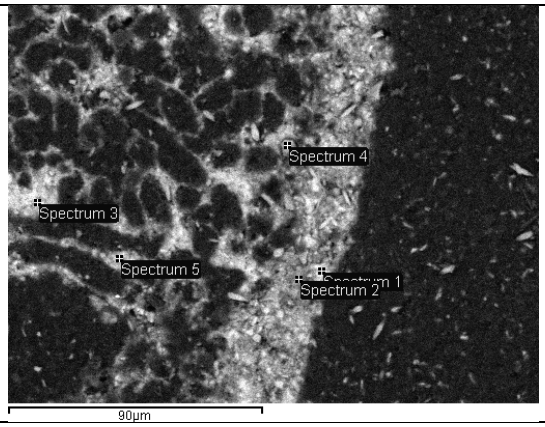
The morphology observed on the thin sections of the trionychid of Gefira concur with the results of Scheyer (2007). They show the typical features of the ecological category II (semi-aquatic to aquatic) but the cortices are quite compact showing tendencies towards category I. As Scheyer (2007) suggests, this could reflect changes to increase the shell stability of these peculiar turtles.

02/16/2016 Ψηφιακή Βιβλιοθήκη Θεόφραστος - Τμήμα Γεωλογίας - Α.Π.Θ.

Table 6.2. SEM analysis of the trionychid section LGPUT GAS 8b

External Cortex





1

Element	Line	App. Conc	k ratio	Intensity corrn.			Weight%	Weight% sigma	Atomic%	Compound%	Formula	Number of ions	Standard
P	K_SERIES	13.55	0.08023	1.3290	18.83	0.66	14.63	43.14	P2O5	7.68	GaP	1-Jun-1999 12:00 AM	
Ca	K_SERIES	22.04	0.19799	1.0016	40.64	0.77	24.40	56.86	CaO	12.81	Wollastonite	1-Jun-1999 12:00 AM	
O				40.53	0.79	60.97			32.00				
Totals				100.00									
									Cation sum	20.48			

2

Element	Line	App. Conc	k ratio	Intensity corrn.			Weight%	Weight% sigma	Atomic%	Compound%	Formula	Number of ions	Standard
Si	K_SERIES	0.56	0.0045	0.8883	1.99	0.35	1.73	4.25	SiO2	0.93	SiO2	1-Jun-1999 12:00 AM	
P	K_SERIES	4.68	0.0277	1.2984	11.41	0.75	9.00	26.13	P2O5	4.84	GaP	1-Jun-1999 12:00 AM	
S	K_SERIES	1.06	0.00928	0.8726	3.83	0.50	2.92	9.57	SO3	1.57	FeS2	1-Jun-1999 12:00 AM	
K	K_SERIES	2.19	0.01794	1.1008	6.29	0.58	3.93	7.57	K2O	2.11	MAD-10 Feldspar	1-Jun-1999 12:00 AM	
Ca	K_SERIES	11.51	0.10335	0.9716	37.50	1.05	22.87	52.47	CaO	12.29	Wollastonite	1-Jun-1999 12:00 AM	
O				38.99	1.11	59.55			32.00				
Totals				100.00									
									Cation sum	21.73			

3

Element	Line	App. Conc	k ratio	Intensity corrn.			Weight%	Weight% sigma	Atomic%	Compound%	Formula	Number of ions	Standard
P	K_SERIES	12.10	0.07164	1.3275	17.96	0.68	14.05	41.16	P2O5	7.43	GaP	1-Jun-1999 12:00 AM	
Ca	K_SERIES	21.44	0.19259	1.0050	42.05	0.80	25.41	58.84	CaO	13.43	Wollastonite	1-Jun-1999 12:00 AM	
O				39.98	0.82	60.54			32.00				
Totals				100.00									
									Cation sum	20.86			

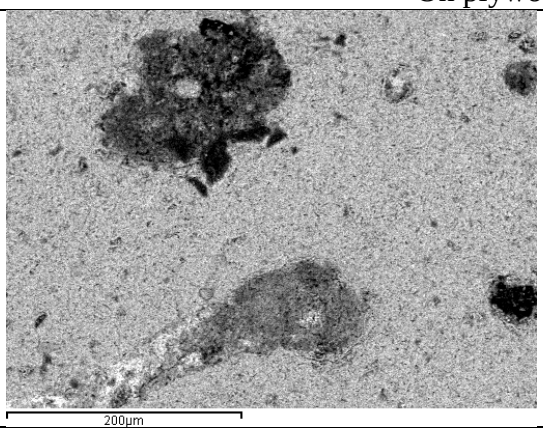
4

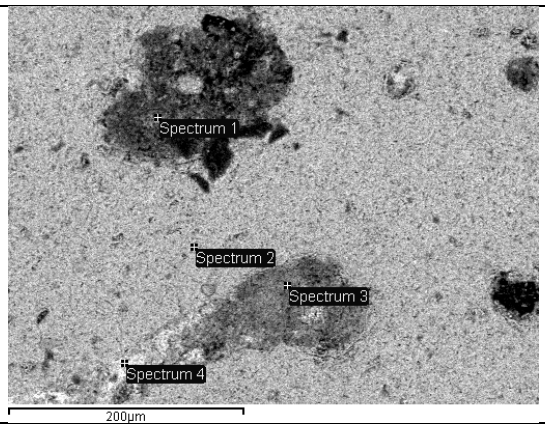
Element	Line	App. Conc	k ratio	Intensity corrn.			Weight%	Weight% sigma	Atomic%	Compound%	Formula	Number of ions	Standard
Si	K_SERIES	45.15	0.36412	0.9552	44.89	0.52	32.18	96.03	SiO2	15.47	SiO2	1-Jun-1999 12:00 AM	
P	K_SERIES	0.82	0.00487	0.7990	0.98	0.23	0.64	2.24	P2O5	0.31	GaP	1-Jun-1999 12:00 AM	
Ca	K_SERIES	1.19	0.01066	0.9121	1.24	0.16	0.62	1.73	CaO	0.30	Wollastonite	1-Jun-1999 12:00 AM	
O				52.90	0.52	66.57			32.00				
Totals				100.00									
									Cation sum	16.07			

5

Element	Line	App. Conc	k ratio	Intensity corrn.			Weight%	Weight% sigma	Atomic%	Compound%	Formula	Number of ions	Standard
P	K_SERIES	12.25	0.07256	1.3284	18.47	0.69	14.39	42.32	P2O5	7.57	GaP	1-Jun-1999 12:00 AM	
Ca	K_SERIES	20.65	0.18545	1.0030	41.22	0.81	24.82	57.68	CaO	13.06	Wollastonite	1-Jun-1999 12:00 AM	
O				40.31	0.83	60.79			32.00				
Totals				100.00									
									Cation sum	20.64			

On plywood structure





1

Element	Line	App. Conc	k ratio	Intensity	corrn.		Weight%	Weight% sigma		Atomic%	Compound%	Formula	Number of ions	Standard
Mg	K_SERIES	0.34	0.00231	0.4764	2.14	0.64	2.54	3.55	MgO	1.45	MgO	1-Jun-1999 12:00 AM		
Al	K_SERIES	0.53	0.0039	0.5811	2.76	0.59	2.95	5.21	Al2O3	1.68	Al2O3	1-Jun-1999 12:00 AM		
Si	K_SERIES	2.55	0.02057	0.6847	11.27	0.82	11.58	24.10	SiO2	6.60	SiO2	1-Jun-1999 12:00 AM		
K	K_SERIES	0.80	0.00653	1.0850	2.22	0.40	1.64	2.67	K2O	0.93	MAD-10 Feldspar	1-Jun-1999 12:00 AM		
Ca	K_SERIES	0.95	0.00855	1.0491	2.75	0.47	1.98	3.84	CaO	1.13	Wollastonite	1-Jun-1999 12:00 AM		
Mn	K_SERIES	9.28	0.09278	0.8758	32.05	1.37	16.83	41.38	MnO	9.60	Mn	1-Jun-1999 12:00 AM		
Fe	K_SERIES	2.97	0.02968	0.8964	10.01	1.05	5.17	12.88	FeO	2.95	Fe	1-Jun-1999 12:00 AM		
Ba	L_SERIES	1.68	0.0157	0.8942	5.69	1.11	1.20	6.35	BaO	0.68	BaF2	1-Jun-1999 12:00 AM		
O				31.11	1.41	56.12				32.00				
Totals				100.00										
									Cation sum	25.02				

2

Element	Line	App. Conc	k ratio	Intensity	corrn.		Weight%	Weight% sigma		Atomic%	Compound%	Formula	Number of ions	Standard
P	K_SERIES	12.64	0.07485	1.3266	17.41	0.63	13.67	39.90	P2O5	7.26	GaP	1-Jun-1999 12:00 AM		
Ca	K_SERIES	23.68	0.21268	1.0072	42.96	0.76	26.07	60.10	CaO	13.85	Wollastonite	1-Jun-1999 12:00 AM		
O				39.63	0.77	60.26				32.00				
Totals				100.00										
									Cation sum	21.11				

3

Element	Line	App. Conc	k ratio	Intensity	corrn.		Weight%	Weight% sigma		Atomic%	Compound%	Formula	Number of ions	Standard
Al	K_SERIES	0.42	0.00311	0.5286	3.49	0.82	3.96	6.59	Al2O3	2.32	Al2O3	1-Jun-1999 12:00 AM		
Si	K_SERIES	0.96	0.00771	0.6324	6.60	0.88	7.21	14.12	SiO2	4.22	SiO2	1-Jun-1999 12:00 AM		
Ca	K_SERIES	0.56	0.00501	1.0691	2.28	0.54	1.74	3.19	CaO	1.02	Wollastonite	1-Jun-1999 12:00 AM		
Fe	K_SERIES	12.43	0.12425	0.9169	59.16	1.69	32.49	76.10	FeO	19.04	Fe	1-Jun-1999 12:00 AM		
O				28.48	1.55	54.60				32.00				
Totals				100.00										
									Cation sum	26.61				

4

Element	Line	App. Conc	k ratio	Intensity	corrn.		Weight%	Weight% sigma		Atomic%	Compound%	Formula	Number of ions	Standard
Mg	K_SERIES	0.21	0.00146	0.4051	1.65	0.53	2.23	2.74	MgO	1.36	MgO	1-Jun-1999 12:00 AM		
Si	K_SERIES	0.56	0.00454	0.6535	2.71	0.53	3.17	5.80	SiO2	1.94	SiO2	1-Jun-1999 12:00 AM		
Ca	K_SERIES	0.77	0.00688	1.1210	2.15	0.44	1.76	3.01	CaO	1.08	Wollastonite	1-Jun-1999 12:00 AM		
Ti	K_SERIES	0.66	0.00659	1.0007	2.08	0.55	1.42	3.46	TiO2	0.87	Ti	1-Jun-1999 12:00 AM		
Mn	K_SERIES	12.06	0.12057	0.9154	41.49	1.47	24.78	53.57	MnO	15.16	Mn	1-Jun-1999 12:00 AM		
Fe	K_SERIES	7.26	0.0726	0.9361	24.43	1.35	14.35	31.42	FeO	8.78	Fe	1-Jun-1999 12:00 AM		
O				25.50	1.35	52.29				32.00				
Totals				100.00										
									Cation sum	29.19				

6.3. The histology of the large testudinid, *Titanochelon bacharidisi*

From the large tortoise from Chalkidiki (*Titanochelon bacharidisi*) we sampled a costal plate (LGPUT MIC 308) from the Pliocene site of Nea Michaniona (6.3). The purpose of the sampling is to investigate the histological structure of this large tortoise. The SEM results are given in Appendix.

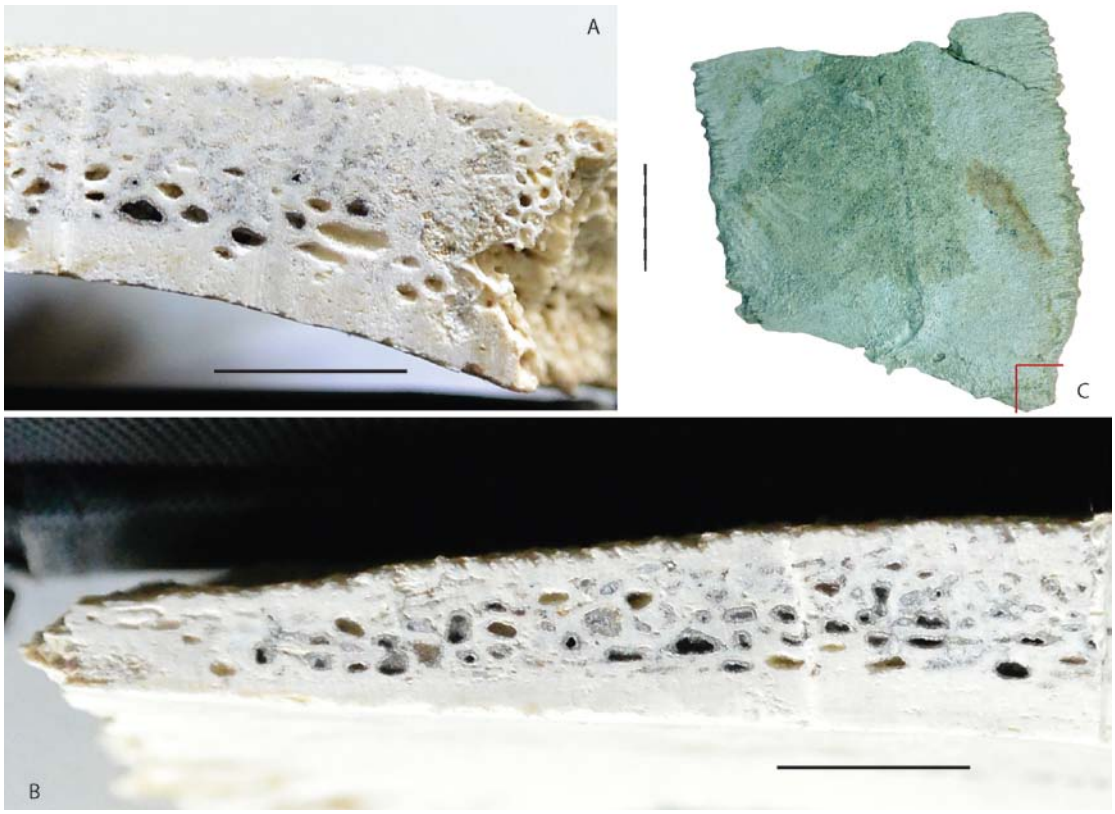


Figure 6.3. Photographs of the sampled sections of the costal plate of *Ti. bacharidisi* from Nea Michaniona (LGPUT MIC 308). A, transversal and B, longitudinal views. Scale bar equals 1 cm. C, The costal plate showing the sampled positions (Scale bar equals 10 cm).

All sampled shell bones show a diploe structure with external cortex (ECO) and internal cortex (ICO) framing an interior area of cancellous bone (CB). A particular alteration of the tissues impedes to study the sections under polarized light. Nevertheless, the bone tissues are well observed under normal light and the nature of the primary bone can be discerned by features as the density, shape and arrangement of the bone cell lacunae. The external cortex consists of parallel fibered bone tissue. A stratified pattern is clearly observed in the compacta, with several bright lines closely spaced, which appear to correspond with lines of arrested growth. These lines are not straight, but they exhibit gentle and irregular undulated shape. These extrinsic fibres are oriented perpendicularly to the external surface. In the cancellous bone, the bone trabeculae are secondarily remodelled. Longitudinally oriented vascular spaces, organized as primary osteons, are scattered in the cortex. Secondary (Haversian) osteons are also present. The external surface is slightly rough, with primary osteons and canals opening up as small foramina. Sharpey's fibres are abundant and densely distributed throughout the whole of the external cortex. Scattered secondary osteons are present at the transition where the external cortex grades into the cancellous bone.

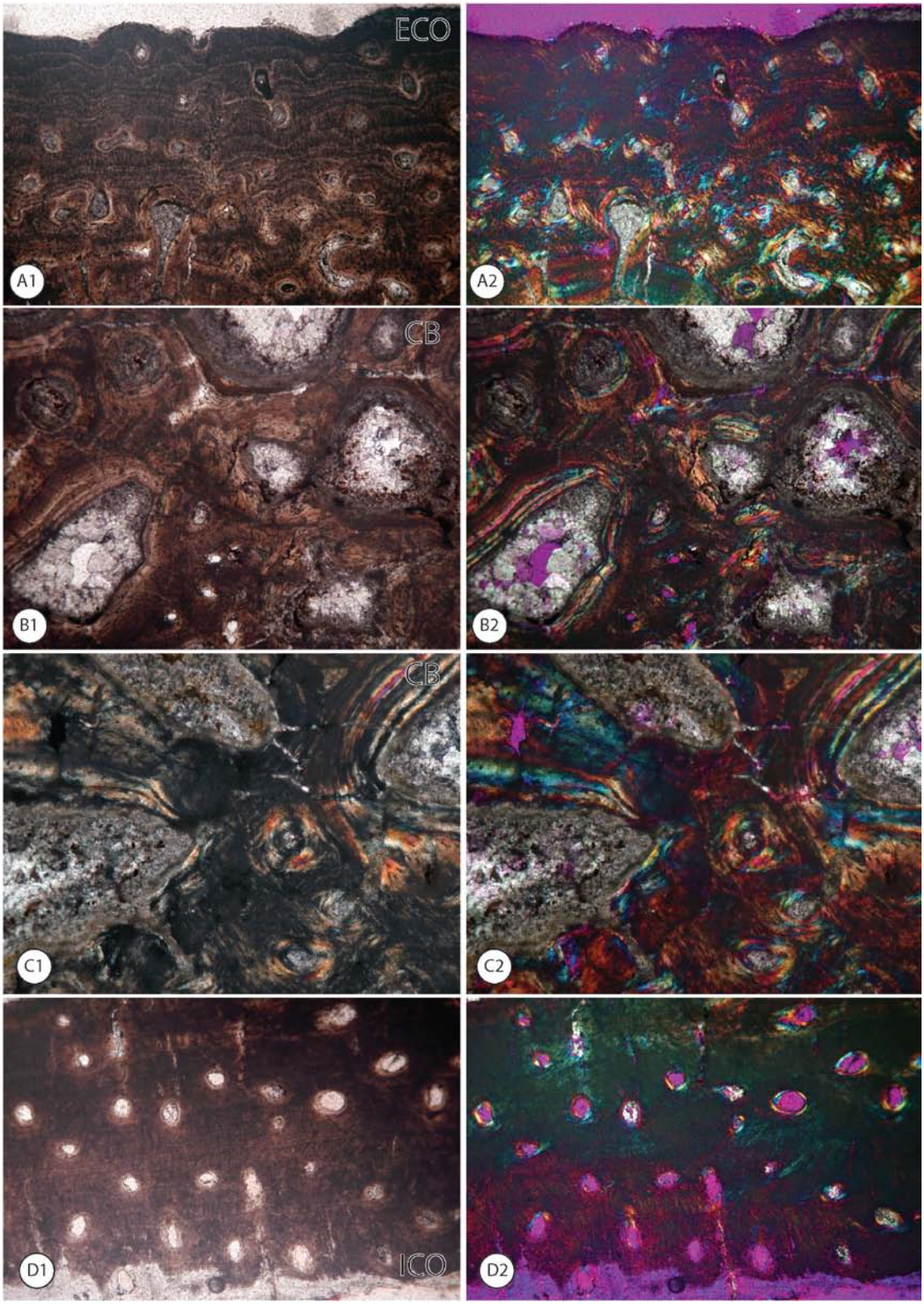


Figure 6.4. Bone shell histology of *Titanochelon bacharidisi* from Nea Michaniona locality, Pliocene, N. Greece. LGPUT MIC 308, A, outer region of the external cortex in (A1) normal transmitted light and (A2) cross-polarized light with lambda compensator. B, cancellous bone in (B1) normal transmitted light and (B2) cross-polarized light with lambda compensator. C, detailed view of the cancellous bone showing the osteons in (C1) normal transmitted light and (C2) cross-polarized light with lambda compensator. D, internal cortex in (D1) normal transmitted light and (D2) cross-polarized light with lambda compensator. Abbreviations: CB: cancellous bone; ECO: external cortex; ICO: internal cortex.

The interior cancellous bone consists of secondarily formed bone trabeculae and cavities of variable size. The bone trabeculae are lined with secondary lamellar bone towards the bone cavities. Flattened and elongated bone cell lacunae follow the centripetally deposited lamellar bone linings. Intertrabecular spaces possess sub-rounded and irregular shapes. The internal cortex is entirely formed by parallel fibred bone. Two different zones (inner and outer) can be discerned in one of the sections. In the inner zone (located toward the cancellous bone), bone cell lacunae exhibit a strongly flattened appearance. Conversely, in the outer zone, these lacunae are rounded in shape. Although an important variation in the extinction pattern between both zones cannot be observed under polarized light (possibly due to diagenetic alteration), the variation in the bone cell lacunae appears to be related with the intrinsic fibre orientation. In the other section, a clear dark and light banding pattern is observed under polarized light, but the variation in the bone cell lacunae shape is not so strong. Based on this pattern, we interpret that the bone corresponds with a lamellar tissue, in which the intrinsic fibres change their orientation in each successive lamella and they possess discoidal bone cell lacunae. Vascularization is low and mostly consists of small primary osteons longitudinally oriented. The vascular spaces are commonly distributed forming laminae. Sharpey's fibres are visible as fibres or fibre bundles that extend perpendicular or in angles into the parallel fibred bone matrix. Several growth marks are formed in the compacta.

The histology of the sections of *Ti. bacharidisi* resembles the condition of the category I (sensu Scheyer, 2007), being terrestrial, with a tendency towards the testudinoid type II, with growth marks in the compacta and increased vascularization.

6.4. Concluding remarks

The histological sections presented here are the first attempts to analyse the histology of extinct Greek chelonians. The results clearly show that histology of even small fragments can provide important information that allows inferring the paleoecology of extinct turtles. The use of turtles and tortoises to infer the ecological features of past ecosystems has been limited. Mostly, the identification of mammalian taxa and their comparison with their extant representatives allows inference of the past ecology. Also, the use of micro- and mesowear analysis on mammalian herbivore teeth allows in-depth knowledge of the vegetation of past ecosystems. Therefore is common to use the mammalian fossil taxa to understand how the past environment looked like. The use of turtles for such studies has been limited so far, but they could potentially be of use for the following reasons: turtles and tortoises show an extensive fossil record that spans in nearly every environment such as terrestrial ecosystems, river systems, pond and lakes, littoral, estuarine and of course truly marine habitats. Moreover, the morphology of the shell of these groups is quite distinct and in many cases even small fragments could be identified at the family or genus level. Finally, turtles and tortoises are sensitive to climate changes in temperature and precipitation.

This page has been left intentionally blank

Chapter 7. Conclusions

CONCLUSIONS

The studied fossil fauna of the chelonians of Greece is the most important paleochelonofauna in the South Balkans. This topic has received little attention up to now both in paleontological and archaeological sites, but its detailed study produced important new results on the systematics and evolution of this group and its contribution to the biostratigraphy and paleoecology of Greece. The present thesis deals with the study of more than 1200 chelonian specimens of Greece that belong to several clades (Fig. 7.1), mainly focusing on the detailed description of the available specimens including many new fossils and nearly all the previously published ones (some remains were not traced or were not available for revision). Also, these taxa were placed into a phylogenetic context, and some hypotheses were generated on the distribution, while the role of chelonians in biostratigraphy and paleoecology is investigated.

The conclusions on each objective listed in the introduction are provided below. Furthermore, additional conclusions that emerged over the course of the present thesis are given. In the end, areas that future research should be focused on are highlighted.

Conclusions on the Objectives

Objective 1: Paleontological study and description of new specimens of turtles and tortoises.

Conclusions: As "new specimens" we consider: a) specimens emerged from recent excavations on new localities; b) unknown specimens housed in various museums are recognized and described for the first time, marking the presence of turtles and tortoises in localities with fossil mammalian remains, c) specimens that derived from localities with previously described chelonian fossils and d) specimens that have only been listed in published papers. In this sense, the present thesis provides valuable information on the following new specimens:

a) Material emerged from recent excavations on new localities: new material of *Testudo* cf. *graeca* from the new Late Miocene locality of Platania, Drama; new material of *Titanochelon* sp. from the Late Miocene localities of Kryopigi and Fourka, Kassandra Peninsula, Chalkidiki. From the Pliocene is reported, new material of *Ti. bacharidisi* from the Pliocene of Epanomi, Nea Michaniona and Nea Kallikratia; new material of *Testudo* sp. nov., *Mauremys* sp. and *Titanochelon* sp. from the Late Pliocene locality of Milia, Greece; new material of Trionychidae from the new Pliocene locality of Gefira, lower Axios Valley, N. Greece. From the Pleistocene times is reported, new material of *Testudo* cf. *marginata* from the Pleistocene of Xerias, Kavala.

b) Previously unidentified specimens housed in various museums are recognized and described for the first time: from the Miocene times is reported, new material of *Mauremys* sp. and Trionychidae from the MN7/8 of Plakias, southern Crete; new material of *Testudo* sp. from the Miocene of Serres basin. From the Pleistocene is reported, new material of *Te. marginata* from Boetia and Kythera; new material of *Testudo* sp. and *Mauremys* sp. from Kos Island; new material of '*Testudo*' *hermanni* from Potidea.

02/16/2016 Ψηφιακή Βιβλιοθήκη Θεόφραστος - Τμήμα Γεωλογίας - Α.Π.Θ.

c) Specimens that derived from localities with previously described chelonian fossils: new material of *Ti. schafferi* from the Late Miocene of Samos; New material of *Testudo* sp. nov. from the Late Miocene of Samos; new material of *Titanochelon* sp. and *Testudo* sp. from the Late Miocene of Pikermi; new material *Testudo graeca* from the Pliocene of Aggelochori/Megalo Emvolon; new material of *Mauremys* sp. nov. from the Latest Miocene/Earliest Pliocene of Allatini; new material of *Te. marginata* from Charkadio cave, Tilos Island.

d) Specimens that have only been listed in published papers: material of *Testudo* sp. from the Mio-Pliocene boundary of Maramena, Serres; material of *Testudo* sp. and *Mauremys* sp. nov. from the Mio-Pliocene boundary of Nea Silata, Thessaloniki; material of *Mauremys rivulata* and *Te. marginata* from the Pleistocene of Gerani, Zourida, Koumpes, Liko, Mavro Mouri IV, Simonelli caves and Sitia in Crete; material of *Te. graeca* from the Pleistocene of Petralona Cave, Chalkidiki; material of *Testudo* cf. *hermanni* and *Emys orbicularis* from the Pleistocene/Holocene of Franchthi Cave, Peloponnesus.

This new material has provided further information on the geographic and temporal distribution of Greek chelonians as well as their taxonomic diversity.

Objective 2: Discovery of new taxa of turtles and tortoises from Greece.

Conclusions: The detailed description of new specimens and the revision of previously published material allow the distinction of at least three new species of turtles and tortoises. These new taxa are currently on the process of publication, but they can be briefly summarized as follows:

- The new small testudinid material from the Late Pliocene of Milia (Grevena) is identified here as a new species of *Testudo*, due to the presence of a posteriorly flared carapacial margin without an elongated posterior carapace. The preliminary phylogenetic analysis presented here, places this taxon in the clade *Testudo*, and one synapomorphy unites this taxon with *Te. marginata*.

- The new small testudinid material from the Late Miocene of Samos Island, could belong to a new species of '*Testudo'*, based on the morphology of the posterior costal plates and the morphology of the scutes of the plastron. The preliminary phylogenetic analysis presented here places this taxon in the stem of the clade *Testudo*.

- The new geoemydid material from the Mio-Pliocene boundary of Nea Silata and Allatini, is identified here as a new species of *Mauremys*, based, amongst other features, on the wide and short pleural scutes. The preliminary phylogenetic analysis presented here places this taxon within the clade *Mauremys*.

Objective 3: Revision of previously published specimens from Greece.

Conclusions: Nearly all previously published specimens from Greece have been revised based on new direct observations, and detailed descriptions, and updated

figuration is provided. In detail, the revision of the previously published specimens allows the following conclusions:

- The lost testudinid material from the Middle Miocene of Chios has been analyzed based on the published photographs and is found similar with the material of the new species of '*Testudo'* from the Late Miocene of Samos.

- The material of the large testudinid from the Late Miocene of Liossati (Kiourka) is here identified as *Titanochelon* sp. The preservation status of this individual is poor and is not possible to draw further conclusions.

- The material of the large testudinid from the Late Miocene of Pikermi, previously identified as cf. *Cheirogaster* cf. *schafferi*, is revised in the light of new, previously not described, specimens as *Titanochelon* sp. This taxon is most probably different from the Late Miocene *Titanochelon schafferi* from Samos Island.

- The status of the Late Miocene *Te. marmorum* from the Late Miocene of Pikermi is re-affirmed and new detailed descriptions are given. Some specimens however, attributed by Bachmayer & Symeonidis (1970) as belonging to the marble tortoise, are recognized here as hingeless. Therefore, a detailed description and updated figuration is given, allowing attribution to '*Testudo*' sp., increasing the turtle diversity of Pikermi.

- The material from Pylea and Allatini, previously described as "*Te*." *amiatae*, is hereby revised, described and figured in detail, allowing attribution to *Te. graeca*. The taxon "*Te*." *amiatae* is not recognized as present in Greece and is now restricted only in its type locality (Cinigiano) in Italy.

- The material from Megalo Emvolon, previously identified as *Te.* cf. *graeca*, is hereby revised and is identified as *Te. graeca*.

- The material from the Pliocene of Epanomi, Nea Kallikratia and Nea Michaniona, previously identified as '*Cheirogaster*' *bacharidisi*, is hereby revised as *Titanochelon bacharidisi*, aided by the description of new specimens from Nea Michaniona and Nea Kallikratia. The cranium of the holotype from Epanomi, has been CT-scanned and the results allow the description of its morphology in more detail, providing evidence of some sutures among the cranial bones.

- *Titanochelon bacharidisi* is further identified in Aggelochori/Megalo Emvolon, revising material previously identified as *Testudo* sp.

- The material from Salonique (sensu Arambourg & Piveteau, 1929) is revised in detail, with descriptions and figuration. The stratigraphic provenance of the specimens is not known precisely. The small testudinid material, previously identified as *Testudo* sp., is identified here as *Te. graeca*. The large testudinid material, previously identified as cf. *Cheirogaster* sp., is identified here as *Titanochelon* cf. *bacharidisi*.

- The type material of *Te. marginata cretensis* from the caves Gerani and Zourida from the Pleistocene of Crete has been re-examined, re-described and figured in detail. The comparison with all known fossil material and several extant specimens of the marginated tortoise has shown that the subspecific distinction by Bachmayer et al. (1975) is not justified. This material is hereby referred to *Te. marginata*.

- The published material of *Te. marginata* from Charkadio Cave, Tilos Island has been re-described, along with the description of new specimens from the cave. This assemblage was proposed to have been created by human interactions due to the supposed lack of shell specimens. Here, the recovered shell specimens from the cave are described and figured, and a taphonomical analysis and comparison with sites with human interaction on turtles seem to refute the human interaction on the chelonian material of Charkadio Cave.

- The material from Megalopolis has been previously identified as *Clemmys caspica*. Although not located over the course of this thesis, the published original figuration by Melentis (1966) allows the identification of two taxa, *M. rivulata* and *E. orbicularis*.

Objective 3: Documentation of the diversity of the fossil chelonians of Greece.

Conclusions: The present thesis documents for the first time the diversity of the fossil chelonians from Greece in detail, that is significantly different than previously thought. The information presented here allows revising the taxonomic diversity in great respect, as briefly summarized below:

- Fossil trionychids in Greece are reported here for the first time. Although only two localities (Gefira, Pliocene; Plakias, late Middle Miocene) preserve few fragmented fossils, these specimens can be clearly identified as trionychids based on the distinctive sculpturing on the dorsal surface of the carapace. In the case of Gefira locality, this attribution has been further confirmed by histological sections that revealed the “plywood” structure (sensu Scheyer, 2007) that is considered as an autapomorphy of the trionychids.

- The taxonomic status of the large testudinids, previously attributed to the Late Eocene genus *Cheirogaster*, are hereby revised as belonging to the newly named genus *Titanochelon* Pérez-García & Vlachos, 2014. For the definition of this clade, material presented in this thesis played an important role. Also, in the present thesis, the distinction of the large testudinids from the Neogene of Europe is further established and the phylogenetic relationships of *Titanochelon* are analyzed in a large scale.

- The diversity of large testudinids has been further established, as containing at least two different species: the Pliocene *Titanochelon bacharidisi* distributed in Northern Greece and the Late Miocene *Titanochelon schafferi* from Samos Island. Although many more specimens from large testudinids have been described by new and previously known localities, these specimens cannot be identified to the species level based on the available information. It seems possible, however, that the large testudinid from Pikermi could represent a

new species but more specimens are certainly needed. This diversity could be explained by the paleogeographical changes that occurred in Neogene times, as the Samos form could be closer with the Minor Asian large testudinids than with the forms from the South Balkans.

- '*Testudo' amiatae*, a small testudinid taxon first described from Italy but previously reported from the Late Miocene/Early Pliocene of Pylea and Allatini. The updated morphological information on the Pylea specimen indicate the presence of a hypo-xiphiplastral hinge in the plastron, a feature absent in '*Te*.' *amiatae*. The overall morphology of the specimens from Pylea and Allatini allows their attribution to *Te. graeca*. Since no other specimens from Greece were identified as close to '*Te*.' *amiatae*, this taxon is considered absent from the Greek paleofauna.

- The Late Miocene *Testudo marmorum* is revised and diagnosed here and is considered a valid species. Some specimens from Pikermi that have been previously attributed to this taxon, are shown here as belonging to a different lineage, given that they are hingeless.

- The type specimens and new material of the endemic subspecies *Testudo marginata cretensis* from the Pleistocene of Crete are revised here, showing no important differences compared to *Te. marginata*. Therefore, the validity of this subspecies is refuted and all those Cretan specimens are now referred to *Te. marginata*.

- The actual taxonomic diversity of the Greek chelonians is even greater, as this work showed the possible presence of new taxa that are summarized above.

Table 7.1. Summary of the changes in the composition of the fossil fauna of chelonians in Greece, based on the present thesis.

Locality	Age	First description	Present study	Institution
		New Material		
Gerani Cave, Crete Island	Holocene?	-	*Mauremys* sp.	AMPG
Liko Cave, Crete Island	Pleistocene	-	*Mauremys rivulata*	AMPG
Koumpes Cave, Crete Island	Pleistocene	-	*Mauremys rivulata*	AMPG
Mavro Mouri IV, Crete Island	Pleistocene	-	*Mauremys rivulata*	AMPG
Kythera Island	Pleistocene	-	*Testudo marginata*	LGPUT?
Kos Island	Pleistocene	-	*Mauremys rivulata*	NHMC
Kos Island	Pleistocene	-	*Testudo marginata*	NHMC
Potidea, Chalkidiki	Pleistocene	-	*Testudo graeca*	LGPUT
Xerias, Kavala	Pleistocene	-	*Testudo* cf. *marginata*	LGPUT
Chalkidiki	Pleistocene	-	*Testudo hermanni*	LGPUT
Gefira, Axios valley	Pliocene	-	Trionychidae indet.	LGPUT
Milia, Grevena	Late Pliocene	-	*Testudo* sp. nov.	LGPUT
Milia, Grevena	Late Pliocene	-	*Mauremys* sp.	LGPUT
Milia, Grevena	Late Pliocene	-	*Titanochelon* sp.	LGPUT
Epanomi	Pliocene	-	*Titanochelon bacharidisi*	LGPUT
Nea Michaniona	Pliocene	-	*Titanochelon bacharidisi*	LGPUT
Nea Kallikratia	Pliocene	-	*Titanochelon bacharidisi*	LGPUT
Allatini,	Latest	-	*Mauremys* sp.	LGPUT

Thessaloniki	Miocene/ Earliest Pliocene			
Nea Silata	Latest Miocene/ Earliest Pliocene	-	*Testudo* sp.	LGPUT
Nea Silata	Latest Miocene/ Earliest Pliocene	-	*Mauremys* sp. nov.	LGPUT
Plakias, Crete island	Late Miocene	-	*Mauremys* sp.	NHMC
Plakias, Crete island	Late Miocene	-	Trionychidae indet.	NHMC
Platania, Drama	Late Miocene	-	*Testudo* cf. *graeca*	LGPUT
Kryopigi, Kassandra peninsula	Late Miocene	-	*Titanochelon* sp.	LGPUT
Fourka, Kassandra peninsula	Late Miocene	-	*Titanochelon* sp.	LGPUT
Samos Island	Late Miocene	-	*Testudo* sp. nov.	AMPG; GNHM
Serres	Late Miocene	-	*Testudo* sp.	AMPG
Material Mentioned but never studied				
Franchthi Cave, Peloponnesus	Pleistocene/ Holocene	*Testudo* (in Stiner & Munro, 2011)	*Testudo* cf. *hermanni*	D' Ephorate of Archaeology, Nafplion
Franchthi Cave, Peloponnesus	Pleistocene/ Holocene	*Emys/Maurymys* [sic] (in Stiner & Munro, 2011)	*Emys orbicularis*	D' Ephorate of Archaeology, Nafplion
Vraona Cave	Recent	*Emys orbicularis* (in Rauscher, 1995)	*Emys orbicularis*	IPUW
Vraona Cave	Recent	*Clemmys caspica* (in Rauscher, 1995)	*Mauremys rivulata*	IPUW
Gerani Cave, Crete Island	Pleistocene	*Testudo marginata cretensis* (in Bachmayer et al., 1975)	*Testudo marginata*	AMPG
Zourida Cave, Crete Island	Pleistocene	*Testudo marginata cretensis* (in Bachmayer et al., 1975)	*Testudo marginata*	AMPG
Liko Cave, Crete Island	Pleistocene	*Testudo marginata cretensis* (in Brinkerink, 1996)	*Testudo marginata*	AMPG
Koumpes Cave, Crete Island	Pleistocene	*Testudo marginata cretensis* (in Brinkerink, 1996)	*Testudo marginata*	AMPG
Mavro Mouri IV, Crete Island	Pleistocene	*Testudo* (in Brinkerink, 1996)	*Testudo marginata*	AMPG
Sitia, Crete Island	Pleistocene	*Clemmys* cf. *caspica* (in Mayhew, 1997)	*Mauremys rivulata*	AMPG
Rethymnon fissure, Crete Island	Pleistocene	cf. *Emys orbicularis* (in Brinkerink, 1996)	*Mauremys rivulata*	AMPG
Bate Cave, Crete Island	Pleistocene	*Testudo marginata cretensis* (in Kotsakis, 1977)	*Testudo marginata*	Roma Tre
Maramena	Latest Miocene/ Earliest Pliocene	Testudinidae indet (in Schmidt-Kittler et al., 1995)	*Testudo* sp.	Mainz
Published Material Revised				
Charkadio Cave, Tilos Island	Latest Pleistocene	*Testudo marginata* (in Bachmayer & Symeonidis, 1975)	*Testudo marginata*	AMPG
Petralona Cave	Pleistocene	*Testudo graeca* (in Kretzoi, 1977)	*Testudo graeca*	Museum of Petralona Cave
Simonelli Cave, Crete Island	Pleistocene	*Testudo marginata* (in Malatesta et al., 1980)	*Testudo marginata*	AMPG
Megalopolis basin, Peloponnesus	Pleistocene	*Clemmys caspica* (in Melentis, 1966)	*Mauremys rivulata*	AMPG
Megalopolis basin,	Pleistocene	*Clemmys caspica*	*Emys orbicularis*	AMPG

Peloponnesus		(in Melentis, 1966)		
Vatera-F site, Lesvos Island	Early Pleistocene	cf. *Cheirogaster* aff. *schafferi* (in Lapparent de Broin, 2002)	*Titanochelon* sp.	VM
Vatera-T site, Lesvos Island	Early Pleistocene	*Testudo* cf. *graeca ibera* (in Lapparent de Broin, 2002)	*Testudo graeca*	VM
Korydallos	Pleistocene	*Testudo* sp. (in Paraskevaidis, 1961)	*Testudo* sp.	unknown
Lakonia	Pleistocene	*Testudo marginata* (in Schleich, 1982)	*Testudo marginata*	BSPG (cast)
Aggelochori/ Megalo Emvolon, Thessaloniki	Pliocene	*Testudo* cf. *graeca* (in Bachmayer et al., 1979)	*Testudo graeca*	NHMW; AMPG
Aggelochori/ Megalo Emvolon, Thessaloniki	Pliocene	*Testudo* sp. (in Bachmayer et al., 1979)	*Titanochelon bacharidisi*	LGPUT; AMPG
Apolakkia, Rhodes Island	Early Pliocene	Testudoolithidae indet (in Mueller-Töwe et al., 2011)	*Testudoolithus* sp.	AMPG
Apolakkia, Rhodes Island	Early Pliocene	*Remains of a chelonian taxon* (in Mueller-Töwe et al., 2011)	cf. *Testudo* sp.	AMPG
"Salonique"	Late Miocene – Pliocene?	*Testudo* sp. (small size) (in Arambourg & Piveteau, 1929)	*Testudo graeca*	MNHN
"Salonique"	Late Miocene – Pliocene?	*Testudo* sp. (large size) (in Arambourg & Piveteau, 1929)	*Titanochelon* cf. *bacharidisi*	MNHN
Allatini, Thessaloniki	Latest Miocene/ Earliest Pliocene	*Testudo amiatae* (in Bachmayer & Symeonidis, 1970)	*Testudo graeca*	AMPG
Pylea, Thessaloniki	Latest Miocene/ Earliest Pliocene	*Testudo amiatae* (in del Campana, 1917)	*Testudo graeca*	IGF
Pylea, Thessaloniki	Latest Miocene/ Earliest Pliocene	*Identified as turtle eggs* (in del Campana, 1919)	Testudoolithidae indet	IGF
Pikermi, Attica	Late Miocene	*Testudo marmorum* (in Gaudry, 1862a,b)	*Testudo marmorum*	AMPG
Pikermi, Attica	Late Miocene	*Testudo* sp. (in Bachmayer, 1967)	*Titanochelon* sp.	AMPG
Pikermi, Attica	Late Miocene	*Testudo marmorum* (in Bachmayer & Symeonidis, 1970)	*Testudo* sp. (hingeless)	AMPG
Liossati, Kiourka	Late Miocene	*Testudo* sp. (in Bachmayer & Symeonidis, 1977)	*Titanochelon* sp.	AMPG
Samos Island	Late Miocene	*Testudo schafferi* (in Szalai, 1931)	*Titanochelon schafferi*	NHMW
Thymiana?, Chios Island	Middle Miocene	*Testudo* sp. I & II (in Paraskevaidis, 1955)	cf. *Testudo* sp. nov. (Samos)	BSPG (lost)
Halmyropotamos, Evia Island	Late Miocene	*Testudo marmorum* (in Melentis, 1970)	Not located	unknown
Nostimo, Kastoria	Early Miocene	*Nostimochelone lampra* (in Georgalis et al., 2013)	*Nostimochelone lampra*	NM

Objective 5: Description of the evolution of the chelonian clades in Greece, from the Miocene up to the present.

Conclusions: The updated information on the morphology, taxonomy and distribution of the Greek fossil chelonians allows observing the evolution of the various chelonian clades in Greece. Briefly, the results emerged from this study show that the evolution of the Greek chelonian clades could be tied with regional (and sometimes larger-

scale) geotectonic and climate events. The testudinid taxa belong to two different clades, whose closest common ancestor could be traced back in the Eocene times. These two clades show a different evolutionary history. The small testudinids are nested within the *Testudona* clade, which shows a tendency towards small-sized individuals. This clade is found around the Mediterranean area, a region with several major tectonic events in the Cenozoic. Therefore, the results presented here indicate a complex evolutionary history for the clade *Testudo*, at least since the Late Miocene times, which needs to be further investigated with the inclusion of more fossil taxa from other countries. On the other hand, the large testudinids from Greece (clade *Titanochelon*) are nested within a larger clade with several small, large and giant extinct and extant taxa from Europe, Africa and Asia, indicating an even more complex biogeographical history for these large testudinids. The clade *Titanochelon* is strongly supported here as monophyletic, and it appears that the presence of giantism could be lineage-specific for this clade, resulting in several large and giant forms. This phenomenon can be observed in Greece, in which large forms (from 80 to 120 cm) characterize the Pliocene, following the truly gigantic forms of the Late Miocene (more than 150 cm).

The clades of the aquatic taxa (*Mauremys* and *Emys*) also show a different evolutionary history. *Mauremys* can be confidently traced since the limit of Middle and Late Miocene, evolving in several different taxa in the Miocene, Pliocene and Pleistocene. This clade also shows a large distribution in Continental Greece, as well as in several islands. On the other hand, the *Emys* clade shows a much smaller geographical (confidently identified in Peloponnesus in pre-Holocene times) and temporal distribution, found only during the Late Pleistocene and the boundary Pleistocene-Holocene. These results are in accordance with the suggestion that South Balkans served as a Glacial refugee for this taxon. During the Glacial, the range of *Mauremys* is also reduced compared to the Pliocene times.

Objective 6: Phylogenetic analysis of the small testudinid taxa of Greece.

Conclusions: The establishment of a new set of characters for the analysis of testudinids (see below) has allowed the phylogenetic analysis of the small testudinid taxa of Greece, within a larger ingroup of testudinid taxa. The results of the analysis are in accordance with molecular data (e.g. Parham et al., 2006; Le et al., 2006; Fritz & Bininda-Emmonds, 2007). The Greek taxa are nested within *Testudona*, and especially the Late Miocene *Te. marmorum* is nested within the *Chersus* clade along with *Te. marginata* and *Te. kleinmanni*. This pushes the origin of *Testudo* prior the Late Miocene, agreeing with the results of Parham et al. (2006) and pointing the antiquity of the *Te. graeca* lineage. *'Testudo' hermanni* (in contrast with Parham et al. 2006 and in agreement with Le et al., 2006 and Fritz & Bininda-Emmonds, 2007) is grouped with *Testudo* and not with *Indotestudo*, being placed in the stem of *Testudo* (sensu Parham et al., 2006).

Objective 7: Phylogenetic analysis of the large testudinid taxa of Greece.

Conclusions: The establishment of a new set of characters for the analysis of testudinids (see below) has allowed the phylogenetic analysis of the large testudinid taxa of Greece and Europe, within a larger ingroup of testudinid taxa. Due to the preservation status, the Late Miocene taxon *Ti. schafferi* could not be confidently analyzed. Instead, the inclusion of *Ti. bacharidisi* in the analysis re-affirmed the

distinction of the Neogene large testudinids from the Late Eocene *Cheirogaster*, confirming their inclusion in the new clade *Titanochelon* Pérez-García & Vlachos, 2014. *Titanochelon bacharidisi* is the sister-group of *Ti. perpiniana*. The clade *Titanochelon* is nested within a larger clade containing most large testudinid taxa, suggesting that the evolution of giantism could be lineage-specific in some cases. Also, this analysis is the first to suggest a morphological sister-group relationship of the South American *Chelonoidis* with African taxa. It seems likely that the main testudinid lineages were already established in the Eocene but their biogeographic history is still complicated. The Dispersal-Evolution-Cladogenesis analysis (DEC) performed (without any dispersal constrains) showed almost equal low possibilities of a Palearctic or African origin for these clades. Both hypotheses have been previously suggested (e.g. Lapparent de Broin, 2001 and Le et al., 2006 respectively).

Objective 8: Phylogenetic analysis of the freshwater taxa of Greece.

Conclusions: From the freshwater taxa, *Mauremys* is the clade with the most numerous representatives in the Greek fossil record. In the present thesis the phylogenetic relationships are explored within the European geoemydids, based on the character/taxon matrix introduced by Hervet (2003). In this matrix, the *Mauremys* taxon from Nea Silata and Allatini, that could be a new taxon is scored and added. Also the possible synonymies in the fossil taxa erected by Hervet (2003), which have been suggested by Claude & Tong (2004) are discussed. The analysis presented here shows that the taxonomy of the European geoemydids is still poorly understood, as the inclusion of the synonymies suggested by Claude & Tong (2004) create paraphyletic and polyphyletic groups. Also, it is showed that the characters in this matrix are not adequate to fully resolve the relationships in the specific level. In order to solve these problems, several options are suggested here: to include in future analyses more European fossil taxa (e.g. geoemydids with wide vertebrals) and Asian fossil and extinct taxa that are largely missing. Also the inclusion of more characters could allow solving several polytomies within clades. Finally, the combination of the morphological parsimony analysis with molecular data (either as constrains or in a total evidence analysis) should provide robust results.

Another aquatic taxon that its phylogenetic relationships are explored within Podocnemidoidea is the oldest chelonian and the only known pleurodire from Greece, *Nostimochelone lampra*. Although the morphological information of this only known specimen is limited, it is possible to score this taxon within the large-scale pleurodire matrices of Gaffney et al. (2006 and 2011 respectively). Its inclusion in the matrix of Gaffney et al. (2011), that is centered around podocnemidids did not produce any results allowing to discern the affinities of this pleurodire. The results in the matrix of Gaffney et al. (2006) however, are significantly better and show that *N. lampra* bears some clear bothremydid affinities in the morphology of carapace and plastron. Hopefully, these results will allow a better analysis of this poorly understood taxon in the future.

Objective 9: Study of the bone histology of several taxa.

Conclusions: In the present thesis the first histological sampling of Greek chelonian material has been performed. In particular, the nuchal and costal plates of the Gefira trionychid and a costal fragment of the large testudinid *Ti. bacharidisi* from Nea Michaniona are sampled and studied. In the trionychid samples, the presence of the

"plywood" structure (sensu Scheyer, 2007) has been verified, confirming the identification of these fragmented plates as soft-shelled turtles. Also, the histology of these plates clearly indicate the aquatic affinities of this extinct turtle. On the other hand, the sections of the large testudinid showed the main histological features of a terrestrial taxon. Furthermore, these sections are marked by the presence of possible lines of arrested growth and of large vascular spaces. Possibly these features could be related with the evolution of the large size on this clade, but further sampling of extinct and extant taxa are needed to provide detailed results. The conclusions resulted from the histological sections are promising towards an increased use of numerous chelonian fragmented specimens in the fossil record for paleoecological reconstructions.

Objective 10: Comparison of the Greek chelonians with those from Minor Asia, Italy, South Balkans and adjacent areas.

Conclusions: The comparison of the Greek chelonians with those from Italy showed that the Italian chelonian fossil record is much more diverse in general, as it contains several pleurodires and truly marine taxa that have not been found in Greece. On the other hand, the testudinid fossil record of Greece is richer in number of taxa compared to the Italian one, especially in the presence of hinged and large testudinids. These results could reflect the differences in the type and diversity of fossil localities between the two Mediterranean countries. Compared to the fossil record of the South Balkans and Minor Asia, the fossil chelonian record of Greece is the richest up to now. In the present thesis the Greek record is found even richer and more diverse than previously thought, with several new testudinid and geoemydid taxa that are going to be described in the near future. On the other hand, the testudinid record of Minor Asia could be of similar or even greater richness than the Greek one, but the Turkish material is poorly studied up to now.

Objective 11: Study of the contribution of the fossil chelonians to the biostratigraphy of the Neogene – Quaternary of South Balkans.

Conclusions: The contribution of the fossil chelonians to the biostratigraphy of the Neogene – Quaternary of South Balkans is limited compared to the results that could be inferred by the study of fossil mammals, that show a more rapid evolution. However, the emerging picture from the present thesis is that the fossil turtles and tortoise could be used in biostratigraphy to confidently identify an assemblage in the Epoch level. Given that the fossil record of chelonians is rich, and even small fragments can be identified in lower taxonomic levels, the contribution of chelonians in the biostratigraphy of Greece seems to be potentially significant in the future.

Conclusions on the evolution of Testudinidae

Especially for the Testudinidae, the new information inferred by the description of new testudinid material and its comparison with extinct and extant forms, has allowed the establishment of a new matrix on morphological characters for the analysis of this clade. This new matrix contains 81 characters from the carapace, plastron, skull and appendicular skeleton, and is the product of combining previously published and new characters. This new set of characters has been described in detail,

accompanied by descriptive drawings of character states based on real specimens for further explanation. For the first time, 36 extant and extinct taxa from all major global lineages have been analyzed. The inclusion of numerous shell characters has allowed the analysis of several fossil taxa that have been previously left out of several analyses that focused on the cranium. Therefore, with this analysis we are able to place several taxa into a phylogenetic context for the first time.

Both the unconstrained and the constrained (based on molecular studies) results are promising, as all the major clades known by molecular studies are recovered. Also, although normally the morphological signal of testudinids is considered weak, homoplastic and complex, the inclusion of many fossil taxa in the analysis produces positive results. For example, even in the unconstrained analysis, most of the phylogenetically defined clades within Testudinidae (e.g. *Testudona*, *Indotestudo*, *Testudo*; sensu Parham et al., 2006) are recovered, a result that provides the confidence that this matrix can be further expanded in the future in order to produce more results. Also, some taxa from the Paleogene of France (‘*Achilemys’ cassouleti* and ‘*Hadrianus’ castrensis*) are identified for the first time as belonging to the stem of Testudinidae, pointing out the necessity of revising these poorly known taxa in order to elucidate the early history of testudinids.

This preliminary global phylogenetic analysis of the testudinids allows identifying the establishment of the major testudinid lineages in the Eocene and the possible African origin of many clades within Testudinidae, as is broadly accepted based on both the fossil record and molecular studies. Also, another promising result is the relatively recent origin of *Testudona* in the Late Miocene, an idea suggested by Parham et al. (2006).

Plotting the evolution of the shell size results in an interesting scenario: it seems most parsimonious that the major testudinid lineages were small in the Eocene, and giantism has evolved independently in several clades. One clade, which contains the African extinct taxa *Gigantochersina ammon*, *Impregnochelys pachytestis* and the extant *Astrochelys radiata* and *Kinixys erosa*, as well as the European *Cheirogaster maurini* and ‘*Testudo’ gigas*, shows a different scenario, in which large size is the plesiomorphic condition and small forms have re-appeared. In some lineages (*Titanochelon*) the large size could be lineage-specific, being developed in the Miocene times. These results are in accordance with climatic data (e.g. Zachos et al. 2001), such as the favorable conditions for giantism in the Paleocene-Eocene due to the warm and humid climate at this period. The onset of glaciations in the Oligocene that triggered a global cooling up to present could explain the trend towards nanism (e.g. *Testudona*), whereas the Miocene Climatic Optimum would explain the presence of large testudinids during the Miocene. These results agree with similar conclusions on the evolution of varanids and horses (Gould & McFadden, 2004) that contrast the generally accepted “Cope’s rule” on gradual increase of size within a clade.

Further research: The results obtained from this study indicate several areas for future research:

- A main point of focus in the future is the description of more new specimens that will allow a better understanding of the chelonian diversity in Greece. At the same time, efforts should increase in better dating of the localities and the specimens. These future results would allow a precise placement of the

various specimens biostratigraphically, providing more detailed results on the evolution of the chelonian clades in South Balkans.

- The Greek fossil chelonian fauna is the most complete and diverse in South Balkans. Hopefully, the results obtained from this study would spur the description of new specimens from adjacent areas (e.g. Minor Asia), which may allow a better knowledge of the evolution of turtles and tortoises in the eastern part of Mediterranean. This region appears to be important for the early and recent evolution of testudinids.

- The new matrix of morphological characters for the analysis of testudinids presented here shows several promising results. Hopefully, future works will expand the number of characters and will include more fossil and extant taxa in a global scale. By achieving this, we will be able to analyze in more detail compared to the present thesis several open questions such as the evolution of shell size and the biogeographic history of testudinids during the Cenozoic.

-

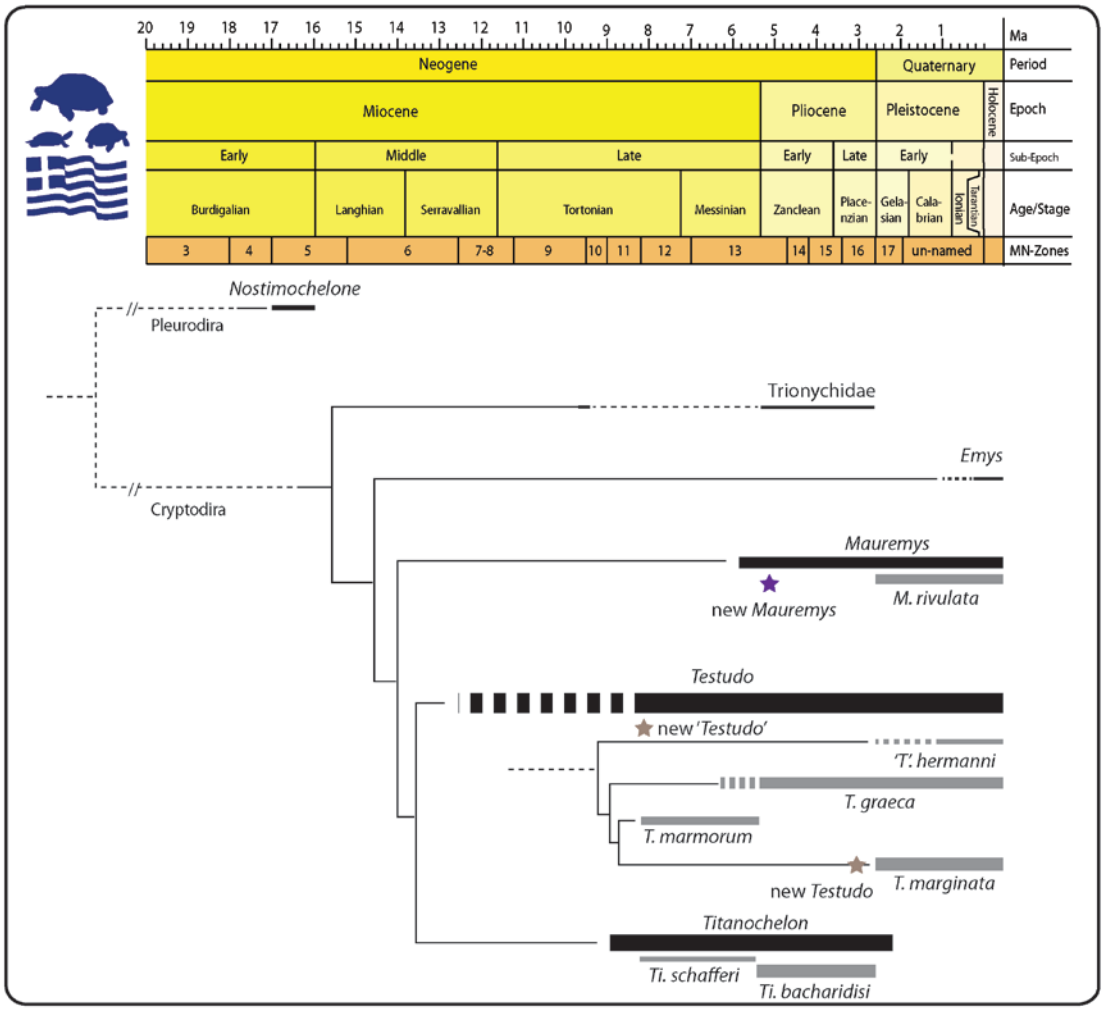


Figure 7.1. Graphical summary of the diversity and temporal distribution of the fossil turtles and tortoises of Greece. Stars indicate the position of new taxa suggested in the present thesis.

- The results presented here show that our understanding of the taxonomy and phylogenetic relationships of fossil geoemydids is rather poor. Future research should focus in the establishment of a detailed matrix of cranial, shell and appendicular characters, which will allow the phylogenetic analysis of geoemydids in a global scale. Possibly, such efforts could be combined with the above mentioned testudinid matrix and a matrix on emydids, allowing the detailed analysis within Testudinoidea.

- Based on the results presented here, it seems most parsimonious that giantism appeared independently in various clades in the Cenozoic. The reasons that led to this phenomenon remain unclear. It is possible that histology could provide further insights on this matter, with sampling of large-sized extinct and extant testudinids and comparing with the histology of small-sized tortoises.

- Lastly, the results obtained on this study regarding the evolution of the chelonian clades (from a taxonomic, phylogenetic, geographic and temporal point of view) in the last 20 million years, should be compared in the future with the evolution of other members of the paleoherpetofauna of Greece.

02/16/2016 Ψηφιακή Βιβλιοθήκη Θεόφραστος - Τμήμα Γεωλογίας - Α.Π.Θ.

Chapter 8. Extended Summary in Greek

Εκτεταμμένη Περίληψη

ΟΙ ΑΠΟΛΙΘΩΜΕΝΕΣ ΧΕΛΩΝΕΣ ΤΗΣ ΕΛΛΑΔΑΣ
ΣΥΣΤΗΜΑΤΙΚΗ-ΕΞΕΛΙΞΗ-ΣΤΡΩΜΑΤΟΓΡΑΦΙΑ-ΠΑΛΑΙΟΟΙΚΟΛΟΓΙΑ

Η παρούσα διδακτορική διατριβή διαπραγματεύεται τη μελέτη του μέχρι σήμερα διαθέσιμου υλικού της παλαιοπανίδας των χελωνών της Ελλάδας. Συγκεκριμένα, εστιάζει στην αναλυτική περιγραφή μορφολογικών στοιχείων νέων δειγμάτων και στη συστηματική αναθεώρηση δειγμάτων που είχαν δημοσιευτεί παλαιότερα. Τα περισσότερα δείγματα που ήταν διαθέσιμα μελετήθηκαν μέσα από προσωπικές παρατηρήσεις σε συλλογές και σε μουσεία. Ορισμένα από τα απολιθώματα χελωνών που είχαν δημοσιευτεί κατά το παρελθόν δεν κατέστη δυνατό να εντοπιστούν για διαφόρους λόγους. Ωστόσο, για όσα οι διαθέσιμες πληροφορίες ήταν αρκετές (περιγραφές, φωτογραφίες κ.λπ.), συμπεριλήφθηκαν ως ένα βαθμό στην παρούσα διατριβή. Όλα τα δείγματα παρουσιάζονται με ομοιόμορφο τρόπο, με φωτογραφίες, επεξηγηματικά σκίτσα και διαγράμματα, περιγραφή και τεκμηρίωση.

Το πρώτο κεφάλαιο περιλαμβάνει ορισμένες εισαγωγικές πληροφορίες για τον αναγνώστη, όπως τους σκοπούς και στόχους της διατριβής, το υλικό που μελετήθηκε, τις μεθόδους που ακολουθήθηκαν, πληροφορίες για τα σημερινά είδη χελωνών που επιβιώνουν στον ελληνικό χώρο και μια συνοπτική ιστορική αναθεώρηση της μελέτης των απολιθωμένων χελωνών στην Ελλάδα.

Το δεύτερο κεφάλαιο παρουσιάζει συνοπτικά γεωλογικά στοιχεία των θέσεων εύρεσης του υλικού το οποίο αναλύεται στην παρούσα διατριβή.

Το τρίτο κεφάλαιο αποτελεί το κύριο μέρος της παρούσας διατριβής, καθώς περιλαμβάνει την ανάλυση του συνόλου του υλικού, λεπτομερή περιγραφή, φωτογραφική τεκμηρίωση, μορφολογική εικονογράφηση και συζήτηση.

Στο τέταρτο κεφάλαιο παρουσιάζονται διάφορα στοιχεία για την εξελικτική ιστορία των ελληνικών χελωνών. Αρχικά ορίζεται ένας νέος πίνακας μορφολογικών χαρακτήρων για τη φυλογενετική ανάλυση των χερσαίων χελωνών. Οι νέοι χαρακτήρες περιγράφονται και τεκμηριώνονται σχηματικά. Στη συνέχεια παρουσιάζεται η φυλογενετική ανάλυση των μεγάλων και μικρών χερσαίων χελωνών. Επιπλέον, με βάση δημοσιευμένους πίνακες χαρακτήρων από προηγούμενους ερευνητές, αναλύονται οι φυλογενετικές σχέσεις ορισμένων υδρόβιων απολιθωμένων ειδών.

Στο πέμπτο κεφάλαιο γίνεται η σύνθεση των στοιχείων που αφορούν τη χωρική και χρονική εξάπλωση των χελωνών του Ελληνικού χώρου και ερευνάται η συνεισφορά των απολιθωμένων χελωνών στη βιοστρωματογραφία της Ελλάδας.

Στο έκτο κεφάλαιο πραγματοποιείται η μελέτη ιστολογικών τομών του πρώτου τριόνυχα της Ελλάδας (υδρόβιο είδος) και ενός είδους χερσαίας γιγαντιαίας χελώνας, δεδομένα που συνεισφέρουν στη γνώση της παλαιοοικολογίας αυτών των εξαφανισμένων ειδών.

Στο έβδομο κεφάλαιο παρουσιάζονται τα συμπεράσματα της παρούσας διδακτορικής διατριβής.

Στο παράρτημα δίνονται πίνακες μετρήσεων δειγμάτων και η ανάλυση όλων των στοιχεία που αναπτύχθηκαν στο τέταρτο κεφάλαιο της φυλογενετικής ανάλυσης.

Νέο Υλικό

Στην παρούσα διατριβή μελετώνται για πρώτη φορά νέα δείγματα απολιθωμένων χελωνών από την Ελλάδα. Ως «νέα δείγματα» θεωρούνται: Α) Δείγματα από απολιθωματοφόρες θέσεις που παρουσιάζονται για πρώτη φορά. Β) Νέα δείγματα από γνωστές θέσεις, οι οποίες είχαν δώσει στο παρελθόν δείγματα

απολιθωμένων χελωνών. Γ) Δείγματα τα οποία περιγράφονται για πρώτη φορά, αλλά είχαν αναφερθεί στο παρελθόν σε δημοσιευμένους καταλόγους ή εργασίες, αλλά δεν είχαν μελετηθεί ποτέ. Συγκεκριμένα:

Α) Υλικό από διάφορες νέες θέσεις με ευρήματα χελωνών παρουσιάζεται για πρώτη φορά. Αυτό το υλικό προέρχεται κυρίες από ανασκαφικές έρευνες, αλλά και από διάφορες συλλογές. Χρονολογικά, από την εποχή του Μειόκαινου παρουσιάζονται δείγματα *Mauremys* sp. και Trionychidae από την MN7/8 του Πλακιά στη Ν. Κρήτη. Νέο υλικό της *Testudo* cf. *graeca* από τη νέα θέση Πλατανιά, από το Άνω Μειόκαινο της Δράμας. Νέο υλικό της *Testudo* sp. από το Άνω Μειόκαινο της λεκάνης των Σερρών. Νέο υλικό της γιγαντιαίας χελώνας *Titanochelon* sp. από τις ανωμειοκαινικές θέσεις Κρυοπηγή και Φούρκα στη χερσόνησο της Κασσάνδρας Χαλκιδικής. Από την εποχή του Πλειόκαινου, αναφέρονται νέα δείγματα *Testudo* sp. nov., *Mauremys* sp. και *Titanochelon* sp. από την ανωπλειοκαινική θέση της Μηλιάς στα Γρεβενά. Νέο υλικό Trionychidae από την πλειοκαινική θέση της Γέφυρας, στην κοιλάδα του Αξιού. Από την εποχή του Πλειστόκαινου, νέα δείγματα της *Testudo* cf. *marginata* παρουσιάζονται από τη θέση Ξεριάς στην Καβάλα, *Te. marginata* από θέσεις στη Βοιωτία και στα Κύθηρα, *Testudo* sp. και *Mauremys* sp. από την Κω, ‘*Testudo*’ *hermanni* από την Ποτίδαια.

Β) Νέο υλικό χελωνών από γνωστές θέσεις με ευρήματα χελωνών κατά το παρελθόν. Συγκεκριμένα, παρουσιάζεται νέο υλικό της γιγαντιαίας χελώνας *Ti. schafferi* από το Άνω Μειόκαινο της Σάμου. Νέο υλικό *Testudo* sp. nov. από το Άνω Μειόκαινο της Σάμου. Νέο υλικό *Titanochelon* sp. και *Testudo* sp. από το Άνω Μειόκαινο του Πικερμίου. Νέο υλικό της γιγαντιαίας χελώνας *Ti. bacharidisi* από το Πλειόκαινο του Αγγελοχωρίου/Μεγάλου Εμβόλου, της Νέας Μηχανιώνας και της Νέας Καλλικράτειας. Νέο υλικό *Testudo graeca* από το Πλειόκαινο του Αγγελοχωρίου/Μεγάλου Εμβόλου. Νέο υλικό *Mauremys* sp. nov. από το όριο Μειόκαινου/Πλειόκαινου του Αλλατίνι. Νέο υλικό της *Te. marginata* από το Σπήλαιο Χαρκαδιό στην Τήλο.

Γ) Αρκετό υλικό απολιθωμένων χελωνών είχε απλώς αναφερθεί κατά το παρελθόν αλλά περιγράφεται για πρώτη φορά στην παρούσα διατριβή. Συγκεκριμένα περιγράφεται για πρώτη φορά το υλικό από *Testudo* sp. από το όριο Μειόκαινου/Πλειόκαινου των Μαραμένων, στη λεκάνη των Σερρών. Υλικό *Testudo* sp. και *Mauremys* sp. nov. από το όριο Μειόκαινου/Πλειόκαινου των Νέων Σιλάτων, στην περιοχή της Θεσσαλονίκης. Υλικό *Mauremys rivulata* και *Te. marginata* από πλειστοκαινικές θέσεις της Κρήτης, και συγκεκριμένα από τα σπήλαια Γεράνι, Ζούριδα, Κούμπες, Λύκο, Μαύρο Μουρί 4 και Σιμονέλλι, αλλά και από την ανοιχτή θέση Σητεία. Υλικό *Te. graeca* από το Πλειστόκαινο του Σπηλαίου των Πετραλώνων. Υλικό *Testudo* cf. *hermanni* και *Emys orbicularis* από το όριο Πλειστόκαινου/Ολόκαινου του Σπηλαίου Φράγχθι στην Πελοπόννησο.

Το νέο αυτό υλικό προσφέρει πολύτιμα συμπεράσματα σχετικά με τη γεωγραφική και βιοστρωματογραφική εξάπλωση των απολιθωμένων χελωνών της Ελλάδας, όπως επίσης και για την ταξινομική τους ποικιλία.

Νέα Είδη

Η λεπτομερής περιγραφή νέου και αναθεωρημένου, δημοσιευμένου παλαιότερα, υλικού απολιθωμένων χελωνών από την Ελλάδα, οδήγησε στον προσδιορισμό τουλάχιστον τριών νέων ειδών. Αυτά προσδιορίστηκαν ως sp. nov., η μορφολογία τους και τα νέα χαρακτηριστικά αναλύθηκαν με λεπτομέρεια στην παρούσα διατριβή και βρίσκονται σε διαδικασία δημοσίευσης. Συγκεκριμένα:

- Το νέο υλικό από μια μικρή σε μέγεθος χερσαία χελώνα από το Άνω Πλειόκαινο της Μηλιάς (Γρεβενά) προσδιορίζεται ως ένα νέο είδος του κλάδου *Testudo*, με βάση την παρουσία ενός εκτεταμένου οπίσθιου χείλους του ραχιαίου θυρεού, αλλά χωρίς ένα επιμηκυσμένο χελώνιο όπως στην *Te. marginata*. Η προκαταρκτική φυλογενετική ανάλυση του υλικού, τοποθετεί το νέο αυτό είδος στον κλάδο *Testudo*, ενώ με βάση μια συναπομορφία ορίζεται ως συγγενής-ομάδα (sister-group) με την *Te. marginata*.

- Το νέο υλικό από μια μικρή σε μέγεθος χελώνα από το Άνω Μειόκαινο της Σάμου, πιθανότατα ανήκει σε ένα νέο είδος του '*Testudo'*, με βάση τη διαφορετική μορφολογία των οστέινων πλακών στο οπίσθιο τμήμα του ραχιαίου θυρεού και τη μορφολογία των κεράτινων πλακών του κοιλιακού θυρεού. Η προκαταρκτική φυλογενετική ανάλυση τοποθετεί το είδος αυτό στο stem του κλάδου *Testudo*.

- Το νέο υλικό νεροχελώνας από τις θέσεις Νέα Σίλατα και Αλλατίνι στο όριο Μειόκαινου-Πλειόκαινου, αναφέρεται στην παρούσα διατριβή ως ένα νέο είδος του *Mauremys*. Ανάμεσα σε αρκετούς χαρακτήρες, το είδος αυτό χαρακτηρίζεται από κεντρικές κεράτινες πλάκες που έχουν μικρό μήκος και μεγάλο πλάτος. Η προκαταρκτική φυλογενετική ανάλυση του υλικού τοποθετεί το είδος αυτό μέσα στον κλάδο *Mauremys*.

Αναθεώρηση Δημοσιευμένου Υλικού

Στο πλαίσιο της παρούσας διατριβής αναθεωρήθηκε και μελετήθηκε από την αρχή το σύνολο του δημοσιευμένου υλικού απολιθωμένων χελωνών της Ελλάδας και παρουσιάζεται μετά από προσωπικές παρατηρήσεις με λεπτομερείς περιγραφές και φωτογραφική τεκμηρίωση. Συγκεκριμένα, η αναθεώρηση του διαθέσιμου δημοσιευμένου υλικού οδήγησε στην εξαγωγή των παρακάτω νέων συμπερασμάτων:

- Το χαμένο υλικό από μικρές χερσαίες χελώνες από το Μέσο Μειόκαινο της Χίου, αναλύθηκε με βάση τις δημοσιευμένες φωτογραφίες. Πιθανότατα ανήκει στο νέο είδος που προσδιορίστηκε από το Άνω Μειόκαινο της Σάμου.

- Το υλικό της γιγαντιαίας χελώνας από το Άνω Μειόκαινο της θέσης Λιοσσάτη (Κιούρκα) στην Αττική, προσδιορίζεται ως *Titanochelon* sp.

- Το υλικό της γιγαντιαίας χελώνας από το Άνω Μειόκαινο του Πικερμίου, το οποίο είχε προηγουμένως προσδιοριστεί ως cf. *Cheirogaster* cf. *schafferi*, αναθεωρείται και με την προσθήκη νέου υλικού προσδιορίζεται ως *Titanochelon* sp. Το υλικό αυτό πιθανότατα ανήκει σε ένα είδος διαφορετικό από το επίσης ανωμειοκαινικό *Titanochelon schafferi* από τη Σάμο.

- Η συστηματική κατάσταση του είδους *Te. marmorum* από το Άνω Μειόκαινο του Πικερμίου επανεξετάζεται μέσα από νέες περιγραφές και φωτογραφική τεκμηρίωση. Το είδος αυτό θεωρείται ως έγκυρο, αλλά ορισμένα δείγματα που αποδόθηκαν στο είδος αυτό από τους Bachmayer & Symeonidis (1970), διαπιστώθηκε ότι δεν διαθέτουν κινητό αρμό στον κοιλιακό θυρεό. Επομένως τα δείγματα αυτά τοποθετούνται προσωρινά στο είδος '*Testudo*' sp., αυξάνοντας την ταξινομική ποικιλία της θέσης του Πικερμίου.

- Το υλικό από τις θέσεις Πυλαία και Αλλατίνι, το οποίο είχε προηγουμένως περιγραφεί ως "*Te*." *amiatae*, αναθεωρείται, περιγράφεται με λεπτομέρεια, και προσδιορίζεται ως *Te. graeca*. Το είδος "*Te*." *amiatae* δεν εντοπίζεται πλέον στην Ελλάδα και περιορίζεται μόνο στην τυπική του θέση στην Ιταλία.

- Το υλικό από το Μεγάλο Έμβολο, το οποίο είχε προσδιοριστεί αρχικά ως *Te.* cf. *graeca*, αναθεωρείται και προσδιορίζεται ως *Te. graeca*.

- Το υλικό από τη θέση Salonique (κατά Arambourg & Piveteau, 1929), αναθεωρείται, περιγράφεται και απεικονίζεται με λεπτομέρεια για πρώτη φορά. Η στρωματογραφική προέλευση των δειγμάτων δεν είναι γνωστή. Το μικρό σε μέγεθος είδος, το οποίο αρχικά είχε προσδιοριστεί ως *Testudo* sp., αναθεωρείται ως *Te. graeca*. Το υλικό της μεγάλης σε μέγεθος χελώνας, το οποίο αποδιδόταν στο είδος cf. *Cheirogaster* sp., αναθεωρείται ως *Titanochelon* cf. *bacharidisi*.

- Με βάση νέο υλικό από το Πλειόκαινο της Επανωμής, Νέας Καλλικράτειας και Νέας Μηχανιώνας, το οποίο αρχικά είχε προσδιοριστεί ως '*Cheirogaster*' *bacharidisi*, αναθεωρείται ως *Titanochelon bacharidisi*. Το κρανίο του ολότυπου από την Επανωμή αναλύθηκε με τη χρήση αξονικής τομογραφίας (CT-scan) και τα αποτελέσματα βοήθησαν να περιγραφεί το δείγμα με περισσότερη λεπτομέρεια και να καταστεί δυνατή η αναγνώριση ορισμένων γραμμών ραφής ανάμεσα στα οστά του κρανίου.

- Το *Ti. bacharidisi* προσδιορίζεται επιπλέον και στις θέσεις Αγγελοχώρι/Μεγάλο Έμβολο, μέσα από την αναθεώρηση υλικού το οποίο προηγουμένως είχε προσδιοριστεί ως *Testudo* sp.

- Το τυπικό υλικό του υποείδους *Te. marginata cretensis* από τα σπήλαια Γεράνι και Ζούριδα από του Πλειστόκαινο της Κρήτης επανεξετάζεται και παρουσιάζονται νέες λεπτομερείς περιγραφές και φωτογραφική τεκμηρίωση. Η σύγκριση με το γνωστό υλικό από την κρασπεδωτή χελώνα φανερώνει ότι ο διαχωρισμός σε ένα διαφορετικό υποείδος από τους Bachmayer et al. (1975) δεν επιβεβαιώνεται με βάση τη μορφολογία. Για αυτό το λόγο, όλο το σχετικό υλικό από το Πλειστόκαινο της Κρήτης προσδιορίζεται ως *Te. marginata*.

- Το δημοσιευμένο υλικό της *Te. marginata* από το Σπήλαιο Χαρκαδιό της Τήλου επανεξετάζεται, ταυτόχρονα με την περιγραφή νέου υλικού από το σπήλαιο. Η υποτιθέμενη απουσία δειγμάτων από το χελώνιο είχε οδηγήσει σε μια παλαιότερη θεωρία ότι το υλικό συγκεντρώθηκε από ανθρώπινη δραστηριότητα. Στην παρούσα διατριβή παρουσιάζονται διάφορα τμήματα από το χελώνιο, τα οποία βρέθηκαν μέσα στο σπήλαιο από ανασκαφές κατά

την περίοδο (1992-2014, Γ. Θεοδώρου, προσ. επικ.). Η ταφονομική ανάλυση του ανεσκαμμένου υλικού και η σύγκριση με άλλες θέσεις από την Ελλάδα όπου έχει ταυτοποιηθεί η ανθρώπινη παρέμβαση, απορρίπτει την υπόθεση της συγκέντρωσης του υλικού από ανθρώπινη παρέμβαση.

- Το υλικό από τη λεκάνη της Μεγαλόπολης είχε προσδιοριστεί ως *Clemmys caspica*. Παρότι το υλικό δεν ήταν δυνατό να εντοπιστεί, με βάση τις δημοσιευμένες πληροφορίες από τον Melentis (1966), προσδιορίστηκαν δύο είδη, το *M. rivulata* και *E. orbicularis*.

Η Ελληνική παλαιο-χελωνοπανίδα

Συνολικά, αναλύθηκε απολιθωμένο υλικό από πάνω από 45 θέσεις, το οποίο αποκαλύπτει ότι η ταξονομική σύνθεση της ελληνικής παλαιο-χελωνοπανίδας είναι σημαντική, περισσότερο πλούσια και αρκετά διαφορετική από ότι γνωρίζαμε πριν:

- Μέλη των Trionychidae δεν απαντώνται στη σημερινή Ελληνική ερπετοπανίδα, παρά μόνο ως τυχαία ευρήματα στα ανοιχτά ύδατα ανάμεσα στα ελληνικά νησιά και τα παράλια της Τουρκίας. Επίσης δεν έχουν αναφερθεί μέχρι τώρα απολιθωμένα δείγματα αυτής της οικογένειας. Στην παρούσα διατριβή παρουσιάζονται τα πρώτα απολιθώματα τριόνυχων από την Ελλάδα, από τις θέσεις Γέφυρα (Πλειόκαινο) και Πλακιάς (τέλος του Μέσου Μειόκαινου). Τα δείγματα αυτά προσδιορίζονται ως μέλη των Trionychidae με βάση τη χαρακτηριστική ανάγλυφη επιφάνεια του ραχιαίου και του κοιλιακού θυρεού. Περαιτέρω τεκμηρίωση δίνεται με βάση τη μελέτη ιστολογικών τομών από τα δείγματα της Γέφυρας Αξιού, στα οποία παρατηρείται η χαρακτηριστική δομή «σανίδας» (plywood κατά Scheyer, 2007), που θεωρείται αυταπομορφική για αυτήν την οικογένεια.

- Η συστηματική θέση των γιγαντιαίων χελωνών αναθεωρείται πλήρως. Οι γιγαντιαίες χελώνες του Νεογενούς της Ευρώπης μέχρι πρόσφατα συμπεριλαμβανόταν στο γένος *Cheirogaster* από το Ηώκαινο της Γαλλίας (de Broin, 1977; Lapparent de Broin, 2001; 2002). Με βάση υλικό που παρουσιάζεται στην παρούσα διατριβή, αλλά και υλικό από την Ισπανία, ορίστηκε από τους Pérez-García & Vlachos (2014) το νέο γένος *Titanochelon*, στο οποίο συμπεριλαμβάνονται οι γιγαντιαίες χελώνες της Ευρώπης, αλλά και της Ελλάδας. Νέο υλικό που παρουσιάζεται στην παρούσα διατριβή ενισχύει αυτήν την άποψη, ενώ επιπλέον οι φυλογενετικές σχέσεις αυτού του κλάδου αναλύονται σε ένα γενικότερο πλαίσιο.

- Η ταξινομική ποικιλία των γιγαντιαίων χελωνών εδραιώνεται, αποτελούμενη από δύο τουλάχιστον διαφορετικά είδη: το *Titanochelon bacharidisi* από το Πλειόκαινο της Βόρειας Ελλάδας και το *Titanochelon schafferi* από το Άνω Μειόκαινο της Σάμου. Στην παρούσα διατριβή παρουσιάζονται ακόμη περισσότερα δείγματα γιγαντιαίων χελωνών, αλλά στις περισσότερες περιπτώσεις δεν μπορούν να προσδιοριστούν σε επίπεδο είδους. Ωστόσο, η γιγαντιαία χελώνα από το Άνω Μειόκαινο του Πικερμίου ενδεχομένως να αποτελεί ένα νέο είδος, αλλά περισσότερα δείγματα χρειάζονται για ένα ασφαλές συμπέρασμα. Αυτή η ταξινομική ποικιλία πιθανώς εξηγείται από τις παλαιογεωγραφικές αλλαγές που έχουν συμβεί κατά το Νεογενές στην

περιοχή του Αιγαίου, καθώς το είδος της Σάμου είναι πιθανότατα πιο συγγενές με είδη από τη Μικρά Ασία, αντί με το είδος από τα Νότια Βαλκάνια.

- Το είδος '*Testudo' amiatae*, ένα μικρό σε μέγεθος testudinid από την Ιταλία είχε αναφερθεί από το Άνω Μειόκαινο/Κάτω Πλειόκαινο του Αλλατίνι και της Πυλαίας, δεν υπάρχει στην Ελλάδα. Η επανεξέταση του υλικού αυτού δείχνει την παρουσία ενός κινητού αρμού ανάμεσα από τα υπόπλαστρα και τα ξιφίπλαστρα, ένα χαρακτηριστικό που απουσιάζει από το είδος '*Te.' amiatae*. Αντίθετα, η συνολική μορφολογία των δειγμάτων του Αλλατίνι και της Πυλαίας οδηγεί στον προσδιορισμό των δειγμάτων αυτών ως *Te. graeca*. Καθώς κανένα άλλο δείγμα από τον ελληνικό χώρο δεν διατηρεί τους χαρακτήρες του '*Te.' amiatae,* συμπεραίνεται ότι αυτό το είδος απουσιάζει από την ελληνική παλαιοχελωνοπανίδα.

- Το είδος του Άνω Μειόκαινου *Testudo marmorum* αναθεωρείται πλήρως, και θεωρείται ένα έγκυρο είδος. Ταυτόχρονα αναλύονται οι φυλογενετικές του σχέσεις, φανερώνοντας ότι ανήκει στον κλάδο *Testudo* και εμφανίζει στενή σχέση με το αφρικανικό *Testudo kleinmanni*. Ορισμένα δείγματα από το Πικέρμι που είχαν προσδιοριστεί ως *Te. marmorum* κατά το παρελθόν, αναθεωρούνται και θεωρούνται μέλη άλλου κλάδου χελωνών (Pan-*Testudo*), οι οποίες δεν εμφανίζουν κινητό αρμό ανάμεσα από τα υπόπλαστρα και ξιφίπλαστρα.

- Τα τυπικά δείγματα και επιπλέον υλικό που κατά το παρελθόν είχαν αποδοθεί στο ενδημικό υποείδος από το Πλειστόκαινο της Κρήτης, *Testudo marginata cretensis,* αναθεωρήθηκαν στην παρούσα διατριβή. Μορφολογικά δεν εμφανίζουν σημαντικές διαφορές σε σχέση με αρτίγονα και απολιθωμένα δείγματα του είδους *Te. marginata*. Για το λόγο αυτό, η εγκυρότητα του υποείδους αυτού αμφισβητείται στην παρούσα διατριβή και το υλικό της Κρήτης προσδιορίζεται ως *Te. marginata*.

Με βάση τα αποτελέσματα που προκύπτουν από την παρούσα διατριβή φαίνεται ότι η εξέλιξη των διαφόρων κλάδων χελωνών στην Ελλάδα σχετίζεται με τοπικές και μεγαλύτερης κλίμακας γεωλογικές, γεωγραφικές και κλιματικές αλλαγές.

Φυλογενετικές Σχέσεις

Αναπτύχθηκε ένας πίνακας μορφολογικών χαρακτήρων από το κρανίο, το χελώνιο και τον σκελετό, με σκοπό την ανάλυση των φυλογενετικών σχέσεων των χερσαίων χελωνών του Καινοζωικού σε παγκόσμιο επίπεδο. Ο νέος αυτός πίνακας επέτρεψε την ανάλυση 38 ειδών (απολιθωμένων και σύγχρονων) με βάση 81 χαρακτήρες. Οι χερσαίες χελώνες της Ελλάδας χωρίζονται σε δύο κλάδους, με τον τελευταίο κοινό τους πρόγονο να εντοπίζεται στο Ηώκαινο. Οι μικρές σε μέγεθος χελώνες ανήκουν στον κλάδο *Testudona*, ο οποίος χαρακτηρίζεται από την παρουσία μικρών σε μέγεθος ειδών. Τα μέλη του κλάδου αυτού εντοπίζονται στην ευρύτερη περιοχή της Μεσογείου, φανερώνοντας μια πολύπλοκη εξελικτική ιστορία μέσα από τις σημαντικές γεωλογικές και παλαιογεωγραφικές αλλαγές της περιοχής κατά τον Καινοζωικό. Τα αποτελέσματα της παρούσας διατριβής για τον κλάδο *Testudo*, δείχνουν ότι πιθανότατα αναπτύχθηκε τουλάχιστον κατά το Άνω Μειόκαινο και

πρέπει να αναλυθούν με λεπτομέρεια σε μελλοντικές έρευνες. Από την άλλη πλευρά, οι γιγαντιαίες χελώνες της Ελλάδας (κλάδος *Titanochelon*) τοποθετούνται σε ένα ευρύτερο κλάδο που περιλαμβάνει διάφορα είδη απολιθωμένων και αρτίγονων χελωνών μικρού, μεσαίου και μεγάλου μεγέθους από την Ευρώπη, Αφρική και Ασία. Τα αποτελέσματα αυτά δείχνουν μια ακόμη περισσότερο πολύπλοκη εξελικτική ιστορία για τις γιγαντιαίες χελώνες. Ο κλάδος *Titanochelon* εντοπίζεται ως μια μονοφυλετική ομάδα, και είναι πιθανό ότι ο γιγαντισμός είναι χαρακτηριστικό αυτού του κλάδου, με μεγάλες και γιγαντιαίες μορφές. Αυτό είναι ιδιαίτερα εμφανές στην Ελλάδα καθώς το Πλειόκαινο χαρακτηρίζεται από είδη μεγάλου μεγέθους (80 έως 120 cm), τα οποία ακολουθούν τις πραγματικά γιγαντιαίες χελώνες του Άνω Μειόκαινου (πάνω από 150 cm).

Με βάση τον νέο πίνακα μορφολογικών χαρακτήρων κατέστη δυνατή η ανάλυση των φυλογενετικών σχέσεων των Testudinidae σε ένα ευρύτερο πλαίσιο. Τα αποτελέσματα των φυλογενετικών αναλύσεων συμφωνούν σε μεγάλο βαθμό με αυτά που προκύπτουν από την ανάλυση γενετικών δεδομένων (e.g. Parham et al., 2006; Le et al., 2006; Fritz & Bininda-Emmonds, 2007). Τα είδη της Ελλάδας βρίσκονται μέσα στον κλάδο *Testudona*, ενώ το ανωμειοκαινικό είδος *Te. marmorum* τοποθετείται μέσα στον κλάδο *Chersus* μαζί με τα είδη *Te. marginata* και *Te. kleinmanni*. Αυτό τοποθετεί την προέλευση του κλάδου *Testudo* πριν από το Άνω Μειόκαινο, το οποίο βρίσκεται σε συμφωνία με τα αποτελέσματα των Parham et al., 2006. Αυτό επίσης δείχνει ότι ο κλάδος της *Te. graeca* εκτείνεται αρκετά πίσω στο χρόνο. Το είδος *'Testudo' hermanni* (σε αντίθεση με τους Parham et al. 2006, αλλά σε συμφωνία με τους Le et al., 2006 και Fritz & Bininda-Emmonds, 2007) σχετίζεται με τον κλάδο *Testudo* και όχι τον κλάδο *Indotestudo*. Συγκεκριμένα εντοπίζεται στο stem του *Testudo* (κατά Parham et al., 2006).

Η φυλογενετική ανάλυση των μεγάλων σε μέγεθος ελληνικών χελωνών, έδωσε τη δυνατότητα της φυλογενετικής τοποθέτησης του κλάδου *Titanochelon* και των ελληνικών αντιπροσώπων του σε ένα ευρύτερο πλαίσιο. Εξαιτίας του περιορισμένου αριθμού δειγμάτων και της κατάστασης διατήρησης, το είδος του Άνω Μειόκαινου *Ti. schafferi* δεν κατέστη δυνατό να αναλυθεί με ασφάλεια. Αντίθετα η ανάλυση του *Ti. bacharidisi*, μαζί με τα υπόλοιπα είδη αυτού του κλάδου, επιβεβαιώνει την άποψη των Pérez -García & Vlachos (2014) ότι οι μεγάλες χελώνες του Νεογενούς της Ευρώπης διαφέρουν σημαντικά από το είδος *Cheirogaster* του Άνω Ηωκαίνου. Το *Titanochelon bacharidisi* εντοπίζεται ως ο συγγενής-ομάδα της *Ti. perpiniana*. Ο κλάδος *Titanochelon* εντοπίζεται ανάμεσα σε ένα ευρύτερο κλάδο μεγάλων και γιγαντιαίων χελωνών, γεγονός που οδηγεί στην υπόθεση ότι η ανάπτυξη του γιγαντισμού ίσως χαρακτηρίζει αυτόν τον κλάδο. Ο κλάδος *Titanochelon* σχετίζεται φυλογενετικά τόσο με τις χερσαίες χελώνες της Νοτίου Αμερικής όσο και με αρκετά Αφρικανικά είδη. Επιπλέον είναι φανερό ότι οι διάφοροι κλάδοι των χερσαίων χελωνών είχαν ήδη κάνει την εμφάνισή τους από το Ηώκαινο. Όπως φανερώνει και η ανάλυση DEC (Dispersal – Evolution – Cladogenesis, χωρίς παραμετροποίηση των μεταναστεύσεων), η παλαιογεωγραφική ιστορία των κλάδων αυτών είναι πολύπλοκη, καθώς η Παλαιοαρκτική και η Αφρικανική προέλευση στηρίζεται με παρόμοια χαμηλές πιθανότητες. Και οι δύο υποθέσεις έχουν προταθεί κατά το παρελθόν (Lapparent de Broin, 2001 και Le et al., 2006 αντίστοιχα).

Τόσο η φυλογενετική ανάλυση χωρίς περιορισμούς, όσο και η ανάλυση με περιορισμούς (με βάση γενετικές αναλύσεις) δίνει ενθαρρυντικά αποτελέσματα.

Σχεδόν όλοι οι κύριοι κλάδοι των χερσαίων χελωνών που εντοπίζονται στην παρούσα διατριβή συμφωνούν με τα γενετικά δεδομένα. Παρόλο που συνήθως η πληροφορία που προκύπτει από την ανάλυση μορφολογικών χαρακτήρων χερσαίων χελωνών θεωρείται αδύναμη και ομοπλαστική, η συμπερίληψη αρκετών απολιθωμένων ειδών στην ανάλυση έδωσε θετικά αποτελέσματα. Για παράδειγμα, ακόμη και στην ανάλυση χωρίς περιορισμούς, κατέστη δυνατή η ανακάλυψη των περισσότερων κλάδων που έχουν οριστεί φυλογενετικά ανάμεσα στα Testudinidae (π.χ. *Testudona*, *Indotestudo*, *Testudo*, κατά Parham et al., 2006). Αυτό το αποτέλεσμα προτείνει με ασφάλεια την επέκταση του συγκεκριμένου πίνακα με περισσότερα είδη και χαρακτήρες στο μέλλον. Επίσης, ορισμένα είδη του Παλαιογενούς (‘*Achilemys’ cassouleti* και ‘*Hadrianus’ castrensis*) προσδιορίζονται για πρώτη φορά ως stem Testudinidae, τονίζοντας την ανάγκη της λεπτομερούς αναθεώρησής του ώστε να περιγραφούν με λεπτομέρεια τα πρώτα εξελικτικά στάδια των Testudinidae.

Η ανάλυση της εξέλιξης του μεγέθους του χελωνίου δίνει ένα ενδιαφέρον αποτέλεσμα: είναι περισσότερο parsimonious ότι οι αντιπρόσωποι των διαφόρων κλάδων κατά το Ηώκαινο ήταν μικροί σε μέγεθος και ότι ο γιγαντισμός αναπτύχθηκε ανεξάρτητα σε διάφορους κλάδους. Ένας από τους μεγάλους κλάδους, αυτός που περιλαμβάνει τα Αφρικανικά απολιθωμένα είδη *Gigantochersina ammon*, *Impregnochelys pachytestis* και τα αρτίγονα *Astrochelys radiata* και *Kinixys erosa*, όπως επίσης και τα ευρωπαϊκά *Cheirogaster maurini* και ‘*Testudo’ gigas*, δείχνει ένα διαφορετικό σενάριο. Σε αυτόν τον κλάδο, το μεγάλο μέγεθος είναι πιθανότατα η πλησιομορφική κατάσταση, ενώ το μικρό μέγεθος επανεμφανίζεται. Σε ορισμένες γενεαλογίες (*Titanochelon*) το μεγάλο μέγεθος ίσως είναι χαρακτηριστικό του κλάδου, το οποίο εμφανίζεται κατά το Μειόκαινο. Όλα αυτά τα αποτελέσματα είναι σε συμφωνία με κλιματικά δεδομένα μεγάλης κλίμακας (π.χ. Zachos et al. 2001), όπως οι ιδανικές συνθήκες για την ανάπτυξη του γιγαντισμού κατά το Παλαιόκαινο – Ηώκαινο χάρη στο θερμό και υγρό κλίμα αυτής της χρονικής περιόδου. Η έναρξη των παγετώνων του Ολιγοκαίνου, που οδήγησαν σε μια πτώση της θερμοκρασίας σε παγκόσμιο επίπεδο, ίσως εξηγούν την τάση κλάδων από το Ολιγόκαινο και μετά προς νανισμό (π.χ. *Testudona*). Αντίθετα το Miocene Climatic Optimum πιθανότατα σχετίζεται με την εμφάνιση και την εξάπλωση των μεγάλων σε μέγεθος testudinids κατά το Μειόκαινο, όπως της Ελλάδας. Επιπλέον, αυτά τα αποτελέσματα συμφωνούν με αντίστοιχα σε σαύρες και ιπποειδή (Gould & McFadden, 2004) που διαφωνούν με την γενική αποδοχή του “Cope’s rule”, δηλαδή τη σταδιακή αύξηση του μεγέθους.

Οι κλάδοι των υδρόβιων χελωνών της Ελλάδας (*Mauremys* και *Emys*) εμφανίζουν μια διαφορετική εξελικτική ιστορία. Ο κλάδος *Mauremys* εντοπίζεται με ασφάλεια από την έναρξη του Άνω Μειόκαινου, και εξελίσσεται σε διάφορα είδη κατά το Πλειόκαινο και Πλειστόκαινο. Αυτός ο κλάδος παρουσιάζει μια ευρεία εξάπλωση στην ηπειρωτική Ελλάδα, καθώς και σε διάφορα νησιά. Αντίθετα, ο κλάδος *Emys* εμφανίζει μια σαφώς μικρότερη γεωγραφική (έχει προσδιοριστεί με ασφάλεια μόνο στην Πελοπόννησο πριν από το Ολόκαινο) και χρονική εξάπλωση, καθώς έχει εντοπιστεί μόνο από το Άνω Πλειστόκαινο μέχρι σήμερα. Αυτά τα αποτελέσματα συμφωνούν με την προϋπάρχουσα άποψη ότι τα Νότια Βαλκάνια αποτέλεσαν ένα καταφύγιο για το είδος αυτό κατά τις παγετώδεις περιόδους. Κατά το ίδιο διάστημα, και η εξάπλωση του *Mauremys* ελαττώνεται.

Από τους υδρόβιους κλάδους, ο κλάδος *Mauremys* εμφανίζει τους περισσότερους αντιπροσώπους στο απολιθωμένο αρχείο της Ελλάδας. Στην παρούσα διατριβή παρουσιάζεται μια φυλογενετική ανάλυση των Ευρωπαϊκών Geoemydidae με βάση τον πίνακα χαρακτήρων/ειδών της Hervet (2003). Σε αυτόν τον πίνακα

προστέθηκε το πιθανό νέο είδος από τα Νέα Σίλατα και το Αλλατίνι. Επιπλέον συζητείται η εγκυρότητα των πιθανών συνονυμιών που προτάθηκαν για τα νέα είδη της Hervet (2003), από τους Claude & Tong (2004). Η ανάλυση αυτή φανερώνει ότι η ταξινόμηση και οι φυλογενετικές σχέσεις των Ευρωπαϊκών γεωέμυδων δεν είναι καλά γνωστές, καθώς η συμπερίληψη των συνωνυμιών των Claude & Tong (2004) οδηγεί σε διάφορες παραφυλετικές και πολυφυλετικές ομάδες. Έτσι προτείνεται η διεύρυνση του πίνακα χαρακτήρων/ειδών με περισσότερους χαρακτήρες που θα βοηθήσουν την επίλυση των σχέσεων σε επίπεδο είδους. Επιπλέον, η προσθήκη περισσότερων Ευρωπαϊκών και Ασιατικών ειδών είναι αναγκαία για την αναπαράσταση της εξελικτικής ιστορίας αυτού του μεγάλου κλάδου.

Τέλος, επιχειρήθηκε η ανάλυση των φυλογενετικών σχέσεων της παλαιότερης ελληνικής χελώνας και του μοναδικού πλευρόδειρου, της *Nostimochelone lampra*. Παρόλο που η διαθέσιμη μορφολογική πληροφορία είναι περιορισμένη στο μοναδικό δημοσιευμένο δείγμα, η συμπερίληψή του στον πίνακα των Gaffney et al. (2006) έδωσε ενθαρρυντικά αποτελέσματα. Αυτή η αινιγματική χελώνα έχει σαφείς σχέσεις με τα Bothremydidae, καθώς με βάση τη διαθέσιμη πληροφορία εντοπίζεται σταθερά μέσα σε αυτόν τον κλάδο. Η ανακάλυψη και η μελέτη νέων δειγμάτων από αυτήν την ομάδα θα βοηθήσει σημαντικά στην αποσαφήνιση των σχέσεων αυτού του είδους.

Παλαιοοικολογικές παρατηρήσεις

Στην παρούσα διατριβή πραγματοποιήθηκαν για πρώτη φορά ιστολογικές τομές ραχιαίου θυρεού ελληνικών απολιθωμένων ειδών. Συγκεκριμένα, η δειγματοληψία έγινε σε δείγματα του τριόνυχα από τη θέση Γέφυρα Αξιού και στη γιγαντιαία χελώνα από τη θέση Νέα Μηχανιώνα. Στα δείγματα του τριόνυχα εντοπίστηκε η χαρακτηριστική δομή “plywood” (κατά Scheyer, 2007), γεγονός που επιβεβαιώνει τον προσδιορισμό των δειγμάτων αυτών ως Trionychidae. Επιπλέον, η ιστολογική δομή υποδεικνύει τις σαφείς υδρόβιες τάσεις αυτής της απολιθωμένης χελώνας. Από την άλλη πλευρά, η ιστολογική μορφολογία των δειγμάτων της γιγαντιαίας χελώνας φανερώνει τις σαφείς χερσαίες τάσεις αυτού του είδους. Σε αυτά τα δείγματα δείχνουν την παρουσία αρκετών γραμμών ανάπτυξης και μεγάλων κενών, χαρακτηριστικά που πιθανότατα σχετίζονται με την ανάπτυξη του γιγαντισμού σε αυτήν την ομάδα. Τα αποτελέσματα πάνω στην ιστολογική ανάλυση δείχνουν ότι αυτή η μέθοδος μπορεί να αποδειχθεί ιδιαίτερα χρήσιμη στις παλαιοοικολογικές αναπαραστάσεις, ακόμη και πάνω σε θραύσματα του χελωνίου.

Βιοστρωματογραφία

Μέχρι στιγμής, η χρήση των απολιθωμένων χελωνών στη μελέτη της βιοστρωματογραφίας του Νεογενούς – Τεταρτογενούς των Νοτίων Βαλκανίων είναι ελάχιστη. Ωστόσο, με βάση τα αποτελέσματα της παρούσας διατριβής, είναι φανερό ότι οι απολιθωμένες χελώνες της Ελλάδας μπορούν να συνεισφέρουν στη βιοχρονολόγηση, τουλάχιστον σε επίπεδο Εποχής. Το απολιθωμένο αρχείο χελωνών είναι άφθονο σε θραύσματα, και τις περισσότερες φορές υπάρχει το πλεονέκτημα ότι ακόμη και τα μικρότερα δείγματα μπορούν να προσδιοριστούν με λεπτομέρεια. Με βάση τα παραπάνω, η μελέτη των απολιθωμένων χελωνών μπορεί να συνεισφέρει σημαντικά στη βιοστρωματογραφία του Νεογενούς/Τεταρτογενούς της Ελλάδας.

References

Abbazzi, L., Carboni, S., Delfino, M., Gallai, G., Lecca, L., Rook, L., 2008. Fossil vertebrates (Mammalia and Reptilia) from Capo Mannu formation (late Pliocene, Sardinia, Italy), with description of a new *Testudo* (Chelonii, Testudinidae) species. Rivista italiana di paleontologia e stratigrafia, 114 (1), 119.

Agassiz, L. 1857. Contributions to the Natural History of the United States of America. First Monograph. Vol. I. Part I. Essay on Classification. Part II. North American Testudinata. Boston: Little, Brown and Co., Vol. I, 1–452.

Amiranashvili, N. G., 2000. Differences in shell morphology of *Testudo graeca* and *Testudo hermanni*, based on material from Bulgaria. Amphibia Reptilia, 21, 67–82.

Andrews, C. W., 1906. A descriptive Catalog of the Tertiary Vertebrata of the Fayum. Egypt: I–XXXVII, London: Trustees British Museum (Natural History), 324 pp.

Arambourg, C., Piveteau, J. J., 1929. Les Vertébrés du Pontien de Salonique. Annales de Paléontologie, 18, 59–138.

Armour-Brown, A., De Bruijn, H., Maniati, C., Siatos, G., Niesen, P., 1979. The geology of the Neogene sediments north of Serrai and the use of rodent faunas for biostratigraphic control. Proceedings of the VI Colloquium on the Geology of the Aegean Region, 2, 612–622.

Athanassiou, A., 2004. On a *Deinotherium* (Proboscidea) finding in the Neogene of Crete. Carnets de Géologie/Notebooks on Geology, Brest, Letter, 5, 1–7.

Athanassiou, A., Kostopoulos, D., 2010. On Pliocene mammal remains in the area of Epanomi (Macedonia, Greece). Scientific Annals, School of Geology, Aristotle University of Thessaloniki, Proceedings of the 19th CBGA Congress, Thessaloniki, Greece, Special Volume 99, 63–68.

Auffenberg, W., 1974. Checklist of fossil land tortoises (Testudinidae). Bulletin of the Florida State Museum, 18, 121–253.

Bachmayer, F., 1967. Eine Riesenschildkröte aus den altpliozänen Shichten von Pikermi (Griechenland). Praktika Akademiae Athenae, 42, 303–317.

Bachmayer, F., Symeonidis, N., 1970. Die fossilen Schildkrötenreste des geologisch-paläontologischen Institutes der Universität von Athen. Annales Géologiques des Pays Helléniques, 22, 227-246.

Bachmayer, F., Symeonidis, N., 1975. Schildkrötenreste (*Testudo marginata* SCHOEPFF) aus der Höhle „Charkadio“ auf der Insel Tilos (Dodekanes, Griechenland). Annales Géologiques des Pays Helléniques, 26, 324–327.

Bachmayer, F., Symeonidis, N., 1977. Eine neue „Pikermi“ Fundstelle im Gebiet von Liossati (Kiourka) nördlich von Athen (Griechenland)(Beschreibung einer Riesenschildkröte). Annales Géologiques des Pays Helléniques, 28, 8–16.

Bachmayer, F., Brinkerink, J. P., Symeonidis, N., 1975. Pleistozäne Schildkröten aus Höhlen der Insel Kreta. Annales Geologiques des Pays Helleniques, 27, 110–122.

Bachmayer, F., Mlynarski, M., Symeonidis, N., 1979. Fossile Schildkröten aus dem Pliozän von Megalo Emvolo (Karaburun) bei Saloniki (Griechenland). Annales Géologiques des Pays Helléniques, 29, 267–276.

Bachmayer, F., Symeonidis N., Zapfe, H., 1984. Die Ausgrabungen in der Zwergelefantenhöhle der Insel Tilos (Dodekanes, Griechenland) im Jahr 1983. Sitzungsberichte Österreichse Akademie der Wissenschaften Mathem. Naturw. Kl., Abt. I, 193. (6–10), 321–328, Wien.

Bader, T., Riegler, C., Grillitsch, H., 2009. The herpetofauna of the Island of Rhodes (Dodecanese, Greece). Herpetozoa, 21, 147–169.

Badgley, C., 1986. Counting individuals in mammalian fossil assemblages from fluvial environments. Palaios, 328–338.

Barth, D., Bernhard, D., Fritzsch, G., Fritz, U., 2004. The freshwater turtle genus *Mauremys* (Testudines, Geoemydidae)—a textbook example of an east–west disjunction or a taxonomic misconcept? Zoologica Scripta, 33, 213–221.

Baryshnikov, G. F., Tsoukala, E., 2010. New analysis of the Pleistocene carnivores from Petralona Cave (Macedonia, Greece) based on the Collection of the Thessaloniki Aristotle University. Geobios, 43, 389–402.

Bate, D., 1914. Remains of a gigantic land tortoise (*T. gymnesicus* n. sp.) from the Pleistocene of Menorca. Geological Magazine 4, 100–107.

Batsch, A.J., 1788. Versuch einer Anleitung, zur Kenntniß und Geschichte der Thiere und Mineralien. Akademische Buchhandlung, Jena, 528 pp.

Baur, G., 1893. Notes on the classification of the Cryptodira. American Naturalist, 27, 672–674.

Behrensmeyer, A. K., 1978. Taphonomic and ecologic information from bone weathering. Paleobiology, 150–162.

Bell, T., 1825. A monograph of the tortoises having a moveable sternum with remarks on their arrangement and affinities. Zoological Journal, 2, 299 –310.

Bergounioux, F., 1935. Contribution à l'étude paléontologique des Chéloniens. Chéloniens fossiles du Bassin d'Aquitaine. Mémoires de la Société Géologique de France, 25, 1–216.

Bibron, G., Bory de Saint–Vincent, J., 1832. Vertébrés à sang froid. Reptiles et poissons.: Geoffroy Saint– Hilaire, E, Ed.). Expédition Scientifique de Morée, Vol. 3, Part 1, 57–80.

Biedermann, W. G. A., 1862. Petrefakten aus der Umgegend von Winterthur. I. Schildkröten. Winterthur, S. Bleuler–Hausheer, 16 pp.

Boev, Z., 2008. First finds of giant land tortoises discovered in Bulgaria. Bulletin of Bulgarian Academy of Sciences, 4(56), 2–4.

Böhme M., Ilg A., 2003. fosFARbase, www.wahre–staerke.com/ (6 December 2014)

Bonin, F., Devaux, B., Dupré, A., 2006. Turtles of the World. JHU Press. 416 pp.

Bonis, L. D., Bouvrain, G., Melentis, I., 1977. Les gisements de Vertébrés de la basse Vallée de l'Axios. Scientific Annals of the School of Geology, 17, 203–209.

Bonis, L. D., Bouvrain, G., Koufos, G. D., 1988. Late Miocene mammal localities of the lower Axios valley (Macedonia, Greece) and their stratigraphic significance. Modern Geology, 13, 141–147.

Bory de Saint–Vincent, J., 1833. Vertébrés à sang froid. Reptiles et poissons.: Geoffroy Saint–Hilaire, E., Ed.). Expédition Scientifique de Morée, Vol. 3, Part 1, Atlas, pl. 6.

Bour, R., 1996. Une nouvelle espèce de tortue terrestre dans le Péloponnèse (Grèce). Dumerilia, 2 (1995), 23–54.

Bourgat, R., Bour, R., 1983. La Tortue géante de Perpignan. Société Agricole, Scientifique et Littéraire des Pyrénées–Orientales, 21, 167–177.

Brinkerink, H. P., 1996. Tortoises and turtles from the Pleistocene of Crete. Pleistocene and Holocene Fauna of Crete and Its First Settlers, Monographs in World Archaeology (Ed. D. Reese), 28, 207–209.

Broin, F. de, 1977. Contribution à l'étude des Chéloniens. Chéloniens continentaux du Crétacé et du Tertiaire de France. Mémoires du Muséum National d'Histoire Naturelle, C, 38, I–IX, 1–366.

Broggi, M., 2006. Feuchtgebiete auf Skyros (Nördliche Sporaden–Griechenland)–ihre Beschreibung und einige ornithologische und herpetologische Inselbeobachtungen. Berichtc der Botanisch Zoologischen Gesellschaft Liechtenstein–Sargans¬ Werdenberg, Vaduz, 31, 1–6.

Broggi, M. F., 2007. Herpetological notes on the island of Amorgos (Cyclades, Greece). Herpetozoa, 20, 94–96.

Broggi, M. F., 2012. The Balkan Terrapin *Mauremys rivulata* (Valenciennes, 1833), in the Aegean islands. Threats, conservation aspects and the situation on the island of Kea (Cyclades) as a case study. Herpetozoa, 24, 149–163.

Brunn, J.H., 1956. Contribution à l'étude géologique du Pinde septentrional et d'une partie de la Macédoine occidentale. Annales Géologiques des Pays Helléniques, Athens 7, 1–358.

Chesi, F., 2008. Il registro fossile italiano dei cheloni. Unpublished PhD thesis. Università degli Studi di Firenze, Italy, 178 pp. [in Italian]

Chesi, F., Delfino, M., Abbazzi, L., Carboni, S., Lecca, L., Rook, L., 2007. New fossil vertebrate remains from San Giovanni di Sinis (Late Pleistocene, Sardinia): the last *Mauremys* (Reptilia, Testudines) in the central Mediterranean. Rivista Italiana di Paleontologia e Stratigrafia, 113, 287–297.

Chesi, F., Delfino, M., Rook, L., 2009. Late Miocene *Mauremys* (Testudines, Geoemydidae) from Tuscany (Italy): evidence of terrapin persistence after a mammal turnover. Journal of Paleontology, 83, 379–388.

Claude, J., Tong, H., 2004. Early Eocene testudinoid turtles from Saint–Papoul, France, with comments on the early evolution of modern Testudinoidea. Oryctos 5, 3–45.

Claude J., Tong H., Suteethorn V., 2007. Turtles from the Late Eocene–Early Oligocene of the Krabi Basin (Thailand). Bulletin de la Société Géologique de France, 178, 305–316.

Cope, E. D., 1868. On the Origin of Genera. Proceedings of the Academy of Natural Sciences of Philadelphia, 20, 242–300.

Corsini, J. A., Böhme, M., Joyce, W. G, 2014. Reappraisal of *'Testudo' antiqua* (Testudines, Testudinidae) from the Miocene of Hohenhöwen, Germany. Journal of Paleontology, 88, 948–966.

Crawford, N. G., Parham, J. F., Sellas, A. B., Faircloth, B. C., Glenn, T. C., Papenfuss, T. J., Simison, W. B., 2014. A phylogenomic analysis of turtles. Molecular phylogenetics and evolution, 1-8.

Crégut–Bonnoure, E., Tsoukala, E., 2014. Bovidae and Cervidae of the Early Villafranchian site of Milia (Grevena, Macedonia, Greece). Abstract Book of the VIth International Conference on Mammoths and their Relatives. Scientific Annals, School of Geology, Aristotle University, Special Volume 102, 3, Thessaloniki.

Crumly, C. R, 1982. A cladistic analysis of *Geochelone* using cranial osteology. Journal of Herpetology, 16, 215–234.

Crumly, C. R., 1984. The evolution of land tortoises (Family Testudinidae). Ph.D dissertation. Rutgers University, Newark, 584 pp.

Danilov, I., 2005. Die fossilen Schildkröten Europas, in U Fritz (ed.) Handbuch der Reptilien und Amphibien Europas. Schildkröten (Testudines) II, Cheloniidae, Dermochelyidae, Fossile Schildkröten Europas). Wiebelsheim, Germany, AULA–Verlag, 329–448 pp.

De Bruijn, H., Meulenkamp, J. E., 1972. Late Miocene rodents from the Pandanassa formation (Prov. Rethymnon), Crete, Greece. Proceedings Koninklijke Nederlandse Akademie van Wetenschappen, Series B, 75, 54–60.

De Bruijn, H., Doukas, C. S., van den Hoek Ostende, L. W., Zachariasse, W. J., 2012. New finds of rodents and insectivores from the Upper Miocene at Plakias (Crete, Greece). Swiss Journal of Palaeontology, 131, 61–75.

De Vos, J., 1979. The endemic Pleistocene deer of Crete. Proceedings of the Koninklijke Akademie van Wetenschappen, Series B, 82, 59–90.

De Vos, J., Van der Made, J., Athanassiou, A., Lyras, G., Sondaar, P. Y., Dermitzakis, M. D. 2002. Preliminary note on the late Pliocene fauna from Vatera (Lesvos, Greece). Annales Géologiques des Pays Helléniques, 39, 37–70.

Del Campana, D., 1917. Resti di "*Testudo*" nel Miocene Superiore di Capudjlar presso Salonicco. Bollettino della Società Geologica Italiana, 36, 1–6.

Del Campana, D., 1919. Uova fossili di chelonio nel Miocene Superiore di Capudjlar presso Salonicco. Bollettino della Società Geologica Italiana, 38, 69–78.

Delfino, M., 2002. Erpetofaune Italiane del Neogene e del Quaternario. PhD Thesis, Università degli Studi di Modena e Reggio Emilia, 417pp.

Delfino, M., Chesi, F., Fritz, U., 2009. Shell morphology of the Egyptian tortoise, *Testudo kleinmanni* Lortet, 1883, the osteologically least–known *Testudo* species. Zoological Studies, 48, 850–860.

Delfino, M., Scheyer, T. M., Chesi, F., Fletcher, T., Gemel, R., MacDonald, S., Rabi, M., Salisbury, S. W., 2013. Gross morphology and microstructure of type locality ossicles of

Psephophorus polygonus Meyer, 1847 (Testudines, Dermochelyidae). Geological Magazine, 150, 767–782.

Depéret, C., 1885. Description géologique du Bassin tertiaire du Roussillon. Paris: G. Masson. 254 pp.

Depéret, C., 1890. Sur la découverte d'une Tortue de terre géante au mont Léberon. Comptes Rendus des Séances de l'Académie des Sciences, Paris, 60, 915–917.

Dimaki, M., 2002. Herpetofauna of Rhodes and the rest of the Dodecanese. Island of deer, natural history of the Fallow Deer of Rhodes and of the vertebrates of the Dodecanese (Greece), 63–69.

Dormoy, I., Peyron, O., Combourieu Nebout, N., Goring, S., Kotthoff, U., Magny, M., Pross, J., 2009. Terrestrial climate variability and seasonality changes in the Mediterranean region between 15000 and 4000 years BP deduced from marine pollen records. Climate of the Past, 5, 615–632.

Doukas, C. S., Athanassiou, A., 2003. Review of the Pliocene and Pleistocene Proboscidea (Mammalia) from Greece. Deinsea, 9, 97–110.

Drinia, H., Dermitzakis, M. D., Kouli, K., Tsourou, T., 2002. Sedimentary facies analysis and paleonenvironmental interpretations of Vatera Formation, Lesvos Island, Greece. Annales Géologiques des Pays Helléniques, 34, 15–35.

Dubois, A., Bour, R., 2010. The distinction between family–series and class–series nomina in zoological nomenclature, with emphasis on the nomina created by Batsch (1788, 1789) and on the higher nomenclature of turtles. Bonn Zoological Bulletin, 57, 149–171.

Duméril, A.M. 1805. Zoologie Analytique, ou Méthode Naturelle de Classification des Animaux. Paris: Perronneau, 344 pp.

Ernst, C.H., Barbour, R.W., 1989. Turtles of the World.

Escapa, I. H., Pol, D., 2011. Dealing with incompleteness: new advances for the use of fossils in phylogenetic analysis. Palaios, 26, 121–124.

Estes, R., Hutchison, H. J., 1980. Eocene lower vertebrates from Ellesmere Island, Canadian Arctic Archipelago. Palaeogeography, Palaeoclimatology, Palaeoecology, 30, 325–347.

Fitzinger, L., 1826. Neue Classification der Reptilien, nach ihren Natürlichen Verwandtschaften nebst einer Verwandtschafts– Tafel und einem Verzeichnisse der Reptilien–Sammlung des k.k. Zoologischen Museum zu Wien. Wien: J.G. Hübner Verlagen, 66 pp.

Fitzinger, L., 1843. Systema Reptilium. Fasciculus Primus: Amblyglossae. Vindobonae: Braumuller und Seidel, 106 pp.

Fritz, U., Wischuf, T., 1997. Zur Systematik westasiatisch–südosteuropäischer Bachschildkröten (Gattung *Mauremys*)(Reptilia: Testudines: Bataguridae). Zoologische Abhandlungen–Staatliches Museum fur Tierkunde in Dresden, 49, 223–260.

Fritz, U., Bininda–Emonds, O. R., 2007. When genes meet nomenclature: Tortoise phylogeny and the shifting generic concepts of *Testudo* and *Geochelone*. Zoology, 110, 298–307.

Fritz, U., Široký, P., Kami, H., Wink, M., 2005. Environmentally caused dwarfism or a valid species—Is *Testudo weissingeri* Bour, 1996 a distinct evolutionary lineage? New evidence from mitochondrial and nuclear genomic markers. Molecular Phylogenetics and Evolution, 37, 389–401.

Fritz, U., Auer, M., Bertolero, A., Cheylan, M., Fattizzo, T., Hundsdörfer, A. K., Sampayo, M.M., Pretus, J., Široký, P., Wink, M., 2006. A rangewide phylogeography of Hermann's tortoise, *Testudo hermanni* (Reptilia: Testudines: Testudinidae): implications for taxonomy. Zoologica Scripta, 35, 531–543.

Fritz, U., Guicking, D., Kami, H., Arakelyan, M., Auer, M., Ayaz, D., Fernández, C., Bakiev, A., Celani, A., Džukic, G., Fahd, S., Havaš, P., Joger, U., Khabibullin, V., Mazanaeva, L., Široký, P., Tripepi, S., Vélez, A., Antón, G., Wink, M., 2007a. Mitochondrial phylogeography of European pond turtles (*Emys orbicularis*, *Emys trinacris*)–an update. Amphibia Reptilia, 28, 418–426.

Fritz, U., Hundsdörfer, A.K., Široký, P., Auer, M., Kami, H., Lehmann, J., Mazanaeva, L.F., Türkozan, O., Wink, M., 2007b. Phenotypic plasticity leads to incongruence between morphology–based taxonomy and genetic differentiation in western Palaearctic tortoises (*Testudo graeca* complex; Testudines, Testudinidae). Amphibia– Reptilia, 28, 97–121.

Fritz, U., Ayaz, D., Buschbom, J., Kami, H. G., Mazanaeva, L. F., Aloufi, A. A., Auer, M., Rifai, L., Šilić, T. & Hundsdörfer, A. K., 2008. Go east: phylogeographies of *Mauremys caspica* and *M. rivulata*–discordance of morphology, mitochondrial and nuclear genomic markers and rare hybridization. Journal of Evolutionary Biology, 21, 527–540.

Fritz, U., Harris, J.D., Fahd, S., Rouag, R., Gracià Martinez, E., Giménez Casalduero, A., Široký, P., Kalboussi, M., Jdeidi, T., Hundsdörfer, A.K., 2009. Mitochondrial phylogeography of *Testudo graeca* in the Western Mediterranean: Old complex divergence in North Africa and recent arrival in Europe. Amphibia– Reptilia, 30, 63–80.

Gaffney, E. S., 1972. An illustrated glossary of turtle skull nomenclature. American Museum Novitates, 2486, 1–33.

Gaffney, E. S., Tong, H., Meylan, P. A., 2006. Evolution of the side–necked turtles: the families Bothremydidae, Euraxemydidae, and Araripemydidae. Bulletin of the American Museum of Natural History, 300, 1–698.

Gaffney, E. S., Meylan, P. A., Wood, R. C., Simons, E., Campos, D. A., 2011. Evolution of the side–necked turtles: The family Podocnemididae. Bulletin of the American Museum of Natural History, 350, 1–236.

García, G., Lapparent de Broin, F., de Bonis, L., Koufos, G.D., Valentin, X., Kostopoulos, D., Merceron, G., 2011. A new terrestrial Testudinidae from the Late Miocene hominoid locality ‘‘Ravin de la Pluie’’ (Axios Valley, Macedonia, Greece). In Van der Geer, A., Athanassiou, A. (Eds.), 9th Annual Meeting of the European Association of Vertebrate Palaeontologists, Program and Abstracts. Natural History Museum of Crete, Heraklion, pp. 26–27.

Gardner, J. D., Russell, A. P., 1994. Carapacial variation among soft–shelled turtles (Testudines: Trionychidae), and its relevance to taxonomic and systematic studies of fossil taxa. Neues Jahrbuch fur Geologie und Paläontologie–Abhandlungen, 193, 209–244.

Gaudry, A., 1862a. Résultats des fouilles exécutées en Grèce sous les auspices de l’Académie. Comptes Rendus de l’Académie des Sciences, Paris, 52, 297–300.

Gaudry, A., 1862b. Note sur les débris d’Oiseaux et de Reptiles trouvés à Pikermi, Grèce, suivie de quelques remarques de paléontologie générale. Bulletin de la Societé Géologique de France, 19, 633–635.

Gaudry, A., 1862–1867. Animaux fossiles et geologie de l'Attique. Paris, Savy, 475 pp.

Geer, A. V. D., Lyras, G. A., MacPhee, R. D. E., Lomolino, M. V., Drinia, H., 2014. Mortality in a predator–free insular environment: the dwarf deer of Crete. American Museum Novitates, 3807, 1–26.

Gerlach, J., 2001. Tortoise phylogeny and the ‘*Geochelone*’ problem. Phelsuma, 9 (Suplement A), 1–24.

Georgalis, G., Kear, B., 2013. The fossil turtles of Greece: an overview of taxonomy and distribution. Geobios, 46, 299–311.

Georgalis, G. L., Velitzelos, E., Velitzelos, D. E., Kear, B. P., 2013. *Nostimochelone lampra* gen. et sp. nov., an Enigmatic New Podocnemidoidean Turtle from the Early Miocene of Northern Greece. In Morphology and Evolution of Turtles, Proceedings of the Gaffney Turtle Symposium, (Eds.) D. Brinkman, P. Holroyd, and J. Gardner, 277–287. Dordrecht: Springer.

Gervais, P., 1848–1852. Zoologie et Paléontologie Françaises (Animaux vertébrés). Paris, Bertrand, 271 pp.

Gervais, P., 1859. Zoologie et Paléontologie Françaises. Bertrand, Paris, 544 pp.

Gilbert, S. F., Loredo, G. A., Brukman, A., Burke, A. C., 2001. Morphogenesis of the turtle shell: the development of a novel structure in tetrapod evolution. Evolution & Development, 3, 47–58.

Gmelin, J., 1789. Caroli a Linné, Systema Naturae per regna tria naturae secundum classes, ordines, genera, species, cum characteribus, differentiis, synonymis, locis. Ed. 13. Tom. I. Pars III. Leipzig: G.E. Beer, Ed. 13, 1(3), 1033–1516.

Gmira, S., Broin, F. D. L. D., Geraads, D., Lefèvre, D., Mohib, A., Raynal, J. P., 2013. Les Tortues Du Pliocène d'Ahl al Oughlam (Casablanca, Maroc) et de localités Mio–Pliocènes avoisinantes. Geodiversitas, 35, 691–733.

Goloboff, P. A., Farris, J. S., Nixon, K. C., 2008a. TNT, a free program for phylogenetic analysis. Cladistics, 24, 774–786.

Goloboff, P., Farris, J., Nixon, K., 2008b. TNT: tree analysis using new technology, version 1.1 (Willi Hennig Society Edition). Program and documentation.

Gómez de Soler, B., Vall–Llosera, G. C., Van der Made, J., Oms, O., Agustí, J., Sala, R., Blain, H. A., Burjachs, F., Claude, J., García Catalán, S., Riba, D., Rosillo, R., 2012. A new key locality for the Pliocene vertebrate record of Europe: the Camp dels Ninots maar (NE Spain). Geologica Acta, 10, 1–17.

Gould, G. C., & McFadden, B. J., 2004. Gigantism, Dwarfism, and Cope's Rule: "Nothing in Evolution Makes Sense without a Phylogeny". Bulletin of the American Museum of Natural History, 285, 219–237.

Gray, J.E., 1825. A synopsis of the genera of reptiles and amphibia, with a description of some new species. Annals of Philosophy, 26, 193–217.

Gray, J.E., 1869. Description of *Mauremys laniaria*, a new freshwater tortoise. Proceedings of the Zoological Society of London, 1869, 499–500.

Grillitch, H., Tiedemann, F., 1984. Zur Herpetofauna der griechischen Inseln Kea, Spanopoula, Kith–nos, Sifnos, Kitriani (Cycladen), Alonissos und Piperi (Nördliche Sporaden). Annalen der Naturhistorischen Museum in Wien, 86, 7–28.

Guérin, C., Tsoukala, E., 2013. The Tapiridae, Rhinocerotidae and Suidae (Mammalia) of the Early Villafranchian site of Milia (Grevena, Macedonia, Greece). Geodiversitas, 35, 447–489.

Hammer, Ø., Harper, D. A. T., Ryan, P. D., 2001. PAST: Paleontological Statistics Software Package for education and data analysis. Palaeontolia Electronica, 4, 1–9.

Harrison, T., 2011. Tortoises (Chelonii, Testudinidae). Paleontology and Geology of Laetoli: Human Evolution in Context (pp. 479–503). Springer Netherlands.

Harvati, K., Darlas, A., Bailey, S. E., Rein, T. R., El Zaatari, S., Fiorenza, L., Kullmer, O., Psathi, E., 2013. New Neanderthal remains from Mani peninsula, Southern Greece: The Kalamakia Middle Paleolithic cave site. Journal of Human Evolution, 64(6), 486–499.

Hernández–Pacheco, E., 1917. Hallazgo de tortugas gigantes en el Mioceno de Alcalá de Henares. Boletín de la Real Sociedad Española de Historia Natural, 17, 194–202.

Hervet, S., 2003. Le groupe "*Palaeochelys* sensu lato–*Mauremys*" dans le contexte systématique des Testudinoidea aquatiques du Tertiaire d'Europe occidentale: Apports à la biostratigraphie et à la paléobiogéographie (Doctoral dissertation, Paris, Muséum National d'Histoire Naturelle).

Hervet, S., 2004. Systématique du groupe «*Palaeochelys* sensu lato–*Mauremys*» (Chelonii, Testudinoidea) du Tertiaire d'Europe occidentale: principaux résultats. Annales de Paléontologie, 90, 13–78.

Hirasawa, T., Nagashima, H., Kuratani, S., 2013. The endoskeletal origin of the turtle carapace. Nature communications, 4, 1–7, doi:10.1038.

Hirsch, K. F., 1996. Parataxonomic classification of fossil chelonian and gecko eggs. Journal of Vertebrate Paleontology, 16, 752–762.

Hirsch, K.F., Lopez–Jurado, L.F., 1987. Pliocene chelonian fossil eggs from Gran Canaria, Canary islands. Journal of Vertebrate Paleontology, 7, 96–99.

Hofstra, J., 2008. An addition to the herpetofauna of the Greek island Lesbos. Podarcris, 9, 1–10.

Holroyd, P. A., Hutchison, J. H., Strait, S. G, 2001. Turtle diversity and abundance through the lower Eocene Willwood Formation of the southern Bighorn Basin. University of Michigan Papers on Paleontology, 33, 97–107.

Hooijer, D. A., 1971. Giant Land Tortoise, *Geochelone atlas* (Falconer & Cautley), from Pleistocene of Timor. Proceedings Of The Koninklijke Nederlandse Akademie van Wetenschappen Series B–Physical Sciences, 74, 504–517.

Itescu, Y., Karraker, N. E., Raia, P., Pritchard, P. C., Meiri, S., 2014. Is the island rule general? Turtles disagree. Global Ecology and Biogeography, 23, 689–700.

Iverson, J. B., 1992. A Checklist with Distribution Maps of the Turtles of the World. Richmond, 363 pp.

Joyce, W., Bell, D., 2004. A review of the comparative morphology of extant testudinoid turtles (Reptilia: Testudines). Asiatic Herpetological Research, 10, 53–109.

Joyce, W., Gauthier, J., 2004. Palaeoecology of Triassic stem turtles sheds new light on turtle origins. Proceedings of Royal Society of London B, 271, 1–5.

Joyce, W. G., Parham, J. F., Gauthier, J. A., 2004. Developing a protocol for the conversion of rank–based taxon names to phylogenetically defined clade names, as exemplified by turtles. Journal of Paleontology, 78, 989–1013.

Konidaris, G. E., Roussiakis, S. J., Theodorou, G. E., Koufos, G. D., 2014. The Eurasian occurrence of the shovel–tusker *Konobelodon* (Mammalia, Proboscidea) as illuminated by its presence in the Late Miocene of Pikermi (Greece). Journal of Vertebrate Paleontology, 34, 1437–1453.

Kostopoulos, D. S., Koufos, G. D., Sylvestrou, I. A., Syrides, G. E., Tsompachidou, E., 2009. The Late Miocene Mammal Faunas of the Mytilinii Basin, Samos Island, Greece: New Collection. 2. Lithostratigraphy and Fossiliferous Sites. Beiträge zur Paläontologie, 31, 13–26.

Kotsakis, T., 1977. I resti di anfibi e rettili pleistocenici della grotta "Bate" (Rethymnon, Creta). Rendivoti dell' Accademia Nazionale dei Lincei, serie 8(63), 571–582.

Koufos, G. D., 2006a. The Neogene mammal localities of Greece: Faunas, chronology and biostratigraphy. Hellenic Journal of Geosciences, 41(1), 183–214.

Koufos, G. D., 2006b. The large mammals from the Miocene/Pliocene locality of Silata, Macedonia, Greece with implications about the latest Miocene palaeoecology. Beitrage zur Paläontologie, 30, 293–313.

Koufos, G. D., 2009. The Late Miocene Mammal Faunas of the Mytilinii Basin, Samos Island, Greece: New Collection. 1. History of the Samos Fossil Mammals. Beiträge zur Paläontologie, 31, 1–12.

Koufos, G.D., Pavlides, S.B., 1988. Correlation between the continental deposits of the lower Axios valley and Ptolemais basin. Bulletin of Geological Society of Greece, 20(2), 9–19.

Koufos, G. Tsoukala, E., 2007. Petralona Cave. Editions Aristotle University, Thessaloniki, 134 pp.

Koufos, G., Syrides, G., Koliadimou, K., 1991. A Pliocene primate from Macedonia (Greece). Journal of Human Evolution, 21, 283–294.

Koufos, G. D., de Bonis, L., Sen, S., 1995. *Lophocyon paraskevaidisi*, a new viverrid (Carnivora, Mammalia) from the Middle Miocene of Chios island, Greece. Geobios, 28(4), 511-523.

Koufos, G. D., Kostopoulos, D. S., Vlachou, D., 2009. The Late Miocene Mammal Faunas of the Mytilinii Basin, Samos Island, Greece: New Collection. 16. Chronology. Beiträge zur Paläontologie, 31, 397–408.

Kretzoi, M., 1977. The fauna of small vertebrates of the Middle Pleistocene at Petralona. Anthropos, 4, 131–143.

Kretzoi, M., Poulianos, N. A., 1981. Remarks on the Middle and Lower Pleistocene Vertebrate Fauna in the Petralona Cave. The Third European Congress of Anthropology. Anthropos, 8, 57–72.

Kuratani, S., Kuraku, S., Nagashima, H., 2011. Evolutionary developmental perspective for the origin of turtles: the folding theory for the shell based on the developmental nature of the carapacial ridge. Evolution & Development, 13, 1–14.

Kurtén, B., Poulianos, A. N., 1977. New stratigraphic and faunal material from Petralona Cave, with special reference to the Carnivora. Anthropos, 4, 47–130.

Kuss, S. E., 1970. Abfolge nud Alter der Pleistozanen Sangetierfannen der Insel Kreta. Berichte Naturforschemte Gesellschaft zu Freiburg i. Br., 60, 35–81.

Kuss, S. E., 1973. Die pleistozänen Säugetierfaunen der ostmediterranen Inseln. Ihr Alter und ihre Herkunft. Berichte Naturforschemte Gesellschaft zu Freiburg i. Br., 63, 49–71.

Lapparent de Broin, F. de, 2000. African chelonians from the Jurassic to the Present: phases of development and Preliminary catalogue of the fossil record. Palaeontologia Africana, 36, 43–82.

Lapparent de Broin, F. de, 2001. The European turtle fauna from the Triassic to the Present. Dumerilia, 4(3), 155–217.

Lapparent de Broin, F. de, 2002. A giant tortoise from the Late Pliocene of Lesvos Island (Greece) and its possible relationships. Annales Géologiques des Pays Helléniques, 34, 99–130.

Lapparent de Broin, F. de, 2003. Miocene chelonians from southern Namibia. Memoir of the Geological Survey of Namibia, 19, 67–102.

Lapparent de Broin, F. de., 2008. Miocene chelonians from south–western Namibia. Memoir of the Geological Survey of Namibia, 20, 107–145.

Lapparent de Broin, F. de, van Dijk, P.P., 1999. Chelonia from the Late Miocene Baynunah Formation, Emirate of Abu Dhabi, United Arab Emirates: palaeogeographic implications; pp. 136–162 in P. J. Whybrow and A. Hill (eds), Fossil Vertebrates of Arabia. Yale University Press, New Haven and London.

Lapparent de Broin, F. de, Murelaga, X., 1999. Turtles from the upper cretaceous of Laño (Iberian peninsula). Estudios del Museo de Ciencias Naturales de Alava, 14, 135–211.

Lapparent de Broin, F., Bour, R., Parham, J. F., Perälä, J., 2006a. Eurotestudo, a new genus for the species *Testudo hermanni* Gmelin, 1789 (Chelonii, Testudinidae). Comptes Rendus Palevol, 5, 803–811.

Lapparent de Broin, F., Bour, R., Perälä, J., 2006b. Morphological definition of *Eurotestudo* (Testudinidae, Chelonii): First part. Annales de Paléontologie, 92, 255–304.

Lapparent de Broin, F. D., Bour, R., Perälä, J., 2006c. Morphological definition of *Eurotestudo* (Testudinidae, Chelonii): second part. Annales de Paléontologie, 92, 325–357.

Lazaridis, G., Tsoukala, E., 2014a. *Hipparion phlegrae*, sp. nov. (Mammalia, Perissodactyla): a new species from the Turolian locality of Kryopigi (Kassandra, Chalkidiki, Greece). Journal of Vertebrate Paleontology, 34(1), 164–178.

Lazaridis, G., Tsoukala, E., 2014b. Short note on the Equidae of the Early Villafranchian site of Milia (Grevena, Macedonia, Greece). Abstract Book of the VIth International Conference on Mammoths and their Relatives. Scientific Annals, School of Geology, Aristotle University, Special Volume, 102, 8.

Le, M., Raxworthy, C. J., McCord, W. P., Mertz, L., 2006. A molecular phylogeny of tortoises (Testudines: Testudinidae) based on mitochondrial and nuclear genes. Molecular Phylogenetics and Evolution, 40, 517–531.

Lenk, P., Fritz, U., Joger, U., Wink, M., 1999. Mitochondrial phylogeography of the European pond turtle, *Emys orbicularis* (Linnaeus, 1758). Molecular Ecology, 8, 1911–1922.

Linnaeus, C., 1758. Systema Naturae, per Regna Tria Naturae, secundum Classes, Ordines, Genera, Species, cum Characteribus, Differentiis, Synonymis, Locis. Tomus I. Editio Decima, Reformata. [10th Ed.]. Holmiae [Stockholm]: Laurentii Salvii, 824 pp.

Lortet, L., 1883. Poissons et reptiles du lac de Tibériade et de quelques autres parties de la Syrie. Archives du Muséum d'Histoire Naturelle de Lyon, 3, 99–194.

Lourenço, J. M., Claude, J., Galtier, N., Chiari, Y., 2012. Dating cryptodiran nodes: origin and diversification of the turtle superfamily Testudinoidea. Molecular Phylogenetics and Evolution, 62(1), 496–507.

Luján, À. H., Alba, D. M., Fortuny, J., Carmona, R., Delfino, M., 2014. First cranial remains of *Cheirogaster richardi* (Testudines: Testudinidae) from the Late Miocene of Ecoparc de Can Mata (Vallès–Penedès Basin, NE Iberian Peninsula): taxonomic and phylogenetic implications. Journal of Systematic Palaeontology, 12, 833–864.

Lyras, G. A., van der Geer, A. A., 2007. The Late Pliocene vertebrate fauna of Vatera (Lesvos Island, Greece). Cranium, 24, 11–24.

Lyson, T. R., Bever, G. S., Bhullar, B. A. S., Joyce, W. G., Gauthier, J. A., 2010. Transitional fossils and the origin of turtles. Biology Letters, rsbl20100371, 1, 1–4.

Lyson, T. R., Bever, G. S., Scheyer, T. M., Hsiang, A. Y., Gauthier, J. A., 2013. Evolutionary origin of the turtle shell. Current Biology, 23, 1113–1119.

Maddison, W. P., Maddison, D., 2001. Mesquite: a modular system for evolutionary analysis.

Makris, Ch., 1969. The Cave "Gerani", Rethymnon. Bulletin of the Speleological Society of Greece, 10 (3–4), 95–101. [in Greek]

Malatesta, A., Angelelli, F., Caloi, L., Kotsakis, T., 1980. Dwarf deer and other Late Pleistocene fauna of the Simonelli cave in Crete. Quaderni dell'Accademia Nazionale dei Lincei, 209, 122 pp.

Mantziou, G., Poulakakis, N., Lymberakis, P., Valakos, E., Mylonas, M., 2004. The inter–and intraspecific status of Aegean *Mauremys rivulata* (Chelonia, Bataguridae) as inferred by mitochondrial DNA sequences. Herpetological journal, 14, 35–46.

Mayhew, D. F., 1977. Endemic Pleistocene Murids of Crete. Proceedings of the Koninklijke Nederlandse Akademie van Wetenschappen Series B, 80, 1–204.

Mein, P., 1989. Updating of MN zones. In European Neogene Mammal Chronology (pp. 73-90). Springer US.

Melentis, J. K., 1966. *Clemmys caspica* aus dem Pleistozän des Beckens von Megalopolis im Peloponnes (Griechenland). Annales Géologiques des Pays Helléniques, 17, 169–181.

Melentis, J. K., 1968. Palaeontological excavations at Samos Island, a preliminary report. Praktika Akadimias Athinon, 43, 344–349.

Melentis, J. K., 1970a. Die Pikermifauna von Halmyropotamos (Euböa, Griechenland)–1. Teil: Odontologie und Kraniologie. Annales Géologiques des Pays Helléniques, 21, 217–306.

Melentis, J. K., 1970b. Die Pikermifauna von Halmyropotamos (Euböa, Griechenland)–2. Teil: Osteologie. Annales Géologiques des Pays Helléniques, 19, 285–411.

Melentis, J. K., Tobien, H., 1967. Paläontologische Ausgrabungen auf der Insel Chios (eine vorläufige Mitteilung). Praktika Akademias Athenon, 42, 147–152.

Meulenkamp, J. E., de Mulder, E. F., van de Weerd, A., 1972. Sedimentary history and paleogeography of the late Cenozoic of the island of Rhodos. Zeitschrift der Deutschen Geologischen Gesellschaft, 123, 541–553.

Meylan, P.A., 1987. The phylogenetic relationships of soft-shelled turtles (family Trionychidae). Bulletin of the AMNH; v. 186, article 1.

Meylan, P.A., 2006. Introduction to the Softshell Turtles: Family Trionychidae. Chelonian Research Monographs, 3, 158–159.

Meylan, P.A., Sterrer, W., 2000. *Hesperotestudo* (Testudines: Testudinidae) from the Pleistocene of Bermuda, with comments on the phylogenetic position of the genus. Zoological Journal of the Linnean Society, 128, 51–76.

Michailidis, D., Mitsopoulou, V., Roussiakis, S., Theodorou, G., 2014. The taphonomic study of Charkadio Cave, Tilos Island. Evidence from elephant and avian remains. Abstract Book of the VIth International Conference on Mammoths and their Relatives. Scientific Annals, School of Geology, Aristotle University, Special Volume, 102, 129.

Miller, J.F., 1779. Icones animalium et plantarum. London. Letterpress, 10 pp.

Mlynarski, M., 1966. Morphology of the shell of *Agrionemys horsfieldii* (Gray, 1844)(Testudines, Reptilia). Acta Biologica Cracoviensia, 9, 219–223.

Mlynarski, M., 1976. Handbuch der Paläoherpetologie. Part 7, Testudines. Gustav Fischer, Stuttgart, 130 pp.

Moen, D. S., 2006. Cope's rule in cryptodiran turtles: do the body sizes of extant species reflect a trend of phyletic size increase? Journal of Evolutionary Biology, 19, 1210–1221.

Mojsisovics, A., 1889. Zoogeographische Notizen über Süd–Ungarn aus den Jahren 1886–1888. III. Nachtrag zur “Fauna von Béllye und Darda”. Mitteilungen des Naturwissenschaftlichen Vereines für Steiermark, Graz 25(1888)[1889], 233–269.

Morales Pérez, J. V., Serra, A. S., 2009. The Quaternary fossil record of the genus *Testudo* in the Iberian Peninsula. Archaeological implications and diachronic distribution in the western Mediterranean. Journal of Archaeological Science, 36, 1152–1162.

Mueller–Töwe, I. J., Kjeldahl–Vallon, T. A., Milàn, J., Vallon, L. H., Theodorou, G., Lindgren, J., Roussiakis, S., Bromley, R. G., 2011. First chelonian eggs and carapace fragments from the Pliocene of Rhodes, Greece. Neues Jahrbuch für Geologie und Paläontologie–Abhandlungen, 262, 309–322.

Nicholas, P., 1978. New deposit of vertebrates in Chersonian–West Kutchuk–Tchekmedje (Turkish Thrace). Comptes Rendus Hebdomadaires des Seances de l’Academie des Sciences, Serie D, 287, 455–458.

N.I.G.M.R., 1974. Geological map, Krinidhes sheet, 1:50.000. Mapping by P. Kronberg, during 1962–1970.

Oppel, M., 1811. Die Ordnungen, Familien und Gattungen der Reptilien als Prodrom einer Naturgeschichte derselben. München: J. Lindauer, 86 pp.

Pafilis, P., 2010. A brief history of Greek herpetology. Bonn Zoological Bulletin, 57, 329–345.

Pallas, P., 1814. Zoographia Rosso–Asiatica. III. Animalia Monocardia seu Frigidi Sanguinis Imperii Rosso–Asiatici. Petropolis: Officina Caes. Academiae Scientiarum, 428 pp.

Pantanelli, D., 1893a. *Testudo amiatae* sp. n. Atti della Società Toscana di Scienze Naturali, Memorie, 12, 128–138.

Pantanelli, D., 1893b. Ulteriori notizie sul giacimento della *Testudo amiatae* Pant. Atti della Società Toscana di Scienze Naturali, Processi Verbali, 8, 90–91.

Paraskevaidis, I., 1955. Zwei schildkrötenreste aus dem obermiozän von Chios. Annales Géologiques des Pays Helléniques, 6, 133–141.

Paraskevaidis, I., 1961. Neue Funde Quartärer Wirbeltierreste in Attika. Annales Géologiques des Pays Helléniques, 12, 149–152, Athens.

Parham, J. F., Macey, J. R., Papenfuss, T. J., Feldman, C. R., Türkozan, O., Polymeni, R., Boore, J., 2006. The phylogeny of Mediterranean tortoises and their close relatives based on complete mitochondrial genome sequences from museum specimens. Molecular Phylogenetics and Evolution, 38, 50–64.

Parham J.F., Donoghue P.C.J., Bell C.J., Calway T.D., Head J.J., Holroyd, P.A., Inoue J.G., Irmis R.B., Joyce W.G., Ksepka D.T., Patané J.S.L., Smith N.D., Tarver J.E., van Tuinen M., Yang Z., Angielczyk K.D., Greenwood J.M., Hipsley C.A., Jacobs L., Makovicky P.J., Müller J., Smith K.T., Theodor J.M., Warnock R.C.M., Benton M.J., 2012. Best practices for justifying fossil calibrations. Systematic Biology, 61, 346–359.

Pašic, M., Klinčarski, V. 1954. Nalazak fosilne kornjače u sedimentima gornjeg eocena okoline Štipa (Makedonija). Kolektivi rad članova Geol. Institute Srp. Akad. Nauka, 61–72.

Perälä, J., 2001. Morphological variation among Middle Eastern *Testudo graeca* L., 1758 (sensu lato), with a focus on taxonomy. Chelonii, 3, 78–108.

Pérez–García, A., 2012. Las tortugas mesozoicas de la Península Ibérica. Doctoral dissertation, PhD thesis. Universidad Complutense de Madrid, Spain.

Pérez–García, A., Murelaga, X., 2013. Las tortugas del Vallesiense Superior del Cerro de los Batallones (Madrid, España): nuevos datos sobre el escasamente conocido género *Paleotestudo*. Ameghiniana, 50, 335–353.

Pérez–García, A., Vlachos, E., 2014. New generic proposal for the European Neogene large testudinids (Cryptodira) and the first phylogenetic hypothesis for the medium and large representatives of the European Cenozoic record. Zoological Journal of the Linnean Society, 172, 653–719.

Petrochilou, A., 1980. The Cave "Gerani" of Rethymnon, Crete. Bulletin of the Speleological Society of Greece, 17 (1), 51–58. [in Greek]

Petrochilou, A., 1981. The Cave "Zourida" of Rethymnon, Crete. Bulletin of the Speleological Society of Greece, 18 (1–2), 418–426. [in Greek]

Peyer, B., 1946. Fossile Riesenschildkröten aus der oberen Süsswassermolasse der Umgebung von Zurich. Abhandlungen der Schweizerischen Paläontologischen Gesellschaft, 63, 1–47.

Pictet, F. J., Humbert, A., 1856. Monographie des chéloniens de la mollasse suisse. J. Kessmann.

Poulakakis, N., Mylonas, M., Lymberakis, P., Fassoulas, C., 2002. Origin and taxonomy of the fossil elephants of the island of Crete (Greece): problems and perspectives. Palaeogeography, Palaeoclimatology, Palaeoecology, 186, 163–183.

Poulakakis, N., Lymberakis, P., Fassoulas, C., 2005. *Deinotherium giganteum* (Proboscidea, Deinotheriidae) from the Late Miocene of Crete. Journal of Vertebrate Paleontology, 25, 732–736.

Plummer, M. V., Krementz, D. G., Powell, L. A., Mills, N. E., 2008. Effects of habitat disturbance on survival rates of softshell turtles (*Apalone spinifera*) in an urban stream. Journal of Herpetology, 42, 555–563.

Pol, D., Norell, M. A., 2001. Comments on the Manhattan stratigraphic measure. Cladistics, 17(3), 285–289.

Pol, D., Norell, M. A., 2006. Uncertainty in the age of fossils and the stratigraphic fit to phylogenies. Systematic Biology, 55, 512–521.

Pol, D., & Escapa, I. H., 2009. Unstable taxa in cladistic analysis: identification and the assessment of relevant characters. Cladistics, 25, 515–527.

Popov, S. V., Shcherba, I. G., Ilyina, L. B., Nevesskaya, L. A., Paramonova, N. P., Khondkarian, S. O., & Magyar, I., 2006. Late Miocene to Pliocene palaeogeography of the Paratethys and its relation to the Mediterranean. Palaeogeography, Palaeoclimatology, Palaeoecology, 238(1), 91–106.

Rabeder, G., Tsoukala, E., 1990. Morphodynamic analysis of some cave–bear teeth from Petralona cave (Chalkidiki, North–Greece). Beiträge zur Paläontologie von Österreich, 16, 103–109.

Rafinesque, C., 1815. Analyse de la Nature ou Tableau de l'Univers et des Corps Organisés. Palermo: 223 pp.

Rauscher, K. L., 1995. Die herpetofauna der Vraona–Hoehle (Attika) in Griechenland. Annales Géologiques des Pays Helléniques, 36, 39–41.

Razzetti, E., Bader, T., Bilek, K., Delfino, M., Di Cerbo, A. R., Duda, M., Hill, J., 2006. A contribution to the knowledge of the herpetofauna of the Greek island of Corfu. Societas Herpetologica Italica: Atti del V Congresso Nazionale, Calci (Pisa), 29, 207–216.

Ree, R. H., Smith, S. A., 2008. Maximum likelihood inference of geographic range evolution by dispersal, local extinction, and cladogenesis. Systematic Biology, 57, 4–14.

Reese, D.S., Belluomini, G., Ikeya, M., 1996. Absolute dates for the Pleistocene fauna of Crete. In D.S. Reese (editor), Pleistocene and Holocene fauna of Crete and its first settlers. Monographs in World Archaeology, 28, 47–51. Madison WI: Prehistory Press.

Reynoso, V. H., Montellano–Ballesteros, M., 2004. A new giant turtle of the genus *Gopherus* (Chelonia: Testudinidae) from the Pleistocene of Tamaulipas, Mexico, and a review of the phylogeny and biogeography of gopher tortoises. Journal of Vertebrate Paleontology, 24(4), 822–837.

Rögl, F., 1999. Mediterranean and Paratethys. Facts and hypotheses of an Oligocene to Miocene paleogeography (short overview). Geologica Carpathica, 50, 339–349.

Rook, L., Croitor, R., Delfino, M., Ferretti, M. P., Gallai, G., & Pavia, M., 2013. The Upper Valdarno Plio-Pleistocene vertebrate record: an historical overview, with notes on palaeobiology and stratigraphic significance of some important taxa. Italian Journal of Geosciences, 132, 104–125.

Rovereto, C., 1914. Los Estratos Araucanos y sus fósiles. Anales del Museo de Historia Natural Buenos Aires, 25, 1–24.

Savoyat E., Monopolis, D., 1972. Geological Map 1: 50.000. Grevena Sheet, Institute of Geological Survey and Research (I.G.S.R.).

Scheyer, T., 2007. Comparative Bone Histology of the Turtle Shell (carapace and plastron) Morphology and Turtle Origins: Implications for Turtle Systematics, Functional Morphology and Turtle Origins. PhD Thesis.

Scheyer, T. M., Sander, P. M., 2004. Histology of ankylosaur osteoderms: implications for systematics and function. Journal of Vertebrate Paleontology, 24, 874–893.

Scheyer, T. M., Sander, P., Joyce, W. G., Böhme, W., Witzel, U., 2007. A plywood structure in the shell of fossil and living soft–shelled turtles (Trionychidae) and its evolutionary implications. Organisms Diversity & Evolution, 7, 136–144.

Scheyer, T. M., Mörs, T., Einarsson, E., 2012. First record of soft–shelled turtles (Cryptodira, Trionychidae) from the Late Cretaceous of Europe. Journal of Vertebrate Paleontology, 32, 1027–1032.

Schleich, H., 1981. Jungtertiäre Schildkröten Süddeutschlands unter besonderer Berücksichtigung der Fundstelle Sandelzhauzen. Courier Forschunginstitut Senckenberg, 48, 1–372.

Schleich, H., 1982. *Testudo marginata* Schoepff aus plio/pleistozänen ablagerungen SE–Lakoniens (Peloponnes, Griechenland). Paläontologische Zeitschrift, 56(3), 259–264.

Schmidt–Kittler, N., (Ed.) 1995. The vertebrate locality Maramena (Macedonia, Greece) at the Turolian–Ruscinian boundary (Neogene). Pfeil., 185 pp.

Schoepff, J., 1793. Historia Testudinum Iconibus Illustrata. Erlangae: Ioannis Iacobi Palm, 136 pp. [Fasciculus III and IV:33–80, pls. 11–16, 17B–20].

Sen, S., Koufos, G. D., Kondopoulou, D., De Bonis, L. D., 2000. Magnetostratigraphy of late Miocene continental deposits of the Lower Axios valley, Macedonia, Greece. Bulletin of the Geological Society of Greece, 9, 197–206.

Sillero, N., Campos, J., Bonardi, A., Corti, C., Creemers, R., Crochet, P. A., Isailović, J., Denoël, M., Ficetola, G., Gonçalves, J., Kuzmin, S., Lymberakis, P., de Pous, P. Rodríguez, A., Sindaco, R., Speybroeck, J., Toxopeus, B., Vieites, B., Vences, M., 2014. Updated distribution and biogeography of amphibians and reptiles of Europe. Amphibia-Reptilia, 35, 1-31.

Simpson, G. G., 1942. A Miocene tortoise from Patagonia. American Museum Novitates, 1209, 1–6.

Sommer, R. S., Persson, A., Wieseke, N., Fritz, U., 2007. Holocene recolonization and extinction of the pond turtle, *Emys orbicularis* (L., 1758), in Europe. Quaternary Science Reviews, 26(25), 3099–3107.

Sondaar, P.Y., Van der Geer, A.A.E. 2005. Evolution and Extinction of Plio-Pleistocene Island Ungulates. In: E. Crégut-Bonnoure (ed.). Les ongulés holarctiques du Pliocène et du Pléistocene. Quaternaire, International Journal of the French, Quaternary Association, hors-série 2005, 2: 241-256. Paris: Maison de la Géologie

Spinks, P.Q., Bradley Shaffer, H., Iverson, J.B., McCord, W.P., 2004. Phylogenetic hypotheses for the turtle family Geoemydidae. Molecular Phylogenetics and Evolution, 32, 164–182.

Staesche, K., Karl, H. V., Staesche, U., 2007. Fossile Schildkröten aus der Türkei. In Staesche U, Ed.), Fossile Schildkröten aus drei Kontinenten, Geologisches Jahrbuch, 98, 91–149.

Starkovich, B. M., 2012. Densification of small game resources at Klissoura Cave 1 (Peloponnese, Greece) from the Middle Paleolithic to Mesolithic. Quaternary International, 264, 17–31.

Steinhauser, G., Hujer, W., Sterba, J. H., Seemann, R., Bichler, M., Symeonidis, N., 2008. On strontium and barium anomalies in the sediments of Charkadio Cave (Tilos Island, Dodekanese, Greece). Journal of Radioanalytical and Nuclear Chemistry, 276, 167–173.

Stevanovic, P., 1961. Beitrag kenntnis der kaspibrackinschen Pontischen molluskenfauna aus Griechenland und deren stratigraphische bedeutung. GLA Academie Serbe Sciences Arts CCXLIX, 22, 67–102.

Stiner, M. C., Munro, N. D., 2011. On the evolution of diet and landscape during the Upper Paleolithic through Mesolithic at Franchthi Cave (Peloponnese, Greece). Journal of Human Evolution, 60, 618–636.

Stojanov, A., 2009. Erster Nachweis einer Riesenlandschildkröte (*Geochelone* s.l. Gray, 1872) aus Bulgarien. Revue de Paléobiologie, 28, 457–470.

Stringer, C. B., Howell, F. C., Melentis, J. K., 1979. The significance of the fossil hominid skull from Petralona, Greece. Journal of Archaeological Science, 6, 235–253.

Symeonidis, N., Rabeder, G. (Eds.) 1993–1995. Das Jungpleistozän in der «Höhle» von Vraona auf Attica in Griechenland. Annales Géologiques des Pays Helléniques, 36, 1–109.

Syrides, G. E., 1990. Lithostratigraphic, biostratigraphic and palaeogeographic study of the Neogene–Quaternary sedimentary deposits of Chalkidiki Peninsula, Macedonia, Greece. Ph.D. thesis, Aristotle University of Thessaloniki, School of Geology, Scientific Annals 1(11), 243 pp.

Szalai, T., 1931. *Testudo schafferi* nov. sp. eine Riesenschildkröte aus dem Pliozän von Samos. Annalen des Naturhistorischen Museums im Wien, 46, 153–163.

Takahashi, A., Otsuka, H., Hirayama, R., 2003. A new species of the genus *Manouria* (Testudines: Testudinidae) from the Upper Pleistocene of the Ryukyu Islands, Japan. Paleontological Research, 7(3), 195–217.

Takahashi, A., Ōki, K., Ishido, T., & Hirayama, R., 2013. A new species of the genus *Ocadia* (Testudines: Geoemydidae) from the middle Miocene of Tanegashima Island, southwestern Japan and its paleogeographic implications. Zootaxa, 3647, 527–540.

Taskavak, E., Akcinar, S. C., 2009. Marine records of the Nile soft–shelled turtle, *Trionyx triunguis* from Turkey. Marine Biodiversity Records, 2, e9.

Taskavak, E., Reimann, M.J., Polder, W.N., 1999. First record of *Trionyx triunguis* from Kos Island, Greece with comments on its occurrence in the eastern Mediterranean. Chelonian Conservation and Biology, 3, 510–512.

Theobald, W., 1868. Catalogue of Reptiles in the Museum of the Asiatic Society of Bengal. Journal of the Asiatic Society, Extra Number, 88 pp.

Theodorou, G., 1983. The fossil dwarf elephants of Charkadio Cave at Insel Tilos. PhD thesis, 232 pp.

Theodorou, G. E., Symeonidis, N., Stathopoulou, E., 2007. *Elephas tiliensis* n. sp. from Tilos Island (Dodecanese, Greece). Hellenic Journal of Geosciences, 42, 19–32.

Theodorou, G. E., Roussiakis, S. J., Athanassiou, A., & Filippidi, A., 2010. Mammalian remains from a new site near the classical locality of Pikermi (Attica, Greece). Scientific Annals, School of Geology, Aristotle University of Thessaloniki, 99, 09–119.

Tóth, T., Krecsák, L., Madsen, T., Újvári, B., 2002. Herpetofaunal locality records on the Greek Island of Corfu. Herpetozoa, 15, 149–169.

Tsoukala, E., 1989. Contribution to the study of the Pleistocene fauna of large mammals (Carnivora, Perissodactyla, Artiodactyla) from Petralona Cave, Chalkidiki (N. Greece). PhD thesis. Aristotle University of Thessaloniki, School of Geology, Scientific Annals 1, 1–360.

Tsoukala, E., 1990. Contribution to the study of the Pleistocene fauna of large mammals (Carnivora, Perissodactyla, Artiodactyla) from Petralona Cave, Chalkidiki (N. Greece). Preliminary report. Comptes Rendus hebdomadaires des Séances de l'Académie des Sciences de Paris (2) 312, 331–336.

Tsoukala, E., 1991. A *Coelodonta antiquitatis praecursor* GUERIN (Mammalia, Rhinocerotidae, zone 24) from the lower Axios valley deposits (Gephyra, Macedonia, N. Greece). Bulletin Geological Society of Greece, 25, 473–485.

Tsoukala, E., 1992. Quaternary faunas of Greece. Courier Forschungsinstitut Senckenberg, 153, 79–92.

Tsoukala, E., 2000. Remains of a Pliocene *Mammut borsoni* (Hays, 1834)(Proboscidea, Mammalia), from Milia (Grevena, W. Macedonia, Greece). Annales de Paléontologie, 86, 165–191.

Tsoukala, E., 2005. Paleontological research in Grevena Proboscideans through time–gigantism–the longest tusks? In: Short papers and Abstracts, Agenbroad, L.D. and Symington, R.L. (Eds.), 2nd World of Elephants Congress, Mammoth Site of Hot Springs, South Dakota.

Tsoukala, E., Bartsiokas, A., 2008. New *Mesopithecus pentelicus* specimens from Kryopigi, Macedonia, Greece. Journal of Human Evolution, 54, 448–451.

Tsoukala, E., Mol, D., in press. The Proboscidea of the Early Villafranchian site of Milia (Grevena, Macedonia, Greece). Quaternary International, 22 pp.

Tsoukala, E., Mol, D., Pappa, S., Vlachos, E., van Logchem, W., Vaxevanopoulos, M., Reumer, J., 2011. *Elephas antiquus* in Greece: New finds and a reappraisal of older material (Mammalia, Proboscidea, Elephantidae). Quaternary International, 245(2), 339–349.

Tsoukala, E., van Logchem, W., Lazaridis, G., Mol, D., 2014. Carnivores of the Early Villafranchian site of Milia (Grevena, Macedonia, Greece). Abstract Book of the VIth International Conference on Mammoths and their Relatives. Scientific Annals, School of Geology, Aristotle University, Special Volume, 102, 6–7.

van Dijk, P. P., Iverson, J. B., Shaffer, H. B., Bour, R., Rhodin, A. G. J. Turtle Taxonomy Working Group: Turtles of the world, 2012 update. Annotated checklist of taxonomy, synonymy, distribution, and conservation status. Conservation Biology of Freshwater Turtles and Tortoises: A Compilation Project of the IUCN/SSC Tortoise and Freshwater Turtle Specialist Group. Chelonian Research Monographs No, 5.

Valakos, E. D., Pafilis, P., Sotiropoulos, K., Lymberakis, P., Marangou, P., Foufopoulos, J., 2008. Amphibians and Reptiles of Greece, Chimaira Publications, Frankfurt am Mainz.

van Vugt, N., de Bruijn, H., van Kolfschoten, M., Langereis, C.G., Okuda, M., 2000. Magneto- and cyclostratigraphy and mammal-fauna's of the Pleistocene lacustrine Megalopolis Basin, Peloponnesos, Greece. Geologica Ultrajectina, 189: chapter 3.

Van Logchem, W., Tsoukala, E., Mol, D., 2010. Milia (Grevena, Macedonia, Greece): A dangerous area for *Mammut borsoni*?. Quaternaire, Hors série (3), 192–194.

Vandelli, D., 1761. Epistola de Holothurio, et Testudine Coriacea ad Celeberrimum Carolum Linnaeum. Patavii [Padova]: Conzatti, 12 pp.

Vasileiadou, K. V., Koufos, G., Syrides, G., 2003. Silata, a new locality with micromammals from the Miocene/Pliocene boundary of the Chalkidiki peninsula, Macedonia, Greece. In J.W.F Reumer and W. Wessels (Eds.), Distribution and Migration of Tertiary Mammals in Eurasia, Deinsea, 10, 549–562.

Verginis, S., 1993–1995. Geomorphologie und Geologie im Bereich der Höhle von Vraona. Annales Géologiques des Pays Helléniques, 36, 8–15.

Vitek, N., Danilov, I., 2012. Cretaceous Trionychids from Asia: an expanded review of their record and biogeography. In Morphology and Evolution of Turtles, Proceedings of the Gaffney Turtle Symposium (Eds.) D. Brinkman, P. Holroyd, and J. Gardner, 419–438. Dordrecht: Springer.

Vlachos, E., 2007. Contribution to the study of the gigantic tortoise from Epanomi, Thessaloniki. Unpublished diploma thesis, School of Geology, Aristotle University of Thessaloniki, Greece.

Vlachos, E., 2011. The contribution of the study of giant tortoises in the stratigraphy and palaeoecology of the Neogene of Macedonia, Greece. Unpublished Master Thesis, School of Geology, Aristotle University of Thessaloniki.

Vlachos, E., 2014. Between the feet of elephants: turtles as a common element of the associated fauna of proboscideans. Abstract Book of the VIth International Conference on Mammoths and their Relatives. Scientific Annals, School of Geology, Aristotle University, Special Volume 102, 9, Thessaloniki.

Vlachos E., Tsoukala, E., in press. *Testudo* cf. *graeca* from the new Late Miocene locality of Platania (Drama basin, N. Greece) and a reappraisal of previously published specimens. Bulletin of the Geological Society of Greece.

Vlachos, E., Tsoukala, E., Corsini, J., 2014. *Cheirogaster bacharidisi*, sp. nov., a new species of a giant tortoise from the Pliocene of Thessaloniki (Macedonia, Greece). Journal of Vertebrate Paleontology, 34, 560–575.

Vlachos, E., Delfino, M., Kotsakis, T., in press. The chelonians from the latest Miocene-earliest Pliocene locality of Allatini and Pylea (east Thessaloniki, Macedonia, Greece). Comptes Rendus Palevol.

Weesie, P. D. M., 1982. A Pleistocene endemic island form within the genus *Athene*: *Athene cretensis* n. sp. (Aves, Strigiformes) from Crete. Proceedings of the Koninslijke Akademie van Weterschappen, series B, 85, 323–336.

White, A. W., Worthy, T. H., Hawkins, S., Bedford, S., Spriggs, M., 2010. Megafaunal meiolaniid horned turtles survived until early human settlement in Vanuatu, Southwest Pacific. Proceedings of the National Academy of Sciences, 107(35), 15512–15516.

Wied, M., 1839. Reise in des innere Nord-America in den Jahren 1832 bis 1834. Coblenz: J. Hoelscher, 213 pp.

Wilson, M. J., 2006. Herpetological observations on the Greek islands of Kefallinia and Zakynthos. Herpetological Bulletin, 19–28.

Wilson, M. J., Grillitsch, H., 2009. The herpetofauna of Simi (Dodecanese, Greece). Herpetozoa, 22, 99–113.

Zacarías, G. G., de la Fuente, M. S., Fernández, M. S., Zurita, A. E., 2013. Nueva especie de tortuga terrestre gigante del género *Chelonoidis* Fitzinger, 1835 (Cryptodira: Testudinidae), del miembro inferior de la formación Toropí/Yupoí (Pleistoceno Tardío/Lujanense), Bella Vista, Corrientes, Argentina. Ameghiniana, 50, 298–318.

Zachos, J., Pagani, M., Sloan, L., Thomas, E., Billups, K., 2001. Trends, rhythms, and aberrations in global climate 65 Ma to present. Science, 292, 686–693.

Zangerl, R., 1969. The turtle shell. In A. d'A. Bellairs and T. S. Parsons (Eds.), The Biology of the Reptilia 1, Morphology A, 311–339. Academic Press, London and New York.

List of Tables

Table 1.1. List of papers and abstracts that are related with this doctoral thesis 3

Table 3.1. Measurements of the preserved parts of the Gefira trionychid carapace 50

Table 3.2. Skeletal element representation of the *Testudo marginata* from Charkadio Cave, Tilos 187

Table. 3.3. Measurements of the left anterior plastron MIL 1753 of Testudo sp. nov. from Milia. 220

Table 3.4. Skeletal element representation of the chelonian material from Franchthi Cave 275

Table 3.5. Summary of the fossil chelonians from Greece, with additional information about the locality, age, initial description and institution. 285

Table 4.1. Morphological characters used in the analysis, based on Hervet (2003: 201-237; original characters in French) 335

Table 5.1. Comparisons between the Greek and Italian fossil chelonians (based on Chesi, 2008) 350

Table 5.2. Presence/Absence (1/0) data of the Greek fossil chelonians 352

Table 6.1. Ecological categories of turtles, based on their bone histology (based on Scheyer, 2007) 356

Table 6.2. SEM analysis of the trionychid section LGPUT GAS 8b 361

Table 7.1. Summary of the changes in the composition of the fossil fauna of chelonians in Greece, based on the present thesis. 372

List of Figures

Chapter 1

Figure 1.1. Comparative morphology of the carapace and plastron of *Testudo graeca* and '*Testudo' hermanni* 12

Figure 1.2. Comparative morphology of the carapace and plastron of *Emys orbicularis* and *Mauremys rivulata*. The dorsal carapace is figured on the top, the ventral plastron on the bottom 14

Figure 1.3. The distribution of the extant species of *Testudo* in Greece 16

Figure 1.4. The distribution of the extant freshwater turtle species in Greece 16

Chapter 2

Figure 2.1. Map of Greece containing the localities with fossils of turtles and tortoises. (A), detail of the Thessaloniki – Chalkikidi area. (B) detail of Crete Island 23

Figure 2.2. Chronological distribution of the main localities with chelonian material from Greece 24

Figure 2.3. The new Late Miocene locality of Platania, Drama basin, Northern Greece 26

Figure 2.4. A, the position of Pylea and Allatini, east of Thessaloniki city, including other sites containing fossils of turtles and tortoises 31

Figure 2.5. The large testudinid sites in Western Chalkidiki peninsula 32

Figure 2.6. Geology of Western Chalkidiki peninsula 33

Figure 2.7. The new specimen of large testudinid from the Pliocene of Nea Kallikratia. 34

Figure 2.8. The Pliocene locality of Gefira, in lower Axios valley 35

Figure 2.9. The Late Pliocene site of Milia, near Grevena (NW Greece) 36

Chapter 3

Figure 3.1. The holotype and only known specimen of *Nostimochelone lampra* Georgalis et al. (2012) from the Late Burdigalian of Nostimo, Kastoria. 46

Figure 3.2. Schematic drawings on *Nostimochelone lampra* Georgalis et al. (2012), showing the available character scoring from the matrix of Gaffney et al. (2006). 46

Figure 3.3. Carapace plates of Trionychidae from Gefira locality, Late Pliocene, N. Greece 48

Figure 3.4. Carapace plates of Trionychidae from Gefira locality, Late Pliocene, N. Greece 49

Figure 3.5. Trionychid plates from the Late Miocene site of Plakias, Crete (NHMC collection). 51

Figure 3.6. Shell remains from the holotype of *Titanochelon bacharidisi* (Vlachos et al., 2014) from the Pliocene of Epanomi (Thessaloniki) 57

Figure 3.7. LGPUT EPN 102, the cranium of the holotype of *Titanochelon bacharidisi* (Vlachos et al., 2014) from the Pliocene of Epanomi (Thessaloniki) 59

Figure 3.8. LGPUT EPN 102, the cranium of the holotype of *Titanochelon bacharidisi* (Vlachos et al., 2014) from the Pliocene of Epanomi (Thessaloniki) 60

Figure 3.9. Appendicular elements of the holotype of *Titanochelon bacharidisi* (Vlachos et al., 2014) from the Pliocene of Epanomi (Thessaloniki) 62

Figure 3.10. The anterior limb associations of the holotype of *Titanochelon bacharidisi* (Vlachos et al., 2014) from the Pliocene of Epanomi (Thessaloniki) 63

Figure 3.11. The right posterior limb association of the holotype of *Titanochelon bacharidisi* (Vlachos et al., 2014) from the Pliocene of Epanomi (Thessaloniki) 67

Figure 3.12. Carpal and tarsal elements of the holotype of *Titanochelon bacharidisi* (Vlachos et al., 2014) from the Pliocene of Epanomi (Thessaloniki) 68

Figure 3.13. LGPUT EPN 184, thigh bony tubercle of the holotype of *Titanochelon bacharidisi* (Vlachos et al., 2014) from the Pliocene of Epanomi (Thessaloniki) 69

Figure 3.14. Shell remains of the paratype of *Titanochelon bacharidisi* (Vlachos et al., 2014) from the Pliocene of Epanomi (Thessaloniki). 72

Figure 3.15. Anterior limb elements of the paratype of *Titanochelon bacharidisi* (Vlachos et al., 2014) from the Pliocene of Epanomi (Thessaloniki). 73

Figure 3.16. Carpal elements of the paratype of *Titanochelon bacharidisi* (Vlachos et al., 2014) from the Pliocene of Epanomi (Thessaloniki). 74

Figure 3.17. Posterior limb elements of the paratype of *Titanochelon bacharidisi* (Vlachos et al., 2014) from the Pliocene of Epanomi (Thessaloniki). 75

Figure 3.18. LGPUT EPN 99, left femur of another individual of *Titanochelon bacharidisi* (Vlachos et 77

02/16/2016 Ψηφιακή Βιβλιοθήκη Θεόφραστος - Τμήμα Γεωλογίας - Α.Π.Θ.

al., 2014) from Epanomi (Thessaloniki).

Figure 3.19. Material of *Titanochelon bacharidisi* (Vlachos et al., 2014) from the Pliocene of Nea Kallikratia (Thessaloniki). 78

Figure 3.20. LGPUT KLK 500, plastron of the KLK II individual of *Titanochelon bacharidisi* (Vlachos et al., 2014) from the Pliocene of Nea Kallikratia. 80

Figure 3.21. Material of *Titanochelon bacharidisi* from the Pliocene of Nea Michaniona (Thessaloniki). 82

Figure 3.22. Material of *Titanochelon bacharidisi* (Vlachos et al., 2014) from the Pliocene of Nea Michaniona (Thessaloniki). 83

Figure. 3.23. A diaphysis of a femur of *Titanochelon bacharidisi* (Vlachos et al., 2014) from the Pliocene of Aggelochori/Megalo Emvolon (Thessaloniki; LGPUT collection). 84

Figure 3.24. Shell material of *Titanochelon bacharidisi* (Vlachos et al., 2014) from Aggelochori/ Megalo Emvolon (Thessaloniki; AMPG collection). 85

Figure 3.25. Elements of *Titanochelon bacharidisi* (Vlachos et al., 2014) from the Pliocene of Aggelochori/ Megalo Emvolon (Thessaloniki; AMPG collection). 87

Figure 3.26. Osteoderms of of *Titanochelon bacharidisi* (Vlachos et al., 2014) from the Pliocene of Aggelochori/ Megalo Emvolon (Thessaloniki; AMPG collection). 89

Figure 3.27. MNHN 1921-5-SLQ-995, the cranium of *Titanochelon* cf. *bacharidisi* from Salonique (sensu Arambourg & Piveteau, 1929) 93

Figure 3.28. MNHN 1921-5-SLQ-995, the cranium of *Titanochelon* cf. *bacharidisi* from Salonique (sensu Arambourg & Piveteau, 1929) 94

Figure 3.29. Appendicular elements of *Titanochelon* cf. *bacharidisi* from Salonique (sensu Arambourg & Piveteau, 1929). 95

Figure 3.30. Ungual and osteoderms of *Titanochelon* cf. *bacharidisi* from Salonique (sensu Arambourg & Piveteau, 1929). 96

Figure 3.31. NHMW 2009z0103/0001, the skull of *Titanochelon schafferi* (Szalai, 1931) from the Late Miocene of Samos Island 99

Figure 3.32. NHMW 2009z0103/0001, the skull of *Titanochelon schafferi* (Szalai, 1931) from the Late Miocene of Samos Island 100

Figure 3.33. Appendicular elements of *Titanochelon schafferi* (Szalai, 1931) from the Late Miocene of Samos Island. 102

Figure 3.34. Shell elements of *Titanochelon* sp. from the Late Miocene of Pikermi (Attica). 104

Figure 3.35. Appendicular elements of *Titanochelon* sp. from the Late Miocene of Pikermi (Attica). 105

Figure 3.36. Osteoderms of *Titanochelon* sp. from the Late Miocene of Pikermi (Attica). 107

Figure 3.37. AMPG 1868/91, shell material of a juvenile individual from the Late Miocene of Pikermi (Attica). 109

Figure 3.38. Material from the giant tortoise from the Late Miocene of Kiourka (Liossati), near Pikermi (Attica). 110

Figure 3.39. Giant tortoise remains from the Late Pliocene of Milia (Grevena). 113

Figure 3.40. Giant tortoise material from the Late Miocene of Kassandra peninsula (Chalkidiki, Thessaloniki). 114

Figure 3.41. LGPUT MP 40, '*Testudo*' *hermanni* Gmelin, 1789 from the ?Pleistocene of Chalkidiki 119

Figure. 3.42. The partial anterior carapace of *Testudo* cf. *hermanni* from the Epigravettian (Occupation phase 4, unit 168) of Franchthi Cave (Peloponnesus) 121

Figure 3.43. *Testudo graeca* Linnaeus, 1758 from the Pleistocene of Petralona Cave (Chalkidiki). 124

Figure 3.44. *Testudo graeca* Linnaeus, 1758 from the Pleistocene of Petralona Cave (Chalkidiki). 126

Figure 3.45. *Testudo graeca* Linnaeus, 1758 from the Pleistocene of Petralona Cave (Chalkidiki). 127

Figure 3.46. *Testudo graeca* Linnaeus, 1758 from the Pleistocene of Potidea (Chalkidiki). 129

Figure 3.47. *Testudo graeca* Linnaeus, 1758 from the Pliocene of Megalo Emvolon - Aggelochori (Thessaloniki). 131

Figure 3.48. *Testudo graeca* Linnaeus, 1758 from the Pliocene of Megalo Emvolon - Aggelochori (Thessaloniki). 132

Figure 3.49. *Testudo graeca* Linnaeus, 1758 from the Pliocene of "Salonique" (sensu Arambourg & Piveteau, 1929). 135

Figure 3.50. *Testudo graeca* Linnaeus, 1758 from the uppermost Miocene – lowermost Pliocene of Pylea 137

(Thessaloniki).
Figure 3.51. *Testudo graeca* Linnaeus, 1758 from the uppermost Miocene – lowermost Pliocene of Allatini, Thessaloniki, Greece. 140
Figure 3.52. *Testudo graeca* Linnaeus, 1758 from the Early Pleistocene of Vatera, Lesvos Island 141
Figure 3.53. The partial shell of the specimen of *Testudo* cf. *graeca* from the Late Miocene of Platania (Drama basin, Northern Greece) 146
Figure 3.54. The plastron of the specimen of *Testudo* cf. *graeca* from the Late Miocene of Platania (Drama basin, Northern Greece) 147
Figure 3.55. Proximal part of the right humerus (LGPUT PLD 71) of the specimen of *Testudo* cf. *graeca* from the Late Miocene of Platania (Drama basin, Northern Greece) 148
Figure 3.56. The holotype of *Testudo marginata cretensis* Bachmayer et al., 1975 (AMPG 3/1974) from the Pleistocene of Gerani Cave (Crete) 152
Figure 3.57. The holotype of *Testudo marginata cretensis* Bachmayer et al., 1975 (AMPG 3/1974) from the Pleistocene of Gerani Cave (Crete) 153
Figure 3.58. The paratype of *Testudo marginata cretensis* Bachmayer et al., 1975 from the Pleistocene of Zourida Cave (Crete) 154
Figure 3.59. Additional material of *Testudo marginata* Schoepff, 1793 from the Pleistocene of Zourida Cave (Crete) 156
Figure 3.60. Shell material of *Testudo marginata* Schoepff, 1793 from the Pleistocene of Koumpes Cave (Crete) 158
Figure 3.61. Additional material of *Testudo marginata* Schoepff, 1793 from the Pleistocene of Koumpes Cave (Crete) 159
Figure 3.62. Carapace material of *Testudo marginata* Schoepff, 1793 from the Pleistocene of Liko Cave (Crete) 161
Figure 3.63. Plastron material of *Testudo marginata* Schoepff, 1793 from the Pleistocene of Liko Cave (Crete) 163
Figure 3.64. Appendicular elements of *Testudo marginata* Schoepff, 1793 from the Pleistocene of Liko Cave (Crete) 166
Figure 3.65. Shell and appendicular elements of *Testudo marginata* Schoepff, 1793 from the Pleistocene of Mavro Mouri IV Cave (Crete) 171
Figure 3.66. Shell and appendicular elements of *Testudo marginata* Schoepff, 1793 from the Pleistocene of Mavro Mouri IV Cave (Crete) 174
Figure 3.67. New appendicular elements of *Testudo marginata* Schoepff, 1793 from the Pleistocene of Simonelli Cave (Crete) 180
Figure 3.68. NHMC FS38/8, right hyoplastron of *Testudo marginata* Schoepff, 1793 from the Pleistocene of Kos Island 180
Figure 3.69. Shell material of *Testudo marginata* Schoepff, 1793 from the Pleistocene/Holocene of Charkadio Cave (Tilos Island) 182
Figure 3.70. Appendicular elements of *Testudo marginata* Schoepff, 1793 from the Pleistocene/Holocene of Charkadio Cave (Tilos Island) 183
Figure 3.71. Humerus of *Testudo marginata* Schoepff, 1793 from the Pleistocene/Holocene of Charkadio Cave (Tilos Island) 185
Figure 3.72. Femur of *Testudo marginata* Schoepff, 1793 from the Pleistocene/Holocene of Charkadio Cave (Tilos Island) 186
Figure 3.73. Skeletal element representation of the shell fragments and appendicular elements from *Testudo marginata* Schoepff, 1793 from Charkadio Cave, Tilos Island 188
Figure 3.74. Skeletal element representation of the left and right humeri from *Testudo marginata* Schoepff, 1793 from Charkadio Cave, Tilos Island 189
Figure 3.75. Skeletal element representation of the left and right femora from *Testudo marginata* Schoepff, 1793 from Charkadio Cave, Tilos Island 190
Figure 3.76. Material from *Testudo marginata* Schoepff, 1793 from the Pleistocene of Poulion Cave in Boetia 192
Figure 3.77. Material from *Testudo marginata* Schoepff, 1793 from the Pleistocene of Kythera Island 194
Figure 3.78. LGPUT XEK 1, partial shell of *Testudo* cf. *marginata* from the Pleistocene of Xerias (Kavala) 198

Figure 3.79. MNHN PIK 3683, the holotype of *Testudo marmorum* Gaudry, 1861 from the Late Miocene of Pikermi (Attica) 201
Figure 3.80. MNHN PIK 3683, the holotype of *Testudo marmorum* Gaudry, 1861 from the Late Miocene of Pikermi (Attica) 202
Figure 3.81. MNHN PIK 3683, the paratype of *Testudo marmorum* Gaudry, 1861 from the Late Miocene of Pikermi (Attica) 203
Figure 3.82. AMPG PIK 1970b, a partial shell of *Testudo marmorum* Gaudry, 1861 from the Late Miocene of Pikermi (Attica) 204
Figure 3.83. AMPG PIK 1970d, a partial shell of *Testudo marmorum* Gaudry, 1861 from the Late Miocene of Pikermi (Attica) 206
Figure 3.84. AMPG PIK 1970e, elements of a partial shell of *Testudo marmorum* Gaudry, 1861 from the Late Miocene of Pikermi (Attica) 207
Figure 3.85. AMPG PIK 1970g, a partial shell of *Testudo marmorum* Gaudry, 1861 from the Late Miocene of Pikermi (Attica) 208
Figure 3.86. AMPG PIK 1970a, a partial shell of a hingeless *Testudo* sp. from the Late Miocene of Pikermi (Attica) 211
Figure 3.87. AMPG PIK 1970c, a partial plastron of *Testudo* sp. from the Late Miocene of Pikermi (Attica) 212
Figure 3.88. AMPG PIK 1970f, a partial shell of a hingeless *Testudo* sp. from the Late Miocene of Pikermi (Attica) 213
Figure 3.89. AMPG PIK 1630, a partial shell of a hingeless *Testudo* sp. from the Late Miocene of Pikermi (Attica) 214
Figure 3.90. MIL 495, partial carapace of *Testudo* sp. from the Late Pliocene of Milia (Grevena) 217
Figure 3.91. MIL 1753, partial plastron of *Testudo* sp. from the Late Pliocene of Milia (Grevena) 218
Figure 3.92. Additional shell material of *Testudo* sp. from the Late Pliocene of Milia (Grevena) 219
Figure 3.93. Comparison of the morphology of the posterior carapace of (A) *Testudo graeca*, (B) *Testudo marginata* and (C) the Milia testudinid 221
Figure 3.94. The partial shell of *Testudo* sp. from the Late Miocene of Samos Island (AMPG collection) 224
Figure 3.95. MFGUI 22, the partial shell of *Testudo* sp. from the Late Miocene of Samos Island 225
Figure 3.96. The specimens from the ?Middle Miocene of Thymiana, Chios described as *Testudo* sp. I (A) and *Testudo* sp. II (B) by Paraskevaidis (1955) 227
Figure 3.97. Material of *Testudo* sp. from the Miocene/Piocene boundary of Maramena (Serres) 229
Figure 3.98. *Testudo* sp. from the Miocene of Serres basin (AMPG collection) 231
Figure 3.99. Shell elements of *Testudo* sp. from the Late Miocene-Early Pliocene of Nea Silata (Thessaloniki) 233
Figure 3.100. *Mauremys rivulata* Vallenciennes *in* Bory de Saint-Vincent, 1833 from Gerani Cave and Rethymnon fissure (Crete) 237
Figure 3.101. *Mauremys rivulata* Vallenciennes *in* Bory de Saint-Vincent, 1833 from the Pleistocene of Koumpes Cave (Crete). 238
Figure 3.102. *Mauremys rivulata* Vallenciennes *in* Bory de Saint-Vincent, 1833 from the Pleistocene of Mavro Mouri IV Cave (Crete) 238
Figure 3.103. *Mauremys rivulata* Vallenciennes *in* Bory de Saint-Vincent, 1833 from the Pleistocene of Liko Cave (Crete) 239
Figure 3.104. Carapace remains of *Mauremys rivulata* Vallenciennes *in* Bory de Saint-Vincent, 1833 from the Pleistocene of Sitia (Crete). 241
Figure 3.105. Plastron remains of *Mauremys rivulata* Vallenciennes *in* Bory de Saint-Vincent, 1833 from the Pleistocene of Sitia (Crete) 244
Figure 3.106. *Mauremys rivulata* Vallenciennes *in* Bory de Saint-Vincent, 1833 from the Pleistocene of Kos Island 247
Figure 3.107. Fossil turtle material from the Pleistocene of Megalopolis (Peloponnesus) 248
Figure 3.108. *Mauremys* sp. from the Late Pliocene of Milia (Grevena) 251
Figure 3.109. *Mauremys* sp. from the Late Miocene of Plakias (Crete Island) 253
Figure 3.110. Carapace plates of *Mauremys* sp. from the Mio-Pliocene boundary of Nea Silata (Thessaloniki) 260

Figure 3.111. Peripheral plates of *Mauremys* sp. from the Mio-Pliocene boundary of Nea Silata (Thessaloniki) 263
Figure 3.112. Plastron plates of *Mauremys* sp. from the Mio-Pliocene boundary of Nea Silata (Thessaloniki) 266
Figure 3.113. The Thessaloniki specimen (LGPUT GG 23) of *Mauremys* sp. from the uppermost Miocene – lowermost Pliocene of Allatini, Thessaloniki, Greece 271
Figure 3.114. Geoemydid taxa with wide vertebral scutes 273
Figure 3.115. *Emys orbicularis* Linnaeus, 1758 (blue) and *Testudo* cf. *hermanii* (brown), from the Pleistocene – Holocene times of Franchthi Cave (Pelopponessus) 277
Figure 3.116. (See caption of Fig. 3.115). Franchthi Cave (Pelopponessus) 277
Figure 3.117. (See caption of Fig. 3.115). Franchthi Cave (Pelopponessus) 278
Figure 3.118. (See caption of Fig. 3.115). Franchthi Cave (Pelopponessus) 278
Figure 3.119. Distribution of the chelonians from Franchthi Cave (Pelopponessus) 279
Figure 3.120. A-F, Clutch of possible giant tortoise eggs (IGF 11603) from the uppermost Miocene – lowermost Pliocene of Pylea (Thessaloniki) 283
Figure 3.121. Clutch of giant tortoise eggs (AMPG 515-519) from the Pliocene of Apolakkia, Rhodes Island 284

Chapter 4

Figure 4.1. Illustration of the different states of the character NUCHAL 1 291
Figure 4.2. Illustration of the different states of the character NUCHAL 2 291
Figure 4.3. Illustration of the different states of the character NUCHAL 3 292
Figure 4.4. Illustration of the different states of the character NUCHAL 4 292
Figure 4.5. Illustration of the different states of the character CERVICAL 293
Figure 4.6. Illustration of the different states of the character NEURAL NUMBER 294
Figure 4.7. Illustration of the different states of the character NEURAL 1 294
Figure 4.8. Illustration of the different states of the character NEURAL 2 295
Figure 4.9. Illustration of the different states of the character NEURAL 3 295
Figure 4.10. Illustration of the different states of the character NEURAL 4 296
Figure 4.11. Illustration of the different states of the character NEURAL 5 296
Figure 4.12. Illustration of the different states of the character COSTAL 296
Figure 4.13. Illustration of the different states of the character SUPRAPYGAL 297
Figure 4.14. Illustration of the different states of the character PYGAL 297
Figure 4.15. Illustration of the different states of the character VERTEBRAL 1 298
Figure 4.16. Illustration of the different states of the character VERTEBRAL 2 298
Figure 4.17. Illustration of the different states of the character SUPRACAUDAL 1 299
Figure 4.18. Illustration of the different states of the character SUPRACAUDAL 2 299
Figure 4.19. Illustration of the different states of the character COINCIDENCE 299
Figure 4.20. Illustration of the different states of the character PERIPHERAL 300
Figure 4.21. Illustration of the different states of the character MARGINAL 1 300
Figure 4.22. Illustration of the different states of the character MARGINAL 2 301
Figure 4.23. Illustration of the different states of the character MARGINAL 3 301
Figure 4.24. Illustration of the different states of the character MARGINAL 4 301
Figure 4.25. Illustration of the different states of the character CARAPACIAL HINGE 302
Figure 4.26. Illustration of the different states of the character BORDER 302
Figure 4.27. Illustration of the different states of the character ANTERIOR LOBE 303
Figure 4.28. Illustration of the different states of the character GULAR PROTRUSION 303
Figure 4.29. Illustration of the different states of the character EPIPLASTRON 1 304
Figure 4.30. Illustration of the different states of the character EPIPLASTRON 2 304
Figure 4.31. Illustration of the different states of the character GULARS 1 304
Figure 4.32. Illustration of the different states of the character GULARS 2 305

Figure 4.33. Illustration of the different states of the character HUMERALS 305
Figure 4.34. Illustration of the different states of the character HUMERO-PECTORAL 1 305
Figure 4.35. Illustration of the different states of the character HUMERO-PECTORAL 2 306
Figure 4.36. Illustration of the different states of the character PECTORALS 306
Figure 4.37. Illustration of the different states of the character PLASTRAL HINGE 306
Figure 4.38. Illustration of the different states of the character FEMORO-ANAL 307
Figure 4.39. Illustration of the different states of the character MEDIAN LENGTH OF ANAL SCUTE 307
Figure 4.40. Illustration of the different states of the character FRONTAL 1 308
Figure 4.41. Illustration of the different states of the character FRONTAL 2 308
Figure 4.42. Illustration of the different states of the character INFERIOR DESCENDING PROCESSES OF THE FRONTAL 309
Figure 4.43. Illustration of the different states of the character SULCUS OLFACTORIUS 309
Figure 4.44. Illustration of the different states of the character position of FOSSA ORBITALIS 310
Figure 4.45. Illustration of the different states of LOWER TEMPORAL EMARGINATION 310
Figure 4.46. Illustration of the different states of MAXILLA-PREMAXILLA SYMPHYSIS HEIGHT 311
Figure 4.47. Illustration of the different states of PREMAXILLA RIDGE 311
Figure 4.48. Illustration of the different states of PREMAXILLARY PIT 311
Figure 4.49. Illustration of the different states of PREMAXILLA-MAXILLA RIDGE 312
Figure 4.50. Illustration of the different states of NUMBER OF TRITURATING RIDGES 312
Figure 4.51. Illustration of the different states of EXTENT OF LINGUAL RIDGE 312
Figure 4.52. Illustration of the different states of LABIAL RIDGE 313
Figure 4.53. Illustration of the different states of POSTERIOR MAXILLARY PROCESS 313
Figure 4.54. Illustration of the different states of MEDIAN MAXILLARY RIDGE 314
Figure 4.55. Illustration of the different states of MAXILLARY RIDGES 314
Figure 4.56. Illustration of the different states of VOMER RIDGE 314
Figure 4.57. Illustration of the different states of VOMER 315
Figure 4.58. Illustration of the different states of CONTACT PTERYGOID-BASIOCCIPITAL 315
Figure 4.59. Illustration of the different states of FORAMEN PRAEPALATINUM 315
Figure 4.60. Illustration of the different states of EXTENSION OF SQUAMOSALS 316
Figure 4.61. Illustration of the different states of CRISTA SUPRAOCCIPITALIS 1 316
Figure 4.62. Illustration of the different states of CRISTA SUPRAOCCIPITALIS 2 317
Figure 4.63. Illustration of the different states of CRISTA SUPRAOCCIPITALIS 3 317
Figure 4.64. Illustration of the different states of PARIETAL 318
Figure 4.65. Illustration of the different states of OPISTHOTIC 318
Figure 4.66. Illustration of the different states of PROCESSUS TROCHLEARIS OTICUM 318
Figure 4.67. The strict consensus of 6 MPT of several extant and extinct testudinid taxa, based on the character defined above 322
Figure 4.68. The same analysis with the molecular constrains from Fritz & Bininda-Emmonds (2007) 323
Figure 4.69. The time calibrated constrained tree of the Analysis #2 324
Figure 4.70. The taxonomy of Testudinidae based on the present analysis 326
Figure 4.71. The Dispersal-Evolution-Cladogenesis (DEC) analysis on the (A) constrained and (B) unconstrained analysis of the testudinids 329
Figure 4.72. Mapping of the shell size on the constrained analysis and comparison with the global climatic evolution from Zachos et al. (2001) 331
Figure 4.73. Phylogenetic analyses of the Milia and Samos testudinids 333
Figure 4.74. Strict consensus tree of the phylogenetic analysis of the Nea Silata geoemydid with many European fossil geoemydids 338
Figure 4.75. A composite cladogram from the 4 MPT of the *Nostimochelone lampra* in the matrix of Gaffney et al. (2006), showing the two positions of the taxon within Bothremydidae 341

Chapter 5

Figure 5.1. The geographical distribution of the chelonian lineages during Quaternary/Neogene 344

Figure 5.2. The geographical distribution of the main chelonian clades through time 346

Figure 5.3. The main events marking the chelonian lineages of Greece 347

Figure 5.4. The biostratigraphical distribution of the Greek chelonian taxa 349

Figure 5.5. Diversity curves of the Greek chelonian taxa diversity through time 351

Chapter 6

Figure 6.1. The costal 3 of the Gefira trionychid, showing the external (ECO) and the internal (ICO) cortex, surrounding the cancellous bone (CB) 357

Figure 6.2. Bone shell histology of Trionychidae from Gefira locality, Pliocene, N. Greece 358

Figure 6.3. Photographs of the sampled sections of the costal plate of *Ti. bacharidisi* from Nea Michaniona (LGPUT MIC 308) 363

Figure 6.4. Bone shell histology of *Titanochelon bacharidisi* from Nea Michaniona locality, Pliocene, N. Greece 364

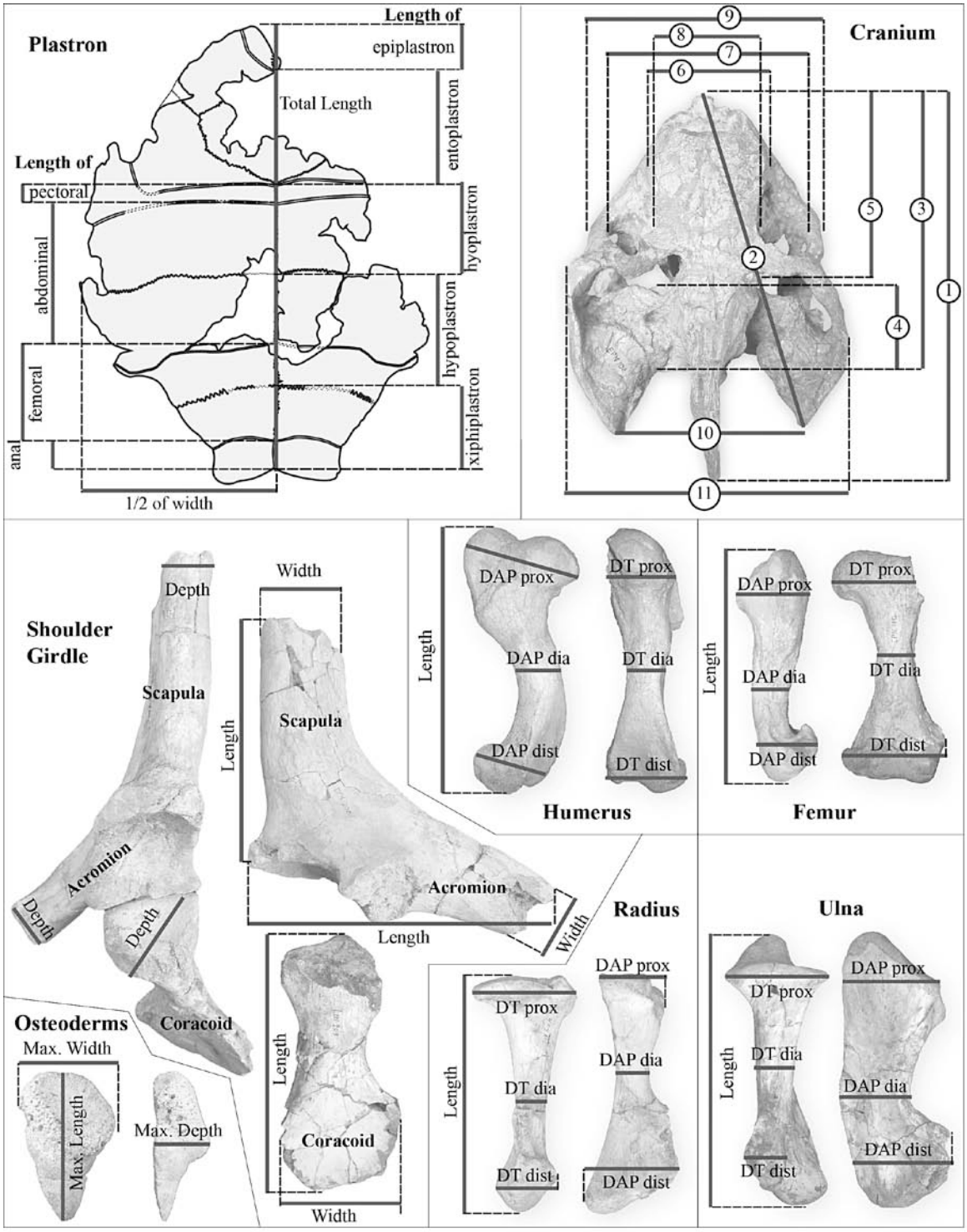
Chapter 7

Figure 7.1. Graphical summary of the diversity and distribution of the fossil turtles and tortoises of Greece, as presented in this thesis 379

02/16/2016 Ψηφιακή Βιβλιοθήκη Θεόφραστος - Τμήμα Γεωλογίας - Α.Π.Θ.

Appendix

Tables of measurements of the studied material of large testudinids. Measurements were taken using a BMI caliper (0.01 mm precision) for bone elements and meter tape for shell elements. In most cases an explanatory drawing is given. Proximal refers to the part of the bone closer to the axial skeleton, in contrast with distal. Diaphysis' measurements were taken at the minimum part of the midshaft. DAP (anteroposterior diameter of the bone) was measured at dorsal view. DT (transversal diameter), was measured at anterior view. For graphical explanation see Figure 9S. Abbreviations—ca., calculated; dia, diaphysis; dist, distal; l, left; pr., preserved; prox, proximal; r, right.



Measurements of testudinid crania for comparison (mm)												
	1	2	3	4	5	6	7	8	9	10	11	12
EPN 102	210	200	165	53	125	49	112	64	129	95	148	65
Samos (NHMW)	257	260	205	68,7	128	66	138	82	185	157,5	185	75
Perpignan (MNHN)	190	180	155	57,3	93,3	55	112	67	130	125	130	70
Thessaloniki (MNHN)	200	197	174	43	113	47,5	110	58	132	144	144	66
1, maximum length; 2, length prosthion–squamosal; 3, length prosthion–opisthotic; 4, length prootic–opisthotic; 5, length prosthion–postorbital; 6, width across frontals; 7, width across ectorbital; 8, width across prefrontals; 9, width across jugals; 10, width across squamosals; 11, maximum width; 12, maximum height (not figured). Prosthion refers to sutural point of the premaxilae; ectorbital refers to the most lateral point posterior to the orbits.												

Measurements of the plastron (mm), measured across the midline												
		Bony Plates					Horny Scutes					
	Length	Ep	En	Hyo	Hypo	Xi	Gu	Hu	Pec	Abd	Fe	An
EPN 101	1150	ca. 190	ca. 150	300	340	170	?	?	?	?	?	?
EPN 285	1120	ca. 140	ca. 210	210	340	220	?	?	50	380	240	80
abd, abdominals; an, annals; ca., calculated; ep, epiplastron; en, entoplastron; fe, femorals; gu, gulars; hu, humerals; hyo, hyoplastron; hypo, hypoplastron; pec, pectorals; xi, xiphiplastron.												

Measurements of shoulder girdle (mm)						
	Left EPN 208			Right EPN 206		
	Length	Width	Depth	Length	Width	Depth
Scapula	180	58,2	29,7 – 16,3	150	60	30,8 – 17,2
Acromion	150	50,8	33,8 – 23,6	140	50,7	38 – 23,3
Coracoid	160	67,2	55,9	70	63	64,5
Articular surface: 93,8 x 62,1				Articular surface: 92 x 67		

Measurements of humerus (mm)							
		Proximal		Diaphysis		Distal	
	Length	DT	DAP	DT	DAP	DT	DAP
EPN 103 (r)	308	74,79	138,49	44,41	55,28	98,14	65,25
EPN 104 (l)	ca. 305	–	–	42	52,68	ca. 95	64,78
EPN 200 (r)	pr. 227	–	–	44,3	55,3	92,3	69
EPN 203(l)	pr. 215	–	–	43,5	53	–	–

KLK 503 (l)	pr. 125	95	112	–	–	–	–

Measurements of radius (mm)							
		Proximal		Diaphysis		Distal	
	Length	DT	DAP	DT	DAP	DT	DAP
EPN 113 (r)	141,91	51,97	47,25	23,64	24,16	37,21	56,86
EPN 114 (l)	150,33	41,96	38,45	24,3	24,73	34,66	63,5
EPN 201 (r)	178	46	79,7	27,3	25,4	73,3	46
EPN 204 (l)	pr. 85	–	–	27,9	28,9	–	–

Measurements of ulna (mm)							
		Proximal		Diaphysis		Distal	
	Length	DT	DAP	DT	DAP	DT	DAP
EPN 202 (r)	190	69,3	67,8	50	24,6	21,1	82,8
EPN 205 (l)	pr. 101,7	–	–	–	–	–	85,9

Measurements of femur (mm)							
		Proximal		Diaphysis		Distal	
	Length	DT	DAP	DT	DAP	DT	DAP
EPN 107 (r)	230	99,5	112	39,6	44,6	106	56
EPN 110 (l)	237,77	93,3	pr. 80,91	42,5	46,89	108,49	58,78
EPN 212 (r)	pr. 139	–	–	39,2	46,6	–	–
MIC 301 (l)	pr. 146	–	–	46,6	60,2	130	70
Measurements of tibia (mm)							
		Proximal		Diaphysis		Distal	
	Length	DT	DAP	DT	DAP	DT	DAP
EPN 108 (r)	160	71	62,4	33,5	27,4	45,6	29,6
EPN 111 (l)	pr. 144	66,91	61,29	26,36	27,19	–	–
EPN 213 (r)	pr. 104,5	–	–	30,3	36,5	–	–
MIC 302 (l)	pr. 104,5	96	74,5	35,7	34	–	–

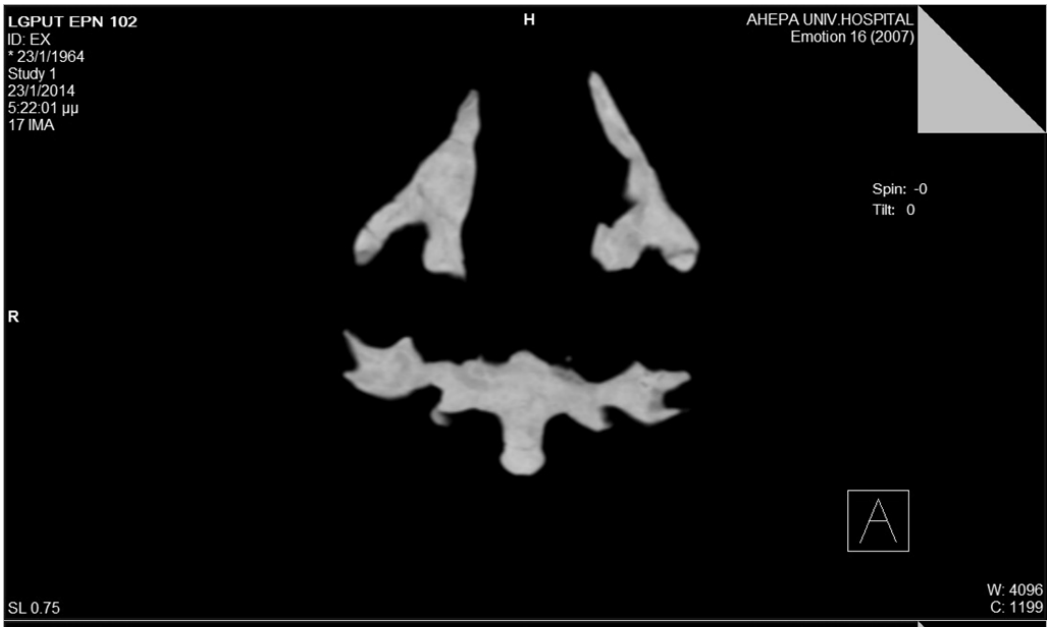
Measurements of fibula (mm)							
		Proximal		Diaphysis		Distal	
	Length	DT	DAP	DT	DAP	DT	DAP
EPN 109 (r)	142	22,6	36	14,6	23,3	21,3	43,3

EPN 112 (l)	147,15	22,75	38,04	21,33	14,51	26,96	44,06
MIC 303 (l)	pr. 89,9	43,7	34,2	29,8	19,9	–	–

Measurements of osteoderms (mm)									
EPN	Maximum Length	Maximum Width	Maximum Depth	Description	EPN	Maximum Length	Maximum Width	Maximum Depth	Description
140	43,4	26	8,4	Anterior limb	237	49,85	57,67	18,95	Anterior limb
142	49,6	31,7	17,5	Half pointed	263	32,58	37,53	10,66	Anterior limb
134	57,9	34	18,8	Half pointed	232	54,45	53,12	19,12	Half pointed
199a	37,5	46,15	15,3	Half pointed	233	47,18	49,21	28,41	Half pointed
199b	34,5	30,3	9,3	Half pointed	239	55,73	39,48	20,87	Half pointed
199c	33,2	26,2	10,4	Half pointed	240	50,3	43,11	21,48	Half pointed
157	29,6	34,7	12	Posterior limb	241	57,06	37,96	17,17	Half pointed
199d	19	18,3	5,3	Posterior limb	242	55,77	47,67	20,88	Half pointed
199e	29,04	24,5	12,8	Posterior limb	243	43,67	42,96	24,46	Half pointed
199f	55,4	42,5	23,6	Pointed	248	48,44	40,91	14,98	Half pointed
199g	34,6	36,1	32,5	Pointed	250	45,52	43,02	23,94	Half pointed
199h	28,8	36,2	31	Pointed	253	41,88	38,74	21,02	Half pointed
199i	62,4	47,6	44,4	Pointed	254	44,1	31,07	17,25	Half pointed
255	40,16	31,26	14,41	Crural	260	47,22	34,68	17,05	Half pointed
257	25,36	22,04	14,01	Crural	231	61,09	45,85	25,45	Pointed
258	34,8	30,45	15,67	Crural	234	54,74	45,24	25	Pointed
259	30,27	32,2	12,45	Crural	235	72,07	52,98	25,63	Pointed
261	24,58	28,36	11,71	Crural	236	58,69	47,4	22,98	Pointed
262	22,13	22,21	10,8	Crural	238	72,5	53,52	24,08	Pointed
265	33,97	24,15	15,16	Crural	244	57,28	39,84	24,26	Pointed
266	30,34	21,93	8,32	Crural	245	55,19	42,06	21,9	Pointed
267	22,53	18,5	10,03	Crural	247	50,46	39,07	31,89	Pointed
268	25,82	31,64	11,63	Crural	251	52,64	42	22,13	Pointed
269	39,55	24,92	13,4	Crural	252	65,37	39,26	18,43	Pointed
270	36,2	29,27	21,63	Crural					

CT SCANS OF LGPUT EPN 102, Cranium of *Titanochelon bacharidisi* (Horizontal Sections)




LGPUT EPN 102
ID: EX
* 23/1/1964
Study 1
23/1/2014
5:22:01 μμ
17 IMA
H
AHEPA UNIV.HOSPITAL
Emotion 16 (2007)
Spin: -0
Tilt: 0
R
A
W: 4096
C: 1199
SL 0.75

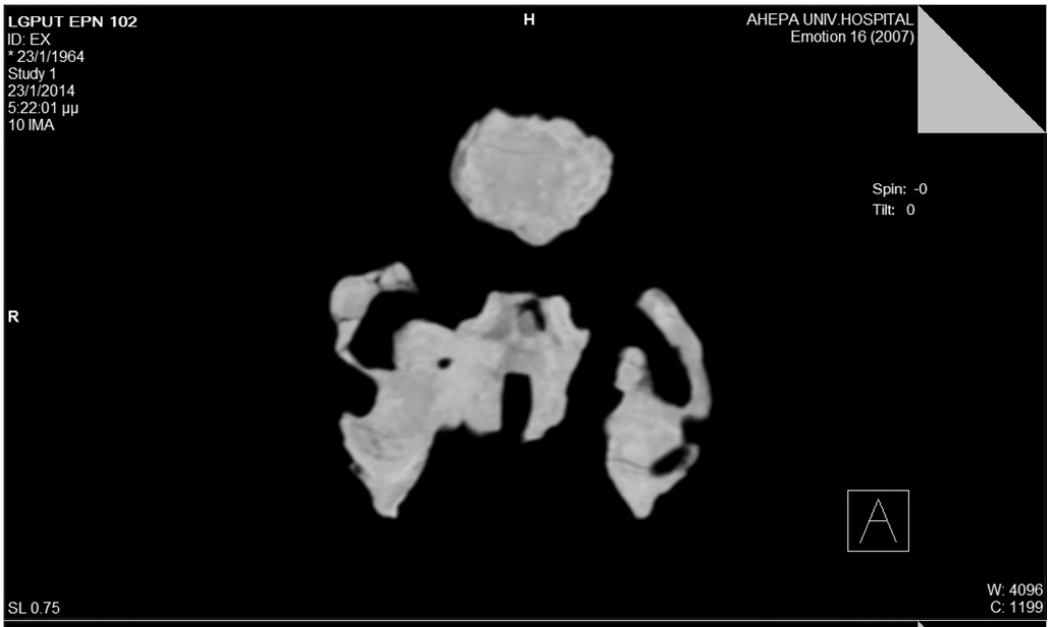

LGPUT EPN 102
ID: EX
* 23/1/1964
Study 1
23/1/2014
5:22:01 μμ
16 IMA
H
AHEPA UNIV.HOSPITAL
Emotion 16 (2007)
Spin: -0
Tilt: 0
R
A
W: 4096
C: 1199
SL 0.75


LGPUT EPN 102
ID: EX
* 23/1/1964
Study 1
23/1/2014
5:22:01 μμ
15 IMA
H
AHEPA UNIV.HOSPITAL
Emotion 16 (2007)
Spin: -0
Tilt: 0
R
A
W: 4096
C: 1199
SL 0.75


LGPUT EPN 102
ID: EX
* 23/1/1964
Study 1
23/1/2014
5:22:01 μμ
13 IMA
H
AHEPA UNIV.HOSPITAL
Emotion 16 (2007)
Spin: -0
Tilt: 0
R
A
SL 0.75
W: 4096
C: 1199

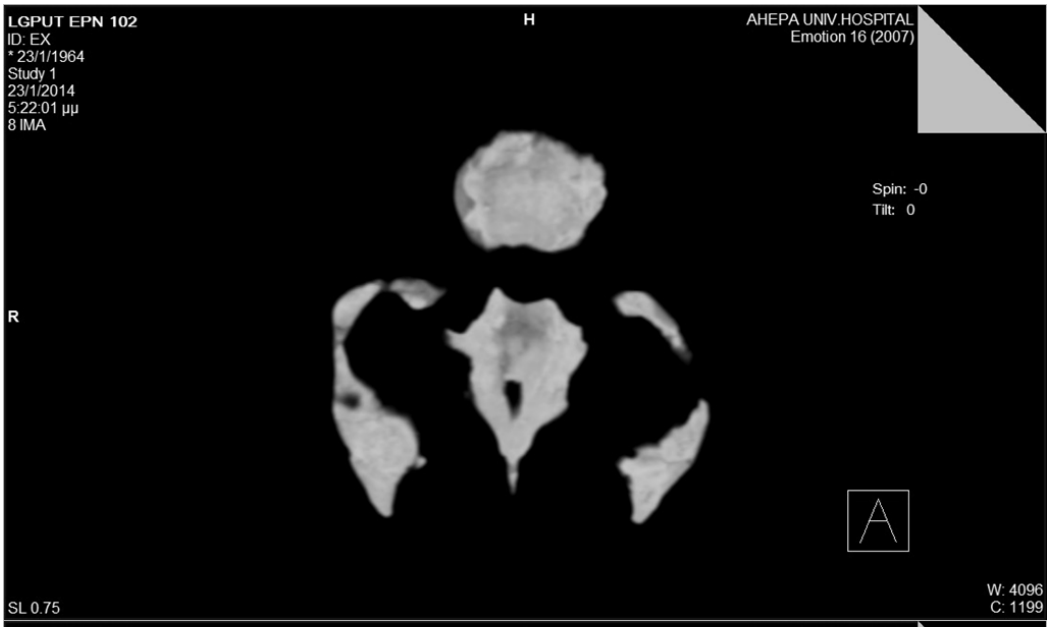

LGPUT EPN 102
ID: EX
* 23/1/1964
Study 1
23/1/2014
5:22:01 μμ
12 IMA
H
AHEPA UNIV.HOSPITAL
Emotion 16 (2007)
Spin: -0
Tilt: 0
R
A
SL 0.75
W: 4096
C: 1199


LGPUT EPN 102
ID: EX
* 23/1/1964
Study 1
23/1/2014
5:22:01 μμ
11 IMA
H
AHEPA UNIV.HOSPITAL
Emotion 16 (2007)
Spin: -0
Tilt: 0
R
A
SL 0.75
W: 4096
C: 1199


LGPUT EPN 102
ID: EX
* 23/1/1964
Study 1
23/1/2014
5:22:01 μμ
10 IMA
H
AHEPA UNIV.HOSPITAL
Emotion 16 (2007)
Spin: -0
Tilt: 0
R
A
SL 0.75
W: 4096
C: 1199


LGPUT EPN 102
ID: EX
* 23/1/1964
Study 1
23/1/2014
5:22:01 μμ
9 IMA
H
AHEPA UNIV.HOSPITAL
Emotion 16 (2007)
Spin: -0
Tilt: 0
R
A
SL 0.75
W: 4096
C: 1199

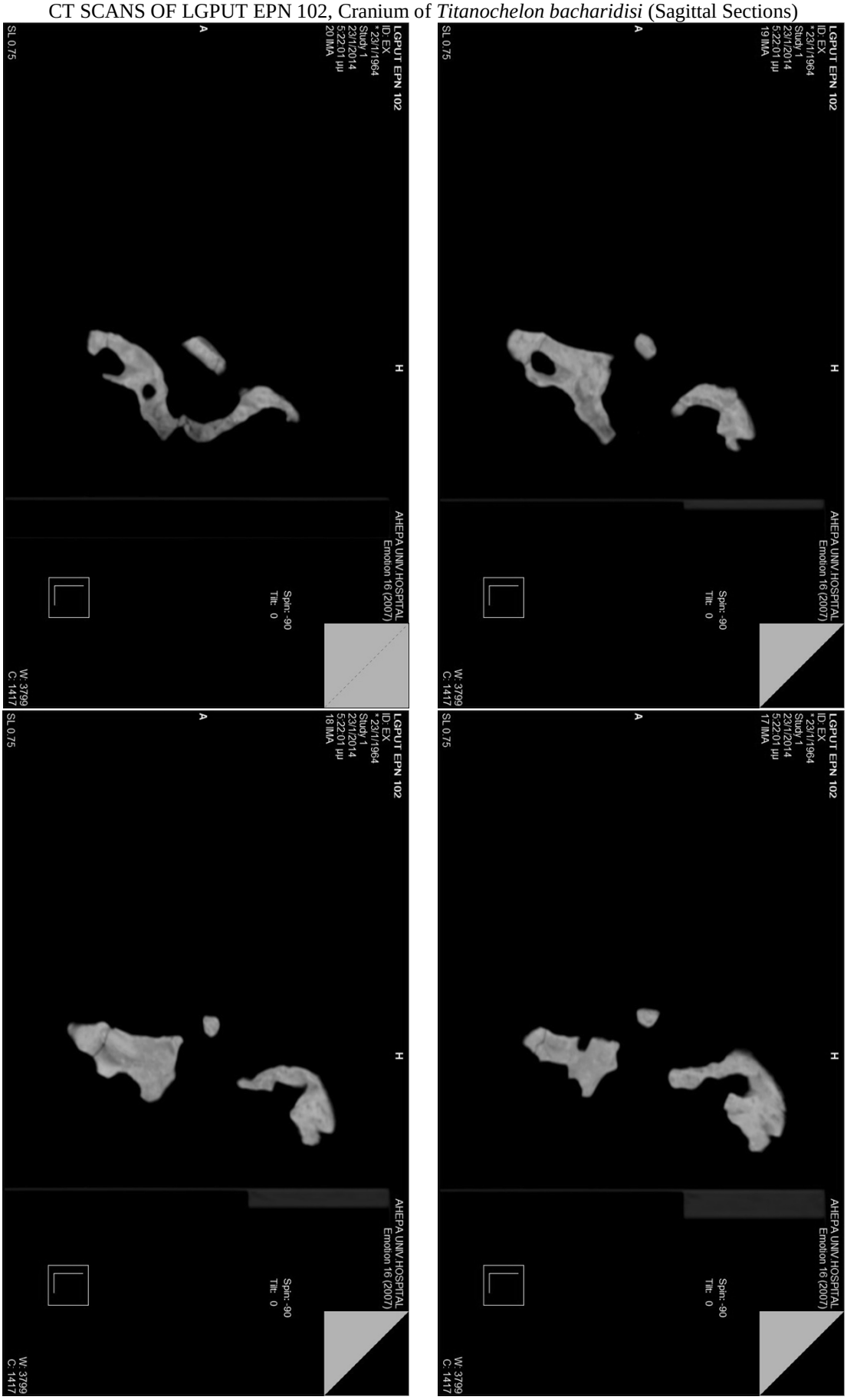

LGPUT EPN 102
ID: EX
* 23/1/1964
Study 1
23/1/2014
5:22:01 μμ
8 IMA
H
AHEPA UNIV.HOSPITAL
Emotion 16 (2007)
Spin: -0
Tilt: 0
R
A
SL 0.75
W: 4096
C: 1199


LGPUT EPN 102
ID: EX
* 23/1/1964
Study 1
23/1/2014
5:22:01 μμ
8 IMA
H
AHEPA UNIV.HOSPITAL
Emotion 16 (2007)
Spin: -0
Tilt: 0
R
A
SL 0.75
W: 4096
C: 1199


LGPUT EPN 102
ID: EX
* 23/1/1964
Study 1
23/1/2014
5:22:01 μμ
7 IMA
H
AHEPA UNIV.HOSPITAL
Emotion 16 (2007)
Spin: -0
Tilt: 0
R
A
SL 0.75
W: 4096
C: 1199


LGPUT EPN 102
ID: EX
* 23/1/1964
Study 1
23/1/2014
5:22:01 μμ
6 IMA
H
AHEPA UNIV.HOSPITAL
Emotion 16 (2007)
Spin: -0
Tilt: 0
R
A
SL 0.75
W: 4096
C: 1199

CT SCANS OF LGPUT EPN 102, Cranium of *Titanochelon bacharidisi* (Sagittal Sections)



LGPUT EPN 102
ID: EX
*23/1/1964
Study 1
23/1/2014
5.22.01 μμ
15 IMA
H
AHEPA UNIV.HOSPITAL
Emotion 16 (2007)
Spin: -90
Tilt: 0
A
W: 3799
C: 1417
SL 0.75
LGPUT EPN 102
ID: EX
*23/1/1964
Study 1
23/1/2014
5.22.01 μμ
13 IMA
H
AHEPA UNIV.HOSPITAL
Emotion 16 (2007)
Spin: -90
Tilt: 0
A
W: 3799
C: 1417
SL 0.75
LGPUT EPN 102
ID: EX
*23/1/1964
Study 1
23/1/2014
5.22.01 μμ
16 IMA
H
AHEPA UNIV.HOSPITAL
Emotion 16 (2007)
Spin: -90
Tilt: 0
A
W: 3799
C: 1417
SL 0.75
LGPUT EPN 102
ID: EX
*23/1/1964
Study 1
23/1/2014
5.22.01 μμ
14 IMA
H
AHEPA UNIV.HOSPITAL
Emotion 16 (2007)
Spin: -90
Tilt: 0
A
W: 3799
C: 1417
SL 0.75

LGPUT EPN 102
ID: EX
*23/1/1964
Study 1
23/1/2014
5.22.01 μμ
9 mA
H
AHEPA UNIV.HOSPITAL
Emotion 16 (2007)
Spin: -90
Tilt: 0
A
W: 3799
C: 1417
SL 0.75
LGPUT EPN 102
ID: EX
*23/1/1964
Study 1
23/1/2014
5.22.01 μμ
11 mA
H
AHEPA UNIV.HOSPITAL
Emotion 16 (2007)
Spin: -90
Tilt: 0
A
W: 3799
C: 1417
SL 0.75
LGPUT EPN 102
ID: EX
*23/1/1964
Study 1
23/1/2014
5.22.01 μμ
5 mA
H
AHEPA UNIV.HOSPITAL
Emotion 16 (2007)
Spin: -90
Tilt: 0
A
W: 3799
C: 1417
SL 0.75
LGPUT EPN 102
ID: EX
*23/1/1964
Study 1
23/1/2014
5.22.01 μμ
8 mA
H
AHEPA UNIV.HOSPITAL
Emotion 16 (2007)
Spin: -90
Tilt: 0
A
W: 3799
C: 1417
SL 0.75

TNT file used for the analysis of the testudinids.

```
xread
81 38

Chrysemys_picta
        02000111010020000000000000000021001010111000000101000101110110 1?00000001110000110
Mauremys_caspica
        00200112010000000000110000?10021021000001000000010000001100010 1?000??????????0???
Manouria_impressa
        00210102010010120011000000111010101102000000010001001100200111000000000??????[0 1]???
Geochelone_elegans
        10211102121010011110000000101100102100000000010001011110300111000000??????????????
Stigmochelys_pardalis
        00111103121010111111000?0000111110210101010001000101 0?012010112010 1??????????[0 1]???
Indotestudo_elongata
        00130113121010221111000000001120021101000100020001000101200010000000??????????[0 1]???
Indotestudo_forstenii
        00100113121010121110000000001120011101000100010001100101200110000011001010110[0 1]?10
Centrochelys_sulcata
        12121102121 0?02?111000??00111001102101010100010011011101200011001110011111110[0 1]111
Agrionemys_horsfieldii
        10110213121000111110000000001121020100100100000001001101200000000100??????????[2 3]???
Testudo_hermanni
        10100203121021220111000000001121010100101100000000100110200010201101001010110 2110
Testudo_graeca  001102131210[0 1 2]0121111000000[0 1]01121110122000000010001001101 2?00102111010111101 10[0 1 2 3]110
Testudo_marginata 00100[1 2]13121[0 1][0 2]0121[0 1]11000001[0 1]01121110122??????????????????????????????????101111101??2110
Milia_testudinid  ????????12102012111?????01001121100 1??????????????????????????????????????????????????????
Testudo_kleinmanni  0003021312102012[0 1]1100000000011211001201??????????????????????????????????????????????10
Testudo_marmorum
        02010113121 0?0121100000?000011211001221??????????????????????????????????????????
Samos_testudinid  00210113121010 12??1000000?0011210101?????????????????????????????????????????????
Testudo_antiqua  00[0 1]00[1 2]131[0 1 2]10102211100000000011211001000?????????????????????????????????????????
Kinixys_erosa
        02231101010020101101000011201100100000001101011000000001100111200 00?????????????
Gopherus_agassizii 00200113121010 0111[0 1]0000000311011100101001010111001101101100010001 01??????????[0 2]???
Gopherus_polyphemus  00200113121000011110001100[2 3]11010100002001110101001101101101110101 01??????????[0 2]???
Astrochelys_radiata
        00200103121010011100000000011100101101000100000011011101101110001 11?????????????
Chelonoidis_chilensis  0221111301[0 1]0100111100000001111[0 1]010110[0 1]01110001011101110120101020210000111011000 10
Chelonoidis_nigra  1222111301[0 1]0100111100000001011200021020001000101110111111201011202100011111110011 0
Chelonoidis_carbonaria  01[1 2]01113121010021110000000111[0 2]0101101001100010111001201200011202 1??????????????
Chelonoidis_denticulata
        01201113121010021110000000011100102101001100010111011201201011002 1??????????????
Titanochelon_bolivari  01101113121010211110001100[0 1 2][0 1]11211021010001000101110011 0??00112??1?01111111[0 1]0?1?0
Titanochelon_vitodurana
        02101?131210??21??1000110?00112110210?0?????????????????????????????????????
Titanochelon_perpiniana
        01101113121010211110 0?100001101112101 0????00?????????????0???????00111111??????
Titanochelon_bacharidisi  ???????????010?11110???1000[0 1]11111121010001011 1?1???01?0????1111??1?0011111110?1?1
Achilemys_cassouleti
        00000100200000200000000000001000100001 1??????????????????????????????????????????
Gigantochersina_ammon
        00200103121010111?10000000011?21122101 0??????????????????????????????????????????
Namibchersus_namaquensis
```

```
	02200113121010011110000000001121102100??????????????????????????????????????????
Testudo_gigas	??021????????0??1?000?000000112110010100??????????????????????????????????????????
Paleotestudo_canetoniana	00[0
1]00113121010221111000000001121000000100??????????????????????????????????????????
Ergilemys_bruneti
	01130113121010011011000000000120102120??????????????????????????????????????????
Hadrianus_castrensis
	01130002110010110?000000001110200200010??????????????????????????????????????????
Cheirogaster_maurini
	02221?131100001???00110?00111?201000010??????????????????????????????????????????
Impregnochelys_pachytestis
	???00???????10?????0??????01112100110100??????????????????????????????????11???????
;

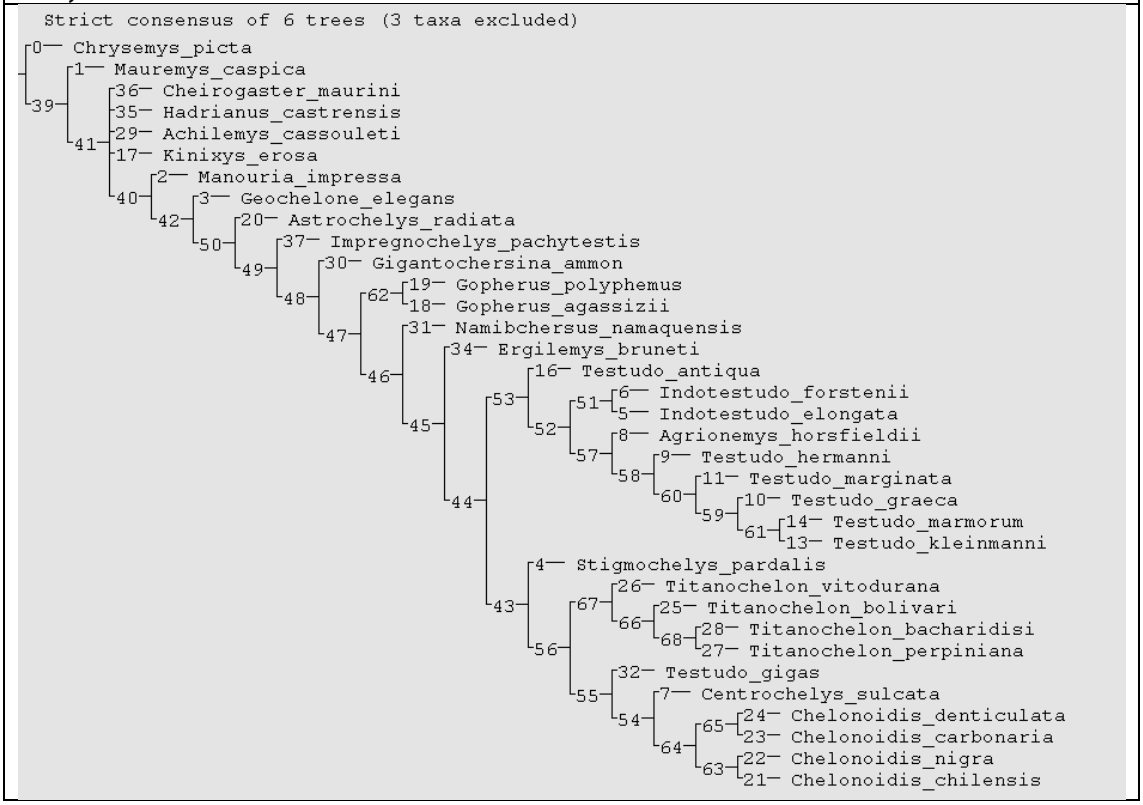
cnames

{0 NUCHAL_1 hexagonal_ octagonal_;
{1 NUCHAL_2 markedly_wider_than_long_ slightly_wider_than_long_or_as_long_as_wide_
markedly_longer_than_wide;
{2 NUCHAL_3 first_pleural_overlaps_postero-lateral_parts_of_the_nuchal
first_pleural_touches,_but_it_does_not_overlap_the_nuchal_ first_pleural_is_not_in_contact_with_the_nuchal_;
{3 NUCHAL_4 notch_absent_ shallow_ deep_ significant_medial_protrusion_present_;
{4 CERVICAL dorsally_present_ absent_;
{5 NEURAL_NUMBER nine_neurals_ eight_neurals_ seven_neurals_or_less_;
{6 NEURAL_1 hexagonal,_short_sides_positioned_posteriorly_ rectangular_;
{7 NEURAL_2 rectangular hexagonal,_short_sides_positioned_anteriorly_
hexagonal,_short_sides_positioned_posteriorly octagonal_;
{8 NEURAL_3 hexagonal_ rectangular_ octagonal_;
{9 NEURAL_4 rectangular_ hexagonal_ octagonal_;
{10 NEURAL_5 hexagonal_ rectangular_;
{11 COSTAL Medial_contact_absent present_;
{12 SUPRAPYGAL
two,_the_contact_between_the_suprapygals_is_straight_and_perpendicular_to_the_axial_plane
two,_both_suprapygals_constitute_one_trapeze_and_the_first_suprapygal_embrassing_the_lenticular_second_one
_ one,_suprapygals_fused,_constituting_one_trapeze_;
{13 PYGAL quadrangular_(without_small_latero-anterior_borders)
quadrangular_or_hexagonal_with_small_latero-anterior_borders;
{14 VERTEBRAL_1 wide_vertebrals,_wider_than_the_pleurals_ wide_vertebrals,_almost_equal_to_the_pleurals
narrow_vertebrals,_narrower_than_the_pleurals;
{15 VERTEBRAL_2 he_posterior_sulcus_of_the_fifth_vertebral_overlaps_the_anterior_part_of_the_pygal
the_posterior_sulcus_of_the_fifth_vertebral_crosses_the_suprapygal_transversely
the_posterior_sulcus_of_the_fifth_vertebral_coincides_with_the_suprapygal-pygal_suture_;
{16 SUPRACAUDAL_1 two_twelfth_marginals_present_dorsally_
twelfth_marginals_fused_into_a_supracaudal_dorsally;
{17 SUPRACAUDAL_2 two_twelfth_marginals_present_viscerally_
twelfth_marginals_fused_into_a_supracaudal_viscerally;
{18 COINCIDENCE absent_ present_;
{19 PERIPHERAL absent_or_poorly_developed_ well_developed_;
{20 MARGINAL_2_with_NUCHAL absent_ present_;
{21 MARGINAL_2_with_VERTEBRAL_1 absent_ present_;
{22 MARGINAL_4_with_PLEURAL_2 absent_ present_;
{23 MARGINAL_6_with_PLEURAL_3 absent_ present_;
{24 CARAPACIAL_HINGE absent_ present_;
{25 BORDER posterior_border_curved_inwards_ posterior_border_posteriorly_flared_;
{26 ANTERIOR_LOBE subrounded_to_straight_ medially_notched_ trilobed_ triagonal_;
{27 GULAR_PROTRUSION absent_ present_;
{28 EPIPLASTRAL_LIP absent_or_poorly_developed_ present_;
{29 EPIPLASTRAL_LIP_SHAPE concave_ convex_to_flat_;
{30 GULARS_vs_ENTOPLASTRON not_in_contact_ in_contact_with_the_anterior_margin_
covering_the_anterior_area;
{31 GULARS_ANGLE 45?_or_more_obtuse_ more_acute_;
{32 HUMERAL_LENGTH humerals_equal_or_smaller_than_the_gulars_ humerals_longer_than_the_gulars_;
{33 HUMEROPECTORAL_POSITION posterior_to_the_entoplastron_
coinciding_medially_with_the_posterior_suture_of_the_entoplastron crossing_the_entoplastron_;
{34 HUMEROPECTORAL_SHAPE
not_perpendicular_to_the_axial_plane,_rounded_or_forming_a_wide_angle_
perpendicular_to_the_axial_plane,_relatively_straight_throughout_its_width_
```

perpendicular_to_the_axial_plane,_with_a_well-developed_lateral_change_of_curvature;
{35 PECTORAL_LENGTH long short;
{36 PLASTRAL_HINGE absent_ present,_between_hyoplastra_and_hypoplastra_
present,_between_hypoplastra_and_xiphiplastra;
{37 FEMOROANAL_SHAPE acute_angle_with_the_axial_plane_
straight_or_slightly_rounded,_developed_mainly_perpendicular_with_the_axial_plane forms_S-
shaped_curve_laterally;
{38 ANAL_LENGTH shorter_than_the_median_length_of_femoral_
longer_than_the_medial_length_of_femoral_;
{39 FRONTAL_vs_ORBIT participates_to_the_formation_of_the_orbital_rim_ excluded_from_the_orbit;
{40 FRONTAL_vs_PREFRONTALS frontals_longer_than_prefrontals_ prefrontals_longer_than_frontals;
{41 DESCENDING_FRONTAL absent,_or_very_small_ present,_well-developed_;
{42 SULCUS_OLFACTURIUS ventrally_open_ ventrally_nearly_closed_;
{43 FOSSA_ORBITALIS_POSITION anterior_to_middle_ posterior_;
{44 VENTRAL_TEMPORAL_EMARGINATION small_ extensive_;
{45 MAX-PRE_SYMPHYSIS_HEIGHT short,_shorter_than_the_height_of_fossa_nasalis_
short,_shorter_than_the_height_of_fossa_nasalis,_but_with_the_development_of_a_dorsal_projection_
high,_taller_than_the_height_of_fossa_nasalis;
{46 PREMAX_RIDGE absent_ present_;
{47 PREMAX_PIT absent_ present_;
{48 MAX-PREMAX_RIDGE absent_ present_;
{49 TRITURATING_RIDGES one,_labial_only three;
{50 LINGUAL_RIDGE restricted_to_maxilla_ extending_onto_premaxillae_;
{51 LABIAL_RIDGE absent_ present_;
{52 POSTERIOR_MAX_PROCESS absent_ present_;
{53 MEDIAN_MAX_RIDGE absent_ present,_restricted_to_maxilla present,_extending_to_premaxilla;
{54 MAX_RIDGE absent_ present_;
{55 VOMER_RIDGE absent_ present_;
{56 VOMER vomer_short,_not_dividing_the_palatines_ vomer_dividing_the_palatines,_not_the_pterygoids
vomer_diving_part_of_the_pterygoids,_not_reaching_the_basisphenoid_
vomer_dividing_palatines_and_pterygoids,_reaching_the_basisphenoid_;
{57 PTERYGOID-BASIOCCIPITAL present_ absent_;
{58 FORAMEN_PRAEPALATINUM visible_ not_visible_in_ventral_view_-
_foramina_may_be_concealed_by_lingual_extensions_of_the_maxillary_alveolar_ridges_;
{59 SQUAMOSALS not_extending_ extending_beyond_the_condylus_occipitalis_;
{60 CRISTA_SUPRAOCCIPITALIS_LENGTH not_extending_ extending_beyond_the_condylus_occipitalis_;
{61 CRISTA_SUPRAOCCIPITALIS_KEELS absent_ present_;
{62 CRISTA_SUPRAOCCIPITALIS_SHAPE straight_ bended_inwards_ elevated_posteriorly_;
{63 PARIETAL_vs_QUADRATE_contact absent_ present_;
{64 OPISTHOTIC not_expanded,_fenestra_postotica_open_ expanded,_could_contact_exoccipital
expanded,_contacting_the_pterygoid_;
{65 PROCESSUS_TROCHLEARIS_OTICUM absent,_or_small_ large;
{66 FORAMEN_NERVI_TRIGEMINI one two;
{67 HUMERUS_DIAPHYSIS slightly_curved_ well-developed_curvature_;
{68 HUMERUS_DISTAL_END symmetric_ asymmetric_;
{69 HUMERUS_SCAR absent_or_reduced_ present_;
{70 HUMERUS_MAJOR_TROCHANTER short,_not_extending_beyond_the_humeral_head_
long,_extending_beyond_the_humeral_head_;
{71 SCAPULA_GLENOID_FOSSA relatively_short_ elongated_;
{72 CORACOID long_and_narrow fan-shaped;
{73 FEMUR_HEAD_ANGLE relatively_large_angle_
femoral_head_developed_almost_perpendicular_to_the_diaphysis_;
{74 FEMUR_TROCHANTERS not_fused fused_;
{75 MED_+_LAT_CENTRALE not_fused fused_;
{76 ULN_+_INTERMEDIUM not_fused fused_;
{77 MANUS two_phalanges_in_all_digits_ one_phalanx_in_fifth_finger_ one_phalanx_in_first_and_fifth_finger
one_phalanx_in_second_and_fifth_finger_;
{78 AS_+_CAL not_fused fused_;
{79 PES_5th_PHALANX present_ absent;
{80 THIGH_SPURS absent present_;
;

proc /;
comments 0
;

Analysis #1: Number of nodes



Analysis #1: Common synapomorphies

Synapomorphies common to 6 trees
(Node numbers refer to nodes in consensus)

Chrysemys_picta :
All trees:
-No autapomorphies:

Mauremys_caspica :
All trees:
-MARGINAL_2_with_NUCHAL (20): absent_ --> present_
-MARGINAL_2_with_VERTEBRAL_1 (21): absent_ --> present_
-HUMEROPECTORAL_POSITION (33): posterior_to_the_entoplastron_ --> crossing_the_entoplastron_
-MAX-PREMAX_RIDGE (48): absent_ --> present_
-SQUAMOSALS (59): extending_beyond_the_condylus_occipitalis_ --> not_extending_
Some trees:
-GULAR_PROTRUSION (27): absent_ --> present_

Manouria_impressa :
All trees:
-VERTEBRAL_2 (15): the_posterior_sulcus_of_the_fifth_vertebral_crosses_the_suprapygal_transversely --> the_posterior_sulcus_of_the_fifth_vertebral_coincides_with_the_suprapygal-pygal_suture_
-PERIPHERAL (19): absent_or_poorly_developed_ --> well_developed_
-FEMOROANAL_SHAPE (37): acute_angle_with_the_axial_plane_, or straight_or_slightly_rounded,_developed_mainly_perpendicular_with_the_axial_plane --> forms_S-shaped_curve_laterally
-VOMER (56): vomer_dividing_the_palatines,_not_the_pterygoids --> vomer_diving_part_of_the_pterygoids,_not_reaching_the_basisphenoid_
Some trees:
-NEURAL_3 (8): rectangular_ --> hexagonal_
-GULARS_vs_ENTOPLASTRON (30): not_in_contact_ --> in_contact_with_the_anterior_margin_

Geochelone_elegans :
All trees:
-NUCHAL_1 (0): hexagonal_ --> octagonal_
-CERVICAL (4): dorsally_present_ --> absent_
-GULAR_PROTRUSION (27): present_ --> absent_
-HUMEROPECTORAL_SHAPE (34): perpendicular_to_the_axial_plane,_relatively_straight_throughout_its_width_ --> perpendicular_to_the_axial_plane,_with_a_well-developed_lateral_change_of_curvature

-MAX_RIDGE (54): absent_ --> present_
-VOMER (56): vomer_dividing_the_palatines,_not_the_pterygoids -->
vomer_dividing_palatines_and_pterygoids,_reaching_the_basisphenoid_
Some trees:
-FEMOROANAL_SHAPE (37): straight_or_slightly_rounded,_developed_mainly_perpendicular_with_the_axial_plane -->
acute_angle_with_the_axial_plane_

Stigmochelys_pardalis :
All trees:
-NUCHAL_4 (3): notch_absent_ --> shallow_
-NEURAL_1 (6): rectangular_ --> hexagonal,_short_sides_positioned_posteriorly_
-PERIPHERAL (19): absent_or_poorly_developed_ --> well_developed_
-GULARS_vs_ENTOPLASTRON (30): covering_the_anterior_area --> in_contact_with_the_anterior_margin_
-FRONTAL_vs_ORBIT (39): participates_to_the_formation_of_the_orbital_rim_ --> excluded_from_the_orbit
-POSTERIOR_MAX_PROCESS (52): present_ --> absent_
-FORAMEN_PRAEPALATINUM (58): visible_ --> not_visible_in_ventral_view_-
_foramina_may_be_concealed_by_lingual_extensions_of_the_maxillary_alveolar_ridges_

Indotestudo_elongata :
All trees:
-NUCHAL_4 (3): notch_absent_ --> significant_medial_protrusion_present_
-PERIPHERAL (19): absent_or_poorly_developed_ --> well_developed_
-MAX-PRE_SYMPHYSIS_HEIGHT (45):
short,_shorter_than_the_height_of_fossa_nasalis,_but_with_the_development_of_a_dorsal_projection_ -->
high,_taller_than_the_height_of_fossa_nasalis

Indotestudo_forstenii :
All trees:
-LINGUAL_RIDGE (50): restricted_to_maxilla_ --> extending_onto_premaxillae_
-SQUAMOSALS (59): not_extending_ --> extending_beyond_the_condylus_occipitalis_

Centrochelys_sulcata :
All trees:
-NUCHAL_1 (0): hexagonal_ --> octagonal_
-NEURAL_1 (6): rectangular_ --> hexagonal,_short_sides_positioned_posteriorly_
-NEURAL_2 (7): octagonal_ --> hexagonal,_short_sides_positioned_posteriorly
-EPIPLASTRAL_LIP_SHAPE (29): convex_to_flat_ --> concave_
-FRONTAL_vs_ORBIT (39): participates_to_the_formation_of_the_orbital_rim_ --> excluded_from_the_orbit
-CRISTA_SUPRAOCCIPITALIS_SHAPE (62): elevated_posteriorly_ --> straight_
-THIGH_SPURS (80): absent --> present_

Agrionemys_horsfieldii :
All trees:
-NUCHAL_4 (3): notch_absent_ --> shallow_
-VERTEBRAL_2 (15): the_posterior_sulcus_of_the_fifth_vertebral_coincides_with_the_suprapygal-pygal_suture_ -->
the_posterior_sulcus_of_the_fifth_vertebral_crosses_the_suprapygal_transversely
-CRISTA_SUPRAOCCIPITALIS_LENGTH (60): extending_beyond_the_condylus_occipitalis_ --> not_extending_

Testudo_hermanni :
All trees:
-NEURAL_1 (6): rectangular_ --> hexagonal,_short_sides_positioned_posteriorly_
-PYGAL (13): quadrangular_(without_small_latero-anterior_borders) --> quadrangular_or_hexagonal_with_small_latero-
anterior_borders
-SUPRACAUDAL_1 (16): twelfth_marginals_fused_into_a_supracaudal_dorsally -->
two_twelfth_marginals_present_dorsally_
-FRONTAL_vs_PREFRONTALS (40): frontals_longer_than_prefrontals_ --> prefrontals_longer_than_frontals

Testudo_graeca :
All trees:
-ANAL_LENGTH (38): longer_than_the_medial_length_of_femoral_ --> shorter_than_the_median_length_of_femoral_

Testudo_marginata :
All trees:
-BORDER (25): posterior_border_curved_inwards_ --> posterior_border_posteriorly_flared_

Testudo_kleinmanni :
All trees:
-NUCHAL_4 (3): shallow_ --> significant_medial_protrusion_present_
-FEMOROANAL_SHAPE (37): forms_S-shaped_curve_laterally --> acute_angle_with_the_axial_plane_

Testudo_marmorum :
All trees:

-NUCHAL_2 (1): markedly_wider_than_long_ --> markedly_longer_than_wide
-NEURAL_NUMBER (5): seven_neurals_or_less_ --> eight_neurals_
-COINCIDENCE (18): present_ --> absent_

Testudo_antiqua :
All trees:
-No autapomorphies:

Kinixys_erosa :
All trees:
-PERIPHERAL (19): absent_or_poorly_developed_ --> well_developed_
-CARAPACIAL_HINGE (24): absent_ --> present_
-BORDER (25): posterior_border_curved_inwards_ --> posterior_border_posteriorly_flared_
Some trees:
-CERVICAL (4): dorsally_present_ --> absent_
-SUPRAPYGAL (12): two,_the_contact_between_the_suprapygals_is_straight_and_perpendicular_to_the_axial_plane --> one,_suprapygals_fused,_constituting_one_trapeze_
-SUPRACAUDAL_1 (16): two_twelfth_marginals_present_dorsally_ --> twelfth_marginals_fused_into_a_supracaudal_dorsally
-SUPRACAUDAL_2 (17): two_twelfth_marginals_present_viscerally_ --> twelfth_marginals_fused_into_a_supracaudal_viscerally
-ANTERIOR_LOBE (26): subrounded_to_straight_, or medially_notched_ --> trilobed_
-EPIPLASTRAL_LIP_SHAPE (29): concave_ --> convex_to_flat_
-FEMOROANAL_SHAPE (37): straight_or_slightly_rounded,_developed_mainly_perpendicular_with_the_axial_plane --> acute_angle_with_the_axial_plane_
-DESCENDING_FRONTAL (41): absent,_or_very_small_ --> present,_well-developed_
-FOSSA_ORBITALIS_POSITION (43): anterior_to_middle_ --> posterior_
-PREMAX_RIDGE (46): absent_ --> present_

Gopherus_agassizii :
All trees:
-DESCENDING_FRONTAL (41): present,_well-developed_ --> absent,_or_very_small_

Gopherus_polyphemus :
All trees:
-SUPRAPYGAL (12): two,_both_suprapygals_constitute_one_trapeze_and_the_first_suprapygal_embrassing_the_lenticular_second_one_ --> two,_the_contact_between_the_suprapygals_is_straight_and_perpendicular_to_the_axial_plane
-MARGINAL_4_with_PLEURAL_2 (22): absent_ --> present_
-MARGINAL_6_with_PLEURAL_3 (23): absent_ --> present_
-GULARS_ANGLE (31): more_acute_ --> 45?_or_more_obtuse_
-PECTORAL_LENGTH (35): short --> long
-FEMOROANAL_SHAPE (37): straight_or_slightly_rounded,_developed_mainly_perpendicular_with_the_axial_plane --> forms_S-shaped_curve_laterally
-MAX-PRE_SYMPHYSIS_HEIGHT (45): short,_shorter_than_the_height_of_fossa_nasalis,_but_with_the_development_of_a_dorsal_projection_ --> short,_shorter_than_the_height_of_fossa_nasalis_
-FORAMEN_PRAEPALATINUM (58): visible_ --> not_visible_in_ventral_view_-_foramina_may_be_concealed_by_lingual_extensions_of_the_maxillary_alveolar_ridges_
-CRISTA_SUPRAOCCIPITALIS_SHAPE (62): straight_ --> bended_inwards_

Astrochelys_radiata :
All trees:
-COINCIDENCE (18): present_ --> absent_
-MAX-PRE_SYMPHYSIS_HEIGHT (45): short,_shorter_than_the_height_of_fossa_nasalis,_but_with_the_development_of_a_dorsal_projection_ --> short,_shorter_than_the_height_of_fossa_nasalis_
-MAX-PREMAX_RIDGE (48): absent_ --> present_
-FORAMEN_PRAEPALATINUM (58): visible_ --> not_visible_in_ventral_view_-_foramina_may_be_concealed_by_lingual_extensions_of_the_maxillary_alveolar_ridges_
-PROCESSUS_TROCHLEARIS_OTICUM (65): absent,_or_small_ --> large

Chelonoidis_chilensis :
All trees:
-NUCHAL_4 (3): deep_ --> shallow_
-HUMEROPECTORAL_SHAPE (34): perpendicular_to_the_axial_plane,_with_a_well-developed_lateral_change_of_curvature --> perpendicular_to_the_axial_plane,_relatively_straight_throughout_its_width_
-FRONTAL_vs_ORBIT (39): participates_to_the_formation_of_the_orbital_rim_ --> excluded_from_the_orbit
-CRISTA_SUPRAOCCIPITALIS_KEELS (61): present_ --> absent_
-HUMERUS_SCAR (69): present_ --> absent_or_reduced_
-FEMUR_HEAD_ANGLE (73): femoral_head_developed_almost_perpendicular_to_the_diaphysis_ --> relatively_large_angle_
-AS_+_CAL (78): fused_ --> not_fused

Chelonoidis_nigra :
All trees:
-NUCHAL_1 (0): hexagonal_ --> octagonal_
-GULAR_PROTRUSION (27): present_ --> absent_
-GULARS_vs_ENTOPLASTRON (30): not_in_contact_ --> covering_the_anterior_area
-HUMERAL_LENGTH (32): humerals_longer_than_the_gulars_ --> humerals_equal_or_smaller_than_the_gulars_
-FEMOROANAL_SHAPE (37): straight_or_slightly_rounded,_developed_mainly_perpendicular_with_the_axial_plane --> forms_S-shaped_curve_laterally
-MAX_RIDGE (54): absent_ --> present_

Chelonoidis_carbonaria :
All trees:
-HUMEROPECTORAL_SHAPE (34): perpendicular_to_the_axial_plane,_with_a_well-developed_lateral_change_of_curvature --> perpendicular_to_the_axial_plane,_relatively_straight_throughout_its_width_
-LABIAL_RIDGE (51): present_ --> absent_

Chelonoidis_denticulata :
All trees:
-CRISTA_SUPRAOCCIPITALIS_SHAPE (62): elevated_posteriorly_ --> straight_

Titanochelon_bolivari :
All trees:
-HUMERUS_DISTAL_END (68): symmetric_ --> asymmetric_

Titanochelon_vitodurana :
All trees:
-No autapomorphies:

Titanochelon_perpiniana :
All trees:
-No autapomorphies:

Titanochelon_bacharidisi :
All trees:
-FOSSA_ORBITALIS_POSITION (43): anterior_to_middle_ --> posterior_
-VENTRAL_TEMPORAL_EMARGINATION (44): small_ --> extensive_
-SQUAMOSALS (59): not_extending_ --> extending_beyond_the_condylus_occipitalis_

Achilemys_cassouleti :
All trees:
-NEURAL_4 (9): hexagonal_ --> rectangular_
Some trees:
-NUCHAL_3 (2): first_pleural_is_not_in_contact_with_the_nuchal_ --> first_pleural_overlaps_postero-lateral_parts_of_the_nuchal
-NEURAL_2 (7): hexagonal,_short_sides_positioned_anteriorly_, or hexagonal,_short_sides_positioned_posteriorly --> rectangular
-NEURAL_3 (8): hexagonal_ --> octagonal_
-VERTEBRAL_1 (14): wide_vertebrals,_almost_equal_to_the_pleurals --> narrow_vertebrals,_narrower_than_the_pleurals
-ANAL_LENGTH (38): shorter_than_the_median_length_of_femoral_ --> longer_than_the_medial_length_of_femoral_

Gigantochersina_ammon :
All trees:
-VERTEBRAL_1 (14): wide_vertebrals,_wider_than_the_pleurals_ --> wide_vertebrals,_almost_equal_to_the_pleurals
-HUMEROPECTORAL_POSITION (33): posterior_to_the_entoplastron_ --> crossing_the_entoplastron_

Namibchersus_namaquensis :
All trees:
-NUCHAL_2 (1): markedly_wider_than_long_ --> markedly_longer_than_wide

Testudo_gigas :
All trees:
-NUCHAL_3 (2): first_pleural_touches,_but_it_does_not_overlap_the_nuchal_ --> first_pleural_overlaps_postero-lateral_parts_of_the_nuchal
-COINCIDENCE (18): present_ --> absent_
-HUMEROPECTORAL_SHAPE (34): perpendicular_to_the_axial_plane,_with_a_well-developed_lateral_change_of_curvature --> not_perpendicular_to_the_axial_plane,_rounded_or_forming_a_wide_angle_

Ergilemys_bruneti :
All trees:
-NUCHAL_2 (1): markedly_wider_than_long_ --> slightly_wider_than_long_or_as_long_as_wide_
-NUCHAL_4 (3): notch_absent_ --> significant_medial_protrusion_present_

-SUPRACAUDAL_2 (17): twelfth_marginals_fused_into_a_supracaudal_viscerally -->
two_twelfth_marginals_present_viscerally_
-PERIPHERAL (19): absent_or_poorly_developed_ --> well_developed_
-EPIPLASTRAL_LIP (28): present_ --> absent_or_poorly_developed_
-GULARS_ANGLE (31): more_acute_ --> 45?_or_more_obtuse_
-PLASTRAL_HINGE (36): absent_ --> present,_between_hypoplastra_and_xiphiplastra

Hadrianus_castrensis :
All trees:
-NUCHAL_3 (2): first_pleural_is_not_in_contact_with_the_nuchal_ -->
first_pleural_touches,_but_it_does_not_overlap_the_nuchal_
-HUMERAL_LENGTH (32): humerals_longer_than_the_gulars_ --> humerals_equal_or_smaller_than_the_gulars_
-HUMEROPECTORAL_POSITION (33): posterior_to_the_entoplastron_ --> crossing_the_entoplastron_
Some trees:
-NUCHAL_2 (1): markedly_wider_than_long_ --> slightly_wider_than_long_or_as_long_as_wide_
-NEURAL_NUMBER (5): eight_neurals_ --> nine_neurals_

Cheirogaster_maurini :
All trees:
-MARGINAL_2_with_NUCHAL (20): absent_ --> present_
-MARGINAL_2_with_VERTEBRAL_1 (21): absent_ --> present_
Some trees:
-NUCHAL_4 (3): significant_medial_protrusion_present_ --> deep_
-CERVICAL (4): dorsally_present_ --> absent_
-NEURAL_1 (6): hexagonal,_short_sides_positioned_posteriorly_ --> rectangular_
-NEURAL_2 (7): hexagonal,_short_sides_positioned_anteriorly_, or hexagonal,_short_sides_positioned_posteriorly -->
octagonal_

Impregnochelys_pachytestis :
All trees:
-HUMERAL_LENGTH (32): humerals_longer_than_the_gulars_ --> humerals_equal_or_smaller_than_the_gulars_

Node 39 :
All trees:
-No synapomorphies

Node 40 :
All trees:
-COINCIDENCE (18): absent_ --> present_
-HUMEROPECTORAL_SHAPE (34): not_perpendicular_to_the_axial_plane,_rounded_or_forming_a_wide_angle_ -->
perpendicular_to_the_axial_plane,_relatively_straight_throughout_its_width_
-PECTORAL_LENGTH (35): long --> short
Some trees:
-NUCHAL_4 (3): significant_medial_protrusion_present_ --> shallow_

Node 41 :
All trees:
-EPIPLASTRAL_LIP (28): absent_or_poorly_developed_ --> present_
-GULARS_ANGLE (31): more_acute_ --> 45?_or_more_obtuse_
-HUMERAL_LENGTH (32): humerals_equal_or_smaller_than_the_gulars_ --> humerals_longer_than_the_gulars_
-HUMEROPECTORAL_SHAPE (34): perpendicular_to_the_axial_plane,_relatively_straight_throughout_its_width_ -->
not_perpendicular_to_the_axial_plane,_rounded_or_forming_a_wide_angle_
Some trees:
-NEURAL_1 (6): rectangular_ --> hexagonal,_short_sides_positioned_posteriorly_
-VERTEBRAL_1 (14): wide_vertebrals,_wider_than_the_pleurals_ --> wide_vertebrals,_almost_equal_to_the_pleurals
-GULARS_vs_ENTOPLASTRON (30): covering_the_anterior_area --> not_in_contact_
-FEMOROANAL_SHAPE (37): acute_angle_with_the_axial_plane_ -->
straight_or_slightly_rounded,_developed_mainly_perpendicular_with_the_axial_plane
-MAX-PRE_SYMPHYSIS_HEIGHT (45): short,_shorter_than_the_height_of_fossa_nasalis_ -->
short,_shorter_than_the_height_of_fossa_nasalis,_but_with_the_development_of_a_dorsal_projection_
-CRISTA_SUPRAOCCIPITALIS_KEELS (61): absent_ --> present_

Node 42 :
All trees:
-NEURAL_4 (9): hexagonal_ --> octagonal_
-NEURAL_5 (10): hexagonal_ --> rectangular_
-VERTEBRAL_1 (14): wide_vertebrals,_almost_equal_to_the_pleurals --> wide_vertebrals,_wider_than_the_pleurals_
-SUPRACAUDAL_1 (16): two_twelfth_marginals_present_dorsally_ -->
twelfth_marginals_fused_into_a_supracaudal_dorsally
-EPIPLASTRAL_LIP_SHAPE (29): concave_ --> convex_to_flat_
Some trees:
-SUPRACAUDAL_2 (17): two_twelfth_marginals_present_viscerally_ -->

twelfth_marginals_fused_into_a_supracaudal_viscerally

Node 43 :
All trees:
-CERVICAL (4): dorsally_present_ --> absent_
-FEMOROANAL_SHAPE (37): acute_angle_with_the_axial_plane_ -->
straight_or_slightly_rounded,_developed_mainly_perpendicular_with_the_axial_plane
-CRISTA_SUPRAOCCIPITALIS_KEELS (61): absent_ --> present_
-CRISTA_SUPRAOCCIPITALIS_SHAPE (62): straight_ --> elevated_posteriorly_

Node 44 :
All trees:
-VERTEBRAL_1 (14): wide_vertebrals,_wider_than_the_pleurals_ --> wide_vertebrals,_almost_equal_to_the_pleurals, or
narrow_vertebrals,_narrower_than_the_pleurals

Node 45 :
All trees:
-NUCHAL_3 (2): first_pleural_is_not_in_contact_with_the_nuchal_ -->
first_pleural_touches,_but_it_does_not_overlap_the_nuchal_

Node 46 :
All trees:
-GULAR_PROTRUSION (27): present_ --> absent_
-FEMOROANAL_SHAPE (37): straight_or_slightly_rounded,_developed_mainly_perpendicular_with_the_axial_plane -->
acute_angle_with_the_axial_plane_

Node 47 :
All trees:
-NEURAL_1 (6): hexagonal,_short_sides_positioned_posteriorly_ --> rectangular_

Node 48 :
All trees:
-HUMEROPECTORAL_SHAPE (34): perpendicular_to_the_axial_plane,_relatively_straight_throughout_its_width_ -->
perpendicular_to_the_axial_plane,_with_a_well-developed_lateral_change_of_curvature

Node 49 :
All trees:
-GULARS_ANGLE (31): 45?_or_more_obtuse_ --> more_acute_
Some trees:
-GULARS_vs_ENTOPLASTRON (30): not_in_contact_ --> covering_the_anterior_area

Node 50 :
All trees:
-NEURAL_2 (7): hexagonal,_short_sides_positioned_posteriorly --> octagonal_
-ANTERIOR_LOBE (26): medially_notched_ --> subrounded_to_straight_
-DESCENDING_FRONTAL (41): absent,_or_very_small_ --> present,_well-developed_
-CRISTA_SUPRAOCCIPITALIS_KEELS (61): present_ --> absent_
-OPISTHOTIC (64): not_expanded,_fenestra_postotica_open_ --> expanded,_could_contact_exoccipital
-FORAMEN_NERVI_TRIGEMINI (66): one --> two
Some trees:
-NUCHAL_4 (3): shallow_ --> notch_absent_

Node 51 :
All trees:
-GULARS_ANGLE (31): more_acute_ --> 45?_or_more_obtuse_
-HUMEROPECTORAL_SHAPE (34): not_perpendicular_to_the_axial_plane,_rounded_or_forming_a_wide_angle_ -->
perpendicular_to_the_axial_plane,_relatively_straight_throughout_its_width_
-FEMOROANAL_SHAPE (37): acute_angle_with_the_axial_plane_ -->
straight_or_slightly_rounded,_developed_mainly_perpendicular_with_the_axial_plane
-POSTERIOR_MAX_PROCESS (52): present_ --> absent_
-OPISTHOTIC (64): expanded,_could_contact_exoccipital --> not_expanded,_fenestra_postotica_open_

Node 52 :
All trees:
-HUMERAL_LENGTH (32): humerals_longer_than_the_gulars_ --> humerals_equal_or_smaller_than_the_gulars_
-HUMEROPECTORAL_POSITION (33): posterior_to_the_entoplastron_ -->
coinciding_medially_with_the_posterior_suture_of_the_entoplastron, or crossing_the_entoplastron_

Node 53 :
All trees:
-VERTEBRAL_2 (15): the_posterior_sulcus_of_the_fifth_vertebral_crosses_the_suprapygal_transversely -->
the_posterior_sulcus_of_the_fifth_vertebral_coincides_with_the_suprapygal-pygal_suture_

-HUMEROPECTORAL_SHAPE (34): perpendicular_to_the_axial_plane,_with_a_well-developed_lateral_change_of_curvature --> not_perpendicular_to_the_axial_plane,_rounded_or_forming_a_wide_angle_

Node 54 :
All trees:
-GULAR_PROTRUSION (27): absent_ --> present_
-GULARS_vs_ENTOPLASTRON (30): covering_the_anterior_area --> not_in_contact_

Node 55 :
All trees:
-NUCHAL_4 (3): notch_absent_ --> deep_

Node 56 :
All trees:
-NUCHAL_2 (1): markedly_wider_than_long_ --> markedly_longer_than_wide
-MAX-PREMAX_RIDGE (48): absent_ --> present_
-PROCESSUS_TROCHLEARIS_OTICUM (65): absent,_or_small_ --> large

Node 57 :
All trees:
-NEURAL_NUMBER (5): eight_neurals_ --> seven_neurals_or_less_
-ANAL_LENGTH (38): shorter_than_the_median_length_of_femoral_ --> longer_than_the_medial_length_of_femoral_
-MANUS (77): two_phalanges_in_all_digits_ --> one_phalanx_in_first_and_fifth_finger

Node 58 :
All trees:
-PERIPHERAL (19): absent_or_poorly_developed_ --> well_developed_
-CRISTA_SUPRAOCCIPITALIS_SHAPE (62): straight_ --> elevated_posteriorly_
-PROCESSUS_TROCHLEARIS_OTICUM (65): absent,_or_small_ --> large

Node 59 :
All trees:
-NUCHAL_4 (3): notch_absent_ --> shallow_

Node 60 :
All trees:
-HUMERAL_LENGTH (32): humerals_equal_or_smaller_than_the_gulars_ --> humerals_longer_than_the_gulars_
-PLASTRAL_HINGE (36): absent_ --> present,_between_hypoplastra_and_xiphiplastra
-FEMOROANAL_SHAPE (37): acute_angle_with_the_axial_plane_ --> forms_S-shaped_curve_laterally
-HUMERUS_SCAR (69): absent_or_reduced_ --> present_

Node 61 :
All trees:
-NUCHAL_3 (2): first_pleural_touches,_but_it_does_not_overlap_the_nuchal_ --> first_pleural_overlaps_postero-lateral_parts_of_the_nuchal
-PERIPHERAL (19): well_developed_ --> absent_or_poorly_developed_
-HUMEROPECTORAL_POSITION (33): coinciding_medially_with_the_posterior_suture_of_the_entoplastron --> posterior_to_the_entoplastron_

Node 62 :
All trees:
-ANTERIOR_LOBE (26): subrounded_to_straight_ --> triagonal_
-EPIPLASTRAL_LIP_SHAPE (29): convex_to_flat_ --> concave_
-GULARS_vs_ENTOPLASTRON (30): covering_the_anterior_area --> in_contact_with_the_anterior_margin_
-HUMEROPECTORAL_SHAPE (34): perpendicular_to_the_axial_plane,_with_a_well-developed_lateral_change_of_curvature --> not_perpendicular_to_the_axial_plane,_rounded_or_forming_a_wide_angle_
-FRONTAL_vs_PREFRONTALS (40): frontals_longer_than_prefrontals_ --> prefrontals_longer_than_frontals
-SULCUS_OLFACTURIUS (42): ventrally_open_ --> ventrally_nearly_closed_
-VENTRAL_TEMPORAL_EMARGINATION (44): small_ --> extensive_
-PREMAX_RIDGE (46): absent_ --> present_
-LINGUAL_RIDGE (50): restricted_to_maxilla_ --> extending_onto_premaxillae_

Node 63 :
All trees:
-NEURAL_3 (8): rectangular_ --> hexagonal_
-NEURAL_4 (9): octagonal_ --> hexagonal_

Node 64 :
All trees:
-NUCHAL_3 (2): first_pleural_touches,_but_it_does_not_overlap_the_nuchal_ --> first_pleural_is_not_in_contact_with_the_nuchal_
-VERTEBRAL_1 (14): narrow_vertebrals,_narrower_than_the_pleurals --> wide_vertebrals,_wider_than_the_pleurals_

-GULARS_ANGLE (31): more_acute_ --> 45?_or_more_obtuse_
-OPISTHOTIC (64): expanded,_could_contact_exoccipital --> expanded,_contacting_the_pterygoid_

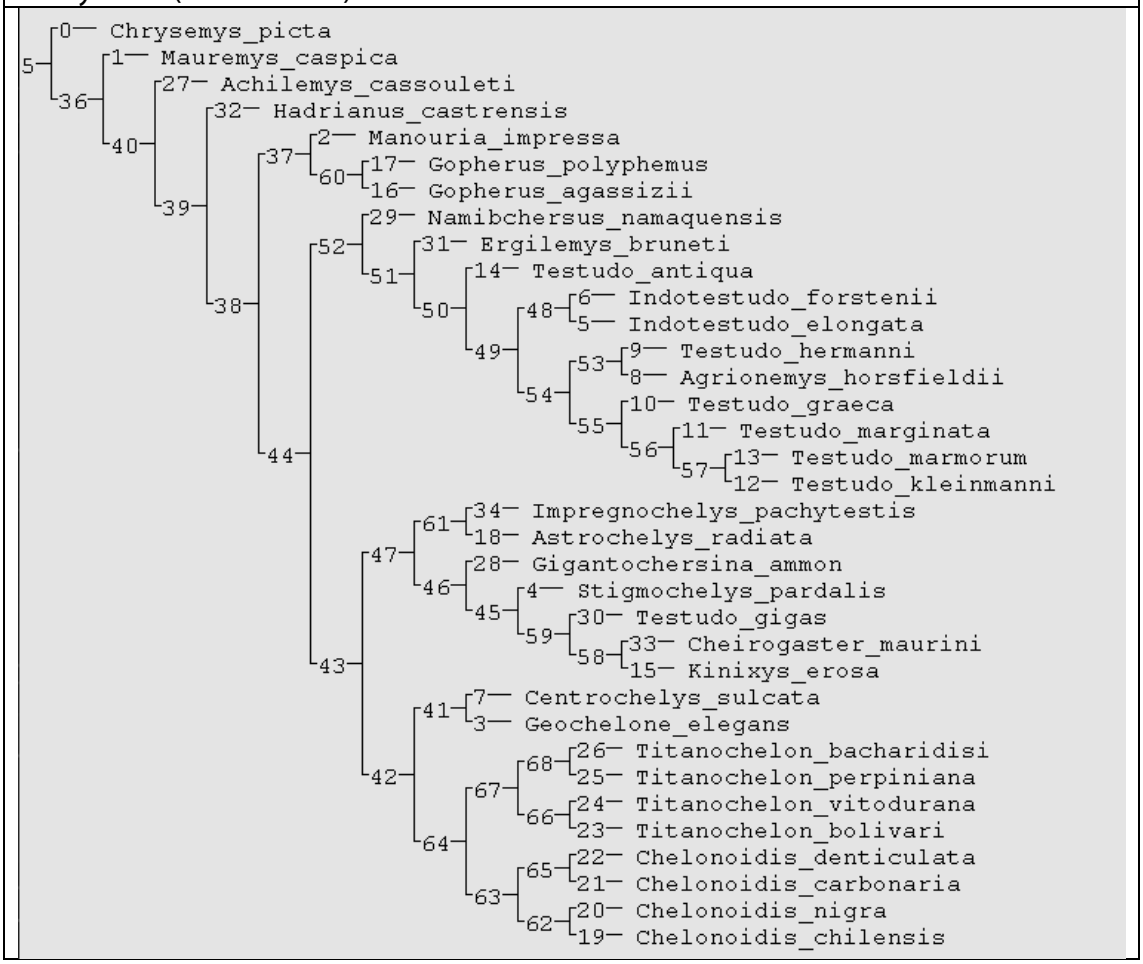
Node 65 :
All trees:
-NUCHAL_2 (1): markedly_longer_than_wide --> slightly_wider_than_long_or_as_long_as_wide_
-NUCHAL_4 (3): deep_ --> notch_absent_
-VERTEBRAL_2 (15): the_posterior_sulcus_of_the_fifth_vertebral_crosses_the_suprapygal_transversely -->
the_posterior_sulcus_of_the_fifth_vertebral_coincides_with_the_suprapygal-pygal_suture_
-MEDIAN_MAX_RIDGE (53): present,_restricted_to_maxilla --> present,_extending_to_premaxilla

Node 66 :
All trees:
-NUCHAL_2 (1): markedly_longer_than_wide --> slightly_wider_than_long_or_as_long_as_wide_

Node 67 :
All trees:
-MARGINAL_4_with_PLEURAL_2 (22): absent_ --> present_
-MARGINAL_6_with_PLEURAL_3 (23): absent_ --> present_

Node 68 :
All trees:
-HUMEROPECTORAL_POSITION (33): posterior_to_the_entoplastron_ -->
coinciding_medially_with_the_posterior_suture_of_the_entoplastron

Analysis #2 (Constrained): Number of Nodes



Analysis #2 (Constrained): List of synapomorphies

Synapomorphies common to 1 trees

(Node numbers refer to nodes in consensus)

Chrysemys_picta :
-No autapomorphies:

Mauremys_caspica :
-MARGINAL_2_with_NUCHAL (20): absent_ --> present_
-MARGINAL_2_with_VERTEBRAL_1 (21): absent_ --> present_
-HUMEROPECTORAL_POSITION (33): posterior_to_the_entoplastron_ --> crossing_the_entoplastron_
-MAX-PREMAX_RIDGE (48): absent_ --> present_
-TRITURATING_RIDGES (49): three --> one,_labial_only
-MEDIAN_MAX_RIDGE (53): present,_restricted_to_maxilla --> absent_

Manouria_impressa :
-NUCHAL_4 (3): notch_absent_ --> shallow_
-NEURAL_3 (8): rectangular_ --> hexagonal_
-VERTEBRAL_1 (14): wide_vertebrals,_wider_than_the_pleurals_ --> wide_vertebrals,_almost_equal_to_the_pleurals
-VERTEBRAL_2 (15): the_posterior_sulcus_of_the_fifth_vertebral_crosses_the_suprapygal_transversely -->
the_posterior_sulcus_of_the_fifth_vertebral_coincides_with_the_suprapygal-pygal_suture_
-PERIPHERAL (19): absent_or_poorly_developed_ --> well_developed_
-HUMEROPECTORAL_SHAPE (34): not_perpendicular_to_the_axial_plane,_rounded_or_forming_a_wide_angle_ -->
perpendicular_to_the_axial_plane,_relatively_straight_throughout_its_width_
-VOMER_RIDGE (55): present_ --> absent_
-CRISTA_SUPRAOCCIPITALIS_KEELS (61): absent_ --> present_

Geochelone_elegans :
-GULAR_PROTRUSION (27): present_ --> absent_

-GULARS_ANGLE (31): more_acute_ --> 45?_or_more_obtuse_
-FEMOROANAL_SHAPE (37): straight_or_slightly_rounded,_developed_mainly_perpendicular_with_the_axial_plane --> acute_angle_with_the_axial_plane_
-DESCENDING_FRONTAL (41): present,_well-developed_ --> absent,_or_very_small_
-MAX_RIDGE (54): absent_ --> present_
-VOMER_RIDGE (55): present_ --> absent_
-VOMER (56): vomer_diving_part_of_the_pterygoids,_not_reaching_the_basisphenoid_ --> vomer_dividing_palatines_and_pterygoids,_reaching_the_basisphenoid_

Stigmochelys_pardalis :
-NUCHAL_3 (2): first_pleural_is_not_in_contact_with_the_nuchal_ --> first_pleural_touches,_but_it_does_not_overlap_the_nuchal_
-PERIPHERAL (19): absent_or_poorly_developed_ --> well_developed_
-GULARS_vs_ENTOPLASTRON (30): covering_the_anterior_area --> in_contact_with_the_anterior_margin_
-FRONTAL_vs_ORBIT (39): participates_to_the_formation_of_the_orbital_rim_ --> excluded_from_the_orbit

Indotestudo_elongata :
-NUCHAL_4 (3): notch_absent_ --> significant_medial_protrusion_present_
-HUMEROPECTORAL_POSITION (33): coinciding_medially_with_the_posterior_suture_of_the_entoplastron --> crossing_the_entoplastron_
-MAX-PRE_SYMPHYSIS_HEIGHT (45): short,_shorter_than_the_height_of_fossa_nasalis,_but_with_the_development_of_a_dorsal_projection_ --> high,_taller_than_the_height_of_fossa_nasalis

Indotestudo_forstenii :
-LINGUAL_RIDGE (50): restricted_to_maxilla_ --> extending_onto_premaxillae_
-FORAMEN_NERVI_TRIGEMINI (66): one --> two

Centrochelys_sulcata :
-NUCHAL_2 (1): markedly_wider_than_long_ --> markedly_longer_than_wide
-NUCHAL_3 (2): first_pleural_is_not_in_contact_with_the_nuchal_ --> first_pleural_touches,_but_it_does_not_overlap_the_nuchal_
-VERTEBRAL_1 (14): wide_vertebrals,_wider_than_the_pleurals_ --> narrow_vertebrals,_narrower_than_the_pleurals
-EPIPLASTRAL_LIP_SHAPE (29): convex_to_flat_ --> concave_
-FRONTAL_vs_ORBIT (39): participates_to_the_formation_of_the_orbital_rim_ --> excluded_from_the_orbit
-FORAMEN_NERVI_TRIGEMINI (66): one --> two

Agrionemys_horsfieldii :
-SUPRAPYGAL (12): one,_suprapygals_fused,_constituting_one_trapeze_ --> two,_the_contact_between_the_suprapygals_is_straight_and_perpendicular_to_the_axial_plane
-VERTEBRAL_2 (15): the_posterior_sulcus_of_the_fifth_vertebral_coincides_with_the_suprapygal-pygal_suture_ --> the_posterior_sulcus_of_the_fifth_vertebral_crosses_the_suprapygal_transversely
-HUMEROPECTORAL_POSITION (33): coinciding_medially_with_the_posterior_suture_of_the_entoplastron --> crossing_the_entoplastron_
-CRISTA_SUPRAOCCIPITALIS_LENGTH (60): extending_beyond_the_condylus_occipitalis_ --> not_extending_

Testudo_hermanni :
-NEURAL_1 (6): rectangular_ --> hexagonal,_short_sides_positioned_posteriorly_
-PYGAL (13): quadrangular_(without_small_latero-anterior_borders) --> quadrangular_or_hexagonal_with_small_latero-anterior_borders
-SUPRACAUDAL_1 (16): twelfth_marginals_fused_into_a_supracaudal_dorsally --> two_twelfth_marginals_present_dorsally_
-FRONTAL_vs_PREFRONTALS (40): frontals_longer_than_prefrontals_ --> prefrontals_longer_than_frontals

Testudo_graeca :
-No autapomorphies:

Testudo_marginata :
-BORDER (25): posterior_border_curved_inwards_ --> posterior_border_posteriorly_flared_

Testudo_kleinmanni :
-FEMOROANAL_SHAPE (37): forms_S-shaped_curve_laterally --> acute_angle_with_the_axial_plane_

Testudo_marmorum :
-NUCHAL_2 (1): markedly_wider_than_long_ --> markedly_longer_than_wide
-NEURAL_NUMBER (5): seven_neurals_or_less_ --> eight_neurals_
-COINCIDENCE (18): present_ --> absent_

Testudo_antiqua :
-No autapomorphies:

Kinixys_erosa :

-NUCHAL_4 (3): deep_ --> significant_medial_protrusion_present_
-NEURAL_2 (7): octagonal_ --> hexagonal,_short_sides_positioned_anteriorly_
-NEURAL_3 (8): rectangular_ --> hexagonal_
-PERIPHERAL (19): absent_or_poorly_developed_ --> well_developed_
-CARAPACIAL_HINGE (24): absent_ --> present_
-BORDER (25): posterior_border_curved_inwards_ --> posterior_border_posteriorly_flared_
-GULARS_vs_ENTOPLASTRON (30): covering_the_anterior_area --> not_in_contact_
-FEMOROANAL_SHAPE (37): straight_or_slightly_rounded,_developed_mainly_perpendicular_with_the_axial_plane --> acute_angle_with_the_axial_plane_

Gopherus_agassizii :
-GULARS_ANGLE (31): 45?_or_more_obtuse_ --> more_acute_

Gopherus_polyphemus :
-SUPRAPYGAL (12):
two,_both_suprapygals_constitute_one_trapeze_and_the_first_suprapygal_embrassing_the_lenticular_second_one_ --> two,_the_contact_between_the_suprapygals_is_straight_and_perpendicular_to_the_axial_plane
-MARGINAL_4_with_PLEURAL_2 (22): absent_ --> present_
-MARGINAL_6_with_PLEURAL_3 (23): absent_ --> present_
-PECTORAL_LENGTH (35): short --> long
-DESCENDING_FRONTAL (41): absent,_or_very_small_ --> present,_well-developed_
-MAX-PRE_SYMPHYSIS_HEIGHT (45):
short,_shorter_than_the_height_of_fossa_nasalis,_but_with_the_development_of_a_dorsal_projection_ --> short,_shorter_than_the_height_of_fossa_nasalis_
-FORAMEN_PRAEPALATINUM (58): visible_ --> not_visible_in_ventral_view_-_foramina_may_be_concealed_by_lingual_extensions_of_the_maxillary_alveolar_ridges_
-CRISTA_SUPRAOCCIPITALIS_SHAPE (62): straight_ --> bended_inwards_

Astrochelys_radiata :
-GULARS_vs_ENTOPLASTRON (30): covering_the_anterior_area --> not_in_contact_
-GULARS_ANGLE (31): more_acute_ --> 45?_or_more_obtuse_

Chelonoidis_chilensis :
-HUMEROPECTORAL_SHAPE (34): perpendicular_to_the_axial_plane,_with_a_well-developed_lateral_change_of_curvature --> perpendicular_to_the_axial_plane,_relatively_straight_throughout_its_width_
-FRONTAL_vs_ORBIT (39): participates_to_the_formation_of_the_orbital_rim_ --> excluded_from_the_orbit
-CRISTA_SUPRAOCCIPITALIS_KEELS (61): present_ --> absent_
-HUMERUS_SCAR (69): present_ --> absent_or_reduced_
-FEMUR_HEAD_ANGLE (73): femoral_head_developed_almost_perpendicular_to_the_diaphysis_ --> relatively_large_angle_
-AS_+_CAL (78): fused_ --> not_fused

Chelonoidis_nigra :
-NUCHAL_1 (0): hexagonal_ --> octagonal_
-GULAR_PROTRUSION (27): present_ --> absent_
-GULARS_vs_ENTOPLASTRON (30): not_in_contact_ --> covering_the_anterior_area
-HUMERAL_LENGTH (32): humerals_longer_than_the_gulars_ --> humerals_equal_or_smaller_than_the_gulars_
-FEMOROANAL_SHAPE (37): straight_or_slightly_rounded,_developed_mainly_perpendicular_with_the_axial_plane --> forms_S-shaped_curve_laterally
-MAX_RIDGE (54): absent_ --> present_

Chelonoidis_carbonaria :
-HUMEROPECTORAL_SHAPE (34): perpendicular_to_the_axial_plane,_with_a_well-developed_lateral_change_of_curvature --> perpendicular_to_the_axial_plane,_relatively_straight_throughout_its_width_
-LABIAL_RIDGE (51): present_ --> absent_

Chelonoidis_denticulata :
-CRISTA_SUPRAOCCIPITALIS_SHAPE (62): elevated_posteriorly_ --> straight_

Titanochelon_bolivari :
-No autapomorphies:

Titanochelon_vitodurana :
-NUCHAL_2 (1): slightly_wider_than_long_or_as_long_as_wide_ --> markedly_longer_than_wide

Titanochelon_perpiniana :
-No autapomorphies:

Titanochelon_bacharidisi :
-GULARS_vs_ENTOPLASTRON (30): not_in_contact_ --> in_contact_with_the_anterior_margin_
-FOSSA_ORBITALIS_POSITION (43): anterior_to_middle_ --> posterior_
-VENTRAL_TEMPORAL_EMARGINATION (44): small_ --> extensive_
-SQUAMOSALS (59): not_extending_ --> extending_beyond_the_condylus_occipitalis_

Achilemys_cassouleti :
-NEURAL_2 (7): hexagonal,_short_sides_positioned_posteriorly --> rectangular
-NEURAL_4 (9): hexagonal_ --> rectangular_
-VERTEBRAL_1 (14): wide_vertebrals,_wider_than_the_pleurals_ --> narrow_vertebrals,_narrower_than_the_pleurals
-GULARS_vs_ENTOPLASTRON (30): covering_the_anterior_area --> not_in_contact_

Gigantochersina_ammon :
-HUMEROPECTORAL_POSITION (33): posterior_to_the_entoplastron_ --> crossing_the_entoplastron_

Namibchersus_namaquensis :
-NUCHAL_2 (1): markedly_wider_than_long_ --> markedly_longer_than_wide

Testudo_gigas :
-NUCHAL_3 (2): first_pleural_is_not_in_contact_with_the_nuchal_ --> first_pleural_overlaps_postero-lateral_parts_of_the_nuchal

Ergilemys_bruneti :
-NUCHAL_2 (1): markedly_wider_than_long_ --> slightly_wider_than_long_or_as_long_as_wide_
-NUCHAL_4 (3): notch_absent_ --> significant_medial_protrusion_present_
-SUPRACAUDAL_2 (17): twelfth_marginals_fused_into_a_supracaudal_viscerally --> two_twelfth_marginals_present_viscerally_
-EPIPLASTRAL_LIP (28): present_ --> absent_or_poorly_developed_
-GULARS_ANGLE (31): more_acute_ --> 45?_or_more_obtuse_
-PLASTRAL_HINGE (36): absent_ --> present,_between_hypoplastra_and_xiphiplastra

Hadrianus_castrensis :
-NUCHAL_2 (1): markedly_wider_than_long_ --> slightly_wider_than_long_or_as_long_as_wide_
-NUCHAL_4 (3): notch_absent_ --> significant_medial_protrusion_present_
-NEURAL_NUMBER (5): eight_neurals_ --> nine_neurals_
-VERTEBRAL_1 (14): wide_vertebrals,_wider_than_the_pleurals_ --> wide_vertebrals,_almost_equal_to_the_pleurals
-HUMEROPECTORAL_POSITION (33): posterior_to_the_entoplastron_ --> crossing_the_entoplastron_

Cheirogaster_maurini :
-NEURAL_1 (6): hexagonal,_short_sides_positioned_posteriorly_ --> rectangular_
-MARGINAL_2_with_NUCHAL (20): absent_ --> present_
-MARGINAL_2_with_VERTEBRAL_1 (21): absent_ --> present_
-GULAR_PROTRUSION (27): absent_ --> present_

Impregnochelys_pachytestis :
-HUMERAL_LENGTH (32): humerals_longer_than_the_gulars_ --> humerals_equal_or_smaller_than_the_gulars_

Node 36 :
-No synapomorphies

Node 37 :
-GULARS_vs_ENTOPLASTRON (30): covering_the_anterior_area --> in_contact_with_the_anterior_margin_

Node 38 :
-COINCIDENCE (18): absent_ --> present_
-PECTORAL_LENGTH (35): long --> short

Node 39 :
-SUPRAPYGAL (12): two,_the_contact_between_the_suprapygals_is_straight_and_perpendicular_to_the_axial_plane --> two,_both_suprapygals_constitute_one_trapeze_and_the_first_suprapygal_embrassing_the_lenticular_second_one_
-VERTEBRAL_2 (15): he_posterior_sulcus_of_the_fifth_vertebral_overlaps_the_anterior_part_of_the_pygal --> the_posterior_sulcus_of_the_fifth_vertebral_crosses_the_suprapygal_transversely

Node 40 :
-NEURAL_1 (6): rectangular_ --> hexagonal,_short_sides_positioned_posteriorly_
-EPIPLASTRAL_LIP (28): absent_or_poorly_developed_ --> present_
-GULARS_ANGLE (31): more_acute_ --> 45?_or_more_obtuse_
-HUMEROPECTORAL_SHAPE (34): perpendicular_to_the_axial_plane,_relatively_straight_throughout_its_width_ --> not_perpendicular_to_the_axial_plane,_rounded_or_forming_a_wide_angle_
-FEMOROANAL_SHAPE (37): acute_angle_with_the_axial_plane_ --> straight_or_slightly_rounded,_developed_mainly_perpendicular_with_the_axial_plane

Node 41 :
-NUCHAL_1 (0): hexagonal_ --> octagonal_
-NEURAL_2 (7): octagonal_ --> hexagonal,_short_sides_positioned_posteriorly
-ANTERIOR_LOBE (26): subrounded_to_straight_ --> medially_notched_

Node 42 :
-CERVICAL (4): dorsally_present_ --> absent_
-GULARS_vs_ENTOPLASTRON (30): covering_the_anterior_area --> not_in_contact_

Node 43 :
-LABIAL_RIDGE (51): absent_ --> present_

Node 44 :
-EPIPLASTRAL_LIP_SHAPE (29): concave_ --> convex_to_flat_
-GULARS_ANGLE (31): 45?_or_more_obtuse_ --> more_acute_
-HUMEROPECTORAL_SHAPE (34): not_perpendicular_to_the_axial_plane,_rounded_or_forming_a_wide_angle_ --> perpendicular_to_the_axial_plane,_with_a_well-developed_lateral_change_of_curvature
-DESCENDING_FRONTAL (41): absent,_or_very_small_ --> present,_well-developed_
-HUMERUS_MAJOR_TROCHANTER (70): short,_not_extending_beyond_the_humeral_head_ --> long,_extending_beyond_the_humeral_head_

Node 45 :
-CERVICAL (4): dorsally_present_ --> absent_
-GULAR_PROTRUSION (27): present_ --> absent_

Node 46 :
-VERTEBRAL_1 (14): wide_vertebrals,_wider_than_the_pleurals_ --> wide_vertebrals,_almost_equal_to_the_pleurals

Node 47 :
-GULARS_ANGLE (31): more_acute_ --> 45?_or_more_obtuse_
-HUMEROPECTORAL_SHAPE (34): not_perpendicular_to_the_axial_plane,_rounded_or_forming_a_wide_angle_ --> perpendicular_to_the_axial_plane,_relatively_straight_throughout_its_width_
-FEMOROANAL_SHAPE (37): acute_angle_with_the_axial_plane_ --> straight_or_slightly_rounded,_developed_mainly_perpendicular_with_the_axial_plane
-POSTERIOR_MAX_PROCESS (52): present_ --> absent_

Node 48 :
-HUMEROPECTORAL_POSITION (33): posterior_to_the_entoplastron_ --> coinciding_medially_with_the_posterior_suture_of_the_entoplastron

Node 49 :
-VERTEBRAL_2 (15): the_posterior_sulcus_of_the_fifth_vertebral_crosses_the_suprapygal_transversely --> the_posterior_sulcus_of_the_fifth_vertebral_coincides_with_the_suprapygal-pygal_suture_
-HUMEROPECTORAL_SHAPE (34): perpendicular_to_the_axial_plane,_with_a_well-developed_lateral_change_of_curvature --> not_perpendicular_to_the_axial_plane,_rounded_or_forming_a_wide_angle_

Node 50 :
-NUCHAL_3 (2): first_pleural_is_not_in_contact_with_the_nuchal_ --> first_pleural_touches,_but_it_does_not_overlap_the_nuchal_

Node 51 :
-NEURAL_1 (6): hexagonal,_short_sides_positioned_posteriorly_ --> rectangular_
-GULAR_PROTRUSION (27): present_ --> absent_
-FEMOROANAL_SHAPE (37): straight_or_slightly_rounded,_developed_mainly_perpendicular_with_the_axial_plane --> acute_angle_with_the_axial_plane_

Node 52 :
-NUCHAL_1 (0): hexagonal_ --> octagonal_
-MAX-PRE_SYMPHYSIS_HEIGHT (45): short,_shorter_than_the_height_of_fossa_nasalis,_but_with_the_development_of_a_dorsal_projection_ --> short,_shorter_than_the_height_of_fossa_nasalis_

Node 53 :
-NEURAL_NUMBER (5): eight_neurals_ --> seven_neurals_or_less_
-SUPRAPYGAL (12): two,_both_suprapygals_constitute_one_trapeze_and_the_first_suprapygal_embrassing_the_lenticular_second_one_ --> one,_suprapygals_fused,_constituting_one_trapeze_
-MANUS (77): two_phalanges_in_all_digits_ --> one_phalanx_in_first_and_fifth_finger

Node 54 :
-PLASTRAL_HINGE (36): absent_ --> present,_between_hypoplastra_and_xiphiplastra
-FEMOROANAL_SHAPE (37): acute_angle_with_the_axial_plane_ --> forms_S-shaped_curve_laterally
-HUMERUS_SCAR (69): absent_or_reduced_ --> present_

Node 55 :
-NUCHAL_3 (2): first_pleural_touches,_but_it_does_not_overlap_the_nuchal_ --> first_pleural_overlaps_postero-lateral_parts_of_the_nuchal

-HUMEROPECTORAL_POSITION (33): coinciding_medially_with_the_posterior_suture_of_the_entoplastron --> posterior_to_the_entoplastron_

Node 56 :
-GULARS_ANGLE (31): more_acute_ --> 45?_or_more_obtuse_
-PECTORAL_LENGTH (35): short --> long

Node 57 :
-COINCIDENCE (18): present_ --> absent_
-HUMEROPECTORAL_SHAPE (34): perpendicular_to_the_axial_plane,_with_a_well-developed_lateral_change_of_curvature --> not_perpendicular_to_the_axial_plane,_rounded_or_forming_a_wide_angle_

Node 58 :
-NEURAL_1 (6): hexagonal,_short_sides_positioned_posteriorly_ --> rectangular_
-SULCUS_OLFACTURIUS (42): ventrally_open_ --> ventrally_nearly_closed_
-VENTRAL_TEMPORAL_EMARGINATION (44): small_ --> extensive_
-PREMAX_RIDGE (46): absent_ --> present_
-LINGUAL_RIDGE (50): restricted_to_maxilla_ --> extending_onto_premaxillae_
-FORAMEN_NERVI_TRIGEMINI (66): one --> two

Node 59 :
-HUMEROPECTORAL_SHAPE (34): perpendicular_to_the_axial_plane,_with_a_well-developed_lateral_change_of_curvature --> perpendicular_to_the_axial_plane,_relatively_straight_throughout_its_width_

Node 60 :
-NUCHAL_2 (1): slightly_wider_than_long_or_as_long_as_wide_ --> markedly_longer_than_wide
-NEURAL_3 (8): rectangular_ --> hexagonal_
-NEURAL_4 (9): octagonal_ --> hexagonal_
-ANTERIOR_LOBE (26): subrounded_to_straight_ --> medially_notched_

Node 61 :
-GULARS_ANGLE (31): more_acute_ --> 45?_or_more_obtuse_

Node 62 :
-NUCHAL_2 (1): markedly_wider_than_long_ --> slightly_wider_than_long_or_as_long_as_wide_
-NEURAL_1 (6): hexagonal,_short_sides_positioned_posteriorly_ --> rectangular_
-PREMAX_PIT (47): absent_ --> present_
-CRISTA_SUPRAOCCIPITALIS_SHAPE (62): straight_ --> elevated_posteriorly_

Node 63 :
-VERTEBRAL_2 (15): the_posterior_sulcus_of_the_fifth_vertebral_crosses_the_suprapygal_transversely --> the_posterior_sulcus_of_the_fifth_vertebral_coincides_with_the_suprapygal-pygal_suture_
-MEDIAN_MAX_RIDGE (53): present,_restricted_to_maxilla --> present,_extending_to_premaxilla

Node 64 :
-GULARS_vs_ENTOPLASTRON (30): not_in_contact_ --> covering_the_anterior_area

Node 65 :
-NUCHAL_3 (2): first_pleural_is_not_in_contact_with_the_nuchal_ --> first_pleural_touches,_but_it_does_not_overlap_the_nuchal_
-VERTEBRAL_1 (14): wide_vertebrals,_wider_than_the_pleurals_ --> narrow_vertebrals,_narrower_than_the_pleurals
-MARGINAL_6_with_PLEURAL_3 (23): absent_ --> present_
-GULAR_PROTRUSION (27): present_ --> absent_
-LABIAL_RIDGE (51): present_ --> absent_

Node 66 :
-HUMEROPECTORAL_POSITION (33): posterior_to_the_entoplastron_ --> coinciding_medially_with_the_posterior_suture_of_the_entoplastron

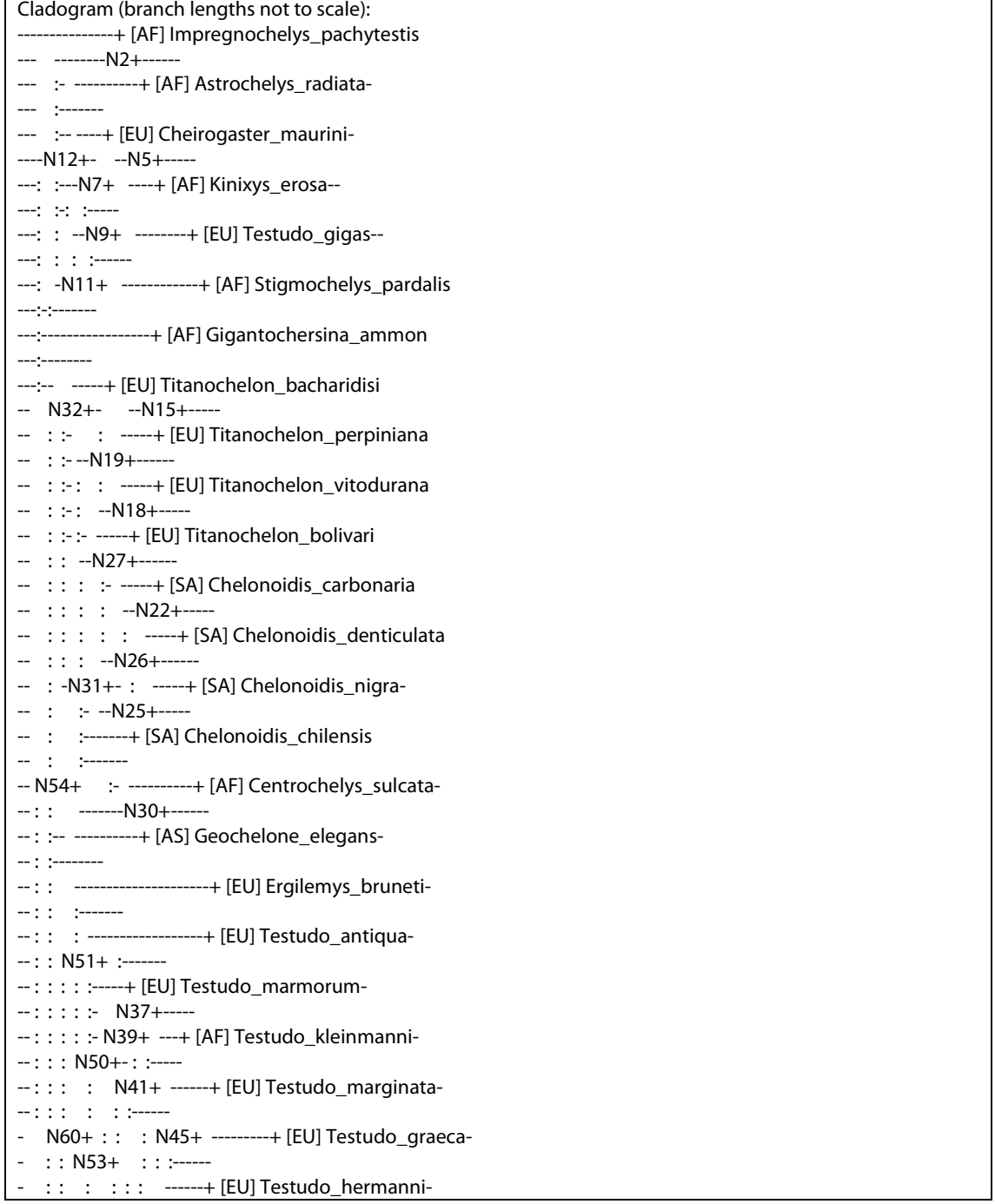
Results of the DEC analysis on the constrained tree

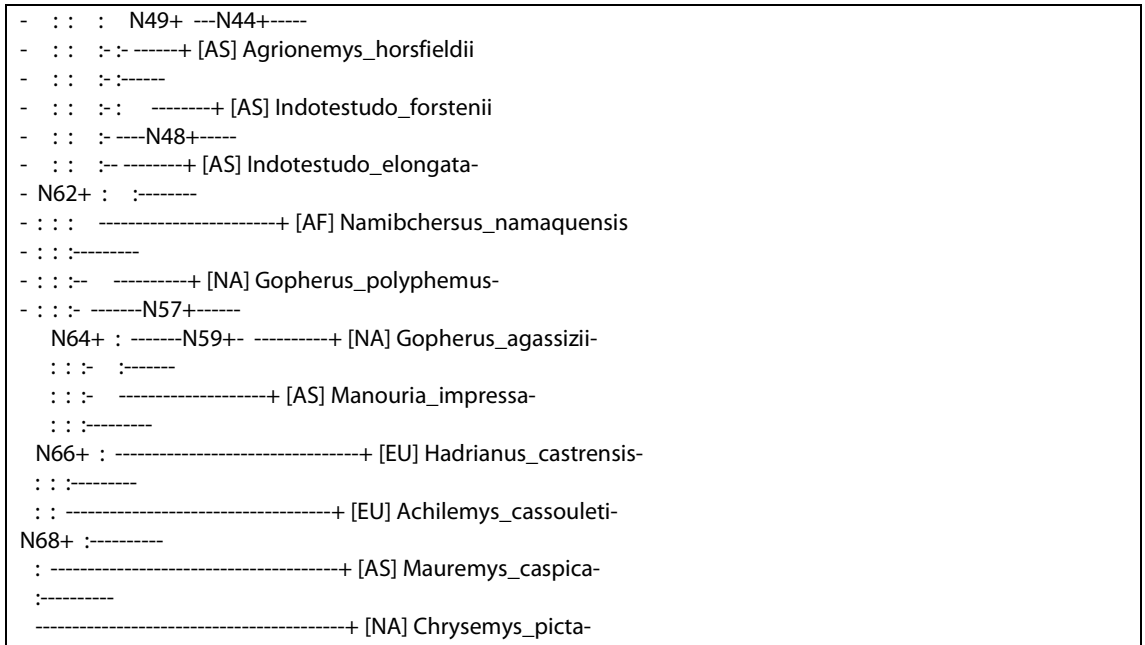
Lagrange: likelihood analysis of geographic range evolution
Version: 20130526
Author: Richard Ree <rree@fieldmuseum.org>
https://github.com/rhr/lagrange-python

Newick tree with interior nodes labeled:
(((((((((Impregnochelys_pachytestis:1.07142857143,Astrochelys_radiata:23.5714285714)N2:17.1428571429,((((Cheirogaster_maurini:1.07142857143,Kinixys_erosa:36.4285714286)N5:1.07142857143,Testudo_gigas:4.28571428571)N7:1.07142857143,Stigmochelys_pardalis:38.5714285714)N9:1.07142857143,Gigantochersina_ammon:6.42857142857)N11:1.07142857143)N12:1.07142857143,((((Titanochelon_bacharidisi:1.07142857143,Titanoch

elon_perpiniana:1.07142857143)N15:10.7142857143,(Titanochelon_vitodurana:1.07142857143,Titanochelon_bolivari:1.07142857143)N18:1.07142857143)N19:1.07142857143,((Chelonoidis_carbonaria:1.07142857143,Chelonoidis_denticulata:1.07142857143)N22:1.07142857143,(Chelonoidis_nigra:1.07142857143,Chelonoidis_chilensis:1.07142857143)N25:1.07142857143)N26:12.8571428571)N27:1.07142857143,(Centrochelys_sulcata:1.07142857143,Geochelone_elegans:1.07142857143)N30:15.0)N31:25.7142857143)N32:1.07142857143,((Ergilemys_bruneti:1.07142857143,(Testudo_antiqua:1.07142857143,(((((Testudo_marmorum:1.07142857143,Testudo_kleinmanni:5.35714285714)N37:1.07142857143,Testudo_marginata:6.42857142857)N39:1.07142857143,Testudo_graeca:5.35714285714)N41:1.07142857143,(Testudo_hermanni:1.07142857143,Agrionemys_horsfieldii:1.07142857143)N44:7.5)N45:1.07142857143,(Indotestudo_forstenii:1.07142857143,Indotestudo_elongata:1.07142857143)N48:8.57142857143)N49:3.21428571429)N50:10.7142857143)N51:10.7142857143,Namibchersus_namaquensis:1.07142857143)N53:8.57142857143)N54:1.07142857143,((Gopherus_polyphemus:1.07142857143,Gopherus_agassizii:1.07142857143)N57:1.07142857143,Manouria_impressa:2.14285714286)N59:41.7857142857)N60:1.07142857143,Hadrianus_castrensis:5.35714285714)N62:12.8571428571,Achilemys_cassouleti:1.07142857143)N64:1.07142857143,Mauremys_caspica:58.9285714286)N66:1.07142857143,Chrysemys_picta:60.0)N68:0.0;

Cladogram (branch lengths not to scale):





Global ML at root node:
-lnL = 64.88
dispersal = 0.0351
extinction = 0.02243

Ancestral range subdivision/inheritance scenarios ('splits') at internal nodes.

* Split format: [left|right], where 'left' and 'right' are the ranges inherited by each descendant branch (on the printed tree, 'left' is the upper branch, and 'right' the lower branch).

* Only splits within 2 log-likelihood units of the maximum for each node are shown. 'Rel.Prob' is the relative probability (fraction of the global likelihood) of a split.

		At node N68:	At node N66:
		split-lnL Rel.Prob [EU|EU] -66.17 0.2744 [EU|AS] -66.39 0.2211 [EU+AS|AS] -66.85 0.139 [EU|EU+AS] -67.03 0.1169 [EU|AF] -67.96 0.04573 [AS|AS] -68.1 0.03984 [EU+AS|EU] -68.43 0.02875 [EU|EU+AF] -68.5 0.02674 [EU+AF|AF] -68.74 0.02102 [EU+AF|EU] -68.74 0.02102 [AS|AS+NA] -69.02 0.01584	split-lnL Rel.Prob [EU|EU] -65.28 0.6687 [EU|EU+AS] -67.09 0.1093 [EU|AS] -67.19 0.09906 [EU|AF] -68.61 0.02394 [EU|EU+AF] -68.74 0.02097 [AS|AS] -68.78 0.02023 [EU+AS|AS] -69.04 0.01562
At node N64: split-lnL Rel.Prob [EU|EU] -64.97 0.9144 [EU+AS|EU] -68.18 0.03698	At node N62: split-lnL Rel.Prob [EU|EU] -65.58 0.4944 [AF|EU] -66.48 0.2016 [EU+AF|EU] -66.89 0.1339 [EU+AS|EU] -67.37 0.08319 [AS|EU] -68.3 0.03256 [AF|EU+AF] -68.48 0.02724	At node N60: split-lnL Rel.Prob [EU|EU] -65.71 0.437 [AF|AF] -66.4 0.2185 [EU|AS] -67.65 0.06289 [EU+AF|EU] -67.9 0.04865 [EU+AF|AF] -67.9 0.04865 [AF|EU] -67.95 0.04646 [EU|EU+AS] -68.29 0.03287 [AF|EU+AF] -68.63 0.02345 [AS|AS] -68.86 0.01874 [AF|AS] -69 0.01619	At node N54: split-lnL Rel.Prob [EU|EU] -65.66 0.4573 [AF|AF] -66.07 0.3029 [AF|EU+AF] -67.53 0.07067 [EU+AF|AF] -67.97 0.04546 [EU|EU+AF] -68.49 0.02692 [EU+AF|EU] -68.62 0.02379 [AF|EU] -68.96 0.01684 [EU|AF] -69.28 0.01225
At node N32: split-lnL Rel.Prob	At node N12: split-lnL Rel.Prob	At node N2: split-lnL Rel.Prob	At node N11: split-lnL Rel.Prob

[EU|EU] -65.74 0.4241 [AF|AF] -65.88 0.3671 [EU+AF|EU] -67.68 0.06057 [AF|EU] -68.11 0.03959 [EU+AF|AF] -68.47 0.02756 [AF|EU+AF] -68.76 0.02057 [AF|AS] -69.1 0.01467	[AF|AF] -65.73 0.4286 [EU|EU] -66.12 0.2897 [AF|EU+AF] -66.61 0.1776 [EU|EU+AF] -68.17 0.03733 [EU+AF|AF] -68.79 0.01993	[AF|AF] -65.25 0.6906 [AF|EU+AF] -66.65 0.1701 [AF|AF+AS] -67.74 0.05723 [AF|EU] -67.76 0.05601	[AF|AF] -65.9 0.3593 [EU|AF] -66.39 0.2198 [EU+AF|AF] -66.53 0.1912 [EU|EU] -66.58 0.1818
At node N9: split-lnL Rel.Prob [EU|EU] -65.72 0.4311 [EU|AF] -66.51 0.1959 [EU|EU+AF] -66.52 0.1929 [AF|AF] -67.05 0.1142 [EU+AF|AF] -68.15 0.03782	At node N7: split-lnL Rel.Prob [EU|EU] -65.06 0.8337 [EU+AF|EU] -66.89 0.1336	At node N5: split-lnL Rel.Prob [EU|EU] -65.07 0.8255 [EU|AF] -67.37 0.08259 [EU|EU+AF] -67.42 0.07897	At node N31: split-lnL Rel.Prob [EU+AS|AS] -65.57 0.5008 [AS|AF+AS] -66.81 0.1456 [EU|AF] -67.42 0.07882 [AS|AS] -67.48 0.0744 [AS|AF] -67.83 0.05248 [EU+AS|EU] -68.29 0.03311 [EU|AS] -68.39 0.02993 [AS+NA|AS] -68.64 0.02335 [EU|EU+AF] -69.09 0.01476
At node N27: split-lnL Rel.Prob [EU|AS] -65.26 0.6833 [AS|AS] -67.59 0.06653 [AS|NA] -67.63 0.06416 [EU+AS|AS] -67.64 0.06343 [EU|EU] -67.77 0.05549 [EU|EU+AS] -68.02 0.04305	At node N19: split-lnL Rel.Prob [EU|EU] -65.07 0.825 [EU+AS|EU] -66.93 0.1291	At node N15: split lnL Rel.Prob [EU|EU] -64.89 0.9857	At node N18: split lnL Rel.Prob [EU|EU] -64.88 0.9943
At node N26: split-lnL Rel.Prob [SA|SA] -65.02 0.8693 [NA+SA|SA] -67.63 0.06378 [SA|NA+SA] -67.63 0.06378	At node N22: split lnL Rel.Prob [SA|SA] -64.9 0.9827	At node N25: split lnL Rel.Prob [SA|SA] -64.9 0.9827	At node N30: split-lnL Rel.Prob [AF|AS] -64.93 0.9475 [AF|AF+AS] -68.62 0.02379
At node N53: split-lnL Rel.Prob [EU|AF] -65.45 0.5622 [EU+AF|AF] -66.49 0.1999 [AF|AF] -66.57 0.1843 [AS|AF] -68.41 0.02913	At node N51: split-lnL Rel.Prob [EU|EU] -65.14 0.7712 [EU|EU+AF] -67.2 0.09794 [EU|EU+AS] -67.39 0.08137	At node N50: split-lnL Rel.Prob [EU|EU] -65.35 0.6253 [EU|EU+AS] -66.11 0.2934 [EU|AS] -67.87 0.05012	At node N49: split-lnL Rel.Prob [EU|EU] -66.08 0.3 [EU|AS] -66.14 0.2832 [EU+AS|AS] -66.18 0.2733 [EU|EU+AS] -67.43 0.07801 [AS|AS] -68.59 0.02452
At node N45: split-lnL Rel.Prob [EU|EU] -65.29 0.6647 [EU|EU+AS] -66.2 0.2678 [EU|AS] -67.83 0.05247	At node N41: split lnL Rel.Prob [EU|EU] -64.9 0.975	At node N39: split-lnL Rel.Prob [EU|EU] -64.97 0.9143 [EU+AF|EU] -67.46 0.07584	At node N37: split-lnL Rel.Prob [EU|EU] -65.45 0.5663 [EU|AF] -65.88 0.369 [EU|EU+AF] -67.88 0.04986
At node N44: split-lnL Rel.Prob [EU|AS] -64.93 0.9459 [EU|EU+AS] -68.62 0.02375	At node N48: split lnL Rel.Prob [AS|AS] -64.92 0.9562	At node N59: split-lnL Rel.Prob [NA|AS] -64.97 0.9123 [NA|AS+NA] -67.92 0.04782	At node N57: split lnL Rel.Prob [NA|NA] -64.89 0.9884

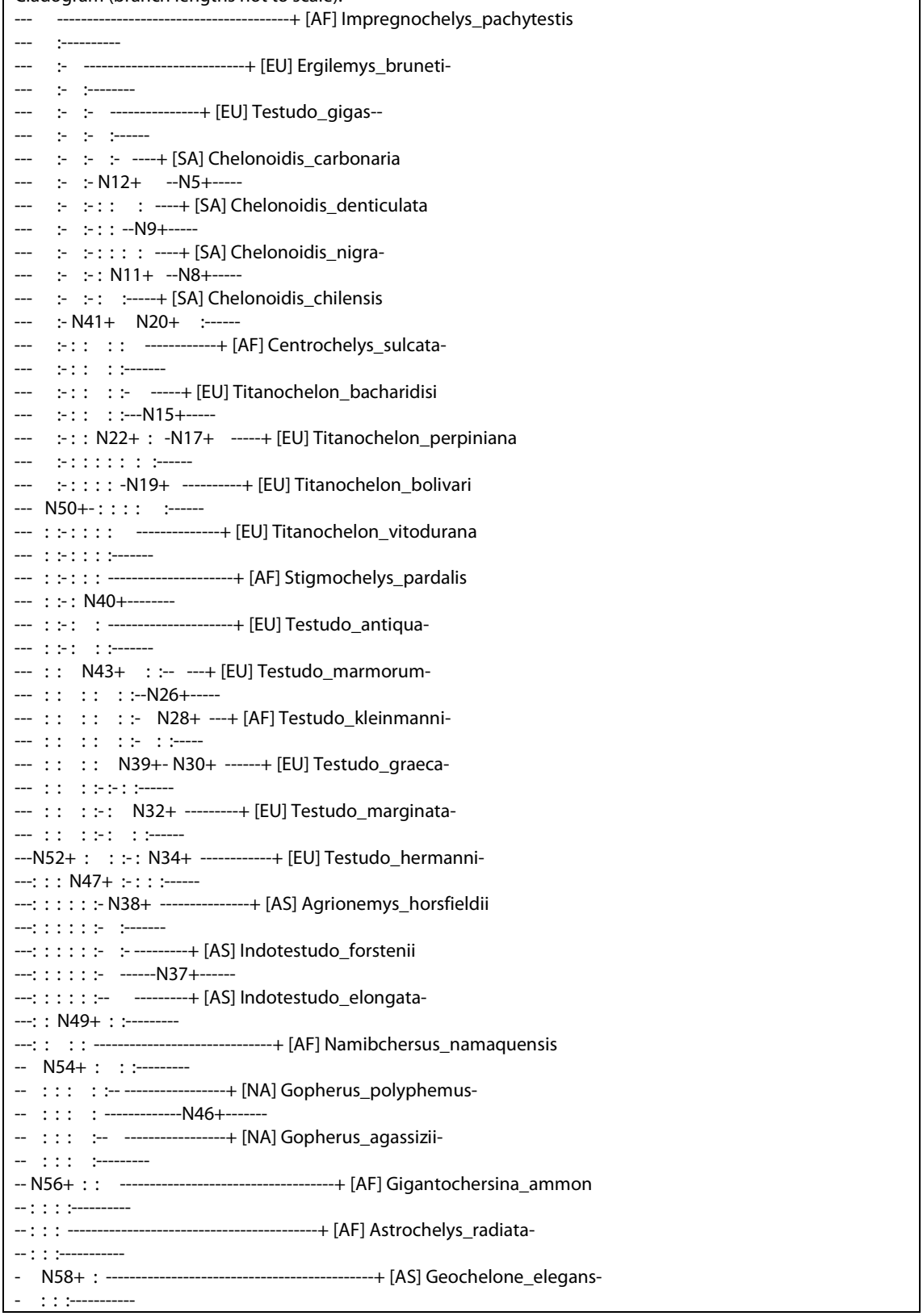
Results of the DEC analysis on the unconstrained tree

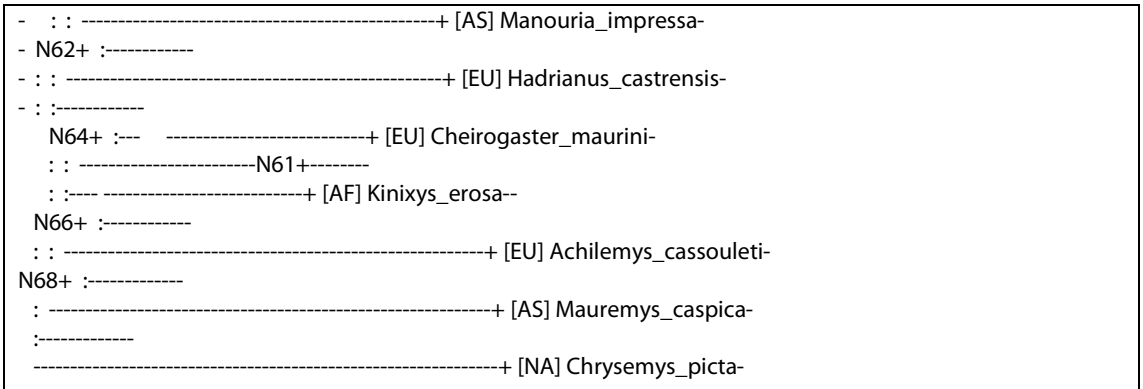
Lagrange: likelihood analysis of geographic range evolution
Version: 20130526
Author: Richard Ree <rree@fieldmuseum.org>
https://github.com/rhr/lagrange-python

Newick tree with interior nodes labeled:
(((((((((Impregnochelys_pachytestis:20.3571428571,((((Ergilemys_bruneti:16.0714285714,((((Testudo_gigas:1.07142857143,(((Chelonoidis_carbonaria:1.07142857143,Chelonoidis_denticulata:1.07142857143)N5:1.07142857143,(Chelonoidis_nigra:1.07142857143,Chelonoidis_chilensis:1.07142857143)N8:1.07142857143)N9:1.07142857143,Centrochelys_sulcata:3.21428571429)N11:31.0714285714)N12:1.07142857143,(((Titanochelon_bacharidisi:1.07142857143,Titanochelon_perpiniana:1.07142857143)N15:9.64285714286,Titanochelon_bolivari:1.07142857143)N17:1.07142857143,Titanochelon_vitodurana:2.14285714286)N19:21.4285714286)N20:1.07142857143,Stigmochelys_pardalis:36.4285714286)N22:1.07142857143,(Testudo_antiqua:1.07142857143,((((((Testudo_marmorum:1.07142857143,Testudo_kleinmanni:5.35714285714)N26:1.07142857143,Testudo_graeca:4.285714285771)N28:1.07142857143,Testudo_marginata:7.5)N30:1.07142857143,Testudo_hermanni:8.57142857143)N32:1.07142857143,Agrionemys_horsfieldii:9.64285714286)N34:1.07142857143,(Indotestudo_forstenii:1.07142857143,Indotestudo_elongata:1.07142857143)N37:9.64285714286)N38:2.14285714286)N39:24.6428571429)N40:1.07142857143)N41:1.07142857143,Namibchersus_namaquensis:6.42857142857)N43:1.07142857143,(Gopherus_polyphemus:1.07142857143,Gopherus_agassizii:1.07142857143)N46:39.6428571429)N47:1.07142857143,Gigan

tochersina_ammon:8.57142857143)N49:1.07142857143)N50:1.07142857143,Astrochelys_radiata:43.9285714286)N52:1.07142857143,Geochelone_elegans:45.0)N54:1.07142857143,Manouria_impressa:46.0714285714)N56:1.07142857143,Hadrianus_castrensis:7.5)N58:1.07142857143,(Cheirogaster_maurini:1.07142857143,Kinixys_erosa:36.4285714286)N61:11.7857142857)N62:9.64285714286,Achilemys_cassouleti:1.07142857143)N64:1.07142857143,Mauremys_caspica:58.9285714286)N66:1.07142857143,Chrysemys_picta:60.0)N68:0.0;

Cladogram (branch lengths not to scale):





Global ML at root node:
-lnL = 76.15
dispersal = 0.0273
extinction = 0.02421

Ancestral range subdivision/inheritance scenarios ('splits') at internal nodes.

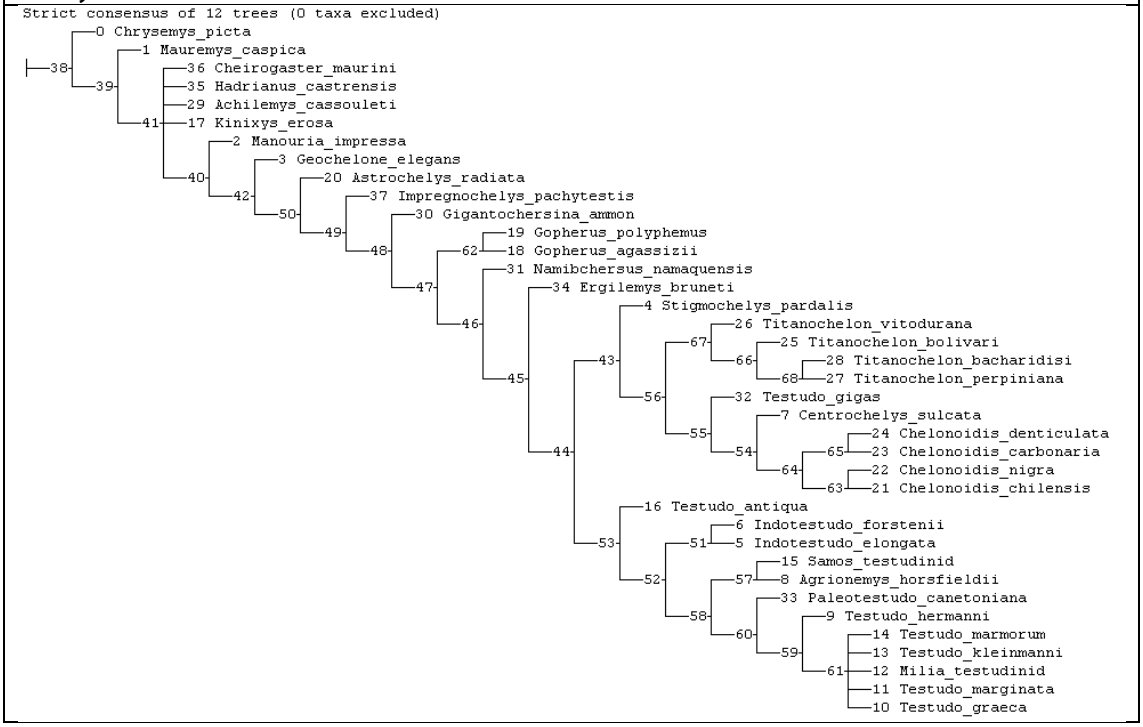
* Split format: [left|right], where 'left' and 'right' are the ranges inherited by each descendant branch (on the printed tree, 'left' is the upper branch, and 'right' the lower branch).

* Only splits within 2 log-likelihood units of the maximum for each node are shown. 'Rel.Prob' is the relative probability (fraction of the global likelihood) of a split.

	At node N68: split-lnL Rel.Prob [EU|EU] -77.51 0.2557 [EU|AS] -77.58 0.2381 [EU+AS|AS] -78 0.1564 [EU|EU+AS] -78.22 0.126 [EU|AF] -79.3 0.04262 [AS|AS] -79.56 0.03298 [EU+AS|EU] -79.72 0.028 [EU|EU+AF] -79.81 0.02552 [EU+AF|AF] -80.06 0.0199 [EU+AF|EU] -80.06 0.0199 [AS|AS+NA] -80.42 0.01393	At node N66: split-lnL Rel.Prob [EU|EU] -76.53 0.6774 [EU|EU+AS] -78.29 0.1172 [EU|AS] -78.4 0.1053 [EU|AF] -80.02 0.02087 [EU|EU+AF] -80.13 0.01866 [AS|AS] -80.44 0.0136	At node N64: split-lnL Rel.Prob [EU|EU] -76.21 0.9358 [EU+AS|EU] -79.83 0.02505
At node N62: split-lnL Rel.Prob [EU|EU] -76.61 0.6269 [EU+AF|EU] -77.88 0.1761 [EU+AF|AF] -79.18 0.04807 [EU|EU+AF] -79.42 0.03798 [EU+AS|EU] -79.69 0.02885 [EU|EU+AS] -80.05 0.02021 [AF|EU+AF] -80.09 0.01945	At node N58: split-lnL Rel.Prob [EU|EU] -76.69 0.5804 [AF|EU] -77.75 0.2017 [EU+AF|EU] -78.5 0.09508 [AF|EU+AF] -79.36 0.04026 [AF|AF] -79.67 0.02935 [AS|EU] -79.82 0.02537	At node N56: split-lnL Rel.Prob [EU|EU] -77.07 0.3951 [AF|AF] -77.46 0.2693 [AF|EU] -78.5 0.09538 [AF|EU+AF] -78.77 0.07214 [EU+AF|EU] -79.3 0.04262 [EU+AF|AF] -79.3 0.04262 [AS|AS] -79.84 0.0248 [AS|EU+AS] -80.78 0.00973	At node N54: split-lnL Rel.Prob [AF|AF] -76.96 0.4415 [EU|EU] -77.55 0.2462 [AF|EU] -78.5 0.09459 [AF|EU+AF] -78.8 0.07027 [EU+AF|AF] -79.47 0.03585 [EU+AF|EU] -79.47 0.03585 [AS|AS] -80.1 0.01913 [AF|AF+AS] -80.3 0.01576
At node N52: split-lnL Rel.Prob [AF|AF] -76.6 0.6363 [EU|EU] -78.25 0.1214 [AF|EU+AF] -78.46 0.09899 [AF|EU] -79.28 0.04358 [EU+AF|AF] -79.37 0.0398 [EU+AF|EU] -80.18 0.01772	At node N50: split-lnL Rel.Prob [AF|AF] -76.38 0.7937 [AF|EU+AF] -78.79 0.07078 [EU|EU] -78.97 0.05955 [EU+AF|AF] -79.58 0.0324	At node N49: split-lnL Rel.Prob [AF|AF] -76.37 0.8022 [EU+AF|AF] -78.46 0.09881 [EU|EU] -79.55 0.03329 [EU|AF] -79.72 0.02806	At node N47: split-lnL Rel.Prob [AF|AF] -76.6 0.6327 [EU+AF|AF] -78.42 0.1032 [EU+AF|EU] -78.42 0.1032 [EU|EU] -79 0.05733 [AF|AS] -79.23 0.04577 [AF|AF+AS] -80.23 0.01683
At node N43: split-lnL Rel.Prob [EU|AF] -76.99 0.4289 [AF|AF] -77.2 0.3481 [EU+AF|AF] -78.67 0.08042 [EU|EU+AF] -78.77 0.07259	At node N41: split-lnL Rel.Prob [EU|EU] -76.69 0.582 [EU+AF|EU] -78.04 0.1511 [EU|EU+AF] -78.29 0.1172 [AF|AF] -78.63 0.08296	At node N40: split-lnL Rel.Prob [EU|EU] -76.42 0.7612 [EU+AF|EU] -78.49 0.09599 [EU|EU+AF] -79.3 0.04262 [AF|AF] -79.36 0.04007	At node N22: split-lnL Rel.Prob [EU|EU] -76.37 0.8 [EU|AF] -78.78 0.0721 [EU|EU+AF] -78.86 0.06599 [AF|AF] -80.09 0.01946

[EU|EU] -79.09 0.05284	[AF|EU] -79.65 0.03007	[EU+AF|AF] -80.37 0.01458	
At node N20: split-lnL Rel.Prob [EU|EU] -76.22 0.929 [EU|EU+AF] -80 0.02121	At node N12: split lnL Rel.Prob [EU|EU] -76.26 0.8914 [EU|AS] -78.97 0.05922	At node N11: split lnL Rel.Prob [NA|AS] -76.27 0.8805 [AS|AF] -79.09 0.05256 [SA|NA] -79.83 0.02511	At node N9: split-lnL Rel.Prob [SA|SA] -76.79 0.5252 [NA+SA|SA] -77.6 0.2327 [SA|NA+SA] -77.6 0.2327
At node N5: split-lnL Rel.Prob [SA|SA] -76.21 0.9388 [NA+SA|SA] -79.65 0.03017	At node N8: split-lnL Rel.Prob [SA|SA] -76.21 0.9388 [NA+SA|SA] -79.65 0.03017	At node N19: split lnL Rel.Prob [EU|EU] -76.18 0.9671	At node N17: split lnL Rel.Prob [EU|EU] -76.16 0.983
At node N15: split lnL Rel.Prob [EU|EU] -76.15 0.9941	At node N39: split-lnL Rel.Prob [EU|EU+AS] -76.83 0.5052 [EU|EU] -77.13 0.373 [EU|AS] -78.41 0.1035	At node N38: split-lnL Rel.Prob [EU+AS|AS] -76.67 0.5893 [EU|EU] -78.11 0.1399 [EU|AS] -78.35 0.1105 [AS|AS] -78.64 0.08264 [EU|EU+AS] -79.54 0.03371	At node N38: split-lnL Rel.Prob [EU+AS|AS] -76.67 0.5893 [EU|EU] -78.11 0.1399 [EU|AS] -78.35 0.1105 [AS|AS] -78.64 0.08264 [EU|EU+AS] -79.54 0.03371
At node N34: split-lnL Rel.Prob [EU|AS] -76.79 0.5258 [EU|EU] -77.54 0.2483 [EU|EU+AS] -78.02 0.1535 [EU+AS|AS] -79.27 0.04384	At node N32: split-lnL Rel.Prob [EU|EU] -76.2 0.945 [EU|EU+AS] -79.52 0.03423	At node N30: split lnL Rel.Prob [EU|EU] -76.17 0.9752	At node N28: split-lnL Rel.Prob [EU|EU] -76.23 0.9223 [EU+AF|EU] -78.78 0.07152
At node N26: split-lnL Rel.Prob [EU|EU] -76.69 0.5819 [EU|AF] -77.18 0.3547 [EU|EU+AF] -79.15 0.04943	At node N37: split lnL Rel.Prob [AS|AS] -76.17 0.9763	At node N46: split lnL Rel.Prob [NA|NA] -76.19 0.9573	At node N61: split-lnL Rel.Prob [EU|EU] -76.61 0.6298 [EU|AF] -78.01 0.155 [EU|EU+AF] -78.1 0.1418 [EU|AS] -79.39 0.03881

Analysis #3, strict consensus tree with nodes



Analysis #3, synapomorphies of the strict consensus tree

Synapomorphies common to 1 trees
(Node numbers refer to nodes in consensus)

Chrysemys_picta :
-No autapomorphies:

Mauremys_caspica :

-MARGINAL_2_with_NUCHAL (20): absent_ --> present_
-MARGINAL_2_with_VERTEBRAL_1 (21): absent_ --> present_
-HUMEROPECTORAL_POSITION (33): posterior_to_the_entoplastron_ --> crossing_the_entoplastron_
-MAX-PREMAX_RIDGE (48): absent_ --> present_
-SQUAMOSALS (59): extending_beyond_the_condylus_occipitalis_ --> not_extending_

Manouria_impressa :
-PERIPHERAL (19): absent_or_poorly_developed_ --> well_developed_
-FEMOROANAL_SHAPE (37): straight_or_slightly_rounded,_developed_mainly_perpendicular_with_the_axial_plane --> forms_S-shaped_curve_laterally
-VOMER (56): vomer_dividing_the_palatines,_not_the_pterygoids --> vomer_diving_part_of_the_pterygoids,_not_reaching_the_basisphenoid_

Geochelone_elegans :
-NUCHAL_1 (0): hexagonal_ --> octagonal_
-CERVICAL (4): dorsally_present_ --> absent_
-GULAR_PROTRUSION (27): present_ --> absent_
-HUMEROPECTORAL_SHAPE (34): perpendicular_to_the_axial_plane,_relatively_straight_throughout_its_width_ --> perpendicular_to_the_axial_plane,_with_a_well-developed_lateral_change_of_curvature
-FEMOROANAL_SHAPE (37): straight_or_slightly_rounded,_developed_mainly_perpendicular_with_the_axial_plane --> acute_angle_with_the_axial_plane_
-MAX_RIDGE (54): absent_ --> present_
-VOMER (56): vomer_dividing_the_palatines,_not_the_pterygoids --> vomer_dividing_palatines_and_pterygoids,_reaching_the_basisphenoid_

Stigmochelys_pardalis :
-NUCHAL_4 (3): notch_absent_ --> shallow_
-NEURAL_1 (6): rectangular_ --> hexagonal,_short_sides_positioned_posteriorly_
-VERTEBRAL_1 (14): narrow_vertebrals,_narrower_than_the_pleurals --> wide_vertebrals,_almost_equal_to_the_pleurals
-PERIPHERAL (19): absent_or_poorly_developed_ --> well_developed_
-GULARS_vs_ENTOPLASTRON (30): covering_the_anterior_area --> in_contact_with_the_anterior_margin_
-FRONTAL_vs_ORBIT (39): participates_to_the_formation_of_the_orbital_rim_ --> excluded_from_the_orbit
-POSTERIOR_MAX_PROCESS (52): present_ --> absent_
-FORAMEN_PRAEPALATINUM (58): visible_ --> not_visible_in_ventral_view_-_foramina_may_be_concealed_by_lingual_extensions_of_the_maxillary_alveolar_ridges_

Indotestudo_elongata :
-NUCHAL_4 (3): notch_absent_ --> significant_medial_protrusion_present_
-PERIPHERAL (19): absent_or_poorly_developed_ --> well_developed_
-MAX-PRE_SYMPHYSIS_HEIGHT (45): short,_shorter_than_the_height_of_fossa_nasalis,_but_with_the_development_of_a_dorsal_projection_ --> high,_taller_than_the_height_of_fossa_nasalis

Indotestudo_forstenii :
-VERTEBRAL_1 (14): narrow_vertebrals,_narrower_than_the_pleurals --> wide_vertebrals,_almost_equal_to_the_pleurals
-LINGUAL_RIDGE (50): restricted_to_maxilla_ --> extending_onto_premaxillae_
-SQUAMOSALS (59): not_extending_ --> extending_beyond_the_condylus_occipitalis_

Centrochelys_sulcata :
-NUCHAL_1 (0): hexagonal_ --> octagonal_
-NEURAL_1 (6): rectangular_ --> hexagonal,_short_sides_positioned_posteriorly_
-NEURAL_2 (7): octagonal_ --> hexagonal,_short_sides_positioned_posteriorly
-EPIPLASTRAL_LIP_SHAPE (29): convex_to_flat_ --> concave_
-FRONTAL_vs_ORBIT (39): participates_to_the_formation_of_the_orbital_rim_ --> excluded_from_the_orbit
-CRISTA_SUPRAOCCIPITALIS_SHAPE (62): elevated_posteriorly_ --> straight_
-THIGH_SPURS (80): absent --> present_

Agrionemys_horsfieldii :
-NUCHAL_1 (0): hexagonal_ --> octagonal_
-NEURAL_NUMBER (5): eight_neurals_ --> seven_neurals_or_less_
-SUPRAPYGAL (12): two,_both_suprapygals_constitute_one_trapeze_and_the_first_suprapygal_embrassing_the_lenticular_second_one_ --> two,_the_contact_between_the_suprapygals_is_straight_and_perpendicular_to_the_axial_plane
-VERTEBRAL_2 (15): the_posterior_sulcus_of_the_fifth_vertebral_coincides_with_the_suprapygal-pygal_suture_ --> the_posterior_sulcus_of_the_fifth_vertebral_crosses_the_suprapygal_transversely

Testudo_hermanni :
-NUCHAL_1 (0): hexagonal_ --> octagonal_
-NEURAL_1 (6): rectangular_ --> hexagonal,_short_sides_positioned_posteriorly_
-PYGAL (13): quadrangular_(without_small_latero-anterior_borders) --> quadrangular_or_hexagonal_with_small_latero-anterior_borders
-SUPRACAUDAL_1 (16): twelfth_marginals_fused_into_a_supracaudal_dorsally -->

two_twelfth_marginals_present_dorsally_
-FRONTAL_vs_PREFRONTALS (40): frontals_longer_than_prefrontals_ --> prefrontals_longer_than_frontals

Testudo_graeca :
-ANAL_LENGTH (38): longer_than_the_medial_length_of_femoral_ --> shorter_than_the_median_length_of_femoral_

Testudo_marginata :
-BORDER (25): posterior_border_curved_inwards_ --> posterior_border_posteriorly_flared_

Milia_testudinid :
-BORDER (25): posterior_border_curved_inwards_ --> posterior_border_posteriorly_flared_

Testudo_kleinmanni :
-NUCHAL_3 (2): first_pleural_touches,_but_it_does_not_overlap_the_nuchal_ --> first_pleural_overlaps_postero-lateral_parts_of_the_nuchal
-NUCHAL_4 (3): notch_absent_, or shallow_ --> significant_medial_protrusion_present_
-PERIPHERAL (19): well_developed_ --> absent_or_poorly_developed_
-FEMOROANAL_SHAPE (37): forms_S-shaped_curve_laterally --> acute_angle_with_the_axial_plane_

Testudo_marmorum :
-NUCHAL_2 (1): markedly_wider_than_long_ --> markedly_longer_than_wide
-NUCHAL_3 (2): first_pleural_touches,_but_it_does_not_overlap_the_nuchal_ --> first_pleural_overlaps_postero-lateral_parts_of_the_nuchal
-NEURAL_NUMBER (5): seven_neurals_or_less_ --> eight_neurals_
-COINCIDENCE (18): present_ --> absent_
-PERIPHERAL (19): well_developed_ --> absent_or_poorly_developed_

Samos_testudinid :
-NUCHAL_3 (2): first_pleural_touches,_but_it_does_not_overlap_the_nuchal_ --> first_pleural_is_not_in_contact_with_the_nuchal_

Testudo_antiqua :
-No autapomorphies:

Kinixys_erosa :
-CERVICAL (4): dorsally_present_ --> absent_
-NEURAL_2 (7): hexagonal,_short_sides_positioned_posteriorly --> hexagonal,_short_sides_positioned_anteriorly_
-SUPRAPYGAL (12): two,_the_contact_between_the_suprapygals_is_straight_and_perpendicular_to_the_axial_plane --> one,_suprapygals_fused,_constituting_one_trapeze_
-SUPRACAUDAL_1 (16): two_twelfth_marginals_present_dorsally_ --> twelfth_marginals_fused_into_a_supracaudal_dorsally
-SUPRACAUDAL_2 (17): two_twelfth_marginals_present_viscerally_ --> twelfth_marginals_fused_into_a_supracaudal_viscerally
-PERIPHERAL (19): absent_or_poorly_developed_ --> well_developed_
-CARAPACIAL_HINGE (24): absent_ --> present_
-BORDER (25): posterior_border_curved_inwards_ --> posterior_border_posteriorly_flared_
-ANTERIOR_LOBE (26): medially_notched_ --> trilobed_
-GULAR_PROTRUSION (27): present_ --> absent_
-EPIPLASTRAL_LIP_SHAPE (29): concave_ --> convex_to_flat_
-FEMOROANAL_SHAPE (37): straight_or_slightly_rounded,_developed_mainly_perpendicular_with_the_axial_plane --> acute_angle_with_the_axial_plane_
-DESCENDING_FRONTAL (41): absent,_or_very_small_ --> present,_well-developed_
-FOSSA_ORBITALIS_POSITION (43): anterior_to_middle_ --> posterior_
-PREMAX_RIDGE (46): absent_ --> present_

Gopherus_agassizii :
-DESCENDING_FRONTAL (41): present,_well-developed_ --> absent,_or_very_small_

Gopherus_polyphemus :
-SUPRAPYGAL (12): two,_both_suprapygals_constitute_one_trapeze_and_the_first_suprapygal_embrassing_the_lenticular_second_one_ --> two,_the_contact_between_the_suprapygals_is_straight_and_perpendicular_to_the_axial_plane
-MARGINAL_4_with_PLEURAL_2 (22): absent_ --> present_
-MARGINAL_6_with_PLEURAL_3 (23): absent_ --> present_
-GULARS_ANGLE (31): more_acute_ --> 45?_or_more_obtuse_
-PECTORAL_LENGTH (35): short --> long
-FEMOROANAL_SHAPE (37): straight_or_slightly_rounded,_developed_mainly_perpendicular_with_the_axial_plane --> forms_S-shaped_curve_laterally
-MAX-PRE_SYMPHYSIS_HEIGHT (45): short,_shorter_than_the_height_of_fossa_nasalis,_but_with_the_development_of_a_dorsal_projection_ --> short,_shorter_than_the_height_of_fossa_nasalis_
-FORAMEN_PRAEPALATINUM (58): visible_ --> not_visible_in_ventral_view_-

_foramina_may_be_concealed_by_lingual_extensions_of_the_maxillary_alveolar_ridges_
-CRISTA_SUPRAOCCIPITALIS_SHAPE (62): straight_ --> bended_inwards_

Astrochelys_radiata :
-COINCIDENCE (18): present_ --> absent_
-MAX-PRE_SYMPHYSIS_HEIGHT (45):
short,_shorter_than_the_height_of_fossa_nasalis,_but_with_the_development_of_a_dorsal_projection_ -->
short,_shorter_than_the_height_of_fossa_nasalis_
-MAX-PREMAX_RIDGE (48): absent_ --> present_
-FORAMEN_PRAEPALATINUM (58): visible_ --> not_visible_in_ventral_view_-
_foramina_may_be_concealed_by_lingual_extensions_of_the_maxillary_alveolar_ridges_
-PROCESSUS_TROCHLEARIS_OTICUM (65): absent,_or_small_ --> large

Chelonoidis_chilensis :
-NUCHAL_4 (3): deep_ --> shallow_
-HUMEROPECTORAL_SHAPE (34): perpendicular_to_the_axial_plane,_with_a_well-developed_lateral_change_of_curvature
--> perpendicular_to_the_axial_plane,_relatively_straight_throughout_its_width_
-FRONTAL_vs_ORBIT (39): participates_to_the_formation_of_the_orbital_rim_ --> excluded_from_the_orbit
-CRISTA_SUPRAOCCIPITALIS_KEELS (61): present_ --> absent_
-HUMERUS_SCAR (69): present_ --> absent_or_reduced_
-FEMUR_HEAD_ANGLE (73): femoral_head_developed_almost_perpendicular_to_the_diaphysis_ --> relatively_large_angle_
-AS_+_CAL (78): fused_ --> not_fused

Chelonoidis_nigra :
-NUCHAL_1 (0): hexagonal_ --> octagonal_
-GULAR_PROTRUSION (27): present_ --> absent_
-GULARS_vs_ENTOPLASTRON (30): not_in_contact_ --> covering_the_anterior_area
-HUMERAL_LENGTH (32): humerals_longer_than_the_gulars_ --> humerals_equal_or_smaller_than_the_gulars_
-FEMOROANAL_SHAPE (37): straight_or_slightly_rounded,_developed_mainly_perpendicular_with_the_axial_plane -->
forms_S-shaped_curve_laterally
-MAX_RIDGE (54): absent_ --> present_

Chelonoidis_carbonaria :
-HUMEROPECTORAL_SHAPE (34): perpendicular_to_the_axial_plane,_with_a_well-developed_lateral_change_of_curvature
--> perpendicular_to_the_axial_plane,_relatively_straight_throughout_its_width_
-LABIAL_RIDGE (51): present_ --> absent_

Chelonoidis_denticulata :
-CRISTA_SUPRAOCCIPITALIS_SHAPE (62): elevated_posteriorly_ --> straight_

Titanochelon_bolivari :
-HUMERUS_DISTAL_END (68): symmetric_ --> asymmetric_

Titanochelon_vitodurana :
-No autapomorphies:

Titanochelon_perpiniana :
-No autapomorphies:

Titanochelon_bacharidisi :
-FOSSA_ORBITALIS_POSITION (43): anterior_to_middle_ --> posterior_
-VENTRAL_TEMPORAL_EMARGINATION (44): small_ --> extensive_
-SQUAMOSALS (59): not_extending_ --> extending_beyond_the_condylus_occipitalis_

Achilemys_cassouleti :
-NUCHAL_3 (2): first_pleural_is_not_in_contact_with_the_nuchal_ --> first_pleural_overlaps_postero-
lateral_parts_of_the_nuchal
-NEURAL_2 (7): hexagonal,_short_sides_positioned_posteriorly --> rectangular
-NEURAL_3 (8): hexagonal_, or rectangular_ --> octagonal_
-NEURAL_4 (9): hexagonal_ --> rectangular_
-VERTEBRAL_1 (14): wide_vertebrals,_almost_equal_to_the_pleurals --> narrow_vertebrals,_narrower_than_the_pleurals
-ANTERIOR_LOBE (26): medially_notched_ --> subrounded_to_straight_
-GULAR_PROTRUSION (27): present_ --> absent_
-ANAL_LENGTH (38): shorter_than_the_median_length_of_femoral_ --> longer_than_the_medial_length_of_femoral_

Gigantochersina_ammon :
-VERTEBRAL_1 (14): wide_vertebrals,_wider_than_the_pleurals_ --> wide_vertebrals,_almost_equal_to_the_pleurals
-HUMEROPECTORAL_POSITION (33): posterior_to_the_entoplastron_ --> crossing_the_entoplastron_

Namibchersus_namaquensis :
-NUCHAL_2 (1): markedly_wider_than_long_ --> markedly_longer_than_wide

Testudo_gigas :
-NUCHAL_3 (2): first_pleural_touches,_but_it_does_not_overlap_the_nuchal_ --> first_pleural_overlaps_postero-lateral_parts_of_the_nuchal
-COINCIDENCE (18): present_ --> absent_
-HUMEROPECTORAL_SHAPE (34): perpendicular_to_the_axial_plane,_with_a_well-developed_lateral_change_of_curvature --> not_perpendicular_to_the_axial_plane,_rounded_or_forming_a_wide_angle_

Paleotestudo_canetoniana :
-PECTORAL_LENGTH (35): short --> long

Ergilemys_bruneti :
-NUCHAL_2 (1): markedly_wider_than_long_ --> slightly_wider_than_long_or_as_long_as_wide_
-NUCHAL_4 (3): notch_absent_ --> significant_medial_protrusion_present_
-SUPRACAUDAL_2 (17): twelfth_marginals_fused_into_a_supracaudal_viscerally --> two_twelfth_marginals_present_viscerally_
-PERIPHERAL (19): absent_or_poorly_developed_ --> well_developed_
-EPIPLASTRAL_LIP (28): present_ --> absent_or_poorly_developed_
-GULARS_ANGLE (31): more_acute_ --> 45?_or_more_obtuse_
-PLASTRAL_HINGE (36): absent_ --> present,_between_hypoplastra_and_xiphiplastra

Hadrianus_castrensis :
-NUCHAL_2 (1): markedly_wider_than_long_, or markedly_longer_than_wide --> slightly_wider_than_long_or_as_long_as_wide_
-NUCHAL_3 (2): first_pleural_is_not_in_contact_with_the_nuchal_ --> first_pleural_touches,_but_it_does_not_overlap_the_nuchal_
-NEURAL_NUMBER (5): eight_neurals_ --> nine_neurals_
-SUPRAPYGAL (12): two,_the_contact_between_the_suprapygals_is_straight_and_perpendicular_to_the_axial_plane --> two,_both_suprapygals_constitute_one_trapeze_and_the_first_suprapygal_embrassing_the_lenticular_second_one_
-VERTEBRAL_2 (15): he_posterior_sulcus_of_the_fifth_vertebral_overlaps_the_anterior_part_of_the_pygal --> the_posterior_sulcus_of_the_fifth_vertebral_crosses_the_suprapygal_transversely
-HUMERAL_LENGTH (32): humerals_longer_than_the_gulars_ --> humerals_equal_or_smaller_than_the_gulars_
-HUMEROPECTORAL_POSITION (33): posterior_to_the_entoplastron_ --> crossing_the_entoplastron_

Cheirogaster_maurini :
-NUCHAL_4 (3): notch_absent_, or significant_medial_protrusion_present_ --> deep_
-CERVICAL (4): dorsally_present_ --> absent_
-NEURAL_1 (6): hexagonal,_short_sides_positioned_posteriorly_ --> rectangular_
-NEURAL_2 (7): hexagonal,_short_sides_positioned_posteriorly --> octagonal_
-MARGINAL_2_with_NUCHAL (20): absent_ --> present_
-MARGINAL_2_with_VERTEBRAL_1 (21): absent_ --> present_

Impregnochelys_pachytestis :
-HUMERAL_LENGTH (32): humerals_longer_than_the_gulars_ --> humerals_equal_or_smaller_than_the_gulars_

Node 39 :
-No synapomorphies

Node 40 :
-SUPRAPYGAL (12): two,_the_contact_between_the_suprapygals_is_straight_and_perpendicular_to_the_axial_plane --> two,_both_suprapygals_constitute_one_trapeze_and_the_first_suprapygal_embrassing_the_lenticular_second_one_
-COINCIDENCE (18): absent_ --> present_
-HUMEROPECTORAL_SHAPE (34): not_perpendicular_to_the_axial_plane,_rounded_or_forming_a_wide_angle_ --> perpendicular_to_the_axial_plane,_relatively_straight_throughout_its_width_
-PECTORAL_LENGTH (35): long --> short
-FRONTAL_vs_PREFRONTALS (40): prefrontals_longer_than_frontals --> frontals_longer_than_prefrontals_
-POSTERIOR_MAX_PROCESS (52): absent_ --> present_

Node 41 :
-NEURAL_1 (6): rectangular_ --> hexagonal,_short_sides_positioned_posteriorly_
-VERTEBRAL_1 (14): wide_vertebrals,_wider_than_the_pleurals_ --> wide_vertebrals,_almost_equal_to_the_pleurals
-EPIPLASTRAL_LIP (28): absent_or_poorly_developed_ --> present_
-GULARS_ANGLE (31): more_acute_ --> 45?_or_more_obtuse_
-HUMERAL_LENGTH (32): humerals_equal_or_smaller_than_the_gulars_ --> humerals_longer_than_the_gulars_
-HUMEROPECTORAL_SHAPE (34): perpendicular_to_the_axial_plane,_relatively_straight_throughout_its_width_ --> not_perpendicular_to_the_axial_plane,_rounded_or_forming_a_wide_angle_
-FEMOROANAL_SHAPE (37): acute_angle_with_the_axial_plane_ --> straight_or_slightly_rounded,_developed_mainly_perpendicular_with_the_axial_plane
-MAX-PRE_SYMPHYSIS_HEIGHT (45): short,_shorter_than_the_height_of_fossa_nasalis_ --> short,_shorter_than_the_height_of_fossa_nasalis,_but_with_the_development_of_a_dorsal_projection_
-CRISTA_SUPRAOCCIPITALIS_KEELS (61): absent_ --> present_

Node 42 :

-NEURAL_4 (9): hexagonal_ --> octagonal_
-NEURAL_5 (10): hexagonal_ --> rectangular_
-VERTEBRAL_1 (14): wide_vertebrals,_almost_equal_to_the_pleurals --> wide_vertebrals,_wider_than_the_pleurals_
-SUPRACAUDAL_1 (16): two_twelfth_marginals_present_dorsally_ -->
twelfth_marginals_fused_into_a_supracaudal_dorsally
-SUPRACAUDAL_2 (17): two_twelfth_marginals_present_viscerally_ -->
twelfth_marginals_fused_into_a_supracaudal_viscerally
-EPIPLASTRAL_LIP_SHAPE (29): concave_ --> convex_to_flat_

Node 43 :
-CERVICAL (4): dorsally_present_ --> absent_
-FEMOROANAL_SHAPE (37): acute_angle_with_the_axial_plane_ -->
straight_or_slightly_rounded,_developed_mainly_perpendicular_with_the_axial_plane
-CRISTA_SUPRAOCCIPITALIS_KEELS (61): absent_ --> present_
-CRISTA_SUPRAOCCIPITALIS_SHAPE (62): straight_ --> elevated_posteriorly_

Node 44 :
-VERTEBRAL_1 (14): wide_vertebrals,_wider_than_the_pleurals_ --> narrow_vertebrals,_narrower_than_the_pleurals

Node 45 :
-NUCHAL_3 (2): first_pleural_is_not_in_contact_with_the_nuchal_ -->
first_pleural_touches,_but_it_does_not_overlap_the_nuchal_

Node 46 :
-GULAR_PROTRUSION (27): present_ --> absent_
-FEMOROANAL_SHAPE (37): straight_or_slightly_rounded,_developed_mainly_perpendicular_with_the_axial_plane -->
acute_angle_with_the_axial_plane_

Node 47 :
-NEURAL_1 (6): hexagonal,_short_sides_positioned_posteriorly_ --> rectangular_

Node 48 :
-HUMEROPECTORAL_SHAPE (34): perpendicular_to_the_axial_plane,_relatively_straight_throughout_its_width_ -->
perpendicular_to_the_axial_plane,_with_a_well-developed_lateral_change_of_curvature

Node 49 :
-GULARS_ANGLE (31): 45?_or_more_obtuse_ --> more_acute_

Node 50 :
-NEURAL_2 (7): hexagonal,_short_sides_positioned_posteriorly --> octagonal_
-ANTERIOR_LOBE (26): medially_notched_ --> subrounded_to_straight
-DESCENDING_FRONTAL (41): absent,_or_very_small_ --> present,_well-developed_
-CRISTA_SUPRAOCCIPITALIS_KEELS (61): present_ --> absent_
-OPISTHOTIC (64): not_expanded,_fenestra_postotica_open_ --> expanded,_could_contact_exoccipital
-FORAMEN_NERVI_TRIGEMINI (66): one --> two

Node 51 :
-GULARS_ANGLE (31): more_acute_ --> 45?_or_more_obtuse_
-HUMEROPECTORAL_SHAPE (34): not_perpendicular_to_the_axial_plane,_rounded_or_forming_a_wide_angle_ -->
perpendicular_to_the_axial_plane,_relatively_straight_throughout_its_width_
-FEMOROANAL_SHAPE (37): acute_angle_with_the_axial_plane_ -->
straight_or_slightly_rounded,_developed_mainly_perpendicular_with_the_axial_plane
-POSTERIOR_MAX_PROCESS (52): present_ --> absent_
-OPISTHOTIC (64): expanded,_could_contact_exoccipital --> not_expanded,_fenestra_postotica_open_

Node 52 :
-HUMERAL_LENGTH (32): humerals_longer_than_the_gulars_ --> humerals_equal_or_smaller_than_the_gulars_

Node 53 :
-VERTEBRAL_2 (15): the_posterior_sulcus_of_the_fifth_vertebral_crosses_the_suprapygal_transversely -->
the_posterior_sulcus_of_the_fifth_vertebral_coincides_with_the_suprapygal-pygal_suture_
-HUMEROPECTORAL_SHAPE (34): perpendicular_to_the_axial_plane,_with_a_well-developed_lateral_change_of_curvature
--> not_perpendicular_to_the_axial_plane,_rounded_or_forming_a_wide_angle_

Node 54 :
-GULAR_PROTRUSION (27): absent_ --> present_
-GULARS_vs_ENTOPLASTRON (30): covering_the_anterior_area --> not_in_contact_

Node 55 :
-NUCHAL_4 (3): notch_absent_ --> deep_

Node 56 :

-NUCHAL_2 (1): markedly_wider_than_long_ --> markedly_longer_than_wide
-MAX-PREMAX_RIDGE (48): absent_ --> present_
-PROCESSUS_TROCHLEARIS_OTICUM (65): absent,_or_small_ --> large

Node 57 :
-NUCHAL_4 (3): notch_absent_ --> shallow_
-VERTEBRAL_1 (14): narrow_vertebrals,_narrower_than_the_pleurals --> wide_vertebrals,_almost_equal_to_the_pleurals

Node 58 :
-ANAL_LENGTH (38): shorter_than_the_median_length_of_femoral_ --> longer_than_the_medial_length_of_femoral_
-MANUS (77): two_phalanges_in_all_digits_ --> one_phalanx_in_first_and_fifth_finger

Node 59 :
-NEURAL_NUMBER (5): eight_neurals_ --> seven_neurals_or_less_
-SUPRAPYGAL (12):
two,_both_suprapygals_constitute_one_trapeze_and_the_first_suprapygal_embrassing_the_lenticular_second_one_ -->
one,_suprapygals_fused,_constituting_one_trapeze_

Node 60 :
-PERIPHERAL (19): absent_or_poorly_developed_ --> well_developed_

Node 61 :
-VERTEBRAL_1 (14): narrow_vertebrals,_narrower_than_the_pleurals --> wide_vertebrals,_almost_equal_to_the_pleurals
-HUMERAL_LENGTH (32): humerals_equal_or_smaller_than_the_gulars_ --> humerals_longer_than_the_gulars_
-PLASTRAL_HINGE (36): absent_ --> present,_between_hypoplastra_and_xiphiplastra
-FEMOROANAL_SHAPE (37): acute_angle_with_the_axial_plane_ --> forms_S-shaped_curve_laterally
-HUMERUS_SCAR (69): absent_or_reduced_ --> present_

Node 62 :
-ANTERIOR_LOBE (26): subrounded_to_straight_ --> triagonal_
-EPIPLASTRAL_LIP_SHAPE (29): convex_to_flat_ --> concave_
-GULARS_vs_ENTOPLASTRON (30): covering_the_anterior_area --> in_contact_with_the_anterior_margin_
-HUMEROPECTORAL_SHAPE (34): perpendicular_to_the_axial_plane,_with_a_well-developed_lateral_change_of_curvature
--> not_perpendicular_to_the_axial_plane,_rounded_or_forming_a_wide_angle_
-FRONTAL_vs_PREFRONTALS (40): frontals_longer_than_prefrontals_ --> prefrontals_longer_than_frontals
-SULCUS_OLFACTURIUS (42): ventrally_open_ --> ventrally_nearly_closed_
-VENTRAL_TEMPORAL_EMARGINATION (44): small_ --> extensive_
-PREMAX_RIDGE (46): absent_ --> present_
-LINGUAL_RIDGE (50): restricted_to_maxilla_ --> extending_onto_premaxillae_

Node 63 :
-NEURAL_3 (8): rectangular_ --> hexagonal_
-NEURAL_4 (9): octagonal_ --> hexagonal_

Node 64 :
-NUCHAL_3 (2): first_pleural_touches,_but_it_does_not_overlap_the_nuchal_ -->
first_pleural_is_not_in_contact_with_the_nuchal_
-VERTEBRAL_1 (14): narrow_vertebrals,_narrower_than_the_pleurals --> wide_vertebrals,_wider_than_the_pleurals_
-GULARS_ANGLE (31): more_acute_ --> 45?_or_more_obtuse_
-OPISTHOTIC (64): expanded,_could_contact_exoccipital --> expanded,_contacting_the_pterygoid_

Node 65 :
-NUCHAL_2 (1): markedly_longer_than_wide --> slightly_wider_than_long_or_as_long_as_wide_
-NUCHAL_4 (3): deep_ --> notch_absent_
-VERTEBRAL_2 (15): the_posterior_sulcus_of_the_fifth_vertebral_crosses_the_suprapygal_transversely -->
the_posterior_sulcus_of_the_fifth_vertebral_coincides_with_the_suprapygal-pygal_suture_
-MEDIAN_MAX_RIDGE (53): present,_restricted_to_maxilla --> present,_extending_to_premaxilla

Node 66 :
-NUCHAL_2 (1): markedly_longer_than_wide --> slightly_wider_than_long_or_as_long_as_wide_

Node 67 :
-MARGINAL_4_with_PLEURAL_2 (22): absent_ --> present_
-MARGINAL_6_with_PLEURAL_3 (23): absent_ --> present_

Node 68 :
-HUMEROPECTORAL_POSITION (33): posterior_to_the_entoplastron_ -->
coinciding_medially_with_the_posterior_suture_of_the_entoplastron

TNT file for the analysis of the geoemydids

xread

```
54 30

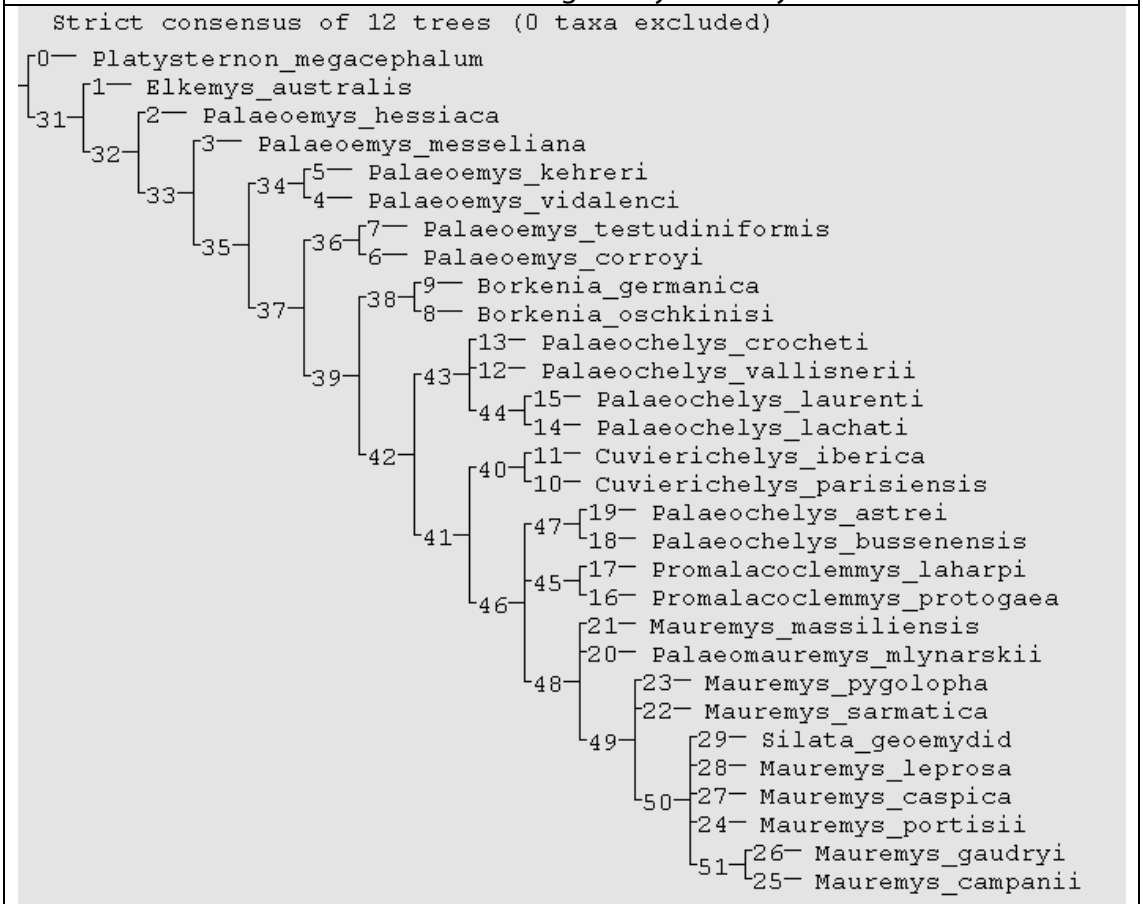
Platysternon_megacephalum 00000?101?1100000010000000000000000000000000??2?0000
Elkemys_australis 0??0??000?00???10000100101011??020101110000111000210 00
Palaeoemys_hessiaca 1110?000200000010000?1101000100201000000001110010 1001
Palaeoemys_messeliana 1110100000000??100000011120 00??020100000000111002 11?01
Palaeoemys_vidalenci 1110200000?0001?000??11????120010100000000111010 11001
Palaeoemys_kehreri 1110200000000001000000111 20?120010100000000111?1021001
Palaeoemys_corroyi 1110200000000001?0011?11???113102010000000011101111001
Palaeoemys_testudiniformis 1110200000000??100011211201 1?1?201000000001110111 1?01
Borkenia_oschkinisi 1110100010001001000???21???113101010000000011111221001
Borkenia_germanica 11101000100010010 00?122112011310101000000001111121 1001
Cuvierichelys_parisiensis 1110?110110?1021000?0221??011311101000000011122103 1101
Cuvierichelys_iberica 1?10?1?0110????2?0?00122112011311101000?000111221021101
Palaeochelys_vallisnerii 1??021101000100 1?00100211201130020101000001111210 31001
Palaeochelys_crocheti 1210?0?0000????110010?21???10300201 0?00000111121031001
Palaeochelys_lachati 1??0211010001?01?11??02112011300201010000011 11?1021001
Palaeochelys_laurenti 12102110 1?00??011111022112011300201010000011 1121031001
Promalacoclemmys_protogaea 12?0222111201??100110031120113102111111000211211021101
Promalacoclemmys_laharpi 1??022211120111100011031120113002011111000111111021?01
Palaeochelys_bussenensis ?????1201000???1?00?0131121??????????????????????????????
Palaeochelys_astrei ????212010001??10000113112 1??????????????????????????????
Palaeomauremys_mlynarskii ?21?211011101??10001023112 1??????????????????????????????
Mauremys_massiliensis 1??12110111?1??1100?023112111320211111011 12?122103?111
Mauremys_sarmatica 13212110111101110001023112111320212111011 1222221041111
Mauremys_pygolopha 13112110 1?1?0111000?123112111320212111011 1222221031111
Mauremys_portisii 1??02111011111??1100102311 3?11?2?212111011 1222221031?11
Mauremys_campanii 14?122211111111?110110[0 1 2]3112111?2?212111?11122222104??11
Mauremys_gaudryi 14?1222111111111101002311321 1???212111011122222104??11
Mauremys_caspica 1421211111111111100102311321132021211101 1222221042111
Mauremys_leprosa 1421211111111111100102311321132021211101 1222221042111
Silata_geoemydid 1??121???12111???0???2311321132021211101 1122222104?111
;

cnames
{0 Inframarginals;
{1 axillary_process;
{2 inguinal_process;
{3 inguinal_&_axillary_notches;
{4 anterior_notch;
{5 V1;
{6 V1_width;
{7 contact_V1_and_M2;
{8 shape_of_V1;
{9 vertebrals_vs_the_nuchal;
{10 vertebrals_vs_the_costals;
{11 V4/V5;
{12 cervical_covering;
{13 cervical_viscerally;
{14 MA1_in_nuchal;
{15 PL1-2_vs_peripherals;
{16 pleurals_vs_peripherals;
{17 marginals_vs_peripherals;
{18 marginals_vs_pleurals;
{19 C2-3_vs_marginals;
{20 C4-V5_vs_marginals;
{21 V5_vs_PY_SPY;
{22 length_of_nuchal;
{23 neural_series;
{24 Shape_of_SP1;
{25 shape_of_SP2;
{26 shape_of_pygal;
{27 shape_of_ant_lobe;
{28 size_of_plastron;
```

```
{29 dorsal_gular_lip;
{30 GU-HU_vs_HU;
{31 gulars_epiplastron;
{32 gulars_vs_entoplastron;
{33 length_vs_width_of_gulars;
{34 angle_of_gulars;
{35 Shape_of_GU-HU;
{36 strengthening_of_ant_lobe;
{37 shape_of_anterior_border_of_plastron;
{38 FEM_vs_ABD;
{39 medial_HU-PEC;
{40 medial_GU_HUM;
{41 medial_HUM_vs_entoplastron;
{42 medial_length_GU_vs_the_ant_lobe;
{43 shape_of_entoplastron;
{44 epi-hyo_suture;
{45 epiplastron_length;
{46 medial_length_hyo;
{47 hyo_length_vs_ant_lobe;
{48 shape_hu-pec;
{49 position_of_hu_pec;
{50 length_bridge_vs_plastron;
{51 hu_fem_viscerally;
{52 anal_notch;
{53 Anals_vs_xiphi;
;

proc /;
comments 0
;
```

The nodes on the strict consensus of the geoemydid analysis



Geoemydid analysis: List of synapomorphies of the strict consensus tree

Synapomorphies common to 12 trees

(Node numbers refer to nodes in consensus)

Platysternon_megacephalum :
All trees:
-No autapomorphies:

Elkemys_australis :
All trees:
-C4-V5_vs_marginals (20): 0 --> 1
-shape_of_ant_lobe (27): 0 --> 1
-size_of_plastron (28): 0 --> 1
-strengthening_of_ant_lobe (36): 0 --> 1
-shape_of_anterior_border_of_plastron (37): 0 --> 1
-FEM_vs_ABD (38): 0 --> 1

Palaeoemys_hessiaca :
All trees:
-shape_of_V1 (8): 0 --> 2
-shape_hu-pec (48): 0, or 2 --> 1

Palaeoemys_messeliana :
All trees:
-No autapomorphies:

Palaeoemys_vidalenci :
All trees:
-No autapomorphies:

Palaeoemys_kehreri :
All trees:

-position_of_hu_pec (49): 1 --> 2

Palaeoemys_corroyi :
All trees:
-No autapomorphies:

Palaeoemys_testudiniformis :
All trees:
-No autapomorphies:

Borkenia_oschkinisi :
All trees:
-position_of_hu_pec (49): 1 --> 2

Borkenia_germanica :
All trees:
-No autapomorphies:

Cuvierichelys_parisiensis :
All trees:
-No autapomorphies:

Cuvierichelys_iberica :
All trees:
-C4-V5_vs_marginals (20): 0 --> 1
-position_of_hu_pec (49): 3 --> 2

Palaeochelys_vallisnerii :
All trees:
-No autapomorphies:

Palaeochelys_crocheti :
All trees:
-V1 (5): 1 --> 0
-shape_of_V1 (8): 1 --> 0
-size_of_plastron (28): 1 --> 0

Palaeochelys_lachati :
All trees:
-position_of_hu_pec (49): 3 --> 2

Palaeochelys_laurenti :
All trees:
-No autapomorphies:

Promalacoclemmys_protogaea :
All trees:
-marginals_vs_pleurals (18): 0 --> 1

Promalacoclemmys_laharpi :
All trees:
-C4-V5_vs_marginals (20): 0 --> 1
-GU-HU_vs_HU (30): 1 --> 0
-epiplastron_length (45): 2 --> 1

Palaeochelys_bussenensis :
All trees:
-No autapomorphies:

Palaeochelys_astrei :
All trees:
-C4-V5_vs_marginals (20): 0 --> 1

Palaeomauremys_mlynarskii :
All trees:
-No autapomorphies:

Mauremys_massiliensis :
All trees:
-pleurals_vs_peripherals (16): 0 --> 1

Mauremys_sarmatica :

Some trees:
-position_of_hu_pec (49): 3 --> 4

Mauremys_pygolopha :
All trees:
-C4-V5_vs_marginals (20): 0 --> 1

Mauremys_portisii :
All trees:
-inguinal_&_axillary_notches (3): 1 --> 0
Some trees:
-shape_of_V1 (8): 1 --> 0
-position_of_hu_pec (49): 4 --> 3

Mauremys_campanii :
Some trees:
-shape_of_SP2 (25): 3 --> 2
-shape_of_pygal (26): 2 --> 1

Mauremys_gaudryi :
All trees:
-C2-3_vs_marginals (19): 1 --> 0

Mauremys_caspica :
All trees:
-No autapomorphies:

Mauremys_leprosa :
All trees:
-No autapomorphies:

Silata_geoemydid :
All trees:
-vertebrals_vs_the_costals (10): 1 --> 2

Node 31 :
All trees:
-No synapomorphies

Node 32 :
All trees:
-Inframarginals (0): 0 --> 1
-length_of_nuchal (22): 0 --> 1
-Anals_vs_xiphi (53): 0 --> 1

Node 33 :
All trees:
-Shape_of_SP1 (24): 0 --> 1
-shape_of_SP2 (25): 1 --> 2

Node 34 :
All trees:
-gulars_vs_entoplastron (32): 2 --> 1

Node 35 :
All trees:
-size_of_plastron (28): 0 --> 1
-hyo_length_vs_ant_lobe (47): 0 --> 1

Node 36 :
All trees:
-shape_hu-pec (48): 0, or 2 --> 1

Node 37 :
All trees:
-C2-3_vs_marginals (19): 0 --> 1
-V5_vs_PY_SPY (21): 0 --> 2
-GU-HU_vs_HU (30): 0 --> 1

Node 38 :
All trees:
-anterior_notch (4): 2 --> 1

-gulars_vs_entoplastron (32): 2 --> 1

Node 39 :
All trees:
-shape_of_V1 (8): 0 --> 1
-cervical_covering (12): 0 --> 1
-length_of_nuchal (22): 1 --> 2

Node 40 :
All trees:
-gulars_epiplastron (31): 0 --> 1
-gulars_vs_entoplastron (32): 2 --> 1

Node 41 :
All trees:
-vertebrals_vs_the_nuchal (9): 0 --> 1
-epiplastron_length (45): 1 --> 2
-hu_fem_viscerally (51): 0 --> 1

Node 42 :
All trees:
-V1 (5): 0 --> 1
-V1_width (6): 0 --> 1
-medial_length_GU_vs_the_ant_lobe (42): 0 --> 1
-position_of_hu_pec (49): 1 --> 3

Node 43 :
All trees:
-GU-HU_vs_HU (30): 1 --> 0
Some trees:
-pleurals_vs_peripherals (16): 0 --> 1

Node 44 :
All trees:
-marginals_vs_peripherals (17): 0 --> 1
-marginals_vs_pleurals (18): 0 --> 1

Node 45 :
All trees:
-V1 (5): 1 --> 2
-contact_V1_and_M2 (7): 0 --> 1
-vertebrals_vs_the_costals (10): 0 --> 2
Some trees:
-V5_vs_PY_SPY (21): 2 --> 0
-FEM_vs_ABD (38): 0 --> 1
-medial_length_hyo (46): 2 --> 1
-position_of_hu_pec (49): 3 --> 2

Node 46 :
All trees:
-cervical_viscerally (13): 0 --> 1
-length_of_nuchal (22): 2 --> 3
-Shape_of_GU-HU (35): 0 --> 1
-shape_of_anterior_border_of_plastron (37): 0 --> 1

Node 47 :
All trees:
-vertebrals_vs_the_nuchal (9): 1 --> 0
Some trees:
-V5_vs_PY_SPY (21): 2 --> 1

Node 48 :
All trees:
-vertebrals_vs_the_costals (10): 0 --> 1
Some trees:
-inguinal_&_axillary_notches (3): 0 --> 1
-GU-HU_vs_HU (30): 1 --> 2
-medial_HU-PEC (39): 0 --> 1
-medial_GU_HUM (40): 0 --> 1
-medial_HUM_vs_entoplastron (41): 0 --> 1
-anal_notch (52): 0 --> 1

Node 49 :
Some trees:
-axillary_process (1): 2 --> 3
-V4/V5 (11): 0 --> 1
-angle_of_gulars (34): 1 --> 2
-epi-hyo_suture (44): 1 --> 2

Node 50 :
All trees:
-contact_V1_and_M2 (7): 0 --> 1
-pleurals_vs_peripherals (16): 0 --> 1
Some trees:
-axillary_process (1): 3 --> 4
-shape_of_SP2 (25): 2 --> 3
-shape_of_pygal (26): 1 --> 2

Node 51 :
All trees:
-V1 (5): 1 --> 2
-V1_width (6): 1 --> 2
-marginals_vs_pleurals (18): 0 --> 1

Iter PCR results on the geoemydid analysis

```
The following reduced consensus is obtained after prunning the most unstable
taxa:

================================================================================
======

Note: for consensus calculation, trees will be

temporarily collapsed (when min. branch length = 0)


Strict consensus of 12 trees

   -ƒƒ Platysternon_megacephalum

   ≥ ⁄ƒ El kemys_aust r al i s

√ƒƒ¥ ≥ /ƒƒ Pal aeoemys_hessi aca

   ┐ƒƒ¥ ≥ ⁄ƒ Pal aeoemys_messel i ana

      ┐ƒƒ¥ ≥ ⁄ƒ Pal aeoemys_kehr er i

         ≥ ≥ ⁄ƒ¡ƒƒ Pal aeoemys_vi dal enci

         ┐ƒƒ¥ ≥ ⁄ƒ Pal aeoemys_t est udi ni f or mi s

            ≥ ≥ ⁄ƒ¡ƒƒ Pal aeoemys_cor r oyi

            ┐ƒƒ¥ ≥ ⁄ƒ Bor keni a_ger mani ca

               ≥ ≥ ⁄ƒ¡ƒƒ Borkenia_oschkinisi

               ┐ƒƒ¥ ≥ ⁄ƒ Pal aeochel ys_cr ocheti

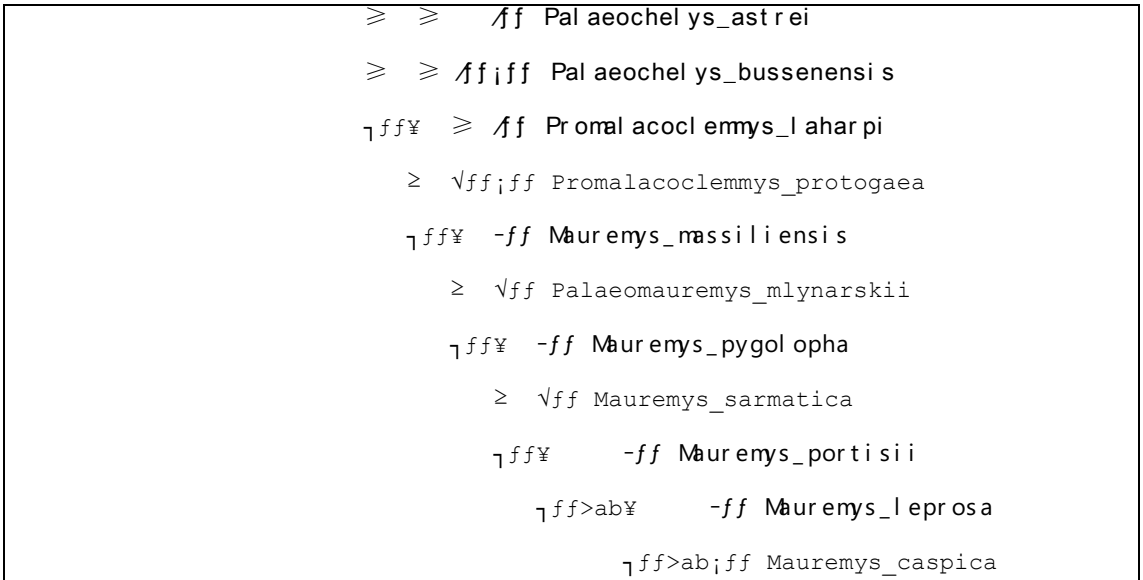
                  ≥ ≥ √ƒƒ Palaeochelys_vallisnerii

                  ┐ƒƒ¥ -ƒƒ¥ -ƒƒ Pal aeochel ys_l aur enti

                     ≥ ≥ ┐ƒƒ¡ƒƒ Palaeochelys_lachati

                     ≥ ≥ ⁄ƒ Cuvi er i chel ys_i ber i ca

                     ┐ƒƒ¥ -ƒƒ¡ƒƒ Cuvi er i chel ys_par i si ensi s
```



Legends:

a: Silata_geoemydid (29)

b: node 51 of consensus

Mauremys_gaudryi

Mauremys_campanii

The following taxa are unstable and collapse nodes in the strict consensus:

Silata_geoemydid

Scoring the following characters may help to resolve its position:

1 2 8 50

Node 51 of the strict consensus

This node includes the following taxa: 26 25

The following characters support alternative positions in different trees:

1 2 3 7 8 12 16 25 26 49 50

==========

EVALUATING CHARACTERS INVOLVED IN ALTERNATIVE POSITIONS OF UNSTABLE TAXA TOOK 3 SECONDS

==========

TNT script of the analysis of *Nostimochelone*

```
xread
175 46

Synapsida_Diapsida 000000[0 1]0000000000[0
1]00000000000000000000000000000000000000000000000000000000000[0
1]00000000000000000000000000000000000000000000000000000000000?????????????????????????????????????
Proganochelys
000000100000000000000000000000000000000000000000000000000000000000000000000000000000000000000000000000000000000000?000000000000000000000000000000000000000000000000000000000000000000000000000000000000000000000000000000000000000000000000????000000100000000000000000?0000
Australochelys
??0?00???00??0??????????000???0?0?0000??0?1???1????0000?000?01010111???00???????1000????0?????
??010??????00?11?1?????????????????????????????????????????????????????????????????????
Palaeochersis
??0?00?0??00?0??0???0??????????0??0??????????1????00000??0?01111111100000???????1000????0??????
?010?0????1??11?10?????0?????0??00000?00000??0??????????0???????000?00???00???000
Kayentachelys
011000011000000000100000000010010000000000011100003000000000111111100001000000011110000001?0100001110001001101102100000001 0?1000000110000?000200011010002001020010101000000?000004
Chelidae 0110000010[0 1]000001010000000010001000[0 1]024000001101003200020101111111100110030[0 1]010112100001[0 1]110000011000100120110210000[0 1]0010011[0 1]1222111111110[1 2 3]2[0 1 2 3 4][1 2][0 1][0 1 3][2 3 4][1 2 3]2[1 2][1 2]0210[0 1]120[1 3]11111?[0 1][0 1]01101[0 1]111
Pelomedusidae 111100[0 1]0100001101010000000010001000[0 1]00300[0 1]012121003200020101111111100110030101011211000111100000110000[0 1]12011021100[0 1][0 1]00100110121211111111[1 2]2[1 2 3]1002[1 2][1 2][0 1]2[0 1]2100120[1 2]11111000011010[0 1]11
Araripemys
11110?00101001101010000000010001000003000??1?10130000201011111111001100300110 11[12]10000101100000110000013?110211000100110111121011111111114202022[0 1]3020211112030111100 0?21?12015
Euraxemys
1111000010001010101000000001000100010030000011010030000101011111111001100410?010111021010110010011100000 11?11?2110001001001111212111111111120?00212?2?2100120211111 00?011011011
Dirqadim
1111000010001000101000000001010100010030000??1?10030000101011111111001100410?110111021010110010011100000 11?11?2??????????????????????????????????????????????????????????????????????????
Podocnemididae 11110000100010101[1 2]0100[0 1]00000100[0 1]10[0 1 2]0[0 1]00300001[1 2]1[0 2]10032000[0 1 2]0111111111101110041001011210001111100200111000011201102 11[0 1]000[0 1]1101211121211111111[1 2]2[1 2 3]1002[2 3]1[1 2][0 1 2][0 1]2100120211111[0 1]11[0 1]11010011
Hamadachelys
1111000010001010?0100000000100 01?000003000011101003200020111111111101110410 41?0101121000111?10020011100001 12?11?2?10000001002??????????????????????????????????????????????????????????
Brasilemys
??1??????0000???101000000001 0????000003??00??1??003000010111111111111011?0041?01?11110301 1??100200??10000112?11?2?1000?0010?2???1?????1?1??12?11002222?121001?????????????????
Cearachelys 11110000100002101011000000011 0?1010001000 00?1101013[0 2]0000011011111111[0 1]011004110111111111011 0?1102[0 1]011101101110110 2?1101010100 01?12?2???111111[1 3]20?0121[1 2]?2?2100120211111000011010014
Galianemys_emringeri 1111[0
1]000100002101012000000111011010001000 00??1?10131101001101111111101100411011111101011011102101110110111011102??????????????????????????????????????????????????????????????????????
Galianemys_whitei
1111000010000210101200000011101 1?10001000000110101311010011011111110011004 1?011111010110111020011101110111011 02??????????????????????????????????????????????????????????????????????
Kurmademys
1111000010000111101000000011001101000130000 1?1?10131101201111111111101100201011112010110?10021011110101120 11?2??10101010001??2??11?111?111231102311212100 12?2?????011111??0?11
Sankuchemys
11110???10??011??010??0?????001??1010??00?011101?????????1111111111001?0?41?0??11?1?10110?1??210??1????112?11?2??????????????????????????????????????????????????????????????
Foxemys
1111100010010010101000010011101102000100010011010131000011101111111201 10041?011111
```

1110110?111210??1101011?11?2?11010110110111?2??11?111111222[1 2]10222121210012?211111111[0 1]11010111
Polysternon
111110?0100?001??010000?00??1011?100010000???1??0131000011111111111201?0041?0?1111111 0110?1??200??1101?112?11?2?????0?????????????1?1??1222[1 2]10222121210112?211111011111010113
Araiochelys
111101101001001??0100011001111220110?100000110?011110001110111111100110011?1?11121 110110?1112001111010111?11?2?1111001011?????????1?????????043212121???2?2?1????10111??0?11
Zolhafah
11111?00100???????10??1???1??01102100??000001101013110?111011111110??0051?0101121?1? 110?11?200??1101?11101102??
Rosasia
111110001001?0?0101000?1??11?021021001100000110101?11?001110111111110???041?01111?1?? 0?1??111200??110??1110110?????????????????????1????1122?10221?2?2101???2?11111000?10?0111
Bothremys_cooki
1111111010111???120100?1???11?12202101??111001101011?????????????????1001?0???101?????????1?? ?????????????????1?11102??11101???1???
Bothremys_maghrebiana 1111111010110011201000110[0 1]1111220[1 2]10[0 1]1111[0 1]00110101111000111011111111001100110011111111211101101111200111101[0 1]21111102?11110[0 1]10110??
Bothremys_kellyi
1111111010?001??0100?11001111120210?1?1100???1??0111100011101111111100??0?51?0?1112111 011??11?2001?11011211?11?2??
Bothremys_arabicus
??1?1??0?01????12??0??1????1??1??210?????0?0110?01?11?00?11011111111001??011???1?12?1101107 11?20???110??211?11?2??
Chedighaii_hutchisoni
1111111010110011201000010011 1?1??200110000011101017110001110111111100110011?0111121 110110?1112001111011211?11?2??
Chedighaii_barberi
11111??0101?????201?0?010?1???2??100???0000??1???1111?0011?0111?11100???011?0?1?121?1011 0?111200??1101121111102??1110110 1?01112????1111111123210221121210112021111111001107?0111
Taphrosphys_sulcatus
1?1100???00?20???01????0111?00?11???????0????1????311100?111111111100???15110?01121110010 1111200111101011 2?1112?????????????1112??1111111111122210222[1 2]21210012021111111107?211?1012
Taphrosphys_congolensis
111100?0100?201??0101?00111200?11000001000???1?1?0?11?00111111111111001?0?51?0?0112111 0110?111200?1110101120110 2??000?0?????????????????????222??22????1?10????2??1?1?1012?1???12
Taphrosphys_ippolitoi
111100?0100??01??0101100 1112?0111000001000 1??1?1?0311100111111111111?0110151?01011211 10110?1??2001111010112?1112??
Azabbaremys
1111000010000010101001000012110100000010001111111021100011101111111100??0011?010112 1110110?1112001111010211011 02???
Labrostochelys 1111011010 0?201?10101?0111??012200000001200101101001111001110111111100110 0[16]0?1101121110110?111200?1110102 11?1?2??
Phosphatochelys
1111000011002011111001001112001210001023000??1?1103111001110111111100110111?010112 1110110?1112001111010[1 2]12?11?2??
Ummulisani 1111010?110020?0?1100100111200121000102300 0??????02111001111111111001?01[16][0 1]?[0 1]10012111011 0?1112001111 0?0112?1??2??211111110021 1?1?12
Rhothonemys
111100?0?00??01??1100???1?12?1?2?0001??300???1????311100????1111111????0????0?01121??????? 11???0?????1??1??11????0000010?10??
Nigeremys
1?1100???000001??010??0????1?01100000??000?0110?1?2110001112111111201?00???1??1121??0? 1??1??200??110?0214?11?2???0??
Arenila
??110????00?????10100?0???11?0???0000??000001101?0211?0??1121111111201???41?11??12111?11 0?111200??1?010214?11???
Proterochersis
???

Platychelys
????????????????????1?????????????????????

{41 Maxilla,_ventral_rim_of_orbit;
{42 Maxilla,_exposure_in_orbital_floor;
{43 Vomer,_maxilla-vomer_contact;
{44 Vomer;
{45 Vomer,_vomerine_teeth;
{46 Vomer,_central_bar;
{47 Palatine,_foramen_palatinum_pterius;
{48 Palatine,_dorsally_arched_palate
{49 Palatine,_palatine_contribution_to_triturating_surface;
{50 Quadrate,_antrum_postoticum;
{51 Quadrate,_incisura_columellae_auris;
{52 Quadrate,_stapes_contained_in_bony_canal;
{53 Quadrate,_trough_on_incisura_columellae_auris_ridge;
{54 Quadrate,_trough_on_incisura_columellae_auris_ridge;
{55 Quadrate,_fossa_precolumellaris;
{56 Quadrate,_shelf_below_cavum_tympani;
{57 Quadrate,_medial_process_contacting_braincase_elements_and_underlying_cranioquadrate_space;
{58 Quadrate,_quadrate-basioccipital_contact;
{59 Quadrate,_condylus_mandibularis_position;
{60 Quadrate,_fully_formed_cavum_tympani;
{61 Quadrate,_cavum_tympani_with_acute_posterior_edge;
{62 Quadrate,_middle_ear_with_complete_lateral_wall;
{63 Quadrate,_cavum_tympani_curved_dorsally;
{64 Quadrate,_covers_opisthotic_laterally;
{65 Quadrate,_pocket_for_stapes_articulation;
{66 Quadrate,_cranioquadrate_space;
{67 Pterygoid,_fossa_pterygoidea;
{68 Pterygoid,_cavum_pterygoidei;
{69 Pterygoid,_processus_trochlearis_pterygoidei;
{70 Pterygoid,_posteroventral_flange_along_lateral_edge,_medial_to_processus_trochlearis_pterygoidei;
{71 Pterygoid,_processus_pterygoideus_externus;
{72 Pterygoid,_trigeminal_ridge;
{73 Pterygoid,_position_of_the_foramen_posterius_canalis_carotici_interni;
{74 Pterygoid,_posterior_margin_of_pterygoid_forms_part_of_foramen_posterius_canalis_carotici_interni;
{75 Pterygoid,_foramen_caroticum_laterale;
{76 Pterygoid,_midline_contact;
{77 Epipterygoid,_absent;
{78 Supraoccipital,_supraoccipital-quadrate_contact;
{79 Supraoccipital,_crista_supraoccipitalis;
{80 Supraoccipital,_wide_occipital_plate;
{81 Exoccipital,_foramen_jugulare_posterius;
{82 Exoccipital,_recessus_scalae_tympani;
{83 Exoccipital,_condylus_occipitalis;
{84 Exoccipital,_exoccipital-quadrate_contact;
{85 Exoccipital,_ventral_process;
{86 Basioccipital,_basioccipital_short;
{87 Basioccipital,_basioccipital_thick;
{88 Basioccipital,_basioccipital-opisthotic_contact;
{89 Prootic,_hyomandibular_branch_of_facial_nerve_lies_in_its_own_canal;
{90 Prootic,_foramen_stapedio-temporale;
{91 Prootic,_foramen_stapedio-temporale_opens_anteriorly;
{92 Prootic,_foramen_stapedio-temporale_and_foramen_nervi_trigemini;
{93 Prootic,_ventral_exposure;
{94 Prootic,_quadrate-pterygoid-basisphenoid_exposure;
{95 Prootic,_processus_trochlearis_oticum;
{96 Prootic,_plane_of_fenestra_ovalis;
{97 Opisthotic,_processus_interfenestralis_expanded_ventrally;
{98 Opisthotic,_processus_interfenestralis_covered_in_ventral_view;
{99 Opisthotic,_fenestra_postotica_closed_medially;
{100 Opisthotic,_fenestra_postotica_short_horizontal_slit;
{101 Opisthotic,_processus_paroccipitalis;
{102 Opisthotic,_thin_horizontal_flange
{103 Basisphenoid,_basisphenoid-quadrate_contact;
{104 Basisphenoid,_interpterygoid_vacuity;

{105 Basisphenoid,_ventral_outline;
{106 Basisphenoid,_processus_clinoideus;
{107 Basisphenoid,_skull_akinetic;
{108 Basisphenoid,_cultriform_process;
{109 Basisphenoid,_sella_turcica/dorsum_sellae;
{110 Basisphenoid,_ventral_tubercle;
{111 Columella_auris,_footplate;
{112 Splenial:
{113 Dentary,_high_lingual_ridge;
{114 Dentary,_dentary_pits;
{115 Dentary,_U-shaped_lingual_ridges_on_symphysis;
{116 Dentary,_symphysis;
{117 Dentary,_triturating_surfaces;
{118 Dentary,_widely_exposed_on_lateral_surface;
{119 Surangular,_foramen_nervi_auriculotemporalis;
{120 Coronoid,_wide_lateral_exposure;
{121 Prearticular,_fossa_meckelii_open_anteriorly;
{122 Articular,_processus_retroarticularis;
{123 Vertebrae,_cervical_ribs;
{124 Vertebrae,_cervical_postzygapophyses_fused;
{125 Vertebrae,_cervical_postzygapophyses_elevated;
{126 Vertebrae,_cervical_centra;
{127 Vertebrae,_cervical_articulation_pattern;
{128 Vertebrae,_caudal_articulation_pattern;
{129 Shoulder_girdle,_coracoid_foramen;
{130 Shoulder_girdle,_coracoid_shape;
{131 Pelvic_girdle,_tenth_thoracic_centrum;
{132 Pelvic_girdle,_pelvis_sutured_to_shell;
{133 Pelvic_girdle,_dorsal_part_of_ilium_columnar;
{134 Pelvic_girdle,_pelvis_narrow;
{135 Pelvic_girdle,_thyroid_fenestra;
{136 Humerus,_shoulder_on_lateral_side_of_head;
{137 Carapace,_cervical_scale;
{138 Carapace,_nuchal_bone_width;
{139 Carapace,_pygal_notch;
{140 Carapace,_neural_series_completeness;
{141 Carapace,_iliac_scar_position;
{142 Carapace,_first_costal_length;
{143 Carapace,_position_of_four-sided_neural;
{144 Carapace,_neural_series_pattern;
{145 Carapace,_neural_number;
{146 Carapace,_length_of_contact_between_peripheral_1_and_costal_1_in_dorsal_view;
{147 Carapace,_axillary_process_contacts_first_costal;
{148 Carapace,_axillary_process_extent_on_ventral_surface_of_peripherals;
{149 Carapace,_inguinal_buttress;
{150 Carapace,_supramarginal_scales;
{151 Carapace,_vertebral_scale_width;
{152 Carapace,_vertebral_scale_1_reaches_anterior_margin_of_shell;
{153 Carapace,_nuchal_embayment;
{154 Carapace,_first_thoracic_rib;
{155 Carapace,_costovertebral_tunnel;
{156 Carapace,_articulation_facet_on_thoracic_rib_1;
{157 Plastron,_mesoplastra;
{158 Plastron,_trapezoidal_entoplastron;
{159 Plastron,_epiplastra_meet_on_midline;
{160 Plastron,_dorsal_epiplastral_process;
{161 Plastron,_intergular_scales;
{162 Plastron,_gular_projections;
{163 Plastron,_anterior_lobe_of_plastron_short,_wide_at_base,_and_semicircular_in_outline;
{164 Plastron,_pectoral_scales_on_entoplastron;
{165 Plastron,_pectoral_scales_on_epiplastron;
{166 Plastron,_pectoral-abdominal_scale_sulcus_crosses_mesoplastron;
{167 Plastron,_size_and_shape_of_ischial_suture;
{168 Plastron,_posterior_lobe_wider_than_pelvis;

{169 Plastron,_intergular_scale;
{170 Plastron,_axillary/inguinal_scales;
{171 Plastron,_abdominal_scale_narrow;
{172 Plastron,_anterior_lobe_reaches_carapace_edge;
{173 Plastron,_anal_notch;
{174 Shell,_surface_texture;
;

proc /;
comments 0
;

SEM results of the thin sections of the Gefira trionychid

Sample 1

3a

1

Element	Line	App. Conc	k ratio	Intensity corrn.			Weight%	Weight% sigma	Atomic%	Compound%	Formula	Number of ions	Standard
P	K_SERIES	13.55	0.08023	1.3290	18.83	0.66	14.63	43.14	P2O5	7.68	GaP	1-Jun-1999 12:00 AM	
Ca	K_SERIES	22.04	0.19799	1.0016	40.64	0.77	24.40	56.86	CaO	12.81	Wollastonite	1-Jun-1999 12:00 AM	
O				40.53	0.79	60.97			32.00				
Totals				100.00									
								Cation sum		20.48			

Processing option : Oxygen by stoichiometry (Normalised)
Number of iterations : 2
Sample is polished.
Sample is coated with Carbon - thickness (nm): 15.0, density (g/cm3): 2.25
Detector efficiency : Calculation

2

Element	Line	App. Conc	k ratio	Intensity corrn.			Weight%	Weight% sigma	Atomic%	Compound%	Formula	Number of ions	Standard
Si	K_SERIES	0.56	0.0045	0.8883	1.99	0.35	1.73	4.25	SiO2	0.93	SiO2	1-Jun-1999 12:00 AM	
P	K_SERIES	4.68	0.0277	1.2984	11.41	0.75	9.00	26.13	P2O5	4.84	GaP	1-Jun-1999 12:00 AM	
S	K_SERIES	1.06	0.00928	0.8726	3.83	0.50	2.92	9.57	SO3	1.57	FeS2	1-Jun-1999 12:00 AM	
K	K_SERIES	2.19	0.01794	1.1008	6.29	0.58	3.93	7.57	K2O	2.11	MAD-10 Feldspar	1-Jun-1999 12:00 AM	
Ca	K_SERIES	11.51	0.10335	0.9716	37.50	1.05	22.87	52.47	CaO	12.29	Wollastonite	1-Jun-1999 12:00 AM	
O				38.99	1.11	59.55			32.00				
Totals				100.00									
								Cation sum		21.73			

Processing option : Oxygen by stoichiometry (Normalised)
Number of iterations : 2
Sample is polished.
Sample is coated with Carbon - thickness (nm): 15.0, density (g/cm3): 2.25
Detector efficiency : Calculation

3

Element	Line	App. Conc	k ratio	Intensity corrn.			Weight%	Weight% sigma	Atomic%	Compound%	Formula	Number of ions	Standard
P	K_SERIES	12.10	0.07164	1.3275	17.96	0.68	14.05	41.16	P2O5	7.43	GaP	1-Jun-1999 12:00 AM	
Ca	K_SERIES	21.44	0.19259	1.0050	42.05	0.80	25.41	58.84	CaO	13.43	Wollastonite	1-Jun-1999 12:00 AM	
O				39.98	0.82	60.54			32.00				
Totals				100.00									
								Cation sum		20.86			

Processing option : Oxygen by stoichiometry (Normalised)
Number of iterations : 2
Sample is polished.
Sample is coated with Carbon - thickness (nm): 15.0, density (g/cm3): 2.25
Detector efficiency : Calculation

4

Element	Line	App. Conc	k ratio	Intensity corrn.			Weight%	Weight% sigma	Atomic%	Compound%	Formula	Number of ions	Standard
Si	K_SERIES	45.15	0.36412	0.9552	44.89	0.52	32.18	96.03	SiO2	15.47	SiO2	1-Jun-1999 12:00 AM	
P	K_SERIES	0.82	0.00487	0.7990	0.98	0.23	0.64	2.24	P2O5	0.31	GaP	1-Jun-1999 12:00 AM	
Ca	K_SERIES	1.19	0.01066	0.9121	1.24	0.16	0.62	1.73	CaO	0.30	Wollastonite	1-Jun-1999 12:00 AM	
O				52.90	0.52	66.57			32.00				
Totals				100.00									
								Cation sum		16.07			

Processing option : Oxygen by stoichiometry (Normalised)
Number of iterations : 2
Sample is polished.
Sample is coated with Carbon - thickness (nm): 15.0, density (g/cm3): 2.25
Detector efficiency : Calculation

5

Element	Line	App. Conc	k ratio	Intensity corrn.			Weight%	Weight% sigma	Atomic%	Compound%	Formula	Number of ions	Standard
P	K_SERIES	12.25	0.07256	1.3284	18.47	0.69	14.39	42.32	P2O5	7.57	GaP	1-Jun-1999 12:00 AM	
Ca	K_SERIES	20.65	0.18545	1.0030	41.22	0.81	24.82	57.68	CaO	13.06	Wollastonite	1-Jun-1999 12:00 AM	
O				40.31	0.83	60.79			32.00				
Totals				100.00									
								Cation sum		20.64			

Processing option : Oxygen by stoichiometry (Normalised)
Number of iterations : 2
Sample is polished.
Sample is coated with Carbon - thickness (nm): 15.0, density (g/cm3): 2.25
Detector efficiency : Calculation

4a

1

Element	Line	App. Conc	k ratio	Intensity	corrn.		Weight%	Weight% sigma	Atomic%	Compound%	Formula	Number of ions	Standard
P	K_SERIES	13.13	0.07773	1.3282	18.35	0.65	14.31	42.05	P2O5	7.54	GaP	1-Jun-1999 12:00 AM	
Ca	K_SERIES	22.38	0.20104	1.0035	41.42	0.77	24.96	57.95	CaO	13.15	Wollastonite	1-Jun-1999 12:00 AM	
O				40.23	0.78	60.73			32.00				
Totals				100.00									
								Cation sum		20.69			

Processing option : Oxygen by stoichiometry (Normalised)
Number of iterations : 2
Sample is polished.
Sample is coated with Carbon - thickness (nm): 15.0, density (g/cm3): 2.25
Detector efficiency : Calculation

2

Element	Line	App. Conc	k ratio	Intensity	corrn.		Weight%	Weight% sigma	Atomic%	Compound%	Formula	Number of ions	Standard
Si	K_SERIES	0.55	0.00445	0.8871	1.57	0.35	1.35	3.36	SiO2	0.72	SiO2	1-Jun-1999 12:00 AM	
P	K_SERIES	8.43	0.04991	1.2999	16.34	0.75	12.79	37.45	P2O5	6.79	GaP	1-Jun-1999 12:00 AM	
Ca	K_SERIES	16.88	0.1516	1.0058	42.30	0.92	25.58	59.19	CaO	13.58	Wollastonite	1-Jun-1999 12:00 AM	
O				39.78	0.95	60.27			32.00				
Totals				100.00									
								Cation sum		21.09			

Processing option : Oxygen by stoichiometry (Normalised)
Number of iterations : 2
Sample is polished.
Sample is coated with Carbon - thickness (nm): 15.0, density (g/cm3): 2.25
Detector efficiency : Calculation

3

Element	Line	App. Conc	k ratio	Intensity	corrn.		Weight%	Weight% sigma	Atomic%	Compound%	Formula	Number of ions	Standard
P	K_SERIES	12.44	0.07364	1.3280	17.56	0.65	13.79	40.24	P2O5	7.33	GaP	1-Jun-1999 12:00 AM	
K	K_SERIES	0.61	0.00502	1.1135	1.03	0.27	0.64	1.24	K2O	0.34	MAD-10 Feldspar	1-Jun-1999 12:00 AM	
Ca	K_SERIES	22.33	0.20054	1.0011	41.82	0.79	25.38	58.52	CaO	13.50	Wollastonite	1-Jun-1999 12:00 AM	
O				39.58	0.80	60.18			32.00				
Totals				100.00									
								Cation sum		21.17			

Processing option : Oxygen by stoichiometry (Normalised)
Number of iterations : 2
Sample is polished.
Sample is coated with Carbon - thickness (nm): 15.0, density (g/cm3): 2.25
Detector efficiency : Calculation

5a

1

Element	Line	App. Conc	k ratio	Intensity	corrn.		Weight%	Weight% sigma	Atomic%	Compound%	Formula	Number of ions	Standard
P	K_SERIES	11.99	0.071	1.3257	16.92	0.64	13.34	38.76	P2O5	7.11	GaP	1-Jun-1999 12:00 AM	
Ca	K_SERIES	23.61	0.21208	1.0091	43.77	0.78	26.66	61.24	CaO	14.22	Wollastonite	1-Jun-1999 12:00 AM	
O				39.32	0.79	60.00			32.00				
Totals				100.00									
								Cation sum		21.33			

Processing option : Oxygen by stoichiometry (Normalised)
Number of iterations : 2
Sample is polished.
Sample is coated with Carbon - thickness (nm): 15.0, density (g/cm3): 2.25
Detector efficiency : Calculation

2

Element	Line	App. Conc	k ratio	Intensity	corrn.		Weight%	Weight% sigma	Atomic%	Compound%	Formula	Number of ions	Standard
P	K_SERIES	11.21	0.0664	1.3256	16.82	0.68	13.27	38.53	P2O5	7.08	GaP	1-Jun-1999 12:00 AM	
Ca	K_SERIES	22.31	0.20042	1.0095	43.93	0.82	26.78	61.47	CaO	14.30	Wollastonite	1-Jun-1999 12:00 AM	
O				39.25	0.83	59.95			32.00				
Totals				100.00									
								Cation sum		21.38			

Processing option : Oxygen by stoichiometry (Normalised)
Number of iterations : 2
Sample is polished.
Sample is coated with Carbon - thickness (nm): 15.0, density (g/cm3): 2.25
Detector efficiency : Calculation

3

Element	Line	App. Conc	k ratio	Intensity	corrn.		Weight%	Weight% sigma	Atomic%	Compound%	Formula	Number of ions	Standard
P	K_SERIES	13.44	0.07956	1.3286	18.13	0.63	14.17	41.55	P2O5	7.49	GaP	1-Jun-1999 12:00 AM	
K	K_SERIES	0.44	0.00359	1.1089	0.71	0.24	0.44	0.85	K2O	0.23	MAD-10 Feldspar	1-Jun-1999 12:00 AM	
Ca	K_SERIES	22.97	0.20633	1.0006	41.17	0.77	24.87	57.60	CaO	13.15	Wollastonite	1-Jun-1999 12:00 AM	
O				39.99	0.78	60.52			32.00				
Totals				100.00									
								Cation sum		20.87			

Processing option : Oxygen by stoichiometry (Normalised)
Number of iterations : 2
Sample is polished.
Sample is coated with Carbon - thickness (nm): 15.0, density (g/cm3): 2.25
Detector efficiency : Calculation

8a

1

Element	Line	App. Conc	k ratio	Intensity	corrn.		Weight%	Weight% sigma	Atomic%	Compound%	Formula	Number of ions	Standard
Si	K_SERIES	0.88	0.00706	0.8932	1.76	0.30	1.50	3.77	SiO2	0.78	SiO2	1-Jun-1999 12:00 AM	
P	K_SERIES	13.11	0.07762	1.3008	18.14	0.66	13.96	41.57	P2O5	7.26	GaP	1-Jun-1999 12:00 AM	
S	K_SERIES	0.13	0.00113	0.8144	0.28	0.23	0.21	0.71	SO3	0.11	FeS2	1-Jun-1999 12:00 AM	
Cl	K_SERIES	0.09	0.00095	0.7581	0.22	0.23	0.15	0.00		0.08	KCl	1-Jun-1999 12:00 AM	
Ca	K_SERIES	21.23	0.19073	0.9958	38.40	0.78	22.83	53.72	CaO	11.88	Wollastonite	1-Jun-1999 12:00 AM	
O				41.19	0.83	61.35			31.92				
Totals				100.00									
								Cation sum		20.03			

Processing option : Oxygen by stoichiometry (Normalised)
Number of iterations : 2
Sample is polished.
Sample is coated with Carbon - thickness (nm): 15.0, density (g/cm3): 2.25
Detector efficiency : Calculation

2

Element	Line	App. Conc	k ratio	Intensity corrn.			Weight%	Weight% sigma	Atomic%	Compound%	Formula	Number of ions	Standard
P	K_SERIES	8.45	0.05003	1.3304	18.54	0.85	14.45	42.48	P2O5	7.57	GaP	1-Jun-1999 12:00 AM	
Cl	K_SERIES	0.17	0.00169	0.7683	0.64	0.34	0.43	0.00		0.23	KCl	1-Jun-1999 12:00 AM	
Ca	K_SERIES	13.93	0.12512	1.0004	40.65	1.00	24.49	56.88	CaO	12.84	Wollastonite	1-Jun-1999 12:00 AM	
O				40.17	1.03	60.62			31.77				
Totals				100.00									
									Cation sum	20.41			

Processing option : Oxygen by stoichiometry (Normalised)
Number of iterations : 2
Sample is polished.
Sample is coated with Carbon - thickness (nm): 15.0, density (g/cm3): 2.25
Detector efficiency : Calculation

3

Element	Line	App. Conc	k ratio	Intensity corrn.			Weight%	Weight% sigma	Atomic%	Compound%	Formula	Number of ions	Standard
P	K_SERIES	11.03	0.06532	1.3290	18.21	0.71	14.22	41.72	P2O5	7.49	GaP	1-Jun-1999 12:00 AM	
Cl	K_SERIES	0.12	0.00121	0.7704	0.34	0.28	0.23	0.00		0.12	KCl	1-Jun-1999 12:00 AM	
Ca	K_SERIES	18.93	0.17004	1.0028	41.41	0.85	24.99	57.94	CaO	13.16	Wollastonite	1-Jun-1999 12:00 AM	
O				40.04	0.86	60.55			31.88				
Totals				100.00									
									Cation sum	20.65			

Processing option : Oxygen by stoichiometry (Normalised)
Number of iterations : 2
Sample is polished.
Sample is coated with Carbon - thickness (nm): 15.0, density (g/cm3): 2.25
Detector efficiency : Calculation

4

Element	Line	App. Conc	k ratio	Intensity corrn.			Weight%	Weight% sigma	Atomic%	Compound%	Formula	Number of ions	Standard
P	K_SERIES	11.69	0.06921	1.3273	17.82	0.70	13.95	40.84	P2O5	7.39	GaP	1-Jun-1999 12:00 AM	
Ca	K_SERIES	21.00	0.18865	1.0056	42.28	0.82	25.58	59.16	CaO	13.54	Wollastonite	1-Jun-1999 12:00 AM	
O				39.89	0.84	60.47			32.00				
Totals				100.00									
									Cation sum	20.92			

Processing option : Oxygen by stoichiometry (Normalised)
Number of iterations : 2
Sample is polished.
Sample is coated with Carbon - thickness (nm): 15.0, density (g/cm3): 2.25
Detector efficiency : Calculation

5

Element	Line	App. Conc	k ratio	Intensity corrn.			Weight%	Weight% sigma	Atomic%	Compound%	Formula	Number of ions	Standard
P	K_SERIES	11.81	0.06994	1.3287	18.65	0.70	14.51	42.72	P2O5	7.63	GaP	1-Jun-1999 12:00 AM	
Ca	K_SERIES	19.56	0.17571	1.0023	40.94	0.82	24.61	57.28	CaO	12.94	Wollastonite	1-Jun-1999 12:00 AM	
O				40.42	0.84	60.88			32.00				
Totals				100.00									
									Cation sum	20.56			

Processing option : Oxygen by stoichiometry (Normalised)
Number of iterations : 2
Sample is polished.
Sample is coated with Carbon - thickness (nm): 15.0, density (g/cm3): 2.25
Detector efficiency : Calculation

6

Element	Line	App. Conc	k ratio	Intensity corrn.			Weight%	Weight% sigma	Atomic%	Compound%	Formula	Number of ions	Standard
P	K_SERIES	12.86	0.07617	1.3282	18.39	0.67	14.34	42.14	P2O5	7.55	GaP	1-Jun-1999 12:00 AM	
Ca	K_SERIES	21.85	0.19623	1.0033	41.35	0.78	24.91	57.86	CaO	13.12	Wollastonite	1-Jun-1999 12:00 AM	
O				40.26	0.80	60.75			32.00				
Totals				100.00									
									Cation sum	20.67			

Processing option : Oxygen by stoichiometry (Normalised)
Number of iterations : 2
Sample is polished.
Sample is coated with Carbon - thickness (nm): 15.0, density (g/cm3): 2.25
Detector efficiency : Calculation

7

Element	Line	App. Conc	k ratio	Intensity corrn.			Weight%	Weight% sigma	Atomic%	Compound%	Formula	Number of ions	Standard
P	K_SERIES	9.68	0.05731	1.3245	16.20	0.70	12.84	37.12	P2O5	6.89	GaP	1-Jun-1999 12:00 AM	
Ca	K_SERIES	20.51	0.18426	1.0120	44.94	0.85	27.53	62.88	CaO	14.77	Wollastonite	1-Jun-1999 12:00 AM	
O				38.86	0.86	59.63			32.00				
Totals				100.00									
									Cation sum	21.66			

Processing option : Oxygen by stoichiometry (Normalised)
Number of iterations : 2
Sample is polished.
Sample is coated with Carbon - thickness (nm): 15.0, density (g/cm3): 2.25
Detector efficiency : Calculation

8

Element	Line	App. Conc	k ratio	Intensity corrn.			Weight%	Weight% sigma	Atomic%	Compound%	Formula	Number of ions	Standard
Si	K_SERIES	0.76	0.00616	0.8892	2.00	0.36	1.72	4.28	SiO2	0.90	SiO2	1-Jun-1999 12:00 AM	
P	K_SERIES	9.33	0.05524	1.2939	16.80	0.74	13.06	38.50	P2O5	6.89	GaP	1-Jun-1999 12:00 AM	
Ca	K_SERIES	17.59	0.15801	1.0024	40.90	0.89	24.57	57.22	CaO	12.96	Wollastonite	1-Jun-1999 12:00 AM	
O				40.30	0.92	60.65			32.00				
Totals				100.00									
									Cation sum	20.76			

Processing option : Oxygen by stoichiometry (Normalised)
Number of iterations : 2
Sample is polished.
Sample is coated with Carbon - thickness (nm): 15.0, density (g/cm3): 2.25
Detector efficiency : Calculation

9a

1

Element	Line	App.	Conc	k ratio	Intensity	corrn.	Weight%	Weight% sigma	Atomic%	Compound%	Formula	Number of ions	Standard
Mg	K_SERIES		0.34	0.00231	0.4764	2.14	0.64	2.54	3.55	MgO	1.45	MgO	1-Jun-1999 12:00 AM
Al	K_SERIES		0.53	0.0039	0.5811	2.76	0.59	2.95	5.21	Al2O3	1.68	Al2O3	1-Jun-1999 12:00 AM
Si	K_SERIES		2.55	0.02057	0.6847	11.27	0.82	11.58	24.10	SiO2	6.60	SiO2	1-Jun-1999 12:00 AM
K	K_SERIES		0.80	0.00653	1.0850	2.22	0.40	1.64	2.67	K2O	0.93	MAD-10 Feldspar	1-Jun-1999 12:00 AM
Ca	K_SERIES		0.95	0.00855	1.0491	2.75	0.47	1.98	3.84	CaO	1.13	Wollastonite	1-Jun-1999 12:00 AM
Mn	K_SERIES		9.28	0.09278	0.8758	32.05	1.37	16.83	41.38	MnO	9.60	Mn	1-Jun-1999 12:00 AM
Fe	K_SERIES		2.97	0.02968	0.8964	10.01	1.05	5.17	12.88	FeO	2.95	Fe	1-Jun-1999 12:00 AM
Ba	L_SERIES		1.68	0.0157	0.8942	5.69	1.11	1.20	6.35	BaO	0.68	BaF2	1-Jun-1999 12:00 AM
O					31.11	1.41	56.12			32.00			
Totals					100.00								
									Cation sum		25.02		

Processing option : Oxygen by stoichiometry (Normalised)
Number of iterations : 2
Sample is polished.
Sample is coated with Carbon - thickness (nm): 15.0, density (g/cm3): 2.25
Detector efficiency : Calculation

2

Element	Line	App.	Conc	k ratio	Intensity	corrn.	Weight%	Weight% sigma	Atomic%	Compound%	Formula	Number of ions	Standard
P	K_SERIES		12.64	0.07485	1.3266	17.41	0.63	13.67	39.90	P2O5	7.26	GaP	1-Jun-1999 12:00 AM
Ca	K_SERIES		23.68	0.21268	1.0072	42.96	0.76	26.07	60.10	CaO	13.85	Wollastonite	1-Jun-1999 12:00 AM
O					39.63	0.77	60.26			32.00			
Totals					100.00								
									Cation sum		21.11		

Processing option : Oxygen by stoichiometry (Normalised)
Number of iterations : 2
Sample is polished.
Sample is coated with Carbon - thickness (nm): 15.0, density (g/cm3): 2.25
Detector efficiency : Calculation

3

Element	Line	App.	Conc	k ratio	Intensity	corrn.	Weight%	Weight% sigma	Atomic%	Compound%	Formula	Number of ions	Standard
Al	K_SERIES		0.42	0.00311	0.5286	3.49	0.82	3.96	6.59	Al2O3	2.32	Al2O3	1-Jun-1999 12:00 AM
Si	K_SERIES		0.96	0.00771	0.6324	6.60	0.88	7.21	14.12	SiO2	4.22	SiO2	1-Jun-1999 12:00 AM
Ca	K_SERIES		0.56	0.00501	1.0691	2.28	0.54	1.74	3.19	CaO	1.02	Wollastonite	1-Jun-1999 12:00 AM
Fe	K_SERIES		12.43	0.12425	0.9169	59.16	1.69	32.49	76.10	FeO	19.04	Fe	1-Jun-1999 12:00 AM
O					28.48	1.55	54.60			32.00			
Totals					100.00								
									Cation sum		26.61		

Processing option : Oxygen by stoichiometry (Normalised)
Number of iterations : 2
Sample is polished.
Sample is coated with Carbon - thickness (nm): 15.0, density (g/cm3): 2.25
Detector efficiency : Calculation

4

Element	Line	App.	Conc	k ratio	Intensity	corrn.	Weight%	Weight% sigma	Atomic%	Compound%	Formula	Number of ions	Standard
Mg	K_SERIES		0.21	0.00146	0.4051	1.65	0.53	2.23	2.74	MgO	1.36	MgO	1-Jun-1999 12:00 AM
Si	K_SERIES		0.56	0.00454	0.6535	2.71	0.53	3.17	5.80	SiO2	1.94	SiO2	1-Jun-1999 12:00 AM
Ca	K_SERIES		0.77	0.00688	1.1210	2.15	0.44	1.76	3.01	CaO	1.08	Wollastonite	1-Jun-1999 12:00 AM
Ti	K_SERIES		0.66	0.00659	1.0007	2.08	0.55	1.42	3.46	TiO2	0.87	Ti	1-Jun-1999 12:00 AM
Mn	K_SERIES		12.06	0.12057	0.9154	41.49	1.47	24.78	53.57	MnO	15.16	Mn	1-Jun-1999 12:00 AM
Fe	K_SERIES		7.26	0.0726	0.9361	24.43	1.35	14.35	31.42	FeO	8.78	Fe	1-Jun-1999 12:00 AM
O					25.50	1.35	52.29			32.00			
Totals					100.00								
									Cation sum		29.19		

Processing option : Oxygen by stoichiometry (Normalised)
Number of iterations : 2
Sample is polished.
Sample is coated with Carbon - thickness (nm): 15.0, density (g/cm3): 2.25
Detector efficiency : Calculation

10a

1

Element	Line	App.	Conc	k ratio	Intensity	corrn.	Weight%	Weight% sigma	Atomic%	Compound%	Formula	Number of ions	Standard
Al	K_SERIES		0.46	0.00341	0.5275	2.51	0.58	2.89	4.75	Al2O3	1.71	Al2O3	1-Jun-1999 12:00 AM
Si	K_SERIES		1.49	0.01205	0.6391	6.69	0.65	7.38	14.30	SiO2	4.36	SiO2	1-Jun-1999 12:00 AM
K	K_SERIES		0.42	0.00345	1.0929	1.10	0.34	0.87	1.32	K2O	0.51	MAD-10 Feldspar	1-Jun-1999 12:00 AM
Ca	K_SERIES		0.59	0.00526	1.0670	1.57	0.38	1.22	2.20	CaO	0.72	Wollastonite	1-Jun-1999 12:00 AM
Mn	K_SERIES		1.10	0.01097	0.8990	3.49	0.64	1.97	4.51	MnO	1.16	Mn	1-Jun-1999 12:00 AM
Fe	K_SERIES		18.22	0.18216	0.9192	56.68	1.40	31.48	72.92	FeO	18.58	Fe	1-Jun-1999 12:00 AM
O					27.96	1.26	54.20			32.00			
Totals					100.00								
									Cation sum		27.05		

Processing option : Oxygen by stoichiometry (Normalised)
Number of iterations : 2
Sample is polished.
Sample is coated with Carbon - thickness (nm): 15.0, density (g/cm3): 2.25
Detector efficiency : Calculation

2

Element	Line	App. Conc	k ratio	Intensity	corrn.		Weight%	Weight% sigma	Atomic%	Compound%	Formula	Number of ions	Standard
Mg	K_SERIES	0.45	0.00311	0.4546	3.03	0.74	3.80	5.02	2.23	MgO	MgO	1-Jun-1999 12:00 AM	
Al	K_SERIES	0.61	0.00451	0.5532	3.36	0.61	3.80	6.35	2.23	Al2O3	Al2O3	1-Jun-1999 12:00 AM	
Si	K_SERIES	1.05	0.00846	0.6567	4.85	0.65	5.27	10.38	3.10	SiO2	SiO2	1-Jun-1999 12:00 AM	
P	K_SERIES	0.20	0.00119	1.0128	0.60	0.49	0.59	1.38	0.35	P2O5	GaP	1-Jun-1999 12:00 AM	
S	K_SERIES	0.13	0.00114	0.8211	0.48	0.42	0.46	1.20	0.27	SO3	FeS2	1-Jun-1999 12:00 AM	
Cl	K_SERIES	0.13	0.00133	0.7708	0.52	0.39	0.45	0.00	0.26	KCl	KCl	1-Jun-1999 12:00 AM	
K	K_SERIES	0.47	0.00383	1.1056	1.28	0.39	1.00	1.54	0.59	K2O	MAD-10 Feldspar	1-Jun-1999 12:00 AM	
Ca	K_SERIES	1.07	0.00959	1.0754	3.02	0.45	2.29	4.22	1.35	CaO	Wollastonite	1-Jun-1999 12:00 AM	
Mn	K_SERIES	11.68	0.11683	0.8897	39.88	1.55	22.14	51.49	13.01	MnO	Mn	1-Jun-1999 12:00 AM	
Fe	K_SERIES	2.73	0.02729	0.9106	9.10	1.11	4.97	11.71	2.92	FeO	Fe	1-Jun-1999 12:00 AM	
Ba	L_SERIES	1.68	0.01564	0.9176	5.54	1.18	1.23	6.19	0.72	BaO	BaF2	1-Jun-1999 12:00 AM	
O				28.34	1.53	54.01			31.74				
Totals				100.00									
								Cation sum	26.76				

Processing option : Oxygen by stoichiometry (Normalised)
Number of iterations : 2
Sample is polished.
Sample is coated with Carbon - thickness (nm): 15.0, density (g/cm3): 2.25
Detector efficiency : Calculation

3

Element	Line	App. Conc	k ratio	Intensity	corrn.		Weight%	Weight% sigma	Atomic%	Compound%	Formula	Number of ions	Standard
Al	K_SERIES	0.38	0.00279	0.5717	2.95	0.76	3.13	5.57	1.74	Al2O3	Al2O3	1-Jun-1999 12:00 AM	
Si	K_SERIES	1.26	0.01013	0.6759	8.28	0.91	8.46	17.71	4.69	SiO2	SiO2	1-Jun-1999 12:00 AM	
P	K_SERIES	0.59	0.00352	0.9919	2.67	0.73	2.47	6.11	1.37	P2O5	GaP	1-Jun-1999 12:00 AM	
Cl	K_SERIES	0.33	0.00336	0.7456	1.99	0.56	1.61	0.00	0.90	KCl	KCl	1-Jun-1999 12:00 AM	
Ca	K_SERIES	1.30	0.01171	1.0388	5.59	0.67	4.00	7.82	2.22	CaO	Wollastonite	1-Jun-1999 12:00 AM	
Fe	K_SERIES	9.50	0.09505	0.8959	47.25	1.76	24.27	60.79	13.47	FeO	Fe	1-Jun-1999 12:00 AM	
O				31.27	1.65	56.06			31.10				
Totals				100.00									
								Cation sum	23.49				

Processing option : Oxygen by stoichiometry (Normalised)
Number of iterations : 2
Sample is polished.
Sample is coated with Carbon - thickness (nm): 15.0, density (g/cm3): 2.25
Detector efficiency : Calculation

11a

1

Element	Line	App. Conc	k ratio	Intensity	corrn.		Weight%	Weight% sigma	Atomic%	Compound%	Formula	Number of ions	Standard
Al	K_SERIES	0.50	0.00367	0.5323	1.99	0.44	2.47	3.75	1.47	Al2O3	Al2O3	1-Jun-1999 12:00 AM	
Si	K_SERIES	0.59	0.00473	0.6481	1.92	0.44	2.29	4.11	1.36	SiO2	SiO2	1-Jun-1999 12:00 AM	
P	K_SERIES	1.25	0.0074	1.0371	2.55	0.47	2.76	5.85	1.64	P2O5	GaP	1-Jun-1999 12:00 AM	
Ca	K_SERIES	2.33	0.02093	1.1064	4.46	0.42	3.73	6.25	2.22	CaO	Wollastonite	1-Jun-1999 12:00 AM	
Mn	K_SERIES	15.35	0.15346	0.8986	36.20	1.21	22.08	46.75	13.13	MnO	Mn	1-Jun-1999 12:00 AM	
Fe	K_SERIES	7.57	0.07566	0.9204	17.42	1.07	10.45	22.41	6.21	FeO	Fe	1-Jun-1999 12:00 AM	
Ba	L_SERIES	4.29	0.04008	0.9336	9.75	1.02	2.38	10.88	1.41	BaO	BaF2	1-Jun-1999 12:00 AM	
O				25.70	1.18	53.83			32.00				
Totals				100.00									
								Cation sum	27.44				

Processing option : Oxygen by stoichiometry (Normalised)
Number of iterations : 2
Sample is polished.
Sample is coated with Carbon - thickness (nm): 15.0, density (g/cm3): 2.25
Detector efficiency : Calculation

2

Element	Line	App. Conc	k ratio	Intensity	corrn.		Weight%	Weight% sigma	Atomic%	Compound%	Formula	Number of ions	Standard
Al	K_SERIES	0.90	0.00663	0.5482	4.64	0.65	5.39	8.76	3.22	Al2O3	Al2O3	1-Jun-1999 12:00 AM	
Si	K_SERIES	0.70	0.00564	0.6445	3.06	0.59	3.42	6.55	2.04	SiO2	SiO2	1-Jun-1999 12:00 AM	
K	K_SERIES	0.41	0.00339	1.1239	1.04	0.33	0.83	1.25	0.50	K2O	MAD-10 Feldspar	1-Jun-1999 12:00 AM	
Ca	K_SERIES	0.78	0.00698	1.0957	2.00	0.40	1.56	2.80	0.94	CaO	Wollastonite	1-Jun-1999 12:00 AM	
Ti	K_SERIES	0.74	0.00738	0.9750	2.13	0.48	1.40	3.56	0.83	TiO2	Ti	1-Jun-1999 12:00 AM	
Mn	K_SERIES	10.88	0.1088	0.9043	33.95	1.34	19.36	43.83	11.57	MnO	Mn	1-Jun-1999 12:00 AM	
Fe	K_SERIES	8.47	0.08471	0.9250	25.84	1.29	14.50	33.24	8.66	FeO	Fe	1-Jun-1999 12:00 AM	
O				27.34	1.32	53.55			32.00				
Totals				100.00									
								Cation sum	27.76				

Processing option : Oxygen by stoichiometry (Normalised)
Number of iterations : 2
Sample is polished.
Sample is coated with Carbon - thickness (nm): 15.0, density (g/cm3): 2.25
Detector efficiency : Calculation

3

Element	Line	App. Conc	k ratio	Intensity	corrn.		Weight%	Weight% sigma	Atomic%	Compound%	Formula	Number of ions	Standard
Mg	K_SERIES	0.34	0.00231	0.4111	2.24	0.74	3.19	3.71	2.01	MgO	MgO	1-Jun-1999 12:00 AM	
Al	K_SERIES	0.54	0.00396	0.5116	2.87	0.62	3.69	5.42	2.32	Al2O3	Al2O3	1-Jun-1999 12:00 AM	
Ca	K_SERIES	1.16	0.01039	1.1262	2.80	0.40	2.43	3.92	1.53	CaO	Wollastonite	1-Jun-1999 12:00 AM	
Mn	K_SERIES	15.69	0.1569	0.9121	46.95	1.50	29.68	60.62	18.65	MnO	Mn	1-Jun-1999 12:00 AM	
Fe	K_SERIES	4.27	0.04269	0.9335	12.48	1.15	7.76	16.06	4.88	FeO	Fe	1-Jun-1999 12:00 AM	
Ba	L_SERIES	3.24	0.03023	0.9609	9.20	1.14	2.33	10.27	1.46	BaO	BaF2	1-Jun-1999 12:00 AM	
O				23.46	1.31	50.92			32.00				
Totals				100.00									
								Cation sum	30.84				

Processing option : Oxygen by stoichiometry (Normalised)
Number of iterations : 2
Sample is polished.
Sample is coated with Carbon - thickness (nm): 15.0, density (g/cm3): 2.25
Detector efficiency : Calculation

4

Element	Line	App. Conc	k ratio	Intensity	corrn.		Weight%	Weight% sigma	Atomic%	Compound%	Formula	Number of ions	Standard
Mg	K_SERIES	0.34	0.00231	0.4119	2.07	0.66	2.90	3.43	1.79	MgO	MgO	1-Jun-1999 12:00 AM	
Al	K_SERIES	0.45	0.00335	0.5128	2.24	0.57	2.83	4.23	1.74	Al2O3	Al2O3	1-Jun-1999 12:00 AM	
Si	K_SERIES	0.54	0.00438	0.6271	2.19	0.48	2.66	4.68	1.64	SiO2	SiO2	1-Jun-1999 12:00 AM	
Ca	K_SERIES	0.61	0.00544	1.1164	1.37	0.36	1.17	1.92	0.72	CaO	Wollastonite	1-Jun-1999 12:00 AM	
Mn	K_SERIES	14.99	0.14989	0.9097	41.61	1.40	25.88	53.73	15.91	MnO	Mn	1-Jun-1999 12:00 AM	
Fe	K_SERIES	6.10	0.06102	0.9306	16.56	1.13	10.13	21.30	6.23	FeO	Fe	1-Jun-1999 12:00 AM	
Ba	L_SERIES	3.65	0.03409	0.9599	9.61	1.11	2.39	10.73	1.47	BaO	BaF2	1-Jun-1999 12:00 AM	
O				24.37	1.29	52.04			32.00				
Totals				100.00									
								Cation sum	29.49				

Processing option : Oxygen by stoichiometry (Normalised)
Number of iterations : 2
Sample is polished.
Sample is coated with Carbon - thickness (nm): 15.0, density (g/cm3): 2.25
Detector efficiency : Calculation

5

Element	Line	App. Conc	k ratio	Intensity	corrn.		Weight%	Weight% sigma	Atomic%	Compound%	Formula	Number of ions	Standard
Al	K_SERIES	0.49	0.00362	0.5287	3.20	0.67	3.75	6.05	2.20	Al2O3	Al2O3	1-Jun-1999 12:00 AM	
Si	K_SERIES	1.16	0.00937	0.6341	6.31	0.74	7.09	13.49	4.16	SiO2	SiO2	1-Jun-1999 12:00 AM	
Ca	K_SERIES	0.71	0.00634	1.0778	2.25	0.45	1.77	3.15	1.04	CaO	Wollastonite	1-Jun-1999 12:00 AM	
Mn	K_SERIES	2.42	0.0242	0.8960	9.29	0.99	5.34	11.99	3.13	MnO	Mn	1-Jun-1999 12:00 AM	
Fe	K_SERIES	12.55	0.12549	0.9166	47.10	1.66	26.61	60.59	15.63	FeO	Fe	1-Jun-1999 12:00 AM	
Ba	L_SERIES	1.14	0.01064	0.9297	4.22	1.16	0.97	4.71	0.57	BaO	BaF2	1-Jun-1999 12:00 AM	
O				27.63	1.47	54.48			32.00				
Totals				100.00									
								Cation sum	26.74				

Processing option : Oxygen by stoichiometry (Normalised)
Number of iterations : 2
Sample is polished.
Sample is coated with Carbon - thickness (nm): 15.0, density (g/cm3): 2.25
Detector efficiency : Calculation

6

Element	Line	App. Conc	k ratio	Intensity	corrn.		Weight%	Weight% sigma	Atomic%	Compound%	Formula	Number of ions	Standard
Al	K_SERIES	0.55	0.00408	0.5386	3.16	0.69	3.72	5.98	2.22	Al2O3	Al2O3	1-Jun-1999 12:00 AM	
Si	K_SERIES	0.74	0.00597	0.6471	3.52	0.63	3.98	7.53	2.38	SiO2	SiO2	1-Jun-1999 12:00 AM	
Ca	K_SERIES	0.65	0.00581	1.1067	1.80	0.41	1.42	2.52	0.85	CaO	Wollastonite	1-Jun-1999 12:00 AM	
Ti	K_SERIES	0.70	0.00697	0.9870	2.17	0.53	1.44	3.62	0.86	TiO2	Ti	1-Jun-1999 12:00 AM	
Mn	K_SERIES	10.13	0.10129	0.9087	34.31	1.41	19.84	44.30	11.84	MnO	Mn	1-Jun-1999 12:00 AM	
Fe	K_SERIES	8.46	0.08464	0.9292	28.03	1.41	15.95	36.06	9.51	FeO	Fe	1-Jun-1999 12:00 AM	
O				27.01	1.41	53.64			32.00				
Totals				100.00									
								Cation sum	27.65				

Processing option : Oxygen by stoichiometry (Normalised)
Number of iterations : 2
Sample is polished.
Sample is coated with Carbon - thickness (nm): 15.0, density (g/cm3): 2.25
Detector efficiency : Calculation

7

Element	Line	App. Conc	k ratio	Intensity	corrn.		Weight%	Weight% sigma	Atomic%	Compound%	Formula	Number of ions	Standard
Al	K_SERIES	0.56	0.0041	0.5223	3.75	0.72	4.36	7.09	2.59	Al2O3	Al2O3	1-Jun-1999 12:00 AM	
Si	K_SERIES	0.87	0.00702	0.6253	4.91	0.74	5.48	10.50	3.26	SiO2	SiO2	1-Jun-1999 12:00 AM	
Ca	K_SERIES	0.59	0.00529	1.0789	1.93	0.44	1.51	2.69	0.90	CaO	Wollastonite	1-Jun-1999 12:00 AM	
Mn	K_SERIES	1.16	0.01163	0.9028	4.54	0.85	2.59	5.86	1.54	MnO	Mn	1-Jun-1999 12:00 AM	
Fe	K_SERIES	15.04	0.15039	0.9229	57.41	1.60	32.23	73.86	19.16	FeO	Fe	1-Jun-1999 12:00 AM	
O				27.47	1.44	53.83			32.00				
Totals				100.00									
								Cation sum	27.45				

Processing option : Oxygen by stoichiometry (Normalised)
Number of iterations : 2
Sample is polished.
Sample is coated with Carbon - thickness (nm): 15.0, density (g/cm3): 2.25
Detector efficiency : Calculation

13a

1

Element	Line	App. Conc	k ratio	Intensity	corrn.		Weight%	Weight% sigma	Atomic%	Compound%	Formula	Number of ions	Standard
Al	K_SERIES	0.54	0.00401	0.5176	2.84	0.60	3.51	5.36	2.11	Al2O3	Al2O3	1-Jun-1999 12:00 AM	
Si	K_SERIES	0.90	0.00723	0.6272	3.86	0.62	4.59	8.25	2.76	SiO2	SiO2	1-Jun-1999 12:00 AM	
Ca	K_SERIES	0.52	0.00465	1.1005	1.27	0.37	1.06	1.77	0.64	CaO	Wollastonite	1-Jun-1999 12:00 AM	
Mn	K_SERIES	7.89	0.07894	0.9070	23.47	1.17	14.27	30.30	8.59	MnO	Mn	1-Jun-1999 12:00 AM	
Fe	K_SERIES	12.53	0.12526	0.9278	36.40	1.38	21.77	46.83	13.10	FeO	Fe	1-Jun-1999 12:00 AM	
Ba	L_SERIES	2.37	0.02211	0.9525	6.70	1.05	1.63	7.49	0.98	BaO	BaF2	1-Jun-1999 12:00 AM	
O				25.47	1.29	53.17			32.00				
Totals				100.00									
								Cation sum	28.18				

2

Element	Line	App. Conc	k ratio	Intensity	corrn.	Weight%	Weight% sigma	Atomic%	Compound%	Formula	Number of ions	Standard
Al	K_SERIES	0.53	0.00388	0.5205	2.68	0.53	3.08	5.07	Al2O3	1.80	Al2O3	1-Jun-1999 12:00 AM
Si	K_SERIES	1.69	0.01365	0.6308	7.10	0.64	7.84	15.19	SiO2	4.59	SiO2	1-Jun-1999 12:00 AM
Fe	K_SERIES	21.60	0.21602	0.9224	61.98	1.27	34.39	79.74	FeO	20.13	Fe	1-Jun-1999 12:00 AM
O				28.23	1.17	54.69				32.00		
Totals				100.00								
									Cation sum	26.51		

Processing option : Oxygen by stoichiometry (Normalised)
Number of iterations : 2
Sample is polished.
Sample is coated with Carbon - thickness (nm): 15.0, density (g/cm3): 2.25
Detector efficiency : Calculation

3

Element	Line	App. Conc	k ratio	Intensity	corrn.	Weight%	Weight% sigma	Atomic%	Compound%	Formula	Number of ions	Standard
Al	K_SERIES	0.49	0.00359	0.5370	3.90	0.84	4.32	7.37	Al2O3	2.48	Al2O3	1-Jun-1999 12:00 AM
Si	K_SERIES	1.28	0.01035	0.6361	8.65	0.92	9.20	18.51	SiO2	5.29	SiO2	1-Jun-1999 12:00 AM
Fe	K_SERIES	12.29	0.12294	0.9150	57.62	1.68	30.81	74.12	FeO	17.70	Fe	1-Jun-1999 12:00 AM
O				29.83	1.55	55.68				32.00		
Totals				100.00								
									Cation sum	25.47		

Processing option : Oxygen by stoichiometry (Normalised)
Number of iterations : 2
Sample is polished.
Sample is coated with Carbon - thickness (nm): 15.0, density (g/cm3): 2.25
Detector efficiency : Calculation

4

Element	Line	App. Conc	k ratio	Intensity	corrn.	Weight%	Weight% sigma	Atomic%	Compound%	Formula	Number of ions	Standard
Al	K_SERIES	0.57	0.00416	0.5190	2.80	0.58	3.24	5.28	Al2O3	1.91	Al2O3	1-Jun-1999 12:00 AM
Si	K_SERIES	1.51	0.01215	0.6288	6.15	0.64	6.84	13.15	SiO2	4.04	SiO2	1-Jun-1999 12:00 AM
Ca	K_SERIES	0.52	0.00467	1.0743	1.24	0.33	0.97	1.74	CaO	0.57	Wollastonite	1-Jun-1999 12:00 AM
Fe	K_SERIES	22.30	0.22302	0.9222	62.05	1.29	34.73	79.83	FeO	20.49	Fe	1-Jun-1999 12:00 AM
O				27.76	1.18	54.23				32.00		
Totals				100.00								
									Cation sum	27.01		

Processing option : Oxygen by stoichiometry (Normalised)
Number of iterations : 2
Sample is polished.
Sample is coated with Carbon - thickness (nm): 15.0, density (g/cm3): 2.25
Detector efficiency : Calculation

5

Element	Line	App. Conc	k ratio	Intensity	corrn.	Weight%	Weight% sigma	Atomic%	Compound%	Formula	Number of ions	Standard
Al	K_SERIES	0.45	0.00334	0.5258	3.39	0.79	3.87	6.40	Al2O3	2.27	Al2O3	1-Jun-1999 12:00 AM
Si	K_SERIES	1.06	0.00858	0.6306	6.61	0.85	7.25	14.15	SiO2	4.25	SiO2	1-Jun-1999 12:00 AM
Ca	K_SERIES	0.41	0.00367	1.0699	1.50	0.48	1.15	2.10	CaO	0.67	Wollastonite	1-Jun-1999 12:00 AM
Fe	K_SERIES	14.09	0.14088	0.9189	60.13	1.65	33.14	77.35	FeO	19.43	Fe	1-Jun-1999 12:00 AM
O				28.37	1.51	54.59				32.00		
Totals				100.00								
									Cation sum	26.62		

Processing option : Oxygen by stoichiometry (Normalised)
Number of iterations : 2
Sample is polished.
Sample is coated with Carbon - thickness (nm): 15.0, density (g/cm3): 2.25
Detector efficiency : Calculation

6

Element	Line	App. Conc	k ratio	Intensity	corrn.	Weight%	Weight% sigma	Atomic%	Compound%	Formula	Number of ions	Standard
Al	K_SERIES	0.49	0.00358	0.5345	3.62	0.80	4.12	6.85	Al2O3	2.42	Al2O3	1-Jun-1999 12:00 AM
Si	K_SERIES	1.02	0.00823	0.6372	6.38	0.86	6.97	13.64	SiO2	4.09	SiO2	1-Jun-1999 12:00 AM
Ca	K_SERIES	0.58	0.00518	1.0745	2.14	0.48	1.64	2.99	CaO	0.96	Wollastonite	1-Jun-1999 12:00 AM
Mn	K_SERIES	2.01	0.0201	0.8990	8.91	1.09	4.98	11.50	MnO	2.92	Mn	1-Jun-1999 12:00 AM
Fe	K_SERIES	11.66	0.11656	0.9190	50.54	1.71	27.78	65.01	FeO	16.30	Fe	1-Jun-1999 12:00 AM
O				28.42	1.56	54.52				32.00		
Totals				100.00								
									Cation sum	26.70		

Processing option : Oxygen by stoichiometry (Normalised)
Number of iterations : 2
Sample is polished.
Sample is coated with Carbon - thickness (nm): 15.0, density (g/cm3): 2.25
Detector efficiency : Calculation

14a

1

Element	Line	App. Conc	k ratio	Intensity	corrn.	Weight%	Weight% sigma	Atomic%	Compound%	Formula	Number of ions	Standard
P	K_SERIES	11.42	0.06763	1.3263	17.22	0.66	13.54	39.45	P2O5	7.20	GaP	1-Jun-1999 12:00 AM
Ca	K_SERIES	21.82	0.19595	1.0079	43.27	0.80	26.30	60.55	CaO	13.99	Wollastonite	1-Jun-1999 12:00 AM
O				39.51	0.81	60.16				32.00		
Totals				100.00								
									Cation sum	21.19		

Processing option : Oxygen by stoichiometry (Normalised)
Number of iterations : 2
Sample is polished.
Sample is coated with Carbon - thickness (nm): 15.0, density (g/cm3): 2.25
Detector efficiency : Calculation

2

Element	Line	App. Conc	k ratio	Intensity	corrn.		Weight%	Weight% sigma	Atomic%	Compound%	Formula	Number of ions	Standard
Si	K_SERIES	0.44	0.00357	0.6583	1.58	0.42	1.94	3.38	1.17	SiO2	SiO2	1-Jun-1999 12:00 AM	
P	K_SERIES	1.14	0.00675	1.0552	2.54	0.49	2.82	5.81	1.70	P2O5	GaP	1-Jun-1999 12:00 AM	
Ca	K_SERIES	2.81	0.02528	1.1174	5.91	0.49	5.09	8.27	3.07	CaO	Wollastonite	1-Jun-1999 12:00 AM	
Mn	K_SERIES	16.04	0.16037	0.9009	41.80	1.32	26.26	53.98	15.83	MnO	Mn	1-Jun-1999 12:00 AM	
Fe	K_SERIES	5.22	0.05223	0.9232	13.28	1.04	8.21	17.09	4.95	FeO	Fe	1-Jun-1999 12:00 AM	
Ba	L_SERIES	4.09	0.0382	0.9353	10.27	1.09	2.58	11.47	1.56	BaF2	BaF2	1-Jun-1999 12:00 AM	
O				24.61	1.19	53.09			32.00				
Totals				100.00									
								Cation sum	28.28				

Processing option : Oxygen by stoichiometry (Normalised)
Number of iterations : 2
Sample is polished.
Sample is coated with Carbon - thickness (nm): 15.0, density (g/cm3): 2.25
Detector efficiency : Calculation

3

Element	Line	App. Conc	k ratio	Intensity	corrn.		Weight%	Weight% sigma	Atomic%	Compound%	Formula	Number of ions	Standard
Al	K_SERIES	0.40	0.00297	0.5201	2.50	0.63	3.04	4.73	1.82	Al2O3	Al2O3	1-Jun-1999 12:00 AM	
Si	K_SERIES	0.86	0.00691	0.6323	4.37	0.67	5.09	9.34	3.06	SiO2	SiO2	1-Jun-1999 12:00 AM	
Ca	K_SERIES	0.86	0.00775	1.0941	2.54	0.46	2.08	3.55	1.25	CaO	Wollastonite	1-Jun-1999 12:00 AM	
Mn	K_SERIES	5.02	0.0502	0.9039	17.90	1.17	10.67	23.11	6.41	MnO	Mn	1-Jun-1999 12:00 AM	
Fe	K_SERIES	12.11	0.12107	0.9247	42.19	1.58	24.75	54.28	14.86	FeO	Fe	1-Jun-1999 12:00 AM	
Ba	L_SERIES	1.31	0.01222	0.9432	4.47	1.20	1.07	4.99	0.64	BaF2	BaF2	1-Jun-1999 12:00 AM	
O				26.03	1.42	53.31			32.00				
Totals				100.00									
								Cation sum	28.03				

Processing option : Oxygen by stoichiometry (Normalised)
Number of iterations : 2
Sample is polished.
Sample is coated with Carbon - thickness (nm): 15.0, density (g/cm3): 2.25
Detector efficiency : Calculation

4

Element	Line	App. Conc	k ratio	Intensity	corrn.		Weight%	Weight% sigma	Atomic%	Compound%	Formula	Number of ions	Standard
Al	K_SERIES	0.68	0.00502	0.5442	4.58	0.73	5.20	8.65	3.06	Al2O3	Al2O3	1-Jun-1999 12:00 AM	
Si	K_SERIES	0.97	0.00783	0.6394	5.55	0.74	6.05	11.87	3.56	SiO2	SiO2	1-Jun-1999 12:00 AM	
Ca	K_SERIES	0.75	0.00677	1.0806	2.55	0.49	1.95	3.57	1.15	CaO	Wollastonite	1-Jun-1999 12:00 AM	
Mn	K_SERIES	4.72	0.04724	0.9001	19.19	1.26	10.69	24.78	6.30	MnO	Mn	1-Jun-1999 12:00 AM	
Fe	K_SERIES	10.00	0.1	0.9201	39.74	1.58	21.78	51.12	12.83	FeO	Fe	1-Jun-1999 12:00 AM	
O				28.39	1.47	54.32			32.00				
Totals				100.00									
								Cation sum	26.91				

Processing option : Oxygen by stoichiometry (Normalised)
Number of iterations : 2
Sample is polished.
Sample is coated with Carbon - thickness (nm): 15.0, density (g/cm3): 2.25
Detector efficiency : Calculation

5

Element	Line	App. Conc	k ratio	Intensity	corrn.		Weight%	Weight% sigma	Atomic%	Compound%	Formula	Number of ions	Standard
Si	K_SERIES	0.93	0.00751	0.6598	8.15	1.04	9.07	17.43	5.24	SiO2	SiO2	1-Jun-1999 12:00 AM	
Cl	K_SERIES	0.26	0.00265	0.7604	2.00	0.70	1.76	0.00	1.02	KCl	KCl	1-Jun-1999 12:00 AM	
Ca	K_SERIES	0.47	0.00421	1.0658	2.54	0.68	1.98	3.56	1.14	CaO	Wollastonite	1-Jun-1999 12:00 AM	
Mn	K_SERIES	0.55	0.00555	0.8974	3.57	1.03	2.03	4.61	1.17	MnO	Mn	1-Jun-1999 12:00 AM	
Fe	K_SERIES	8.95	0.0895	0.9180	56.28	1.99	31.50	72.41	18.19	FeO	Fe	1-Jun-1999 12:00 AM	
O				27.46	1.76	53.65			30.98				
Totals				100.00									
								Cation sum	25.75				

Processing option : Oxygen by stoichiometry (Normalised)
Number of iterations : 2
Sample is polished.
Sample is coated with Carbon - thickness (nm): 15.0, density (g/cm3): 2.25
Detector efficiency : Calculation

6

Element	Line	App. Conc	k ratio	Intensity	corrn.		Weight%	Weight% sigma	Atomic%	Compound%	Formula	Number of ions	Standard
Al	K_SERIES	0.48	0.00353	0.5420	3.01	0.68	3.34	5.69	1.93	Al2O3	Al2O3	1-Jun-1999 12:00 AM	
Si	K_SERIES	1.60	0.01293	0.6481	8.43	0.81	8.99	18.03	5.20	SiO2	SiO2	1-Jun-1999 12:00 AM	
Ca	K_SERIES	0.95	0.00857	1.0632	3.06	0.48	2.29	4.28	1.32	CaO	Wollastonite	1-Jun-1999 12:00 AM	
Mn	K_SERIES	0.84	0.00844	0.8910	3.23	0.73	1.76	4.17	1.02	MnO	Mn	1-Jun-1999 12:00 AM	
Fe	K_SERIES	14.09	0.14094	0.9112	52.72	1.55	28.28	67.83	16.36	FeO	Fe	1-Jun-1999 12:00 AM	
O				29.55	1.41	55.33			32.00				
Totals				100.00									
								Cation sum	25.83				

Processing option : Oxygen by stoichiometry (Normalised)
Number of iterations : 2
Sample is polished.
Sample is coated with Carbon - thickness (nm): 15.0, density (g/cm3): 2.25
Detector efficiency : Calculation

7

Element	Line	App. Conc	k ratio	Intensity	corrn.		Weight%	Weight% sigma	Atomic%	Compound%	Formula	Number of ions	Standard
Si	K_SERIES	0.65	0.00522	0.6606	3.37	0.65	3.95	7.21	2.39	SiO2	SiO2	1-Jun-1999 12:00 AM	
Ca	K_SERIES	0.83	0.00749	1.1209	2.56	0.49	2.10	3.58	1.27	CaO	Wollastonite	1-Jun-1999 12:00 AM	
Ti	K_SERIES	0.81	0.00809	0.9954	2.79	0.61	1.92	4.66	1.16	TiO2	Ti	1-Jun-1999 12:00 AM	
Mn	K_SERIES	10.13	0.1013	0.9133	38.14	1.52	22.88	49.25	13.83	MnO	Mn	1-Jun-1999 12:00 AM	
Fe	K_SERIES	7.46	0.07457	0.9345	27.44	1.48	16.20	35.30	9.79	FeO	Fe	1-Jun-1999 12:00 AM	
O				25.70	1.42	52.94			32.00				
Totals				100.00									
								Cation sum	28.45				

Processing option : Oxygen by stoichiometry (Normalised)
Number of iterations : 2
Sample is polished.
Sample is coated with Carbon - thickness (nm): 15.0, density (g/cm3): 2.25
Detector efficiency : Calculation

SEM results of the thin sections of the large testudinid from Nea Michaniona

Sample 2

2a

1

calcite

Element	Line	App. Conc	k ratio	Intensity corrn.		Weight%	Weight% sigma	Atomic%	Standard
O	K_SERIES	1.71	0.00614	0.2153	32.45	3.84	54.61	SiO2	1-Jun-1999 12:00 AM
Ca	K_SERIES	17.73	0.15925	1.0725	67.55	3.84	45.39	Wollastonite	1-Jun-1999 12:00 AM
Totals				100.00					

Processing option : All elements analyzed (Normalised)
Number of iterations : 3
Sample is polished.
Sample is coated with Carbon - thickness (nm): 15.0, density (g/cm3): 2.25
Detector efficiency : Calculation

2

quartz

Element	Line	App. Conc	k ratio	Intensity corrn.		Weight%	Weight% sigma	Atomic%	Compound%	Formula	Number of ions	Standard
Si	K_SERIES	19.68	0.15868	0.9576	46.74	0.76	33.33	100.00	SiO2	16.00	SiO2	1-Jun-1999 12:00 AM
O				53.26	0.76	66.67		32.00				
Totals				100.00								
								Cation sum		16.00		

Processing option : Oxygen by stoichiometry (Normalised)
Number of iterations : 2
Sample is polished.
Sample is coated with Carbon - thickness (nm): 15.0, density (g/cm3): 2.25
Detector efficiency : Calculation

3

calcite

Element	Line	App. Conc	k ratio	Intensity corrn.		Weight%	Weight% sigma	Atomic%	Compound%	Formula	Number of ions	Standard
Ca	K_SERIES	17.53	0.15744	1.0774	71.47	0.99	50.00	100.00	CaO	32.00	Wollastonite	1-Jun-1999 12:00 AM
O				28.53	0.99	50.00		32.00				
Totals				100.00								
								Cation sum		32.00		

Processing option : Oxygen by stoichiometry (Normalised)
Number of iterations : 2
Sample is polished.
Sample is coated with Carbon - thickness (nm): 15.0, density (g/cm3): 2.25
Detector efficiency : Calculation

4

apatite

Element	Line	App. Conc	k ratio	Intensity corrn.		Weight%	Weight% sigma	Atomic%	Compound%	Formula	Number of ions	Standard
P	K_SERIES	8.00	0.04739	1.3258	16.95	0.80	13.36	38.83	P2O5	7.12	GaP	1-Jun-1999 12:00 AM
Ca	K_SERIES	15.71	0.14112	1.0090	43.72	0.96	26.63	61.17	CaO	14.20	Wollastonite	1-Jun-1999 12:00 AM
O				39.34	0.97	60.02		32.00				
Totals				100.00								
								Cation sum		21.32		

Processing option : Oxygen by stoichiometry (Normalised)
Number of iterations : 2
Sample is polished.
Sample is coated with Carbon - thickness (nm): 15.0, density (g/cm3): 2.25
Detector efficiency : Calculation

3a

1

calcite

2
apatite

Element	Line	App. Conc	k ratio	Intensity corrn.		Weight%	Weight% sigma	Atomic%	Compound%	Formula	Number of ions	Standard
P	K_SERIES	8.27	0.04896	1.3270	17.67	0.78	13.85	40.49	P2O5	7.34	GaP	1-Jun-1999 12:00 AM
Ca	K_SERIES	15.09	0.13554	1.0062	42.53	0.95	25.76	59.51	CaO	13.65	Wollastonite	1-Jun-1999 12:00 AM
O				39.80	0.96	60.39		32.00				
Totals				100.00								
								Cation sum		20.99		

Processing option : Oxygen by stoichiometry (Normalised)
Number of iterations : 2
Sample is polished.
Sample is coated with Carbon - thickness (nm): 15.0, density (g/cm3): 2.25
Detector efficiency : Calculation

3

multiple phases

4

calcite

5a

1

Element	Line	App.	Conc	k ratio	Intensity	corrn.	Weight%	Weight% sigma	Atomic%	Compound%	Formula	Number of ions	Standard
Al	K_SERIES		0.89	0.00656	0.7718	6.08	0.76	5.06	11.48	Al2O3	2.61	Al2O3	1-Jun-1999 12:00 AM
Si	K_SERIES		4.23	0.03415	0.7988	27.90	1.27	22.33	59.68	SiO2	11.51	SiO2	1-Jun-1999 12:00 AM
K	K_SERIES		0.46	0.00377	0.9968	2.43	0.59	1.39	2.92	K2O	0.72	MAD-10 Feldspar	1-Jun-1999 12:00 AM
Ca	K_SERIES		1.49	0.01338	0.9512	8.24	0.85	4.62	11.53	CaO	2.38	Wollastonite	1-Jun-1999 12:00 AM
Fe	K_SERIES		1.77	0.01773	0.8350	11.18	1.28	4.50	14.39	FeO	2.32	Fe	1-Jun-1999 12:00 AM
O					44.18	1.51	62.08			32.00			
Totals					100.00								
										Cation sum	19.54		

Processing option : Oxygen by stoichiometry (Normalised)
Number of iterations : 2
Sample is polished.
Sample is coated with Carbon - thickness (nm): 15.0, density (g/cm3): 2.25
Detector efficiency : Calculation

2

Element	Line	App.	Conc	k ratio	Intensity	corrn.	Weight%	Weight% sigma	Atomic%	Compound%	Formula	Number of ions	Standard
Si	K_SERIES		0.90	0.00723	0.8576	5.92	0.76	5.62	12.66	SiO2	3.41	SiO2	1-Jun-1999 12:00 AM
Ca	K_SERIES		11.62	0.10442	1.0549	62.42	1.31	41.56	87.34	CaO	25.18	Wollastonite	1-Jun-1999 12:00 AM
O					31.66	1.24	52.81			32.00			
Totals					100.00								
										Cation sum	28.59		

Processing option : Oxygen by stoichiometry (Normalised)
Number of iterations : 2
Sample is polished.
Sample is coated with Carbon - thickness (nm): 15.0, density (g/cm3): 2.25
Detector efficiency : Calculation

3
calcite

Element	Line	App.	Conc	k ratio	Intensity	corrn.	Weight%	Weight% sigma	Atomic%	Compound%	Formula	Number of ions	Standard
Ca	K_SERIES		13.86	0.12451	1.0774	71.47	1.12	50.00	100.00	CaO	32.00	Wollastonite	1-Jun-1999 12:00 AM
O					28.53	1.12	50.00			32.00			
Totals					100.00								
										Cation sum	32.00		

Processing option : Oxygen by stoichiometry (Normalised)
Number of iterations : 2
Sample is polished.
Sample is coated with Carbon - thickness (nm): 15.0, density (g/cm3): 2.25
Detector efficiency : Calculation

7a

1

calcite

Element	Line	App.	Conc	k ratio	Intensity	corrn.	Weight%	Weight% sigma	Atomic%	Compound%	Formula	Number of ions	Standard
Ca	K_SERIES		12.50	0.11231	1.0774	71.47	1.18	50.00	100.00	CaO	32.00	Wollastonite	1-Jun-1999 12:00 AM
O					28.53	1.18	50.00			32.00			
Totals					100.00								
										Cation sum	32.00		

Processing option : Oxygen by stoichiometry (Normalised)
Number of iterations : 2
Sample is polished.
Sample is coated with Carbon - thickness (nm): 15.0, density (g/cm3): 2.25
Detector efficiency : Calculation

2

Element	Line	App.	Conc	k ratio	Intensity	corrn.	Weight%	Weight% sigma	Atomic%	Compound%	Formula	Number of ions	Standard
Al	K_SERIES		0.24	0.00177	0.7499	2.25	0.73	2.16	4.25	Al2O3	1.28	Al2O3	1-Jun-1999 12:00 AM
Si	K_SERIES		0.88	0.0071	0.8392	7.37	0.96	6.82	15.77	SiO2	4.05	SiO2	1-Jun-1999 12:00 AM
Ca	K_SERIES		8.49	0.07626	1.0438	57.16	1.60	37.06	79.98	CaO	21.98	Wollastonite	1-Jun-1999 12:00 AM
O					33.22	1.51	53.95			32.00			
Totals					100.00								
										Cation sum	27.31		

Processing option : Oxygen by stoichiometry (Normalised)
Number of iterations : 2
Sample is polished.
Sample is coated with Carbon - thickness (nm): 15.0, density (g/cm3): 2.25
Detector efficiency : Calculation

3
calcite

Element	Line	App.	Conc	k ratio	Intensity	corrn.	Weight%	Weight% sigma	Atomic%	Compound%	Formula	Number of ions	Standard
Ca	K_SERIES		12.48	0.11208	1.0774	71.47	1.18	50.00	100.00	CaO	32.00	Wollastonite	1-Jun-1999 12:00 AM
O					28.53	1.18	50.00			32.00			
Totals					100.00								
										Cation sum	32.00		

Processing option : Oxygen by stoichiometry (Normalised)
Number of iterations : 2
Sample is polished.
Sample is coated with Carbon - thickness (nm): 15.0, density (g/cm3): 2.25
Detector efficiency : Calculation

4

calcite

Element	Line	App. Conc	k ratio	Intensity corrn.		Weight%	Weight% sigma	Atomic%	Compound%	Formula	Number of ions	Standard
Al	K_SERIES	0.21	0.00152	0.7372	1.66	0.62	1.65	3.13	Al2O3	Al2O3	1.01	1-Jun-1999 12:00 AM
Si	K_SERIES	0.53	0.0043	0.8376	3.76	0.73	3.60	8.05	SiO2	SiO2	2.21	1-Jun-1999 12:00 AM
Ca	K_SERIES	11.36	0.10205	1.0588	63.48	1.42	42.54	88.81	CaO	Wollastonite	26.07	1-Jun-1999 12:00 AM
O				31.10	1.33	52.21			32.00			
Totals				100.00								
									Cation sum		29.29	

Processing option : Oxygen by stoichiometry (Normalised)
Number of iterations : 2
Sample is polished.
Sample is coated with Carbon - thickness (nm): 15.0, density (g/cm3): 2.25
Detector efficiency : Calculation

7a

1

Element	Line	App. Conc	k ratio	Intensity corrn.		Weight%	Weight% sigma	Atomic%	Compound%	Formula	Number of ions	Standard
Si	K_SERIES	0.49	0.00395	0.8878	2.07	0.41	1.78	4.43	SiO2	SiO2	0.94	1-Jun-1999 12:00 AM
P	K_SERIES	5.58	0.03304	1.2919	16.20	0.88	12.64	37.12	P2O5	GaP	6.70	1-Jun-1999 12:00 AM
Ca	K_SERIES	11.19	0.1005	1.0045	41.78	1.10	25.20	58.46	CaO	Wollastonite	13.36	1-Jun-1999 12:00 AM
O				39.95	1.12	60.37			32.00			
Totals				100.00								
									Cation sum		21.00	

Processing option : Oxygen by stoichiometry (Normalised)
Number of iterations : 2
Sample is polished.
Sample is coated with Carbon - thickness (nm): 15.0, density (g/cm3): 2.25
Detector efficiency : Calculation

2

Element	Line	App. Conc	k ratio	Intensity corrn.		Weight%	Weight% sigma	Atomic%	Compound%	Formula	Number of ions	Standard
Ca	K_SERIES	13.18	0.1184	1.0774	71.47	1.13	50.00	100.00	CaO	Wollastonite	32.00	1-Jun-1999 12:00 AM
O				28.53	1.13	50.00			32.00			
Totals				100.00								
									Cation sum		32.00	

Processing option : Oxygen by stoichiometry (Normalised)
Number of iterations : 2
Sample is polished.
Sample is coated with Carbon - thickness (nm): 15.0, density (g/cm3): 2.25
Detector efficiency : Calculation

3

Element	Line	App. Conc	k ratio	Intensity corrn.		Weight%	Weight% sigma	Atomic%	Compound%	Formula	Number of ions	Standard
Al	K_SERIES	1.48	0.01092	0.7894	6.81	0.60	5.89	12.87	Al2O3	Al2O3	3.08	1-Jun-1999 12:00 AM
Si	K_SERIES	1.82	0.01467	0.8132	8.11	0.69	6.74	17.35	SiO2	SiO2	3.52	1-Jun-1999 12:00 AM
P	K_SERIES	2.85	0.0169	1.1228	9.21	0.80	6.94	21.11	P2O5	GaP	3.63	1-Jun-1999 12:00 AM
K	K_SERIES	0.56	0.00461	1.0735	1.90	0.41	1.13	2.29	K2O	MAD-10 Feldspar	0.59	1-Jun-1999 12:00 AM
Ca	K_SERIES	7.13	0.06402	0.9902	26.11	0.98	15.21	36.54	CaO	Wollastonite	7.95	1-Jun-1999 12:00 AM
Ti	K_SERIES	1.23	0.01234	0.7584	5.90	0.68	2.88	9.84	TiO2	Ti	1.50	1-Jun-1999 12:00 AM
O				41.95	1.23	61.21			32.00			
Totals				100.00								
									Cation sum		20.28	

Processing option : Oxygen by stoichiometry (Normalised)
Number of iterations : 2
Sample is polished.
Sample is coated with Carbon - thickness (nm): 15.0, density (g/cm3): 2.25
Detector efficiency : Calculation

8a
1

Element	Line	App. Conc	k ratio	Intensity corrn.		Weight%	Weight% sigma	Atomic%	Compound%	Formula	Number of ions	Standard
Ca	K_SERIES	12.16	0.10926	1.0774	71.47	1.18	50.00	100.00	CaO	Wollastonite	32.00	1-Jun-1999 12:00 AM
O				28.53	1.18	50.00			32.00			
Totals				100.00								
									Cation sum		32.00	

Processing option : Oxygen by stoichiometry (Normalised)
Number of iterations : 2
Sample is polished.
Sample is coated with Carbon - thickness (nm): 15.0, density (g/cm3): 2.25
Detector efficiency : Calculation

2

Element	Line	App. Conc	k ratio	Intensity corrn.		Weight%	Weight% sigma	Atomic%	Compound%	Formula	Number of ions	Standard
Ca	K_SERIES	12.76	0.11465	1.0774	71.47	1.15	50.00	100.00	CaO	Wollastonite	32.00	1-Jun-1999 12:00 AM
O				28.53	1.15	50.00			32.00			
Totals				100.00								
									Cation sum		32.00	

Processing option : Oxygen by stoichiometry (Normalised)
Number of iterations : 2
Sample is polished.
Sample is coated with Carbon - thickness (nm): 15.0, density (g/cm3): 2.25
Detector efficiency : Calculation

3

Element	Line	App. Conc	k ratio	Intensity	corrn.	Weight%	Weight% sigma	Atomic%	Compound%	Formula	Number of ions	Standard
Ca	K_SERIES	13.61	0.1222	1.0774	71.47	1.11	50.00	100.00	CaO	32.00	Wollastonite	1-Jun-1999 12:00 AM
O				28.53	1.11	50.00			32.00			
Totals				100.00								
								Cation sum		32.00		

Processing option : Oxygen by stoichiometry (Normalised)
Number of iterations : 2
Sample is polished.
Sample is coated with Carbon - thickness (nm): 15.0, density (g/cm3): 2.25
Detector efficiency : Calculation

10a

1

Element	Line	App. Conc	k ratio	Intensity	corrn.	Weight%	Weight% sigma	Atomic%	Compound%	Formula	Number of ions	Standard
Mg	K_SERIES	0.47	0.00324	0.6902	2.98	0.59	2.65	4.94	MgO	1.36	MgO	1-Jun-1999 12:00 AM
Al	K_SERIES	1.73	0.01271	0.7721	9.72	0.82	7.78	18.36	Al2O3	4.00	Al2O3	1-Jun-1999 12:00 AM
Si	K_SERIES	4.90	0.03955	0.7570	28.13	1.19	21.63	60.18	SiO2	11.13	SiO2	1-Jun-1999 12:00 AM
K	K_SERIES	0.95	0.0078	0.9676	4.27	0.57	2.36	5.15	K2O	1.21	MAD-10 Feldspar	1-Jun-1999 12:00 AM
Fe	K_SERIES	1.70	0.017	0.8358	8.84	1.06	3.42	11.37	FeO	1.76	Fe	1-Jun-1999 12:00 AM
O				46.06	1.40	62.17			32.00			
Totals				100.00								
								Cation sum		19.47		

Processing option : Oxygen by stoichiometry (Normalised)
Number of iterations : 2
Sample is polished.
Sample is coated with Carbon - thickness (nm): 15.0, density (g/cm3): 2.25
Detector efficiency : Calculation

2

Element	Line	App. Conc	k ratio	Intensity	corrn.	Weight%	Weight% sigma	Atomic%	Compound%	Formula	Number of ions	Standard
Ca	K_SERIES	12.49	0.11218	1.0774	71.47	1.15	50.00	100.00	CaO	32.00	Wollastonite	1-Jun-1999 12:00 AM
O				28.53	1.15	50.00			32.00			
Totals				100.00								
								Cation sum		32.00		

Processing option : Oxygen by stoichiometry (Normalised)
Number of iterations : 2
Sample is polished.
Sample is coated with Carbon - thickness (nm): 15.0, density (g/cm3): 2.25
Detector efficiency : Calculation

3

Element	Line	App. Conc	k ratio	Intensity	corrn.	Weight%	Weight% sigma	Atomic%	Compound%	Formula	Number of ions	Standard
Al	K_SERIES	0.22	0.00159	0.7292	2.23	0.73	2.16	4.21	Al2O3	1.28	Al2O3	1-Jun-1999 12:00 AM
Si	K_SERIES	0.86	0.00696	0.8218	7.92	0.99	7.38	16.94	SiO2	4.36	SiO2	1-Jun-1999 12:00 AM
Ca	K_SERIES	7.23	0.06494	1.0432	52.30	1.72	34.16	73.18	CaO	20.16	Wollastonite	1-Jun-1999 12:00 AM
Fe	K_SERIES	0.47	0.00472	0.8091	4.40	1.12	2.06	5.67	FeO	1.22	Fe	1-Jun-1999 12:00 AM
O				33.15	1.62	54.23			32.00			
Totals				100.00								
								Cation sum		27.01		

Processing option : Oxygen by stoichiometry (Normalised)
Number of iterations : 2
Sample is polished.
Sample is coated with Carbon - thickness (nm): 15.0, density (g/cm3): 2.25
Detector efficiency : Calculation

4

Element	Line	App. Conc	k ratio	Intensity	corrn.	Weight%	Weight% sigma	Atomic%	Compound%	Formula	Number of ions	Standard
Ca	K_SERIES	12.00	0.10778	1.0774	71.47	1.21	50.00	100.00	CaO	32.00	Wollastonite	1-Jun-1999 12:00 AM
O				28.53	1.21	50.00			32.00			
Totals				100.00								
								Cation sum		32.00		

Processing option : Oxygen by stoichiometry (Normalised)
Number of iterations : 2
Sample is polished.
Sample is coated with Carbon - thickness (nm): 15.0, density (g/cm3): 2.25
Detector efficiency : Calculation

5

Element	Line	App. Conc	k ratio	Intensity	corrn.	Weight%	Weight% sigma	Atomic%	Compound%	Formula	Number of ions	Standard
Ca	K_SERIES	12.37	0.11108	1.0774	71.47	1.18	50.00	100.00	CaO	32.00	Wollastonite	1-Jun-1999 12:00 AM
O				28.53	1.18	50.00			32.00			
Totals				100.00								
								Cation sum		32.00		

Processing option : Oxygen by stoichiometry (Normalised)
Number of iterations : 2
Sample is polished.
Sample is coated with Carbon - thickness (nm): 15.0, density (g/cm3): 2.25
Detector efficiency : Calculation

6

Element	Line	App. Conc	k ratio	Intensity corrn.			Weight%	Weight% sigma	Atomic%	Compound%	Formula	Number of ions	Standard
Si	K_SERIES	0.41	0.00332	0.6653	3.44	0.74	4.13	7.35	2.10	SiO2	SiO2	1-Jun-1999 12:00 AM	
P	K_SERIES	0.62	0.00367	1.0337	3.33	0.75	3.63	7.62	1.84	P2O5	GaP	1-Jun-1999 12:00 AM	
S	K_SERIES	1.13	0.00993	0.8118	7.72	0.81	8.14	19.28	4.14	SO3	FeS2	1-Jun-1999 12:00 AM	
Ca	K_SERIES	2.40	0.02159	1.0661	12.51	0.99	10.55	17.51	5.36	CaO	Wollastonite	1-Jun-1999 12:00 AM	
Ba	L_SERIES	6.63	0.0619	0.8525	43.21	2.13	10.63	48.24	5.41	BaO	BaF2	1-Jun-1999 12:00 AM	
O				29.80	1.76	62.92							
Totals				100.00									
									Cation sum		18.85		

Processing option : Oxygen by stoichiometry (Normalised)
Number of iterations : 2
Sample is polished.
Sample is coated with Carbon - thickness (nm): 15.0, density (g/cm3): 2.25
Detector efficiency : Calculation

11a

1

Element	Line	App. Conc	k ratio	Intensity corrn.			Weight%	Weight% sigma	Atomic%	Compound%	Formula	Number of ions	Standard
Mg	K_SERIES	0.25	0.00172	0.4237	2.71	0.95	3.83	4.49	2.34	MgO	MgO	1-Jun-1999 12:00 AM	
Al	K_SERIES	0.10	0.00074	0.5176	0.89	0.72	1.13	1.68	0.69	Al2O3	Al2O3	1-Jun-1999 12:00 AM	
Si	K_SERIES	0.50	0.00403	0.6410	3.56	0.74	4.37	7.62	2.66	SiO2	SiO2	1-Jun-1999 12:00 AM	
Ca	K_SERIES	0.25	0.00225	1.1224	1.02	0.46	0.87	1.43	0.53	CaO	Wollastonite	1-Jun-1999 12:00 AM	
Mn	K_SERIES	10.79	0.10794	0.9076	54.34	1.93	34.05	70.17	20.76	MnO	Mn	1-Jun-1999 12:00 AM	
Ba	L_SERIES	2.75	0.02571	0.9609	13.09	1.53	3.28	14.62	2.00	BaO	BaF2	1-Jun-1999 12:00 AM	
O				24.39	1.66	52.47							
Totals				100.00									
									Cation sum		28.99		

Processing option : Oxygen by stoichiometry (Normalised)
Number of iterations : 2
Sample is polished.
Sample is coated with Carbon - thickness (nm): 15.0, density (g/cm3): 2.25
Detector efficiency : Calculation

2

Element	Line	App. Conc	k ratio	Intensity corrn.			Weight%	Weight% sigma	Atomic%	Compound%	Formula	Number of ions	Standard
S	K_SERIES	2.43	0.02137	0.8383	14.51	1.13	16.13	36.23	7.80	SO3	FeS2	1-Jun-1999 12:00 AM	
Ca	K_SERIES	0.75	0.00676	1.0673	3.53	0.62	3.14	4.94	1.52	CaO	Wollastonite	1-Jun-1999 12:00 AM	
Fe	K_SERIES	0.47	0.00472	0.8596	2.75	0.87	1.75	3.54	0.85	FeO	Fe	1-Jun-1999 12:00 AM	
Ba	L_SERIES	8.79	0.0821	0.8884	49.52	2.01	12.85	55.29	6.22	BaO	BaF2	1-Jun-1999 12:00 AM	
O				29.69	1.69	66.13							
Totals				100.00									
									Cation sum		16.39		

Processing option : Oxygen by stoichiometry (Normalised)
Number of iterations : 2
Sample is polished.
Sample is coated with Carbon - thickness (nm): 15.0, density (g/cm3): 2.25
Detector efficiency : Calculation

3

Element	Line	App. Conc	k ratio	Intensity corrn.			Weight%	Weight% sigma	Atomic%	Compound%	Formula	Number of ions	Standard
Si	K_SERIES	2.36	0.01907	0.8563	18.71	1.17	16.36	40.03	9.00	SiO2	SiO2	1-Jun-1999 12:00 AM	
Ca	K_SERIES	5.51	0.04951	1.0097	37.00	1.50	22.66	51.77	12.47	CaO	Wollastonite	1-Jun-1999 12:00 AM	
Fe	K_SERIES	0.77	0.00768	0.8161	6.38	1.22	2.80	8.20	1.54	FeO	Fe	1-Jun-1999 12:00 AM	
O				37.91	1.53	58.18							
Totals				100.00									
									Cation sum		23.00		

Processing option : Oxygen by stoichiometry (Normalised)
Number of iterations : 2
Sample is polished.
Sample is coated with Carbon - thickness (nm): 15.0, density (g/cm3): 2.25
Detector efficiency : Calculation

4

Element	Line	App. Conc	k ratio	Intensity corrn.			Weight%	Weight% sigma	Atomic%	Compound%	Formula	Number of ions	Standard
Ca	K_SERIES	11.73	0.10534	1.0774	71.47	1.21	50.00	100.00	32.00	CaO	Wollastonite	1-Jun-1999 12:00 AM	
O				28.53	1.21	50.00							
Totals				100.00									
									Cation sum		32.00		

Processing option : Oxygen by stoichiometry (Normalised)
Number of iterations : 2
Sample is polished.
Sample is coated with Carbon - thickness (nm): 15.0, density (g/cm3): 2.25
Detector efficiency : Calculation